

Case No. 84739

IN THE SUPREME COURT OF THE STATE OF NEVADA

Electronically Filed
Nov 08 2022 04:38 p.m.
Elizabeth A. Brown
Clerk of Supreme Court

ADAM SULLIVAN, P.E., NEVADA
STATE ENGINEER, et al.

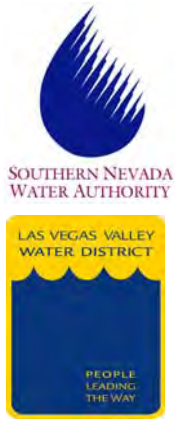
Appellants,

vs.

LINCOLN COUNTY WATER
DISTRICT, et al.

JOINT APPENDIX

VOLUME 20 OF 49



Assessment of Water Resource Conditions in the Lower White River Flow System

October 2018

This document's use of trade, product, or firm names is for descriptive purposes only and does not imply endorsement by the Southern Nevada Water Authority. Although trademarked names are used, a trademark symbol does not appear after every occurrence of a trademarked name. Every attempt has been made to use proprietary trademarks in the capitalization style used by the manufacturer.

Suggested citation: Southern Nevada Water Authority and Las Vegas Valley Water District, 2018, Assessment of Water Resource Conditions in the Lower White River Flow System: Southern Nevada Water Authority, Las Vegas, Nevada, Doc. No. WRD-ED-0051, 116 p.

SE ROA 37698

CONTENTS

List of Figures	iii
List of Tables	v
List of Acronyms and Abbreviations	vii
1.0 Introduction.....	1-1
1.1 Background.....	1-1
1.1.1 Order 1169	1-1
1.1.2 2006 Memorandum of Agreement.....	1-3
1.1.3 Order 1169 Aquifer Test and Order 1169A.....	1-4
1.1.4 NSE Rulings Nos. 6254 through 6261.....	1-4
1.2 Purpose and Scope	1-4
1.3 Approach.....	1-5
2.0 Sources of Information.....	2-1
2.1 Previous Investigations.....	2-1
2.1.1 Order 1169 Reports	2-1
2.1.2 Annual Data Reports (2013-2018).....	2-3
2.1.3 Other Reports	2-4
2.2 Data Sources.....	2-4
3.0 LWRFS Description.....	3-1
3.1 Physiography	3-1
3.2 Climate	3-1
3.3 Hydrogeology.....	3-1
3.3.1 Structural Setting	3-3
3.3.2 Hydrogeologic Setting.....	3-5
3.4 Hydrology.....	3-6
3.4.1 Surface Water.....	3-6
3.4.2 Groundwater.....	3-10
3.4.2.1 Aquifer Types and Conditions	3-10
3.4.2.2 Occurrence and Movement	3-12
4.0 Natural and Anthropogenic Stresses.....	4-1
4.1 Natural Stresses.....	4-1
4.2 Anthropogenic Stresses.....	4-5
4.2.1 Surface-Water Diversions above Muddy River near Moapa, NV Gage ..	4-5
4.2.2 Groundwater Production	4-5
4.2.2.1 Muddy River Springs Area	4-6
4.2.2.2 Carbonate Aquifer	4-8
5.0 Hydrologic Responses	5-1
5.1 Evaluation of Muddy River Streamflow Declines	5-1
5.1.1 Climate Variability.....	5-1



CONTENTS (CONTINUED)

5.1.2 Historical Land Use in the MRSA 5-2

5.1.3 MRSA Surface-Water Diversions 5-3

5.1.4 MRSA Groundwater Production 5-4

5.2 Carbonate-Aquifer Responses to Climate Variability and Pumping Stresses 5-6

5.2.1 Responses to Climate Variability 5-6

5.2.2 Groundwater Production - NSE Order 1169 Aquifer Test and Recovery 5-9

5.3 Water-Resource Implications 5-14

6.0 Summary and Conclusions 6-1

7.0 References 7-1

Appendix A - Site Table for Wells

Appendix B - Surface Water Diversions above the Moapa Gage

Appendix C - Groundwater Production Data

FIGURES

NUMBER	TITLE	PAGE
1-1	Area of Interest and Lower White River Flow System	1-2
3-1	Physiography of the Area of Interest including the LWRFS	3-2
3-2	Hydrogeologic Map of the Lower White River Flow System	3-4
3-3	Spring Complexes, Streams, Diversions, and Gaging Stations within the Headwaters of the Muddy River	3-7
3-4	Pederson Spring near Moapa, NV - Daily Discharge Record (1986 to present)	3-8
3-5	Warm Springs West near Moapa, NV - Daily Discharge Record (1985 to present)	3-9
3-6	Muddy River near Moapa, NV (1945 to 2017)	3-10
3-7	Conceptualization of the Lower White River Flow System.	3-13
4-1	Nevada Division 4 Climate Zone	4-2
4-2	Climate Division 4 Precipitation with Trendline	4-3
4-3	Nevada Climate Division 4 Precipitation.	4-4
4-4	Surface-Water Diversions above the MR Moapa Gage	4-6
4-5	Locations of Production Wells in the LWRFS.	4-7
4-6	Annual Groundwater Production from the MRSA Alluvial Reservoir	4-8
4-7	Carbonate-Aquifer Groundwater Production	4-9
5-1	Natural Flow Record at MR Moapa Gage (1993 - 2017).	5-3
5-2	Annual ET Reduced by Precipitation for Muddy River Springs Area (2001 -2012).	5-3
5-3	MR Flow Deficit (1993 - 2017)	5-4
5-4	MR Flow Deficit and Coyote Spring Valley and MRSA Groundwater Production	5-5
5-5	Water-Level Responses in Representative Carbonate Wells	5-7
5-6	Water-Level Responses in Representative Carbonate Wells	5-8



FIGURES (CONTINUED)

NUMBER	TITLE	PAGE
5-7	MRSA Spring Discharge and Carbonate-Aquifer Groundwater Production	5-10
5-8	Carbonate-Aquifer Water Levels and Groundwater Production	5-11
5-9	Carbonate-Aquifer Water Levels and Groundwater Production	5-12
5-10	Carbonate-Aquifer Water Levels and Groundwater Production	5-13
5-11	Elevation of Selected Springs and LIDAR Digital Elevation Model within the MRSA	5-16

TABLES

NUMBER	TITLE	PAGE
1-1	Trigger Ranges at Warm Springs West Gage and Corresponding Pumping Restrictions	1-3
3-1	USGS Gaging Stations in the Headwaters of the Muddy River	3-8
A-1	Site Table for Wells	A-1
B-1	Surface Water Diversions above the Moapa Gage in the MRSA	B-1
C-1	Shallow Alluvial Wells in the Muddy River Springs Area Pumped by Nevada Energy	C-1
C-2	Groundwater Diversions in MRSA and CSV	C-2
C-3	Groundwater Production	C-3



This Page Left Intentionally Blank

ACRONYMS

BLM	Bureau of Land Management
CSI	Coyote Springs Investment, LLC
CSV	Coyote Springs Valley
ET	Evapotranspiration
HA	Hydrographic Area
HRT	Hydrologic Review Team
LDS	The Church of Jesus Christ of Latter-day Saints
LVVWD	Las Vegas Valley Water District
LVVSZ	Las Vegas Valley Shear Zone
LWRFS	Lower White River Flow System
MBPI	Moapa Band of Paiute Indians
METRIC	Mapping EvapoTranspiration at high Resolution with Internalized Calibration
MOA	Memorandum of Agreement
MRSA	Muddy River Springs Area
MR	Muddy River
MVWD	Moapa Valley Water District
NSE	Nevada State Engineer
NDWR	Nevada Division of Water Resources
NDVI	Normalized Difference Vegetation Index
NPS	National Park Service
NOAA	National Oceanic and Atmospheric Administration
NV	Nevada
NVE	Nevada Energy
NWIS	National Water Information System
PRISM	Parameter-elevation Regressions on Independent Slopes Model
PSZ	Pahranagat Shear Zone
SNWA	Southern Nevada Water Authority
USGS	U.S. geological Survey
USFWS	U.S. Fish and Wildlife Service
WRCC	Western Region Climate Center
WRFS	White River Flow System

ABBREVIATIONS

° C	degrees Celsius
° F	degrees Fahrenheit
af	acre-foot
afy	acre-feet per year
cfs	cubic feet per second
ft	foot [feet]
ft amsl	feet above mean sea level
gpm	gallons per minute
in.	inch [inches]
Ma	million years ago

1.0 INTRODUCTION

This report was prepared to supplement the October 5, 2018, *Comment Letter to the State Engineer Regarding Administrative Order for LWRFS* (Comment Letter) submitted on behalf of the Las Vegas Valley Water District (LVVWD) and Southern Nevada Water Authority (SNWA) in response to the Nevada State Engineer's (NSE) Draft Order concerning the Lower White River Flow System (LWRFS). This report addresses in greater detail the points raised in the Comment Letter concerning water-resource conditions in the LWRFS and the imminent conflicts with senior water rights that would result from increased groundwater production. The NSE is urged to consider this report in making any temporary or final order concerning the administration of water rights and management of groundwater development in the LWRFS.

The Nevada Division of Water Resources (NDWR) defines the LWRFS as the hydrographic areas (HA) of Coyote Spring Valley (HA 210), Hidden Valley (HA 217), Garnet Valley (HA 216), California Wash (HA 218) Muddy River Springs Area (HA 219), and the northwest portion of the Black Mountains Area (HA 215) (NDWR, 2018a). [Figure 1-1](#) presents the boundary of the LWRFS. Kane Springs Valley is included within the area of interest because it contributes to the local recharge and is tributary to the LWRFS. The remainder of this section presents background information about the LWRFS and the purpose and scope of the work described in this document.

1.1 Background

In 1989, the LVVWD filed applications with the NDWR to appropriate groundwater in Coyote Spring Valley. The NSE held administrative hearings on these applications and other applications filed by Coyote Springs Investment, LLC (CSI) during 2001. Subsequent to these hearings, several NSE orders, stakeholder agreements, and NSE rulings were issued. The pertinent details of the relevant documents are summarized in the following sections.

1.1.1 Order 1169

In 2002, the NSE issued Order 1169 holding in abeyance all pending and new applications for the appropriation of groundwater from the carbonate-rock aquifer underlying Coyote Spring, Hidden, Garnet, and Lower Moapa valleys, and the Muddy River Springs and Black Mountains areas. In addition, the NSE required a five-year study during which at least 50 percent of the existing groundwater rights in Coyote Spring Valley would be pumped for at least two consecutive years. The NSE stated the purpose of the study and aquifer test was to “...*determine if the pumping of those water rights will have any detrimental impacts on existing water rights or the environment.*” (NSE, 2002). The NSE directed the following entities to complete the study:

- LVVWD

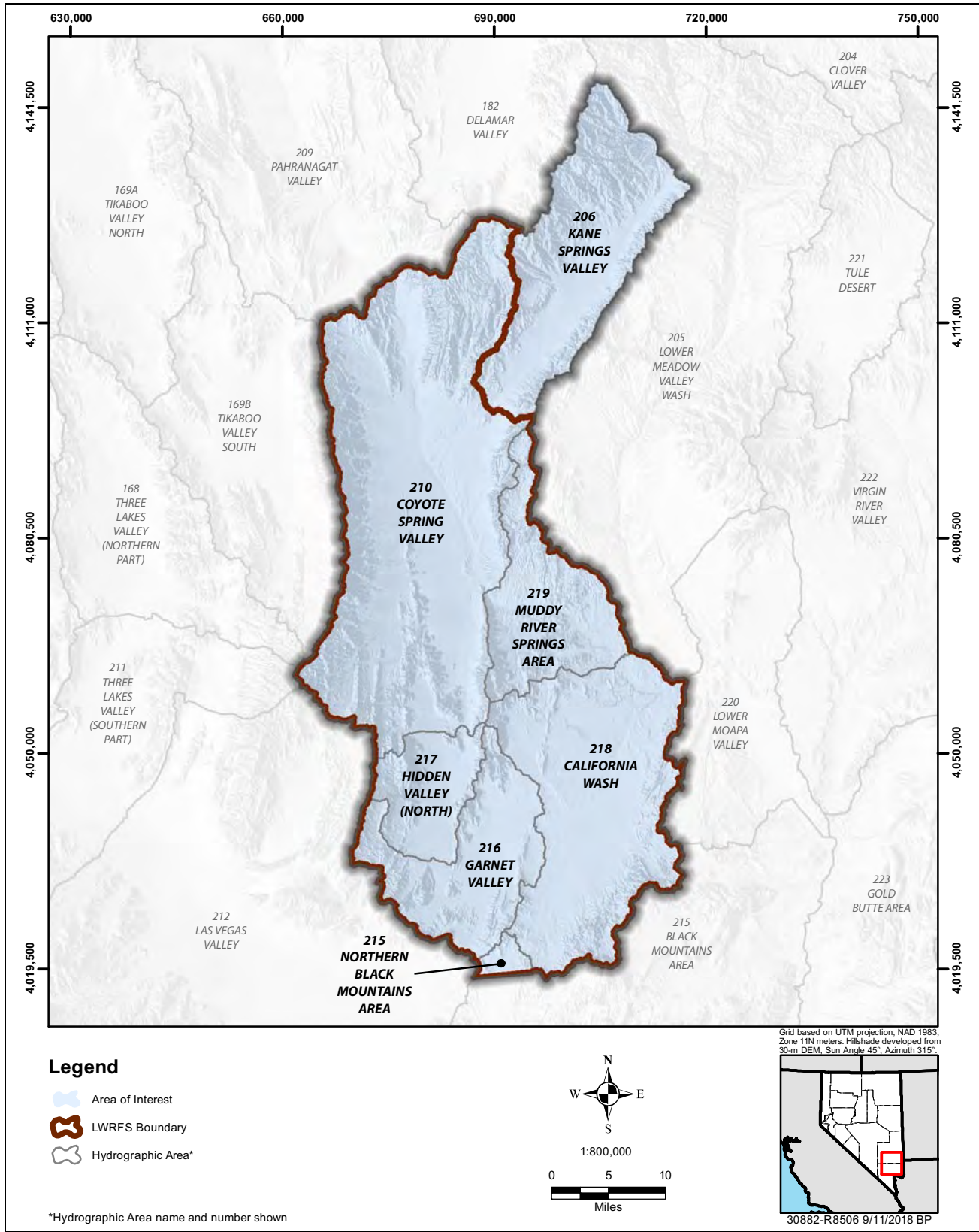


Figure 1-1
Area of Interest and Lower White River Flow System

- SNWA
- CSI
- Nevada Power Company (hereinafter referred to as Nevada Energy)
- Moapa Valley Water District (MVWD)

Order 1169 also instituted hydrologic monitoring and reporting requirements for the study participants and other water-right owners with points of diversion located in Garnet Valley and the Black Mountains Area. In April of 2002, the NSE granted requests by the Moapa Band of Paiute Indians (MBPI) and the U.S. Department of Interior to allow the Bureau of Indian Affairs, Fish and Wildlife Service (USFWS), and National Park Service (NPS) to participate in the study.

1.1.2 2006 Memorandum of Agreement

In 2006, to facilitate implementation of the Order 1169 study and aquifer test and to ensure protections of senior water rights and the endangered Moapa dace, the SNWA, CSI, USFWS, MBPI and MVWD entered into a Memorandum of Agreement (MOA) that instituted, among other things, Trigger Ranges associated with flows at the Warm Springs West gage under which pumping restrictions would apply (SNWA, 2006). These Trigger Ranges and the corresponding pumping restrictions are listed in [Table 1-1](#).

**Table 1-1
Trigger Ranges at Warm Springs West Gage and Corresponding
Pumping Restrictions**

	SNWA ¹	CSI ¹	MVWD ²	MBPI ³
Water Rights considered under MOA (afy)	9,000	4,600	--	2,500
Trigger Ranges (cfs)	Pumping Restrictions (acre-feet per year [afy])			
3.2 or less	Parties meet to discuss and interpret data and plan mitigation measures			
3.0 or less	SNWA & CSI take actions to redistribute pumping		--	--
3.0 - <2.9	< 8,050		--	--
2.9 - <2.8	< 6,000		--	< 2,000
2.8 - <2.7	< 4,000		--	< 1,700
≤2.7	< 724		--	< 1,250

¹ SNWA and CSI production from wells MX-5, RW-2, CS-1, CS-2 and other CSI wells in Coyote Spring Valley

² MVWD pumping restriction were only for the duration of the test

³ MBPI pumping under permit no. 54075

In addition, the MOA established a Hydrologic Review Team (HRT) composed of representatives of each MOA signatory. The HRT is tasked with analyzing hydrologic data and determining, on an annual basis, whether the pumping restrictions under each Trigger Range should be modified.



1.1.3 Order 1169 Aquifer Test and Order 1169A

Pumping associated with the aquifer test began in accordance with Order 1169 on November 15 2010. The aquifer test was completed on December 31, 2012; however, production from SNWA's MX-5 well continued into April 2013.

During the test, pumping rates of the SNWA MX-5 well ranged from 3,300 to 3,800 gpm and constituted the single largest stress on the carbonate aquifer in LWRFS. Equipment issues associated with the water treatment facility connected to the well resulted in periods of non-pumping during the test. Production volumes from the MX-5 well totaled 4,131 af and 3,961 af for calendar years 2011 and 2012, respectively. Combined with CSI pumping from wells CSI-1 through CSI-4, a total of 5,331 and 5,102 af were pumped in Coyote Spring Valley during calendar years 2011 and 2012, respectively. Additional production from the carbonate aquifer occurred during the test by MVWD in the Muddy River Springs Area (MRSA) and by several entities in Garnet Valley. A historical accounting of groundwater production in the LWRFS is presented in [Section 4.0](#). Prior to and during the aquifer test, the study participants implemented a comprehensive hydrologic monitoring program under the direction of NDWR. Data were submitted quarterly to NDWR in electronic form and made available to all study participants and the public.

The State Engineer issued amended Order 1169A on December 21, 2012 (NSE, 2012). In Order 1169A, the NSE declared the aquifer test completed as of December 31, 2012 and solicited information from the study participants regarding the test, impacts, and the availability of water pursuant to the pending applications held in abeyance by Order 1169. The reports submitted by the MOA signatories are summarized in [Section 2.0](#).

1.1.4 NSE Rulings Nos. 6254 through 6261

In January 2014, the NSE issued Rulings 6254 through 6261 (NSE, 2014a through h). In these rulings the NSE denied all pending applications in the LWRFS and found that “...*the Order 1169 test measurably reduced flows in headwater springs of the Muddy River.*” Based on the test results, the NSE ruled that there is no unappropriated groundwater and that the applications would conflict with existing rights and threaten to prove detrimental to the public interest. The NSE also ruled that the basins composing the LWRFS would be jointly managed.

1.2 Purpose and Scope

The purpose of the work presented in this document is to summarize the current state of knowledge of the LWRFS, including spring discharge and perennial streamflow in the MRSA. Specific objectives are as follows:

- Evaluate hydrologic responses to the variable stress conditions affecting the LWRFS;
- Evaluate the recovery responses associated with the cessation of the 2-year aquifer test; and
- Identify trends in the behavior of key hydrologic variables.

The scope of work includes a survey of the available information; compilation and analysis of time-series data; and the creation of various maps, tables, and charts to support the analyses and conclusions.

1.3 Approach

The objectives of this work were achieved by completing the following steps:

1. Performing a survey of the information available regarding the flow system, including hydrologic stress conditions and responses ([Section 2.0](#)).
2. Describing the flow system using the available information, including the interpretations derived from the data collected during the two-year aquifer test ([Section 3.0](#)).
3. Compiling and analyzing historical time-series data for natural and anthropogenic stresses affecting the hydrology of the LWRFS ([Section 4.0](#)).
4. Using historical time-series data to analyze the hydrologic responses of several variables that describe the historical conditions of the flow system over a period of decades ([Section 5.0](#)).
5. Summarizing the assessment of current water-resource conditions of the LWRFS ([Section 6.0](#)).



This Page Left Intentionally Blank

2.0 SOURCES OF INFORMATION

The assessment described in this document required a review of the existing literature and the use of large quantities of data acquired from various sources.

2.1 Previous Investigations

Previous investigations completed by LVVWD/SNWA and others that are relevant to this assessment are summarized in this section. Such investigations started with the reconnaissance studies initiated in the late 1940s and have continued since. Only relevant studies documented after the issuance of NSE's Order 1169A in December 2012 are summarized in this section.

2.1.1 Order 1169 Reports

In the months following the completion of the 2-year aquifer test mandated by NSE Order 1169, the various stakeholders, including the MOA signatories, evaluated the test results and documented their interpretations, conclusions, and recommendations in reports submitted to the NSE in June of 2013. It should be noted that these reports relied upon only a few months of recovery data that were influenced by the SNWA MX-5 well which continued pumping through mid-April 2013 (see [Section 5.2.2](#) of this report for a more detailed explanation).

SNWA (2013)

SNWA (2013) presents the data collected before and during the test, as well as interpretations of aquifer responses and water availability. Based on their analysis of the pre-test and test data, the major conclusions made by SNWA (2013) are as follows:

- Changes in groundwater levels are affected by both groundwater pumping from the carbonate aquifer and changes in prevailing hydrologic conditions before and after the aquifer test.
- The aquifer test confirmed that extensive hydraulic connectivity exists in the carbonate aquifer. However, the presence of boundaries and spatial variations in hydraulic conductivity affect the carbonate aquifer's response depending on location. For example, no discernible responses were observed north of the Kane Springs Fault and west of the MX-5 and CSI wells near the eastern front of the Las Vegas Range (note: the lack of responses cited in SNWA (2013), referred to wells CSVM-3 and CSVM-5; see [Sections 5.2.1](#) and [5.2.2](#) of this report for a more detailed explanation).
- Relatively minor declines in spring flow were observed at the highest elevation springs (Pederson and Pederson East springs) during the test. However, no changes were discerned in



the flows of the Muddy River at the U.S. Geological Survey (USGS) Muddy River near Moapa, Nevada gage, as these flows are mainly affected by local alluvial pumping in the MRSA.

- Pumping the existing groundwater rights in Coyote Spring Valley (CSV) during the test did not result in an unreasonable lowering of the groundwater table. Furthermore, recovery began when pumping was reduced to pre-test levels.
- It remains unclear if additional resource development beyond existing permitted rights could take place in Coyote Spring Valley at selected locations.

USFWS, Bureau of Land Management (BLM), and NPS (2013)

The USFWS, BLM, and NPS prepared a similar report in 2013. Their analyses included a numerical groundwater flow model developed by Tetra Tech (2012a and b) and SeriesSEE analysis. They attempted to calibrate the model using the data from the 2-year aquifer test and used the resulting model to make predictions. The SeriesSEE analysis was conducted to segregate the drawdowns caused by the MX-5 pumping well from those caused by the other pumping wells. Their main conclusions are as follows:

- Pumping at MX-5 caused drawdowns of about the same magnitude in the portion of the carbonate aquifer underlying Coyote Spring Valley, the MRSA, Hidden and Garnet valleys, and California Wash at the end of the test.
- Using the results of the SeriesSEE analyses, USFWS et al. (2013) delineated the connected portion of the carbonate aquifer, which they state includes the source of the Muddy River Springs and majority source of the Muddy River.
- Based on these analyses, USFWS et al. (2013) concluded that pumping from the connected portion of the carbonate aquifer causes drawdowns of about the same magnitude throughout the delineated area.
- Based on previous information and the results of their analysis of the test data, they also concluded that no additional groundwater is available for appropriation.

Johnson and Mifflin (2013)

Johnson and Mifflin (2013) also prepared a report of the analysis of the 2-year aquifer test data. Based on their analysis, they found that (1) the portion of the WRFS located south of Pahrnagat Valley consists of two separate flow fields, the northern and southern flow fields, that responded differently to the pumping in Coyote Spring Valley; and (2) the variations in the Muddy River baseflow caused by natural stresses are of the same order of magnitude as the pumping stresses in Coyote Spring Valley during the two-year aquifer test. Based on their analyses, they made the following four recommendations:

- At least four of the basins that include and extend upgradient from the MRSA should be combined into one water-management unit.

- The pending LVVWD water rights applications in this area should be denied on the grounds that they would impact senior rights by the full amount.
- The existing undeveloped permits located within the combined area must be mostly revoked, restricted, or very carefully managed to avoid periods of eliminated Muddy River base flows in the Springs-area headwater reaches in the future.
- A large interim pumping test should be conducted in the northern portion of the Southern Flow Field to better evaluate the water-resource potential of this portion of the flow system.

CSI (2013)

CSI (2013) conducted a qualitative analysis of the 2-year aquifer test and concluded that the effects of pumping during the test generated a shallow drawdown cone that extends miles from the MX-5 well. Using the observations from the test and monitoring data collected by SNWA, CSI (2013) concluded the following:

- The Kane Spring fault acts as a groundwater barrier to groundwater flowing from north to south in Coyote Spring Valley and may also serve as a barrier to pumping from wells located north of the fault.
- Based on supporting information from SNWA's Annual Monitoring Reports, additional groundwater is available for appropriation in Coyote Spring Valley.
- Water-right applications submitted by CSI and SNWA should be fully or partly granted.

Myers (2013)

Myers (2013) describes an analysis of the 2-year aquifer test and a review of the groundwater flow model developed by Tetra Tech for the southern White River Flow System (WRFS) (Tetra Tech, 2012a and b). Myers (2013) concluded the following:

- The Order 1169 aquifer test data and the Tetra Tech groundwater flow model predictions indicate that pumping from existing groundwater rights in Coyote Springs Valley and the MRSA will cause the spring discharge to decrease to dangerous levels.
- Any additional water rights potentially granted in the future will cause the spring discharge to decrease further below the required target rates, and may eventually dry up some or all of the springs in the MRSA.

2.1.2 Annual Data Reports (2013-2018)

This assessment relied upon the annual data reports prepared by the Order 1169 study participants and others who submit quarterly data to NDWR. Among these reports are the ones prepared by SNWA, MVWD, NVE and the HRT.



SNWA Annual Monitoring Reports

SNWA prepares and submits annual monitoring reports in satisfaction of water-right permit terms for groundwater and surface-water sites throughout the LWRFS. The reports of particular interest are the ones prepared after the completion of the aquifer test as they contain data characterizing the recovery responses to the pumping stresses imposed during the 2-year aquifer test (SNWA, 2013 through 2018).

HRT Annual Determination Reports

Also relevant to this assessment are the annual reports prepared by the HRT after the completion of the test (2013 through 2018). The MOA signatories collect and analyze data and share their findings to satisfy the objectives of the MOA. Since the MOA was signed in 2006, extensive data collection and analysis efforts have been performed, including those associated with the Order 1169 study. The HRT annual reports include descriptions of previous monitoring activities and interpretations prepared by the signatories in the form of appendices. Based on the findings of each year, the HRT makes recommendations about the action levels associated with the Trigger Ranges. As in all previous reports, HRT (2018) recommended that no changes be made to the existing pumping restrictions listed in the MOA (SNWA, 2006) and presented in [Table 1-1](#).

2.1.3 Other Reports

A few other relevant reports have been issued since the completion of the 1169 aquifer test including the following:

Huntington et al. (2013)

Huntington et al. (2013) prepared a technical memorandum for SNWA containing estimates of evapotranspiration (ET) for the MRSA from 2001-2012. This work was part of a larger project designed to identify trends in ET over the period of 2001-2012 and the potential impacts that land management practices and vegetation changes may have on ET.

Rowley et al. (2017)

Rowley et al. (2017) published a comprehensive report describing the geology and geophysics of a large area including parts of eastern Nevada and western Utah, and comprising the LWRFS. The report includes geologic maps at a scale of 1:250,000 based on various published and unpublished geologic maps, site studies and new local geologic maps. Their report includes 25 new geologic cross sections at the same scale and interpretations of new geophysical data collected by the U.S. Geological Survey.

2.2 Data Sources

Data relevant to this evaluation of the water resource conditions of the LWRFS were obtained from many project-related sources as well as regional and national sources. Monitoring of hydrologic conditions and reporting of surface-water diversions and groundwater production has been on-going in the LWRFS for decades. Through the collective efforts of water-right owners, several monitoring

programs have been implemented to comply with monitoring and reporting requirements associated with permit terms. In addition, the NDWR instituted comprehensive monitoring and reporting requirements associated with the Order 1169 study to ensure pertinent data were collected and reported in a timely manner. These data are summarized in annual data reports and are accessible on the NDWR website at <http://water.nv.gov/Order1169Menu.aspx>.

In addition, SNWA and NDWR participate in joint funding agreements with the USGS to fund operation and maintenance of several important surface-water and groundwater sites located within the LWRFS. These data are accessible through the USGS National Water Information System and Groundwater Site Inventory database (NWIS) (USGS, 2018). Additional data were compiled from the NDWR drillers log database (NDWR, 2018b), published reports documenting well completions or hydrologic studies. However, the majority of the data presented in this report were collected and reported by the 2006 MOA signatories and Order 1169 study participants.

Climate records spanning long periods were necessary for this assessment are not available for meteorological stations located within the LWRFS. Thus, climate data were obtained from the following agencies:

- Western Region Climate Center (WRCC) at <https://wrcc.dri.edu/summary/Climsmnv.html>
- National Oceanic and Atmospheric Administration (NOAA) at <https://www.noaa.gov/climate>
- Parameter-elevation Regressions on Independent Slopes Model (PRISM) at <http://www.prism.oregonstate.edu/>



This Page Left Intentionally Blank

3.0 LWRFS DESCRIPTION

The boundary of the LWRFS was initially described in NSE Rulings 6254 through 6261 (NSE, 2014a through h), inclusive, and a figure attached to the rulings that identified the Order 1169 basins. The boundary of the LWRFS is depicted in [Figure 1-1](#). This section presents the physiography, climate, and hydrogeology of the LWRFS, and a description of the surface-water and groundwater hydrology.

3.1 Physiography

The LWRFS is within the Basin and Range physiographic province of the Great Basin, which is characterized by a series of parallel to sub-parallel, north-trending mountain ranges separated by elongated alluvial valleys (Fenneman, 1931). The western margin of the LWRFS is defined by the Sheep Range in the north and the Las Vegas Range in the south. The Sheep Range is the highest range in the LWRFS with peak elevations ranging from 7,000 to nearly 10,000 ft amsl. The eastern boundary of the LWRFS is defined by the Muddy and North Muddy mountains in the south and by the Meadow Valley and Delamar mountains in the north. Adjacent to the LWRFS, in Kane Springs Valley, elevations in the Delamar Mountains exceed 7,000 ft amsl. Included within the LWRFS are the Coyote Spring, Elbow, Arrow Canyon, and Dry Lake ranges all having elevations less than 6,000 ft amsl ([Figure 3-1](#)). During the Pleistocene Epoch, the White River flowed through Coyote Spring Valley entering the valley from southern Pahrangat Valley and traveling south and then southeast between the Arrow Canyon Range and the Meadow Valley Mountains where it continued along the present course of the Muddy River (Eakin, 1964). The elevations along this ancestral feature range from just above 3,000 ft amsl where it enters Coyote Spring Valley to 1,420 ft amsl where the river leaves California Wash near Glendale, Nevada.

3.2 Climate

The climate of the LWRFS is typical of southern Nevada ranging between arid and semi-arid conditions. This climate is characterized by small amounts of precipitation occurring mostly on the surrounding mountains, and high summer temperatures and evaporation rates. Winter-season precipitation occurs as snow at the higher elevations of the Sheep and Delamar Ranges and serves as the primary source of local recharge. During the summer months, precipitation occurs as a result of local storms. Air temperatures vary greatly on a daily and seasonal basis. Climate variations constitute natural stresses to the hydrologic system of the LWRFS and are discussed in more detail in [Section 4.0](#).

3.3 Hydrogeology

The hydrogeology of the LWRFS is characterized by the complex geology of the area, which ranges in age from Precambrian siliciclastic rocks to Tertiary and Quaternary alluvial deposits that have been

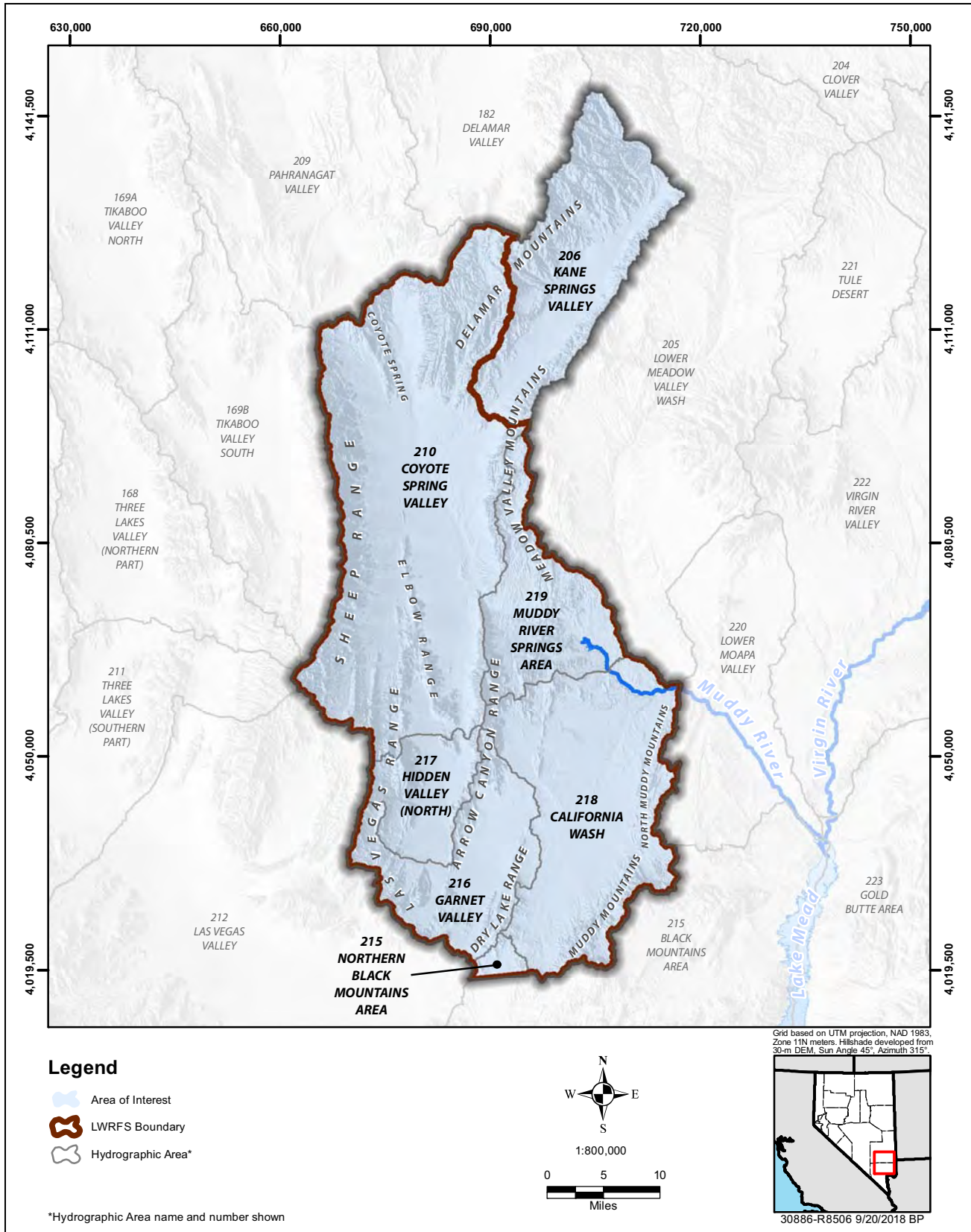


Figure 3-1
Physiography of the Area of Interest including the LWRFS

structurally deformed during several tectonic episodes (Rowley et al., 2017). Three tectonic episodes as well as extensive volcanism have affected the region. The Antler deformation and Sevier deformation resulted in east-verging thrust sheets in which Paleozoic carbonate rocks were placed over the top of each other as well as over younger rocks producing thick sequences of carbonate rocks in the region. The third tectonic episode is the middle Miocene to Holocene basin-range deformation that shaped the current topography of the Great Basin. In this episode, basin-range faulting produced horst and graben topography resulting in typically deep basins and relatively high mountain ranges that are generally oriented north-south (Rowley et al., 2017).

The following sections summarize the structural setting and hydrogeology of the LWRFS, with reference to the 1:250,000 scale hydrogeologic map of Rowley et al. (2011) presented in [Figure 3-2](#). The map is based on a geologic map and cross sections for a region including portions of White Pine, Lincoln, and Clark counties in Nevada, and adjacent areas.

3.3.1 Structural Setting

Major structural episodes have caused faulting within the LWRFS. These episodes have influenced the distribution and thickness of geologic units and the geometry of the basins and ranges. Major fault structures within the area are described in the following sections.

Thrust Faults

Thrust faults within the LWRFS include the Muddy Mountain thrust in the Muddy Mountains, the Dry Lake thrust in the Dry Lake Range, and the Gass Peak thrust in the eastern Sheep Range ([Figure 3-2](#)). As previously stated, the importance of these faults is that they create very thick carbonate rock sequences that, as a result of compression and transport, have significant fracture development and therefore increased permeabilities (Heilweil and Brooks, 2011; Page et al., 2005). However, the thrust faults themselves may act as barriers to groundwater flow (Page et al., 2005).

Strike-Slip Faults

The left-lateral strike-slip fault of the Pahrangat Shear Zone (PSZ) and the right-lateral strike-slip fault of the Las Vegas Valley Shear Zone (LVVSZ) occur just to the north and south of the LWRFS, respectively. Faults of the PSZ, provide a partial barrier to southward flow from southern Pahrangat and Delamar valleys into the LWRFS (Rowley et al., 2011). Groundwater likely flows south through the barrier into Coyote Spring Valley along north-trending normal faults and fractures (Rowley et al., 2011). The LVVSZ has been interpreted to be a barrier to southward groundwater flow (Heilweil and Brooks, 2011).

The Kane Springs Wash Fault Zone is a left-lateral and normal down-to-the-west oblique fault that occurs in Kane Springs Valley and the northern portion of Coyote Spring Valley ([Figure 3-2](#)). The oblique fault along with the Kane Springs caldera and thrust faults likely prevent groundwater flow between Kane Springs Valley and Meadow Valley Wash (Rowley et al., 2011). In Coyote Spring Valley the Kane Springs Wash Fault may act as a partial barrier to flow, impeding flow across the fault from north to south.

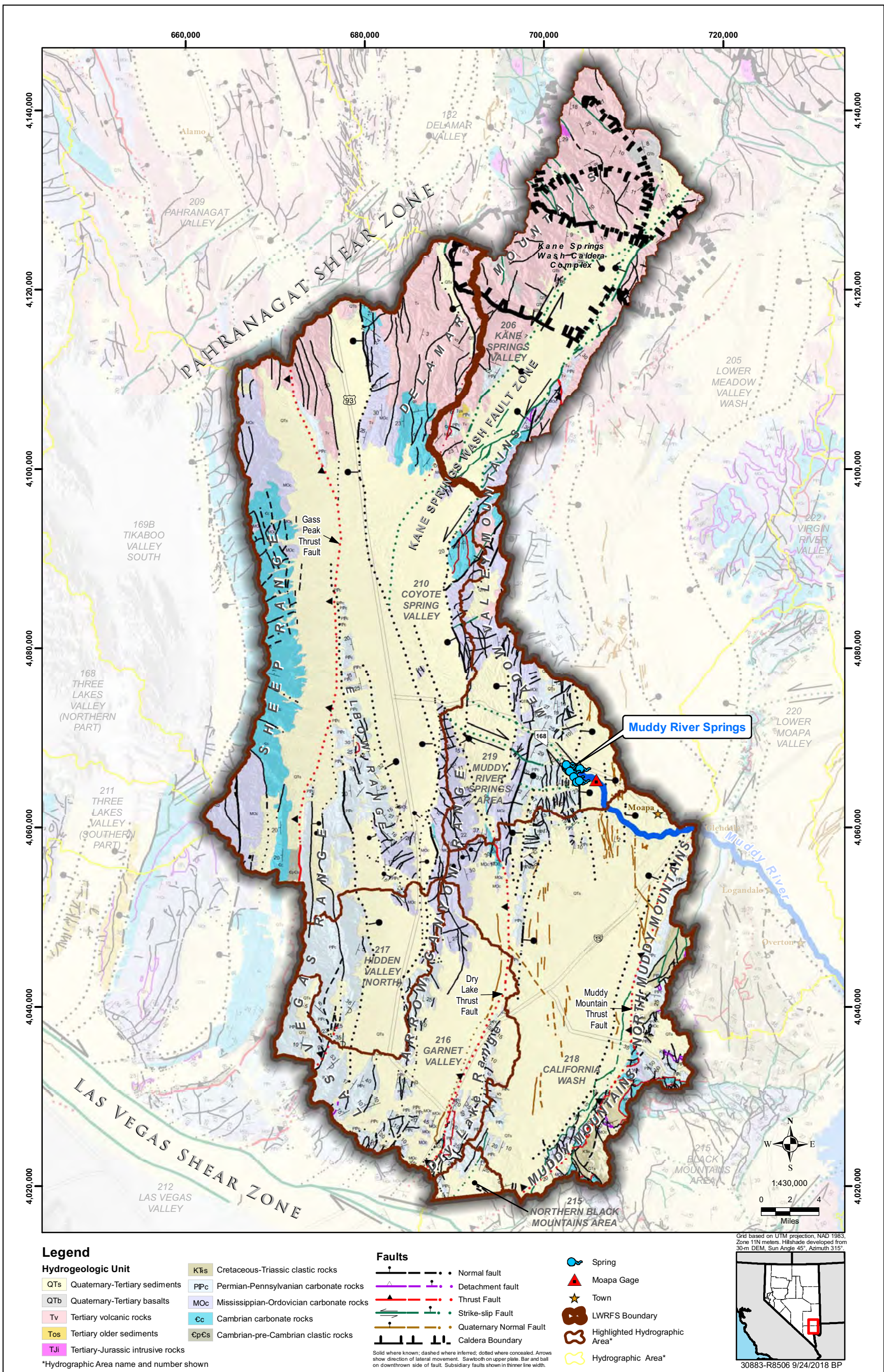


Figure 3-2
Hydrogeologic Map of the Lower White River Flow System

Normal Faults

The main phase of Basin and Range deformation which began around 10 Ma, is characterized by steeply-dipping, north-striking, normal faulting (Rowley et al., 2017). This faulting is responsible for the formation of the present-day physiography of north-trending basins and ranges forming the LWRFS (Page et al., 2011). The many Basin and Range faults that underlie and define the sides of Coyote Spring Valley provide the pathways for southward groundwater flow (Harrill et al., 1988; Schmidt and Dixon, 1995). A major part of that groundwater flows southeast, between the northern end of the Arrow Canyon Range and the southwestern end of the Meadow Valley Mountains along what has been referred to as the east Arrow Canyon Range fault zone (Page et al., 2011; Rowley et al., 2011). East-striking faults intersect the north-striking faults likely increasing the permeability of carbonate rocks in the MRSA (Page et al., 2011; Rowley et al., 2017). It is well known that the southeast-flowing groundwater is the principal source of many large springs in the MRSA, which currently create the perennial flow of the Muddy River (Schmidt and Dixon, 1995; Donovan et al., 2004; Buqo, 2007; Donovan, 2007; Johnson, 2007).

3.3.2 Hydrogeologic Setting

The hydrogeologic map presented in [Figure 3-2](#) was constructed by grouping geologic units with similar hydrologic properties into hydrogeologic units. The following sections summarize the geology and hydrogeology of the mountain ranges within and at the boundaries of the LWRFS.

Delamar Mountains

The Delamar Mountains at the northern LWRFS boundary are dominated by Tertiary caldera complexes including the Kane Springs Wash caldera complex (Rowley et al., 1995; Scott and Swadley, 1995; Scott et al., 1996; Dixon et al., 2007). The main bounding fault of the Delamar Mountains is the down-to-the-west normal fault on the western side, which is joined from the southwest by several splays of the left-lateral and normal PSZ (Ekren et al., 1977). In Kane Springs Valley, the bounding fault is the oblique (left-lateral and normal down-to-the-west) Kane Springs Wash fault zone (Swadley et al., 1994). Tertiary caldera complexes forming the northern boundary of Kane Springs are effective barriers to groundwater flow. The calderas are barriers primarily because of their underlying intracaldera intrusions and both hydrothermal clays and contact-metamorphic rocks formed by emplacement of the intrusions into intracaldera tuffs (Rowley et al., 2011). Groundwater likely enters the LWRFS from southern Delamar Valley along the PSZ to Pahranaagat Valley and then through the PSZ and along north-striking normal faults into Coyote Springs Valley ([Figure 3-2](#)).

Southern Sheep Range, Las Vegas Range, and Elbow Range

The southern Sheep Range is underlain by mostly Cambrian and Ordovician carbonate rocks that dip eastward (Guth, 1980). The range is a large tilt block uplifted along major north-striking, basin-range normal faults on its western side. The range is on the upthrown western side of the low-angle, west-dipping Gass Peak thrust. The thrust transported Neoproterozoic to Cambrian quartzite and Cambrian to Devonian carbonate rocks eastward over Cambrian to Mississippian rocks (Dohrenwend et al., 1996).



The Las Vegas Range is defined by the Gass Peak thrust, which transported rocks as old as the Cambrian Wood Canyon Formation eastward over Mississippian, Pennsylvanian, and Permian carbonate rocks of the Bird Spring Formation (Maldonado and Schmidt, 1991). Most of the range is made up of folded Bird Spring limestone, with the Gass Peak thrust exposed along its western side (Maldonado and Schmidt, 1991; Page, 1998). The small Elbow Range, which bounds the Las Vegas Range on the northeast, is made up of thrust and folded Bird Spring Formation that has been uplifted as a horst (Page and Pampeyan, 1996).

Meadow Valley Mountains

The Meadow Valley Mountains constitutes a narrow, generally low, north-northeast-trending range about 40-mi-long. The northern 30 mi of the range consists mostly of outflow ash-flow tuffs and part of the Kane Springs Wash caldera complex. The southern end of the Meadow Valley Mountains, just east of Coyote Spring Valley, is made up of mostly thrust-faulted and normally faulted Paleozoic rocks (Pampeyan, 1993; Swanson and Wernicke, 2017).

Arrow Canyon Range

The Arrow Canyon Range is a sharp, narrow, north-trending range consisting of a syncline of Cambrian to Mississippian carbonate rocks. It is uplifted along its western side by normal faults of the Arrow Canyon Range fault zone (Schmidt and Dixon, 1995; Page and Pampeyan, 1996; Page, 1998). The trace of the north-striking Dry Lake thrust, which carries Cambrian rocks over Silurian through Permian carbonate rocks, is exposed and projected north just east of the range (Page et al., 1992; Schmidt and Dixon, 1995; Beard et al., 2007).

North Muddy Mountains, Muddy Mountains, and Dry Lake Range

The southeastern corner of the LWRFS contains the Cretaceous-Triassic clastic rocks of the North Muddy Mountains and the Muddy Mountains (Bohannon, 1983). West of the Muddy Mountains and east of the Apex Industrial Park, is the small Dry Lake Range. This range is made up mostly of Bird Spring carbonate rocks. A narrow arm of bedrock extending west from Apex connects with the southern Arrow Canyon Range/Las Vegas Range. Basin-fill sediments to the northeast along the I-15 corridor (California Wash area) belong to an east-tilted half graben that reaches depths of 9,000 to 12,000 ft (Langenheim et al., 2001, 2010; Scheirer et al., 2006).

3.4 Hydrology

The hydrology of the LWRFS is presented in this section including descriptions of prominent surface-water features and associated time-series records of discharge; as well as descriptions of groundwater characteristics including aquifer types and conditions, and occurrence and movement. The sources of the data utilized in this section are described in [Section 2.0](#).

3.4.1 Surface Water

The primary surface-water features of the LWRFS are located within the MRSA where five spring-complexes and numerous gaining stream reaches form the headwaters of the Muddy River, the only perennial stream within the LWRFS ([Figure 3-3](#)). There are additional small springs in Coyote

Spring and Kane Springs valleys which discharge groundwater sourced from local recharge; however, these springs are not described in this report.

The source of water for the springs and the gaining stream reaches that form the headwaters of the Muddy River is the regional carbonate aquifer (Eakin, 1964; Rowley et al., 2017). Discharge from the springs coalesce with the gaining reaches to form the main channel of the Muddy River just above the USGS Muddy River near Moapa, Nevada (NV) gaging station. Figure 3-3 depicts the location of this gaging station and several other USGS gaging stations. Also depicted are the locations of metered surface-water diversions in the headwaters area. Table 3-1 lists the periods of record for each of the gaging stations.

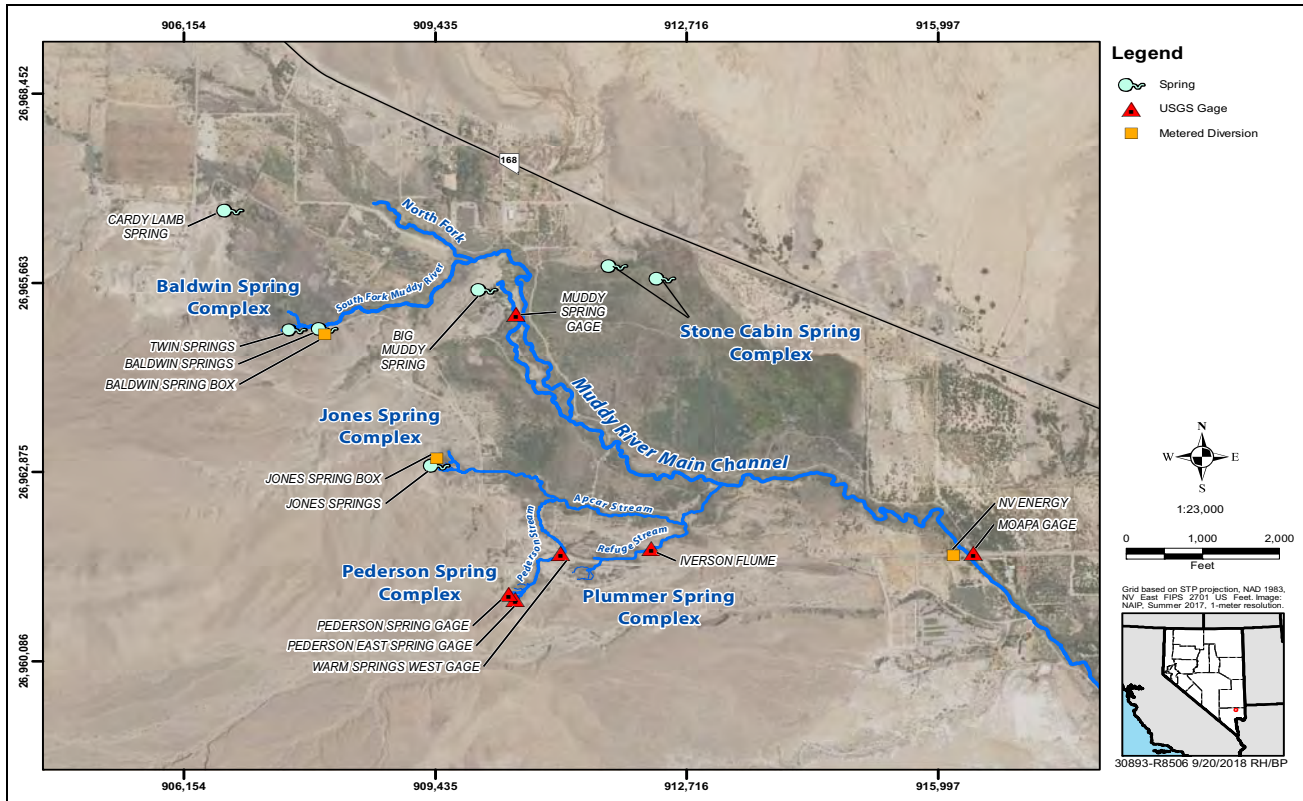


**Figure 3-3
Spring Complexes, Streams, Diversions, and Gaging Stations
within the Headwaters of the Muddy River**

There are three gaging stations that are critical to the analyses presented in this report. Two are associated with the Pederson Spring Complex: Pederson Spring near Moapa, NV and Warm Springs West near Moapa, NV. The Pederson Spring gage is important because it measures flow from the highest elevation spring within the MRSA representing groundwater discharge from the regional carbonate aquifer. The Warm Springs West gage is important because flow triggers have been established at the gage as part of the 2006 MOA (see Table 1-1). The Muddy River near Moapa gage is important because the streamflow at this location is a measure of the regional spring discharge and has the longest period of record. Details for each are presented in the following sections.



**Table 3-1
USGS Gaging Stations in the Headwaters of the Muddy River**

USGS Station Number	Gaging Station Name	Period of Record for Daily Average flow
09415900	Muddy Springs at LDS Farm near Moapa, NV (LDS gage)	August 1985 to Present
09415908	Pederson East Spring near Moapa, NV (Pederson East gage)	May 2000 to Present
09415910	Pederson Spring near Moapa, NV (Pederson gage)	October 1986 to Present ¹
09415920	Warm Springs West near Moapa, NV (Warm Springs West gage)	August 1985 to Present ²
09415927	Warm Springs Confluence at Iverson Flume near Moapa, NV (Iverson Flume gage)	October 2001 to Present
09416000	Muddy River near Moapa, NV (Moapa gage)	July 1913 to September 1915 May 1916 to September 1918 October 1944 to Present

Note: ¹Flow data in the latter half of 2003 through April 2004 reflects flows bypassing the gage through a leak in the weir. The weir was replaced in April 2004.

²Flow records prior to 1996 were influenced by agricultural diversion above the gage.

Pederson Spring Complex

The Pederson Spring near Moapa, NV gage (09415910) measures spring discharge from the highest elevation spring in the Muddy River headwaters area. The gage record begins in 1986, but is missing data from 1994 to 1996. It includes underreported records from 2003 until April 2004 during which time discharge was observed bypassing the gage. The gage was replaced in April 2004. [Figure 3-4](#) presents the flow record for the gage for the period 1986 to present. As the highest-elevation spring, it is considered to be the most sensitive to changes in groundwater conditions associated with the regional carbonate aquifer, and, therefore, a good indicator of how these changes affect spring discharge in the MRSA.

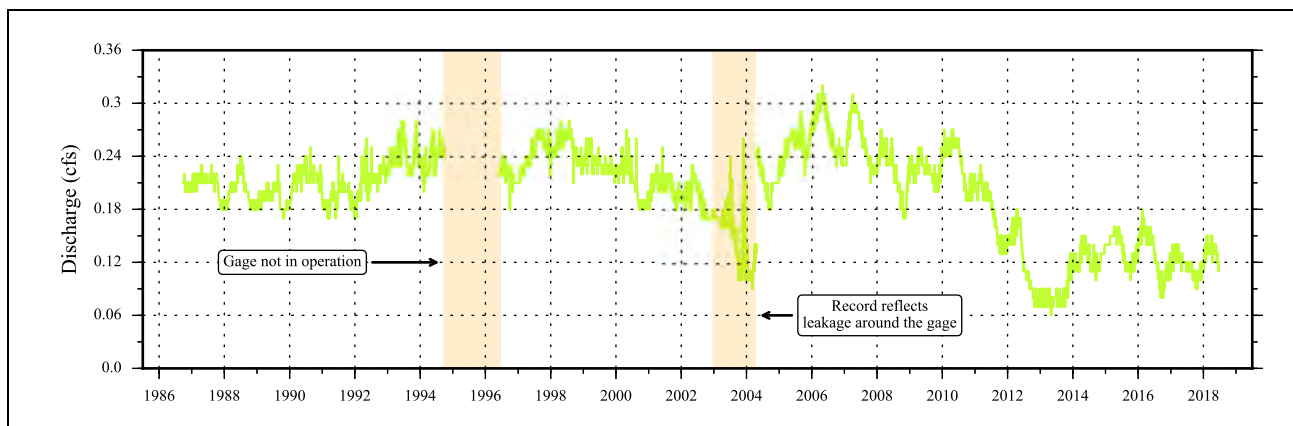


**Figure 3-4
Pederson Spring near Moapa, NV - Daily Discharge Record (1986 to present)**

Warm Springs West near Moapa, NV Gage (09415920)

The Warm Springs West near Moapa, NV gage (09415920) is a parshall flume that measures the total discharge from the Pederson Spring complex. The period of record ranges from 1985 to present. Gage records prior to October 1997 are considered unreliable because the flows were influenced by an unmetered agricultural diversion above the gage. Figure 3-5 presents the flow measured at the gage for the period of record. Trigger Ranges at various flow rates have been established at the gage for the purpose of initiating water management actions per the 2006 MOA. These actions are designed to protect instream flow rights and habitat for the endangered Moapa dace.

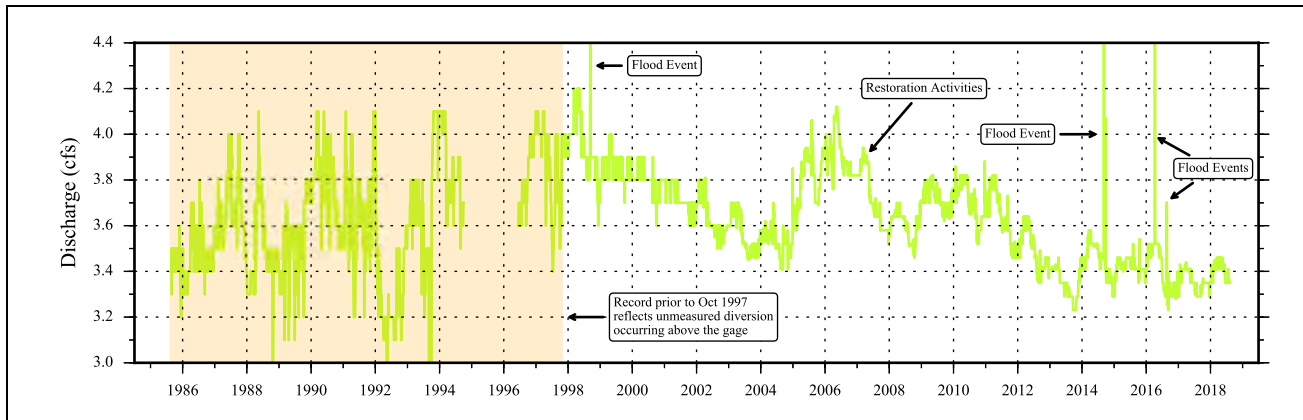


Figure 3-5
Warm Springs West near Moapa, NV - Daily Discharge Record (1985 to present)

Muddy River near Moapa, NV Gage (09416000)

The USGS Muddy River near Moapa, NV gage (Station No. 09416000; hereinafter referred to as the MR Moapa gage) measures the streamflow contributions from spring complexes, gaining reaches and intermittent flood flows. Streamflow is directly affected by surface-water diversions and evapotranspiration occurring above the gage. Figure 3-6 presents a time-series chart of the annual streamflow measured at the MR Moapa gage for the period 1945 to 2017. Also presented on the chart is a record of these flows that has been adjusted to remove the influence of intermittent flood flows. These influences were removed from the daily mean flow record using a method that replaces the identified flood flow with the median monthly flow as described in Johnson (1999). The resulting flow record is more representative of actual baseflow conditions at the gage. The flood-adjusted flow record is used in the analyses presented in this report.

The mean annual flow measured at the MR Moapa gage in 1946 was 46.8 cfs (33,900 af). This flow rate is considered the pre-development baseflow because it predates municipal and industrial surface-water diversions and exports by NVE and MVWD, as well as groundwater development within the MRSA. This baseflow also matches the average mean annual flow when the gage was operated intermittently between 1913 and 1918. During two intervals covering 3-years (July 1, 1913 to June 30, 1915 and October 1, 1916 to September 30, 1917) the average flood-adjusted mean annual flow was 47.0 cfs (34,000 afy), a difference of 100 afy from the 1946 flow rate.

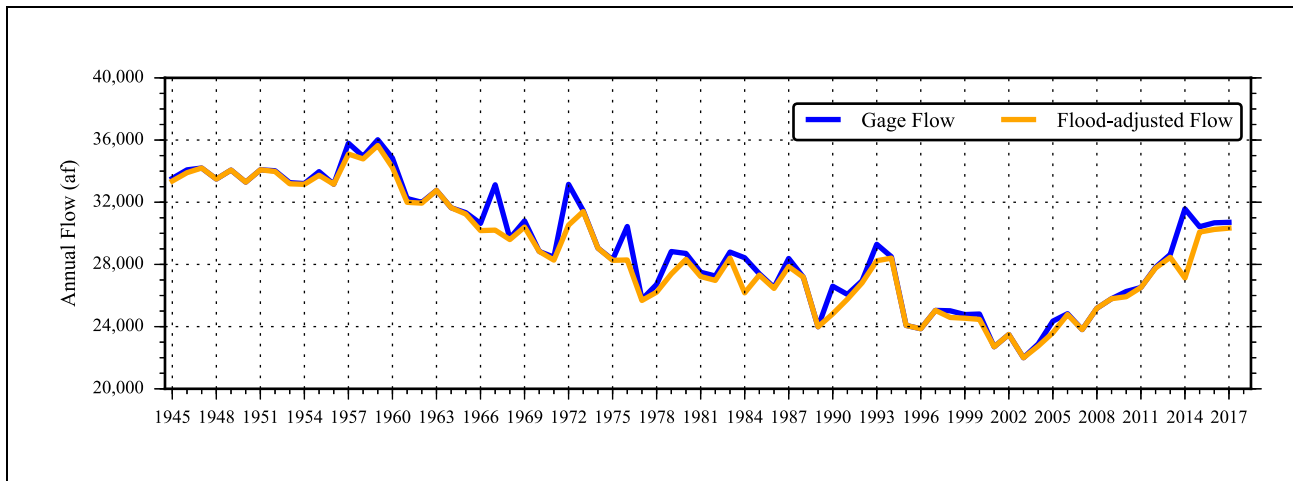


Figure 3-6
Muddy River near Moapa, NV (1945 to 2017)

The 1946 pre-development baseflow also corresponds with information compiled by Eakin (1964). Eakin (1964) reported a 25-year average flood-adjusted mean annual flow of 46.4 cfs (33,600 afy) using intermittent data between 1914 and 1962. In addition, Eakin (1964) estimated that approximately 2,000 to 3,000 afy of spring flow was being consumed by phreatophytes between the spring orifices and the gage, which infers that the pre-development groundwater discharge above the gage was approximately 36,000 to 37,000 afy (50 to 51 cfs).

As illustrated by [Figure 3-6](#), the gage flow during pre-development conditions only varied by about 1,000 afy from 1945 to 1955. Starting in the early 1960s, Muddy River streamflow began to decline from the 33,900 afy pre-development baseflow. This decreasing trend continued, reaching a low of about 22,000 af in 2003. By this time, streamflow had declined by over one-third of the pre-development baseflow. Streamflow has since recovered, and by the end of 2017 the mean annual flood-adjusted flow was 30,300 af. The causes of this decline and subsequent recovery are analyzed in [Section 5.0](#).

3.4.2 Groundwater

Descriptions of the groundwater characteristics of the LWRFS, including aquifer types and conditions and groundwater occurrence and movement are presented in this Section.

3.4.2.1 Aquifer Types and Conditions

The hydrogeology described in [Section 3.3](#) can be further simplified into a groundwater system composed of a regional carbonate aquifer interconnecting the basins of the LWRFS and one or more areas where saturated basin-fill is present. The regional carbonate aquifer is contiguous throughout the basins, while the saturated basin fill occurs primarily within the basin centers.

Regional Carbonate Aquifer

The identification of the regional carbonate aquifer was made by Eakin (1964, 1966) who noted that the large discharge from the springs located within the MRSA could not be supported by the relatively small local recharge. As a result, Eakin (1966) concluded that the springs were discharging groundwater originating from basins located upgradient. Eakin (1966) developed a water balance for thirteen basins located within south-eastern Nevada, ending with the MRSA. Based on the results, he concluded that recharge in these basins contributes to the discharge of the Muddy River springs and that the Paleozoic carbonate rocks must be the primary system that is transmitting water between these basins. Investigations conducted after Eakin (1966) revealed that the hydraulic connection of the carbonate aquifer extends to basins located south of the MRSA (SNWA, 2009; Burns and Drisci, 2011; SNWA, 2013).

The regional carbonate aquifer is predominantly composed of thick sequences of Paleozoic and Mesozoic carbonate rocks that have well-developed fracture networks (Heilweil and Brooks, 2011). As described in [Section 3.3.2](#), thick sequences of carbonate rocks occur throughout the LWRFS as thrust faulting has placed carbonate rocks sequences on top of other carbonate rock sequences. The compressional and transport processes that are involved with thrusting may lead to significant fracture development (Heilweil and Brooks, 2011). Carbonate rocks typically have a low permeability but may have very high secondary permeabilities as result of dissolution of the carbonate minerals along faults, fractures, and bedding planes (Schaefer et al., 2005).

Basin-Fill Aquifers

Saturated basin-fill may form aquifers in the LWRFS. Where they occur, these aquifers generally overlie the regional carbonate aquifer system and are typically separated from one another by mountain ranges composed of consolidated rocks (Schaefer et al., 2005). The aquifers are composed of Tertiary sediments consisting of eroded limestone, conglomerate, sandstones, as well as Quaternary alluvium, colluvium, playa deposits, and eolian deposits (Page et al., 2011). Basin-fill can be composed of many sediment types with different grain sizes and levels of sorting, and, consequently, can have a large range of permeabilities (Heilweil and Brooks, 2011). Basin-fill aquifers within the LWRFS occur at great depths above the carbonate aquifer, as perched, or as semi-perched systems.

MRSA Alluvial Reservoir

The interbedded fine- and coarse-grained sediments in the MRSA, that overlay the Muddy Creek Formation, form a highly transmissive shallow, alluvial aquifer that comprises at least the top 125 feet of basin fill based on well driller's logs. This local aquifer acts as a reservoir whose storage and outflow is sourced from the regional carbonate aquifer. The water table of this shallow alluvial reservoir is generally within a few feet of land surface, and outflow occurs as spring discharge, seepage to gaining reaches of the Muddy River, or as ET.



3.4.2.2 Occurrence and Movement

Figure 3-7 is a map presenting the current conceptualization of groundwater occurrence and movement within the LWRFS. The map depicts areas of potential local recharge and primary groundwater discharge, groundwater flow directions, and current aquifer conditions observed at selected monitor wells during January to March, 2018, a period when pumping is at its lowest during the year. The areas of potential recharge were approximated by areas where normal precipitation is greater than 8 in. The PRISM 800-meter normal precipitation grid was used for this purpose (Daly et al., 1994, 1997, 1998, 2008). Aquifer conditions are represented by measurements of static or near-static water-level elevations on the map (Figure 3-7). Depth-to-water and water-level elevation data are presented in Table A-1 (Appendix A). The existing well data are insufficient for the development of potentiometric contour maps. Thus, the discussion is based on the well data presented in this section, supplemented by information from previous interpretive reports.

As stated above, within the LWRFS, groundwater occurs in basin-fill and carbonate-rock aquifers. Within many of the LWRFS basins, groundwater in the basin fill occurs at great depths, or as perched as is the case in the extreme northern area of Coyote Spring Valley (Eakin, 1964). The alluvial reservoir of the MRSA constitutes an exception in the LWRFS. Depth to water within the basin fill ranges between about 3-4 ft at the LDS Central well in the MRSA to about 751 ft bgs (02/14/2018) at the CSV3011M well in Coyote Spring Valley (Appendix A). The shallower depths to water occur within the alluvial reservoir, downgradient from the Muddy River springs. The greater depths to water in the basin fill occur in northern and southern Coyote Spring Valley. Groundwater also occurs at substantial depths in other basins of the LWRFS. For example, the Byron Well completed in the basin fill within California Wash basin has a depth to water of about 238 ft bgs (10/09/2018) (Appendix A).

Depth to groundwater within the carbonate aquifer of the LWRFS varies significantly. In general, depth to water is near the surface in the MRSA and much deeper in the other basins. A better understanding of the deeper groundwater that occurs in the carbonate aquifer of the LWRFS was developed based on the water-level responses, which are discussed in greater detail in Section 5.0. The responses depend on the relative locations of the wells with respect to the range-front faults located at the base of the mountain ranges (Figure 3-2). These faults have created structural basins where most of the wells are located.

Within the Coyote Spring Valley structural basin, water-level elevations are higher in the northern portion of the valley and decrease to the south. Wells located within the structural blocks of the mountain ranges are significantly higher (e.g., CSVM-3 and CSVM-5). Well CSVM-3, which has a depth to water of 444 ft bgs (02/14/2018), is located to the far north of the valley and within a different structural block composing the southern Delamar Mountains. Water levels in this structural block are greater than 320-ft higher than those observed in wells CSVM-4 and KMW-1 to the southeast that are completed within the Kane Spring fault zone. Well CSVM-5 is located high off the valley floor and within the structural block of the Sheep Range and has a depth to water of 1,080 ft bgs (02/14/2018). At the CSVM-5 site, the Gass Peak thrust fault has influenced the geologic setting by causing the bedding orientation of the carbonate strata to be nearly vertical at the surface. Except for these two wells, water levels throughout the LWRFS respond in the same manner. This indicates a

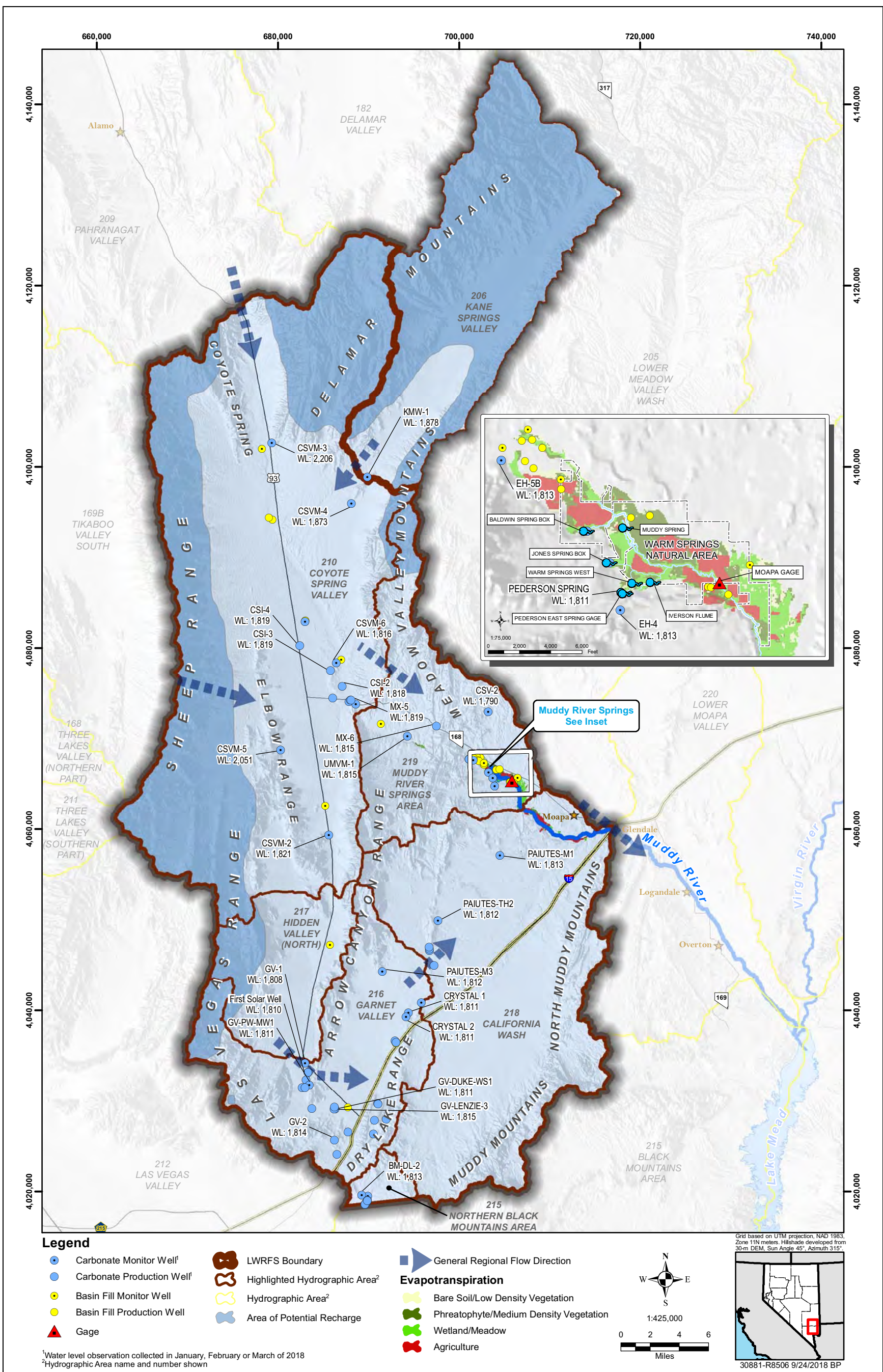


Figure 3-7
Conceptualization of the Lower White River Flow System

high-degree of hydraulic continuity between the structural basins of the LWRFS, including Kane Springs Valley.

Based on the well data described in this section and presented in [Figure 3-7](#) and [Appendix A](#), the minimum depth to water measured within the connected portion of the carbonate aquifer was about 31 ft bgs (03/16/2018) measured at well EH-5B in the MRSA. The maximum depth to water of 970 ft bgs (02/14/2018) was measured at well CSVN-4 in northern Coyote Springs Valley. Measured depth-to-water values in Garnet Valley range from about 259 to 883 ft bgs, all measured in early 2018. Despite the large differences in depth to water across the LWRFS, groundwater elevations in the carbonate aquifer near the center of the valleys only vary by approximately six feet between central Coyote Spring Valley, and Garnet Valley and Black Mountains Area to the south, and the MRSA and California Wash to the east. These minor differences in groundwater elevation across such a broad area are indicative of a high degree of hydraulic connection as demonstrated by the results of the NSE Order 1169 aquifer test.

In general, groundwater flows from areas of natural recharge at high elevations to lower-elevation areas of discharge. The source of natural recharge for the carbonate aquifer underlying the LWRFS is a combination of regional groundwater inflow from the upper portion of the WRFS including Pahrnagat, Delamar, and Kane Springs valleys; and from local recharge in the mountain ranges bounding the LWRFS ([Figure 3-7](#)). The potential areas of local recharge shown on the map are approximated by areas where annual precipitation is greater than 8 in. Such areas occur mainly on the higher elevations of the Delamar Mountains in Kane Springs Valley and northern Coyote Spring Valley, and the Sheep Range along the western boundary of Coyote Spring Valley. As shown on the map ([Figure 3-7](#)), natural groundwater discharge in the LWRFS occurs through springs and seeps located in the MRSA and through ET from riparian and phreatophytic vegetation. Groundwater contributing to the headwaters of the Muddy River leaves the flow system in the form of surface water along this stream.

Groundwater flow directions in the regional carbonate aquifer have been defined based on a detailed analysis of groundwater measurements and the hydrogeology of the WRFS described in SNWA (2009) and Burns and Drici (2011) and are shown as red arrows in [Figure 3-7](#). Groundwater flow within Coyote Spring Valley is to the south-southeast, primarily to the regional springs in the MRSA. However, some groundwater in Coyote Spring Valley is also believed to flow to the south (to Hidden and Garnet valleys) based on groundwater elevations, accommodating hydrogeology, and the results of the NSE Order 1169 aquifer test. In the southern portion of the LWRFS (i.e., Garnet Valley), groundwater flow is to the northeast and California Wash. Groundwater discharge from the carbonate aquifer in the MRSA saturates the local alluvial reservoir.



This Page Left Intentionally Blank

4.0 NATURAL AND ANTHROPOGENIC STRESSES

Groundwater levels, spring discharges, and perennial streamflow in the LWRFS are affected by many natural and anthropogenic stresses. The effects of these stresses depend on their magnitude, duration, and frequency, and can be classified as short- or long-term.

4.1 Natural Stresses

Natural stresses on a given hydrologic system include precipitation, air temperature, barometric pressure, earth tides, and earthquakes. Barometric pressure, earth tides, and earthquakes are considered to be short-term effects and are not given further consideration in this analysis. Air temperature, which is a controlling factor of ET, changes seasonally causing seasonal fluctuations in ET which may affect groundwater levels and discharge where ET occurs. In the LWRFS and its tributary basins, precipitation is the main source of recharge and is, therefore, the main driver of its hydrology. Changes in precipitation can cause both short- and long-term effects in the groundwater levels and discharge from the area.

The LWRFS is within the Nevada Division 4 climate zone (Division 4) as defined by the National Oceanic and Atmospheric Administration's (NOAA) Climate Divisional Database ([Figure 4-1](#)). Divisional climate data are reported as average monthly values derived from daily climate observations within each climate division. Precipitation and air temperature data are of particular importance to the hydrology of the area of interest and were obtained from the on-line database (NOAA, 2018).

Annual precipitation within Nevada Division 4 was compiled for the period 1895 to 2018. Winter precipitation in the LWRFS is understood to be the dominant source of local recharge. Winograd et al. (1998) demonstrated that winter precipitation (October through June) in the Spring Mountains of southern Nevada comprised two-thirds of the total precipitation for the area and was responsible for the majority of recharge to the hydrologic system, with summer precipitation comprising only a small fraction (perhaps 10 percent) of the recharge.

Division 4 winter-season precipitation, defined as the total precipitation occurring during the months of October through March, was used for the analyses presented in this report. These months were selected because most precipitation occurring during the warmer months (April through September) evaporates or is consumed by vegetation due to the high rates of potential ET, averaging 7.27 feet per year (ft/yr) from 2001 to 2012 at Overton (Huntington et al., 2013). These rates are largely dependent upon air temperature. Based on Division 4 period of record, the high temperatures for the months of April through September ranged from 58.9 to 93°F, averaging 76.3°F, while during the months of October through March, they ranged from 33.9 to 68°F, averaging 62.7°F. [Figure 4-2](#) depicts the

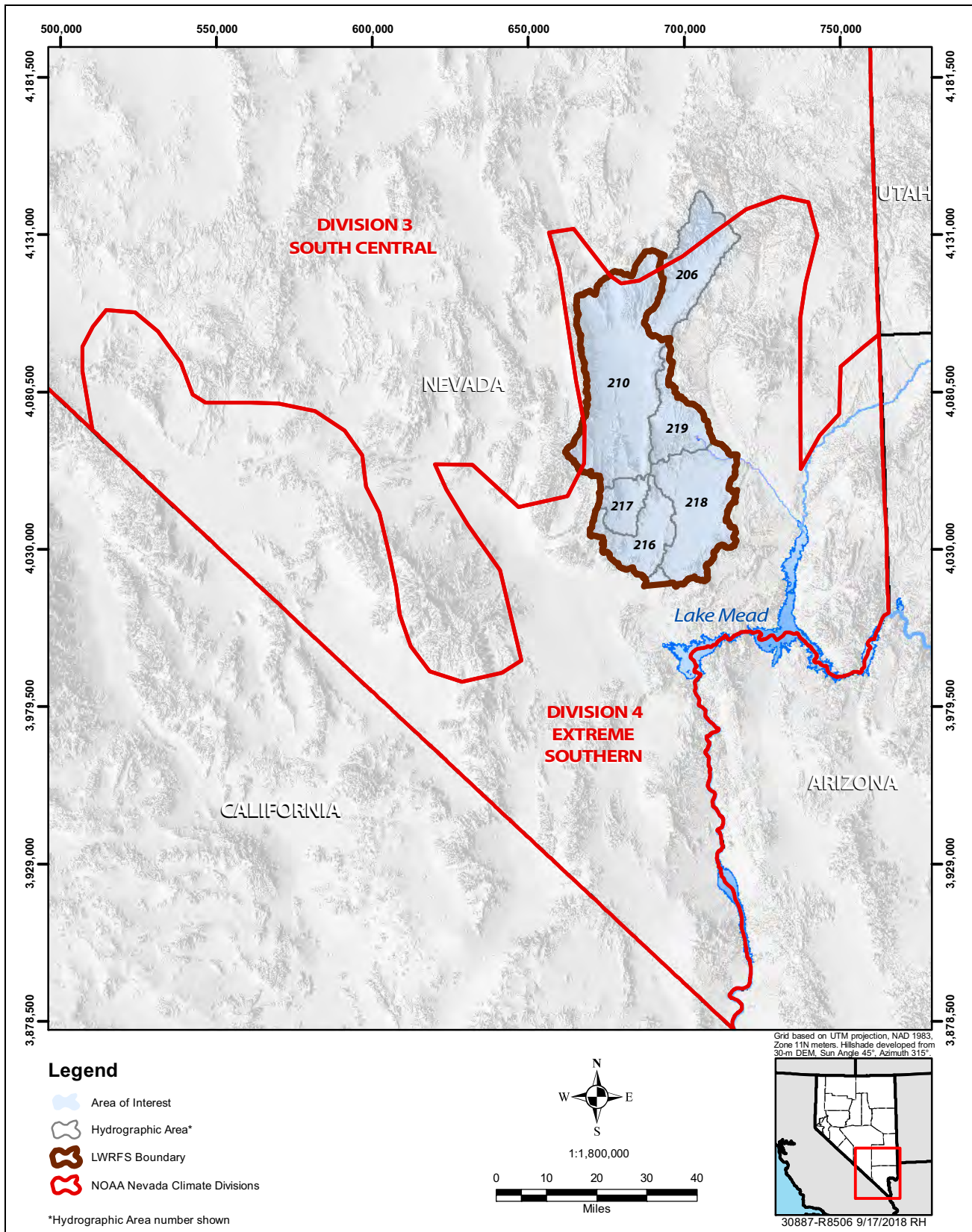


Figure 4-1
Nevada Division 4 Climate Zone

winter precipitation (October through March) from 1895 to 2018 with a linear-regression indicating a positive slope, but essentially no trend.

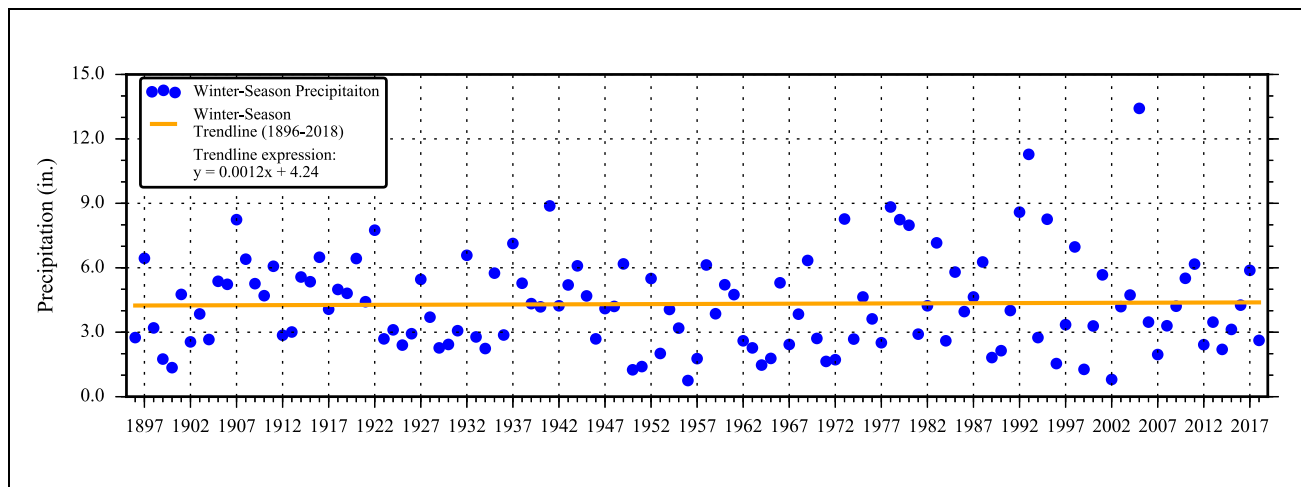
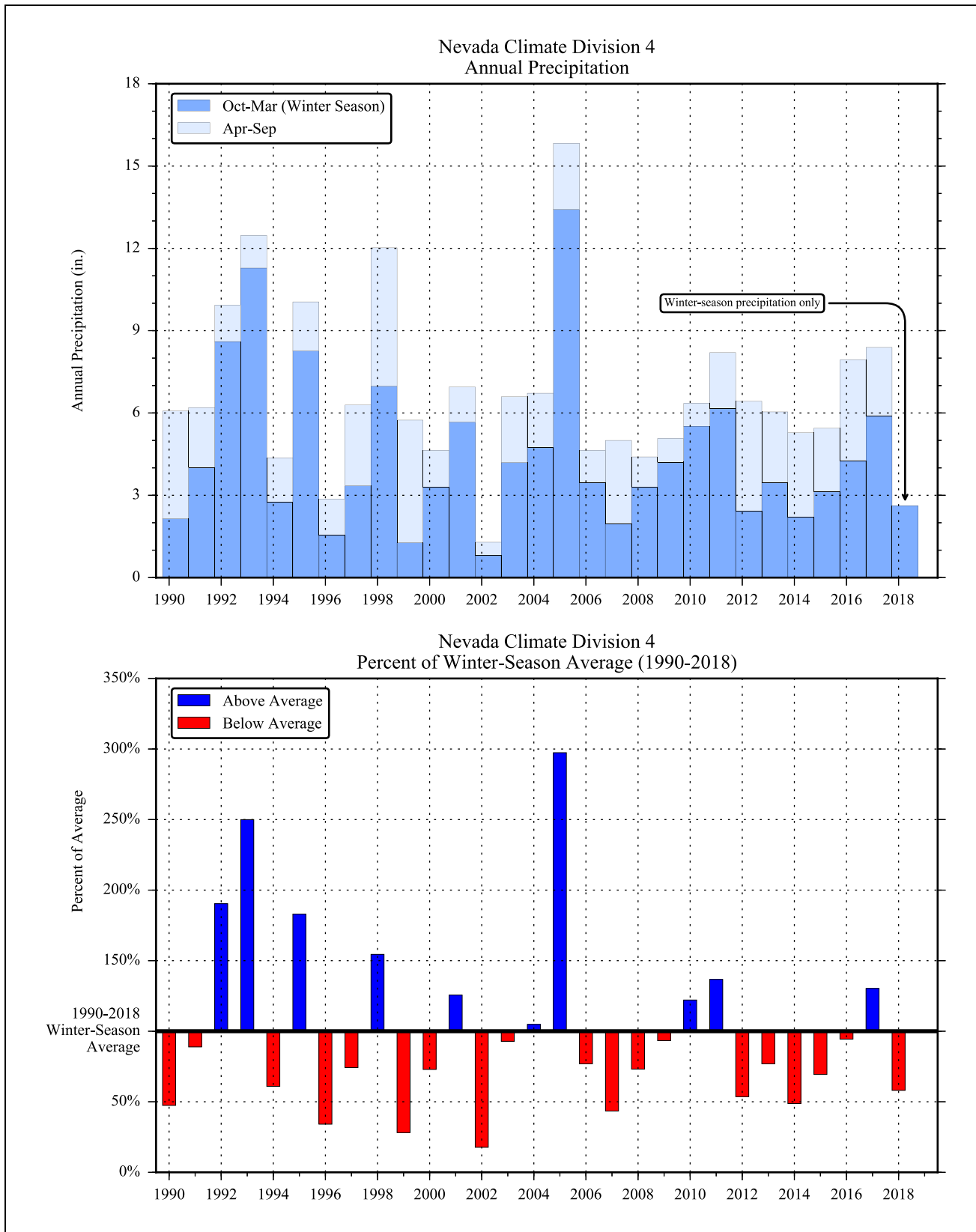


Figure 4-2
Climate Division 4 Precipitation with Trendline

Annual precipitation data were analyzed for the period 1990 to 2018, which is the period for which complete data sets are available for other LWRFS hydrologic and water-use records. [Figure 4-3](#) presents the annual total precipitation as winter-season (October through March) and summer-season (April through September) totals. During this period, the winter- and summer-season precipitation averaged 4.51 and 2.25 in., respectively. For calendar year 2018, only winter-season precipitation is shown, since the summer-season record was incomplete at the time this report was written.

Precipitation data were evaluated by computing the annual percent of winter-season average for the period analyzed. These values are presented in [Figure 4-3](#), with positive values (blue bars) representing above-average precipitation and negative values (red bars) representing below-average precipitation. There are several observations that can be made from [Figure 4-3](#):

- Winter seasons of 1992, 1993, 1995, and 2005 were extraordinarily high, with values of 190, 250, 183 and 297 percent of average, respectively.
- Winter seasons of 1996, 1999, and 2002 were extraordinarily low, with values of 34, 28, and 18 percent of average, respectively.
- The period from 2006 through 2018 was mostly below average, with 10 of the 13 seasons below average.



**Figure 4-3
Nevada Climate Division 4 Precipitation**

4.2 Anthropogenic Stresses

The primary anthropogenic stresses that have influenced surface-water and groundwater conditions within the LWRFS include surface-water diversions above the MR Moapa gage, groundwater production from both the regional carbonate aquifer and MRSA alluvial reservoir, and land use. These stresses have occurred over different time periods and durations. Records of surface-water diversions, groundwater production, and groundwater levels were compiled from all available sources for the entire LWRFS. Historical information on MRSA land use and water development was assembled from the literature. The following sections present time-series data for MRSA surface-water diversions (see [Figure 3-3](#) for locations) and groundwater production from the regional carbonate aquifer and the MRSA alluvial reservoir. The sources of data were described in [Section 2.0](#).

4.2.1 Surface-Water Diversions above Muddy River near Moapa, NV Gage

There are three primary surface-water diversions above the MR Moapa gage that are of significance to this assessment. These are the MVWD diversions at the Pipeline-Jones and Baldwin springs, and the NVE Muddy River diversion directly above the gage. The locations of the diversions are depicted in [Figure 3-3](#). The MVWD has diverted spring flow from the Pipeline-Jones and Baldwin springs since 1959 and 1975, respectively. Diversions by NVE began in 1968 when the agency started leasing decreed Muddy River water rights from the Muddy Valley Irrigation Company. The MVWD diversions supply water to users within the MVWD service area, primarily outside the MRSA. The NVE diversions were historically exported out of the MRSA to supply industrial uses at the Reid Gardner Generating Station in the California Wash basin. In addition, SNWA owns and leases surface-water rights above the gage, but water associated with these rights is not diverted and eventually flows into Lake Mead.

Detailed records of surface-water diversions by NVE and MVWD began in 1978 and 1992, respectively, and are provided in [Table B-1](#) of [Appendix B](#). Historically, these two entities have been the principal surface-water diverters above the MR Moapa gage. With the gradual closure of the Reid Gardner Generating Station, which began in 2014 and was completed in March 2017, NVE has not diverted surface water since 2015. There have been, and still are, other minor diversions and uses of surface water above the gage. However, these diversions are small and no records exist to determine their quantity; therefore, they are not accounted for in this analysis. [Figure 4-4](#) presents the historical surface-water diversions above the MR Moapa gage for the period in which records are available.

4.2.2 Groundwater Production

Groundwater is produced from two primary sources within the LWRFS: the MRSA alluvial reservoir and the regional carbonate aquifer underlying the six basins. As described in [Section 3.4.2.2](#), the regional carbonate aquifer is also the source of water for the alluvial reservoir. [Figure 4-5](#) depicts the locations of production wells within the LWRFS using symbology to differentiate between the sources (i.e., carbonate aquifer vs. alluvial reservoir). This section summarizes groundwater production from wells located within the MRSA and from wells located in the other LWRFS basins with completions in the carbonate aquifer.

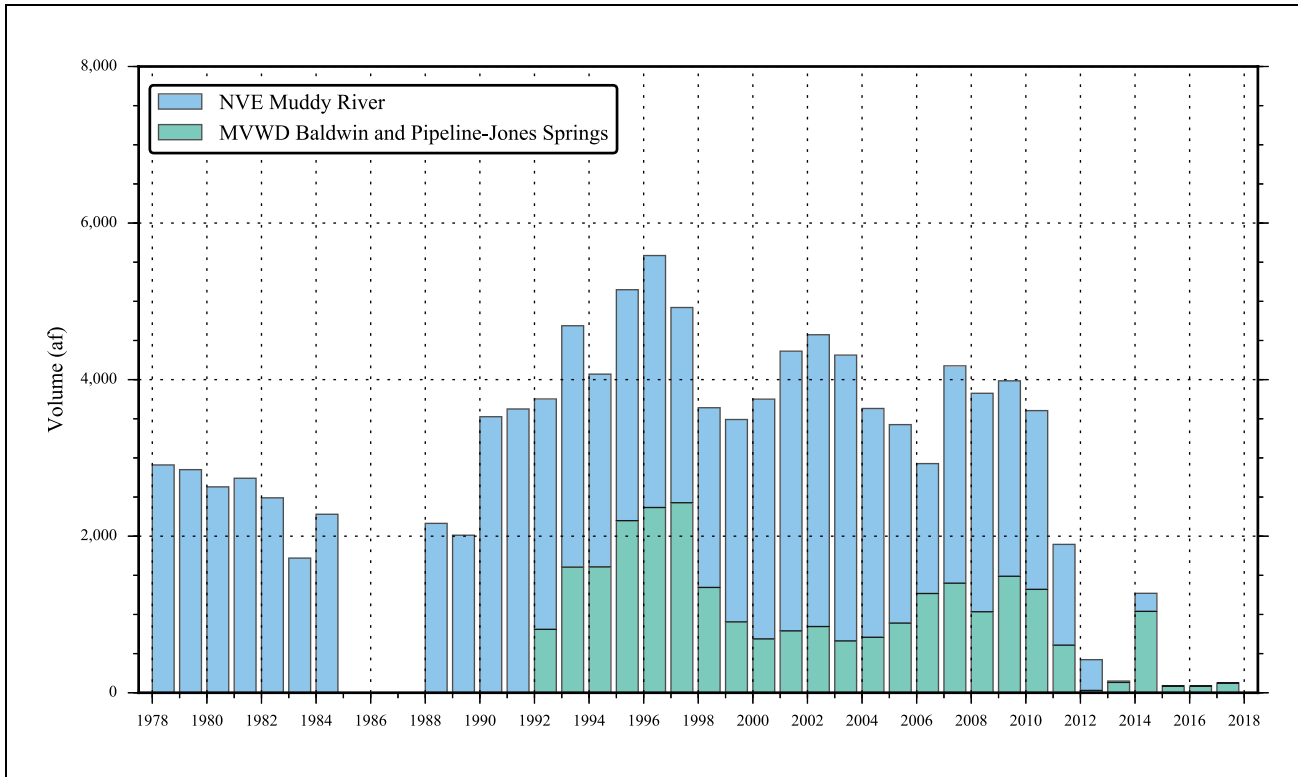


Figure 4-4
Surface-Water Diversions above the MR Moapa Gage

4.2.2.1 Muddy River Springs Area

Groundwater production within the MRSA began around 1948 when the first well was constructed (Eakin, 1964; NDWR, 2018b). Eakin (1964) estimated groundwater production ranged from 2,000 to 3,000 af from about 12 wells completed in the alluvial reservoir. The water was used for irrigation. Several of these wells (Lewis 1 through 5) were purchased by NVE and were used to supply water for the Reid Gardner Generating Station in the California Wash basin. NVE augmented the production from its Lewis well field using its Perkins and Behmer wells and by leasing water produced from three wells owned by the Corporation of the Presiding Bishop of the Church of Jesus Christ of Latter-Day Saints (LDS): LDS East, LDS Central, and LDS West. All of these production wells are completed to shallow depths in the alluvial reservoir ranging from 50 to 135 ft bgs. Well construction details are provided in Table C-1 of Appendix C. NVE began reporting production data from these wells in 1987 (Table C-2 of Appendix C). Figure 4-6 presents the annual production from the wells grouped by well field (Lewis Wells, LDS Wells, and Perkins and Behmer wells).

The groundwater production by NVE constitutes the vast majority of production from the MRSA alluvial reservoir. However, there have been, and still are, other minor users within the area. These uses are small and no long-term records exist to determine their quantity; therefore, they were not accounted for in this analysis.

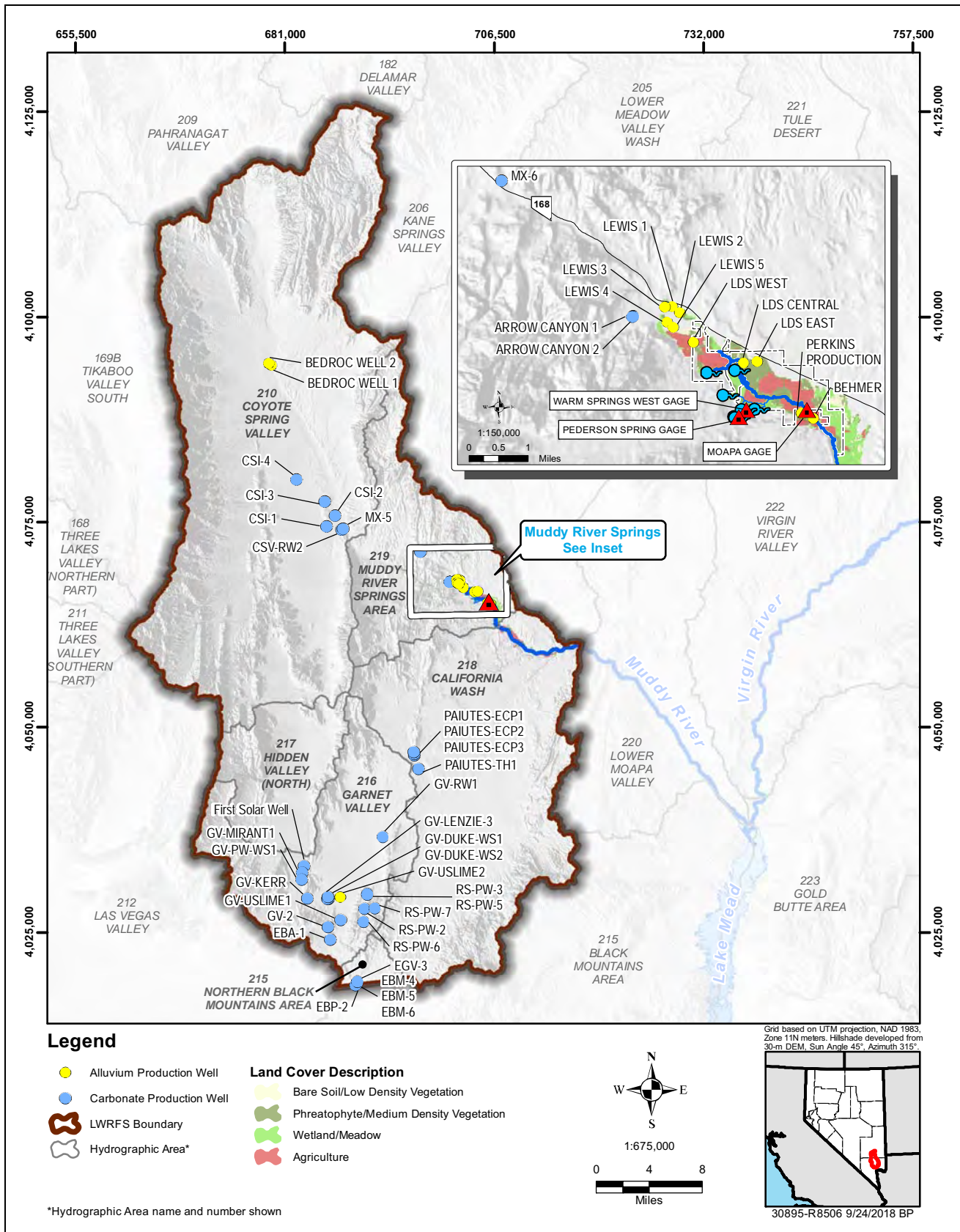


Figure 4-5
Locations of Production Wells in the LWRFS

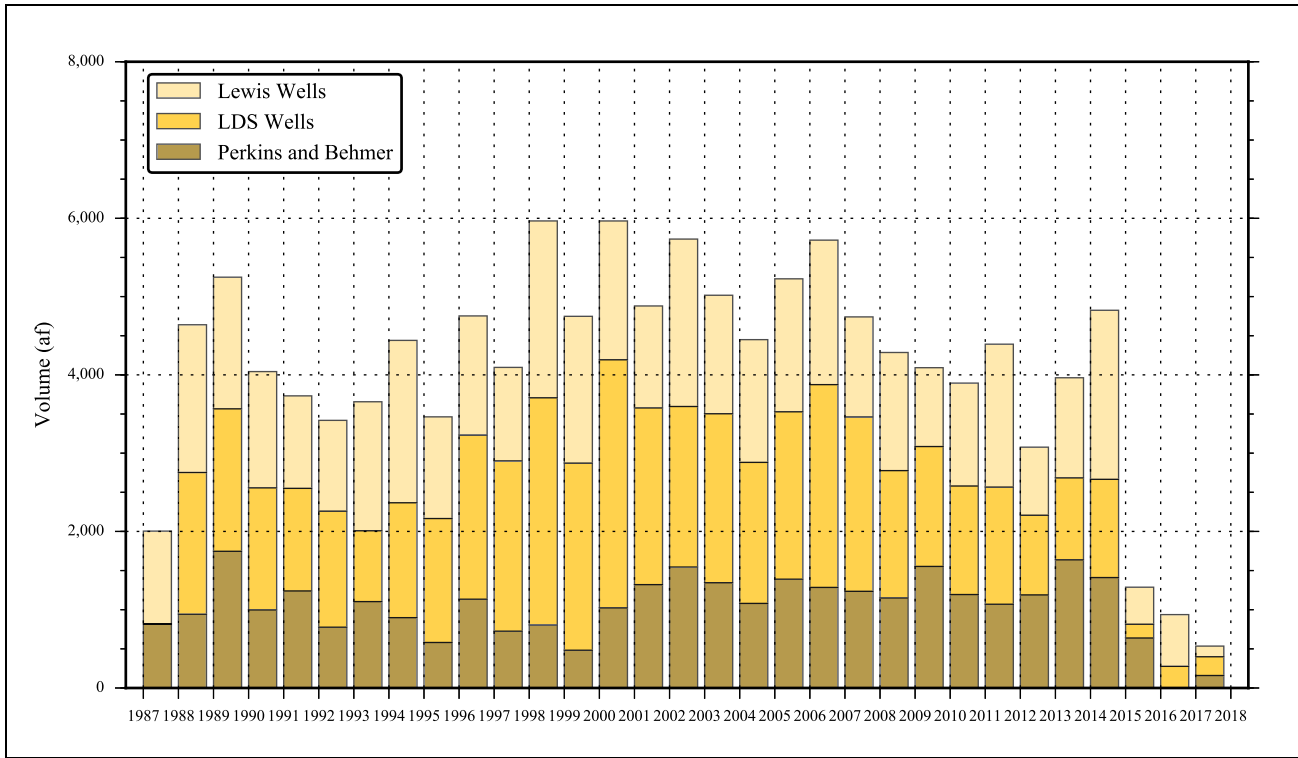
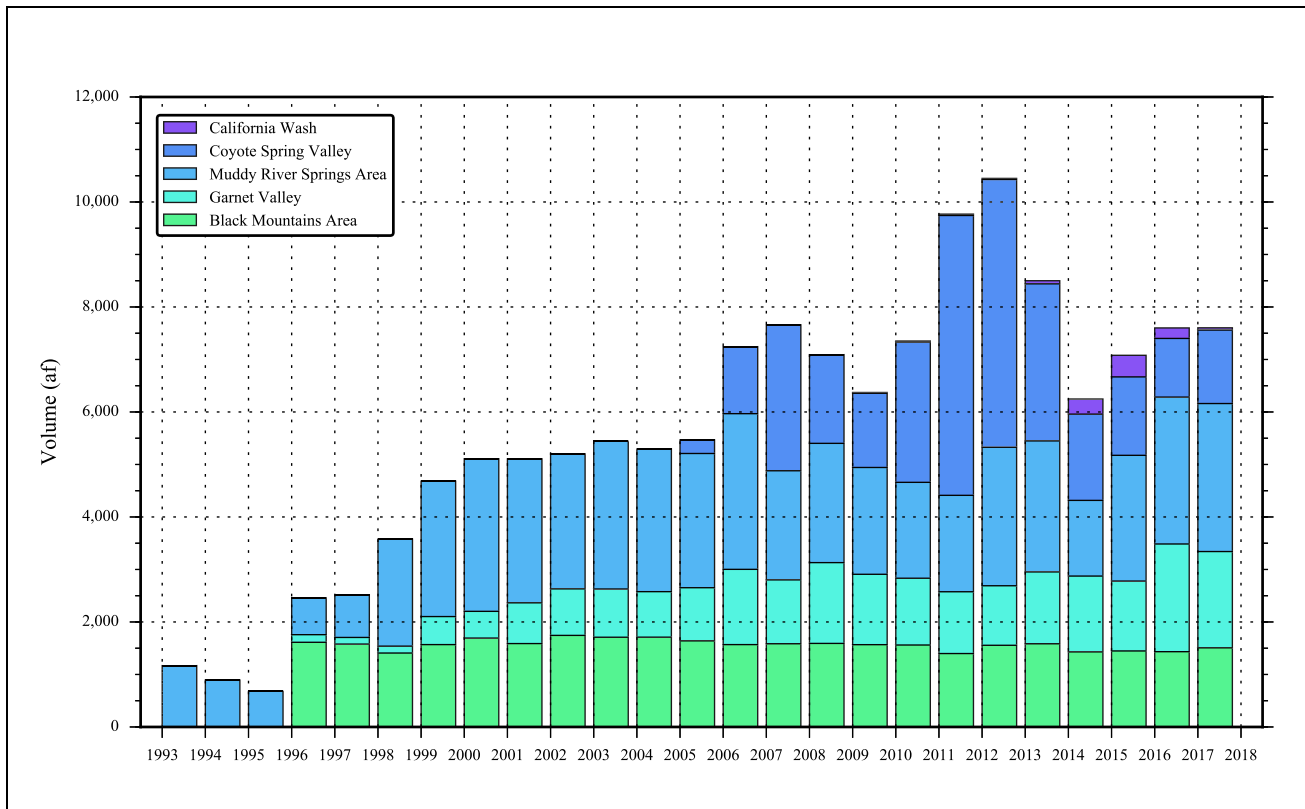


Figure 4-6 Annual Groundwater Production from the MRSA Alluvial Reservoir

The MVWD produces groundwater from three wells completed in the regional carbonate aquifer within the MRSA. These wells, Arrow Canyon 1, Arrow Canyon 2, and MX-6, are located adjacent to and upgradient of the Muddy River headwaters (Figure 4-5). The wells are used to supply water for uses within the MVWD service area, primarily outside the MRSA. MVWD began reporting groundwater production totals from these wells in 1992 (Table C-2 of Appendix C). The groundwater production totals are presented in Figure 4-7 along with total production from the carbonate aquifer in the other LWRFS basins.

4.2.2.2 Carbonate Aquifer

As described in Section 3.4.2.1, the LWRFS is defined by the interconnected nature of the underlying carbonate aquifer that provides hydraulic continuity between the basins. Production wells completed in the carbonate aquifer have some of the highest yields making it an attractive water-supply source. As a result, there has been significant development of the aquifer in various locations throughout the LWRFS. As stated in Section 1.0, one of the objectives of this assessment is to evaluate how the aquifer has responded to different stresses, in particular the long-term pumping stresses. This section summarizes annual groundwater production from the carbonate aquifer by LWRFS basin. The locations of the associated production wells are depicted in Figure 4-5. Site information and well construction data for these wells are provided in Table A-1 of Appendix A.



**Figure 4-7
Carbonate-Aquifer Groundwater Production**

Coyote Spring Valley

Groundwater production started in 2005 when CSI began using water for construction purposes related to their Coyote Springs development. CSI has constructed four wells, CSI-1, CSI-2, CSI-3, and CSI-4, and has used them to support operation and maintenance of an 18-hole golf course and implementation of the NSE Order 1169 aquifer test. SNWA owns and operates the MX-5 well which was used as the primary production well during the NSE Order 1169 aquifer test. Annual production volumes for Coyote Spring Valley are provided in [Table C-3 of Appendix C](#).

Garnet and Hidden Valleys

Groundwater production in Garnet Valley has predominantly been associated with mineral mining, electrical power generation, and industrial uses. There are several utility companies that lease groundwater rights owned by SNWA who have constructed production wells and operate them to supply water for industrial uses at their respective facilities. These entities report monthly production totals to SNWA who in turn reports them to NDWR on a quarterly basis. In addition, Republic Services operates several wells in support of their landfill operations in the southeast part of the valley, however, records are unavailable prior to 1999. Records for well EBA-1 are unverified for the period 1996 to 2000, and unavailable for wells GV-USLIME 1 and 2, Harvey, and GV-KERR prior to 1999. There has been no groundwater development in Hidden Valley. Annual production volumes for Garnet Valley are provided in [Table C-3 of Appendix C](#).



Black Mountains Area

There are several wells completed in the carbonate aquifer in the northern portion of the Black Mountains Area that is a designated part of the LWRFS. Two of these wells, owned by Dry Lake Water, were constructed as production wells but have never been operational. The other wells, owned by Nevada Cogeneration Associates, have been used to supply water to a power generating station. Annual production volumes for the Black Mountains Area of the LWRFS are provided in [Table C-3](#) of [Appendix C](#).

California Wash

The MBPI has produced groundwater in the California Wash basin to supply municipal uses. Production has been relatively small as compared to other uses in the LWRFS. Annual production volumes for California Wash basin are provided in [Table C-3](#) of [Appendix C](#).

5.0 HYDROLOGIC RESPONSES

Using the time-series data compiled in [Sections 3.0](#) and [4.0](#), hydrologic responses to natural and anthropogenic stresses were evaluated for the LWRFS. First, observed declines in Muddy River streamflow were evaluated. Second, responses to climate variability and carbonate-aquifer groundwater production were evaluated for representative wells in the LWRFS and high-elevation springs in the MRSA.

5.1 Evaluation of Muddy River Streamflow Declines

The Muddy River streamflow is measured near Moapa, NV as described in [Section 3.4.1](#) and depicted in [Figure 3-6](#). The flood-adjusted flow record was used in this analysis and compared to the average annual pre-development baseflow of 33,900 afy. By this comparison, a long-term trend of decreasing streamflow since the early 1960s was identified ([Figure 3-6](#)). Although groundwater production was occurring in the MRSA during the early 1960s and before, the uses remained in the basin. In 1965, NVE began exporting water to supply industrial uses in the California Wash basin. The disparity between the pre-development baseflow and gage record indicates there have been factors impacting the flow over time. These may include one or more of the following: (1) climate variability, (2) changes in land use above the gage, (3) surface-water diversions above the gage, and (4) capture of spring and streamflows by production wells. These factors are evaluated in the following sections.

5.1.1 Climate Variability

To investigate the effects of climate variability on the Muddy River streamflow, an evaluation of the historical precipitation record was performed. Only precipitation is considered in this analysis because it is the main climate variable affecting hydrology in the study area.

The winter-season precipitation record from 1895 to 2018 presented in [Figure 4-2](#) was analyzed and a simple-linear regression indicated a positive slope, but essentially no trend. The precipitation record was also used to assess climate conditions before and after 1965. This year was selected to distinguish two periods of record for analysis that represented pre- and post-exports of water from the area, even though groundwater production in the MRSA had already been occurring since around 1947 (Eakin, 1964). Eakin (1964) reported that the groundwater production during this intervening period was relatively small, and had no discernible affect on the gage record.

The average annual winter-season precipitation was computed for each period and used as a metric to evaluate climate differences. The average annual winter-season precipitation was 4.17 and 4.50 in/yr, pre- and post-1965, respectively. Based on these values and because the post-1965 average is slightly higher, it is concluded that the historical trend in climate conditions have not been a primary factor



causing the long-term trend of declining streamflow. The seasonal and annual variations in precipitation and temperature may, however, explain the short-term variability observed in the streamflow record.

5.1.2 Historical Land Use in the MRSA

Pre-development ET within the MRSA was estimated to be between 2,000 and 3,000 afy (Eakin, 1964). Land-use changes presumably have some impact on the consumptive use of water due to an increase or decrease in vegetative cover. An increase in vegetative cover would increase consumptive use, making less water available in the system. Conversely, if vegetative cover decreased, consumptive use would also decrease and more water would be available. Examples of land-use change include:

- replacing natural vegetation with agriculture lands
- fallowing agricultural lands
- restoring natural landscapes (e.g., removal of palm trees and replacing with natural vegetation)
- fires
- stream restoration

To evaluate conditions in the MRSA and the influence of land-use changes in the early 2000s, SNWA funded the DRI to compile and analyze satellite imagery and associated vegetation indices to estimate ET for the period 2001 through 2012 (Huntington et al., 2013). The study area encompassed the spring complexes, agricultural lands, and phreatophytes within the Muddy River headwaters, where most of the changes have occurred.

The study applied two methods to derive ET estimates. The first method used Mapping EvapoTranspiration at high Resolution with Internalized Calibration (METRIC), and the second used the Normalized Difference Vegetation Index (NDVI). Both methods relied upon Landsat multispectral data. Precipitation was subtracted from the ET estimates to yield results that are more comparable from one year to the next, and also allow for the evaluation of changes independent of precipitation influences.

The study results for each method are presented in [Figure 5-1](#) which depicts the annual ET reduced by annual precipitation for the study period. High and low values are observed in the estimates from both methods and correspond with observed conditions that would be expected to have an impact on ET rates in the area. The high estimate of 2005 is associated with increased vegetation density due to above normal precipitation. Even though the precipitation falling directly on the ET area was subtracted from the ET volume, the effects of the extraordinarily large precipitation of 2005 can be seen in [Figure 5-1](#). These effects are due to the increased recharge resulting from the increased precipitation. During 2004-2005, precipitation was about 300 percent of the 2001-2012 average. The low estimate of 2010 is associated with a major fire that burned more than 600 acres. During the years analyzed, other more gradual and subtle changes occurred involving landscape restoration and the removal of palm trees and weeds in the Warm Springs Natural Area. These changes may have contributed to the decline observed over the analysis period.

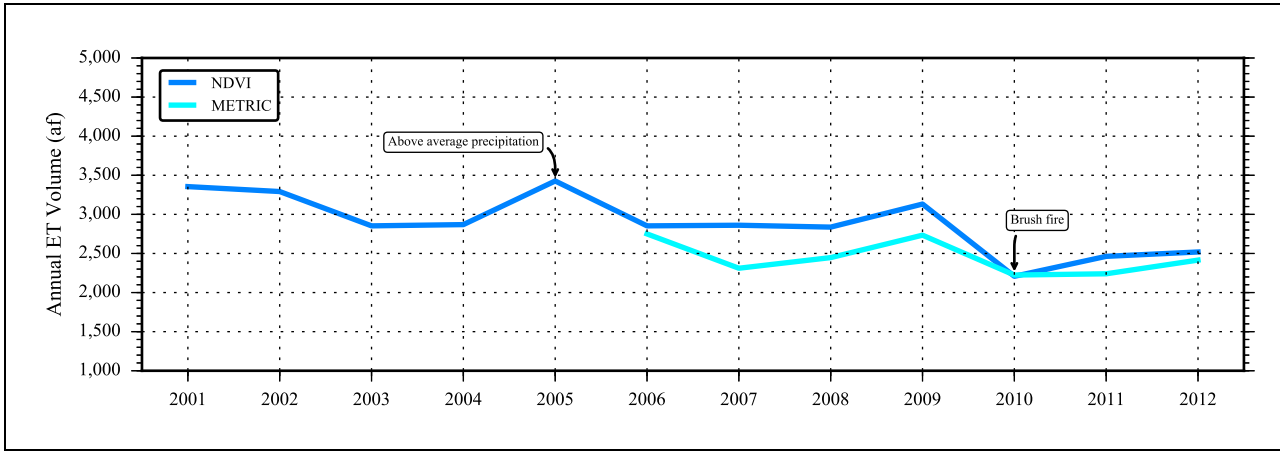


Figure 5-1
Annual ET Reduced by Precipitation for Muddy River Springs Area (2001 -2012)

Although there were land-use changes observed during the years analyzed, the range of ET estimates closely aligns with the pre-development estimate of Eakin (1964). Estimates ranged from about 2,200 to 3,400 afy, and the estimates declined over the period of analysis by about 600 to 900 afy based on the METRIC and NDVI methods, respectively. These changes are relatively small compared to the measured flow of the Muddy River and appear to be within the range of seasonal variability observed during the period of pre-development baseflow from 1945 to 1955 (Figure 3-6).

5.1.3 MRSA Surface-Water Diversions

A natural-flow record was constructed for the period 1993 through 2017 by adding the total annual diversions above the MR Moapa gage to the flood-adjusted record (Figure 5-2). This period of record was selected because diversion data for the years prior to 1993 were incomplete or based on estimated values as opposed to metered records.

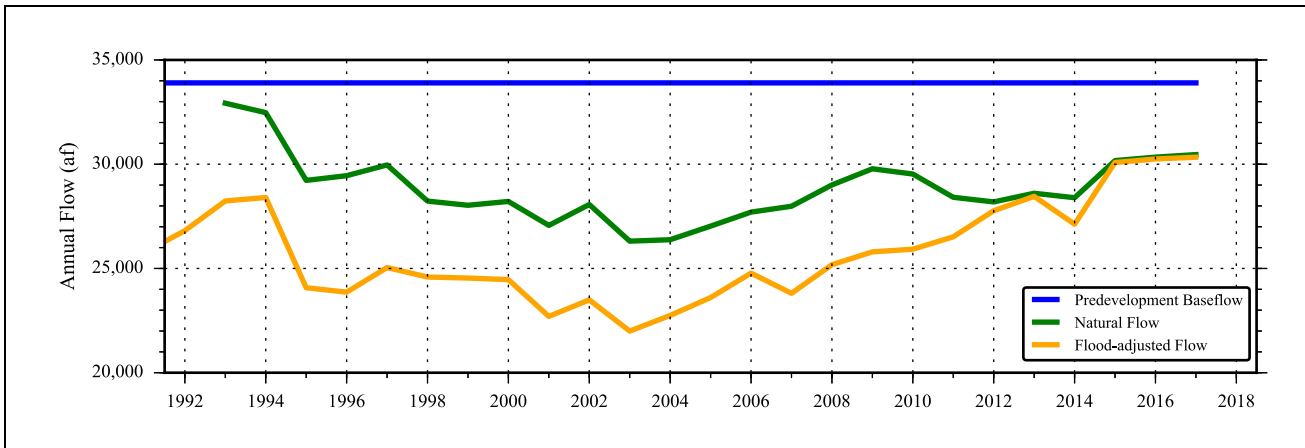


Figure 5-2
Natural Flow Record at MR Moapa Gage (1993 - 2017)



The diversion data used to construct the natural flow record include the MVWD diversions at Baldwin and Pipeline-Jones springs and the NVE diversion directly above the gage (Figure 4-4). Water associated with these diversions was exported out of the basin to supply municipal uses within the MVWD service area and NVE industrial uses in California Wash basin. Figure 5-2 compares the natural flow record to the pre-development baseflow flow of 33,900 afy. Long-term climate variability and MRSA land-use were determined not to be primary factors causing the long-term trend of declining streamflow. Therefore, the difference between the pre-development baseflow and the natural flow record must be mostly associated with groundwater production within the MRSA.

5.1.4 MRSA Groundwater Production

MRSA groundwater production and its influence on Muddy River streamflow was evaluated by quantifying the difference between the pre-development baseflow, 33,900 afy, and the natural flow record (hereinafter referred to as the “MR Flow Deficit” depicted in Figure 5-3), and determining whether the difference and source of the deficit is equivalent to the annual groundwater production within the MRSA. Like the surface-water diversion data, groundwater-production records from 1993 through 2017 were used in the analysis.

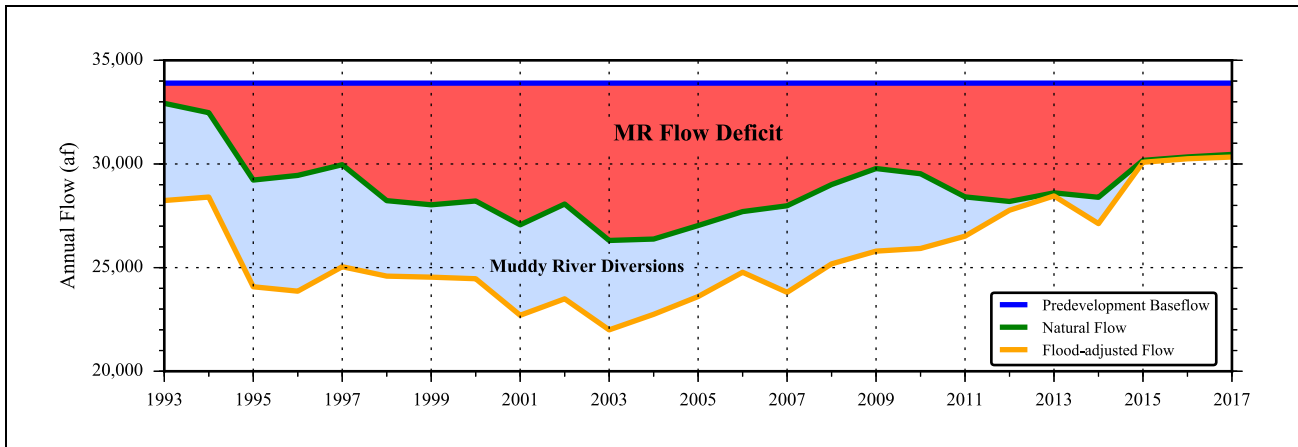


Figure 5-3
MR Flow Deficit (1993 - 2017)

As described in Section 4.2.2.1, there are several alluvial wells in the MRSA that are completed to shallow depths within the headwaters of the Muddy River. NVE has operated these wells to supply water for industrial uses in California Wash basin. Operation of the wells creates cones of depression that induce flow to the wells, capturing water from reservoir storage, springs, and seeps on the valley floor, and gaining stream reaches above the gage. Conceptually, the wells capture water that would otherwise compose the flows measured at the gage during pre-development conditions. The locations of these wells and their historical production are presented in Figures 4-5 and 4-6, respectively.

In addition to the shallow alluvial wells operated by NVE, MVWD operates three municipal wells within the MRSA and northwest of the alluvial basin (i.e., Arrow Canyon 1, Arrow Canyon 2, and MX-6). These wells produce groundwater to supply municipal uses within the MVWD service area, but primarily to locations outside the MRSA. The locations of these wells and their historical production are presented in Figure 4-5 and 4-7, respectively.

Figure 5-4 presents a time-series chart of the MR Flow Deficit and MRSA groundwater production. Production from two wells, Perkins and Behmer, was excluded from the total because of their location in proximity to the MR Moapa gage. These wells are located downstream of the gage and are unlikely to influence the streamflow above the gage. As Figure 5-4 illustrates, groundwater production within the MRSA can fully account for the MR Flow Deficit observed for the period of analysis. Included on the chart is groundwater production by CSI and SNWA from production wells located farther away within Coyote Spring Valley and upgradient of the MRSA.

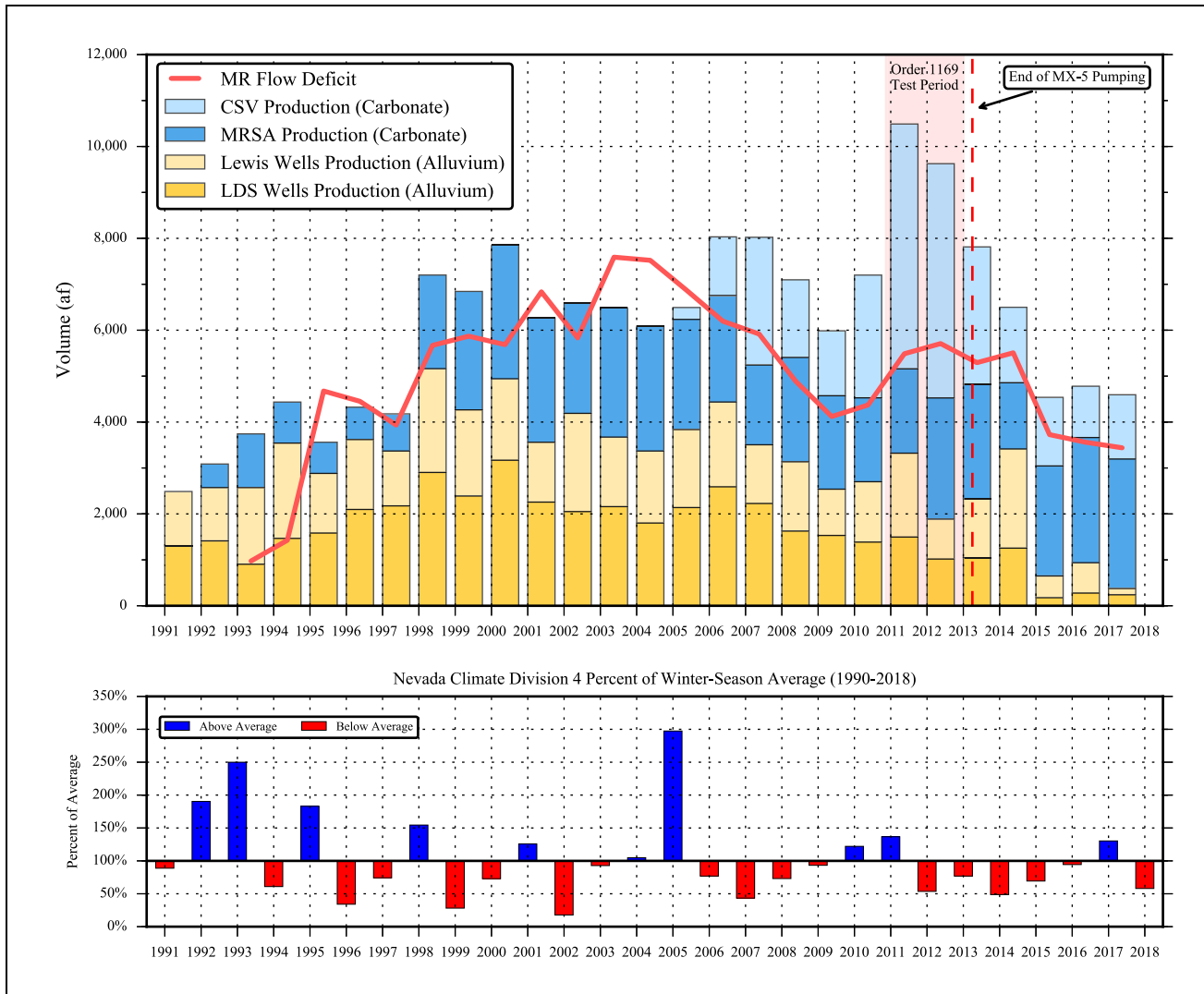


Figure 5-4
MR Flow Deficit and Coyote Spring Valley and MRSA Groundwater Production

There are certain years when the MR Flow Deficit appears to be too low (1993 and 1994) or too high (2003 and 2004) with respect to the annual groundwater production. This can be explained, in part, by the fluctuations in Muddy River streamflow caused by short-term variability in climate conditions as compared to the constant pre-development baseflow. During years of above average flow, the MR Deficit is apparently low because the difference between the pre-development baseflow and the



above-average streamflow is smaller. Conversely, in years that the streamflow is below average, the MR Flow Deficit is apparently high because the difference is larger.

Regardless of the streamflow variability, the results of this analysis conclusively demonstrate the impacts MRSA groundwater production has on MR streamflow. Groundwater production from the MRSA alluvial reservoir depletes MR streamflow on a 1:1 basis because the production wells are within the MR headwaters and capture water that would otherwise flow into the river and past the MR Moapa gage. This is supported by the fact the production volumes fall beneath the MR Flow Deficit line as depicted in [Figure 5-4](#). In similar fashion, MRSA production wells completed in the carbonate aquifer capture water that would otherwise replenish the alluvial reservoir through diffuse subsurface flow or via discrete springs. Capturing this groundwater ultimately depletes the source of supply to the alluvial reservoir and springs; thereby, depleting the MR streamflow. Based on the accounting depicted in [Figure 5-4](#), the carbonate production wells deplete the MR streamflow approaching a 1:1 basis.

5.2 Carbonate-Aquifer Responses to Climate Variability and Pumping Stresses

Throughout the LWRFS, there are many groundwater sites that are monitored and provide information on groundwater conditions regarding the carbonate aquifer. These sites include production and monitor wells completed in the carbonate aquifer and various springs in the MRSA. In this section, an evaluation of the hydrologic responses to climate variability and groundwater production at wells and springs representative of the carbonate aquifer is presented.

5.2.1 Responses to Climate Variability

An extensive database of groundwater levels exists for wells located in the LWRFS. These data were analyzed to evaluate current groundwater conditions, hydraulic gradients, and flow directions as described in [Section 3.4.2](#), and aquifer responses to climate variability in this section.

Time-series charts of water-level data for representative carbonate wells located in each of the basins composing the LWRFS were constructed and are presented in [Figure 5-5](#) for wells CSVM-1, GV-1, BM-DL-2, PAIUTES-TH2, and EH-4. As these charts illustrate, groundwater levels respond in the same manner throughout the LWRFS. The responses are indicative of a high degree of hydraulic connection within the aquifer and across all of the basins. Based on a review of all of the data, the only apparent exception is within Coyote Spring Valley for wells CSVM-3 and CSVM-5 (SNWA, 2018). These two wells are different because of their geologic setting and completion in the upthrown structural blocks of the southern Delamar Mountains and Sheep Range, respectively, as described in [Section 3.4.2](#). Time-series charts for these two wells, CSVM-4 and KMW-1, which are completed within the Kane Springs fault zone, and CSMV-1 are presented in [Figure 5-6](#). As [Figure 5-6](#) illustrates, the wells within the Coyote Spring structural basin respond in the same manner, although responses in CSVM-4 and KMW-1 appear to be slightly attenuated by the Kane Springs fault. Responses observed in CSVM-3 and CSVM-5 are distinctly different.

The time-series charts are presented with precipitation data from the Nevada Division 4 as described in [Section 4.1](#). In this figure, annual winter-season precipitation is represented as a percentage of

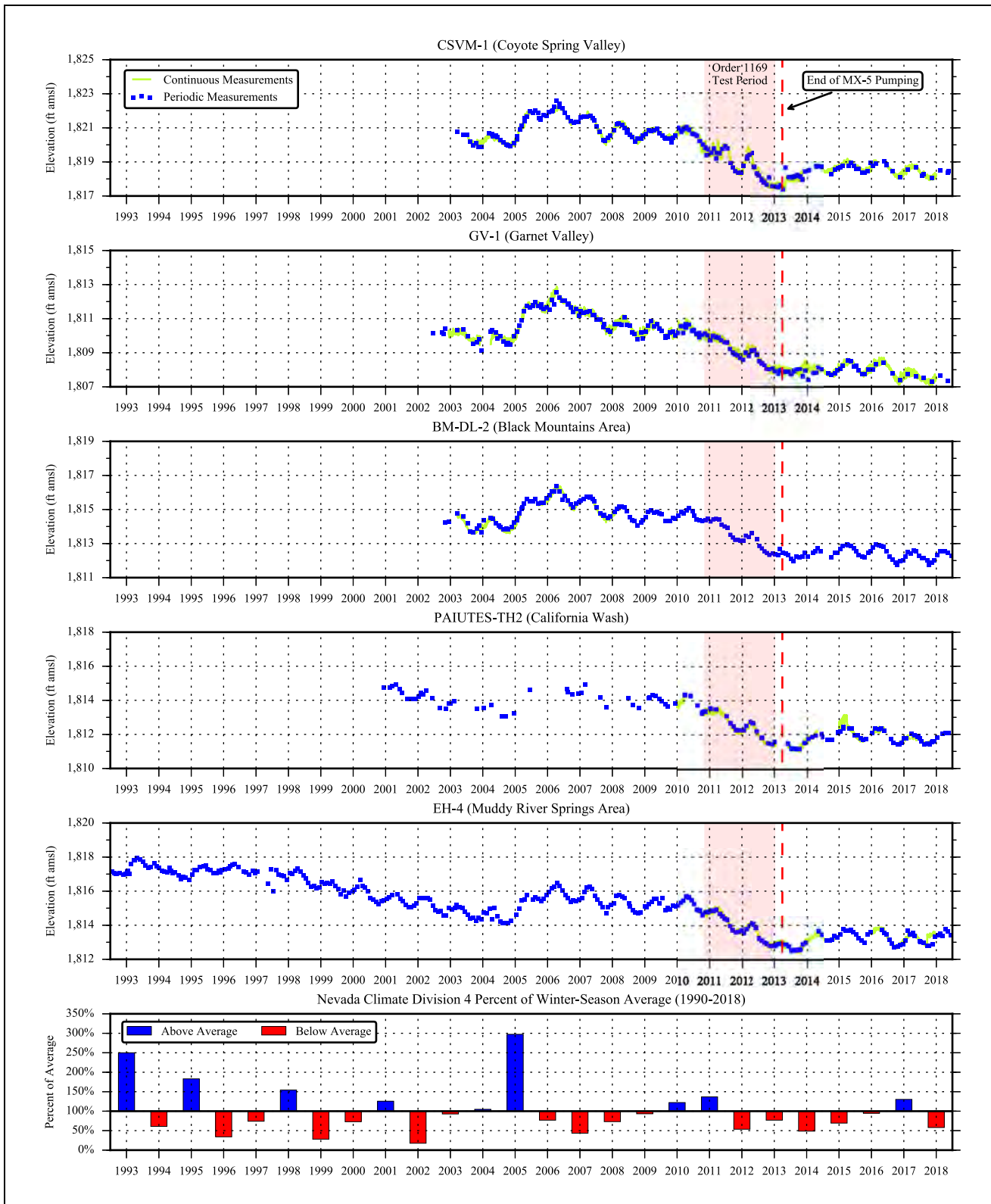


Figure 5-5
Water-Level Responses in Representative Carbonate Wells

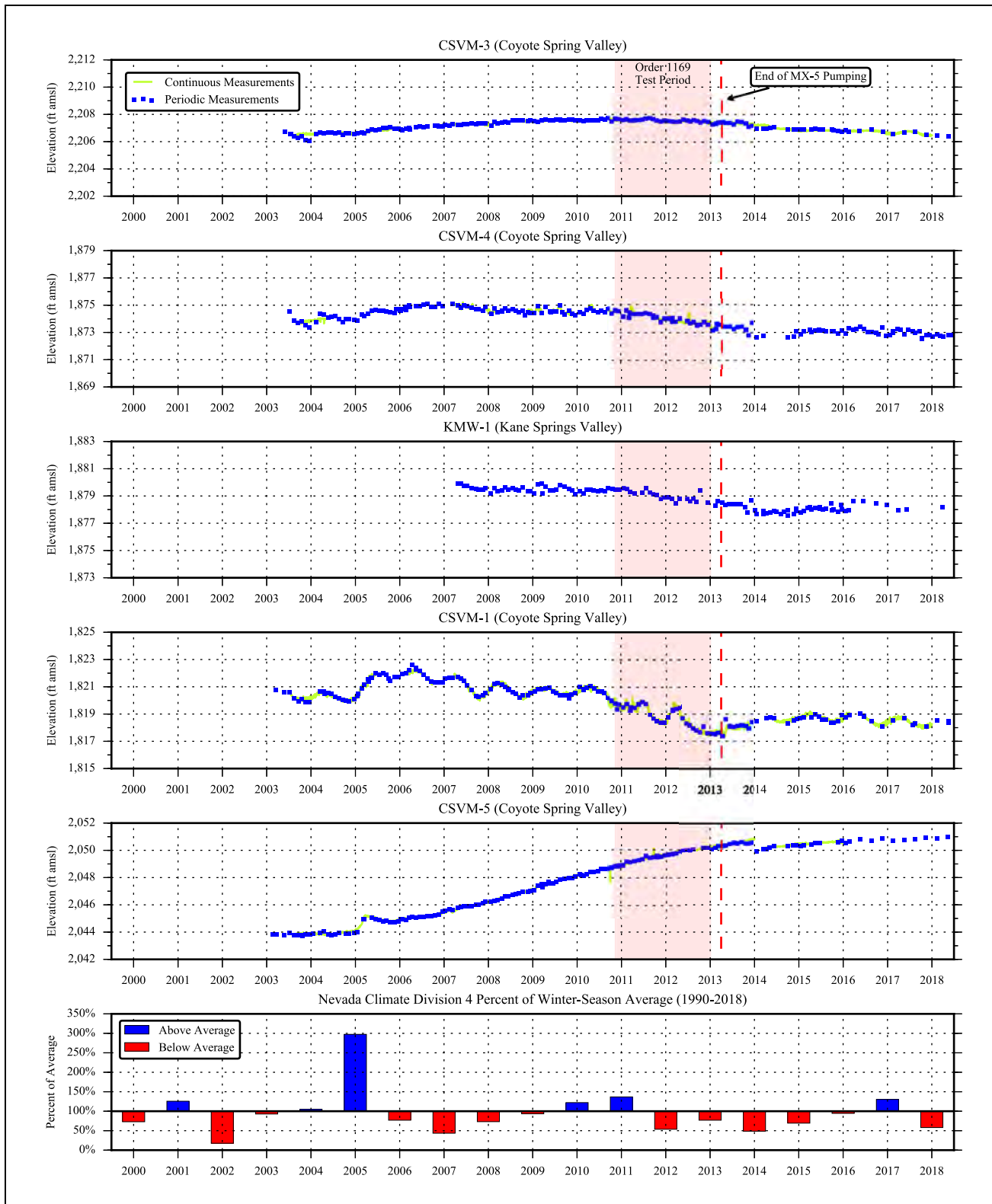


Figure 5-6
Water-Level Responses in Representative Carbonate Wells

average winter-season precipitation for the period 1990 through 2018. The charts illustrate the seasonal responses of groundwater levels to recharge pulses, with levels typically achieving their annual peak in April. The amplitudes of these seasonal fluctuations are generally consistent except for years when the percent of average precipitation is extraordinary, like in 2004-2005. For the winter months spanning October 2004 through March 2005, the percent of average precipitation was nearly 300 percent, the highest percentage for the 1895 to 2018 period of record. Water levels in all carbonate wells increased accordingly in 2005, and by the spring of 2006 most wells reached their period of record high. After 2006, water levels declined and appeared to stabilize from 2008 through 2010, prior to the start of the NSE Order 1169 aquifer test.

In the MRSA, the Pederson Spring and the Warm Springs West gage records are used as indicators of how changes in aquifer conditions affect discharge from the regional springs in the area. These records are described in detail in [Section 4.0](#) and are presented in [Figure 5-7](#) with the percent of average precipitation and groundwater production from the carbonate aquifer. The gage records respond in the same manner as the carbonate-aquifer water levels, reaching peak discharge levels in the spring of 2006 after the extraordinary precipitation during 2004-2005. Like the groundwater levels, after 2006 the spring discharge declined, then stabilized prior to the start of the NSE Order 1169 aquifer test.

5.2.2 Groundwater Production - NSE Order 1169 Aquifer Test and Recovery

Groundwater production from the carbonate aquifer is described in [Section 4.2.2.2](#) and presented by basin in [Figure 4-7](#). Regional responses to local pumping stresses are difficult to discern in the water-level records which typically only vary about 6 ft throughout the entire LWRFS over the various periods of record. On an annual basis, the typical seasonal fluctuations from recharge pulses are less than 2 ft. These seasonal responses and longer-term trends associated with climate variability mask the subtle effects of gradual changes in the relatively consistent pumping regime. Only abrupt and significant changes to the pumping regime, such as those implemented as part of the NSE Order 1169 aquifer test, cause responses that are discernible in the water-level and spring-discharge records ([Figures 5-7](#) through [5-10](#)). These responses and interpretations of the test results are documented in several reports that were submitted to the NSE in 2013 and summarized in [Section 2.0](#). In summary, water-levels in the carbonate aquifer declined from 1.0 to 2.5 ft throughout the LWRFS as a result of the stresses imposed during the aquifer test, including Kane Springs Valley.

In general, responses to groundwater production are even more difficult to discern in the spring discharge records. The measurement accuracy of the Pederson and Warm Springs West gages and the variability of discharge due to seasonal fluctuations and long-term trends associated with the carbonate aquifer make it difficult to identify responses to pumping stresses. However, responses to pumping stresses imposed during the Order 1169 aquifer test were very apparent in these records. As [Figure 5-7](#) illustrates, by the end of the 2-year test, discharge from Pederson Spring was reduced to about one-third of its pre-test flow, from 0.21 to 0.07 cfs. Discharge measured at the Warm Springs West gage declined about 8 percent, from 3.70 to 3.41 cfs. After the test, discharge at the Warm Springs West gage continued to decline and, had the test or operation of the MX-5 well continued, the initial trigger of 3.2 cfs at the Warm Springs West gage would have been reached before the end of 2014.

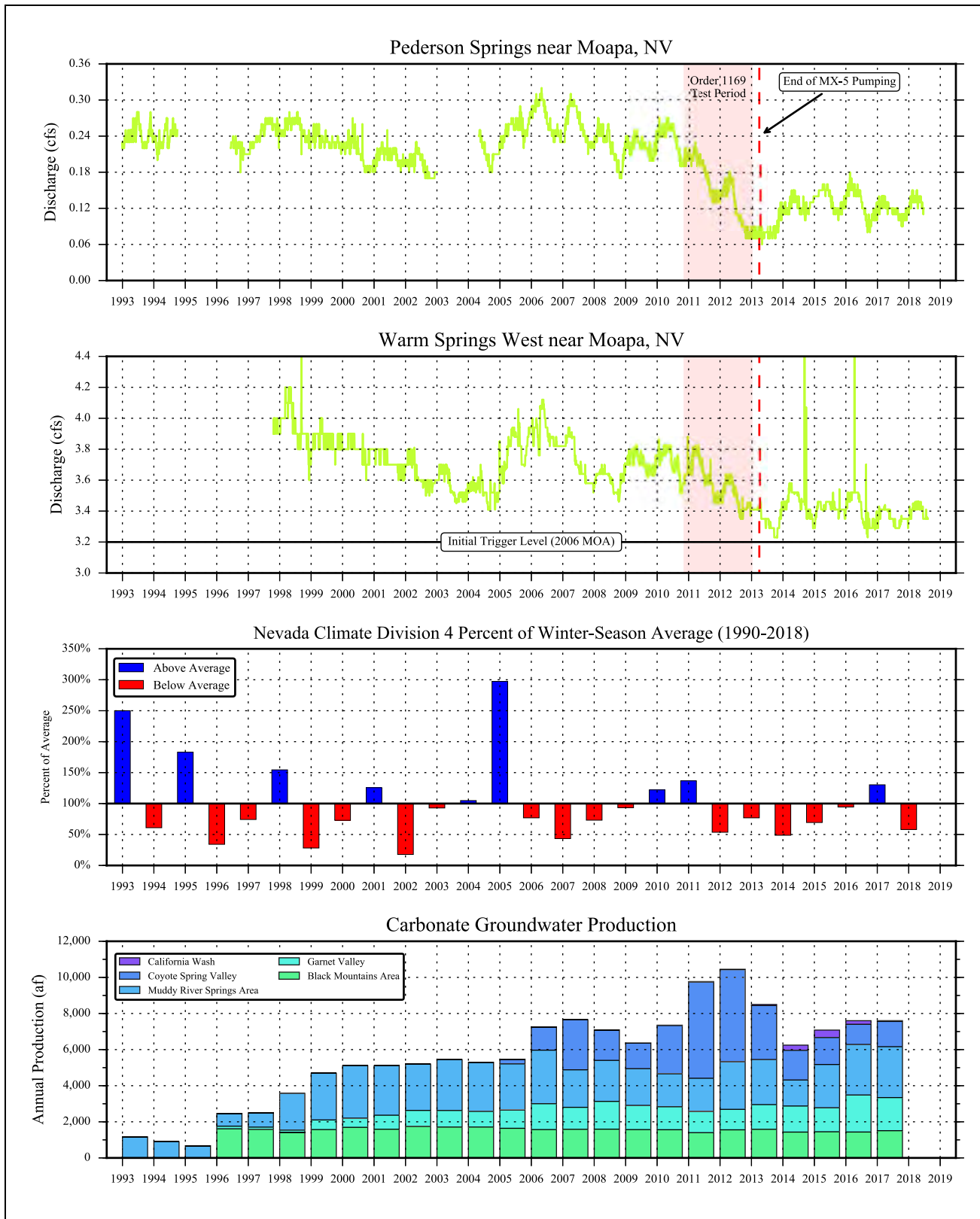


Figure 5-7
MRSA Spring Discharge and Carbonate-Aquifer Groundwater Production

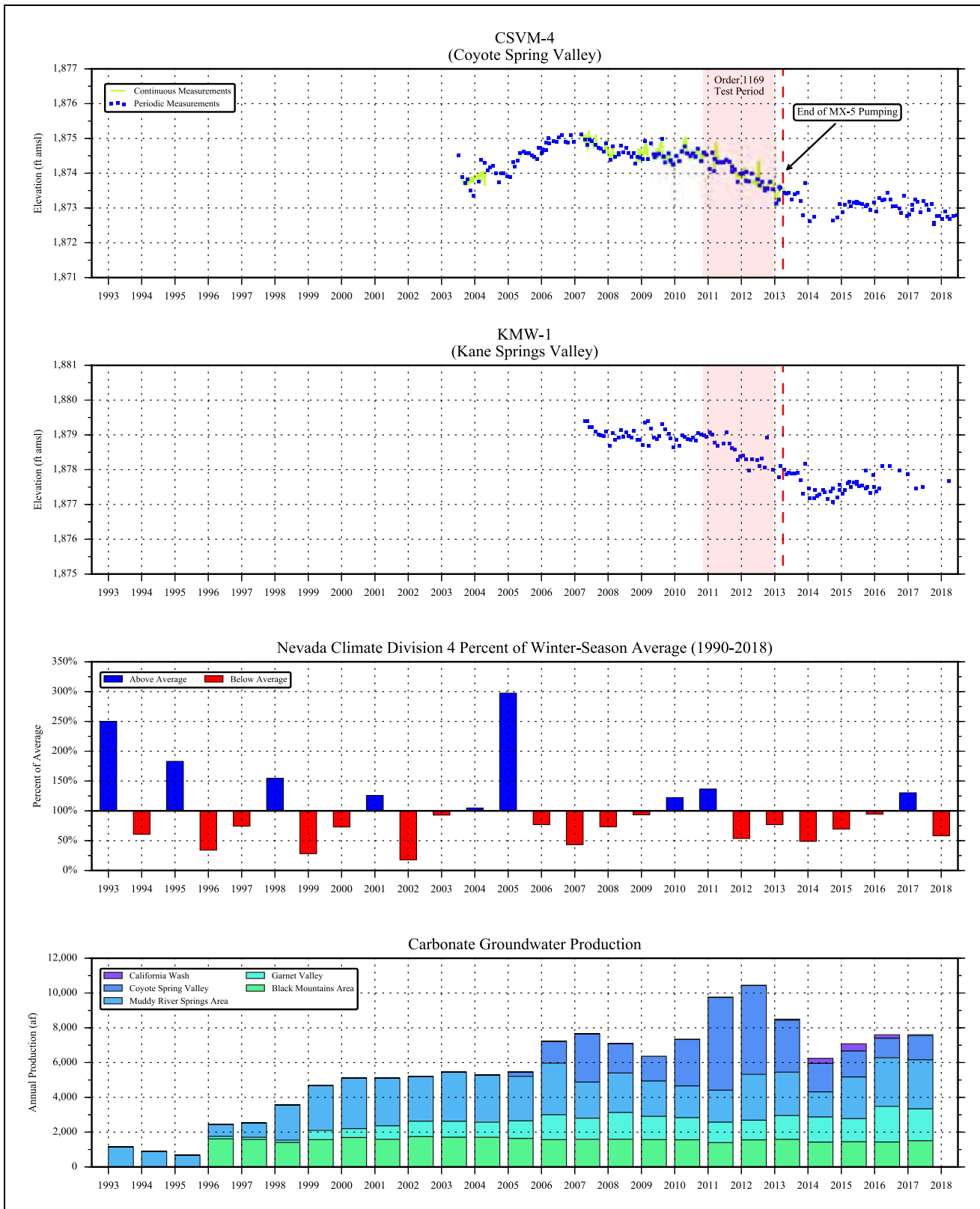


Figure 5-8
Carbonate-Aquifer Water Levels and Groundwater Production

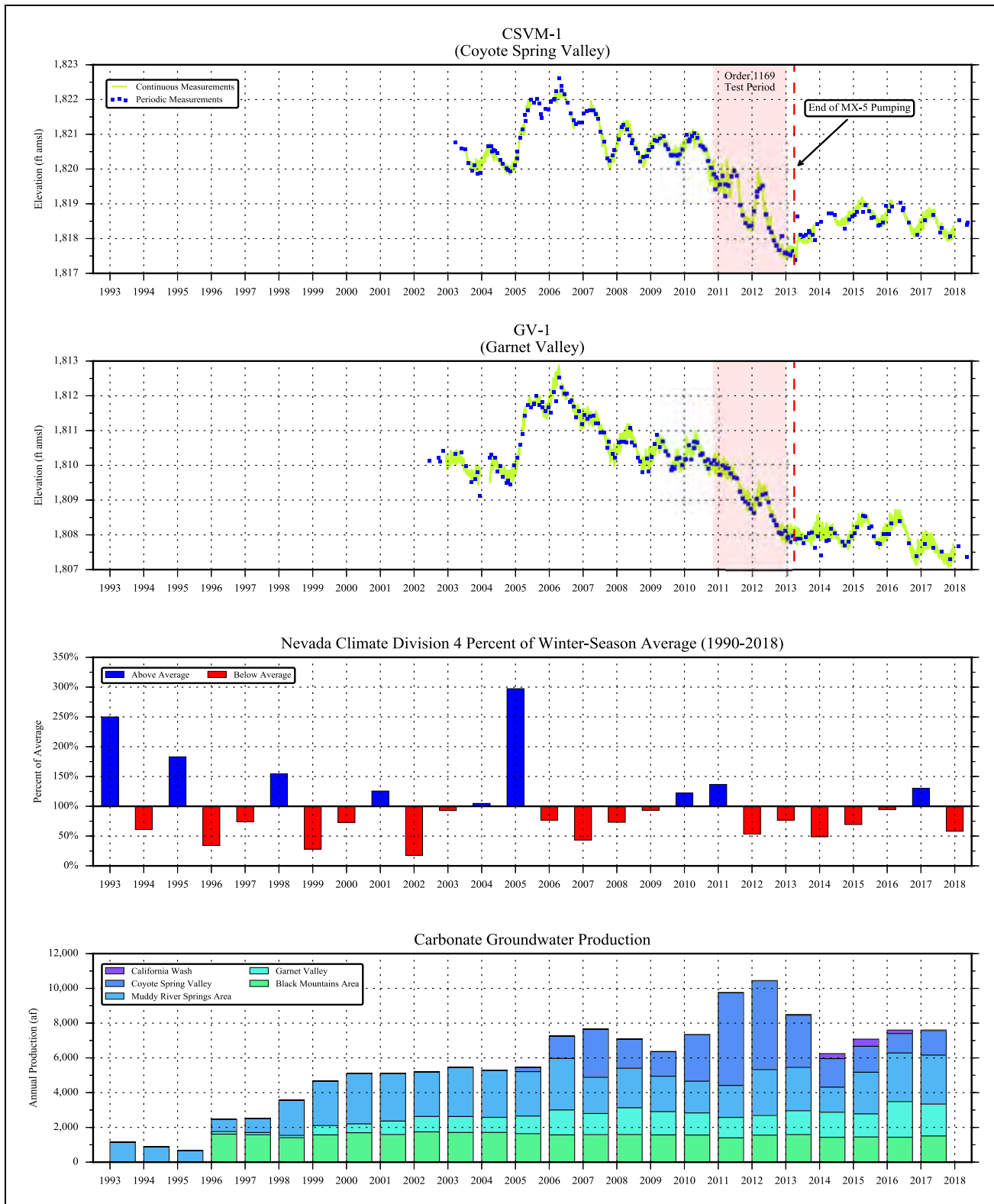


Figure 5-9
Carbonate-Aquifer Water Levels and Groundwater Production

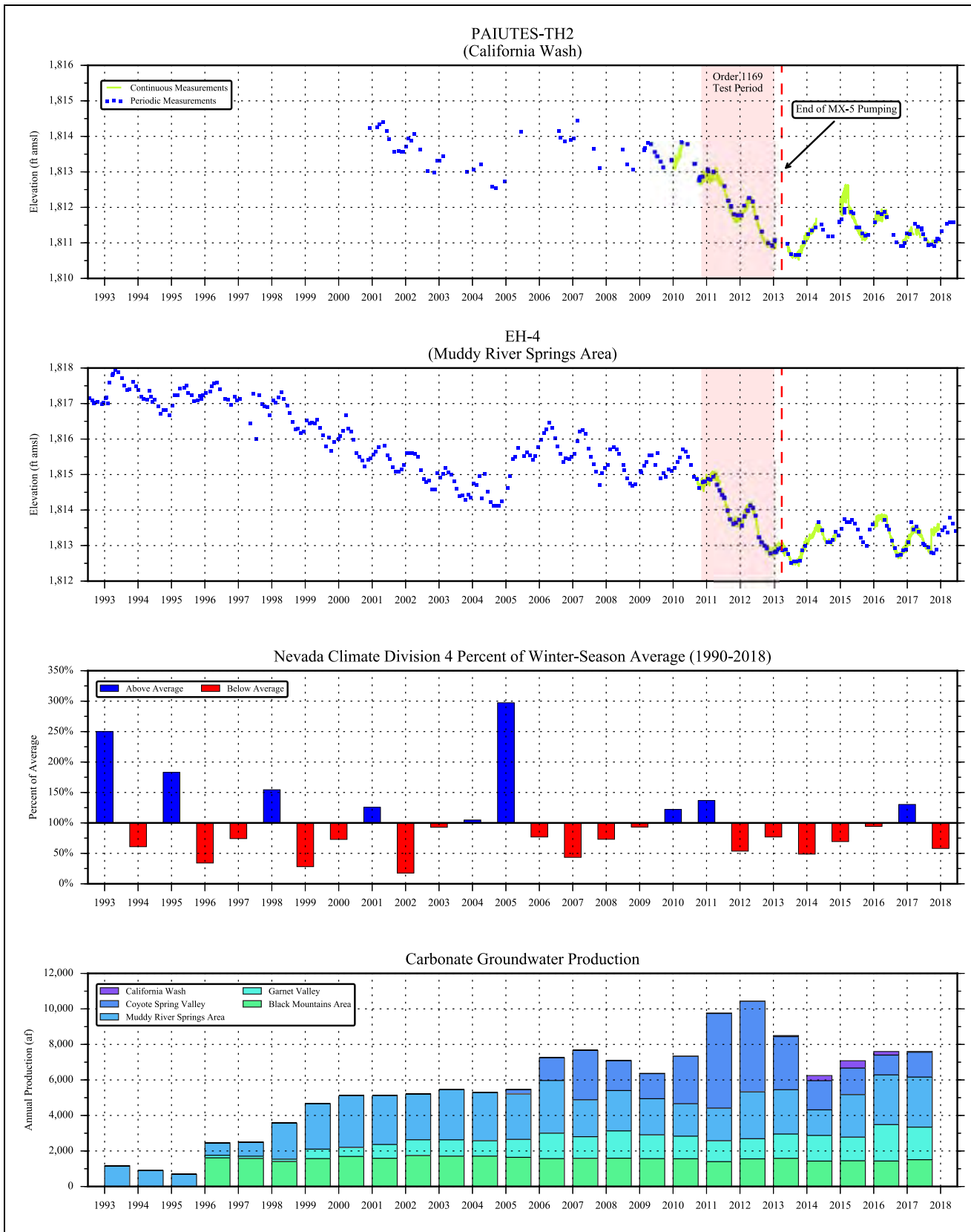


Figure 5-10
Carbonate-Aquifer Water Levels and Groundwater Production



Recovery from the pumping stresses imposed during the aquifer test was less than expected, and never reached pre-test levels. There were two primary factors that influenced the initial recovery record observed during 2013: (1) continued pumping of the MX-5 well and (2) the seasonal responses to recharge pulses. Continued pumping of the MX-5 well muted the recovery response during a period in which water levels increase to their typical season high in April. After the MX-5 well was shut down in mid-April 2013, the recovery response was attenuated by the seasonal water-level decline that starts in May and reaches a low in October. Although these factors complicated the 2013 record, the subsequent years of monitoring provided a clear picture of the recovery response and the following observations are made:

- Carbonate-aquifer water levels have not recovered to pre-test levels.
- Spring flows measured at the Pederson Spring and Warm Springs West gages have not recovered to pre-test levels.
- Recovery achieved its maximum levels between the first quarters of 2015 and 2016.

5.3 Water-Resource Implications

The carbonate aquifer composing the LWRFS extends into Kane Springs Valley, and recharge derived locally within the basin flows into northern Coyote Spring Valley. Responses to natural and anthropogenic stresses observed in monitor wells located in northern Coyote Spring Valley (CSVM-4) and southwest Kane Springs Valley (KMW-1) indicate there is hydraulic continuity within the aquifer between this area and production wells in southern Coyote Spring Valley. The effects of groundwater production in Kane Springs Valley will propagate into Coyote Spring Valley and be additive to any effects caused by pumping stresses elsewhere in the LWRFS, even if the effects are attenuated by the Kane Springs fault. Spring flows from high-elevation springs in the MRSA are highly sensitive to small changes in hydraulic head, and to ensure the long-term protection of these flows and senior water-rights, Kane Springs Valley should be included as part of the LWRFS administrative unit.

As previously discussed, the carbonate aquifer is the source of all perennial springs and seeps in the MRSA that sustain the local alluvial reservoir and Muddy River streamflow. Based on the analysis described in [Section 5.2](#), groundwater levels (i.e., hydraulic heads) in the carbonate aquifer are highly sensitive to natural and anthropogenic stresses. Discharge from the MRSA springs also responds to these stresses; however, the responses are highly dependent on the elevations of the spring orifices. The elevation of a spring orifice controls the hydraulic potential (hydraulic head in the carbonate aquifer minus spring-orifice elevation) driving its discharge. The hydraulic potential driving spring discharge decreases with increasing spring elevation, resulting in increasing levels of sensitivity to natural and anthropogenic stresses affecting groundwater levels in the carbonate aquifer.

[Figure 5-11](#) presents the MRSA spring locations with Light Detection and Ranging (LIDAR) elevation data to illustrate the distribution of spring complexes and stream reaches with respect to ground-surface elevations. Spring orifices and gaining stream reaches occurring at higher elevations are more susceptible to changes in groundwater levels than lower elevations. For instance, discharge from high-elevation springs in the MRSA respond in a manner that is consistent with changes in the groundwater levels in the carbonate aquifer. Small changes in groundwater levels during the NSE

Order 1169 aquifer test resulted in reduced discharge from the Pederson Spring Complex. Springs that occur at lower elevations have a greater hydraulic potential and are less sensitive to such changes.

Since 2016, carbonate groundwater levels and discharge measured at Pederson Spring and Warm Springs West gages have declined. A significant increase in carbonate groundwater production, such as that which occurred during the NSE Order 1169 aquifer test, will increase the rate of decline (see [Figures 5-7 through 5-10](#)) so that the 2006 MOA trigger ranges are encountered much sooner. In this case, groundwater production would be restricted per the annual volumes listed in [Table 1-1](#).

It is unclear whether the observed declines since 2016 are mainly caused by the slight increase in carbonate groundwater production, a sequence of below average precipitation since the end of the aquifer test, or a combination of the two. However, it should be noted that the declines occurred even though the 2017 winter-season precipitation was above average. Precipitation can neither be predicted nor controlled; therefore, monitoring the response of the flow system and managing groundwater production is the only way to avoid reaching the protective triggers and impacting senior water rights. Based on this assessment, the following conclusions are made:

- Flow measured at the Warm Springs West gage will reach trigger ranges sooner and at lower production rates than initially contemplated;
- Given the current rates of carbonate groundwater production, recovery of groundwater levels and spring discharge to pre-test levels is not possible without extraordinary hydrology such as the 2004-2005 winter-season precipitation; and
- Even with such extraordinary hydrology, subsequent years of lesser precipitation with similar groundwater production volumes will result in a resumption of declining trends as has been observed in the historical record.

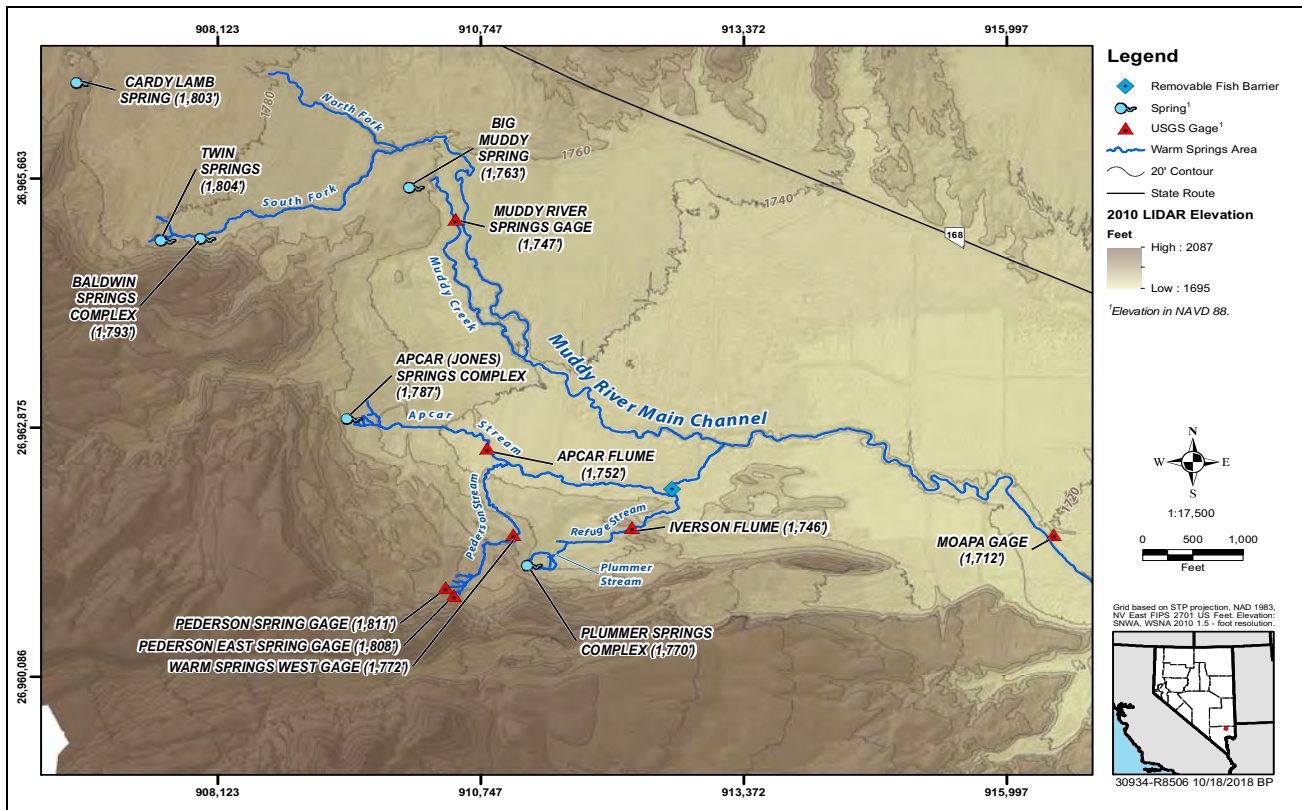


Figure 5-11

Elevation of Selected Springs and LIDAR Digital Elevation Model within the MRSA

6.0 SUMMARY AND CONCLUSIONS

An assessment of the current water-resource conditions for the LWRFS was performed and an analysis was completed to evaluate hydrologic responses to natural and anthropogenic stresses observed at various locations of interest. The analysis considered time-series data for several variables that describe the historical conditions of the hydrologic system over a period of decades. The objectives of the analysis were to assess the following:

- Evaluate hydrologic responses to the variable stress conditions affecting the LWRFS;
- Evaluate the recovery responses associated with the cessation of the 2-year aquifer test; and
- Identify trends in the behavior of key hydrologic variables.

The analysis focused on the historical behavior of the Muddy River streamflow and the carbonate system composing the LWRFS. The results and conclusions from this assessment are summarized in the following sections.

Muddy River Stream Flow

An evaluation of Muddy River streamflow was performed to identify the likely causes of a long-term trend of declining streamflows observed at the MR Moapa gage since the early 1960s. Long-term climate variability and changes in land use were ruled out as major contributors to the decline. Annual records of winter-season precipitation, a reflection of climate conditions, indicate that the average annual precipitation during the period of declining streamflow (post-1965) is not substantively different than the average for the period prior to the decline (pre-1965). Land-use changes during this period may have had very short-term effects, but the incremental changes in consumptive uses above the gage have been minimal. The most likely causes of streamflow declines have been surface-water diversions and MRSA groundwater production above the MR Moapa gage.

A period from 1993 to 2017, in which comprehensive records of Muddy River streamflow, surface-water diversions and groundwater production are available, was analyzed to estimate the MR Flow Deficit. An average annual natural-flow record was constructed by adding annual surface-water diversions to the flood-adjusted flow record of the MR Moapa gage. The annual MR Flow Deficit was estimated by computing the difference between the average annual pre-development flow of the Muddy River and the natural-flow record. An analysis was performed to determine whether MRSA groundwater production could account for the MR Flow Deficit. The results of the analysis yielded the following observations and conclusions:

- Muddy River streamflow declined from a pre-development condition of 33,900 afy to a minimum of about 22,000 af in 2002.



- Since 2002, streamflow has steadily increased to its current rate of over 30,000 afy as a result of reduced surface-water diversions and MRSA groundwater production.
- The MR Flow Deficit peaked at about 7,500 af in 2003, and was about 3,500 af in 2017.
- MRSA groundwater production above the MR Moapa gage peaked in 2000 at 7,850 af, and was 3,200 af in 2017.
- Groundwater production from the MRSA alluvial reservoir depletes Muddy River streamflow on a 1:1 basis.
- Groundwater production from MRSA carbonate wells deplete Muddy River streamflow approaching a 1:1 basis.

Hydrologic Responses to Natural and Anthropogenic Stresses

An analysis of the hydrologic responses to natural and anthropogenic stresses at wells and springs representative of the carbonate aquifer was performed for the LWRFS. Time-series charts of groundwater levels and gage records for the Pederson Spring and Warm Springs West gages were prepared for the period 1993 to 2018. To assess groundwater-level and spring-discharge responses to climate variability and pumping stresses, these charts were compared to time-series of average annual winter-season precipitation and annual carbonate-aquifer groundwater production. The analysis observations and conclusions are listed below:

- Aquifer responses to climate variability are uniform across the entire LWRFS.
- Widespread responses to pumping stresses associated with the NSE Order 1169 aquifer test were observed in groundwater-level and spring-discharge records.
- By the end of the aquifer test, discharge from Pederson Spring decreased by about 0.15 cfs (to about 1/3 of baseflow).
- Spring discharge as measured at the Warms Springs West gage decreased about 0.3 cfs (< 10% of baseflow).
- Continuation of the aquifer-test or pumping from the MX-5 well would have reduced flows at the Warm Springs West gage to the initial 2006 MOA trigger level (3.2 cfs).
- Groundwater levels and spring discharge rates have not recovered to pre-test levels.
- Recovery achieved its maximum levels between the first quarters of 2015 and 2016.
- Groundwater levels and spring discharge-rates have declined since 2016.

Water-Resource Implications

Based on the data evaluation and analysis, the following water-resource implications associated with current conditions and the prospects of future groundwater development were identified:

- Kane Springs Valley should be included as part of the LWRFS administrative unit because the carbonate aquifer extends beneath the basin, recharge derived locally within the basin flows into Coyote Spring Valley, and responses to natural and anthropogenic stresses observed in monitor wells located in northern Coyote Spring Valley (CSVM-4) and southwest Kane Springs Valley (KMW-1) indicate there is hydraulic continuity within the aquifer between this area and production wells in southern Coyote Spring Valley.
- High-elevation springs in the MRSA are highly sensitive to changes in carbonate groundwater levels and are most susceptible to carbonate groundwater production;
- A significant increase in carbonate groundwater production, such as that which occurred during the NSE Order 1169 aquifer test, will cause sharp groundwater-level and spring-discharge declines;
- Flow measured at the Warm Springs West gage will reach trigger ranges sooner and at lower production rates than initially contemplated;
- Given the current rates of carbonate groundwater production, recovery of groundwater levels and spring discharge to pre-test levels is not possible without extraordinary hydrology such as the 2004-2005 winter-season precipitation; and
- Even with such extraordinary hydrology, subsequent years of lesser precipitation with similar groundwater production volumes will result in a resumption of declining trends as has been observed in the historical record.



This Page Left Intentionally Blank

7.0 REFERENCES

- Beard, L.S. , Anderson, R.E., Block, D.L., Bohannon, R.G., Brady, R.J., Castor, S.B., Duebendorfer, E.M., Faulds, J.E., Felger, T.J., Howard, K.A., Kuntz, M.A., and Williams, V.S., 2007, Preliminary Geologic Map of the Lake Mead 30' x 60' Quadrangle, Clark County, Nevada, and Mohave County, Arizona: U.S. Geological Survey Open-File Report 2007-1010, 109 p.
- Bohannon, R.G., 1983, Geologic map, tectonic map and structure sections of the Muddy and northern Black Mountains, Clark County, Nevada: U.S. Geological Survey Miscellaneous Investigations Series Map I-1406, scale 1:62,500, two sheets.
- Buqo, T., 2007, Carbonate development in the Muddy Springs area, in Coache, R., ed., Regional tour of the carbonate system guidebook: Nevada Water Resources Association, Clark County, Nevada, June 18-20, 2007, p. 5-6.
- Burns, A.G., and Drici, W., 2011, Hydrology and water resources of Spring, Cave, Dry Lake, and Delamar valleys, Nevada and vicinity: Presentation to the Office of the Nevada State Engineer: Southern Nevada Water Authority, Las Vegas, Nevada.
- Coyote Springs Land, 2013, Letter from Carl D. Savely to Jason King (Nevada State Engineer), regarding Report of Coyote Springs Investment LLC, Pursuant to Nevada State Engineer Order 1169A, dated June 14, 2013.
- CSI, see Coyote Springs Land AKA Coyote Springs Investment, LLC.
- Daly, C., Neilson, R.P., and Phillips, D.L., 1994, A statistical-topographic model for mapping climatological precipitation over mountainous terrain: *Journal of Applied Meteorology*, Vol. 33, No. 2, p. 140-158.
- Daly, C., Taylor, G., and Gibson, W., 1997, The PRISM approach to mapping precipitation and temperature: American Meteorological Society, Proceedings of the 10th AMS Conference on Applied Climatology, Reno, Nevada, October 20-23, 1997, p. 10-12.
- Daly, C., Taylor, G.H., Gibson, W.P., and Parzybok, T., 1998, Development of high-quality spatial climate datasets for the United States: Proceedings of the First International Conference on Geospatial Information in Agriculture and Forestry, Lake Buena Vista, Florida, June 1-3, 1998, p. I-512-I-519.



- Daly, C., Halbleib, M., Smith, J.I., Gibson, W.P., Doggett, M.K., Taylor, G.H., Curtis, J., and Pasteris, P.A., 2008, Physiographically sensitive mapping of climatological temperature and precipitation across the conterminous United States: *International Journal of Climatology*, Vol. 28, p. 2031-2064.
- Dixon, G.L., Donovan, D.J., and Rowley, P.D., 2007, Geology of Oak Springs Summit, in Coache, R., ed., *Regional tour of the carbonate system guidebook: Nevada Water Resources Association, Clark County, Nevada, June 18-20, 2007*, p. 71-72.
- Dohrenwend, J.C., Schell, B.A., Menges, C.M., Moring, B.C., and McKittrick, M.A., 1996, Reconnaissance photogeologic map of young (Quaternary and late Tertiary) faults in Nevada, in Singer, D.A., ed., *An analysis of Nevada's metal-bearing mineral resources: Nevada Bureau of Mines and Geology Open-File Report 96-2*, p. 9-1-9-12.
- Donovan, D.J., 2007, Geology of Muddy River Springs, in Coache, R., ed., *Regional tour of the carbonate system guidebook: Nevada Water Resources Association, Clark County, Nevada, June 18-20, 2007*, p. 1-2.
- Donovan, D.J., Dixon, G.L., and Rowley, P.D., 2004, Detailed geologic mapping in the Muddy Springs area, Clark County, Nevada [abs.]: Nevada Water Resources Association Annual Conference, Mesquite, Nevada, February 24-26, 2004, p. 23.
- Eakin, T. E., 1964, Ground-water appraisal of Coyote Spring and Kane Spring Valleys and Muddy River Springs area, Lincoln and Clark Counties, Nevada: Nevada Department of Conservation and Natural Resources, Ground-Water Resources Reconnaissance Series, Report 25, 40 p.
- Eakin, T.E., 1966, A Regional Inter-basin Ground-water System in the White River Area, Southeastern Nevada, published in *Water Resources Research*, Vol. 2, No. 2, pp. 251-271.
- Ekren, E.B., Orkild, P.P., Sargent, K.A., and Dixon, G.L., 1977, Geologic map of Tertiary rocks, Lincoln County, Nevada: U.S. Geological Survey Miscellaneous Investigations Series Map -1041, scale 1:250,000.
- Fenneman, N. M., 1931, *Physiography of the western United States: Chapter 8: Basin and Range Province*. First edition(?): New York, McGraw Hill Book Company, p. 326-395.
- Guth, P.L., 1980, Geology of the Sheep Range, Clark County, Nevada: Massachusetts Institute of Technology, Cambridge, Massachusetts, unpublished Ph.D. dissertation, 189 p.
- Harrill, J.R., Gates, J.S., and Thomas, J.M., 1988, Major ground-water flow systems in the Great Basin region of Nevada, Utah, and adjacent states: U.S. Geological Survey Hydrologic Investigations Atlas HA-694-C, scale 1:1,000,000.
- Heilweil, V.M., and Brooks, L.E., eds., 2011, Conceptual model of the Great Basin carbonate and alluvial aquifer system: U.S. Geological Survey Scientific Investigations Report 2010-5193, 191 p.

- Huntington, J. Morton, C., Bromley, M. and Liebert, R., 2013, Analysis of Evapotranspiration along the Muddy River and Warm Springs Natural Area, Desert Research Institute Technical Memo Prepared for Southern Nevada Water Authority.
- Hydrologic Review Team, 2013, 2013 Annual Determination Report, prepared by the Hydrologic Review Team established under the Memorandum of Agreement dated April 20, 2006. Las Vegas, NV.
- Hydrologic Review Team, 2014, 2014 Annual Determination Report, prepared by the Hydrologic Review Team established under the Memorandum of Agreement dated April 20, 2006. Las Vegas, NV.
- Hydrologic Review Team, 2015, 2015 Annual Determination Report, prepared by the Hydrologic Review Team established under the Memorandum of Agreement dated April 20, 2006. Las Vegas, NV.
- Hydrologic Review Team, 2016, 2016 Annual Determination Report, prepared by the Hydrologic Review Team established under the Memorandum of Agreement dated April 20, 2006. Las Vegas, NV.
- Hydrologic Review Team, 2017, 2017 Annual Determination Report, prepared by the Hydrologic Review Team established under the Memorandum of Agreement dated April 20, 2006. Las Vegas, NV.
- Hydrologic Review Team, 2018, 2018 Annual Determination Report, prepared by the Hydrologic Review Team established under the Memorandum of Agreement dated April 20, 2006. Las Vegas, NV.
- Johnson, C., and M. Mifflin. 2013. Summary of Order 1169 Testing Impacts, per Order 1169A: A Report Prepared in Cooperation with the Moapa Band of Paiutes. Submitted to Nevada Division Water Resources per Order 1169A, June 2013.
- Johnson, J., 1999, Estimation of stormwater flows in Las Vegas Wash, Nevada and potential stormwater capture: In Las Vegas Wash Coordination Committee, (2000), Las Vegas Wash Comprehensive Adaptive Management Plan, Appendix 2.1, p. 1-31.
- Johnson, J.A., 2007, Hydrology of Muddy River Springs, in Coache, R., ed., Regional tour of the carbonate system guidebook: Nevada Water Resources Association, Clark County, Nevada, June 18-20, 2007, p. 3-4. Langenheim et al., 2001, 2010;
- Langenheim, V.E., Beard, L.S., and Faulds, J.E., 2010, Implications of geophysical analysis on basin geometry and fault offsets in the northern Colorado River extensional corridor and adjoining Lake Mead region, Nevada and Arizona, in Umhoefer, P.J., Beard, L.S., and Lamb, M.A., editors, Miocene tectonics of the Lake Mead region, central Basin and Range: Geological Society of America Special Paper 463, p. 39-59.



- Langenheim, V.E., Miller, J.J., Page, W.R., and Grow, J.A., 2001, Thickness and geometry of Cenozoic deposits in California Wash area, Nevada, based on gravity and seismic-reflection data: U.S. Geological Survey Open-File Report 01-393, 26 p.
- Maldonado, F., and Schmidt, D.L., 1991, Geologic map of the southern Sheep Range, Fossil Ridge, and Castle Rock area, Clark County, Nevada: U.S. Geological Survey Miscellaneous Investigations Series Map I-2086, scale 1:24,000.
- Myers, T., 2013, Comments on carbonate Order 1169 Pump Test Data and the Groundwater Flow System in Coyote Springs and Muddy River Springs Valley, Nevada; Technical Memorandum dated June 12, 2013 Prepared For Great Basin Water Network, Baker, NV.
- National Oceanic and Atmospheric Administration, 2018, Climate Division 4 Monthly Precipitation and Temperature Data for Period of Record (1895-2018), accessed September, 2018. Webpage: <https://www.ncdc.noaa.gov/cag/divisional/time-series>.
- NDWR, See Nevada Division of Water Resources.
- Nevada Division of Water Resources, 2018a, Letter from Micheline N. Fairbank to Water Right Owners in the Lower White River Flow System regarding Public Workshop Regarding Existing Water Right Use and Groundwater Pumping in the Lower White River Flow System, dated June 14, 2018.
- Nevada Division of Water Resources, 2018b, Well Log Database [Internet], accessed multiple times between September 3 and September 14, 2018, available from <http://water.nv.gov/welllogquery.aspx>
- Nevada State Engineer, 2002, Order 1169, Holding in abeyance carbonate-rock aquifer system groundwater applications pending or to be filed in Coyote Springs Valley (Basin 210), Black Mountains Area (Basin 215), Garnet Valley (Basin 216), Hidden Valley (Basin 217), Muddy River Springs aka Upper Moapa Valley (Basin 219), Lower Moapa Valley (Basin 220), and for further study of the appropriation of water from the carbonate rock aquifer system, Lincoln and Clark Counties, Nevada. March 8, 2002. 11 p.
- Nevada State Engineer, 2012, Order 1169A, Nevada State Engineer Order 1169A (1) Declaring the pumping test completed as of December 31, 2012; (2) Rescinding the update of Exhibit No. 54; and (3) Stating that study participants may file a report addressing the information obtained from the study/pumping test and the availability of water, Carson City, NV, 3 p.
- Nevada State Engineer, 2014a, Ruling 6254, In The Matter Of Applications 54055, 54056, 54057, 54058, 54059, 63272, 63273, 63274, 63275, 63276, 63867, 63868, 63869, 63870, 63871, 63872, 63873, 63874, 63875 And 63876 Filed To Appropriate The Underground Waters Of The Coyote Spring Valley Hydrographic Basin (210), Clark County And Lincoln County, Nevada.

Nevada State Engineer, 2014b, Ruling 6255, In The Matter Of Applications 64039, 64186, 64187, 64188, 64189, 64190, 64191, 64192, 67892, 71031, 72838, 72839, 72840, 72841, 79296, 79297, 79298, 79299, 79300, 79497, 79498 And 79518 Filed To Appropriate The Underground Waters Of The Coyote Spring Valley Hydrographic Basin (210), Clark County And Lincoln) County, Nevada.

Nevada State Engineer, 2014c, Ruling 6256, N The Matter Of Applications 54130, 54484, 62996, 62998, 64040, 64045, 64222, 64223, 67894, 79354, 79687, 79688, 79689, 79691 And 79903 Filed To Appropriate The Underground Waters Of The Garnet Valley) Hydrographic Basin (216), Clark County, Nevada.

Nevada State Engineer, 2014d, Ruling 6257, In The Matter Of Applications 62997, 62999, 64038, 66162, 67895, 68501, 79355, 79692 And 79693 Filed To Appropriate The Underground Waters Of The Hidden Valley Hydrographic Basin (217), Clark County, Nevada.

Nevada State Engineer, 2014e, Ruling 6258, In The Matter Of Applications 54076, 54634, 64037, 65197, 65944, 65945, 65946, 65947, 65948, 65949, 65954, 65955, 66473, 66474, 66475, 66476, 67896 And 79690 Filed To Appropriate The Underground Waters Of The California Wash Hydrographic Basin (218), Clark County, Nevada.

Nevada State Engineer, 2014f, Ruling 6259, In The Matter Of Application 59369 Filed To Appropriate The Underground Waters) Of The Muddy River Springs Area Aka Upper Moapa Valley Hydrographic Basin (219), Clark County, Nevada.

Nevada State Engineer, 2014g, Ruling 6260, In The Matter Of Applications 58592, 58593, 58594, 64041 And 67893 Filed To Appropriate) The Underground Waters Of The Black Mountains Area Hydrographic Basin) (215), Clark County, Nevada.

Nevada State Engineer, 2014h, Ruling 6261, In The Matter Of Applications 59368, 59370, 59371, And 81019 Filed To Appropriate The Underground Waters Of The Lower Moapa Valley Hydrographic Basin (220), Clark County, Nevada.

NOAA, see National Oceanic and Atmospheric Administration.

NSE, see Nevada State Engineer.

Page, W.R., 1998, Geologic map of the Arrow Canyon NW quadrangle, Clark County, Nevada:U.S. Geological Survey Geologic Quadrangle Map GQ-1776, scale 1:24,000.

Page, W.R., and Pampeyan, E.H., 1996, Preliminary geologic map of the Paleozoic rocks in the Wildcat Wash SE and Wildcat Wash SW quadrangles, Lincoln and Clark Counties, Nevada: U.S. Geological Survey Open-File Report 96-26, 18 p., scale 1:24,000.

Page, W.R., Dixon, G.L., and Ash, S.R., 1992, Northern terminus of Mesozoic Dry Lake thrust fault, Arrow Canyon range, southeastern Nevada: Geological Society of America, Rocky Mountain Section, Abstracts with Programs, Vol. 24, No. 6, p. 56.



- Page, W.R., Dixon, G.L., Rowley, P.D., and Brickey, D.W., 2005, Geologic map of parts of the Colorado, White River, and Death Valley groundwater flow systems-Nevada, Utah, and Arizona: Nevada Bureau of Mines and Geology Map 150, scale 1:250,000.
- Page, W.R., Scheirer, D.S., Langenheim, V.E., and Berger, M.A., 2011, Revised geologic cross sections of parts of the Colorado, White River, and Death Valley regional groundwater flow systems, Nevada, Utah, and Arizona: U.S. Geological Survey Open-File Report 2006-1040.
- Pampeyan, E.H., 1993, Geologic map of the Meadow Valley Mountains, Lincoln and Clark Counties, Nevada: U.S. Geological Survey Miscellaneous Investigations Series Map I-2173, scale 1:50,000.
- Rowley, P.D., Dixon, G.L., Burns, A.G., Pari, K.T., Watrus, J.M., and Ekren, E.B., 2011, Geology and geophysics of Spring, Cave, Dry Lake, and Delamar valleys, White Pine and Lincoln Counties and adjacent areas, Nevada and Utah: The geologic framework of regional groundwater flow systems: Presentation to the Office of the Nevada State Engineer: Southern Nevada Water Authority, Las Vegas, Nevada.
- Rowley, P.D., Dixon, G.L., Mankinen, E.A., Pari, K.T., McPhee, D.K., McKee, E.H., Burns, A.G., Watrus, J.M., Ekren, E.B., Patrick, W.G., and Brandt, J.M., 2017, Geology and Geophysics of White Pine and Lincoln Counties, Nevada, and Adjacent Parts of Nevada and Utah: The Geologic Framework of Regional Groundwater Flow Systems, Nevada Bureau of Mines and Geology Report 56, Prepared cooperatively by Geologic Mapping, Inc., New Harmony, Utah, U.S. Geological Survey, Menlo Park, California, Southern Nevada Water Authority, Las Vegas, Nevada and Private consultant, White Sulphur Springs, Montana.
- Rowley, P.D., Nealey, L.D., Unruh, D.M., Snee, L.W., Mehnert, H.H., Anderson, R.E., and Grommé, C.S., 1995, Stratigraphy of Miocene ash-flow tuffs in and near the Caliente Caldera Complex, southeastern Nevada and southwestern Utah, in Scott, R.B., and Swadley, W.C., eds., Geologic studies in the Basin and Range-Colorado Plateau transition in southeastern Nevada, southwestern Utah, and northwestern Arizona: U.S. Geological Survey Bulletin 2056, p. 47-88.
- Schaefer, D.H., Thiros, S.A., and Rosen, M.R., 2005; Ground-water quality in the Carbonate-Rock Aquifer of the Great Basin, Nevada and Utah, 2003: U.S. Geological Survey Scientific Investigations Report 2005-5232, 41 p.
- Scheirer, D.S., Page, W.R., and Miller, J.J., 2006, Geophysical studies based on gravity and seismic data of Tule Desert, Meadow Valley Wash, and California Wash basins, southern Nevada, U.S. Geological Survey Open-File Report 2006-1396, 44 p.
- Schmidt, D.L., and Dixon, G.L., 1995, Geology and aquifer system of the Coyote Spring Valley area, southeastern Nevada: U.S. Geological Survey Open-File Report 95-579, 47 p.
- Scott, R.B., and Swadley, W.C., eds., 1995, Geologic studies in the Basin and Range-Colorado Plateau transition in southeastern Nevada, southwestern Utah, and northwestern Arizona, 1992: U.S. Geological Survey Bulletin 2056, p. 5-42.

Scott, R.B., Rowley, P.D., Snee, L.W., Anderson, R.E., Harding, A.E., Unruh, D.M., Nealey, L.D., Hudson, M.R., Swadley, W.C., and Ferris, D.E., 1996, Synchronous Oligocene and Miocene extension and magmatism in the vicinity of caldera complexes in southeastern Nevada, in Thompson, R.A., Hudson, M.R., and Pillmore, C.L., eds., Geologic excursions to the Rocky Mountains and beyond-Field trip guidebook for the 1996 annual meeting, Geological Society of America, Denver, Colorado, October 28-31: Colorado Geological Survey Special Publication 44, (CD-ROM), 36 p.

SNWA, See Southern Nevada Water Authority.

Southern Nevada Water Authority, 2006, Memorandum of Agreement, dated April 20, 2006 for Muddy River: Las Vegas, NV: Southern Nevada Water Authority, 26 p.

Southern Nevada Water Authority, 2009, Conceptual model of groundwater flow for the Central Carbonate-Rock Province—Clark, Lincoln, and White Pine Counties Groundwater Development Project: Southern Nevada Water Authority, Las Vegas, Nevada, 416 p.

Southern Nevada Water Authority, 2013, Monitoring Report for Southern Nevada Water Authority and Las Vegas Valley Water District's Groundwater Right Permits and Applications in Coyote Spring Valley, Hidden Valley and Garnet Valley within Clark and Lincoln Counties, Nevada - Calendar Year 2012. Southern Nevada Water Authority, Las Vegas, Nevada.

Southern Nevada Water Authority, 2013, Nevada State Engineer Order 1169 and 1169A Study Report: Southern Nevada Water Authority, Las Vegas, Nevada, Doc. No, WMP-ED-0001, 51 p.

Southern Nevada Water Authority, 2014, 2013 Annual Monitoring Report for Southern Nevada Water Authority and Las Vegas Valley Water District Groundwater Permits in Coyote Spring, Garnet, and Hidden Valleys, Clark and Lincoln Counties, Nevada: Southern Nevada Water Authority, Las Vegas, Nevada, Doc. No. WMP-ED-0002, 67 p.

Southern Nevada Water Authority, 2015, 2014 Annual Monitoring Report for Southern Nevada Water Authority Groundwater Permits in Coyote Spring, Garnet, and Hidden Valleys, Clark and Lincoln Counties, Nevada: Las Vegas, Nevada, Doc. No. WRD-ED-0029 72 p.

Southern Nevada Water Authority, 2016: 2015 Annual SNWA Monitoring Report for Coyote Spring, Garnet, and Hidden Valleys, Clark and Lincoln Counties, Nevada: Las Vegas, Nevada, Doc. No. WRD-ED-0036, 72 p.

Southern Nevada Water Authority, 2017: 2016 Annual SNWA Monitoring Report for Coyote Spring, Garnet, and Hidden Valleys, Clark and Lincoln Counties, Nevada: Las Vegas, Nevada, Doc. No. WRD-ED-0042, 68 p.

Southern Nevada Water Authority, 2018, 2017 Annual monitoring report for SNWA groundwater permits in Coyote Spring, Garnet, and Hidden valleys, Clark and Lincoln counties, Nevada: Las Vegas, Nevada, Doc. No. WRD-ED-0048, 69 p.



Swadley, W.C., Page, W.R., Scott, R.B., and Pampeyan, E.H., 1994, Geologic map of the Delamar 3 SE quadrangle, Lincoln County, Nevada: U.S. Geological Survey Geologic Quadrangle Map-GQ-1754, scale 1:24,000.

Swanson, E., and Wernicke, B.P., 2017, Geologic map of the east-central Meadow Valley Mountains, and implications for reconstruction of the Mormon Peak detachment, Nevada: *Geosphere*, v. 13, no. 4, p. 1234-1253.

Tetra Tech, 2012a. Development of a numerical groundwater flow model of selected basins within the Colorado Regional Groundwater Flow System, Southeastern Nevada. Prepared for NPS, USFWS, and BLM. Prepared by Tetra Tech Inc., Louisville, CO.

Tetra Tech, 2012b. Predictions of the effects of groundwater pumping in the Colorado Regional Groundwater Flow System, Southeastern Nevada. Prepared for NPS, USFWS, and BLM. Prepared by Tetra Tech Inc., Louisville, CO.

United States Fish and Wildlife Service, Bureau of Land Management, National Park Service, 2013, Test Impacts and Availability of Water Pursuant to Applications Pending Under Order 1169, Presentation to the Office of the Nevada State Engineer, 92 p.

United States Geological Survey, 2018, National Water Information System, accessed multiple times in September 2018 at <https://waterdata.usgs.gov/nwis>

USFWS, see United States Fish and Wildlife Service.

USGS, see United States Geological Survey.

Western Regional Climate Center, 2018, Cooperative Climatological Data Summaries. Website: https://wrcc.dri.edu/Climate/west_coop_summaries.php, accessed on 10/16/2018: Reno, Nevada.

Winograd, I. J., Riggs, A. C., Coplen, T. B. 1998. The Relative Contributions of Summer and Cool-Season Precipitation to Groundwater Recharge, Spring Mountains, Nevada, USA, *Hydrogeology Journal*, Volume 6 p. 77-93, New York, NY: Published by Springer - Verlag.

WRCC, see Western Regional Climate Center.

Appendix A
Site Table for Wells

Table A-1
Site Table for Wells
 (Page 1 of 3)

Site Name	UTM Northing (m)	UTM Easting (m)	Surface Elevation (ft amsl)	Drill Depth (ft bgs)	Well Depth (ft bgs)	Well Type ¹	Well Completion	Water Level Obs. Date	Depth to Water (ft-bgs)	Water Level Elevation (ft amsl)
Kane Springs Valley (HA 206)										
KMW-1	4,098,863	689,882	2,870.60	---	---	M	Carbonate	3/6/2018	992.42	1,878.18
COYOTE SPRING VALLEY (HA 210)										
BEDROC 1	4,094,151	679,399	2,492.44	---	---	P	Basin Fill	---	---	---
BEDROC 2	4,094,374	679,009	2,529	---	---	P	Basin Fill	---	---	---
CE-VF-1	4,083,038	683,025	2,468.34	714	714	M	Basin Fill	2/14/2018	551.37	1,916.97
CE-VF-2	4,082,892	683,007	2,468.35	1,221	1,221	M	Carbonate	2/14/2018	600.41	1,867.94
CSI-1	4,074,459	686,044	2,278.05	935	920	P	Carbonate	---	---	---
CSI-2	4,075,780	687,084	2,208.94	1,019	1,015	P	Carbonate	3/12/2018	390.95	1,818
CSI-3	4,077,518	685,809	2,334.51	1,156	1,152	P	Carbonate	3/12/2018	515.88	1,818.63
CSI-4	4,080,224	682,409	2,511.88	---	---	P	Carbonate	3/12/2018	693.35	1,818.53
CSV-1	4,071,630	691,378	2,160.25	765	765	M	Basin Fill	3/7/2018	350.46	1,809.79
CSV-2	4,072,967	703,217	2,188.68	---	478	M	Carbonate	2/22/2018	395.43	1,790.47
CSV-3	4,062,583	685,222	2,415.93	780	780	M	Basin Fill	2/14/2018	594.95	1,820.98
CSV3009M	4,094,987	681,079	2,595.08	1,580	1,578	M	Basin Fill	2/14/2018	493.95	2,101.14
CSV3011M	4,094,873	684,075	2,665.72	1,580	1,555	M	Basin Fill	2/14/2018	751.11	1,914.61
CSVM-1	4,073,793	688,602	2,160.60	1,060	1,040	M	Carbonate	2/14/2018	342.08	1,818.52
CSVM-2	4,059,370	685,625	2,572.74	1,425	1,400	M	Carbonate	2/14/2018	751.72	1,821.02
CSVM-3	4,102,600	679,319	2,650.68	1,230	1,200	M	Carbonate	2/14/2018	444.22	2,206.46
CSVM-4	4,095,971	688,086	2,842.38	1,605	1,600	M	Carbonate	3/12/2018	969.63	1,872.75
CSVM-5	4,068,774	680,295	3,130.70	1,783	1,780	M	Carbonate	2/14/2018	1,079.83	2,050.87
CSVM-6	4,078,333	686,453	2,251.66	1,200	1,180	M	Carbonate	2/14/2018	435.59	1,816.07
CSVM-7	4,101,968	678,234	2,692.08	610	607	M	Basin Fill	2/14/2018	444.22	2,247.86
CSV-RW2	4,074,082	687,862	2,200.06	720	710	P	Carbonate	3/16/2018	383.48	1,816.58
DF-1	4,078,687	686,980	2,229.22	---	170	M	Basin Fill	---	---	---
MX-4	4,074,276	688,003	2,177.02	669	669	M	Carbonate	---	---	---
MX-5	4,074,219	688,084	2,176.13	628	628	P	Carbonate	2/14/2018	357.37	1,818.76
BLACK MOUNTAINS AREA (HA 215)										
BM-DL-1	4,019,493	689,926	2,467.94	1,400	1,400	M	Carbonate	---	---	---
BM-DL-2	4,019,591	689,270	2,487.56	1,800	1,800	M	Carbonate	3/12/2018	675.03	1,812.53
BM-ONCO-1	4,010,748	702,650	2,055.83	1,291	1,291	M	Basin Fill	---	---	---
BM-ONCO-2	4,010,722	702,054	2,098.17	1,575	1,570	M	Basin Fill	---	---	---
EBM-3	4,018,550	689,601	2,390.18	1,241	900	M	Carbonate	3/1/2018	740	1,648.4
EBM-4	4,018,828	689,782	2,391.36	1,134	1,129	P	Carbonate	---	---	---
EBM-5	4,019,030	689,858	2,440.7	1,400	1,014	P	Carbonate	---	---	---
EBM-6	4,018,803	689,765	2,421.3	1,401	1,000	P	Carbonate	---	---	---
EBP-2	4,018,604	689,629	2,442.456	1,214	1,214	P	Carbonate	---	---	---
EGV-3	4,019,000	689,857	2,434.21	960	955	P	Carbonate	---	---	---



Table A-1
Site Table for Wells
(Page 2 of 3)

Site Name	UTM Northing (m)	UTM Easting (m)	Surface Elevation (ft amsl)	Drill Depth (ft bgs)	Well Depth (ft bgs)	Well Type ¹	Well Completion	Water Level Obs. Date	Depth to Water (ft-bgs)	Water Level Elevation (ft amsl)
GARNET VALLEY (HA 216)										
CRYSTAL 1	4,039,716	694,389	2,072.67	497	497	M	Carbonate	3/16/2018	261.81	1,810.65
CRYSTAL 2	4,039,284	694,146	2,068.52	465	465	M	Carbonate	3/16/2018	258.76	1,811.15
EBA-1	4,024,108	686,513	2,426.99	1,598	1,200	P	Carbonate	---	---	---
FIRST SOLAR	4,033,129	683,330	2,603.216	2,000	1,990	P	Carbonate	1/8/2018	792.89	1,810.33
GARNET	4,036,387	693,046	2,096.68	500	---	M	Basin Fill	---	---	---
GV-1	4,034,143	682,983	2,691.14	1,400	1,400	M	Carbonate	2/12/2018	883.46	1,807.68
GV-2	4,025,690	686,227	2,424.08	1,232	1,232	P	Carbonate	3/12/2018	609.94	1,814.14
GV-DUKE-WS1	4,029,104	686,286	2,243.50	685	685	P	Carbonate	3/12/2018	432.73	1,810.77
GV-DUKE-WS2	4,029,097	686,199	2,246.721	2,020	1,965	P	Carbonate	3/12/2018	432.57	1,814.15
GV-KERR	4,029,147	683,738	2,404.601	1,145	1,145	P	Carbonate	---	---	---
GV-LENZIE-3 ¹²	4,029,329	686,247	2,247	1,940	1,920	P	Carbonate	3/12/2018	432.16	1,814.84
GV-MIRANT1	4,032,318	683,115	2,567.87	2,007	1,979	P	Carbonate	---	---	---
GV-PW-MW1	4,031,730	683,460	2,502.27	1,500	1,500	M	Carbonate	2/12/2018	691.6	1,810.67
GV-PW-MW2	4,031,488	682,652	2,524.79	1,500	1,500	M	Carbonate	3/12/2018	714.83	1,809.96
GV-PW-WS1	4,031,435	683,005	2,532.28	2,000	2,000	P	Carbonate	3/12/2018	733.44	1,798.84
GV-RW1	4,036,645	692,928	2,069.2	870	833	P	Carbonate	---	---	---
GV-USLIME1	4,026,564	687,748	2,286.48	860	860	P	Carbonate	---	---	---
GV-USLIME2	4,029,329	687,739	2,155.333	500	500	P	Basin Fill	---	---	---
PAIUTES-M3	4,044,302	691,536	2,237.69	670	670	M	Carbonate	3/11/2018	423.11	1,811.89
RS-PW-1	4,028,841	690,787	2,240	---	860	P	Clastic	3/13/2018	516.28	1,723.72
RS-PW-2	4,027,890	690,674	2,412	---	---	P	Carbonate	---	---	---
RS-PW-3	4,029,719	691,026	2,162	720	720	P	Carbonate	---	---	---
RS-PW-5	4,029,626	691,053	2,175	---	---	P	Carbonate	---	---	---
RS-PW-6	4,026,318	690,552	2,471	---	---	P	Carbonate	---	---	---
RS-PW-7	4,027,940	691,938	2,423	940	940	P	Carbonate	---	---	---
HIDDEN VALLEY (HA 217)										
SHV-1	4,047,256	685,751	2,650.32	920	920	M	Basin Fill	---	---	---
CALIFORNIA WASH (HA 218)										
BYRON	4,051,282	710,993	1,903.06	1,095	1,095	M	Basin Fill	3/8/2018	238.5	1,664.56
PAIUTES-ECP1	4,046,590	696,729	2,233.8	1,170	1,125	P	Carbonate	---	---	---
PAIUTES-ECP2	4,046,742	696,723	2,228.33	---	---	P	Carbonate	---	---	---
PAIUTES-ECP3	4,046,984	696,714	2,243.08	---	---	P	Carbonate	---	---	---
PAIUTES-M1	4,057,109	704,517	1,898.09	400	400	M	Carbonate	2/17/2018	82.22	1,813.47
PAIUTES-M2	4,040,876	695,836	2,108.53	680	680	M	Carbonate	2/17/2018	298.13	1,810.37
PAIUTES-TH1	4,044,959	697,234	2,169.95	---	---	P	Carbonate	---	---	---
PAIUTES-TH2	4,049,916	697,684	2,340.59	---	1,200	M	Carbonate	3/11/2018	526.06	1,812.03

Table A-1
Site Table for Wells
 (Page 3 of 3)

Site Name	UTM Northing (m)	UTM Easting (m)	Surface Elevation (ft amsl)	Drill Depth (ft bgs)	Well Depth (ft bgs)	Well Type ¹	Well Completion	Water Level Obs. Date	Depth to Water (ft-bgs)	Water Level Elevation (ft amsl)
MUDDY RIVER SPRINGS AREA (HA 219)										
ABBOTT	4,065,656	706,443	1,715.284	101	100	M	Basin Fill	3/16/2018	12.65	1,699.69
ARROW CANYON	4,067,763	701,108	1,860.7	565	565	P	Carbonate	---	---	---
ARROW CANYON 2	4,067,750	701,083	1,860.7	746	742	P	Carbonate	---	---	---
BEHMER	4,065,080	706,031	1,715.77	115	115	P	Basin Fill	3/30/2018	9.3	1,707.29
CSV-1	4,071,630	691,378	2,160.25	765	765	M	Basin Fill	3/7/2018	350.46	1,809.79
CSV-2	4,072,967	703,217	2,188.68	---	478	M	Carbonate	2/22/2018	395.43	1,790.47
EH-4	4,064,736	703,929	1,933.93	285	285	M	Carbonate	3/16/2018	120.56	1,813.37
EH-5B	4,067,619	701,569	1,844.8	265	264	M	Carbonate	3/16/2018	31.41	1,813.39
LDS CENTRAL	4,066,544	704,114	1,762.15	106	106	P	Basin Fill	---	---	---
LDS EAST	4,066,594	704,479	1,752.61	195	195	P	Basin Fill	3/16/2018	7.16	1,745.97
LDS WEST	4,067,083	702,746	1,807.26	80	80	P	Basin Fill	3/16/2018	19.18	1,788.62
LEWIS 1	4,068,043	702,164	1,823.069	80	80	P	Basin Fill	---	---	---
LEWIS 1 OLD	4,068,229	702,077	1,828.71	58	58	M	Basin Fill	3/16/2018	29.64	1,799.07
LEWIS 2	4,067,886	702,365	1,825.45	66	66	P	Basin Fill	3/16/2018	26.25	1,799.79
LEWIS 3	4,068,022	701,963	1,825.078	70	70	P	Basin Fill	---	---	---
LEWIS 4	4,067,618	702,029	1,832.874	97	97	P	Basin Fill	---	---	---
LEWIS 5	4,067,484	702,195	1,828.109	93	88	P	Basin Fill	---	---	---
LEWIS NORTH	4,067,872	701,589	1,844.71	70	70	M	Basin Fill	3/16/2018	34.57	1,810.14
LEWIS SOUTH	4,067,266	702,737	1,809.61	91	90	M	Basin Fill	3/16/2018	14.38	1,793.72
MX-6	4,071,381	697,482	2,277.94	937	937	P	Carbonate	3/27/2018	463.4	1,814.71
PERKINS OLD	4,065,223	705,637	1,728.51	150	70	M	Basin Fill	3/16/2018	20.81	1,707.7
PERKINS PRODUCTION	4,065,206	705,693	1,734.861	---	---	P	Basin Fill	3/16/2018	21.67	1,713.191
UMVM-1	4,070,248	694,305	2,061.88	1,785	1,780	M	Carbonate	3/7/2018	247.34	1,814.54

¹Well Type: M = Monitoring well, P = Production well

³GV-LENZIE-3 is the replacement well for GV-DUKE-WS2, which was plugged and abandoned in 2016

Appendix B

Surface Water Diversions above the Moapa Gage

Table B-1
Surface Water Diversions above the Moapa Gage in the MRSA

Year	NVE Muddy River just above Moapa Gage (afy)	MVWD Baldwin Springs (afy)	MVWD Jones Spring (afy)
1993	2,871	922	684
1994	2,462	948	660
1995	2,950	1,449	750
1996	3,219	1,707	659
1997	2,494	1,771	656
1998	2,296	646	700
1999	2,585	250	656
2000	3,063	53	635
2001	3,573	101	690
2002	3,727	210	635
2003	3,651	9	653
2004	2,923	44	664
2005	2,535	248	642
2006	1,659	569	699
2007	2,776	719	681
2008	2,791	332	702
2009	2,496	1,166	322
2010	2,283	1,119	202
2011	1,287	605	3
2012	393	27	3
2013	17	131	1
2014	230	990	50
2015	0	92	0
2016	0	89	0
2017	0	126	0

Appendix C
Groundwater Production Data

Table C-1
Shallow Alluvial Wells in the Muddy River Springs Area
Pumped by Nevada Energy

Well Name	Well Log	Township	Range	Section	Section Quarter	Depth Cased (a)	Top Perf (a)	Bottom Perf (a)	Well Finish Date
Lewis 1	27268	14S	65E	8	SW NE	91	30	90	07-Mar-86
Lewis 2	62870	14S	65E	8	SE NE	100	35	100	22-Jun-72
Lewis 3	12727	14S	65E	8	SE NE	100	35	100	22-Jun-72
Lewis 4	10853	14S	65E	8	NW SE	97	38	88	12-Apr-69
Lewis 5	10852	14S	65E	8	NW SE	93	38	88	06-May-69
Perkins Production	31969	14S	65E	22	NE NE	135	25	125	16-Jun-88
Behmer	15623	14S	65E	23	NW NW	115	30	115	20-May-76
LDS East	102501	14S	65E	15	NW NW	77	17	77	15-Jun-88
LDS Central	102500	14S	65E	16	NE NE	50	25	50	15-Jun-88
LDS West	62880	14S	65E	9	SW SW	80	10	80	26-Nov-68

^aDepth cased, Top Perf (top of perforations) and Bottom Perf (bottom of perforations) depths are in feet below land surface.

^bWell completion dates listed are the most recent well restoration/repair dates and may not reflect installation dates.



**Table C-2
Groundwater Diversions in MRSA and CSV**

Year	Alluvial Well Development (afy)			Carbonate Well Development (afy)		
	NVE Lewis Wells	NVE, LDS Wells	Perkins & Behmer Wells	MVWD Wells	CSI Development ¹	SNWA Development ²
1993	1,648	958	1048	1,169	---	---
1994	2,075	1,467	886	894	---	---
1995	1,299	1,583	581	678	---	---
1996	1,522	2,097	1,134	705	---	---
1997	1,194	2,175	726	808	---	---
1998	2,259	2,903	804	2,039	---	---
1999	1,876	2,390	482	2,579	---	---
2000	1,774	3,169	1,044	2,908	---	---
2001	1,303	2,257	1,350	2,743	---	---
2002	2,139	2,051	1,601	2,573	---	---
2003	1,514	2,159	1,460	2,816	---	---
2004	1,568	1,802	1,130	2,609	---	---
2005	1,699	2,138	1,417	2,557	258	---
2006	1,846	2,591	1,285	2,325	1,277	---
2007	1,278	2,227	1,298	2,079	2,781	---
2008	1,509	1,626	1,150	2,272	1,660	30
2009	1,008	1,532	1,553	2,034	1,398	15
2010	1,315	1,386	1,194	1,834	1,288	1,384
2011	1,826	1,496	1,070	1,836	1,199	4,131
2012	869	1,018	1,189	2,638	1,140	3,961
2013	1,279	1,047	1,637	2,496	1,222	1,770
2014	2,159	1,255	1,411	1,442	1,216	426
2015	473	176	639	2,396	1,108	385
2016	661	276	0	2,795	1,117	0
2017	136	240	159	2,823	1,399	0
2018 ³	0	0	0	1,012	800	4

¹ Combined development of CSI wells in Coyote Springs Valley including CSI-1, CSI-2, CSI-3, and CSI-4

² Total includes development of the MX-5 well in Coyote Springs Valley.

³ Production data as of June 2018.

**Table C-3
Groundwater Production
(Page 1 of 30)**

Hydrographic Area	Well Name	Aquifer Material	Year	Production (gallons)	Production (af)	Comments	Source
210	BEDROC WELL 1	Alluvium	2015	83,492,912	256.23	Combined BEDROC WELL 1, 3, 5, and 7	Western Elite, 2018
210	BEDROC WELL 1	Alluvium	2016	100,088,525	307.16	Combined BEDROC WELL 1, 3, 5, and 7	Western Elite, 2018
210	BEDROC WELL 1	Alluvium	2017	89,964,321	276.09	Combined BEDROC WELL 1, 3, 5, and 7	Western Elite, 2018
210	BEDROC WELL 2	Alluvium	2015	122,904,642	377.18	Combined BEDROC WELL 2, 4, and 6	Western Elite, 2018
210	BEDROC WELL 2	Alluvium	2016	100,544,717	308.56	Combined BEDROC WELL 2, 4, and 6	Western Elite, 2018
210	BEDROC WELL 2	Alluvium	2017	91,772,796	281.64	Combined BEDROC WELL 2, 4, and 6	Western Elite, 2018
210	CSI-1	Carbonate	2005	70,382,000	215.99		NDWR, 2018a
210	CSI-1	Carbonate	2006	235,338,000	722.23		NDWR, 2018a
210	CSI-1	Carbonate	2007	247,947,000	760.92		NDWR, 2018a
210	CSI-1	Carbonate	2008	14,273,000	43.80		NDWR, 2018a
210	CSI-1	Carbonate	2009	0	0.00		NDWR, 2018a
210	CSI-1	Carbonate	2010	0	0.00		NDWR, 2018a
210	CSI-1	Carbonate	2011	0	0.00		NDWR, 2018a
210	CSI-1	Carbonate	2012	6,885,242	21.13		NDWR, 2018a
210	CSI-1	Carbonate	2013	386,506,510	1,186.14		NDWR, 2018a
210	CSI-1	Carbonate	2014	294,814,000	904.75		NDWR, 2018a
210	CSI-1	Carbonate	2015	186,961,000	573.76		NDWR, 2018a
210	CSI-1	Carbonate	2016	233,857,000	717.68		NDWR, 2018a
210	CSI-1	Carbonate	2017	399,700,000	1,226.63		NDWR, 2018a
210	CSI-1	Carbonate	2018	125,970,000	386.59		NDWR, 2018a
210	CSI-2	Carbonate	2005	13,851,000	42.51		NDWR, 2018a
210	CSI-2	Carbonate	2006	170,586,000	523.51		NDWR, 2018a
210	CSI-2	Carbonate	2007	489,531,000	1,502.32		NDWR, 2018a
210	CSI-2	Carbonate	2008	313,515,000	962.14		NDWR, 2018a
210	CSI-2	Carbonate	2009	4,180,000	12.83		NDWR, 2018a
210	CSI-2	Carbonate	2010	0	0.00		NDWR, 2018a
210	CSI-2	Carbonate	2011	0	0.00		NDWR, 2018a
210	CSI-2	Carbonate	2012	0	0.00		NDWR, 2018a

**Table C-3
Groundwater Production
(Page 2 of 30)**

Hydrographic Area	Well Name	Aquifer Material	Year	Production (gallons)	Production (af)	Comments	Source
210	CSI-2	Carbonate	2013	0	0.00		NDWR, 2018a
210	CSI-2	Carbonate	2014	0	0.00		NDWR, 2018a
210	CSI-2	Carbonate	2015	0	0.00		NDWR, 2018a
210	CSI-2	Carbonate	2016	0	0.00		NDWR, 2018a
210	CSI-2	Carbonate	2017	0	0.00		NDWR, 2018a
210	CSI-2	Carbonate	2018	125,682,000	385.70		NDWR, 2018a
210	CSI-3	Carbonate	2006	10,164,000	31.19		NDWR, 2018a
210	CSI-3	Carbonate	2007	160,672,000	493.08		NDWR, 2018a
210	CSI-3	Carbonate	2008	209,739,000	643.67		NDWR, 2018a
210	CSI-3	Carbonate	2009	263,978,000	810.12		NDWR, 2018a
210	CSI-3	Carbonate	2010	340,371,348	1,044.56		NDWR, 2018a
210	CSI-3	Carbonate	2011	233,891,372	717.79		NDWR, 2018a
210	CSI-3	Carbonate	2012	183,781,356	564.00		NDWR, 2018a
210	CSI-3	Carbonate	2013	11,779,752	36.15		NDWR, 2018a
210	CSI-3	Carbonate	2014	0	0.00		NDWR, 2018a
210	CSI-3	Carbonate	2015	0	0.00		NDWR, 2018a
210	CSI-3	Carbonate	2016	0	0.00		NDWR, 2018a
210	CSI-3	Carbonate	2017	0	0.00		NDWR, 2018a
210	CSI-3	Carbonate	2018	0	0.00		NDWR, 2018a
210	CSI-4	Carbonate	2007	7,898,000	24.24		NDWR, 2018a
210	CSI-4	Carbonate	2008	3,339,000	10.25		NDWR, 2018a
210	CSI-4	Carbonate	2009	187,369,000	575.01		NDWR, 2018a
210	CSI-4	Carbonate	2010	79,486,396	243.93		NDWR, 2018a
210	CSI-4	Carbonate	2011	156,854,000	481.37		NDWR, 2018a
210	CSI-4	Carbonate	2012	180,845,000	554.99		NDWR, 2018a
210	CSI-4	Carbonate	2013	0	0.00		NDWR, 2018a
210	CSI-4	Carbonate	2014	101,517,000	311.54		NDWR, 2018a
210	CSI-4	Carbonate	2015	174,209,000	534.63		NDWR, 2018a



**Table C-3
Groundwater Production
(Page 3 of 30)**

Hydrographic Area	Well Name	Aquifer Material	Year	Production (gallons)	Production (af)	Comments	Source
210	CSI-4	Carbonate	2016	130,213,000	399.61		NDWR, 2018a
210	CSI-4	Carbonate	2017	56,300,000	172.78		NDWR, 2018a
210	CSI-4	Carbonate	2018	9,116,000	27.98		NDWR, 2018a
210	CSV-RW2	Carbonate	2000	0	0.00		NDWR, 2018a
210	CSV-RW2	Carbonate	2001	0	0.00		NDWR, 2018a
210	CSV-RW2	Carbonate	2002	0	0.00		NDWR, 2018a
210	CSV-RW2	Carbonate	2003	0	0.00		NDWR, 2018a
210	CSV-RW2	Carbonate	2004	0	0.00		NDWR, 2018a
210	CSV-RW2	Carbonate	2005	0	0.00		NDWR, 2018a
210	CSV-RW2	Carbonate	2006	0	0.00		NDWR, 2018a
210	CSV-RW2	Carbonate	2007	0	0.00		NDWR, 2018a
210	CSV-RW2	Carbonate	2008	0	0.00		NDWR, 2018a
210	CSV-RW2	Carbonate	2009	0	0.00		NDWR, 2018a
210	CSV-RW2	Carbonate	2010	0	0.00		NDWR, 2018a
210	CSV-RW2	Carbonate	2011	0	0.00		NDWR, 2018a
210	CSV-RW2	Carbonate	2012	0	0.00		NDWR, 2018a
210	CSV-RW2	Carbonate	2013	0	0.00		NDWR, 2018a
210	CSV-RW2	Carbonate	2014	0	0.00		NDWR, 2018a
210	CSV-RW2	Carbonate	2015	0	0.00		NDWR, 2018a
210	CSV-RW2	Carbonate	2016	0	0.00		NDWR, 2018a
210	CSV-RW2	Carbonate	2017	0	0.00		NDWR, 2018a
210	CSV-RW2	Carbonate	2018	0	0.00		NDWR, 2018a
210	MX-5	Carbonate	2008	9,819,500	30.13		SNWA, 2010
210	MX-5	Carbonate	2009	5,017,300	15.40		SNWA, 2010
210	MX-5	Carbonate	2010	450,905,191	1,383.78		NDWR, 2018a
210	MX-5	Carbonate	2011	1,346,243,737	4,131.47		NDWR, 2018a
210	MX-5	Carbonate	2012	1,290,557,441	3,960.58		NDWR, 2018a
210	MX-5	Carbonate	2013	576,659,399	1,769.70		NDWR, 2018a

**Table C-3
Groundwater Production
(Page 4 of 30)**

Hydrographic Area	Well Name	Aquifer Material	Year	Production (gallons)	Production (af)	Comments	Source
210	MX-5	Carbonate	2014	138,903,080	426.28		NDWR, 2018a
210	MX-5	Carbonate	2015	125,583,895	385.40		NDWR, 2018a
210	MX-5	Carbonate	2016	0	0.00		NDWR, 2018a
210	MX-5	Carbonate	2017	0	0.00		NDWR, 2018a
210	MX-5	Carbonate	2018	1,265,648	3.88		NDWR, 2018a
215	EBM-4	Carbonate	1996	209,745,000	643.68		NDWR, 2018b
215	EBM-4	Carbonate	1997	252,361,100	774.47		NDWR, 2018b
215	EBM-4	Carbonate	1998	240,830,000	739.08		NDWR, 2018b
215	EBM-4	Carbonate	1999	243,225,000	746.43		NDWR, 2018b
215	EBM-4	Carbonate	2000	259,923,000	797.67		NDWR, 2018a
215	EBM-4	Carbonate	2001	277,466,000	851.51		NDWR, 2018a
215	EBM-4	Carbonate	2002	281,379,000	863.52		NDWR, 2018a
215	EBM-4	Carbonate	2003	176,807,000	542.60		NDWR, 2018a
215	EBM-4	Carbonate	2004	235,330,000	722.20		NDWR, 2018a
215	EBM-4	Carbonate	2005	250,208,000	767.86		NDWR, 2018a
215	EBM-4	Carbonate	2006	247,516,000	759.60		NDWR, 2018a
215	EBM-4	Carbonate	2007	253,668,000	778.48		NDWR, 2018a
215	EBM-4	Carbonate	2008	99,584,000	305.61		NDWR, 2018a
215	EBM-4	Carbonate	2009	208,401,000	639.56		NDWR, 2018a
215	EBM-4	Carbonate	2010	312,428,000	958.81		NDWR, 2018a
215	EBM-4	Carbonate	2011	253,605,000	778.29		NDWR, 2018a
215	EBM-4	Carbonate	2012	230,985,264	708.87		NDWR, 2018a
215	EBM-4	Carbonate	2013	218,728,708	671.25		NDWR, 2018a
215	EBM-4	Carbonate	2014	224,975,000	690.42		NDWR, 2018a
215	EBM-4	Carbonate	2015	116,017,840	356.05		NDWR, 2018a
215	EBM-5	Carbonate	2015	93,435,000	286.74		NDWR, 2018a
215	EBM-5	Carbonate	2016	244,061,013	749.00		NDWR, 2018a
215	EBM-5	Carbonate	2017	271,995,048	834.72		NDWR, 2018a



**Table C-3
Groundwater Production
(Page 5 of 30)**

Hydrographic Area	Well Name	Aquifer Material	Year	Production (gallons)	Production (af)	Comments	Source
215	EBM-5	Carbonate	2018	22,341,064	68.56		NDWR, 2018a
215	EBM-6	Carbonate	2015	65,970,000	202.45		NDWR, 2018a
215	EBM-6	Carbonate	2016	194,914,456	598.17		NDWR, 2018a
215	EBM-6	Carbonate	2017	208,396,543	639.55		NDWR, 2018a
215	EBM-6	Carbonate	2018	136,469,056	418.81		NDWR, 2018a
215	EBP-2	Carbonate	1996	64,080,000	196.65		NDWR, 2018b
215	EBP-2	Carbonate	1997	33,070,000	101.49		NDWR, 2018b
215	EBP-2	Carbonate	1998	9,314,000	28.58		NDWR, 2018b
215	EBP-2	Carbonate	1999	36,840,000	113.06		NDWR, 2018b
215	EBP-2	Carbonate	2000	21,987,000	67.48		NDWR, 2018a
215	EBP-2	Carbonate	2001	1,179,000	3.62		NDWR, 2018a
215	EBP-2	Carbonate	2002	23,157,000	71.07		NDWR, 2018a
215	EBP-2	Carbonate	2003	166,841,000	512.02		NDWR, 2018a
215	EBP-2	Carbonate	2004	56,501,000	173.40		NDWR, 2018a
215	EBP-2	Carbonate	2005	483,000	1.48		NDWR, 2018a
215	EBP-2	Carbonate	2006	33,961,000	104.22		NDWR, 2018a
215	EBP-2	Carbonate	2007	171,000	0.52		NDWR, 2018a
215	EBP-2	Carbonate	2008	200,241,000	614.52		NDWR, 2018a
215	EBP-2	Carbonate	2009	23,172,000	71.11		NDWR, 2018a
215	EBP-2	Carbonate	2010	59,286,000	181.94		NDWR, 2018a
215	EBP-2	Carbonate	2011	795,000	2.44		NDWR, 2018a
215	EBP-2	Carbonate	2012	10,324,000	31.68		NDWR, 2018a
215	EBP-2	Carbonate	2013	41,058,893	126.01		NDWR, 2018a
215	EBP-2	Carbonate	2014	1,954,000	6.00		NDWR, 2018a
215	EBP-2	Carbonate	2015	77,104,404	236.62		NDWR, 2018a
215	EBP-2	Carbonate	2016	28,249,904	86.70		NDWR, 2018a
215	EBP-2	Carbonate	2017	10,769,028	33.05		NDWR, 2018a
215	EBP-2	Carbonate	2018	95,386,568	292.73		NDWR, 2018a

**Table C-3
Groundwater Production
(Page 6 of 30)**

Hydrographic Area	Well Name	Aquifer Material	Year	Production (gallons)	Production (af)	Comments	Source
215	EGV-3	Carbonate	1996	251,694,000	772.42		NDWR, 2018b
215	EGV-3	Carbonate	1997	228,981,000	702.72		NDWR, 2018b
215	EGV-3	Carbonate	1998	208,759,000	640.66		NDWR, 2018b
215	EGV-3	Carbonate	1999	231,181,000	709.47		NDWR, 2018b
215	EGV-3	Carbonate	2000	269,747,000	827.82		NDWR, 2018a
215	EGV-3	Carbonate	2001	238,938,000	733.27		NDWR, 2018a
215	EGV-3	Carbonate	2002	263,821,000	809.64		NDWR, 2018a
215	EGV-3	Carbonate	2003	213,277,000	654.52		NDWR, 2018a
215	EGV-3	Carbonate	2004	265,500,000	814.79		NDWR, 2018a
215	EGV-3	Carbonate	2005	283,714,000	870.69		NDWR, 2018a
215	EGV-3	Carbonate	2006	229,758,000	705.10		NDWR, 2018a
215	EGV-3	Carbonate	2007	262,651,000	806.05		NDWR, 2018a
215	EGV-3	Carbonate	2008	218,745,000	671.30		NDWR, 2018a
215	EGV-3	Carbonate	2009	279,226,000	856.91		NDWR, 2018a
215	EGV-3	Carbonate	2010	136,945,232	420.27		NDWR, 2018a
215	EGV-3	Carbonate	2011	201,293,696	617.75		NDWR, 2018a
215	EGV-3	Carbonate	2012	265,637,176	815.21		NDWR, 2018a
215	EGV-3	Carbonate	2013	256,576,104	787.40		NDWR, 2018a
215	EGV-3	Carbonate	2014	239,081,000	733.71		NDWR, 2018a
215	EGV-3	Carbonate	2015	119,275,720	366.04		NDWR, 2018a
216	EBA-1	Carbonate	1996	47,268,400	145.06	Unverified. Records received from Georgia Pacific.	
216	EBA-1	Carbonate	1997	41,192,100	126.41	Unverified. Records received from Georgia Pacific.	
216	EBA-1	Carbonate	1998	42,663,100	130.93	Unverified. Records received from Georgia Pacific.	
216	EBA-1	Carbonate	1999	48,703,500	149.47	Unverified. Records received from Georgia Pacific.	
216	EBA-1	Carbonate	2000	12,835,500	39.39	Unverified. Records received from Georgia Pacific.	



**Table C-3
Groundwater Production
(Page 7 of 30)**

Hydrographic Area	Well Name	Aquifer Material	Year	Production (gallons)	Production (af)	Comments	Source
216	EBA-1	Carbonate	2001	48,831,300	149.86		NDWR, 2001
216	EBA-1	Carbonate	2002	45,366,300	139.22		NDWR, 2002
216	EBA-1	Carbonate	2003	61,443,600	188.56		NDWR, 2003
216	EBA-1	Carbonate	2004	60,837,000	186.70		NDWR, 2004
216	EBA-1	Carbonate	2005	49,268,500	151.20		NDWR, 2005
216	EBA-1	Carbonate	2006	45,460,300	139.51		NDWR, 2006
216	EBA-1	Carbonate	2007	48,388,874	148.50		NDWR, 2007
216	EBA-1	Carbonate	2008	47,417,838	145.52		NDWR, 2008
216	EBA-1	Carbonate	2009	36,641,945	112.45		NDWR, 2009
216	EBA-1	Carbonate	2010	40,539,123	124.41		NDWR, 2010
216	EBA-1	Carbonate	2011	43,426,163	133.27		NDWR, 2011
216	EBA-1	Carbonate	2012	35,921,814	110.24		NDWR, 2012
216	EBA-1	Carbonate	2013	47,486,266	145.73		NDWR, 2013
216	EBA-1	Carbonate	2014	22,666,196	69.56		NDWR, 2014
216	EBA-1	Carbonate	2015	38,202,771	117.24		NDWR, 2015
216	EBA-1	Carbonate	2016	37,062,293	113.74		NDWR, 2016
216	EBA-1	Carbonate	2017	30,717,974	94.27		NDWR, 2017
216	First Solar Well	Carbonate	2016	30,045,051	92.20		NDWR, 2018a
216	First Solar Well	Carbonate	2017	70,833,966	217.38		NDWR, 2018a
216	First Solar Well	Carbonate	2018	45,156,000	138.58		NDWR, 2018a
216	GV-2	Carbonate	2007	0	33.40		NDWR, 2007
216	GV-2	Carbonate	2008	40,620,000	124.66		NDWR, 2018a
216	GV-2	Carbonate	2009	5,560,000	17.06		NDWR, 2018a
216	GV-2	Carbonate	2010	3,232,442	9.92		NDWR, 2010
216	GV-2	Carbonate	2011	4,077,300	12.51		NDWR, 2018a
216	GV-2	Carbonate	2012	13,170,000	40.42		NDWR, 2018a
216	GV-2	Carbonate	2013	4,307,750	13.22		NDWR, 2013
216	GV-2	Carbonate	2014	5,112,602	15.69		NDWR, 2014

**Table C-3
Groundwater Production
(Page 8 of 30)**

Hydrographic Area	Well Name	Aquifer Material	Year	Production (gallons)	Production (af)	Comments	Source
216	GV-2	Carbonate	2015	96,679,999	29.67		NDWR, 2015
216	GV-2	Carbonate	2016	11,300,513	34.68		NDWR, 2016
216	GV-2	Carbonate	2017	9,765,754	29.97		NDWR, 2017
216	GV-DUKE-WS1	Carbonate	2000	0	0.00		NDWR, 2018a
216	GV-DUKE-WS1	Carbonate	2001	0	0.00		NDWR, 2018a
216	GV-DUKE-WS1	Carbonate	2002	36,984,037	113.50		NDWR, 2018a
216	GV-DUKE-WS1	Carbonate	2003	0	0.00		NDWR, 2018a
216	GV-DUKE-WS1	Carbonate	2004	281,760	0.86		NDWR, 2018a
216	GV-DUKE-WS1	Carbonate	2005	27,866,150	85.52		NDWR, 2018a
216	GV-DUKE-WS1	Carbonate	2006	35,739,890	109.68		NDWR, 2018a
216	GV-DUKE-WS1	Carbonate	2007	75,670,000	232.22		NDWR, 2018a
216	GV-DUKE-WS1	Carbonate	2008	75,467,718	231.60		NDWR, 2018a
216	GV-DUKE-WS1	Carbonate	2009	48,129,840	147.71		NDWR, 2018a
216	GV-DUKE-WS1	Carbonate	2010	20,223,182	62.06		NDWR, 2018a
216	GV-DUKE-WS1	Carbonate	2011	18,432,325	56.57		NDWR, 2018a
216	GV-DUKE-WS1	Carbonate	2012	31,851,607	97.75		NDWR, 2018a
216	GV-DUKE-WS1	Carbonate	2013	43,496,700	133.49		NDWR, 2018a
216	GV-DUKE-WS1	Carbonate	2014	59,018,943	181.12		NDWR, 2018a
216	GV-DUKE-WS1	Carbonate	2015	23,200,200	71.20		NDWR, 2018a
216	GV-DUKE-WS1	Carbonate	2016	28,956,200	88.86		NDWR, 2018a
216	GV-DUKE-WS1	Carbonate	2017	7,806,300	23.96		NDWR, 2018a
216	GV-DUKE-WS1	Carbonate	2018	3,241,100	9.95		NDWR, 2018a
216	GV-DUKE-WS2	Carbonate	2000	0	0.00		NDWR, 2018a
216	GV-DUKE-WS2	Carbonate	2001	0	0.00		NDWR, 2018a
216	GV-DUKE-WS2	Carbonate	2002	3,312,100	10.16		NDWR, 2018a
216	GV-DUKE-WS2	Carbonate	2003	0	0.00		NDWR, 2018a
216	GV-DUKE-WS2	Carbonate	2004	0	0.00		NDWR, 2018a
216	GV-DUKE-WS2	Carbonate	2005	20,176,000	61.92		NDWR, 2018a



**Table C-3
Groundwater Production
(Page 9 of 30)**

Hydrographic Area	Well Name	Aquifer Material	Year	Production (gallons)	Production (af)	Comments	Source
216	GV-DUKE-WS2	Carbonate	2006	52,927,802	162.43		NDWR, 2018a
216	GV-DUKE-WS2	Carbonate	2007	33,780,000	103.67		NDWR, 2018a
216	GV-DUKE-WS2	Carbonate	2008	54,572	0.17		NDWR, 2018a
216	GV-DUKE-WS2	Carbonate	2009	95,265,432	292.36		NDWR, 2018a
216	GV-DUKE-WS2	Carbonate	2010	101,809,227	312.44		NDWR, 2018a
216	GV-DUKE-WS2	Carbonate	2011	103,242,291	316.84		NDWR, 2018a
216	GV-DUKE-WS2	Carbonate	2012	102,565,323	314.76		NDWR, 2018a
216	GV-DUKE-WS2	Carbonate	2013	31,273,855	95.98		NDWR, 2018a
216	GV-DUKE-WS2	Carbonate	2014	1,767,473	5.42		NDWR, 2018a
216	GV-DUKE-WS2	Carbonate	2015	66,944,359	205.44		NDWR, 2018a
216	GV-DUKE-WS2	Carbonate	2016	43,864,896	134.62		NDWR, 2018a
216	GV-DUKE-WS2	Carbonate	2017	0	0.00		NDWR, 2018a
216	GV-DUKE-WS2	Carbonate	2018	0	0.00		NDWR, 2018a
216	GV-KERR	Carbonate	2001	681,029	2.09		NDWR, 2001
216	GV-KERR	Carbonate	2002	1,029,689	3.16		NDWR, 2002
216	GV-KERR	Carbonate	2003	1,798,698	5.52		NDWR, 2003
216	GV-KERR	Carbonate	2004	3,287,837	10.09		NDWR, 2004
216	GV-KERR	Carbonate	2005	3,173,789	9.74		NDWR, 2005
216	GV-KERR	Carbonate	2006	1,358,799	4.17		NDWR, 2006
216	GV-KERR	Carbonate	2007	984,070	3.02		NDWR, 2007
216	GV-KERR	Carbonate	2008	1,309,921	4.02		NDWR, 2008
216	GV-KERR	Carbonate	2009	1,238,234	3.80		NDWR, 2009
216	GV-KERR	Carbonate	2010	2,078,929	6.38		NDWR, 2010
216	GV-KERR	Carbonate	2011	2,078,929	6.38		NDWR, 2011
216	GV-KERR	Carbonate	2012	3,245,476	9.96		NDWR, 2012
216	GV-KERR	Carbonate	2013	3,196,598	9.81		NDWR, 2013
216	GV-KERR	Carbonate	2014	3,509,415	10.77		NDWR, 2014
216	GV-KERR	Carbonate	2015	5,774,080	17.72		NDWR, 2015

**Table C-3
Groundwater Production
(Page 10 of 30)**

Hydrographic Area	Well Name	Aquifer Material	Year	Production (gallons)	Production (af)	Comments	Source
216	GV-KERR	Carbonate	2016	18,002,000	55.25		NDWR, 2018a
216	GV-KERR	Carbonate	2017	8,965,852	27.52		NDWR, 2018a
216	GV-KERR	Carbonate	2018	9,670,000	29.68		NDWR, 2018a
216	GV-LENZIE-3	Carbonate	2016	152,261,653	467.27		NDWR, 2018a
216	GV-LENZIE-3	Carbonate	2017	145,347,533	446.06		NDWR, 2018a
216	GV-LENZIE-3	Carbonate	2018	56,897,304	174.61		NDWR, 2018a
216	GV-MIRANT1	Carbonate	2000	0	0.00		NDWR, 2018a
216	GV-MIRANT1	Carbonate	2001	0	0.00		NDWR, 2018a
216	GV-MIRANT1	Carbonate	2002	24,939,000	76.53		NDWR, 2018a
216	GV-MIRANT1	Carbonate	2003	40,659,000	124.78		NDWR, 2018a
216	GV-MIRANT1	Carbonate	2004	14,411,400	44.23		NDWR, 2018a
216	GV-MIRANT1	Carbonate	2005	17,529,000	53.79		NDWR, 2018a
216	GV-MIRANT1	Carbonate	2006	20,102,000	61.69		NDWR, 2018a
216	GV-MIRANT1	Carbonate	2007	15,940,000	48.92		NDWR, 2018a
216	GV-MIRANT1	Carbonate	2008	20,270,000	62.21		NDWR, 2018a
216	GV-MIRANT1	Carbonate	2009	21,790,000	66.87		NDWR, 2018a
216	GV-MIRANT1	Carbonate	2010	11,780,000	36.15		NDWR, 2018a
216	GV-MIRANT1	Carbonate	2011	10,610,000	32.56		NDWR, 2018a
216	GV-MIRANT1	Carbonate	2012	5,160,000	15.84		NDWR, 2018a
216	GV-MIRANT1	Carbonate	2013	8,610,000	26.42		NDWR, 2018a
216	GV-MIRANT1	Carbonate	2014	13,850,000	42.50		NDWR, 2018a
216	GV-MIRANT1	Carbonate	2015	18,425,000	56.54		NDWR, 2018a
216	GV-MIRANT1	Carbonate	2016	25,815,000	79.22		NDWR, 2018a
216	GV-MIRANT1	Carbonate	2017	30,400,000	93.29		NDWR, 2018a
216	GV-MIRANT1	Carbonate	2018	10,940,000	33.57		NDWR, 2018a
216	GV-PW-WS1	Carbonate	2000	0	0.00		NDWR, 2018a
216	GV-PW-WS1	Carbonate	2001	0	0.00		NDWR, 2018a
216	GV-PW-WS1	Carbonate	2002	24,628,280	75.58		NDWR, 2018a



**Table C-3
Groundwater Production
(Page 11 of 30)**

Hydrographic Area	Well Name	Aquifer Material	Year	Production (gallons)	Production (af)	Comments	Source
216	GV-PW-WS1	Carbonate	2003	15,721,736	48.25		NDWR, 2018a
216	GV-PW-WS1	Carbonate	2004	46,332,890	142.19		NDWR, 2018a
216	GV-PW-WS1	Carbonate	2005	43,064,719	132.16		NDWR, 2018a
216	GV-PW-WS1	Carbonate	2006	51,438,313	157.86		NDWR, 2018a
216	GV-PW-WS1	Carbonate	2007	54,400,000	166.95		NDWR, 2018a
216	GV-PW-WS1	Carbonate	2008	45,994,581	141.15		NDWR, 2018a
216	GV-PW-WS1	Carbonate	2009	48,684,769	149.41		NDWR, 2018a
216	GV-PW-WS1	Carbonate	2010	52,966,620	162.55		NDWR, 2018a
216	GV-PW-WS1	Carbonate	2011	43,557,511	133.67		NDWR, 2018a
216	GV-PW-WS1	Carbonate	2012	45,994,240	141.15		NDWR, 2018a
216	GV-PW-WS1	Carbonate	2013	45,222,054	138.78		NDWR, 2018a
216	GV-PW-WS1	Carbonate	2014	37,660,958	115.58		NDWR, 2018a
216	GV-PW-WS1	Carbonate	2015	50,122,548	153.82		NDWR, 2018a
216	GV-PW-WS1	Carbonate	2016	56,162,212	172.36		NDWR, 2018a
216	GV-PW-WS1	Carbonate	2017	62,814,431	192.77		NDWR, 2018a
216	GV-PW-WS1	Carbonate	2018	16,329,566	50.11		NDWR, 2018a
216	GV-RW1	Carbonate	2000	0	0.00		NDWR, 2018a
216	GV-RW1	Carbonate	2001	15,779,600	48.43		NDWR, 2018a
216	GV-RW1	Carbonate	2002	0	0.00		NDWR, 2018a
216	GV-RW1	Carbonate	2003	0	0.00		NDWR, 2018a
216	GV-RW1	Carbonate	2004	0	0.00		NDWR, 2018a
216	GV-RW1	Carbonate	2005	355,830	1.09		NDWR, 2018a
216	GV-RW1	Carbonate	2006	12,440,900	38.18		NDWR, 2018a
216	GV-RW1	Carbonate	2007	0	0.00		NDWR, 2018a
216	GV-RW1	Carbonate	2008	61,017,090	187.25		NDWR, 2018a
216	GV-RW1	Carbonate	2009	55,146,664	169.24		NDWR, 2018a
216	GV-RW1	Carbonate	2010	21,402,649	65.68		NDWR, 2018a
216	GV-RW1	Carbonate	2011	40,395,489	123.97		NDWR, 2018a

**Table C-3
Groundwater Production
(Page 12 of 30)**

Hydrographic Area	Well Name	Aquifer Material	Year	Production (gallons)	Production (af)	Comments	Source
216	GV-RW1	Carbonate	2012	28,555,356	87.63		NDWR, 2018a
216	GV-RW1	Carbonate	2013	82,926,540	254.49		NDWR, 2018a
216	GV-RW1	Carbonate	2014	117,003,648	359.07		NDWR, 2018a
216	GV-RW1	Carbonate	2015	88,709,326	272.24		NDWR, 2018a
216	GV-RW1	Carbonate	2016	193,028,250	592.38		NDWR, 2018a
216	GV-RW1	Carbonate	2017	43,062,364	132.15		NDWR, 2018a
216	GV-RW1	Carbonate	2018	19,080,000	58.55		NDWR, 2018a
216	GV-USLIME1	Carbonate	2000	0	0.00		NDWR, 2018a
216	GV-USLIME1	Carbonate	2001	33,388,170	102.46		NDWR, 2018a
216	GV-USLIME1	Carbonate	2002	35,554,390	109.11		NDWR, 2018a
216	GV-USLIME1	Carbonate	2003	33,117,643	101.63		NDWR, 2018a
216	GV-USLIME1	Carbonate	2004	38,606,818	118.48		NDWR, 2018a
216	GV-USLIME1	Carbonate	2005	36,171,110	111.01		NDWR, 2018a
216	GV-USLIME1	Carbonate	2006	42,614,870	130.78		NDWR, 2018a
216	GV-USLIME1	Carbonate	2007	41,089,881	126.10		NDWR, 2018a
216	GV-USLIME1	Carbonate	2008	32,559,872	99.92		NDWR, 2018a
216	GV-USLIME1	Carbonate	2009	27,974,570	85.85		NDWR, 2018a
216	GV-USLIME1	Carbonate	2010	24,452,529	75.04		NDWR, 2018a
216	GV-USLIME1	Carbonate	2011	23,470,206	72.03		NDWR, 2018a
216	GV-USLIME1	Carbonate	2012	19,097,000	58.61		NDWR, 2018a
216	GV-USLIME1	Carbonate	2013	26,117,000	80.15		NDWR, 2018a
216	GV-USLIME1	Carbonate	2014	19,720,000	60.52		NDWR, 2018a
216	GV-USLIME1	Carbonate	2015	23,665,000	72.63		NDWR, 2018a
216	GV-USLIME1	Carbonate	2016	17,327,967	53.18		NDWR, 2018a
216	GV-USLIME1	Carbonate	2017	18,111,927	55.58		NDWR, 2018a
216	GV-USLIME1	Carbonate	2018	11,278,340	34.61		NDWR, 2018a
216	GV-USLIME2	Alluvium	2000	0	0.00		NDWR, 2018a
216	GV-USLIME2	Alluvium	2001	41,921,670	128.65		NDWR, 2018a



**Table C-3
Groundwater Production
(Page 13 of 30)**

Hydrographic Area	Well Name	Aquifer Material	Year	Production (gallons)	Production (af)	Comments	Source
216	GV-USLIME2	Alluvium	2002	47,303,000	145.17		NDWR, 2018a
216	GV-USLIME2	Alluvium	2003	43,273,269	132.80		NDWR, 2018a
216	GV-USLIME2	Alluvium	2004	41,337,821	126.86		NDWR, 2018a
216	GV-USLIME2	Alluvium	2005	35,416,070	108.69		NDWR, 2018a
216	GV-USLIME2	Alluvium	2006	39,206,320	120.32		NDWR, 2018a
216	GV-USLIME2	Alluvium	2007	51,732,669	158.76		NDWR, 2018a
216	GV-USLIME2	Alluvium	2008	43,563,740	133.69		NDWR, 2018a
216	GV-USLIME2	Alluvium	2009	26,844,877	82.38		NDWR, 2018a
216	GV-USLIME2	Alluvium	2010	27,664,227	84.90		NDWR, 2018a
216	GV-USLIME2	Alluvium	2011	32,362,077	99.32		NDWR, 2018a
216	GV-USLIME2	Alluvium	2012	36,961,000	113.43		NDWR, 2018a
216	GV-USLIME2	Alluvium	2013	20,719,000	63.58		NDWR, 2018a
216	GV-USLIME2	Alluvium	2014	23,136,000	71.00		NDWR, 2018a
216	GV-USLIME2	Alluvium	2015	39,594,000	121.51		NDWR, 2018a
216	GV-USLIME2	Alluvium	2016	29,348,314	90.07		NDWR, 2018a
216	GV-USLIME2	Alluvium	2017	38,183,670	117.18		NDWR, 2018a
216	GV-USLIME2	Alluvium	2018	16,880,022	51.80		NDWR, 2018a
216	RS-PW-1	Clastic	1999	528,600	1.62		NDWR, 2018b
216	RS-PW-1	Clastic	2000	0	0.00		NDWR, 2018a
216	RS-PW-1	Clastic	2001	0	0.00		NDWR, 2018a
216	RS-PW-1	Clastic	2002	0	0.00		NDWR, 2018a
216	RS-PW-1	Clastic	2003	0	0.00		NDWR, 2018a
216	RS-PW-1	Clastic	2004	0	0.00		NDWR, 2018a
216	RS-PW-1	Clastic	2005	0	0.00		NDWR, 2018a
216	RS-PW-1	Clastic	2006	0	0.00		NDWR, 2018a
216	RS-PW-1	Clastic	2007	0	0.00		NDWR, 2018a
216	RS-PW-1	Clastic	2008	0	0.00		NDWR, 2018a
216	RS-PW-1	Clastic	2009	0	0.00		NDWR, 2018a

**Table C-3
Groundwater Production
(Page 14 of 30)**

Hydrographic Area	Well Name	Aquifer Material	Year	Production (gallons)	Production (af)	Comments	Source
216	RS-PW-1	Clastic	2010	0	0.00		NDWR, 2018a
216	RS-PW-1	Clastic	2011	46,502,300	142.71		NDWR, 2018a
216	RS-PW-1	Clastic	2012	30,563,900	93.80		NDWR, 2018a
216	RS-PW-1	Clastic	2013	9,566,000	29.36		NDWR, 2018a
216	RS-PW-1	Clastic	2014	8,560,074	26.27		NDWR, 2018a
216	RS-PW-1	Clastic	2015	6,572,526	20.17		NDWR, 2018a
216	RS-PW-1	Clastic	2016	1,450,728	4.45		NDWR, 2018a
216	RS-PW-1	Clastic	2017	0	0.00		NDWR, 2018a
216	RS-PW-1	Clastic	2018	0	0.00		NDWR, 2018a
216	RS-PW-2	Carbonate	1999	46,625,400	143.09		NDWR, 2018b
216	RS-PW-2	Carbonate	2000	29,818,300	91.51		NDWR, 2018a
216	RS-PW-2	Carbonate	2001	22,497,650	69.04		NDWR, 2018a
216	RS-PW-2	Carbonate	2002	33,203,350	101.90		NDWR, 2018a
216	RS-PW-2	Carbonate	2003	52,891,600	162.32		NDWR, 2018a
216	RS-PW-2	Carbonate	2004	44,666,500	137.08		NDWR, 2018a
216	RS-PW-2	Carbonate	2005	8,323,200	25.54		NDWR, 2018a
216	RS-PW-2	Carbonate	2006	16,073,000	49.33		NDWR, 2018a
216	RS-PW-2	Carbonate	2007	20,714,700	63.57		NDWR, 2018a
216	RS-PW-2	Carbonate	2008	39,794,700	122.13		NDWR, 2018a
216	RS-PW-2	Carbonate	2009	39,974,400	122.68		NDWR, 2018a
216	RS-PW-2	Carbonate	2010	37,954,200	116.48		NDWR, 2018a
216	RS-PW-2	Carbonate	2011	40,543,400	124.42		NDWR, 2018a
216	RS-PW-2	Carbonate	2012	41,012,700	125.86		NDWR, 2018a
216	RS-PW-2	Carbonate	2013	34,236,700	105.07		NDWR, 2018a
216	RS-PW-2	Carbonate	2014	33,442,918	102.63		NDWR, 2018a
216	RS-PW-2	Carbonate	2015	11,947,708	36.67		NDWR, 2018a
216	RS-PW-2	Carbonate	2016	0	0.00		NDWR, 2018a
216	RS-PW-2	Carbonate	2017	0	0.00		NDWR, 2018a



**Table C-3
Groundwater Production
(Page 15 of 30)**

Hydrographic Area	Well Name	Aquifer Material	Year	Production (gallons)	Production (af)	Comments	Source
216	RS-PW-2	Carbonate	2018	0	0.00		NDWR, 2018a
216	RS-PW-3	Carbonate	1999	0	0.00		NDWR, 2018b
216	RS-PW-3	Carbonate	2000	0	0.00		NDWR, 2018a
216	RS-PW-3	Carbonate	2001	0	0.00		NDWR, 2018a
216	RS-PW-3	Carbonate	2002	0	0.00		NDWR, 2018a
216	RS-PW-3	Carbonate	2003	0	0.00		NDWR, 2018a
216	RS-PW-3	Carbonate	2004	0	0.00		NDWR, 2018a
216	RS-PW-3	Carbonate	2005	0	0.00		NDWR, 2018a
216	RS-PW-3	Carbonate	2006	0	0.00		NDWR, 2018a
216	RS-PW-3	Carbonate	2007	0	0.00		NDWR, 2018a
216	RS-PW-3	Carbonate	2008	0	0.00		NDWR, 2018a
216	RS-PW-3	Carbonate	2009	0	0.00		NDWR, 2018a
216	RS-PW-3	Carbonate	2010	0	0.00		NDWR, 2018a
216	RS-PW-3	Carbonate	2011	0	0.00		NDWR, 2018a
216	RS-PW-3	Carbonate	2012	0	0.00		NDWR, 2018a
216	RS-PW-3	Carbonate	2013	0	0.00		NDWR, 2018a
216	RS-PW-3	Carbonate	2014	0	0.00		NDWR, 2018a
216	RS-PW-3	Carbonate	2015	0	0.00		NDWR, 2018a
216	RS-PW-3	Carbonate	2016	0	0.00		NDWR, 2018a
216	RS-PW-3	Carbonate	2017	0	0.00		NDWR, 2018a
216	RS-PW-3	Carbonate	2018	0	0.00		NDWR, 2018a
216	RS-PW-5	Carbonate	1999	17,869,200	54.84		NDWR, 2018b
216	RS-PW-5	Carbonate	2000	83,063,400	254.91		NDWR, 2018a
216	RS-PW-5	Carbonate	2001	58,488,000	179.49		NDWR, 2018a
216	RS-PW-5	Carbonate	2002	39,610,100	121.56		NDWR, 2018a
216	RS-PW-5	Carbonate	2003	55,826,300	171.32		NDWR, 2018a
216	RS-PW-5	Carbonate	2004	44,048,100	135.18		NDWR, 2018a
216	RS-PW-5	Carbonate	2005	70,927,700	217.67		NDWR, 2018a

**Table C-3
Groundwater Production
(Page 16 of 30)**

Hydrographic Area	Well Name	Aquifer Material	Year	Production (gallons)	Production (af)	Comments	Source
216	RS-PW-5	Carbonate	2006	37,547,900	115.23		NDWR, 2018a
216	RS-PW-5	Carbonate	2007	29,339,400	90.04		NDWR, 2018a
216	RS-PW-5	Carbonate	2008	78,452,840	240.76		NDWR, 2018a
216	RS-PW-5	Carbonate	2009	58,241,500	178.74		NDWR, 2018a
216	RS-PW-5	Carbonate	2010	45,005,000	138.12		NDWR, 2018a
216	RS-PW-5	Carbonate	2011	6,445,500	19.78		NDWR, 2018a
216	RS-PW-5	Carbonate	2012	11,561,900	35.48		NDWR, 2018a
216	RS-PW-5	Carbonate	2013	23,462,900	72.00		NDWR, 2018a
216	RS-PW-5	Carbonate	2014	33,141,107	101.71		NDWR, 2018a
216	RS-PW-5	Carbonate	2015	39,001,222	119.69		NDWR, 2018a
216	RS-PW-5	Carbonate	2016	31,413,123	96.40		NDWR, 2018a
216	RS-PW-5	Carbonate	2017	88,328,611	271.07		NDWR, 2018a
216	RS-PW-5	Carbonate	2018	64,831,056	198.96		NDWR, 2018a
216	RS-PW-6	Carbonate	1999	60,764,900	186.48		NDWR, 2018b
216	RS-PW-6	Carbonate	2000	40,254,200	123.54		NDWR, 2018a
216	RS-PW-6	Carbonate	2001	58,762,200	180.33		NDWR, 2018a
216	RS-PW-6	Carbonate	2002	42,952,100	131.82		NDWR, 2018a
216	RS-PW-6	Carbonate	2003	37,063,000	113.74		NDWR, 2018a
216	RS-PW-6	Carbonate	2004	33,310,199	102.23		NDWR, 2018a
216	RS-PW-6	Carbonate	2005	46,520,700	142.77		NDWR, 2018a
216	RS-PW-6	Carbonate	2006	26,403,000	81.03		NDWR, 2018a
216	RS-PW-6	Carbonate	2007	40,707,000	124.93		NDWR, 2018a
216	RS-PW-6	Carbonate	2008	58,169,300	178.52		NDWR, 2018a
216	RS-PW-6	Carbonate	2009	45,197,400	138.71		NDWR, 2018a
216	RS-PW-6	Carbonate	2010	39,948,000	122.60		NDWR, 2018a
216	RS-PW-6	Carbonate	2011	24,497,000	75.18		NDWR, 2018a
216	RS-PW-6	Carbonate	2012	39,346,900	120.75		NDWR, 2018a
216	RS-PW-6	Carbonate	2013	42,697,000	131.03		NDWR, 2018a



**Table C-3
Groundwater Production
(Page 17 of 30)**

Hydrographic Area	Well Name	Aquifer Material	Year	Production (gallons)	Production (af)	Comments	Source
216	RS-PW-6	Carbonate	2014	32,231,721	98.92		NDWR, 2018a
216	RS-PW-6	Carbonate	2015	42,679,916	130.98		NDWR, 2018a
216	RS-PW-6	Carbonate	2016	55,796,378	171.23		NDWR, 2018a
216	RS-PW-6	Carbonate	2017	68,200,752	209.30		NDWR, 2018a
216	RS-PW-6	Carbonate	2018	20,124,640	61.76		NDWR, 2018a
216	RS-PW-7	Carbonate	1999	39,430	0.12		NDWR, 2018b
216	RS-PW-7	Carbonate	2000	0	0.00		NDWR, 2018a
216	RS-PW-7	Carbonate	2001	0	0.00		NDWR, 2018a
216	RS-PW-7	Carbonate	2002	0	0.00		NDWR, 2018a
216	RS-PW-7	Carbonate	2003	0	0.00		NDWR, 2018a
216	RS-PW-7	Carbonate	2004	0	0.00		NDWR, 2018a
216	RS-PW-7	Carbonate	2005	0	0.00		NDWR, 2018a
216	RS-PW-7	Carbonate	2006	0	0.00		NDWR, 2018a
216	RS-PW-7	Carbonate	2007	0	0.00		NDWR, 2018a
216	RS-PW-7	Carbonate	2008	0	0.00		NDWR, 2018a
216	RS-PW-7	Carbonate	2009	0	0.00		NDWR, 2018a
216	RS-PW-7	Carbonate	2010	27,310	0.08		NDWR, 2018a
216	RS-PW-7	Carbonate	2011	7,850	0.02		NDWR, 2018a
216	RS-PW-7	Carbonate	2012	152,300	0.47		NDWR, 2018a
216	RS-PW-7	Carbonate	2013	541,800	1.66		NDWR, 2018a
216	RS-PW-7	Carbonate	2014	432,500	1.33		NDWR, 2018a
216	RS-PW-7	Carbonate	2015	5,390,581	16.54		NDWR, 2018a
216	RS-PW-7	Carbonate	2016	27,925,361	85.70		NDWR, 2018a
216	RS-PW-7	Carbonate	2017	22,153,234	67.99		NDWR, 2018a
216	RS-PW-7	Carbonate	2018	31,553,066	96.83		NDWR, 2018a
218	PAIUTES-ECP1	Carbonate	2011	1,928,600	5.92		NDWR, 2018a
218	PAIUTES-ECP1	Carbonate	2012	0	0.00		NDWR, 2018a
218	PAIUTES-ECP1	Carbonate	2013	7,610,000	23.35		NDWR, 2018a

**Table C-3
Groundwater Production
(Page 18 of 30)**

Hydrographic Area	Well Name	Aquifer Material	Year	Production (gallons)	Production (af)	Comments	Source
218	PAIUTES-ECP1	Carbonate	2014	57,130,000	175.33		NDWR, 2018a
218	PAIUTES-ECP1	Carbonate	2015	95,700,000	293.69		NDWR, 2018a
218	PAIUTES-ECP1	Carbonate	2016	44,510,000	136.60		NDWR, 2018a
218	PAIUTES-ECP1	Carbonate	2017	4,190,000	12.86		NDWR, 2018a
218	PAIUTES-ECP1	Carbonate	2018	0	0.00		NDWR, 2018a
218	PAIUTES-ECP3	Carbonate	2015	28,360,000	87.03		NDWR, 2018a
218	PAIUTES-ECP3	Carbonate	2016	9,620,000	29.52		NDWR, 2018a
218	PAIUTES-ECP3	Carbonate	2017	0	0.00		NDWR, 2018a
218	PAIUTES-ECP3	Carbonate	2018	0	0.00		NDWR, 2018a
218	PAIUTES-TH1	Carbonate	2009	5,000,000	15.34		NDWR, 2018a
218	PAIUTES-TH1	Carbonate	2010	6,300,000	19.33		NDWR, 2018a
218	PAIUTES-TH1	Carbonate	2011	6,470,000	19.86		NDWR, 2018a
218	PAIUTES-TH1	Carbonate	2012	6,790,000	20.84		NDWR, 2018a
218	PAIUTES-TH1	Carbonate	2013	11,670,000	35.81		NDWR, 2018a
218	PAIUTES-TH1	Carbonate	2014	36,830,000	113.03		NDWR, 2018a
218	PAIUTES-TH1	Carbonate	2015	10,020,000	30.75		NDWR, 2018a
218	PAIUTES-TH1	Carbonate	2016	11,040,000	33.88		NDWR, 2018a
218	PAIUTES-TH1	Carbonate	2017	9,806,313	30.09		NDWR, 2018a
218	PAIUTES-TH1	Carbonate	2018	3,510,000	10.77		NDWR, 2018a
219	ARROW_CANYON	Carbonate	1992	167,289,000	513.39		MVWD, 2018
219	ARROW_CANYON	Carbonate	1993	335,084,000	1,028.34		MVWD, 2018
219	ARROW_CANYON	Carbonate	1994	164,219,000	503.97		MVWD, 2018
219	ARROW_CANYON	Carbonate	1995	99,050,000	303.97		MVWD, 2018
219	ARROW_CANYON	Carbonate	1996	89,388,000	274.32		MVWD, 2018
219	ARROW_CANYON	Carbonate	1997	163,354,000	501.32		MVWD, 2018
219	ARROW_CANYON	Carbonate	1998	641,596,000	1,968.99		MVWD, 2018
219	ARROW_CANYON	Carbonate	1999	793,268,000	2,434.45		MVWD, 2018
219	ARROW_CANYON	Carbonate	2000	904,935,000	2,777.14		MVWD, 2018



**Table C-3
Groundwater Production
(Page 19 of 30)**

Hydrographic Area	Well Name	Aquifer Material	Year	Production (gallons)	Production (af)	Comments	Source
219	ARROW_CANYON	Carbonate	2001	793,065,000	2,433.83		MVWD, 2018
219	ARROW_CANYON	Carbonate	2002	737,673,750	2,263.84		MVWD, 2018
219	ARROW_CANYON	Carbonate	2003	804,304,520	2,468.32		MVWD, 2018
219	ARROW_CANYON	Carbonate	2004	816,215,000	2,504.87		MVWD, 2018
219	ARROW_CANYON	Carbonate	2005	679,303,000	2,084.70		MVWD, 2018
219	ARROW_CANYON	Carbonate	2006	641,990,508	1,970.20		MVWD, 2018
219	ARROW_CANYON	Carbonate	2007	416,343,000	1,277.71		MVWD, 2018
219	ARROW_CANYON	Carbonate	2008	583,101,000	1,789.47		MVWD, 2018
219	ARROW_CANYON	Carbonate	2009	461,027,733	1,414.84		MVWD, 2018
219	ARROW_CANYON	Carbonate	2010	375,264,540	1,151.64		MVWD, 2018
219	ARROW_CANYON	Carbonate	2011	547,436,576	1,680.02		MVWD, 2018
219	ARROW_CANYON	Carbonate	2012	641,920,168	1,969.98		MVWD, 2018
219	ARROW_CANYON	Carbonate	2013	613,093,890	1,881.52		MVWD, 2018
219	ARROW_CANYON	Carbonate	2014	379,141,924	1,163.54		MVWD, 2018
219	ARROW_CANYON	Carbonate	2015	655,291,990	2,011.02		MVWD, 2018
219	ARROW_CANYON	Carbonate	2016	736,378,979	2,259.86		MVWD, 2018
219	ARROW_CANYON	Carbonate	2017	748,223,000	2,296.21		MVWD, 2018
219	ARROW_CANYON	Carbonate	2018	249,540,000	765.81		MVWD, 2018
219	ARROW_CANYON_2	Carbonate	2005	66,440,000	203.90		MVWD, 2018
219	ARROW_CANYON_2	Carbonate	2006	261,000	0.80		MVWD, 2018
219	ARROW_CANYON_2	Carbonate	2007	184,622,000	566.58		MVWD, 2018
219	ARROW_CANYON_2	Carbonate	2008	32,129,000	98.60		MVWD, 2018
219	ARROW_CANYON_2	Carbonate	2009	201,394,403	618.06		MVWD, 2018
219	ARROW_CANYON_2	Carbonate	2010	216,208,406	663.52		MVWD, 2018
219	ARROW_CANYON_2	Carbonate	2011	50,554,746	155.15		MVWD, 2018
219	ARROW_CANYON_2	Carbonate	2012	159,785,076	490.36		MVWD, 2018
219	ARROW_CANYON_2	Carbonate	2013	117,203,061	359.68		MVWD, 2018
219	ARROW_CANYON_2	Carbonate	2014	90,609,576	278.07		MVWD, 2018

**Table C-3
Groundwater Production
(Page 20 of 30)**

Hydrographic Area	Well Name	Aquifer Material	Year	Production (gallons)	Production (af)	Comments	Source
219	ARROW_CANYON_2	Carbonate	2015	125,232,959	384.33		MVWD, 2018
219	ARROW_CANYON_2	Carbonate	2016	175,395,278	538.27		MVWD, 2018
219	ARROW_CANYON_2	Carbonate	2017	170,436,287	523.05		MVWD, 2018
219	ARROW_CANYON_2	Carbonate	2018	214,718,278	658.95		MVWD, 2018
219	BEHMER	Alluvium	1993	200,429,800	615.10	Combined Behmer 14" and 8" production.	Mifflin and Adenle, 1994
219	BEHMER	Alluvium	1994	75,445,300	231.53	Combined Behmer 14" and 8" production.	Mifflin and Adenle, 1995
219	BEHMER	Alluvium	1995	139,805,760	429.05	Combined Behmer 14" and 8" production.	Pohlmann, 1996
219	BEHMER	Alluvium	1996	222,068,000	681.50	Combined Behmer 14" and 8" production.	Pohlmann and Russell, 1997
219	BEHMER	Alluvium	1999	78,801,740	241.83	Combined Behmer 14" and 8" production.	Kleinfelder, 2000
219	BEHMER	Alluvium	2000	180,081,000	552.65	Production from Behmer 14".	NDWR, 2018a
219	BEHMER	Alluvium	2001	270,722,000	830.82	Combined Behmer 14" and 8" production.	Converse, 2002
219	BEHMER	Alluvium	2002	267,153,000	819.86	Production from Behmer 14".	Converse, 2003
219	BEHMER	Alluvium	2003	209,306,000	642.34	Production from Behmer 14".	Converse, 2004
219	BEHMER	Alluvium	2004	181,153,440	555.94	Production from Behmer 14".	Converse, 2005
219	BEHMER	Alluvium	2005	214,128,000	657.13	Production from Behmer 14".	NDWR, 2018a
219	BEHMER	Alluvium	2006	166,359,000	510.54	Production from Behmer 14".	NDWR, 2018a
219	BEHMER	Alluvium	2007	170,896,000	524.46	Production from Behmer 14".	NDWR, 2018a
219	BEHMER	Alluvium	2008	156,091,000	479.03	Production from Behmer 14".	NDWR, 2018a
219	BEHMER	Alluvium	2009	295,797,000	907.77		NDWR, 2018a
219	BEHMER	Alluvium	2010	199,527,000	612.33		NDWR, 2018a
219	BEHMER	Alluvium	2011	141,521,000	434.31		NDWR, 2018a
219	BEHMER	Alluvium	2012	141,012,500	432.75		NDWR, 2018a
219	BEHMER	Alluvium	2013	202,634,000	621.86		NDWR, 2018a
219	BEHMER	Alluvium	2014	200,741,453	616.05		NDWR, 2018a
219	BEHMER	Alluvium	2015	94,933,000	291.34		NDWR, 2018a
219	BEHMER	Alluvium	2016	20,000	0.06		NDWR, 2018a



**Table C-3
Groundwater Production
(Page 21 of 30)**

Hydrographic Area	Well Name	Aquifer Material	Year	Production (gallons)	Production (af)	Comments	Source
219	BEHMER	Alluvium	2017	28,760,000	88.26		NDWR, 2018a
219	BEHMER	Alluvium	2018	0	0.00		NDWR, 2018a
219	LDS Central	Alluvium	1990	172,457,000	529.25		Mifflin, Adenle, and Johnson, 1991
219	LDS Central	Alluvium	1993	67,869,000	208.28		Mifflin and Adenle, 1994
219	LDS Central	Alluvium	1994	98,137,000	301.17		Mifflin and Adenle, 1995
219	LDS Central	Alluvium	1995	159,600,000	489.79		Pohlmann, 1996
219	LDS CENTRAL	Alluvium	1996	180,549,000	554.08		Pohlmann and Russell, 1997
219	LDS CENTRAL	Alluvium	1999	238,859,000	733.03		Kleinfelder, 2000
219	LDS CENTRAL	Alluvium	2000	315,045,000	966.84		NDWR, 2018a
219	LDS CENTRAL	Alluvium	2001	310,055,000	951.52		NDWR, 2018a
219	LDS CENTRAL	Alluvium	2002	296,357,000	909.49		NDWR, 2018a
219	LDS CENTRAL	Alluvium	2003	317,365,000	973.96		NDWR, 2018a
219	LDS CENTRAL	Alluvium	2004	237,541,000	728.99		NDWR, 2018a
219	LDS CENTRAL	Alluvium	2005	252,015,000	773.41		NDWR, 2018a
219	LDS CENTRAL	Alluvium	2006	287,471,000	882.22		NDWR, 2018a
219	LDS CENTRAL	Alluvium	2007	230,442,000	707.20		NDWR, 2018a
219	LDS CENTRAL	Alluvium	2008	198,628,000	609.57		NDWR, 2018a
219	LDS CENTRAL	Alluvium	2009	267,394,000	820.60		NDWR, 2018a
219	LDS CENTRAL	Alluvium	2010	231,525,000	710.52		NDWR, 2018a
219	LDS CENTRAL	Alluvium	2011	161,742,000	496.37		NDWR, 2018a
219	LDS CENTRAL	Alluvium	2012	77,824,000	238.83		NDWR, 2018a
219	LDS CENTRAL	Alluvium	2013	128,674,000	394.89		NDWR, 2018a
219	LDS CENTRAL	Alluvium	2014	68,333,661	209.71		NDWR, 2018a
219	LDS CENTRAL	Alluvium	2015	5,190,000	15.93		NDWR, 2018a
219	LDS CENTRAL	Alluvium	2016	19,670,000	60.37		NDWR, 2018a

**Table C-3
Groundwater Production
(Page 22 of 30)**

Hydrographic Area	Well Name	Aquifer Material	Year	Production (gallons)	Production (af)	Comments	Source
219	LDS CENTRAL	Alluvium	2017	0	0.00		NDWR, 2018a
219	LDS CENTRAL	Alluvium	2018	0	0.00		NDWR, 2018a
219	LDS East	Alluvium	1990	137,505,000	421.99		Mifflin, Adenle, and Johnson, 1991
219	LDS East	Alluvium	1993	92,336,000	283.37		Mifflin and Adenle, 1994
219	LDS East	Alluvium	1994	100,962,000	309.84		Mifflin and Adenle, 1995
219	LDS East	Alluvium	1995	175,869,000	539.72		Pohlmann, 1996
219	LDS EAST	Alluvium	1996	171,100,000	525.09		Pohlmann and Russell, 1997
219	LDS EAST	Alluvium	1999	191,588,000	587.96		Kleinfelder, 2000
219	LDS EAST	Alluvium	2000	363,754,000	1,116.32		NDWR, 2018a
219	LDS EAST	Alluvium	2001	197,351,000	605.65		NDWR, 2018a
219	LDS EAST	Alluvium	2002	124,970,000	383.52		NDWR, 2018a
219	LDS EAST	Alluvium	2003	213,657,000	655.69		NDWR, 2018a
219	LDS EAST	Alluvium	2004	183,984,500	564.63		NDWR, 2018a
219	LDS EAST	Alluvium	2005	140,928,000	432.49		NDWR, 2018a
219	LDS EAST	Alluvium	2006	127,973,000	392.73		NDWR, 2018a
219	LDS EAST	Alluvium	2007	207,036,000	635.37		NDWR, 2018a
219	LDS EAST	Alluvium	2008	165,261,000	507.17		NDWR, 2018a
219	LDS EAST	Alluvium	2009	63,551,000	195.03		NDWR, 2018a
219	LDS EAST	Alluvium	2010	52,720,000	161.79		NDWR, 2018a
219	LDS EAST	Alluvium	2011	196,639,000	603.46		NDWR, 2018a
219	LDS EAST	Alluvium	2012	188,436,000	578.29		NDWR, 2018a
219	LDS EAST	Alluvium	2013	177,234,000	543.91		NDWR, 2018a
219	LDS EAST	Alluvium	2014	195,257,868	599.22		NDWR, 2018a
219	LDS EAST	Alluvium	2015	13,710,000	42.07		NDWR, 2018a
219	LDS EAST	Alluvium	2016	0	0.00		NDWR, 2018a



**Table C-3
Groundwater Production
(Page 23 of 30)**

Hydrographic Area	Well Name	Aquifer Material	Year	Production (gallons)	Production (af)	Comments	Source
219	LDS EAST	Alluvium	2017	60,100,000	184.44		NDWR, 2018a
219	LDS EAST	Alluvium	2018	0	0.00		NDWR, 2018a
219	LDS West	Alluvium	1990	198,115,000	607.99		Mifflin, Adenle, and Johnson, 1991
219	LDS West	Alluvium	1993	134,620,000	413.13		Mifflin and Adenle, 1994
219	LDS West	Alluvium	1994	279,092,000	856.50		Mifflin and Adenle, 1995
219	LDS West	Alluvium	1995	180,481,000	553.88		Pohlmann, 1996
219	LDS WEST	Alluvium	1996	331,528,000	1,017.42		Pohlmann and Russell, 1997
219	LDS WEST	Alluvium	1999	348,289,000	1,068.86		Kleinfelder, 2000
219	LDS WEST	Alluvium	2000	353,827,000	1,085.86		NDWR, 2018a
219	LDS WEST	Alluvium	2001	228,110,000	700.04		NDWR, 2018a
219	LDS WEST	Alluvium	2002	246,938,000	757.82		NDWR, 2018a
219	LDS WEST	Alluvium	2003	172,354,000	528.94		NDWR, 2018a
219	LDS WEST	Alluvium	2004	165,522,000	507.97		NDWR, 2018a
219	LDS WEST	Alluvium	2005	303,863,000	932.52		NDWR, 2018a
219	LDS WEST	Alluvium	2006	428,686,000	1,315.59		NDWR, 2018a
219	LDS WEST	Alluvium	2007	288,217,000	884.51		NDWR, 2018a
219	LDS WEST	Alluvium	2008	166,099,000	509.74		NDWR, 2018a
219	LDS WEST	Alluvium	2009	168,098,000	515.87		NDWR, 2018a
219	LDS WEST	Alluvium	2010	167,529,000	514.13		NDWR, 2018a
219	LDS WEST	Alluvium	2011	129,219,000	396.56		NDWR, 2018a
219	LDS WEST	Alluvium	2012	65,323,000	200.47		NDWR, 2018a
219	LDS WEST	Alluvium	2013	35,166,000	107.92		NDWR, 2018a
219	LDS WEST	Alluvium	2014	145,313,981	445.95		NDWR, 2018a
219	LDS WEST	Alluvium	2015	38,379,000	117.78		NDWR, 2018a
219	LDS WEST	Alluvium	2016	70,410,000	216.08		NDWR, 2018a

**Table C-3
Groundwater Production
(Page 24 of 30)**

Hydrographic Area	Well Name	Aquifer Material	Year	Production (gallons)	Production (af)	Comments	Source
219	LDS WEST	Alluvium	2017	17,970,000	55.15		NDWR, 2018a
219	LDS WEST	Alluvium	2018	0	0.00		NDWR, 2018a
219	LEWIS 1	Alluvium	1993	135,885,000	417.02		Mifflin and Adenle, 1994
219	LEWIS 1	Alluvium	1994	185,686,000	569.85		Mifflin and Adenle, 1995
219	LEWIS 1	Alluvium	1995	59,146,000	181.51		Pohlmann, 1996
219	LEWIS 1	Alluvium	1996	79,882,000	245.15		Pohlmann and Russell, 1997
219	LEWIS 1	Alluvium	1999	117,567,000	360.80		Kleinfelder, 2000
219	LEWIS 1	Alluvium	2000	101,913,332	312.76		NDWR, 2018a
219	LEWIS 1	Alluvium	2001	35,630,000	109.34		NDWR, 2018a
219	LEWIS 1	Alluvium	2002	123,094,000	377.76		NDWR, 2018a
219	LEWIS 1	Alluvium	2003	93,257,000	286.20		NDWR, 2018a
219	LEWIS 1	Alluvium	2004	100,527,000	308.51		NDWR, 2018a
219	LEWIS 1	Alluvium	2005	92,664,000	284.38		NDWR, 2018a
219	LEWIS 1	Alluvium	2006	86,734,000	266.18		NDWR, 2018a
219	LEWIS 1	Alluvium	2007	77,139,000	236.73		NDWR, 2018a
219	LEWIS 1	Alluvium	2008	103,418,000	317.38		NDWR, 2018a
219	LEWIS 1	Alluvium	2009	17,407,000	53.42		NDWR, 2018a
219	LEWIS 1	Alluvium	2010	44,258,000	135.82		NDWR, 2018a
219	LEWIS 1	Alluvium	2011	133,139,200	408.59		NDWR, 2018a
219	LEWIS 1	Alluvium	2012	71,765,700	220.24		NDWR, 2018a
219	LEWIS 1	Alluvium	2013	64,453,800	197.80		NDWR, 2018a
219	LEWIS 1	Alluvium	2014	89,944,300	276.03		NDWR, 2018a
219	LEWIS 1	Alluvium	2015	0	0.00		NDWR, 2018a
219	LEWIS 1	Alluvium	2016	0	0.00		NDWR, 2018a
219	LEWIS 1	Alluvium	2017	0	0.00		NDWR, 2018a
219	LEWIS 1	Alluvium	2018	0	0.00		NDWR, 2018a



**Table C-3
Groundwater Production
(Page 25 of 30)**

Hydrographic Area	Well Name	Aquifer Material	Year	Production (gallons)	Production (af)	Comments	Source
219	LEWIS 2	Alluvium	1993	76,466,000	234.67		Miffilin and Adenle, 1994
219	LEWIS 2	Alluvium	1994	70,949,000	217.73		Miffilin and Adenle, 1995
219	LEWIS 2	Alluvium	1995	73,164,000	224.53		Pohlmann, 1996
219	LEWIS 2	Alluvium	1996	64,856,000	199.04		Pohlmann and Russell, 1997
219	LEWIS 2	Alluvium	1999	72,835,000	223.52		Kleinfelder, 2000
219	LEWIS 2	Alluvium	2000	103,158,000	316.58		NDWR, 2018a
219	LEWIS 2	Alluvium	2001	6,180,000	18.97		NDWR, 2018a
219	LEWIS 2	Alluvium	2002	78,513,000	240.95		NDWR, 2018a
219	LEWIS 2	Alluvium	2003	68,188,000	209.26		NDWR, 2018a
219	LEWIS 2	Alluvium	2004	102,914,000	315.83		NDWR, 2018a
219	LEWIS 2	Alluvium	2005	100,377,000	308.05		NDWR, 2018a
219	LEWIS 2	Alluvium	2006	74,216,000	227.76		NDWR, 2018a
219	LEWIS 2	Alluvium	2007	116,889,000	358.72		NDWR, 2018a
219	LEWIS 2	Alluvium	2008	108,228,000	332.14		NDWR, 2018a
219	LEWIS 2	Alluvium	2009	97,690,000	299.80		NDWR, 2018a
219	LEWIS 2	Alluvium	2010	113,247,000	347.54		NDWR, 2018a
219	LEWIS 2	Alluvium	2011	127,704,000	391.91		NDWR, 2018a
219	LEWIS 2	Alluvium	2012	35,537,000	109.06		NDWR, 2018a
219	LEWIS 2	Alluvium	2013	26,465,000	81.22		NDWR, 2018a
219	LEWIS 2	Alluvium	2014	44,022,000	135.10		NDWR, 2018a
219	LEWIS 2	Alluvium	2015	0	0.00		NDWR, 2018a
219	LEWIS 2	Alluvium	2016	0	0.00		NDWR, 2018a
219	LEWIS 2	Alluvium	2017	0	0.00		NDWR, 2018a
219	LEWIS 2	Alluvium	2018	0	0.00		NDWR, 2018a
219	LEWIS 3	Alluvium	1993	129,001,000	395.89		Miffilin and Adenle, 1994

**Table C-3
Groundwater Production
(Page 26 of 30)**

Hydrographic Area	Well Name	Aquifer Material	Year	Production (gallons)	Production (af)	Comments	Source
219	LEWIS 3	Alluvium	1994	256,934,000	788.50		Mifflin and Adenle, 1995
219	LEWIS 3	Alluvium	1995	118,406,000	363.37		Pohlmann, 1996
219	LEWIS 3	Alluvium	1996	81,207,000	249.22		Pohlmann and Russell, 1997
219	LEWIS 3	Alluvium	1999	205,279,000	629.98		Kleinfelder, 2000
219	LEWIS 3	Alluvium	2000	152,499,000	468.00		NDWR, 2018a
219	LEWIS 3	Alluvium	2001	141,026,000	432.79		NDWR, 2018a
219	LEWIS 3	Alluvium	2002	238,372,000	731.54		NDWR, 2018a
219	LEWIS 3	Alluvium	2003	136,780,000	419.76		NDWR, 2018a
219	LEWIS 3	Alluvium	2004	121,044,000	371.47		NDWR, 2018a
219	LEWIS 3	Alluvium	2005	101,789,000	312.38		NDWR, 2018a
219	LEWIS 3	Alluvium	2006	145,098,000	445.29		NDWR, 2018a
219	LEWIS 3	Alluvium	2007	105,172,300	322.76		NDWR, 2018a
219	LEWIS 3	Alluvium	2008	52,951,600	162.50		NDWR, 2018a
219	LEWIS 3	Alluvium	2009	53,981,600	165.66		NDWR, 2018a
219	LEWIS 3	Alluvium	2010	60,061,000	184.32		NDWR, 2018a
219	LEWIS 3	Alluvium	2011	114,042,000	349.98		NDWR, 2018a
219	LEWIS 3	Alluvium	2012	75,691,000	232.29		NDWR, 2018a
219	LEWIS 3	Alluvium	2013	111,242,000	341.39		NDWR, 2018a
219	LEWIS 3	Alluvium	2014	173,058,834	531.10		NDWR, 2018a
219	LEWIS 3	Alluvium	2015	3,830,000	11.75		NDWR, 2018a
219	LEWIS 3	Alluvium	2016	63,890,000	196.07		NDWR, 2018a
219	LEWIS 3	Alluvium	2017	0	0.00		NDWR, 2018a
219	LEWIS 3	Alluvium	2018	0	0.00		NDWR, 2018a
219	LEWIS 4	Alluvium	1993	144,441,000	443.27		Mifflin and Adenle, 1994
219	LEWIS 4	Alluvium	1994	89,080,000	273.38		Mifflin and Adenle, 1995



**Table C-3
Groundwater Production
(Page 27 of 30)**

Hydrographic Area	Well Name	Aquifer Material	Year	Production (gallons)	Production (af)	Comments	Source
219	LEWIS 4	Alluvium	1995	107,707,000	330.54		Pohlmann, 1996
219	LEWIS 4	Alluvium	1996	175,769,000	539.42		Pohlmann and Russell, 1997
219	LEWIS 4	Alluvium	1999	78,307,000	240.32		Kleinfelder, 2000
219	LEWIS 4	Alluvium	2000	81,103,000	248.90		NDWR, 2018a
219	LEWIS 4	Alluvium	2001	111,354,000	341.73		NDWR, 2018a
219	LEWIS 4	Alluvium	2002	203,322,400	623.97		NDWR, 2018a
219	LEWIS 4	Alluvium	2003	88,076,400	270.30		NDWR, 2018a
219	LEWIS 4	Alluvium	2004	107,038,100	328.49		NDWR, 2018a
219	LEWIS 4	Alluvium	2005	130,254,900	399.74		NDWR, 2018a
219	LEWIS 4	Alluvium	2006	133,886,400	410.88		NDWR, 2018a
219	LEWIS 4	Alluvium	2007	103,962,300	319.05		NDWR, 2018a
219	LEWIS 4	Alluvium	2008	108,001,400	331.44		NDWR, 2018a
219	LEWIS 4	Alluvium	2009	67,665,100	207.66		NDWR, 2018a
219	LEWIS 4	Alluvium	2010	89,094,000	273.42		NDWR, 2018a
219	LEWIS 4	Alluvium	2011	87,828,000	269.53		NDWR, 2018a
219	LEWIS 4	Alluvium	2012	45,697,000	140.24		NDWR, 2018a
219	LEWIS 4	Alluvium	2013	61,536,000	188.85		NDWR, 2018a
219	LEWIS 4	Alluvium	2014	154,217,229	473.28		NDWR, 2018a
219	LEWIS 4	Alluvium	2015	15,250,000	46.80		NDWR, 2018a
219	LEWIS 4	Alluvium	2016	17,310,000	53.12		NDWR, 2018a
219	LEWIS 4	Alluvium	2017	680,000	2.09		NDWR, 2018a
219	LEWIS 4	Alluvium	2018	0	0.00		NDWR, 2018a
219	LEWIS 5	Alluvium	1993	51,249,000	157.28		Mifflin and Adenle, 1994
219	LEWIS 5	Alluvium	1994	73,265,000	224.84		Mifflin and Adenle, 1995
219	LEWIS 5	Alluvium	1995	64,863,000	199.06		Pohlmann, 1996

**Table C-3
Groundwater Production
(Page 28 of 30)**

Hydrographic Area	Well Name	Aquifer Material	Year	Production (gallons)	Production (af)	Comments	Source
219	LEWIS 5	Alluvium	1996	94,302,000	289.40		Pohlmann and Russell, 1997
219	LEWIS 5	Alluvium	1999	137,169,000	420.96		Kleinfelder, 2000
219	LEWIS 5	Alluvium	2000	139,206,000	427.21		NDWR, 2018a
219	LEWIS 5	Alluvium	2001	130,284,000	399.83		NDWR, 2018a
219	LEWIS 5	Alluvium	2002	53,624,000	164.57		NDWR, 2018a
219	LEWIS 5	Alluvium	2003	107,017,000	328.42		NDWR, 2018a
219	LEWIS 5	Alluvium	2004	79,409,000	243.70		NDWR, 2018a
219	LEWIS 5	Alluvium	2005	128,429,000	394.13		NDWR, 2018a
219	LEWIS 5	Alluvium	2006	161,538,500	495.74		NDWR, 2018a
219	LEWIS 5	Alluvium	2007	13,424,600	41.20		NDWR, 2018a
219	LEWIS 5	Alluvium	2008	119,084,000	365.46		NDWR, 2018a
219	LEWIS 5	Alluvium	2009	91,462,000	280.69		NDWR, 2018a
219	LEWIS 5	Alluvium	2010	121,690,000	373.45		NDWR, 2018a
219	LEWIS 5	Alluvium	2011	132,237,000	405.82		NDWR, 2018a
219	LEWIS 5	Alluvium	2012	54,629,000	167.65		NDWR, 2018a
219	LEWIS 5	Alluvium	2013	153,055,672	469.71		NDWR, 2018a
219	LEWIS 5	Alluvium	2014	242,481,080	744.15		NDWR, 2018a
219	LEWIS 5	Alluvium	2015	135,082,000	414.55		NDWR, 2018a
219	LEWIS 5	Alluvium	2016	134,160,000	411.72		NDWR, 2018a
219	LEWIS 5	Alluvium	2017	43,690,000	134.08		NDWR, 2018a
219	LEWIS 5	Alluvium	2018	0	0.00		NDWR, 2018a
219	MX-6	Carbonate	1993	45,945,000	141.00		MVWD, 2018
219	MX-6	Carbonate	1994	127,033,000	389.85		MVWD, 2018
219	MX-6	Carbonate	1995	122,008,000	374.43		MVWD, 2018
219	MX-6	Carbonate	1996	140,352,000	430.72		MVWD, 2018
219	MX-6	Carbonate	1997	100,087,000	307.16		MVWD, 2018
219	MX-6	Carbonate	1998	22,782,800	69.92		MVWD, 2018



**Table C-3
Groundwater Production
(Page 29 of 30)**

Hydrographic Area	Well Name	Aquifer Material	Year	Production (gallons)	Production (af)	Comments	Source
219	MX-6	Carbonate	1999	47,099,500	144.54		MVWD, 2018
219	MX-6	Carbonate	2000	42,504,600	130.44		MVWD, 2018
219	MX-6	Carbonate	2001	100,855,300	309.51		MVWD, 2018
219	MX-6	Carbonate	2002	100,644,540	308.87		MVWD, 2018
219	MX-6	Carbonate	2003	113,150,568	347.25		MVWD, 2018
219	MX-6	Carbonate	2004	69,423,000	213.05		MVWD, 2018
219	MX-6	Carbonate	2005	87,378,000	268.15		MVWD, 2018
219	MX-6	Carbonate	2006	324,073,000	994.54		MVWD, 2018
219	MX-6	Carbonate	2007	76,330,000	234.25		MVWD, 2018
219	MX-6	Carbonate	2008	125,056,000	383.78		MVWD, 2018
219	MX-6	Carbonate	2009	507,102	1.56		MVWD, 2018
219	MX-6	Carbonate	2010	3,645,192	11.19		MVWD, 2018
219	MX-6	Carbonate	2011	460,864	1.41		MVWD, 2018
219	MX-6	Carbonate	2012	57,878,530	177.62		MVWD, 2018
219	MX-6	Carbonate	2013	82,912,071	254.45		MVWD, 2018
219	MX-6	Carbonate	2014	0	0.00		MVWD, 2018
219	MX-6	Carbonate	2015	0	0.00		MVWD, 2018
219	MX-6	Carbonate	2016	0	0.00		MVWD, 2018
219	MX-6	Carbonate	2017	0	0.00		MVWD, 2018
219	MX-6	Carbonate	2018	0	0.00		MVWD, 2018
219	PERKINS PRODUCTION	Alluvium	1993	159,155,000	488.43		Mifflin and Adenle, 1994
219	PERKINS PRODUCTION	Alluvium	1994	217,349,000	667.02		Mifflin and Adenle, 1995
219	PERKINS PRODUCTION	Alluvium	1995	49,595,000	152.20		Pohlmann, 1996
219	PERKINS PRODUCTION	Alluvium	1996	147,494,000	452.64		Pohlmann and Russell, 1997
219	PERKINS PRODUCTION	Alluvium	1999	78,396,000	240.59		Kleinfelder, 2000
219	PERKINS PRODUCTION	Alluvium	2000	153,475,000	471.00		NDWR, 2018a

**Table C-3
Groundwater Production
(Page 30 of 30)**

Hydrographic Area	Well Name	Aquifer Material	Year	Production (gallons)	Production (af)	Comments	Source
219	PERKINS PRODUCTION	Alluvium	2001	159,530,000	489.58		NDWR, 2018a
219	PERKINS PRODUCTION	Alluvium	2002	236,304,000	725.19		NDWR, 2018a
219	PERKINS PRODUCTION	Alluvium	2003	228,829,000	702.25		NDWR, 2018a
219	PERKINS PRODUCTION	Alluvium	2004	170,913,000	524.51		NDWR, 2018a
219	PERKINS PRODUCTION	Alluvium	2005	238,755,000	732.71		NDWR, 2018a
219	PERKINS PRODUCTION	Alluvium	2006	252,270,000	774.19		NDWR, 2018a
219	PERKINS PRODUCTION	Alluvium	2007	231,534,000	710.55		NDWR, 2018a
219	PERKINS PRODUCTION	Alluvium	2008	218,774,000	671.39		NDWR, 2018a
219	PERKINS PRODUCTION	Alluvium	2009	210,205,000	645.10		NDWR, 2018a
219	PERKINS PRODUCTION	Alluvium	2010	189,468,000	581.46		NDWR, 2018a
219	PERKINS PRODUCTION	Alluvium	2011	207,057,000	635.43		NDWR, 2018a
219	PERKINS PRODUCTION	Alluvium	2012	246,502,000	756.49		NDWR, 2018a
219	PERKINS PRODUCTION	Alluvium	2013	330,911,000	1,015.53		NDWR, 2018a
219	PERKINS PRODUCTION	Alluvium	2014	258,918,323	794.59		NDWR, 2018a
219	PERKINS PRODUCTION	Alluvium	2015	113,142,000	347.22		NDWR, 2018a
219	PERKINS PRODUCTION	Alluvium	2016	0	0.00		NDWR, 2018a
219	PERKINS PRODUCTION	Alluvium	2017	23,170,000	71.11		NDWR, 2018a
219	PERKINS PRODUCTION	Alluvium	2018	0	0.00		NDWR, 2018a



References

- Converse Consultants, 2000, Groundwater level monitoring program 1999 annual report Moapa, Nevada, Prepared for Nevada Power Company, 14 p.
- Converse Consultants, 2001, Groundwater level monitoring program 2000 annual report Moapa, Nevada, Prepared for Nevada Power Company, 24 p.
- Converse Consultants, 2002, Production Well Construction and Testing, RW-2 Well, Coyote Spring Valley, Clark County, Nevada, Prepared for Nevada Power Company, June 2002.
- Converse Consultants, 2004, Groundwater level monitoring program 2003 annual report Moapa, Nevada, Prepared for Nevada Power Company, 26 p.
- Converse Consultants, 2005, Groundwater level monitoring program 2004 annual report Moapa, Nevada, Prepared for Nevada Power Company, 27 p.
- Kleinfelder, 2000, 1999 Hydrologic Impacts from Groundwater Withdrawals in the Upper Muddy River Valley, Nevada, February 2000, 22 p.
- Mifflin, M.D., Adenle, O.A., and Johnson, R.J., 1991, Effects of 1989 and 1990 Ground-Water Withdrawals on Muddy River Flows, Upper Muddy River Valley, Nevada, for Nevada Power Company, Las Vegas, Nevada, 160 p.
- Mifflin, M.D., and Adenle, O.A., 1994, 1993 Hydrologic Impacts from Groundwater Withdrawals in the Upper Muddy River Valley, Nevada.
- Mifflin, M.D., and Adenle, O.A., 1995, 1994 Hydrologic Impacts from Groundwater Withdrawals in the Upper Muddy River Valley, Nevada.
- Moapa Valley Water District, 2018, Personal communication of September 14 to J. Johnson (Southern Nevada Water Authority) regarding pumpage data, Overton, Nevada.
- MVVWD, see Moapa Valley Water District.
- NDWR, see Nevada Division of Water Resources.
- Nevada Division of Water Resources, 2001-2017, Nevada Division of Water Resources Pumpage Inventories as accessed at <http://water.nv.gov/PumpageInventoryFiles.aspx> during October, 2018.
- Nevada Division of Water Resources, 2018a, Nevada Division of Water Resources Pumpage Records as accessed at <http://water.nv.gov/Order1169Menu.aspx> during October, 2018.



- Nevada Division of Water Resources, 2018b, Personal communication of September, 19 from M. Dillon to J. Johnson (Southern Nevada Water Authority) regarding pumpage data, Carson City, Nevada.
- Pohlmann, K.F., 1996, Moapa Valley Ground-water Level Monitoring Program 1995 Annual Report: Desert Research Institute, Water Resources Center, Prepared for the Nevada Power Company, 48 p.
- Pohlmann, K.F., Russell, C.E., 1997, Moapa Valley Ground-water Level Monitoring Program 1996 Annual Report: Desert Research Institute, Water Resources Center, Prepared for the Nevada Power Company, 55 p.
- Pohlmann, K.F., Wert, B.L., 1992, Moapa Valley Ground-water Level Monitoring Program 1991 Annual Report: Desert Research Institute, Water Resources Center, Prepared for the Nevada Power Company, 72 p.
- Pohlmann, K.F., Wert, B.L., 1993, Moapa Valley Ground-water Level Monitoring Program 1992 Annual Report: Desert Research Institute, Water Resources Center, Prepared for the Nevada Power Company, 72 p.
- SNWA, see Southern Nevada Water Authority.
- Southern Nevada Water Authority, 2010, Monitoring Report for Southern Nevada Water Authority and Las Vegas Valley Water District's Groundwater Right Permits and Applications in Coyote Spring Valley, Hidden Valley, and Garnet Valley within Clark and Lincoln Counties, Nevada, 79 p.
- Western Elite, 2018, Personal communication of March 15, 2018 from D. Muaina to J. Watrus (Southern Nevada Water Authority) regarding details of BEDROC, LLC, Las Vegas, Nevada.



Geologic map of the east-central Meadow Valley Mountains, and implications for reconstruction of the Mormon Peak detachment, Nevada

E. Swanson and B.P. Wernicke

Division of Geological and Planetary Sciences, California Institute of Technology, Pasadena, California 91125, USA

ABSTRACT

The role of low-angle faults in accommodating extension within the upper crust remains controversial because the existence of these faults markedly defies extant continuum theories of how crustal faults form, and once initiated, how they continue to slip. Accordingly, for many proposed examples, basic kinematic problems like slip direction, dip angle while active, and magnitude of offset are keenly debated. A well-known example is the Miocene Mormon Peak detachment and overlying Mormon Peak allochthon of southern Nevada (USA), whose origin and evolution have been debated for several decades. Here, we use geologic mapping in the Meadow Valley Mountains to help define the geometry and kinematics of emplacement of the Mormon Peak allochthon, the hanging wall of the Mormon Peak detachment. Pre-extension structural markers, inherited from the east-vergent Sevier thrust belt of Mesozoic age, are well suited to constrain the geometry and kinematics of the detachment. In this study, we add to these markers a newly mapped Sevier-age monoclinial flexure preserved in the hanging wall of the detachment. The bounding axial surfaces of the flexure can be readily matched to the base and top of the frontal Sevier thrust ramp, which is exposed in the footwall of the detachment to the east in the Mormon Mountains and Tule Springs Hills. Multiple proxies for the slip direction of the detachment, including the mean tilt direction of hanging wall fault blocks, the trend of striations measured on the fault plane, and other structural features, indicate that it is approximately $S77^{\circ}W$ (257°). Given the observed structural separation lines between the hanging wall and footwall, this slip direction indicates 12–13 km of horizontal displacement on the detachment (14–15 km net slip), lower than a previous estimate of 20–22 km, which was based on erroneous assumptions in regard to the geometry of the thrust system. Based on a new detailed map compilation of the region and recently published low-temperature thermochronologic data, palinspastic constraints also preclude earlier suggestions that the Mormon Peak allochthon is a composite of diachronously emplaced, surficial landslide deposits. Although earlier suggestions that the initiation angle of the detachment in the central Mormon Mountains is $\sim 20^{\circ}$ – 25° remain valid, the geometry of the Sevier-age monocline in the Meadow Valley Mountains and other structural data suggest that the initial

dip of the detachment steepens toward the north beneath the southernmost Clover Mountains, where the hanging wall includes kilometer-scale accumulations of volcanic and volcanoclastic strata.

INTRODUCTION

In materials obeying Coulombic- or Byerlee-type failure laws, both the initiation and continued slip on normal fault planes dipping $<30^{\circ}$ is prohibited, assuming the maximum principal stress direction is subvertical (e.g., Collettini and Sibson, 2001; Axen, 2004). Extensional detachments (nominally, low-angle normal faults with displacements of kilometers to tens of kilometers) are widely described in the literature and currently accepted by most earth scientists as fundamental tectonic elements (e.g., Lister and Davis, 1989; Abers, 1991; Rigo et al., 1996; Chiaraluce et al., 2007; Bidgoli et al., 2015). However, they are problematic, not only from a mechanical point of view, but also from the point of view of historical seismicity, which is dominated by slip on planes steeper than 30° (e.g., Jackson and White, 1989; Wernicke, 1995; Elliott et al., 2010; Styron and Hetland, 2014). Thus, despite general acceptance, the very existence of low-angle normal faults continues to be challenged, in some cases even on geological grounds (e.g., Miller et al., 1999; Anders et al., 2006; Wong and Gans, 2008).

A frequently cited example of an upper-crustal normal fault that both initiated and slipped at low angle (20° – 25°) throughout its evolution is the middle Miocene Mormon Peak detachment of southern Nevada (USA), which localized near the frontal thrust ramp of the Cretaceous Sevier fold-and-thrust belt (Figs. 1 and 2; Wernicke et al., 1985; Wernicke and Axen, 1988; Axen et al., 1990; Wernicke, 1995; Axen, 2004; Anderson et al., 2010). This interpretation has been challenged by several workers who contend that the hanging wall of the detachment constitutes one or more large-scale landslide or rock avalanche deposits (e.g., Carpenter et al., 1989; Anders et al., 2006; Walker et al., 2007).

Because the detachment is superimposed on the frontal ramp of a décollement fold-and-thrust belt, numerous potential structural markers provide constraints on both the initial dip and net displacement along the detachment. The most important of these include (1) the axial surfaces of the frontal ramp syncline and anticline, (2) footwall cutoffs of Paleozoic and Mesozoic stratigraphic

SE ROA 37813

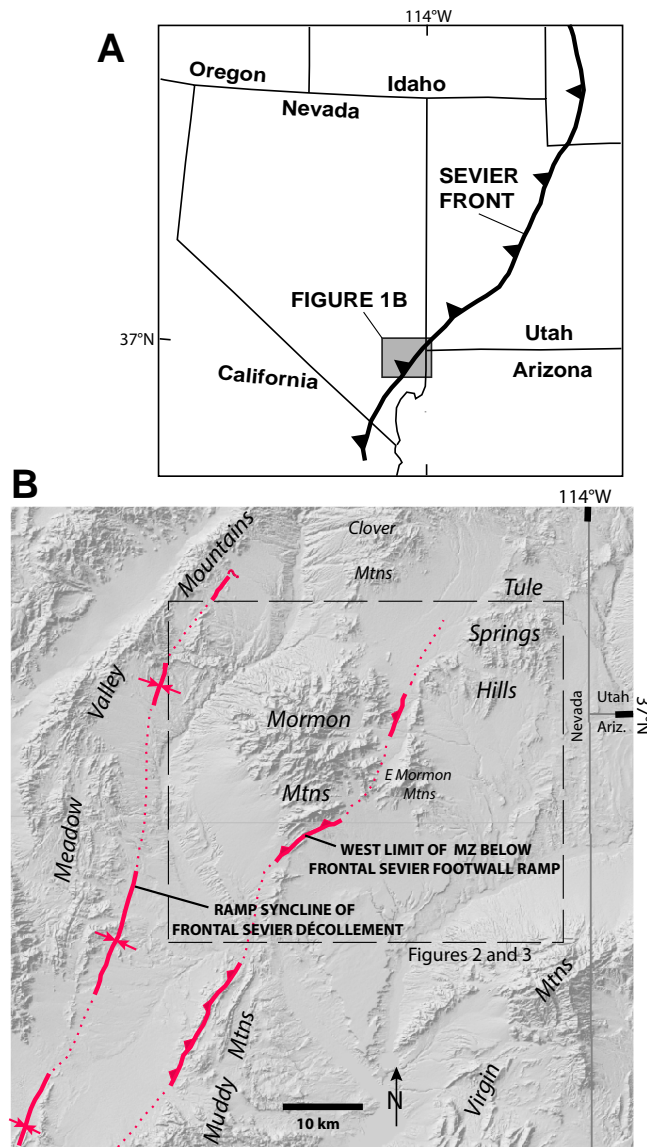


Figure 1. (A) Map showing the trace of the Sevier orogenic front (western USA) and location of B. (B) Shaded relief map showing the surface traces (solid) and subsurface projections (dotted) of the positions of selected elements of the frontal Sevier thrust fault in southern Nevada and environs, and the location of Figures 2 and 3. MZ—Mesozoic; Ariz.—Arizona.

units by the ramp zone, and (3) stratigraphic mismatch between the footwall and hanging wall of the detachment. Although some of these features were previously described in detail from the footwall of the detachment in the Mormon Mountains and Tule Springs Hills area (Fig. 1; Wernicke et al., 1985; Axen et al., 1990), potential offset counterparts in the Meadow Valley Mountains, immediately to the west of the Mormon Mountains, have to date only been mapped in reconnaissance (Tschanz and Pampeyan, 1970; Pampeyan, 1993). These maps depict a large-scale, monoclinial flexure in Paleozoic and Mesozoic strata overlain in angular unconformity by a succession of mid-Tertiary lacustrine and volcanic strata. Based on the regional geology of the frontal Sevier ramp zone in southern Nevada (Longwell et al., 1965; Burchfiel et al., 1974, 1982, 1997; Carr, 1983; Axen, 1984), the monoclinial flexure constrains the geometry of the frontal thrust ramp that generated it (e.g., Axen et al., 1990). In this paper, we present new 1:24,000-scale mapping, cross-sections, and structural reconstructions of the central Meadow Valley Mountains, targeted toward documenting the heretofore poorly constrained geometry of the frontal ramp zone above the detachment. We then examine these data in light of previous structural and thermochronological studies in the Mormon Mountains and Tule Springs Hills and explore implications for the existence, geometry, and kinematics of the Mormon Peak detachment as a typical low-angle normal fault.

■ GEOLOGIC SETTING

The Sevier front in the southern Nevada region (Fig. 1) is primarily expressed by a décollement thrust formed in Middle Cambrian dolostones, which can be traced along a strike length of >200 km (Fig. 1; Burchfiel et al., 1982; Bohannon, 1983; Axen et al., 1990). In the northern 50 km of exposure, the thrust trace is comparatively straight, striking NNE (Fig. 1), except where strongly overprinted by Miocene fault systems, such as the Mormon Peak detachment and other normal faults (Fig. 2). The most readily identifiable structural element along the entire trace of the thrust is the frontal ramp, where the thrust cuts upsection in the footwall from lower Paleozoic to Jurassic strata. The ramp zone is variably accompanied by a footwall syncline and thin duplex slices. The hanging wall of the thrust is invariably detached within a restricted stratigraphic interval within Middle Cambrian dolostones, near the boundary between the Papoose Lake and Banded Mountain Members of the Bonanza King Formation (Burchfiel et al., 1982; Bohannon, 1983; Wernicke et al., 1985; Axen et al., 1990).

The three structural elements of Sevier age that are most useful as potential offset markers along the Miocene detachment are (1) the base of the ramp and associated ramp syncline; (2) the intersection of the ramp and the top of footwall Mississippian strata; and (3) the top of the ramp and associated ramp anticline (Fig. 3). Based on previous mapping, the positions of the first two of these elements is well known. The top of the ramp in the footwall of the detachment is also well exposed, but the corresponding ramp anticline in the hanging wall of the detachment had not been recognized (Fig. 3).

SE ROA 37814

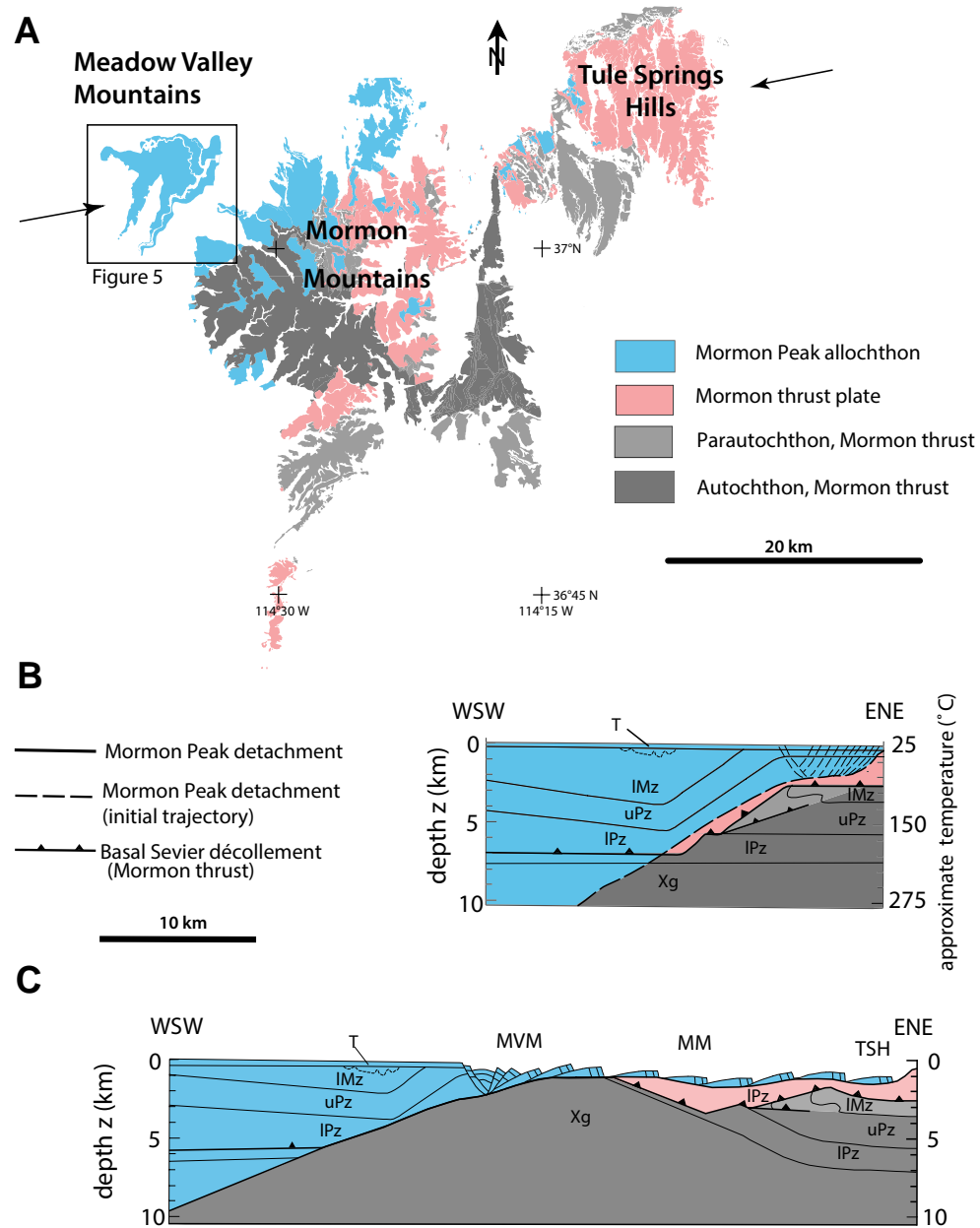


Figure 2. Structural map (A) and schematic cross-sections, restored (B) and un-restored (C) with respect to Miocene extension, of the Meadow Valley Mountains (MVM), Mormon Mountains (MM), and Tule Spring Hills (TSH) of Nevada. Arrows show the cross-section location. Xg—Proterozoic gneiss; IPz—lower Paleozoic strata; uPz—upper Paleozoic strata; IMz—lower Mesozoic strata; T—Tertiary strata. Map location is shown on Figure 1B. Black outline in A indicates the area of Figure 5.

SE ROA 37815

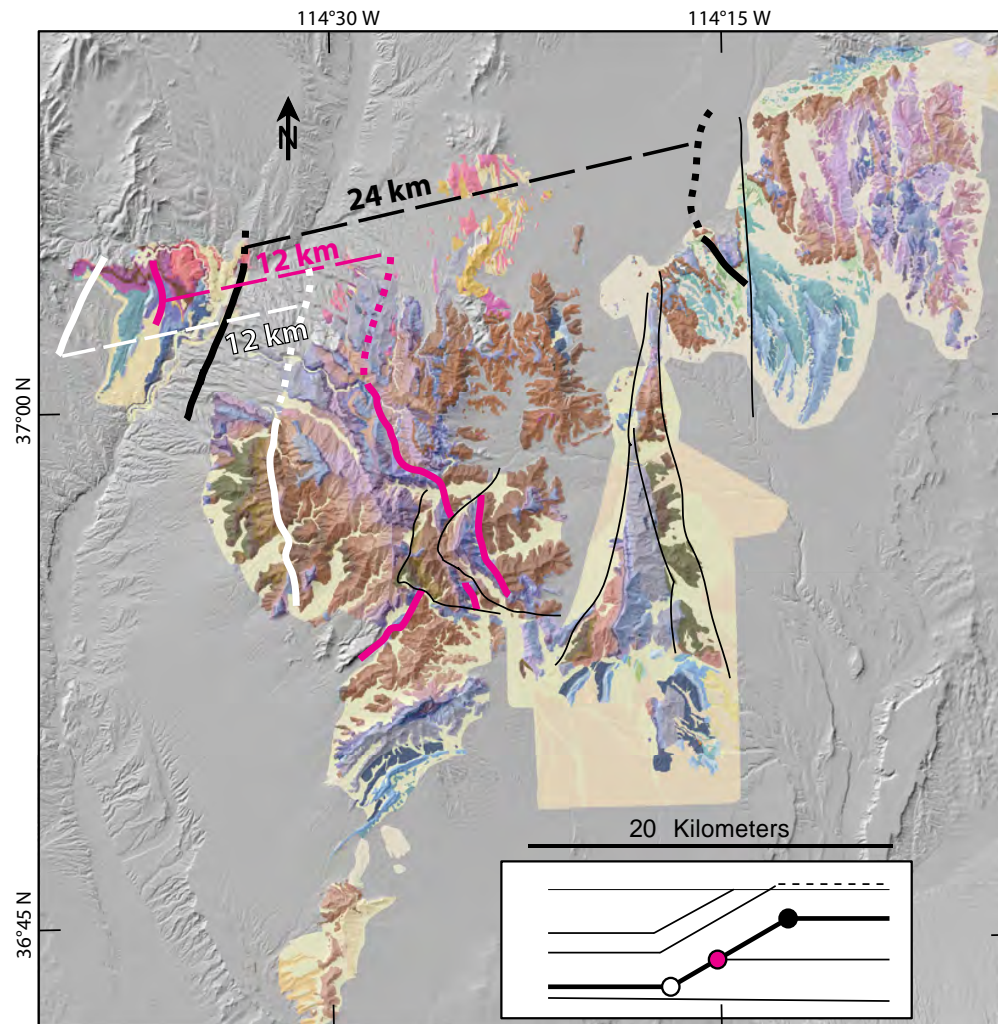


Figure 3. Map of the same area in Figure 2A showing locations of the Sevier ramp syncline (white line), thrust truncation of the top of Mississippian strata in the footwall (pink line), and the ramp anticline (thick black line). The three lines in north-western corner of the map are above the detachment; lines in the central and eastern part of the map are below the detachment. Lines are dotted where projected. Thin black lines show major post-detachment normal faults. Dashed lines show offsets of structural features along the Mormon Peak detachment slip direction. Inset shows a schematic cross-section of a thrust ramp, showing positions of the offset thrust ramp features. Colors: Olive, Proterozoic basement; browns, Cambrian–Ordovician; lavender and blues, Devonian–Permian; greens, Mesozoic; purples and orange, Tertiary; yellow, Quaternary.

The Paleozoic and Mesozoic strata involved in thrusting lie along the eastern margin of the Cordilleran miogeocline. The hanging wall of the frontal thrust contains a section transitional between thin cratonic facies to the east and thick continental shelf deposits to the west (e.g., Burchfiel et al., 1974). Among a number of systematic across-strike stratigraphic features near the thrust ramp, the westward erosive pinchout of some 400 m of Permian car-

bonates (Toroweap and Kaibab Formations), below an unconformity at the base of the Lower Triassic Virgin Limestone Member of the Moenkopi Formation, is the most conspicuous (Burchfiel et al., 1974; Tschanz and Pampeyan, 1970). The pinchout occurs within the west-facing monoclinial flexure formed by the ramp and is best exposed in the central Meadow Valley Mountains and the Spring Mountains to the southwest.

SE ROA 37816

The Mormon Mountains are a topographic and structural dome, veneered by klippen of the Mormon Peak detachment (Fig. 2). It is geometrically similar to a Cordilleran metamorphic core complex, except the level of footwall exhumation has not unroofed metamorphic rocks to the surface (Wernicke et al., 1985; Bidgoli et al., 2015). The footwall geology of the detachment is a 6–8-km-thick, variably east-tilted crustal section through the frontal thrust ramp zone. Below the detachment, the structurally deeper, western part of the Mormon Mountains exposes autochthonous Proterozoic basement and nonconformably overlying Cambrian through Mississippian strata. In the central part of the range, Middle Cambrian strata of the Cretaceous Mormon thrust plate (as distinct from the Tertiary Mormon Peak allochthon, described below) are thrust over Mississippian strata. In the eastern part of the range, the thrust ramps upward at an angle of 30°–40° relative to bedding in the autochthon (Fig. 2). Both the thrust and the Mormon Peak detachment are rotated eastward and cut by a younger set of west-dipping normal faults, known as the Tule Springs detachment system, described further below (Axen et al., 1990; Axen, 1993).

The hanging wall of the Mormon Peak detachment, hereafter referred to as the Mormon Peak allochthon, is composed of moderately to strongly tilted imbricate normal fault blocks (Fig. 2). The fault blocks are composed primarily of Cambrian through Pennsylvanian carbonates, all derived from the Mormon thrust plate. Along the northern flank of the range, the Pennsylvanian carbonates are concordantly overlain by interstratified gravels, rock avalanche deposits, and volcanic strata of Tertiary age, locally as much as 2000 m thick but generally much thinner (Anderson et al., 2010). Most of these strata are coeval with eruption of the middle Miocene Kane Wash Tuff (ca. 14–15 Ma), but locally, strata as old as the late Oligocene Leach Canyon Member of the Condor Canyon Formation (ca. 24 Ma) are preserved in the Tertiary section (Anderson et al., 2010). Apatite and zircon (U-Th)/He ages indicate that the footwalls of both the Tule Springs and Mormon Peak systems were unroofed primarily in middle Miocene time (ca. 14 Ma), contemporaneous with the extrusion of the Kane Wash tuffs and emplacement of rock avalanche deposits in the hanging wall of the Mormon Peak detachment (Bidgoli et al., 2015).

Stratal tilt directions within the Mormon Peak allochthon form a systematic pattern. The eastern and northern part of the allochthon contains blocks tilted to the east or northeast, and the westernmost part contains blocks tilted to the west or southwest (Figs. 2 and 4). Where the boundary between the east- and west-tilted domains intersects the northwest boundary of the Mormon Mountains, Tertiary strata are disconformable on Bird Spring Formation strata and exhibit both east and west tilts along with the underlying Paleozoic strata. Therefore, the difference in tilt directions within the allochthon in the Mormon Mountains is primarily a consequence of Miocene deformation (Anderson et al., 2010).

The Meadow Valley Mountains, immediately to the west of the Mormon Mountains (Figs. 1, 2 and 5), are separable into two distinct structural domains on the basis of the age of the youngest strata below the basal Tertiary unconformity. In the southern part of the range, the ramp syncline is cored by folded upper Paleozoic strata no younger than the Permian Kaibab Formation, overlain in angular unconformity by the Kane Wash Tuff (Pampeyan, 1993).

Farther north, strata as young as the Jurassic Kayenta Formation are preserved beneath the Tertiary unconformity, suggesting at least a 1500 m difference in Mesozoic structural level near the axis of the syncline. In the northern area (central Meadow Valley Mountains), strata on the east limb of the syncline are overlain in angular unconformity by the Leach Canyon Member and younger strata. Toward the east, the sub-Tertiary unconformity progressively cuts downsection to the Bird Spring Formation of late Paleozoic age. Tertiary strata in the easternmost Meadow Valley Mountains lie in mild angular unconformity on the Bird Spring Formation. Still farther east in the northern Mormon Mountains, this same relationship (Oligocene unconformable on Bird Spring strata or overlying Permian red beds) holds for all exposures of Tertiary strata (Anderson et al., 2010).

METHODS

Geologic mapping of part of the Meadow Valley Mountains was done during the spring of 2011 and spring of 2012, using 1:12,000-scale base maps (Fig. 5). The following source geologic maps and unpublished field mapping were compiled and digitized in ArcGIS software: Meadow Valley Mountains mapping from this report (Fig. 5), Wernicke et al. (1985), Axen et al. (1990), Axen (1991, 1993), Taylor (1984), Ellis (1985), Olmore (1971), Skelly (1987), and Anderson et al. (2010); unpublished mapping in the northeastern Mormon Mountains (G. Axen, M. Skelly, and B. Wernicke, 1987); and unpublished mapping in the northwestern Mormon Mountains (B. Wernicke, B. Ellis, and W. Taylor, 1983). Stereograms of bedding and foliations within the field areas were prepared using the freeware Stereonet 8 program (Cardozo and Allmendinger, 2013; Allmendinger et al., 2013).

STRUCTURES

Faults within the mapped areas of the Meadow Valley Mountains (Fig. 5) are predominantly NNE- to NNW-trending high-angle normal faults with moderate offsets (tens to hundreds of meters). Tertiary volcanic units are truncated by these faults, indicating a Tertiary age. There is a tight, pre-Tertiary anticline with a northwest trend in the central part of the mapped area. Subvertical orientations of the Permian strata in the core of the anticline directly underlie subhorizontal Tertiary strata.

The general orientations of strata within the southwestern half of the map area are different from those in the northeastern half, with the transition occurring across a zone of north-south-trending faults located in the middle of the map area (Fig. 5). The Paleozoic and Mesozoic units in the southwestern half form a homocline that on average dips ~40°NW, overlain by subhorizontal Tertiary strata. In the northeastern half, dips of pre-Tertiary strata are more variable but average 10°–20°NE. Tertiary strata generally dip 25°–50°NE, somewhat more steeply than underlying pre-Tertiary strata.

SE ROA 37817

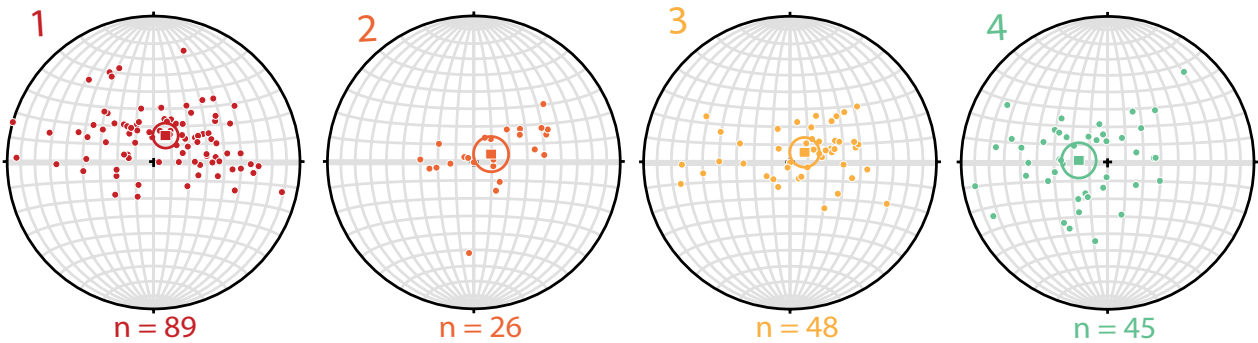
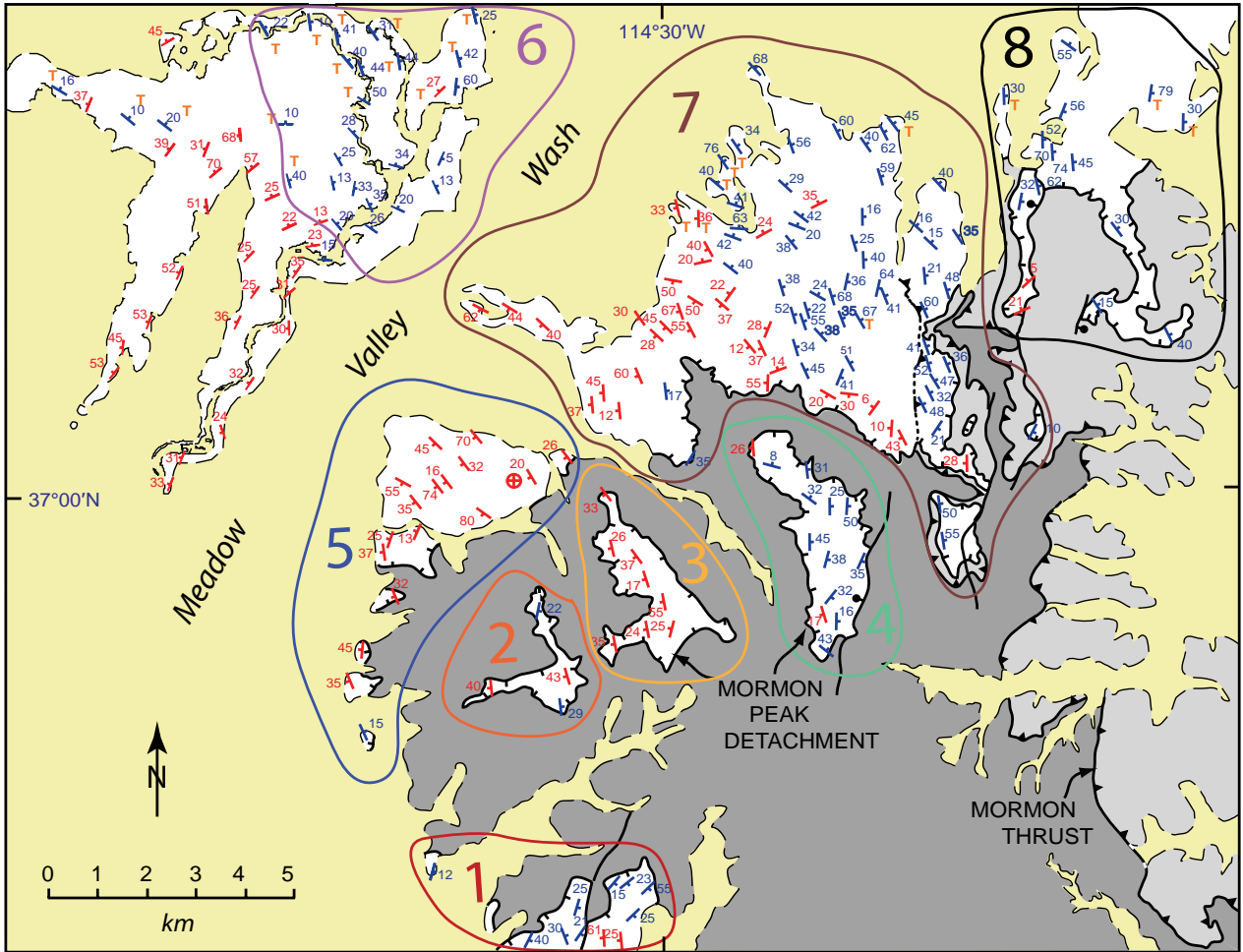
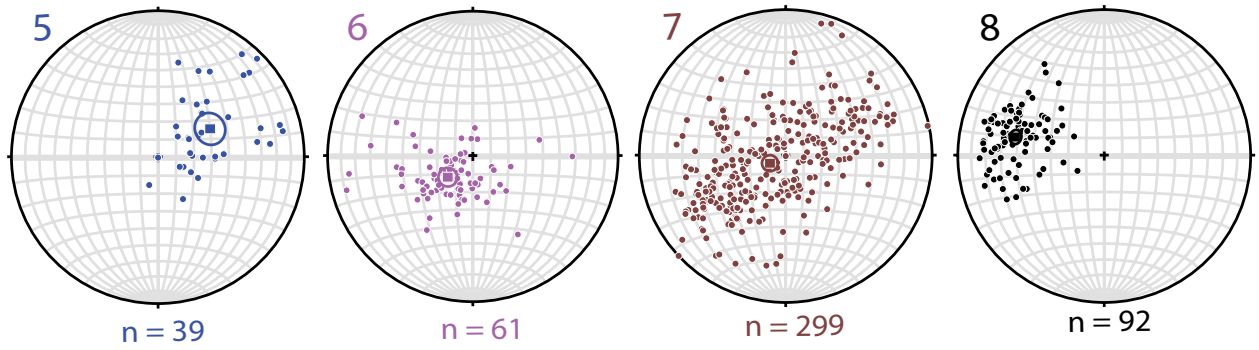


Figure 4. Map showing representative orientations of hanging-wall strata of the Mormon Peak detachment, with stereograms showing all measurements, grouped by areal domains. On the map, red symbols indicate west-dipping strata; blue symbols indicate east-dipping strata. Measurements within Tertiary strata are labeled with an orange T. Stereonet plots show orientations of poles to bedding, with each areal domain marked on the map by a number and boundary of the same color.

SE ROA 37818

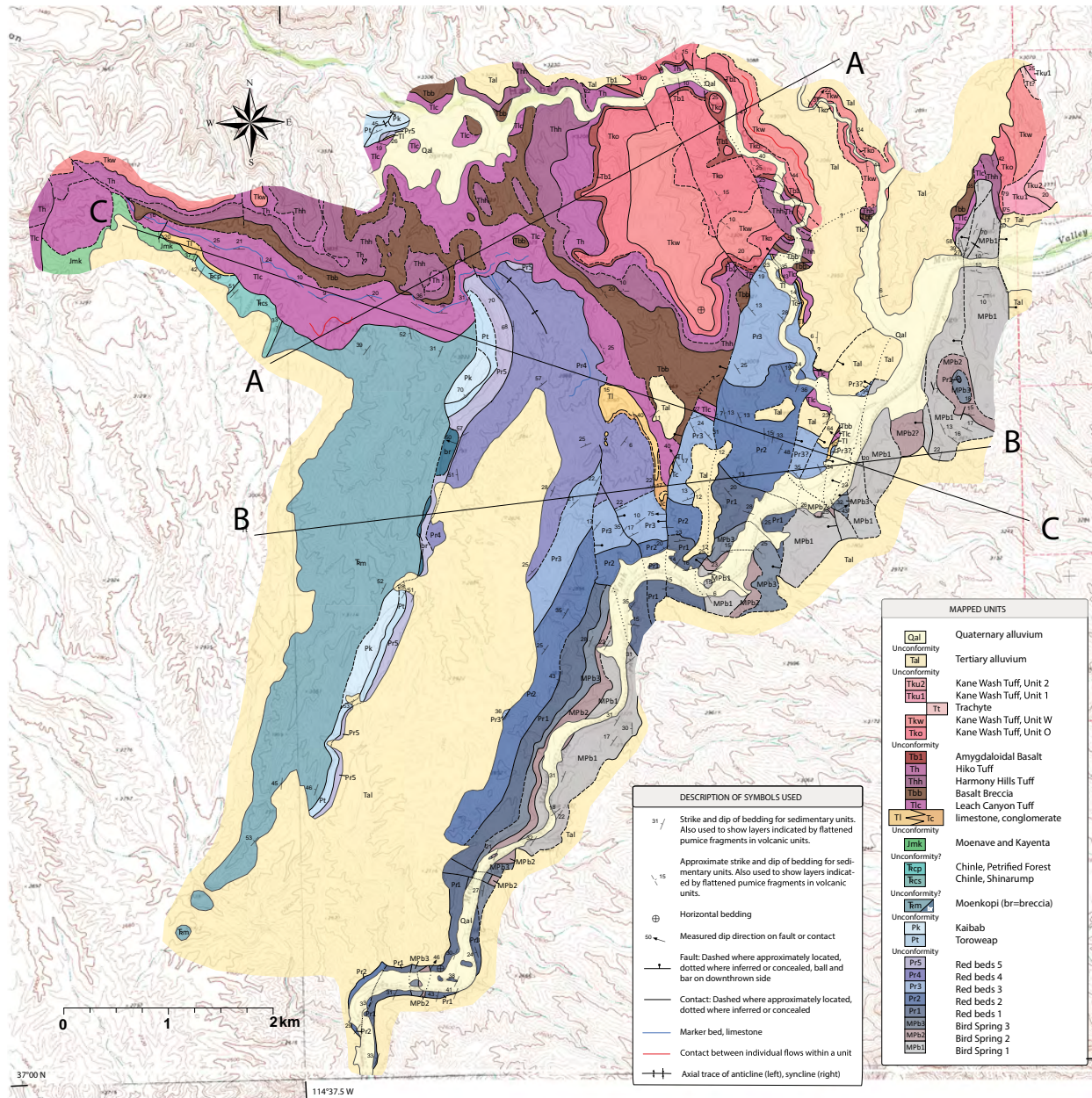


Figure 5. Geologic map of the Meadow Valley Mountains. All units are stratified, with ages indicated using standard North American symbols; see Appendix for unit descriptions. See Figure 2 for location. Cross-sections are shown in Figure 6.

SE ROA 37819

The oldest exposed Tertiary units are assigned to the lower Quichapa Group (Leach Canyon and Bauers Members of the Condor Canyon Formation), locally overlying basal Tertiary conglomerate or lacustrine limestone (Pampeyan, 1993, and references therein). Leach Canyon tuffs overlie northwest-tilted Triassic and Jurassic formations in the west and cut downsection to the middle of the Permian red beds in the east. In the northeastern corner of the mapped area (Fig. 5), the Leach Canyon and Harmony Hills tuffs directly overlie Bird Spring strata, but it is unclear whether the contact is depositional or faulted. There appears to be a slight angular unconformity beneath and within Kane Wash units in the north-central part of the mapped area, suggesting that some tilting may have occurred between individual flows, but the difference in dip is too slight to be definitive.

Two cross-sections drawn perpendicular to the strike of Tertiary bedding (Figs. 6A and 6C) show the increase in Tertiary-age tilting toward the east. Reconstructions that untilt Tertiary strata and restore Tertiary fault offsets (Figs. 6B and 6D) show an eastward decrease in angle between the pre-Tertiary and Tertiary strata from west to east. Thus the area records the formation of a WNW-facing monoclinical flexure prior to deposition of the Tertiary section (Figs. 6B and 6D). After deposition, the flexure was overprinted by a NNW-trending extensional rollover structure, imparting an ENE dip onto the initial shallow west dip of the pre-Tertiary flexure. The pre-Tertiary monoclinical flexure is better shown by a cross-section, C-C', drawn perpendicular to the strike of the monoclinical section (Fig. 6E). The section and its reconstruction (Fig. 6F) show the true dips of the Paleozoic and Mesozoic section before and after Tertiary tilting. They also reveal that the structural relief of the monocline is at least 4100 m, discussed in more detail below.

As noted above, orientations of bedding in the hanging wall of the Mormon Peak detachment show an abrupt transition from predominantly east dips to predominantly west dips in both the Meadow Valley Mountains and the Mormon Mountains (Fig. 4). The boundary between the two domains has an apparent separation of ~5 km left-laterally across a narrow swath of alluvial cover in Meadow Valley Wash (Fig. 4). The strike of bedding in fault blocks on the northwestern edge of the Mormon Mountains, closest to Meadow Valley Wash, is more westerly than in the interior of the Mormon Mountains, with the dip direction transitioning gradually between the two areas (Fig. 4).

As a potential proxy for the slip direction on the detachment, we compiled Tertiary tilt directions in the Mormon Peak allochthon, subdivided into eight domains (including the eastern domain in the Meadow Valley Mountains), with each domain denoted with variously colored and numbered enclosures in Figure 4. We do not include dips of hanging-wall strata in the western domain in the Meadow Valley Mountains, because these strata lie in sharp angular unconformity below subhorizontal Tertiary strata, and therefore their dips do not record the Tertiary tilt direction of fault blocks. In contrast, as mentioned earlier, west-dipping strata in the Mormon Mountains do contain Tertiary strata that are as strongly tilted westward as the underlying Paleozoic strata, and hence these are included in the compilation. Each klippe of the detachment is shown separately, except those with <20 measurements, which were com-

bined with nearby klippen. Stereograms showing a total of 717 attitudes of bedding define a fabric in tilt directions oriented ENE-WSW. The main exception to this overall pattern is the strong east to ESE tilt in the northernmost Mormon Mountains (domain 8, Fig. 4).

The pre-Tertiary monoclinical flexure is apparent not only in the restorations of cross-sections through the Meadow Valley Mountains (Figs. 6B, 6D, and 6F), but also in stereographic restoration of Tertiary tilting of pre-Miocene strata in the greater hanging-wall area of the Mormon Peak allochthon (Fig. 7). Domains 7 and 8 (Fig. 4) in the northern Mormon Mountains, and the northeastern and southwestern portions of the Meadow Valley Mountains (domain 6 and the unnumbered area, respectively, in Fig. 4), all have Tertiary strata in depositional contact with underlying Paleozoic units. We calculated the mean Tertiary attitude in each domain and used it to estimate attitudes of bedding in Paleozoic and Mesozoic units in each domain prior to Tertiary deposition (Fig. 7). These restored dips define a northwest-facing monocline, with dips shallowing to a subhorizontal orientation in the northwestern Mormon Mountains (domain 7, Fig. 4). Restored dips in the westernmost Meadow Valley Mountains average ~35°NW, in the eastern Meadow Valley Mountains ~20°NW, and in the northwestern Mormon Mountains <10°. The reconstructed dips from the northernmost Mormon Mountains (domain 8) vary from this pattern, dipping ~25°S. Regardless of this complexity, the observation that the Tertiary section typically rests on the lower part of the Bird Spring Formation throughout the northern Mormon Mountains suggests limited overall pre-Tertiary structural relief east of the monoclinical flexure.

We can reconstruct offset on the Mormon Peak detachment at the latitude of the study area by relating the footwall and hanging-wall structural cutoffs (Fig. 3). The footwall cutoffs are exposed at the surface in the Mormon Mountains, and the location of hanging-wall cutoffs may be estimated by the downward projection of structural elements in the cross-sections in the Meadow Valley Mountains (Fig. 8). The geology of the Mormon Mountains and Tule Springs Hills in the footwall of the Mormon Peak detachment is modified from Axen et al. (1990), and the Meadow Valley Mountains geology is based on structural cross-sections from this study.

DISCUSSION

Transport Direction and Timing of Emplacement of the Mormon Peak Allochthon

Tilt Directions

Because the offset features are planar and therefore only permit an estimate of fault separation, proxies for the direction of displacement are necessary in order to estimate the net offset across the Mormon Peak detachment. The average of a number of independent proxies for slip direction suggests that the transport direction is ~S77°W (Table 1). The first proxy is Tertiary tilt

SE ROA 37820

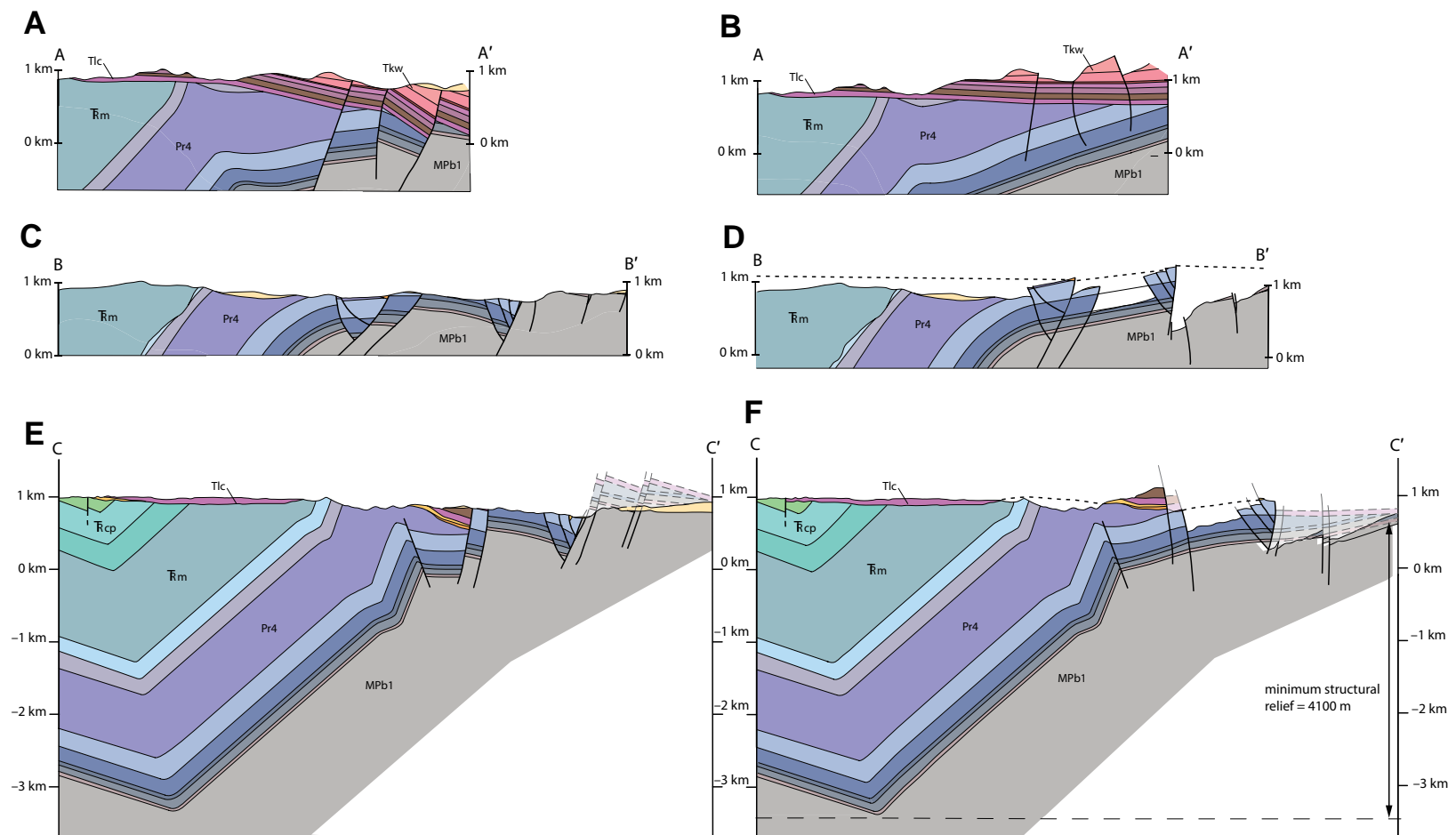


Figure 6. Cross-sections through the Meadow Valley Mountains, and reconstructions to early Miocene structural geometries. See Figure 5 for cross-section locations and legend. (A) Cross-section along line A-A'. (B) Reconstruction of A-A'. (C) Cross-section along line B-B'. (D) Reconstruction of B-B'. (E) Cross-section along line C-C'. (F) Reconstruction of C-C'. Dashed lines indicate projected position of base of Tertiary volcanic section. No vertical exaggeration. Thin dashed lines near point C' indicate positions of late Paleozoic units projected onto the cross section.

directions within the Mormon Peak allochthon, based on the compilation of 717 attitudes of bedding within the hanging wall of the detachment that indicate the tilt directions within the Mormon Peak allochthon (Fig. 4). Studies of imbricate normal fault blocks suggest that the mean tilt direction tends to parallel slickenlines and other transport indicators (e.g., Anderson, 1971; Davis et al., 1980; Davis and Hardy, 1981). Thus, the tilt direction of bedding is often used as a proxy for maximum elongation direction in extensional allochthons,

and for the transport direction on underlying detachments, assuming bedding was subhorizontal at the onset of extension.

The tilt directions reveal a strong preferred orientation. Figure 9A shows the modern orientations of pre-Tertiary strata that were subhorizontal prior to extension (i.e., excluding units from the Sevier thrust ramp in the southwestern Meadow Valley Mountains). The density contours and maximum density of these data show a well-defined ENE-WSW trend, with the best-fit

SE ROA 37821

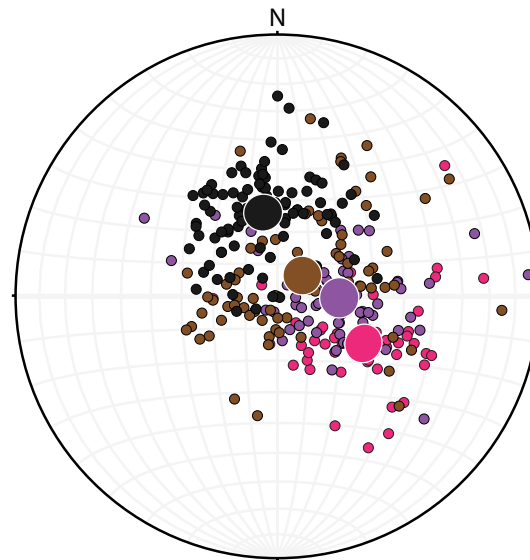


Figure 7. Restored poles to bedding in pre-Tertiary strata, taken from areas where Tertiary strata are exposed in the Mormon Peak allochthon. From west to east, these areas include the western Meadow Valley Mountains (magenta), domain 6 from Figure 4 (purple), domain 7 from Figure 4 (brown), and domain 8 from Figure 4 (black). Attitudes were restored by rotating nearby Tertiary units to the horizontal about the strike of bedding. The larger circles are the average orientation within each group, with the circle diameters scaled to the scatter within the data set. Data define a northeast-trending anticlinal flexure. Sources: this study (purple and magenta groups), B.P. Wernicke et al. (unpub. data; brown group), and Anderson et al. (2010; black group).

circle through them oriented 251°/86° (first number indicates azimuth of dip direction or plunge direction; second number indicates dip or plunge) (Fig. 9B), suggesting a maximum elongation direction and slip direction along the detachment of S71°W (azimuth 251°). In addition, the averages for each spatial domain (Fig. 4) define an array that also aligns along an ENE-WSW trend of S65°W (245°), excluding domain 8. Domain 8 is at the extreme northern edge of the Mormon Mountains. It contains a larger proportion of syntectonic strata and may have experienced complex vertical-axis rotations due to Tertiary strike-slip faulting and/or folding, as suggested by Anderson et al. (2010) and discussed further below.

In Figure 9C, poles to bedding for 90 attitudes measured in Tertiary units in the Mormon Peak allochthon are plotted, along with domain averages (Fig. 4). A unimodal maximum in poles to bedding occurs at S69°W 60° (239°/60°), corresponding to a mean bedding attitude of N31°W, 30°NE. This implies an extension direction and transport of the allochthon of S59°W (239°) (Fig. 9D).

Fault Striations and the Radial Sliding Model

Twenty-six (26) striation measurements on or near the detachment plane, broadly distributed over the surface trace of the Mormon Peak detachment in the Mormon Mountains, are shown on Figure 10 (Walker, 2008). The east-plunging determinations were all measured on the east-dipping trace of the detachment in the eastern Mormon Mountains. As noted above, the detachment there was rotated eastward in Miocene time along imbricate normal fault blocks of the Tule Springs detachment system (Axen et al., 1990; Axen, 1993). The Tule Springs system faults cut, and are therefore slightly younger than, eastern exposures of the Mormon Peak detachment.

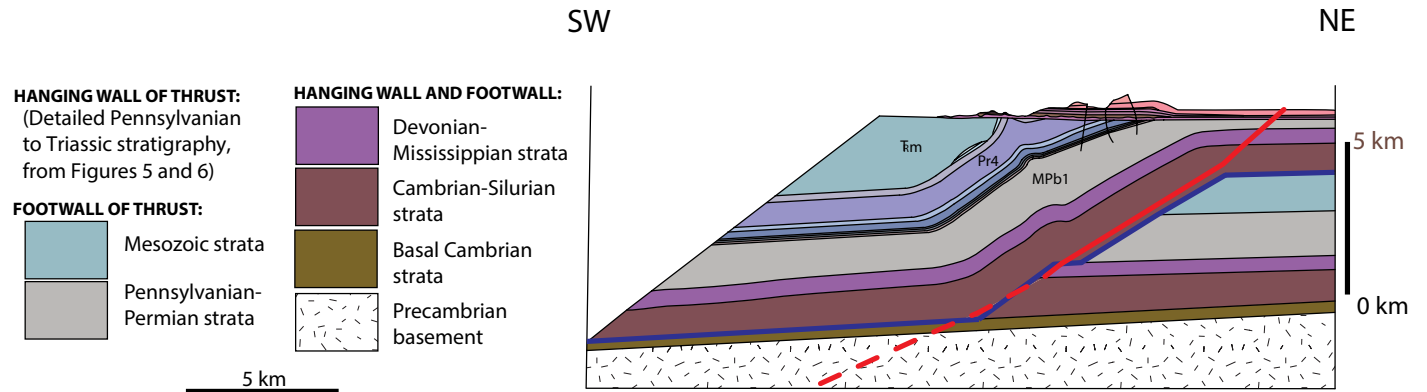


Figure 8. Regional reconstruction of pre-Tertiary structures in the Meadow Valley Mountains, Mormon Mountains, and Tule Springs Hills, drawn parallel to the WNW-ESE extension direction. Blue line is the Mormon thrust; red line is the Mormon Peak detachment. The thrust ramp shown with apparent dip of 32°; true WNW dip is 40°. Hanging-wall geology is based Figures 6B and 6F. Detachment footwall geometry modified from Axen et al. (1990).

SE ROA 37822

TABLE 1. SUMMARY OF SLIP DIRECTION PROXIES, MORMON PEAK DETACHMENT

Data type	Inferred slip direction
Tilt direction in hanging-wall Paleozoic strata	251°
Tilt direction in hanging-wall Tertiary strata	239°
Mean trend of striations on fault surface	270°
Obtuse bisectrix, footwall conjugate fault fabric	260°
Intersecting fault offset direction	262°
Long axis of dome in detachment	250°

Walker et al. (2007) suggested that each of the individual klippen of the Mormon Peak allochthon represents an individual rock avalanche or surficial gravity slide mass that moved at a different time radially off of the modern dome, defined by the topography and by structural contours of the Mormon Peak detachment. They based their hypothesis on the claim that the striations everywhere indicate motion of the klippen down the modern dip direction of the detachment.

Across the eastern half of the topographic and structural dome, the substrate of the detachment is the Mormon thrust plate. The radial gravity slide hypothesis of Walker et al. (2007) is readily falsified by the observation that the oldest strata at the base of the fault blocks across the eastern half of the dome are everywhere younger than strata in the footwall of the detachment. Across this area, the detachment is a footwall décollement within the Bonanza King Formation, 100–200 m stratigraphically below the base of the Dunderberg Shale Member of the Upper Cambrian Nopah Formation (see Axen [1993] for stratigraphic nomenclature). The east-tilted normal fault blocks above the detachment across the eastern two-thirds of the Mormon Mountains are predominantly composed of Ordovician through Pennsylvanian strata, unconformably overlain by Tertiary volcanic and sedimentary strata, with only local preservation of the upper part of the Nopah Formation in some of the fault blocks, mainly in the westernmost blocks well to the west of the range crest (Fig. 11). The detachment level at the base of the hanging-wall blocks is thus stratigraphically at least 100–200 m above the basal beds of “unit Cbb4” (the black marker horizon in the upper part of the Banded Mountain Member of the Bonanza King Formation, as defined in Wernicke [1982], Wernicke et al. [1985, 1989], Axen et al. [1990], and Axen [1993]), ruling out derivation of any of these blocks to the west of their present location, as required by the gravity-slide model. The footwall décollement in unit Cbb4 can be confidently traced on geologic maps from the northeasternmost Mormon Mountains across the East Mormon Mountains and Tule Springs Hills to Jumbled Mountain (Axen et al., 1990; Axen, 1991, 1993). In the Tule Springs Hills, a few kilometers east of the Jumbled Mountain exposure, the detachment is observed to cut rapidly upsection in its footwall, from its unit Cbb4 décollement upward across the Dunderberg Shale Member and into Upper Cambrian and younger strata (Axen, 1993).

Hence, basic palinspastic constraints define a simple stratigraphic separation across the detachment, independent of arguments based on offset

structural markers of Sevier age. This stratigraphic separation constraint indicates that the pre-detachment substrate of fault blocks in the Mormon Peak allochthon lies in the Tule Springs Hills, east of the footwall cutoff of the Dunderberg Shale. This constraint requires the allochthon in its entirety to have been displaced westward, not radially off the crest of the present structural and topographic dome in the Mormon Mountains. The dome lacks a substrate that is compatible for the restoration of the hanging-wall blocks, precluding the top-east motions required by the radial model.

This simple “stratigraphic separation” argument is supported by the observations that (1) the tilted fault blocks in the eastern Mormon Mountains are bounded by faults that cut the Mormon Peak detachment, restoring its initial trajectory to dip uniformly westward (Wernicke et al., 1985; Axen et al., 1990); (2) the structural continuity between the northwest Mormon Mountains and the Meadow Valley Mountains, both of which are composed of ENE-tilted fault blocks of Kane Wash Tuff and older Tertiary strata resting unconformably on the lower part of the Bird Spring Formation (Figs. 3, 4, 5, and 6); (3) all of the blocks in the Mormon Peak allochthon, which are continuously exposed across the northern flank of the range and do not contain any thrust repetitions, are derived from the hanging wall of the Mormon thrust, as noted above; (4) the overall structural continuity of >700 measurements of stratal rotations in the allochthon form a coherent fabric traceable across all of the klippen (Figure 4); and (5) in both hanging wall and footwall, the structural and stratigraphic position of the detachment descends monotonically to the west.

A further difficulty with the surficial sliding model is the presence of a ~2000-m-thick Tertiary section within the Mormon Peak allochthon in the northernmost Mormon Mountains and southern Clover Mountains (Fig. 1; Anderson et al., 2010). This section is steeply tilted to the east and contains within it interstratified rock avalanche deposits. The unlikely implication of the gravity slide model is, therefore, that a slide block near the crest of the dome was, at first, a kilometer-scale depocenter receiving scarp breccias. Then at some later time it was uplifted and then slid into a newly developed depression.

The radial sliding model is also inconsistent with the recent thermochronometric data. These data indicate that the footwall of the detachment in the core of the dome was near the base of the partial retention zone for helium in zircon at ca. 14 Ma (~180 °C) and subsequently unroofed from paleodepths of 5–7 km (Bidgoli et al., 2015), depending on the geothermal gradient. This estimate of paleodepth confirms the cross-sectional reconstructions of Axen et al. (1990). The fault blocks in the allochthon represent at most the uppermost 2 km of the crust in pre-extension, middle Miocene time (e.g., Wernicke, 1995). Any model in which unroofing occurs by intra-range motion of putative slide masses therefore does not account for the magnitude of unroofing.

Against these straightforward kinematic and thermochronological arguments, the only evidence cited in support of radial gravity sliding are the 26 slickenline data, of which ~11 measurements (about 40% of the data collected, mainly along the northwestern flank of the range) plot in the northwest or

SE ROA 37823

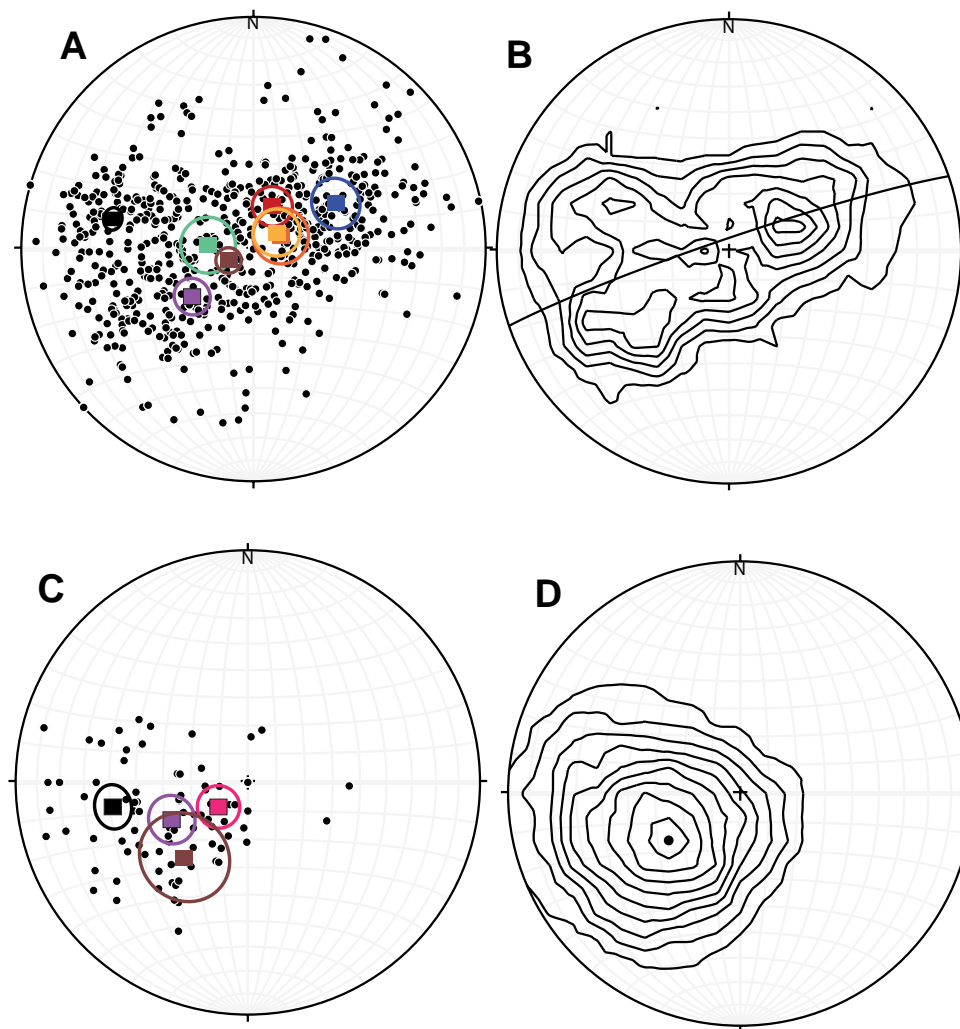


Figure 9. Equal-angle stereograms of orientations of strata within the hanging wall of the Mormon Peak detachment. (A) Poles to bedding of Paleozoic units (small black dots); squares are averages by domain, colored as in Figure 4. Circles show the relative spread of data within each subset. (B) Density contours of all points in A, and best-fit plane of 251/86, S71°W (azimuth 251°, 86°NW). (C) Poles to bedding of Tertiary units (small black dots); squares are averages by domain, colored as in Figure 4, with the addition of magenta for the western Meadow Valley Mountains. Circles show the relative spread of data within each subset. (D) Density contours of points in C, with center plunging S59°W61° (azimuth 239°).

southeast quadrant of a stereogram (Fig. 10B). As elaborated further below, this evidence is best interpreted as supporting arguments based on palinspastic constraints and the coherence of the structural fabric within the allochthon.

Commensurate with the palinspastically constrained westward displacement of the allochthon relative to its substrate, we assume that all of the striations plotted on Figure 10 reflect upper-plate displacement toward the west-

ern hemisphere of the stereogram. Neglecting the effect of post-detachment tilt along the eastern flank of the range, we interpret the western-hemisphere polarity of each of the measured striations to reflect the slip direction. A histogram of the western polarities (Fig. 10A) indicates that the striations define a unimodal population with the peak oriented east-west (270°), with an estimated standard deviation of $\pm 37^\circ$.

SE ROA 37824

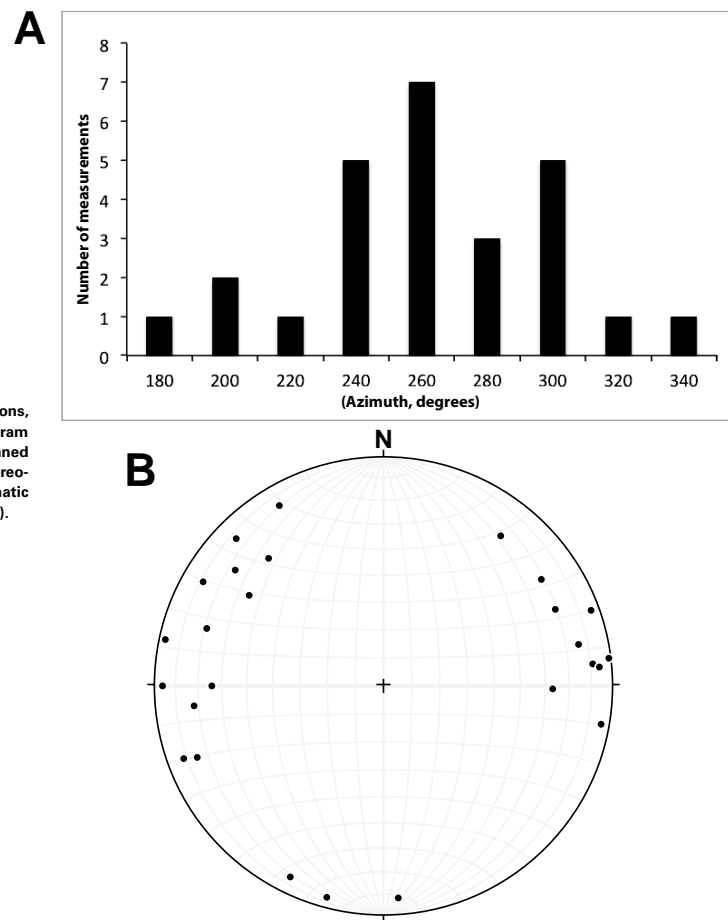


Figure 10. Orientation of fault striations, Mormon Peak detachment. (A) Histogram of kinematic orientation directions, binned in 20° increments. (B) Equal-angle stereogram, showing orientations of kinematic indicators. Data are from Walker (2008).

Other Indicators

Additional lines of evidence for the maximum elongation direction during extensional deformation in the Mormon Mountains (Wernicke et al., 1985) include (1) the observation that two intersecting normal faults in the footwall of the detachment do not offset each other, implying that both have a slip direction along or near the trend and plunge of their intersection, which is S82°W, 25° (262/25); (2) the trend of the obtuse bisector between two sets of syn-detachment, small-displacement high-angle faults in the footwall of the detachment interpreted to be conjugate fractures suggests that the least principal stress direction along the crest of the structural dome during fracture was S80°W

(260°); and (3) the long axis of structurally domiform detachments is generally a reliable proxy for the extension direction along detachment faults (e.g., Davis and Coney, 1979; Spencer and Reynolds, 1991; Livaccari et al., 1993). The orientation of the long axis of the structural dome defined by the detachment is also approximately WSW (~S70°W [250°]); e.g., Walker et al., 2007, their figure 1).

A summary of all available slip direction indicators is presented in Table 1. The mean orientation of these proxies is S77°W (257°). This extensional slip direction is oblique (~40°) to the dip direction of the thrust ramp (N62°W [298°]), requiring caution in interpreting two-dimensional cross-sections depicting the interaction between Sevier-age and Miocene tectonic elements (e.g., Fig. 8). Below, given an overall WSW displacement direction for the Mormon Peak allochthon, we present data bearing on the fault separation of Mesozoic features by the detachment in map view (Fig. 3), so as to better assess the three-dimensional complexities of structural restoration.

Locations of Three Offset Sevier-Age Structural Markers

Above the Mormon Peak Detachment

The geometry of the Sevier-aged thrust ramp is defined by the west-facing monocline in the western part of the mapped area (Figs. 2 and 5). At the level of the basal Tertiary erosion surface, the monoclinical section between the axial surfaces of the bounding folds ranges from the lower Bird Spring Formation (Pennsylvanian) to the Moenave Formation (Jurassic). The reconstruction of a section perpendicular to the Sevier structure (Fig. 6F) shows the base of the MPb2 unit being 4100 m structurally higher at C' than at C (see Fig. 5 for location). This provides a minimum amount of structural relief on the ramp. The total structural relief would be larger by the thickness of Bird Spring that is involved, something that is not readily measurable within the Tertiary fault blocks that are currently exposed in the area. The minimum amount of unit MPb (Bird Spring Formation) involvement would be 200 m, given the thicknesses exposed. The maximum would be 700–1000 m (Pampeyan, 1993; Axen, 1993). Thus, we estimate the total structural relief on the ramp to be between 4300 m and 5100 m.

Structural relief of 4300–5100 m on the monocline accords well with the value predicted by the structural relief on the frontal Sevier thrust ramp exposed in the detachment footwall, which is simply the thickness of the Middle Cambrian through Jurassic section exposed beneath the ramp. According to footwall cross-sections from the Tule Springs Hills and Beaver Dam Mountains to the east, the section is ~5000 m thick (e.g., Axen, 1993, his plate 1; Hintze, 1986, his plate 2A). A value near 5000 m is inconsistent with placing the base of the frontal thrust ramp in Mississippian strata, as depicted in the reconstruction of Axen et al. (1990). This placement predicts structural relief of only 3000 m in the hanging wall of the thrust. Their reconstruction was based on the occurrence of a Cambrian-on-Mississippian décollement segment of the thrust exposed in the central Mormon Mountains, which is cut off by the detachment.

SE ROA 37825

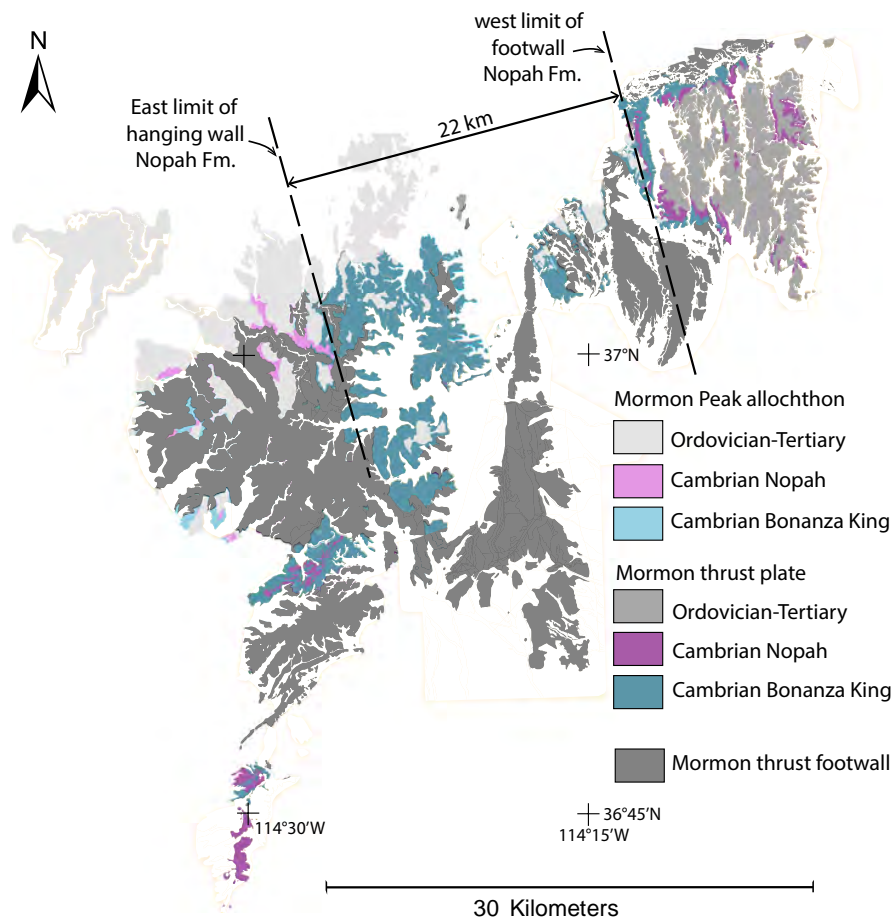


Figure 11. Map showing distributions of Cambrian Bonanza King Formation and Nopah Formation strata in the hanging wall and footwall of the Mormon Peak detachment, excluding autochthonous strata. West limit of footwall Nopah strata is presently 22 km east of the easternmost hanging-wall Nopah strata, defining a 22 km separation across the fault.

The exposed décollement segment is only ~2 km wide in the thrust transport direction. In the northern part of the range, the Mississippian décollement segment may die out altogether. A narrow footwall décollement segment within the Mississippian, however, appears to be useful as a structural marker, because it predicts significant structural effects in the hanging wall of the thrust, as elaborated on below.

A northward pinchout of a footwall décollement segment in Mississippian strata is supported by a change in the exposed structural level that occurs between the southern Meadow Valley Mountains and the area mapped in this study, as described in the Geologic Setting section. Along strike to the south of the area of Figure 5, the sub-Tertiary unconformity, rather than resting on strata

as young as Jurassic, instead rests on strata only as young as the Permian Kaibab Limestone. This difference in stratigraphic position suggests a 1500 m difference in total structural relief on the ramp to the south, from about 4500 m to 3000 m. This difference is readily explained by a lateral ramp in the thrust, where a décollement riding on top of the Mississippian structurally descends to the Middle Cambrian to the north, dropping the structural level of the thrust plate toward the north by 1500 m, about the stratigraphic difference both between the Kaibab and Jurassic strata in the hanging wall, and between the Banded Mountain Member and the upper Mississippian strata in the footwall.

Given these constraints, the first structural marker is delineated by the western edge of the monocline (ramp syncline; Fig. 3). The west-dipping section

SE ROA 37826

above the ramp is complicated by the “East Vigo thrust” and other structural complexities identified by Pampeyan (1993), but it is clear that the structural low is defined by a narrow outcrop belt of Jurassic strata (point C, Fig. 5). The match in structural relief exposed in the central Meadow Valley Mountains and the relief on the footwall ramp also suggests that the axial trace of the syncline is located near the westernmost exposures of Jurassic strata (also near point C on Fig. 5), because a location further west would require more structural relief on the ramp than could be generated by the entire Cambrian through Jurassic section. Additional structural relief would require somehow building up structural relief in the footwall with additional thrusts or other structures, which are not observed in extensive exposures of footwall rocks in the region. Therefore we interpret the ramp syncline to be located at the western edge of the Moenave Formation exposures mapped here, near point C.

The second structural marker, which constitutes the most significant complication in the otherwise homoclinal section from lower Bird Spring to Moenave strata, is a relatively tight backfold that affects the central part of the section, which may have a relationship with the structures below the detachment.

The third structural marker, the trace of the ramp anticline, is located at the top of the ramp where the dip of the reconstructed pre-Tertiary units shallows from 40° to subhorizontal. Within the Meadow Valley Mountains, reconstructed pre-Tertiary units shallow eastward from 40° to 15°, but do not reach 0°, indicating that the anticline is located just east of the easternmost Meadow Valley Mountains exposures (Fig. 6). Consistent with this hypothesis, the stereographic plot of reconstructed dips in pre-Tertiary strata discussed above (Fig. 7) indicates that the hinge of the anticline is located between the Meadow Valley Mountains and the westernmost Mormon Mountains (Figs. 4 through 8).

Below the Mormon Peak Detachment

In the footwall, the first structural marker is the base of the ramp, i.e., the intersection of the axial surface of the ramp syncline with the Mormon thrust. It can be constrained only by its easternmost possible position, because the detachment mainly cuts downward across the thrust autochthon and into Proterozoic basement (Wernicke et al., 1985). The map-view position of the undisturbed, autochthonous base of the Middle Cambrian Banded Mountain Member of the Bonanza King Formation (the detachment horizon for the thrust décollement) marks the easternmost possible position of the base of the ramp (Fig. 3).

The second Sevier-age structural marker below the detachment is the location of the westward cutoff of footwall Mississippian strata by the thrust ramp (Figure 3). As described above, the thrust fault remains within the Mississippian for at least 2 km across strike, and is cut off by the Mormon Peak detachment (Figs. 2 and 8). In the hanging wall, we infer that the narrow Mississippian décollement segment of the thrust served as a nucleation point for the relatively tight anticlinal backfold within hanging-wall Permian strata (Fig. 5), as indicated by the reconstruction in Figure 8.

The third marker below the detachment is the top of the thrust ramp, which is well exposed in the Tule Springs Hills near Jumbled Mountain. To the west of it, the décollement ramps at a moderate angle across upper Paleozoic and lower Mesozoic strata. To the east, the thrust plate is everywhere thrust over the Jurassic Kayenta Formation (Axen, 1993).

Offset Estimates

Offset along the detachment is, in part, based on the six positions of the three Sevier-age structural markers described above, and summarized in Figure 3. Above the detachment, they are the axial traces of the ramp anticline and ramp syncline and the axial trace of a small backfold we infer to be genetically related to the narrow décollement segment of the thrust. Below the detachment, they are the base and top of the thrust ramp, and the intersection or cutoff of Mississippian strata along the thrust ramp. In present geometry, the anticline at the east edge of the Meadow Valley Mountains is 24 km away, as measured along the detachment slip direction, from the top of the thrust ramp at Jumbled Mountain (easternmost thick black line, Fig. 3). This includes the combined offset of (1) the Mormon Peak detachment and (2) younger faults in the footwall of the Mormon Peak detachment, predominantly the Tule Springs detachment system of Axen et al. (1990) and Axen (1993). Axen et al. (1990) estimated 11 km of slip on these faults based on restoration of cross-sections. Subtracting that figure from the 24 km of total separation of the ramp anticline leaves 13 km of horizontal component of slip on the Mormon Peak detachment.

The ramp syncline in the hanging wall is 12 km WSW of the east limit of its possible position in the footwall (Fig. 3). There may be minor strike-slip offset along Meadow Valley Wash, but this is at high angle to the detachment slip direction. Therefore, based on this marker alone, we estimate a maximum of 12 km of horizontal displacement on the detachment at this location. The position of the truncation of the Mississippian by the Sevier thrust and its narrow ramp zone, and its counterpart projected in the subsurface in the Meadow Valley Mountains, also suggests ~12 km of slip on the detachment.

Independent of any considerations of thrust ramp geometry, Anderson et al. (2010) proposed a 10–15 km of offset across the northern part of the Mormon Mountains, which they attribute to displacement on an inferred strike-slip fault. Within the Kane Wash section, they documented scarp breccias derived from both Cambrian- and Jurassic-aged bedrock. They noted that the nearest location where such disparate ages of source material could have been simultaneously exposed to a fault scarp is in the Tule Springs Hills, 10–15 km to the east-northeast. These landslides and interbedded Kane Wash volcanics both dip 70° to the east, a direction that would be expected from block rotation above the Mormon Peak detachment.

Independent of these structural markers, as mentioned above in regard to the uniform displacement direction of the detachment, the stratigraphic offset of the Dunderberg Shale Member of the Nopah Formation is defined by the east limit of Nopah Formation exposures above the detachment and by

SE ROA 37827

the truncation of the Dunderberg below the detachment (Fig. 11). The stratigraphic separation in the direction of transport is at least 22 km. Again, subtracting 11 km of offset along the younger Tule Springs detachment system, the net horizontal offset along the Mormon Peak detachment is at least 11 km.

Given these offsets, the scaling between displacement and fault length of the Mormon Peak detachment is comparable to one of the best known examples of an active low-angle normal fault, the Alto Tiberina fault of central Italy, which has a strike length of at least 70 km and net offset of 10 km (e.g., Mirabella et al., 2011).

Initial Dip of the Detachment

The initial dip of the detachment may be estimated by comparing its orientation with those of various elements in the thrust system, as well as its reconstructed angle with respect to the basal Tertiary unconformity in the area, which pre-dates formation of the detachment (e.g., Wernicke, 1995). In the central Mormon Mountains, the detachment makes an angle of 17° with respect to the autochthonous stratigraphy, based on a restored section ~20 km along strike to the south of our sections (Wernicke et al., 1985, their figure 15). Assuming a gentle west dip of the stratigraphy at the time of initiation of the detachment, then an initial dip of the detachment of 20°–25° is indicated.

Along our sections, the best datum for estimating the initial dip of the detachment is the thrust ramp and its relationship to the sub-Tertiary unconformity. Paleozoic units thrust over the ramp should correspond fairly closely to the dip of the ramp, assuming a simple reconstruction (Fig. 8). Bedding within the western Meadow Valley Mountains dips an average of 40°NW relative to the subhorizontal Tertiary units that overlie it. The base of the thrust ramp is not unambiguously exposed in the footwall in the Mormon Mountains, indicating that it has been (largely or) wholly excised by the detachment, which cuts directly into autochthonous basement in the westernmost Mormon Mountains (Wernicke et al., 1985; Axen et al., 1990). Whatever the case in the central and southern Mormon Mountains where most of the detachment footwall is exposed, relief across the monocline in the Meadow Valley Mountains demands that the ramp cut upward more or less uninterrupted from Middle Cambrian through Jurassic strata in the northernmost Mormon Mountains and southern Clover Mountains, where this area palinspastically restores (Figs. 3 and 8). Hence, if the Mormon Peak detachment is parallel to the ramp, then the initial dip of the Miocene detachment in this area should be ~40°. The reconstruction in Figure 8, oriented parallel to section A-A' (Figs. 5 and 6), depicts the fault and ramp with a dip of 30°, accounting for apparent dip correction between the WSW extension direction and the WNW dip direction of the ramp.

This estimate is 15° steeper than the 20° to 25° initial dip proposed for the central Mormon Mountains (e.g., Wernicke et al., 1985; Wernicke, 1995). Hence, if we presume that the detachment tends to follow the thrust ramp to the north, its initial dip must steepen by 15° along strike toward the north, from 25° to 40°. A steeper detachment to the north, especially at uppermost

crustal levels (<2 km; Fig. 8), would also tend to promote the creation of void space for a deep supradetachment basin, and promote the generation of scarp breccias, as observed in the northernmost Mormon Mountains. Our map compilation indicates that the detachment fault within the northernmost Mormon Mountains is closely parallel to the thrust ramp there. For at least 6.6 km in the inferred transport direction, the detachment is parallel to the ramp section, localized within the lower part of unit Cbb4 of Wernicke et al. (1985).

As noted above, the 1500 m difference in structural relief between the central and southern Meadow Valley Mountains suggests a lateral ramp in the thrust, between an extensive Cambrian flat to the north and a significant Mississippian flat to the south. This lateral ramp would occur between the central and northern Mormon Mountains, and may have influenced the initial dip of the detachment, with a steeper dip of 40° to the north (consistent with the reconstruction in Fig. 8 and the detachment-ramp angle) and shallower dip to the south (consistent with the reconstruction of Axen et al. [1990] and the detachment-autochthon angle). Whereas the shallower, southern segment of the detachment would have had nearly pure dip slip at 25°, the northern segment would have had a strong component of left-oblique slip plunging 30° along a fault plane that dips 40°.

In addition to probable variations in initial dip for the detachment along strike, there may also be significant variation in the dip of the detachment and thrust as a function of depth. The 42° dips within the Moenkopi and Chinle may reflect a steeper, lower part of the thrust ramp, while the 30° dips of the Permian red beds and Bird Spring Formation may reflect a shallower upper ramp.

Post-Miocene Faulting

There is the potential for a few kilometers of left-lateral strike-slip motion to have been accommodated by a fault or faults buried within Meadow Valley Wash between the Meadow Valley Mountains and Mormon Mountains. This is suggested by (1) 5 km apparent offset of the boundary between east- and west-dipping strata noted earlier (Fig. 4) and (2) the apparent sinistral vertical-axis rotation in the dip direction of strata at the northwesternmost edge of the Mormon Mountains, closest to the Meadow Valley Wash. Possible right-lateral faulting in the northernmost Mormon Mountains is suggested by apparent dextral drag folding along an east-west-trending fault concealed beneath alluvium. The existence and timing of motion of these faults is speculative, as none of them have been identified in the field, but other north-trending, left-lateral faults, active after regional Miocene normal faulting, have been identified in the region. These include the Kane Wash fault on the western edge of the Meadow Valley Mountains, and the Tule Corral fault in the central part of the Tule Springs Hills (e.g., Axen, 1993; Anderson and Barnhard, 1993). Assuming one or more sinistral faults exist beneath Meadow Valley Wash, they do not have significant vertical offsets, because blocks on either side of their putative traces lie at the same structural level. On both sides of the wash, Tertiary volcanic rocks rest unconformably on the Bird Spring Formation.

SE ROA 37828

Other Interpretations of the Mormon Peak Detachment

Some researchers have questioned, firstly, whether the Mormon Peak detachment is a “rooted” crustal fault, as opposed to a system of landslide deposits, as noted above (e.g., Anders et al., 2006; Walker et al., 2007); and secondly, whether all of the apparent thinning of the Mormon Peak allochthon is due to faulting, or alternatively, to large-scale dissolution of carbonate rocks (Anderson et al., 2010).

In addition to the stratigraphic and structural arguments against radial sliding described above, several other lines of evidence indicate that the detachment is rooted into the crust and accommodates regional extension. First, stable isotopic data on fault rocks on the detachment (Swanson et al., 2012) indicate that rapid circulation of significant volumes of warm meteoric fluids occurred during motion, from a depth of at least 4 km, too deep to explain with a landsliding mechanism. Second, the 2-km-thick section of multiple rock avalanche deposits interbedded with the Kane Wash Tuff in the hanging wall and their 70° dip toward the east (see Anderson et al., 2010) are suggestive of gradual syntectonic deformation at ca. 14 Ma, and remain poorly explained by catastrophic gravity sliding. Third, the stratigraphy and structural style of the easternmost Meadow Valley Mountains, ENE-tilted normal fault blocks of Bird Spring Formation unconformably overlain by Tertiary tuffs, is the same as that in the nearby Mormon Peak allochthon in the Mormon Mountains, and highly dissimilar to the exposed basement rocks below the detachment. Interpreting the Meadow Valley Mountains block as part of the detachment footwall, a consequence of the radial sliding model, requires the existence of two faults for which there is no evidence: (1) the base of the slide, which would oddly exhibit the same stratigraphy and structural style as its substrate in the runout zone, and (2) a pre-existing high-angle fault with kilometers of structural relief, presumably buried beneath the slide (Walker, 2008). Both putative structural boundaries would be fortuitously concealed beneath the ~2 km width of alluvial cover between the nearest approach of the two ranges (Fig. 4) without resulting in any significant contrast in stratigraphy, structural level, or structural style.

Evidence in favor of the detachment being a rootless fault, as noted above, mostly hinges on the radial orientations of a small number of fault striations measured on or near the detachment (Walker et al., 2007). However, such a distribution of slip directions, even assuming they are representative of a much larger population, does not preclude the detachment from being a rooted fault. Singleton (2013) described kinematic indicators on corrugations of the Buckskin-Rawhide detachment in west-central Arizona showing a radial pattern, which he interpreted as a reflection of a late-stage compressional event perpendicular to the extension direction, promoting flexural slip along the detachment plane. As argued in Wernicke et al. (1985) and Anderson and Barnhard (1993), the north-south component of bending of the Mormon dome resulted from regional north-south shortening during extension and emplacement of the Mormon Peak allochthon, which would promote north or northwest-trending flexural slip along the northern flank of the dome.

The determination of the amount of displacement and thinning accommodated by slip on the detachment, versus dissolution of the hanging wall (e.g., Anderson et al., 2010; Diehl et al., 2010), is more difficult to address directly with our data. Our approach is to present here a kinematic model based on reconstruction of the dismembered Mesozoic thrust system and does not depend on structural reconstruction of individual fault blocks in the Mormon Peak allochthon. Thus, although we acknowledge the central importance of fluid-assisted deformation in the development of the Mormon Peak and other carbonate allochthons (e.g., Swanson et al., 2012, 2016), it is beyond the scope of this paper to address this important issue.

CONCLUSIONS

Based on the mapping of structures within the Meadow Valley Mountains and a regional compilation of geologic data in the neighboring Mormon Mountains, East Mormon Mountains, and Tule Springs Hills, we correlate Sevier-age contractile structures across the Mormon Peak detachment and provide a new, independent estimate of 12–13 km of horizontal displacement at the latitude of the central Meadow Valley Mountains–northern Mormon Mountains. Accounting for a 30° plunge in the slip vector, net slip on the fault is estimated to be 14–15 km. This estimate is in the interpreted slip direction of S77°W (257°), which is based on multiple lines of structural evidence (Table 1).

The observations presented here are broadly consistent with the model of Axen et al. (1990), where a Sevier-age thrust flat-ramp-flat is overprinted and distended by the Mormon Peak detachment as well as by structurally lower, younger detachments. However, our data indicate several significant modifications to their geometric and kinematic model of the detachment. First, structural relief indicates that the flat at the base of the ramp is in Cambrian, not Mississippian strata, within the northernmost Mormon Mountains. Second, the total displacement on the Mormon Peak detachment is significantly less than the estimate of 20–22 km as indicated in the earlier reconstruction, but consistent with recent estimates based on thermochronological data (Bidgoli et al., 2015). Third, assuming the detachment initiated near the thrust ramp, it would have steepened northward from a dip of 20°–25° in the Mormon Mountains to a dip of 40°, over an along-strike distance of 10–20 km to the north.

ACKNOWLEDGMENTS

This research was supported by NSF Grant EAR-1250565 awarded to B. Wernicke and J. Eiler, and by the Caltech Tectonics Observatory of the Gordon and Betty Moore Foundation.

APPENDIX. DESCRIPTION OF MAP UNITS

Descriptions of map units (Fig. 5) are heavily modified from Pampeyan (1993). All potassium-argon (K-Ar) ages cited have been recalculated using the decay constants presented by Steiger and Jäger (1977), resulting in ages 2.7% older than the original published data. Color terminology used in the following descriptions is from the National Research Council Rock Color Chart (Goddard et al., 1948).

SE ROA 37829

Qal: Alluvium (Holocene)—Unconsolidated stream-channel and fan deposits of clay to cobble size. Commonly less than a few meters thick but probably exceeds 10 m in major washes.

Tal: Alluvium (Pleistocene? and Tertiary)—Mildly consolidated stream-channel and coarse basin deposits of sand to cobble size, crudely stratified. Commonly present on former drainage terrace surfaces or perched on older alluvial or lacustrine deposits. Thickness is 100 m at the mouth of Vigo Canyon, but typically thinner.

KANE WASH TUFF (Miocene)—Ash flows are subdivided, from youngest to oldest, into unit 2, unit 1, unit W, and unit O. Adularescent sanidine is diagnostic of this tuff.

Tku2: Unit 2—Thin blue-gray to blue-green devitrified tuff ~1 m thick overlain by brownish-gray-weathering, devitrified ash-flow tuff. Lithic component is mostly flattened pumice. Ranges from a few meters to ~90 m thick. K-Ar age, 14.1 Ma (Novak, 1984).

Tku1: Unit 1—Cliff-forming, crystal-rich, rhyolitic to trachytic ash-flow tuff grading upwards from densely welded, reddish-brown to less welded, brownish-gray lithic-crystal tuff. Contains flattened pumice fragments as large as 2.5 by 15 cm. Sanidine crystals as long as 10 mm, many of them adularescent, decrease in size, but increase in abundance, upwards. K-Ar age, 14.1 Ma (Novak, 1984). May be as thick as 120 m in an escarpment along Kane Springs Wash.

Tt: Trachyte (Miocene)—Black to grayish-purple, blocky-weathering trachyte lavas with a micro-crystalline to glassy matrix that locally shows flow banding. In this map area, it is defined by the very hard layer that crops out in an otherwise poorly exposed slope. Flow is ~5 m thick in its only exposure in the mapped area. This flow is not considered part of the Kane Wash Tuff, but is found between units Tkw and Tku1.

Tkw: Unit W—Pinkish-gray, pale-yellowish-brown-weathering, rhyolite ash-flow tuff. Lower four-fifths of the unit is lithic tuff with non-compacted pumice fragments as much as 15 cm across, cavities, and few crystals; upper one-fifth of the unit is pink to pale-violet, moderately to densely welded cliff-forming devitrified lithic tuff. Thickness ranges from 137 m to zero. K-Ar age, 14.7 Ma (Novak, 1984).

Tko: Unit O—Largely moderate-brown to reddish-brown, densely welded, rhyolite ash-flow tuff easily recognized as forming a thin dark cliff under a thick light-colored slope. Eutaxitic structure is unique to most of this unit, and the flattened pumice fragments can be used for dip measurements. Maximum thickness of the unit is ~79 m in the Kane Springs Wash scarp decreasing to zero along south edge of the volcanic terrane. K-Ar age, 15.6 Ma (Novak, 1984).

Tb1: Amygdaloidal basalt (Miocene)—Dark-gray to grayish-black, brownish-black-weathering olivine basalt in compact to amygdaloidal flows. Single(?) aphanitic flow as much as 4 m thick exposed in the vicinity of Hackberry Canyon lies between the Hiko Tuff (unit Th) and crystal tuff of the Kane Wash Tuff (unit Tku). This basalt locally is coarsely amygdaloidal with epidote- and quartz-lined amygdules up to 1 cm long.

Th: Hiko Tuff (Miocene)—Pinkish- to brownish-gray, brown-weathering, moderately welded vitric-crystal to crystal ash-flow tuff, becoming slightly less welded toward the top of the unit. Basal 10–15 m, where exposed, is white to pale greenish-yellow and light-gray, partially welded, punky lithic-crystal tuff. In the upper half of the section there are local lenses of coarse impure sandstone or wacke as thick as 3 m. Maximum thickness is 43 m near Vigo. Hiko Tuff has yielded K-Ar ages of 18–20 Ma (Armstrong, 1970; Noble and McKee, 1972; Marvin et al., 1970).

Thh: Harmony Hills Tuff (Miocene)—Brownish-gray to pale yellowish-brown, reddish-brown-weathering, crystal-rich, biotite ash-flow tuff. Abundance and size of biotite crystals are diagnostic characteristics as the unit contains more euhedral biotite than any other ash-flow tuff in this region, usually in books as much as 3 mm in diameter and 1–2 mm thick. Total thickness of the Harmony Hills Tuff is ~81 m in Hackberry Canyon, where it rests on a basalt flow breccia (unit Tb1). Radiometric analyses of the Harmony Hills Tuff from the surrounding region yielded an average age of 21 Ma (Armstrong, 1970; Noble and McKee, 1972; Marvin et al., 1970).

Tbb: Basalt breccia (Miocene)—Thick, dark-purple, red, and black, monolithologic basalt flow breccias and flows. Well exposed in Hackberry Canyon and along the south edge of the volcanic terrane. The thickness of this unit is highly variable, with a maximum thickness reported by Cook (1965) of 289 m in an area 3 km west of Vigo; average thickness is closer to 100 m, thinning to zero away from Hackberry Canyon.

LEACH CANYON AND CONDOR CANYON FORMATIONS (Miocene)—In this area, consists of Leach Canyon Formation and Bauers Tuff (undivided), lacustrine limestone, and conglomerate.

Tlc: Leach Canyon Formation and Bauers Tuff, undivided (Miocene)—Bauers Tuff is a pale purple, highly welded tuff up to 8 m thick, but is too thin to show separately and is included with the underlying Leach Canyon Formation (Tlc). Leach Canyon Formation consists of a pale-lavender ash-flow tuff. The Leach Canyon consists of two cooling units locally separated by lenses of light gray, orange-mottled lacustrine limestone up to 5 m thick. Total thickness of unit is ~74 m west of Vigo. Age of the Leach Canyon Formation, based on K-Ar analyses of samples from the surrounding region, is ca. 24.6 Ma (Armstrong, 1970; Rowley et al., 1975).

Tl: Lacustrine limestone (Oligocene?)—Light-gray freshwater limestone in beds 10–30 cm thick, commonly containing algal structures. Thickness ranges from 5 to 30 m; typically 20 m thick. Occurs at the base of the volcanic section, resting unconformably on pre-Tertiary sedimentary rocks, and locally on, or interlayered with, prevolcanic conglomerate (unit Tc). Age is considered to be late Oligocene inasmuch as strata underlie lower Miocene tuffs (Ekren et al., 1977).

Tc: Conglomerate (Tertiary)—Reddish-orange- to reddish-brown-weathering, poorly sorted, syn-orogenic(?) conglomerate occurring in isolated patches filling low areas on the pre-volcanic erosion surface. Appears to interfinger locally with lower lacustrine limestone (unit Tl). Mainly well-rounded cobbles in a silty to coarse sandy matrix, but pebble- to small boulder-size clasts are present, all consisting of Paleozoic carbonate rocks, quartzite, and some chert. Thickness ranges from 0 to ~50 m.

MOENAVE AND KAYENTA FORMATIONS (Jurassic)

Jmk: Moderate-red to dark-red, fine-grained, nonmarine, silty sandstone and shaley sandstone present in poorly exposed, scattered outcrops along south edge of volcanic terrane.

CHINLE FORMATION (Upper Triassic)—Consists of Petrified Forest and Shinarump Members.

ƒcp: Petrified Forest Member—Moderate-red to dusky-red, fine-grained, nonmarine, silty sandstone and shaley sandstone present in scattered outcrops along the south edge of the volcanic terrane. Thickness is 365 m.

ƒcs: Shinarump Member—Grayish-red, dark-brown-weathering, ridge-forming, fine-grained sandstone and chert-pebble conglomerate. Some sandstone is cross-bedded and quartzitic. Fossil wood common elsewhere in the Shinarump was not seen here, and the overall texture of the member is finer than in exposures farther east. The Shinarump Member is observed to be 40 m thick in its sole outcrop within the map area.

ƒm and br: Moenkopi Formation (Middle? and Lower Triassic)—Predominantly gray, pale-brown, and yellowish-brown, grayish-yellow- to grayish-orange-weathering, even-bedded, dense marine limestone, with interbedded red, orange, and brown silty and shaley limestone giving large outcrops a color-banded aspect. Moenkopi rests with slight angular discordance on a variety of units, including br, Pk, and Pt, and locally lies directly on unit Pr5. Unit br is a dark-brown-weathering, chert-rich, sedimentary or karst breccia that is locally present in lenses along the base of the Moenkopi. Upper contact with the Shinarump Member of the Chinle Formation (unit ƒcs) is poorly exposed in an isolated outcrop, but 985 m of Moenkopi is present in the homoclinal section 5 km west of Vigo.

Pk: Kaibab Limestone (Lower Permian)—Gray limestone with ~50% brown-weathering chert. Chert is commonly bedded, but can occur as elongate nodules. Thickness ranges from 40 m to zero.

Pt: Toroweap Formation (Lower Permian)—Pinkish-gray to light gray, cliff-forming limestones with minor chert. Minimum thickness of 60 m lies unconformably between the Moenkopi Formation (unit ƒm) and Permian red beds (unit Pr 5).

RED BEDS (Lower Permian)—Red sandstone unit, subdivided here into units 1–5. Complete red bed section is exposed, with a total thickness of ~552 m. This unit correlates approximately with strata mapped as Coconino Sandstone, Queantoweap Sandstone, and Pakoon Limestone of McNair (1951) in the Beaver Dam Mountains to the east (Reber, 1952; Langenheim and Larson, 1973).

Pr5: Unit 5—Slope-forming, even-bedded, red, coarse-grained sandstone and silty sandstone. Lower contact is drawn at the base of a prominent gray carbonate marker bed that is overlain by yellow sandstone beds. Upper contact is drawn at the discordant contact with either overlying chert breccia of the Toroweap Formation and Kaibab Limestone (units Pt and Pk) or carbonate beds of the Moenkopi Formation. Unit is ~123 m thick.

Pr4: Unit 4—Upper 90 m is red, slope-forming, coarse-grained sandstone containing some inter-layered red siltstone layers, as well as minor resistant beds of gray, fossiliferous limestone. These beds are darker red and more resistant than the sandstone beds of unit Pr5, and have significantly less carbonate than unit Pr3. The lower part of this unit consists of badland-weathering, contorted

SE ROA 37830

beds of red and yellow shaley sandstone and siltstone with interlayered beds of gypsum. Gypsiferous beds up to 6 m thick occur in an area ~1100 m long by 305 m wide (Jones and Stone, 1920) and appear to represent deformed evaporite basin deposits. The thickness of this unit is ~242 m.

Pr3: Unit 3—Even-bedded, pink, white, and gray sandstone and shale, with lesser gray limestone and sandy limestone and cross-bedded pale-brown sandstone. Contains more pink beds and fewer carbonate beds than units Pr1 and Pr2. The upper contact is defined at the top of the highest carbonate bed. This unit is ~90 m thick.

Pr2: Unit 2—Pink, white, and gray sandstone, gray limestone and sandy limestone, cross-bedded pale-brown sandstone, pinkish shale, sandstone, and sandy limestone, with calcareous beds increasing downwards. This unit contains a higher percentage of gray carbonate beds than units Pr1 and Pr3. Thickness is ~50 m.

Pr1: Unit 1—Even-bedded, pink, white, and gray sandstone, gray limestone and sandy limestone, and cross-bedded pale-brown sandstone, with lesser pinkish shale, sandstone, and sandy limestone. This unit has more carbonate beds than units Pr2 and Pr3, and is more pink in color than unit Pr2. Basal contact is drawn at the lowest red sandy bed. Thickness is ~45 m.

BIRD SPRING FORMATION (Pennsylvanian to Mississippian)—Divided into units 1–3.

MPb3: Unit 3—Light to dark-gray limestone, with very little chert. Looks very similar to the top of unit MPb1, and is often distinguished solely on stratigraphic position. Thickness is ~30 m.

MPb2: Unit 2—Very fine-grained, brown-weathering sandy limestone. Well exposed in Meadow Valley Wash near Galt. Thickness is 30–45 m.

MPb1: Unit 1—Interlayered beds of light- to dark-gray limestone, pinkish-gray cherty limestone, reddish-brown sandy, calcareous, and dolomitic limestone, and white to reddish-brown, fine-grained sandstone. Limestone is fine to medium crystalline, thin to medium bedded, and fossiliferous. Sandy beds, some of which are quartzitic, form brownish- to reddish-weathering ledges in even-bedded step-like outcrop. Upper limestone and cherty limestone are middle Wolfcampian in age. The lowermost limestones and cherty limestones are Morrowan in age. A complete continuous section is not exposed anywhere in the Meadow Valley Mountains, but the unit was previously estimated to be ~1310 m thick (Tschanz and Pampeyan, 1970); however, it may be closer to 2000 m thick in the southern Meadow Valley Mountains.

REFERENCES CITED

- Abers, G.A., 1991, Possible seismogenic shallow-dipping normal faults in the Woodlark-D'Entrecasteaux extensional province, Papua New Guinea: *Geology*, v. 19, p. 1205–1208, doi:10.1130/0091-7613(1991)019<1205:PSSDNF>2.3.CO;2.
- Allmendinger, R.W., Cardozo, N.C., and Fisher, D., 2013, Structural Geology Algorithms: Vectors and Tensors: Cambridge, UK, Cambridge University Press, 289 p.
- Anders, M.H., Christie-Blick, N., and Walker, C.D., 2006, Distinguishing between rooted and rootless detachments: A case study from the Mormon Mountains of southeastern Nevada: *The Journal of Geology*, v. 114, p. 645–664, doi:10.1086/507612.
- Anderson, R.E., 1971, Thin-skin distension in Tertiary rocks of southeastern Nevada: *Geological Society of America Bulletin*, v. 82, p. 43–58, doi:10.1130/0016-7606(1971)82[43:TSDITR]2.0.CO;2.
- Anderson, R.E., and Barnhard, T.P., 1993, Aspects of three-dimensional strain at the margin of the extensional orogen, Virgin River depression area, Nevada, Utah, and Arizona: *Geological Society of America Bulletin*, v. 105, p. 1019–1052, doi:10.1130/0016-7606(1993)105<1019:AOTDSA>2.3.CO;2.
- Anderson, R.E., Felger, T.J., Diehl, S.F., Page, W.R., and Workman, J.B., 2010, Integration of tectonic, sedimentary, and geohydrologic processes leading to a small-scale extension model for the Mormon Mountains area north of Lake Mead, Lincoln County, Nevada, in Umhoefer, P.J., Beard, L.S., and Lamb, M.A., eds., *Miocene Tectonics of the Lake Mead Region, Central Basin and Range*: Geological Society of America Special Paper 463, p. 395–426, doi:10.1130/2010.2463(18).
- Armstrong, R.L., 1970, Geochronology of Tertiary igneous rocks, eastern Basin and Range province, western Utah, eastern Nevada, and vicinity, USA: *Geochimica et Cosmochimica Acta*, v. 34, p. 203–232, doi:10.1016/0016-7037(70)90007-4.
- Axen, G.J., 1984, Thrusts in the eastern Spring Mountains, Nevada: Geometry and mechanical implications: *Geological Society of America Bulletin*, v. 95, p. 1202–1207, doi:10.1130/0016-7606(1984)95<1202:TITESM>2.0.CO;2.

Axen, G.J., 1991, Tertiary extension, magmatism, and thrust reactivation in the southern Great Basin, and a mechanical model for detachment faulting [Ph.D. thesis]: Cambridge, Massachusetts, Harvard University, 235 p.

Axen, G.J., 1993, Ramp-flat detachment faulting and low-angle normal reactivation of the Tule Springs thrust, southern Nevada: *Geological Society of America Bulletin*, v. 105, p. 1076–1090, doi:10.1130/0016-7606(1993)105<1076:RFDFA>2.3.CO;2.

Axen, G.J., 2004, Mechanics of low-angle normal faults, in Karner, G.D., Taylor, B., Driscoll, N.W., and Kohlstedt, D.L., eds., *Rheology and Deformation of the Lithosphere at Continental Margins*: New York, Columbia University Press, p. 46–91, doi:10.7312/karn12738-004.

Axen, G.J., Wernicke, B.P., Skelly, M.F., and Taylor, W.J., 1990, Mesozoic and Cenozoic tectonics of the Sevier thrust belt in the Virgin River Valley area, southern Nevada, in Wernicke, B.P., ed., *Basin and Range Extensional Tectonics near the Latitude of Las Vegas, Nevada*: Geological Society of America Memoir 176, p. 123–154, doi:10.1130/MEM176-p123.

Bidgolf, T.S., Stockli, D.F., and Walker, J.D., 2015, Low-temperature thermochronologic constraints on the kinematic histories of the Castle Cliffs, Tule Springs, and Mormon Peak detachments, southwestern Utah and southeastern Nevada: *Geosphere*, v. 11, p. 850–867, doi:10.1130/GES01083.1.

Bohannon, R.G., 1983, Mesozoic and Cenozoic tectonic development of the Muddy, North Muddy, and northern Black Mountains, Clark County, Nevada, in Miller, D.M., Todd, V.R., and Howard, K.A., eds., *Tectonic and Stratigraphic Studies in the Eastern Great Basin*: Geological Society of America Memoir 157, p. 125–148, doi:10.1130/MEM157-p125.

Burchfiel, B.C., Fleck, R.J., Secor, D.T., Vincelette, R.R., and Davis, G.A., 1974, Geology of the Spring Mountains, Nevada: *Geological Society of America Bulletin*, v. 85, p. 1013–1022, doi:10.1130/0016-7606(1974)85<1013:GOTSMN>2.0.CO;2.

Burchfiel, B.C., Wernicke, B., Willemin, J.H., Axen, G.J., and Cameron, S.C., 1982, A new type of decollement thrust: *Nature*, v. 300, p. 513–515, doi:10.1038/300513a0.

Burchfiel, B.C., Cameron, C.S., and Royden, L.H., 1997, Geology of the Wilson Cliffs–Potosi Mountain Area, Southern Nevada: *International Geology Review*, v. 39, p. 830–854, doi:10.1080/00206819709465304.

Cardozo, N., and Allmendinger, R.W., 2013, Spherical projections with OSXStreeonet: *Computers & Geosciences*, v. 51, p. 193–205, doi:10.1016/j.cageo.2012.07.021.

Carpenter, D.G., Carpenter, J.A., Bradley, M.D., Franz, U.A., and Reber, S.J., 1989, Comment on “On the role of isostasy in the evolution of normal fault systems”: *Geology*, v. 17, p. 774–776, doi:10.1130/0091-7613(1989)017<0774:CAROOT>2.3.CO;2.

Carr, M.D., 1983, Geometry and structural history of the Mesozoic thrust belt in the Goodsprings district, southern Spring Mountains, Nevada: *Geological Society of America Bulletin*, v. 94, p. 1185–1198, doi:10.1130/0016-7606(1983)94<1185:GASHOT>2.0.CO;2.

Chiaraluce, L., Chiarabba, C., Collettini, C., Puccinini, L., and Cocco, M., 2007, Architecture and mechanics of an active low-angle normal fault: Alto Tiberina Fault, northern Apennines, Italy: *Journal of Geophysical Research*, v. 112, B10310, doi:10.1029/2007JB005015.

Collettini, C., and Sibson, R.H., 2001, Normal faults, normal friction?: *Geology*, v. 29, p. 927–930, doi:10.1130/0091-7613(2001)029<0927:NFNF>2.0.CO;2.

Cook, E.F., 1965, Stratigraphy of Tertiary volcanic rocks in eastern Nevada: Nevada Bureau of Mines and Geology Report 11, 67 p. (incl. geologic map, scale 1:500,000).

Davis, G.A., Anderson, J.L., Frost, E.G., and Shackelford, T.J., 1980, Mylonitization and detachment faulting in the Whipple-Buckskin-Rawhide Mountains terrane, southeastern California and western Arizona, in Crittenden, M.D., Jr., Coney, P.J., and Davis, G.H., eds., *Cordilleran Metamorphic Core Complexes*: Geological Society of America Memoir 153, p. 79–130, doi:10.1130/MEM153-p79.

Davis, G.H., and Coney, P.J., 1979, Geologic development of Cordilleran metamorphic core complexes: *Geology*, v. 7, p. 120–124, doi:10.1130/0091-7613(1979)7<120:GDOTCM>2.0.CO;2.

Davis, G.H., and Hardy, J.J., 1981, The Eagle Pass detachment, southeastern Arizona: Product of mid-Miocene listric(?) normal faulting in the southern Basin and Range: *Geological Society of America Bulletin*, v. 92, p. 749–762, doi:10.1130/0016-7606(1981)92<749:TEPDSA>2.0.CO;2.

Diehl, S.F., Anderson, R.E., and Humphrey, J.D., 2010, Fluid flow, solution collapse, and massive dissolution at detachment faults, Mormon Mountains, Nevada, in Umhoefer, P.J., Beard, L.S., and Lamb, M.A., eds., *Miocene Tectonics of the Lake Mead Region, Central Basin and Range*: Geological Society of America Special Paper 463, p. 427–441, doi:10.1130/2010.2463(19).

Ekren, E.B., Orkild, P.P., Sargent, K.A., and Dixon, G.L., 1977, Geologic map of Tertiary rocks, Lincoln County, Nevada: U.S. Geological Survey Miscellaneous Investigations Map I-1041, scale 1:250,000.

SE ROA 37831

- Elliott, J.R., Walters, R.J., England, P.C., Jackson, J.A., Li, Z., and Parsons, B., 2010, Extension on the Tibetan plateau: Recent normal faulting measured by InSAR and body wave seismology: *Geophysical Journal International*, v. 183, p. 503–535, doi:10.1111/j.1365-246X.2010.04754.x.
- Ellis, B.J., 1985, Thin-skinned extension superposed on frontal Sevier thrust faults, Mormon Mountains, southern Nevada [M.S. thesis]: Syracuse, New York, Syracuse University, 87 p.
- Goddard, E.N., Trask, P.D., De Ford, R.K., Rove, O.N., Singewald, J.T., and Overbeck, R.M., 1948, Rock-color chart: Boulder, Colorado, Geological Society of America.
- Hintze, L.F., 1986, Stratigraphy and structure of the Beaver Dam Mountains, Utah, in Griffin, D.T., and Phillips, W.R., eds., *Thrusting and Extensional Structures and Mineralization in the Beaver Dam Mountains, Southwestern Utah*: Utah Geological Association Special Publication 15, p. 1–36.
- Jackson, J.A., and White, N.J., 1989, Normal faulting in the upper continental crust: Observations from regions of active extension: *Journal of Structural Geology*, v. 11, p. 15–36, doi:10.1016/0191-8141(89)90033-3.
- Jones, J.C., and Stone, R.W., 1920, Deposits in southern Nevada, in Stone, R.W., et al., eds., *Gypsum Deposits of the United States*: U.S. Geological Survey Bulletin 697, p. 155–160.
- Langenheim, R.L., Jr., and Larson, E.R., 1973, Correlation of Great Basin stratigraphic units: Nevada Bureau of Mines and Geology Bulletin 72, 36 p.
- Lister, G.S., and Davis, G.A., 1989, The origin of core complexes and detachment faults formed during Tertiary continental extension in the northern Colorado River region, USA: *Journal of Structural Geology*, v. 11, p. 65–94, doi:10.1016/0191-8141(89)90036-9.
- Livaccari, R.F., Geissman, J.W., and Reynolds, S.J., 1993, Paleomagnetic evidence for large-magnitude, low-angle normal faulting in a metamorphic core complex: *Nature*, v. 361, p. 56–59, doi:10.1038/361056a0.
- Longwell, C.R., Pampeyan, E.H., Bowyer, B., and Roberts, R.J., 1965, Geology and mineral deposits of Clark County, Nevada: Nevada Bureau of Mines and Geology Bulletin 62, 218 p.
- Marvin, R.F., Byers, F.M., Mehnert, H.H., Orkild, P.P., and Stern, P.W., 1970, Radiometric ages and stratigraphic sequence of volcanic and plutonic rocks, southern Nye and western Lincoln Counties, Nevada: *Geological Society of America Bulletin*, v. 81, p. 2657–2676, doi:10.1130/0016-7606(1970)81[2657:RAASSO]2.0.CO;2.
- McNair, A.H., 1951, Paleozoic stratigraphy of part of northwestern Arizona: *American Association of Petroleum Geologists Bulletin*, v. 35, p. 503–541.
- Miller, E.L., Dumitru, T.A., Brown, R.W., and Gans, P.B., 1999, Rapid Miocene slip on the Snake Range–Deep Creek Range fault system, east-central Nevada: *Geological Society of America Bulletin*, v. 111, p. 886–905, doi:10.1130/0016-7606(1999)111<0886:RMSOTS>2.3.CO;2.
- Mirabella, F., Brozzetti, F., Lupattelli, A., and Barchi, M.R., 2011, Tectonic evolution of a low-angle extensional fault system from restored cross sections in the Northern Apennines (Italy): *Tectonics*, v. 30, TC6002, doi:10.1029/2011TC002890.
- Noble, D.C., and McKee, E.H., 1972, Description and K-Ar ages of volcanic units of the Caliente volcanic field, Lincoln County, Nevada, and Washington County, Utah: *Isochron/West*, no. 5, p. 17–24.
- Novak, S.W., 1984, Eruptive history of the rhyolitic Kane Springs Wash Volcanic Center, Nevada: *Journal of Geophysical Research*, v. 89, p. 8603–8615, doi:10.1029/JB089iB10p08603.
- Olmore, S.D., 1971, Style and evolution of thrusts in the region of the Mormon Mountains, Nevada [Ph.D. thesis]: Salt Lake City, University of Utah, 213 p.
- Pampeyan, E.H., 1993, Geologic map of the Meadow Valley Mountains, Lincoln and Clark Counties, Nevada: U.S. Geological Survey Miscellaneous Investigation Map I-2173, scale 1:50,000.
- Reber, S.J., 1952, Stratigraphy and structure of the south-central and northern Beaver Dam Mountains, Utah, in Thune, H.W., ed., Cedar City, Utah to Las Vegas, Nevada: Intermountain Association of Petroleum Geologists Guidebook to the Geology of Utah 7, p. 101–108.
- Rigo, A., Lyon-Caen, H., Armijo, R., Deschamps, A., Hatzfeld, D., Markropoulos, K., Papadimitriou, P., and Kassaras, I., 1996, A microseismic study of the western part of the Gulf of Corinth (Greece): Implications for large-scale normal faulting mechanism: *Geophysical Journal International*, v. 126, p. 663–688, doi:10.1111/j.1365-246X.1996.tb04697.x.
- Rowley, P.D., Anderson, J.J., and Williams, P.L., 1975, A summary of Tertiary volcanic stratigraphy of the southwestern high plateaus and adjacent Great Basin, Utah: U.S. Geological Survey Bulletin 1405-B, 20 p.
- Singleton, J.S., 2013, Development of extension-parallel corrugations in the Buckskin-Rawhide metamorphic core complex, west-central Arizona: *Geological Society of America Bulletin*, v. 125, p. 453–472, doi:10.1130/B30672.1.
- Skelly, M.F., 1987, The geology of the Moapa Peak area, southern Mormon Mountains, Clark and Lincoln Counties, Nevada [M.S. thesis]: Flagstaff, Northern Arizona University, 150 p.
- Spencer, J.E., and Reynolds, S.J., 1991, Tectonics of mid-Tertiary extension along a transect through west-central Arizona: *Tectonics*, v. 10, p. 1204–1221, doi:10.1029/91TC01160.
- Steiger, R.H., and Jäger, E., 1977, Subcommission on Geochronology: Convention on the use of decay constants in geo- and cosmochronology: *Earth and Planetary Science Letters*, v. 36, p. 359–362, doi:10.1016/0012-821X(77)90060-7.
- Styron, R.H., and Hetland, E.A., 2014, Estimated likelihood of observing a large earthquake on a continental low-angle normal fault and implications for low-angle normal fault activity: *Geophysical Research Letters*, v. 41, p. 2342–2350, doi:10.1002/2014GL059335.
- Swanson, E.M., Wernicke, B.P., Eiler, J.M., and Losh, S., 2012, Temperatures and fluids on faults based on carbonate clumped-isotope thermometry: *American Journal of Science*, v. 312, p. 1–21, doi:10.2475/01.2012.01.
- Swanson, E.M., Wernicke, B.P., and Hauge, T.A., 2016, Episodic dissolution, precipitation, and slip on the Heart Mountain detachment, Wyoming: *The Journal of Geology*, v. 124, p. 75–97, doi:10.1086/684253.
- Taylor, W.J., 1984, Superposition of thin-skinned normal faulting on Sevier orogenic belt thrusts, northern Mormon Mountains, Lincoln County, Nevada [M.S. thesis]: Syracuse, New York, Syracuse University, 80 p.
- Tschanz, C.M., and Pampeyan, E.H., 1970, Geology and mineral deposits of Lincoln County, Nevada: Nevada Bureau of Mines and Geology Bulletin 73, 187 p.
- Walker, C.D., 2008, A gravity slide origin for the Mormon Peak detachment: Re-examining the evidence for extreme extension in the Mormon Mountains, southeastern Nevada, U.S.A. [Ph.D. thesis]: New York, Columbia University, 690 p.
- Walker, C.D., Anders, M.H., and Christie-Blick, N., 2007, Kinematic evidence for down-dip movement on the Mormon Peak detachment: *Geology*, v. 35, p. 259–262, doi:10.1130/G23396A.1.
- Wernicke, B., 1982, Processes of extensional tectonics [Ph.D. thesis]: Cambridge, Massachusetts Institute of Technology, 171 p.
- Wernicke, B., 1995, Low-angle normal faults and seismicity: A review: *Journal of Geophysical Research*, v. 100, p. 20,159–20,174, doi:10.1029/95JB01911.
- Wernicke, B., and Axen, G.J., 1988, On the role of isostasy in the evolution of normal fault systems: *Geology*, v. 16, p. 848–851, doi:10.1130/0091-7613(1988)016<0848:OTROI>2.3.CO;2.
- Wernicke, B., Walker, J.D., and Beaufait, M.S., 1985, Structural discordance between Neogene detachments and frontal Sevier thrusts, central Mormon Mountains, southern Nevada: *Tectonics*, v. 4, p. 213–246, doi:10.1029/TC004i002p00213.
- Wernicke, B., Snow, J.K., Axen, G.J., Burchfiel, B.C., Hodges, K.V., Walker, J.D., and Guth, P.L., 1989, Extensional tectonics in the Basin and Range province between the southern Sierra Nevada and the Colorado Plateau: *American Geophysical Union Field Trip Guidebook T138*, 80 p.
- Wong, M.S., and Gans, P.B., 2008, Geologic, structural, and thermochronologic constraints on the tectonic evolution of the Sierra Mazatán core complex, Sonora, Mexico: New insights into metamorphic core complex formation: *Tectonics*, v. 27, TC4013, doi:10.1029/2007TC002173.

Determining the Flow of Comal Springs at New Braunfels, Texas

By Kenneth L. Wahl¹ and Tony L. Wahl²

Abstract

A computerized base-flow separation method based on 2-day local minimums (the minimum discharge within each 2-day interval) was used to estimate springflow for Comal Springs from daily discharges for the Comal River at New Braunfels, Texas, for the 1933-93 water years. These estimates were compared to the historic estimates (manual separation). The annual springflow from the computer separation averaged about 0.4 percent less than manually-separated values. Daily estimates of springflow were also in good agreement. Thus, the computerized separation method appears to be a viable and objective method of defining the springflows from the river discharges. The study results also show that the water levels in the Comal County and Bexar County index wells are closely related (correlation coefficient of 0.98), and that it is possible to estimate the base flow of the springs from water levels in either well. The Comal County well, however, gave the better result (standard error of estimate of about 16 ft³/s above 623 ft elevation and about 8 ft³/s below).

Introduction

The Edwards aquifer is an important source of water for south-central Texas. In addition to providing water for agriculture, San Antonio and other cities in the area rely on the aquifer as a principal source of their municipal water supplies. Recharge occurs along the outcrop of the Edwards and associated limestones (*fig. 1*); streams that cross the outcrop lose much of their flow to the aquifer (Puente, 1978; Maclay and Land, 1988). Many studies of the geology and hydrology of the Edwards aquifer have been made. The report by Maclay and Land (1988) summarizes these studies and provides an overview of the interconnection of the aquifer and the springs that rise along faults between San Antonio and San Marcos.

¹. Hydrologist, U.S. Geological Survey, Lakewood, CO

². Hydraulic Engineer, U.S. Bureau of Reclamation, Lakewood, CO

The largest of those springs, Comal Springs at New Braunfels, Texas, is the largest group of springs in Texas (Harden, 1988, p. 26) and one of the largest in the southwestern United States. In addition to providing agricultural and municipal water, Comal Springs supports a regional recreation and tourism industry and provides critical habitat for the fountain darter (*Estheostoma fonticola*), an endangered fish that occurs at Comal Springs as well as in parts of the Comal and San Marcos Rivers. The U.S. Fish and Wildlife Service has determined that flows of less than 150 ft³/s from Comal Springs will place the fountain darter in jeopardy (Moore, 1994). As springflows approach this level, users of water from the aquifer will be affected by aquifer management strategies designed to maintain the springflows.

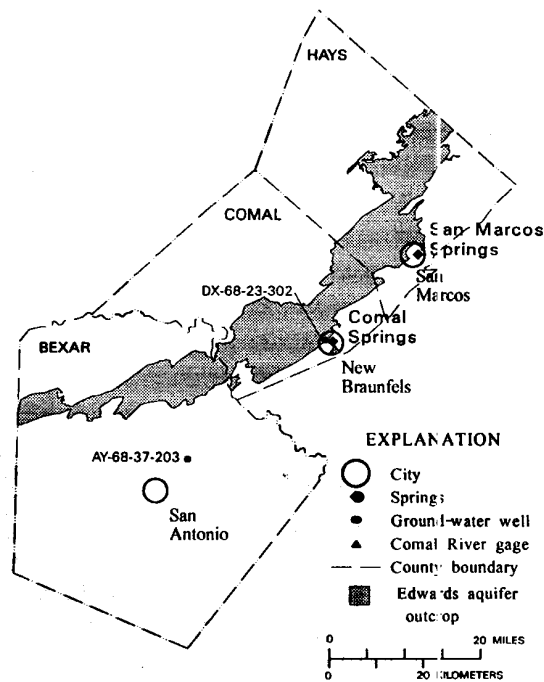


Figure 1. Location map of the study area.

Because Comal Springs rises in numerous orifices, some of which are submerged in pools, direct measurement of the discharge of Comal Springs is not feasible. Historically, estimates of daily springflow have been derived from the daily flow record for the U.S. Geological Survey (USGS) streamflow gaging station on the Comal River at New Braunfels (08169000) using manual methods of base-flow separation. About 95 percent of the time, all flow in the Comal River is derived from Comal Springs. Thunderstorms occasionally produce direct runoff to the river, which has a surface drainage area at the gaging station of 108 mi². The direct runoff is included in the gaged river discharge and must be subtracted from the total flow in order to arrive at the base flow derived from the springs.

There are now two somewhat separate needs for springflow data. Data are needed to define the long-term flow rates of the springs for archival purposes. In addition, there is a need to be able to estimate the real-time (present) flow of the springs. Base-flow separation methods can provide the data for archival purposes, but it is unlikely that those methods can provide real-time estimates of the springflow except during periods of no direct runoff. Therefore, alternative methods are needed, perhaps using local ground-water levels. The present study was undertaken to determine (1) whether computerized base-flow separation methods can provide the daily flow records needed for documentation and archival purposes, and (2) whether real-time estimates of the discharge of the springs during periods of direct runoff can be derived from ground-water levels.

Computerized Base-Flow Separation (BFI Program)

Manual base-flow separation methods are labor intensive and are generally not objective; different analysts given the same data would probably arrive at somewhat different values for base flow.

To overcome the lack of objectivity in manual base-flow separation methods, the Institute of Hydrology (1980a,b) proposed a set of procedures in which the water year is divided into 5-day increments, and the minimum flow during each 5-day period is identified. Minimums are then compared to adjacent minimums to determine turning points on the base-flow hydrograph. If 90 percent of a given minimum is less than both adjacent minimums, then that minimum is a turning point. Straight lines drawn between turning points (on semilogarithmic paper) define the base-flow hydrograph; the area beneath the hydrograph is an estimate of the volume of base flow for the period. The ratio of this volume to the total volume of streamflow for the period is defined as the base-flow index. Although these procedures may not yield the true base flow of the stream, tests in Great Britain (Institute of Hydrology, 1980b), Canada (Swan and Condie, 1983), and the United States (Wahl and Wahl, 1988) suggest that the results are consistent and indicative of the base flow. The procedure is only appropriate for unregulated streams, and thus often cannot be applied to large watersheds.

In contrast to most manual procedures, computerized methods of base-flow separation can handle large amounts of data with relative ease and are objective. A FORTRAN program, BFI (Base Flow Index) that implements the Institute of Hydrology method was initially written for studies of base flow trends in the Oklahoma Panhandle (Wahl and Wahl, 1988) and has been further developed since that time.

How the BFI Program Works

The BFI program accepts data in USGS WATSTORE 2- and 3-card (80-column) format (Hutchinson, 1975) and can process multiple years of data from one or more gage sites. The program produces a table that includes the base flow, total streamflow, and the base-flow index for each water year, as well as summary statistics.

Several refinements have been made to the program to increase its usefulness and provide flexibility. To allow analysis of streams with zero-flow periods, the program uses a linear base-flow recession rather than the standard semilogarithmic relation if a base-flow turning point falls on a zero-flow day. The program can also process continuously through consecutive years so that data near the beginning and end of each water year are not excluded from the analysis. The program checks for errors in the input data, and although it will only calculate a base-flow index for years with complete data, all turning points, daily streamflow and base-flow values can be output to a file for further analysis.

The algorithm proposed by the Institute of Hydrology uses 5-day minimum streamflows and a factor of 0.9 for the test to identify base-flow turning points. Both of these parameters can be varied in the BFI program to permit tuning the algorithm for different watersheds or to match other base-flow separation methods. These parameters are termed N (number of days) and f (turning point test factor). If the year cannot be evenly divided into N -day periods, the last period in the year is lengthened to include the remaining days.

In some cases the method may estimate daily base flows that exceed the actual streamflow. This is often the result of random errors in reported streamflow discharge for streams dominated by base flow. The program makes no adjustments for this situation in its calculations of total annual base flow. However, the daily base-flow values printed in the output file are checked and limited to the actual daily streamflow.

Determining N and f

Tuning of the BFI program is accomplished by varying N and f . The parameter N has the most dramatic effect in most cases. As N is increased, higher-flow days are excluded, and the base flow estimated by the program is reduced. Figure 2 shows the relation between the base-flow index and N for the Comal River at New Braunfels for each of the 1986-88 water years and for the 1933-93 average. The curves show two different behaviors. For 1988, a year with little direct runoff, the relation between BFI and N is basically linear. For the remaining curves, however, increasing N causes a dramatic drop in the estimated base flow as direct runoff is being eliminated. When a critical value of N is reached, all direct runoff has been eliminated, and the drop in estimated base flow becomes less pronounced and essentially linear with increasing N ; any further increase of N causes the method to cut into base flow. Thus, the point of slope change indicates an appropriate value for N . For the Comal River at New Braunfels the slope change occurs at $N = 2$ days. This is consistent with the observation that direct runoff generally ceases within 1-2 days following a storm.

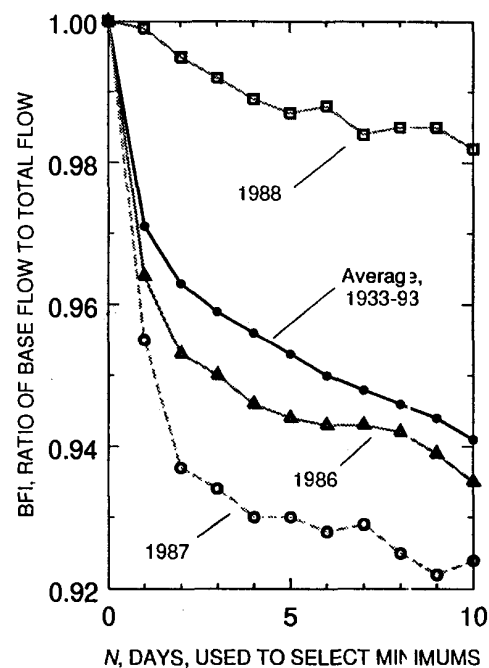


Figure 2. Relation between base flow (BFI) and number of days (N) used to select minimums.

The effect of the f parameter is less definite. If the interval in days between each potential turning point (N -day

minimum) were a constant, the value of f associated with a given N would define limiting rising and recession slopes for the base-flow hydrograph. However, since minimum flows can occur anywhere within each N -day period, the interval between any two N -day minimums can vary from 1 to $(2N-1)$, producing a wide range of slope limits imposed by f within the course of a single application of the program. In practice, the value of 0.9 seems appropriate in most applications for which the BFI method is suitable.

Comparison with Historic Springflow Estimates

The program was used to compute base-flow estimates for the Comal River at New Braunfels for water years 1933-1955 and 1958-1991, using an N of 2 days and an f of 0.9. Water years 1956 and 1957 were excluded because the Comal Springs went dry during these years, and the river flow was supplemented by ground-water pumping, which has not been excluded from the reported daily streamflow. The percentage differences between annual base-flow volumes estimated using the BFI program and the historic estimates based on manual-separation methods are shown in figure 3A and 3B. The annual results compare very favorably, with BFI producing about 0.4 percent less springflow, on average, than was estimated through the historic manual separation. While the annual differences average only about 0.4 percent, the differences appear to be systematically larger from the late 1970's to about 1992 (fig. 3A). These differences are independent of the magnitude of the annual discharge of the river (fig. 3B). This implies a difference in the manual base-flow separation method used to estimate springflow for that period.

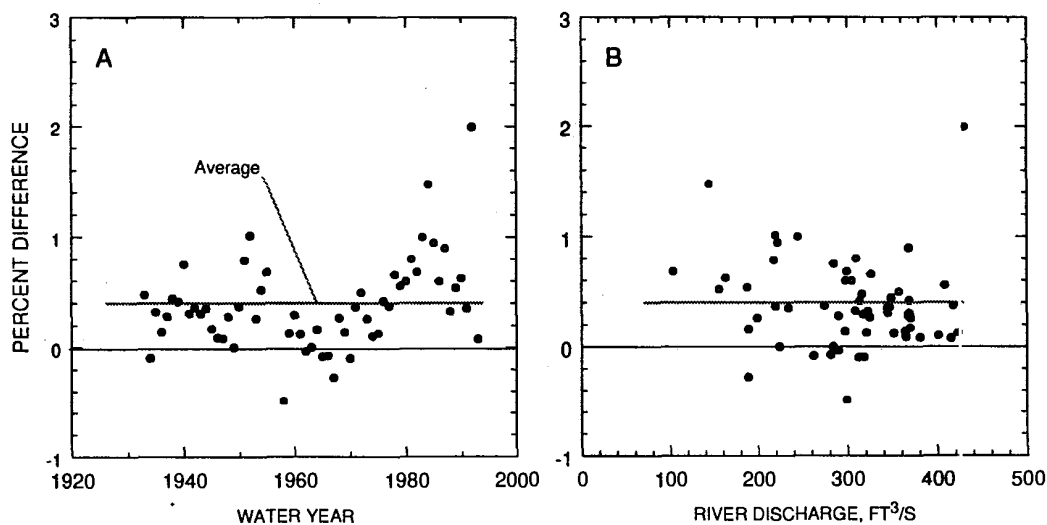


Figure 3. Percent difference between historic springflow estimates (manual separation method) and BFI results using $N = 2$ days as a function of (A) time, and (B) Discharge of the Comal River.

Daily base-flow estimates produced by the BFI program for water years 1986-90 are compared with manually-separated values in *figure 4*. The 1986-90 period was selected as a sample representative of the period of record. The correspondence between daily values is only approximate, confirming previous observations that the method may not yield the true base flow, but provides a consistent indication of longer-term base-flow variations. There is, of course, no assurance that the manually-separated base flows are the true springflows.

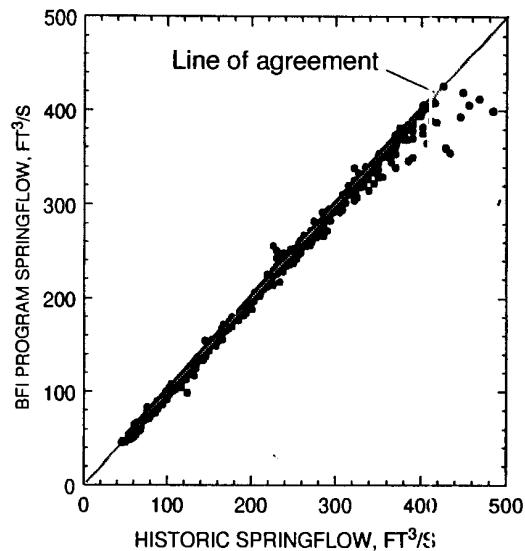


Figure 4. Comparison of daily springflow from the BFI program with historic estimates from manual separation, water years 1986-90.

Relations between Ground-Water Levels and Springflows

The flow of the springs has long been recognized to be directly related to the water levels in the Edwards aquifer. Maclay and Land (1988, p. 20) described the general movement of ground-water in the Edwards aquifer and noted that "Most of the flow in Comal Springs is sustained by ground water along the downthrown side of the Comal Springs fault." Espey (1988) showed the relation between river flows and base flows, and Harden (1988) described the general relation between water level in the aquifer and elevations of the principal springs that issue from the aquifer. However, the relations shown by both Espey (1988) and Harden (1988) were qualitative; no specific estimating relations were shown.

Puente (1976) defined regression relations between water levels in several index wells in the area as well as defining the relations between those water levels and springflow amounts. Among the wells he used were the Comal County index well (DX-68-23-302) located about 300 feet west of Comal Springs and the Bexar County index well (AY-68-37-203) located about 25 mi southwest of Comal Springs.

For the present study, regression relations were defined between the historic springflows (from base-flow separation) and the water-surface elevations of both the Comal County and Bexar County index wells. The Comal County well is nearby and would serve as a convenient index to the springflow. Although this well is near the springs, the well was completed on the upthrown side of the Comal Springs fault (George Ozuna, U.S. Geological Survey, written commun., 1994), and the springs are sustained by ground water along the downthrown side of the fault (Maclay and Land, 1988, p. 20). In addition, the head variation in the Comal County well (about 11 ft) is much less than in upgradient wells that are more distant from the fault and springs. Thus, a relatively small change in water-level elevation in the well could effect a

relatively large change in springflow. The Bexar County well is a widely used index well with a larger range in water-level elevation (about 80 ft), but is located about 25 mi from the springs. The Bexar County well, however, is known to be influenced by development in the San Antonio area (Harden, 1988). Because of this development and the distance to the springs, the Bexar County well may not accurately reflect the hydraulic head driving Comal Springs.

The Relation Between Well Levels

Water-level data are available in computer files of the USGS for both the Comal County well and the Bexar County well. Several wells have served as the Bexar County index well since about 1911; water levels in the USGS computer files represent well AY-68-37-203 only since the spring of 1963. Thus, the current analysis of water levels for the Bexar County index well used data only after 1963.

Puente (1976) developed a linear regression relation between the monthly mean depths (in ft) to water below land surface in the Comal County (D_C) and in the Bexar County (D_B) index wells. The elevations of the land-surface datums are 642.7 ft and 730.81 ft, respectively. A similar relation was developed in the present study using 2,016 daily water-level readings for calendar years 1964-1993. Those relations as well as the equivalent present relation using water-level elevations (E_C and E_B) of the wells are shown in Table 1.

Table 1: Regression relations between water levels in the Comal County and Bexar County index wells.

Variable	Equation	R ²	Standard error, ft	Sample size	Data used
Monthly mean depth to water (Puente, 1976)	$D_C = 8.46 + 0.13 D_B$	0.98	0.22	81	1964-73
Daily depth to water	$D_C = 8.48 + 0.1316 D_B$.97	.39	2,016	1964-93
Daily water-level elevation	$E_C = 538.1 + 0.1316 E_B$.97	.39	2,016	1964-93

The relations between the water-level elevation data are shown in *figure 5*. The excellent agreement between Puente's relation and those defined in the present study using more frequent readings and a longer period of record attest to the stability of the relation between these wells.

Relation between Springflow and Ground-Water Levels

Puente (1976) defined regression relations between the flow of Comal Springs and the ground-water levels in the Comal and Bexar County index wells. Daily and monthly flows were related to the Comal County well, and monthly and annual flows

were related to the Bexar County well. Although his data covered the normal ranges of the variables, the daily-flow relations were based on a relatively small set of data (33 days). Puente concluded that springflow could be estimated accurately by a set of empirical equations. These wells were also used in the present study.

The elevation of Comal Springs is commonly given as 623 ft. That elevation, however, is for the topmost orifice. The springs went dry in 1956 as the water-level elevation in the Comal County well neared 619 ft; the springs remained dry while the water level in the well remained below about 619 ft. Therefore, the elevations of the various orifices of the springs can be assumed to cover a range of about 4 ft. The relation between the water levels in the well and springflow will change as the various orifices cease to flow over a water-level range of about 4 ft. Therefore, separate relations were developed depending on whether the water-level elevation in the Comal County well was above or below 623 ft. The corresponding elevation at the Bexar County well is 645 ft.

Daily springflow discharges (Q) determined from base-flow separation were related to the water levels in both the Comal County and Bexar County wells. Those relations are shown in Table 2 and the data and relations for the Comal County well are shown in *figure 6*. The lower relation for the Comal County well shows the springs to be dry when the water level in the well falls below about 619.3 ft and should not be used below that elevation. The Comal County well produced the better relations, probably by virtue of its proximity to the springs. The relation between the flow from Comal Springs and the Comal County well is good, but there appears to be some minor seasonal fluctuation in some years. That fluctuation may be a result of the response of the well to pumping in the vicinity of the well or to changes in the water level in Landa Lake, which would affect the head difference between the aquifer and the spring orifices.

Table 2: Regression relations between the average daily flow of Comal Springs and water-surface elevations in the Comal County and Bexar County index wells.

Equation	Conditions	R ²	Standard Error, ft ³ /s	Sample Size
$Q = 36.82 + 36.96 (E_C - 619)$	$E_C > 623$	0.94	16.13	813
$Q = -17.03 + 50.5 (E_C - 619)$	$619.3 > E_C < 623$.97	7.92	114
$Q = 52.31 + 4.932 (E_B - 619)$	$E_B > 645$.92	19.22	813
$Q = 11.63 + 6.51 (E_B - 619)$	$619 > E_B < 645$.93	12.52	114

Puente (1976) presented a relation between the daily springflow and the depth below land surface in the Comal County index well that was based on 33 daily values. His relation, recast in the form of the equations in Table 2 was

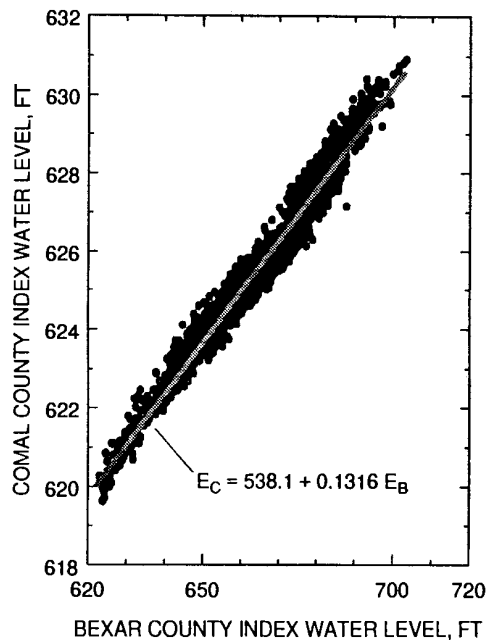


Figure 5. Relation between the water-level elevations in the Bexar and Comal County index wells (1964-93).

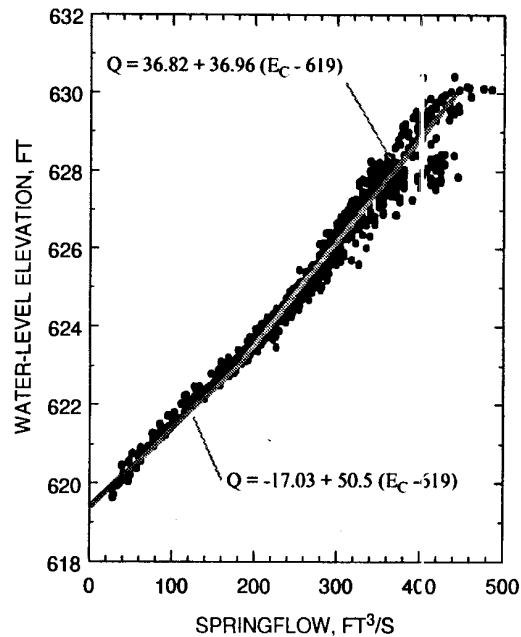


Figure 6. Relation between water level in Comal County index well and flow from Comal Springs (1977-91).

$Q = 12.72 + 44.4 (E_C - 619)$. That equation produces comparable results to those in Table 2 for $E_C = 623$ ft; for $E_C = 630$ ft, Puente's equation gives about 13 percent more springflow.

Summary and Conclusions

The study shows that the springflows that have traditionally been computed by manual separation of the base flow from the daily discharges of the Comal River can be reproduced using a computerized method. The annual percentage differences between the model-produced results and the historic values averaged about 0.4 percent. The computerized method has advantages over the manual method in that the computerized method is fast and objective; that is, given the same set of input data, different analysts would produce the same base-flow (springflow) estimates using the model. There is some evidence that in the past, the methodology used in performing the manual separation has undergone some subtle changes that, while producing relatively small differences, could cause the results to suggest changes that may in fact be artifacts of the changes in methodology. The computer-based separated values do not show this feature.

The study results also show that it is possible to estimate the base flow of the springs from water levels in either the Comal County or the Bexar County index wells. The Comal County well gave the better result (standard error of estimate of about 16 ft^3/s above 623 ft elevation and about 8 ft^3/s below). Using the well record could be particularly useful when the rates of springflow are needed during periods of direct

runoff to the river. During such periods, base-flow separation techniques, both manual and computerized, are ineffective until the river has returned to base-flow conditions.

A possible procedure that could be used to determine springflows in the future would be to (1) use the computerized method ($N=2$ days) to derive the springflows for archival purposes, and (2) use the relation with the water levels in the Comal County index well to estimate the flow in real time during periods of direct runoff. These latter values would be recognized as estimates that could be available immediately for management purposes, but that would be revised and replaced in the database with values from the computer model once the river flow had receded to base-flow conditions.

References

- Espey, W.H., Jr., 1988, Surface Water: Proceedings, San Marcos and Comal Springs Symposium, Southwest Texas State University, San Marcos, Texas, December 2-3, 1988.
- Harden, Rollin, 1988, Ground Water: Proceedings, San Marcos and Comal Springs Symposium, Southwest Texas State University, San Marcos, Texas, December 2-3, 1988.
- Hutchinson, N.E., 1975, WATSTORE user's guide: U.S. Geological Survey Open-File Report 75-426, 6 Vols.
- Institute of Hydrology, 1980, Low flow studies: Wallingford, Oxon, United Kingdom, Report No. 1, 41 p.
- Institute of Hydrology, 1980, Low flow studies: Wallingford, Oxon, United Kingdom, Report No. 3, p. 12-19.
- Maclay, R.W., and Land, L.F., 1988, Simulation of flow in the Edwards aquifer, San Antonio region, Texas, and refinement of storage and flow concepts: U.S. Geological Survey Water-Supply Paper 2336-A, 48 p.
- Moore, J.G., Jr., 1994, Emergency withdrawal reduction plan for the Edwards aquifer: U.S. District Court Report on Sierra Club et al v. Bruce Babbitt et al, Cause No. MO-91-CA-069, 91 p.
- Puente, Celso, 1976, Statistical analyses of water-level, springflow, and streamflow data for the Edwards aquifer in south-central Texas: U.S. Geological Survey Open-File Report 76-393, 58 p.
- Puente, Celso, 1978, Method of estimating natural recharge to the Edwards aquifer in the San Antonio area, Texas: U.S. Geological Survey Water Resources Investigations 78-10, 34 p.
- Swan, D.R., and Condie, R., 1983, Computation of the base flow index: Water Resources Branch Inland Water Directorate, Environment Canada, Ottawa, Ontario, 21 p.
- Wahl, K.L., and Wahl, T.L., 1988, Effects of regional ground-water level declines on streamflow in the Oklahoma Panhandle: Proceedings of Symposium on Water-Use Data for Water Resources Management, American Water Resources Association, August 1988, Tucson, Arizona, pp. 239-249.

Appendix E - BFI



Determining the Flow of Comal Springs at New Braunfels, Texas

By Kenneth L. Wahl
Hydrologist, U.S. Geological Survey, Lakewood, CO
and Tony L. Wahl
Hydraulic Engineer, Bureau of Reclamation, Lakewood, CO

Abstract

A computerized base-flow separation method based on 2-day local minimums (the minimum discharge within each 2-day interval) was used to estimate springflow for Comal Springs from daily discharges for the Comal River at New Braunfels, Texas, for the 1933-93 water years. These estimates were compared to the historic estimates (manual separation). The annual springflow from the computer separation averaged about 0.4 percent less than manually-separated values. Daily estimates of springflow were also in good agreement. Thus, the computerized separation method appears to be a viable and objective method of defining the springflows from the river discharges. The study results also show that the water levels in the Comal County and Bexar County index wells are closely related (correlation coefficient of 0.98), and that it is possible to estimate the base flow of the springs from water levels in either well. The Comal County well, however, gave the better result (standard error of estimate of about 16 ft³/s above 623 ft elevation and about 8 ft³/s below).

Introduction

The Edwards aquifer is an important source of water for south-central Texas. In addition to providing water for agriculture, San Antonio and other cities in the area rely on the aquifer as a principal source of their municipal water supplies. Recharge occurs along the outcrop of the Edwards and associated limestones (fig. 1); streams that cross the outcrop lose much of their flow to the aquifer (Puente, 1978; Maclay and Land, 1988). Many studies of the geology and hydrology of the Edwards aquifer have been made. The report by Maclay and Land (1988) summarizes these studies and provides an overview of the interconnection of the aquifer and the springs that rise along faults between San Antonio and San Marcos.

The largest of those springs, Comal Springs at New Braunfels, Texas, is the largest group of springs in Texas (Harden, 1988, p. 26) and one of the largest in the southwestern United States. In addition to providing agricultural and municipal water, Comal Springs supports a regional recreation and tourism industry and provides critical habitat for the fountain darter (*Estheostoma fonticola*), an endangered fish that occurs at Comal Springs as well as in parts of the Comal and San Marcos Rivers. The U.S. Fish and Wildlife Service has determined that flows of less than 150 ft³/s from Comal Springs will place the fountain darter in jeopardy (Moore, 1994). As springflows approach this level, users of water from the aquifer will be affected by aquifer management strategies designed to maintain the springflows.

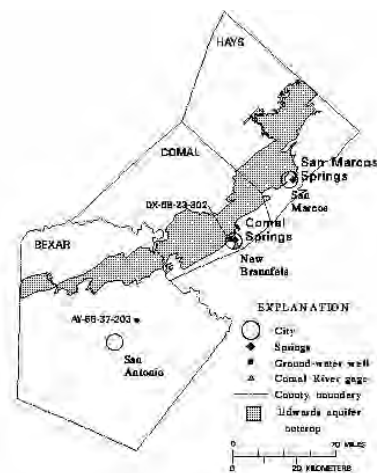


Figure 1. Location map of the study area.

Figure 1. Location map of the study area.

Because Comal Springs rises in numerous orifices, some of which are submerged in pools, direct measurement of the discharge of Comal Springs is not feasible. Historically, estimates of daily springflow have been derived from the daily flow record for the U.S. Geological Survey (USGS) streamflow gaging station on the Comal River at New Braunfels (08169000) using manual methods of base-flow separation. About 95 percent of the time, all flow in the Comal River is derived from Comal Springs. Thunderstorms occasionally produce direct runoff to the river, which has a surface drainage area at the gaging station of 108 mi². The direct runoff is included in the gaged river discharge and must be subtracted from the total flow in order to arrive at the base flow derived from the springs.

There are now two somewhat separate needs for springflow data. Data are needed to define the long-term flow rates of the springs for archival purposes. In addition, there is a need to be able to estimate the real-time (present) flow of the springs. Base-flow separation methods can provide the data for archival purposes, but it is unlikely that those methods can provide real-time estimates of the springflow except during periods of no direct runoff. Therefore, alternative methods are needed, perhaps using local groundwater levels. The present study was undertaken to determine (1) whether computerized base-flow separation methods can provide the daily flow records needed for documentation and archival purposes, and (2) whether real-time estimates of the discharge of the springs during periods of direct runoff can be derived from groundwater levels.

Computerized Base-Flow Separation (BFI Program)

Manual base-flow separation methods are labor intensive and are generally not objective; different analysts given the same data would probably arrive at somewhat different values for base flow.

To overcome the lack of objectivity in manual base-flow separation methods, the Institute of Hydrology (1980a,b) proposed a set of procedures in which the water year is divided into 5-day increments, and the minimum flow during each 5-day period is identified. Minimums are then compared to

SE ROA 37843

adjacent minimums to determine turning points on the base-flow hydrograph. If 90 percent of a given minimum is less than both adjacent minimums, then that minimum is a turning point. Straight lines drawn between turning points (on semilogarithmic paper) define the base-flow hydrograph; the area beneath the hydrograph is an estimate of the volume of base flow for the period. The ratio of this volume to the total volume of streamflow for the period is defined as the base-flow index. Although these procedures may not yield the true base flow of the stream, tests in Great Britain (Institute of Hydrology, 1980b), Canada (Swan and Condie, 1983), and the United States (Wahl and Wahl, 1988) suggest that the results are consistent and indicative of the base flow. The procedure is only appropriate for unregulated streams, and thus often cannot be applied to large watersheds.

In contrast to most manual procedures, computerized methods of base-flow separation can handle large amounts of data with relative ease and are objective. A FORTRAN program, BFI (Base Flow Index) that implements the Institute of Hydrology method was initially written for studies of base flow trends in the Oklahoma Panhandle (Wahl and Wahl, 1988) and has been further developed since that time. How the BFI Program Works

The BFI program accepts data in USGS WATSTORE 2- and 3-card (80-column) format (Hutchinson, 1975) and can process multiple years of data from one or more gage sites. The program produces a table that includes the base flow, total streamflow, and the base-flow index for each water year, as well as summary statistics.

Several refinements have been made to the program to increase its usefulness and provide flexibility. To allow analysis of streams with zero-flow periods, the program uses a linear base-flow recession rather than the standard semilogarithmic relation if a base-flow turning point falls on a zero-flow day. The program can also process continuously through consecutive years so that data near the beginning and end of each water year are not excluded from the analysis. The program checks for errors in the input data, and although it will only calculate a base-flow index for years with complete data, all turning points, daily streamflow and base-flow values can be output to a file for further analysis.

The algorithm proposed by the Institute of Hydrology uses 5-day minimum streamflows and a factor of 0.9 for the test to identify base-flow turning points. Both of these parameters can be varied in the BFI program to permit tuning the algorithm for different watersheds or to match other base-flow separation methods. These parameters are termed N (number of days) and f (turning point test factor). If the year cannot be evenly divided into N-day periods, the last period in the year is lengthened to include the remaining days.

In some cases the method may estimate daily base flows that exceed the actual streamflow. This is often the result of random errors in reported streamflow discharge for streams dominated by base flow. The program makes no adjustments for this situation in its calculations of total annual base flow. However, the daily base-flow values printed in the output file are checked and limited to the actual daily streamflow.

Determining N and f

Tuning of the BFI program is accomplished by varying N and f. The parameter N has the most dramatic effect in most cases. As N is increased, higher-flow days are excluded, and the base flow estimated by the program is reduced. Figure 2 shows the relation between the base-flow index and N for the Comal River at New Braunfels for each of the 1986-88 water years and for the 1933-93 average. The curves show two different behaviors. For 1988, a year with little direct runoff, the relation between BFI and N is basically linear. For the remaining curves, however, increasing N causes a dramatic drop in the estimated base flow as direct runoff is being eliminated. When a critical value of N is reached, all direct runoff has been eliminated, and the drop in estimated base flow becomes less pronounced and essentially linear with increasing N; any further increase of N causes the method to cut into base flow. Thus, the point of slope change indicates an appropriate value for N. For the Comal River at New Braunfels the slope change occurs at N = 2 days. This is consistent with the observation that direct runoff generally ceases within 1-2 days following a storm.

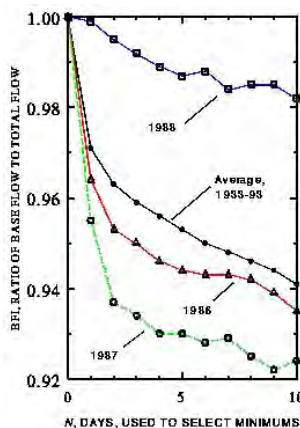


Figure 2. Relation between base flow (BFI) and number of days (N) used to select minimums.

The effect of the f parameter is less definite. If the interval in days between each potential turning point (N-day minimum) were a constant, the value of f associated with a given N would define limiting rising and recession slopes for the base-flow hydrograph. However, since minimum flows can occur anywhere within each N-day period, the interval between any two N-day minimums can vary from 1 to (2N-1), producing a wide range of slope limits imposed by f within the course of a single application of the program. In practice, the value of 0.9 seems appropriate in most applications for which the BFI method is suitable.

Comparison with Historic Springflow Estimates

The program was used to compute base-flow estimates for the Comal River at New Braunfels for water years 1933-1955 and 1958-1991, using an N of 2 days and an f of 0.9. Water years 1956 and 1957 were excluded because the Comal Springs went dry during these years, and the river flow was supplemented by groundwater pumping, which has not been excluded from the reported daily streamflow. The percentage differences between annual base-flow volumes estimated using the BFI program and the historic estimates based on manual-separation methods are shown in figure 3A and 3B. The annual results compare very favorably, with BFI producing about 0.4 percent less springflow, on average, than was estimated through the historic manual separation. While the annual differences average only about 0.4 percent, the differences appear to be systematically larger from the late 1970's to about 1992 (fig. 3A). These differences are independent of the magnitude of the annual discharge of the river (fig. 3B). This implies a difference in the manual base-flow separation method used to estimate springflow for that period.

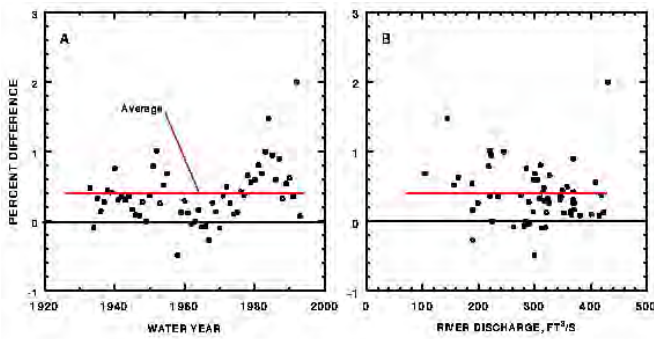


Figure 3. Percent difference between historic springflow estimates (manual separation method) and BFI results using $N = 2$ days as a function of (A) time, and (B) Discharge of the Comal River.

Daily base-flow estimates produced by the BFI program for water years 1986-90 are compared with manually-separated values in figure 4. The 1986-90 period was selected as a sample representative of the period of record. The correspondence between daily values is only approximate, confirming previous observations that the method may not yield the true base flow, but provides a consistent indication of longer-term base-flow variations. There is, of course, no assurance that the manually-separated base flows are the true springflows

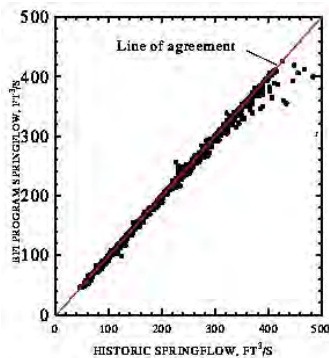


Figure 4. Comparison of daily springflow from the BFI program with historic estimates from manual separation, water years 1986-90.

Figure 4. Comparison of daily springflow from BFI program with historic estimates from manual separation, water years 1986-1990.

Relations between groundwater Levels and Springflows

The flow of the springs has long been recognized to be directly related to the water levels in the Edwards aquifer. Maclay and Land (1988, p. 20) described the general movement of groundwater in the Edwards aquifer and noted that "Most of the flow in Comal Springs is sustained by ground water along the downthrown side of the Comal Springs fault." Espey (1988) showed the relation between river flows and base flows, and Harden (1988) described the general relation between water level in the aquifer and elevations of the principal springs that issue from the aquifer. However, the relations shown by both Espey (1988) and Harden (1988) were qualitative; no specific estimating relations were shown.

Puente (1976) defined regression relations between water levels in several index wells in the area as well as defining the relations between those water levels and springflow amounts. Among the wells he used were the Comal County index well (DX-68-23-302) located about 300 feet west of Comal Springs and the Bexar County index well (AY-68-37-203) located about 25 mi southwest of Comal Springs.

For the present study, regression relations were defined between the historic springflows (from base-flow separation) and the water-surface elevations of both the Comal County and Bexar County index wells. The Comal County well is nearby and would serve as a convenient index to the springflow. Although this well is near the springs, the well was completed on the upthrown side of the Comal Springs fault (George Ozuna, U.S. Geological Survey, written commun., 1994), and the springs are sustained by ground water along the downthrown side of the fault (Maclay and Land, 1988, p. 20). In addition, the head variation in the Comal County well (about 11 ft) is much less than in upgradient wells that are more distant from the fault and springs. Thus, a relatively small change in water-level elevation in the well could effect a relatively large change in springflow. The Bexar County well is a widely used index well with a larger range in water-level elevation (about 80 ft), but is located about 25 mi from the springs. The Bexar County well, however, is known to be influenced by development in the San Antonio area (Harden, 1988). Because of this development and the distance to the springs, the Bexar County well may not accurately reflect the hydraulic head driving Comal Springs.

The Relation Between Well Levels

Water-level data are available in computer files of the USGS for both the Comal County well and the Bexar County well. Several wells have served as the Bexar County index well since about 1911; water levels in the USGS computer files represent well AY-68-37-203 only since the spring of 1963. Thus, the current analysis of water levels for the Bexar County index well used data only after 1963.

Puente (1976) developed a linear regression relation between the monthly mean depths (in ft) to water below land surface in the Comal County (DC) and in the Bexar County (DB) index wells. The elevations of the land-surface datums are 642.7 ft and 730.81 ft, respectively. A similar relation was developed in the present study using 2,016 daily water-level readings for calendar years 1964-1993. Those relations as well as the equivalent present relation using water-level elevations (EC and EB) of the wells are shown in Table 1.

Table 1: Regression relations between water levels in the Comal County and Bexar County index wells.

Variable	Equation	R ²	Standard error, ft.	Sample size	Data used
Monthly mean depth to water (Puente, 1976)	$DC = 8.46 + 0.13 DB$	0.98	0.22	81	1964-73
Daily depth to water	$DC = 8.48 + 0.1316 DB$.97	.39	2,016	1964-93
Daily water-level elevation	$EC = 538.1 + 0.1316 EB$.97	.39	2,016	1964-93

The relations between the water-level elevation data are shown in figure 5. The excellent agreement between Puente's relation and those defined in the present study using more frequent readings and a longer period of record attest to the stability of the relation between these wells.

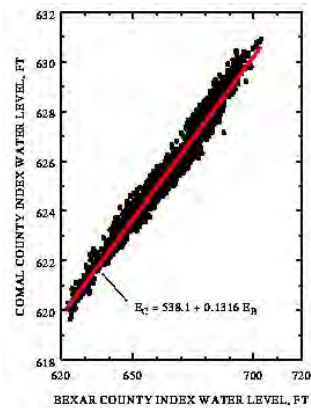


Figure 5. Relation between the water-level elevations in the Bexar and Comal County index wells (1964-93).

Figure 5. Relation between the water-level elevations in the Bexar and Comal County index wells (1964-93).

Relation between Springflow and groundwater Levels

Puente (1976) defined regression relations between the flow of Comal Springs and the groundwater levels in the Comal and Bexar County index wells. Daily and monthly flows were related to the Comal County well, and monthly and annual flows were related to the Bexar County well. Although his data covered the normal ranges of the variables, the daily-flow relations were based on a relatively small set of data (33 days). Puente concluded that springflow could be estimated accurately by a set of empirical equations. These wells were also used in the present study.

The elevation of Comal Springs is commonly given as 623 ft. That elevation, however, is for the topmost orifice. The springs went dry in 1956 as the water-level elevation in the Comal County well neared 619 ft; the springs remained dry while the water level in the well remained below about 619 ft. Therefore, the elevations of the various orifices of the springs can be assumed to cover a range of about 4 ft. The relation between the water levels in the well and springflow will change as the various orifices cease to flow over a water-level range of about 4 ft. Therefore, separate relations were developed depending on whether the water-level elevation in the Comal County well was above or below 623 ft. The corresponding elevation at the Bexar County well is 645 ft.

Daily springflow discharges (Q) determined from base-flow separation were related to the water levels in both the Comal County and Bexar County wells. Those relations are shown in Table 2 and the data and relations for the Comal County well are shown in figure 6.

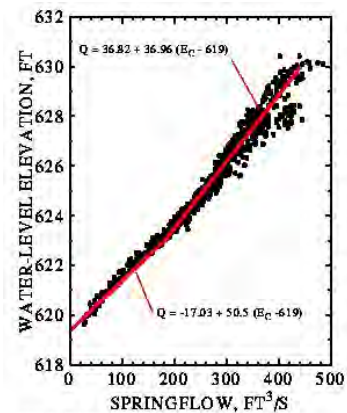


Figure 6. Relation between water level in Comal County index well and flow from Comal Springs (1977-91).

Figure 6. Relation between the water level in the Comal County index well and flow from Comal Springs (1977-91).

The lower relation for the Comal County well shows the springs to be dry when the water level in the well falls below about 619.3 ft and should not be used below that elevation. The Comal County well produced the better relations, probably by virtue of its proximity to the springs. The relation between the flow from Comal Springs and the Comal County well is good, but there appears to be some minor seasonal fluctuation in some years. That fluctuation may be a result of the response of the well to pumping in the vicinity of the well or to changes in the water level in Landa Lake, which would affect the head difference between the aquifer and the spring orifices.

Table 2: Regression relations between the average daily flow of Comal Springs and water-surface elevations in the Comal County and Bexar County index wells.

Equation	Conditions	R ²	Standard Error, ft ³ /s	Sample Size
$Q = 36.82 + 36.96 (EC - 619)$	$EC > 623$	0.94	16.13	813
$Q = -17.03 + 50.5 (EC - 619)$	$619.3 > EC < 623$.97	7.92	114
$Q = 52.31 + 4.932 (EB - 619)$	$EB > 645$.92	19.22	813
$Q = 11.63 + 6.51 (EB - 619)$	$619 > EB < 645$.93	12.52	114

Puente (1976) presented a relation between the daily springflow and the depth below land surface in the Comal County index well that was based on 33 daily values. His relation, recast in the form of the equations in Table 2 was $Q = 12.72 + 44.4 (EC - 619)$. That equation produces comparable results to those in Table 2 for $EC = 623$ ft; for $EC = 630$ ft, Puente's equation gives about 13 percent more springflow.

Summary and Conclusions

The study shows that the springflows that have traditionally been computed by manual separation of the base flow from the daily discharges of the Comal River can be reproduced using a computerized method. The annual percentage differences between the model-produced results and the historic values averaged about 0.4 percent. The computerized method has advantages over the manual method in that the computerized method is fast and objective; that is, given the same set of input data, different analysts would produce the same base-flow (springflow) estimates using the model. There is some evidence that in the past, the methodology used in performing the manual separation has undergone some subtle changes that, while producing relatively small differences, could cause the results to suggest changes that may in fact be artifacts of the changes in methodology. The computer-based separated values do not show this feature.

The study results also show that it is possible to estimate the base flow of the springs from water levels in either the Comal County or the Bexar County index wells. The Comal County well gave the better result (standard error of estimate of about 16 ft³/s above 623 ft elevation and about 8 ft³/s below). Using the well record could be particularly useful when the rates of springflow are needed during periods of direct runoff to the river. During such periods, base-flow separation techniques, both manual and computerized, are ineffective until the river has returned to base-flow conditions.

A possible procedure that could be used to determine springflows in the future would be to (1) use the computerized method (N=2 days) to derive the springflows for archival purposes, and (2) use the relation with the water levels in the Comal County index well to estimate the flow in real time during periods of direct runoff. These latter values would be recognized as estimates that could be available immediately for management purposes, but that would be revised and replaced in the database with values from the computer model once the river flow had receded to base-flow conditions.

References

- Espey, W.H., Jr., 1988,
 Surface Water: Proceedings, San Marcos and Comal Springs Symposium, Southwest Texas State University, San Marcos, Texas, Decem
 Harden, Rollin, 1988,
 Ground Water: Proceedings, San Marcos and Comal Springs Symposium, Southwest Texas State University, San Marcos, Texas, Decem
 Hutchinson, N.E., 1975,
 WATSTORE user's guide: U.S. Geological Survey Open-File Report 75-426, 6 Vols.
 Institute of Hydrology, 1980,
 Low flow studies: Wallingford, Oxon, United Kingdom, Report No. 1, 41 p.
 Institute of Hydrology, 1980,
 Low flow studies: Wallingford, Oxon, United Kingdom, Report No. 3, p. 12-19.
 Maclay, R.W., and Land, L.F., 1988,
 Simulation of flow in the Edwards aquifer, San Antonio region, Texas, and refinement of storage and flow concepts: U.S. Geolog
 Moore, J.G., Jr., 1994,
 Emergency withdrawal reduction plan for the Edwards aquifer: U.S. District Court Report on Sierra Club et al v. Bruce Babbitt
 Puente, Celso, 1976,
 Statistical analyses of water-level, springflow, and streamflow data for the Edwards aquifer in south-central Texas: U.S. Geol
 Puente, Celso, 1978,
 Method of estimating natural recharge to the Edwards aquifer in the San Antonio area, Texas: U.S. Geological Survey Water Reso
 Swan, D.R., and Condie, R., 1983,
 Computation of the base flow index: Water Resources Branch Inland Water Directorate, Environment Canada, Ottawa, Ontario, 21 p
 Wahl, K.L., and Wahl, T.L., 1988,
 Effects of regional groundwater level declines on streamflow in the Oklahoma Panhandle: Proceedings of Symposium on Water-Use

This paper was modified for the web by Alisa Remington, USGS Volunteer for Science

Last reviewed: 10/26/04



PNNL-19775, Rev. 1

Prepared for the U.S. Department of Energy
under Contract DE-AC05-76RL01830

Guide to using Multiple Regression in Excel (MRCX v.1.1) for Removal of River Stage Effects from Well Water Levels

RD Mackley
FA Spane

TC Pulsipher
CH Allwardt

September 2010



Pacific Northwest
NATIONAL LABORATORY

Proudly Operated by Battelle Since 1965

SE ROA 38072

JA_9354

DISCLAIMER

This report was prepared as an account of work sponsored by an agency of the United States Government. Neither the United States Government nor any agency thereof, nor Battelle Memorial Institute, nor any of their employees, makes **any warranty, express or implied, or assumes any legal liability or responsibility for the accuracy, completeness, or usefulness of any information, apparatus, product, or process disclosed, or represents that its use would not infringe privately owned rights.** Reference herein to any specific commercial product, process, or service by trade name, trademark, manufacturer, or otherwise does not necessarily constitute or imply its endorsement, recommendation, or favoring by the United States Government or any agency thereof, or Battelle Memorial Institute. The views and opinions of authors expressed herein do not necessarily state or reflect those of the United States Government or any agency thereof.

PACIFIC NORTHWEST NATIONAL LABORATORY
operated by
BATTELLE
for the
UNITED STATES DEPARTMENT OF ENERGY
under Contract DE-AC05-76RL01830

Printed in the United States of America

Available to DOE and DOE contractors from the
Office of Scientific and Technical Information,
P.O. Box 62, Oak Ridge, TN 37831-0062;
ph: (865) 576-8401
fax: (865) 576 5728
email: reports@adonis.osti.gov

Available to the public from the National Technical Information Service,
U.S. Department of Commerce, 5285 Port Royal Rd., Springfield, VA 22161
ph: (800) 553-6847
fax: (703) 605-6900
email: orders@nits.fedworld.gov
online ordering: <http://www.ntis.gov/ordering.htm>

SE ROA 38073

Guide to using Multiple Regression in Excel (MRCX v.1.1) for Removal of River Stage Effects from Well Water Levels

RD Mackley
FA Spane

TC Pulsipher
CH Allwardt

September 2010

Prepared for
the U.S. Department of Energy
under Contract DE-AC05-76RL01830

Pacific Northwest National Laboratory
Richland, Washington 99352

SE ROA 38074

JA_9356

Summary

A software tool was created in Fiscal Year 2010 (FY11) that enables multiple-regression correction of well water levels for river-stage effects. This task was conducted as part of the Remediation Science and Technology project of CH2M-HILL Plateau Remediation Company (CHPRC). This document contains an overview of the multiple regression convolution/deconvolution methodology and is intended to be a user's manual for the Multiple Regression in Excel (MRCX) v.1.1 software. This document contains a step-by-step tutorial that shows users how to use MRCX to correct river effects in two different wells.

This report is accompanied by an enclosed CD that contains the MRCX installer application and files used in the tutorial exercises.

SE ROA 38076

Acknowledgments

The authors would like to acknowledge the valuable contributions of staff and colleagues who have helped willingly in support of the creation of the MRCX v.1.1 software tool and user's manual. We would like to thank Kyle R. Parker (PNNL) and Robert S. Edrington (CHPRC) for providing water level data. Special thanks to Matt Tonkin and Rachel Shannon (S.S. Papadopulos & Associates, Inc.) for their instructive technical discussion and willingness to share information and data.

We would like to acknowledge the contributions of technical reviewers, including Vince R. Vermeul, and Megan Peters for editing and text processing (PNNL).

SE ROA 38078

Contents

Summary	iii
Acknowledgments.....	v
1.0 Introduction	1.1
1.1 Groundwater Response to Changes in River Stage.....	1.1
1.2 Multiple-Regression Correction.....	1.2
1.2.1 Application to River-Stage Effects.....	1.2
1.2.2 Multiple-Regression Models Issues	1.6
2.0 Software Installation and Configuration.....	2.1
2.1 Installing the MRCX v.1.1 Software Files	2.1
2.2 File Saving and Renaming	2.1
2.3 Configuring the MRCX Workbook Template.....	2.2
2.3.1 Enabling the MRCX VBA Macro in Excel 2007	2.2
3.0 User Interface	3.1
3.1 General Overview	3.1
3.2 Input Data.....	3.3
3.2.1 Copy Paste Special-Values.....	3.3
3.2.2 Training Data.....	3.4
3.2.3 Correction data	3.4
3.2.4 Input Data Requirements.....	3.4
3.3 Model Configuration.....	3.5
3.3.1 Time Filtering.....	3.6
3.3.2 Data Value Option.....	3.6
3.3.3 Lag Option.....	3.7
3.3.4 Maximum Number of Lags	3.8
3.3.5 Trend Adjustment.....	3.9
3.4 Command Buttons.....	3.11
3.4.1 Reset Filter	3.11
3.4.2 Run Multiple Regression on Training Data	3.11
3.5 Results	3.12
4.0 Tutorial Examples.....	4.1
4.1 Example 1: Well 399-1-21A	4.1
4.1.1 Entering the Input Data	4.2
4.1.2 Configuring the Multiple Regression Model.....	4.3
4.1.3 Varying the Maximum Lag Term	4.4
4.1.4 Different Training and Correction Time Periods	4.5
4.1.5 Batch Lag Mode.....	4.6

4.2	Example 2: Well 199-K-112A	4.7
4.2.1	Input Data.....	4.9
4.2.2	Establishing a Suitable Training Period and Maximum Lag Combination.....	4.9
4.2.3	Linear Trend Adjustment	4.13
5.0	References	5.1

Figures

1.1	River-Stage Effects on Well 399-1-21A	1.2
1.2	River Response Function for Well 399-1-21A	1.4
1.3	Observed, Predicted, and Corrected Water Level Results for Well 399-1-21A	1.6
2.1	Macro Security Warning Notification on the Excel 2007 Toolbar Ribbon	2.2
2.2	Enabling Temporary Macro Permission	2.3
3.1	Generalized MRCX Workflow Process Diagram	3.2
3.2	Input Data Worksheet	3.3
3.3	Model Config Worksheet.....	3.5
3.4	Time Filtering Settings	3.6
3.5	Data Value Type Option Configuration Setting	3.7
3.6	Lag Option Configuration Setting	3.8
3.7	Maximum Lag Configuration Setting.....	3.9
3.8	Background Trends in River-Stage and Well Water Level Data.....	3.10
3.9	Linear Trend Adjustment on Predicted Well Water Levels.....	3.10
3.10	Linear Trend Adjustment Configuration Setting	3.11
3.11	Batch Lag Option Dialog Menu.....	3.12
4.1	Site Map of 300 Area Wells.....	4.1
4.2	Paste Values Option in Excel.....	4.2
4.3	Well 399-1-21A Input Data Worksheet.....	4.3
4.4	399-1-21A Config Options	4.3
4.5	Well 399-1-21A Training Data Regression Results 1	4.4
4.6	Well 399-1-21A Training Data Regression Results 2	4.5
4.7	Well 399-1-21A Training and Correction Data Regression Results.....	4.6
4.8	Batch Lag Menu.....	4.7
4.9	Batch Lag Menu.....	4.7
4.10	Site Map of 100-K Wells	4.8
4.11	Average Daily Pumping Rates Data for Extraction Well 199-K-129.....	4.9
4.12	Well 199-K-112A Regression Results 1	4.10
4.13	Well 199-K-112A Regression Results 2.....	4.11
4.14	Well 199-K-112A Regression Results 3.....	4.12
4.15	Well 199-K-112A Regression Results 4.....	4.13
4.16	Well 199-K-112A Regression Results with Linear Trend Adjust Turned Off	4.14

SE ROA 38082

1.0 Introduction

It has long been observed that water levels in groundwater wells fluctuate in response to changes in river stage or ocean tides (e.g., Ferris, 1952 and 1963; Erskine, 1991; Barlow and Moench, 1998). River-stage effects can obscure well/aquifer responses due to pumping or other hydraulic testing and require removal prior to successful analysis. The multiple-regression convolution/deconvolution method used to correct barometric effects on well water levels (Rasmussen and Crawford 1997, Spane 1999, 2002) has been extended similarly and applied in removal of river-stage effects from well response (Vermeul et al., 2009; Spane and Mackley, 2010).

This user's guide documents recent efforts during Fiscal Year 2010 (FY10) to develop a software tool within Microsoft Excel that facilitates river-level correction using the multiple-regression techniques. Multiple Regression Correction in Excel (MRCX) is a user-friendly tool that provides functionality to perform river correction in a single software environment.

This document is meant to serve as a user's guide to MRCX. Basic theory and correction methodology will be introduced in the following document; however, the reader is directed to Spane and Mackley (2010) for a more complete discussion on river-aquifer/well response and using multiple-regression convolution/deconvolution. A tutorial example of using MRCX to correct river-stage effects at two field sites is included to help end users become familiar with the user interface and illustrate technical aspects and guidelines for effective and defensible river correction using this multiple regression technique. Basic guidance and technical details of river correction using convolution/deconvolution within the MRCX software environment will be included for the benefit of the end user. It was intended to make a useful and analytically-straightforward correction technique available to a wide technical audience within the familiar software environment of Excel. However, it is the user's ultimate responsibility to apply the functionality in MRCX appropriately to their specific site conditions and data.

1.1 Groundwater Response to Changes in River Stage

Changes in river stage impart transient pressure groundwater responses within a hydraulically-connected aquifer system (Figure 1.1). The topic of fluctuations and boundary effects of rivers and oceans has been examined by workers in the time and frequency domain for over half a century (e.g., Jacob, 1950; Ferris, 1952 and 1963; Erskine, 1991; Gilmore, 1991; Barlow and Moench, 1998; Zlotnik and Huang, 1999). Refer to and Barlow and Moench (1998) and Spane and Mackley (2010) for a more complete technical discussion and literature review on river/tidal fluctuation and boundary effects.

As note in Spane and Mackley (2010), river response effects in wells are a function of aquifer hydraulic properties, inland distance, well effects, degree of river/aquifer intersection (e.g., fully versus partially penetrating), and the harmonics of the river-stage input stress signal. Based upon derivations of classical heat-flow equations by Ferris (1952, 1963), groundwater responses to cyclical river-stage fluctuations are predicted to be attenuated in magnitude and lagged in time with increasing distance to the river. An example of attenuated and lagged well responses to river-stage changes is illustrated in Figure 1.1.

Transient river-stage effects can often mask or overshadow hydraulic test responses, making it difficult to estimate aquifer hydraulic properties or evaluate the effectiveness of remediation attempts. The next section explains methods used to remove (deconvolve) these effects.

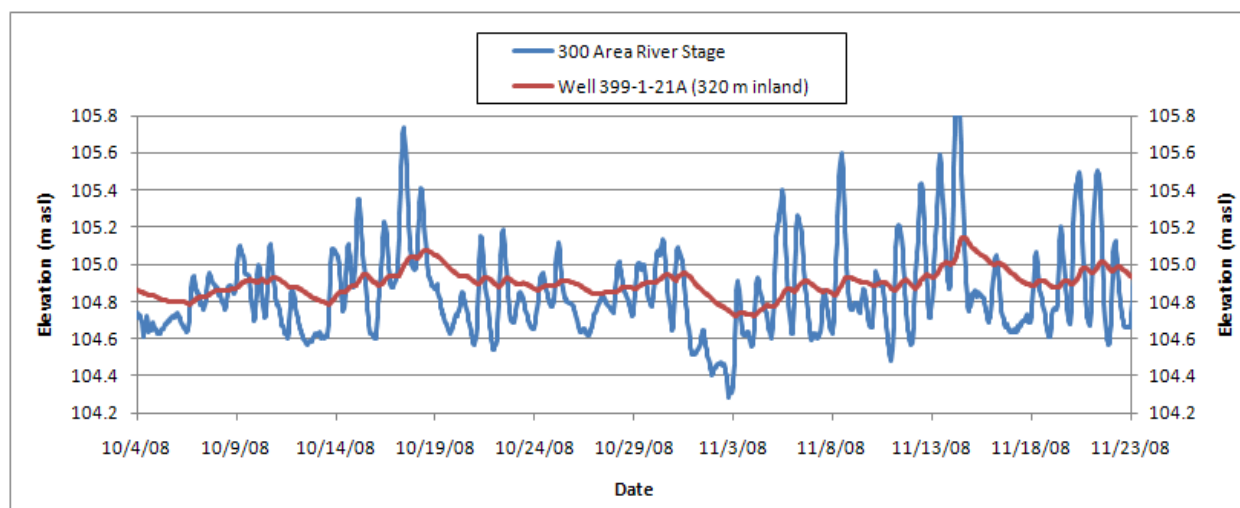


Figure 1.1. River-Stage Effects on Well 399-1-21A

1.2 Multiple-Regression Correction

Correction of river-stage effects from well water levels using multiple-regression convolution/deconvolution is an extension of a removal technique developed for barometric effects. Rasmussen and Crawford (1997) described a multiple-regression technique for removing barometric pressure responses with convolution in the time domain using impulse response functions discussed in Furbish (1991). Although this removal technique was specifically applied in the context of barometric effects, similar and variant regression, multivariate, and convolution techniques have also been used extensively in applications of data forecasting. Associated statistical methods of note include: autoregressive integrated moving average (ARIMA) techniques (Box et al., 2008), distributed-lag transfer functions (Pankratz, 1991), and/or the combinations of these methods; all of which may also produce satisfactory barometric or river-stage correction results.

The multiple regression convolution/deconvolution technique for barometric correction originally presented in Rasmussen and Crawford (1997) involves using linear regression of time-lagged input stresses and observed well water levels to predict well response (convolution). Predicted well responses can then be removed from the observed well responses (deconvolution) to produce a corrected time series. This multiple-regression technique has been used successfully by others (e.g., Spane, 1999 and 2002; McDonald, 2007) to correct for barometric effects.

1.2.1 Application to River-Stage Effects

Recently, the multiple-regression convolution/deconvolution method has been used to identify and correct river-stage fluctuations from affected well water levels (Vermeul et al., 2009; Spane and Mackley, 2010). Since associated groundwater responses to river-stage fluctuations are time-lagged and attenuated (see Ferris 1952, 1963 for mathematical relationship discussion), the multiple regression method of

Rasmussen and Crawford (1997) has direct technical application to river correction. The multiple regression technique implemented in MRCX and applied to river-stage correction involves these four basic steps:

1. Use multiple linear regression to model the time-dependant relation between well water level (W_t) and river stage (R_t) for a specified maximum number of time lags (n). In MRCX, users can choose to run the multiple regression using either a) the original data, or b) the first differences of the original data (change in water level between successive time steps). Rasmussen and Crawford (1997) suggested using the original time series data in the multiple regression correction; however, subsequent workers have chosen to use differenced data (change in water level) in correcting barometric (Spane, 1999 and 2002; Toll and Rasmussen, 2007) and river effects (Vermeul et al., 2009; Spane and Mackley, 2010).

MRCX allows users to select running the regression as either the original or the differenced data, depending upon their preference (see discussion in Section 3.3.2 on the merits of both methods). Equations for both methods are included:

- a. Original Data Option:

$$W_t = \alpha + \beta_0 R_t + \beta_1 R_{t-1} + \beta_2 R_{t-2} + \dots + \beta_n R_{t-n} + \varepsilon \quad (1a)$$

where W_t = well water level
 R_t = river stage
 R_{t-1} = river stage one time step (lag) previously
 R_{t-n} = river stage n time steps (lags) previously
 n = maximum lag (indexed at 0)
 α = regression intercept (offset term)
 $\beta_0 \dots \beta_n$ = regression coefficients corresponding to time lags of 0 to n
 ε = residual error term

- b. Differenced Data (Change in Water Level) Option:

$$\Delta W_t = \alpha + \beta_0 \Delta R_t + \beta_1 \Delta R_{t-1} + \beta_2 \Delta R_{t-2} + \dots + \beta_n \Delta R_{t-n} + \varepsilon \quad (1b)$$

where ΔW_t = change in well water level = $W_t - W_{t-1}$
 ΔR_t = change in river stage = $R_t - R_{t-1}$
 ΔR_{t-1} = change in river stage one time step (lag) previously
 ΔR_{t-n} = change in river stage n time steps (lags) previously
 n = maximum lag (indexed at zero)
 α = regression intercept (linear trend term)
 $\beta_0 \dots \beta_n$ = regression coefficients corresponding to time lags of 0 to n
 ε = residual error term

The regression intercept term (α) in Equation 1b incorporates the background linear trend (i.e., slope) over the model estimation period. There may be situations where it is desirable to ignore the background trend in the training time series (e.g., training and correction periods have different background linear trends). MRCX can be configured to omit the linear trend term ($\alpha = 0$) in Equation 1b. In contrast, the regression intercept term in Equation 1a represents the constant offset term in the multiple regression model – it should never be omitted. The residual error term in both equations

accounts for the inability of the model to fit the observed well water levels with lagged river input. For a more thorough discussion of residual analysis in multiple or dynamic regression see Pankratz (1991).

MRCX uses ordinary-least squares (OLS) linear regression to solve the regression intercept (α) and the coefficients (β_i) using matrix operations described in Stevens (1996). This is accomplished in MRCX using VBA code that calls up functions within a dynamic-link library (.dll) reference developed using C#. The.dll reference utilizes statistical functions contained in the commercially-available code library FoundaStat Pro (FoundaStat 2008).

2. Calculate the cumulative river response function (RRF) as the sum of the individual regression coefficients (β_i) estimated from the multiple regression model. The RRF is calculated the same way regardless which data type is chosen (original or differenced data) according to:

$$RRF_n = \sum_{i=0}^n \beta_i \tag{2}$$

where RRF_n = river response function for n number of time lags
 β_i = regression coefficients corresponding to time lags of 0 to n

RRF's are diagnostic indicators of the nature of the river influence on the well water levels. The RRF illustrated in Figure 1.2 shows about a 0.9 unit increase in well water level after 480 hours (20 days) for a unit increase in river stage for well 399-1-21A (320 meters inland). It is worth mentioning again that the controlling factors for river response function include aquifer hydraulic properties, inland distance, well effects, degree of river/aquifer intersection (e.g. fully vs. partially penetrating), and the harmonics of the river-stage input stress signal. River response functions would need to be normalized for inland distance in order to make direct comparisons between wells – this involves plotting RRF's against the distance-normalized time lag where (time lag divided by the square of the inland distance).

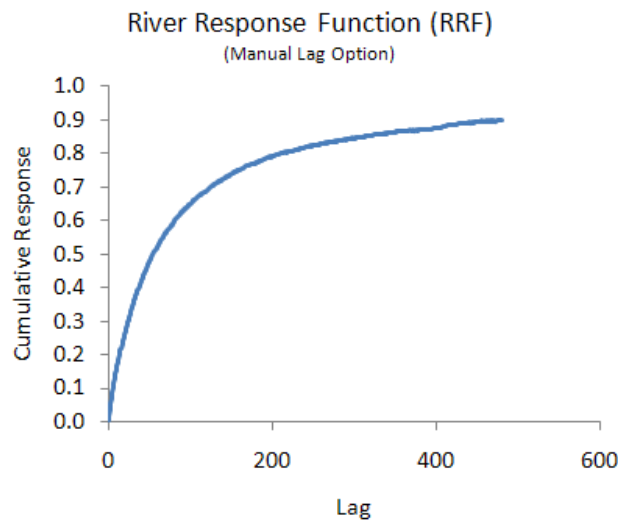


Figure 1.2. River Response Function (RRF) for Well 399-1-21A

Rasmussen and Crawford (1997) suggest increasing the maximum lag term (n) to a value sufficiently high to incorporate long-term responses. Others (Spane, 1999 and 2002; Toll and Rasmussen, 2007) recommend increasing the number of lags until the response function stabilizes. In practice, this is observed as an asymptotic approach in the cumulative response to some maximum response value.

3. Calculate the predicted well water levels (P_t). The process for calculating the predicted water levels for the original data is more straightforward than it is for differenced data. For the original data, summation of the right side of Equation 1a provides the predicted well water levels (P_t). The first water level that can be predicted with Equation 1a occurs $n+1$ records into the original time series data, since the maximum lag, n , indexes (starts) at zero.

For the differenced data, the regression model (Equation 1b) predicts the *change* in water level (ΔP_t), rather than the actual water level (W_t). The predicted water levels at a given point in the time series (P_t) for differenced data are calculated according to:

$$P_t = W_0 + \sum_{i=0}^m \Delta P_{t-i} \quad (3)$$

where
$$\sum_{i=0}^m \Delta P_{t-i} = \Delta P_t + \Delta P_{t-1} + \Delta P_{t-2} + \dots + \Delta P_{t-m}$$

and

P_t	=	predicted water level at a given point in the time series
W_0	=	initial water level ($n+1$ records into original time series)
m	=	number of records in original water level time series
ΔP_t	=	predicted change in water level from Equation 1b
ΔP_{t-1}	=	predicted change in water level at previous time step
ΔP_{t-m}	=	predicted change in water level m time steps previously

Equation 3 defines the predicted water level (P_t) as the initial water level (W_0) plus the cumulative sum change in water level predicted up to that point in time. The initial water level (W_0) term in Equation 3 is the observed water level that occurs $n+1$ records into the time series, since the maximum lag (n) indexes (starts) at zero. The first water level that can be predicted occurs $n+2$ records into the original water level time series, since differencing removes the first value in the time series.

4. Calculate the river-corrected well water levels (C_t) according to:

$$C_t = W_0 + (W_t - P_t) \quad (4)$$

where

C_t	=	river-corrected well water level at a given point in the time series
W_0	=	initial water level ($n+1$ records into original time series)
W_t	=	observed water level at a given point in the time series
P_t	=	predicted water level at a given point in the time series

Equation 4 states that the corrected well water level at a given point in time (C_t) after the initial water level (W_0) is the residual difference between the observed (W_t) and predicted (P_t) value at that point in time.

Figure 1.3 illustrates the observed, predicted, and corrected water level results for well 399-1-21A (located about 320 meters inland) when using the differenced data option and a maximum lag (n) of 480 hours.

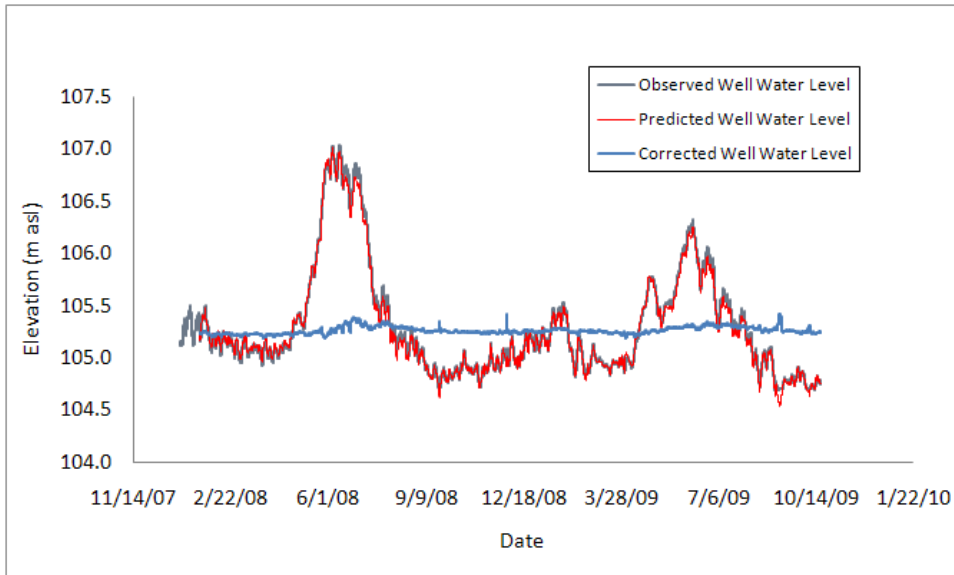


Figure 1.3. Observed, Predicted, and Corrected Water Level Results for Well 399-1-21A

1.2.2 Multiple-Regression Models Issues

There are a number of assumptions and limitations related to multiple regression. Those that are more relevant and obvious are discussed briefly here. The reader is directed to statistical textbooks covering this topic (e.g., Pankratz, 1991) for a more in-depth and comprehensive discussion of multiple regression, its assumptions, and limitations. In multiple regression it is assumed that 1) the input (stress) variables are not perfectly auto correlated with each other and independent from the dependant (response) variable, 2) the regression residuals are normally distributed with a mean of zero, have constant variance, and are not auto correlated/collinear (Pankratz, 1991; Stevens, 1996). It is inevitable that river-stage and well water levels will lack complete independence, due to the open, hydraulically communicative exchange between surface and groundwater. It also expected that the time-lagged input river-stage data are going to have a degree of autocorrelation. Violation of these assumptions does not necessarily preclude the use of multiple regression for the application of river or barometric correction or invalidate the regression estimates (intercept and coefficients); however, it does call into question statistical hypothesis testing. The statistical parameters can be used diagnostically to guide end users in determining the optimum maximum time lag for prediction and correction applications, but they should not be used to signify statistical significance. The well-established conceptual and analytical basis for time-lagged river-stage effects, with responses often requiring extended period of time (e.g., days to months) to become fully manifested in distant, inland wells supports the use of multiple-regression convolution/deconvolution as valid method for identifying and removing their effects (Spane and

Mackley, 2010). However, caution needs to be exercised on the part of the analyst not to put too much confidence in the statistical metrics such as R^2 or p-values when the above-mentioned assumptions are violated.

The goodness-of-fit metrics reported by MRCX include the R^2 , adjusted R^2 , and the MAE of the regression model. Of the three, the MAE is considered the least biased indicator of the goodness-of-fit, with lower values indicating improved model fit. All three serve as diagnostic indicators of the ability of the predictions from the regression model to fit the observed data, but none of them should be used to quantitatively test for statistical significance, due to the above-mentioned assumption violations.

Lastly, it should be reiterated that there may be other frequency-based or time-series techniques in addition to the established method of Rasmussen and Crawford (1997) that could also be used to predict river-stage effects on well water levels. ARIMA (Box et al., 2008) or distributed-lag transfer functions (Pankratz, 1991) might also be effective. Examining and comparing the efficacy of different forecasting techniques, although out of the scope of this task, is a worthwhile research objective.

SE ROA 38090

2.0 Software Installation and Configuration

The Multiple Regression Correction in Excel (MRCX v.1.1) software tool is distributed as a single .MSI Windows Installer file (MRCX_v1.1.MSI). The .MSI installer program installs a collection of dynamic link library (.DLL) files that contain the compiled statistical and processing functions as well as the Excel 2007 macro-enabled workbook template (MRCX_v1.1.xlsm). The installation of the MRCX Windows Installer files is discussed below, followed by instructions for opening of the Excel macro-enabled workbook file.

2.1 Installing the MRCX v.1.1 Software Files

The first step is to install the .MSI Windows Installer file. This will install a collection of .dll files that perform the highly-computation portion of the multiple-regression and place a local copy of the MRCX Excel worksheet template file on your computer. The steps for installing MRCX with the .MSI Windows Installer file are:

1. Remove any previous versions of MRCX using the Add or Remove Programs within the Control Panel in Windows.
2. Exit out of Microsoft Excel prior to attempting the install.
3. Double-click on the MRCX_v1.1.MSI install file. This will bring up Setup Wizard.
4. Click on Next to proceed.
5. Select the installation folder path for the MRCX files.
6. Click on Next. This will bring up the confirmation screen.
7. Click on Next to finish the install.
8. When the program is successfully installed, click on Close to exit the Setup Wizard.

Although you do not need full administrator privileges on the computer you are installing MRCX on, some level of program installation permissions are needed.

2.2 File Saving and Renaming

The MRCX_v1.1.xlsm workbook contains a default data entry and model configuration template and Visual Basic for Applications (VBA) code for performing the river-correction process. Users are encouraged to re-save and rename the template as desired. However, you must save each renamed instance of the MRCX template workbook as an Excel 2007 macro-enabled workbook (.xlsm file format) or the full MRCX river-correction functionality will be lost.

The MRCX Excel software tool will be referred to by its original name (MRCX_v.1.1.xlsm) in this document for consistency. As noted above, you can resave the workbook under a different filename. The guidance and information content herein applies equally to renamed instances of the MRCX workbook as long as the structural contents of the original MRCX_v1.1.xlsm workbook template are retained. The filename does not affect the functionality of the MRCX VBA code.

2.3 Configuring the MRCX Workbook Template

The MRCX_v1.1.xlsm file will be installed into the user-selected folder during the installation described above. This file is an Excel 2007 macro-enabled workbook. It designed to enable the end user the functionality to perform the river correction process within a single software environment. It interacts with the library of .dll files using VBA.

2.3.1 Enabling the MRCX VBA Macro in Excel 2007

Since the Excel template workbook contains VBA code, it is considered a macro-enabled workbook and has the .xlsm file extension. The macro security settings in Excel may need to be adjusted in order to enable the VBA code in the MRCX_v1.1.xlsm file to function, depending upon the user's current settings. Excel 2007 has the following Macro Security Setting Options:

1. Disable all macros without notification
2. Disable all macros with notification
3. Disable all macros except digitally signed macros
4. Enable all macros (not recommended; potentially dangerous code can run)

If the macro security is set to option 1, you will not be able run any type of macro. The other three macro security options allow macros to be enabled either on a case-by-case basis or permanently. Macro security option 2 disables macros from running initially unless the user manually enables the specific file – this is the temporary macro enable option described below. Option 3 restricts all macros except those containing digitally-signed certificates – this is not an option since the MRCX Excel workbook file is not digitally signed. Option 4 allows all macros to be enabled and is not recommended.

If you have your macro security settings configured to option 2 (*Disable all macros with notification*), Excel will initially disable the MRCX code from running when the workbook file is opened. It places a notification in the Excel toolbar Ribbon (Figure 2.1). For instructions on configuring your Excel 2007 macro security settings set to option 2 see the help file in Excel. Once you have set Excel to macro security option 2, you are ready to open the MRCX workbook file and enable temporary access to the MRCX VBA code. To enable temporary access to the VBA code in MRCX, follow the steps below each time you open the workbook:

1. Open the MRCX_v1.1.xlsm workbook file.
2. Click on the Options button on the Security Warning notification on the Excel toolbar ribbon (Figure 2.1)
3. Select the *Enable this content* option (Figure 2.2) to temporarily enable the MRCX VBA macro.

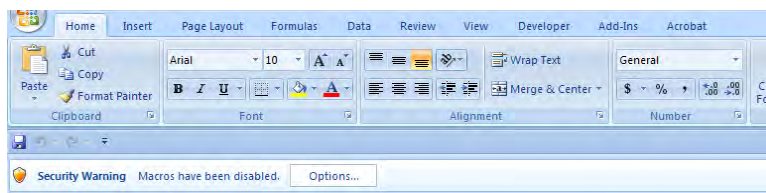


Figure 2.1. Macro Security Warning Notification on the Excel 2007 Toolbar Ribbon

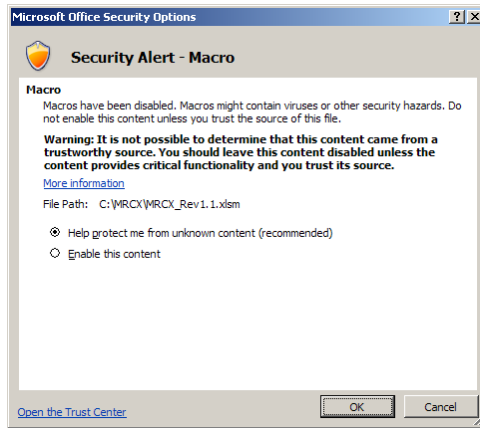


Figure 2.2. Enabling Temporary Macro Permission

4. Click on OK to save and close the macro settings.

The Security Warning notification will no longer be visible on the Excel toolbar ribbon and the MRCX VBA macro should be enabled. You will need to follow the steps listed above every time you open a MRCX macro-enabled workbook.

SE ROA 38094

3.0 User Interface

The MRCX Excel workbook template (MRCX_v1.1.xlsm) was designed as a software tool for a broad audience of end users to perform river correction of well water levels within a single user environment. It contains a collection of worksheets for input data, model configuration, and output results. There are drop-down lists and command buttons that allow the user to configure the multiple-regression convolution/deconvolution correction settings with flexibility.

As noted above, the original MRCX workbook file can be resaved under a different name as desired, with the imposed restriction that it is saved as an Excel 2007 macro-enabled workbook (.xlsm file format). This section introduces the general features and functionality of the MRCX workbook template components. Instructions for utilizing the features of the MRCX software tool then discussed in order of the river-correction process.

3.1 General Overview

The MRCX software tool is a single workbook template organized into four worksheets, organized by workflow process. These include Input Data, Model Config, Training Results, and Correction Results. They contain a mixture of locked and editable cells.

It is important to reiterate that the structural form (rows and columns) is directly tied to the functionality of the VBA code, particularly for the Input Data and Model Config worksheets. Changes to the structural form (e.g., inserting/deleting a column) will alter cell mapping between the worksheets and the VBA code, resulting in loss of functionality or erroneous results. The general workflow process for river correction in MRCX v.1.1 is depicted in Figure 3.1.

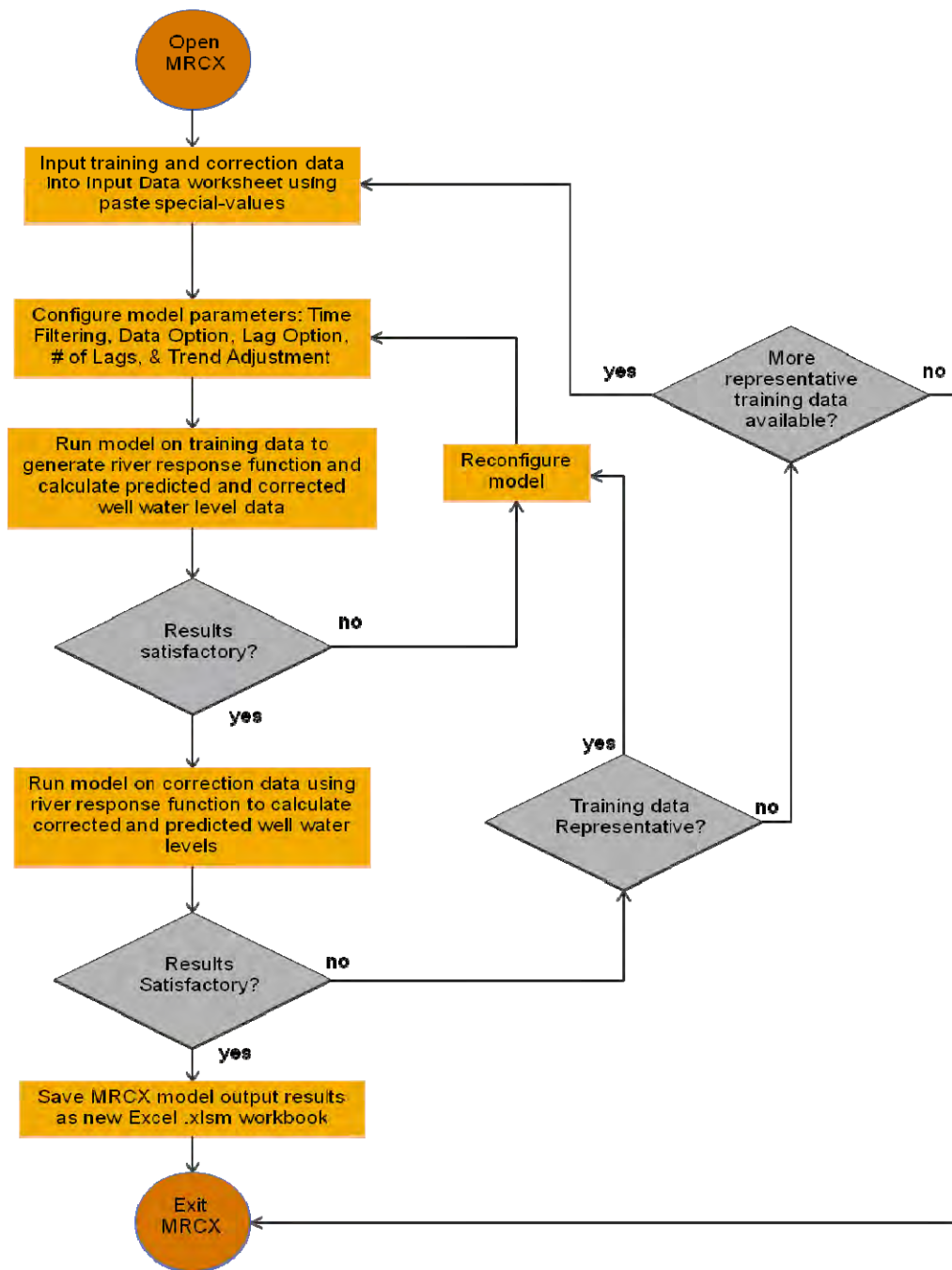


Figure 3.1. Generalized MRCX Workflow Process Diagram

The MRCX workbook can be viewed at any zoom level within Excel; however, the drop-down lists and graphs were sized to be viewed at about 85% zoom level on a 19-inch monitor configured to display at 1280 by 1024 dpi resolution. You may need to adjust the zoom level to your particular monitor screen size and resolution.

3.2 Input Data

The Input Data worksheet contains place holders for the data that will be used in the river-correction process (Figure 3.2). It is organized into Training and Correction ranges. The two time series of data are distinguished from each other in order to extend the flexibility and capability of the MRCX software tool. It is often desirable to “train” the multiple regression convolution/deconvolution model using one set of data, and then make river-level correction on another set of data. For example, you can use several months of water level data preceding a hydraulic test as the training data. The RRF generated from the training data can then be used to correct the data collected during a hydrologic test.

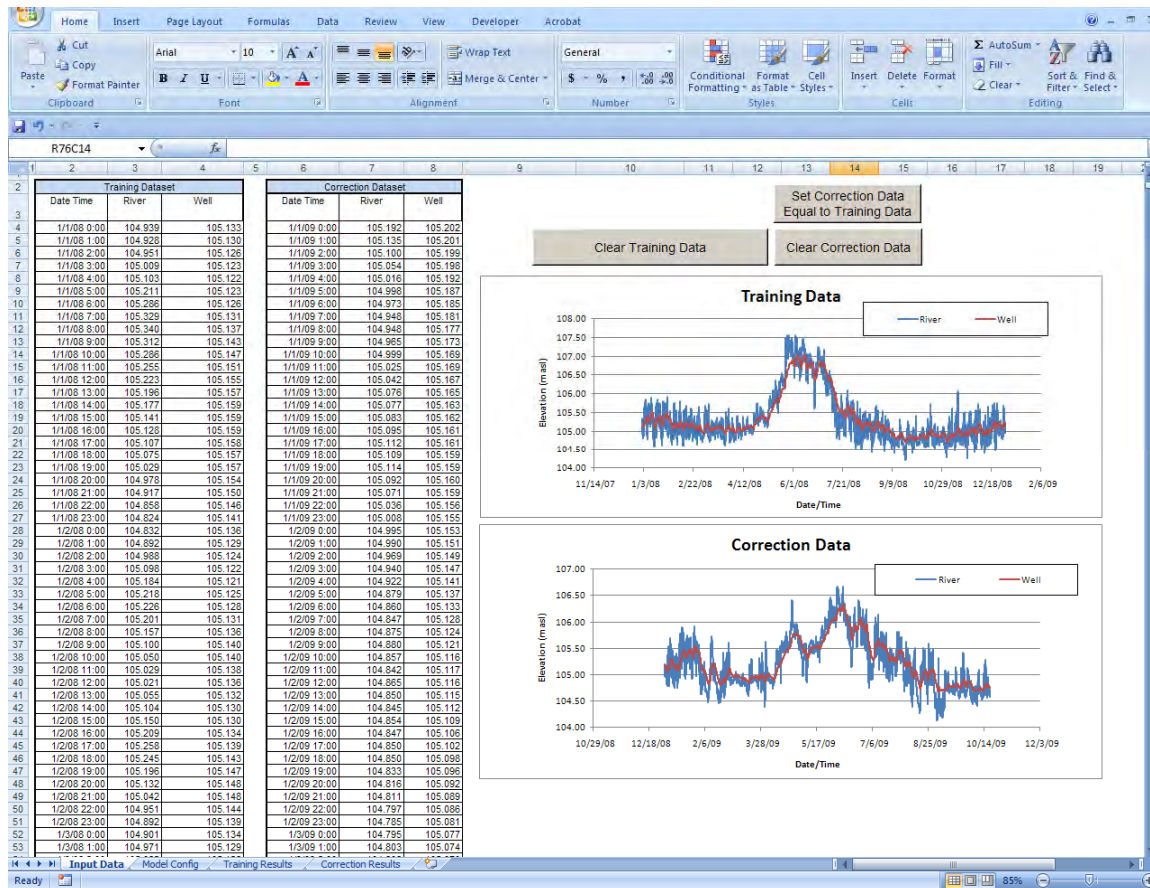


Figure 3.2. Input Data Worksheet

There are three command buttons embedded into the Input Data worksheet for convenience. The ‘Set Correction Data Equal to Training Data’ command button will copy the data from the training to the correction input range. The ‘Clear Training Data’ and ‘Clear Correction Data’ command buttons reset and clear the corresponding input data ranges in the worksheet.

3.2.1 Copy Paste Special-Values

The MRCX workbook template is designed for users to make changes to the values in the data input and model parameter cells as part of the workflow process (Figure 3.1); however, changes to the row and column structure and cell formulas will impact the functionality of MRCX.

It is essential that you use the Copy Paste Special-Values command in Excel when copying the training and correction data into the Data Input worksheet. This will ensure cell formatting remains intact. As noted above, changes to the structural format of the MRCX workbook will cause the program to either fail completely or produce erroneous results. This can easily be avoided by utilizing the Copy Paste Special-Values feature in Excel (refer to the help files in Excel if you are unfamiliar with using this feature).

3.2.2 Training Data

The input data in the Training Dataset range are used to “train” the multiple regression convolution/deconvolution model and generate a RRF that will be used to calculate predicted and corrected well water levels under the influence of river-stage effects. Entering the training data is the first step in the river-correction workflow process within MRCX (Figure 3.1). As mentioned before, these are the primary data used to create the RRF used to predict (convolution) and remove (deconvolution) river-stage effects.

3.2.3 Correction data

The MRCX interface allows users to enter different time-series of data in the Correction Dataset section of the Input Data worksheet. This feature was included to allow greater flexibility with training versus correction periods. The RRF is generated by the training data and can then be extended for use to the separate correction data. The primary difference between the training and correction data is that the correction data can and often do contain groundwater responses from sources other than the river (e.g., pumping test). The response of these non-river input stresses is often obscured in the water level data due to river-stage effects.

Unlike the training data, the correction data does not need be entered into the Input Data worksheet prior to generating the RRF function. It needs to be added prior to running the ‘Run Multiple Regression Model on Correction Data’ command button on the Model Config worksheet (discussed below).

3.2.4 Input Data Requirements

The river-correction method and the code in the MRCX assume the input data meet structural, formatting, and technical requirements. For the MRCX code to work properly, the following general format requirements for the training and correction data sets should be met:

1. Data must be continuous – that is, there are no data gaps or missing intervals of data
2. Data must be chronologically sequenced at a constant interval (e.g., entire time series is on hourly interval)
3. Date values need to be in MM/DD/YYYY HH:MM format (e.g., 01/01/2010 15:00)
4. River stage and well water levels need to be in a number format with values no more than ten decimal places (e.g., 115.215)
5. The number of records (rows) for each time series cannot exceed 32,000. (note: To clarify: this restriction is for each input data type – in other words, the training and correction data can *each* have 32,000 records i.e., rows)

Additionally, the training and correction data need to meet technical assumptions in order to generate effective and scientifically defensible river correction:

1. Have similar well hydrologic conditions between the training and correction data (e.g., saturated aquifer thickness, magnitude and frequency of river-stage changes)
2. Collected in a similar manner (e.g., consistent source of water level data)
3. Training data contain or is of a sufficient time period to adequately capture associated, long-term river-stage responses influence.
4. The maximum lag value must be less than 0.5 times the number of input data records minus two time units. For example, if the input data contains 1,000 hourly-spaced records. The maximum lag value must not exceed 498 hours. This is a technical requirement imposed by the multiple regression function specifically used by MRCX in order to reach a solution for the model estimates.

3.3 Model Configuration

The Model Config worksheet contains the main user interface for MRCX (Figure 3.3). It contains a pre-generated collection of drop-down lists, input cells, command buttons, and diagnostic plots for setting model parameters and running the multiple regression deconvolution/convolution method for river correction. Note: users can add/modify the existing plots (e.g. scale on axes). Unlike the Input Data worksheet, no copying or pasting of data values is necessary in the Model Config worksheet. However, similar to the other MRCX worksheets, changing the structural format of the worksheet will prevent the VBA code from running properly (e.g., inserting/deleting rows or columns).

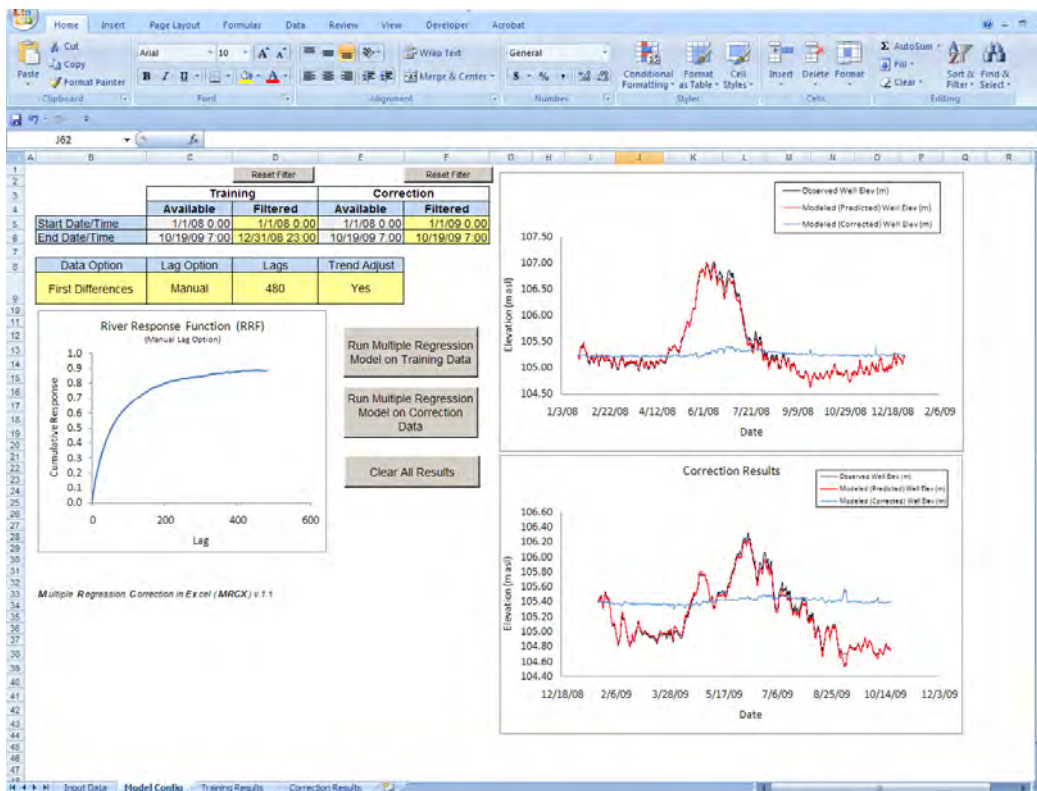


Figure 3.3. Model Config Worksheet

The use of the model configuration features and command buttons will be discussed below in the context of the river-correction workflow process outlined in Figure 3.1. Additional application of these features is contained in the Tutorial Example section.

3.3.1 Time Filtering

It may be desirable to focus on a particular time period of the input data during model training and correction (Figure 3.4). Typically, the training period should consist of a time when well water-level responses are known to be solely responding to river-stage fluctuations and not subjected to other interfering extraneous effects (e.g., pumping activities). The available time range (start and end data/time) is displayed. The input data for both the training and the correction data can be filtered to a customized time range by entering a filter start and end date. The start and end dates must fall within the available time range or an error message will be displayed.

The Reset Filter command buttons above the training and correction time filter options will reset the start and end date/time to the minimum and maximum available values available, respectively. Note: remember to reset the time filtering options each time you copy new data to the Input Data worksheet – they do not automatically reset.

Keep in mind, that you need to set the start date n or $n+1$ time units previously to the date/time you want the output from the regression model to begin, when using the Original Data and First Differences data options, respectively (where n is the maximum time lag). For example, if you want the river correction results to start on 05/01/2010 0:00 using the Differenced Data option and a maximum lag (n) of 480 hours, you would set the start date to 04/10/2010 23:00 (482 hours previously).

	Reset Filter		Reset Filter	
	Training		Correction	
	Available	Filtered	Available	Filtered
Start Date/Time	1/1/08 0:00	1/1/08 0:00	1/1/09 0:00	1/1/09 0:00
End Date/Time	12/31/08 23:00	12/31/08 23:00	10/19/09 7:00	10/19/09 7:00

Figure 3.4. Time Filtering Settings

3.3.2 Data Value Option

MRCX give users the option to run the multiple model using either the original data or first differences of the original data (i.e., changes in river stage and well water level between successive time periods). Rasmussen and Crawford (1997) reported better success with using original data in the regression deconvolution correction of barometric effects. However, others have chosen to use the first differences instead for barometric (Spane 1999 and 2002; Toll and Rasmussen 2007) and river correction (Vermeul et al., 2009; Spane and Mackley, 2010).

Differencing is a common transformation technique used in time-series analysis to minimize systematic changes in the mean (trend) and create a more stationary (constant mean and variance) data set (Pankratz, 1991). One of the advantages to running the model on the first differences is that this method is consistent with the concept that it is the *changes* in river stage and not the actual river-stage elevations themselves that creates the time-lagged and attenuated well water level responses.

The inherent correlation of river-stage and well water elevations might cause the OLS regression model to be less stable when using the original data. However, this has not been fully evaluated by the authors. An advantage of using the original data in the regression is that you can achieve a “rough” prediction and correction using fewer lags, although the response function is less stable and the overall goodness-of-fit is typically lower. Fewer lags means that the training period can be shorter since the training period must have slightly more than two times the number of records as the lag term in order for the regression model to run properly. Both methods may have application depending upon the existing well/aquifer/river communicative conditions. Further evaluation and comparison of the two methods beyond the scope of the development of this software tool is needed to better understand the relative effectiveness of one method over the other. MRCX allows both data options as a means of providing a higher degree of model functionality.

To select the data option, click inside the Data Option cell and select one of the two options from the drop-down list (Figure 3.5).

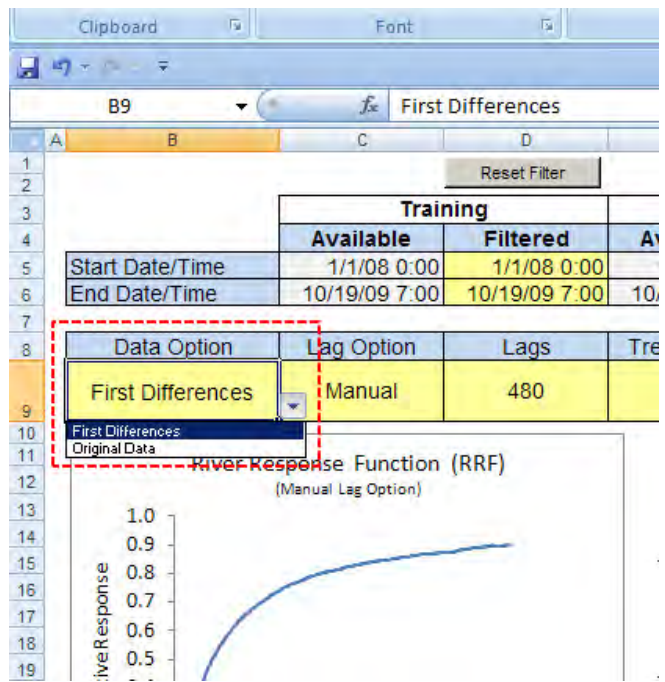


Figure 3.5. Data Value Type Option Configuration Setting

3.3.3 Lag Option

MRCX allows two different lag options for running multiple regression on the specified training data set, Manual and Batch mode. In Manual lag mode, the regression model is run for a single, specified, maximum time-lag value. This is the default mode in MRCX. Alternatively, in Batch lag mode, users can create a list of maximum lag values, and a separate regression model will be run for each lag. In the Batch mode, model results are saved in a separate Excel workbook, with results for each regression model run saved in individual worksheets. The Batch lag option was included in MRCX to allow users to compare regression results for the same training data for varying maximum time-lag values.

MRCX may require up to several minutes to process results for a single multiple-regression model for large data sets and lag values. Processing times will also vary as a function of performance capabilities of the individual computer system running MRCX code. The Batch mode option also allows users to process a large batch of regression training models for various maximum lag values and outputs the regression results into a single external Excel workbook file. This may be preferable to individually changing the maximum time-lag value and comparing regression results in a trial-and-error fashion using the Manual option within the Model Config worksheet.

To select the lag option, click inside the Lag Option cell and select one of the two options from the drop-down list (Figure 3.6).

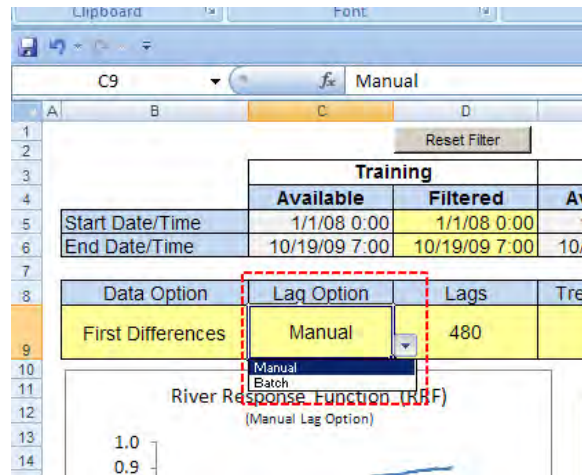


Figure 3.6. Lag Option Configuration Setting

3.3.4 Maximum Number of Lags

The maximum number of time lags (n) to be used in the multiple regression model is specified by entering a value into the Lags input box (Figure 3.7). Maximum lag values are restricted to a single integer value between 0 and 10,000. The lag units are the same as the interval units for the records in the input data. For example, if the training and correction data consist of hourly river-stage and water level measurements, units for the lags will be hours.

As discussed in Section 1.2.1, the maximum number of lags should be increased until either the RRF asymptotically approaches a maximum cumulative response value or there is no major improvement in the model results (Rasmussen and Crawford, 1997; Toll and Rasmussen, 2007; Spane and Mackley, 2010). In practice, maximum lags of several hundred hours or more may be necessary to adequately capture the full river-stage effects in water levels in wells located several hundred meters from the river (e.g., Vermeul et al., 2008; Spane and Mackley, 2010).

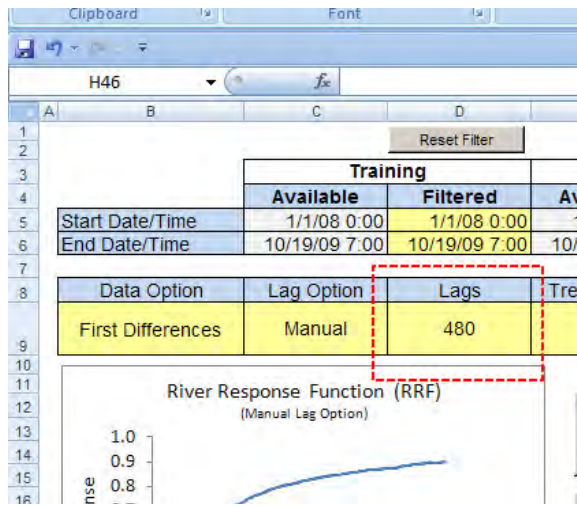


Figure 3.7. Maximum Lag Configuration Setting

3.3.5 Trend Adjustment

River-stage and well water-level time series data may contain background trends. Although the river-stage and groundwater levels for a hydraulically-connected aquifer will usually have similar general trends, the trend magnitudes may vary (Figure 3.8). Trend adjustment is less of an issue when using the original data in the regression model. However, when using the first differences of the data (changes in river-stage and well water level), the linear trend is represented by the inclusion of the additional linear trend term (regression intercept, α) in Equation 1b. The linear trend term adjusts the predicted change in water level (ΔP_t) by a constant value (α) at each time step in the time series. The summation of these step adjustments over the entire time series applies a linear trend adjustment to the predicted water levels (Equation 3). In practice, this generally results in an increased goodness-of-fit between the predicted and the observed well water levels (Figure 3.9). However, it may be useful to see the predicted and corrected results without the trend component included (e.g., when transducer data are suspected to suffer from instrument drift or when hydrologic conditions are different between the training and correction time periods).

Although the river response function (regression coefficients) from the training data are used in the prediction and correction of the correction data, MRCX does fit a separate multiple regression model to the correction data for the purpose of estimating a unique linear trend (regression intercept, α) for the correction data. The correction-data linear trend term is then used in Equation 1b in place of the linear-trend term from the training data. This is helpful when the background linear trends in the training and correction data are significantly different.

To change the linear trend adjustment option in the multiple regression model, click in the Trend Adjust cell in the Model Config worksheet and choose from the drop-down list (Figure 3.10). Note: the Trend Adjust option is set to 'Yes' automatically when the multiple regression model is run with original data.

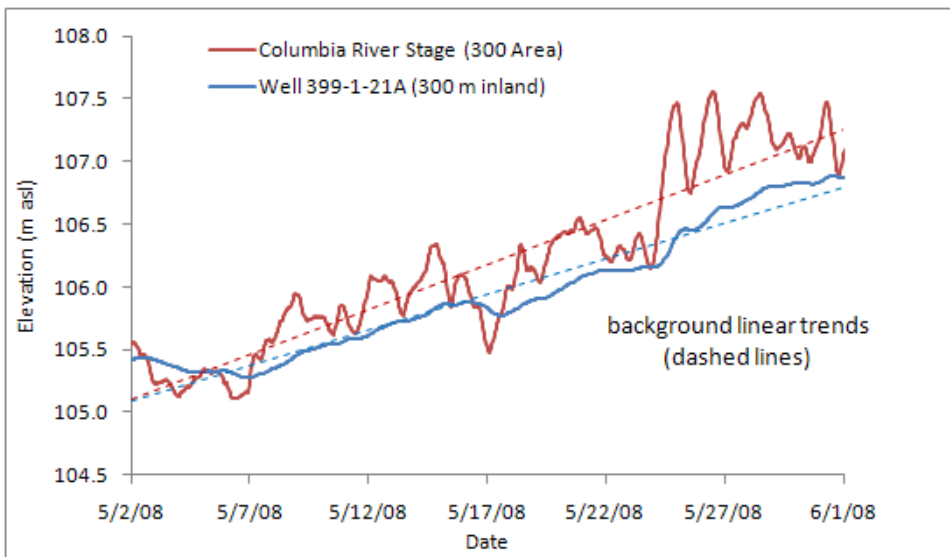


Figure 3.8. Background Trends in River-Stage and Well Water Level Data

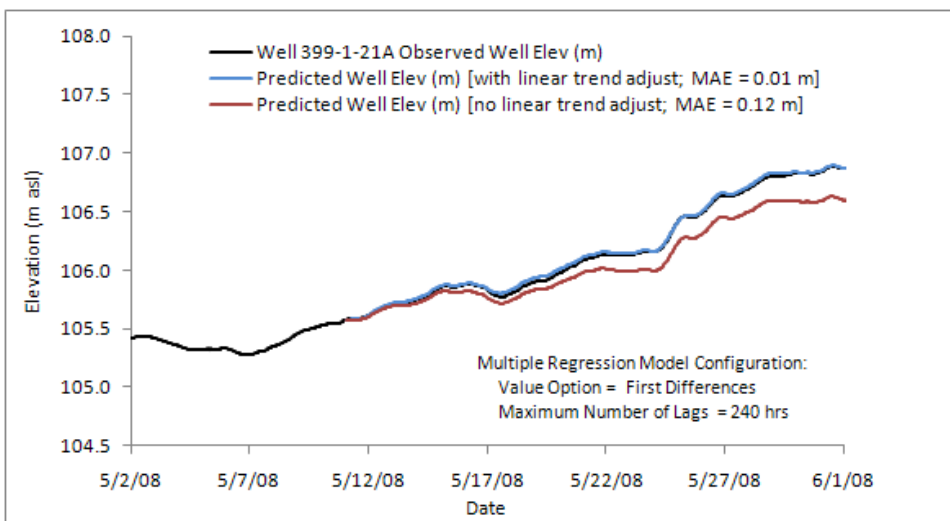


Figure 3.9. Linear Trend Adjustment on Predicted Well Water Levels

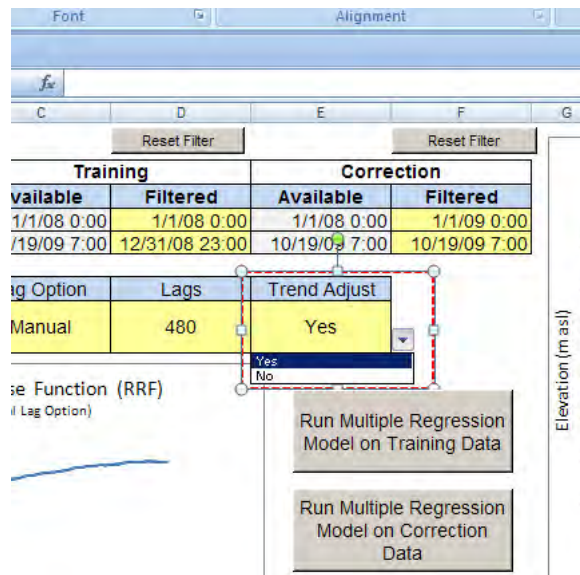


Figure 3.10. Linear Trend Adjustment Configuration Setting

3.4 Command Buttons

There are five command buttons added to the Model Config worksheet that initiate VBA code operations. Click with the left-mouse button on the command buttons to run the corresponding command.

3.4.1 Reset Filter

There are two ‘Reset Filter’ filter command buttons near the top of the worksheet that will reset the Start and End Date/Time values in the filtering option cells to the minimum and maximum date/time values in the Input Data worksheet.

3.4.2 Run Multiple Regression on Training Data

The two main command buttons located to the right of the RRF plot in the Model Config worksheet initiate the multiple regression models for the training and correction data. As noted above, the training data can be run in batch or manual lag option modes. If the lag option is set to ‘Manual’ (default), you can simply click on the ‘Run Multiple Regression on Training Data’ to run the regression model for the training data (steps 1 through 4 in Section 1.2.1). The RRF plot, the training data results plot, and the results worksheet for the training data will be updated automatically once the model processing steps are complete.

If the lag option is set to ‘Batch’ mode, an additional user dialog menu will pop up once the ‘Run Multiple Regression Correction on Training Data’ is clicked (Figure 3.11). Create a range of maximum lag (n) values by entering an integer number into the starting and ending input boxes. When you have specified the starting and ending values, set the interval spacing within the range of lag values by selecting one of the spacing values in the drop-down list. This list will automatically update each time the values in the starting and ending input boxes changes. The list is populated with even multiples of the lag range. When the interval spacing has been selected, click on the ‘Update List’ command button to refresh

the list in the frame on the right side of the menu. Users have the option to output the predicted and corrected results in addition to the summary results by check the option box in the dialog box. Click on the ‘Run Model’ command button to begin the multiple regression for the batch of maximum lags listed. In batch mode, the results will be saved in a new external Excel workbook file. The workbook file contains a summary worksheet and separate worksheets for each maximum lag value in the batch list. Be patient while the batch of regression models is processed – this can take several minutes or longer. The Windows “hour glass” cursor will show while the batch regression is processing. When it is complete, a message box will appear with “Finished Running Batch-Mode Multiple Regression on Training Data.”

It is also possible that your computer will run out of memory and return an error if your batch list is long, the number of records in the input data is large, the maximum lag values are large, and/or you have limited memory resources available on your computer. If this happens, the easiest solution is to decrease the number of maximum lag values in the batch list – in other words, split up your batch list into multiple batches then run them separately.

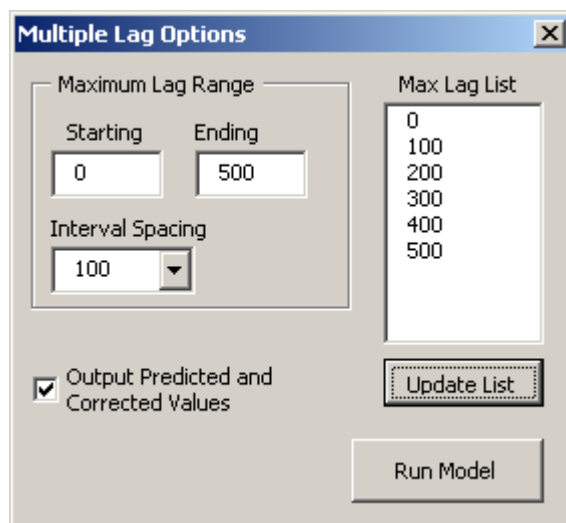


Figure 3.11. Batch (Multiple) Lag Option Dialog Menu

Once the RRF has been generated from the training data, you can click the ‘Run Multiple Regression Model on Correction Data’ command button to run the regression model on the correction data. The correction data results plot and the correction results worksheets will then be automatically updated. Note: the batch maximum lag option is not available for the correction data regression model.

3.5 Results

The results from the multiple regression model are displayed in plots within the Model Config worksheet and stored in worksheets within the MRCX workbook. The observed, predicted, and corrected well water levels for the training and correction data are shown in separate plots in the Model Config worksheet. The RRF generated from the training data is also included for diagnostic purposes. Users are free to customize the plot properties within the Model Config worksheet.

The model results for the training and correction data are automatically output to the corresponding result worksheets in the MRCX workbook. You can quickly clear the results by clicking on the ‘Clear All Results’ command button on the Model Config worksheet.

The individual and cumulative regression coefficients (β_i 's) for each lag (0 to n) from the multiple regression model are included in the results worksheets. The MRCX code is designed to utilize the regression coefficients from the respective training results worksheet when processing the predicted and corrected water levels for the correction data.

Goodness-of-fit statistics and model configuration settings are also included in the model summary section of the results worksheet. The R^2 , adjusted R^2 , and the MAE provide an indication on the ability of the multiple regression model to explain well water levels with time-lagged input from the river. As previously discussed, they should be used as diagnostic indicators and not as quantitative metrics for establishing statistical significance due to non-standard model conditions (e.g., stationarity, collinearity, autocorrelation, etc.).

The results worksheet also contains the river stage, observed, predicted, and corrected well water level time series. Note: the predicted and corrected water levels contain a large number of decimal places. These do not reflect the precision of the model. Keep in mind the goodness-of-fit statistics from the model when interpreting these values and round them to appropriate significant figures.

SE ROA 38108

4.0 Tutorial Examples

This section includes examples of the multiple regression technique from two different Hanford Site field settings. It is written in tutorial form for users to follow step-by-step instructions. It assumes that the user has already successfully installed MRCX v.1.1 onto their local computer and has opened the MRCX workbook in Excel. See Section 2.1 above for instruction on installing MRCX.

The first Hanford Site example is for a test well (399-1-21A) completed in the Hanford formation and exhibits excellent hydraulic communication and high aquifer diffusivity. River-stage effects for this well are easily identified and removed. In contrast, the second Hanford Site example is for a well completed in the lower permeability Ringold Formation and is in close proximity to extraction wells used within the 100-K Area pump-and-treat system. This example demonstrates the difficulties in removing river-stage effects from well response records which may be significantly impacted by extraneous stress effects (i.e., surrounding pumping). The difficulty centers on finding a baseline well record not adversely impacted by extraneous stress effects so that a representative data record can be used as part of the MRCX training analysis for developing an associated river response function. The motivation for including a problematic data set such as this is that end users are likely to encounter similar challenges and need to be aware of the complications associated with such “noisy” data sets and the limitations for removing river-stage effects in wells such as this one.

4.1 Example 1: Well 399-1-21A

The first tutorial example involves removal of river-stage effects for well 399-1-21A, in the 300 Area of the Hanford Site. It is located about 323 meters from the river and is completed in the permeable Hanford formation (Figure 4.1). It provides an excellent example of a well with a highly associated river response behavior ($RRF \geq 0.8$), sufficient to allow for good river correction of well water levels. Spang and Mackley (2010) used this well as a demonstration example of the multiple-regression correction methodology. The following steps will guide you through the process of correcting river-stage effects for this well and highlight some of the different MRCX user options.

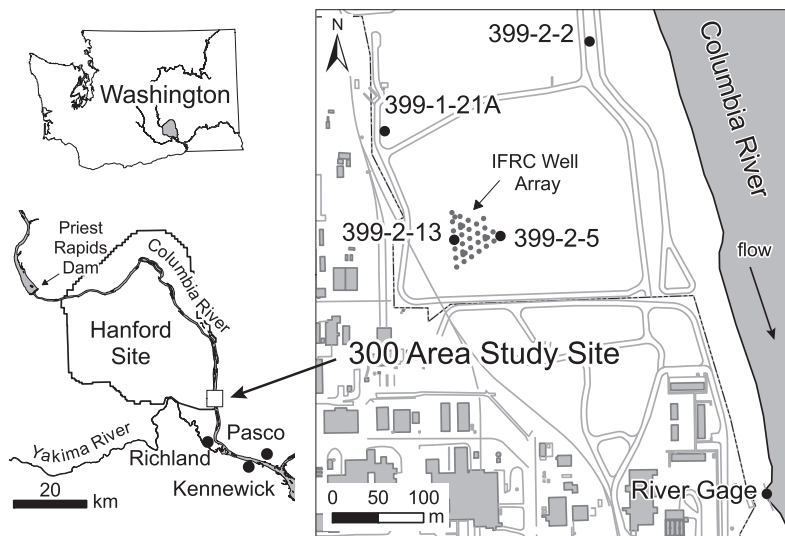


Figure 4.1. Site Map of 300 Area Wells

4.1.1 Entering the Input Data

The first step is to enter the river-stage and well water level data into the MRCX workbook. The time-series data for the 300-Area river gage and well 399-1-21A is located in the \Tutorial subfolder in the MRCX folder created during the initial installation of MRCX.

- Open the 300_Area_Example_InputData.xlsx workbook file from the C:\MRCX\Tutorial\ subfolder. This workbook contains the hourly river gage and well data.
- Select the entire three-column data range (excluding the header).
- Select Copy (Ctrl + C) from the Excel Home Ribbon tab.
- Switch back to the MRCX workbook file.
- Click on cell B4 in the Input Data worksheet to set this as the destination location for the next step.
- Select Paste > Paste Values from the Excel Home Ribbon tab (Figure 4.2). This will paste the input values into the three Training Dataset columns. The Training Data time-series plot now be updated, showing river and well elevations.

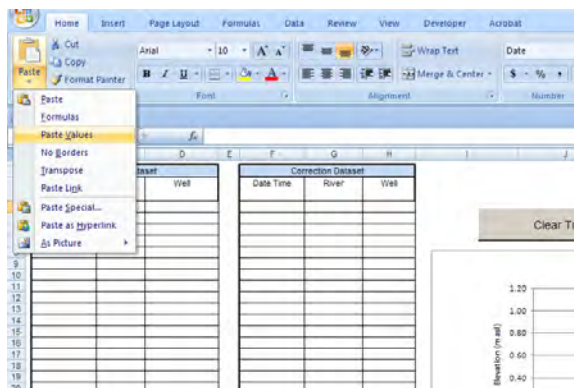


Figure 4.2. Paste Values Option in Excel

- Click on the 'Set Correction Data Equal to Training Data' command button above the time-series plots in the Input Config worksheet. This will copy the data in the Training Dataset section into the Correction Dataset section. The plots for the training and correction data should be similar in appearance (Figure 4.3).

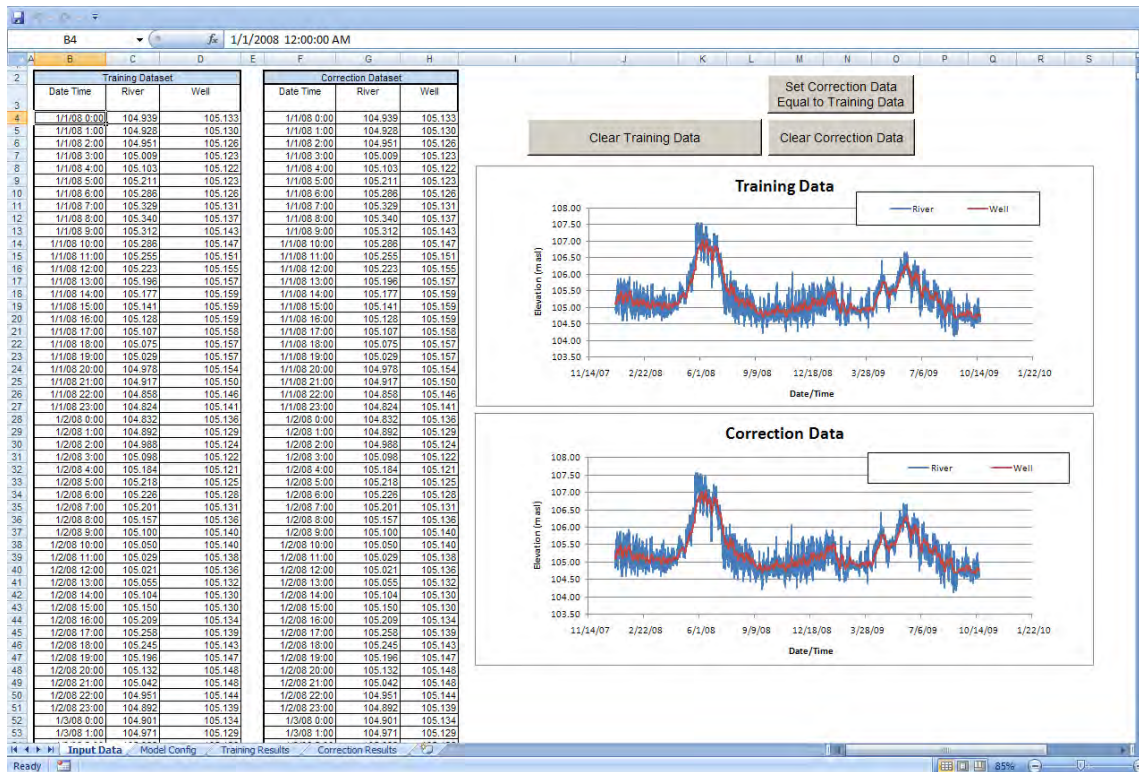


Figure 4.3. Well 399-1-21A Input Data Worksheet

4.1.2 Configuring the Multiple Regression Model

- Activate the Model Config worksheet.
- Click on the ‘Reset Filter’ command buttons, located at the top of the Model Config worksheet, for both the training and correction time periods. It is important to reset the time filters each time you enter new data into the Input Data worksheet. This will ensure the filter start/end dates are within the valid date range of the input data.
- Leave the filter start date default of 1/1/08 0:00 for the training data (cell D5).
- Set the filter end date for the training data to 12/31/08 23:00 (cell D6). This will restrict the training range to only use data from 2008.
- Set the filter start date for the correction data to 1/1/09 0:00 (cell F5).
- Leave the filter end date default of 10/19/09 7:00 for the correction data (cell F6) (Figure 4.4).

			Reset Filter		Reset Filter	
			Training		Correction	
			Available	Filtered	Available	Filtered
5	Start Date/Time	1/1/08 0:00	1/1/08 0:00	1/1/08 0:00	1/1/09 0:00	1/1/09 0:00
6	End Date/Time	10/19/09 7:00	12/31/08 23:00	10/19/09 7:00	10/19/09 7:00	10/19/09 7:00
7						
8	Data Option	Lag Option	Lags	Trend Adjust		

Figure 4.4. 399-1-21A Config Options

- Set the model configuration options to:
 - Data Option (cell B9): First Differences
 - Lag Option (cell C9): Manual
 - Lags (cell D9): 100
 - Trend Adjust (cell E9): Yes
- Click on the ‘Run Multiple Regression Model on Training Data’ command button to run the multiple regression model. You should see the following results (Figure 4.5):

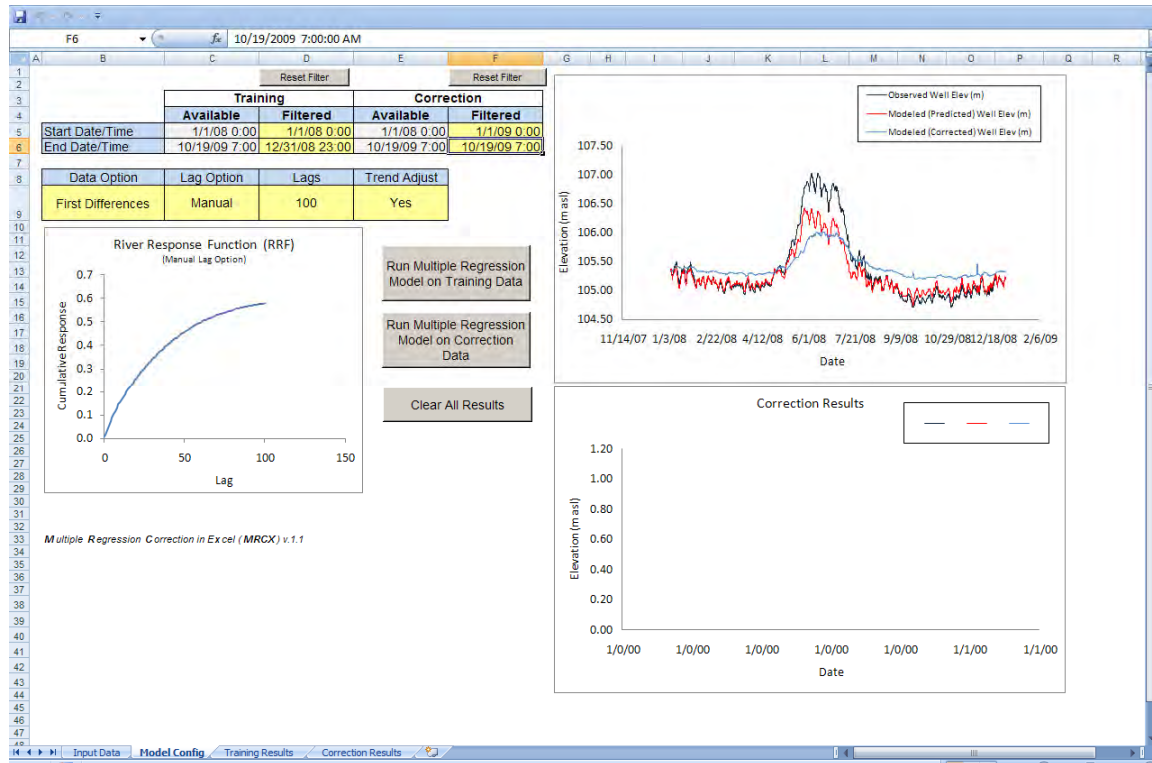


Figure 4.5. Well 399-1-21A Training Data Regression Results 1 (Lag = 100 hrs)

4.1.3 Varying the Maximum Lag Term

The RRF shows a smooth trend when using a maximum time lag of 100 hours; however it only attains a cumulative value of about 0.58. As a general rule of thumb, satisfactory river correction results are achieved when RRF values are ≥ 0.8 . Additionally, the MAE is 0.143 meters, as reported in the model summary section of the Training Results worksheet. The low RRF and relatively high MAE suggest that the maximum lag needs to be increased in order to better capture long-term river responses.

- Set the maximum lag value (cell D9) to 480, and then click on the ‘Run Multiple Regression Model on Training Data’. The plots will update, and you should see the following results (Figure 4.6):

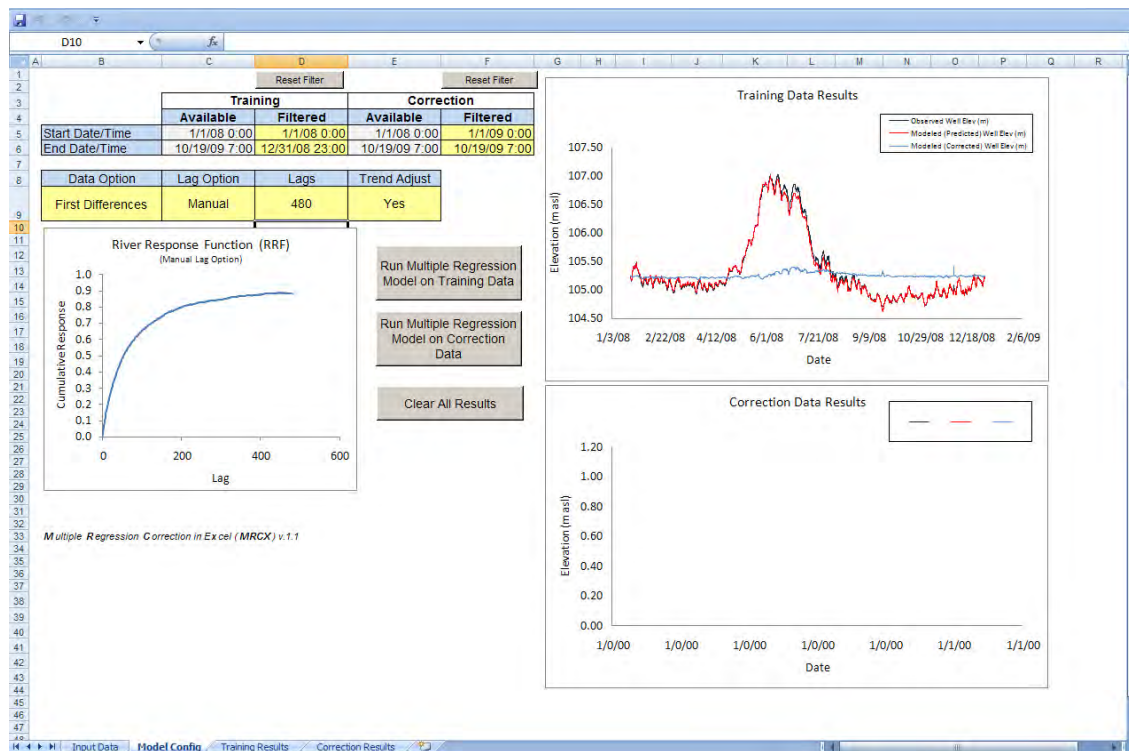


Figure 4.6. Well 399-1-21A Training Data Regression Results 2 (Lag = 480 hrs)

The increase of the lag to 480 hours results in a much improved match between the predicted and the corrected data. The RRF approaches a maximum value of 0.88, and the MAE equals 0.031 meters. This suggests a valid model fitting for the training data, consisting of the data for the entire year of 2008. The model does show under-prediction in the well water levels during the high river-stage period of 2008. There may be a storage effect of the water table increasing on a seasonal time scale that is not fully captured in the average river response function with a maximum time lag of 480 hours.

4.1.4 Different Training and Correction Time Periods

Often, it will be desirable to focus on a particular time period for the correction rather than for the entire data set. In the next step, the objective is to correct river effects during the first four months of 2009. You can use data from the same time period to train the model; however, a more robust application of the correction method is to train the model with data from a different time period than will be corrected. To be representative, the training period should have similar river-stage, well water elevation relationship, and hydrologic conditions as the correction time period. In the next step, data from the first four months of 2008 will be used to train the model and develop the RRF for correction for the first four months of 2009.

- Verify the model configuration options are still set to:
 - Data Option (cell B9): First Differences
 - Lag Option (cell C9): Manual
 - Lags (cell D9): 480
 - Trend Adjust (cell E9): Yes

- Set the start and end dates on the training period to 1/1/08 0:00 and 4/30/08 0:00, respectively (cells D5 and D6).
- Set the start and end dates on the correction period to 12/11/08 23:00 and 4/30/09 0:00, respectively (cells F5 and F6). Remember, you need to set the start date $n+1$ time units previously to the date/time when you want the regression model results to begin if you are using the First Differences (change in water levels) option.
- Create the RRF and the predicted and corrected results for the training data by clicking on the ‘Run Multiple Regression Model on Training Data’ command button.
- Predict and correct the well water levels for the correction period by clicking on the ‘Run Multiple Regression Model on Correction Data’ command button. The Model Config will update the RRF and time-series plots (Figure 4.7):

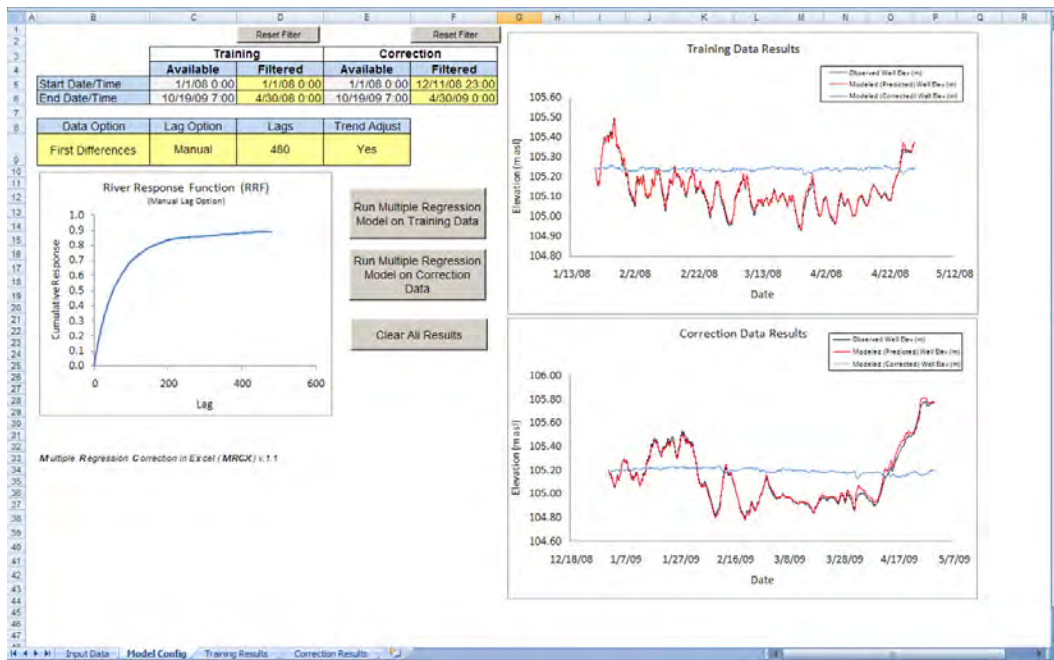


Figure 4.7. Well 399-1-21A Training and Correction Data Regression Results (Lag = 480 hrs)

- Compare the model summary results in the Training and Correction results worksheets.

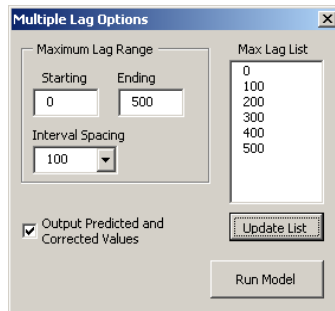
The river response for well 399-1-21A during the first four months of 2008 appears to be representative of the river response a year later based on the model results. The mean MAE for the correction data is 0.019 meters.

4.1.5 Batch Lag Mode

If you would like to run the multiple regression model for a list of maximum lags (n) rather than a single value manually one at a time, you can use the batch mode option in MRCX. This is helpful for comparing the model results for different values of n . To run a batch list of regression results for a list n values:

- Set the Lag Option (cell C9) to Batch using the drop-down list prior to running the regression model for the training data. This will bring up a dialog box containing additional user input options (Figure 4.8).

Figure 4.8. Batch Lag Menu



- Set the Starting and Ending values for the range of maximum lag values to 0 and 500, respectively.
- Select one of the Interval Spacing items in the drop-down list.
- Click on the ‘Update List’ command button to display the list of maximum lag values that will be run in batch mode.
 - Click in the box next to the ‘Output Predicted and Corrected Values’ to include the full results in the output workbook. Disabling this option will output just the summary results for the batch correction.
- Click on the ‘Run Model’ command button to initiate the batch mode. Note: if the list is long and the maximum lag values are large, the batch regression results can take several minutes to process. When complete, a message box will appear letting you know the processing is complete (Figure 4.9).



Figure 4.9. Batch Lag Menu

In batch mode, MRCX creates a new workbook file containing individual worksheets for each item in the batch list of maximum lag values. The result worksheets are named according to the corresponding lag value.

- Click on the ‘Summary’ worksheet to view a table showing a summary of the regression results for each of the values in the maximum lag list.
- Click on each worksheet to compare the results for varying maximum lag values.

4.2 Example 2: Well 199-K-112A

This example will involve using various regression options in MRCX while correcting water level data for well 199-K-112A. As noted above, this well was chosen to highlight the challenges and

limitations of river-stage correction when dealing with a complicated data set that includes extraneous influences such as nearby pumping wells.

Well 199-K-112A is located 115 meters inland from the river shoreline in the 100-K area of the Hanford Site and is screened in the Ringold Formation (Figure 4.10). The Ringold Formation has a relatively lower permeability than the Hanford formation, so the river response might be expected to be more lagged and attenuated than the response observed in the first example for well 399-1-21A. On the other hand, well 199-K-112A is almost three times closer to the river than well 399-1-21A (323 m inland). The river response function would need to be normalized for inland distance to make direct comparisons between wells – this involves plotting RRF's against the distance-normalized time lag where (time lag divided by the square of the inland distance). We will not do that in this exercise, but you might want to explore the comparison on your own.

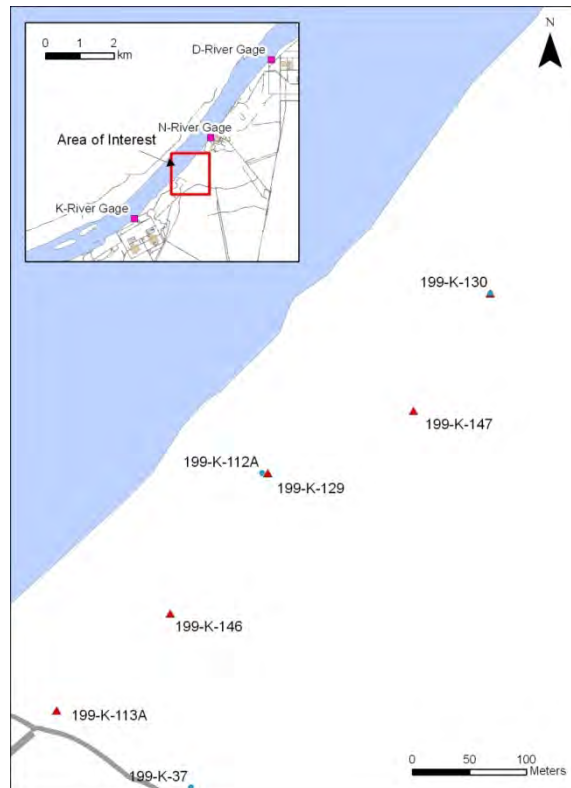


Figure 4.10. Site Map of 100-K Wells

Well 199-K-112A is located 5 meters away from the pump-and-treat extraction well 199-K-129 (also screened in the Ringold Formation) and within a few hundred meters of several other extraction wells. During the 2008 and 2009 time period of interest, well 199-K-129 was mostly running, but experienced intermittent shut-down events. These shut-down events created recovery responses in well 199-K-112A. However, river-stage effects make these recovery responses less obvious and obscure their overall magnitude. This example will illustrate the difficulty in correcting river-stage effects with data that contain non-river input signals.

4.2.1 Input Data

The time-series data for the 100-K river gage and well 199-K-112A is located in \Tutorial subfolder in the MRCX folder created during the initial installation of MRCX.

- Open the 100K_Area_Example_InputData.xlsx workbook file. This workbook contains the hourly river gage and well data in a worksheet named 'Elev Data'. It also contains pumping flow rate data for the adjacent extraction well in a worksheet named 'Flow Data'.
- Open a new instance of the MRCX workbook template, and clear the results and the input data using the command buttons in MRCX if needed.
- Follow the steps outlined in Section 1.1.1 for copying the river-stage and well water level from the source workbook to the target cells in the Input Data worksheet in the MRCX workbook file.
- Use the 'Set Correction Data Equal to Training Data' command button in the Input Data worksheet to copy the data from the training section to the correction sections.

You are now ready to configure the multiple regression model settings in the Model Config worksheet.

4.2.2 Establishing a Suitable Training Period and Maximum Lag Combination

As noted above, the presence of the intermittent pumping of the adjacent extraction well creates additional complexity to the correction process (Figure 4.11). In the following steps, we will attempt to look for a suitable training period that can be used to generate a river response function to correct a select period of time in 2009 when a major shut down even occurred (04/29/08 to 05/17/09). River-stage effects obscure the recovery response to the extraction well shut down. The objective is to remove or minimize river-stage effects in order to better evaluate the recovery response.

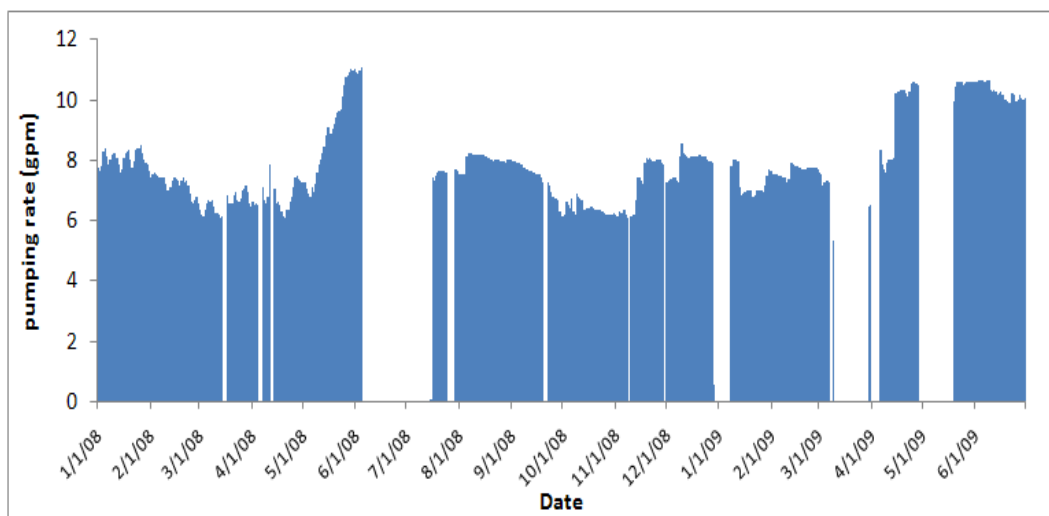


Figure 4.11. Average Daily Pumping Rates Data for Extraction Well 199-K-129

Typically, the ideal scenario would be to train the response function during a period when the extraction well has been shut down for an extended period of time. Unfortunately, the longest shut down

period is only about 40 days (06/5/08 to 07/14/08), which is too short of a time period to adequately incorporate longer-term (e.g., seasonal) river-stage influences. This will become apparent in the results generated in the next steps. To begin:

- Activate the Model Config worksheet, and verify the following options:
 - Data Option (cell B9): First Differences
 - Lag Option (cell C9): Manual
 - Lags (cell D9): 150
 - Trend Adjust (cell E9): Yes
- Set the time filter options to:
 - Training start date: 6/5/08 0:00
 - Training end date: 7/14/08 0:00
 - Correction end date: 4/1/09 0:00
 - Correction start date: 6/15/09 0:00
- Run the multiple regression model on the training data period to generate the RRF.
- Run the multiple regression model on the correction data period.

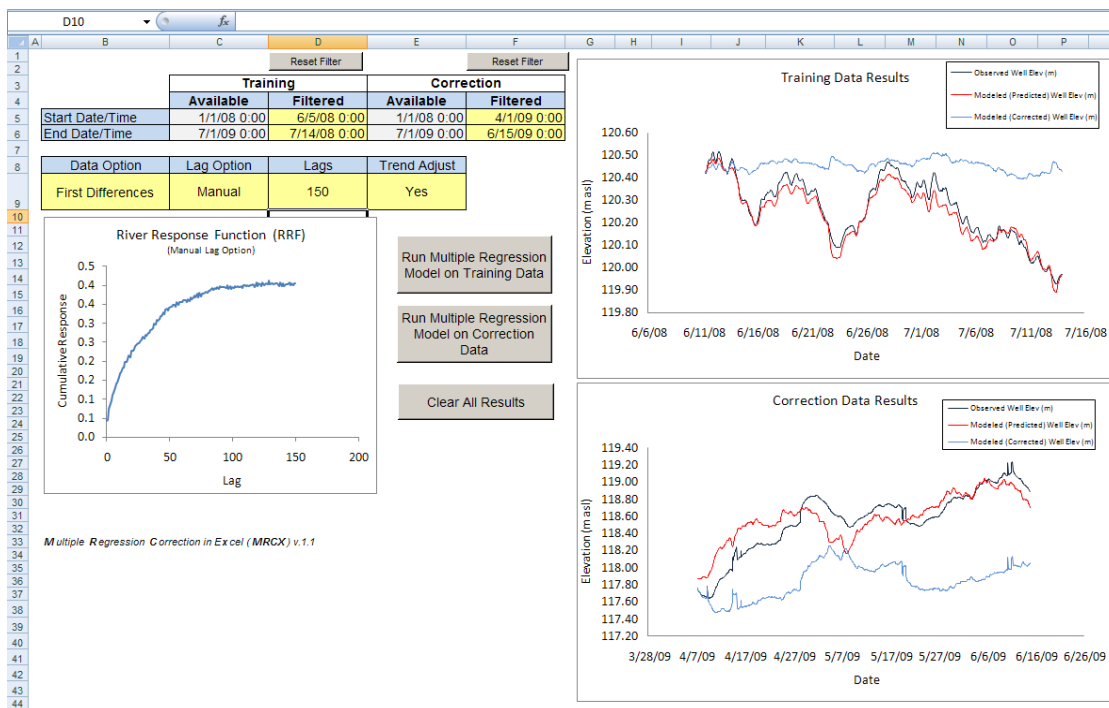


Figure 4.12. Well 199-K-112A Regression Results 1 (Lag = 150 hours)

The river response function has a typical shape; however, it only reaches a maximum response of about 0.4 (Figure 4.12). This indicates either the well has a relatively weak river-stage effect or the maximum lag needs to be increased in order to incorporate longer-time scale river effects. Furthermore, the recovery response in April-May 2009 still contains noticeable river effects.

- Change the Lags (cell D9) value to 300 hrs, and re-run the regression models for the training and correction data.

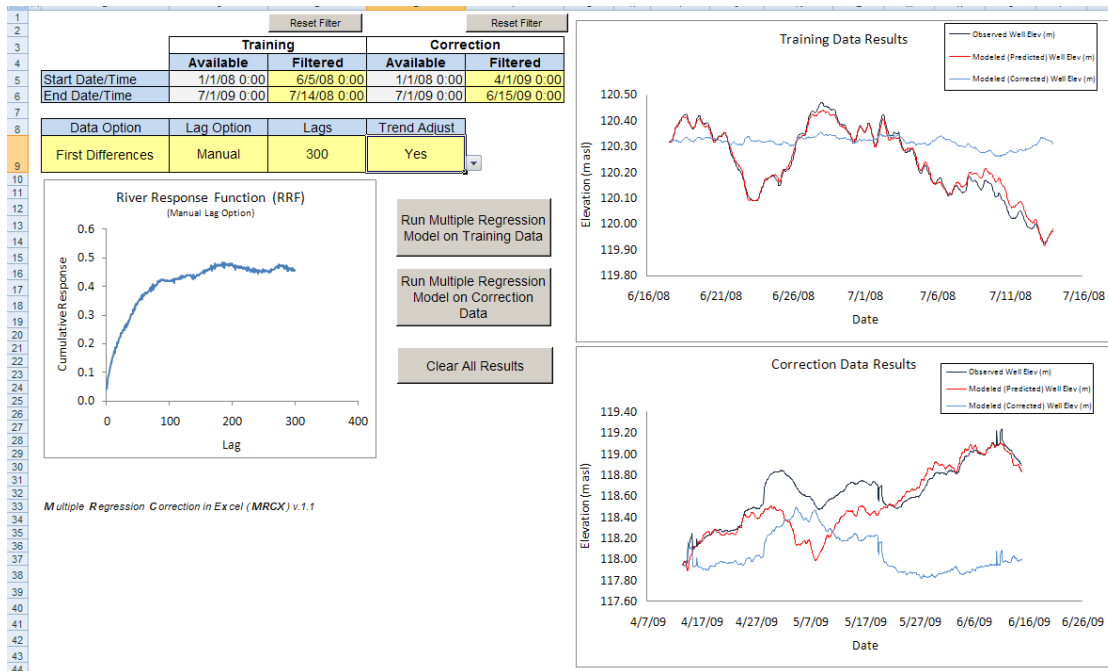


Figure 4.13. Well 199-K-112A Regression Results 2 (Lag = 300 hours)

The RRF increased to 0.46 but now has a less-stable pattern, and the correction of the recovery response in April-May 2009 did not improve (Figure 4.13).

- Try changing the Lags (cell D9) value to 400 (hrs), and re-run the regression models for the training and correction data.

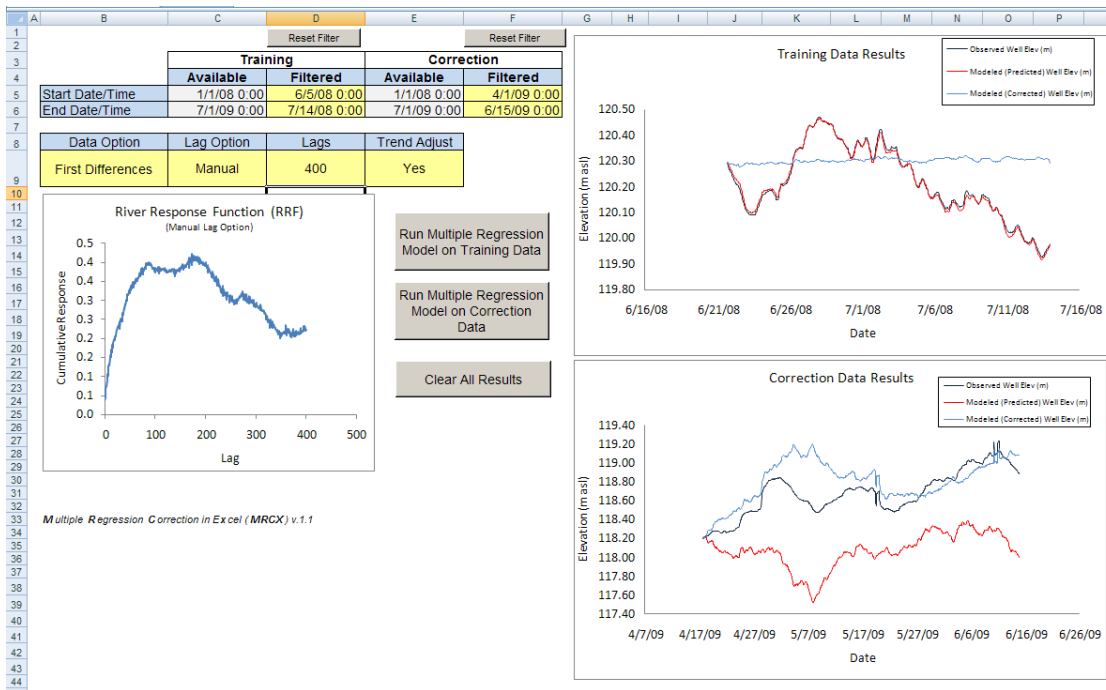


Figure 4.14. Well 199-K-112A Regression Results 3 (Lag = 400 hours)

Although there is a very strong match of the predicted and the observed water levels for the training period, the correction of the recovery response is worse than it was when using 150 or 300 hours for the lag (Figure 4.14). Increasing the maximum lag to 400 hours resulted in a very unstable and non-characteristic pattern in the river response function. It suggests that the maximum lag term is too large for the short training period.

A different approach is to train the model on the entire 2008 and 2009 data set, lumping river and non-river influences in the response function. The advantage to this is that the longer training period can incorporate any longer-term river-stage effects that were absent in the 40-day training period. However, the obvious drawback to this approach is that the response function will contain non-river effects such as the intermittent pumping of well 199-K-129. Normally, this approach would be avoided. However, in the next step we will use *all* of the available data to train the RRF, and use it for correcting the April-May 2009 shut down recovery response. The *caveat* is that the river response function will be highly skewed by the extraneous (non-river) influences and should be interpreted with caution. To proceed:

- Verify the model configuration options are still set to the following:
 - Data Option (cell B9): First Differences
 - Lag Option (cell C9): Manual
 - Lags (cell D9): 400
 - Trend Adjust (cell E9): Yes
- Click the ‘Reset Filter’ command button for the training data in order to set the options to:
 - Training start date: 1/1/08 0:00
 - Training end date: 7/1/09 0:00

- Verify the correction start and end times are still set to the following:
 - Correction end date: 4/1/09
 - Correction start date: 6/15/19
- Re-run the regression models for the training and correction data to generate new results.

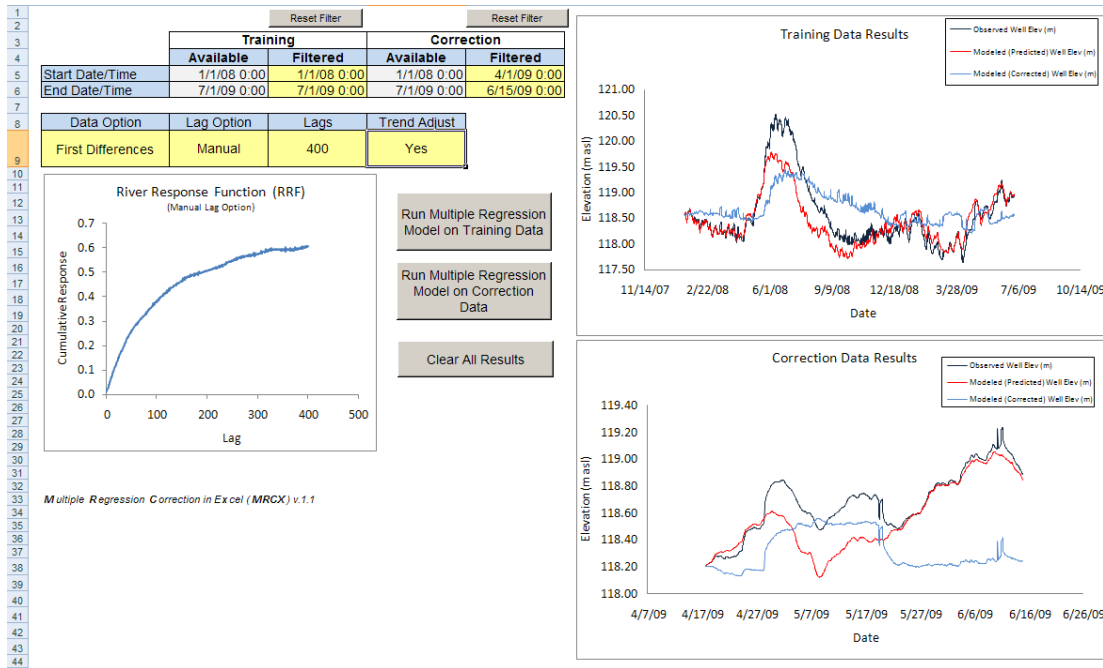


Figure 4.15. Well 199-K-112A Regression Results 4 (Lag = 400 hours)

The RRF increased to a higher value of 0.61 and the correction of the 2009 data improved (Figure 4.15). Although the RRF is still relatively low (indicating a relatively weaker river influence), and there are still residual river-stage effects present in the corrected data for April-May 2009, the recovery response pattern does have a more characteristic pattern. The apparent drop in the observed water levels around 5/6/09, due to a river-stage decrease, is now almost entirely removed.

4.2.3 Linear Trend Adjustment

MRCX allows the option to include or omit a background linear trend coefficient in the regression model. Thus far, we have included the background trend in all the regression models. To see the effect of leaving out the linear trend adjustment on the previous results:

- Change the Linear Adjustment option (cell E9) to No by clicking in drop-down list.
- Re-run the training and correction regression models.

The result of leaving out the background trend adjustment in the model is that the predicted values progressively deviate from the observed water levels with time (Figure 4.16). The corrected data for the 2009 recovery response has a slightly more positive trend compared to the previous results that included the trend adjustment. Although, the difference is small in this instance it may be more significant in other situations. The use of the trend adjustment option is highly dependent upon the situation – it is

recommended that you typically run the model with and without the trend adjustment and compare the results, especially when there is a very noticeable background trend in the observed well water level data.

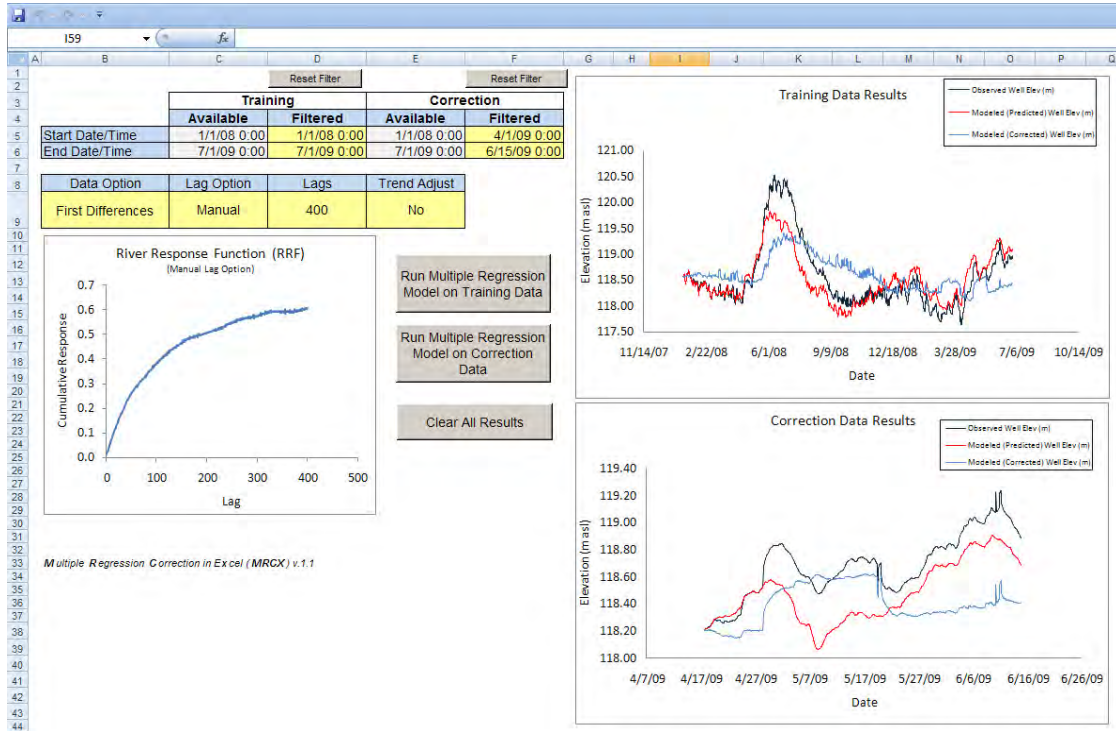


Figure 4.16. Well 199-K-112A Regression Results with Linear Trend Adjust Turned Off

5.0 References

- Barlow PM and AF Moench. 1998. "Analytical solutions and computer programs for hydraulic interaction of stream-aquifer systems." U.S. Geological Survey, Open-File Report 98-415A, 85 p.
- Erskine AD. 1991. "The effect of tidal fluctuation on a coastal aquifer in the UK." *Ground Water*, vol. 29, no. 4, pp. 556–562.
- Box GEP, GM Jenkins, GC Reinsel. 2008. *Time Series Analysis* (4th Edition). John Wiley, New York.
- Ferris JG. 1952. "Cyclic fluctuations of water level as a basis for determining aquifer transmissibility." U.S. Geological Survey, Ground-Water Hydraulics Section, Contribution No. 1, 17 p.
- Ferris JG. 1963. "Cyclic fluctuations of water level as a basis for determining aquifer transmissibility." *Water-Supply Paper 1536-I*, U.S. Geological Survey, pp. 305–318.
- Foundastat .Net Statistics Made Easy. 2008. *FoundaStat Pro*. Accessed (09/15/2010) at <http://www.foundasoft.com/> (last updated 2008).
- Furbish DJ. 1991. "The response of water level in a well to a time series of atmospheric loading under confined conditions." *Water Resources Research*, vol. 27, no. 4, pp. 557–568.
- Gilmore TJ, FA Spane, Jr., DR Newcomer, and CR Sherwood. 1992. Applications of three aquifer test methods for estimating hydraulic properties within the 100-N Area." Pacific Northwest Laboratory, Richland, Washington.
- Jacob CE. 1950. "Flow of groundwater." In *Engineering Hydraulics*, H. Rouse (ed.), John Wiley & Sons, Inc., New York, pp. 321–386.
- McDonald JP. 2007. Water-level barometric response analysis for the Liquid Effluent Retention Facility monitoring wells. SGW-35756, Rev. 0. Fluor Hanford, Inc., Richland, Washington
- Pankratz A. 1983. *Forecasting with univariate Box-Jenkins models: concepts and cases*. John Wiley & Sons, New York.
- Pankratz A. 1991. *Forecasting with dynamic regression models*. John Wiley, New York.
- Rasmussen TC and LA Crawford. 1997. "Identifying and removing barometric pressure effects in confined and unconfined aquifers." *Ground Water*, vol. 35, no. 3, pp. 502–511.
- Spane FA, Jr. 1999. Effects of barometric fluctuations on well water-level measurements and aquifer test data. PNNL-13078, Pacific Northwest National Laboratory, Richland, Washington.
- Spane FA. 2002. "Considering barometric pressure in groundwater flow investigations." *Water Resources Research*, vol. 38, no. 6, pp. 14:1-18.
- Spane FA, and RD Mackley. 2010. "Removal of River-Stage Fluctuations from Well Response Using Multiple-Regression." *Ground Water in press*.

- Stevens J. 1996. Applied Multivariate Statistics for the Social Sciences (3rd Edition). Lawrence Erlbaum Associates, Inc., New Jersey.
- Toll NJ and TC Rasmussen. 2007. "Removal of barometric pressure effects and earth tides from observed water levels." Ground Water, vol. 45, no. 1, pp. 101–105.
- Vermeul VR, BN Bjornstad, BG Fritz, JS Fruchter, RD Mackley, DR Newcomer, DP Mendoza, ML Rockhold, DM Wellman, and MD Williams. 2009. 300 Area uranium stabilization through polyphosphate injection: final report. PNNL-18529, Pacific Northwest National Laboratory, Richland, Washington.
- Zlotnik VA and H. Huang. 1999. "Effect of shallow penetration and streambed sediments on aquifer response to stream stage fluctuations (analytical model)." Ground Water, vo. 37, no. 4, pp. 599–605.

Distribution

No. of Copies

OFFSITE

2 S.S. Papadopoulos & Assoc., Inc
7944 Wisconsin Ave.
Bethesda, MD 20814
Matt Tonkin
Rachel Shannon

ONSITE

12 CH2M-HILL Plateau Remediation
Company, Inc

D.J. Alexander	R3-60
R.S. Edrington	R3-50
D. Erb	R3-60
E.J. Freeman	R3-50
M.J. Hartman	R3-50
K.J. Johnson	R3-50
J.P. McDonald	R3-50
S.W. Petersen (3)	R3-50
J.L. Smoot	R3-50
L.C. Swanson	R3-50

16 Pacific Northwest National Laboratory

C.H. Allwardt	K7-28
K.C. Carroll	K6-96
M.D. Freshley	K9-33
T.J. Gilmore	K6-96
R.D. Mackley (5)	K6-96
R.E. Peterson	K6-75
T.C. Pulsipher	K7-20
F.A. Spane	K6-96
V.R. Vermeul	K6-96
D.R. Newcomer	K6-96
P.D. Thorne	K6-96
M.D. Williams	K6-96



902 Battelle Boulevard
P.O. Box 999
Richland, WA 99352
1-888-375-PNNL (7665)
www.pnl.gov



U.S. DEPARTMENT OF
ENERGY

UNITED STATES
DEPARTMENT OF THE INTERIOR
GEOLOGICAL SURVEY

PRELIMINARY INTERPRETATION OF THERMAL DATA
FROM THE NEVADA TEST SITE

by

J. H. Sass and Arthur H. Lachenbruch

Open-File Report 82-973

1982

This report is preliminary and has not been reviewed for conformity
with U.S. Geological Survey editorial standards and stratigraphic nomenclature.

SE ROA 38127

Abstract

. Analysis of data from 60 wells in and around the Nevada Test Site, including 16 in the Yucca Mountain area, indicates a thermal regime characterized by large vertical and lateral gradients in heat flow. Estimates of heat flow indicate considerable variation on both regional and local scales. The variations are attributable primarily to hydrologic processes involving interbasin flow with a vertical component of (seepage) velocity (volume flux) of a few mm/yr. Apart from indicating a general downward movement of water at a few mm/yr, the results from Yucca Mountain are as yet inconclusive.

INTRODUCTION

The Geothermal Studies Project, USGS, has been periodically measuring temperatures in holes drilled in and near the Nevada Test Site (NTS) in southern Nevada (fig. 1). Our primary motivation has been the measurement of the earth's heat flow. Thus, when we examined temperature profiles within the context of heat flow in the western United States (Sass and others, 1971), we discarded most of the data we had obtained as unsuitable owing to hydrologic disturbances to the conductive heat-flow field. Recently (Lachenbruch and Sass, 1977), we have attempted to refine our interpretation of the variation of heat flow in the western U.S. In particular, we have sought to explain much of the scatter in heat flow within the Great Basin in terms of local water circulation. In addition, we have interpreted the large area of anomalously low heat flow (Eureka Low, EL, fig. 1) as reflecting regional water flow with a downward (seepage) velocity component on the order of a few mm/y (Lachenbruch and Sass, 1977) consistent with regional hydrologic studies (see Winograd and Thordarson, 1975). The regional heat flow from beneath the zone of hydrologic disturbance in the Eureka Low may be the same as that characteristic of the Great Basin in general ($\sim 80 \text{ mWm}^{-2}$, or $\sim 2 \text{ HFU}$) or it could be as high as $\sim 100 \text{ mWm}^{-2}$ ($\sim 2.5 \text{ HFU}$).

In view of the importance of hydrologic processes in determining the suitability of proposed repository sites, and because thermal measurements are extremely sensitive to these processes, we have re-examined our existing data and obtained additional data from Syncline Ridge near the Eleana Range, hole U15K in the Climax Stock, and from all available wells near Yucca Mountain (fig. 2). In this section, we briefly review the thermal data from approximately 60 wells and their implications for regional heat flow. We also

examine in more detail the thermal data from the Yucca Mountain site and their implications for vertical water flow within and adjacent to the proposed nuclear waste repository.

Acknowledgments. Temperature measurements were made by Gordon Greene, Fred Grubb, Tom Moses, Bob Munroe, and Gene Smith. Conductivities were measured by Bob Munroe and Gene Smith. We are grateful to W. E. Wilson and Rick Waddell for their helpful comments and suggestions.

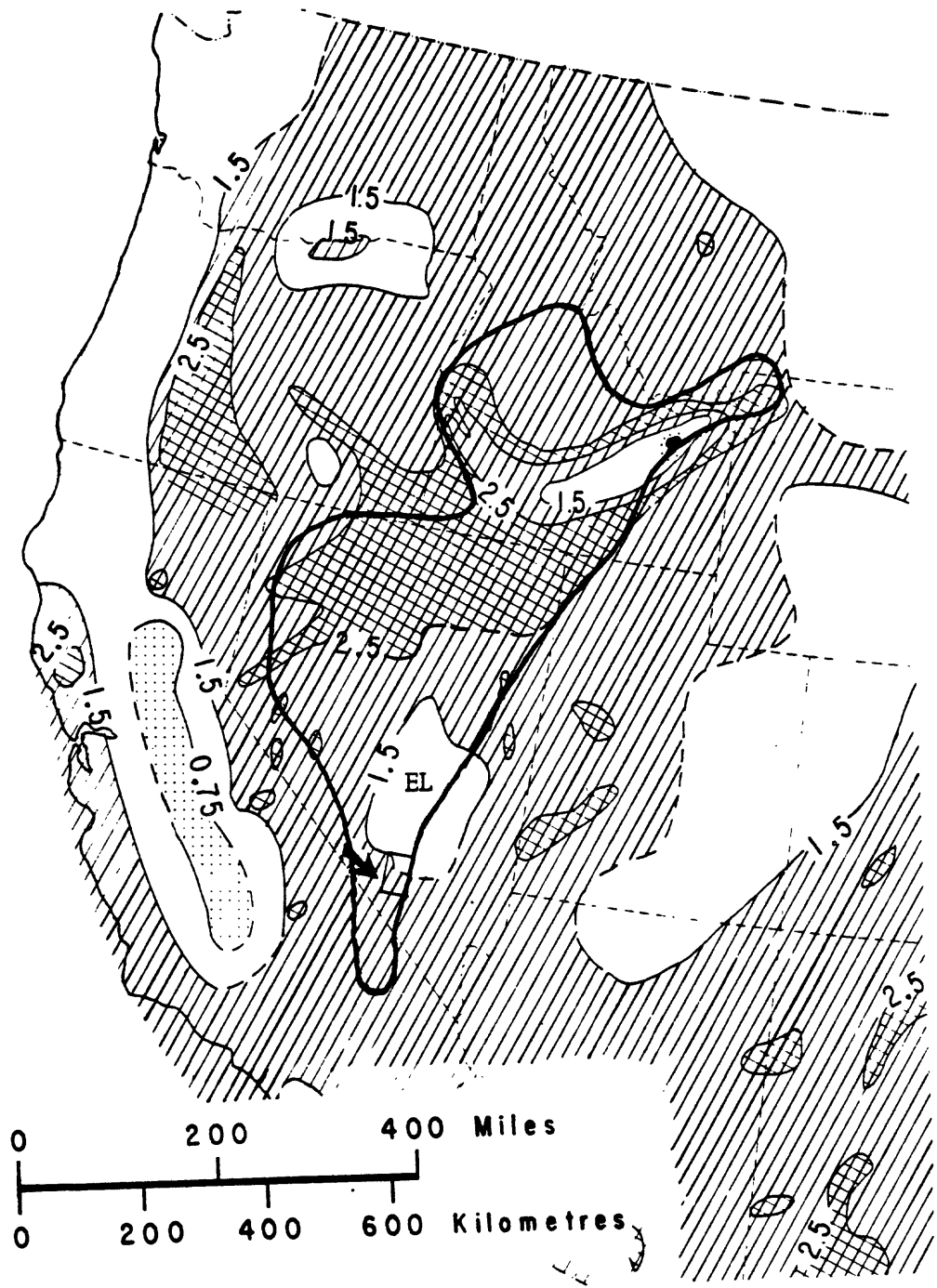


Figure 1. Map of western United States showing heat-flow contours (in HFU) 1 heat-flow unit (HFU) = 41.86 mWm^{-2} . EL is Eureka Low. Arrow indicates outline of approximate boundaries of the Nevada Test Site (NTS). Heavy line is 2.5 HFU contour, based on the empirical relation between silica temperatures and heat flow (Swanberg and Morgan, 1978).

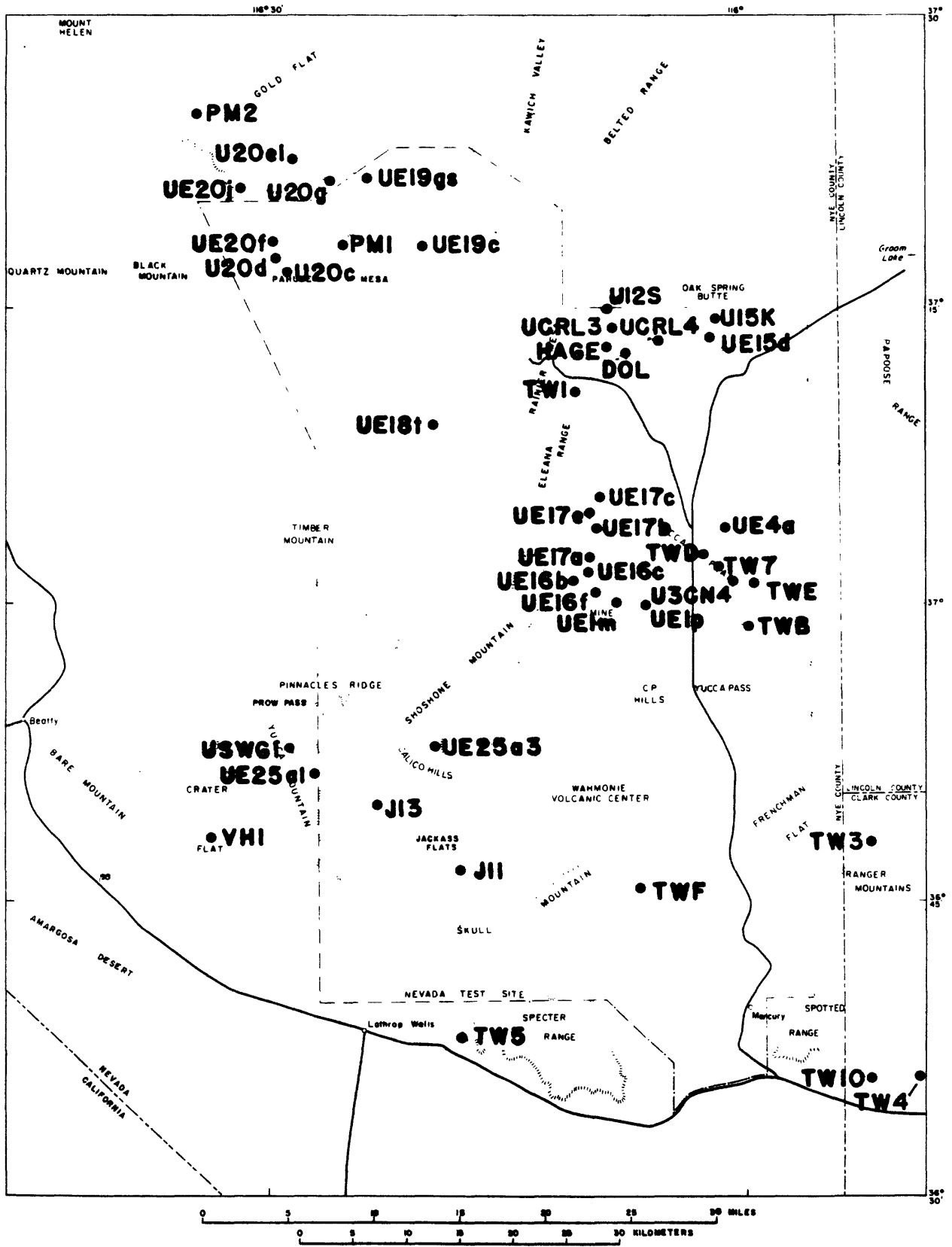


Figure 2. Map of the test-site region showing locations of wells discussed in the text.

REGIONAL HEAT FLOW

Available heat-flow data from the NTS region are summarized in table 1 and figure 3. The data described as "USGS Unpublished" are preliminary and are subject to minor revision (\pm a few percent) upon further study. The data (fig. 3) indicate a typical Basin-and-Range distribution of heat flow in the region immediately surrounding Mercury but a rather complex situation to the north and west. The complexity of the thermal regime is further demonstrated, and can be explained to some extent, by consideration of all temperature data within the region (fig. 2). These data are presented as a series of composite temperature-depth plots ("worm diagrams") for different areas within the region in figures 4 through 8 and 10.

Beneath Pahute Mesa (fig. 4), temperature gradients are fairly low (~ 20 to $25^\circ\text{C}/\text{km}$), and the tuffs within which the wells were drilled have low thermal conductivities (1 to $1.5 \text{ Wm}^{-1} \text{ K}^{-1}$) resulting in anomalously low values of regional heat flow. The deepest log we obtained from NTS was that in Ue20f (fig. 4). In the upper 1.5 km, the temperature gradient is $26^\circ\text{C}/\text{km}$ and the calculated conductive heat flow is less than 40 mWm^{-2} . Below 1.5 km, there is a zone extending to nearly 3 km that is probably disturbed by a complex combination of lateral and vertical water flow. Below 3 km, the temperature profile is linear, and the gradient is $37^\circ\text{C}/\text{km}$. Thermal conductivities in this section are not well characterized, but reasonable values would result in heat-flow values between 80 and 100 mWm^{-2} which is typical of the Basin and Range Province in general. The implication here is that water is carrying off much of the earth's heat in the upper 3 km and delivering it elsewhere. Well PM-2 is a possible exception. Its temperature profile (fig. 4) might indicate regional heat flow or possibly just a local upwelling of convecting water.

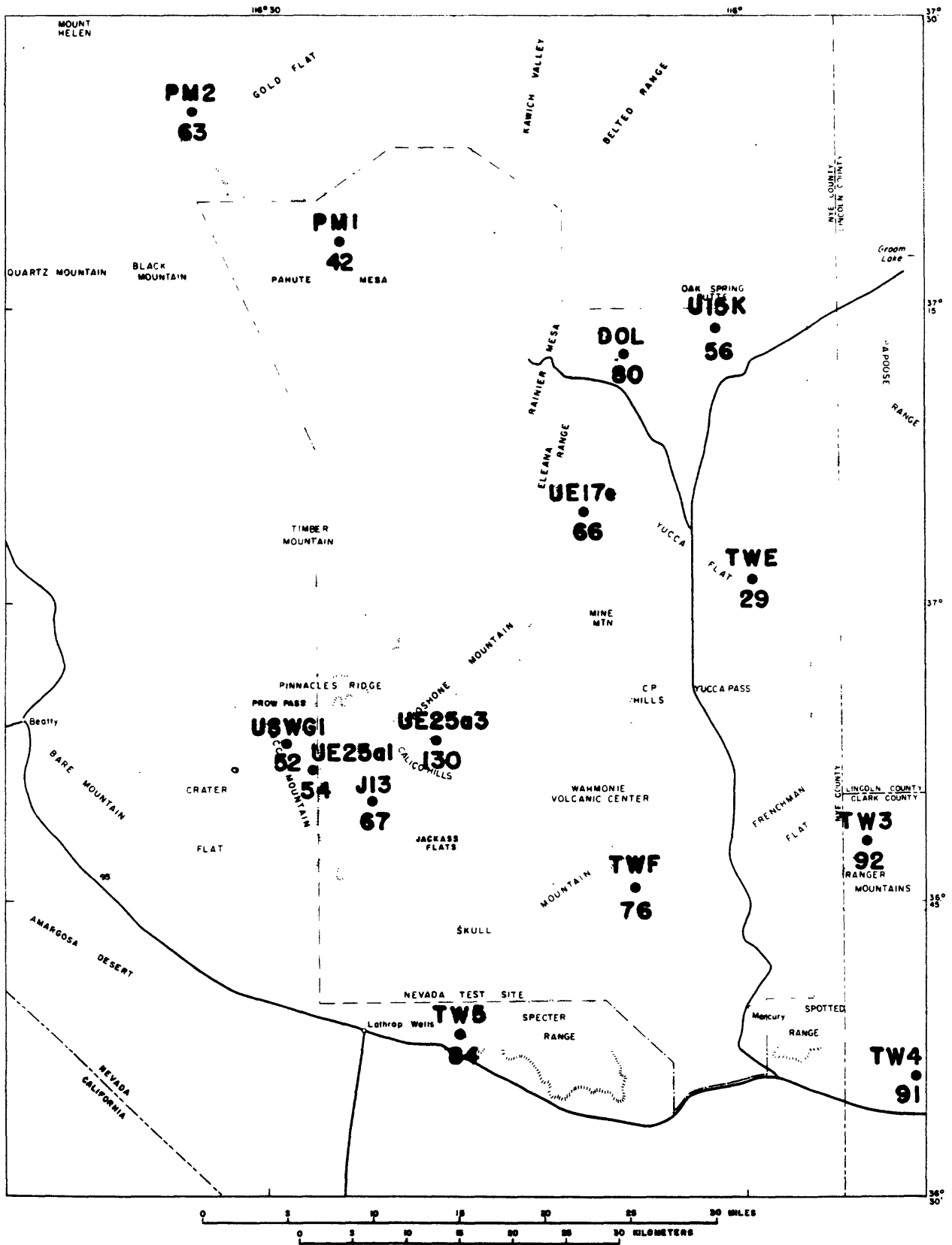


Figure 3. Regional heat-flow values within and adjacent to the Nevada Test Site.

TABLE 1. Heat-flow determinations in and adjacent to the Nevada Test Site (see Figures 2 and 3 for locations)

Well	Heat flow		Reference
	mWm^{-2}	HFU	
PM2	63	1.5	Sass and others, 1971
PM1	42	1.0	Sass and others, 1971
DOL	80	1.9	Sass and others, 1971
U15K	56	1.3	USGS unpublished
Ue17e	66	1.58	USGS unpublished
TWE	29	0.7	Sass and others, 1971
J-13	67	1.6	Sass and others, 1971
Ue25a1	54	1.3	Sass and others, 1980
Ue25b1	47	1.1	USGS unpublished
Ue25a3	130	3.1	Sass and others, 1980
USWG1*	52	1.25	Table 2, this paper
TWF	76	1.81	Sass and others, 1971
TW3	92	2.2	Sass and others, 1971
TW5	84	2.0	Sass and others, 1971
TW4	91	2.2	Sass and others, 1971

*Average heat flow in lowermost ~600 m.

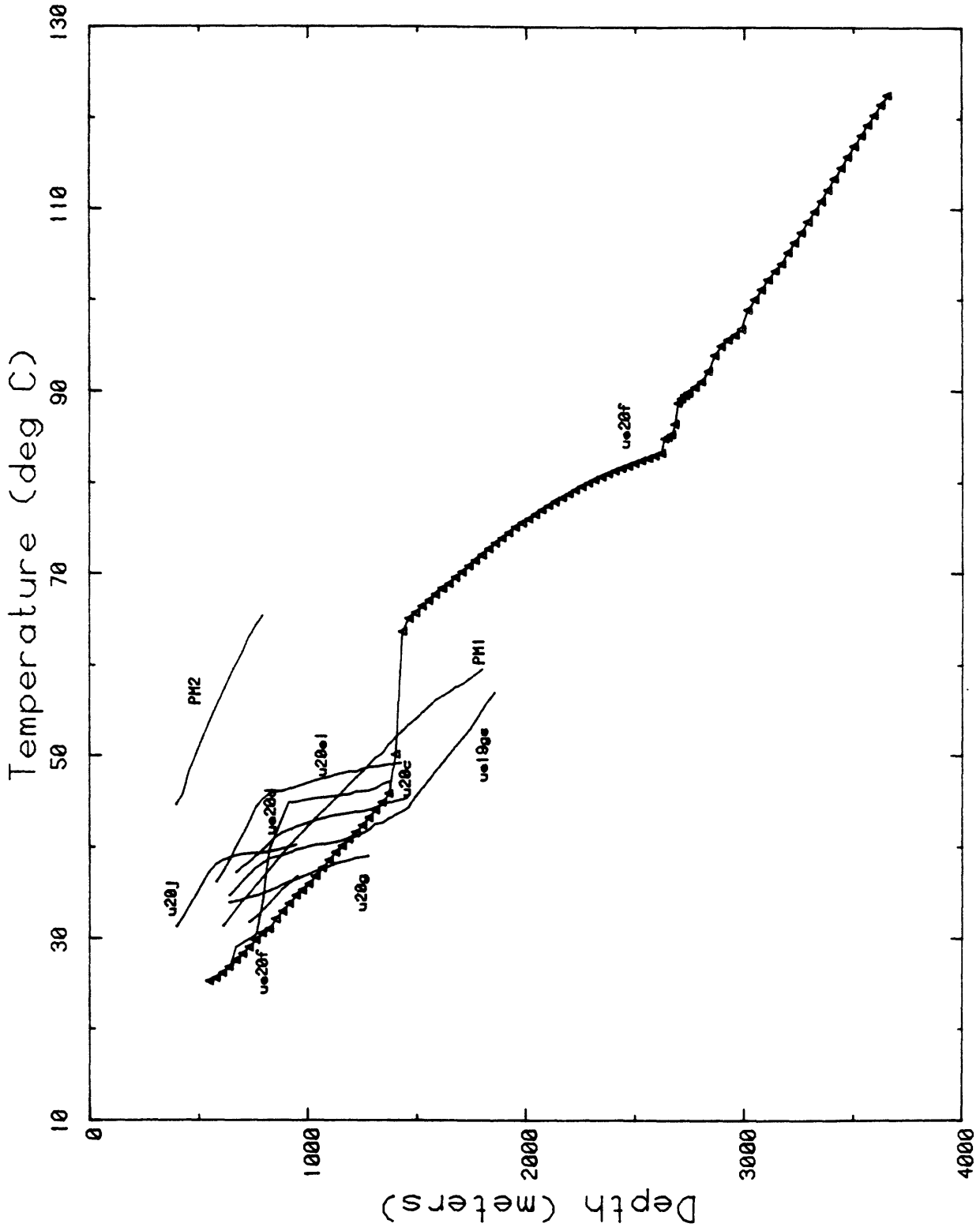


Figure 4. Composite Temperature Profile, Pahute Mesa

Consideration of temperatures from other areas of the NTS (figs. 5 through 8) also suggests lateral variations in heat flow that can be attributed largely to lateral and vertical water movement with vertical seepage velocities probably on the order of 1-10 mm/y.

The most reliable "flux plates" for determination of regional heat flow generally have been granitic bodies. Unfortunately, we have only one such determination (U15k, fig. 3), and even it is uncertain because the hole is relatively shallow (~260 m), and we have only one determination of thermal conductivity. The best documented heat-flux value in this region is that for UE17e (figs. 3 and 7) which was drilled in argillites of the Eleana Formation. This is the only well in this entire study for which we can rule out vertical water movement in the hole, as the access casing was completely grouted in. In other wells, some or all of the perturbations to the steady-state conductive thermal regime may be the result of water movement in the annulus between casing and borehole wall rather than water movement in the formation. Fortunately, however, it is usually possible to distinguish between the two types of flow on the basis of the shape of the disturbed temperature profile.

To characterize adequately the heat flow in this region, we require several holes to depths of several hundred meters, preferably drilled in granitic rocks, and with the annulus between access casing and borehole wall completely sealed off by grout or a similar medium.

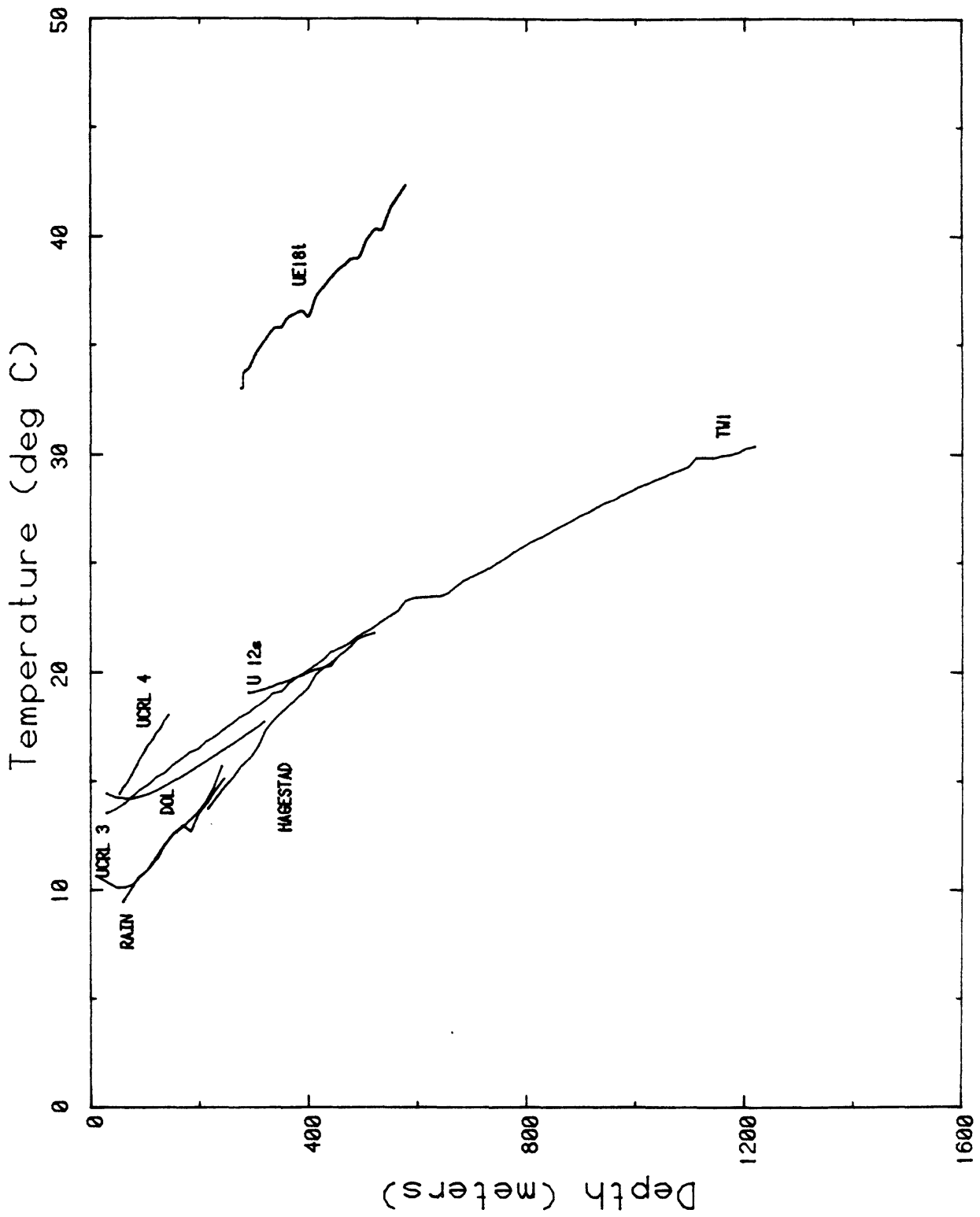


Figure 5. Composite Temperature Profile for Rainier Mesa & Environs.

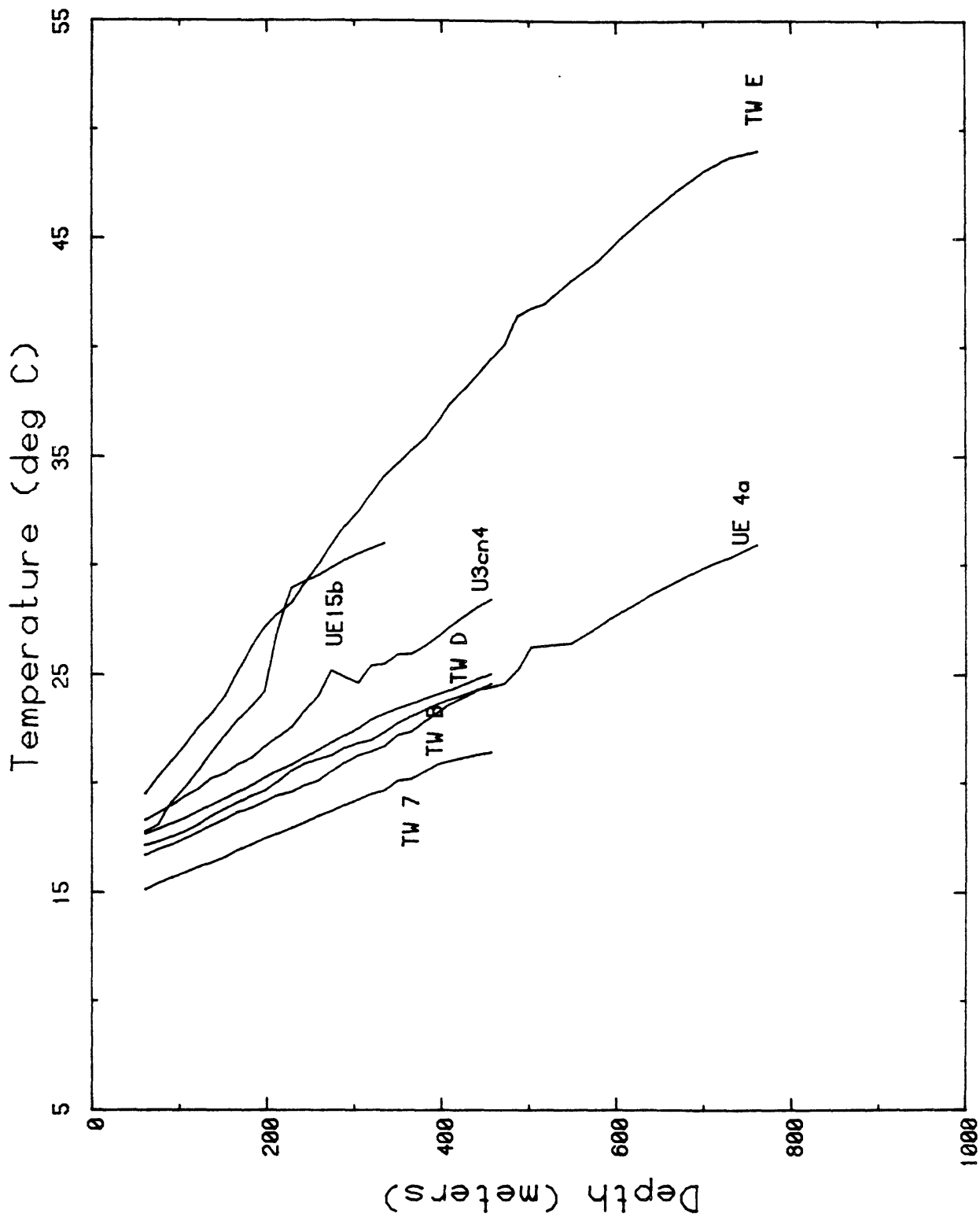


Figure 6. Composite Temperature Profile for Yucca Flat Area

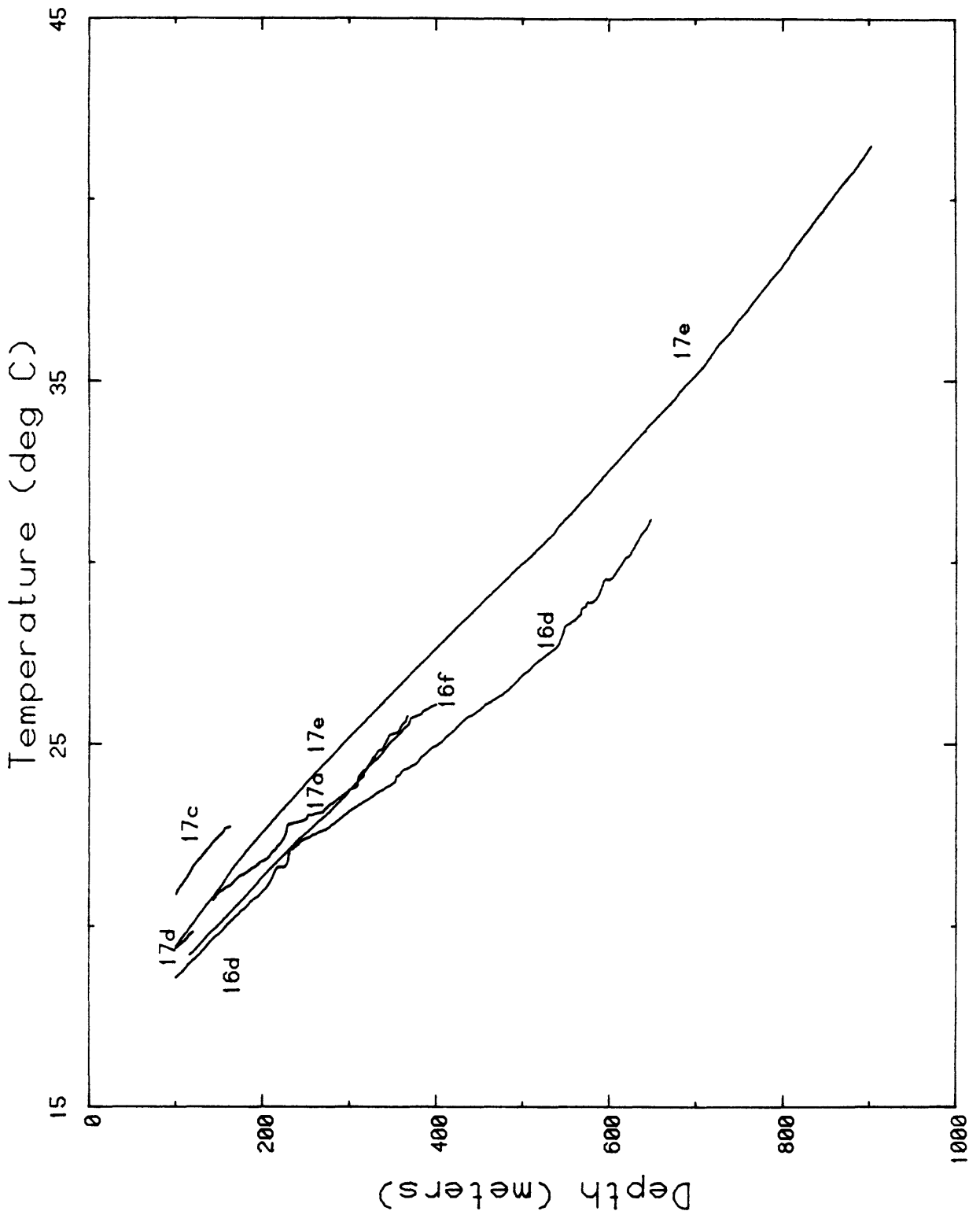


Figure 7. Composite Plot of Temperatures below 100 m, Syncline Ridge Area

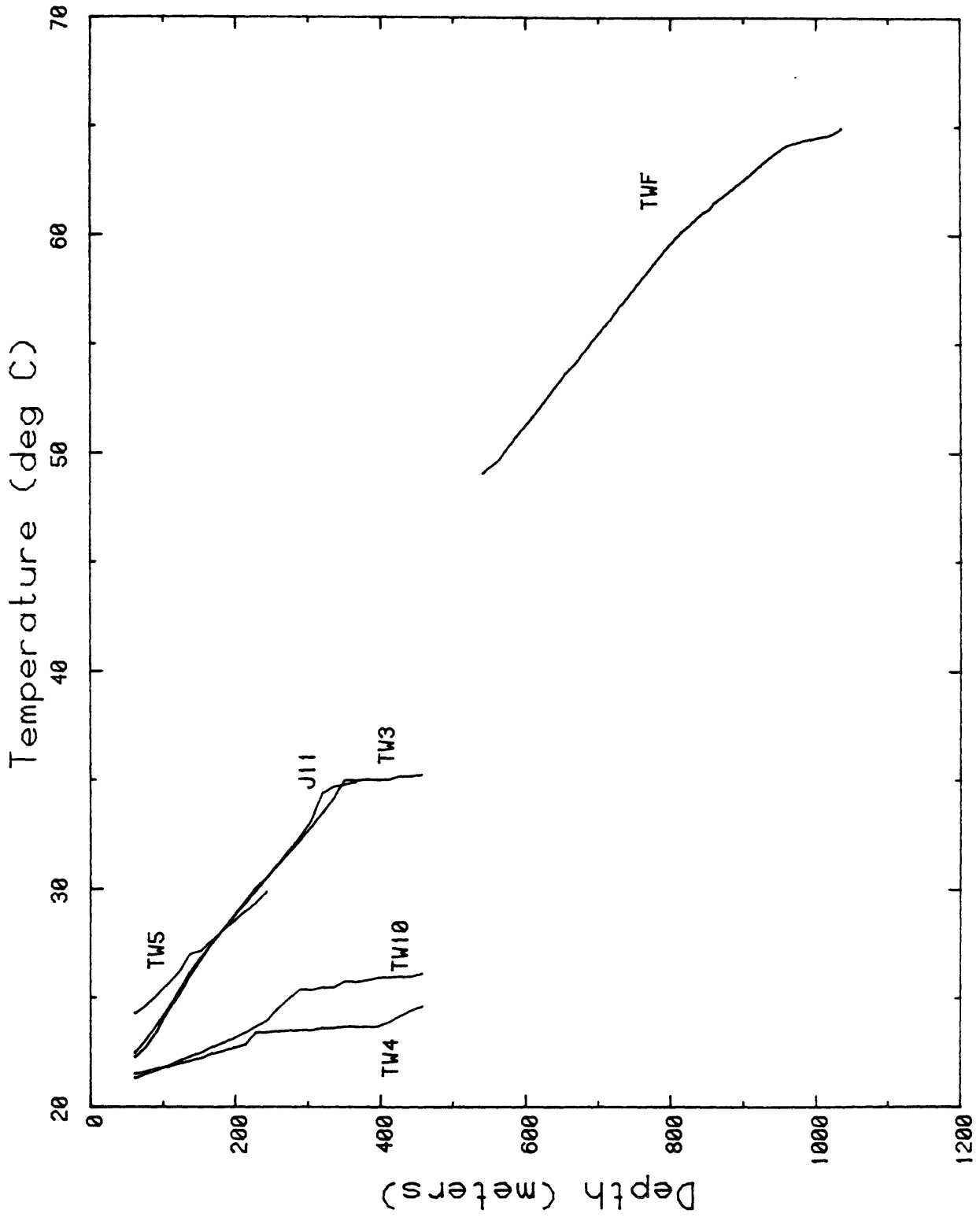


Figure 8. Composite Temperature Profile for the Southern NTS.

THERMAL REGIME OF YUCCA MOUNTAIN

Locations of wells drilled specifically to study the repository site being investigated at Yucca Mountain are shown in figure 9. The most recent temperature profiles from these wells (and some nearby wells, fig. 2) are presented in figures 10 and 11. The hydraulic potentiometric surface beneath Yucca Mountain is deeper than 500 meters. The curves show variations in thermal gradients to about 1,000 m. Thus, hydrologic disturbances to the temperature field may occur both above and below the water table. Some of the extreme variations in thermal gradient above the water table might be explained in terms of two-phase water flow, with the ratio of liquid to vapor varying as a function of depth (see Lachenbruch, 1981). At present, this seems to be the most reasonable physical explanation for the types of variations, both lateral and vertical, in temperature gradients observed in the "conductor holes" (UE25a4, 5, 6, and 7, fig. 9), a closely grouped series of holes drilled entirely within the unsaturated zone. Some, but by no means all, of the variations in gradient for this series (fig. 11) may be explained by long-lived transients resulting from the loss of large quantities of mud during drilling. The holes are, however, effectively in thermal equilibrium, and the gradient variations cannot be ascribed plausibly to variations in thermal conductivity (particularly where there are temperature reversals).

For the deepest wells (G1 and H1, fig. 10), systematic variations in temperature gradient occur without corresponding variations in thermal conductivity. Our preliminary interpretation suggested a systematic downward percolation of ground water through both unsaturated and saturated zones with seepage velocities of a few mm/y. With sufficient thermal conductivity data now available, we are able to test that interpretation quantitatively.

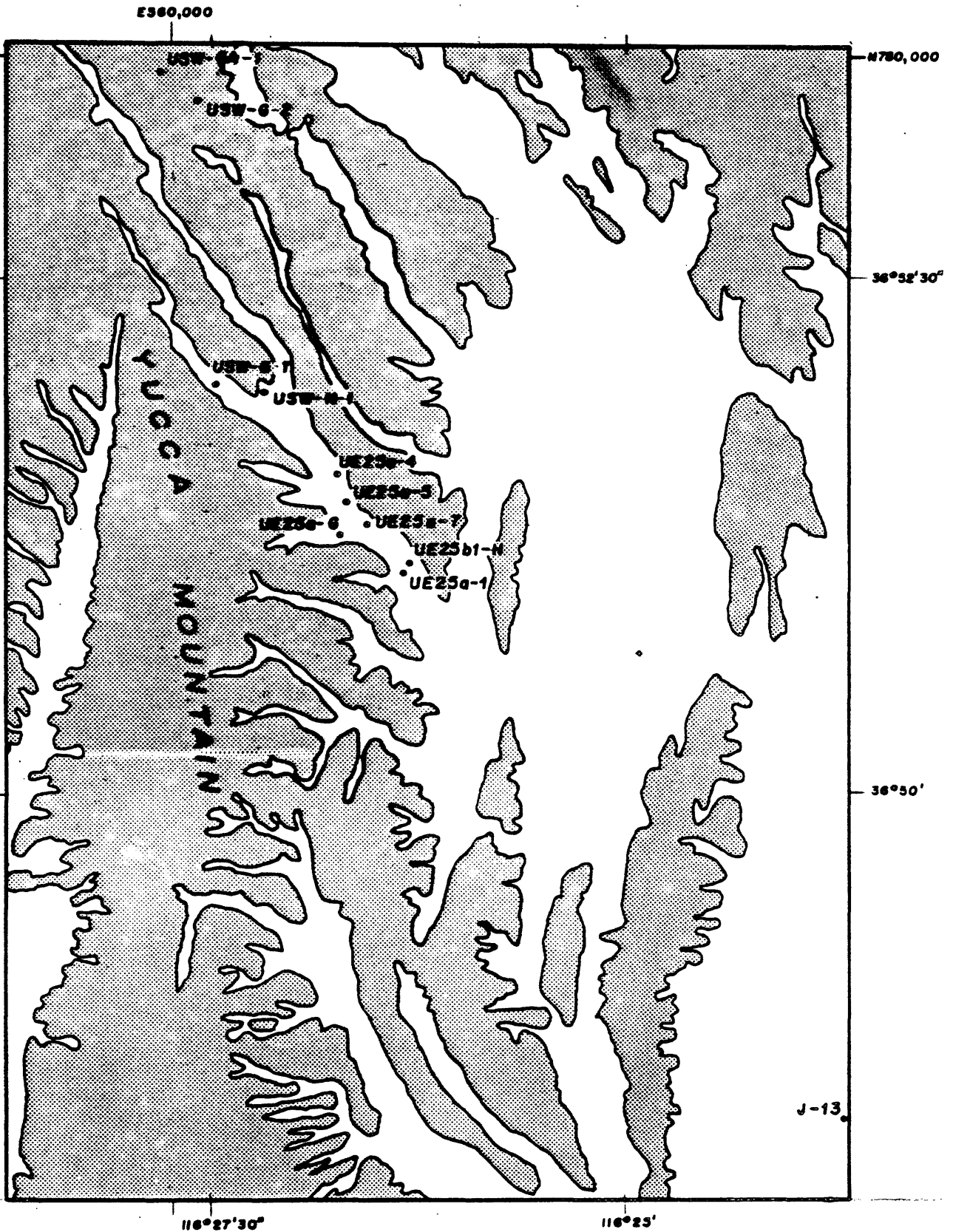


Figure 9. Locations of drill holes near Yucca Mountain.

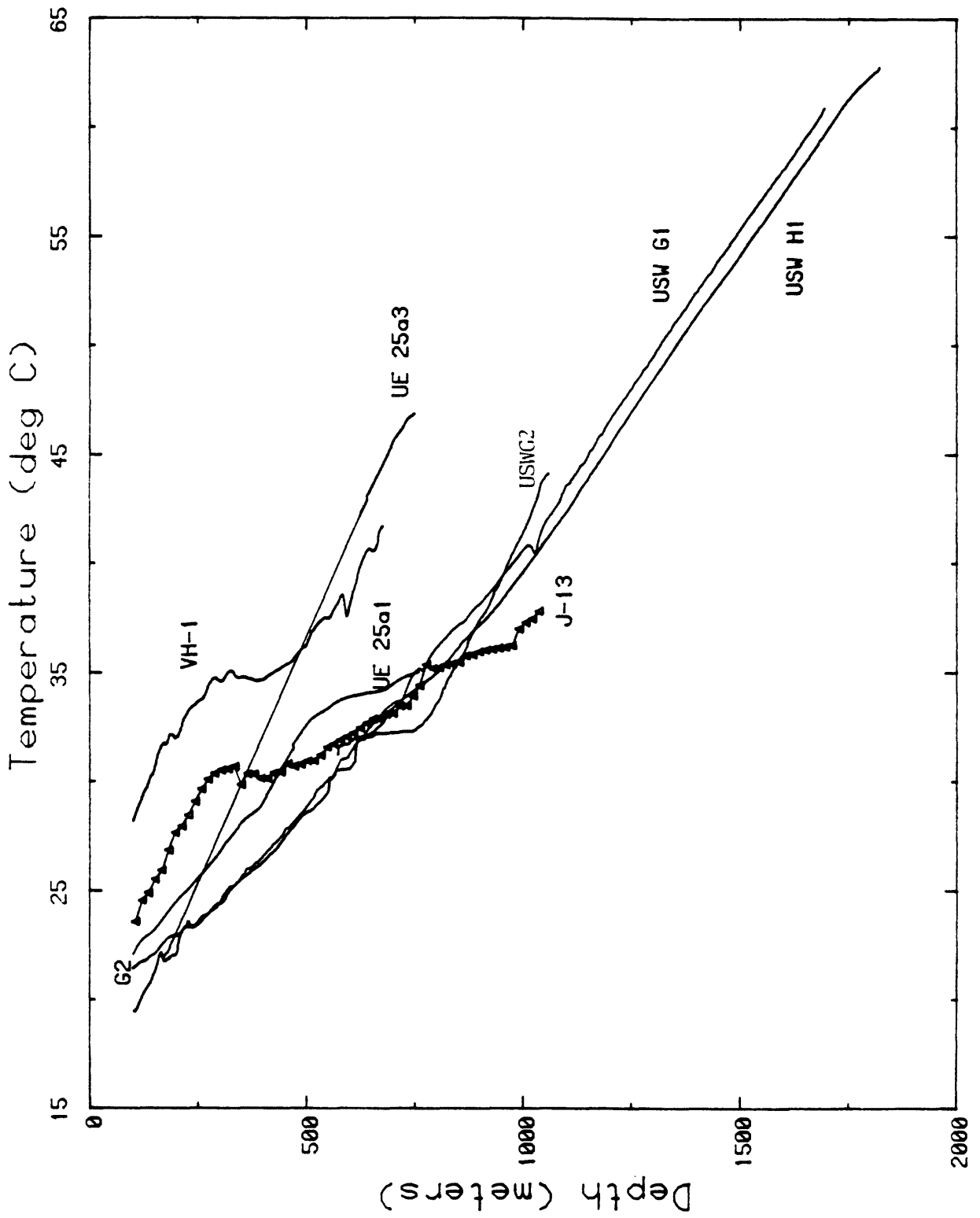


Figure 10. Temperatures in Wells deeper than 600 m, Yucca Mountain

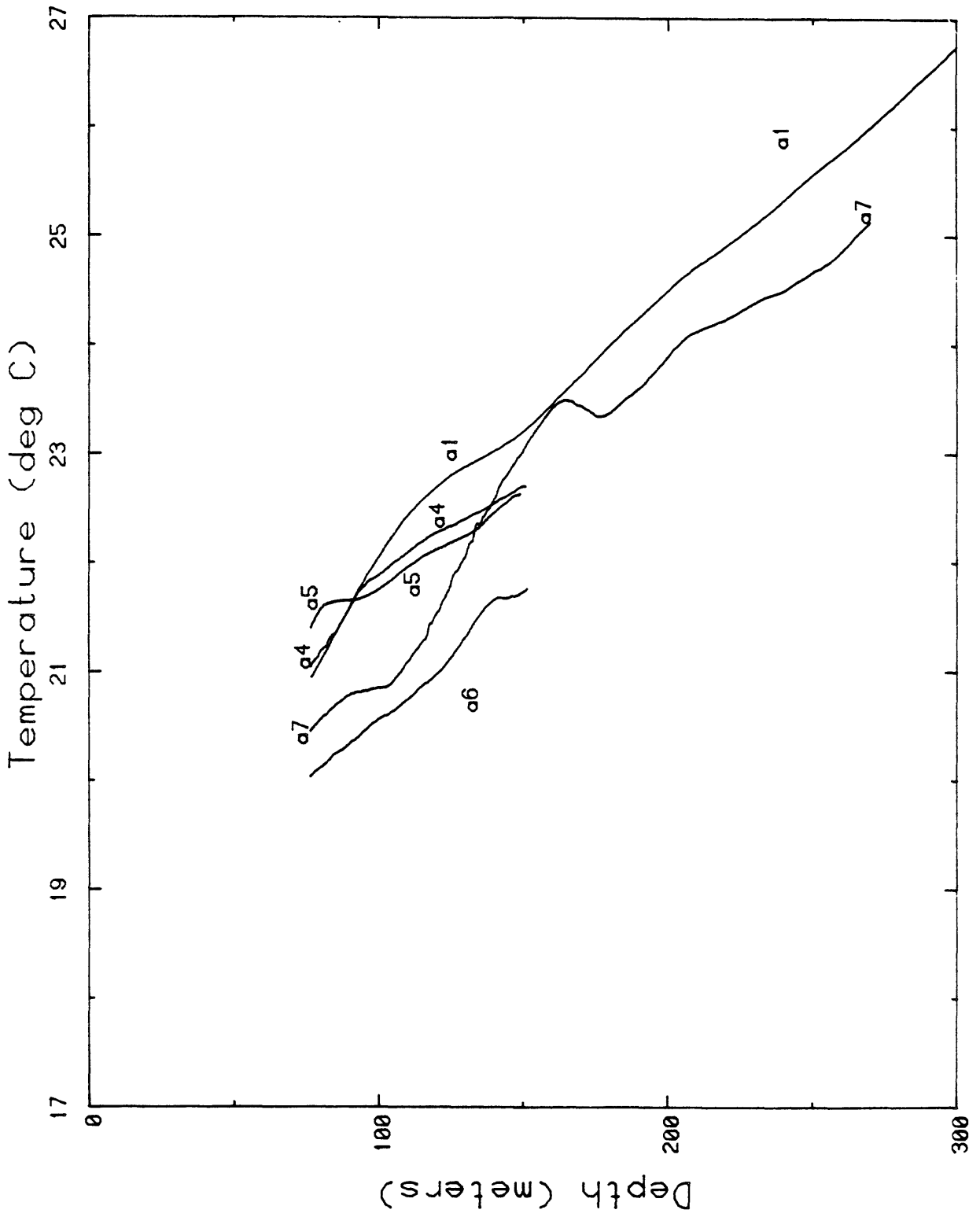


Figure 11. Temperatures from UE25a1 & the "conductor holes", Yucca Mtn.

Temperature gradients within individual formations were combined with thermal conductivity determinations by Lappin and others (1982) (above ~900 m) and our own measurements (below ~900 m) to obtain component conductive heat flows for each formation (table 2). The six interval heat flows increase systematically with depth, lending support to our preliminary interpretation. If we assume that one-dimensional steady-state vertical water flow is responsible for the observed increase in heat flow with depth and that the material is saturated, we may perform a simple calculation to estimate the seepage velocity and penetration depth of the vertical water flow.

For the idealized conditions assumed, conservation of mass and energy requires that the temperature θ be related to the vertical volumetric flow rate of interstitial water V by the differential equation (see e.g., Lachenbruch and Sass, 1977)

$$\frac{d}{dz} k \frac{d\theta}{dz} = -\rho' c' V \frac{d\theta}{dz} \quad (1)$$

where z is depth and V is taken positive for upward flow. Density and specific heat at constant pressure for the water are represented by ρ' and c' , respectively; k is thermal conductivity of the saturated aggregate. Their values are approximately

$$\rho' c' = 1 \text{ cal/cm}^3 \text{ }^\circ\text{C} = 4.2 \times 10^6 \text{ J/m}^3\text{K} \quad (2a)$$

$$k = 4.3 \text{ mcal/cm sec } ^\circ\text{C} = 1.8 \text{ W/m K} \quad (2b)$$

The vertical conductive heat flow q (positive upward) is defined by

$$q = k \frac{d\theta}{dz} \quad (3)$$

Combining (1) and (3) yields a relation between vertical heat flow and volumetric flow velocity V (e.g., cm^3 of water per cm^2 of cross sectional area

TABLE 2. Heat-flow determinations, USWGI

Depth interval m	Formation	Γ^* $^{\circ}\text{C km}^{-1}$	SE	N^{\dagger}	$\langle K \rangle^{\ddagger\dagger}$ $\text{Wm}^{-1} \text{K}^{-1}$	SD	SE	Heat flow mWm^{-2} HFU
91- 427	Paintbrush tuffs	16.32	0.08	0**	1.58	.30	.10	26±2 0.62
427- 549	Calico Hills tuffs	21.51	0.27	16**	1.31	0.11	0.03	28±1 0.67
610-1006	Crater Flat tuffs	23.01	0.08	27	1.65	0.28	0.05	38±1 0.91
1067-1204	Flow Breccia	31.16	0.19	4	1.65	0.26	0.13	51±4 1.23
1219-1524	Lithic-rich tuffs	29.04	0.03	10	1.81	0.13	0.04	53±1 1.26
1524-1697	Older tuffs	28.09	0.09	11	1.93	0.13	0.04	54±1 1.30

* Γ = least-squares temperature gradient \pm Standard Error (SE).

$\dagger N$ = number of samples measured.

**These are estimates from Tables 9 and 10 of Lappin and others (1982).

$\ddagger\dagger$ Harmonic mean thermal conductivity \pm Standard deviation (SD) and Standard Error (SE) over the least-squares interval.

of aggregate per unit time)

$$\frac{dq}{dz} = -Aq \quad (4)$$

where

$$A = \frac{\rho' c' V}{k} \quad (5)$$

According to (4), the conducted heat flow at the surface q_0 , is related to the conducted heat flow $q(z)$ at depth z by

$$q(z) = q_0 e^{-\bar{A}z} \quad (6)$$

where

$$\bar{A} = \frac{1}{z} \int_0^z A dz \quad (7)$$

Thus \bar{A} is a representative value of A in the depth range $[0, z]$.

To obtain an order of magnitude estimate of \bar{A} (and hence V , equation 5), we neglect its variation with depth and fit a curve of form (6) to heat flows $q(z)$ determined over a number of depth intervals in the hole. The interval heat flows were plotted as a function of the depth of the mid-point of the interval (fig. 12) and a least-squares regression curve (also shown in the figure) was calculated. The parameters of equation 6 obtained from the regression analysis are:

$$q_0 = 0.53 \text{ HFU} = 22.4 \text{ mW/m} \quad (8)$$

$$\bar{A} = -6.12 \times 10^{-4} \text{ m}^{-1} \quad (9)$$

The correlation coefficient is 0.95, and the maximum departures from the least-squares line are about $\pm 5 \text{ mW/m}^2$ which we consider reasonable in view of the idealized nature of the model and likely sources of measurement error.

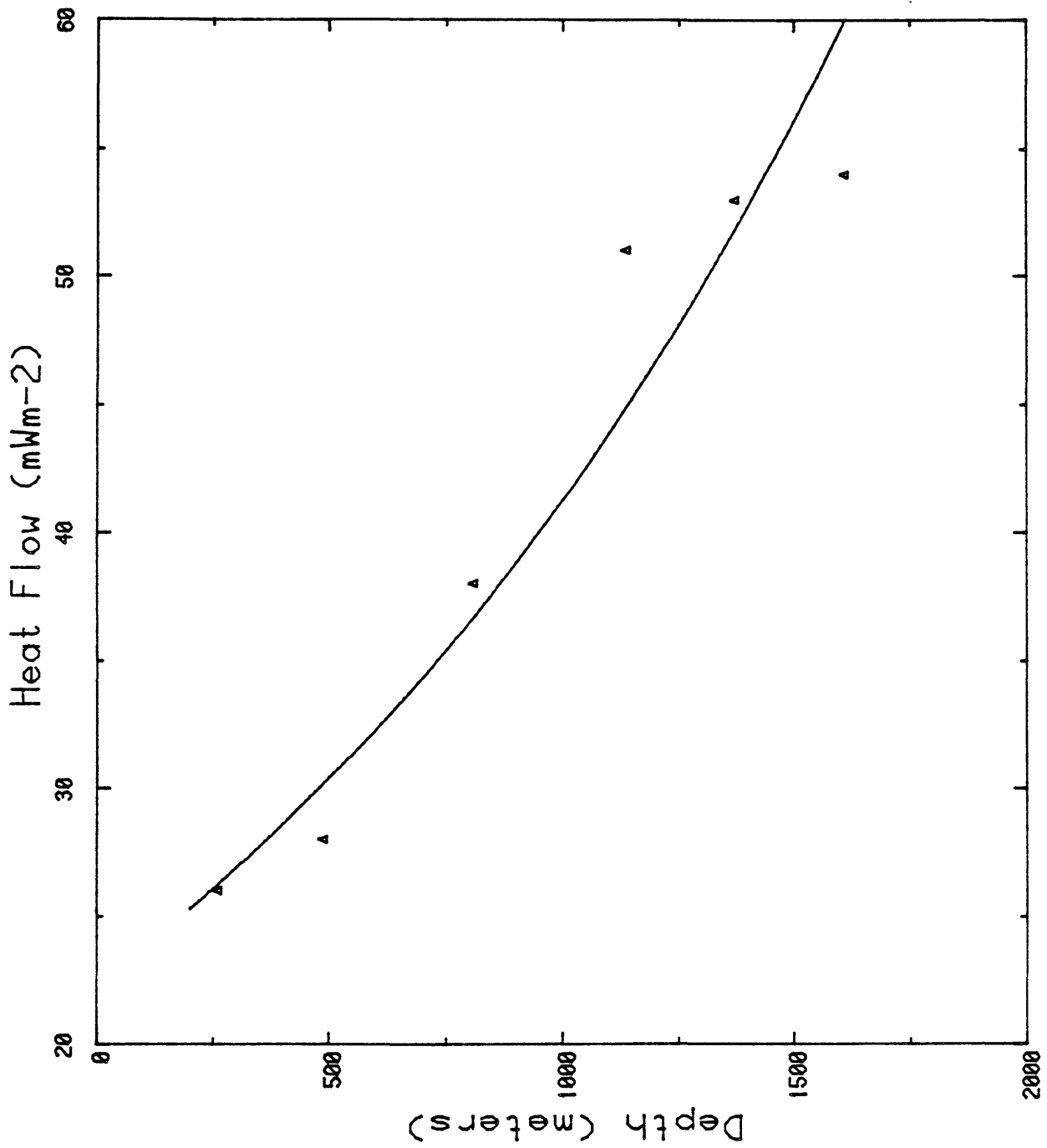


Figure 12. Interval heat flows (from Table 2) as a function of the depth of the midpoint of the interval. The least-squares regression line is $q = 22.4 \exp 0.12 \times 10^{-4} z$.

Combining equations 2, 5, and 9 yields an estimate of the vertical seepage velocity

$$V = \frac{-k}{\rho' c'} \bar{A} \quad (10a)$$

$$= 2.6 \times 10^{-10} \text{ m/s} = 8 \text{ mm/y} \quad (10b)$$

The average particle velocity of the pore water is obtained from V by dividing by the porosity; i.e., it would be 40 mm/yr (40 m/1000 yrs) for a porosity of 20% (10b).

If we assume that this simple flow pattern persists to some depth z^* , beneath which the heat flow is equal to the regional value $q(z^*)$, we can estimate the depth of vertical flow from equations 6, 8, and 9

$$z^* = \frac{-1}{\bar{A}} \ln \frac{q(z^*)}{q_0} \quad (11a)$$

$$\cong 2 \text{ km} \quad \text{if } q(z^*) \cong 80 \text{ mW/m} \sim 2 \text{ HFU} \quad (11b)$$

$$\cong 2.5 \text{ km} \quad \text{if } q(z^*) \cong 100 \text{ mW/m} \sim 2.5 \text{ HFU} \quad (11c)$$

Although this model represents a gross idealization, it leads to numerical values for vertical seepage velocity (10b) and circulation depth (11b and c) that are reasonable in order of magnitude and consistent with other information.

SUMMARY

From thermal measurements in about 60 wells, it appears that over much of the Nevada Test Site, including the Yucca Mountain site, the steady-state, conductive thermal regime has been altered significantly to depths as great as 2 to 3 km by water movement having a vertical component of seepage velocity of several meters per millenium. Regionally, the predominant vertical flow in this depth range is downward, but local upwellings exist. The measurements suggest 2- or 3-dimensional flow which in turn suggests that lateral movement of ground water must also be involved; however, the thermal measurements provide no measure of lateral velocities. In summarizing these results, we emphasize that of all the holes we have studied at NTS, only Ue17e was completed in the manner required for a confident analysis of the thermal effects of natural ground-water flow. In the other holes, the annulus was not blocked with grout, and uncertainties persist regarding possible complications of local vertical flow within the annulus behind the well casing.

In the Yucca Mountain area itself, measurements in wells deeper than 1 km suggest a downward water movement with seepage velocity on the order of 1-10 mm/y.

References

Lachenbruch, A. H., 1981, Temperature effects of varying phase composition during the steady vertical flow of moisture in unsaturated stratified sediments: U.S. Geological Survey Open-File Report 81-1220, 11 p.

Lachenbruch, A. H., and Sass, J. H., 1977, Heat flow in the United States and the thermal regime of the crust, in Heacock, J. H., ed., The Earth's Crust: American Geophysical Union Geophysical Monograph 20, American Geophysical Union, Washington, D. C., p. 626-675.

Lappin, A. R., Van Buskirk, R. G., Enniss, D. O., Butters, S. W., Prater, F. M., Muller, C. S., and Bergosh, J. L., 1982, Thermal conductivity, bulk properties, and thermal stratigraphy of silicic tuffs from the upper portion of hole USW-G1, Yucca Mountain, Nye County, Nevada: Sandia National Laboratories Report SAND 81-1873.

Sass, J. H., Blackwell, D. D. Chapman, D. S., Costain, J. K., Decker, E. R., Lawver, L. A., and Swanberg, C. A., 1981, Heat flow from the crust of the United States, in Touloukian, Y. S., Judd, W. R., and Roy, R. F., eds., Physical Properties of Rocks and Minerals: McGraw-Hill Book Company, p. 503-548.

Sass, J. H., Lachenbruch, A. H., and Mase, C. W., 1980, Analysis of thermal data from drill holes UE25a-3 and UE25a-1, Calico Hills and Yucca Mountain, Nevada Test Site: U.S. Geological Survey Open-File Report 80-826, 25 p.

Sass, J. H., Lachenbruch, A. H., Munroe, R. J., Greene, G. W., and Moses, T. H., Jr., 1971, Heat flow in the western United States: Journal of Geophysical Research, v. 76, p. 6376-6413.

Swanberg, C. A., and Morgan, P., 1978, The linear relation between temperature based on the silica content of groundwater and regional heat flow: A new heat flow map of the United States: Pure and Applied Geophysics, v. 117, p. 227-241.

Winograd, I. J., and Thordarson, W., 1975, Hydrogeologic and hydrochemical framework, South-Central Great Basin, Nevada-California, with special reference to the Nevada Test Site: U.S. Geological Survey Professional Paper 712-C, 126 p.

APPENDIX A-1.

Thermal conductivity, density, and apparent porosity of tuffs
from USWG1 (measured at ~25°C)

TABLE A-1. Thermal conductivity, density, and apparent porosity of tuffs from USWGI (measured at ~25°C)

Depth, m	Formation	Lithology	K Wm ⁻¹ K ⁻¹	ρ^{\dagger} gm cm ⁻³	ϕ^{\ddagger} %
868.1	TcfT	Moderately welded tuff	1.80	2.20	22.2
892.8	TcfT	Moderately welded tuff	1.94	2.34	15.3
892.9	TcfT	Moderately welded tuff	1.87	2.36	15.7
899.8	TcfT	Moderately welded tuff	1.87	2.37	13.7
930.2	TcfT	Moderately welded tuff	1.42	2.11	22.4
940.4	TcfT	Moderately welded tuff	1.54	2.13	20.4
967.3	TcfT	Zeolitized partially welded tuff	1.62	2.29	16.6
983.6	TcfT	Zeolitized non-welded tuff	1.67	NM	NM
1013.8	TcfT	Vitrophyre	1.67	2.29	18.2
1044.5	TcfT	Vitrophyre	2.00	NM	NM
1065.6	TcfT	Vitrophyre	1.80	2.34	15.6
1091.6	Tfb	Flow Breccia	1.86	2.44	12.1
1123.4	Tfb	Flow Breccia	1.43	2.34	14.5
1157.9	Tfb	Flow Breccia	1.95	2.55	3.2
1187.9	Tfb	Flow Breccia	1.49	2.34	12.5
1219.4	Trt	Zeolitized partially welded tuff	1.65	2.19	15.7
1253.6	Trt	Zeolitized partially welded tuff	1.80	2.25	13.6
1280.1	Trt	Zeolitized partially welded tuff	1.88	2.16	16.5
1319.9	Trt	Zeolitized partially welded tuff	1.72	2.24	16.7
1349.2	TrT	Zeolitized partially welded tuff	1.77	2.23	15.4
1389.4	TrT	Zeolitized partially welded tuff	1.86	2.32	14.5
1419.3	TrT	Zeolitized partially welded tuff	1.75	2.27	16.8
1450.7	TrT	Zeolitized partially welded tuff	1.96	2.37	11.0
1477.5	TrT	Zeolitized non-welded tuff	2.10	NM	NM

TABLE A-1. Thermal conductivity, density, and apparent porosity of tuffs from USWGI (measured at ~25°C)--continued

Depth, m	Formation	Lithology	K Wm ⁻¹ K ⁻¹	ρ [†] gm cm ⁻³	φ ^{††} %
1511.6	TrT	Zeolitized non-welded tuff	1.68	NM	NM
1540.0	TtA	Silicic tuff densely welded	1.98	2.30	12.4
1573.0	TtA	Silicic tuff densely welded	1.98	2.28	14.0
1600.0	TtA	Zeolitized tuff densely welded	2.15	2.30	14.8
1632.6	TtB	Zeolitized tuff bedded	2.12	2.35	11.3
1675.7	TtC	Zeolitized non-welded tuff	1.70	NM	NM
1716.9	TtC	Zeolitized tuff densely welded	1.94	2.39	11.2
1747.7	TtC	Devitrified moderately welded tuff	1.91	2.46	9.2
1754.5	TtC	Devitrified moderately welded tuff	1.85	2.43	11.0
1783.3	TtC	Devitrified moderately welded tuff	1.97	2.47	8.6
1813.8	TtC	Silicified moderately welded tuff	1.89	2.49	5.8
1814.0	TtC	Silicified moderately welded tuff	1.86	2.31	13.6

*TcFT, tram unit, Crater Flat tuff

Tfb, Flow Breccia

TrT, Lithic-rich tuff

Tt, older ash-flow and bedded tuff, units A, B, and C

† Saturated density NM, not measured (because of disintegration of specimen).

†† Apparent porosity = $\frac{\text{saturated weight} - \text{dry weight}}{\text{saturated weight}}$ NM, not measured.

UNITED STATES DEPARTMENT OF THE INTERIOR
GEOLOGICAL SURVEY

Temperature, thermal conductivity, and heat flow near Yucca Mountain, Nevada:
Some tectonic and hydrologic implications

by

J. H. Sass¹, A. H. Lachenbruch², W. W. Dudley, Jr.³,
S. S. Priest¹, and R. J. Munroe²

Open File Report 87-649

Prepared in cooperation with the
Nevada Operations Office
U.S. Department of Energy
(Interagency Agreement DE-AI08-78ET44802)

This report is preliminary and has not been reviewed for conformity with U.S. Geological Survey editorial standards and stratigraphic nomenclature. Any use of trade names and trademarks is for descriptive purposes only and does not constitute endorsement by the U.S. Geological Survey.

¹U.S. Geological Survey, Flagstaff, AZ 86001

²U.S. Geological Survey, Menlo Park, CA 94025

³U.S. Geological Survey, Denver, CO 80225

1988

SE ROA 38157

JA_9439

CONTENTS

	<u>page</u>
Abstract	2
Introduction	5
Symbols and Units	7
Temperatures	8
Thermal Conductivity	25
Heat Flow	31
References	50
Appendix 1. Temperature logs from geologic and hydrologic test wells, Yucca Mountain	54
Appendix 2. Temperature measurements in air in the unsaturated zone	83
Appendix 3. Thermal conductivities	106

List of Tables

	<u>page</u>
Table 1. Location, elevation and static water level (SWL) for geologic and hydrologic test wells near Yucca Mountain, Nevada	9
Table 2. Location, elevation and static water level (SWL) for test well UZ-1 and the WT series	10
Table 3. Average thermal conductivities for various tuff units of Yucca Mountain and for Paleozoic rocks from UE-25p1	26
Table 4. Linear regression of thermal conductivity (K , $\text{Wm}^{-1} \text{K}^{-1}$) on compressional wave velocity (V_p , km s^{-1}) for G series wells, Yucca Mountain, Nevada	29
Table 5. Heat-flow estimates from test wells near Yucca Mountain, Nevada	36
Table 6. Heat-flow estimates (\pm SE) from the unsaturated zone in UZ-1 and WT series wells based on average formation conductivities	38

List of Illustrations

	<u>page</u>
Fig. 1	Map of Yucca Mountain and vicinity with selected test well locations 11
Fig. 2	Map showing locations of wells studied 12
Fig. 3	Test wells near Yucca Mountain 13
Fig. 4	Thermal profile, J13-G2 14
Fig. 5	Thermal profile, J13-G4 15
Fig. 6	Thermal profile, H4-G2 16
Fig. 7	Thermal profile, G3-H5 17
Fig. 8	Thermal profile, H6-B1H 18
Fig. 9	Temperature profile, heat-flow calculations above the water table and a one-dimensional model calculation for well USW G-4 22
Fig. 10	Temperature profiles from WT series wells 23
Fig. 11	Histograms of thermal conductivity of tuffs 27
Fig. 12	Thermal conductivity as a function of compressional wave velocity for tuffs from coreholes 30
Fig. 13	Distribution of heat flow in the western United States 32
Fig. 14	Configuration of 63 mW m^{-2} contour in the vicinity of the Nevada Test Site 33
Fig. 15	Conductive heat flow from the unsaturated zone in the vicinity of Yucca Mountain 40
Fig. 16	Heat flow from the unsaturated zone as a function of the thickness of the zone 41
Fig. 17	Comparison of heat-flow estimates for the unsaturated zone with those for the saturated zone using the least-squares gradients and gradients of linear segments 43
Fig. 18	Stratigraphic relationships among hydrostratigraphic units near Yucca Mountain 45

Abstract

Repeated temperature logs were obtained in 18 geologic and hydrologic test wells near Yucca Mountain, Nevada. Single logs were also obtained (using a specially designed sonde with fast response in air) in the air column of 17 wells drilled to monitor water level below and around Yucca Mountain. The temperature data suggest that the thermal regimes of both the saturated and unsaturated zones are strongly influenced by a complex hydrologic regime in the saturated tuffs and underlying Paleozoic carbonate rocks. Temperature gradients in the unsaturated zone (UZ) appear primarily conductive, but they range from about $15^{\circ}\text{C km}^{-1}$ to nearly $60^{\circ}\text{C km}^{-1}$. However, one profile indicates rapid penetration to a depth of 150 m beneath a major channel by water from run-off following a local heavy rain. From the water table (which ranges in depth from about 300 m to over 700 m) to depths of 1 km or more, the temperature gradient in the saturated zone (SZ) typically is very irregular with evidence for locally controlled water movement in the Tertiary volcanic rocks, laterally and both up and down vertically. Vertical seepage velocities inferred from one-dimensional hydrologic models range from a few millimeters to 100 millimeters or more per year. Below depths of 1 km, temperature profiles are linear, suggesting conductive heat flow, but as in the case of the UZ, the gradients are quite variable, suggesting that the heat flux here is being controlled by fluid flow in the Paleozoic carbonate aquifer that underlies Yucca Mountain.

Measurements of thermal conductivity were performed (at room temperature) on 204 carefully preserved specimens of core, mostly from the volcanic rocks. Fifty-seven conductivities from the UZ are bimodally distributed (the modes of 1.0 and $2.1 \text{ Wm}^{-1} \text{ K}^{-1}$ represent nonwelded and welded tuffs, respectively) with a mean of $1.66 \pm 0.06 \text{ Wm}^{-1} \text{ K}^{-1}$.

Conductivities of 134 specimens of tuffs from the SZ are normally distributed with a mean of $1.72 \pm 0.03 \text{ Wm}^{-1} \text{ K}^{-1}$. Variations in conductivity are due primarily to variations in porosity, which is negatively correlated with degree of welding. By contrast, 13 conductivities from the Paleozoic carbonate aquifer average nearly $5.0 \text{ Wm}^{-1} \text{ K}^{-1}$. Conductivities from the SZ correlate well ($R = 0.78$) with compressional wave velocity.

Thermal conductivities were combined with individual thermal gradients for both the UZ and SZ to provide estimates of heat flow. Heat flows from the SZ are variable both laterally and vertically, particularly in the upper 1 km, and apparently are affected both by flow in the annulus between casing and borehole wall and in the adjacent formation. The average conductive heat flow from the SZ at Yucca Mountain, calculated from nine wells, was $40 \pm 9 \text{ mW m}^{-2}$ using least-squares gradients for the entire SZ intervals, including hydrologically disturbed segments, and $49 \pm 8 \text{ mW m}^{-2}$ using short, linear segments of the thermal profiles. The anomaly with respect to the regional heat flow ($\sim 85 \text{ mW m}^{-2}$) is attributed principally to lateral flow with a downward component beneath the depth of exploration, probably in the Paleozoic carbonate aquifer; however, the downward flow required to recharge the carbonate aquifer need not occur at Yucca Mountain and, in fact, is not evident there from the limited hydrologic data currently available.

Heat flows in the UZ also vary but in a systematic fashion, both geographically and as a function of UZ thickness. Considering the limitations on data abundance for the SZ and on data quality, the average heat flow from the UZ ($\sim 41 \text{ mW m}^{-2}$) may be interpreted to be about the same as that from the SZ or perhaps as much as 20% lower. If heat is being removed nonconductively from the UZ, vaporization and advective removal of infiltrating water by air circulating in fractures combined with an as yet

undetermined amount of hydrologic recharge can explain the conductive heat-flow deficiency.

An unambiguous interpretation of the heat-flow field near Yucca Mountain in terms of its hydrologic implications requires data of higher quality. For the UZ, this means reconfiguring the WT series of holes so that temperatures can be measured in water-filled pipes. For the SZ, access pipes must be grouted in to total depth to ensure that all hydrologic disturbances observed are in the formation, and not merely in the annulus between casing and borehole wall.

INTRODUCTION

Among the factors to be evaluated in assessing the suitability of the Yucca Mountain area as a candidate repository for high-level nuclear waste, are the regional tectonic setting and the regional and local hydrologic regimes. Seismic and volcanic hazards are the most directly recognized tectonic factors, and these have been the subject of intense investigations (see Carr and Rogers, 1983; Crowe and others, 1983). Regional heat-flow studies are, however, an important adjunct to the more focused investigations. Regional thermal regimes can help to put contemporary seismic/volcanic activity into an historical perspective (as regards regional tectonics) and local thermal anomalies may help pinpoint magma bodies that have no contemporary surface expression.

Thermal and hydrologic regimes are closely related. In fact, both on local and regional scales, the deep thermal regime can be effectively masked or substantially altered by relatively slow movement of ground water (see Lachenbruch and Sass, 1977; Mase and others, 1982). This, in turn, makes thermal measurements sensitive indicators of fluid movement, and in some instances, allows quantitative estimates of flow velocities.

The Geothermal Studies Project, U.S. Geological Survey, has been actively engaged in thermal studies in and around the Nevada Test Site since the late 1950's (see Lachenbruch, 1958; Lachenbruch and others, 1987). The initial thrust of these studies was to provide high-quality data to define the regional heat-flow field. Hydrologic disturbances were noted in many wells, however, and data from the NTS were instrumental in defining the Eureka Low, a large thermal anomaly, most probably of hydrologic origin, within the Basin and Range province (Sass and others, 1971). Our regional studies

provided a context for a focused study of the Yucca Mountain area (Figures 1 and 2). Preliminary results (Sass and others, 1980; Sass and Lachenbruch, 1982) confirmed that the thermal regime was indeed distorted by the effects of water movement, and provided data complementary to conventional hydrologic studies (Robison, 1984; Czarnecki and Waddell, 1984; Montazer and Wilson, 1984; Waddell and others, 1984).

The present report updates our preliminary results and incorporates detailed suites of temperature logs in all available wells and of thermal conductivity measurements on carefully preserved core. Gradients from linear portions of temperature profiles were combined with the appropriate thermal conductivity data to obtain values of heat flow. These values, in turn, were used to define the local conductive thermal regime and place it in the context of regional heat flow, with some comments on the implications for local water flow.

Techniques and procedures used are described by Sass and others (1971, 1984) and are the subject of Quality Assurance procedures NWM USGS-GPP-02, RO and -GPP-05, R1 (USGS Quality Assurance Manual, 1986). Work was performed in cooperation with the U.S. Department of Energy, Interagency Agreement DE-AI08-78ET44802. We are indebted to Frederick Grubb and Thomas H. Moses, Jr., for assistance in obtaining the temperature data. Eugene P. Smith performed the thermal conductivity measurements. We thank Ken Fox, Parviz Montazer, and D. T. Snow for their helpful comments.

SYMBOLS AND UNITS (SI)

°C	=	Degrees celsius
m	=	Meter (or 10^{-3} as a prefix)
K	=	Degrees Kelvin (or symbol for thermal conductivity in context)
W	=	Watts
SE	=	Standard error
SD	=	Standard deviation
v	=	Seepage velocity $\times 10^{-13}$ m sec or mm/y
V_p	=	Compressional wave velocity km s^{-1}
a	=	"Air"; used as a subscript
w	=	"Water"; used as a subscript
s	=	Seconds
N	=	Number of samples in population
q	=	Heat flow, mWm^{-2}
K	=	Thermal conductivity $\text{Wm}^{-1} \text{K}^{-1}$
Γ	=	Temperature gradient, $^{\circ}\text{C km}^{-1}$

TEMPERATURES

Temperature profiles for all geologic and hydrologic test wells (Table 1) are plotted in Appendix 1. An additional set of temperature logs made in air in test well UZ-1 and the WT series holes (Table 2) is presented as Appendix 2. A brief discussion of the peculiarities of individual wells or groups of wells is also presented in Appendix 1. In this section, we shall look at some topographic, thermal, and hydrologic cross sections (Figure 3) within the study area in an attempt to identify and assess lateral variations in temperature.

The profiles are presented in two parts (Figures 4 through 8). An upper diagram displays all temperature profiles along the line in question plotted with common origin. The reader interested in more details of the temperature log or the thermal recovery history post-drilling of a given well is urged to look up the appropriate figure in Appendix 1. In the lower diagram (Figures 4 through 8), the wells are projected onto a topographic cross section on which is also plotted (as a dotted line) the static water level, or piezometric surface. The depth to a given temperature is indicated at 5°C intervals and every other temperature is joined by a dashed line across the section to show interpolated isothermal surfaces.

The longest cross section is that connecting J-13 in Fortymile Wash to G2, the northernmost geologic corehole (Figures 3 and 4). This section is also presented in two segments (Figures 5 and 6) to allow more detailed consideration of individual wells. The most noteworthy features of this profile are the large lateral hydraulic gradient between G2 and G1 (Figures 4 and 6) and the apparent thermal high (Figures 4 and 5) in the vicinity of UE25p1. This well was drilled into a local basement high to examine the

TABLE 1. Location, elevation and static water level (SWL) for geologic and hydrologic test wells near Yucca Mountain, Nevada

Well	Latitude	Longitude	Elevation (m)	Depth to SWL (m)
USW G-1	36° 51.8'	116° 27.5'	1326	572
USW G-2	36° 53.3'	116° 26.4'	1554	526
USW G-3	36° 50.1'	116° 28.1'	1480	751
USW G-4	36° 51.3'	116° 26.8'	1270	541
USW H-1	36° 52.0'	116° 27.2'	1302	572
USW H-3	36° 49.7'	116° 28.0'	1483	751
USW H-4	36° 50.5'	116° 26.9'	1249	519
USW H-5	36° 51.2'	116° 27.9'	1478	704
USW H-6	36° 50.8'	116° 28.7'	1302	526
UE25a4	36° 51.6'	116° 26.8'	1277	---
UE25a5	36° 51.4'	116° 26.8'	1234	---
UE25a6	36° 51.2'	116° 26.8'	1231	---
UE25a7	36° 51.3'	116° 26.6'	1219	---
UE25b1H	36° 51.1'	116° 26.4'	1200	469
UE25p1	36° 49.5'	116° 25.3'	1114	384
VH-1	36° 47.5'	116° 32.6'	954	56
VH-2	36° 48.4'	116° 34.6'	974	163
J-13	36° 48.5'	116° 23.7'	1011	282

TABLE 2. Location, elevation and static water level (SWL)
for test well UZ-1 and the WT series

Well	Latitude	Longitude	Elevation (m)	Depth to SWL (m)
UZ-1	36° 52.1'	116° 27.7'	1349	---
WT-1	36° 49.3'	116° 27.0'	1202	471
WT-2	36° 50.4'	116° 27.3'	1301	571
WT-3	36° 47.9'	116° 25.0'	1030	300
WT-4	36° 51.7'	116° 26.1'	1167	439
WT-5	36° 50.6'	116° 24.8'	1088	---
WT-6	36° 53.7'	116° 26.75'	1313	284
WT-7	36° 49.5'	116° 28.9'	1197	421
WT-10	36° 48.4'	116° 29.2'	1123	348
WT-11	36° 46.8'	116° 28.1'	1094	364
WT-12	36° 46.9'	116° 26.3'	1075	345
WT-13	36° 49.7'	116° 23.9'	1032	303
WT-14	36° 50.6'	116° 24.6'	1076	346
WT-15	36° 51.3'	116° 23.7'	1083	354
WT-16	36° 52.7'	116° 25.7'	1210	473
WT-17	36° 48.5'	116° 26.5'	1124	395
WT-18	36° 52.25'	116° 26.75'	1336	---

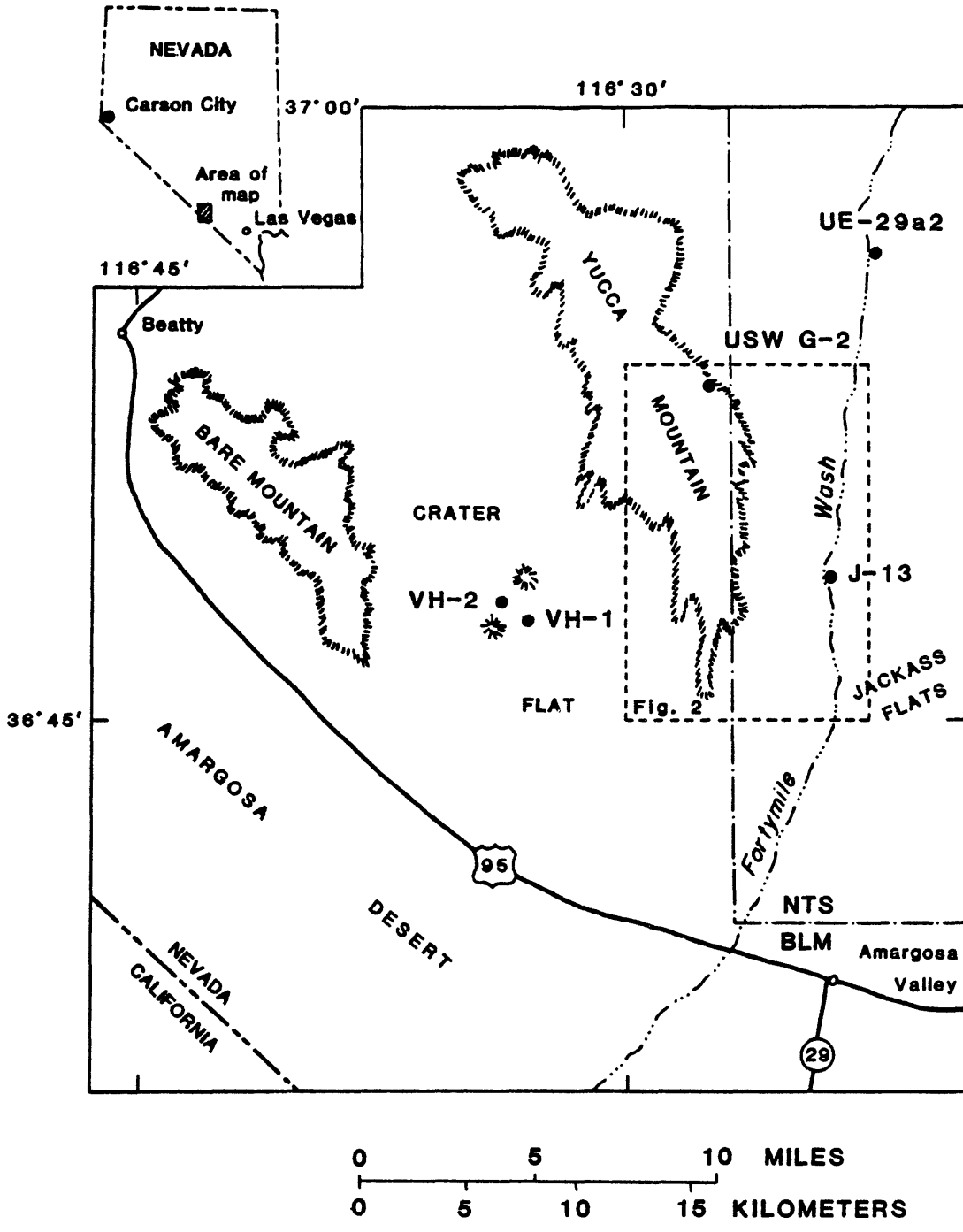


Figure 1. Map of Yucca Mountain and vicinity with selected test well locations.

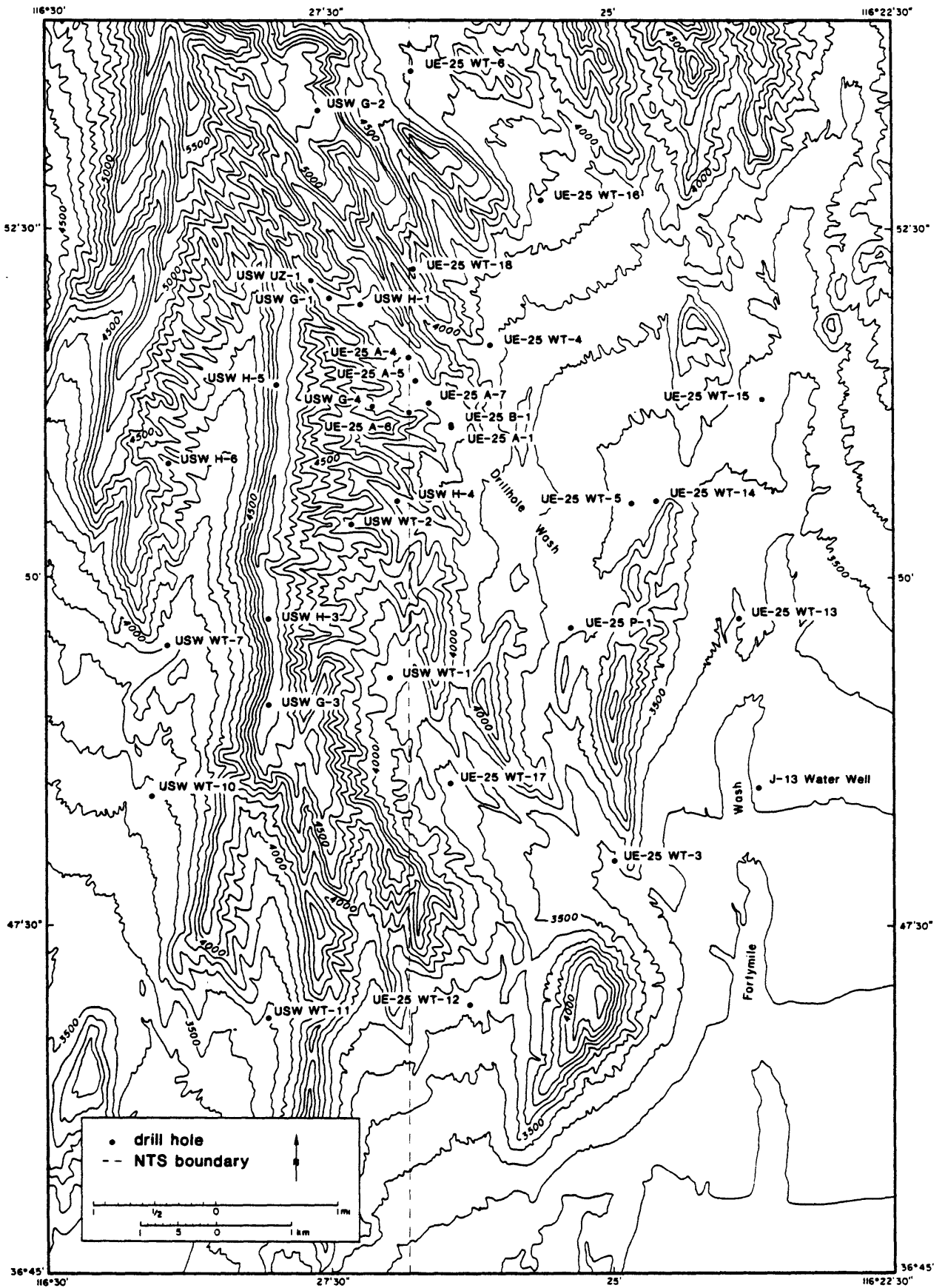


Figure 2. Map showing locations of wells studied (see index, Figure 1).
 Contour interval, 100 ft.

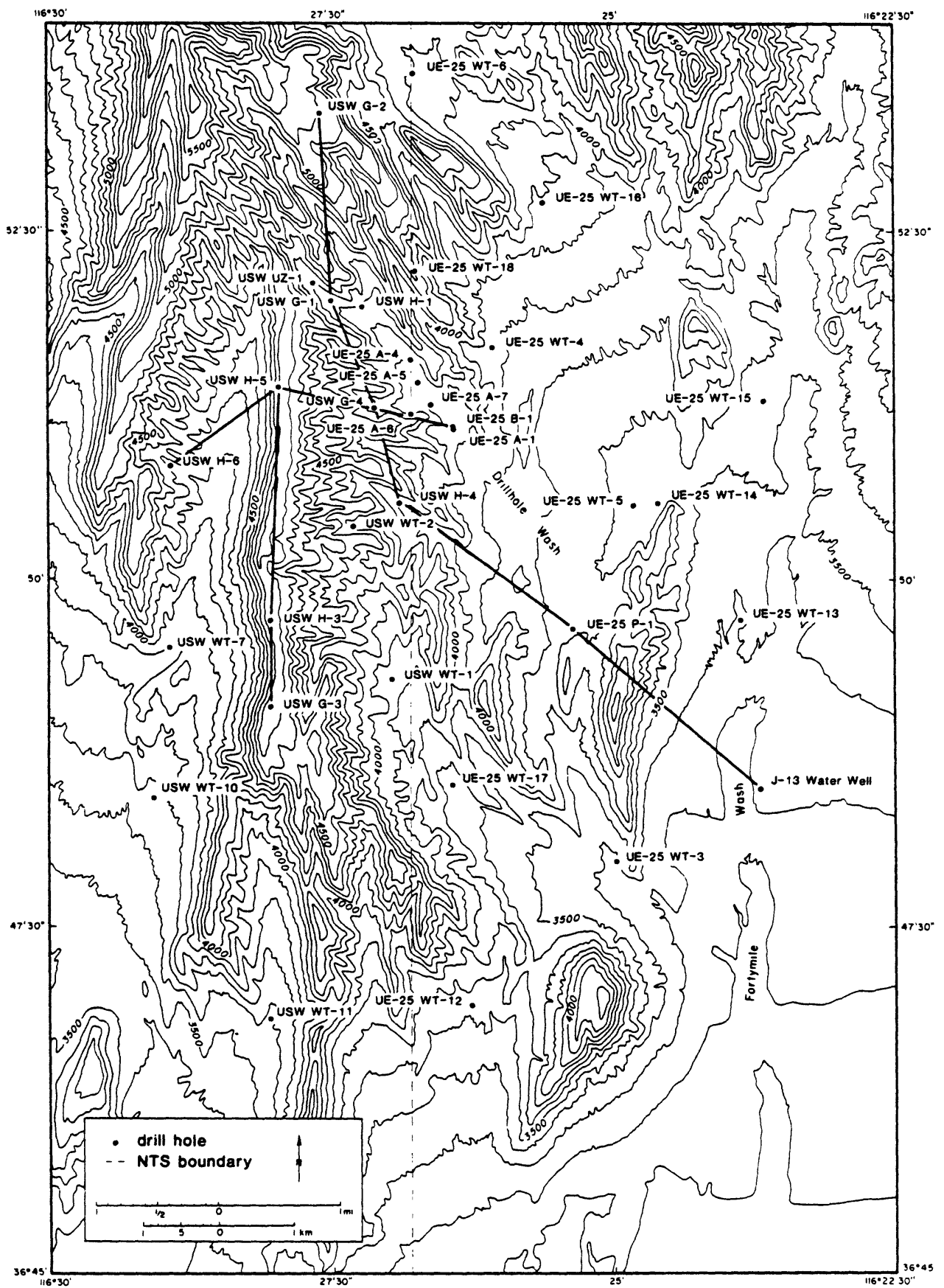


Figure 3. Test wells near Yucca Mountain. Profiles of Figures 4 through 8 are identified by solid lines.

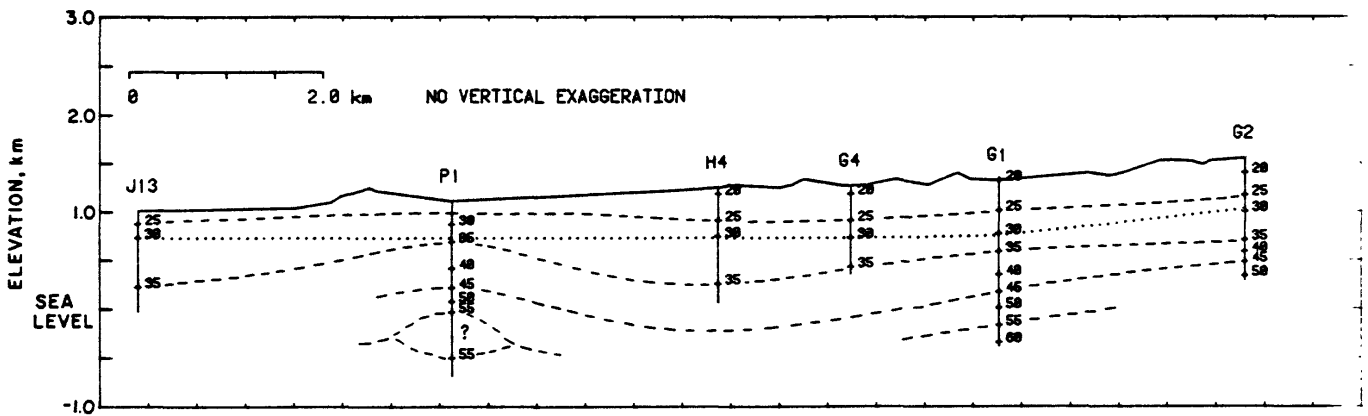
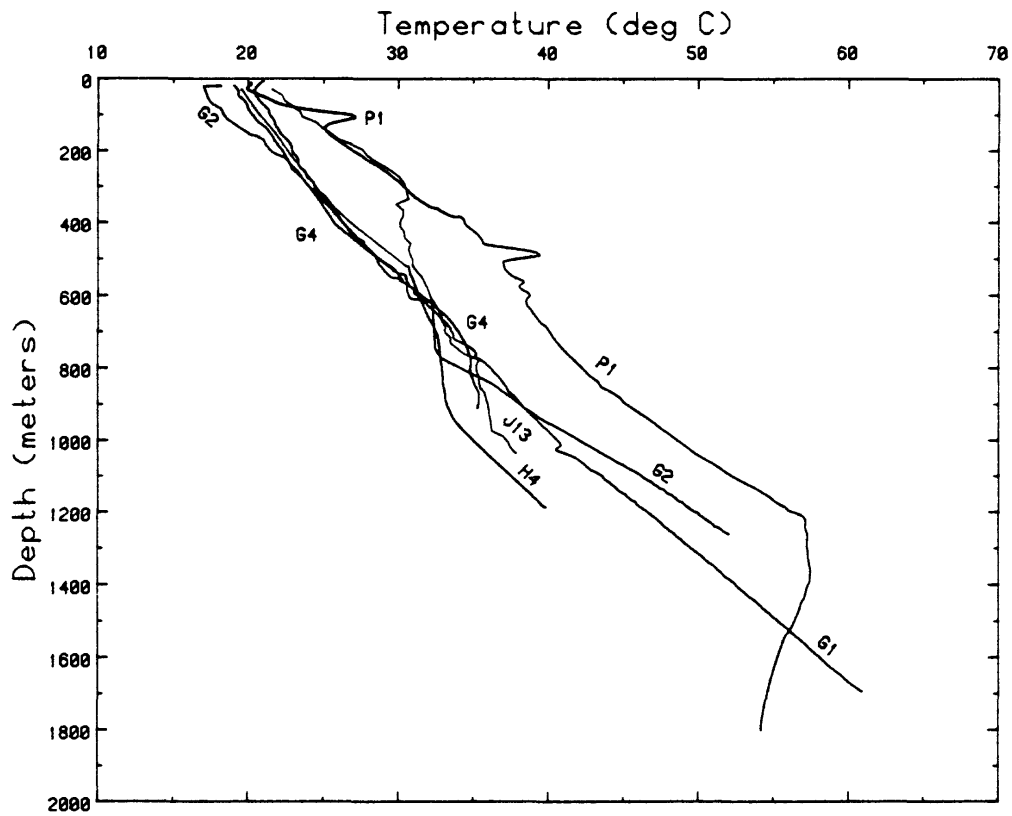


Figure 4. Thermal profile J13-G2 (Figure 3). Temperature profiles are plotted above with common origin. Dashed lines, isotherms; dotted line, static water level.

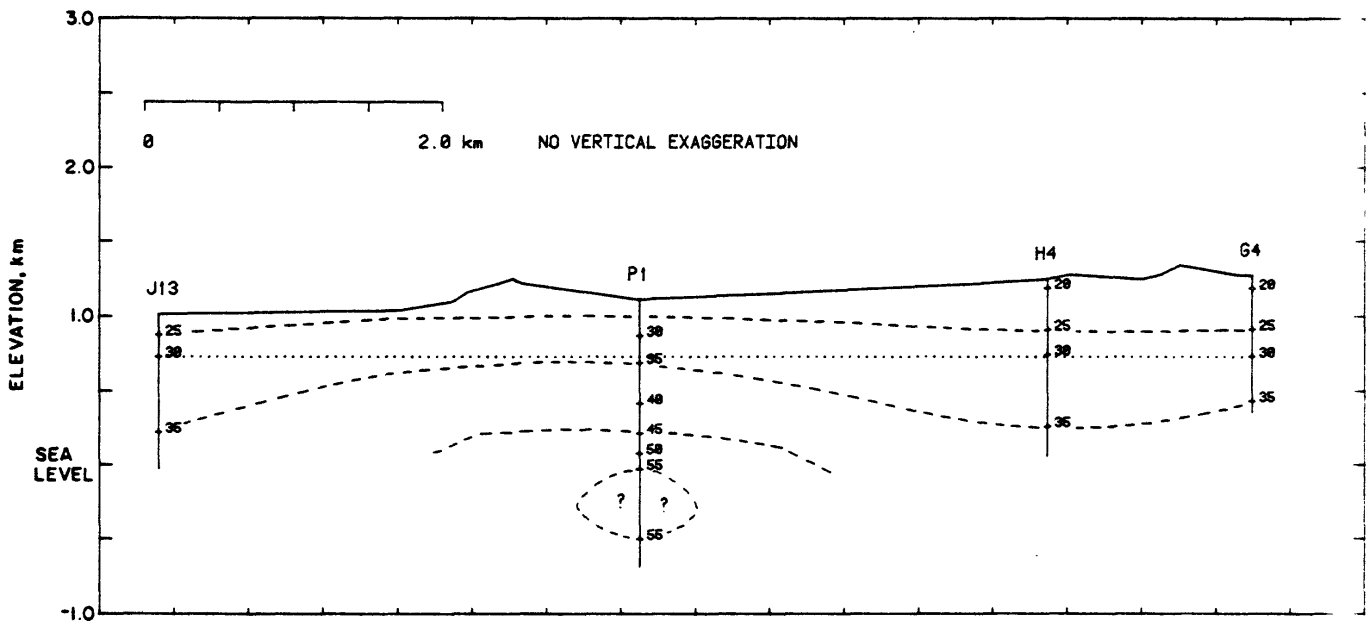
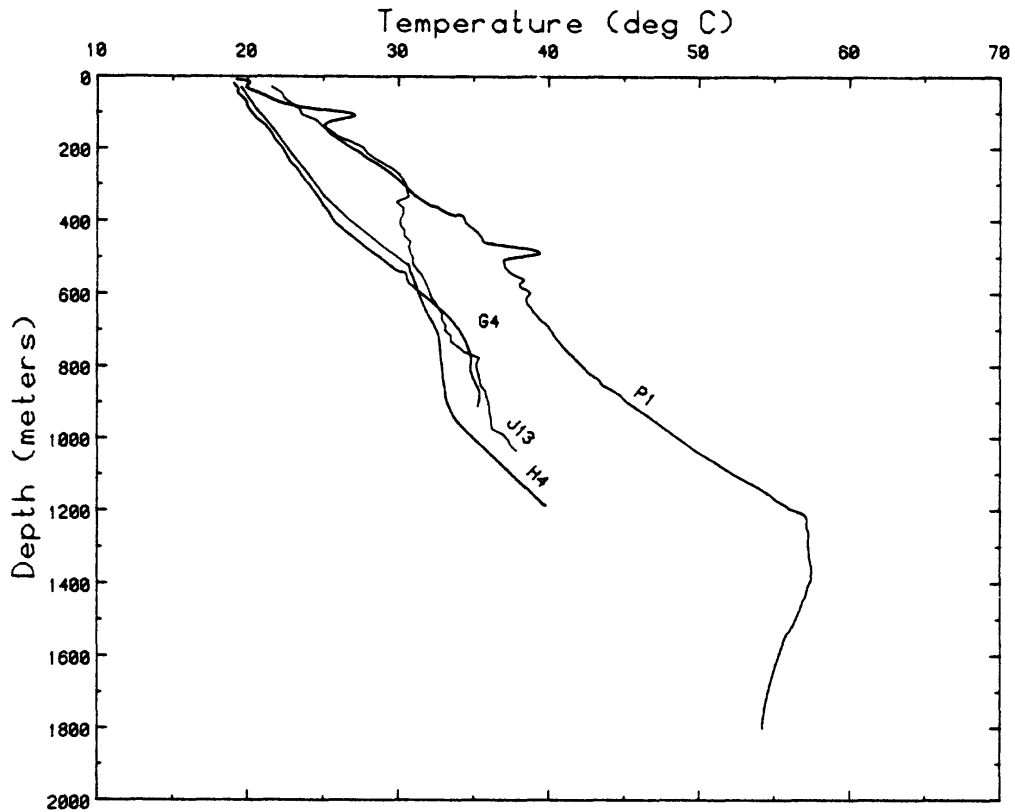


Figure 5. Thermal profile, J13-G4 (Figure 3). Temperature profiles are plotted above with common origin. Dashed lines, isotherms; dotted line, static water level.

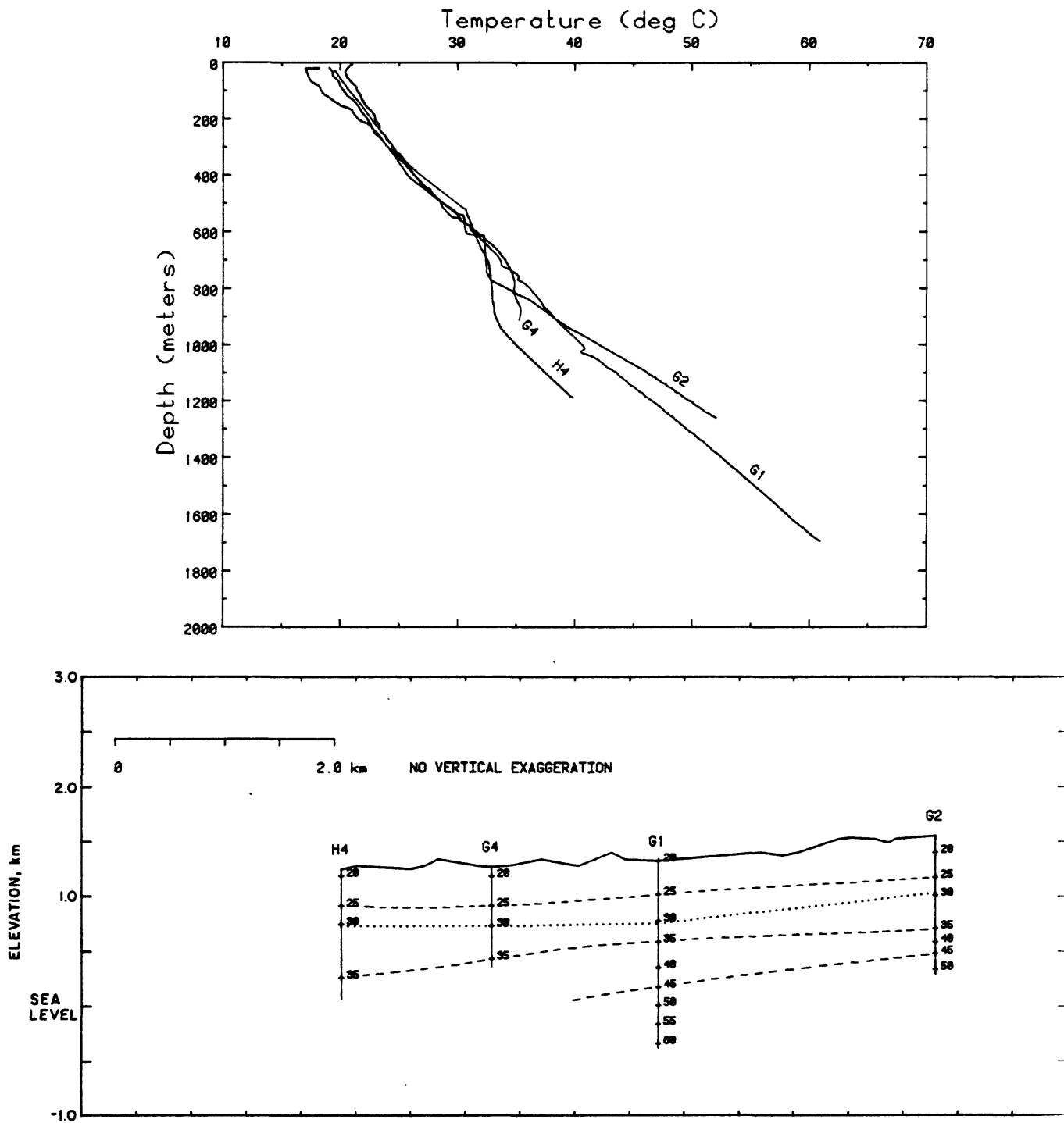


Figure 6. Thermal profile, H4-G2 (Figure 3). Temperature profiles are plotted above with common origin. Dashed lines, isotherms; dotted line, static water level.

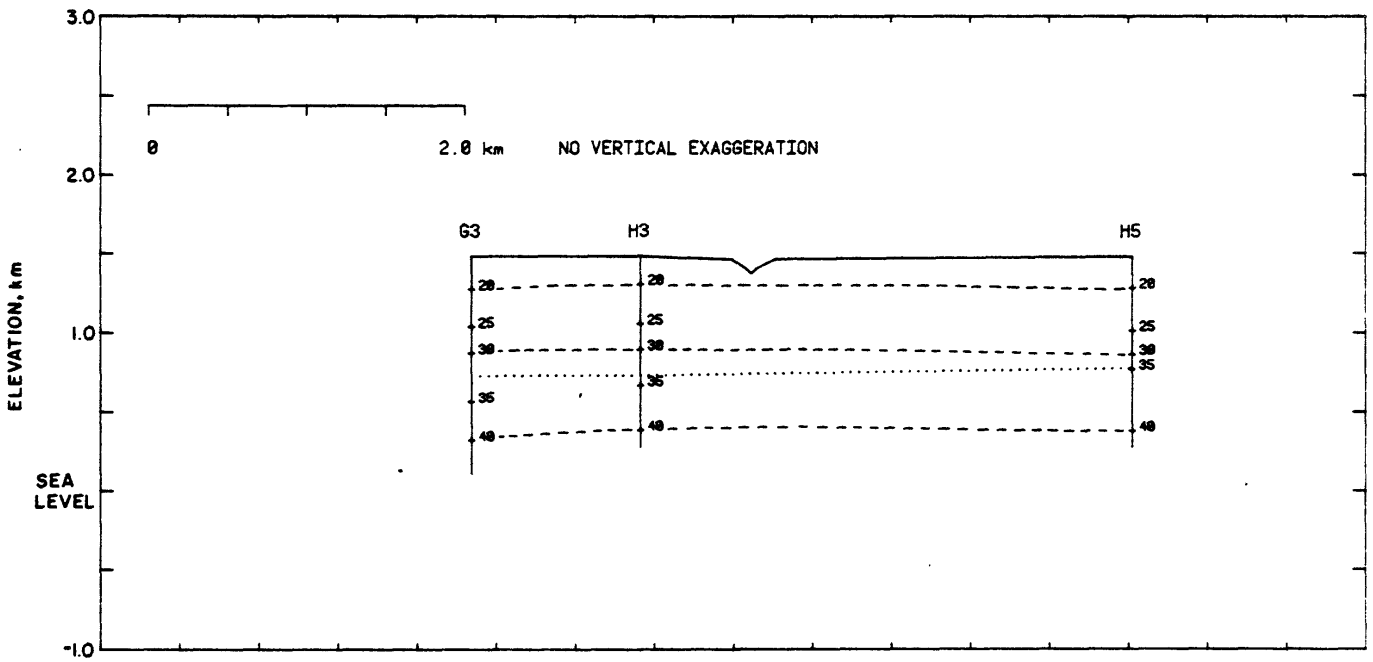
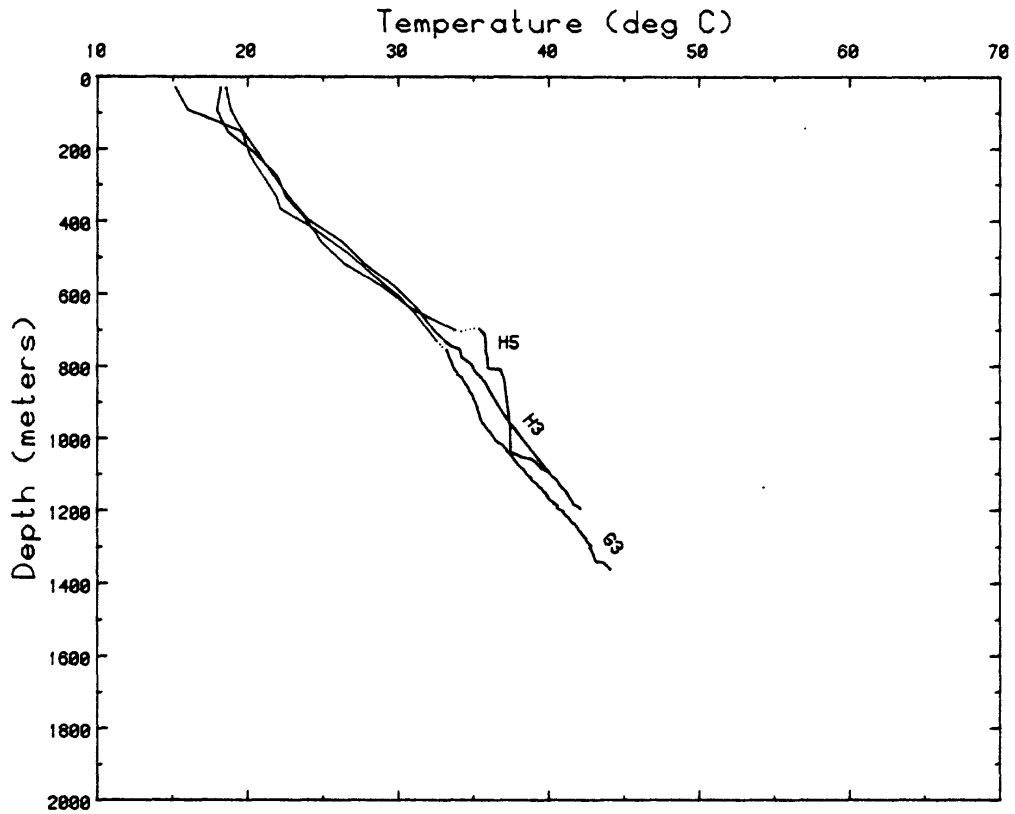


Figure 7. Thermal profile, G3-H5 (Figure 3). Temperature profiles are plotted above with common origin. Dashed lines, isotherms; dotted line, static water level.

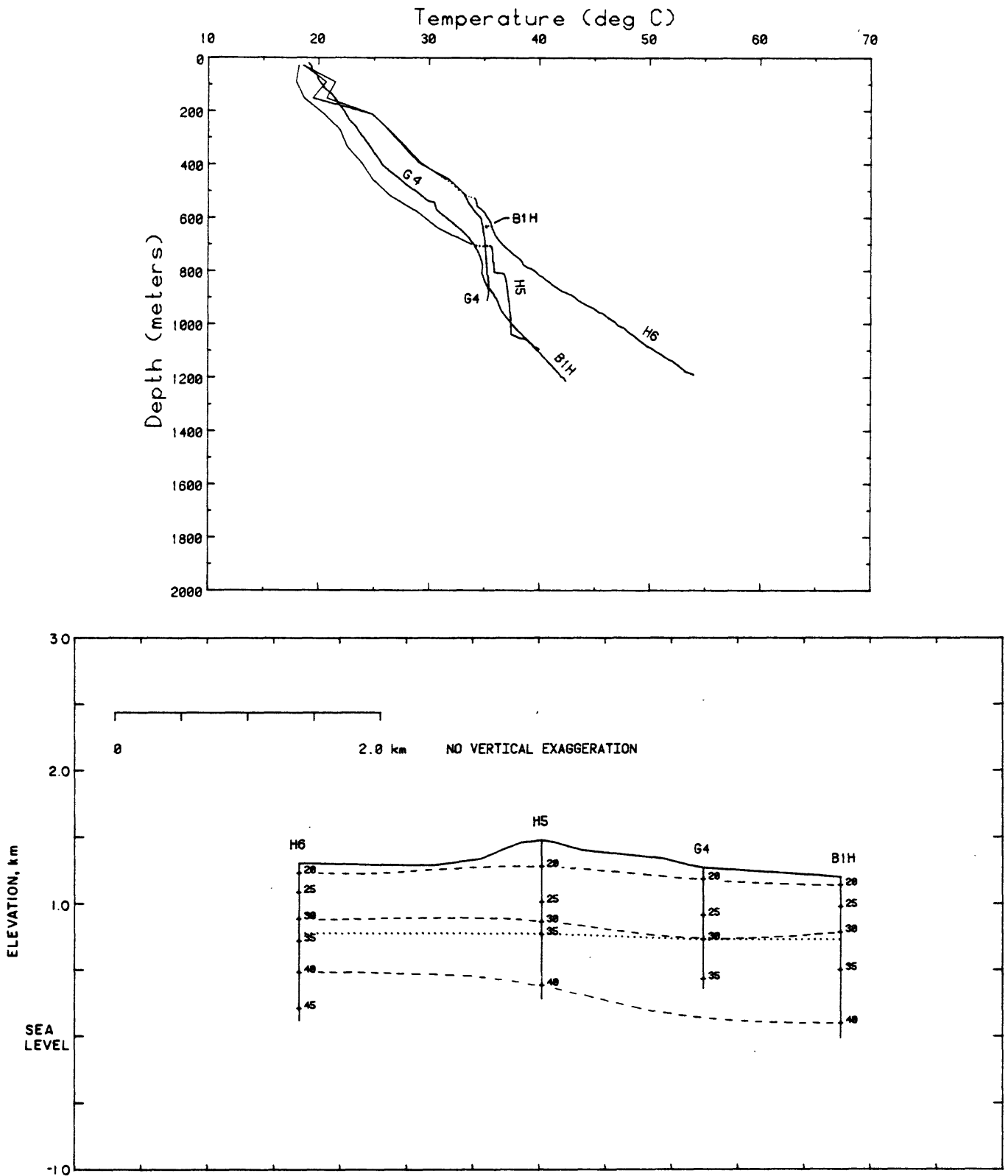


Figure 8. Thermal profile, H6-B1H (Figure 3). Temperature profiles are plotted above with common origin. Dashed lines, isotherms; dotted line, static water level.

SE ROA 38177

geologic, hydrologic, and geophysical properties of the pre-Tertiary rocks, which were identified as Silurian dolomites (Carr and others, 1986) that comprise part of the "lower carbonate aquifer" defined by Winograd and Thordarson (1975). Below the contact between volcanic rocks and that aquifer at a depth of about 1200 m (Figure 4 and 1-19) the temperature profile becomes nearly isothermal, then reverses indicating a complex pattern of lateral throughflow of higher temperature water (cf. profile and cross section, Figures 4 and 5).

We examined the temperature profile from Ue25p1 in the light of hydraulic head and temperature data of Craig and Robison (1984) and of some additional geologic data (Carr and others, 1986). The analysis suggests that the apparent anomaly at this site could be explained in terms of the breaching (by the drill) of a hydraulic barrier in the lower part of the tuffs above the Paleozoic carbonate sequence, causing a relatively long-lived transient thermal response to annular uphole flow previous to our only temperature log in the saturated zone. This suggestion is testable in part by additional thermal profiling but can be resolved completely only by completing a well in the Paleozoic carbonate rocks and grouting in a water-filled access pipe. As this procedure is beyond the scope and timing of the present report, we are retaining a literal interpretation of our observations (Figures 4, 5, and 1-19) with the caveat that further observations may change the interpretation significantly. The important indications of both thermal and hydrologic observations at the Ue25p1 site are that locally, there is a strong potential for a net vertical upflow from the Paleozoic carbonate aquifer. Whether this is actually occurring requires additional observation.

The north-south cross section along the ridge (G3 - H5, Figures 3 and 7) features widely separated isotherms (low temperature gradients) and local

vertical flow below the water table, particularly for USW H5 (see temperature profile, Figure 7). The cross section otherwise is undistinguished with all relevant surfaces nearly parallel to the topography along strike. The section across the ridge (H6 - B1H, Figures 3 and 8) provides some evidence for lateral water flow away from the ridge in an easterly direction. Local upflow with vertical seepage velocity (v) of about 0.1 meter per year is suggested in USW G4 (Figure 9) and both upward and downward components of flow are evident in the profile from UE25B1H (Figure 8 and 1-6). For a detailed review and documentation of the one-dimensional vertical seepage calculation, the reader is referred to Sass and others (1980).

Measurements in air in the WT-series and UZ-1. As the focus of engineering studies shifted from the saturated to the unsaturated zone (UZ), it seemed important to obtain as many thermal data as possible above the water table in support of hydrologic investigations. We routinely logged above the water table in the G- and H-series test wells, the preferred configuration being an access pipe plugged at the bottom and filled with water to allow good thermal contact for the temperature probe and thus a continuous temperature log. In UZ-1, the principal activity was detailed monitoring of the unsaturated zone in its natural state. Thus the risk of introducing water into the system via a leaky coupling was considered too high for our preferred completion. The WT-series was completed with a single, open piezometer to monitor water levels. These wells were thus also unsuitable for water-filled pipes, and we were forced to settle for single point measurements at 100 or 200 foot (30.5 - 61 m) intervals. The measurement technique and method of data reduction are described in detail in Appendix 2 which also contains individual temperature profiles. Thermal gradients in the UZ (Figure 10) vary laterally from about 20°C/km to nearly 60°C/km. In the

absence of corresponding lateral variations in thermal resistivity, this suggests a lateral variation in heat flow which we discuss further in a later section.

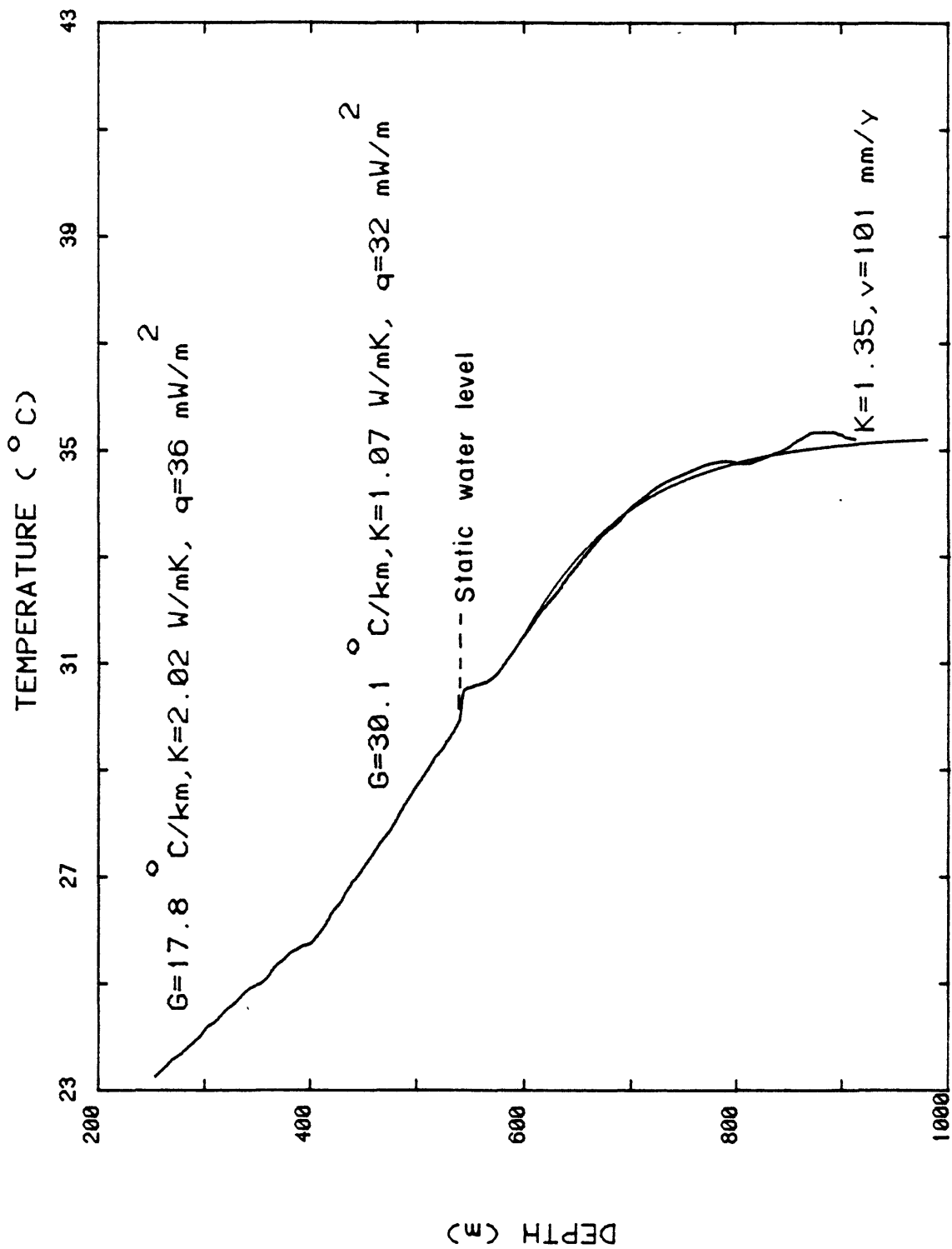


Figure 9. Temperature profile, heat-flow calculations (G is gradient, K is thermal conductivity, q is heat flow) above the water table and a one-dimensional model calculation (smooth curve, see Lachenbruch and Sass, 1977; Sass and others, 1980) for well USW G-4.

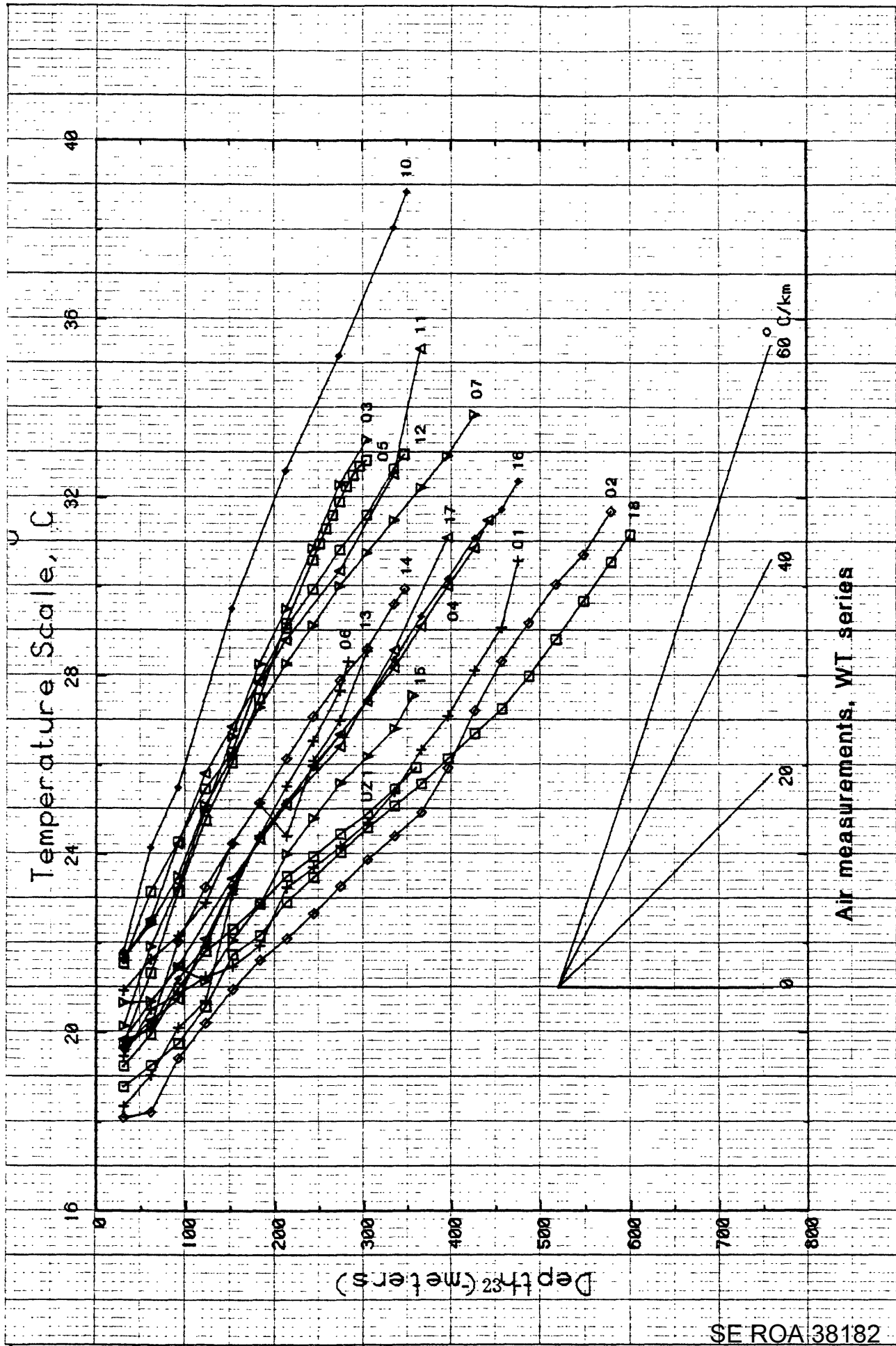


Figure 10. Temperature profiles from WT series wells (see Appendix 2 for individual profiles).

SE ROA 38182

From a consideration of individual temperature profiles in Appendices 1 and 2, we may infer that heat transfer above the water table (i.e., in the unsaturated zone) is primarily by conduction. Most temperature profiles in the UZ are linear or consist of linear segments, the significant exception being "conductor" well UE25a7 in drillhole wash (Figures 1-1 and 1-5), which is discussed in detail in Appendix 1. Ue25a7 apparently responded almost instantaneously to a depth of 150 m to a flash flood following a locally heavy rain. The primary conduit may have been the annulus between casing and borehole wall, but the persistence of the disturbance for at least a year indicates that significant lateral infiltration occurred near or in this well.

The apparent conductive nature of the temperature profiles in the UZ may be the result of the wide separation in data points (see discussion, Appendix 2). Measurements in water-filled access pipes might well reveal significant thermal structure in the UZ on the scale of tens of meters. Linear segments of UZ temperature profiles having different gradients are in rocks of correspondingly different thermal conductivity (see in particular, discussion of G-4 in "heat flow"). By contrast, although portions of many temperature profiles below the water table are linear (particularly below a depth of 1 km), heat transfer in the saturated zone seems to be disturbed by lateral and vertical fluid motion over much of the study area (see individual profiles, Appendix 1 and Figures 4 through 8).

THERMAL CONDUCTIVITY

A total of 204 determinations of thermal conductivity was performed on specimens of solid core from coreholes in the Yucca Mountain area. Individual values of thermal conductivity are tabulated in Appendix 3. The results are summarized in Table 3 by lithologic unit and according to whether the rocks were saturated or unsaturated. For the unsaturated zone, the range of values is greater than that for the saturated zone (Figure 11), but the means are not significantly different. Unsaturated conductivities have a bimodal distribution with peaks at about 1 and 2 $\text{Wm}^{-1} \text{K}^{-1}$, reflecting different degrees of welding. By contrast, the conductivities from the saturated zone have a near-normal distribution, and the deviations from the mean are probably the result of variations in porosity and mineralogy. To the extent that degree of welding and porosity are negatively correlated, and that welded tuffs tend to incorporate minerals of relatively high thermal conductivity, welded saturated tuffs tend also to be more conductive than non-welded. Because of the subjective nature of "degree of welding," however, we choose not to attempt a numerical correlation.

Correlation of thermal conductivity with compressional wave velocity from well logs. A number of workers have attempted correlations between thermal conductivity and various well-log parameters. For monomineralic aggregates or those not containing variable amounts of exotic constituents with extreme values of conductivity, such well-log parameters as neutron porosity (ϕ) and compressional wave velocity V_p can be used with some success as predictors of thermal conductivity.

Goss and Combs (1975) used such relations to predict thermal conductivities for the Imperial Valley in California. We had V_p -log information at depths corresponding to 130 of our conductivity determinations

TABLE 3. Average thermal conductivities for various tuff units of Yucca Mountain and for Paleozoic rocks from UE-25p1

Designation	Unit	Thermal conductivity $Wm^{-1}K^{-1}$							
		N	unsat	S.D.	S.E.	N	sat	S.D.	S.E.
Tpb	Paintbrush Tuff, bedded tuffs	2	0.78	0.13	0.13				
Tpc	Paintbrush Tuff, Tiva Canyon Mem.	5	1.86	0.35	0.15				
Tpp	Paintbrush Tuff, Pah Canyon Mem.	3	1.12	0.36	0.21				
Tpt	Paintbrush Tuff, Topopah Spr. Mem.	31	1.87	0.36	0.07	1	1.16		
Thc	Tuff beds, Calico Hills	7	1.08	0.16	0.06	11	1.22	0.11	0.03
Tcp	Crater Flat Tuff, Prow Pass Mem.	5	1.47	0.62	0.28	12	1.42	0.21	0.06
Tcb	Crater Flat Tuff, Bullfrog Mem.	4	1.94	0.07	0.03	20	1.63	0.26	0.06
Tct	Crater Flat Tuff, Tram Mem.					34	1.72	0.26	0.04
Tfb	Flow breccia					4	1.68	0.26	0.13
Tlr	Lithic Ridge Tuff					27	1.84	0.18	0.03
Tllr	Rhyolitic lava - flow breccia					3	2.25	0.18	0.11
Tllq	Qtz-latic lava - flow breccia					5	2.07	0.24	0.11
Tlld	Latitic lava - flow breccia					3	2.32	0.24	0.14
Tta	Older ash flows - bedded tuffs. Units A, B, and C.	6	2.01	0.15	0.06				
Ttb		1	2.12						
Ttc		7	1.87	0.09	0.03				
Slm	Lone Mtn. dolomite	12	4.90	0.25	0.07				
Srm	Roberts Mtn. Fm.	1	5.47						
All		57	1.66	0.49	0.06	134*	1.72	0.32	0.03

*Excluding Paleozoic rocks from UE25-p1

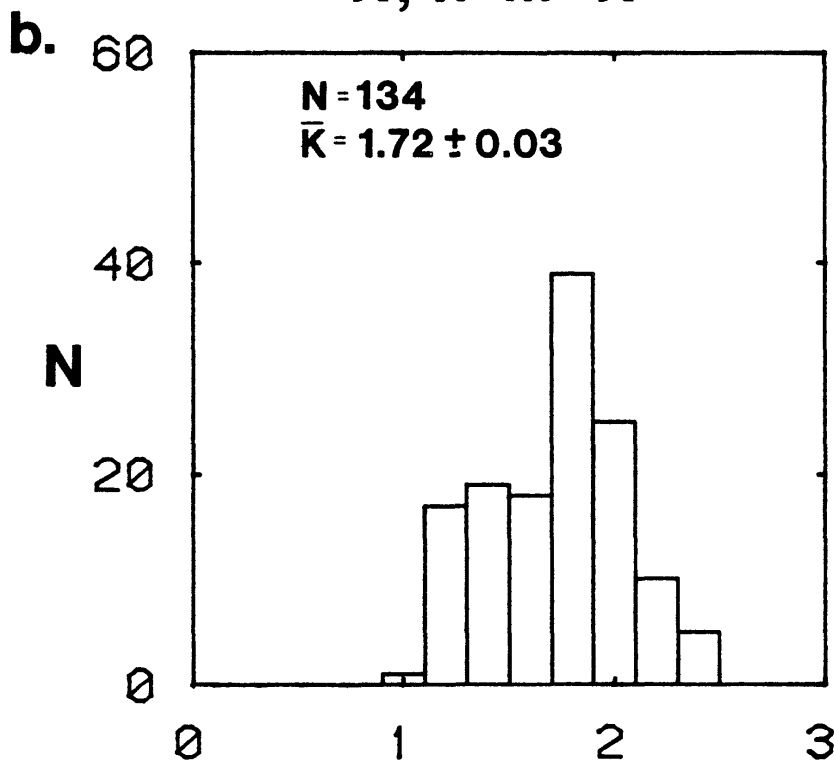
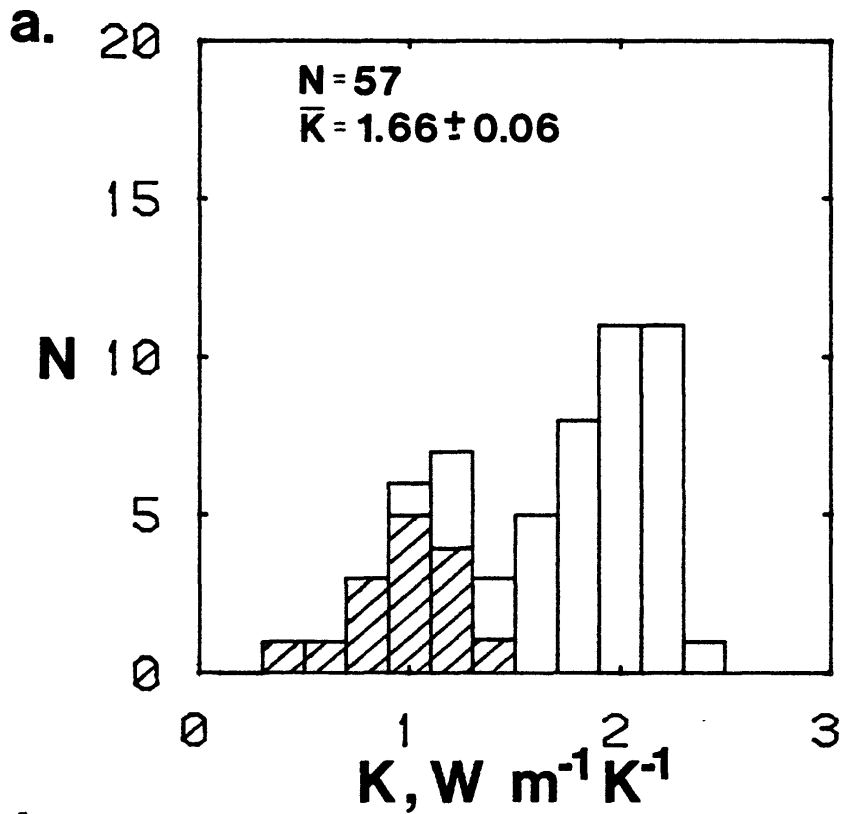


Figure 11. Histograms of thermal conductivity of tuffs from Yucca Mountain, Nevada: (a) unsaturated zone; cross-hatched non-welded, unshaded, welded; (b) saturated zone.

from the G-series wells (Muller and Kibler, 1984; Spengler and Chornack, 1984; D. C. Muller, written commun., 1983, 1984). Coefficients for linear regression of K on V_p are listed for each of the G series wells and for the combined sample in Table 4. The regression line for the combined sample, together with the data plot is shown in Figure 12. There is considerable scatter, but a definite correlation exists. We estimate, based on the RMS residual of $0.2 \text{ Wm}^{-1} \text{ K}^{-1}$ for the general relation (Figure 12) that we can predict thermal conductivity from compressional wave velocity to within ± 10 percent to 15 percent.

TABLE 4. Linear regression of thermal conductivity (K , $\text{Wm}^{-1} \text{K}^{-1}$) on compressional wave velocity (V_p , km s^{-1}) for G series wells, Yucca Mountain, Nevada

Well	N	Coefficient of correlation	Intercept (SE)	Slope (SE)
USW G-1	52	0.65	0.086 (0.08)	0.438 (0.072)
USW G-2	40	0.87	-0.382 (0.04)	0.564 (0.053)
USW G-3	24	0.50	0.406 (0.22)	0.337 (0.125)
USW G-4	14	0.69	0.022 (0.19)	0.430 (0.130)
All wells	130	0.78	-0.197 (0.02)	0.509 (0.036)

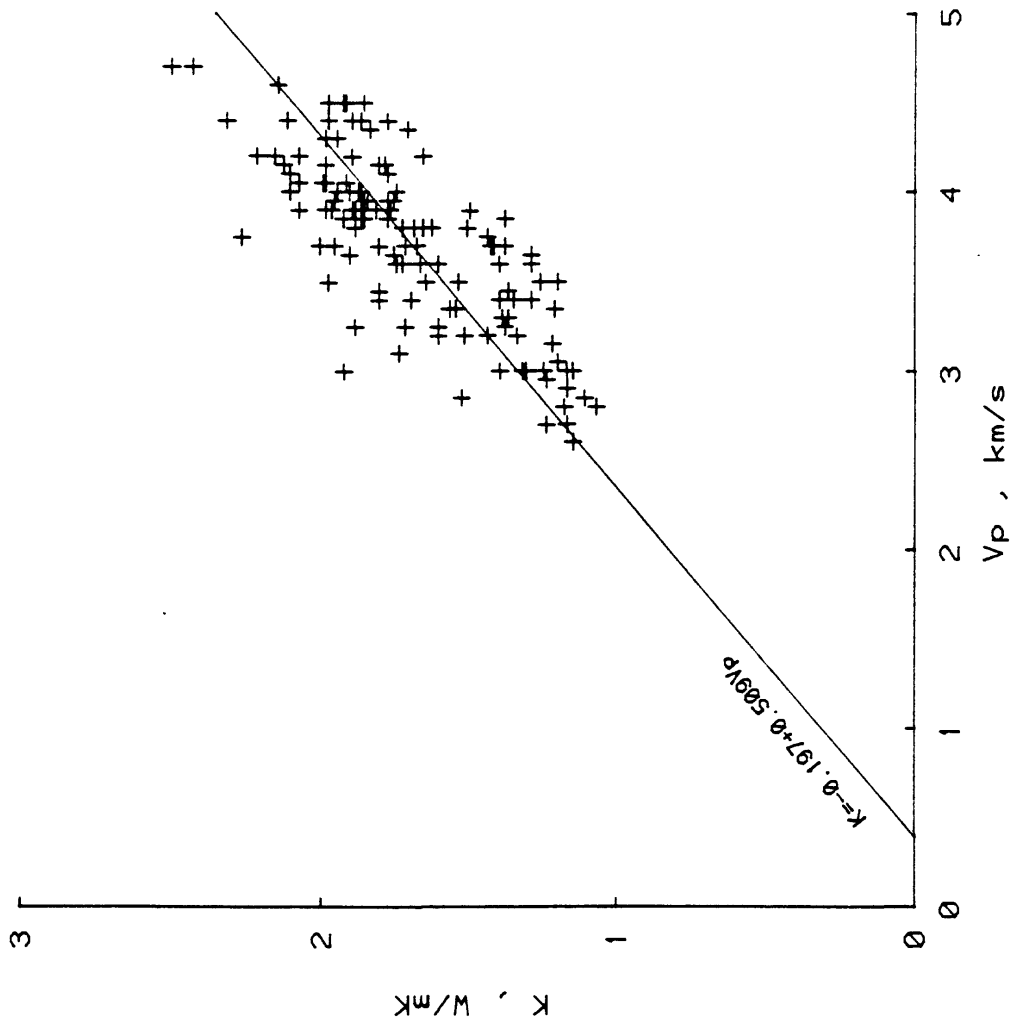


Figure 12. Thermal conductivity (K) as a function of compressional wave velocity (V_p) for tuffs from core holes at Yucca Mountain.

HEAT FLOW

The study area is near the southern boundary of a regional heat-flow anomaly, the Eureka Low (Figure 13). Hydrologic studies of the region (e.g., Winograd and Thordarson, 1975) indicate a complex interbasin flow in Paleozoic carbonate aquifers. This flow has a downward component with seepage velocity on the order of a few centimeters per year to depths as great as 3 km. Flow in the regional aquifer beneath Yucca Mountain discharges by evapotranspiration and perhaps at springs south and southwest of Yucca Mountain (Figure 1). Average heat flow in the Eureka Low is about half that for the adjacent region. Lachenbruch and Sass (1977) calculated that, if the average depth to the interbasin conduit were about 1.4 km, this could be accomplished by downward percolation with seepage velocity of 1 cm/yr. This is consistent with the observations of Winograd and Thordarson (1975) and with a more recent hydrologic study of the Yucca Mountain region by Waddell and others (1984). It is also consistent with a preliminary one-dimensional interpretation of the variation of heat flow with depth in well USWG-1 (Sass and Lachenbruch, 1982). Heat-flow data that were available from near Yucca Mountain in 1981 and earlier (Sass and others, 1980; Sass and Lachenbruch, 1982) were interpreted as a local excursion of the 63 mWm^{-2} contour (1.5 heat-flow units), which defines the boundary of the Eureka Low (Figures 13 and 14). The interpretation of Figure 14, from Sass and Lachenbruch (1982), shows this excursion and includes the Yucca Mountain area within the Eureka Low. It could as easily have been contoured as an isolated thermal sink with then-existing heat-flow data. For either interpretation, the tectonic implications of the heat-flow data are largely inconclusive, inasmuch as the true regional heat flow is obscured by hydrologic processes. The regional data outside the Eureka Low suggest a

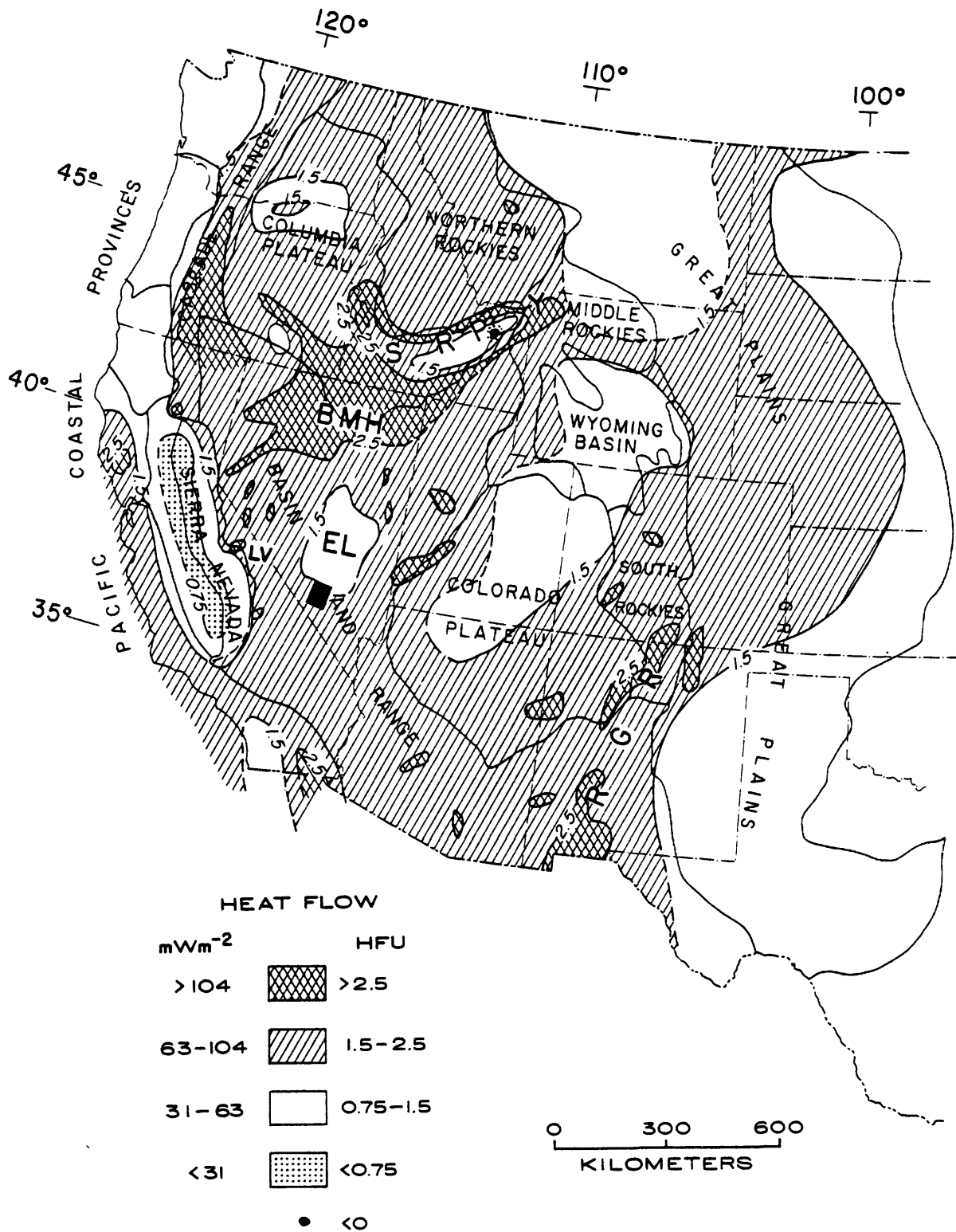


Figure 13. Distribution of heat flow in the western United States (after Sass and others, 1981). Abbreviations: SRP, Snake River Plain; BMH, Battle Mountain High; EL, Eureka Low; RGR, Rio Grande Rift zone; Y, Yellowstone; LV, Long Valley. Black box at the south end of EL is location of Figure 14.

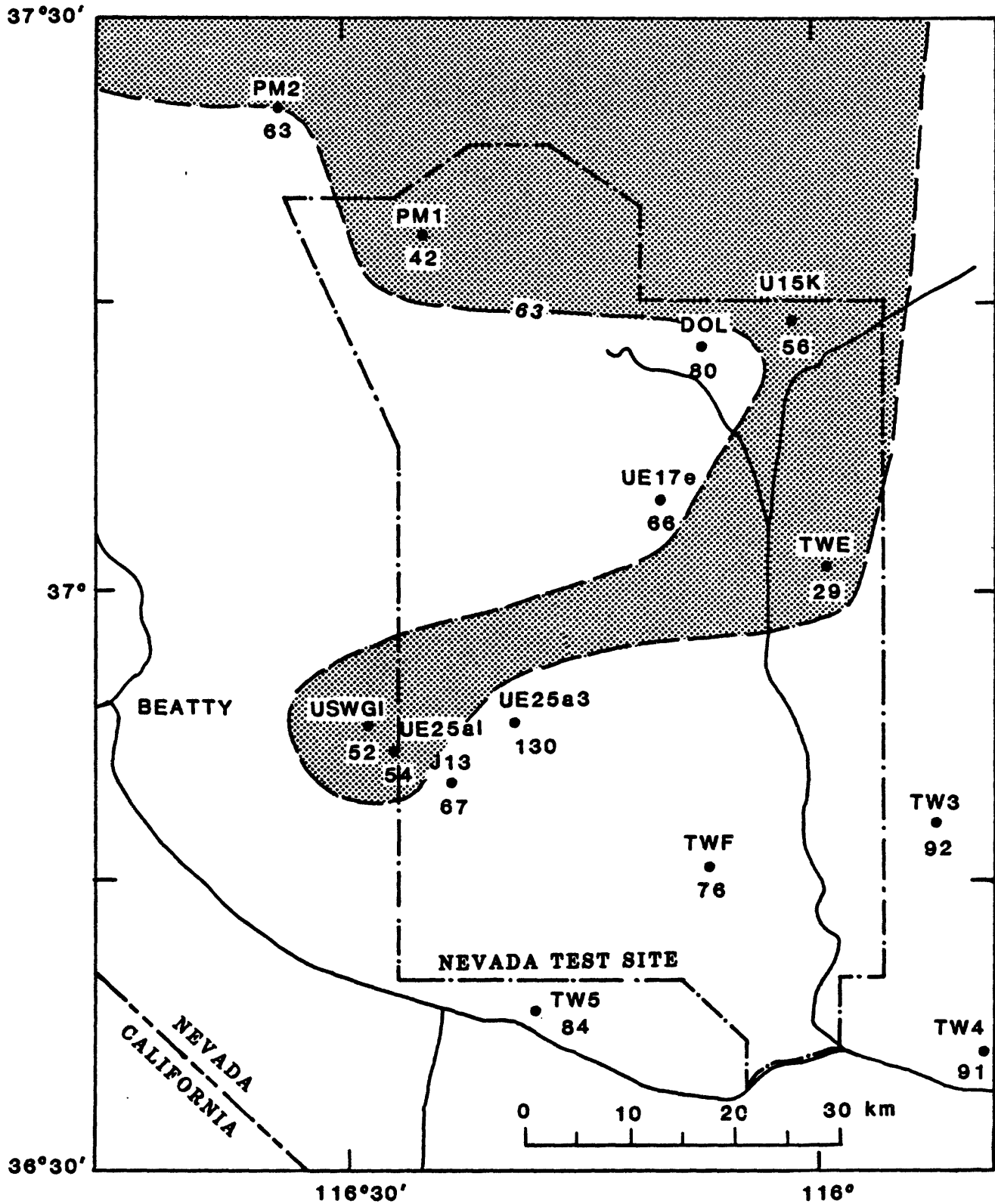


Figure 14. Configuration of 63 mW m⁻² contour (1.5 heat-flow units) in the vicinity of the Nevada Test Site (from Sass and Lachenbruch, 1982). Stippled area has heat flow less than 63 mW m⁻².

regional heat flux (65-90 mWm⁻²) typical of the average for the Basin and Range. However, higher heat flows cannot be ruled out entirely. In fact, Swanberg and Morgan (1978) include the entire Nevada Test Site in a southerly extension of the Battle Mountain High (Figure 13) based on the application of an empirical relation between heat flow and silica geotemperatures. However, the abundance of highly soluble volcanic glass in the rhyolitic rocks of southern Nevada casts serious doubt on the validity of uncompensated silica geotemperatures in this area.

Three methods were applied to the current data from the geologic and hydrologic test wells in order to estimate conductive heat flow (q) for both saturated and unsaturated zones (Table 5). The preferred method is to combine the least-squares thermal gradient, Γ , for a linear interval of a given temperature profile with the harmonic mean thermal conductivity, $\langle K \rangle$, from the same interval according to

$$q = \langle K \rangle \cdot \Gamma \quad (1)$$

Because all thermal conductivity specimens came from the G series of coreholes, this method could be used only in these wells. In the second method, the weighted formation average was substituted for the harmonic mean. Third, where velocity logs were available, the relation between K and V_p (Table 4, Figure 12) was used to estimate the appropriate K. We evaluated the formation average method by comparing values calculated by equation (1) with those calculated using the weighted formation average. Agreement between the two methods was excellent (within about 15%, Table 5), lending credence to our estimates of thermal conductivity in other wells.

Estimates of heat flow from the unsaturated zone were also made in UZ1 and the WT series of wells (Table 6). These values, together with the UZ

heat flow from Table 5, are plotted and contoured in Figure 15; they have a systematic geographic distribution. The southernmost group of wells have heat flows approaching regional values (Figure 15). The lowest heat flows are within a kilometer or two of USWG-4 which is near the location of the planned exploratory shaft and within the area of the proposed repository. We also note that the heat flow in the UZ correlates negatively with the thickness of the UZ (Figure 16). Within the area of Figure 15, this thickness is generally greatest in the proposed repository area. The heat flow from the UZ at G4 is probably the best documented of all. It is based on a large number of measured thermal conductivities and on a thermal profile obtained in water-filled tubing. Between 150 and 400 m (Figure 1-12, Figure 9, Table 5), the gradient is 17.8 ± 0.04 (SE) °C/km and 13 samples of the densely welded Topopah Spring member of the Paintbrush Tuff yield a well constrained average thermal conductivity of 2.02 ± 0.06 W m⁻¹ K⁻¹. The heat flow from equation 1 is 36 ± 1 mWm⁻². Just below 400 m, there is an abrupt increase in gradient to 30.1 ± 0.06 °C/km and a corresponding decrease in conductivity (from eight samples of the unwelded tuffaceous beds of Calico Hills) to 1.07 ± 0.04 resulting in a heat flow of 32 ± 1 mWm⁻². Considering the numerous sources of possible error, the agreement between these two independent heat-flow determinations is excellent, supporting our conclusion that heat flow in the UZ is primarily by conduction. Also of interest is the inference (from the curvature of the temperature profile) that the upward component of seepage velocity in the saturated zone at this site is about 100 mm per year.

For the nine wells providing both SZ and UZ heat-flow estimates, the mean values determined from Table 5 are very similar, 40 mW m⁻² for the SZ and 41 mW m⁻² for the UZ. However, estimates for the SZ are strongly

TABLE 5. Heat-flow estimates from test wells near Yucca Mountain, Nevada

Well	Depth range (m)	Method*	Heat flow mWm^{-2}	
			q_{uns}	q_{sat}
USW G-1	100-527	2	41	
	1067-1697	1		53
USW G-2	200-526	1	42	
		2	45	
	Avg	44		
	610-1250	1		52
		2		54
		Avg		53
USW G-3/GU-3	100-751	1	39	
		2	44	
	Avg	42		
	750-1360	1		27
		2		29
		Avg		28
USW G-4	150-402	1	36	
		2	32	
	Avg	34		
	410-541	1	32	
		2	37	
			34	
USW H-1	80-454	2	34	
	1000-1830	2		54
		3		46
		Avg		50
USW H-3	150-750	2	40	
	750-1200	2		42
		3		52
		Avg		47
USW H-4	65-520	2	34	
	520-1220	2		24
		3		26
		Avg		25

TABLE 5. Heat-flow estimates from test wells near Yucca Mountain, Nevada
(continued)

Well	Depth range (m)	Method*	Heat flow mWm^{-2}	
			q_{uns}	q_{sat}
USW H-5	165-700	2	41	
	720-1220	2		27
USW H-6	100-526	2	49	
	530-1210	2		51
UE25a4	100-150	2	29	
UE25a5	100-150	2	32	
UE25a6	75-150	2	47	
UE25a7	180-270	2	33	
UE25a1 b1H	150-469	2	48	
	470-1220	2		23
UE25p1	80-380	2	62	
J-13	130-262	1	65	
		2	67	
		Avg	66	

*Method 1: Least-squares gradient \times harmonic mean of measured conductivities over same interval.

Method 2: Least-squares gradient \times conductivity calculated from formation means.

Method 3: Least-squares gradient \times harmonic mean of conductivities inferred from K vs. V_p relation.

TABLE 6. Heat-flow estimates (\pm SE) from the unsaturated zone in UZ-1 and WT series wells based on average formation conductivities

Well	Depth range (m)	Member	$Wm^{-1} K^{-1}$	Γ °C km $^{-1}$	q_m mWm $^{-2}$
UZ-1	30-90	Tpp	1.12	28.5	32
	122-350	Tpt	1.87	17.1	32
		Mean			32
WT-1	30-144	Tpc	1.86	15.7	29
	144-422	Tpt	1.87	23.2	43
	422-475	Tht	1.08	41.5	45
		Mean			39 \pm 5
WT-2	82-397	Tpt	1.87	19.7	37
	397-488	Tht	1.08	35.7	39
	488-628	Tcp	1.47	25.3	37
		Mean			38 \pm 1
WT-3	30-112	Tpt	1.87	51.5	96
	112-154	Tht	1.08	55.3	60
	154-257	Tcp	1.47	42.8	63
	257-305	Tcb	1.94	39.7	77
		Mean			74 \pm 8
WT-4	30-86	Tpc	1.86	17.2	32
	86-132	Tpp	1.12	41.7	47
	132-352	Tpt	1.87	26.4	49
	352-442	Tht	1.08	30.4	33
		Mean			40 \pm 5
WT-5	30-180	Tpb	0.78	51.1	40
	180-305	Tpc	1.86	44.4	82
		Mean			61 \pm 21
WT-6	52-117	Tpt	1.87	26.6	50
	117-290	Tht	1.08	43.2	47
		Mean			48 \pm 2
WT-7	30-120	Tpc	1.86	37.1	69
	120-427	Tpt	1.87	27.9	52
		Mean			60 \pm 8
WT-10	46-191	Tpb	0.78	58.6	46
	191-290	Tpc	1.86	42.2	78
	290-350	Tpt	1.87	48.0	90
		Mean			71 \pm 13
WT-11	30-96	Tpc	1.86	42.2	78
	96-366	Tpt	1.87	36.2	68
		Mean			73 \pm 5

TABLE 6. Heat-flow estimates (\pm SE) from the unsaturated zone in UZ-1 and WT series wells based on average formation conductivities (continued)

Well	Depth range (m)	Member	K^* $Wm^{-1} K^{-1}$	Γ $^{\circ}C km^{-1}$	q mWm^{-2}
WT-12	30-110	Tpc	1.86	42.1	78
	110-350	Tpt	1.87	33.2	62
		Mean			<u>70\pm8</u>
WT-13	67-155	Tpc	1.86	21.6	40
	155-305	Tpt	1.87	31.4	59
		Mean			<u>50\pm10</u>
WT-14	33-350	Tpt	1.87	32.6	61
WT-15	128-350	Tpt	1.87	26.9	50
WT-16	175-325	Tpt	1.87	26.9	50
	325-472	Tht	1.08	28.0	30
		Mean			<u>40\pm10</u>
WT-17	30-75	Tpc	1.86	27.2	51
	75-300	Tpt	1.87	27.0	51
	300-371	Tht	1.08	38.4	42
		Mean			<u>48\pm3</u>
WT-18	30-110	Tpc	1.86	15.8	29
	110-214	Tpp	1.12	24.6	27
	214-493	Tpt	1.87	18.0	33
	493-610	Tht	1.08	28.3	31
		Mean			<u>30\pm1</u>

*Average conductivity for member, see Table 3.

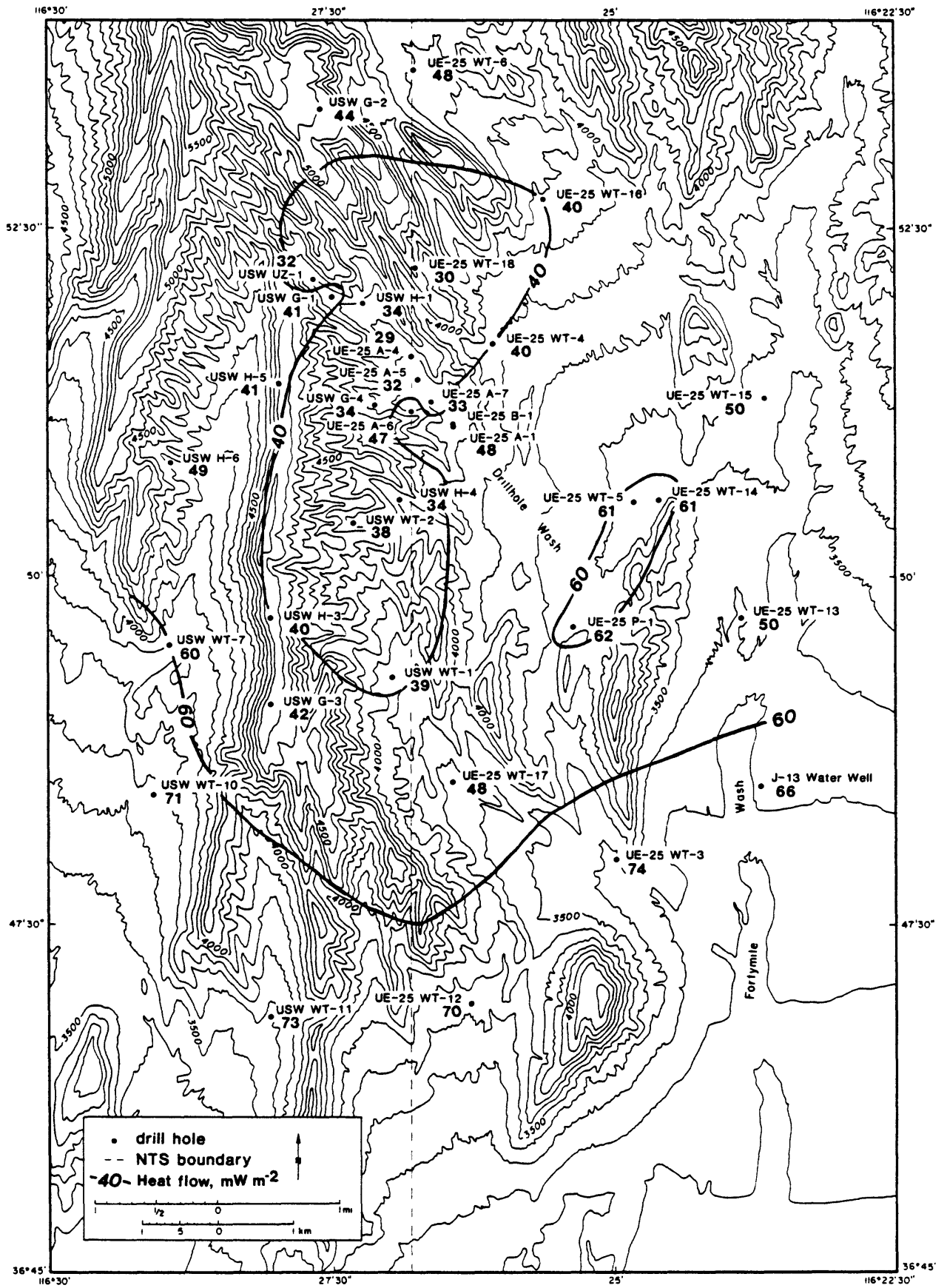


Figure 15. Conductive heat flow from the unsaturated zone in the vicinity of Yucca Mountain (see Index, Figure 1).

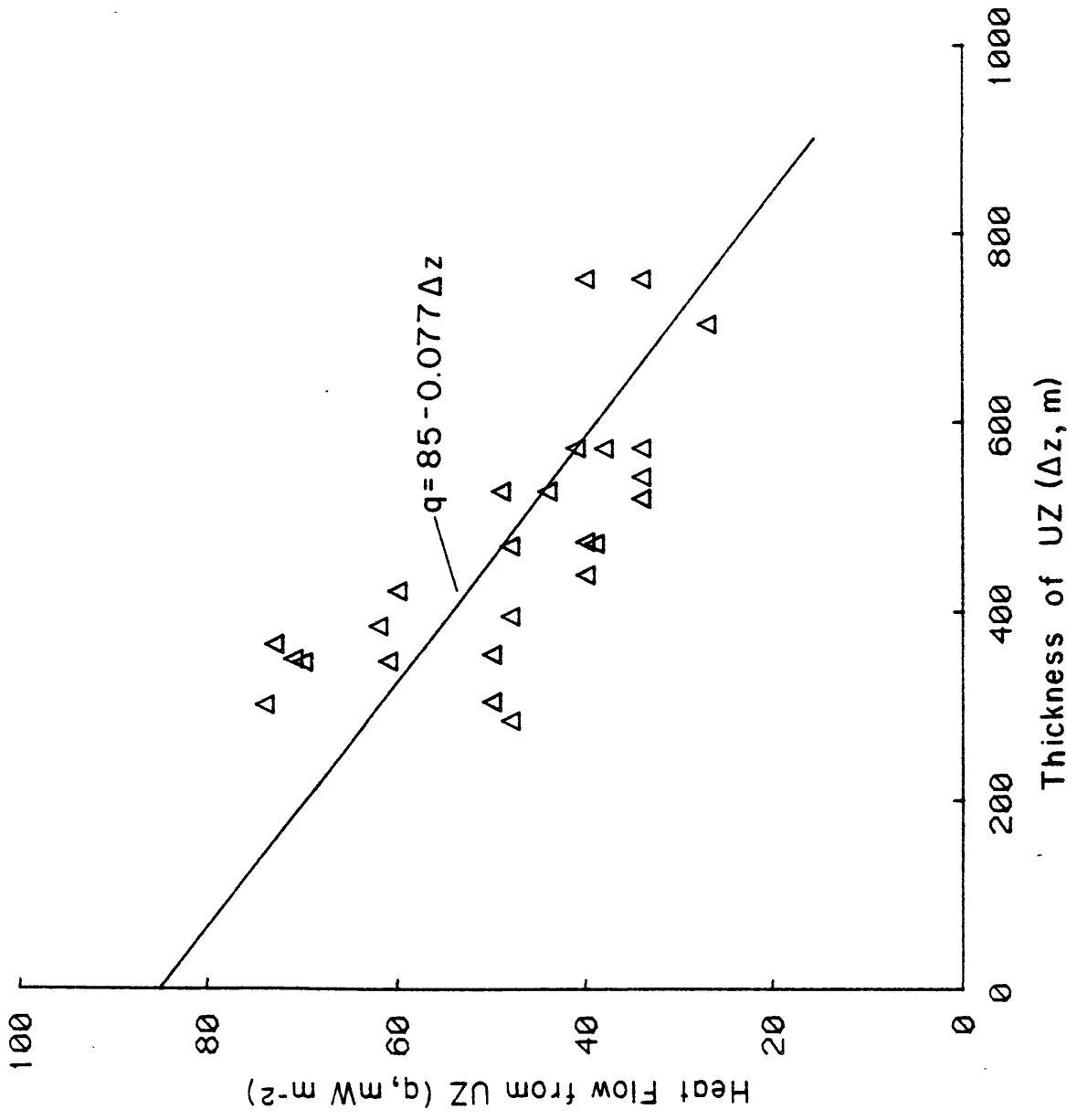


Figure 16. Heat flow from the unsaturated zone as a function of the thickness of the zone.

bimodal (Figure 17B), and those comprising the lower group (USW G-3, USW H-4, USW H-5, and UE25b1) have SZ heat flows that are substantially less than the UZ values (Figure 17C) for the same wells. The temperature profiles in these wells and in USW G-1 and USW H-6) are non-linear, indicating upward or downward flow of water in the well bore or the surrounding formations (see profiles in Appendix 1). The least-squares temperature gradients used to calculate the heat flows on Table 5 were determined for all or most of the SZ parts of the wells. Because flow in either direction generally increases the efficiency of heat transfer, thereby suppressing gradients in the affected interval, the calculated estimates are probably minimum values. We are more confident of the estimates for USW G-1, USW H1, and USW H-3, which were based on gradients defined by long, apparently conductive segments.

An alternative approach to defining gradients on hydraulically disturbed temperature profiles is to force measurements on short linear segments in the deepest parts of the wells, where the probability of significant in-hole flow is least. This procedure involves the risk of including sections of distributed inflow or outflow, as well as the risk of forcing use of the data beyond their limit of reliability. However, hydrologic testing in the Yucca Mountain area indicates that hydraulic conductivity is provided mainly by thin, discrete intervals, which are probably fracture-controlled (Waddell and others, 1984). Under these conditions, the assumption that linear segments of at least several tens of meters represent zones of primarily conductive heat flow may be justified. The depths and thermal gradients of these segments for the wells in question are discussed in Appendix 1.

We calculated alternative heat-flow estimates, using average thermal conductivities (Tables 3-2 and 3-3) for the appropriate depths in USW G-2

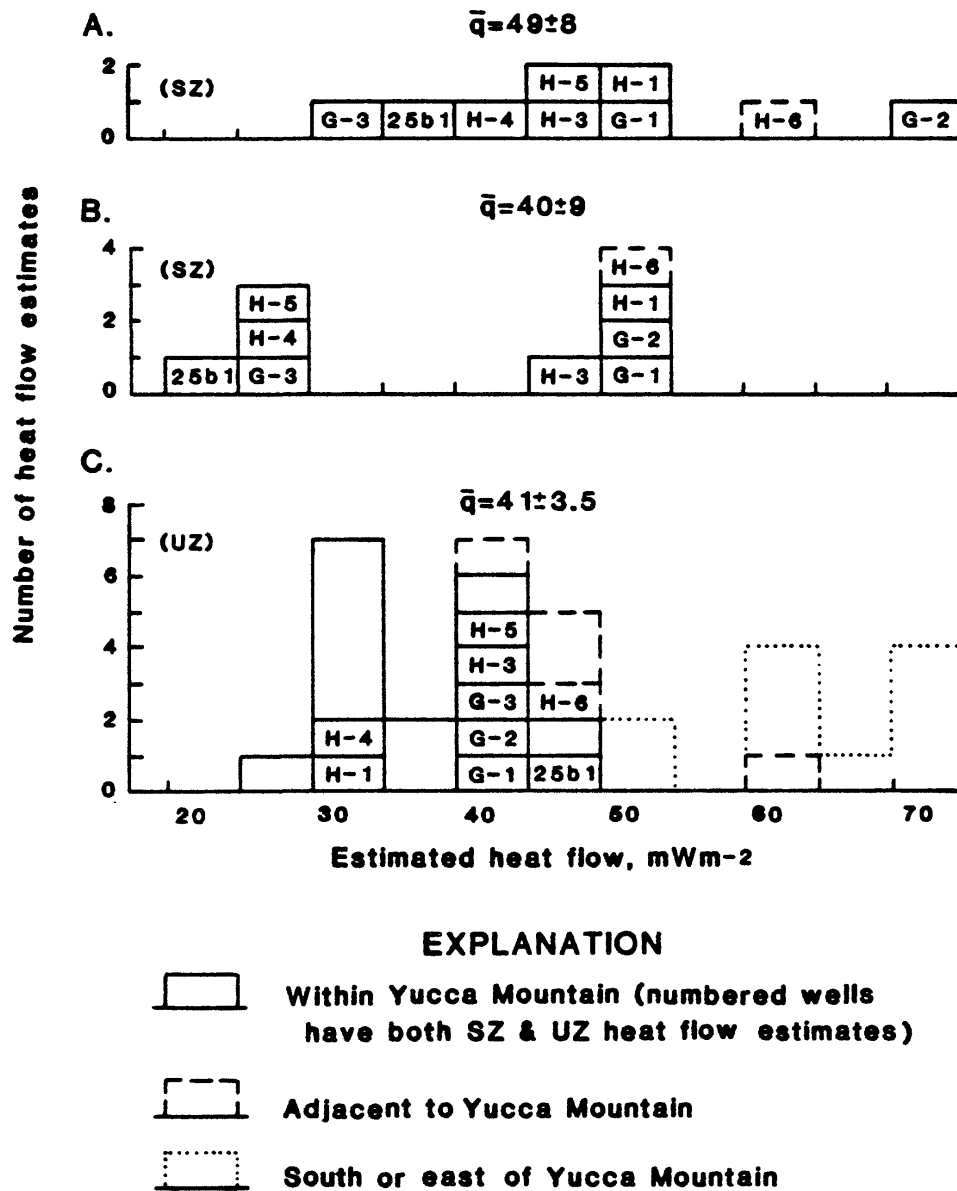


Figure 17. Comparison of heat-flow estimates for the unsaturated zone (C) with those for the saturated zone using the least-squares gradients (B) and gradients of linear segments (A). \bar{q} is average for numbered wells $\pm 95\%$ confidence limits.

and USW G-3 and the weighted formation averages for the other four holes. The revised distribution is shown in Figure 17A, as compared with Figure 17B. Heat flows for the SZ in USW G-3 and UE25b1 are still less than those for the UZ, although the differences are reduced. It is questionable that the gradient (21°C/km) in the interval used for USW G-3 represents the actual, undisturbed conductive gradient, as the interval (1000-1280 m) is considerably above the 1533-m total depth of penetration. In UE25b1, however, the interval used, 1000-1220 m extends to the total drilled depth. The mean for the nine holes is increased to $49 \pm 8 \text{ mW m}^{-2}$ (Figure 17A), however, within the limits of 95% confidence, neither SZ mean is significantly different from that for the UZ (Figure 17).

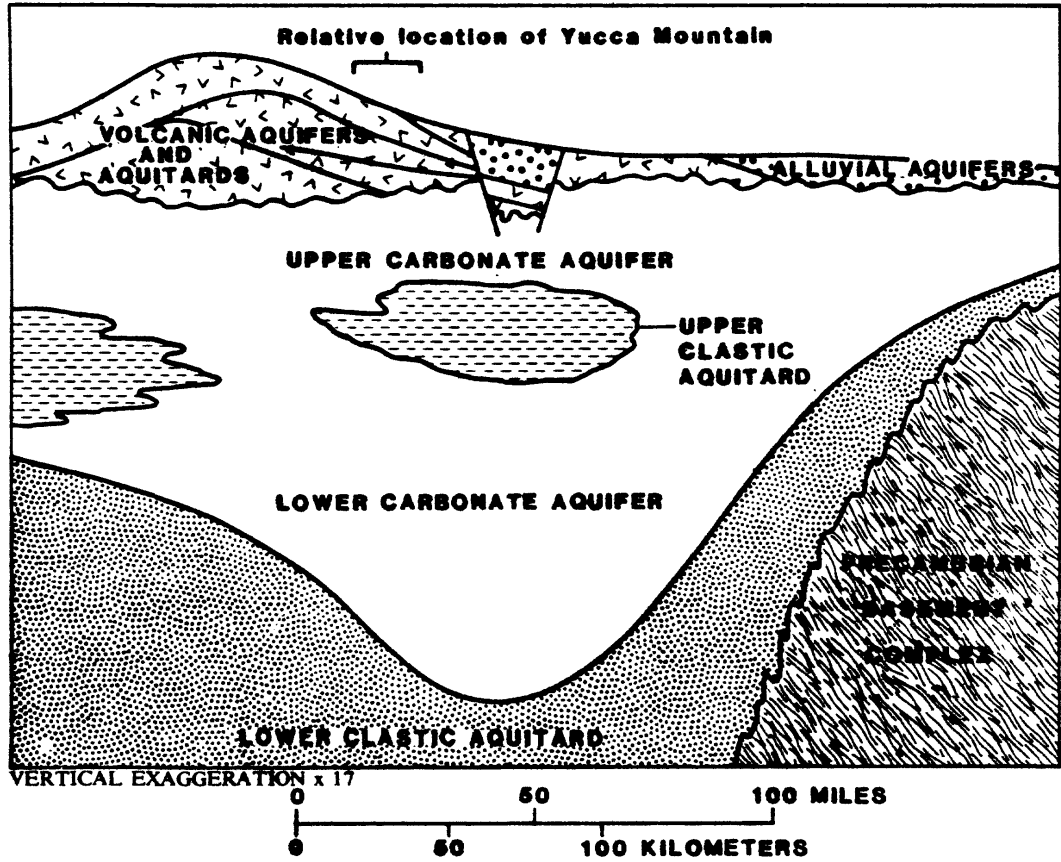
The geographic influence on UZ heat flow is clearly evident in Figure 17C, which includes all of the UZ estimates. Wells that are within the smoothed boundary of Yucca Mountain (Figure 15) have the lowest heat flows. Those that are closely adjacent have intermediate values, and those farther east and south have the highest.

With reference to the regional heat flow (about 85 mW m^{-2}) outside of the Eureka Low, the deficiency at the repository site is $35\text{-}45 \text{ mW m}^{-2}$ for the SZ and $45\text{-}50 \text{ mW m}^{-2}$ for the UZ. We can conclude that 80%, and perhaps all, of the anomaly is attributable to the SZ. The removal of significant amounts of heat from the SZ requires intense lateral flow of relatively cool water in regional aquifers. In active recharge areas, infiltration further reduces surface heat flow according to the one-dimensional relationship (Lachenbruch and Sass, 1977, equation 8),

$$\Delta q [\text{mW/m}^{-2}] \cong 0.14 V_w [\text{mm/yr}] \times G [^\circ\text{C/km}] \times \Delta z [\text{km}], \quad (2)$$

where Δq is the reduction of surface heat flow, V_w is the downward infiltration rate, G is the thermal gradient, and Δz is the depth of infiltration

WEST ← CANDIDATE AREA → EAST



EXPLANATION

- | | | | |
|---|---|---|-----------------------------------|
|  | ALLUVIUM AND LACUSTRINE DEPOSITS |  | SILTSTONE AND SHALE |
|  | CARBONATE ROCKS |  | VOLCANIC ROCKS |
|  | SANDSTONE AND QUARTZITE |  | CRYSTALLINE BASEMENT ROCKS |

Figure 18. Stratigraphic relationships among hydrostratigraphic units near Yucca Mountain (reproduced with permission from Figure 2 of Waddell and others, 1984).

to the regional aquifer. In the previously defined Eureka Low (Figure 13), downward percolation may persist to depths of 4 km or so, and recharge rates of 2 to 3 mm/yr on a regional scale would produce the observed reductions. It is tempting to call upon the same process in explaining the heat-flow anomaly at Yucca Mountain because of its proximity to the Eureka Low, the great depth of the water table, and the probable occurrence of the regional carbonate aquifer at depths of 2-4 km (Figure 18). Downward infiltration of a few mm/yr would account for the anomaly. However, a necessary constraint is that the thermal and hydrologic data that are available must at least be consistent with the dominance of downward components of flow over upward components. Short segments of some of the Yucca Mountain SZ temperature profiles indicate downward flow, but upward flow is indicated by others, most notably and persistently in USW G-4 (Figure 9). Furthermore, Robison (1984) reports significant hydraulic potentials for upward flow at USW H-1, USW H-3 and UE25p1. Hence, the existing limited data do not support pervasive downward flow throughout the vicinity of Yucca Mountain as the principal cause of the average SZ heat-flow deficiency. For the area of Figure 15, pervasive lateral flow in the Paleozoic carbonates with a net downward component of velocity is the most likely principal cause of the anomaly.

Neither the hydrologic nor the thermal data rule out locally heavy recharge within the study area as a significant factor. Heavy infiltration along permeable, high angle fractures at high elevations would produce the observed potential for upward flow in less permeable systems or systems with impermeable caps at lower elevation. This type of gravitationally driven convection is common in many regions of the Basin and Range (see e.g., Mase and others, 1982).

The possible additional reduction of heat flow (5-10 mW m⁻²) in the UZ, if confirmed, could be attributed to the coupled action of three processes. The first, downward infiltration, can be limited by equation 2, using 14°C as the typical produce of $G \times \Delta z$ (Figure 10). This small UZ anomaly could be accounted for by 2-5 mm/yr of infiltration, about an order of magnitude greater than that postulated from hydrologic considerations (Montazer and Wilson, 1984). D. T. Snow and Parviz Montazer (written communications, July and April 1987) have suggested the additional processes of vaporization and of advective transport of heat in upward movement of air (presumably containing water vapor). The latent heat of liquid water is about 580 cal/cm³. Therefore, the vaporization of only 0.1 mm/yr would consume about 5.8 cal/cm²/yr, which is about 8 mW m⁻² or approximately the UZ heat-flow deficiency. Vaporization requires the circulation of air through the mountain. As currently postulated (Parviz Montazer, written communication, April 1987), cool, dry air enters the outcrop of the Topopah Spring member (fractured welded tuff) low on the west side of the mountain and discharges near its crest. By analogy with equation 2 and again using 14°C as the temperature differential, we can estimate an upper limit of the air discharge, V_a , from

$$v_a = \frac{\rho_w C_w}{\rho_a C_a} v_w \quad , \quad (3)$$

where ρ and C denote the densities and heat capacities of water and air, respectively. The required upward discharge of air is about 3,000 times that of water, or about 15 m/yr to produce the small 10 mW m⁻² anomaly if indeed it exists.

Though the thermal profiles in the UZ possibly lack resolution owing to the wide separation in data points, they appear primarily conductive throughout the UZ thickness. This might result from vertically uniform

action of the heat-removing processes discussed above; alternatively, it could be attributed to shallow SZ lateral flow, above depths used to calculate SZ heat flows. The credibility of this alternative is supported by borehole flow surveys while pumping (Benson and others, 1983), which show that most of the water production occurred within a few hundred meters beneath the water table.

The large lateral variability of heat flow over distances of one or two kilometers suggests a relatively shallow, hydrologic source for the observed anomaly, primarily convection in the saturated tuffs and underlying carbonate rocks. Confirmation of this hypothesis or the identification of an alternative will require additional thermal and hydrologic data of higher quality than are currently available.

In summary, the thermal regime of the Yucca Mountain area, based on the data available, seems similar to that of the Eureka Low, a regional heat-flow anomaly of hydrologic origin defined by Sass and others (1971). The large, systematic lateral variations of heat flow in both saturated and unsaturated zones, coupled with thermal and hydrologic indications of vertical head gradients, indicate a complex local hydrologic regime superimposed on the regional interbasin flow in the Paleozoic carbonate rocks.

The quality of the presently available data set does not allow an unambiguous interpretation of heat-flow data from either the UZ or the SZ. Some of the apparent hydrologic activity in the upper part of the SZ could be limited to the annulus between casing and the borehole wall, where water will respond readily to small head differences owing to the high transmissivity of the annulus. The ambiguity can be resolved only by completing some of the presently planned wells with access pipes grouted into place. It will be necessary to have water-filled pipes (also preferably with annulus grouted) to

characterize adequately the thermal state of the UZ. We also encourage thermal measurements in conjunction with hydrologic testing, particularly to correct for water density as a routine part of water-level measurements for the purpose of detecting head variations with depth.

References

Benson, L. V., Robison, J. H., Blankennagel, R. K., and Ogard, A. E., 1983, Chemical composition of ground water and the locations of permeable zones in the Yucca Mountain area, Nevada: U.S. Geological Survey Open-File Report 83-854, 19 p.

Carr, M. D., Waddell, S. J., Vick, G. S., Stock, J. M., Monsen, S. A., Harris, A. G., Cork, B. W., and Byers, F. M., Jr., 1986, Geology of drill hole Ue25p#1: A test hole into pre-Tertiary rocks near Yucca Mountain, southern Nevada: U.S. Geological Survey Open-File Report 86-175, 87 p.

Carr, W. J., and Rogers, A. M., 1983, Tectonics, seismicity, and volcanism of the southern Great Basin, in U.S. Geological Survey Research in Radioactive Waste Disposal--Fiscal Year 1981: U.S. Geological Survey Water Resources Investigations Report 83-4105.

Craig, R. W., and Robison, J. H., 1984, Geohydrology of rocks penetrated by test well UE-25p#1, Yucca Mountain area, Nye County, Nevada: U.S. Geological Survey Water-Resources Investigations Report 84-4248, 57 p.

Crowe, B. M., Amos, R., Perry, F., Self, S., and Vaniman, D. T., 1983, Aspects of potential magmatic disruption of a high-level radioactive waste repository in southern Nevada: *Journal of Geology*, v. 91, p. 259-276.

Czarnecki, J. B., 1984, Simulated effects of increased recharge on the ground-water flow system of Yucca Mountain and vicinity, Nevada-California: U.S. Geological Survey Water-Resources Investigations Report 84-4344, 33 p.

Czarnecki, J. B., and Waddell, R. K., 1984, Finite-element simulation of ground-water flow in the vicinity of Yucca Mountain, Nevada-California: U.S. Geological Survey Water-Resources Investigations Report 84-4349, 38 p.

Goss, R., and Combs, J., 1975, Thermal conductivity measurement and prediction from geophysical well log parameters with borehole application, in United Nations Symposium on the Development and Use of Geothermal Resources, 2nd, San Francisco, CA, May 20-29, 1975, Proceedings, v. 2: Lawrence Berkeley Lab., Univ. of California, p. 1019-1027.

Lachenbruch, A. H., 1958, Thermal measurements in Oak Springs formation, in Properties of Oak Spring Formation in Area 12 at the Nevada Test Site, edited by W. H. Diment and others: U.S. Geological Survey Open-File Report (TEI 672, Chapter 11).

Lachenbruch, A. H., Marshall, B. V., and Roth, E. F., 1987, Thermal measurements in Oak Springs formation at the Nevada Test Site, southern Nevada: U.S. Geological Survey Open-File Report 87-610, 19 p.

Lachenbruch, A. H., and Sass, J. H., 1977, Heat flow in the United States and the thermal regime of the crust, in The Earth's Crust, edited by J. G. Heacock, Geophysical Monograph 20, p. 626-675: American Geophysical Union, Washington, D. C.

Mase, C. W., Sass, J. H., Lachenbruch, A. H., and Munroe, R. J., 1982, Preliminary heat-flow investigations of the California Cascades: U.S. Geological Survey Open-File Report 82-150, 240 p.

Montazer, P., and Wilson, W. E., 1984, Conceptual hydrologic model of flow in the unsaturated zone, Yucca Mountain, Nevada: U.S. Geological Survey Water-Resources Investigations Report 84-4345, 55 p.

Muller, D. C., and Kibler, J. E., 1984, Preliminary analysis of geophysical logs from drill hole UE-25p#1, Yucca Mountain, Nye County, Nevada: U.S. Geological Survey Open-File Report 84-649.

Robison, J. H., 1984, Ground-water level data and preliminary potentiometric-surface maps of Yucca Mountain and vicinity, Nye County, Nevada: U.S. Geological Survey Water-Resources Investigations Report 84-4197, 8 p.

Sass, J. H., Blackwell, D. D., Chapman, D. S., Costain, J. K., Decker, E. R., Lawver, L. A., and Swanberg, C. A., 1981, Heat flow from the crust of the United States, in Touloukian, Y. S., Judd, W. R., and Roy, R. F., editors, Physical Properties of Rocks and Minerals: McGraw-Hill, New York, p. 503-548, 1981.

Sass, J. H., Kennelly, J. P., Smith, E. P., and Wendt, W. E., 1984, Laboratory line-source methods for the measurement of thermal conductivity of rocks near room temperature: U.S. Geological Survey Open-File Report 84-91, 21 p.

Sass, J. H., and Lachenbruch, A. H., 1982, Preliminary interpretation of thermal data from the Nevada Test Site: U.S. Geological Survey Open-File Report 82-973, 30 p.

Sass, J. H., Lachenbruch, A. H., and Mase, C. W., 1980, Analysis of thermal data from drill holes UE25a-3 and UE25a-1, Calico Hills and Yucca Mountain, Nevada Test Site: U.S. Geological Survey Open-File Report 80-826, 25 p.

Sass, J. H., Lachenbruch, A. H., Munroe, R. J., Greene, G. W., and Moses, T. H., Jr., 1971, Heat flow in the western United States: Journal of Geophysical Research, v. 76, p. 6376-6413.

Spengler, R. W., and Chornack, M. P., 1984, Stratigraphic and structural characteristics of volcanic rocks in core hole USW G-4, Yucca Mountain, Nye County, Nevada, with a section on Geophysical logs by D. C. Muller and J. E. Kibler: U.S. Geological Survey Open-File Report 84-789, 77 p.

Spengler, R. W., and Rosenbaum, J. G., 1980, Preliminary interpretations of geologic results obtained from boreholes Ue25a4, -5, -6, and -7, Yucca Mountain, Nevada Test Site: U.S. Geological Survey Open-File Report 80-929, 39 p.

Swanberg, C. A., and Morgan, P., 1978, The linear relation between temperature based on the silica content of groundwater and regional heat flow: A new heat flow map of the United States: Pure and Applied Geophysics, v. 117, p. 227-241.

U.S. Geological Survey, 1986, Quality Assurance Program Plan for Nevada Nuclear Waste Storage Investigations NNWSI-USGS-QAPP-01, R3.

Waddell, R. K., Robison, J. H., and Blankennagel, R. K., 1984, Hydrology of Yucca Mountain and vicinity, Nevada-California--Investigative results through mid-1983: U.S. Geological Survey Water-Resources Investigations Report 84-4267.

Winograd, I. J., and Thordarson, W., 1975, Hydrogeologic and hydrochemical framework, South-Central Great Basin, Nevada-California, with special reference to the Nevada Test Site: U.S. Geological Survey Professional Paper 712-C, C1-C126.

APPENDIX 1. Temperature logs from geologic and hydrologic test wells,
Yucca Mountain

A series of precise temperature logs was obtained from all available wells at the Yucca Mountain site. This appendix contains the latest temperature logs together with time series for wells that have been logged more than once.

NOTES ON PRESENTATION OF DATA

Temperature-depth profiles for all logs are displayed as a time-series. The leftmost profile is the earliest. Later profiles are identified by month and year and are stepped to the right by a sufficient amount relative to the first curve (shown after the date in °C) to separate data from successive logs. All measurements made in air in the unsaturated zone are indicated as discrete symbols joined by straight lines. Where appropriate, the static water level (SWL) is indicated by a horizontal line. It should be noted that this is the level measured by us at the time of the temperature log, and in some instances, it is different from that listed in other publications (e.g., Robison, 1984).

THE CONDUCTOR WELLS

This series of four shallow wells was originally drilled to investigate a geoelectric anomaly within the unsaturated zone in Drill Hole Wash. All but one (UE25a-6) were drilled within the main drainage of the wash (Figure 2). The wells were drilled with mud and water and considerable fluid loss occurred. Early logs showed some quite bizarre departures from the linear temperature profiles characteristic of steady-state one-dimensional heat flow, including temperature reversals (Figures 1-2, through 1-5). Most of the

reversals and high-frequency noise did decay conductively with time, indicating that they were drilling-related. There remain, however, irregularities and large contrasts in thermal gradient that cannot be explained by pure conduction, and must be associated with vertical and lateral movement of fluids (air, water vapor and liquid water) within the unsaturated zone in Drill Hole Wash.

UE25a4 and 5 were not available for logging after December 1981 so that we show only the time series ending then (Figures 1-2 and 1-3). The most prominent steady-state anomalies are the large changes in gradient in the 75-100 m depth range.

UE25a6 which is sited above the main surface drainage of Drill Hole Wash and is close to USWG4, the site of the exploratory shaft (Figure 2), does not show this gradient break and has an average gradient of about $25^{\circ}\text{C km}^{-1}$ below 55 m (Figure 1-4). The time series for UE25a6 is a good example of the conductive decay of thermal transients resulting from the loss of drilling fluid. Temperatures in Ue25a7 (Figure 1-5) still indicate considerable disturbance. In fact, above 150 m, the latest two logs show a remarkable resemblance to the first log made in March 1981. By contrast, temperature disturbances below a vertical depth of 150 m appear to be decaying conductively. We know of no renewed circulation of fluids in this well after December 1981. We can speculate that the remarkable change in the temperature profile above 150 m was the result of lateral water movement in fractures in densely welded tuff of the Topopah Spring Member (Spengler and Rosenbaum, 1980) below the main drainage of Drill Hole Wash, arising from a major storm that occurred a week or so before the March 1983 log was obtained.

UE25b1H. This well is also collared near the main surface drainage of Drill Hole Wash (Figure 2) and some degree of disturbance to the temperature field is evident in the unsaturated zone. Between 610 and 869 m (Figure 1-6), the profile is nearly isothermal and suggests lateral flow with both upward (concave downward) and downward (concave upward) components of water flow over different depth-intervals. Below a depth of 1 km, the profile is linear with a gradient of about $23^{\circ}\text{C km}^{-1}$, possibly indicating conductive heat flow. Temperature profiles from Ue25a1, which was drilled on the same pad are presented in Figure 1-7.

UE29a2. UE29a2 is shown on the index map (Figure 1). It is located some 10 km NW of USWG2 near the main surface drainage of Forty-Mile Wash. Static water level was just below 30 m below which temperatures increased very slightly ($\sim 10^{\circ}\text{C km}^{-1}$) to a depth of nearly 90 m (Figure 1-8) whereupon there was a reversal and erratic temperature variations to the total accessible depth of 168 m. It would appear that the thermal regime at this site is dominated by lateral water movement below Forty-Mile Wash with just over 0.5°C variation in temperature in the accessible portion of the hole.

The "G" Series, Yucca Mountain. These wells were drilled primarily to obtain geologic data, although considerable hydrologic and other information also was obtained from them. They generally were completely cored to allow for detailed studies of lithology, fracture density, and physical properties. We have made thermal conductivity measurements in all of them (see Appendix 3).

USW G-1. Hole G1 has been instrumented by Sandia Corporation and is unavailable for temperature measurements. For completeness sake, we include here the time series comprising complete logs in September 1980 and April 1981 (Figure 1-9). Temperature gradients (which unfortunately had not reached equilibrium by the time of our last log) increase systematically to

1 km or so whereupon they become essentially constant at about $30^{\circ}\text{C km}^{-1}$ yielding a mean heat flux of about 53 mWm^{-2} below 1 km (see Table 2, Sass and Lachenbruch, 1982). Our preliminary interpretation involved downward vertical water movement with seepage velocity of $\sim 1 \text{ cm/y}$ to depths of 2 to 2.5 km, an interpretation that ignores the essentially constant heat flow below 1.1 km in this well but accounts for its anomalously low value.

USW G-2: Temperatures to about 600 m are similar to those in G1 and other deep wells in the area. There is then a step rise in temperatures (Figure 1-10) followed by about 150 m that is nearly isothermal whereupon a quasi-conductive gradient is established to total depth of 1250 m. The least-squares gradient between 800 and 1250 m is about $41 \pm 0.1^{\circ}\text{C km}^{-1}$ which, when combined with the average thermal conductivity of $1.74 \pm 0.04 \text{ Wm}^{-1} \text{ K}^{-1}$, yields a typical Basin and Range heat flux of 71 mWm^{-2} in contrast with the heat flow of 44 mWm^{-2} from the unsaturated zone. Taken literally, this would support our one-dimensional interpretation of high ($\sim 20 \text{ mm/yr}$) rates of downward percolation of groundwater or lower rates combined with vaporization in the unsaturated zone. The high gradient may, however, reflect the anomalously low temperature boundary at 760 m brought on by water moving vertically downward from 600 to 750 m or laterally with a downward component of velocity. An alternative gradient can be obtained by joining the top edge of the "stairstep" at $\sim 600 \text{ m}$ to the bottom-hole temperature. This gradient ($31^{\circ}\text{C km}^{-1}$) yields a heat flow of 54 mWm^{-2} .

USW G-3. This is the most southerly of three wells drilled on the steep ridge immediately to the west of Drill Hole Wash. The water table here is exceptionally deep (Figure 1-11). Below the water table, the temperature profile shows evidence for upward and downward water movement over different intervals. The linear part of the profile between about 1000 and

1280 m has a thermal gradient of about $21^{\circ}\text{C km}^{-1}$. For a mean conductivity in the saturated zone of $1.58 \pm 0.05 \text{ Wm}^{-1} \text{ K}^{-1}$ (25 samples), we estimate a heat flux of 33 mWm^{-2} .

USW G-4. G4 is the most recently completed well and is the proposed site of the exploratory shaft. The temperature gradient (Figure 1-12) increases from about $18^{\circ}\text{C km}^{-1}$ between 150 and 400 m to about $30^{\circ}\text{C km}^{-1}$ between 400 and 536 m (approximate water table). The profile below the water table is nonconductive and is consistent with an upward component of water movement from near the bottom of the well, exiting near the water table.

The "H" series, Yucca Mountain. By contrast with the previous series with which it is interspersed (Figure 2), these wells were drilled primarily for hydrologic studies. As such, they have larger diameters, typically contain a number of piezometer tubes, and have a very limited amount of core available for properties measurements. Between our November 1982 and March 1983 loggings, all of these sites (except H1) were reoccupied and packers were set near the bottom to aid in the estimation of head gradients.

USW H-1. This well is only about 0.5 km WSW of G1 (Figure 2), and it has a similar temperature profile with the exception of the lowermost 150 m. Below 1680 m, the gradient decreases systematically from ~ 30 to less than $20^{\circ}\text{C km}^{-1}$ (Figure 1-13). A piezometer was grouted in to nearly total depth in September(?) of 1982. Post-grout profiles show very little change from pre-grout (Figure 1-13) indicating that water is probably moving upward in the formation in this interval.

USW H-3. The temperature gradient in USWH3 between 975 and 1190 m averages about $19^{\circ}\text{C km}^{-1}$, similar to that observed in the linear portion of USWG3. H3 is about 1.5 km north of G3 on the west ridge of Yucca Mountain

(Figure 2). The temperature profiles (Figure 1-14) illustrate once more the great depth to the water table and the abnormally low thermal gradients found on the ridge.

USW H-4. H4 is located on the flank of the west ridge on one of the eastward drainages (Figure 2). The thermal profile becomes linear and apparently conductive below 1 km (Figure 1-15) with a value of $25.5\text{ }^{\circ}\text{C km}^{-1}$.

USW H-5. This well is the northernmost of the three deep wells on the ridge. Characteristically, the water table is very deep and non-conductive processes predominate to a depth of over 1 km (Figure 1-16). Below this depth, there is a quasi-linear profile with gradient of $28.5\text{ }^{\circ}\text{C km}^{-1}$; the average gradient below the static water level is $\sim 15^{\circ}\text{C km}^{-1}$.

USW H-6. H6 is located on the west and slightly south of H5 in a subsidiary drainage northwest of Crater Flat (Figure 2). Because of its lower elevation, the static water level is higher than for G3, H3, and H5 on the ridge (compare Figures 1-16 and 1-17). Below 880 m, the temperature profile is essentially conductive, with a gradient of $36^{\circ}\text{C km}^{-1}$.

J-13. Well J-13 (formerly Test Well 6) was drilled in Forty-Mile Wash and is used as a water supply well. Below the water table (Figure 1-18), the profile shows signs of hydrologic disturbance. The gradient in the unsaturated zone was used by Sass and others (1971) to calculate a heat flow of 67 mWm^{-2} .

UE25P1. Well UE25P1 was drilled to test a basement high of Paleozoic carbonate rocks. Below the water table (Figure 1-19) the thermal regime is complex and appears dominated by lateral water flow or possibly by vertical flow within the well.

USW VH-1 and VH-2. These two wells are located in Crater Flat (Figure 1) near two Holocene cinder cones. Equilibrium temperature profiles

for both wells (Figures 1-20 and 1-21) indicate a thermal regime dominated by lateral water movement having both upward and downward vertical components. Particularly puzzling is the fact that, even though they are similar in character, the profile in VH-1 is consistently warmer by about 5°C than that in VH-2 (Figure 1-22). This indicates strong lateral gradients between the two wells. In fact, the range of temperatures in VH-2 is very similar to that in USW-H6 which is 330 m higher in elevation (Figure 1-22). This, in turn, suggests that VH-2 is in a region of net downward water flow rather than VH-1 being anomalously hot.

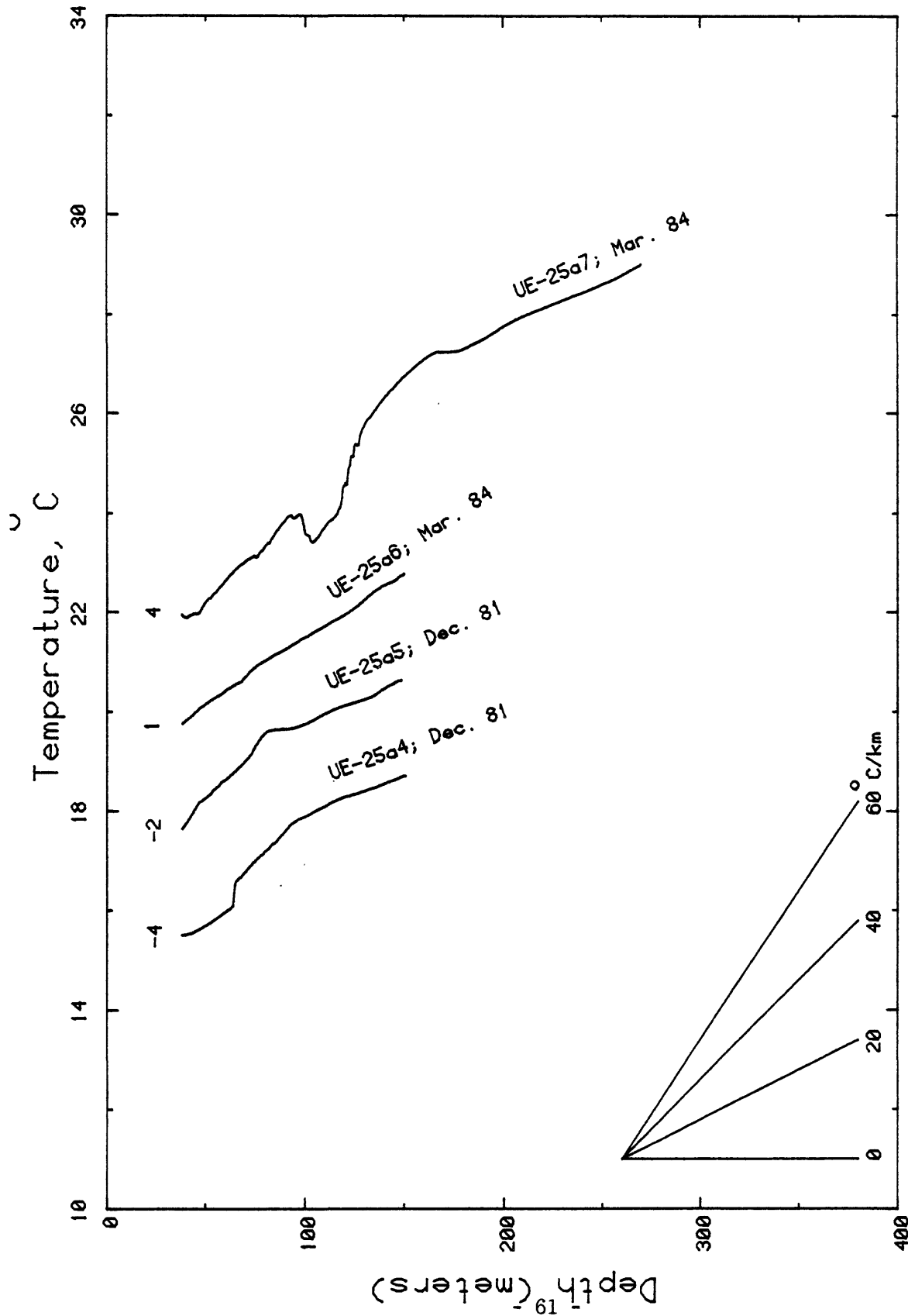


Figure 1-1. Most recent temperature logs from the "conductor" wells. Numbers near the top of each profile indicate the rightward shift of the profile relative to the temperature axis.

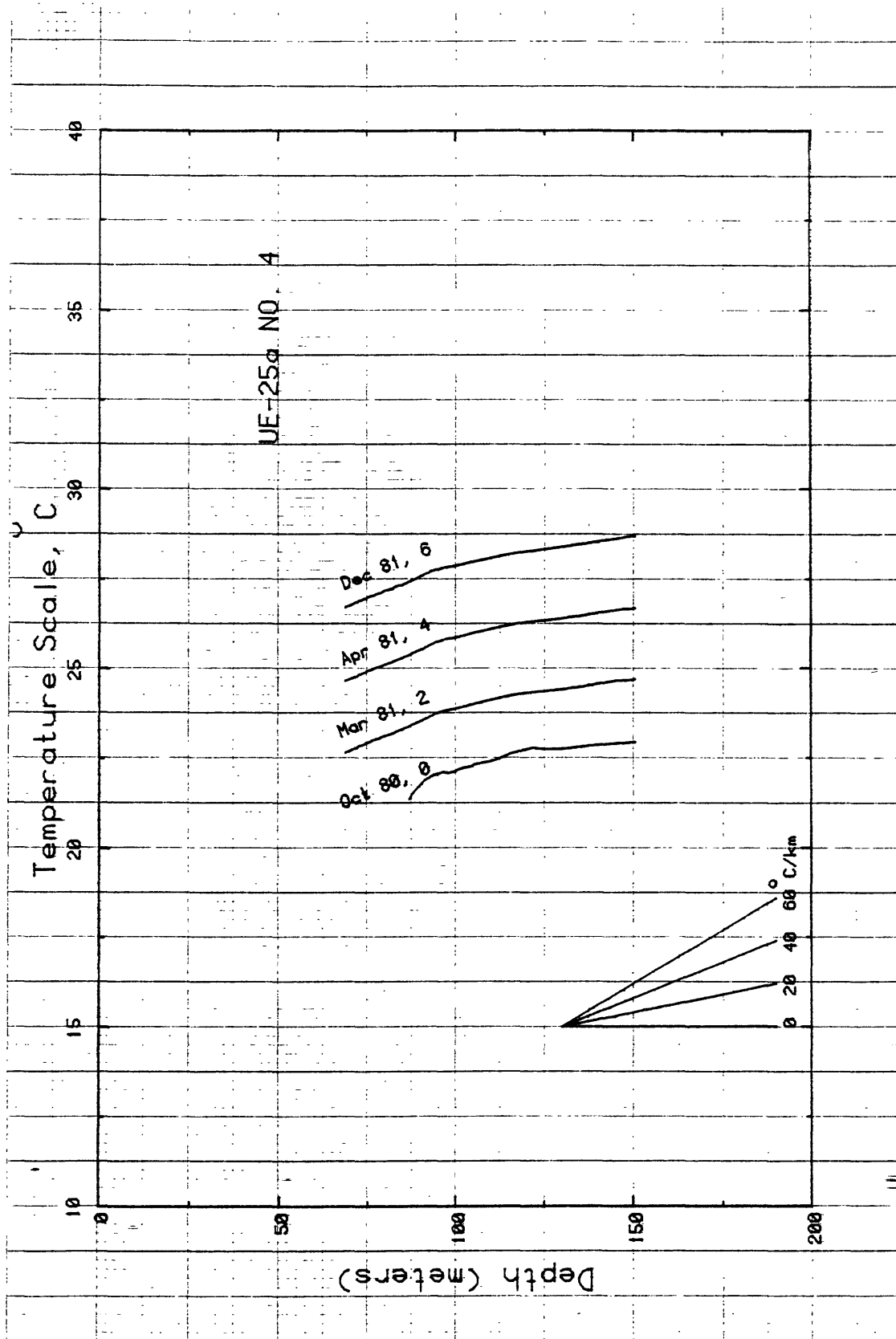


Figure 1-2. Temperature logs from Ue25a4. Numbers after date indicate rightward shift of profile relative to temperature axis.

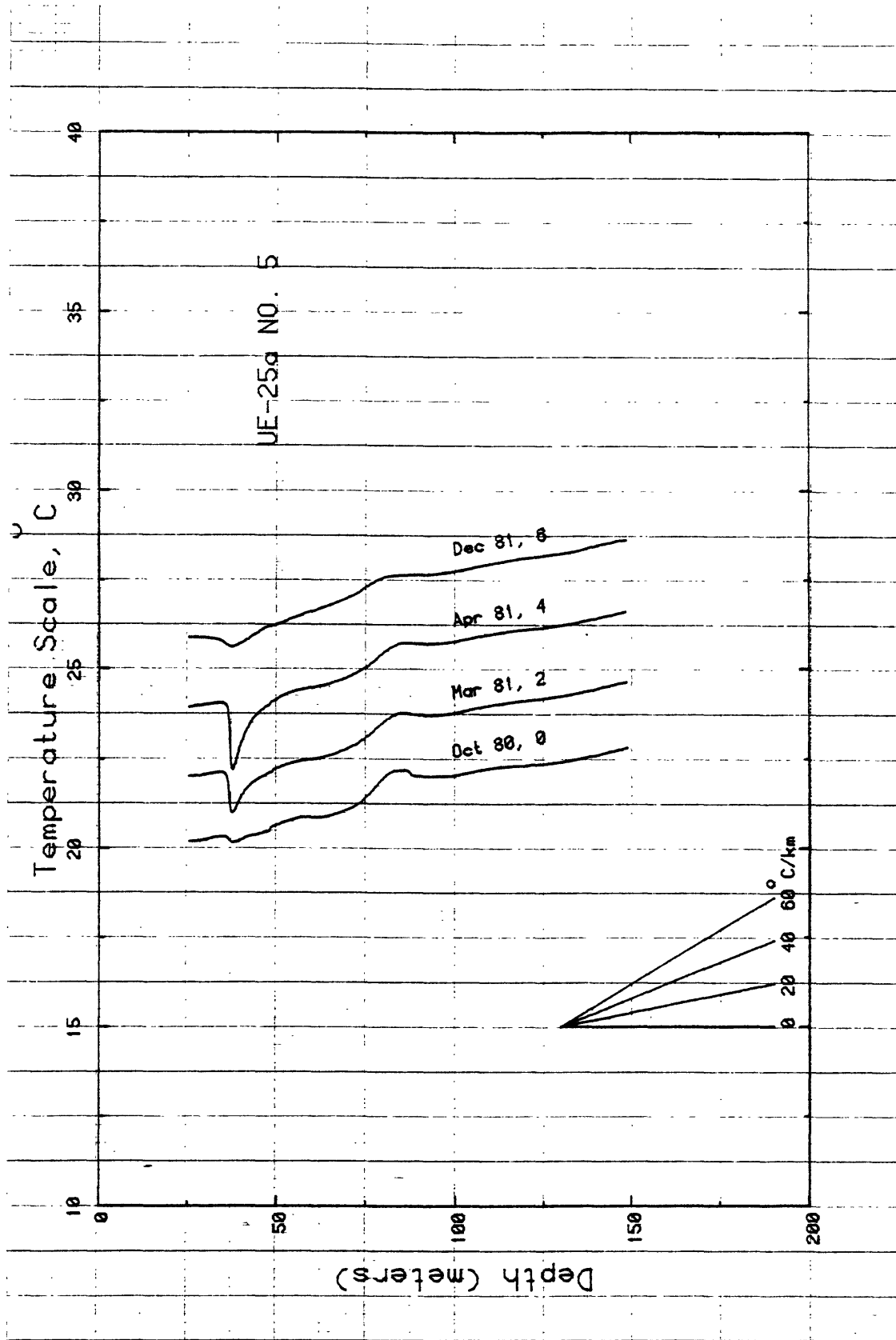


Figure 1-3. Temperature logs from Ue25a5. Numbers after date indicate rightward shift of profile relative to temperature axis.

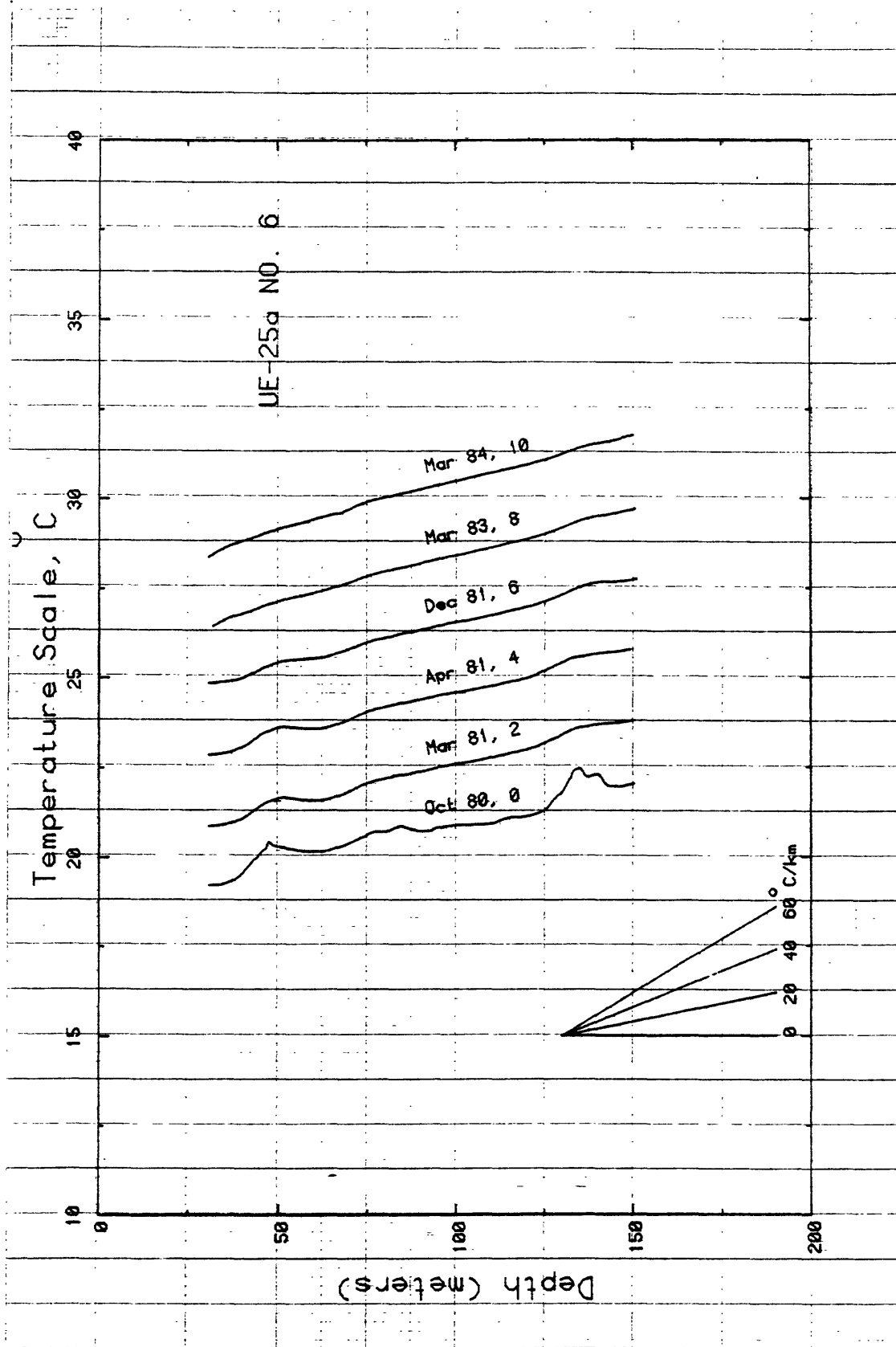


Figure 1-4. Temperature logs from Ue25a6. Numbers after date indicate rightward shift of profile relative to temperature axis.

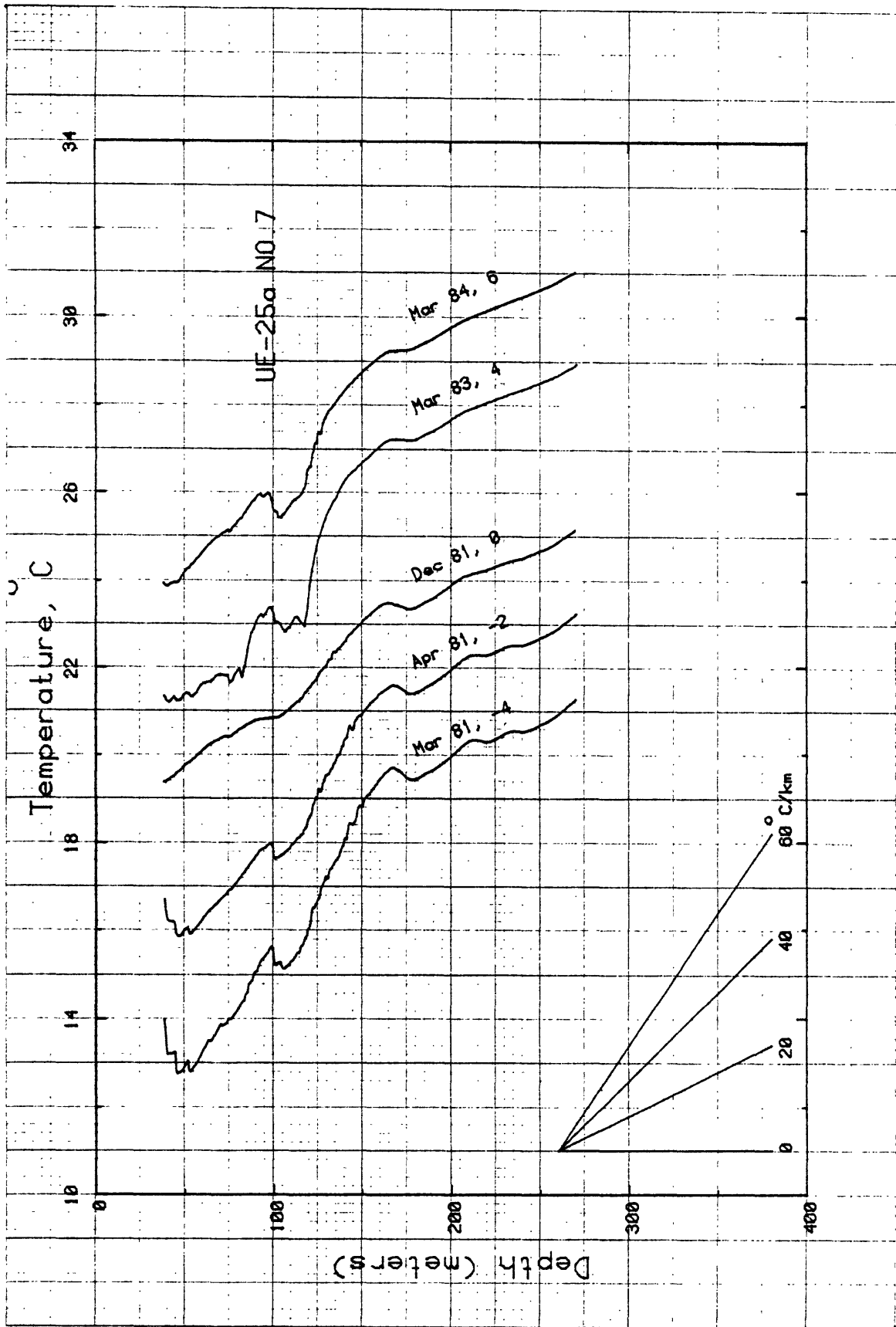


Figure 1-5. Temperature logs from Ue25a7. Numbers after date indicate rightward shift of profile relative to temperature axis.

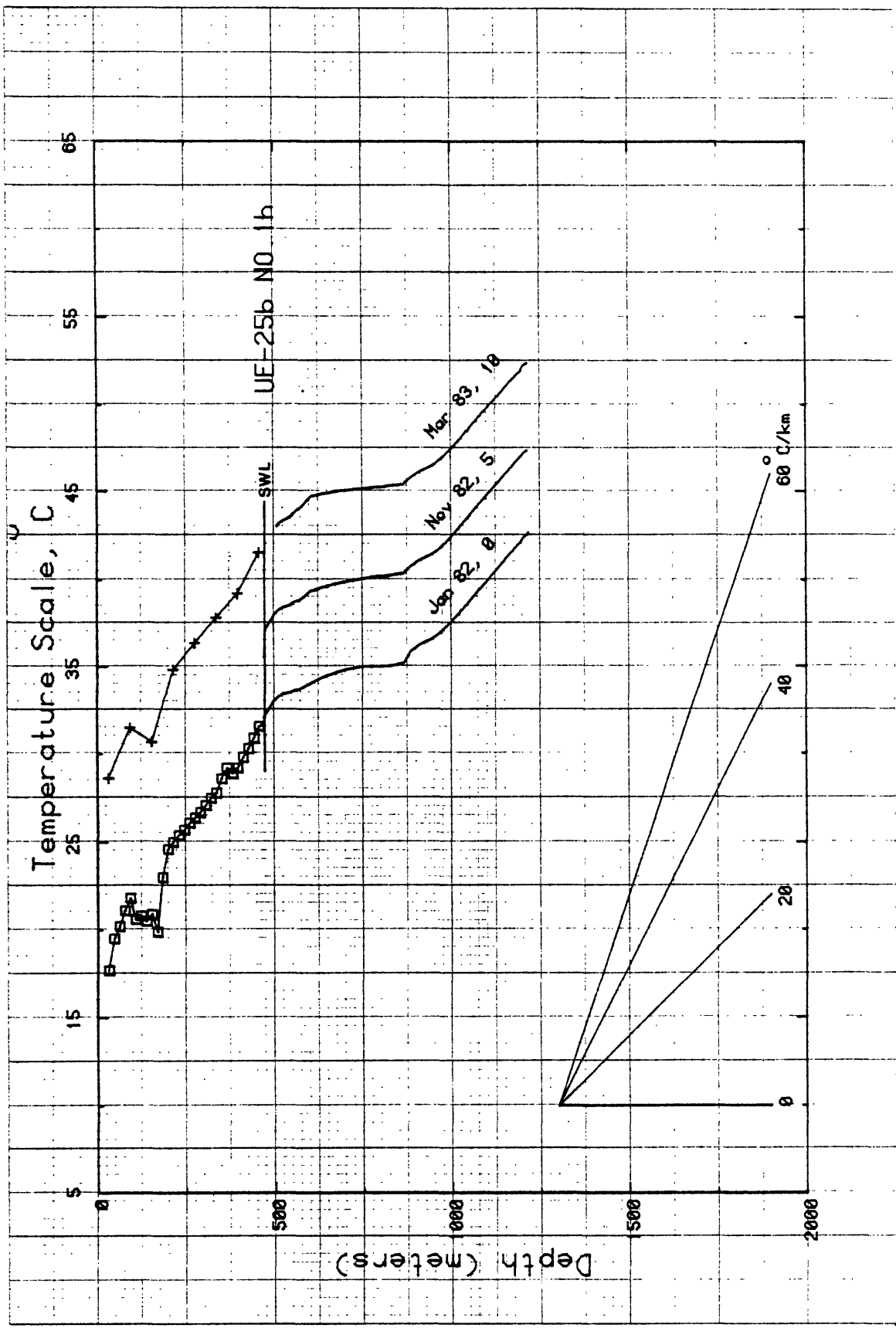


Figure 1-6. Temperature logs from Ue25blh. Numbers after date indicate rightward shift of profile relative to temperature axis. SWL is static water level.

TELETYPE INFORMATION DISPLAY DIVISION 006-1098-00 10 x 75 M. LINEAR

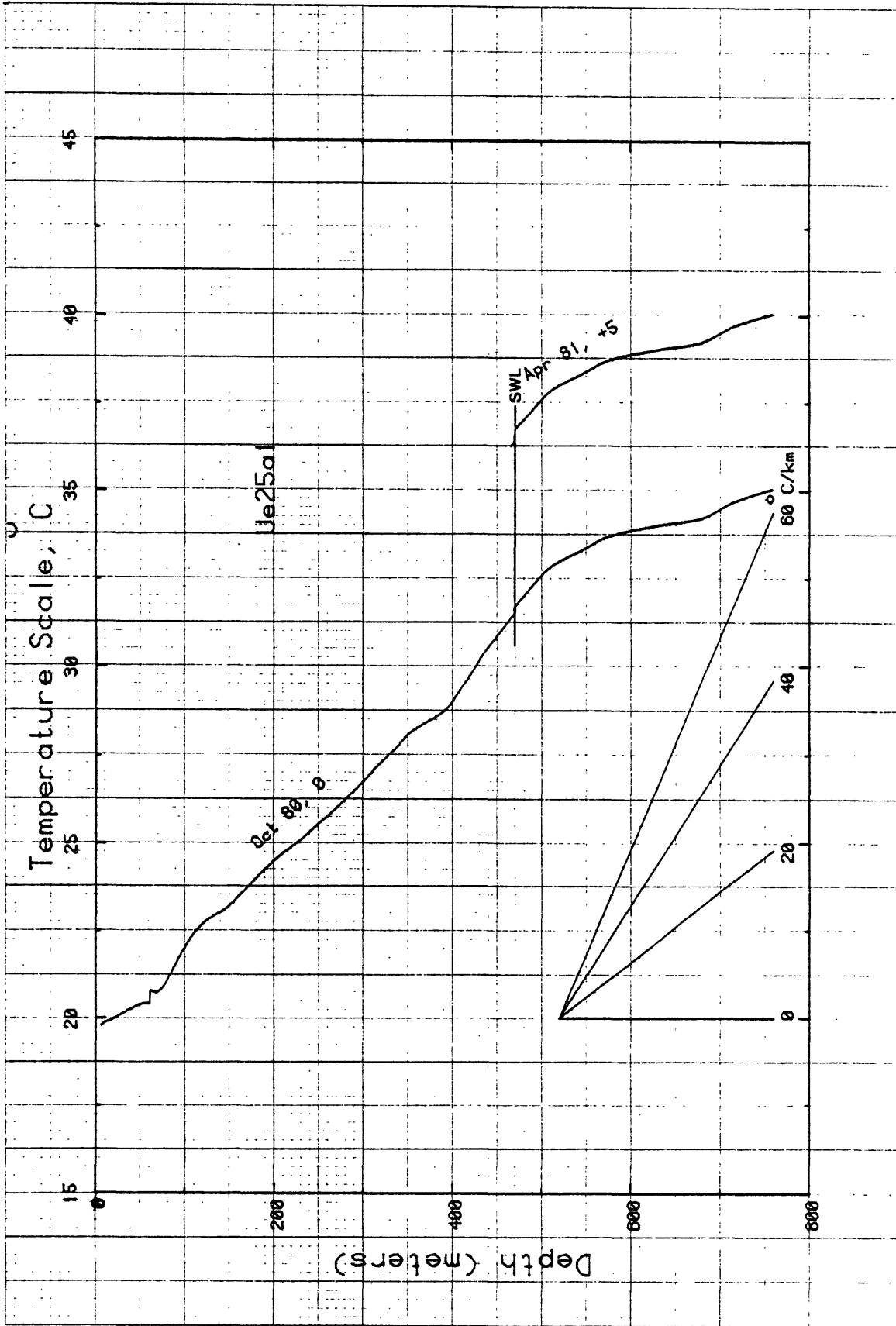


Figure 1-7. Temperature logs from Ue25a1. Numbers after date indicate rightward shift of profile relative to temperature axis. SWL is static water level.

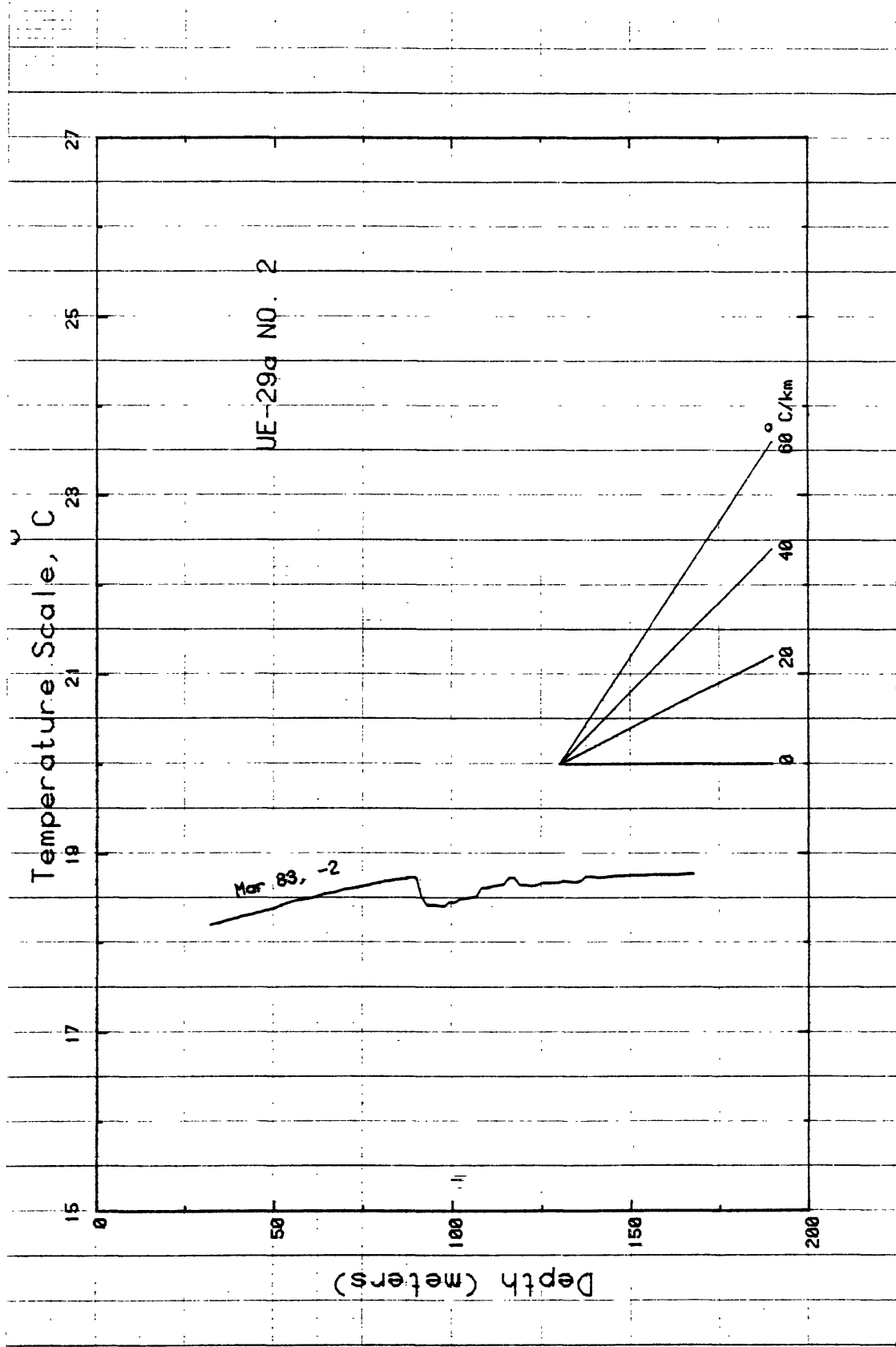


Figure 1-8. Temperature log for U-29a2.

SE ROA 38227

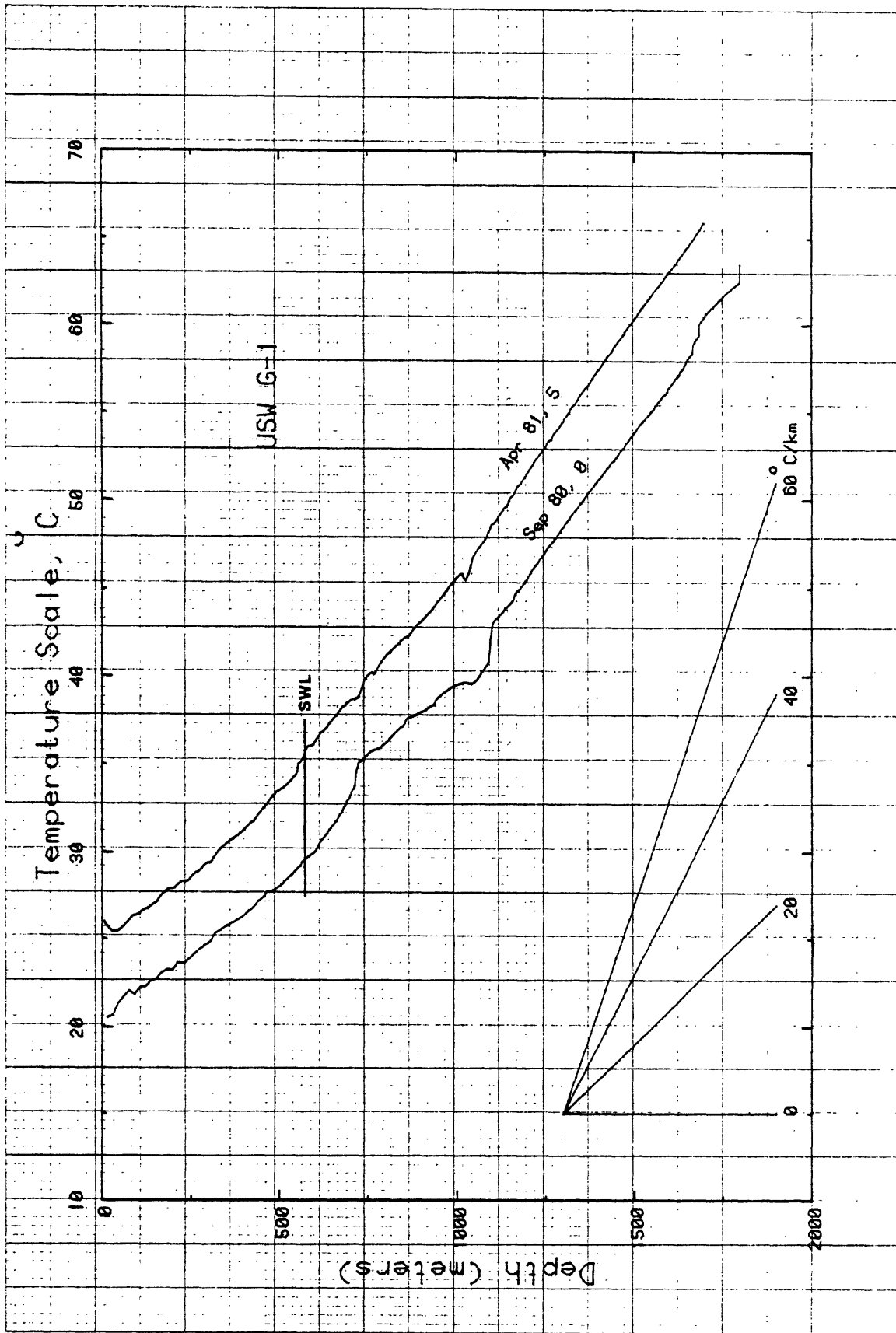


Figure 1-9. Temperature logs from USWG-1. Numbers after date denote the number of °C by which the profile is shifted to the right relative to the temperature axis. SWL is static water level.

TEKTRONIX INFORMATION DISPLAY DIVISION 0081688-00 10 x 15 IN. LINEAR

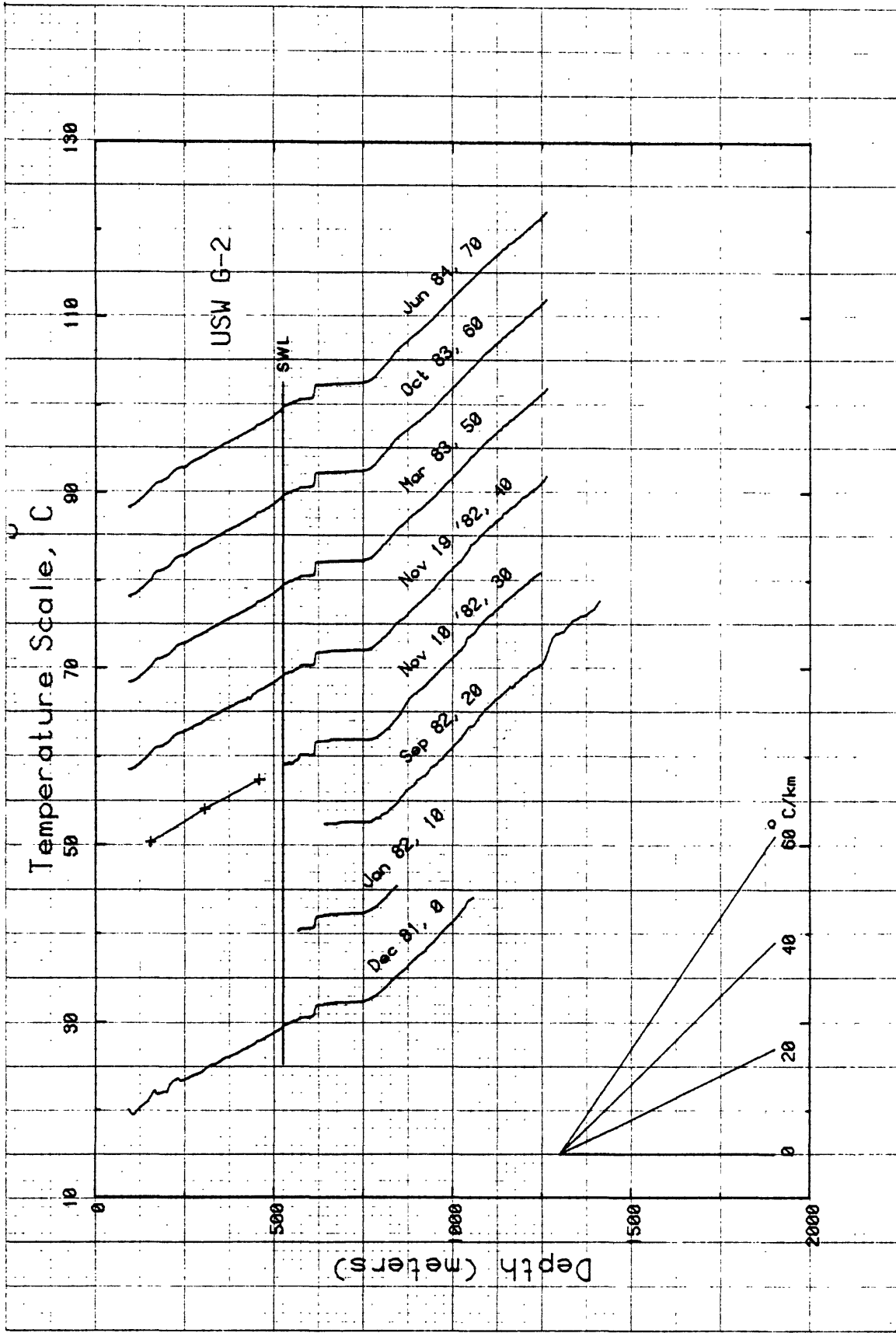


Figure 1-10. Temperature logs from USW G-2. Number after date denotes the amount of rightward shift relative to the temperature axis. SWL is static water level.

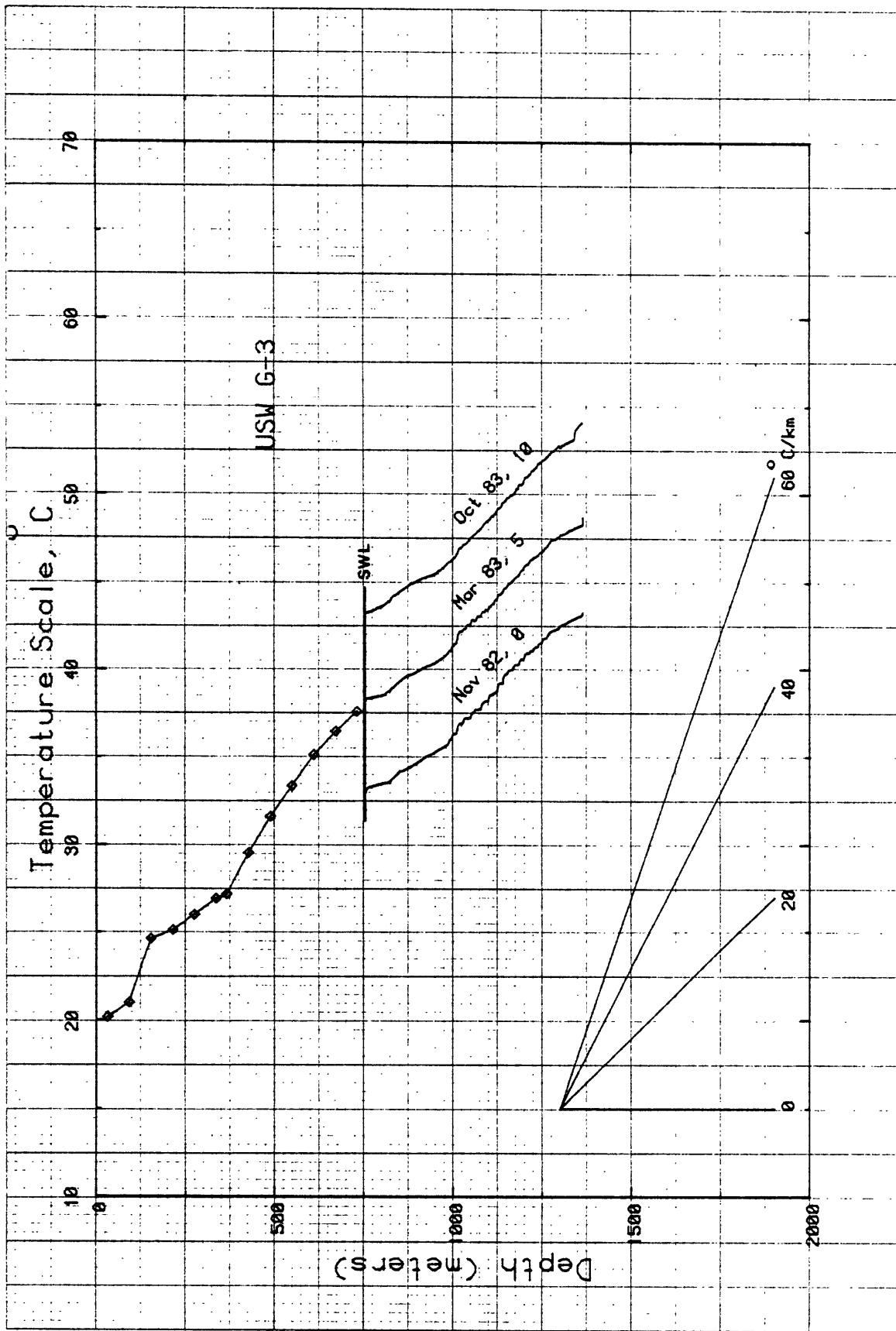


Figure 1-11. Temperature logs for USW G-3. Number after date denotes the amount by which profile is shifted to the right relative to the temperature axis. SWL is static water level.

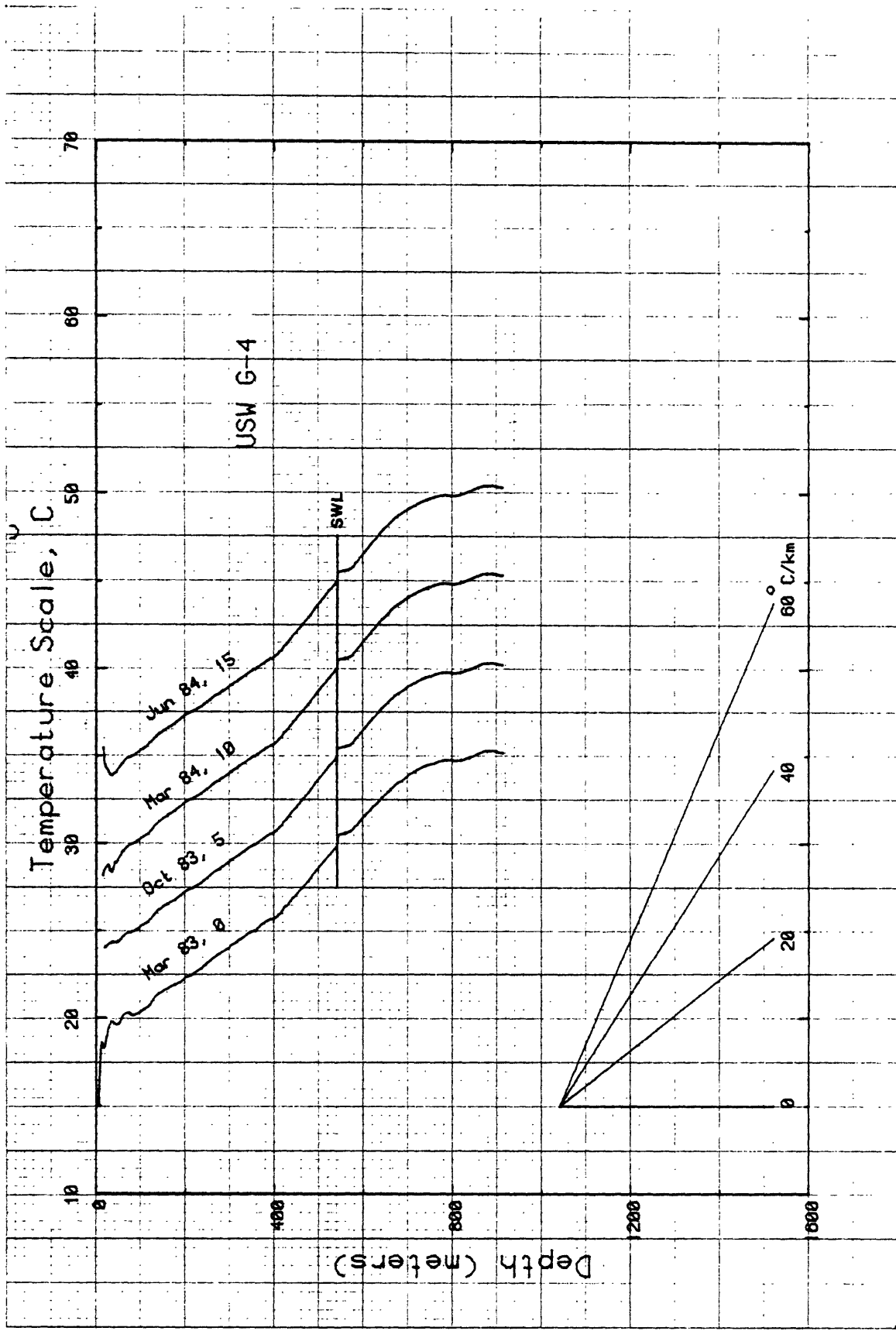


Figure 1-12. Temperature profiles from USW G-4. Number after date denotes the amount of rightward shift (in °C) relative to the temperature axis. SWL is static water level.

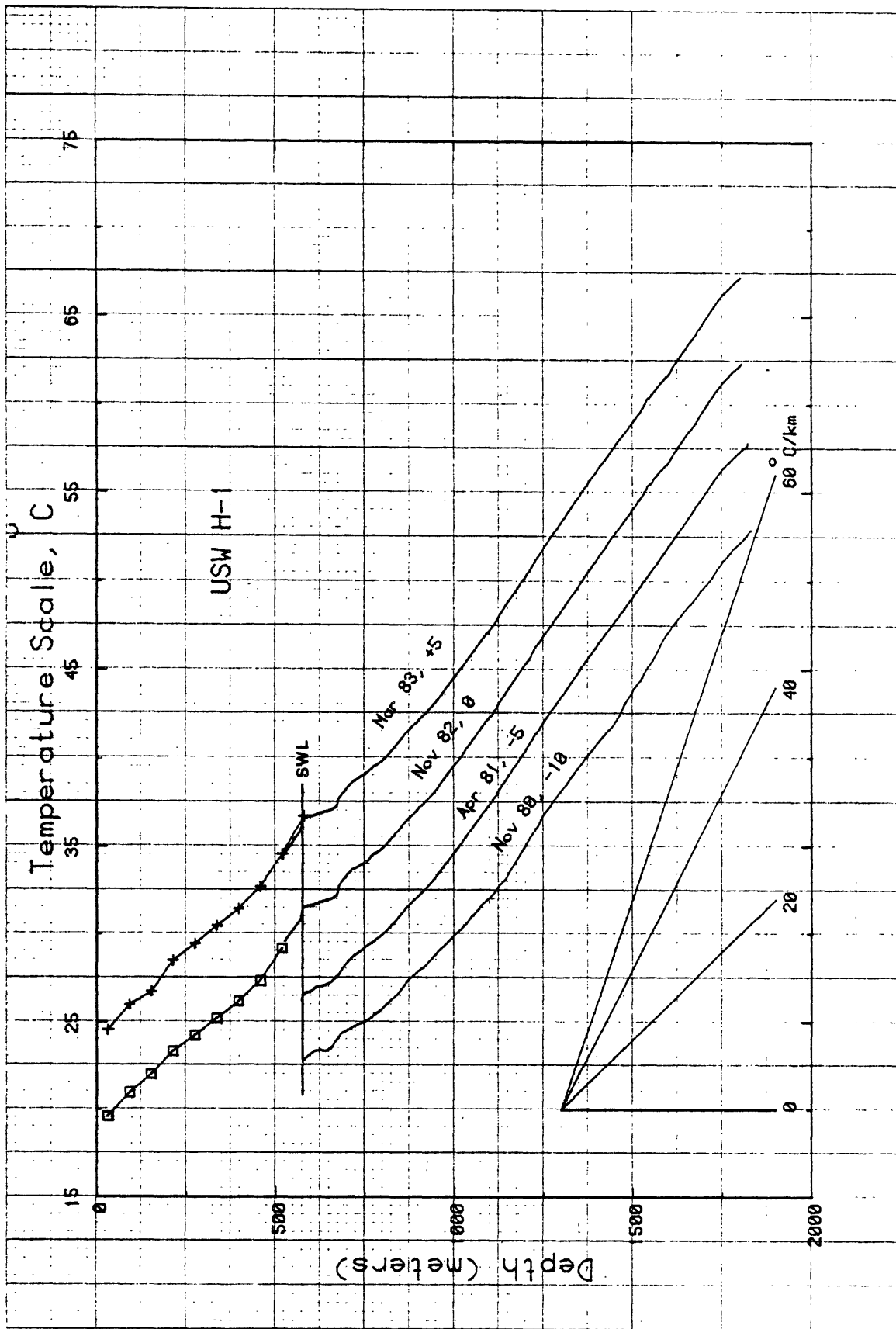


Figure 1-13. Temperature profiles from USW H-1. Number after date indicates the rightward (leftward if negative) shift of the profile relative to the temperature axis. SWL is static water level.

TELETYPE INFORMATION DISPLAY DIVISION 006 1698 00 70 x 15 M. LINEAR

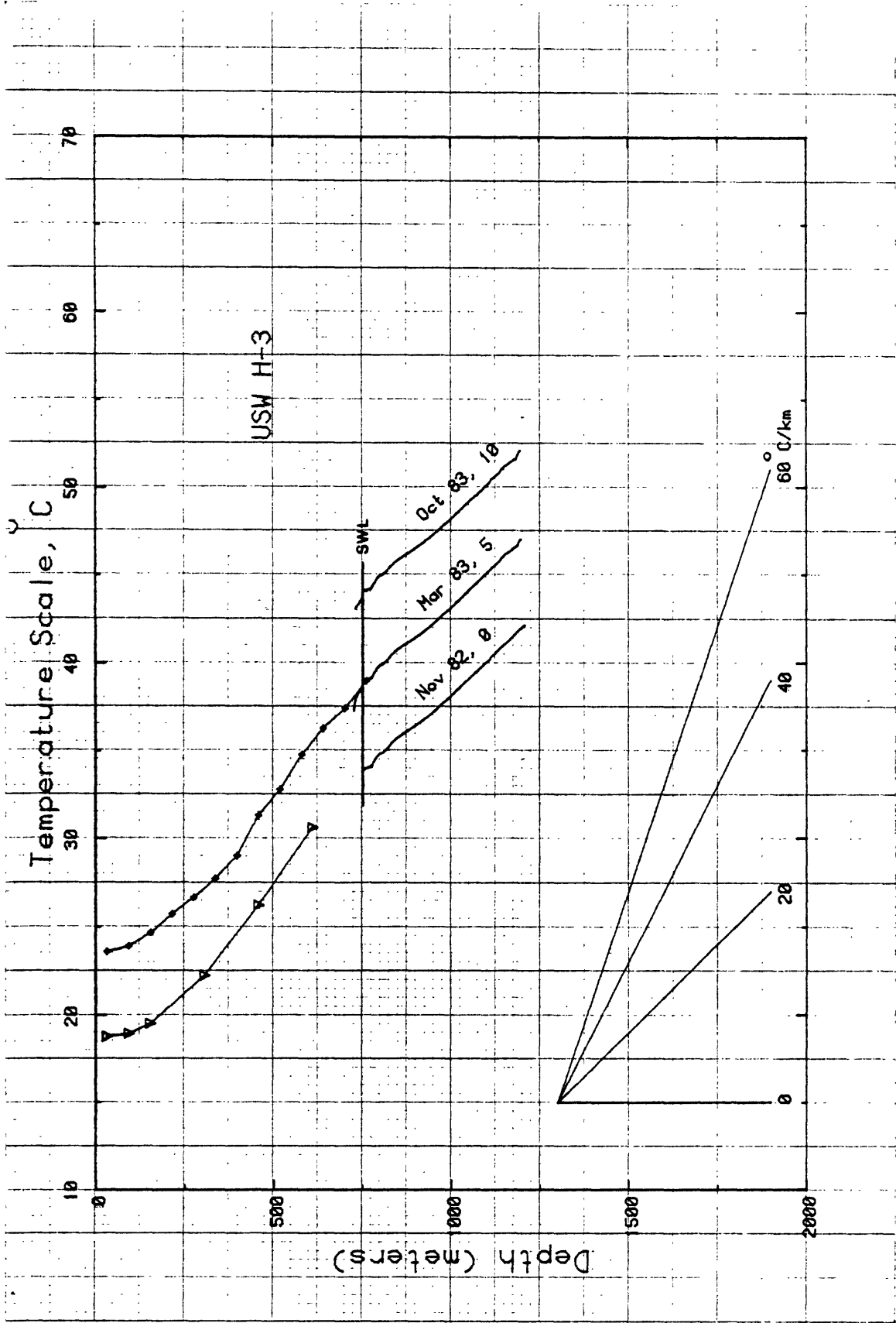


Figure 1-14. Temperature logs in USW H-3. Number after date denotes rightward shift of a profile relative to the temperature origin. SWL is static water level.

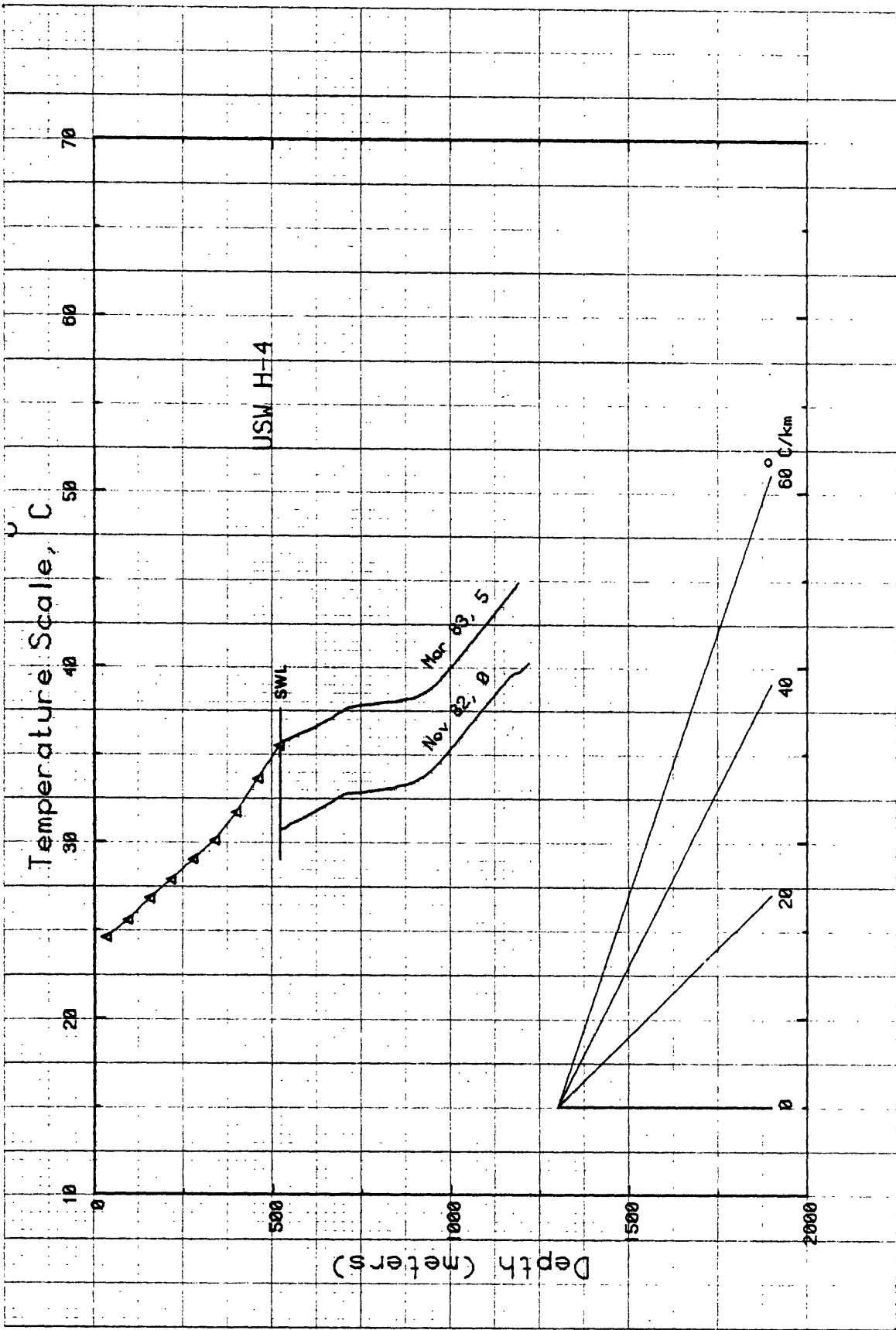


Figure 1-15. Temperature profiles for USW H-4. Number after date represents the rightward shift of the profile relative to the temperature origin. SWL is static water level.

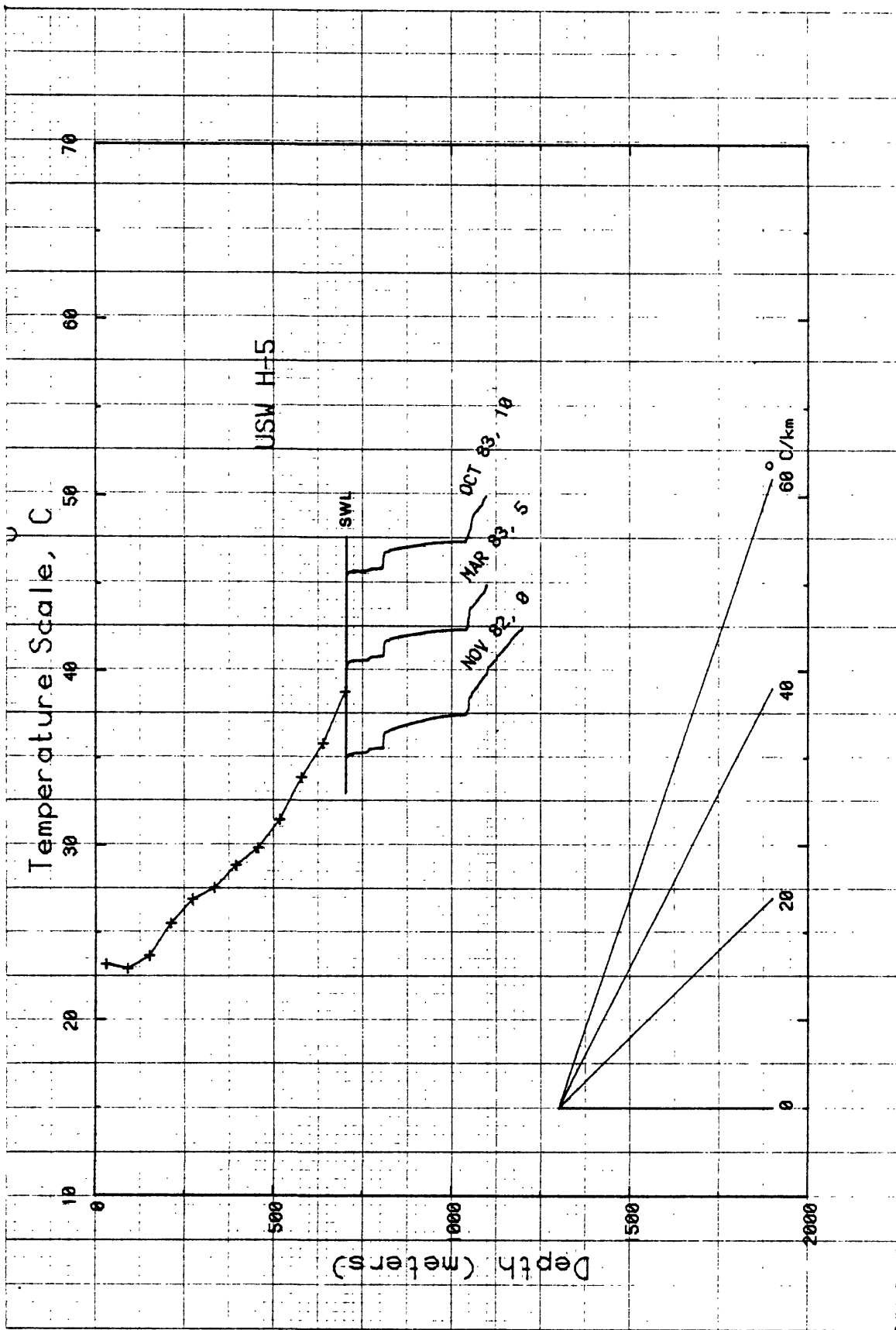


Figure 1-16. Temperature profiles from USW H-5. Number after date is the amount by which profile is shifted to the right. SWL is static water level.

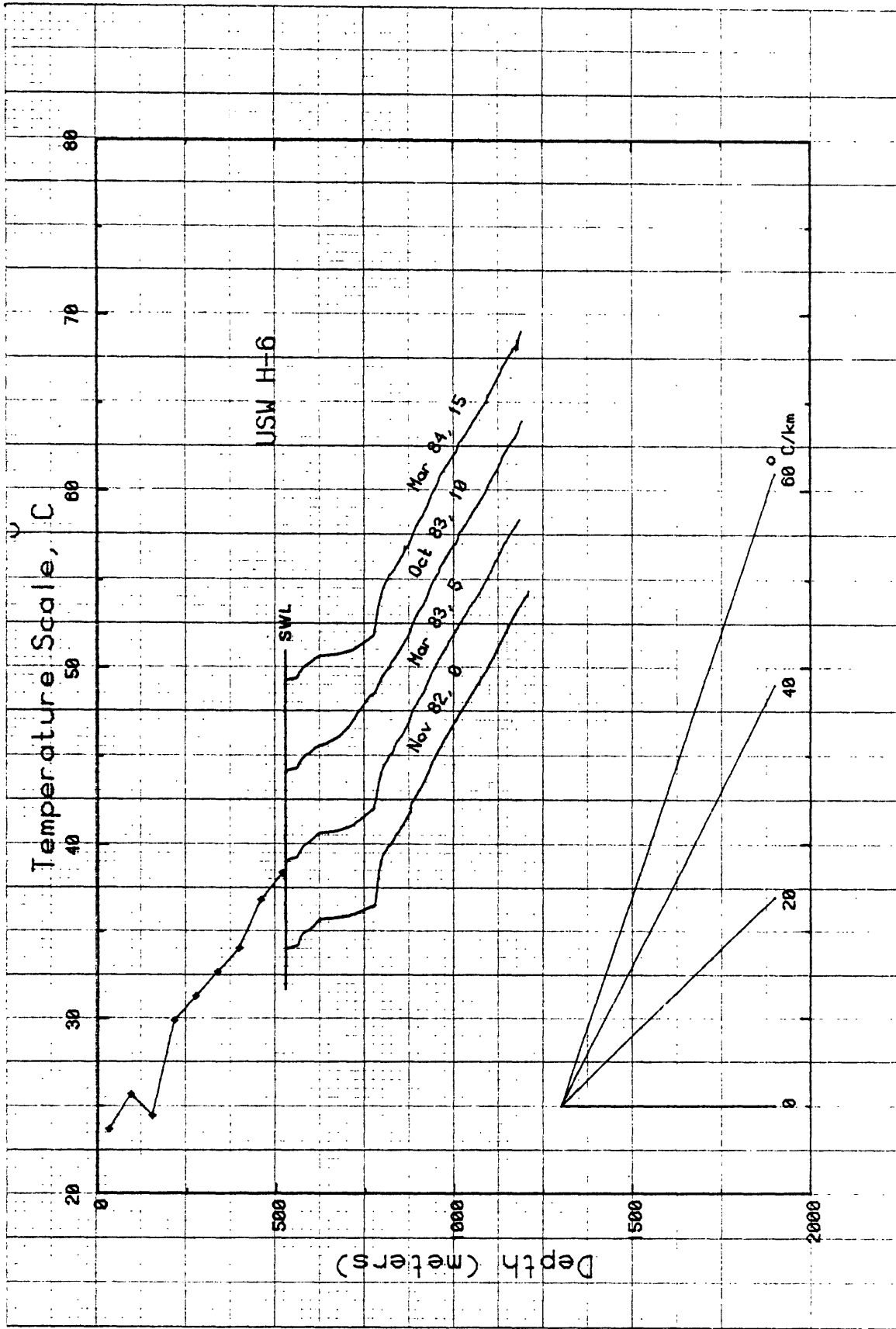


Figure 1-17. Temperature profiles for USW H-6. Number after date of log signifies rightward shift of the profile relative to the temperature origin. SWL is static water level.

TERMINIX INFORMATION DISPLAY DIVISION 006 1858 00 30 x 15 W. LINEAR

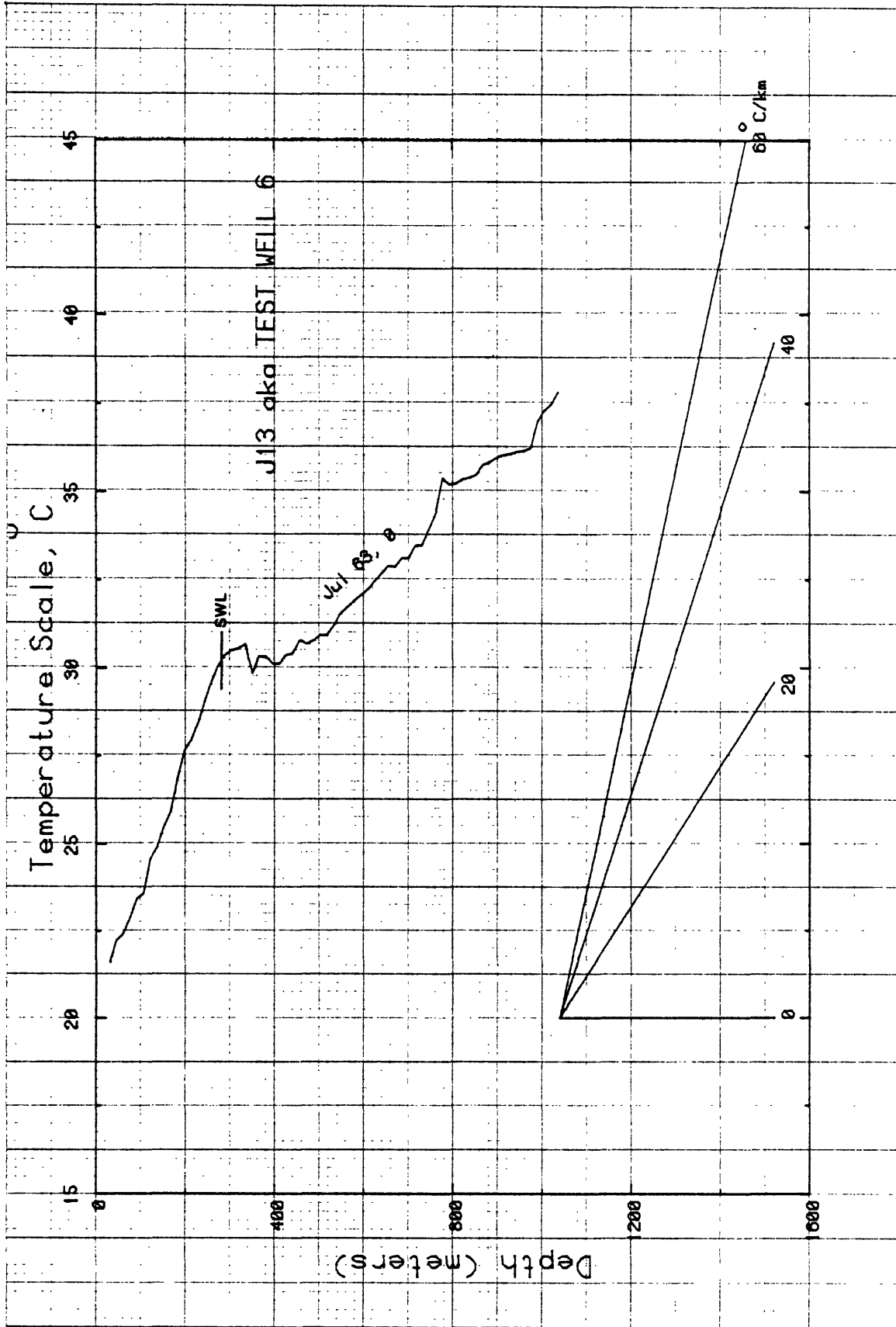


Figure 1-18. Temperature profile in well J-13. SWL is static water level.

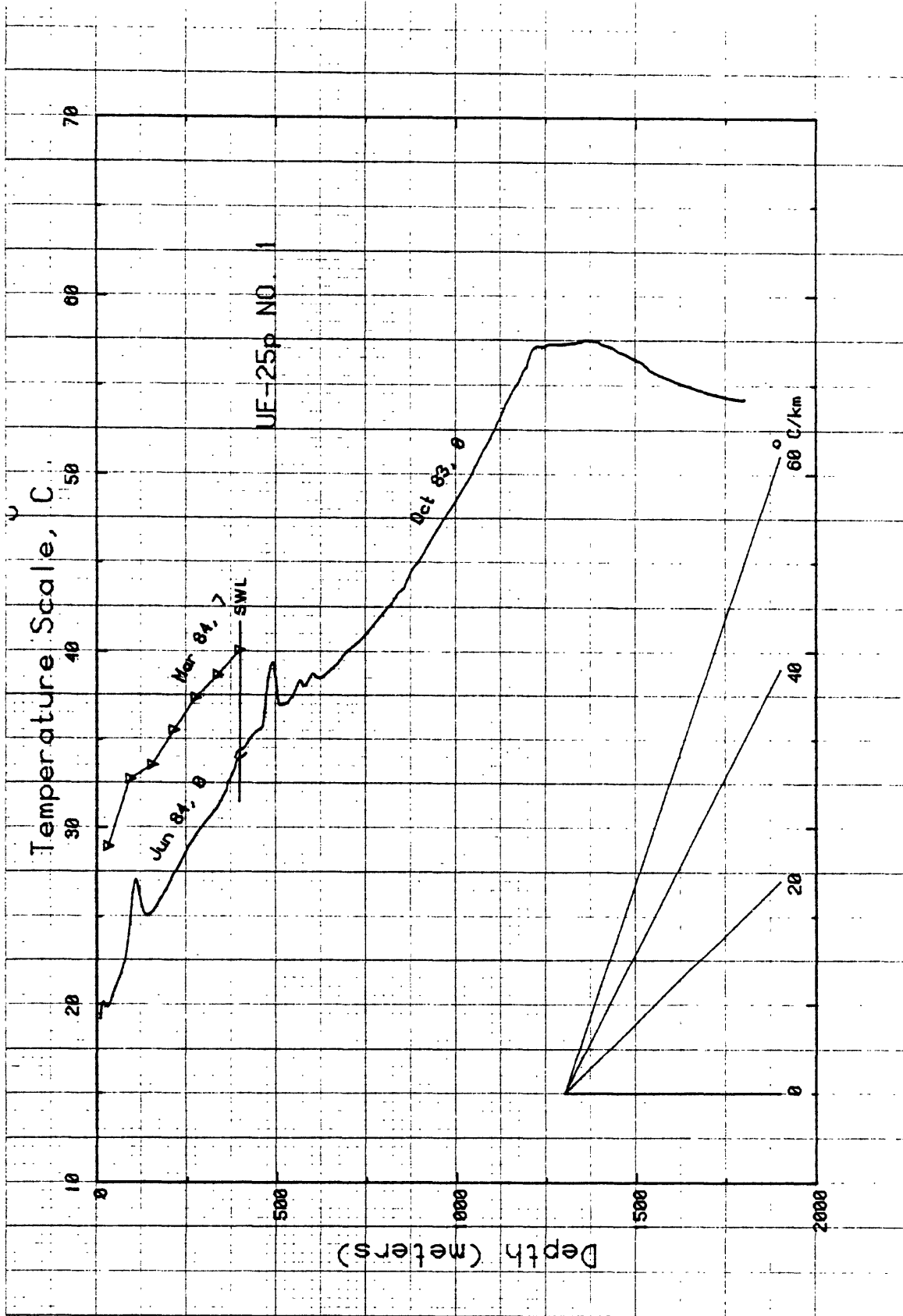


Figure 1-19. Temperature profiles in Ue25p. Rightward shift in profile is indicated by the number after the date. SWL is static water level.

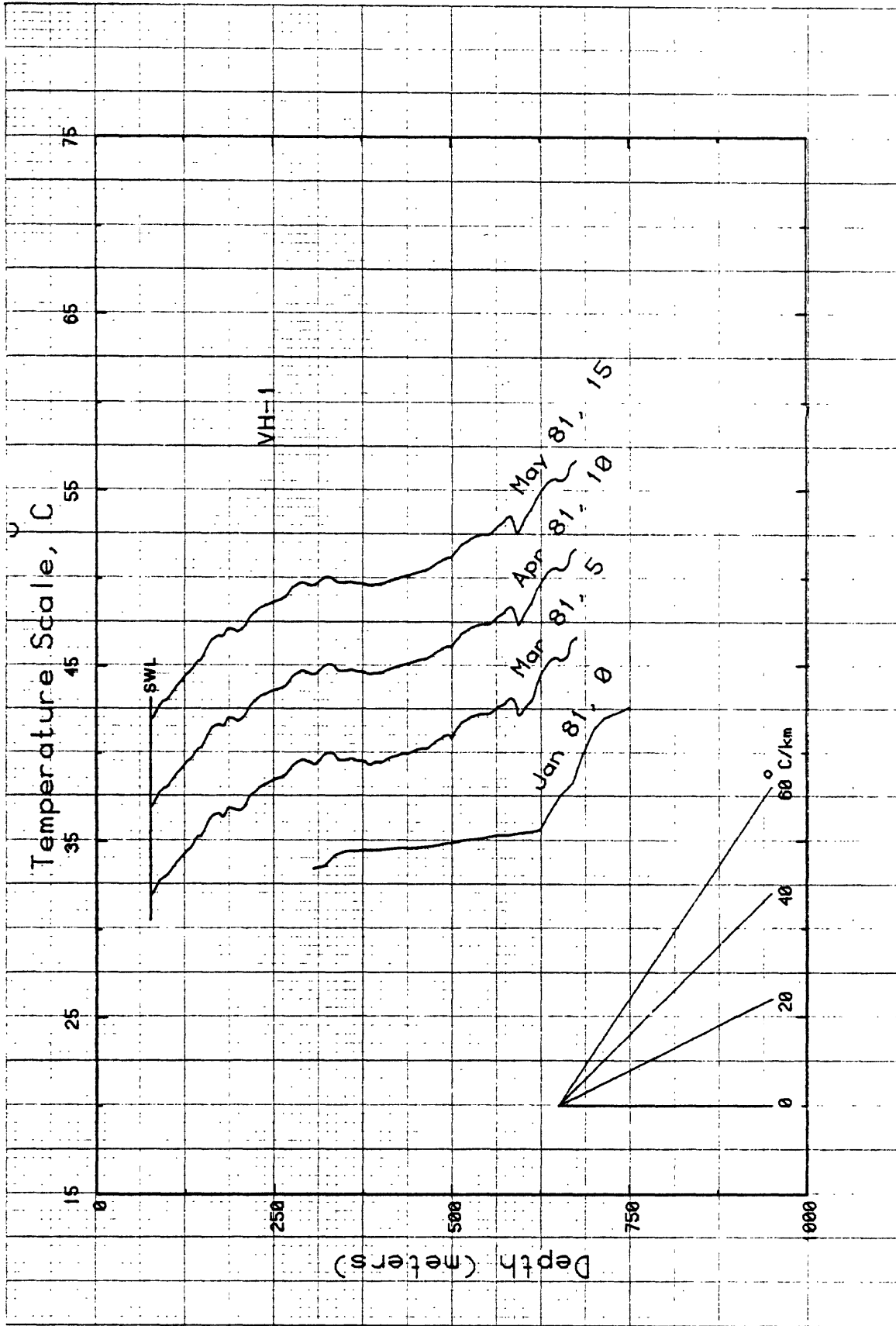


Figure 1-20. Temperature profiles from USW VH-1. Number after date signifies amount of rightward shift relative to temperature origin. SWL is static water level.

TEKTRONIX INFORMATION DISPLAY DIVISION
006 1098 00 10 x 15 IN. LINEAR

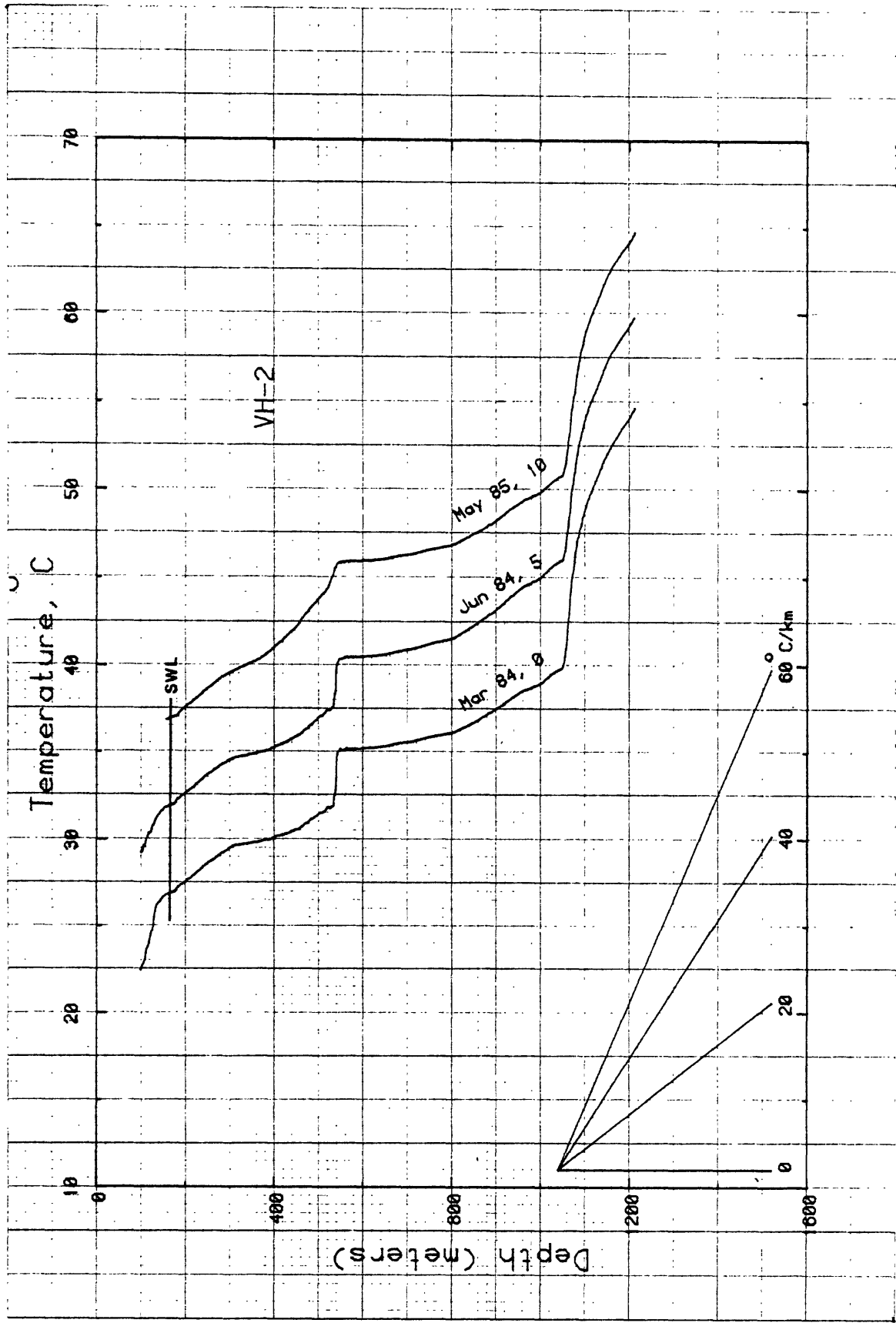
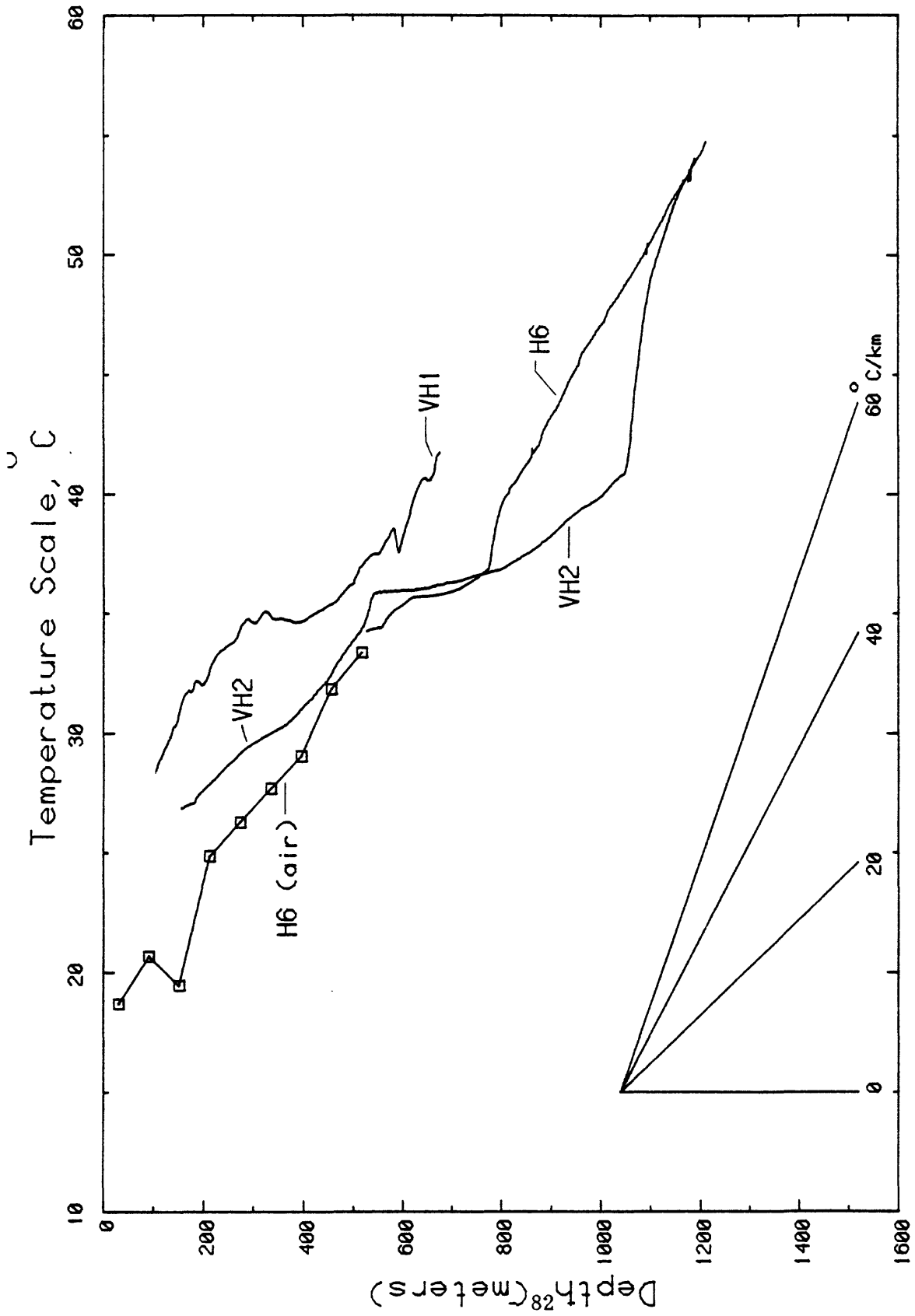


Figure 1-21. Temperature profiles for USW VH-2. Number after date denotes amount of rightward shift relative to temperature origin. SWL is static water level.



CRATER FLAT, NEVADA : USW-VH 1, USW-VH 2 & USW-H 6.

Figure 1-22. Temperature and gradient profiles from USW H-6, VH-1, and VH-2.

SE ROA 38242

JA_9524

APPENDIX 2. Temperature measurements in air in the unsaturated zone

In many wells, we had available an access pipe plugged at the bottom and filled with water. For these (e.g., USW G-2 and USW G-4, figures 1-10 and 1-12), we were able to obtain logs through the unsaturated zone using our standard logging techniques (procedure GPP-02, RO, Sass and others 1971). For various reasons, however, it was not always possible to have such an access pipe and measurements had to be obtained at discrete points in air. Using our standard probe (Fenwall K212E, Sass and others, 1971), such measurements are very time consuming - the time constant of the probe in air is on the order of one hour as compared with a few seconds in water.

Faced with a formidable number of wells from which to obtain such temperature measurements, we elected to design and construct a special thermistor probe having a very small thermal mass. The probe (Figure 2-1) equilibrates with a column of still air to within 1% of a step temperature change in a period of four minutes.

By far the most serious problem in obtaining meaningful air-temperature measurements in a large (~ 0.5 m) diameter well results from convective motion induced by both the thermal instability of the air column (cooler, heavier air lying on top of warmer, lighter air) and by diurnal barometric changes. In the WT series wells, the usual casing configuration involved a large diameter (~ 400 mm) outer casing at the top of which was spot-welded a heavy flange (~ 20 mm thick) which in turn supported a string of smaller diameter tubing (~ 50 - 70 mm o.d.) with a well screen below the water table. It was common for the large casing to be "breathing" through gaps beneath the spot-welded flange, inhaling at certain times, and exhaling at others. When this was occurring, temperature fluctuations of varying periods were superimposed on the simple equilibration process with the result that temperatures were still

varying considerably after 20 minutes. As the magnitude of this problem became apparent, we were able to alleviate the disturbances somewhat by partially sealing the upper part of the large casing using materials that were available to us in the field (filament tape, weather stripping, etc.).

The measurement procedure consisted of lowering the probe in 100 to 200 foot (30.5 to 61 m) increments, then reading thermistor resistances at one-minute intervals until the resistance change in one minute was less than 1% of the accumulated change, or for 20 minutes, whichever was less. Data reduction consisted of converting resistances to temperatures, plotting temperature as a function of the reciprocal of time (t) and extrapolating linearly to $1/t = 0$ ($t = \infty$) for each depth. In this procedure, the time origin is difficult to fix precisely, as we are not dealing with an instantaneous step change in temperature. This is particularly true where the decay of a recent convective overturn is superimposed on the change imposed by moving the probe down in the geothermal gradient. A misplaced time origin is usually manifested as curvature in the later part of the temperature versus $1/t$ curve. When this was observed, we adjusted the time origin empirically (usually by no more than 1 or 2 minutes) so as to minimize the observed curvature.

When the air columns in both the outer casing and the observation tubing were truly stable (Figure 2-2), extrapolation of the θ versus $1/t$ curve resulted in an unambiguous intercept value for temperature (θ) accurate to within a few hundredths of a degree. On the other hand, there is a much larger degree of uncertainty ($\pm 0.1^\circ\text{C}$ or more in the extrapolated temperature for a convecting air column, Figure 2-3), and disturbances with periods of tens to hundreds of minutes may cause undetectable errors of 1°C or more.

We are reasonably certain that the least squares temperature gradient between 100 feet (30.5 m) and the water table is representative of the average thermal gradient in the unsaturated zone. In the "well-behaved" wells, the 30.5 m or 61 m interval-gradients probably also are reliable. It is impossible, however, to apply objective criteria to the data set from the large-diameter wells to distinguish between reliable and unreliable data.

The data for all accessible WT series wells are presented in Figures 2-4 through 2-20. For each depth shown on each of these figures, a graph of the kind illustrated in Figures 2-2 and 2-3 was generated, a suitable interval selected, and an extrapolation to $1/t = 0$ (infinite time) was made. Thus the temperature symbol plotted at each depth represents our interpretation of the most likely equilibrium temperature.

The static water level, in each instance where it was encountered is indicated by the lowermost triangle in each of Figures 2-4 through 2-20. Below that, there is a short "tail" of a few meters to tens of meters continuous temperature depth profile below the water table. As we noted in the "G" and "H" series wells, immediately below the water table, these tails are generally not consistent with the more regular and conductive temperature profiles in the unsaturated zone.

In WT-13 (Figure 2-15) it was consistently difficult to obtain a consistent temperature versus $1/\text{time}$ profile (cf. Figures 2-2 and 2-3). We logged it on two different occasions (June 1 and June 4, 1984) but found it very difficult to get an internally consistent set of data except near the top and near the water table (Figure 2-15). This is a "worst-case" illustration of our contention that, even though the detailed structure of the thermal profiles from this series of wells may be suspect, the least-squares gradient over a ~ 300 m interval does have some status.

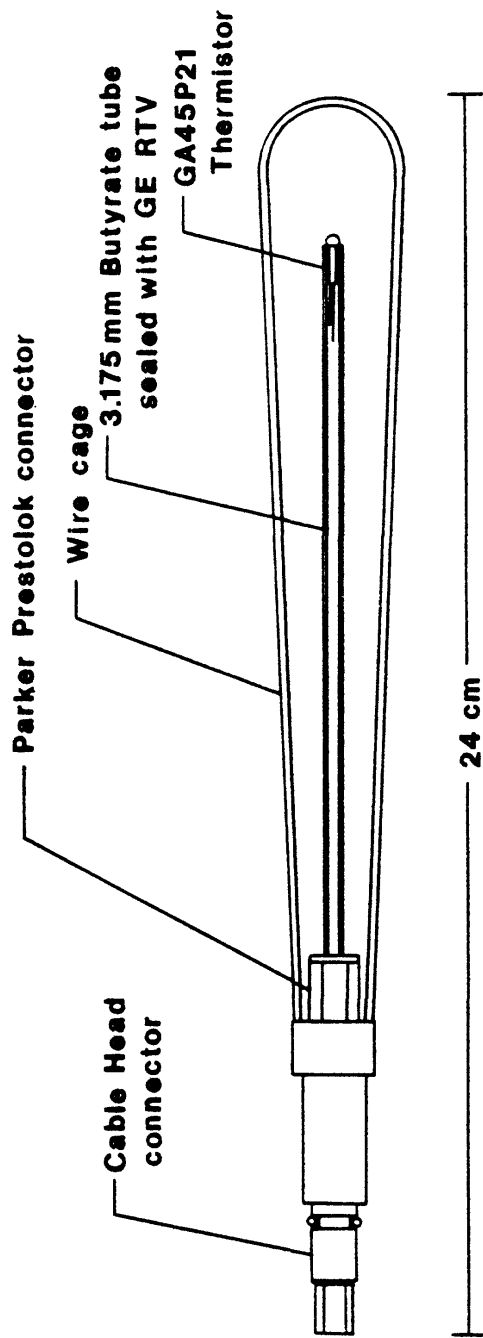


Figure 2-1. Temperature transducer having a low thermal mass for use in air.

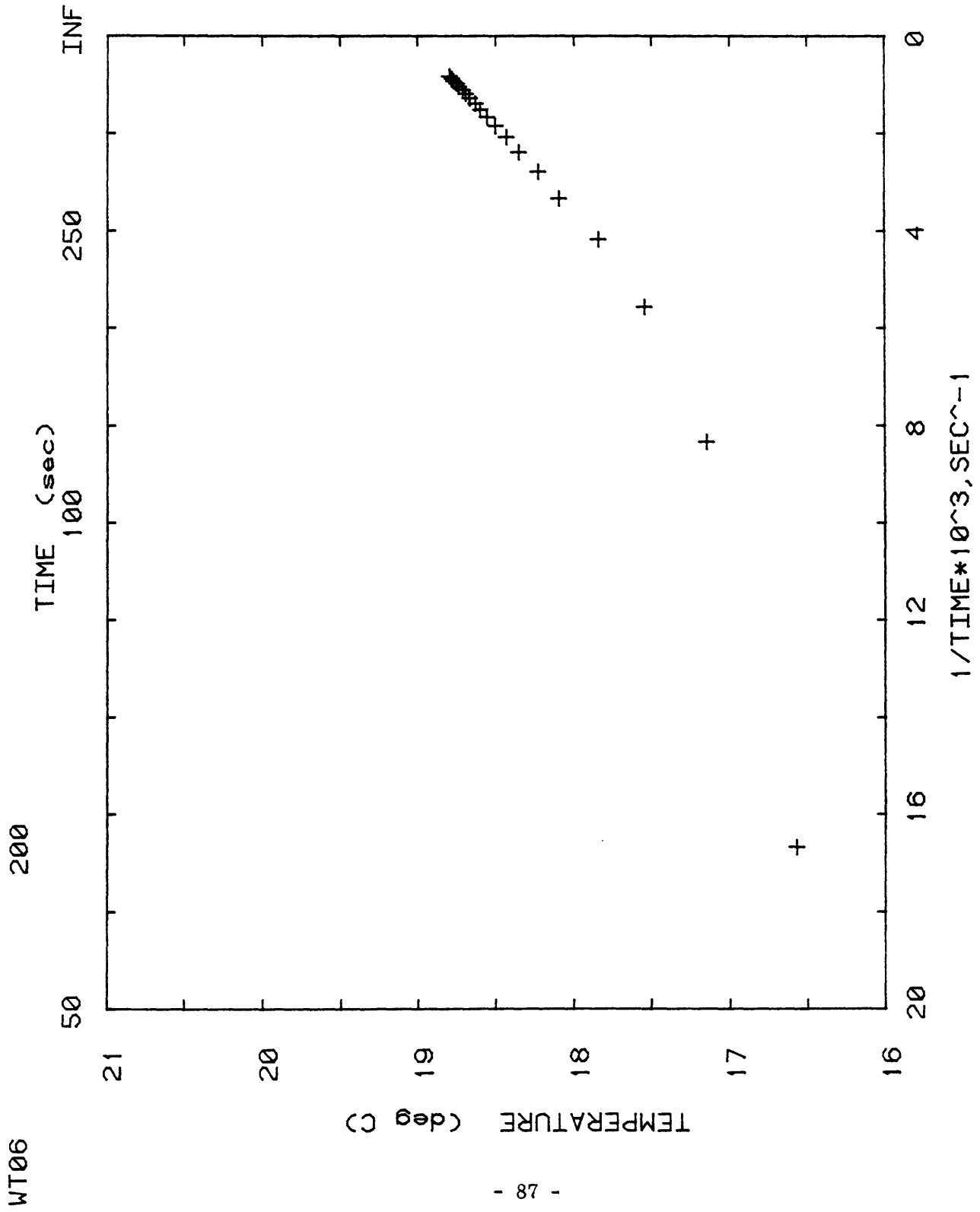


Figure 2-2. Temperature versus reciprocal time (from stopping of probe) for WT06, 200 feet, illustrating approach to equilibrium in a stable air column.

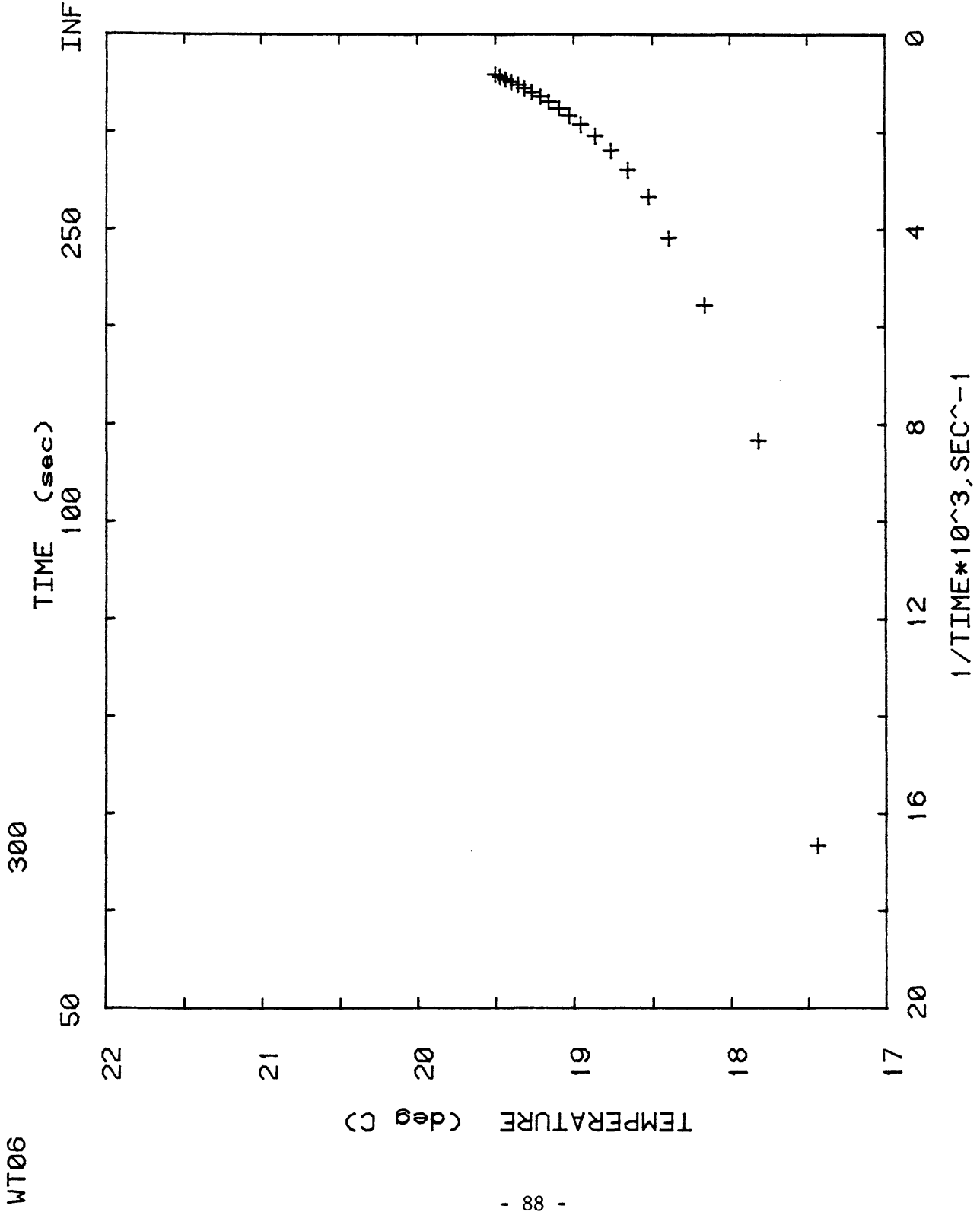
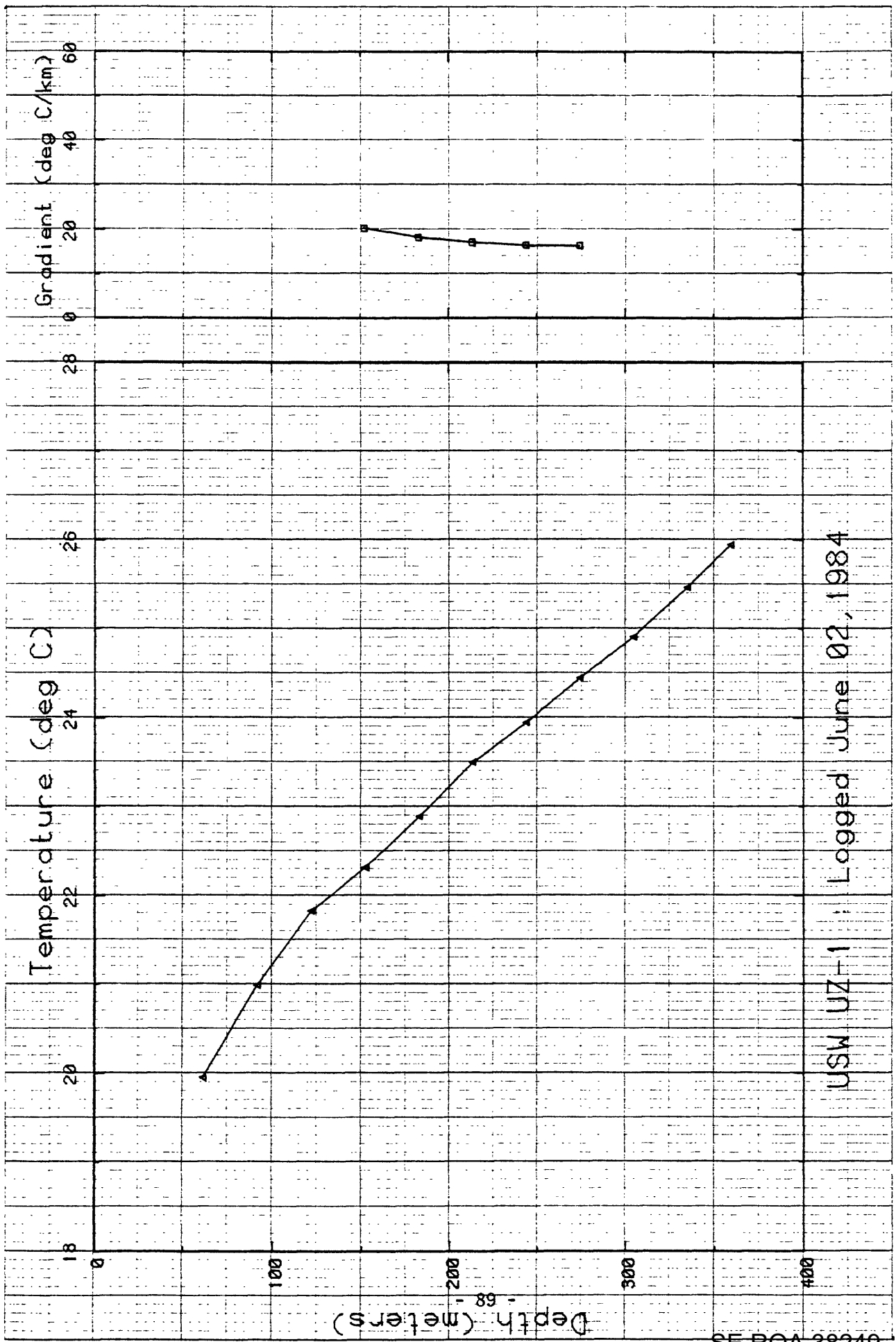


Figure 2-3. Temperature versus reciprocal time (from stopping of probe) for WT06, 300 feet, illustrating the effects of a long-period disturbance superimposed on a simple step change in temperature.



USW UZ-1 : Logged June 02, 1984

SE ROA 38249

TELEPHONE INFORMATION DISPLAY DIVISION 006-9698-00 10 x 15 cm. LINEAR

Figure 2-4.

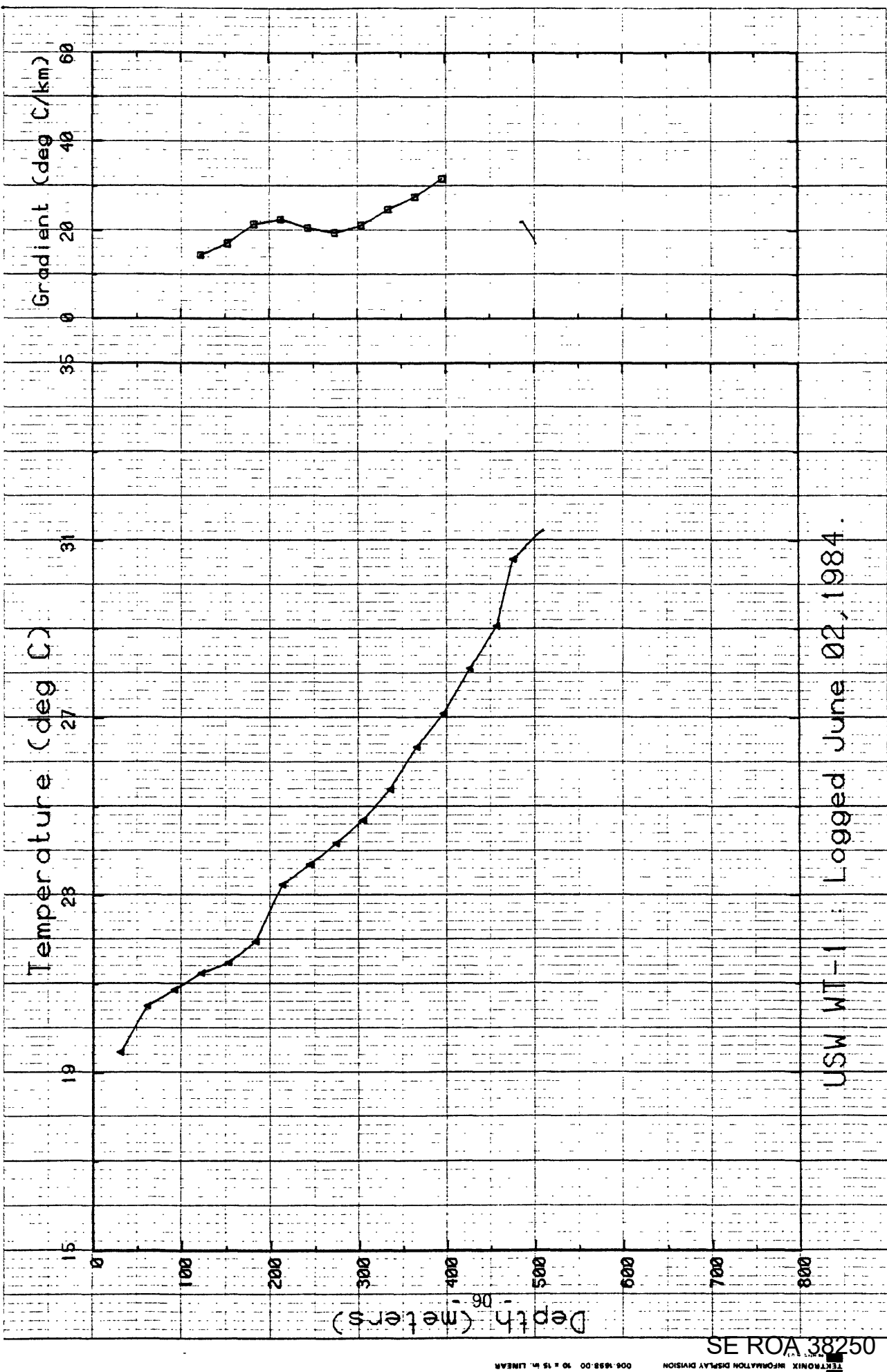
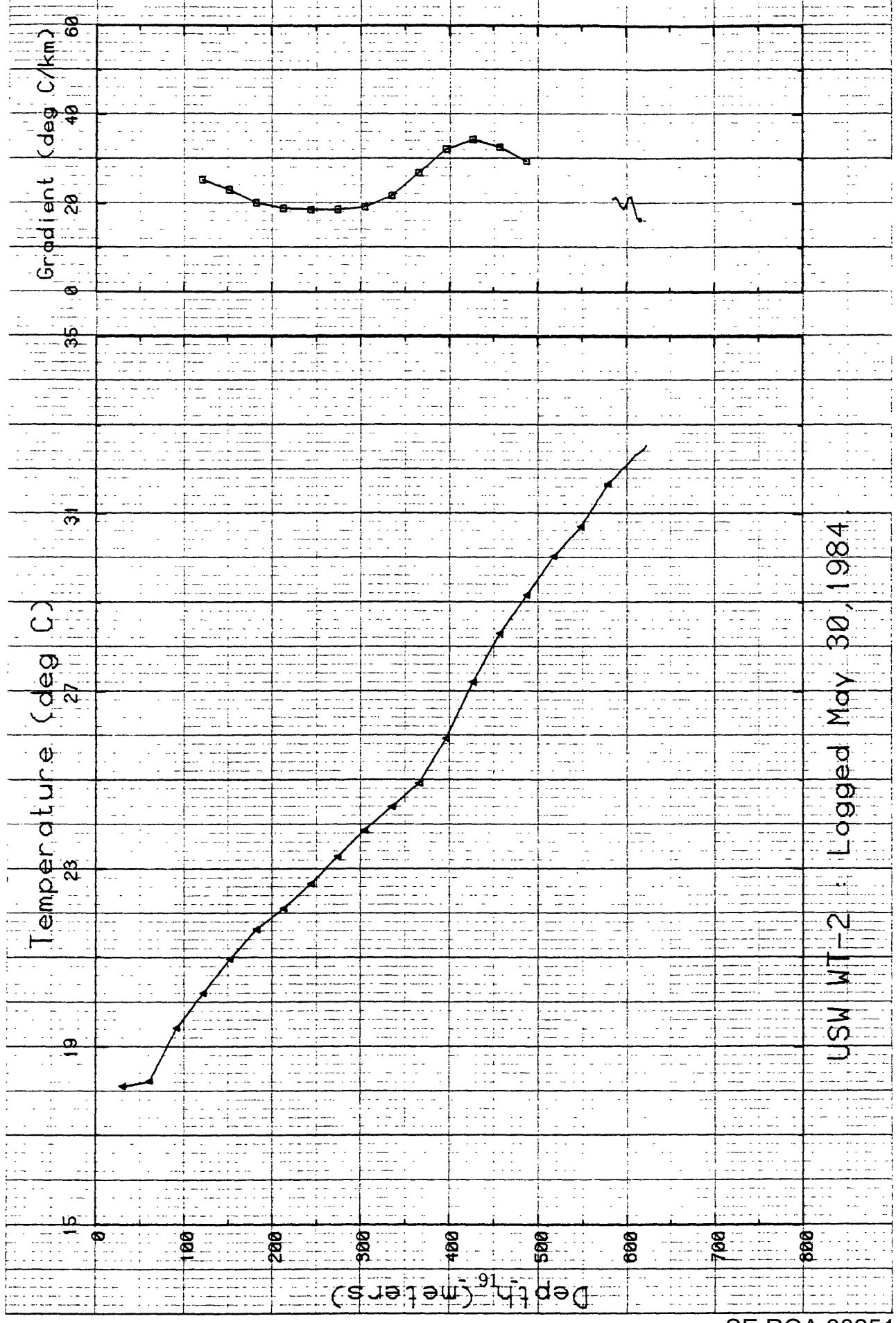


Figure 2-5.

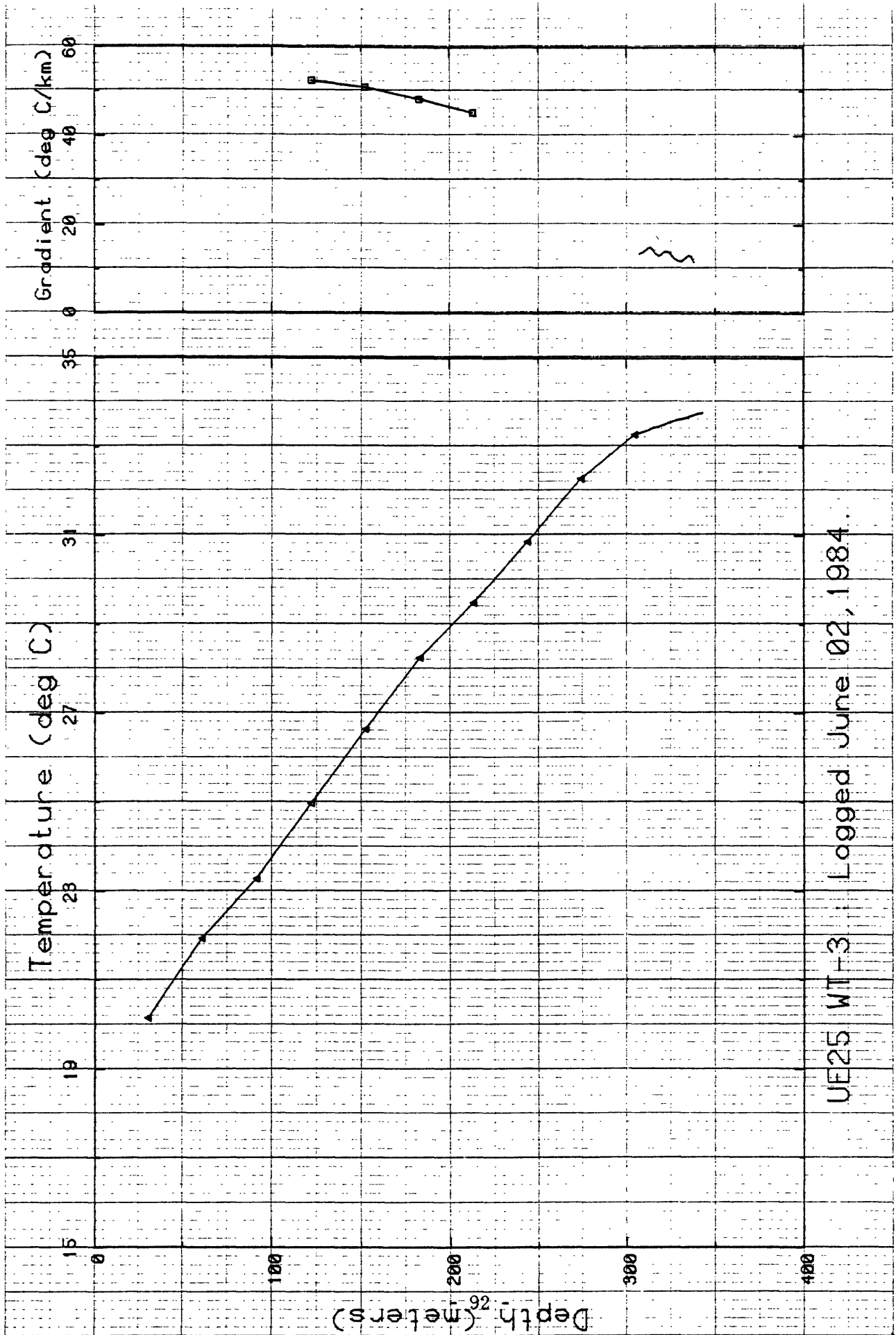


USW WT-2 : Logged May 30, 1984

Figure 2-6.

SE ROA-28251

TELETYPE INFORMATION DISPLAY DIVISION 004-1698 00 10 x 15 in. LINEAR

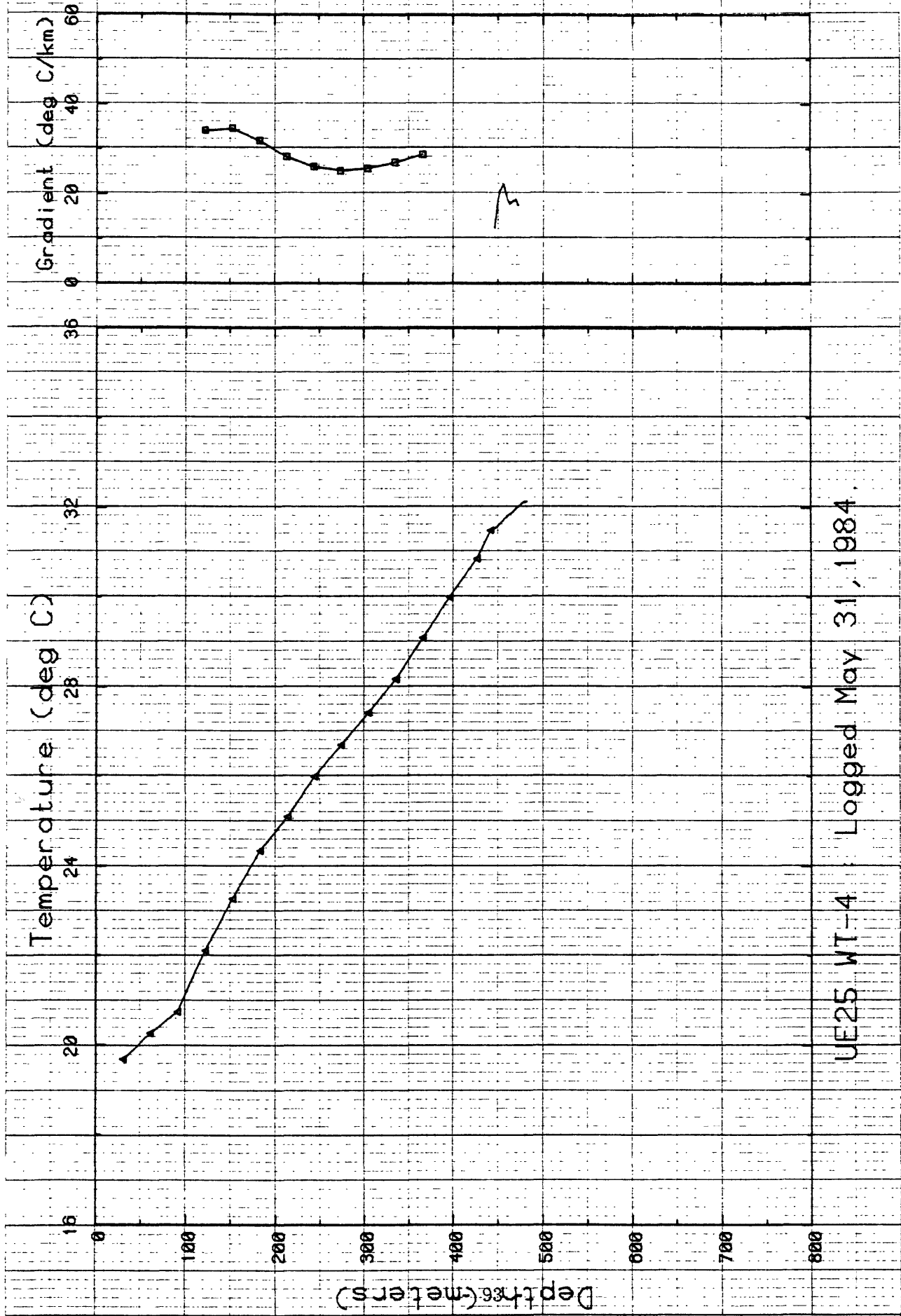


UE25 WT-3 : Logged June 02, 1984.

SE ROA 38252

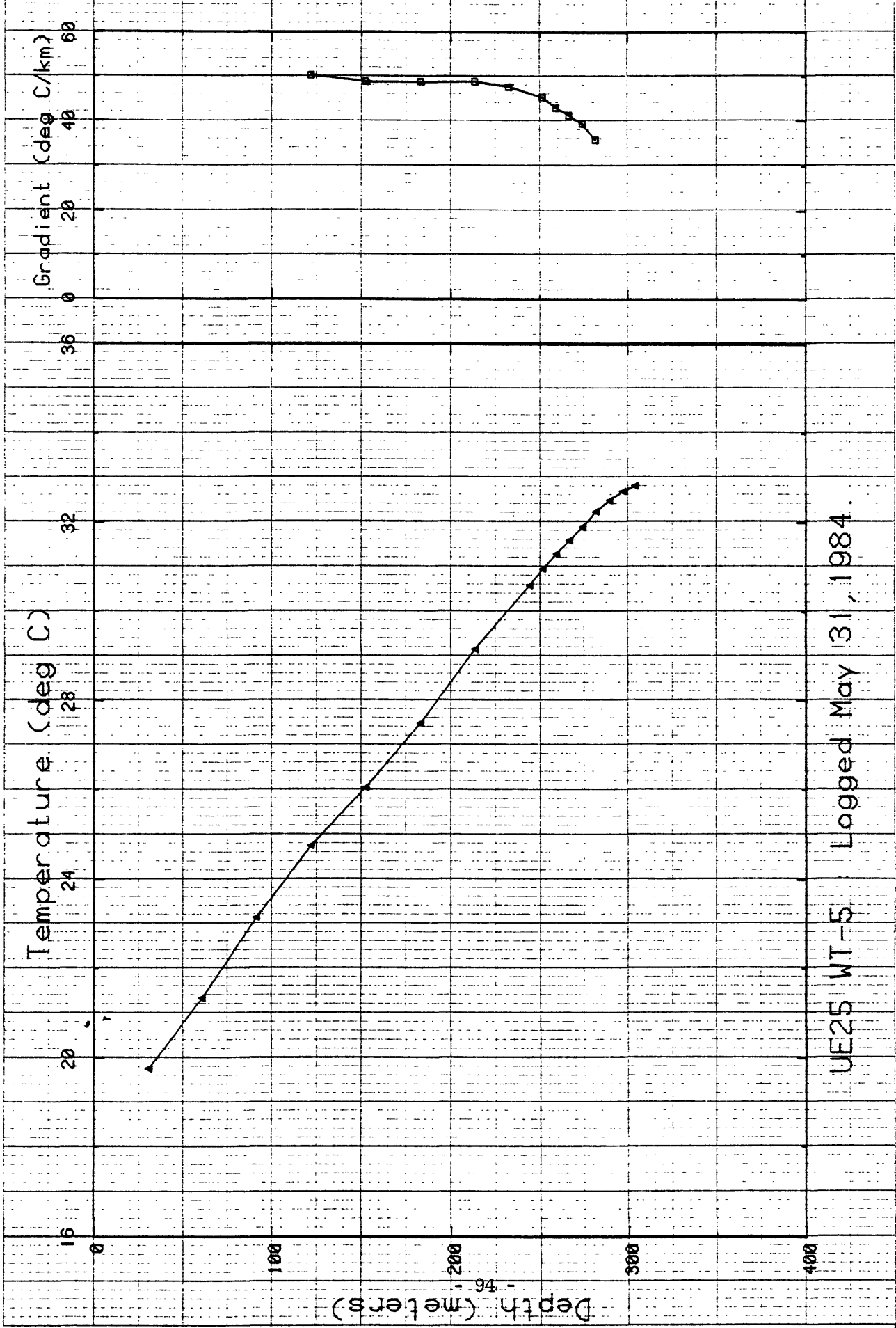
TEKTRONIX INFORMATION DISPLAY DIVISION
006:1898 00 10 x 16 M. LINEAR

Figure 2-7.



UE25 WT-4 Logged May 31, 1984.

Figure 2-8.



UE25 WT-5 Logged May 31, 1984.

Figure 2-9.

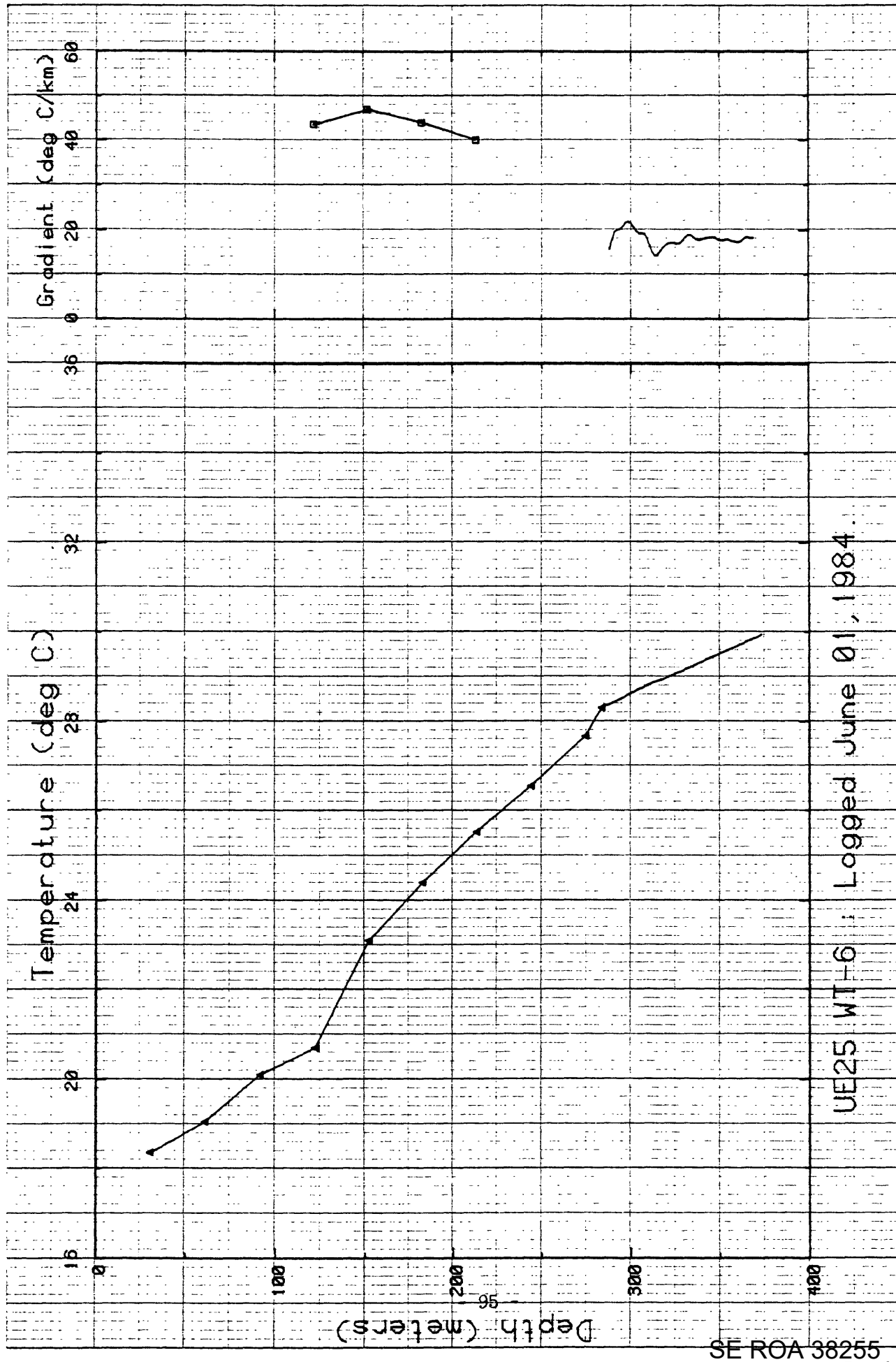


Figure 2-10.

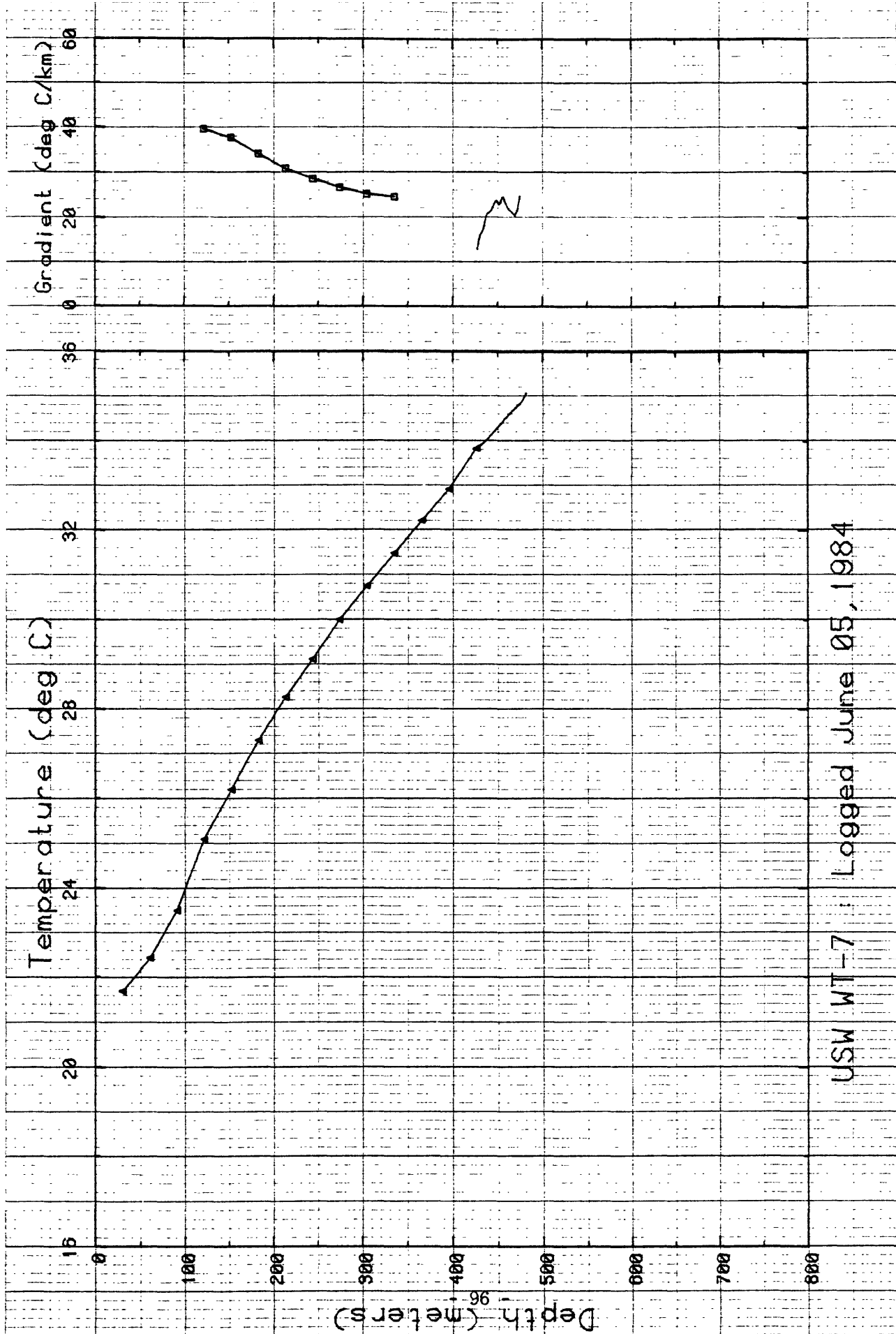
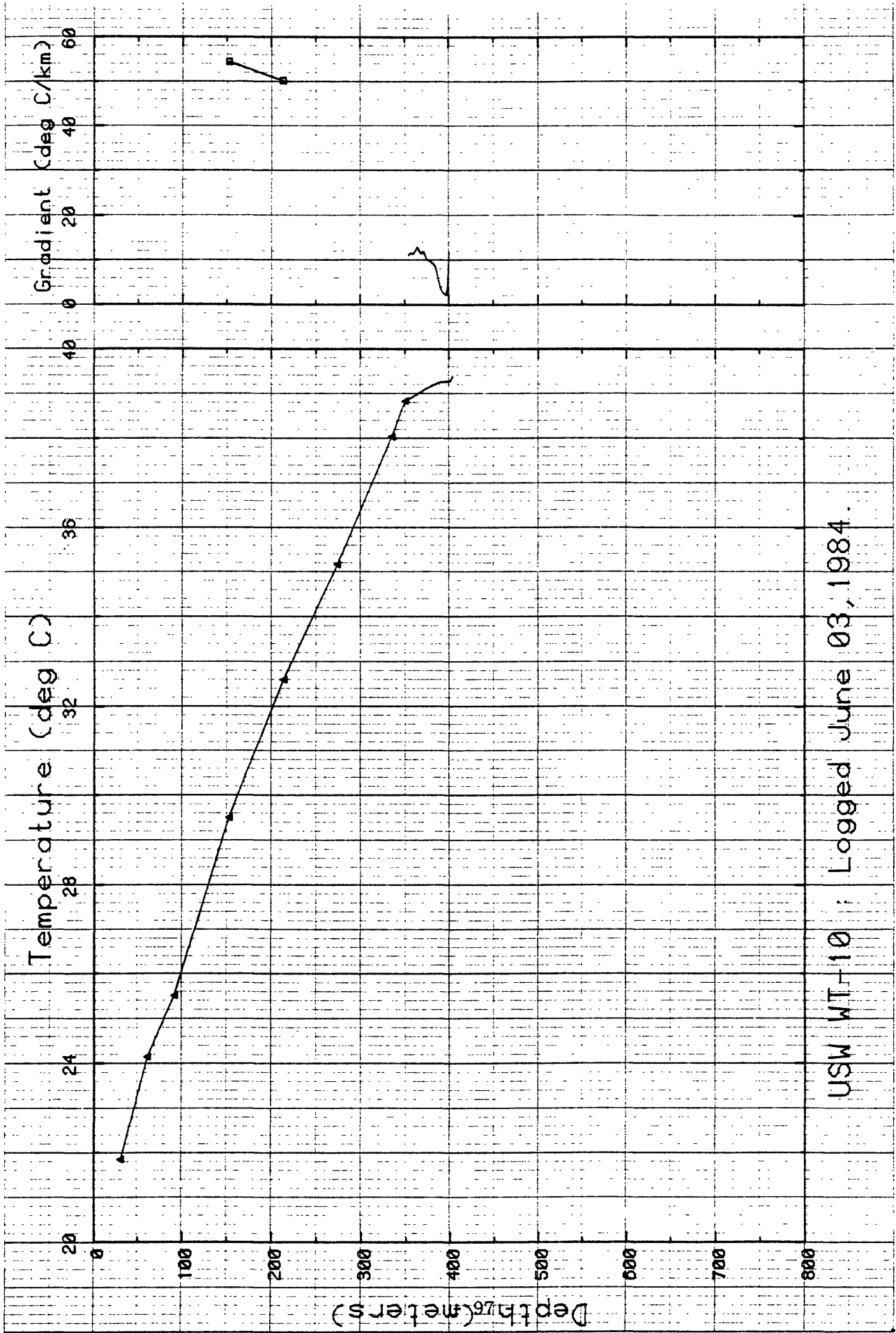
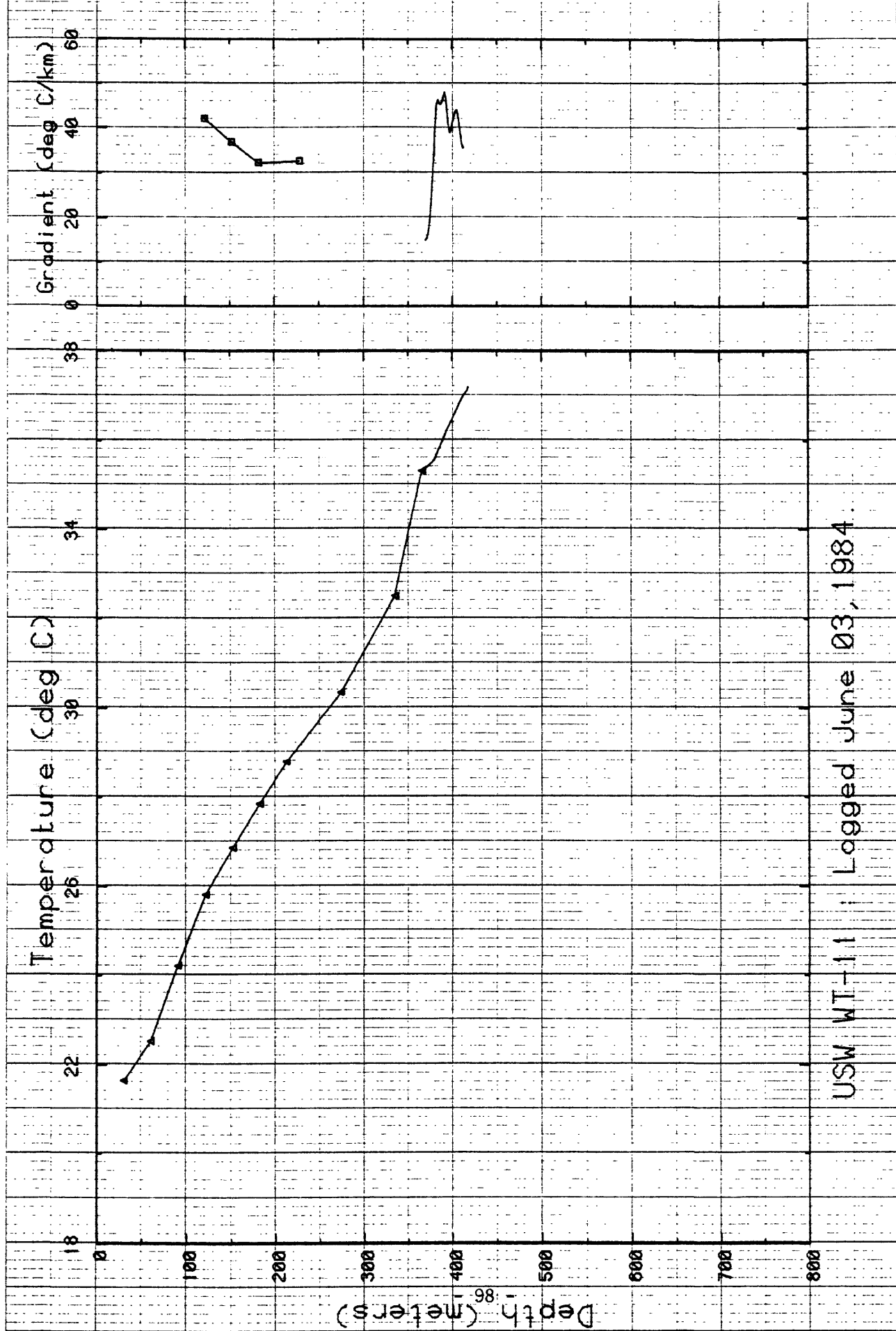


Figure 2-11.



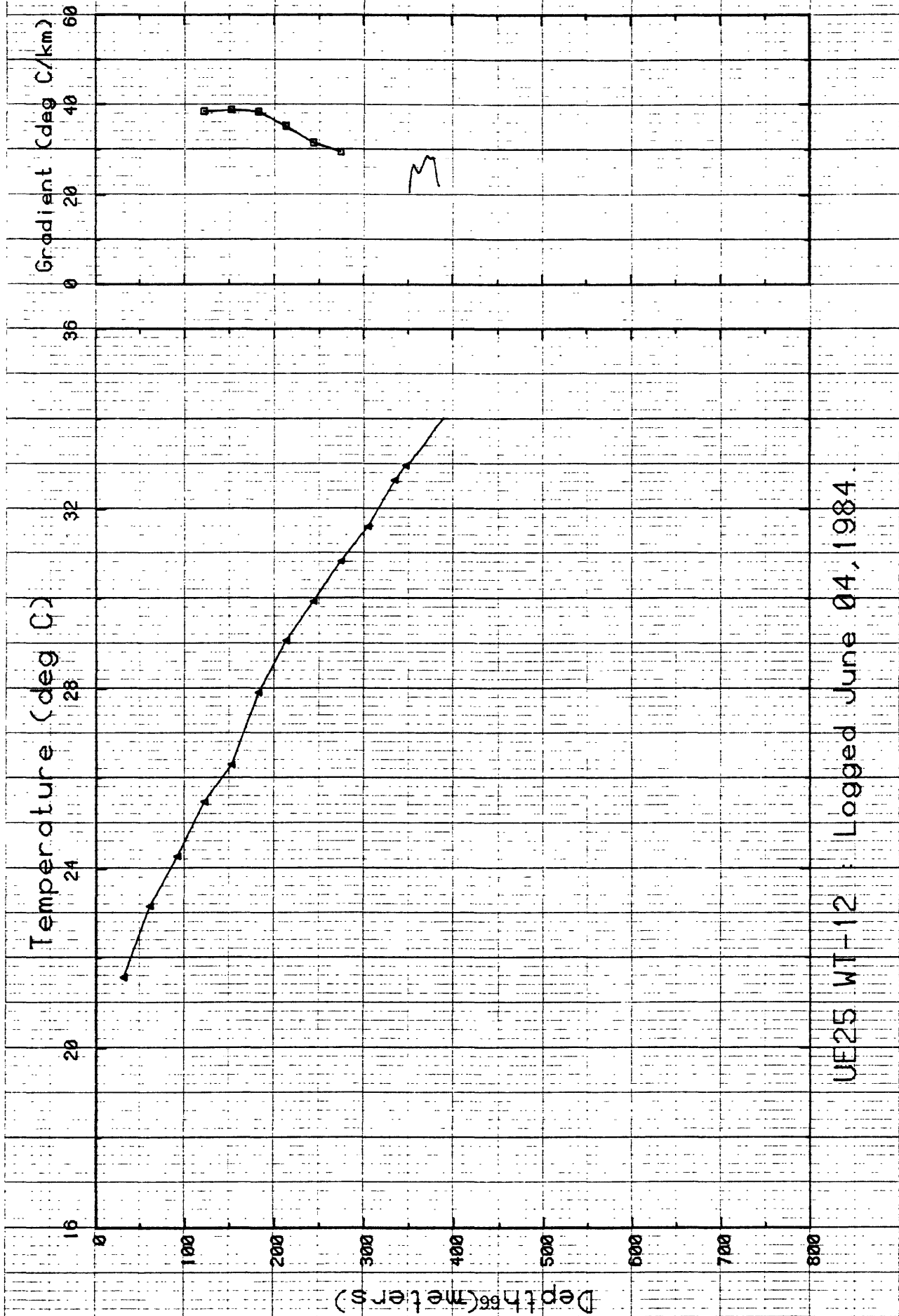
USW WT-10 ; Logged June 03, 1984.

Figure 2-12.



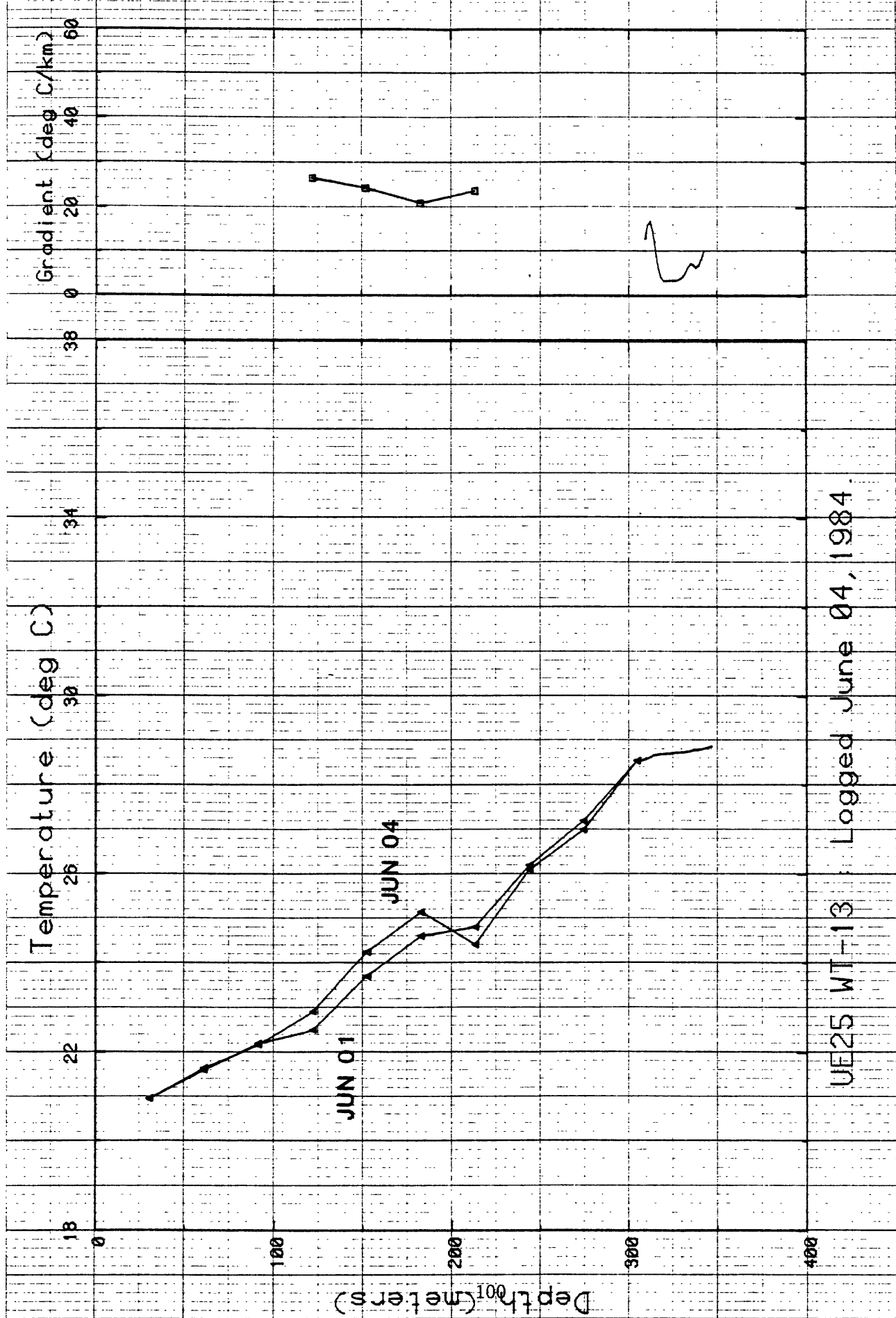
USW WT-1.1 | Logged June 03, 1984.

Figure 2-13.



UE25 WT-12 : Logged June 04, 1984.

Figure 2-14.



UE25 WT-13 : Logged June 04, 1984.

Figure 2-15.

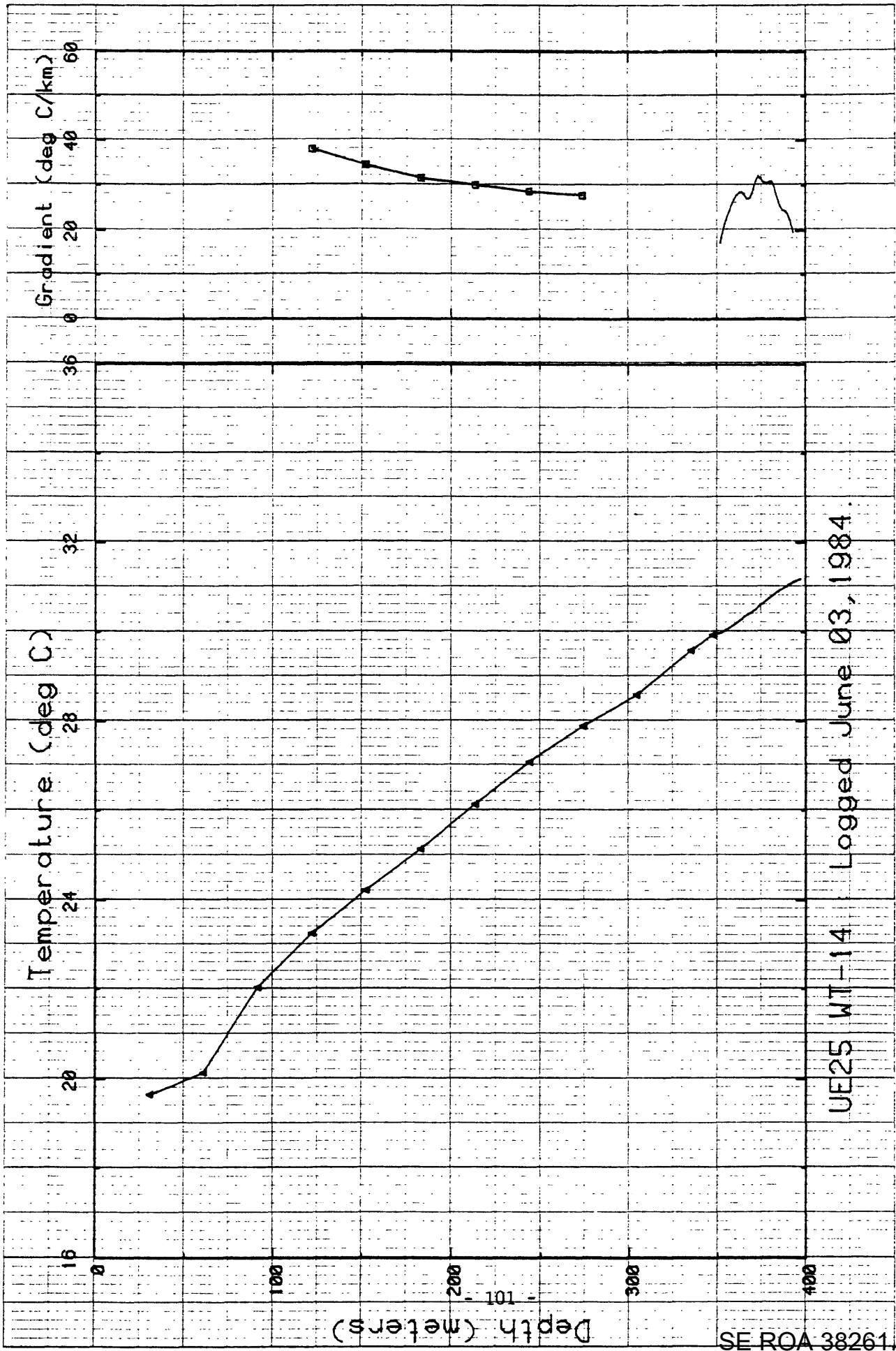


Figure 2-16.

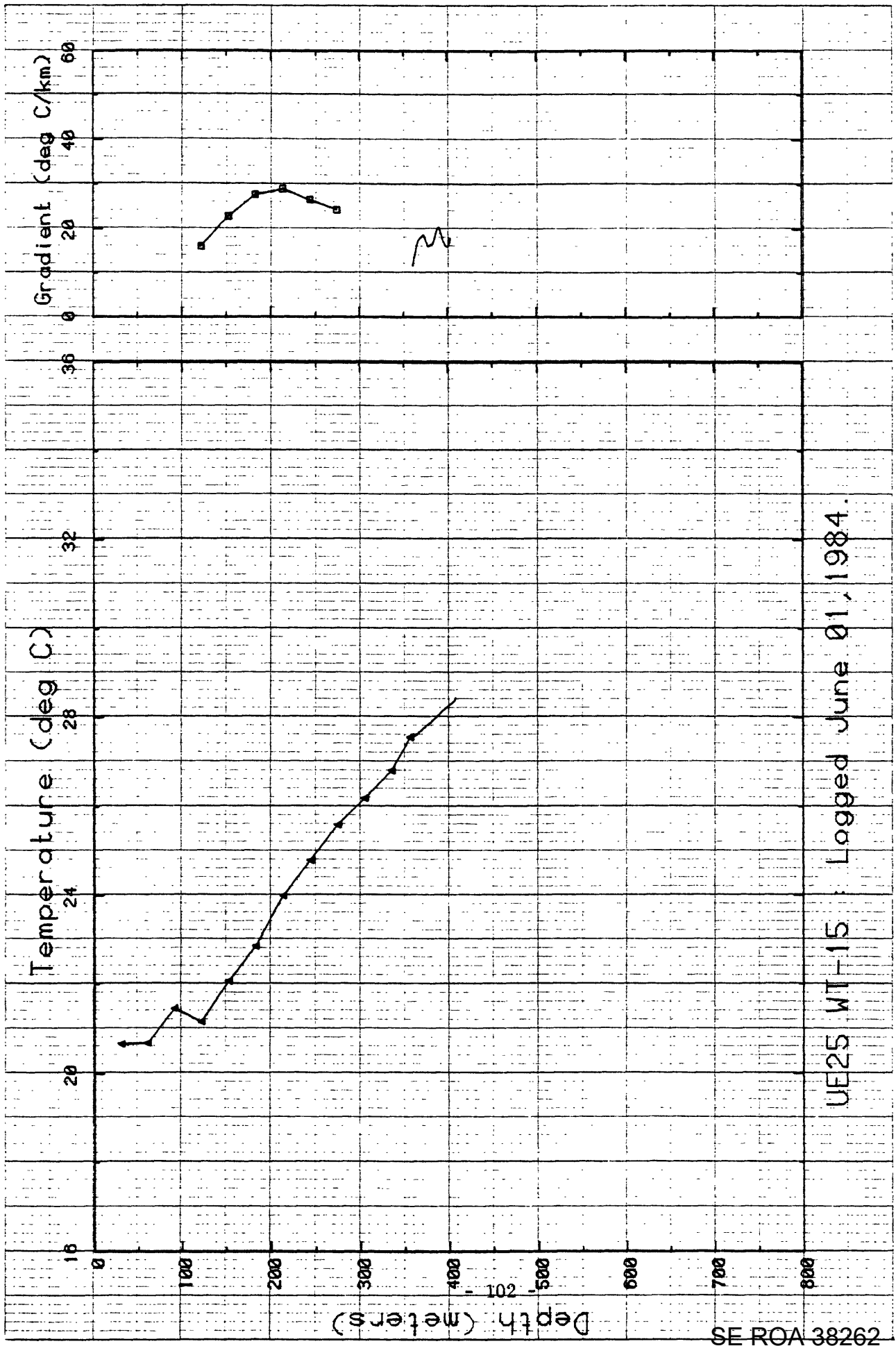


Figure 2-17.

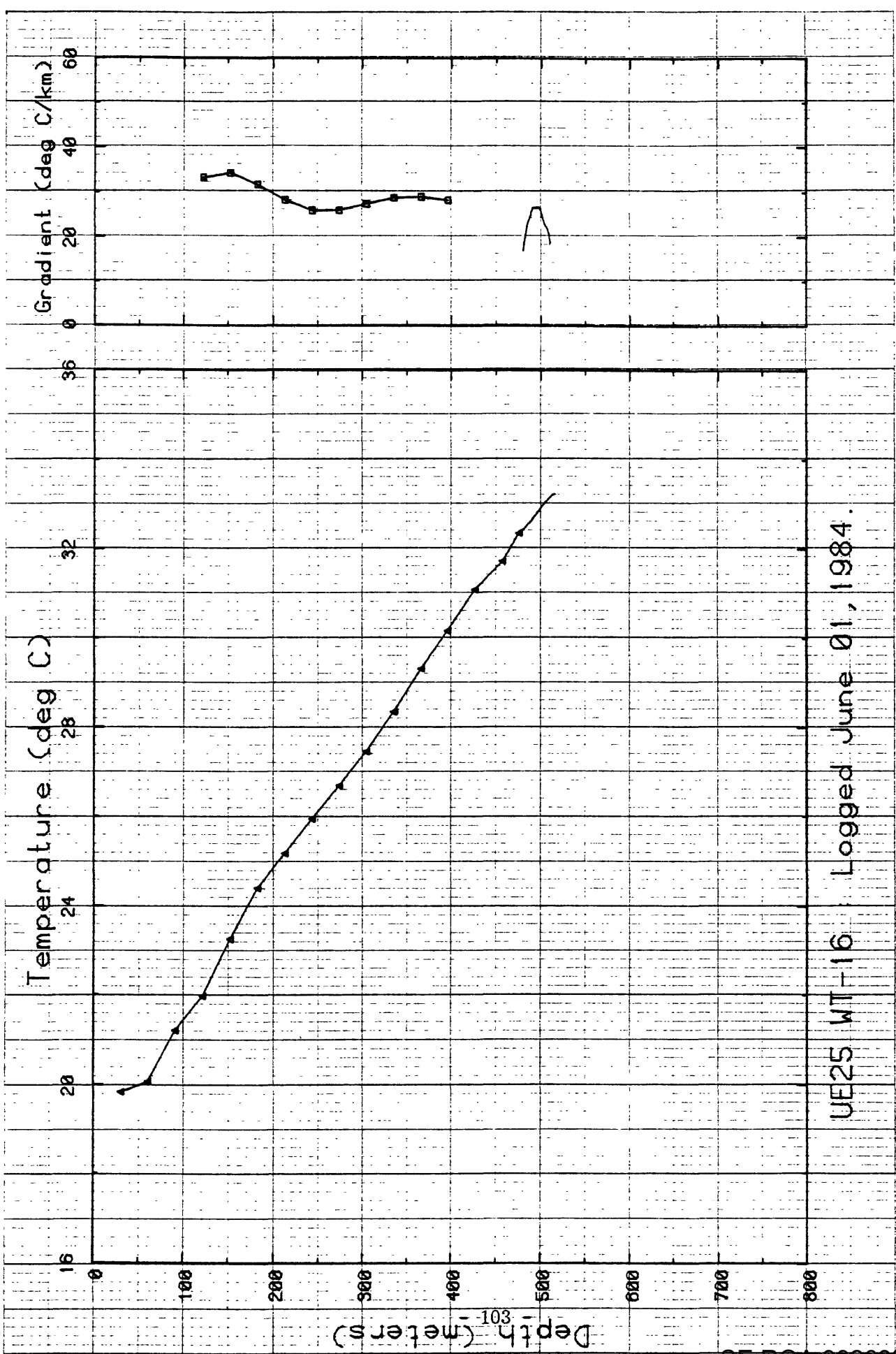


Figure 2-18.

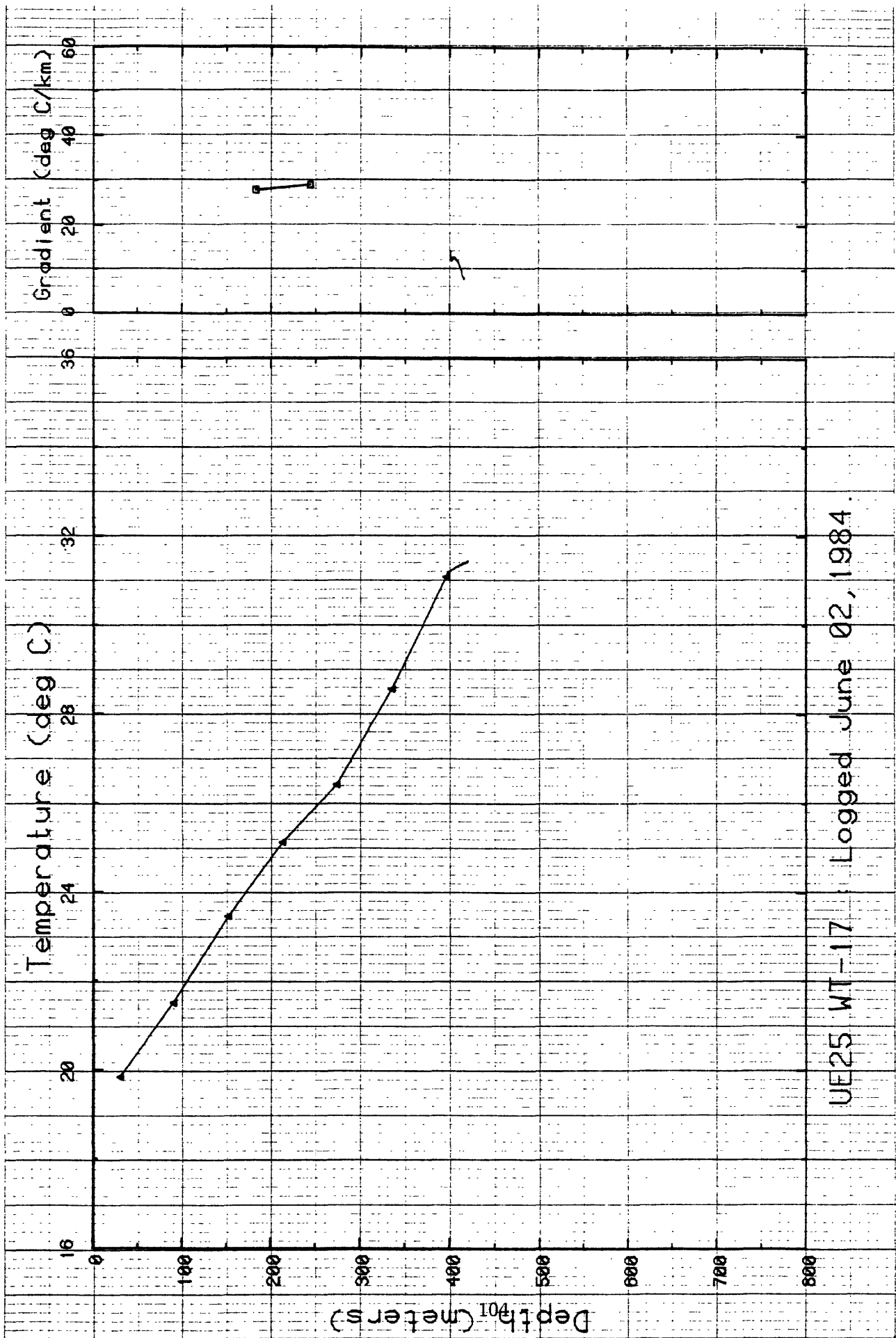


Figure 2-19.

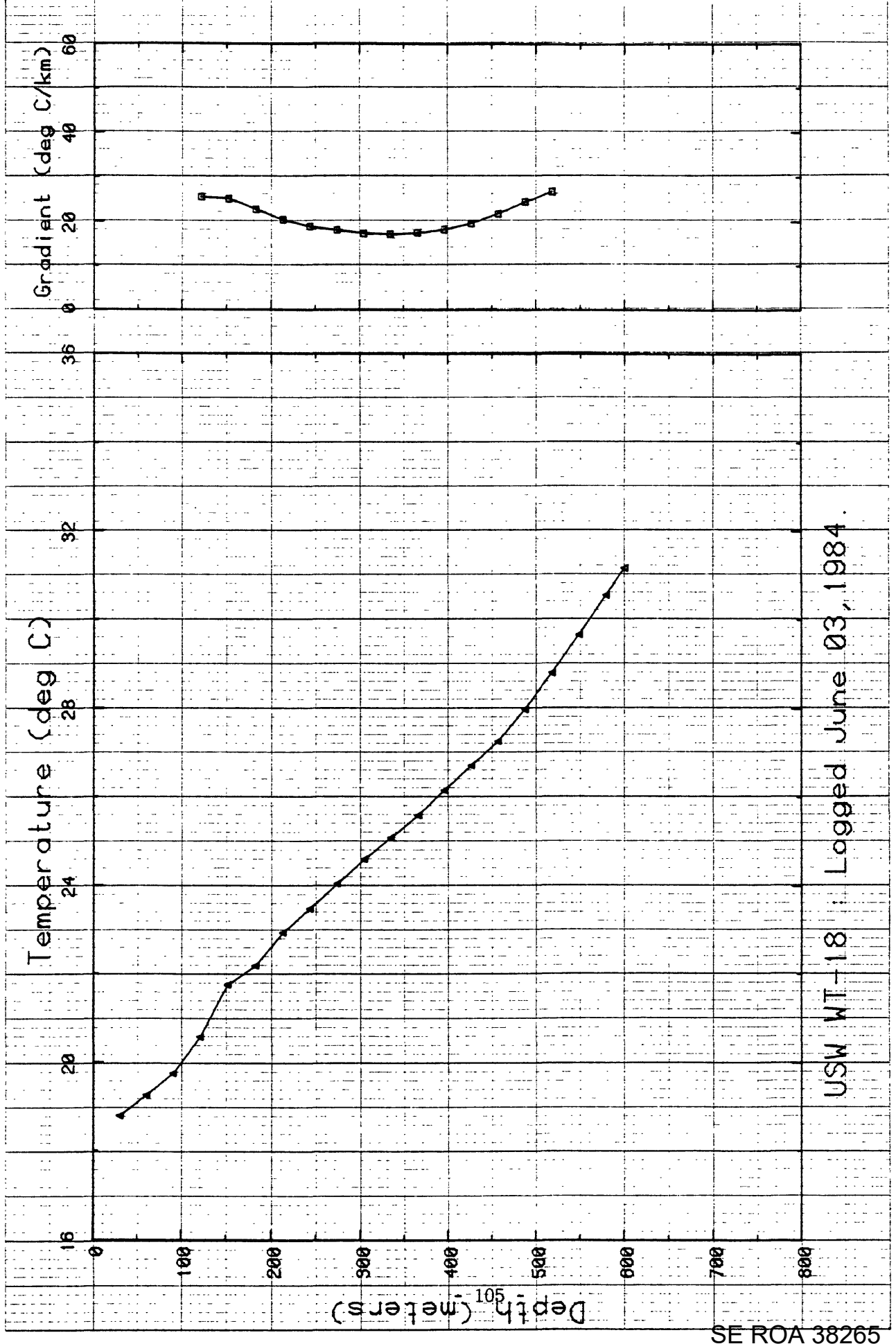


Figure 2-20.

SE ROA 38266

JA_9548

APPENDIX 3. Thermal conductivities

Thermal conductivity measurements were performed on core samples that had been wrapped in aluminum foil and dipped in hot wax to preserve in situ moisture conditions to the fullest extent possible. Thermal conductivity determinations were performed at an ambient temperature of about 25°C using the needle-probe method described by Sass and others (1971, 1984). Conductivity values are presented in Tables 3-1 through 3-5.

TABLE 3-1. Thermal conductivity of volcanic rocks from USW G-1

Depth, m	Formation (member)	Lithology	$\text{Wm}^{-1} \text{K}^{-1}$	K	Saturation
242.3	Paintbrush Tuff (Topopah Spring Member)	Densely welded tuff	2.15		U
405.4		Densely welded tuff	1.18		U
458.1	Tuffaceous beds of Calico Hills	Non-welded tuff	1.30		U
520.0		Non-welded tuff	1.17		U
----- SWL (static water level) -----					
612.6	Crater Flat Tuff (Prow Pass Member)	Partially welded tuff	1.28		S
630.9		Partially welded tuff	1.33		S
693.1	(Bullfrog Member)	Non- to partially welded tuff	1.37		S
704.2		Non- to partially welded tuff	1.38		S
721.7		Partially welded tuff	1.88		S
753.6		Moderately to densely welded tuff	1.80		S
759.9		Moderately to densely welded tuff	1.88		S
773.0		Moderately to densely welded tuff	1.90		S
782.7		Moderately to densely welded tuff	1.36		S
823.3	Crater Flat Tuff (Tram Unit)	Partially to moderately welded tuff	1.39		S
857.7		Partially to moderately welded tuff	2.26		S
868.1*		Partially to moderately welded tuff	1.80		S
892.5		Partially to moderately welded tuff	2.07		S
892.8*		Partially to moderately welded tuff	1.94		S
892.9*		Partially to moderately welded tuff	1.87		S
895.7		Partially to moderately welded tuff	2.10		S
929.6		Partially to moderately welded tuff	1.95		S
930.2*		Partially to moderately welded tuff	1.42		S
940.4		Moderately welded tuff	1.54		S

TABLE 3-1. Thermal conductivity of volcanic rocks from USW G-1 (continued)

Depth, m	Formation (member)	Lithology	K $Wm^{-1}K^{-1}$	Saturation
967.3		Partially welded tuff	1.62	S
983.6		Non-welded tuff	1.67	S
1013.8		Vitrophyre	1.67	S
1044.5	Crater Flat Tuff (Tram Unit)	Vitrophyre	2.00	S
1065.6		Vitrophyre	1.80	S
1091.6	Flow breccia	Flow breccia	1.86	S
1123.4		Flow breccia	1.43	S
1157.9		Flow breccia	1.95	S
1187.9		Flow breccia	1.49	S
1219.4	Lithic Ridge Tuff	Partially welded tuff	1.65	S
1253.6		Partially welded tuff	1.80	S
1280.1		Partially welded tuff	1.88	S
1319.9		Partially welded tuff	1.72	S
1349.2		Partially welded tuff	1.77	S
1389.4		Partially welded tuff	1.86	S
1419.3		Partially welded tuff	1.75	S
1450.7	Lithic Ridge Tuff	Partially welded tuff	1.96	S
1477.5		Non-welded tuff	2.10	S
1511.6		Non-welded tuff	1.68	S
1540.0	Older ash flows to bedded tuffs. Units A, B, and C	Densely welded tuff	1.98	S
1573.0		Densely welded tuff	1.98	S
1600.0		Densely welded tuff	2.15	S
1632.6		Bedded tuffs	2.12	S
1675.7		Non-welded tuff	1.70	S

TABLE 3-1. Thermal conductivity of volcanic rocks from USW G-1 (continued)

Depth, m	Formation (member)	Lithology	$W_{m^{-1} K^{-1}}$	Saturation
1716.9		Densely welded tuff	1.94	S
1747.7		Moderately welded tuff	1.91	S
1754.5		Moderately welded tuff	1.85	S
1783.3		Moderately welded tuff	1.97	S
1813.8		Moderately welded tuff	1.89	S
1814.0		Moderately welded tuff	1.86	S

TABLE 3-2. Thermal conductivity of volcanic rocks from USW G-2

Depth, m	Formation (member)	Lithology	k $Wm^{-1} K^{-1}$	Saturation
110.7	(Paintbrush Tuff)	Non-welded tuff	0.88	U
135.6		Non-welded tuff	0.69	U
166.8	(Pah Canyon Member)	Partially welded tuff	0.85	U
196.6		Moderately welded tuff	1.53	U
230.6		Bedded tuff	0.97	U
259.7	(Topopah Spring Member)	Welded tuff	1.67	U
279.4		Densely welded tuff	1.95	U
309.6		Densely welded tuff	2.01	U
337.2		Densely welded tuff	2.13	U
371.1		Densely welded tuff	2.15	U
394.2		Densely welded tuff	1.74	U
422.2		Densely welded tuff	1.71	U
451.6		Densely welded tuff	2.05	U
481.6		Densely welded tuff	2.09	U
495.5		Densely welded tuff	2.11	U
----- SWL (static water level) -----				
525.8		Bedded tuff	1.16	S
555.4	(Tuffaceous beds of Calico Hills)	Bedded tuff	1.10	S
579.3		Non-welded tuff	1.14	S
586.6		Non-welded tuff	1.06	S
617.4		Non-welded tuff	1.16	S
644.9		Non-welded tuff	1.16	S
675.7		Non-welded tuff	1.31	S

TABLE 3-2. Thermal conductivity of volcanic rocks from USW G-2 (continued)

Depth, m	Formation (member)	Lithology	$\text{Wm}^{-1} \text{K}^{-1}$	Saturation
700.6		Non-welded tuff	1.28	S
731.6		Non-welded tuff	1.19	S
761.8		Non-welded tuff	1.24	S
793.0		Partially welded tuff	1.37	S
822.4		Moderately welded tuff	1.37	S
852.6	Crater Flat tuff (Prow Pass Member)	Moderately welded tuff	1.89	S
885		Partially welded tuff	1.65	S
916.9		Partially welded tuff	1.51	S
951.5		Partially welded tuff	1.43	S
982.1		Non-welded tuff	1.56	S
1010.8	(Bullfrog Member)	Moderately welded tuff	1.83	S
1013.0		Moderately welded tuff	1.78	S
1028.5		Moderately welded tuff	1.89	S
1041.2		Non-welded tuff	1.81	S
1071.6		Bedded tuff	1.60	S
1101.6	(Tram Unit)	Lithic-rich tuff	1.90	S
1137.2		Partially welded tuff	1.60	S
1166.9		Partially welded tuff	1.92	S
1202.7		Bedded tuff	1.97	S
1234.1		Bedded tuff	1.76	S
1294.5	(Tuff of Lithic Ridge)	Partially welded tuff	1.98	S
1324.4		Partially welded tuff	2.07	S
1355.0		Partially welded tuff	1.98	S

TABLE 3-2. Thermal conductivity of volcanic rocks from USW G-2 (continued)

Depth, m	Formation (member)	Lithology	$\frac{K}{\text{m} \cdot \text{K} \cdot \text{K}^{-1}}$	Saturation
1385.1		Partially welded tuff	1.84	S
1416.0		Partially welded tuff	2.04	S
1444.8		Partially welded tuff	2.07	S
1461.9		Partially welded tuff	2.31	S
1498.1	(Rhyolitic lava and flow breccia)	Flow breccia	2.46	S
1535.6		Lava	2.16	S
1560.2		Lava	2.13	S
1588.9	(Quartz latitic lava and flow breccia)	Lava	2.40	S
1622.6		Lava	2.14	S
1650.5		Lava	1.77	S
1681.9		Flow breccia	1.92	S
1711.2		Flow breccia	2.11	S
1734.4	(Dacitic lava and flow breccia)	Lava	2.49	S
1765.8		Lava	2.04	S
1796.4		Bedded tuff	2.42	S
1827.0	(older tuffs of USW G-2)	Moderately welded tuff	2.21	S

TABLE 3-3. Thermal conductivity of volcanic rocks from USW G-3 and USW GU-3

Depth, m	Formation (member)	Lithology	$\text{Wm}^{-1} \text{K}^{-1}$	Saturation
35.7	Paintbrush tuff (Tiva Canyon Member)	Welded tuff	2.03	U
61.0		Welded tuff	2.20	U
96.0		Welded tuff	1.89	U
133.2		Bedded tuff (non-welded)	1.28	U
152.4	(Topopah Spring Member)	Moderately welded tuff	1.54	U
183.3		Moderately welded tuff	1.95	U
214.0		Welded tuff	2.26	U
253.3		Welded tuff	2.22	U
276.5		Welded tuff	2.23	U
311.6		Welded tuff	2.17	U
335.7		Welded tuff	2.01	U
367.3		Densely welded tuff	1.34	U
396.5		Partially welded tuff	1.08	U
453.0	(Tuffaceous beds of Calico Hills?)	Non-welded tuff	0.84	U
457.3		Non-welded tuff	0.91	U
489.4	Crater Flat Tuff (Frow Pass Member)	Non-welded tuff	2.50	U
519.1		Partially welded tuff	1.61	U
549.9		Partially welded tuff	1.02	U
580.6		Partially welded tuff	1.07	U
608.5		Bedded tuff	1.15	U
640.3	Crater Flat Tuff (Bullfrog Member)	Partially welded tuff	1.90	U
669.4		Welded tuff	1.86	U

TABLE 3-3. Thermal conductivity of volcanic rocks from USW G-3 and USW GU-3 (continued)

Depth, m	Formation (member)	Lithology	κ $\text{Wm}^{-1} \text{K}^{-1}$	Saturation
704.1		Welded tuff	1.98	U
734.7		Welded tuff	2.01	U
----- SWL (static water level) -----				
767.1		Moderately welded	1.91	S
791.2		Partially welded	1.31	S
- End GU-3 -				
795.4		Partially welded	1.20	S
829.7	Crater Flat Tuff (Tram Member)	Non- to partially welded tuff	1.73	S
859.9		Bedded tuff	1.69	S
920.6		Moderately welded	1.77	S
949.2		Partially to moderately welded tuff	1.77	S
986.4		Moderately to partially welded tuff	1.97	S
1011.9		Partially to moderately welded tuff	1.39	S
1042.9		Partially to moderately welded tuff	1.39	S
1074.1		Moderately welded tuff	1.66	S
1103.5		Moderately welded tuff	1.41	S
1134.1		Moderately to partially welded tuff	1.50	S
1162.1		Partially to moderately welded tuff	1.37	S
1194.8	Lithic Ridge Tuff	Moderately welded tuff	1.71	S
1224.7		Partially welded tuff	1.53	S
1255.9		Non- to partially welded tuff	1.60	S
1286.7		Partially to moderately welded tuff	1.64	S
1316.6		Partially welded tuff	1.74	S
1347.6		Moderately welded tuff	1.71	S

TABLE 3-3. Thermal conductivity of volcanic rocks from USW G-3 and USW GU-3 (continued)

Depth, m	Formation (member)	Lithology	$\kappa_{\text{m}^{-1} \text{K}^{-1}}$	Saturation
1347.6		Moderately welded tuff	1.71	
1377.6		Partially to moderately welded tuff	1.74	
1407.6		Partially to moderately welded tuff	1.75	
1438.9		Moderately to partially welded tuff	1.85	
1469.6		Moderately to partially welded tuff	1.86	
1499.8	Older tuffs (Unit A?)	Welded tuff	1.92	
1529.5		Welded tuff	1.80	

TABLE 3-4. Thermal conductivity of volcanic rocks from USW G-4

Depth, m	Formation (member)	Lithology	k $Wm^{-1} K^{-1}$	Saturation
27.6	Paintbrush Tuff (Tiva Canyon Member)	Densely welded tuff	1.88	U
77.2	(Tonopah Spring Member)	Densely welded tuff	1.33	U
116.1		Moderate to densely welded tuff	1.72	U
151.3		Densely welded tuff	2.03	U
183.8		Densely welded tuff	2.04	U
214.8		Densely welded tuff	2.17	U
253.0		Densely welded tuff	2.11	U
286.5		Densely welded tuff	2.21	U
324.8		Densely welded tuff	1.69	U
376.1		Densely welded tuff	1.87	U
418.5		Non-welded tuff	0.95	U
448.2	Rhyolite lavas and tuffs of Calico Hills (Tuffaceous beds of Calico Hills)	Non-welded tuff	1.11	U
479.6		Non-welded tuff	1.11	U
511.6		Non-welded tuff	1.14	U
----- SWL (static water level) -----				
544.3	Crater Flat Tuff (Prow Pass Member)	Non-welded tuff	1.23	S
570.8		Partially welded tuff	1.52	S
603.2		Non- to partially welded tuff	1.23	S
627.5		Partially welded tuff	1.21	S
660.5		Partially welded tuff	1.19	S
694.9	Crater Flat Tuff (Bullfrog Member)	Partially welded tuff	1.71	S
721.5		Partially welded tuff	1.25	S

TABLE 3-4. Thermal conductivity of volcanic rocks from USW G-4 (continued)

Depth, m	Formation (member)	Lithology	$W_m^{-1} K^{-1}$	Saturation
752.5		Partially welded tuff	1.36	S
786.1		Partially welded tuff	1.91	S
820.2		Partially welded tuff	1.39	S
849.9	(Tram Member)	Non- to partially welded tuff	1.28	S
873.4		Tuff	1.99	S
905.7		Tuff	1.25	S

TABLE 3-5. Thermal conductivity of rocks from UE25p1

Depth, m	Formation (member)	$\frac{K}{Wm^{-1} K^{-1}}$
1310.4	Lone Mtn. Dolomite	5.36
1330.5	Lone Mtn. Dolomite	5.08
1339.9	Lone Mtn. Dolomite	4.67
1351.6	Lone Mtn. Dolomite	4.91
1367.4	Lone Mtn. Dolomite	5.17
1387.0	Lone Mtn. Dolomite	4.71
1399.1	Lone Mtn. Dolomite	4.93
1414.5	Lone Mtn. Dolomite	4.76
1429.0	Lone Mtn. Dolomite	4.45
1454.1	Lone Mtn. Dolomite	5.09
1479.1	Lone Mtn. Dolomite	4.79
1490.5	Lone Mtn. Dolomite	4.94
1801.6	Roberts Mountains Formation	5.47

SE ROA 38280

JA_9562

ogy, in the form of written text, flow charts, cross sections, block diagrams, and tables. A conceptual model is an expression of the past and current state of the system based on field information from the site, and knowledge available from similar sites (Section 2.2). A more powerful groundwater model is one that quantitatively represents heads in space and time in a simplified representation of the complex hydrogeologic conditions in the subsurface. Broadly speaking, groundwater models can be divided into physical (laboratory) models and mathematical models.

1.2.1 Physical Models

Physical models include laboratory tanks and columns packed with porous material (usually sand) in which groundwater heads and flows are measured directly. For example, in pioneering work Darcy (1856) measured head in sand-packed columns of various diameters and lengths to show that flow in porous media is linearly related to the head gradient. Physical models are mostly used at the laboratory scale (e.g., Mamer and Lowry, 2013; Illman et al., 2012; Sawyer et al., 2012; Fujinawa et al., 2009). Analog models are laboratory models that rely on the flow of electric current (electric analog models; e.g., Skibitzke, 1961) or viscous fluids (Hele-Shaw or parallel plate models; e.g., Collins and Gelhar, 1971) to represent groundwater flow. Analog models of groundwater flow, especially electric analog models, were important in the 1960s before digital computers were widely available (e.g., see Bredehoeft, 2012).

1.2.2 Mathematical Models

We consider two types of mathematical models: data-driven models and process-based models. *Data-driven or "black-box" models* (Box 1.1) use empirical or statistical equations derived from the available data to calculate an unknown variable (e.g., head at the water table) from information about another variable that can be measured easily (e.g., precipitation). *Process-based models* (sometimes called physically based models although that usage is discouraged by Beven and Young, 2013) use processes and principles of physics to represent groundwater flow within the problem domain. Process-based models are either stochastic or deterministic. A model is *stochastic* if any of its parameters have a probabilistic distribution; otherwise, the model is *deterministic*. The focus of our book is process-based deterministic models, although we briefly discuss stochastic models in Boxes 10.1 and 10.4 and Section 12.5.

SE ROA 38281

A process-based mathematical groundwater flow model consists of a *governing equation* that describes the physical processes within the problem domain; *boundary conditions* that specify heads or flows along the boundaries of the problem domain; and for time-dependent problems, *initial conditions* that specify heads within the problem domain at the beginning of the simulation. Mathematical models can be solved analytically or numerically. Mathematical models for groundwater flow are solved for the distribution of head in space and also in time for transient problems.

Analytical models require a high level of simplification of the natural world in order to define a problem that can be solved mathematically to obtain a closed-form solution. The resulting analytical solution is an equation that solves for a dependent variable (e.g., head) in space and for transient problems also in time. Simple analytical solutions can be solved using a hand calculator but more complex solutions are often solved using a spreadsheet or a computer program (e.g., Barlow and Moench, 1998), or special software (e.g., MATLAB, <http://www.mathworks.com/products/matlab/>). Assumptions built into analytical solutions limit their application to relatively simple systems and hence they are inappropriate for most practical groundwater problems. For example, few analytical solutions allow for three-dimensional flow or hydrogeological settings with heterogeneity or boundaries with realistic geometries. Numerical models are even replacing the Theis (1935) analytical solution for aquifer test analysis (e.g., Li and Neuman, 2007; Yeh et al., 2014). Nevertheless, analytical solutions are still useful for some problems

Box 1.1 Data-Driven (Black-Box) Models

Data-driven models use equations that calculate system response (e.g., head) to input stresses (e.g., recharge from precipitation) without quantifying the processes and physical properties of the system. First, a site-specific equation is developed by fitting parameters either empirically or statistically to reproduce the historical record (time series) of fluctuations in water levels (or flows) in response to stresses. Then, the equation is used to calculate the response to future stresses. Data-driven models require a large number of observations of head that ideally encompass the range of all expected stresses to the system. They are used by themselves (e.g., Bakker et al., 2007) or with a process-based model (e.g., Gusyev et al., 2013; Demissie et al., 2009; Szidarovszky et al., 2007).

Early applications of data-driven models analyzed the response of karst aquifers (Dreiss, 1989) and applications to karst systems continue to be popular and successful (Fig. B1.1.1). Artificial neural network (ANN) models are data-driven models that have received much interest in the recent literature (e.g., Sepúlveda, 2009; Feng et al., 2008; Coppola et al., 2005). Data-driven models are also developed using Bayesian networks (e.g., Fienen et al., 2013).

Generally, process-based models are preferred over data-driven models because process-based models can make acceptable forecasts when large numbers of observations are not available and when future conditions lie outside the range of stresses in the historical record, such as response to climate change.

Box 1.1—cont'd

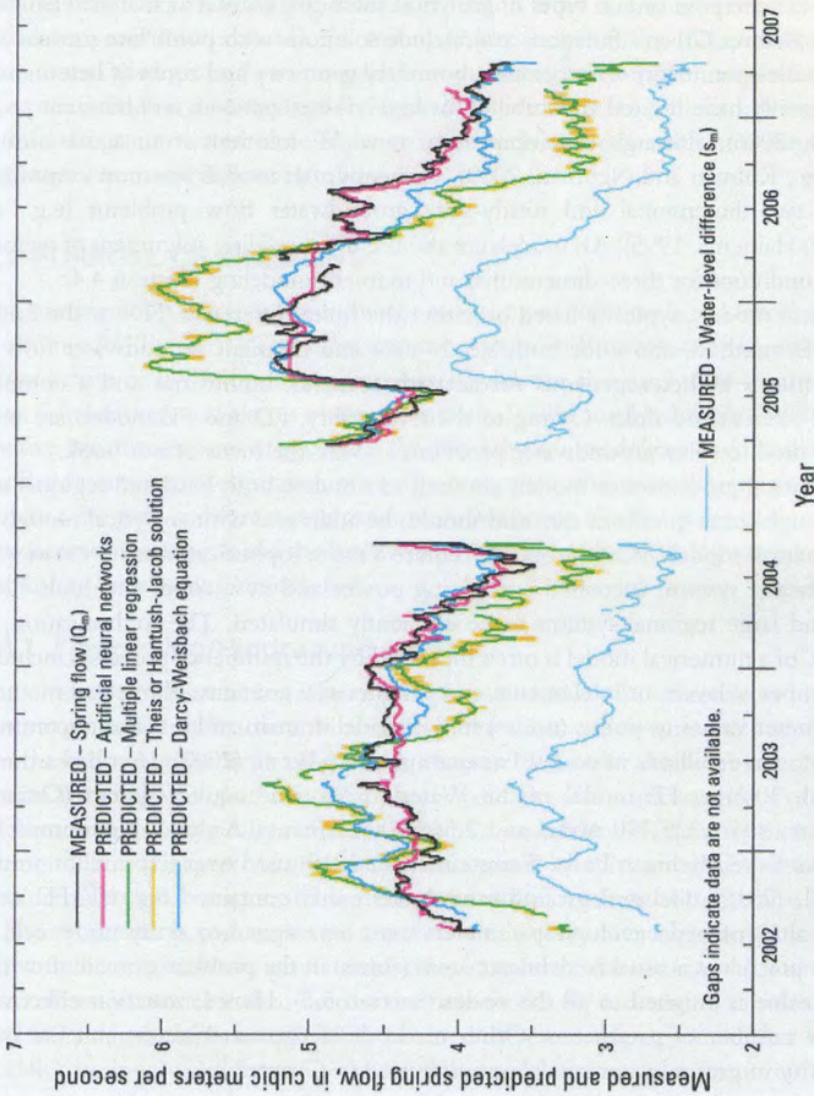


Figure B1.1.1 Springflow calculated using an ANN model and multiple linear regression compared with results from models for continuous porous media (Theis or Hantush-Jacob solutions) and conduit flow (Darcy-Weisbach equation). Springflow is also shown (Sepúlveda, 2009).

SE ROA 38283

and also provide important insight into the behavior of groundwater systems (Box 3.2). Analytical models can be useful interpretive tools to guide construction of more complex numerical models (Haitjema, 2006). Analytical solutions are also used to verify that codes that solve numerical models are programmed correctly (Section 1.6).

The analytic element (AE) method (Haitjema, 1995; Strack, 1989) provides a way to extend analytical solutions to more complex problems. The AE method relies on a computer code to superpose certain types of analytical solutions, known as analytic elements, which are based on Green's functions and include solutions with point/line sources and sinks. AE models can incorporate complex boundary geometry and zones of heterogeneity, but currently have limited applicability for highly heterogeneous and transient problems (Hunt, 2006), although development of new AE solutions is an active area of research (e.g., Kulman and Neuman, 2009). Currently, AE models are most commonly applied to two-dimensional and steady-state groundwater flow problems (e.g., see Hunt, 2006; Haitjema, 1995). AE models are also useful for guiding assignment of regional boundary conditions for three-dimensional and transient modeling (Section 4.4).

Numerical models, typically based on either the finite-difference (FD) or the finite-element (FE) method, allow for both steady-state and transient groundwater flow in three dimensions in heterogeneous media with complex boundaries and a complex network of sources and sinks. Owing to their versatility, FD and FE models are most commonly used to solve groundwater problems and are the focus of our book.

Mathematical groundwater models are used to simulate both local and regional settings. Although some questions can, and should, be addressed with analytical models or simple numerical models, many problems require a more sophisticated representation of the groundwater system. Increased computing power and new codes and tools allow complex and large regional systems to be efficiently simulated. The sophistication, or complexity, of a numerical model is often measured by the number of processes included and the number of layers, cells/elements, and parameters it contains. Numerical methods assign parameter values to points (nodes) in the model domain and it is not uncommon for models to have millions of nodes. For example, Frind et al. (2002) described a three-dimensional, 30-layer FE model of the Waterloo Moraine aquifer system (Ontario, Canada) that used 1,335,790 nodes and 2,568,900 elements. A three-dimensional FD model of the Lake Michigan Basin (Feinstein et al., 2010) used over two million nodes. Kollet et al. (2010) discussed groundwater models that contained 8×10^9 FD cells. Although values of hydrogeologic parameters must be assigned to every node, cell, or element, in practice it is usual to delineate areas (zones) in the problem domain in which a constant value is assigned to all the nodes (Section 5.5). Hence, zonation effectively reduces the number of parameters. Other methods of parameterization and the issue of complexity in groundwater models are discussed in Chapter 9.

We use the term *groundwater model* or model to mean the mathematical representation and associated input data for a specific problem. A *code* is a computer program that

such as flow. A *particle tracking code* takes output from a groundwater flow code and calculates groundwater flowpaths and associated travel times (Chapter 8). Codes are sometimes called groundwater models but we distinguish between a specific application of a code, which is a model, and the code itself, which is the tool for solving the model. A different groundwater model is designed for each application whereas the same code is used to solve many different problems.

1.3 PURPOSE OF MODELING

The starting point of every groundwater modeling application is to identify the purpose of the model (Fig. 1.1). The most common purpose is to forecast the effects of some future action or hydrologic condition, but models are also used to re-create past conditions (hindcasting) and also as interpretive tools. Reilly and Harbaugh (2004, p. 3) identify five broad categories of problems for groundwater modeling: basic understanding of groundwater systems; estimation of aquifer properties; understanding the present; understanding the past; and forecasting the future. We group the first three of these categories into interpretive models and the last two into forecasting/hindcasting models. We discuss forecasting/hindcasting models first.

1.3.1 Forecasting/Hindcasting Models

The objective of the vast majority of groundwater models is to forecast or predict results of a proposed action/inaction. Forecasting simulations are designed to address questions like those listed at the beginning of this chapter. We prefer the term forecast over prediction to emphasize that a forecast always contains some uncertainty. For example, a weather forecast is typically stated in terms of a probability (of rain, for example). Forecasting models (Chapter 10) are typically first tested by comparing model results to field measurements in a history matching exercise that is part of model calibration (Chapter 9). In history matching, parameters are adjusted within acceptable limits until model outputs, primarily heads and flows, give a satisfactory match to field-measured (observed) values. The calibrated model is then used as the base model for forecasting simulations.

Hindcasting (or back-casting) models are used to re-create past conditions. Hindcasting models may involve both a groundwater flow model and a contaminant transport model to simulate the movement of a contaminant plume. Examples of hindcasting models include those used in the well-known Woburn, Massachusetts Trial (Bair, 2001) and

SE ROA 38285

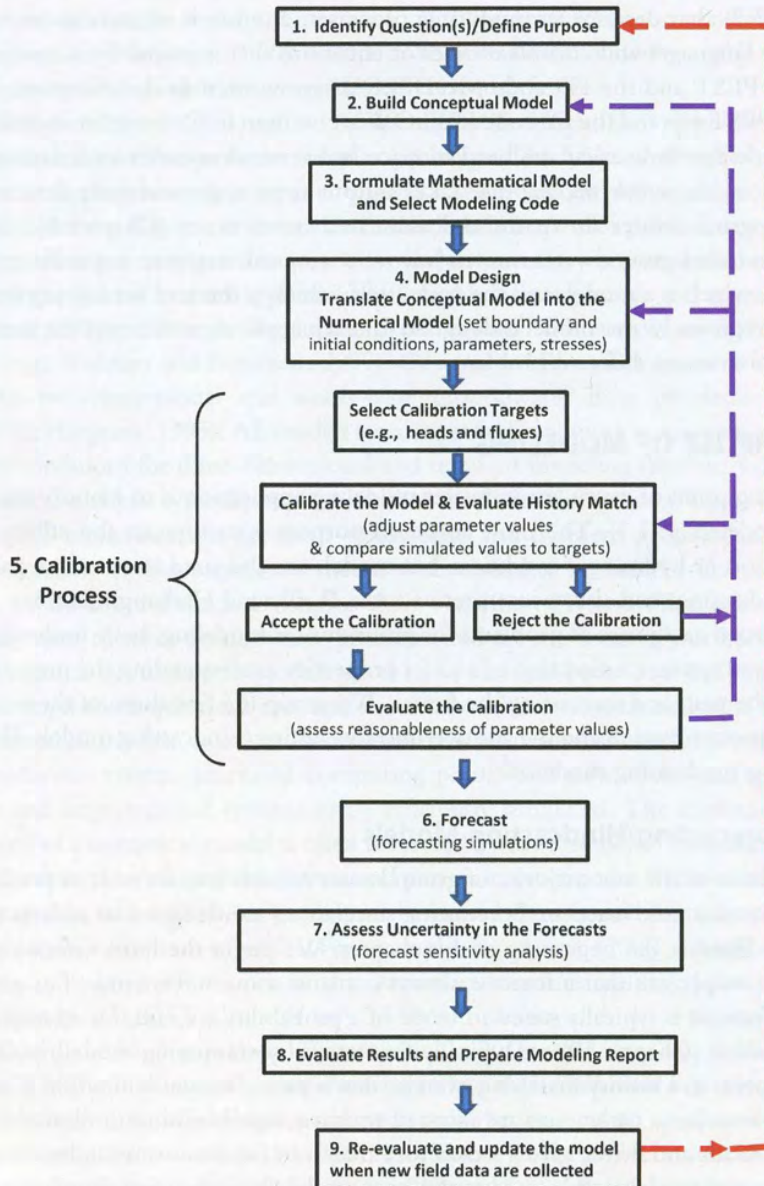


Figure 1.1 Workflow for groundwater modeling. As presented, the workflow assumes the objective of the model is a forecast but the workflow can be adapted for other modeling purposes, as described in the text. Although not shown in the figure, field data are critical for the workflow, especially conceptual model design and the calibration process.

answer to a specific engineering question; (2) *screening models* that help the modeler develop an initial understanding of a groundwater system and/or test hypotheses about the system; (3) *generic models* that explore processes in generic hydrogeologic settings. Models used as engineering calculators and generic models usually are not calibrated. Screening models may or may not be calibrated.

An example application of an interpretive model as an engineering calculator is the use of analytical and numerical models to calculate aquifer parameters from drawdown data obtained in an aquifer (pumping) test. Analytical models and sometimes numerical models are used as engineering calculators to verify new codes (Section 1.6).

A screening model vets a conceptual model or tests hypotheses about the flow system. A screening model might help in designing a more complex numerical model. For example, Hunt et al. (1998) developed a two-dimensional AE model as a screening model to develop boundary conditions for a three-dimensional FD model. Interpretive models also are used to conceptualize system dynamics and provide general insights into controlling parameters or processes at a field site. For example, during a major oil spill from a damaged well in the Gulf of Mexico, Hsieh (2011) quickly developed an interpretive MODFLOW model (adapted to simulate flow in a petroleum reservoir) to determine if measured shut-in pressure in the damaged well was indicative of a potential future catastrophic rupture of the capped well. The results were used to make the decision not to uncapp the well to reduce reservoir pressure, which proved to be the correct course of action.

Generic models are interpretive models applied to idealized groundwater systems. Generic models were used in the early days of numerical modeling of groundwater flow and continue to be useful. For example, Freeze and Witherspoon (1967) and Zlotnik et al. (2011) used two-dimensional generic models to study the effects of heterogeneity on regional groundwater flow in cross section. Woessner (2000) and Sawyer et al. (2012) used generic models to study exchange between groundwater and streams at the aquifer/stream interface (the hyporheic zone). Sheets et al. (2005) used generic models to assess the effect of pumping near regional groundwater divides.

1.4 LIMITATIONS OF MODELS

Groundwater models are simplifications of reality and thus are limited by underlying simplifying approximations as well as by nonuniqueness and uncertainty (Chapters 9

SE ROA 38287

and 10). Groundwater models never uniquely represent the complexity of the natural world. Therefore, groundwater models that represent the natural world have some level of uncertainty that must be evaluated and reported. In that respect, forecasting simulations for groundwater are similar to weather forecasts. Weather forecasts combine extensive datasets, representations of atmospheric physics, meteorology, and real-time satellite images within a highly sophisticated model, but the daily forecast is always given with probabilities. Similarly, results from groundwater models should be qualified by specifying the nature and magnitude of uncertainty associated with a forecast (Section 10.6).

1.4.1 Nonuniqueness

Nonuniqueness in groundwater models means that many different combinations of model inputs produce results that match field-measured data. Consequently, there will always be more than one possible reasonable model. Although early groundwater modeling applications typically reported only one calibrated model and presented only one possible forecast, this is unacceptable practice today. Either multiple calibrated models are carried forward in the analysis or the modeler chooses a preferred calibrated model and constructs error bounds around forecasted outputs. In either case, it is acknowledged that a groundwater model cannot give a single true answer.

Although models are critical tools, professional judgment, guided by modeling intuition and hydrogeological principles, is always required during a modeling project. Recognition of model uncertainty and nonuniqueness motivates the following underlying philosophy of modeling: "...a model cannot promise the right answer. However, if properly constructed, a model can promise that the right answer lies within the uncertainty limits which are its responsibility to construct" (Doherty, 2011).

1.4.2 Uncertainty

Uncertainty in groundwater models (Sections 10.2, 10.3) arises from a number of factors related to representing groundwater processes. In selecting a particular code, the modeler indirectly makes assumptions about the set of hydrologic processes important to the modeling objective because the selection of a code in effect reduces all processes under consideration to only those included in the code. Furthermore, current and future hydrogeologic conditions represented in a model cannot be fully described or quantified. Hunt and Welter (2010) described one source of uncertainty as "unknown unknowns," which are "...things we do not know we don't know" (from Former US. Secretary of Defense Donald Rumsfeld, February 12, 2002 press briefing). In groundwater models, *unknown unknowns* include unexpected (and hence unmodeled) hydrogeologic features such as heterogeneities in subsurface properties, as well as unanticipated future stresses. Bredehoeft (2005) cautioned modelers to anticipate the model "surprise" that occurs when new data reveal system responses caused by unmodeled hydrologic processes. For example, in a forecasting model there is uncertainty over future hydrological

“hydrosense” (Hunt and Zheng, 2012) help a modeler evaluate modeling output and identify flawed results. Modeling processes and results need to undergo rigorous “sensitivity analyses” that are rooted in basic hydrogeologic principles.

1.5 MODELING ETHICS

Ethics refer to pursuing a course of action that leads to morally right outcomes. Ethics in groundwater modeling means that the groundwater modeler acts in a morally responsible manner when planning, designing, and executing models and presenting modeling results. Ethics also means that the modeler remains unbiased and objective and strives to model according to the best available science for the modeling purpose. The modeler must maintain scientific integrity even when the results are not what the client expects, and when models enter regulatory and legal arenas. Tensions can arise between the modeler and teams of interdisciplinary scientists, lawyers, regulators, and stakeholders including industrial clients and the public-at-large. The modeler must resist inappropriate pressure from those groups as well as the pressure of societal, environmental, and regulatory concerns and steadfastly perform ethical modeling.

Modeling may be driven by regulatory concerns or even mandated by regulations. For example, groundwater models are required by the European Water Framework Directive (Hulme et al., 2002) or regulations may be written in such a way that the best (perhaps even only) way to satisfy a regulatory obligation is by groundwater modeling. When models are discussed in the courtroom, the modeler must be especially vigilant to present objective, unbiased results based on sound science. The U.S. Federal Court trial regarding groundwater contamination in Woburn, Massachusetts, which was the subject of a popular book (Harr, 1995) and a movie (*A Civil Action*), was notable for the conflict and confusion that surrounded the interpretation of the hydrogeologic system (Bair, 2001; Bair and Metheny, 2011; also see *Science in the Courtroom: The Woburn Toxic Trial*: <http://serc.carleton.edu/woburn/index.html>). In that case, competing groundwater models (a one-dimensional steady-state model and a three-dimensional, transient model) and differences in opinion among three expert witnesses over the basic hydrogeology and appropriate parameter values led to difficulties in fact-finding needed to reach a verdict.

Ethical issues may arise over decisions about model design (especially as related to model complexity), model bias, presentation of results, and costs of modeling. Each of these is discussed below.

SE ROA 38289

The AEM and Regional Carbonate Aquifer Modeling

by Cady Johnson¹ and Martin Mifflin²

Abstract

The analytic element method (AEM) has been applied to a 15,000-km² area of the Paleozoic carbonate rock terrain of Nevada. The focus is the Muddy River springs area, which receives 1.44 m³/s (51 ft³/s) of regionally derived ground water, and forms the Muddy River. The study was undertaken early in 2000 to support the development of a cooling water supply for a gas-fired generation facility 20 km south of the Muddy River springs. The primary objectives of the AEM modeling were to establish a better understanding of regional fluxes and boundary conditions and to provide a framework for examination of more local transient effects using MODFLOW. Geochemical evidence available in 2000 suggested two separate flow fields, one in the north discharging at the springs, and a southern area of small hydraulic gradients. To be conservative, however, hydraulic continuity between the two areas was maintained in the 2000 AEM model. Using new monitoring well data collected in the south, and analyses confirming that seasonal pumping effects in the north are not propagated to the south, a later AEM model that included a barrier calibrated with relative ease. The analytic element model was well suited for simulating an area larger than the immediate area of interest, was easy to modify as more information became available, and facilitated the stepwise development of multiple conceptual models of the site.

Introduction

In 1989, Las Vegas Valley Water District (LVVWD) filed landmark applications for all unappropriated water, $\sim 2.7 \times 10^6$ m³/d (800,000 acre-ft/year) in 26 hydrographic basins of eastern Nevada, later reduced to a maximum of 6.1×10^5 m³/d (180,800 acre-ft/year) in 17 basins. Alarmed by the potential impacts on springs and associated habitats, the National Park Service (NPS), U.S. Fish and Wildlife Service, Bureau of Land Management, and Bureau of Indian Affairs requested that the USGS quantitatively evaluate the effects of this pumping on regional flow and spring discharge. A highly generalized finite-difference model of the Carbonate Rock Province of the Great Basin was developed, consisting of two layers of 3660 cells, each 8.05 km (5 miles) wide by 12.1 km (7.5 miles) long (Schaefer and Harrill 1995). A flow

reduction on the order of 11% was predicted at the Muddy River springs after 100 years of pumping. Conceptually, these results were not unanticipated but offer no guidance as to where the ground water resources might be developed to minimize or prevent impacts.

Beginning in 2000, the analytic element method (AEM) was adopted as a primary modeling strategy in evaluating flow patterns and boundary conditions in a large (15,000 km²) area of carbonate rock terrain in southeastern Nevada, characterized by interbasin ground water flow and overlapping an area targeted for development by LVVWD. This application of the AEM, using GFLOW 2000 from Haitjema Software, was a departure from traditional methods in the region; previous modeling efforts generally relied on flux estimates based on hydrographic basin water budgets. In the AEM method, fluxes are determined from Darcian and mass conservation principles using aquifer characteristics and water-level data, with measured discharge of the Muddy River springs as a calibration target. The operational challenge of fitting model components to the geologic framework was aided by generally good regional exposures and was anchored by information from four local areas where characteristics of the carbonate aquifer were known from multiwell pumping experiments.

¹Corresponding author: Mifflin & Associates Inc., HCR 38, Box 126, Las Vegas, NV 89124; ircady@yahoo.com; maihydrogeol@starband.net

²Mifflin & Associates Inc., HCR 38, Box 126, Las Vegas, NV 89124

Received June 2003, accepted May 2005.

Copyright © 2005 The Author(s)

Journal compilation © 2006 National Ground Water Association
doi: 10.1111/j.1745-6584.2005.00132.x

The primary objective of the study was to forecast impacts of a 25- to 45-year, 8.6×10^6 m³/year (7000 acre-ft/year) pumping stress. Calpine Corporation would use the water for power generation at the proposed 750-MW Moapa Paiute Energy Center (MPEC). The MPEC wellfield targeted Paleozoic carbonate rocks that underlie much of the western portion of the Reservation. The first test well, ECP-1, yielded $\sim 6.3 \times 10^{-2}$ m³/s (1000 US gallons/min) for a 7-d constant-discharge test. The fundamental question for the Calpine project was the relationship of the carbonate aquifer of the site area to the Muddy River springs, the flows of which support the endemic Moapa dace, an endangered fish that inhabits the spring areas, and to senior water rights on the Muddy River, which originates at the springs and is fully appropriated under Nevada water law. Potential long-term impacts on another major spring complex, Rogers and Blue Point Springs, located ~ 40 km southeast of the MPEC in the Lake Mead National Recreation Area, were a concern of the NPS.

The area extending some 15 km northwest from the Muddy River springs is a zone of extremely high transmissivities, with small hydraulic gradients indicating flow toward the Muddy River springs (Ertec Western Inc. 1981). In contrast, hydraulic gradients between 2 and 30 km south of the springs were not known at the beginning of this study, nor were the properties of the aquifer, so fluxes within the carbonate rock terrain of the Reservation could not be estimated (Mifflin 1992; Dettinger 1989). Ground water flux in the project area is of great practical interest from the standpoint of tribal water rights as the magnitude and pattern may ultimately determine the allowable level of development based on Nevada water law.

The objective of this paper is to describe the application of the AEM to a poorly understood subregional area with hydrogeology dominated by highly transmissive carbonate rock terrain, and supporting analyses that allowed for refinement of subregional boundary conditions. The paper's scope includes monitoring well databases through the end of the year 2002 and brief observations on data acquired since 2002.

Hydrogeology

In the broadest terms, the hydrogeologic setting of the study area is one of ground water discharge from large springs at the southeastern margin of the Carbonate Rock Province of the eastern Great Basin (Figure 1 inset). Thinning and major facies changes in the carbonate rock section occur as a northeast-trending "hinge line" passing through the study area (Tschanz and Pampeyan 1970, 5); the hinge line represents the approximate boundary between the continental shelf and "miogeosyncline" for much of Paleozoic time. Also, overthrusts of the Sevier orogenic belt (Armstrong 1968) are exposed in a corresponding zone that extends from the Spring Mountains to the southwest to east of upper Moapa Valley (Figure 2). Regional-scale thrust faults, dismembered by Tertiary extension (Axen et al. 1990), ramp to the surface and place carbonate rocks above much less permeable Mesozoic red beds along a northeast trend. The combined effects of stratigraphic thinning and structurally induced

damming by Mesozoic and Cenozoic lithologies are thought to induce regional ground water discharge in the study area.

The oasis at the headwaters of the Muddy River, which supplies the entire base flow of this perennial stream, is referred to herein as the Muddy River springs area. The temperature, chemical characteristics, and temporal stability of discharge from these springs clearly indicate the "regional" character of the aquifer system that sustains their flow (Mifflin 1968). Flow in the Muddy River at Warm Springs Road has been monitored intermittently since 1913 by the USGS (site ID 09416000, "Muddy River near Moapa, Nevada") and reported as average daily flow. From the inception of monitoring until the early 1960s, base flow averaged ~ 1.3 m³/s (47 ft³/s).

Figures 1 (inset) and 2 (solid yellow lines) illustrate a series of hydrographic basins in the Carbonate Rock Province (Mifflin 1968, 1988; Dettinger et al. 1995) that were delineated by Eakin (1966) as the combined catchment for the White River flow system (WRFS), with a terminal discharge area at the Muddy River springs (H1 in Figure 1) in upper Moapa Valley (Figures 2 and 3). In Figure 2, Pahrnagat Valley (PV) is the location of three large springs classified as "regional" in the Mifflin (1968) study along with the Muddy River springs. The two northernmost basins of the Eakin (1966) WRFS in Figure 2, Long Valley and Jakes Valley, were subsequently noted by Mifflin and Wheat (1979) to display pluvial-climatic-state hydrologic evidence of leaking to the west into Newark Valley (to balance basin surface water catchment areas with pluvial lake areas in these basins). If these two northernmost basins' contributions are removed from Eakin's (1966) classical water balance that was derived for discharge measured at Muddy River springs, a balance is achieved at Pahrnagat Valley. Eakin's balance requires the majority of discharge for the Muddy River springs to be derived from flow that passes from Pahrnagat Valley south through Coyote Spring Valley and then southeastward to the springs (F3 to K2 to K3 to H1 in Figure 1). Water discharging in Pahrnagat Valley is, however, almost devoid of fluoride and isotopically much lighter than Muddy River springs. Muddy River springs' fluoride and stable isotope compositions are more akin to water in upper (northern) Meadow Valley Wash (Figure 2) than to those in Pahrnagat Valley (Thomas et al. 1996).

The Muddy River spring area hydrology is locally complex, with an alluvial aquifer comprising coarse gravel lenses inset into the fine-grained Muddy Creek Formation (Schmidt et al. 1996). Between 1987 (Mifflin & Associates Inc. 1987) and 1996 (Mifflin and Adenle 1996), the status of known wells and springs in the upper Moapa Valley was documented on a quarterly basis. The alluvial aquifer is supplied by subsurface inflow from the northwest of roughly 8.3×10^4 m³/d (34 ft³/s) from the carbonate rock flow system. An additional 4.1×10^4 m³/d (17 ft³/s), or one third of the total ground water discharge (Figure 4), issues from large springs via carbonate-cemented conduits through the alluvial gravels. Roughly 0.1 m³/s (4 ft³/s) is lost to evapotranspiration on an annualized basis. A well-developed seasonal cone of depression forms around

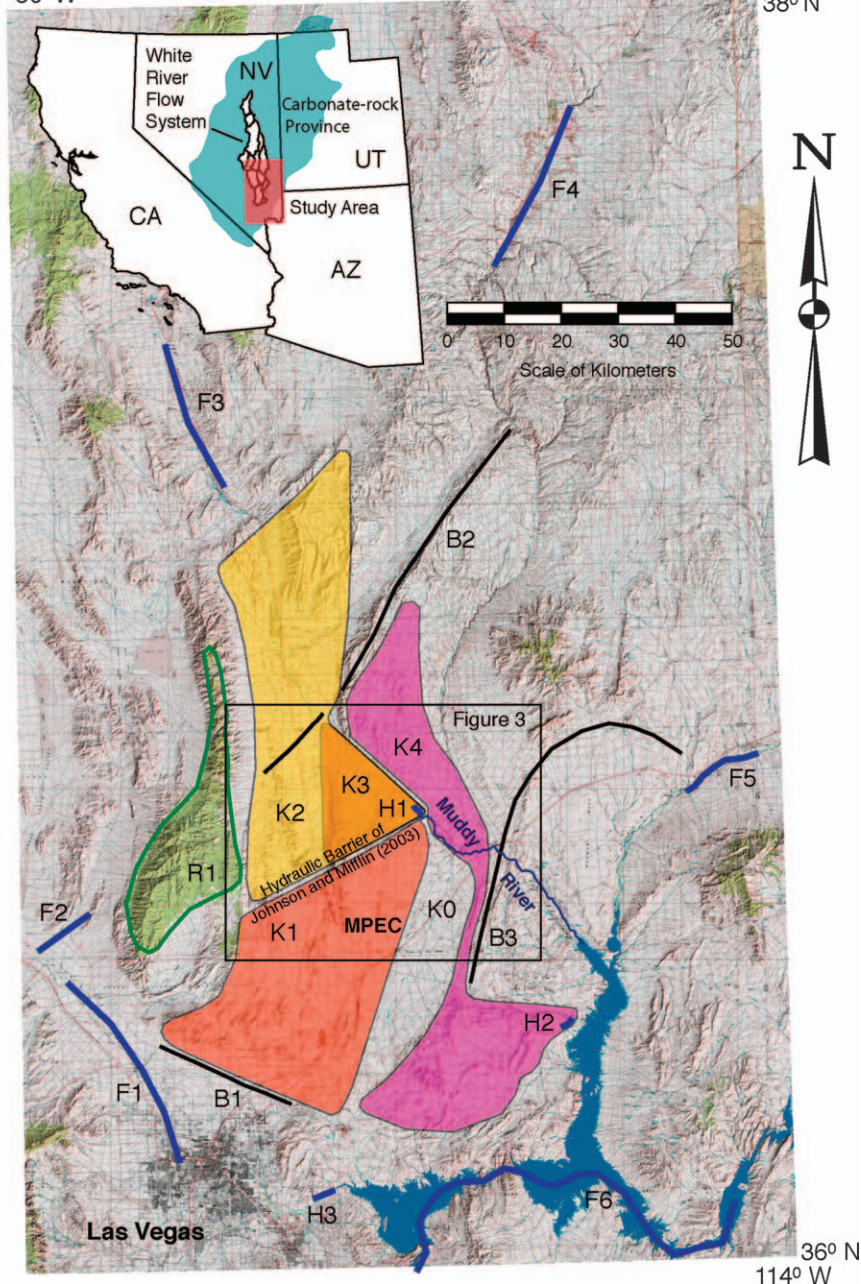


Figure 1. Analytic element representation of the study area, showing hydraulic conductivity domains (K), no-flow barriers (B), far-field features (F), near-field discharge (H), and recharge (R); see reference Table 1 for details.

Nevada Power Company's production wells in the alluvial aquifer and migrates down-valley toward the Muddy River springs during the summer pumping season; there was recovery each winter until 1997. Flow reductions are attributed to effects of the pumping cone on seepage flux from the unconfined alluvial aquifer into the headwaters channels of the Muddy River.

Upstream of the spring area near the Nevada Power Company (NPC) Lewis Well Field (Figure 5), there is local hydraulic continuity between the carbonate aquifer, source for the Arrow Canyon well, and the alluvial aquifer, local source for the Lewis wells. Between this important zone of inflow to the alluvial aquifer and Big Muddy Spring, the alluvial aquifer remains unconfined, but evidence for hydraulic connection with the carbonate aquifer

is absent. Near Big Muddy Spring, the alluvial aquifer discharges via seepage into headwaters channels of the Muddy River, and spring outflow channels combine flows to establish the total discharge represented by the Muddy River gauge (Figure 5). Spring conduits (active and relic) are encased by highly cemented zones and, for the most part, hydraulically isolated from the alluvial aquifer. Two wells (LDS East and Central), finished in conduit-cemented gravels (relic conduits), respond instantaneously to pumping stress changes, suggesting a high degree of hydraulic continuity with the carbonate aquifer based on the response characteristics and elevated temperatures. Downstream of the spring area, the alluvial aquifer becomes confined and hydraulically separated from the river channel and remains so southeastward to where monitoring

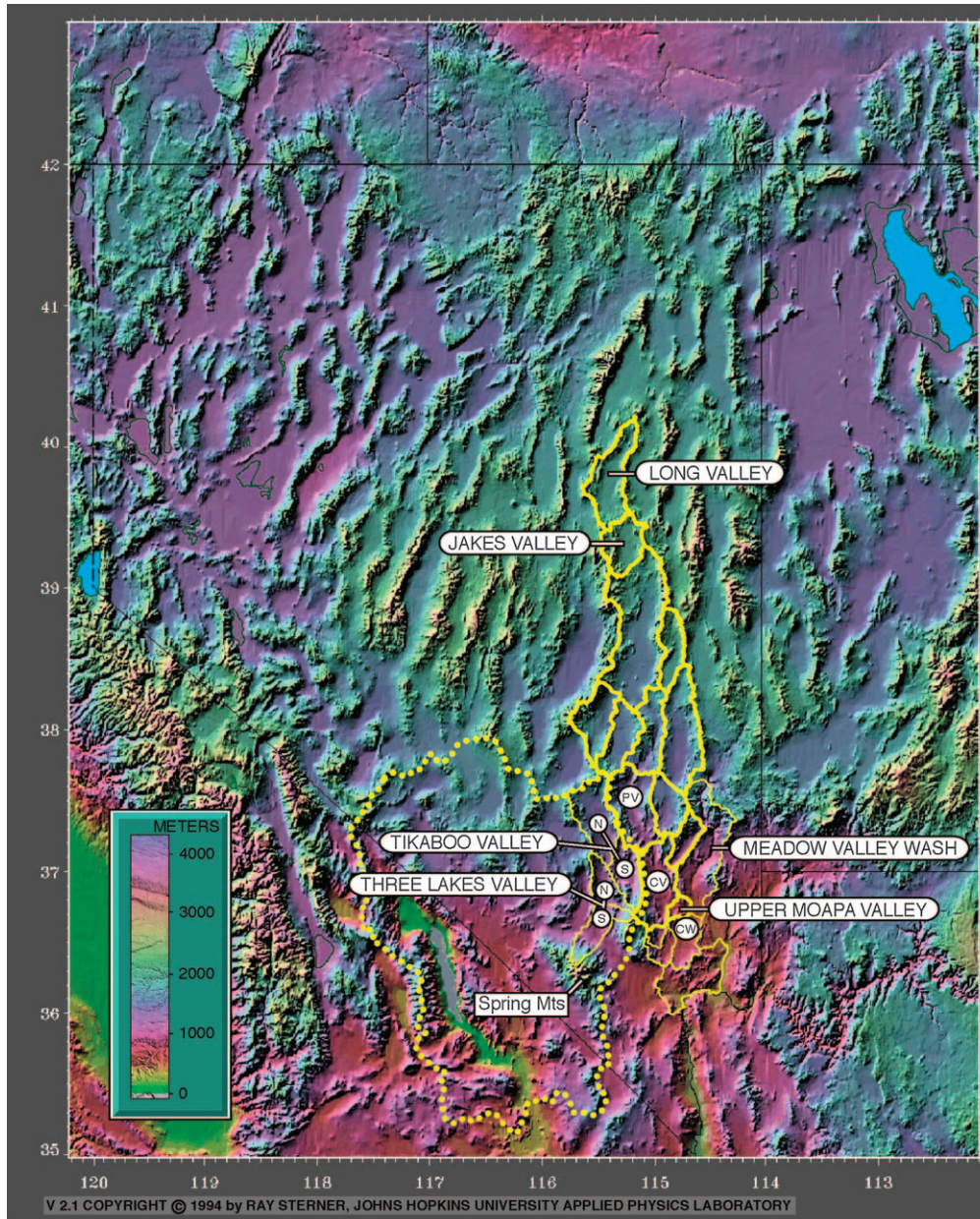


Figure 2. Regional topography showing Eakin's (1966) WRFS delineation (bold outline); flanking southern basins (narrow outline); Death Valley Regional Flow System (dotted) (U.S. Department of Energy 2002); and north (N) and south (S) subdivisions of Tikaboo and Three Lakes Valleys (Southern Nevada Water Authority 2003). PV = Pahrnagat Valley; CV = Coyote Spring Valley; CW = California Wash. Base map mosaic copyright 1994 to 2002 by Andrew D. Birrell, used with permission.

well control ends. The Warm Springs Road Muddy River gauging station is located on the reach where there is no hydraulic continuity between the alluvial aquifer and river channel.

In 1985, NPC expanded its monitoring activities to include carbonate aquifer water levels in addition to monthly production totals from each of its wells in the Muddy River springs area. Monitoring records from carbonate rock aquifers became available in 1986, when NPC wells EH-4 and EH-5b were fitted with chart recorders and the USGS began taking monthly water-level measurements in MX-4. Seasonal fluctuations and long-term decline followed by recovery after the drought years of 1987 to 1992 are evident in all the three records. In the California Wash hydrographic basin (Figure 2), a water

resources appraisal was conducted for LVVWD in 1990 (Wildermuth et al. 1990), but no potentiometric data were available from carbonate rock aquifers within 18 km of the proposed MPEC facility until 1998 (Terracon; unpublished data). Systematic monitoring in this southern area began late in 2000, and the first full year of record was 2001 (Figure 6).

Basin Water Budgets, Interbasin Flow, and Subregional Fluxes

Hydrographic basin water budgets are the fundamental accounting system used by the Nevada Division of Water Resources to administer the State's limited but uncertain ground water resource. Using the Maxey-Eakin

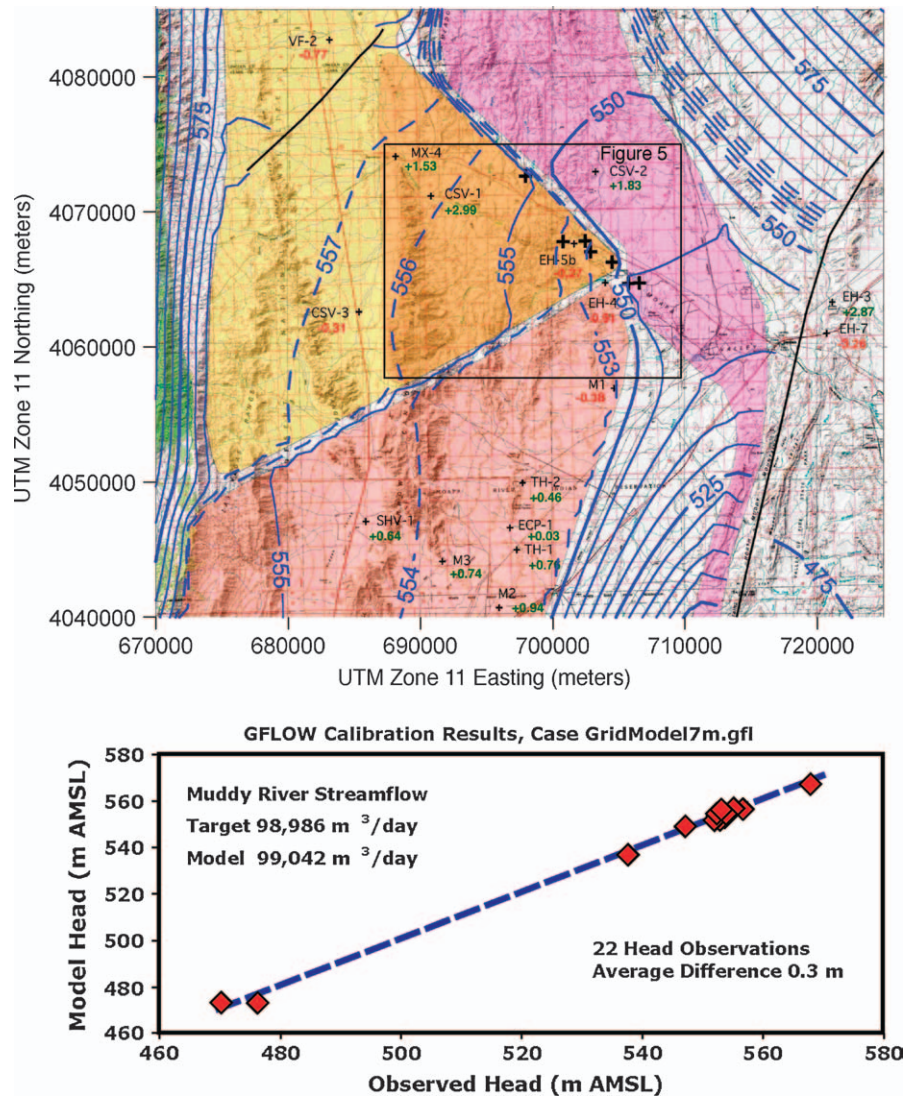


Figure 3. AEM model results for year 2001 conditions with calibration summary, showing head contours (meters above mean sea level) and residuals (meters + or -) at monitoring well locations. Contour interval is 1 m where dashed, 5 m elsewhere. “+” indicates model locations of ground water extraction by Nevada Power Company and Moapa Valley Water District.

method for estimating recharge (Maxey and Eakin 1949), percentages of precipitation falling within elevation zones were designated as recharge, with higher recharge efficiencies associated with the higher elevation (precipitation) zones. The contributions of each elevation zone to recharge were adjusted iteratively so that their sum would balance with discharge estimates in several control basins. Recharge estimates, established in this way as empirical percentages of precipitation assigned to elevation zones in the control basins, were then extrapolated to hydrographic basins throughout the Great Basin. The Maxey-Eakin method relies on two basic assumptions that appear to hold in the control areas:

- The hydrographic basin is also a hydrologically closed basin.
- The efficiency of recharge is uniform regardless of terrain lithology.

However, neither of the above assumptions is necessarily met in the more general case of the Carbonate Rock Province. The carbonate lithologies are likely more efficient in capturing greater percentages of incident

precipitation, and hydrologic closure for many hydrographic basins remains uncertain.

The Eakin (1966) water budget approach is based on a “series” configuration of interbasin flow; water is transferred through a series of discrete compartments (basins) down a regional gradient. The method as generally applied does not accommodate “parallel” configurations, proposed by Tóth (1962, 1963) and explored through modeling analyses by Freeze and Witherspoon (1966, 1967, 1968). In suitable hydrogeologic environments, regional interbasin flow may bypass more localized ground water flow systems. The observed geographic distributions of the “regional”-class springs of Mifflin (1968) suggest that the parallel configuration of interbasin flow may be common and frequently unidentified by the basin water budget analytical procedure.

The efficiency of recharge for a given precipitation zone could be significantly greater in carbonate terrain than assigned in the Maxey-Eakin method, but there has been little comprehensive study to determine how much more efficient. The AEM-derived fluxes are independent

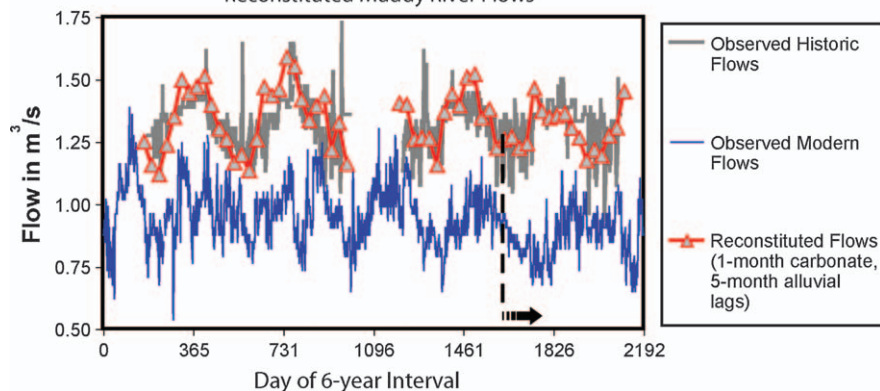


Figure 4. Flow reductions due in part to ground water pumping, accompanied by time lag in occurrence of seasonal discharge pattern of the Muddy River. The Muddy River responds to surface diversions immediately, to pumpage from the carbonate aquifer the following month and does not sense extractions from the alluvial aquifer until 5 months after they occur. Lag relations are attributable to depletion of storage in the alluvial aquifer, observed in monitoring records.

of hydrographic basin water budgets, thereby providing an alternative to Maxey-Eakin-derived flux estimates and their implicitly assumed configurations of interbasin flow. With evidence accumulating that the Muddy River springs are not the terminus of the WRFS (two independent lines of evidence suggest it terminates at Pahranaagat Valley and excludes Jakes Valley and Long Valley), the AEM is elevated in importance for evaluating subregional fluxes related to interbasin flows.

The AEM Model and Supporting Analyses

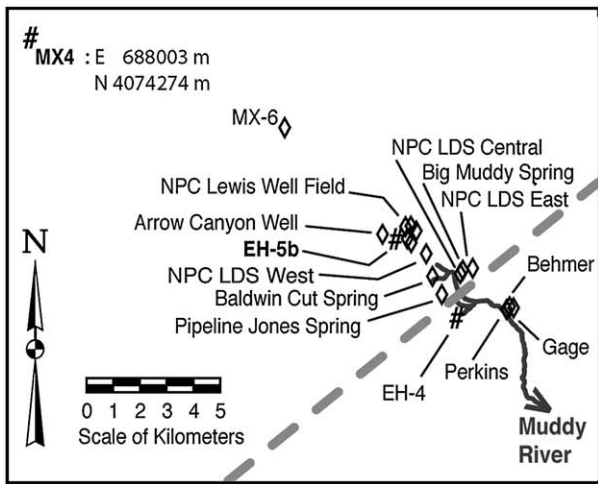
Table 1 summarizes the features and properties of the AEM model as constituted in Figure 1. The AEM was selected to support a fast-track, year-2000 effort to locate a wellfield site, conduct aquifer characterization, establish a monitoring network, and provide an impact assessment for the proposed ground water extraction that would supply MPEC (Johnson et al. 2001). In the subregion of the study area, only four widely spaced areas with aquifer testing in carbonate aquifers were available to suggest material properties for the model (Ertec Western Inc. 1981; Mifflin & Associates Inc. unpublished Bonneville Pacific/Nevada Cogeneration Associates data; Buqo 1994; Johnson et al. 2001). Even less aquifer test data were available from Muddy River alluvium (Mifflin & Associates Inc. 1987) and the Muddy Creek Formation (Johnson et al. 1986). Regional relationships of hydro-chemistry and water temperature (Thomas et al. 1996), a few key continuous monitoring well records (USGS, Nevada Power Company, and Mifflin & Associates Inc. unpublished), and distribution of pumping stress (unpublished data in files of Nevada State Engineer) were also available. Major structural features and the resulting distribution of lithologies are complex, but the carefully documented flux of the Muddy River spring area, pumping records, and Muddy River flow records tightly constrain the magnitude of ground water discharge.

In the early efforts toward constructing an AEM representation of the area, reviews of the regionally estimated fluxes, mixing models based on basin water

budgets, and isotopic mass balance (Kirk and Campana 1990; Thomas et al. 1996, 2001) were considered in efforts to constrain the more troublesome uncertainties, such as recharge fluxes in adjacent mountainous terrain. The result of these efforts, facilitated by stepwise AEM modeling, was a set of revised conceptual models that addressed uncertainties and inconsistencies in prior analyses, some of which (notably Eakin 1966) have stood unquestioned for decades.

The model has been based on an infinite aquifer, 1524 m (5000 feet) in thickness throughout its stages of development. Two primary observations governed the thickness estimate: measured thicknesses of carbonate rock in the stratigraphic section (Longwell et al. 1965) and ground water temperatures in the 29°C to 35°C range (9°C to 15°C above the mean annual temperature) from Coyote Spring Valley to the Muddy River springs area and south beyond the MPEC site (Johnson et al. 2001). Although this is a remarkable thickness for widespread vertical hydraulic continuity, available evidence supports this order of magnitude thickness of transmissive rock and active ground water circulation in the subregion. The fundamental assumption in application of the AEM is that Dupuit-Forchheimer approximation of the flow field (Freeze and Cherry 1979; Haitjema 1995) is appropriate. In considerations of regional flow, where vertical variations in fluid potential are much less than those that occur over the lateral extent of the model domain, calculations based on Dupuit-Forchheimer flow should compare favorably with more rigorous methods (Haitjema 1995).

Monitoring records were instrumental in driving the evolution of the conceptual model of the area and its AEM representation (Figure 3). In 2000, no monitoring records suggestive of the hydraulic barrier between K1 and K3 existed. A feature limiting or blocking southward ground water flow from the Muddy River springs (H1) area was suspected based on incompatible water chemistries between the spring area discharge water and the southern flow field (K1). Available water-level data suggested that any lateral flow from the K3/H1 spring area southward should result in compatible hydrochemical



Well Hydraulics Model with N45E Flow Barrier

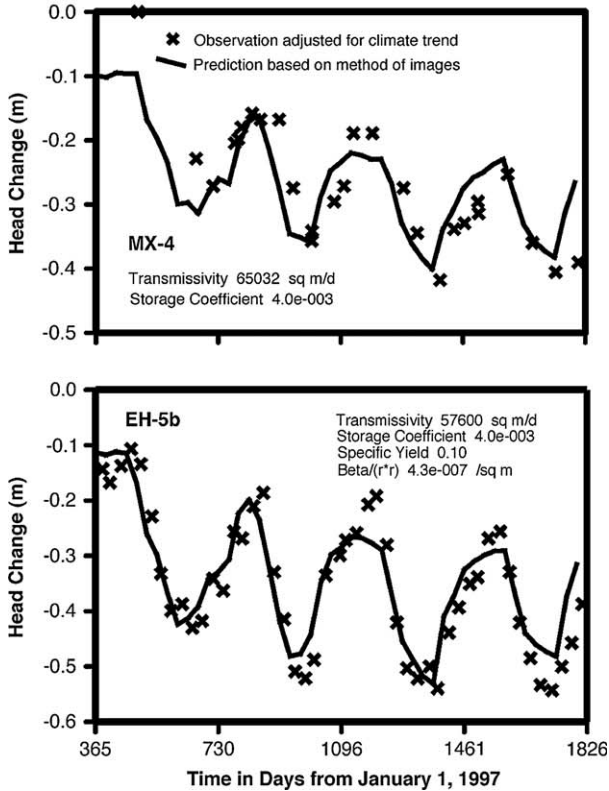


Figure 5. Parameter estimation for Zone K3, based on monthly stress periods, 1997 to 2001, and fitting 1998 to 2001 water levels. Image-well boundary trending N45E through EH-4 location (dashed line) was assumed. Raw measurements by USGS (at MX-4) and NPC (at EH-5b) were detrended to remove -8.32×10^{-2} m/year climate effect, based on southern flow field records (Figure 6).

evolution. A decision was made to adopt a conservative modeling approach by allowing hydraulic continuity to carry through from the northern domain to the southern domain in accord with the apparent continuity of carbonate rock (Schmidt et al. 1996), which, in retrospect, made the early AEM calibration difficult. In this manner, conservative analyses of impacts on spring flows were obtained, and the available evidence suggesting a barrier was discussed but not embedded in the AEM or derivative MODFLOW modeling analyses of the transient pumping impacts (Johnson et al. 2001).

Southern Flow Field Records for 2001, with Distances from Center of Pumping

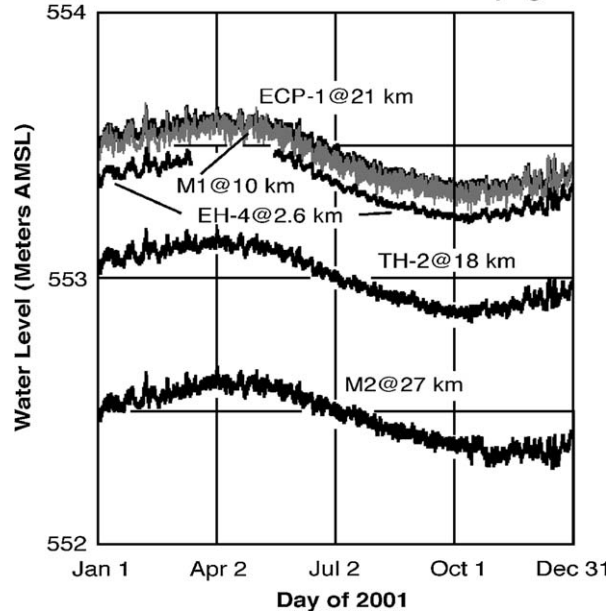


Figure 6. Evidence for hydraulic barrier between southern (Zone K1) and northern flow fields (Zones K2 and K3). Signals are essentially identical from 2.6 to 27 km south of the weighted center of pumping, indicating no distance-drawdown relationship and therefore no pumping effects.

As the Reservation area (northern K1) monitoring records accumulated during 2001, the first physical (as contrasted to hydrochemical) evidence for a barrier between the areas was developing. The characteristic pumping-induced asymmetry of the EH-5b and MX-4 monitoring well hydrographs is not present in those from K1; instead, a uniform annual water-level fluctuation cycle and long-term decline are characteristic of the southern records. Two of these wells (EH-4 and M1) are closer to the pumping area than MX-4, and one (TH-2) is about the same distance; yet, no clearly defined asymmetry of the seasonal pulse is evident in the 2001 data. These observations encouraged further analyses in an attempt to better understand the periodicities and regional multiyear water-level declines. It should be noted that the 2002 to 2004 monitoring records indicate the same downward trend and congruent hydrographs in the K1 domain.

Figure 3, a realization from the second-generation AEM model, incorporates a low-permeability "hydraulic barrier" of K0 material between the K1 and K3 domains in Figure 1. In the model, the barrier terminates at its northeast end against the K4 domain, which supplies the flow to Rogers and Blue Point Springs, H2. The area where the barrier approaches K4 presents the greatest uncertainty in the model, which is quite sensitive to the poorly constrained conditions there. Structural elements responsible for the barrier may in fact continue far to the northeast, the area where the Weiser Syncline (B3) terminates in a large drag fold against the Mormon Mountains (Axen et al. 1990), but no monitoring well records are available to support this idea. The southwestern extent of the barrier is suggested by an abrupt transition between upright and overturned beds in the Arrow Canyon Range,

and the northern termination of the Dry Lake Thrust Fault (Page 1992).

The Figure 3 AEM realization, with a “soft” or “leaky” version of the barrier of Johnson and Mifflin (2003), calibrates well with water-level data and observed spring flow. A hydraulic barrier between K1 and K3 was established as a fundamental model component on the basis of (1) the Figure 4 analyses of sources of ground water pumped in the Muddy River springs area (K3); (2) the Figure 5 parameter estimation based on EH-5b and MX-4

monitoring well hydrographs in K3; and (3) the Figure 6 Reservation area (K1) monitoring well records that became available in 2001. These analyses and monitoring well records, when combined with the geochemical differences between the water of the K1 and K3 domains (Johnson et al. 2001), support the inclusion of the low-permeability zone between these areas depicted in Figures 1 and 3. The northeast-southwest trend passing just north of monitoring well EH-4 is constrained to that location and orientation by the affinity of the EH-4

Table 1
Features and Properties of the MPEC Analytic Element Model (from Figure 1)

Far-Field Controls		
F1	Corn Creek to Las Vegas	Specified heads 892 to 652 m
F2	Divide Well to Cow Camp	Specified heads 895 to 867 m
F3	Pahranagat Valley	Specified heads 1100 to 900 m
F4	Upper Meadow Valley Wash	Specified heads 1500 to 1300 m
F5	Virgin River	Specified heads 500 to 450 m
F6	Colorado River	Specified heads 250 to 200 m
Inhomogeneities		
K0	Far-field zone	$K = 0.064$ m/d, obtained by calibration
K1	Southern flow field	$K = 6.1$ m/d from 7-d aquifer test reported by Johnson et al. (2001). Bounded on south and west by Las Vegas Shear Zone and Gass Peak Thrust, respectively (Longwell et al. 1965); on north by subregional hydraulic barrier described by Johnson and Mifflin (2003 and this study), and on east by down-faulted Tertiary (K0) sediments of California Wash (Johnson et al. 1986; Langenheim et al. 2001, 2002)
K2	Northern flow field	$K = 12.2$ m/d, obtained by calibration. Bounded on west by Gass Peak Thrust, on north by Menard Lake Fault, and on east by Delamar Mountains Thrust and fold belt (Tschanz and Pampeyan 1970)
K3	Arrow Canyon zone	$K = 36.6$ m/d from analysis of seasonal pumping response, 1997 to 2001 (Johnson and Mifflin 2003 and this study). Bounded on west by normal fault on west side of Arrow Canyon Range
K4	Glendale cell	$K = 5.5$ m/d, obtained by calibration. Isotopic data reviewed by Pohlmann et al. (1998)
Near-Field Discharge		
H1	Muddy River springs	Specified heads 536 to 530 m, hydraulic resistance 1.35 d
H2	Rogers/Blue Point Springs	Specified heads 488 to 463 m, hydraulic resistance 2.7 d
H3	Southern receptor zone	Specified heads 450 to 396 m at south end along Las Vegas Wash, hydraulic resistance 2 d
No-flow barriers		
B1	Las Vegas Shear Zone	Accounts for large hydraulic gradient between southern flow field (K1) and Las Vegas Valley, and absence of candidate outflow component in Las Vegas Valley ground water (Johnson et al. 2001)
B2	Kane Springs Wash Fault	Diverts flow from north around area of exposed basement rock in Mormon Mountains (Tschanz and Pampeyan 1970); southwestward extension in Coyote Spring Valley required to fit VF-2 and CSV-3 water levels (Figure 3)
B3	Weiser Syncline	Continuous feature per Axen et al. (1990), bent and rotated clockwise at northern end by Moapa Peak Shear Zone; required to match EH-3 and EH-7 water levels (Figure 3)
Recharge		
R1	Sheep Range	0.7 cm/year in forested highlands, by calibration. Recharge area encompasses 420 km ² , total 2.94×10^6 m ³ /year (2380 acre-ft/year). Previous estimates include 2000 acre-ft/year (Eakin 1966), 5000 to 6000 acre-ft/year (Kirk and Campana 1990) and 14,000 acre-ft/year (Thomas et al. 1996)

hydrograph with several others to the south (Figure 6), which as a group are distinct from those northwest of the barrier (Figure 5), and by the need for a no-flow boundary in close proximity to the center of pumping for the image-well analysis of Figure 5.

Figure 4 reconstitutes Muddy River flows for the period 1997 to 2002 by adding monthly surface water diversions and ground water pumpage to base flows, with carbonate aquifer pumpage delayed 1 month and alluvial aquifer pumpage delayed 5 months. The exercise is simple addition by spreadsheet, with the lags obtained by trial-and-error comparison of trial results with the 1913 to 1918 record. These lag estimates are compatible with a cone of depression that develops each summer in the alluvial aquifer, migrating down-valley over the pumping season until it intersects the headwaters channels of the Muddy River, then recovering completely by the next pumping season (Mifflin and Adenle 1996). The reconstituted record compares remarkably well with the 1913 to 1918 Muddy River record in both timing and magnitude of seasonal flows. Three key relationships are recognized:

- The flux reaching the spring area has remained constant for almost a century.
- The seasonal variability of flows in the 1913 to 1918 record is likely due to evapotranspiration in the heavily vegetated headwaters area of the Muddy River based on the close correlation of flow differences to seasonal temperatures.
- All ground water diversions of the 1997 to 2002 record are manifested by 1:1 decreases in Muddy River discharge.

The latter point, all water is accounted for in the Muddy River springs system, has bearing on the multiyear downward trend observed in all the monitoring wells in K1, K2, K3, and K4 during the 1997 to 2004 drought. When the analysis of Figure 5 was performed, the data in K3 were detrended according to the rate that is characteristic throughout the K1 domain, where the long-term decline is attributed entirely to drought. The analysis, performed with Aquifer^{win32} from Environmental Simulations Inc. (Reinholds, PA) attempted to replicate the pumping-induced hydrographs of monitoring wells EH-5b and MX-4 of the K3 domain. The forcing function for the well hydraulics analysis was based on monthly production totals from 10 wells that produced at a combined average rate of 2.14×10^4 m³/d (8.74 ft³/s) in 2001, a typical year (Table 2) with pumping heavily weighted toward the summer months. To match the hydrographs, a no-flow boundary condition was necessary (from image-well analysis), consistent with the “hydraulic barrier” proposed by Johnson and Mifflin (2003). The derived parameter estimates also proved consistent with the AEM calibration of K3 with Muddy River spring discharge, adding additional confidence in the interpretation of the “barrier” as well as the interpretation of the asymmetrical hydrographs as representing a pumping signal.

Figure 6, the synchronous, but geographically widely distributed 2001 hydrographs of the new monitoring wells in the Reservation area of K1, and EH-4 near the Muddy River spring area, are suggestive of a barrier and

Table 2
Ground Water Diversions, 2001

Well ID	Annualized Q (m ³ /d)
Arrow Canyon	8224
MX-6	1046
Lewis 1	369
Lewis 2	64
Lewis 3	1462
Lewis 4	1243
Lewis 5	1351
LDS West	2365
LDS Central	3215
LDS East	2046
Behmer	2761
Perkins	1654

Note: Behmer and Perkins data were used in the regional AEM model but not in the well hydraulics model since they are located southeast of the image-well boundary.

encouraged the above analyses. The synchronicity, identical amplitudes both near and far from the pumping center, and absence of a hint of the asymmetry seen in the EH-5b and MX-4 signals (Figure 5) suggest that the periodicity in these wells cannot be a porous-media response to seasonal pumping in K3 to the north. On the other hand, a loading or tidal mechanism for this magnitude of annual aquifer response does not seem reasonable. It is conceivable that a seasonal pumping signal could be propagated southward, with little attenuation along fractures of the Hogan Spring Fault Zone (Schmidt et al. 1996), thus supplying a similar response to the larger K1 area. A 7-d aquifer test (Johnson et al. 2001), however, produced a porous-medium response with no evidence of direct fracture connections between ECP-1, TH-1, and TH-2 (Figure 3). Though the periodicity observed in the K1 domain remains enigmatic, the weight of the evidence indicates that the annual periodicity in the southern flow field is not directly related to seasonal pumping in upper Moapa Valley.

Benefits of the AEM Approach

AEM modeling facilitated a realistic, simple beginning of hydrogeologic assessment but also allowed the easy incorporation of complexity as additional data became available. The ability to simulate a large domain was important for maintaining flexibility in the site area while minimizing boundary artifacts and was easily accommodated by the AEM assumption of an infinite aquifer. A strength of the method lies in the mechanics of its implementation, a logical progression from embedding what is known and easily seen at the land surface to exploring the effects of changes to the underlying conceptual models. The ease of adding and deleting analytic elements helps to determine if a conceptual model with added complexity makes sense or should be discarded. In practice, the AEM approach allows many more realizations within a given time frame (project duration) than alternative methods.

Testing multiple conceptual models is critically important for understanding the effects of adding features that may not exist, or omitting key features that do. The more sparse the constraining databases, the more important this insight—as demonstrated by our initial failure to embed the hydraulic barrier between the northern (K3) and southern (K1) flow fields. Hydrochemical evidence alone, however compelling in terms of indicating a non-Muddy River springs-type water source for southern water, was insufficient to negate the possibility of hydraulic continuity between the northern and southern areas. Moreover, assuming a hydraulic barrier on the basis of hydrochemical evidence alone would likely have been challenged due to its importance for estimating impacts of pumping on the regional spring flows. The quantitative framework provided by the AEM model, and the field data collected after the initial modeling, provided a more encompassing and defensible conceptual model for the site area. While the modeling was a critical part of the investigation, the value and information content of the continuous water-level monitoring cannot be overstated.

Conclusion

The AEM proved to be a powerful approach for conceptualizing ground water flow in a large subregion with poorly understood regional flow in carbonate rock aquifers. During the work, two aspects stood out: (1) its suitability for developing regionally appropriate models while removing the potential for boundary condition artifacts on the local scale of interest, and (2) the ease in which minor or major changes are accommodated and conceptual model hypotheses are “tested.” Elements of an existing AEM model were easily modified, removed, or supplemented without starting over. Finally, we believe that the AEM fosters development of a conceptual model that is compact yet complete—a characteristic that is well suited for evaluations of competing models that are often the de facto decision framework for ground water resource management.

Acknowledgments

The authors wish to acknowledge and thank Calpine Corporation, the Moapa Band of Paiute Indians, and Nevada Power Company for support and cooperation during this investigation, and specifically recognize Nevada Power Company for supporting the initial carbonate rock monitoring wells EH-4 and EH-5b, without which these analyses would not have been possible.

References

Armstrong, R.L. 1968. Sevier orogenic belt in Utah. *Geological Society of America Bulletin* 79, no. 4: 429–458.

Axen, G.J., B.P. Wernicke, M.F. Skelly, and W.J. Taylor. 1990. Mesozoic and Cenozoic tectonics of the Sevier thrust belt in the Virgin River Valley area, southern Nevada. *Geological Society of America Memoir* 176, 123–153.

Buqo, T.S. 1994. Results of long-term testing of the Arrow Canyon well. Prepared for Moapa Valley Water District, 22 p. Logandale, Nevada, MVWD (unpublished)

Dettinger, M.D. 1989. Distribution of carbonate-rock aquifers in southern Nevada and the potential for their development—Summary of findings, 1985–1988. Program for the study and testing of carbonate-rock aquifers in eastern and southern Nevada. Summary Report 1.

Dettinger, M.D., J.R. Harrill, D.L. Schmidt, and J.W. Hess. 1995. Distribution of carbonate-rock aquifers and the potential for their development, southern Nevada and adjacent parts of California, Arizona, and Utah. USGS Water-Resources Investigations Report 91-4146.

Eakin, T.E. 1966. A regional interbasin groundwater system in the White River area, southeastern Nevada. *Water Resources Research* 2, no. 2: 251–271.

Ertec Western Inc. 1981. MX siting investigation—Water resources program—Results of regional carbonate aquifer testing—Coyote Spring Valley, Nevada. Unpublished report prepared for U.S. Department of the Air Force, Ballistic Missile Office, Norton Air Force Base, California: 190 p. (unpublished)

Freeze, R.A., and J.A. Cherry. 1979. *Groundwater*. Prentice-Hall, Englewood Cliffs, New Jersey.

Freeze, R.A., and P.A. Witherspoon. 1968. Theoretical analysis of regional groundwater flow: 3. Quantitative interpretations. *Water Resources Research* 4, no. 3: 581–590.

Freeze, R.A., and P.A. Witherspoon. 1967. Theoretical analysis of regional groundwater flow: 2. Effect of water-table configuration and subsurface permeability variation. *Water Resources Research* 3, no. 2: 623–634.

Freeze, R.A., and P.A. Witherspoon. 1966. Theoretical analysis of regional groundwater flow: 1. Analytical and numerical solutions to the mathematical model. *Water Resources Research* 2, no. 4: 641–656.

Haitjema, H.M. 1995. *Analytic Element Modeling of Groundwater Flow*. Academic Press, San Diego, California.

Johnson, C., C. Brick, and S. Tyler. 1986. Construction, development and testing of NPC wells EH-2 and EH-2A. Water Resources Center, Desert Research Institute, University of Nevada system. Reno, Nevada (unpublished)

Johnson, C., and M. Mifflin. 2003. Evidence for a sub-regional hydraulic barrier in southeastern Nevada (abstract). In *Geological Society of America 115th annual meeting*, Seattle, Washington. Geological Society of America, Denver, Colorado.

Johnson, C., M. Mifflin, R.J. Johnson, and H. Haitjema. 2001. Hydrogeologic and groundwater modeling analyses for the Moapa Paiute Energy Center, a Calpine company project in cooperation with the Moapa Band of Paiute Indians, Moapa Indian Reservation, Clark County, Nevada: 218 p. Mifflin and Associates, Inc., Las Vegas, Nevada. (unpublished)

Kirk, S.T., and M.E. Campana. 1990. A deuterium-calibrated groundwater flow model of a regional carbonate-alluvial system. *Journal of Hydrology* 119, no. 4: 357–388.

Langenheim, V.E., J.J. Miller, W.R. Page, and J.A. Grow. 2001. Thickness and geometry of Cenozoic deposits in the California Wash area, Nevada, based on gravity and seismic-reflection data. USGS Open-File Report 01-393.

Langenheim, V.E., W.R. Page, J.J. Miller, and J.A. Grow. 2002. Geophysical and geological constraints on the hydrogeological framework of the California Wash region, southern Nevada (abstract). In *Geological Society of America, Rocky Mountain Section, 54th annual meeting*, May 7–9, 2002. Geological Society of America, Denver, Colorado.

Longwell, C.R., E.H. Pampeyan, B. Bowyer, and R.J. Roberts. 1965. Geology and mineral deposits of Clark County, Nevada. *Nevada Bureau of Mines and Geology Bulletin* 62, 218.

Maxey, G.B., and T.E. Eakin. 1949. Ground water in White River Valley, White Pine, Nye, and Lincoln Counties, Nevada. Nevada State Engineer. *Water Resources Bulletin* 8, 59.

Mifflin & Associates Inc. 1987. Hydrogeologic assessment, upper Muddy River valley, Nevada. Unpublished report prepared

- on behalf of Nevada Power Company and California Department of Water Resources: 396 p. (unpublished)
- Mifflin, M.D. 1992. The Arrow Canyon Range cell, carbonate aquifer and upper Muddy River valley groundwater monitoring—A summary of local and regional evidence and interpretations. Mifflin & Associates Inc., Las Vegas, Nevada: 18 p. (unpublished)
- Mifflin, M.D. 1988. Region 5, Great Basin. In *The Geology of North America: Hydrogeology*, vol. 0–2, ed. W. Back and P.R. Seaber, 69–78. Decade of North American Geology. Geological Society of America, Denver, Colorado.
- Mifflin, M.D. 1968. Delineation of groundwater flow systems in Nevada. Water Resources Center, Desert Research Institute, University of Nevada System. Desert Research Institute, Reno, Nevada. Publication no. 42004.
- Mifflin, M.D., and O.A. Adenle. 1996. 1995 hydrologic impacts from groundwater withdrawals in the upper Muddy River valley, Nevada. Unpublished report prepared for Nevada Power Company. Mifflin & Associates Inc.:227 p. (unpublished)
- Mifflin, M.D., and M.M. Wheat. 1979. Pluvial lakes and estimated pluvial climates of Nevada. *Nevada Bureau of Mines and Geology Bulletin* 94, 57.
- Neuman, S.P. 1972. Theory of flow in unconfined aquifers considering delayed response of the water table. *Water Resources Research* 8, no. 4: 1031–1045.
- Page, W.R. 1992. Preliminary geologic map of the Paleozoic rocks in the Arrow Canyon Range quadrangle, Clark County, Nevada. USGS Open-File Report 92-681.
- Pohlmann, K.F., D.J. Campagna, J.B. Chapman, and S. Earman. 1998. Investigation of the origin of springs in the Lake Mead National Recreation Area. Desert Research Institute, University and Community College System of Nevada, Reno, Nevada. Publication no. 41161.
- Schaefer, D.H., and J.R. Harrill. 1995. Simulated effects of proposed groundwater pumping in 17 basins of east-central and southern Nevada. USGS Water-Resources Investigations Report 95-4173.
- Schmidt, D.L., W.R. Page, and J.B. Workman. 1996. Preliminary geologic map of the Moapa West quadrangle, Clark County, Nevada. USGS Open-File Report 96-521.
- Southern Nevada Water Authority (SNWA). 2003. Hydrology of Tikaboo Valley and Three Lakes Valleys, Clark and Lincoln Counties, Nevada: 70 p. appendix. Las Vegas, Nevada (unpublished)
- Thomas, J.M., S.C. Calhoun, and W.B. Apambire. 2001. A deuterium mass-balance interpretation of ground water sources and flows in southeastern Nevada. Division of Hydrologic Sciences, Desert Research Institute, University and Community College System of Nevada, Reno, Nevada. Publication no. 41169.
- Thomas, J.M., A.H. Welch, and M.D. Dettinger. 1996. Geochemistry and isotope hydrology of representative aquifers in the Great Basin region of Nevada, Utah, and adjacent states. USGS Professional Paper 1409-C.
- Tóth, J. 1963. A theoretical analysis of groundwater flow in small drainage basins. *Journal of Geophysical Research* 68, no. 16: 4795–4812.
- Tóth, J. 1962. A theory of groundwater motion in small drainage basins in central Alberta. *Journal of Geophysical Research* 67, no. 11: 4375–4387.
- Tschanz, C.M., and E.H. Pampeyan. 1970. Geology and mineral deposits of Lincoln County, Nevada. Nevada Bureau of Mines and Geology Bulletin 73. Reno, Nevada.
- U.S. Department of Energy. 2002. Final environmental impact statement for a geologic repository for the disposal of spent nuclear fuel and high-level radioactive waste at Yucca Mountain, Nye County, Nevada. Office of Civilian Radioactive Waste Management. DOE/EIS-0250. Volume I. Impact Analyses.
- Wildermuth, M.J., J.H. Hwang, R. Broadbent, and M.C. Inada. 1990. Cooperative water resources development program, final hydrologic report for California Wash, hydrographic basin 218. James M. Montgomery Consulting Engineers, Inc.: 47 p. Las Vegas, Nevada. (unpublished)

Analysis Progress Report – Order 1169 Impacts Assessment

Cady Johnson
Martin Mifflin
Mifflin & Associates, Inc.

March 17, 2012

Overview

Combining reconstituted Muddy River discharge records and modeling analyses based on the groundwater responses to pumping in Coyote Spring Valley, a quantitative relationship between Order 1169 pumping and decreases in River discharge has been established for the 2010-11 record. Aquifer parameters were derived by matching drawdowns in monitoring wells to theoretical responses to pumping, allowing groundwater storage in Coyote Spring Valley to be accounted for in the analyses. There is an overall lag for impacts but minimal attenuation of pumping effects on the River flows. The influence of natural forcing agents on the Muddy River hydrograph, in particular regional climate and the delayed effects local flood events that cause influxes of storm runoff to groundwater storage in Pahranaagat Wash, appear to be of secondary importance to other effects in the 2010-11 record.

Well Hydraulics Analyses and the Impulse Response Function

The fundamental requirement for confident determinations of flow reductions in the Muddy River related to pumping activities in Coyote Spring Valley is establishing an Impulse Response Function (IRF). The IRF depends on the physical properties of the aquifer, in particular its transmissivity, storage, and volume properties. The aquifer parameters transmissivity (T) and storage coefficient (S) are derived by well hydraulics analyses, which generally rely on infinite-aquifer assumptions. Forward modeling supported by monitoring-well responses to pumping stresses has allowed approximation of real-world boundary conditions. The Order 1169 aquifer testing and derivation of the IRF fulfills the objective of documenting impacts on River flows. Appropriate magnitude, duration, and intermittency of pumping are the fundamental requirements for derivation and refinement of the IRF, which in turn predicts the timing and magnitude of impacts on Muddy River flows resulting from varying pumping schedules.

Approach to the Analysis

Our approach is to assume that MX-5 extracts groundwater from an idealized system with steady-state throughput equal to the nominal discharge at the headwaters of the Muddy River, 50 cubic feet per second (cfs). Assuming that MX-5 taps tributary groundwater that directly sustains the base flow of the River is conservative with respect to placing an upper limit on impacts that are physically possible. After an infinite amount of time has elapsed, the full pumping effect would be expressed as 1:1 flow reductions in the River, but while the system equilibrates to this new condition, release of water from storage will mitigate (reduce) impacts on the River, in accordance with the IRF. One question is if the average pumping rate of 5.4 cfs realized from the first year of operations is theoretically large enough to have produced detectable impacts. The second question is whether the

SE ROA 38301

prescribed rate of 11 cfs and duration of 2 years are necessary to meet the objectives of the Test. From the perspective of flow-system theory, if any impacts (reductions) in River flow can be confidently documented as related to Order-1169 pumping, then 1:1 impacts will develop, over time, from such pumping. From the perspective of Order 1169 objectives, however, both the magnitude and *rate* of impact development are needed for an improved predictive model.

Interpretation of Phase 1 of Order 1169 Test

The first phase of continuous pumping from MX-5 began at about 13:30 PDT on September 21, 2010, and continued until October 14. The average pumping rate was 8.4 cfs, and the USGS real-time (15-minute interval) record from MX-4, 326 feet from MX-5, is available for analysis. Pumping effects are superimposed on a regional water-level trend from which observed water levels are subtracted to obtain drawdown (Figure 1). Analysis of early pumping response in MX-4 suggests an unconfined aquifer with highly transmissive properties and substantial storage near the wells (Figure 2). The pumping response data flatten at late times, suggesting that a higher transmissivity (T) and much lower storage coefficient (S) apply in regions remote from the pumping activity (Figure 3). Very low storage coefficients are typical of confined aquifers.

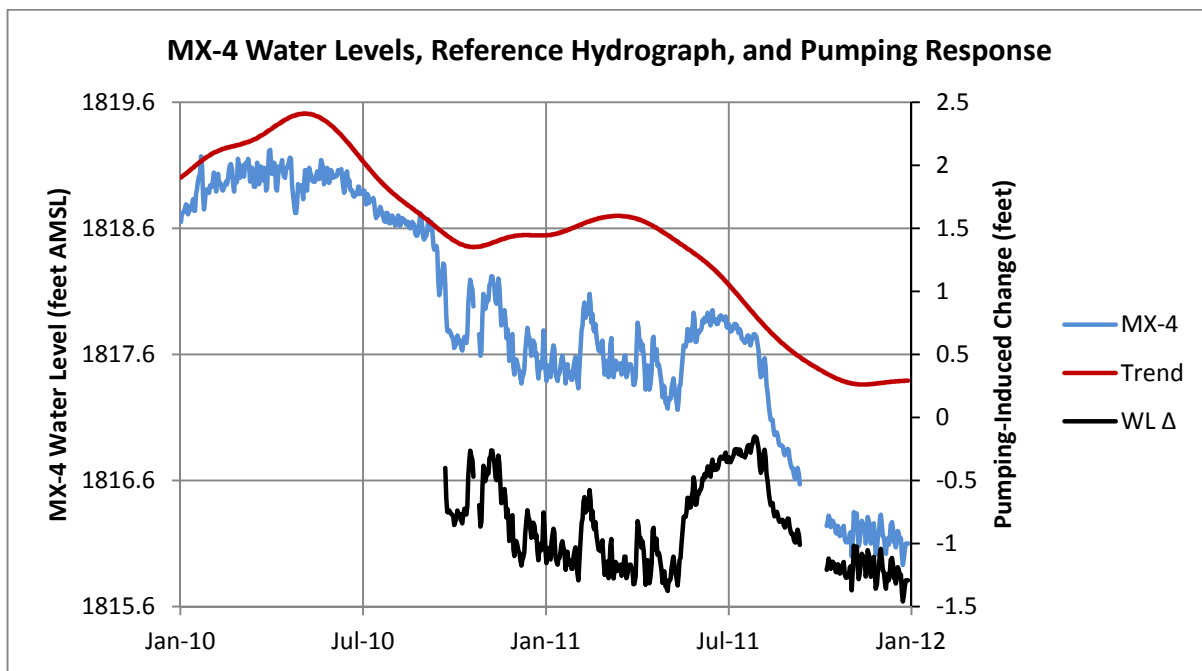


Figure 1. Raw, reference, and adjusted MX-4 hydrographs [file MX5PMX4obs.xlsx, sheet 'MX4daily2010-12']

To explore the validity of test results summarized in Figures 2 and 3, daily water-level records and average pumping rates for 11 stress periods were evaluated with a single-layer, finite-difference model (Figures 4 and 5). The model represents an area of 200 square miles and an aquifer nominally 1000 feet thick, dependent on saturated thickness. The optimized match to daily drawdown data (Figure 6) results in estimated $T=1,008,000 \text{ ft}^2/\text{day}$ and $S=0.0075$, indicating (as do field relations) that

both confined and unconfined conditions prevail locally and that boundaries are influential on pumping response. An infinite aquifer with the same S and T as used to match data in Figure 6 would experience drawdowns roughly half of what has been observed (Figure 7).

To derive impulse response functions for systems of finite extent as represented in Figures 4-6, the approach to equilibrium at the outflow boundary following a step increase in pumping at MX-5 is evaluated. The IRF can be simply characterized by a time constant τ , the time required for the outflow to decrease by 63.2% ($1-e^{-1}$) of the pumping rate. τ is proportional to S/T , and the quantity of groundwater available from storage is dependent on aquifer volume in addition to S . We subscript τ with the area of the model system, e.g. τ_{200} refers to the IRF of the base case 200 mi² grid.

Noting that monitoring well BW-01, 9.7 miles from MX-5, exhibits a very small but finite pumping response (Figure 8), the area of the model domain was doubled to 400 mi² as an alternative case to explore the sensitivity of τ to area. Similarly evaluating a smaller, 80 mi² flow domain leads to the conclusion that the time constant of the boundary outflow IRF, as constrained by pumping response data, is relatively insensitive to the area of a homogeneous and isotropic model domain (Figure 9). The high transmissivity and storage coefficient smaller than is typical of unconfined systems combine to provide ample time for detection of impacts within the first year of testing.

Calibration of the three models (80, 200, and 400 mi²) was accomplished with similar (but not identical) values of T , S , and outflow boundary head, and the very similar curves in Figure 9 are testimony to the non-uniqueness of groundwater models. In this case, for our purposes, all produce equivalent results. We find $\tau_{200} \approx 51$ days, $\tau_{400} \approx 43$ days and $\tau_{80} \approx 36$ days, but uncertainty in matching theoretical response to the noisy dataset of monitoring-well water-level responses shown in Figure 6 suggests the results are similar, with $\tau \approx 1$ -2 months.

If the simple model presented herein is approximately correct, pumping effects from MX-5 should be expressed in the Muddy River hydrograph. Comparison of the two signals (response function and River hydrograph) strongly suggests that this is the case (Figure 10).

Application of Results

From March of 1988 through March of 2005, before any significant groundwater development in Coyote Spring Valley, the average base flow of the Muddy River was 48.2 cfs with a standard deviation of 3.37 cfs, based on the EEMD approximation (Figure 11). Without accounting for pumping in Coyote Spring Valley, the average discharge for 2011 was 47.4 cfs with a standard deviation of 3.56 cfs, 0.8 cfs below the historic average. When CSI and MX-5-related impacts to the River are accounted for with a lag of 6 weeks in accordance with the IRF, the reconstituted average discharge for calendar 2011 was 57.8 cfs with a standard deviation of 1.08 cfs, 9.6 cfs greater than the historic average (Figure 12). Our reconstitution therefore implies a strong influence of antecedent wet conditions on the River hydrograph, consistent with observations of regional climate (Figure 13) and terrestrial water storage (Figure 14). Figure 14 illustrates that at least four years are required for the stored water in the region to dissipate following a particularly wet year or years, two years later than recession of the White River hydrograph.

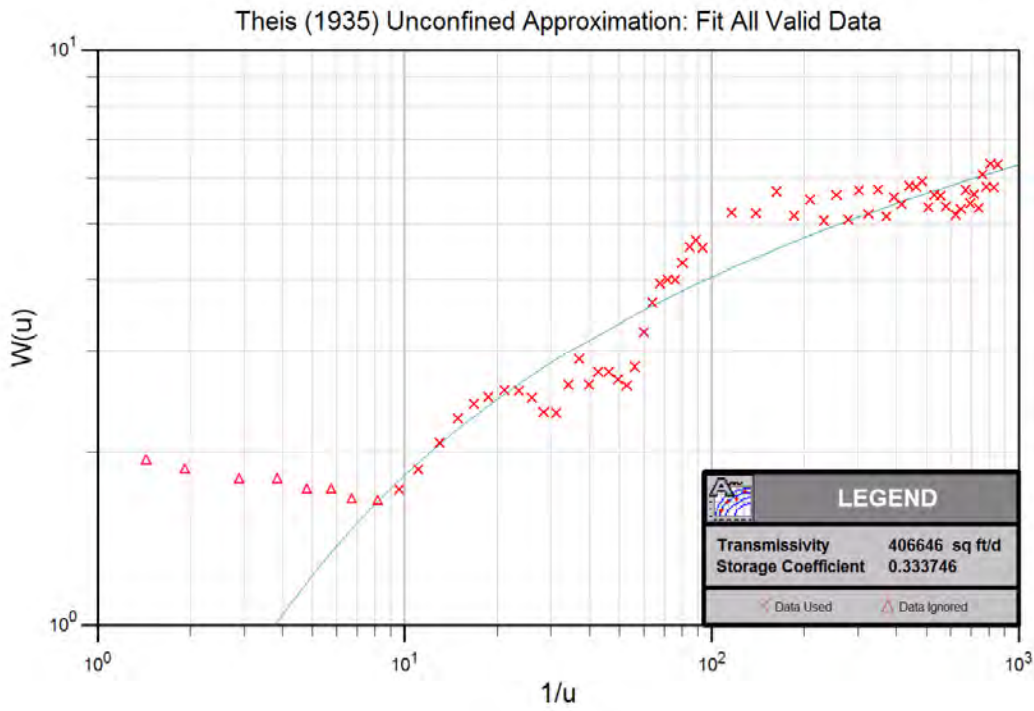


Figure 2. Curve-match solution of Theis equation for T and S, using MX-4 drawdown from pumping interval beginning September 21, 2010 [file MX4phase1fitAllData.tif]

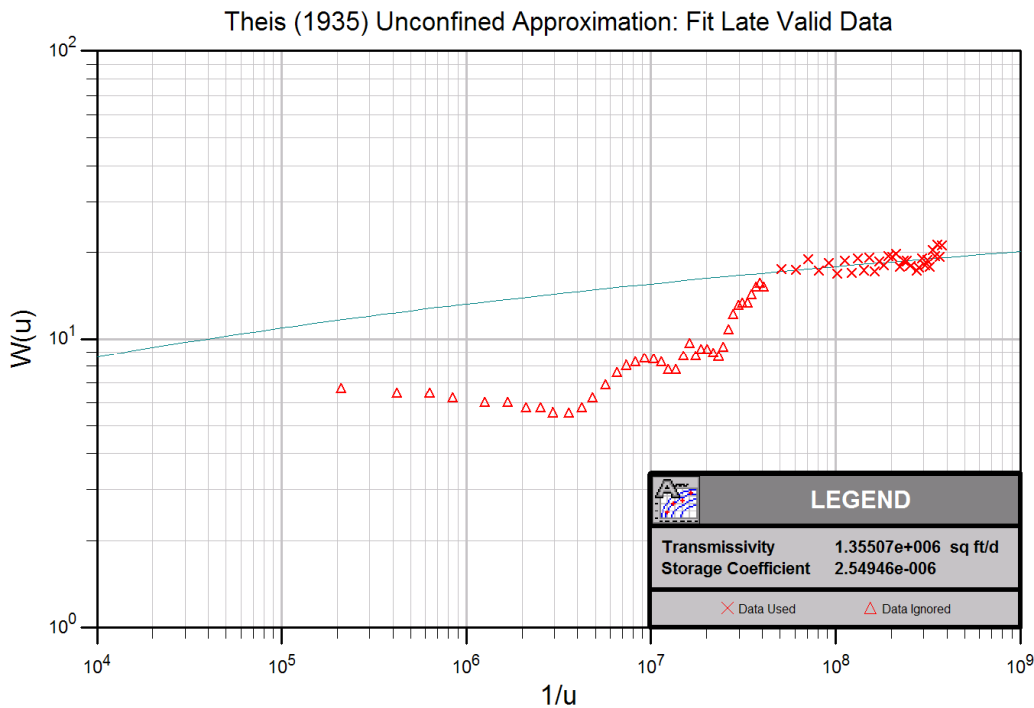


Figure 3. Curve-match solution of Theis equation for T and S, using MX-4 drawdown data from late portion of pumping interval beginning September 21, 2010 [MX4phase1fitLateData.tif]

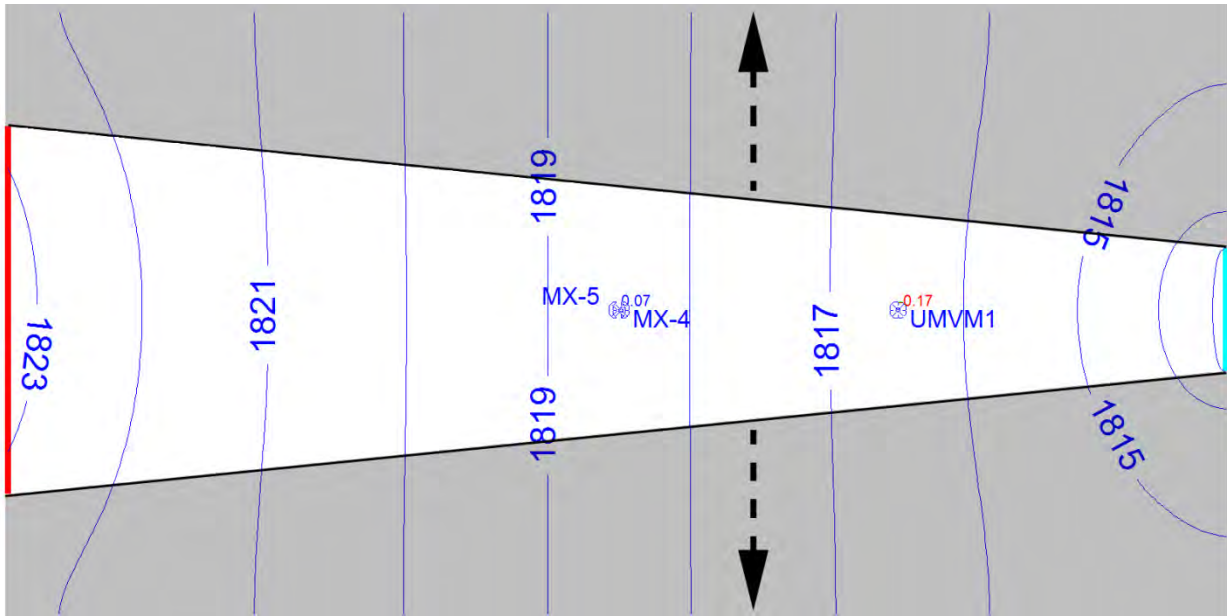


Figure 4. Calibrated, steady-state water levels in 200 mi² model domain, with residuals at two steady-state calibration targets indicated. Shading indicates area removed from model to produce 80 mi² domain; arrows indicate expansion directions to produce 400 mi² domain. Influx at left side of model was specified as 50 cfs (red boundary); head at right side of model (aqua boundary) was specified to match target water levels in monitoring wells MX-4 and UMV-M1 [file CalibSep10SWLlayers.tif]

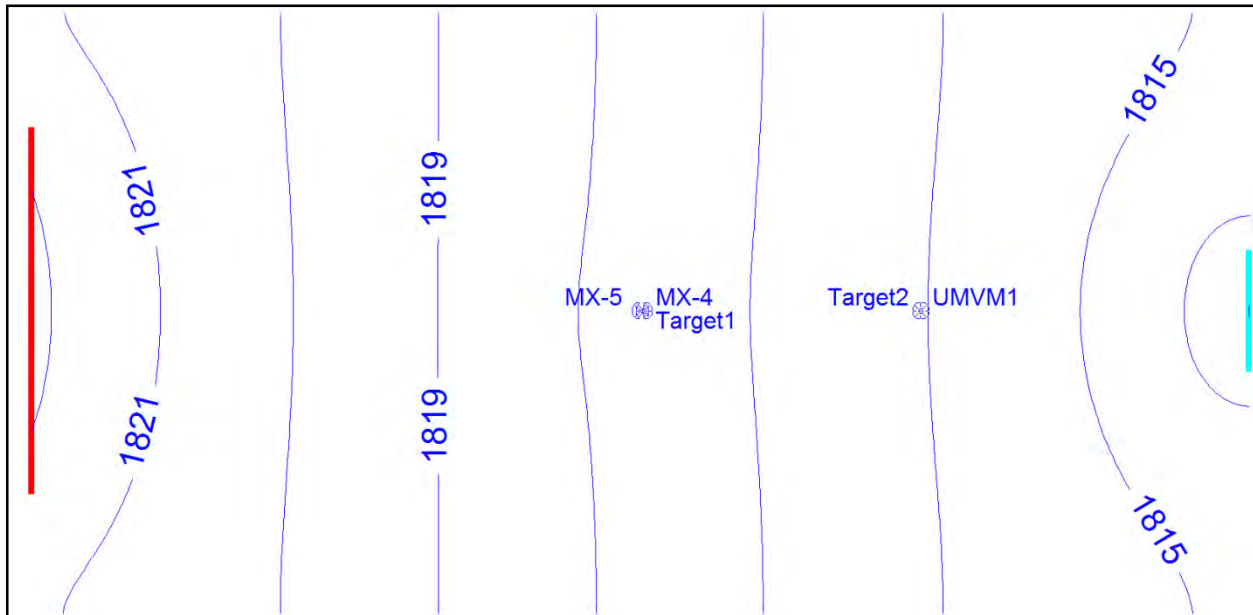


Figure 5. Calibrated, transient water levels representative of December, 2011 at end of 11th pumping stress period in 200 mi² model domain; drawdown histories at MX-4 and UMV-M1 provided calibration targets. Model provided flux vs time at outflow boundary based on MX-5 pumping history from September of 2010 through December of 2011. [file CalibDec11PWL.tif]

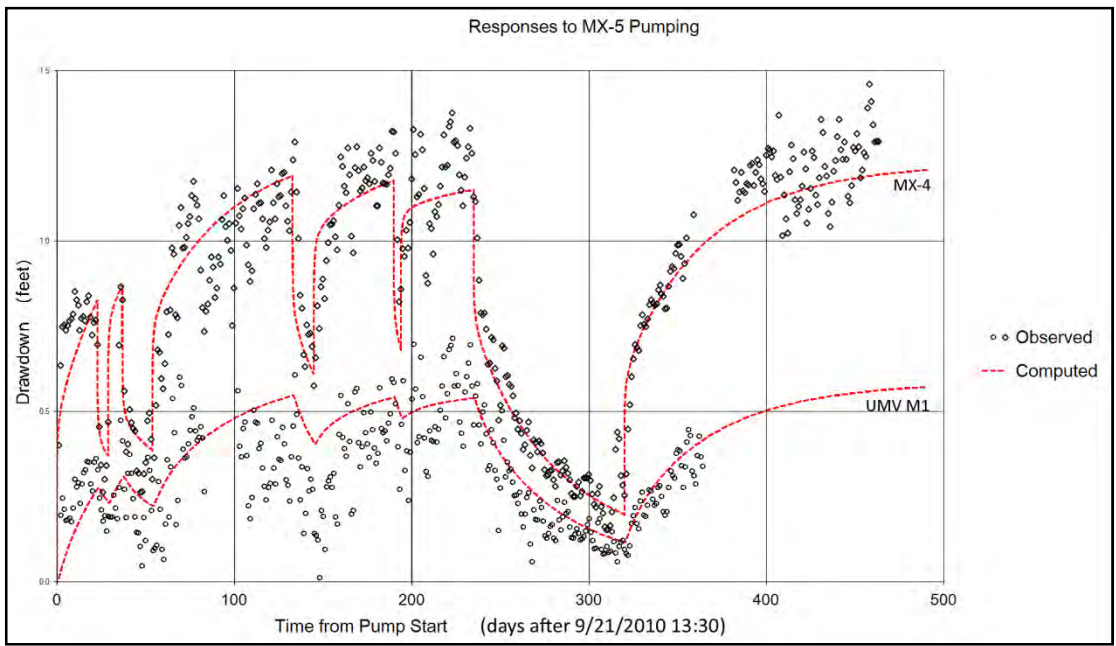


Figure 6. Calibrated prediction of pumping response at monitoring wells MX-4 and UMV M1, in 200 mi² model domain, based on T=1,008,000 ft²/day and S=0.0075, with pumping from MX-5 represented by 11 stress periods varying from 0 to 8.4 cfs [CalibratedComposite.tif]

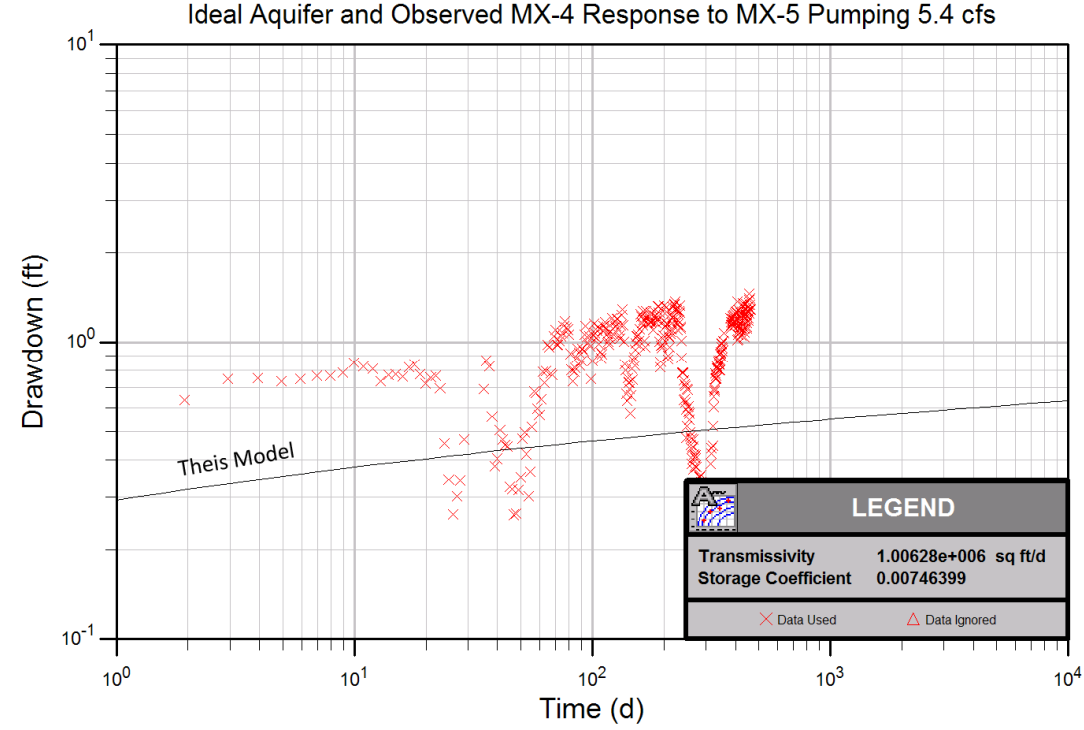


Figure 7. This infinite-aquifer solution based on aquifer parameters derived from data match in bounded system (Figure 6). This equation predicts roughly half the observed drawdown response to annualized pumping rate of 5.4 cfs. [file PredictMX4.tif]

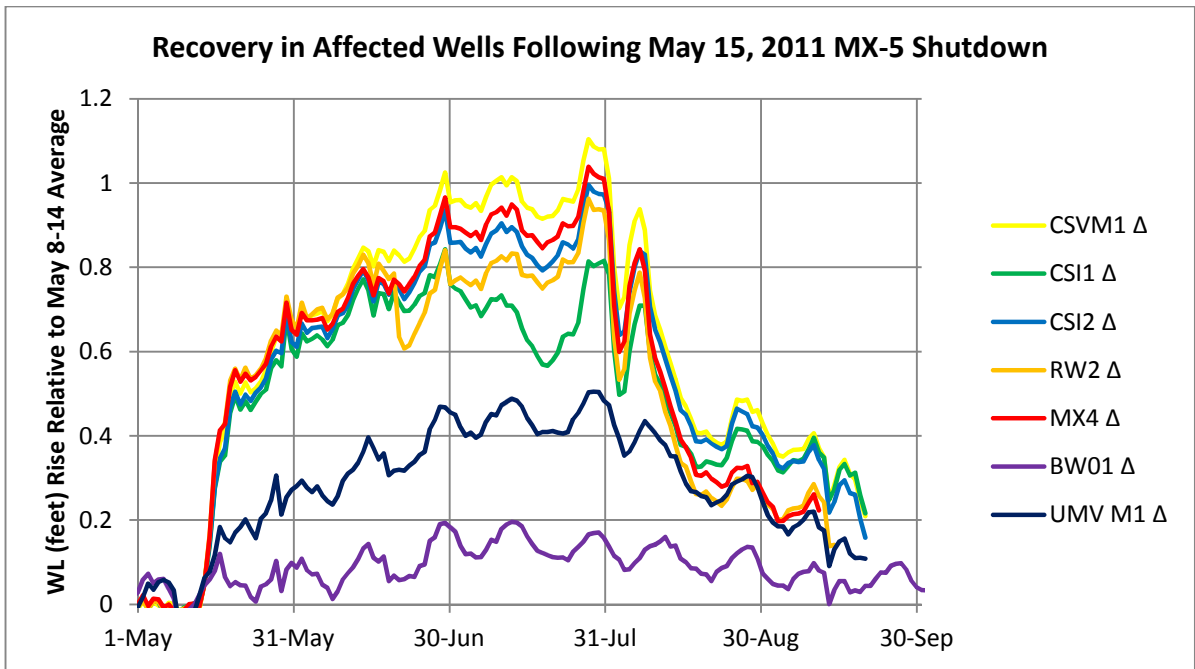


Figure 8. Recovery from differences versus Paiutes M1 [file Drawdown2010-11.xlsx, sheet 'Normalize']

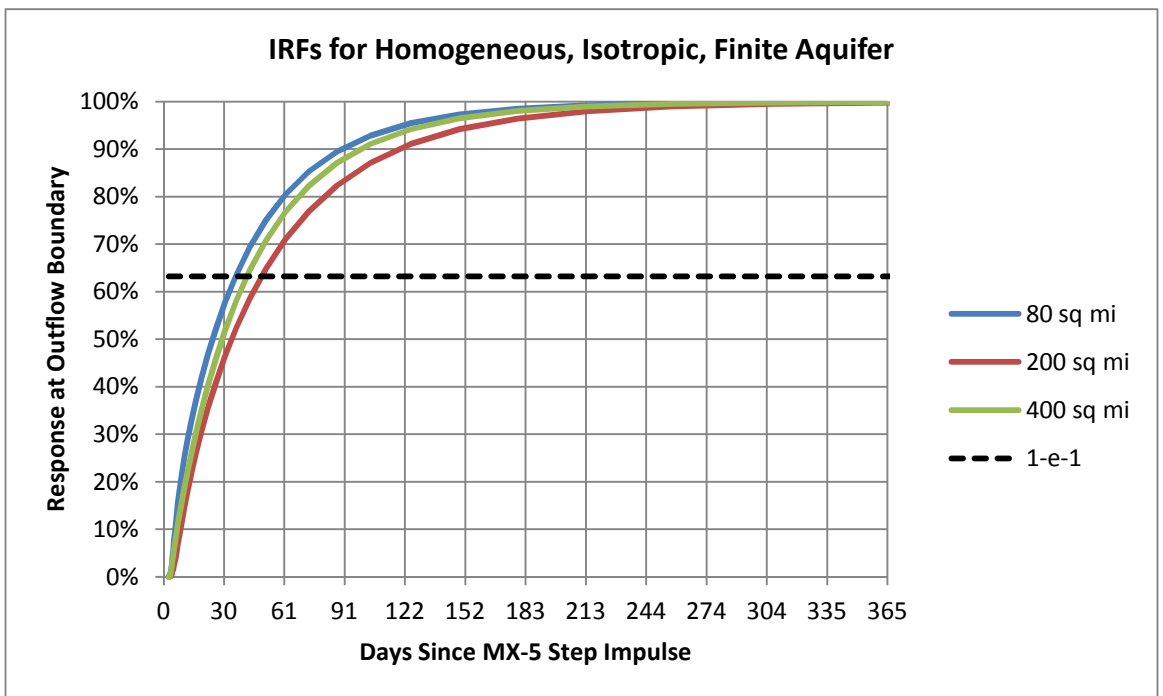


Figure 9. Time constant of boundary impulse response function varies from 36 to 51 days for 3 model flow domains, with T and S derived in individual models by matching field data. [file BaseGHBflux.xlsx]

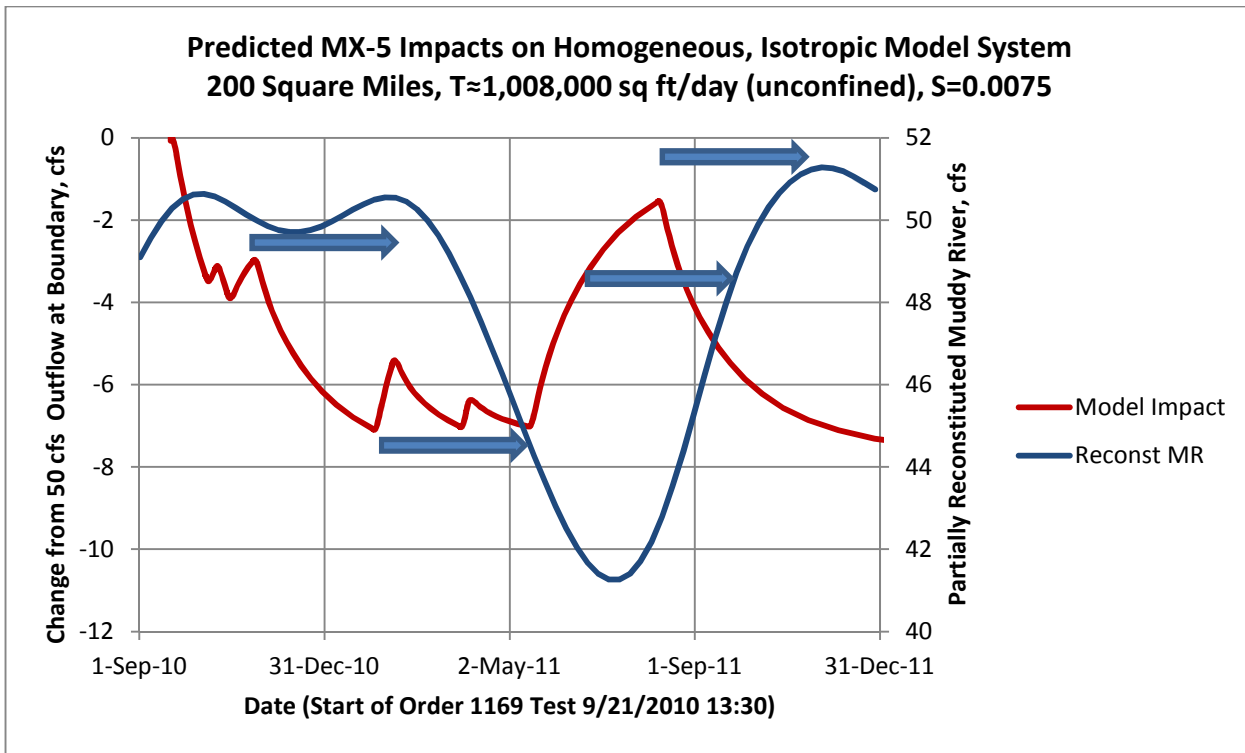


Figure 10. Predicted outflow hydrograph from model system, illustrating changes from initial condition of 50 cfs outflow at model boundary (left vertical axis), and partially reconstituted (Coyote Spring Valley pumping excluded) Muddy River hydrograph (right vertical axis) showing proportional decrease in discharge before accounting for CSI and MX-5 pumping effects. Arrows illustrate the lags between the first stage of pumping and decreasing River discharge (left arrows), and increasing discharge after the May 15 cessation of pumping (right arrows) [file CHBflux200.xlsx]

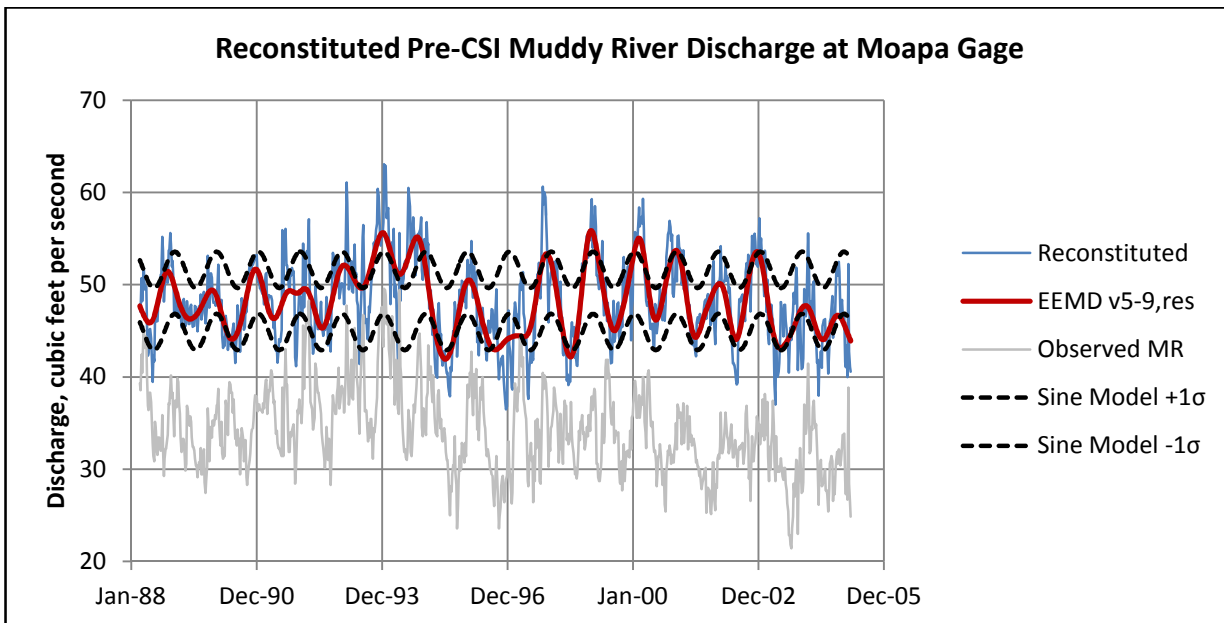


Figure 11. Reconstituted Muddy River hydrograph (red curve) derived by empirical mode decomposition, based on rain-censored weekly data (blue curve). [file BPinReconstEEMD.xlsx]

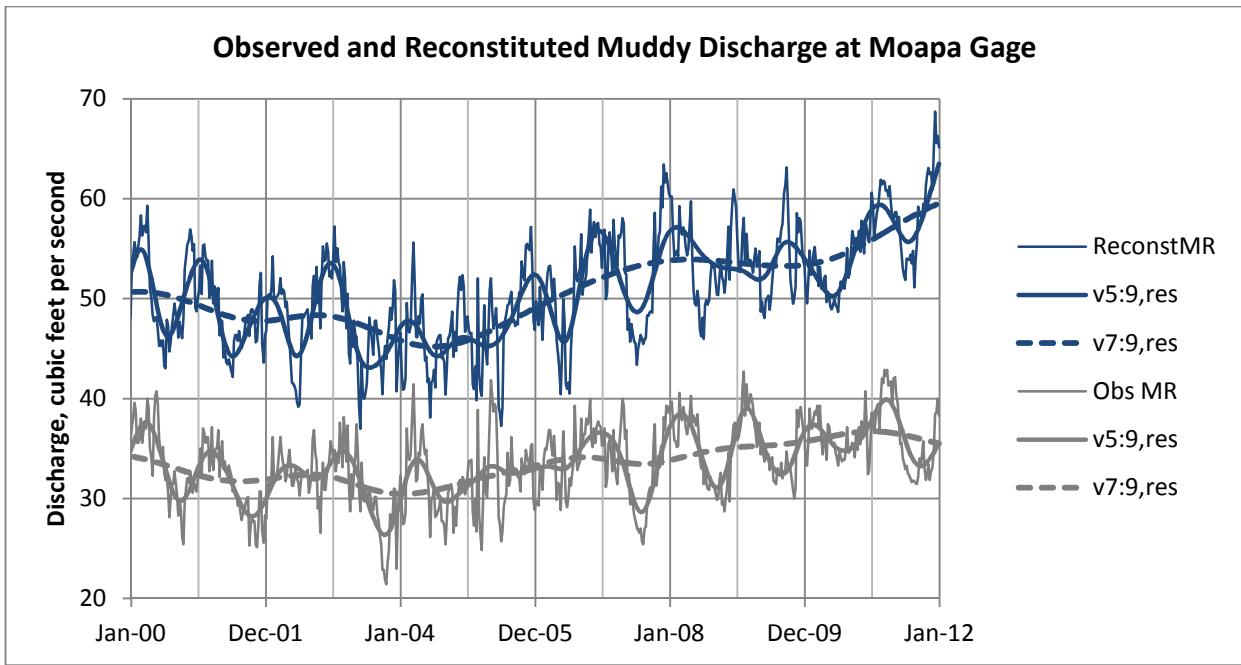


Figure 12. Reconstitution based on rain-censored weekly data, showing trends from combinations of intrinsic mode functions derived by EEMD. Notation in the legend refers to groups of intrinsic mode functions that approximate non-stationary signals, such as the hydrograph, by its low-frequency components. [file 2011MRfinalEEMD.xlsx, sheet 'PlotWithRaw']

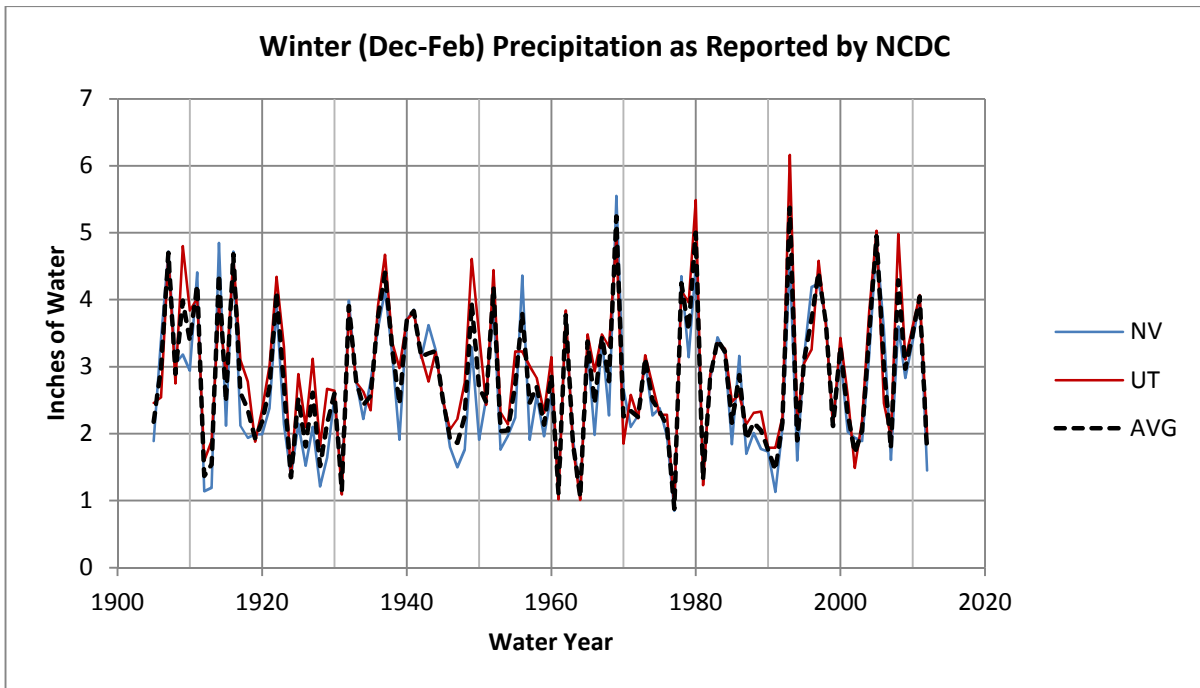


Figure 13. Statewide, winter precipitation totals for Nevada and Utah, as reported by National Climatic Data Center (NCDC) [file ClimateAtGlance.xlsx, sheet 'YearlyNVUT']

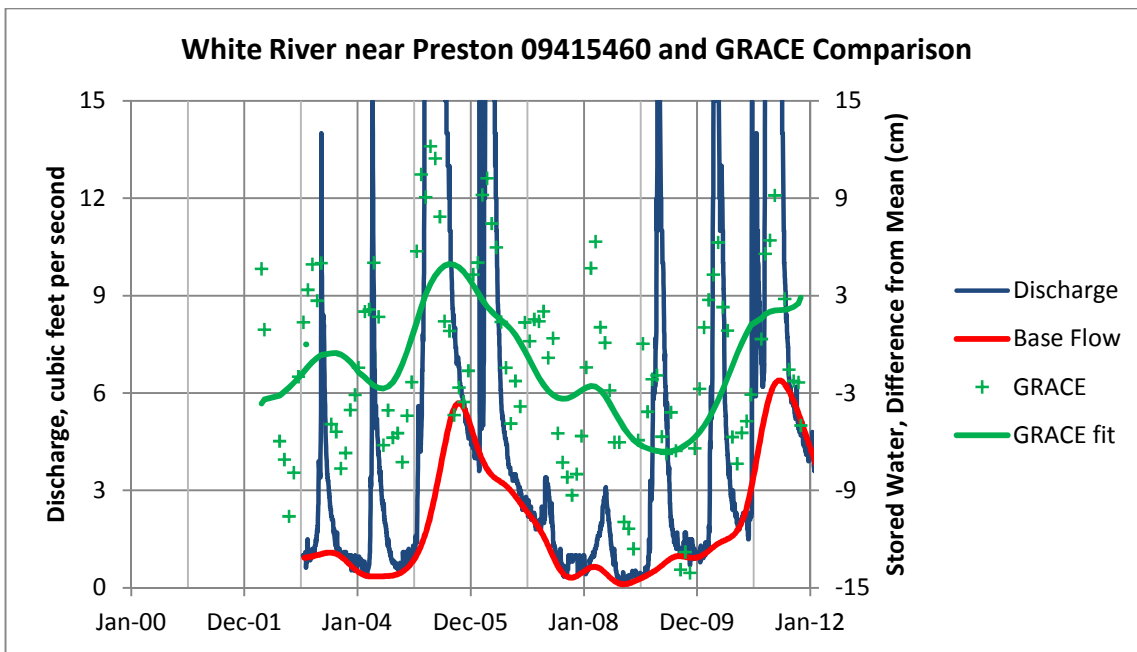


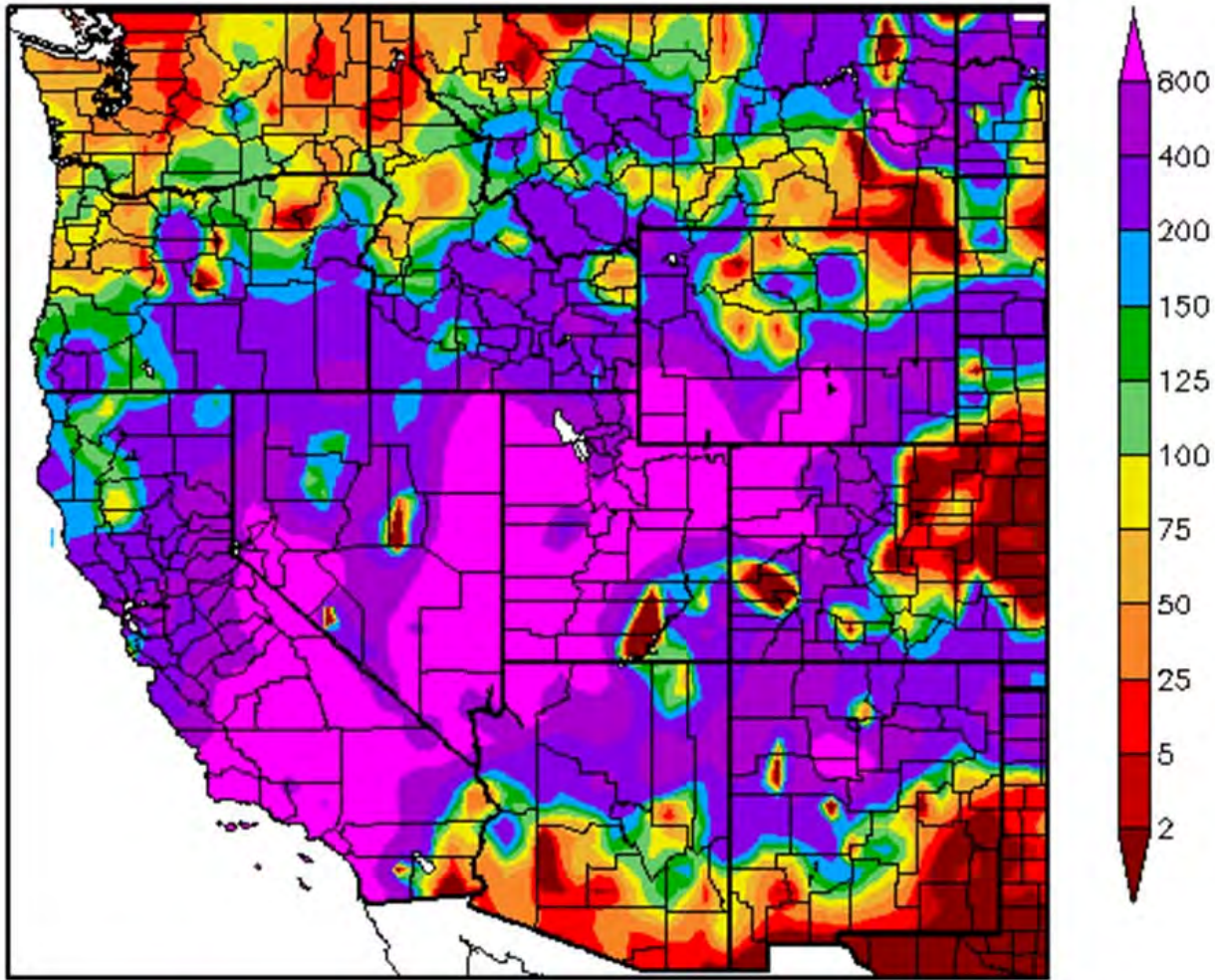
Figure 14. Base flow near headwaters of the White River, and close correspondence shown by stored terrestrial water from Gravity Recovery and Climate Experiment (GRACE) measurements Note the 2-year lag (2007-2009) between the end of the first major recession limb of the White River hydrograph and dissipation of associated terrestrial water. [file WhiteRiverDaily03-12.xlsx, sheet 'BaseFlow']

Discussion

Was 2011 a wet year or a dry year? It was very wet by any measure, with record snowpack and a rare arrival of the “pineapple express” (Arctic Oscillation) in December of 2010, the wettest December on record for Nevada (Figure 15). Over the past century, when precipitation records are detrended to account for changes in the evolving precipitation monitoring networks in Nevada and Utah, the precipitation record is clarified (Figure 16). In Figure 16, there is a striking similarity between the precipitation record from 1995-2012 and the record from 1905-1922, when the Colorado River discharge record used as the basis for allocations under the Colorado River Compact was compiled by the Bureau of Reclamation. It is widely recognized that the long-term average discharge of the Colorado River was significantly over-estimated from those early records, and proportionally comparable fluctuations in Muddy River base flow indicate a similar multi-year response to wet years.

A check on the reconstituted discharge presented in Figure 12 is provided by similar multi-year trends of the hydrograph during successive drought and wet periods (Figure 17). The regional distribution of stored terrestrial water during the “wet” years of 2005 and 2011 was, however, very different (Figure 18). Because groundwater levels (Figure 1) are declining at the same time base flow of the Muddy River is increasing (Figure 12), the mechanism of delivery of recharge to the headwaters of the Muddy River must differ in a fundamental way from recharge of the Arrow Canyon Range Cell as a whole. Until 2011 there was general correspondence between well hydrographs and spring and River discharge records, but the recent divergence illustrates the importance of accounting for local recharge, particularly from major runoff events in Pahranaagat Wash.

Percent of Normal Precipitation (%) 12/15/2010 – 12/21/2010



Source:  <http://www.almanac.com/blog/weather-blog/weather-blog-pineapple-express>

Generated 12/22/2010 at HPRCC using provisional data. Regional Climate Centers

Figure 15. Precipitation anomaly resulting from “pineapple express” event of December, 2010 [file PineappleExpress2010.jpg]

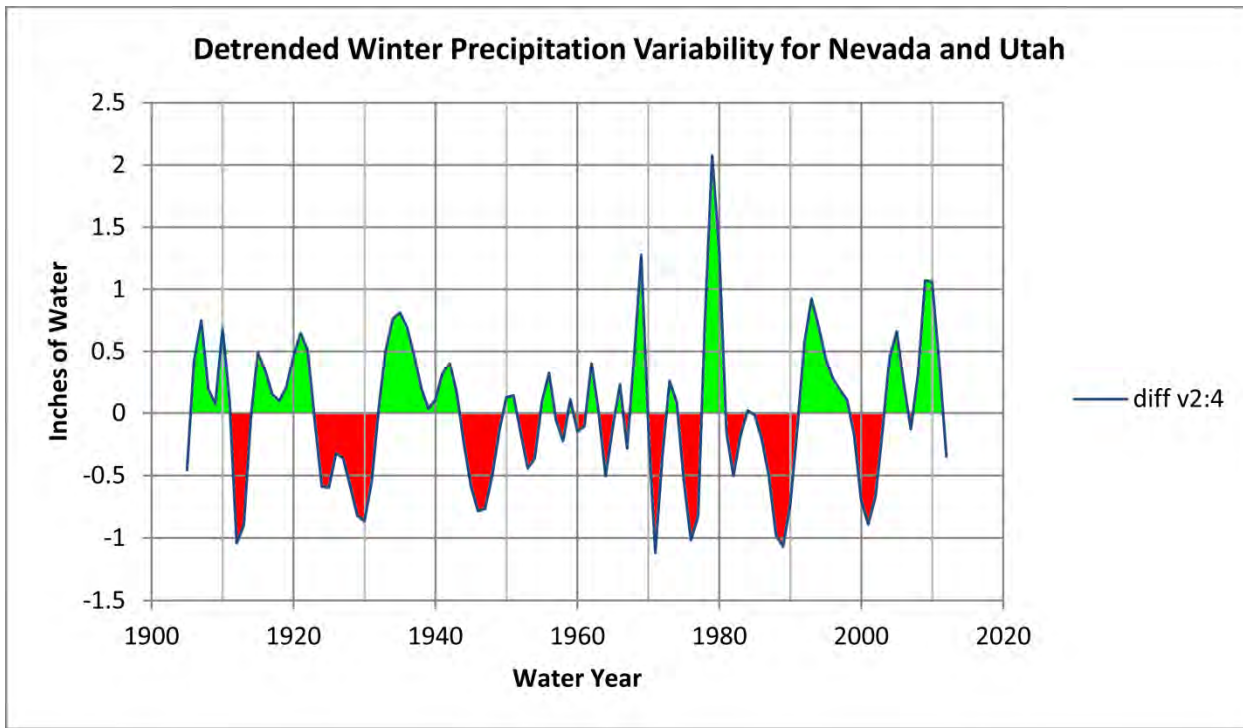


Figure 16. Departures of reported winter precipitation from multi-decadal trends, average of statewide Nevada and Utah records, 1905-2010 [file DetrendedNV&UTwinterPPT.tif]

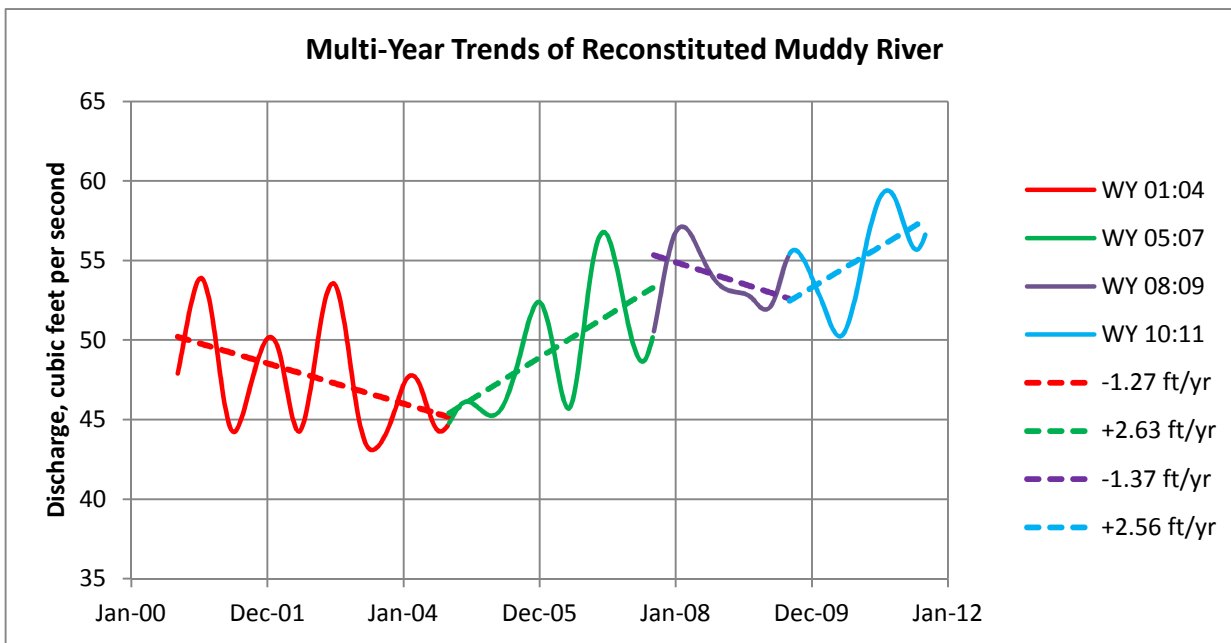


Figure 17. Repetitive, nearly-identical recession and recovery trends in reconstituted Muddy River hydrograph [file 2011MRfinalEEMD.xlsx, sheet 'FitSegment']

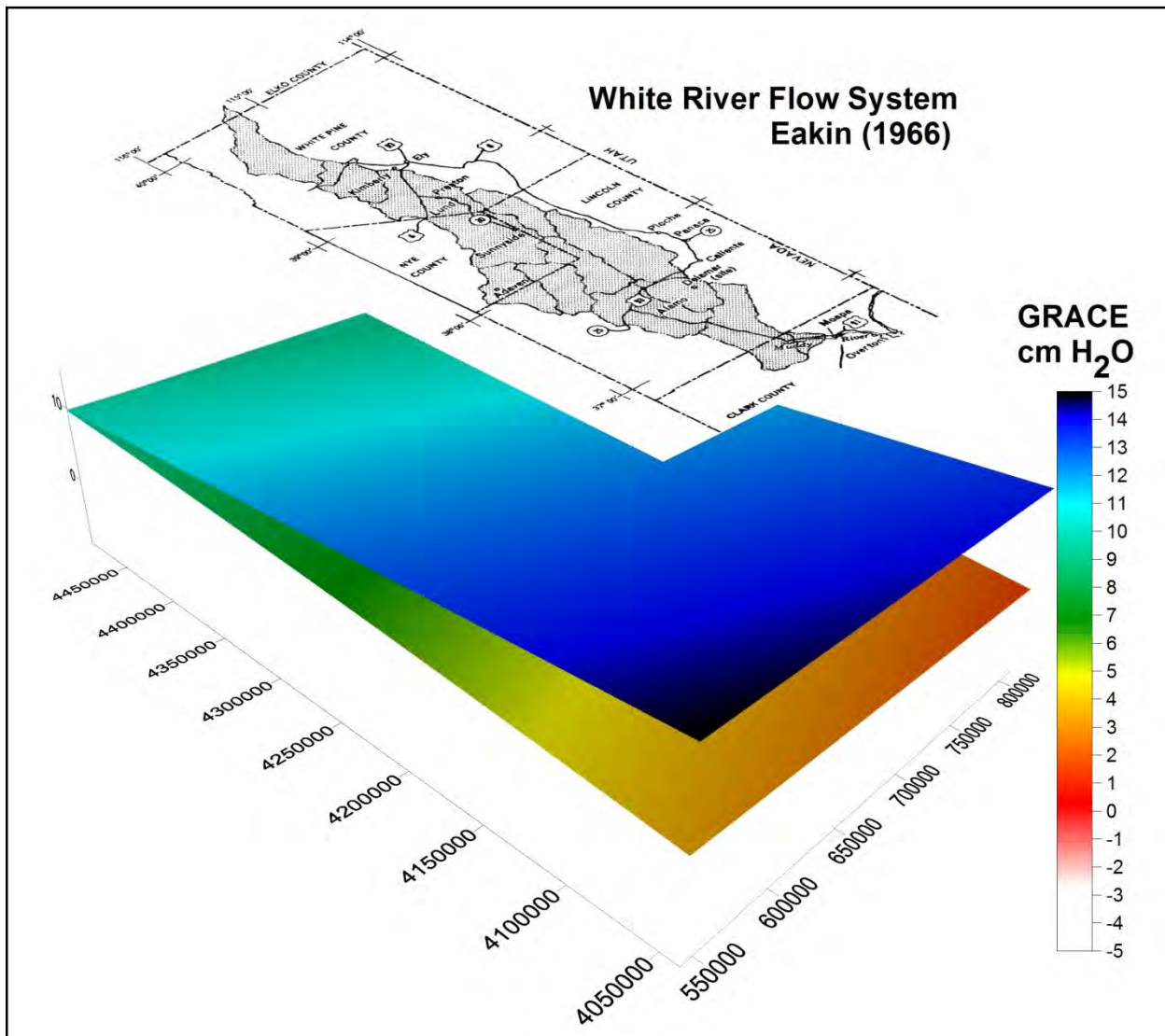


Figure 18. Stored terrestrial water, expressed as centimeters, for April of 2005 (upper surface) and April of 2011 (lower surface). Plot area is bounded by 35.5°N, 40.5°N, 113.5°W, and 116.5°W, which corresponds to limits of UTM coordinates shown along axes, and contains White River Flow System of Eakin (1966), shown for reference. Note that southern area was relatively wet in 2005 but relatively dry in 2011. Superposition of contrasting regional and local (Pahrnagat Wash) effects in 2011 offers an explanation of divergent well and River hydrographs. [file Graceapr05&apr11.jpg]

Figure 10 illustrates that the volume of reduced outflow of the carbonate-rock aquifer model is approximately equal to the volume of water that appears to be “missing” in the partially-reconstituted Muddy River flows (Coyote Spring Valley pumping not added into the reconstitution). Such suggests the simple modeling analysis of pumping-induced impacts forecasts the right amount of impact on Muddy River flow, but not necessarily the timing. Storage effects in the alluvial aquifer of the headwaters area could add weeks or months to the lag characteristic of the carbonate-rock aquifer. This would not be surprising, as about 60% of the measured discharge forming the Muddy River flows in the early 1960’s,

when tributary channels were monitored, was via alluvial-aquifer seepage into headwater channels, and the other 40% was discharge from large springs (Eakin, 1964).

The unconfined portion of the thin (less than 100 feet thick, with highly lenticular gravel zones) alluvial aquifer in and upstream of the Springs area has a much smaller transmissivity (Maxey and others, 1966) than the carbonate-rock aquifer, but due to its unconfined nature, a much larger storage coefficient (two orders of magnitude larger). Such combine to delay sensing of at least 60% of the regional carbonate-rock aquifer discharge at the Moapa Gage. The ~40% discharged from large springs reaches the Muddy River by conduit pathways to the surface, exchanging water with the alluvial-aquifer water in some tributaries. Eakin (1964) attempted to distinguish waters derived from these two fundamental modes of discharge using electrical conductivity (EC), with the higher EC values indicating tributary-channel flow with contributions from the alluvial aquifer.

Conclusion

There are two important questions that require answers if the objectives of Order 1169 are to be satisfied:

1. Did the first year of pumping stresses from Coyote Spring Valley, with about 5.4 cfs produced from MX-5 and less than 2 cfs from CSI -3 and -4 provide large enough and prolonged enough pumping stresses to confidently recognize pumping impacts in the Muddy River flows if they are present?
2. If not, would the Order 1169-prescribed production equivalent to a minimum of 11 cfs for two years be necessary and sufficient to produce recognizable pumping impacts?

Our preliminary conclusion, based on the opportunity provided by the shutdown of MX-5 to develop and incorporate an IRF for the Carbonate-rock aquifer of the production region, is that the pumping stresses *were* large enough (given the fortuitous shutdown event of summer 2011) to produce an analyzable impact to Muddy River flows. Because of distributed pumping stresses (no distinct stress periods), CSI pumping contributes noise to the system and hinders, rather than facilitates, analysis. Furthermore, because of the exceptionally wet winter of 2010-11, undesirable uncertainty with respect to base flow remains. Our final conclusion will depend on obtaining similar results from the January 2012 shutdown, which should become apparent in the summer of 2012. The relationship established for the 2010-11 pumping records should be repeated in 2012 in accordance with the characteristics of a linear, time-invariant (LTI) system. There are two fundamental characteristics of an LTI: experiments performed at different times have the same outcome (time invariance), and additive superposition of effects (linearity). The test, as it appears to be proceeding, should provide a confirmatory period of record.

The outcomes will differ if the alluvial aquifer's ability to delay and attenuate external impacts depends on the extent of dewatered zones (pumping cones) in the gravels, which develop and recover seasonally in response to *local* pumping. By analogy with a variable capacitor in a low-pass filter, the alluvial aquifer would transmit pumping stresses from Coyote Spring Valley to the Muddy River differently depending on the state of saturation related to the seasonal development and recovery of

the pumping cones in the alluvial aquifer. The Order 1169 test offers the prospect of identifying such effects by comparing the results of May and January shutdowns.

The answer to the broader question of test duration and requisite pumping stress depends on *analytical* results (confirmation or ambiguity) by the end of the 2-year interval in November of 2012. There is no question that the initially-prescribed 11 cfs pumping stress, particularly if long periods of shutdowns were incorporated, would eliminate much if not all of the uncertainty created by climate-induced fluctuations in Muddy River flows, which may exceed 5 cfs. Reconstituted Muddy River hydrographs are the only valid measure of base flow, given the signal-to-noise issue resulting from the combined magnitudes (seasonally 20+ cfs) and varied lag times (zero to several months) associated with ongoing water exports from the headwaters area.

References

- Eakin, T.E., 1964, Ground-water appraisal of Coyote Spring and Kane Spring Valleys and Muddy River Springs area, Lincoln and Clark Counties, Nevada: Department of Conservation and Natural Resources, Ground-Water Resources – Reconnaissance Series Report 25, 40 p.
- Maxey, G.B., A.L. Mindling, and P.A. Domenico, 1966, Ground water in upper Muddy River basin: Desert Research Institute, Center for Water Resources Research, University of Nevada, Misc. Report #3, 28 p.

Parameter Estimation for Order 1169

Cady Johnson
Martin Mifflin
Mifflin & Associates, Inc.

August 27, 2012

Introduction

The April 23, 2012 re-start of pumping from MX-5 provides the best opportunity to date for analysis of pumping responses in affected wells for estimation of aquifer parameters. The re-start occurred near the spring water-level maximum in the region; three full days of recovery preceded the re-start; CSI-3, the primary source of interference, was inactive between April 12 and March 14; and pumping was uninterrupted between 9:38:57 (PDT) on April 23 and 16:05:52 (PDT) on May 7 according to SNWA records, with "offscan" reported only once at 12:28:38 (PDT) on April 30. Based on hourly production records for April, the pumping rate on April 23 was steady at 3551 ± 3 gpm, and for April 23-30 was approximately steady at 3513 ± 23 gpm, less than one percent variability. Monitoring records from the Moapa Indian Reservation will allow long-term drawdowns to be derived using difference hydrographs, which remove seasonality from the raw water-level records.

There have been numerous attempts to derive the aquifer parameters transmissivity (T) and storage coefficient (S or S_v) from pumping response in southeastern Coyote Spring Valley, and none have been entirely successful. Ertec Western (1981) and Converse Consultants (2002) conducted the only interference tests (those utilizing observation wells) on record, but neither testing program resolved the storage parameter from pumping response. Ertec obtained an unrealistic (>1) estimate of the storage coefficient from late-time drawdown at MX-4 in response to pumping at MX-5, and Converse was unable to resolve any responses to RW-2 pumping in the MX-4 and MX-5 hydrographs. There are two reasons for these difficulties that we now understand; boundary effects exert the dominant effect on drawdowns after the first few hours of pumping, and barometric and tidal effects must be filtered from observation-well hydrographs to resolve pumping-induced drawdowns from natural noise.

Analytical Approach

Barometric Pressure and Total Head

As summarized by Rasmussen and Crawford (1997), Spane (2002), and Toll and Rasmussen (2007), total head (TH; the sum of water elevation and barometric pressure) is more representative of fluid potential in an aquifer than water-level alone. Total head varies in response to barometric pressure changes; in deep, unconfined aquifers the finite pneumatic diffusivity of the overburden causes a lag between a barometric pressure change that is transmitted instantaneously down an open observation well but delayed in reaching surrounding areas of the aquifer. Methods including BETCO (Toll and Rasmussen, 2007) and MRCX (Mackley and others, 2010) employ multiple regression

SE ROA 38316

(autoregressive moving-average models) to derive lag relations and adjust (correct) heads by removing barometric effects. When air-pressure changes are transmitted through the overburden on time scales shorter than the measurement interval, instantaneous response (barometric efficiency) is the only practical measure of barometric response. Cumulative response functions from several wells (MX-4, CSVM-1, TH-2) indicate that air-pressure changes are fully expressed as total-head changes within 30 minutes in this study area, requiring that barometric efficiency (instantaneous effect) rather than lag-weighted air-pressure effects be used for total-head adjustments.

Tides

Astronomical forcings are known to influence water levels in wells, and since the pioneering work of Bredehoeft (1967) there has been some theoretical justification for applying tidal corrections to well hydrographs, particularly in confined-aquifer systems. The process has become simplified in recent years by tools such as TSOFT (Vauterin and Van Camp, 2011) that produce earth-tide tables, but the mechanical properties of the aquifer are seldom known and must therefore be assumed. Another approach is that of Foremen (1977) as implemented by Caldwell (1998) that fits *observed* tide data to a theoretical model that offers a predictive capability. Even the largest aquifer systems are tiny compared to open-water bodies with measurable tides, but the presence of a tide signal (residual, periodic fluctuations after barometric effects are removed) suggests that an astronomical model that empirically *fits* the candidate well tides has great potential for hydrograph adjustment (correction). We employ the latter method in work described below.

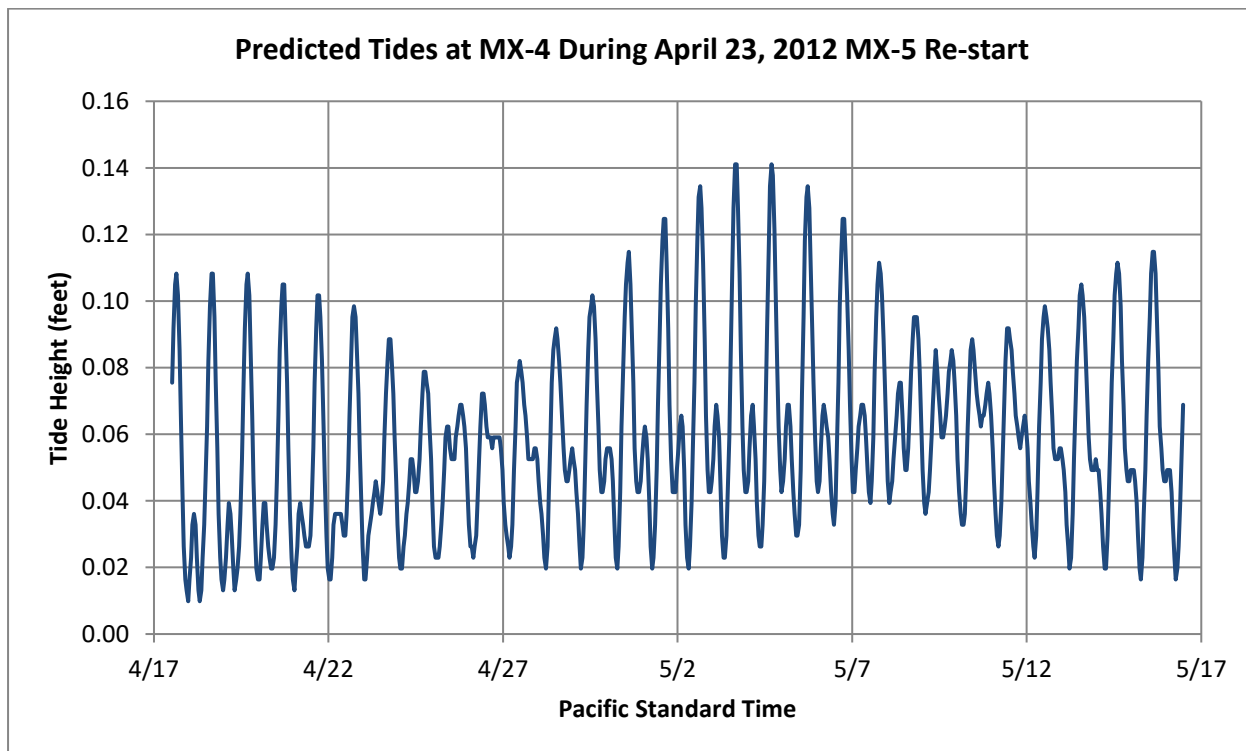


Figure 1. Tides predicted by SLPR2 (Caldwell, 1998) based on 2003-04 tide analysis year [File WT40012cj.xlsx, sheet 'Apr17-May16']

Results Summary

Appendices A, B, and C contain preliminary derivations of transmissivity (T) and storage coefficient (S) from responses of monitoring wells CSVN-1, RW-2, and MX-4, respectively, to the April 23, 2012 re-start of MX-5. Appendix D and E contain our preliminary derivations of T and S from the response of MX-4 and MX-5, respectively, to the March 5-6, 2002 constant-rate test of RW-2. Tide analysis and prediction has only been accomplished for MX-4, pending receipt of additional water-level and barometric-pressure data from SNWA for 2003-04, the most appropriate tide-reference year. The RW-2 test in 2002 pre-dates SNWA monitoring in Coyote Spring Valley, requiring utilization of interpolated barometric-pressure data from Paiutes' TH-2 as the only available alternative to the closer and higher-frequency SNWA monitoring that began late in 2003.

An anisotropic, single-layer finite-difference model (Table 1) provides a fair representation of time-drawdown relations observed in April-May of 2012 (Figure 1). However, the time constant for impacts to arrive at the outflow boundary of the model is only about 14 days (Figure 3), even shorter than the range derived by Johnson and Mifflin (2012) for different domain areas, to which the time constant is insensitive. The time actually required for impacts to occur appears to be related to the seepage velocity, a direct indication of which is evident in temperature records from the EH-4 monitoring well (Figure 4). The extreme rainfall events of the winter of 2010-2011 appear to have caused two distinct reductions of water temperature at EH-4; the first is interpreted to be the result of local infiltration, the second as underflow from up-gradient recharge areas along Pahrangat Wash.

Table 1. Single-Layer Finite-Difference Model Configuration

Domain Extent:	20 miles NW-SE, 10 miles SW-NE		
Grid Origin Location:	E 673742 m, N 4073832 m, UTM Zone 11,NAD83		
Rotation about Origin:	35.62° clockwise		
Number of Cells:	5000		
Cell Dimensions:	x	1056 ft	
	y	1056 ft	
	z	4000 ft	
Parameters:	K _x	329 ft/day	
	K _y	274 ft/day	
	S _y	0.003	
Boundary Conditions:	Inflow	4,320,000 ft ³ /day	50 cfs specified steady-state flux
	Outflow	1846 ft	specified total head
	MX-5	-683615 ft ³ /day	(includes barometric pressure)
			(3551 gpm)
MX-5 Stress Periods:	1	730 days	70 time steps, 1.2 time step multiplier

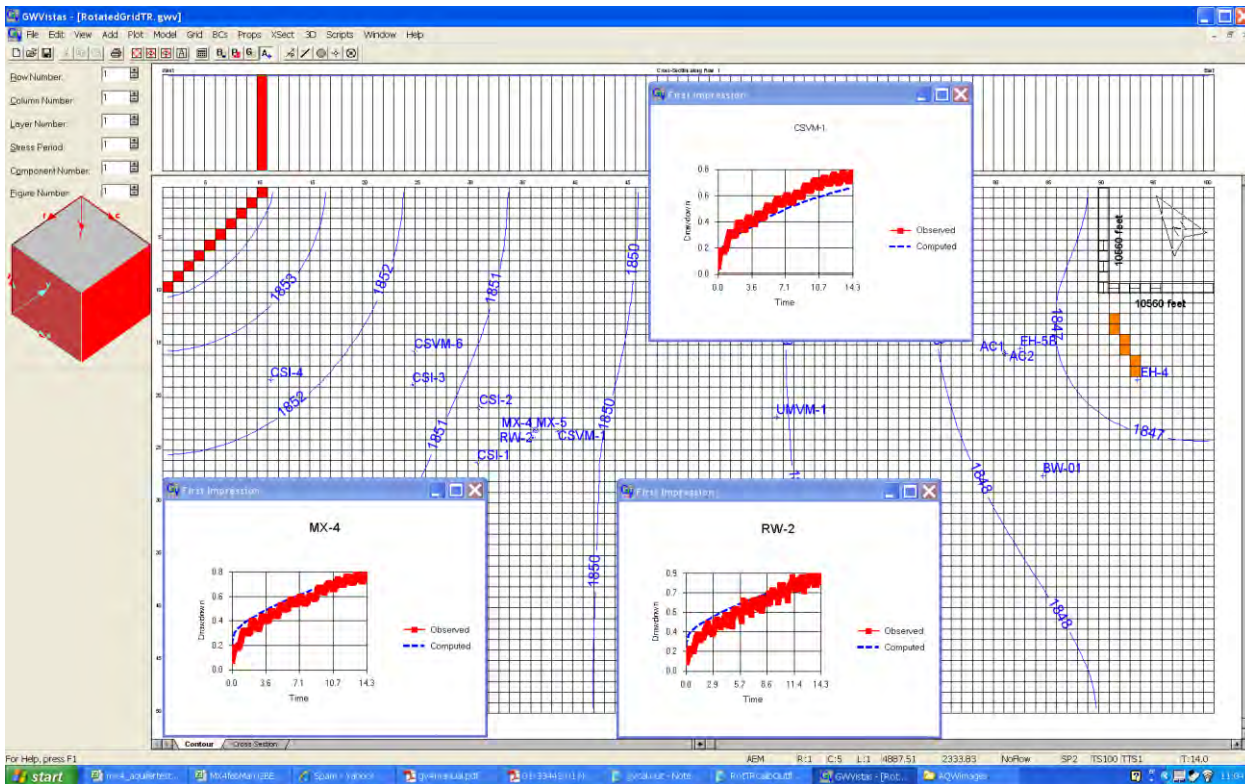


Figure 2. Simulated responses to April 23, 2012 re-start of MX-5 in anisotropic, bounded domain with properties given in Table 1. [File MX42012GWV.tif, screenshot from file RotatedGridTR.gvw]

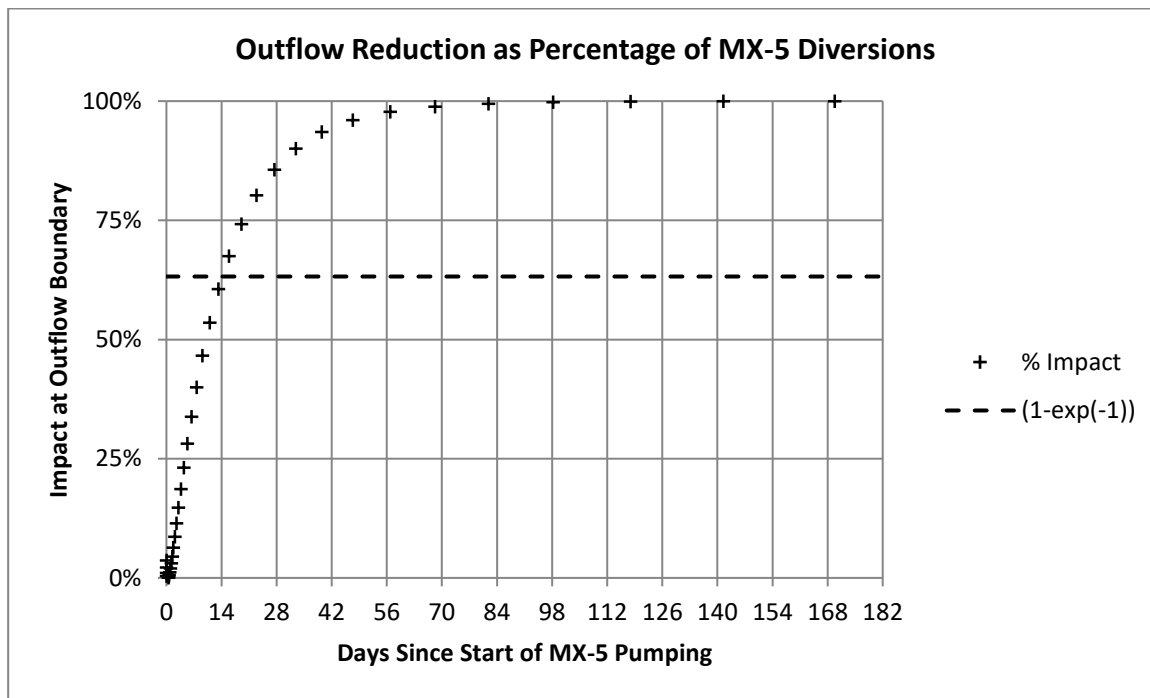


Figure 3. Time required for MX-5 diversions to be expressed as outflow reductions at downstream boundary of model domain (orange cells near right edge of Figure 2). The quantity $(1-\exp(-1))$ defines the time constant for the impulse response function [File RotTRcalibOutflow.xlsx]

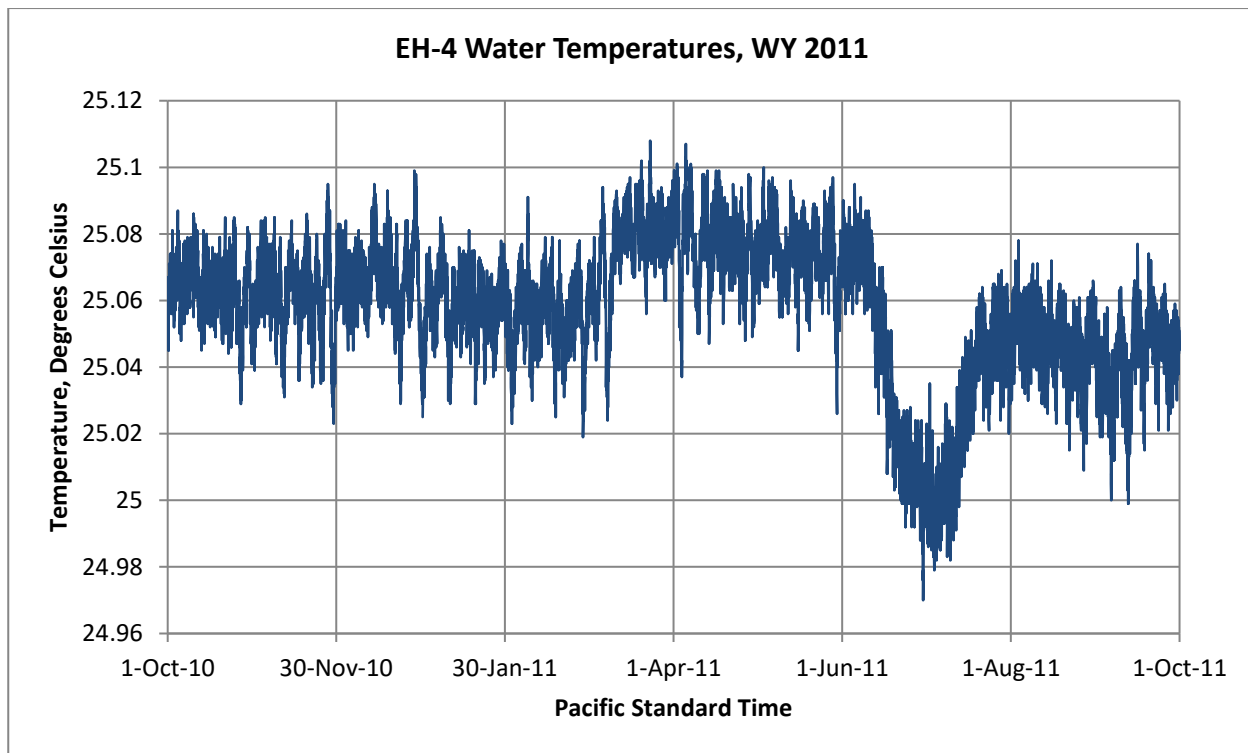


Figure 4. Depression of water temperatures at EH-4 during and following the extremely wet winter of 2010-2011 [File RW-1, RW-2, EH-4, Eh-5b Hourly 2003-2012V2.xlsx, sheet 'Eh-4']

Discussion

A valid model of Order 1169 responses will need to accurately represent drawdowns in observation wells, which develop rapidly, and impacts in Upper Moapa Valley, which require several months to be fully expressed as discharge reductions. Tortuous flow paths, non-Darcian (turbulent) flow, partial penetration of test wells, layering of hydrostratigraphic units, permeability barriers, and yet-unidentified aquifer cells with enhanced storage are potential contributors to the large-scale system inertia that is inconsistent with well-hydraulics analyses. Still, all lines of evidence continue to point to an unconfined groundwater system in southeastern Coyote Spring Valley that is tributary to the Muddy River.

References

- Bredehoeft, J.D., 1967. Response of well-aquifer systems to earth tides: *Journal of Geophysical Research* 72, no. 12, pp. 3075-3087.
- Caldwell, P. 1998. [Sea Level Data Processing on IBM-PC Compatible Computers, Version 3.0 \(Year 2000 Compliant\)](#). JIMAR Contribution No. 319, SOEST, University of Hawaii, 72 pp.
- Converse Consultants, 2002. Production well construction and testing, RW-2 well, Coyote Spring Valley, Clark County, Nevada: unpublished report, Converse Project No. 01-33422-01, June 14, 2002, 86 p.

- Davis, D.R. and Rasmussen, T.C., 1993. A Comparison of Linear Regression With Clark's Method for Estimating Barometric Efficiency of Confined Aquifers: *Water Resources Research*, v. 29, no. 6, pp. 1849-1854.
- Ertec Western, Inc., 1981, MX siting investigation, water resources program, results of regional carbonate aquifer testing, Coyote Spring Valley, Nevada: unpublished report dated December 18, 1981.
- Foreman, M.G.G., 1977. *Manual for Tidal Heights Analysis and Prediction*. Pacific Marine Science Report 77-10, Institute of Ocean Sciences, Patricia Bay, Sidney, B.C., 97 pp.
- Johnson, C. and M. Mifflin, 2012. Analysis Progress Report – Order 1169 Impacts Assessment: unpublished letter report to HRT Participants, March 17, 2012, 15 p.
- Mackley, R.D., T.C. Pulsipher, F.A. Spane, and C.H. Allwardt, 2010. Guide to using Multiple Regression in Excel (MRCX v.1.1) for Removal of River Stage Effects from Well Water Levels: Pacific Northwest National Laboratory, PNNL-19775, Rev. 1, September, 2010, 55 p. (NOTE: MRCX v.1.2 provided by author July 31, 2012)
- Mifflin & Associates, 2010. Order 1169 Impacts (with September 8, 2010 Addendum): unpublished letter report to HRT Participants, dated May 27, 2010 and distributed December 20, 2010, 31 p.
- Mifflin, M.D. 1992. The Arrow Canyon Range cell, carbonate aquifer and upper Muddy River valley groundwater monitoring – a summary of local and regional evidence and interpretations. Mifflin & Associates, Inc.: 18 p. (unpublished)
- Rasmussen, T.C. and L.A. Crawford, 1997, Identifying and Removing Barometric Pressure Effects in Confined and Unconfined Aquifers: *Ground Water*, v. 35, no. 3, May-June, 1997, pp. 502-511.
- Spane, F.A., 2002. Considering barometric pressure in groundwater flow investigations: *Water Resources Research*, v. 38, no. 6, pp. 14-1 – 14-18
- Toll, N.J. and Rasmussen, T.C., 2007. Removal of Barometric Pressure Effects and Earth Tides from Observed Water Levels: *Ground Water*, v. 45, no. 1, pp. 101-105.
- Vauterin, P. and Van Camp, M., 2011, TSoft Manual: Royal Observatory of Belgium, v. 2.1.6 Release date Nov 8, 2011, 58 p.

Appendix A

Responses of CSVM-1 to April, 2012 MX-5 Re-Start

SE ROA 38322

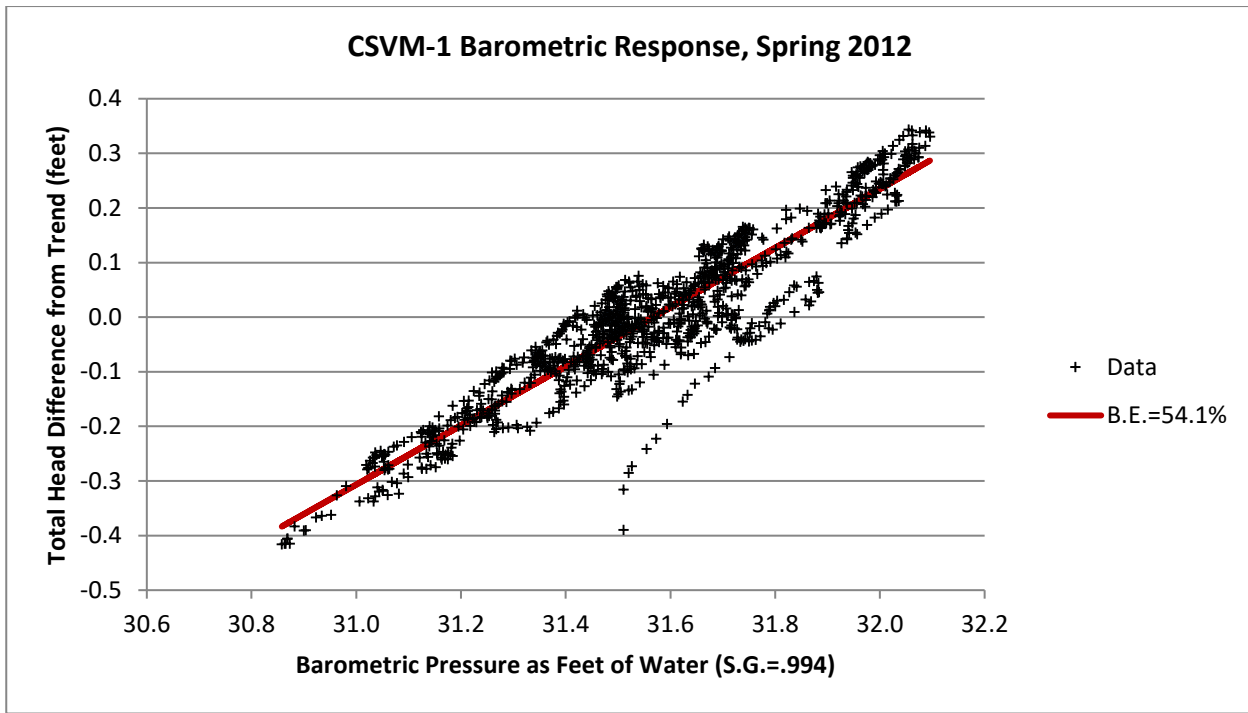


Figure A1. [File CSV1_RawP_2012.xlsx, sheet 'Feb-May']

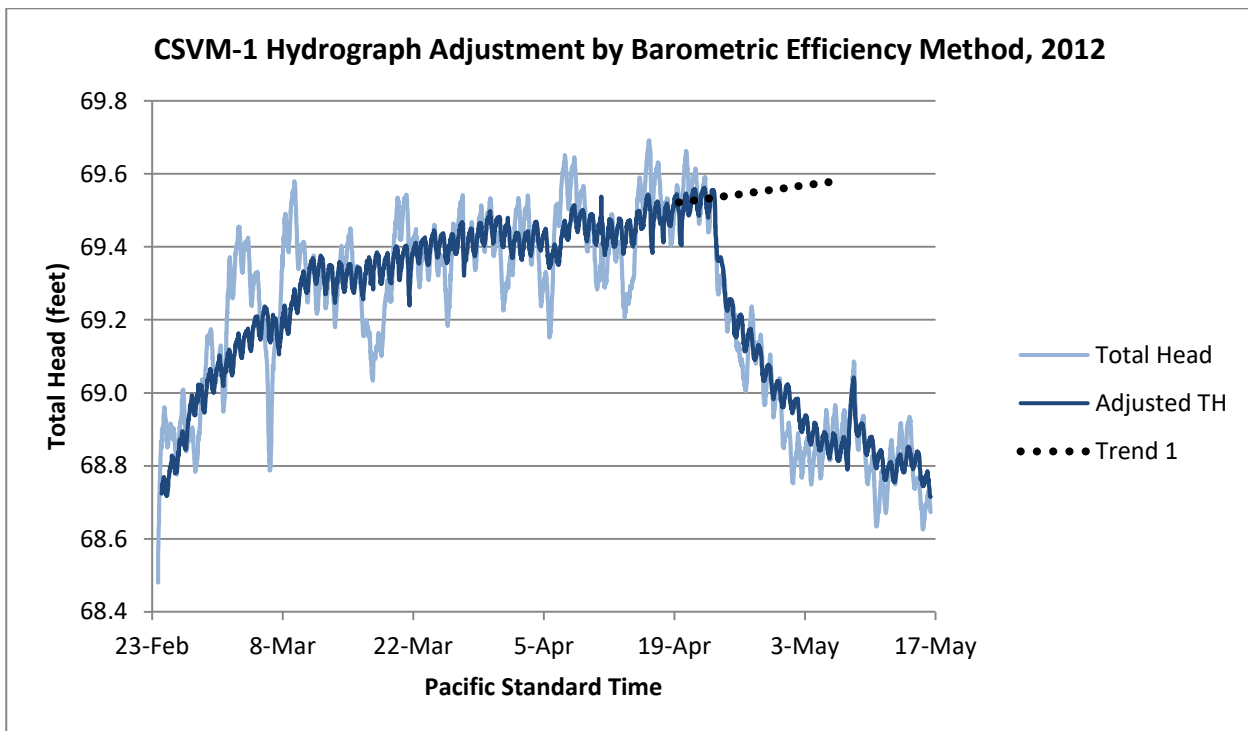


Figure A2. [File CSV1_RawP_2012.xlsx, sheet 'Feb-May']

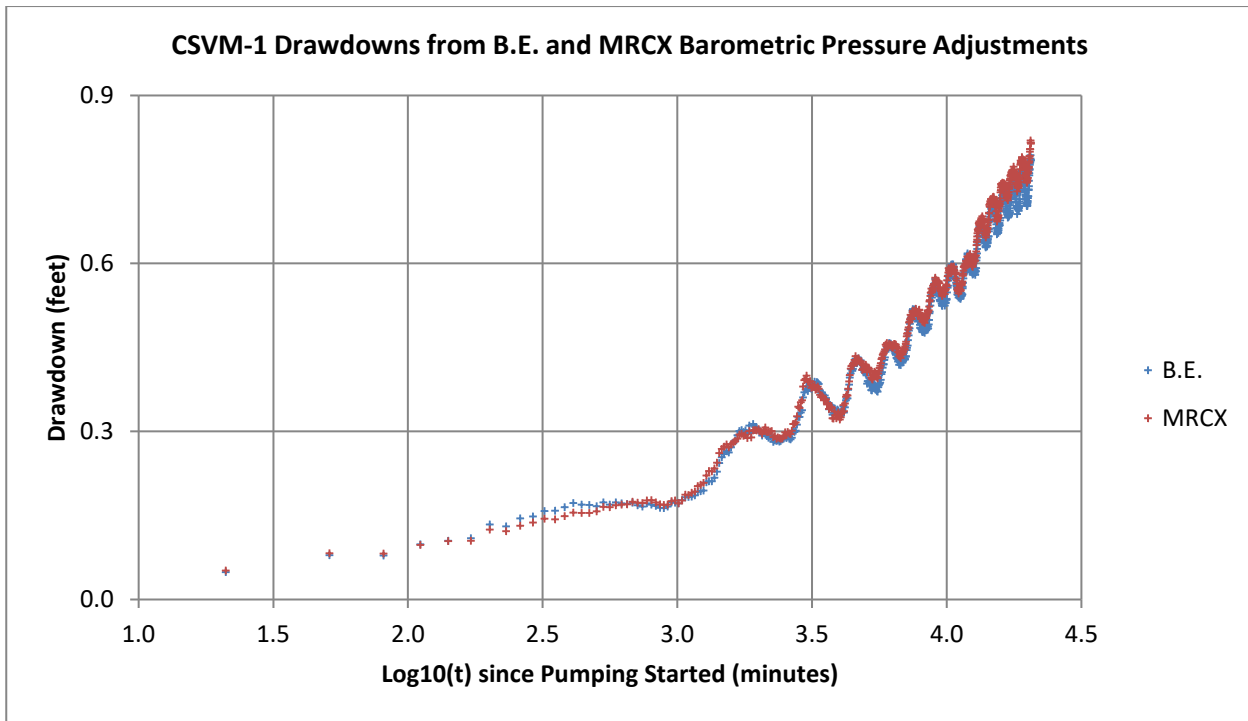


Figure A3. CSV-1 drawdowns, April-May 2012, based on barometric efficiency (B.E.) and multiple regression (MRCX) adjustments of total head [File CSV1_RawP_2012.xlsx, sheet 'TimeDD']

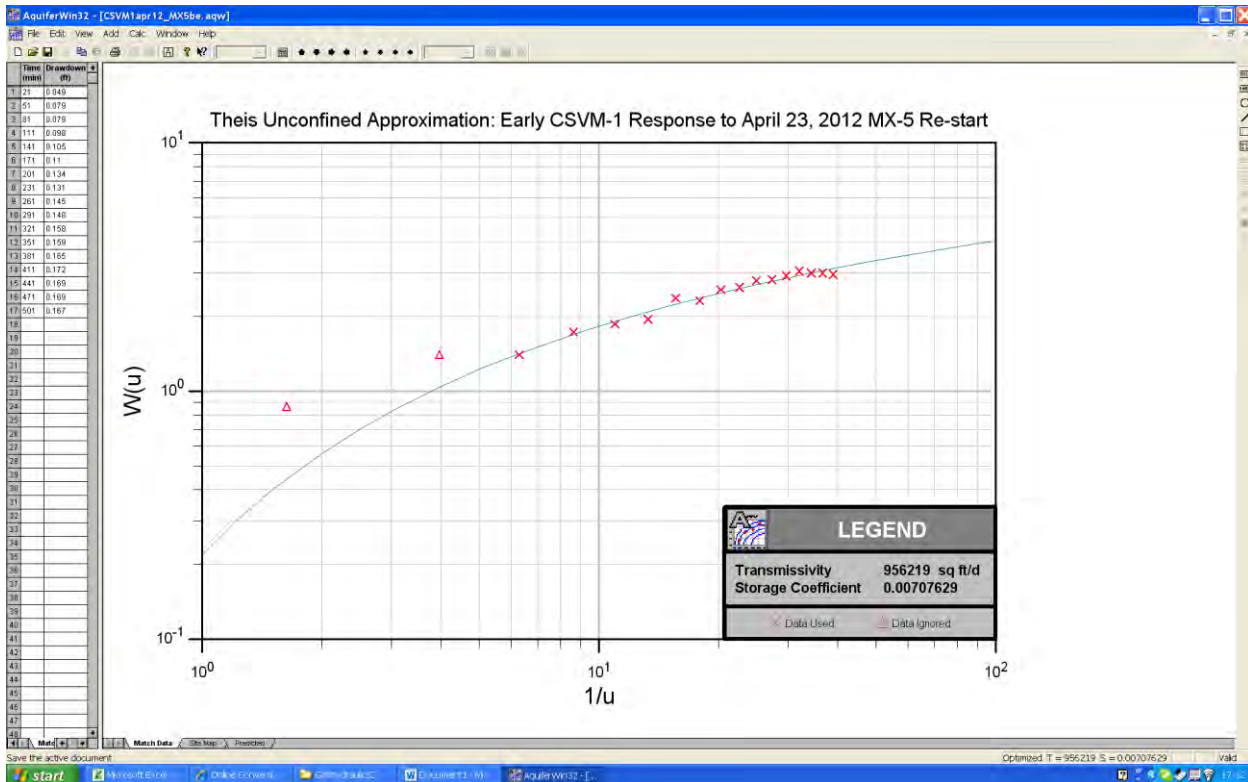


Figure A4. Optimized match to early-time drawdown data, MX-5 pumping rate 3,551 gpm [File CSV120120423be.tif, screenshot from file CSV1apr12_MX5be.aqw]

Appendix B

Responses of RW-2 to April, 2012 MX-5 Re-Start

SE ROA 38325

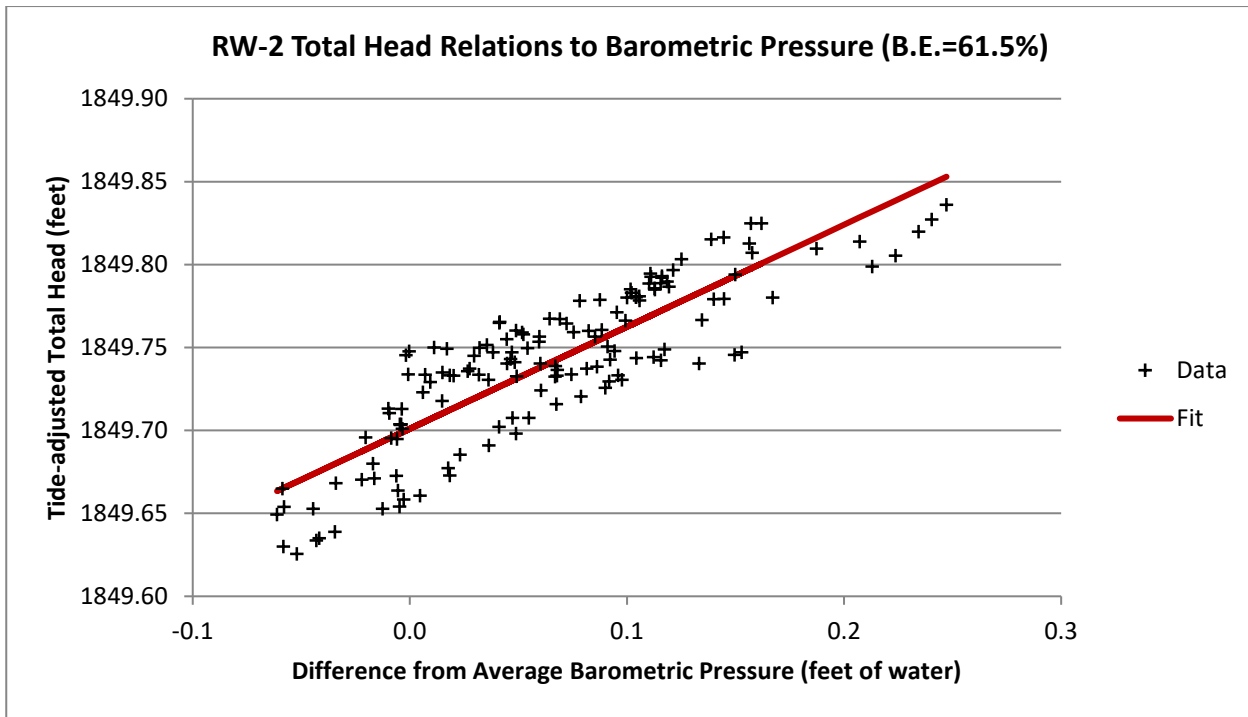


Figure B1. [File RW2responseAprMay12.xlsx, sheet 'AdjData']

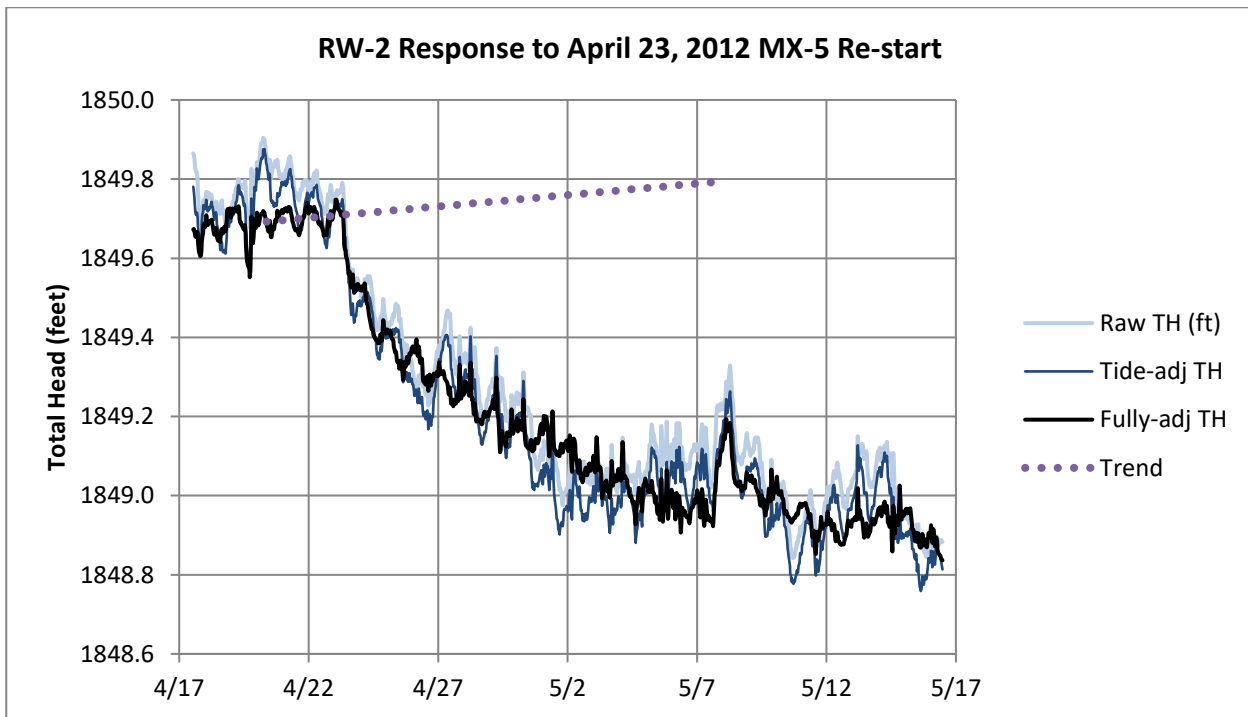


Figure B2. Adjustments to total head at RW-2 based on barometric efficiency method [File RW2responseAprMay12.xlsx, sheet 'AdjData']

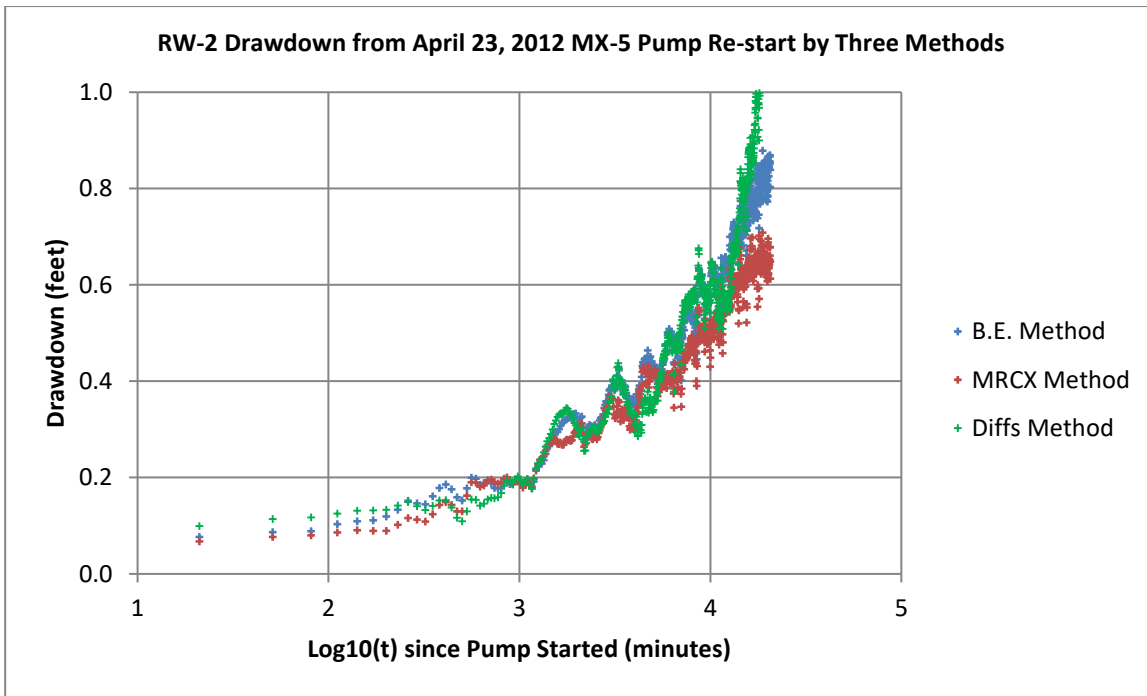


Figure B3. File RW2responseAprMay12.xlsx, sheet 'TimeDD'

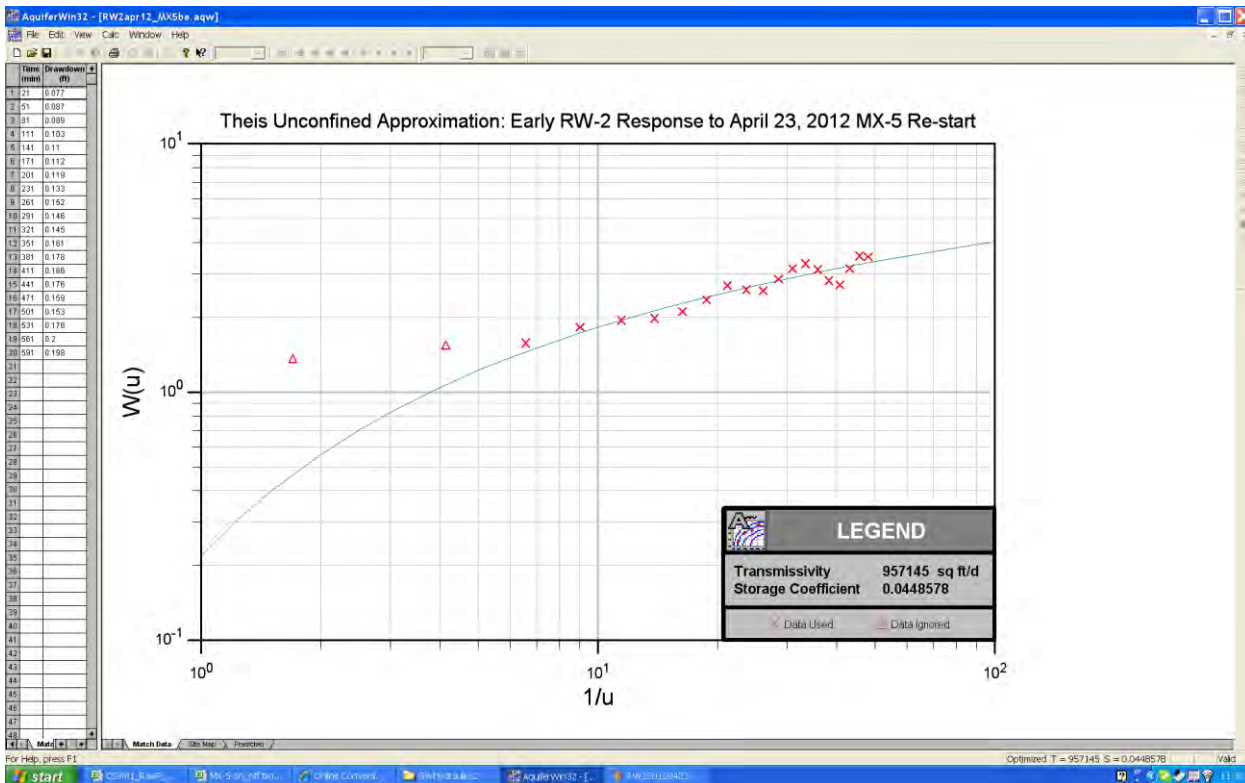


Figure B4. Optimized match to early-time drawdown data, MX-5 pumping rate 3,551 gpm [File RW2120120423be.tif, screenshot from file RW2apr12_MX5be.aqw]

Appendix C

Responses of MX-4 to April, 2012 MX-5 Re-Start

SE ROA 38328

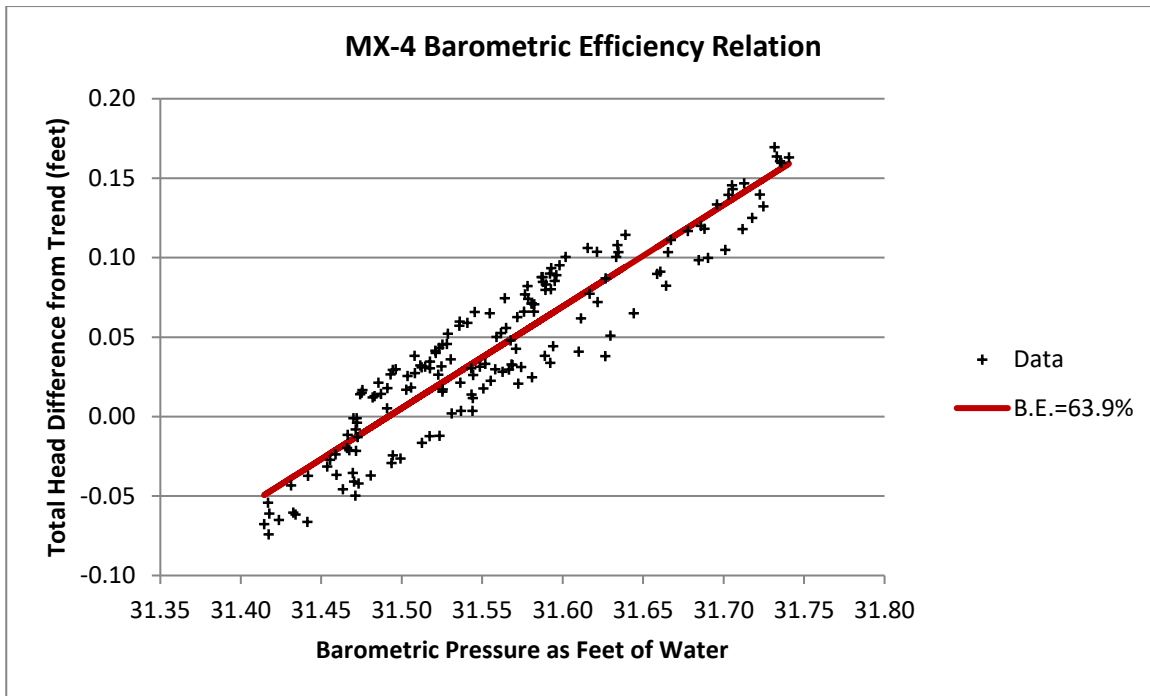


Figure C1. [File MX4_Apr12response.xlsx, sheet 'Feb-May12']

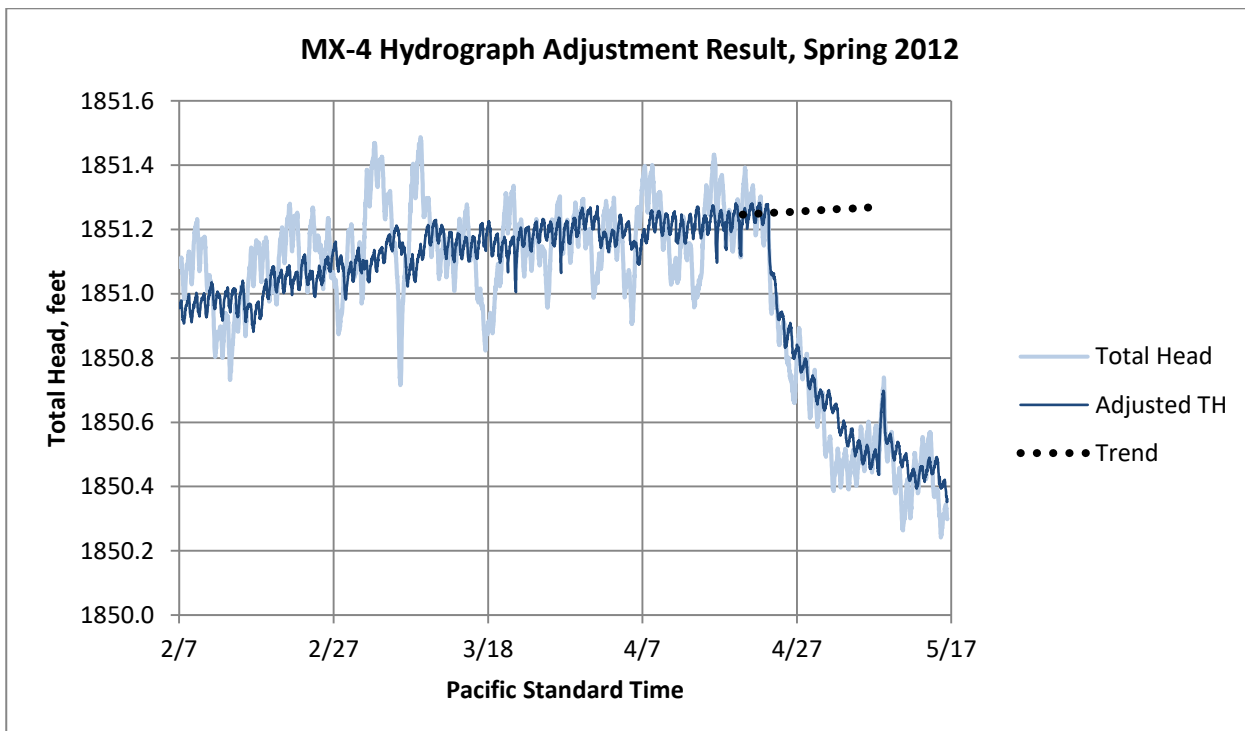


Figure C2. [File MX4_Apr12response.xlsx, sheet 'Feb-May12']

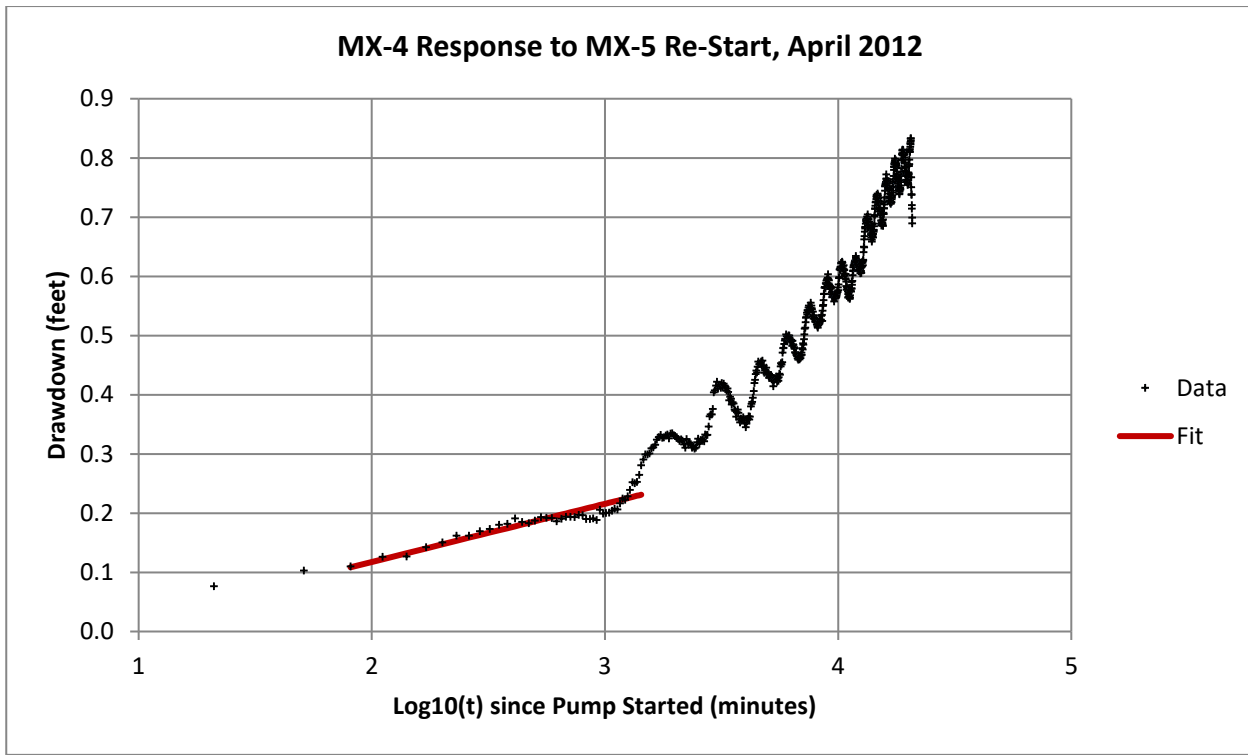


Figure C3. [File MX4_Apr12response.xlsx, sheet 'TimeDD']

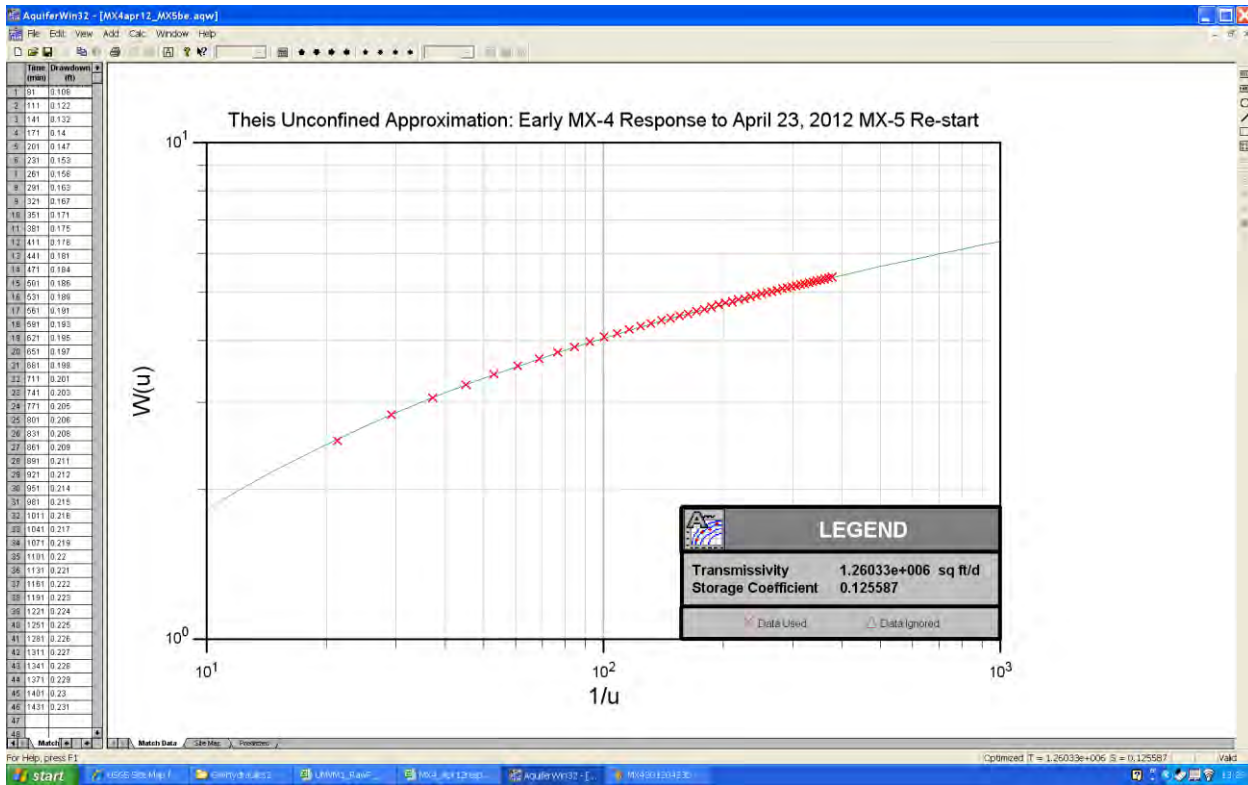


Figure C4. Optimized match to early-time drawdown data, MX-5 pumping rate 3,551 gpm [File MX4120120423be.tif, screenshot from file MX4apr12_MX5be.aqw]

Appendix D

Analysis of MX-4 Response to RW-2 Development and Testing, March 2002

SE ROA 38331

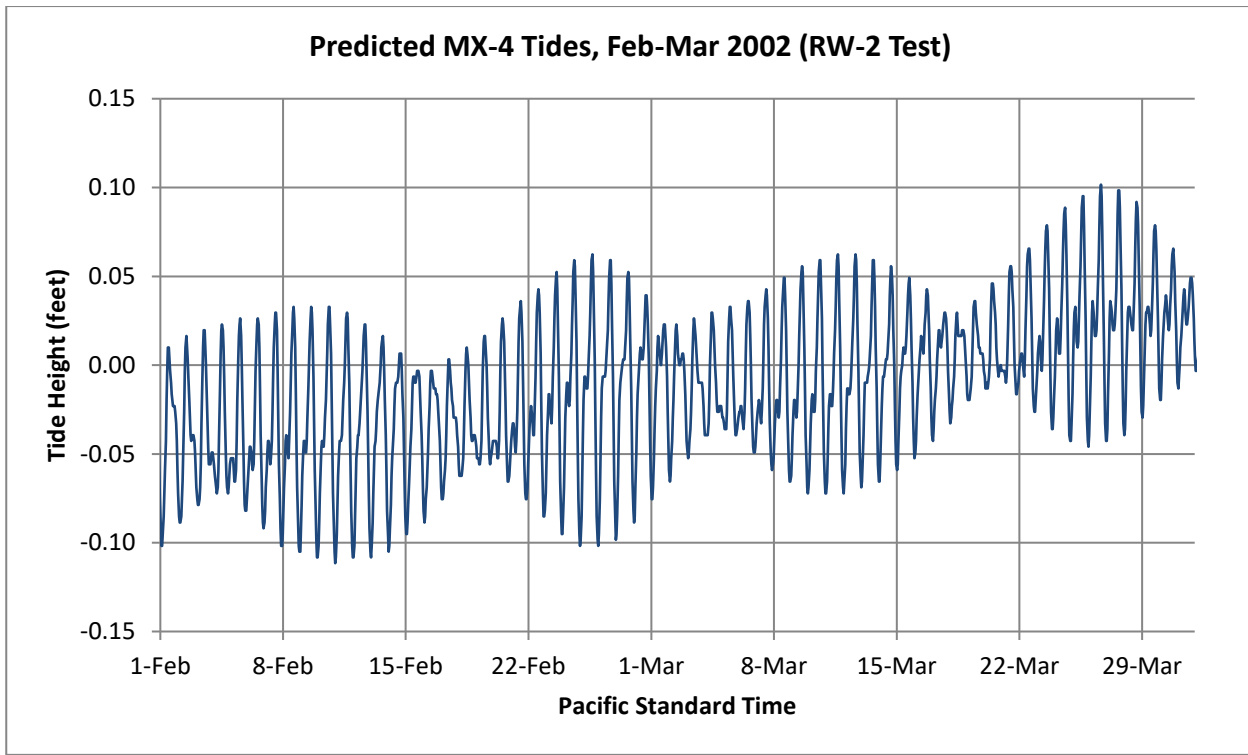


Figure D1. Predicted MX-4 tides from SLPR2 based on 2003-04 reference year [File WT40002cj.xlsx]

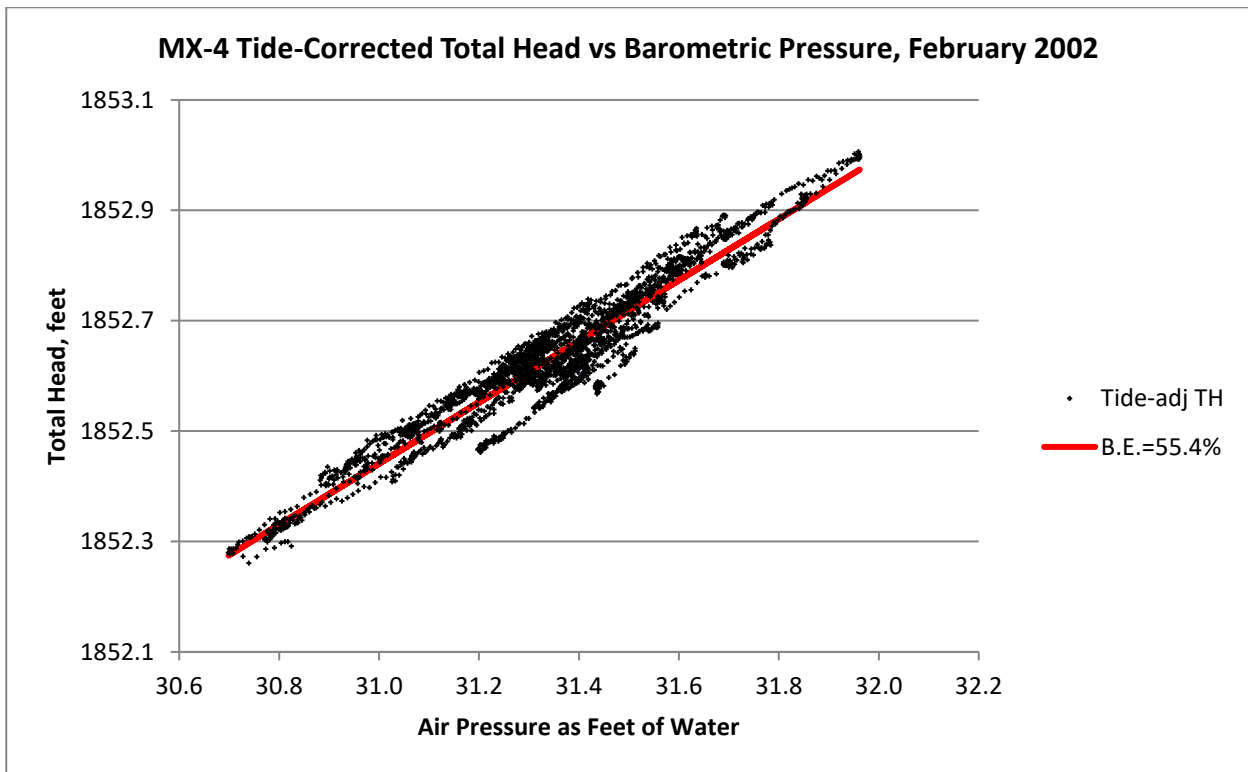


Figure D2. MX-4 barometric efficiency from interpolated TH-2 station pressures File MX4febMar02BE.xlsx, sheet 'AdjData'

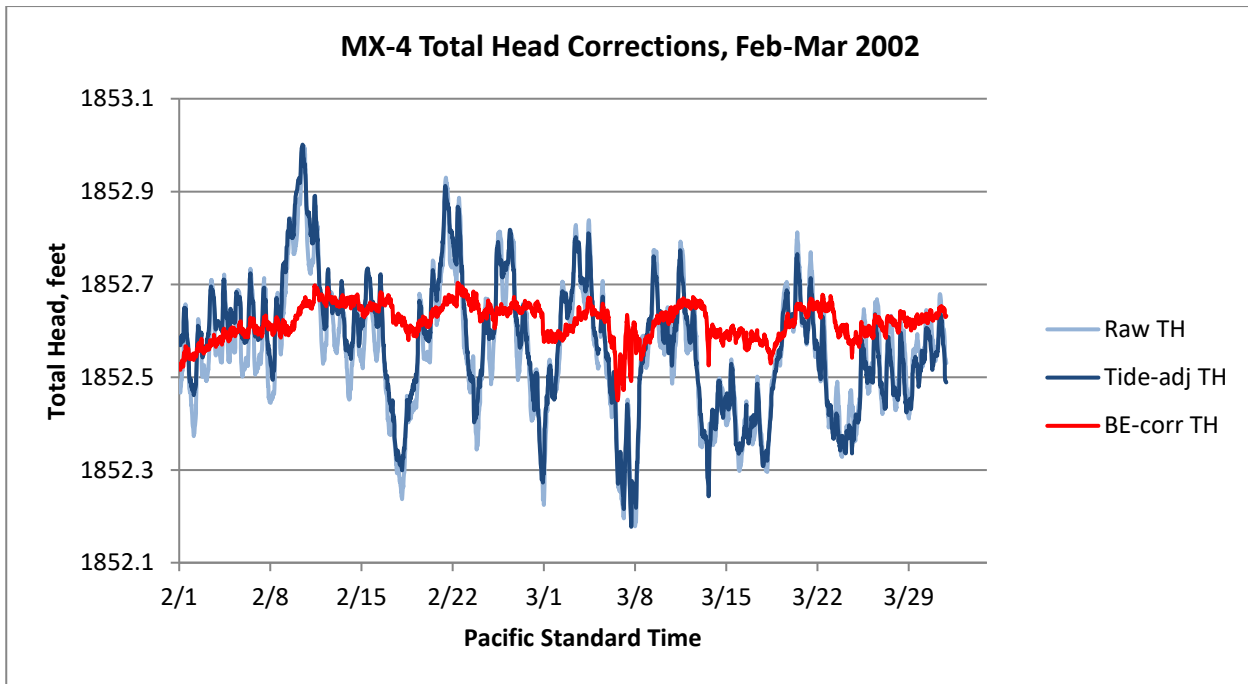


Figure D3. Result of tidal and barometric corrections to MX-4 total heads [File MX4febMar02BE.xlsx, sheet 'AdjData']

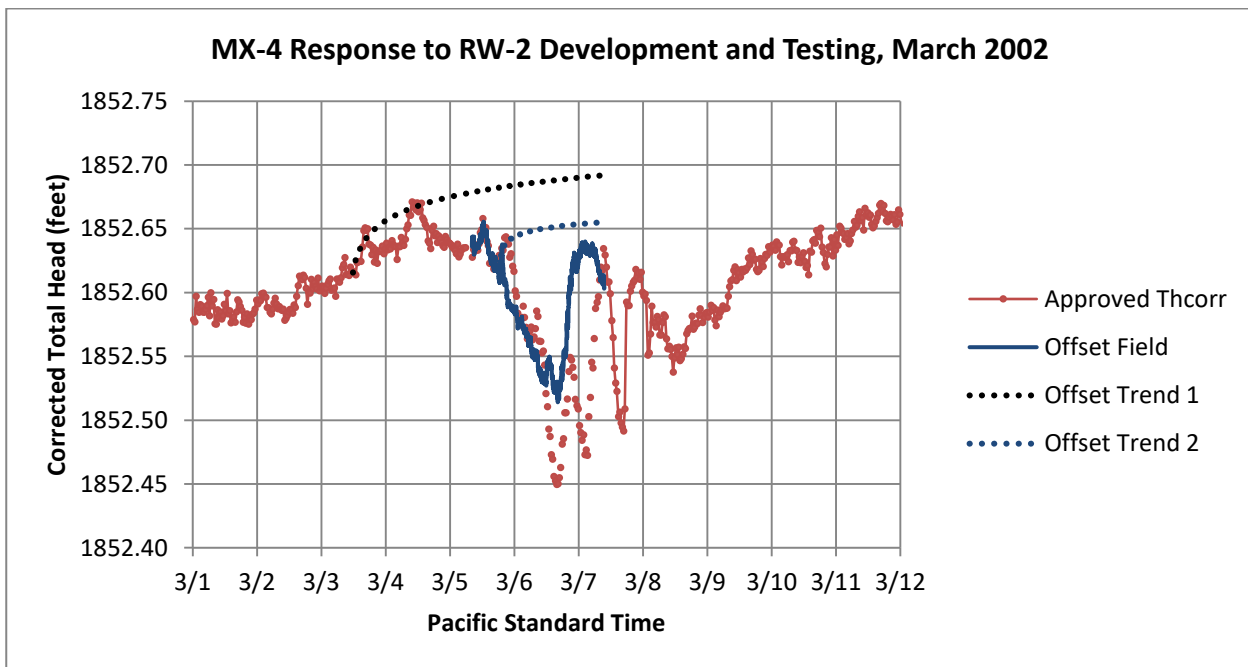


Figure D4. Antecedent trends for overall development and testing interval (Trend 1), and constant-rate test (Trend 2) File MX4febMar02BE.xlsx, sheet 'TimeDD2'

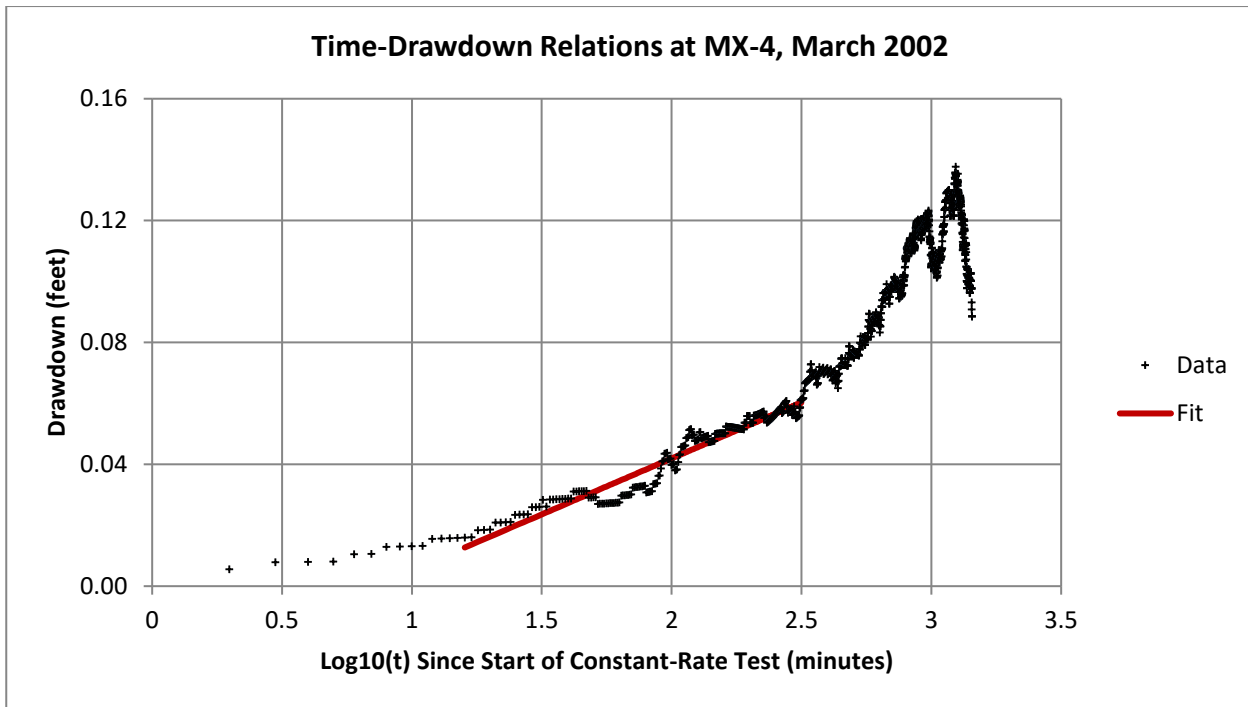


Figure D5. MX-4 pumping response and early-time interval selected for analysis; boundary effects dominate late-time data [File mx4_aquifertest_MARCH2002cj.xlsx, sheet 'TimeDD']

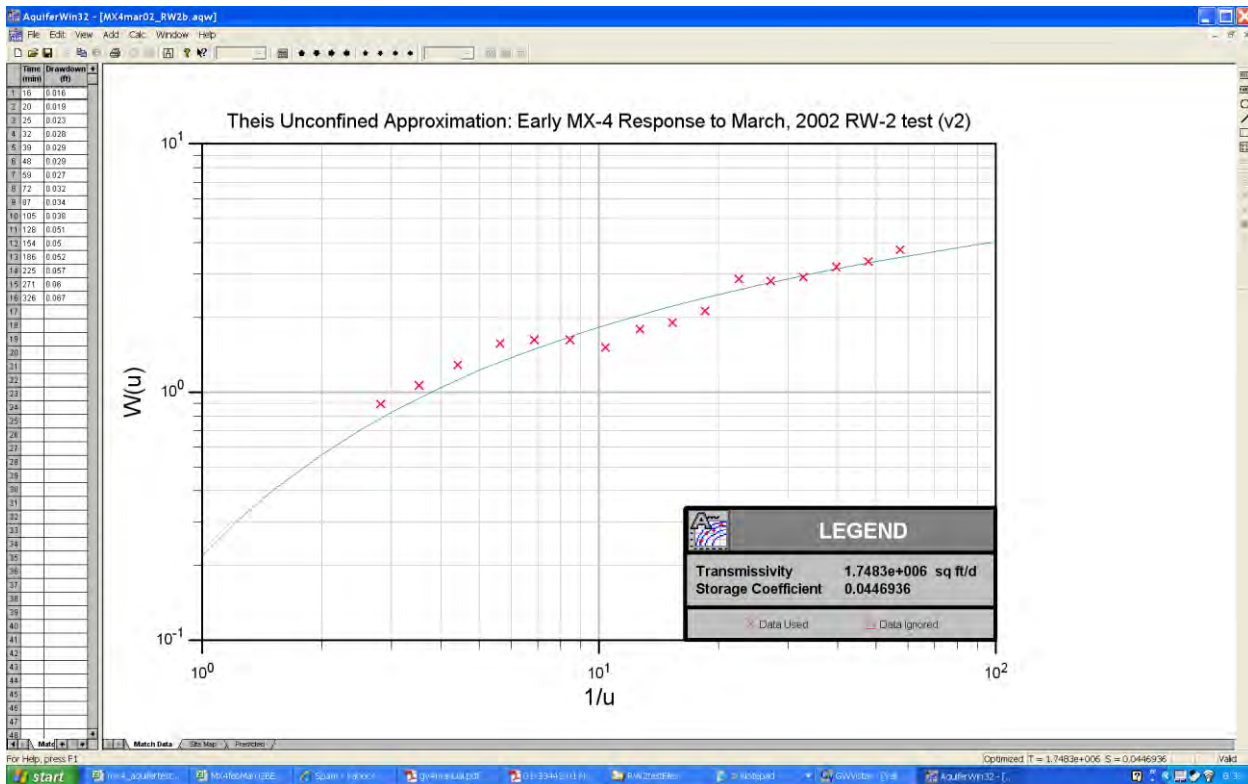


Figure D6. Parameter estimates from early MX-4 response to RW-2 constant-rate test, March 5-6, 2002 [File MX42002RW2v2.tif, screenshot from file MX4mar02_RW2b.aqw]



Figure D7. Simulated response of MX-4 to RW-2 activity March 4-6, 2002 in anisotropic, bounded domain with properties derived from April, 2012 re-start of MX-5 and responses of CSVM-1, RW-2, and MX-4 [File MX42002GWVa.tif, screenshot from ValidateRW2test.gww]

Appendix E

Analysis of MX-5 Response to RW-2 Development and Testing, March 2002

SE ROA 38336

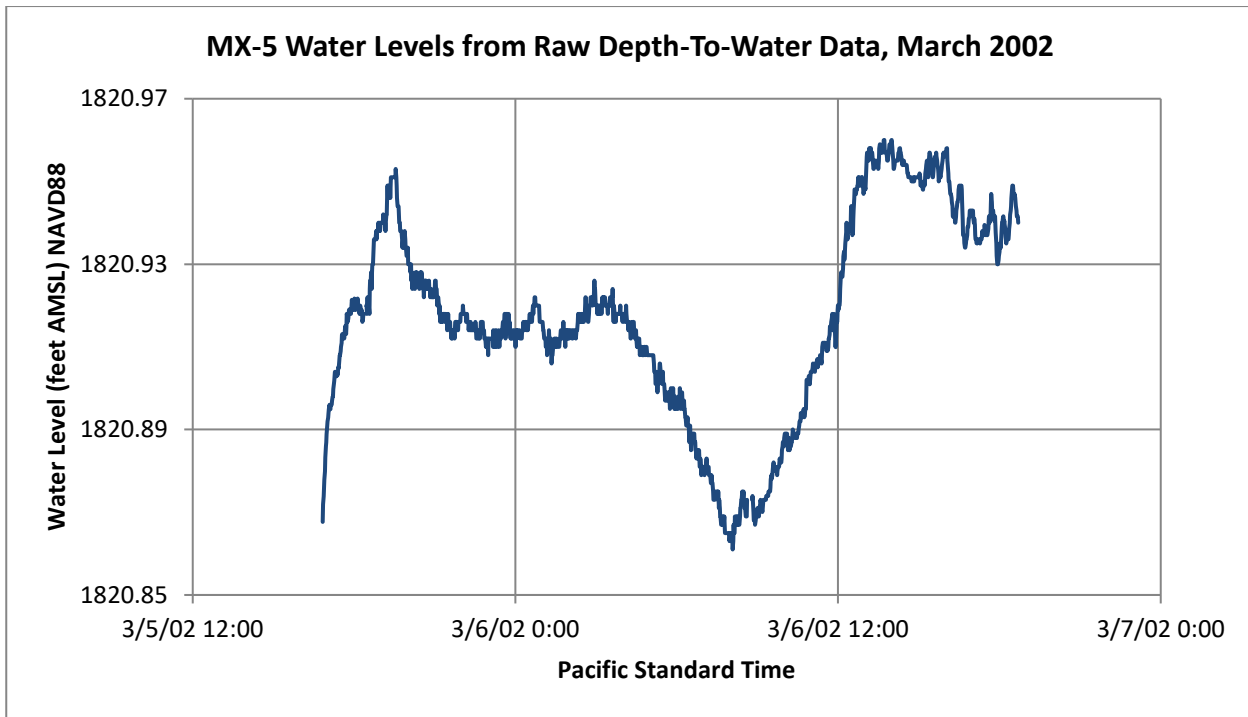


Figure E1. [File MX5allCJ.xlsx, sheet '1-minData']

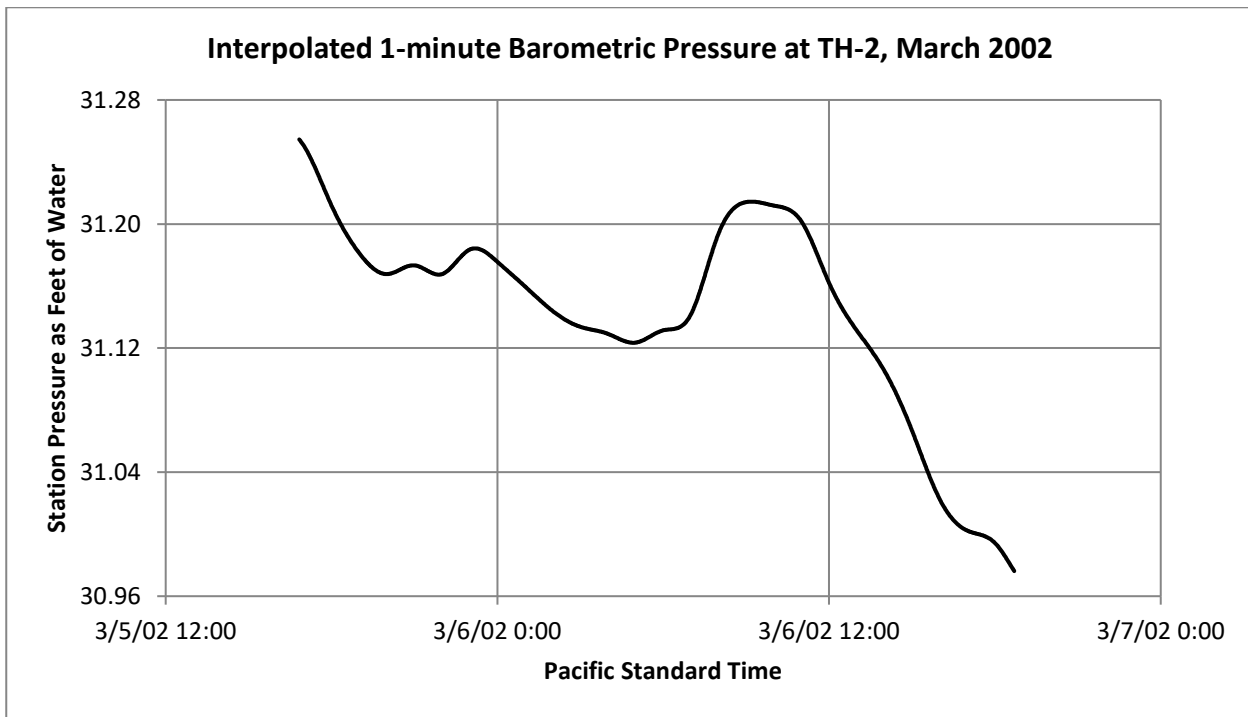


Figure E2. [File MX5allCJ.xlsx, sheet '1-minData']

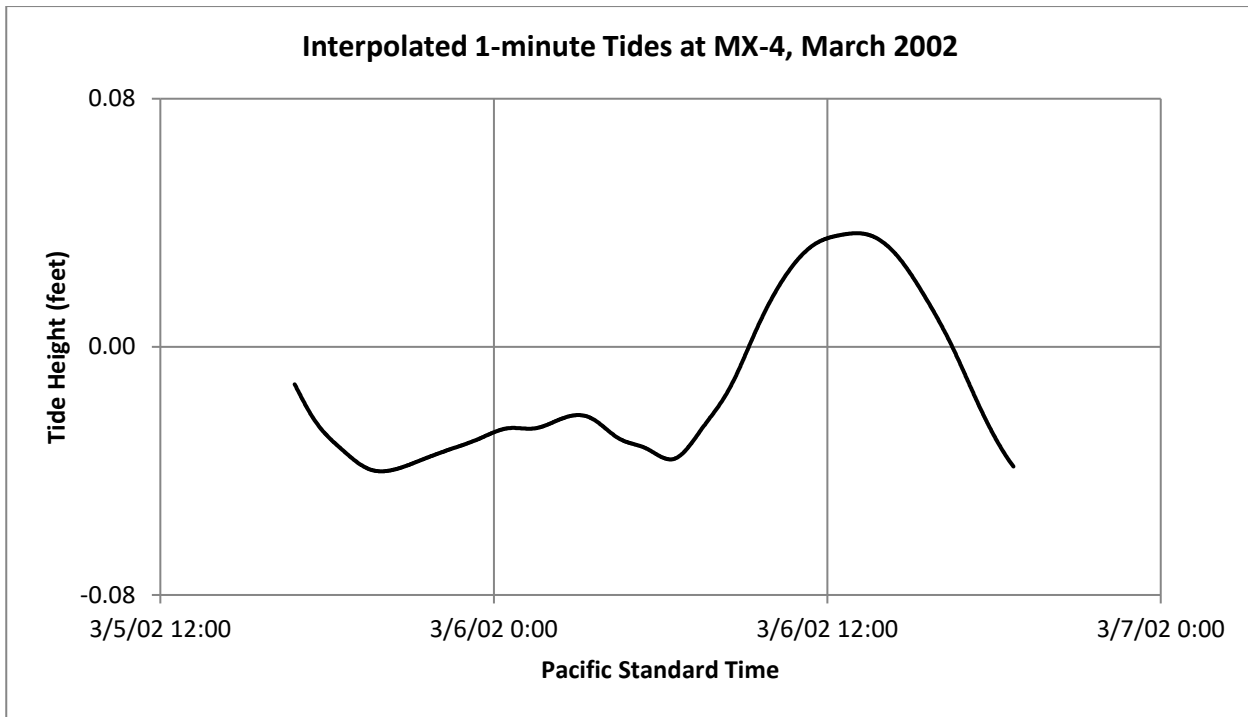


Figure E3. [File MX5allCJ.xlsx, sheet '1-minData']

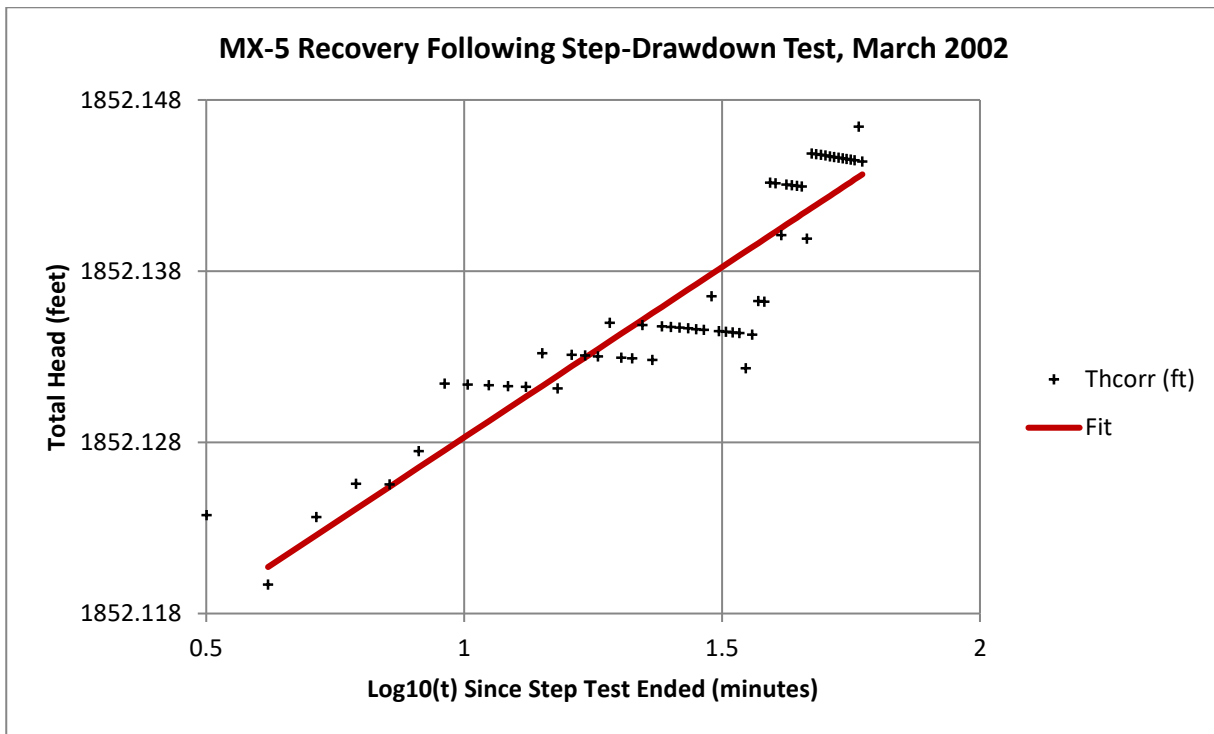


Figure E4. [File MX5allCJ.xlsx, sheet '1-minData']

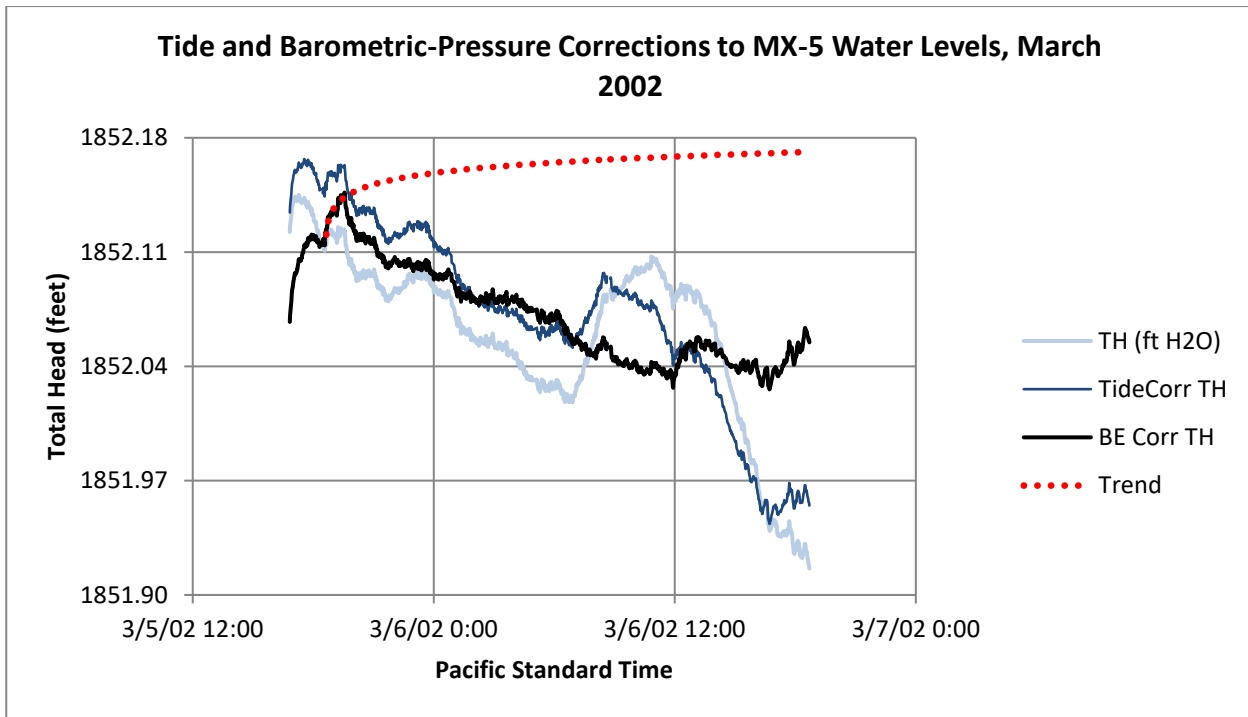


Figure E5. [File MX5allCJ.xlsx, sheet '1-minData']

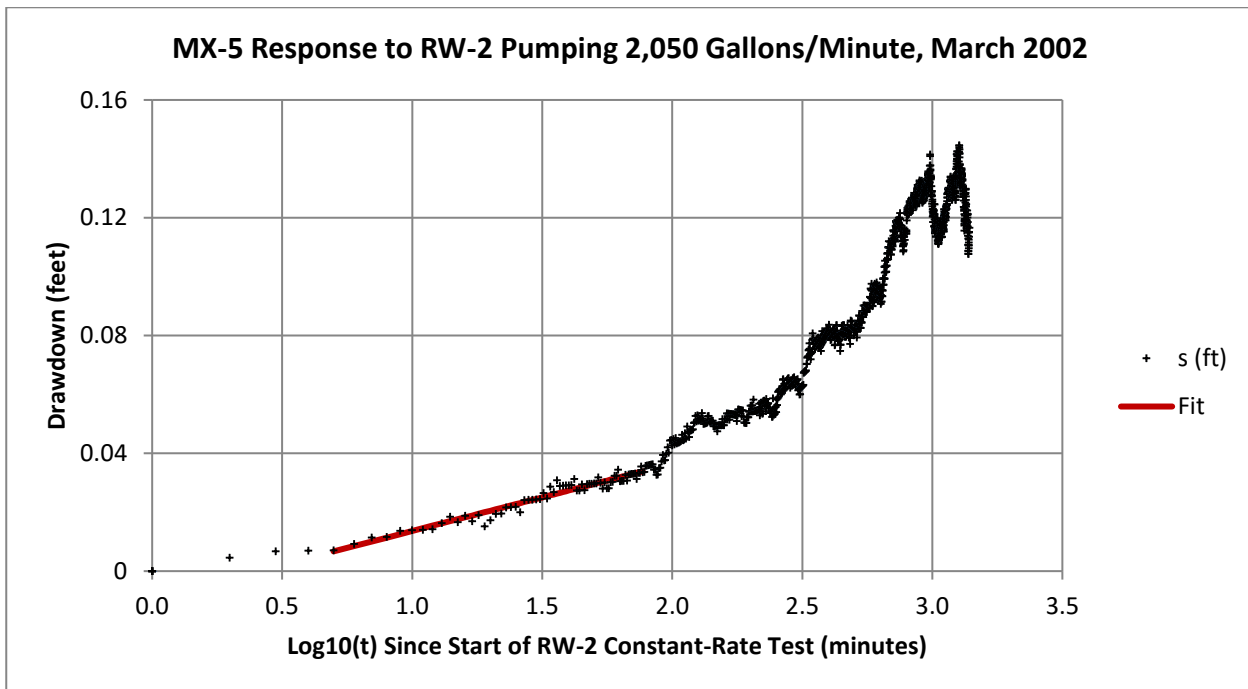


Figure E6. [File MX5allCJ.xlsx, sheet 'TimeDD']

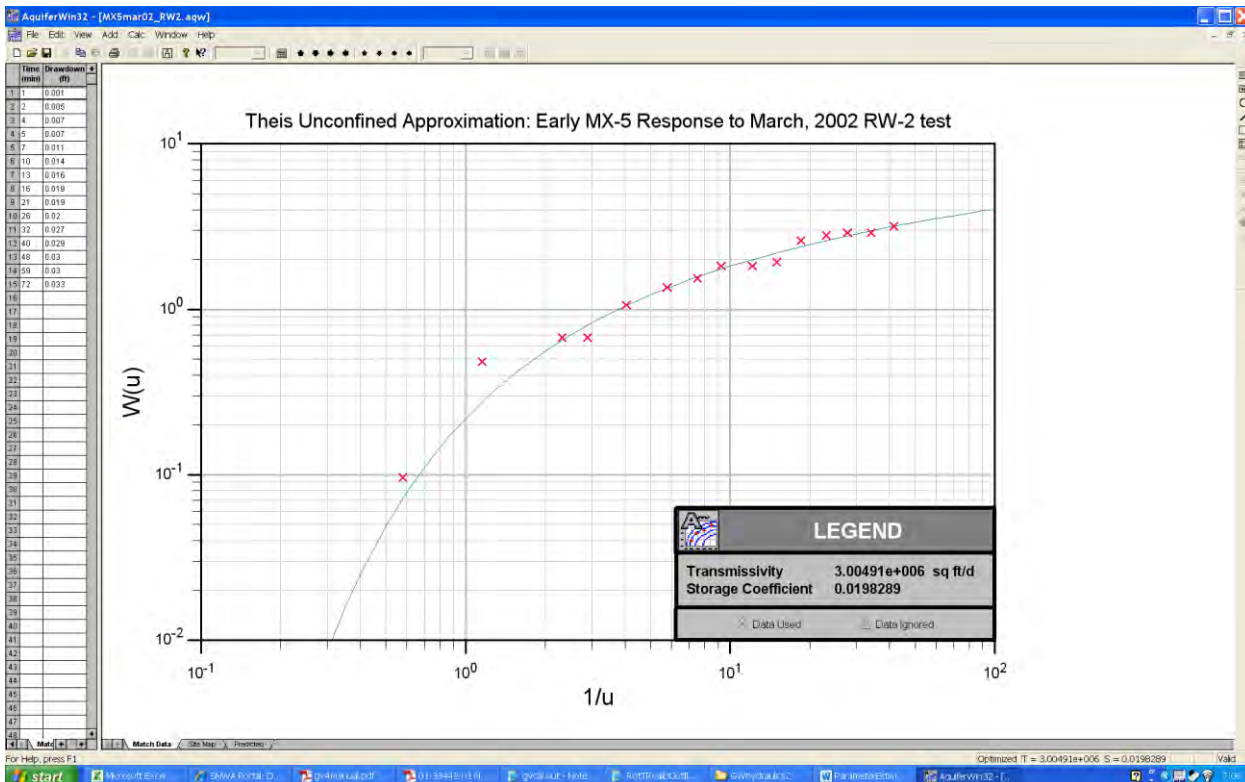


Figure E7. [File MX52002RW2.tif, screenshot from MX5mar02_RW2.aqw]

Order 1169 Impacts (with September 8, 2010 Addendum)

Mifflin & Associates, Inc.
Las Vegas, Nevada

May 27, 2010

Preface by Dr. Martin Mifflin

The Moapa Band of Paiutes' (MBP) hydrogeologic contractor, Mifflin and Associates Inc (MAI) has conducted comprehensive analyses of monitoring records in preparation for the Order 1169 test. Order 1169 was issued to validate the Las Vegas Valley Water District (LVVWD) model docketed as Exhibit 54 (LVVWD, 2001) in the 2001 State Engineer hearing on LVVWD's applications. Based on past analyses of Muddy River Springs area (MRSA) pumpage, 1:1 pumping impacts on Muddy River flows have been shown to occur through water-balance accounting (Johnson and Mifflin, 2006) but specific sources of impacts had been very difficult to confidently identify and measure due to several data-related problems. However, with longer monitoring records now available and better documentation of region-wide annual and multi-year water-level fluctuations, a new analytical strategy – presented here – has been developed by MAI that has proven successful well beyond expectations. The large CSI pumping stresses that began in 2006 have been identified and their impacts confidently resolved in the MRSA monitoring records; the analyses demonstrate 1:1 impacts developing 9-10 months after pumping during the first three years of Coyote Springs Investments (CSI) groundwater development in Coyote Spring Valley. The analytical objectives of Order 1169 have been met: the magnitude and rate of development of impacts have been estimated in the MRSA. Reduction of the monitoring databases into useful formats for analyses has been labor-intensive, but the analytical strategies are straightforward and reproducible.

The results of the MAI analyses are consistent with independent lines of evidence gathered over many years. All developed hydrogeologic evidence, beginning in the 1960's (Eakin, 1966; Mifflin, 1968) indicated Coyote Spring Valley is a direct source basin for Muddy River Springs flow. Databases confirming the transmissive characteristics of the carbonate-rock aquifer and small hydraulic gradients were established by Fugro/Ertec during the MX Program (Ertec Western, 1981) and extended geographically by new CSI production wells, SNWA monitoring wells, and associated monitoring records within Coyote Spring Valley. As far north (and into) Kane Springs Valley, all databases have combined to document a highly transmissive carbonate-rock aquifer in close hydraulic continuity with the Muddy River Springs discharge area. Pump anywhere upgradient of the Springs within this interconnected transmissive zone and 1:1 impacts will develop on flows in the Muddy River Springs discharge area - and now there is a good measure of timing for the rate of development of impacts to a full 1:1 ratio from pumpage in southeastern Coyote Spring Valley.

The rate and magnitude of impacts resulting from CSI pumping stresses applied in Coyote Spring Valley indicate a potential for highly undesirable consequences from the currently proposed design of the Order 1169 pump test. Reduced flows in already marginal Moapa Dace habitats in the Springs area, including in several of the tributary reaches that historically provided the best habitats, and the recent (synchronous with the first large CSI pumping impact) drop in population counts by approximately 60% from 2007 to 2008 (USFWS, 2008) indicate that a choice may exist between development of 50% of permits for two years, as prescribed by Order 1169, or maintaining flows required for the remaining

quality Dace habitats. The 2006 Memorandum of Agreement (MOA) between regional water users and the U.S. Fish and Wildlife Service, with mandated pumping reductions designed to limit existing Dace habitat-flow declines at the Springs to specified trigger levels, is ineffective because of the full development of 1:1 impacts from pumping upgradient from the Springs. Just as important, the impacts persist long after MOA-prescribed actions reduce pumping stresses.

The MOA stipulations related to trigger-level flows and actions to protect in-stream flows of Dace habitat reaches would fail to accomplish such objectives during execution of Order 1169 as currently planned with 8050 ac-ft/yr (11.12 cfs) pumping stress. In fact, MOA stipulations assure that, whatever level of pumping stresses may be adopted for the Order 1169 test, the 1:1 level of impacts from the full initial pumping stress would be acting for many months in the Springs area, perhaps for well over a year even if the final trigger level of 2.7 cfs at the Warm Springs West gage were to be reached or significantly exceeded (as could occur with 11.12 cfs of constant stress and would be even more likely if pumping varies seasonally to achieve an annualized 11.12 cfs). If it requires 9 months for full development of 1:1 impacts in the Springs area flows, it also will take 9 months for the stipulated actions of decreases or termination of the pumping stress in Coyote Spring Valley to fully register in the Springs area flows. Further adding to the problem are the 45 or 90 day periods stipulated before actions are taken, and the number of trigger-level actions required before the pumping stresses in Coyote Spring Valley begin to be reduced. Contrary to the intent of the MOA, the MOA stipulations would act to wipe out Dace habitats and local Dace populations if the initial pumping stress selected for the Order 1169 test proved to be too large. As there seems to be considerable uncertainty in flow requirements, a very cautious approach in applying the initial pumping stresses is warranted.

With these anticipated problems stemming from full-scale Order 1169 implementation, and given that 1:1 impacts are already evident in the existing monitoring records, alternative strategies warrant careful consideration and would be wise in light of these new findings. MAI urges the participants to approach the production requirement of Order 1169 in a step-wise fashion by delaying full-scale pumping until the analyses presented herein have been competently reviewed. Participants are unlikely to accept the MAI analyses without the opportunity for comprehensive review and rebuttal, and will require adequate time for such reviews. The ramifications of the MAI findings are far-reaching, and Order 1169 is effectively in process with lower-level but useful pumping stresses providing sufficient data for impact analyses. Higher-resolution pumping and streamflow data would allow MAI results to be refined, particularly with respect to features that are presently hidden within the very coarse monthly pumping tabulations near the most important monitoring localities, which produce records at 15-minute intervals. Adding on comprehensive documentation of real-time pumping activity and gauging individual low-flow Dace-habitat reaches would provide useful additional information to support a decision of whether the full production level planned in Coyote Spring Valley is necessary, wise, or desirable.

We are confident the results of MAI analyses are as reliable as the existing databases allow. One of the reasons for confidence is internally consistent results obtained from independent analytical steps in the scaling evaluation. Further, one does not need to be an expert in hydrograph analyses to recognize the marked change in pattern of the Muddy River flows and the marked lows in River flows that began during 2007, and continue to the end of data availability. We have recommended refinements in monitoring database collections that would allow more refined analyses. Also, some information used in our analyses (for example, reported daily production from the CSI1 well that at times exceeds the tested capacity of the well) is suspect.

Annual Muddy River flows have declined in lock-step with groundwater production in the MRSA since the early 1960s. Monitoring records now demonstrate the same level of system response to Coyote Spring Valley pumpage. It is not acceptable to ignore these Muddy River Springs-area responses if the remaining Moapa Dace habitats and populations are to be maintained. The issued but undeveloped permits in the Coyote Spring Valley groundwater basin essentially equal the remaining flows of the Muddy River and Muddy River Springs.

Figures 1 and 2, and Figure 16 of the following section tell the story perhaps as well as the analytical methodology and quantitative results. Figure 1 illustrates a period of flows in 1913 to 1918 in the Muddy River at the Moapa gage before flows began to respond to local groundwater development (note peak winter flows at 51-53 cfs). Figure 2 illustrates the current flow regime as well as the various diversions that have prevented water flows from exceeding 40 cfs in recent years. The key relationship that doesn't require an expert to recognize is the change in the pattern of Muddy River flows after 2006. The markedly reduced summer flows occurred during a period when the totals of non-CSI diversions are generally smaller than in previous years. The new pattern of low summer flows begins in the summer of 2007, after the first season of CSI pumping in 2006. Figure 16 of the following section illustrates how the River hydrograph responded to production by CSI, and is quantified in our analyses and derivations of full 1:1 impacts about 9 months (Warm Springs West gage) and 10 months (Muddy River at Moapa gage) after pumping occurs in southeastern Coyote Spring Valley.

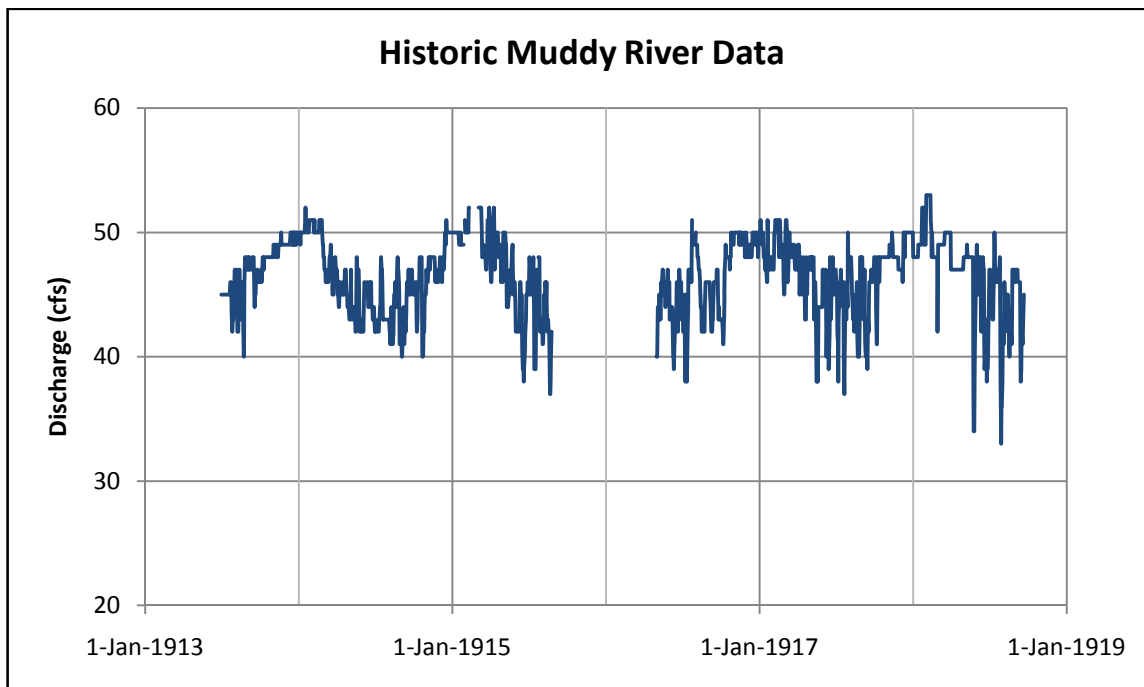


Figure 1. Recorded daily flows of the Muddy River between 1913 and 1918, prior to any known groundwater production from wells. Minor data gaps represent storm surges that have been removed from the record. Note the effects of irrigation diversions during the summer months. [file MuddyRivQ_1913-1918.xls, Sheet NarrowCensor]

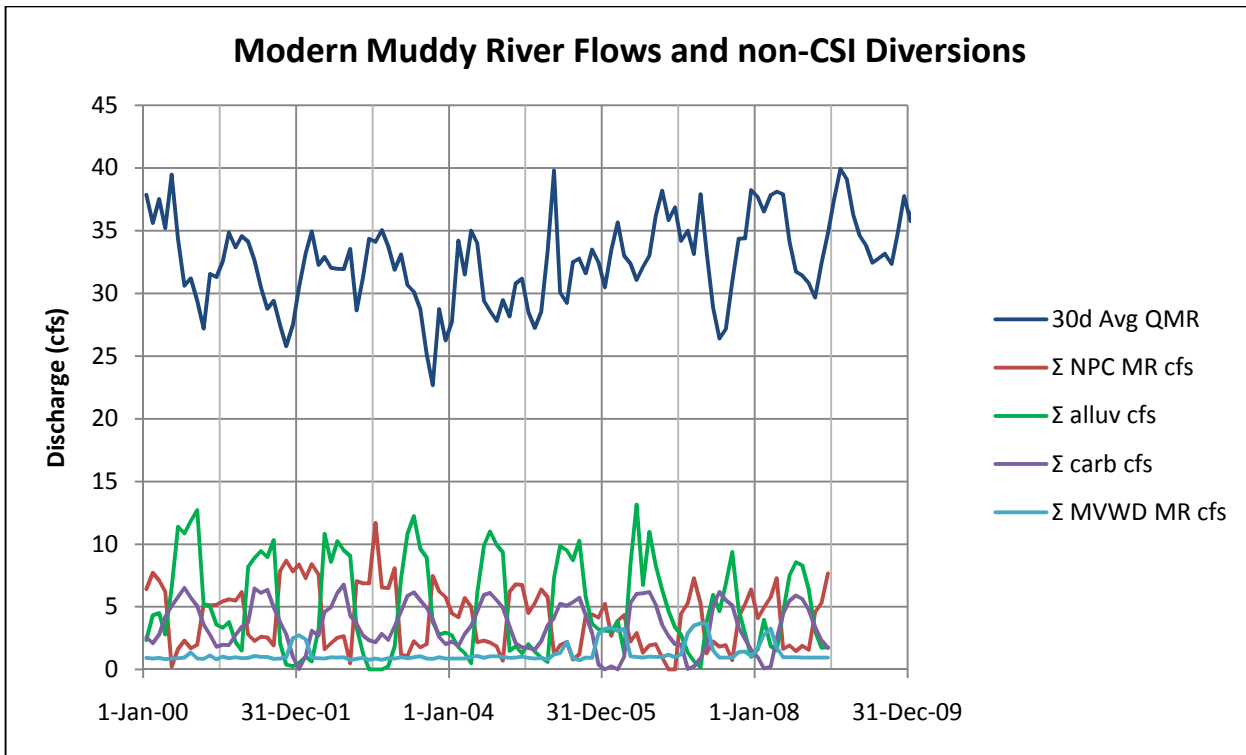


Figure 2. Average monthly flows in the Muddy River from 2000 through 2009, with municipal (MVWD) and industrial (NPC) diversions. Data associated with rain days and associated storm surges have been censored (removed) from the record. “alluv” indicates the alluvial aquifer, “carb” indicates the carbonate-rock aquifer, and “MR” indicates diversions directly from the River or its tributaries. [File MuddyRivQ_2000-2010b.xlsx, Sheet ‘MonthlyRaw’]

MAI offers the following analytical methodology and results to other Order 1169 participants in anticipation of their independent and in-depth analyses, followed by technical exchanges on results. MAI also suggests all involved directly with the Order 1169 pump test should make independent reviews of the implications of MAI analytical results with respect to how effectively the MOA would serve to limit impacts. Perhaps attention should also be focused on the 60% Dace population crash that apparently occurred sometime in 2007 (and continued similar population counts). The CSI pumping resulted in 1:1 impacts in 2007 after the first large CSI production year of 2006 and have continued in subsequent years.

Approach and Analyses by Dr. Cady Johnson

Mifflin & Associates, Inc. (MAI) has carefully analyzed ten years of monitoring records from MBP’s 5-well piezometer network, water levels from the USGS CE-DT-4 (MX-4) and Nevada Energy Company (NPC/NEC) EH-5b monitoring wells, springflow records from Big Muddy Spring and Warm Springs West, stream-gauging data for the Muddy River, production records from NEC and Moapa Valley Water District (MVWD) plus four years of drilling, development, and production records from Coyote Springs Investments (CSI) (Figures 3a, 3b).

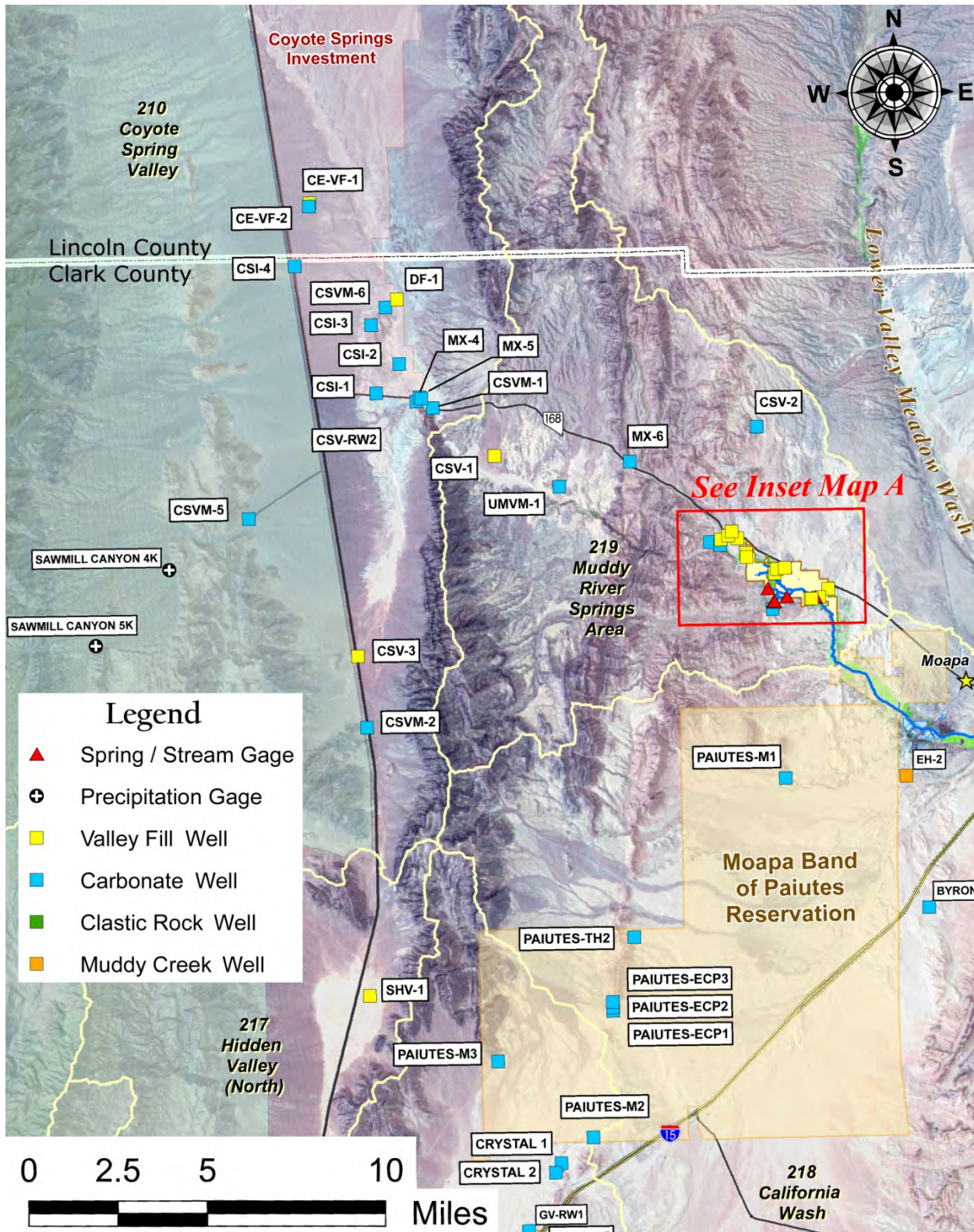


Figure 3a. Location of study area; map and “Inset Map A” (Figure 3b herein) have been modified and corrected from source file “CSI_Monitor_Points_Map.pdf”, which is stored in the SNWA Common Data Repository at www.snwawatershed.org/portal. [file MonitoringPtMapSmallGR83.jpg]

Inset Map A Muddy River Springs Area and Warm Springs Natural Area

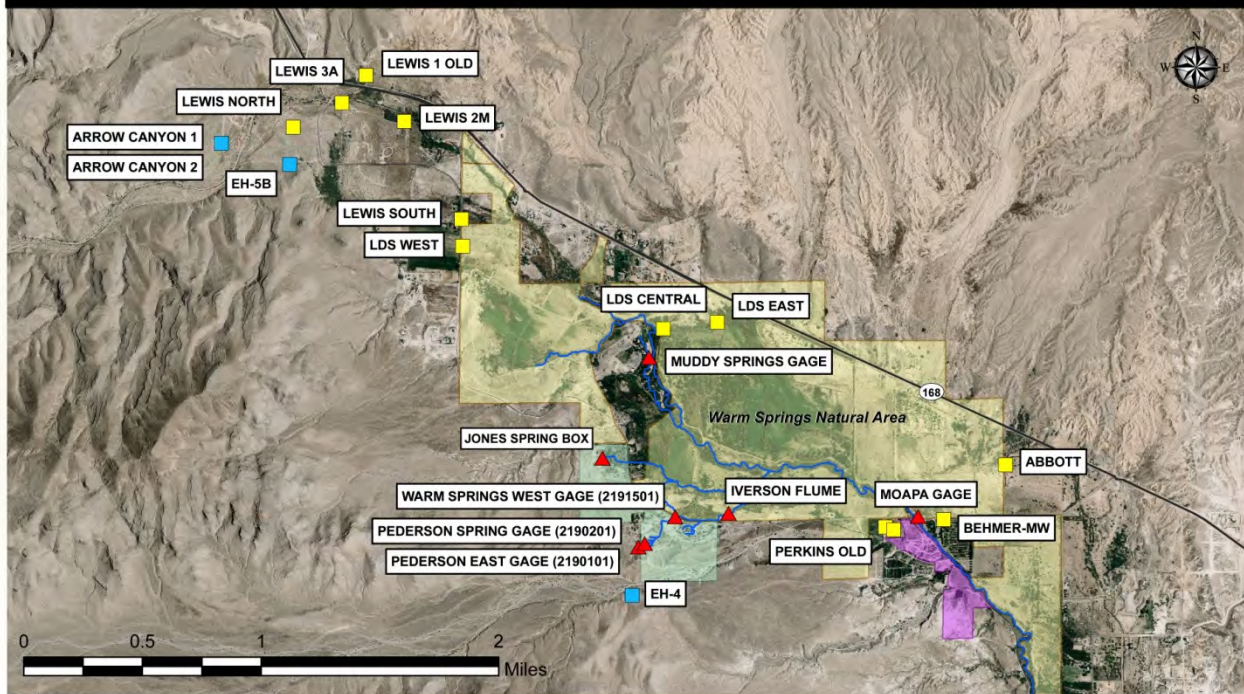


Figure 3b. Detail area from Figure 3a; Legend from Figure 3a applies. Unmodified from source, same as Figure 3a. [file MonitoringPtMapInsetAGR83.jpg]

From the inception of the MBP monitoring program in 2000 until late 2004, yearly-average water levels in the five MBP monitoring wells and several other monitoring wells in the region including MX-4 (monitored by the USGS) and EH-5b (monitored by NVE) were decreasing, with generally sinusoidal, seasonal variations about linear long-term decline trends (Mayer and Congdon, 2008). Seasonal water-level cycles that track those at MX-4, and follow the same pattern as long-term discharge rates at Warm Springs West, dominate the hydrographs. The origins of the sinusoidal component of the MBP hydrographs has long been an issue, but the absence of systematic phase differences or attenuation with distance from known pumping wells suggested that pumping effects were absent, and that climate was solely responsible for the seasonal water-level variations in the MBP wells (Johnson and Mifflin, 2006). The winter of 2004-2005 was unusually wet, and was followed by two years of rising water levels and increasing springflow in upper Moapa Valley. This climatic impulse produced distinctive responses in the hydrographs of the region, and the expectation that climatic responses are more uniform in space than pumping effects presents the opportunity to resolve these two primary influences on water levels using new approaches that we begin to explore here.

The fundamental premise in the following analyses is that springflow is deterministically responsive to regional water levels. There is no other underlying assumption. In a new analytical approach, described below, MAI has developed a *Synthetic Reference Hydrograph* (SRH) based on comparison of the ECP-1 and TH-2 hydrographs with that from MX-4. Subtraction of paired (hourly or daily) data points filters the climatic component from this composite record, producing a *difference* hydrograph (DH) so perturbations in either area can be recognized as a departure from the typical closely-correlated relationship.

The first potential perturbation to be considered was pumping at the MVWD Arrow Canyon #1 Well (ACW) which is usually pumped at about 5 cfs during the peak (summer) season. It was observed that maxima and minima of the ECP-1/MX-4 difference hydrograph bear a close correspondence to the pattern of pumping at ACW until about 2006, and was so similar in 2001-2004 (before CSI activities began) that fortuitous similarity is unlikely (Figure 4). Furthermore, comparison of the best-defined peaks in ACW production and DH response reveals a 4-week lag between cause and effect (caveat: production data are currently reported *monthly*, and although we interpolated to weekly values for this analysis and a 4-week lag is indicated, we do not imply week-scale precision of the lag estimate). Notably, there is a *positive* correlation between the signals illustrated in Figure 4; as pumping increases at the ACW, the difference between MX-4 and ECP-1 water levels also increases. Since pumping would be unlikely to cause the water level in another well to rise systematically, it appears that ECP-1 (which has the lower water level elevation) is experiencing a seasonal drawdown effect from ACW.

Possible influences of NPC/NEC pumping seasonally from the alluvial aquifer of upper Moapa Valley on the DH hydrograph were investigated next. The years 2001-2002 are of particular interest, since the ACW was shut down for most of January, 2002, an atypical event at that time. During the summers of 2001 and 2002 Nevada Power Company (NPC) operated its Lewis and LDS well fields analogously to a square-wave impulse to the hydrologic system that was twice as strong and more sustained than the pattern of pumping by MVWD (Figure 5). The fact that the sawtooth pattern of the DH that was maintained in 2001-2002 demonstrates little or no effect of alluvial pumping on ECP-1, consistent with Johnson and Miffilin (2006). Incorporating the good correspondence that exists between ACW production, lagged four weeks, and the DH, the linear relationship (Figure 6) that explains variations in head difference between MX-4 and ECP-1 as responses to ACW pumping was used to adjust the ECP-1 hydrograph for the ACW effect. This is the Synthetic Reference Hydrograph (Figure 7) a tool that is particularly useful for understanding excursions of springflow from “normal” trends.

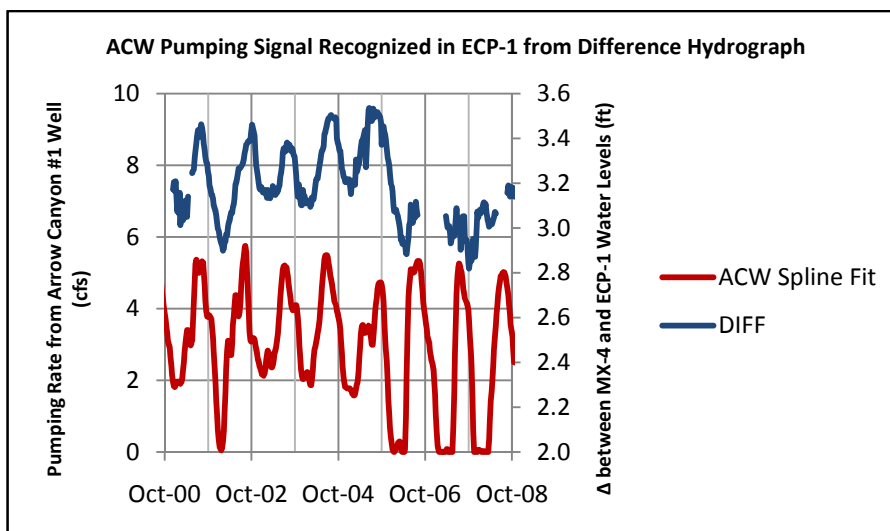


Figure 4. Difference hydrograph, obtained by subtracting weekly average water levels in ECP-1 from those in MX-4, compared with pumping rate of Arrow Canyon #1 well. The monthly well production totals were interpolated to weekly values with a cubic spline approximation. The relationship indicates that as well production increases the difference between the reference hydrographs increases, meaning that water levels in ECP-1 are being lowered relative to MX-4. [file ACW_QmonthsToWeeks.xls, Sheet ‘AllWeeks’]

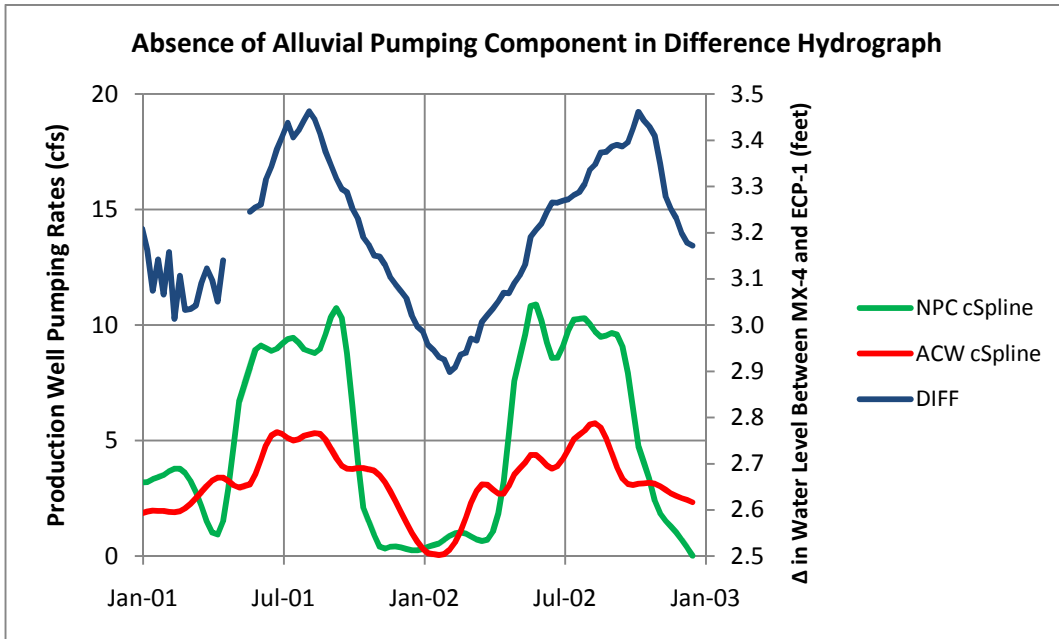


Figure 5. The sawtooth pattern of the difference hydrograph in 2001-2002 closely mimics the pattern of seasonal pumping from the Arrow Canyon #1 well, and is almost completely unaffected by the square-wave alluvial pumping signal that is roughly twice as strong and seasonally more sustained. The data gap in the difference hydrograph is where MX-4 data are missing. Monthly production data were interpolated to weekly values by a cubic spline approximation. [file Production.xls, Sheet 'Diffs00-02']

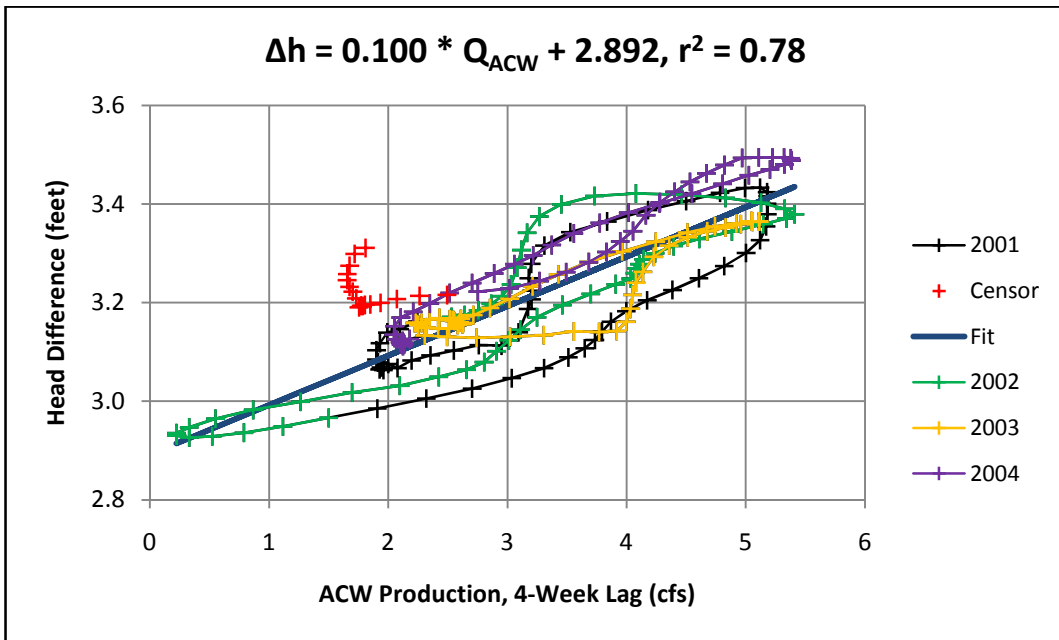


Figure 6. Correlation relations between Arrow Canyon #1 production and head difference between MX-4 and ECP-1 for 2001 through 2004. "Censor" indicates data from late 2004 not considered in the regression; heavy precipitation in that time frame may have caused a water-level rise in MX-4.

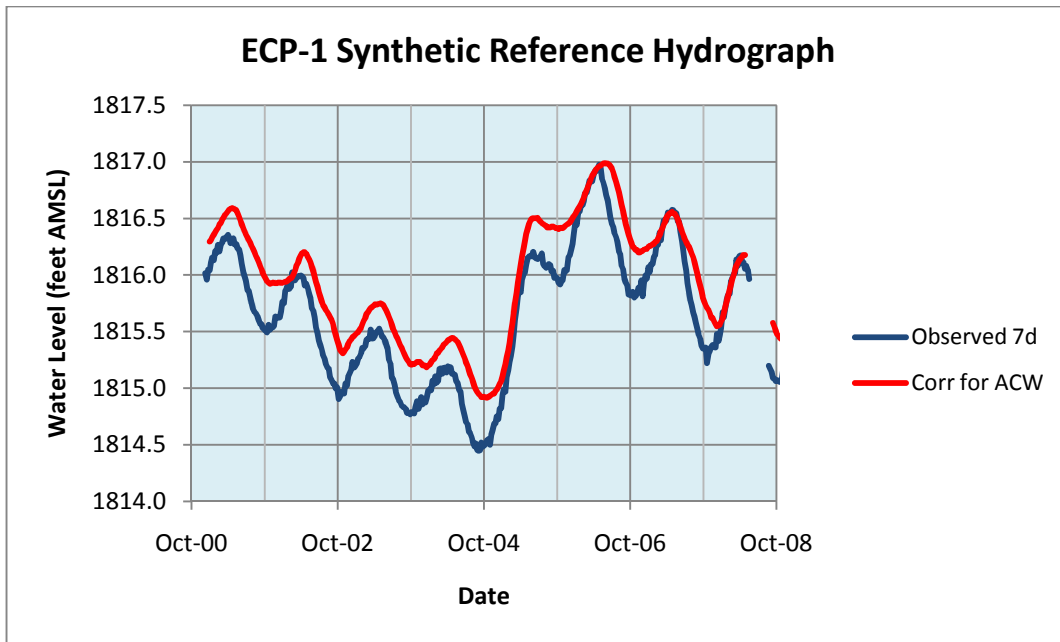


Figure 7. Synthetic reference hydrograph developed from differences in 7-day average ECP-1 water levels relative to the MX-4 monitoring well, with adjustment for pumping stress attributable to the Arrow Canyon #1 well. [file Production.xls, Sheet 'SyntheticHydrograph']

Transformations of the SRH are useful as indicators of baseline flow conditions in individual springs and the Muddy River, after censoring (adjusting) discharge records to eliminate data from rain days (River) and operational disturbances (springs). In the case of the Muddy River, effects of winter precipitation are particularly difficult to remove from the discharge record without introducing large data gaps, resulting in annual maxima that are less uniform in the reconstituted record than annual minima.

Warm Springs West Trend

To utilize the SRH as a reference discharge indicator for springflow, it is necessary to detrend and scale the long-term hydrograph (which has a length dimension) to be proportional to the discharge measurements (volumetric flow rate) by a linear transformation (Figure 8). The process is exploratory, requiring a choice of the time interval that contains the antecedent trends in the hydrographs being compared, then additional choices of how to align the detrended hydrographs in scale (such as fitting maxima or minima) and time (by shifting time scales to account for lags between stimulus and response). These linear transformations are non-unique, but ultimately preserve the form of the original data and provide a basis for quantitative comparison of discharge records and water levels. Appropriately-scaled head data can be considered to be cfs-equivalents in this approach. When fitted to springflow maxima, the scaled SRH should tightly drape the springflow record, matching at times when spring discharge is unaffected by pumping activity. The drape-fit of the SRH on the springflow record (Figure 9) demonstrates a discharge deficit at Warm Springs West after 2006, the year CSI began producing from their CSI1 well. Discharge plotted in Figure 9 is partially reconstituted to account for the influence of the ACW, derived by minimizing the amplitude of the 2001-2004 hydrograph (Figure 10). A scale factor of 0.015, derived interactively by trial-and-error, indicates that for each 1 cfs pumped from the ACW, 0.015 cfs (1.5%) is accounted for by capture from Warm Springs West.

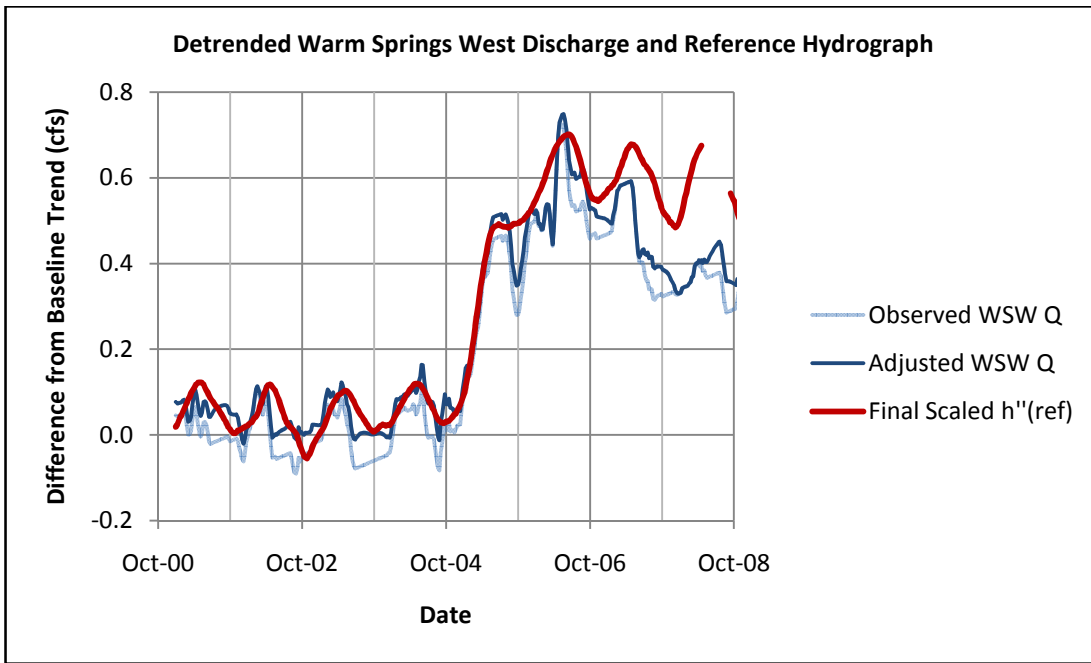


Figure 8. Detrended hydrographs, expressed as differences from their baseline (2001-2004) trends, with synthetic reference hydrograph (SRH) scaled to drape springflow. The adjustment to Warm Springs West discharge removes the effect of the Arrow Canyon #1 well. [File CSI&ACWimpacts3.xls, Sheet Scaling3]

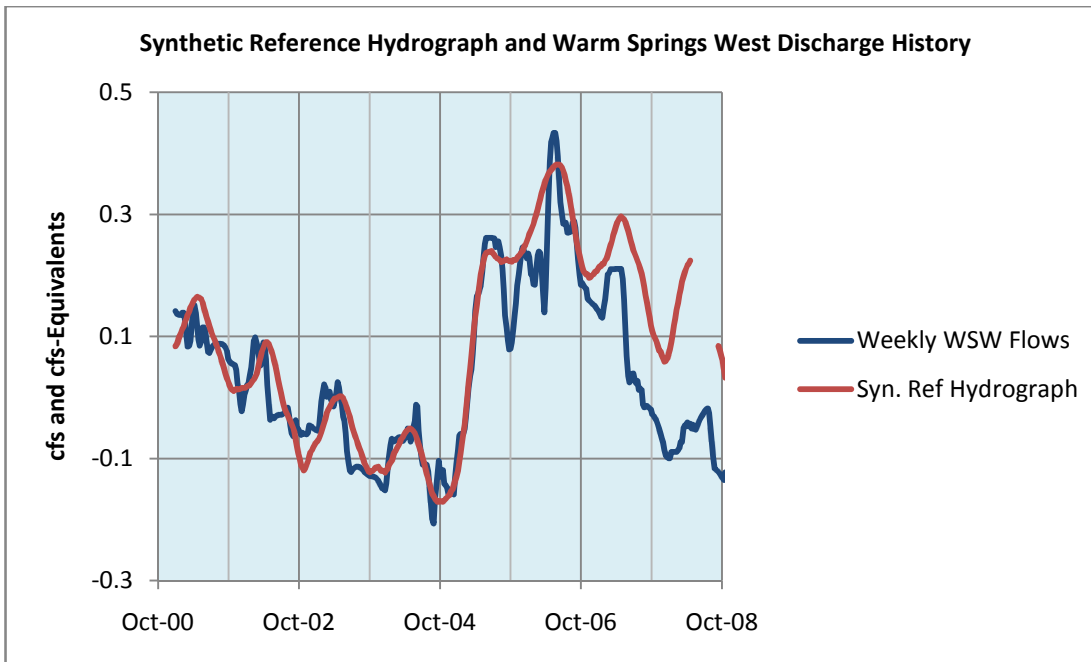


Figure 9. Re-trended hydrographs, showing progressive divergence of Warm Springs West discharge from Synthetic Reference Hydrograph beginning in late 2006, the year that continuous production by Coyote Springs Investments began. [file CSI&ACWimpacts2.xls, Sheet 'Scaling3']

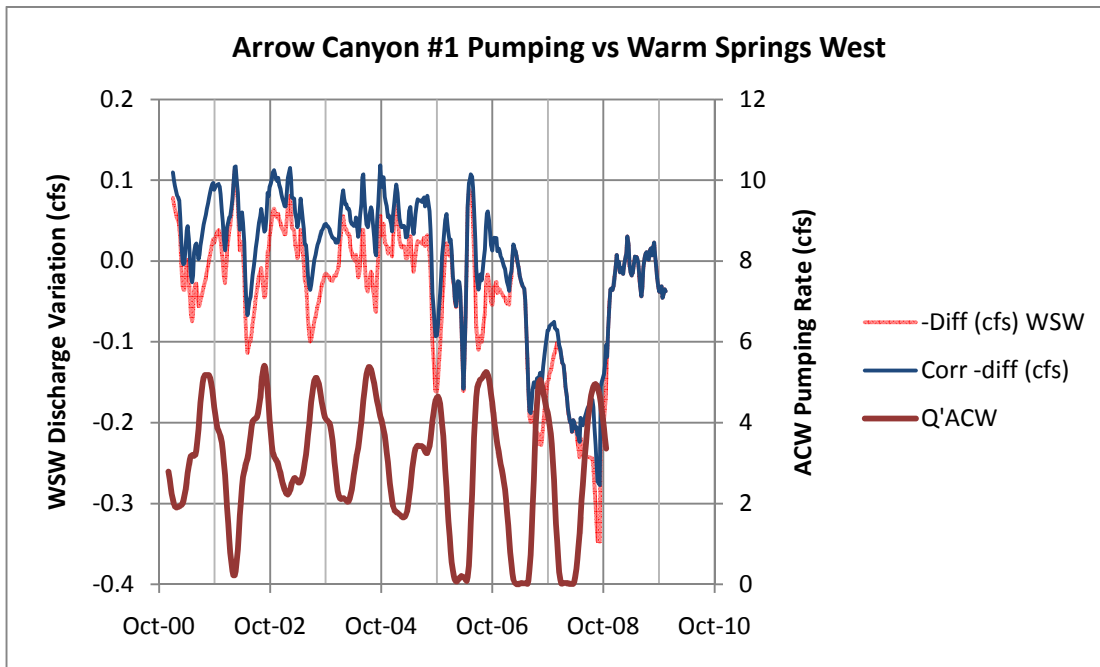


Figure 10. Scale factor of 0.015 minimizes the effects of the Arrow Canyon #1 well on Warm Springs West discharge; for each 1 cfs pumped from the well, 0.015 cfs is accounted for by capture from the Springs. [file CSI&ACWimpacts2.xls, Sheet 'ACWfineTuning']

CSI Impacts at Warm Springs West

Three production wells operated by Coyote Springs Investments were considered as having the potential to capture flow from Warm Springs West. Weekly production data were compiled from records submitted to the Nevada State Engineer (NSE); additional information pertaining to well-development activities is available in reports by Johnson (2005a,b; 2007). Weekly averages were prepared from the production records, since generally the totalizing meters were not read on a daily basis.

Well CSI1 was completed in May of 2005, with development and production testing occurring in the latter half of that same month. CSI1 entered service in January of 2006, primarily for grading and dust control, according to information on file with the NSE. CSI2 was completed in August of 2005; development pumping began on August 29 and production testing ended on October 1. CSI2 entered service in July of 2006. CSI3 was completed in August of 2006, with development and production testing taking place between August 10 and September 14. CSI3 entered service in June of 2007. Johnson (2007, p. A-13) reports development activity at a Well #4, but production from this facility was minor and intermittent through 2008.

The CSI pumping signal is well-expressed in the Warm Springs West discharge record, and lags the actual pumping by 9 months (Figure 11). The proportional reduction of Spring discharge is 5.8%, meaning Springs discharge is reduced by 5.8% of pumpage with a 9 month delay (Figure 12). "Raw CSIT" on the Figure 11 chart represents the time the pumping occurred; "Lag CSIT" presents the pumping data 9 months later to illustrate correspondence of the lagged signal with changes in springflow.

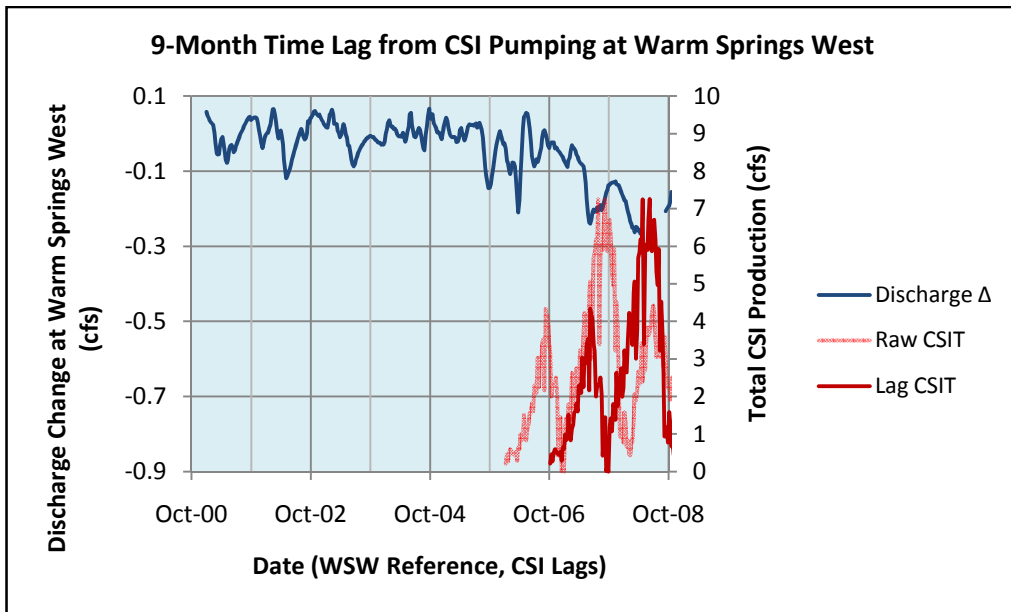


Figure 11. Pumping effects at Warm Springs West attributable to CSI activity, accounting for the 9-month lag that provides the best correspondence between peaks. [file CSI&ACWimpacts3.xls, Sheet 'CSImpacts']

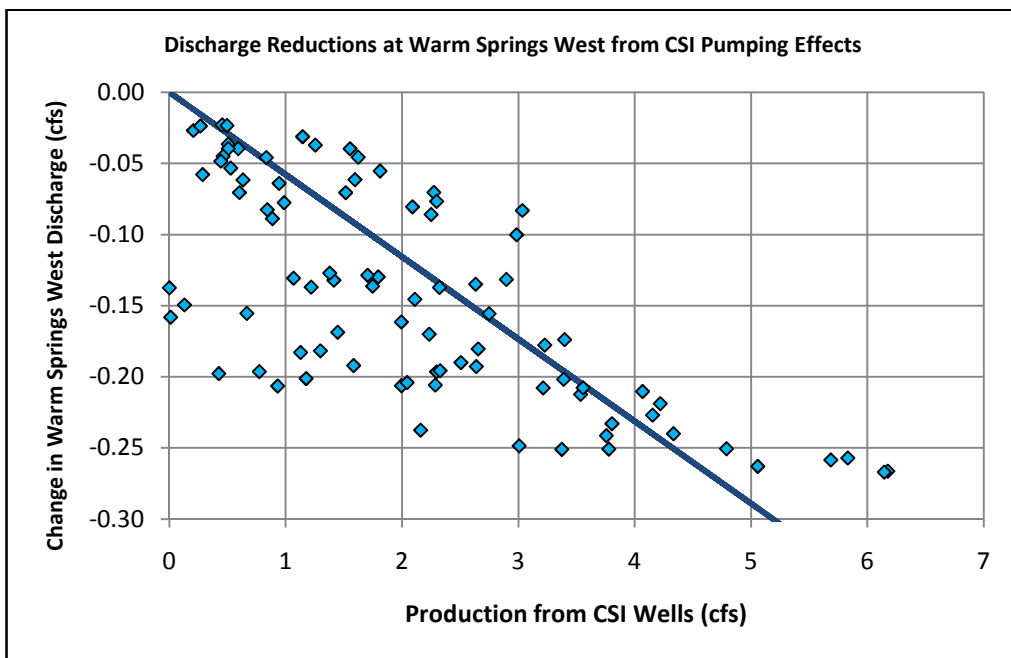


Figure 12. Proportional reduction of discharge at Warm Springs West with respect to groundwater production in Coyote Spring Valley, lagged 9 months; the constant of proportionality is 0.058 cfs reduction per cfs pumped. [file CSI&ACWimpacts3.xls, Sheet 'CSImpacts']

Scaling of Results to the Muddy River Headwaters Area

Discharge of the Muddy River at the Moapa gage is roughly twice as great as the sum of tributary flows derived directly from springs (Eakin, 1968; Beck et al., 2006). The alluvial aquifer, recharged by distributed flux from the carbonate-rock aquifer, stores groundwater and contributes to the base flow of the River in the headwaters area. Storage effects delay the impacts of alluvial pumping on measured River discharge. Adding present-day diversions to the modern, reduced flows of the Muddy River (Figure 2) reproduces the annual cycle seen in 1913-1918 (Figure 1) if appropriate time lags are applied to represent the effects of groundwater storage (Johnson and Mifflin, 2006). In reconstituting the Muddy River to match historic flows, surface-water diversions were applied in the month they are reported, diversions from the carbonate-rock aquifer (MX-6 and Arrow Canyon wells) were lagged one month, and diversions from the alluvial aquifer (Lewis and LDS well fields) were lagged five months. Johnson and Mifflin (2006) analyzed records from 1997-2002, and in the present analysis from 2001-2008 with comparable results. The finding of both analyses is the same, that the net effect of all diversions is a 1:1 reduction of Muddy River discharge, and each category of diversion has a unique imprint upon the discharge record based on the delayed responses of the River.

Mayer and Congdon (2008) hypothesized that higher-elevation springs would prove to be most sensitive to pumping effects based on the assumption that Darcy's law applies in the discharge conduits. Big Muddy Spring is the largest (8 cfs prior to 2005) and lowest elevation spring in the MRSA, with a measuring station elevation of 1745.34 feet AMSL about 0.1 mile downstream from the spring pool (Beck et al., 2006). Detrended discharge from 2001-2002 correlates well with production from the Arrow Canyon #1 well (Figure 13; slope = -0.08669 cfs/cfs or 8.7%, intercept = 8.606 cfs), allowing the discharge record from Big Muddy Spring to be adjusted for the ACW impact effects in subsequent years (Figure 14). We note that the proportional impacts from Arrow Canyon Well pumpage are substantially greater (8.7% of pumpage) at Big Muddy Spring than at Warm Springs West, where ACW impacts are only 1.5% of pumpage, and for which Beck et al. (2006) report a station elevation of 1770.04 feet AMSL.

NOTE: There is inconsistency in usage of the name "Warm Springs West". Beck et al. (2006, Table 4) refer to USGS site 09415920, and their reported elevation of 1770.04 feet corresponds to a staff plate reading of 0.91 feet in the 1-ft Parshall flume at that measurement location, which monitors total flow discharging from all springs associated with the Pederson Springs Groups. Mayer and Congdon (2008, Table 1 and Fig. 10), however, appear to consider Warm Springs West to be "Lower Elevation Springs" (an average of 5 elevations, 1797.9 feet) and Pederson and Pederson East "Higher Elevation Springs". Spring elevations are immaterial to the present analysis, so we leave it to Mayer and Congdon to clarify the confusion.

The average production of the ACW from September 2000 to October 2008 was 2.9 cfs, 5.7% of the estimated 51 cfs total groundwater flux to the MRSA, the 1:1 impact on the overall system in accordance with the water balance of Johnson and Mifflin (2006). Recognition of non-uniform pumping effects from the ACW in the MRSA raises the question of how CSI impacts are distributed. Identification of the spatially variable impacts of the ACW on individual springs and River flows is important because superposed CSI pumping impacts are now incorporated into the gauging records, and the opportunity to consider individual well impact effects in isolation (with other pumping sources "quiet") is no longer available.

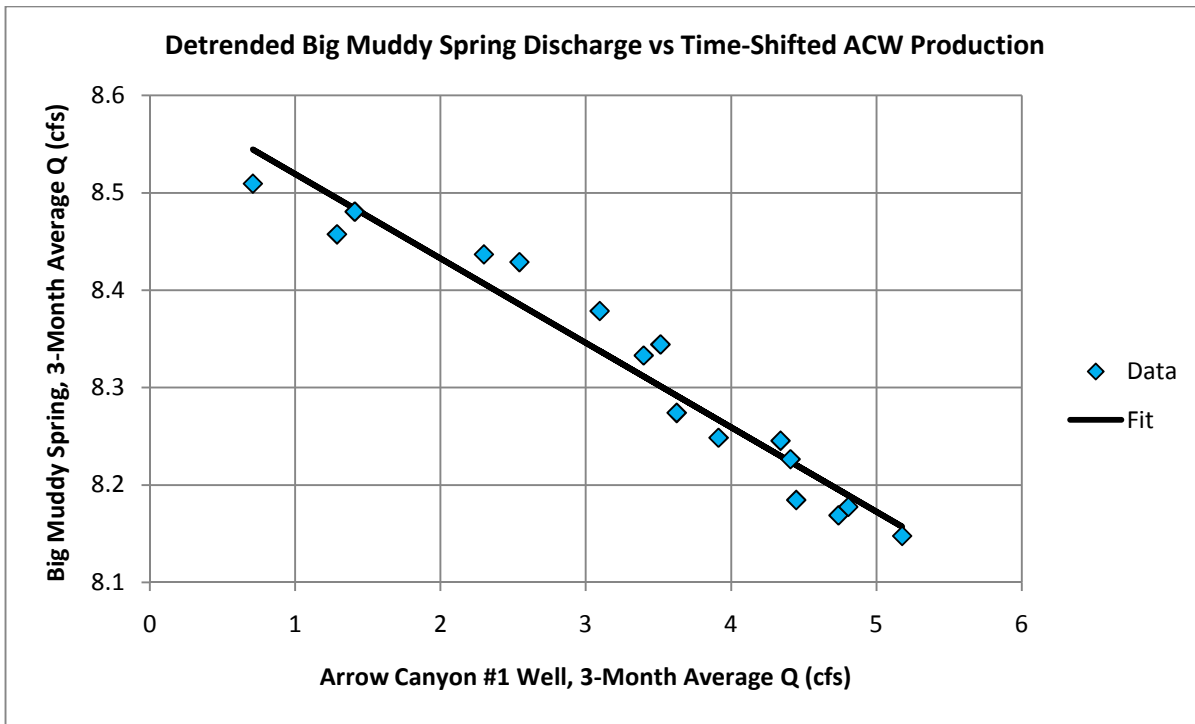


Figure 13. Proportional decreases in discharge from Big Muddy Spring, May 2001 – August 2002. [File FinalSpringflowComponents.xls, Sheet 'Re-startWithACW']

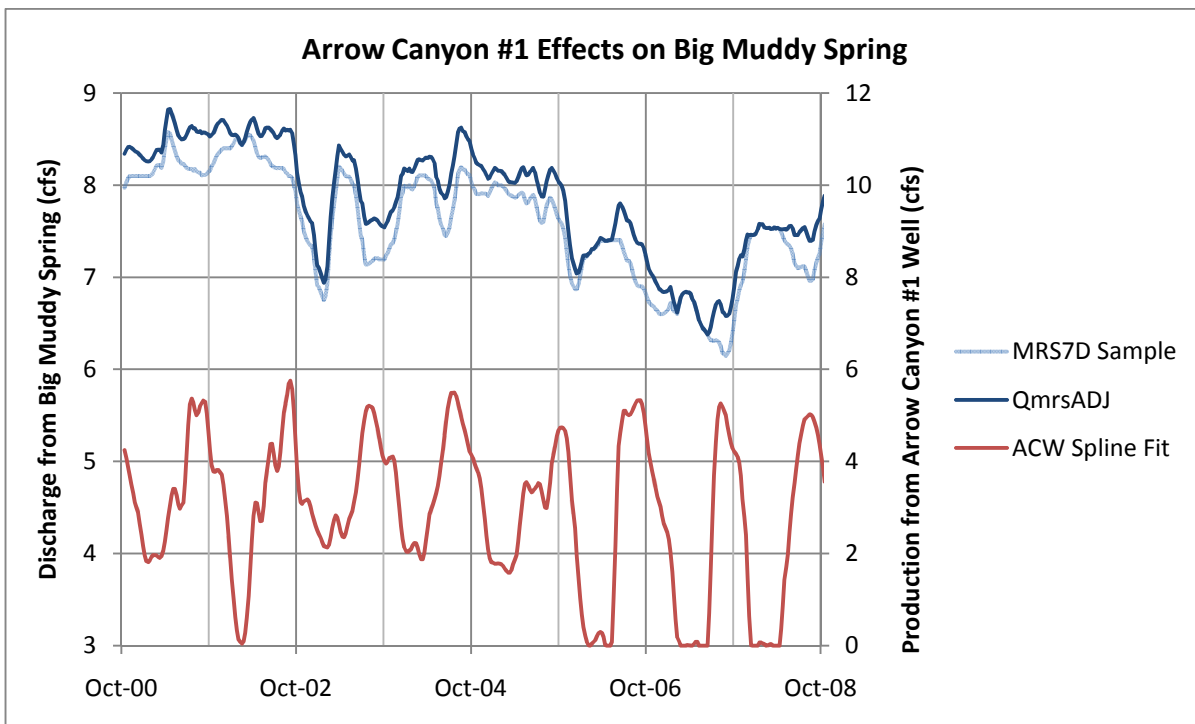


Figure 14. Adjustment of the 7-day average Big Muddy Spring discharge record to remove effects of the Arrow Canyon #1 well. [File BigMuddyLongTerm.xls, Sheet 'WeeklyACW']

As a result of seepage gains from the alluvial aquifer, the Muddy River as a whole might be considered to be dominated by “lower-elevation” discharge, in the parlance of Mayer and Congdon (2008). At an average discharge rate of about 3.7 cfs, Warm Springs West represents only about 7.3% of the long-term average total flux to the Muddy River headwaters in upper Moapa Valley. If the CSI impact results from Warm Springs West (5.8% of CSI pumpage; Figure 12) prove representative of CSI pumping impacts distributed throughout the MRSA, groundwater diverted in Coyote Spring Valley would be manifested as a reduction of the 51 cfs in the proportion of 51 cfs / 3.7 cfs, or about 14 times the impact at Warm Springs West. To date, diversions from Coyote Spring Valley have occurred as three distinct seasonal pulses peaking at approximately 3.7, 6.0, and 3.9 cfs in 2006, 2007, and 2008, respectively (Figure 11). Total CSI diversions are of sufficient magnitude that if pumping effects calculated for Warm Springs West are representative of the MRSA as a whole, it should be possible to measure the total impacts of CSI diversions that have already occurred in the post-2006 record of Muddy River discharge. In other words, if local estimates of pumping impacts derived from springflow data are proportionally representative, these 1:1 impacts would be apparent in Muddy River flows.

To develop a CSI pumping-impact estimate for the MRSA as a whole, the synthetic reference hydrograph (Figure 7) and censored Muddy River hydrograph were detrended based on the 2000-2004 record, and the SRH was scaled to match the minima of the River hydrograph. When comparing River flows with the history of groundwater production from Coyote Spring Valley, there would be a correspondence of River and SRH peaks if the pumping impacts from 2006 lag the actual pumping by 10 months (Figure 15). Moreover, since scaling the SRH to the River hydrograph produces a measure of differences in cfs-equivalents; deficits in River flow have the units of cfs and can be compared directly with the pumping stress suspected of creating the discharge deficits. In the case of the 2006 CSI pumping stresses, the July and August 2007 River discharge deficits have 1:1 correspondence with the CSI pumping stress 10 months earlier. The calculated Warm Springs West impact estimate scales up to the Muddy River as a whole, and the 1:1 impacts of local diversions (Johnson and Mifflin, 2006) also apply to groundwater extracted from southeastern Coyote Spring Valley in 2006.

The raw hydrograph of the Muddy River illustrates changed flow patterns in 2007-2009 that do not require detailed or sophisticated analyses to appreciate (Figure 16). The large production peak from 2007 is primarily due to pumping from the CSI2 well, and appears to be expressed in the River hydrograph with a lag time greater than one year.

Conclusion

Flows at Warm Springs West would be reduced by 0.64 cfs as a direct result of an 11 cfs Order 1169 experiment, 17% of the historic 10-year average of 3.7 cfs or 19% of the minimum flows of 2004. These estimates are subject to considerable uncertainty due to the scatter of data in the regression relation (Figure 12), and the CSI impact would be superposed on seasonal discharge reductions that are attributable to the Arrow Canyon wells, and climate effects. The CSI pumping impacts detected at Warm Springs West are proportional to impacts derived by reconstituting Muddy River flows; if full-scale groundwater production in Coyote Spring Valley of 22 cfs were to occur as a uniform pumping stress, elimination of that full amount from the regional flux to the MRSA would be the result. This discharge reduction would translate directly to flow reductions that approach the minimum flows recorded in 2003, and are well over half the average seasonal minima of the past 10 years. If, however, seasonal pumping typical of the region were to occur, periodic impacts transmitted to the Springs area would be far greater.

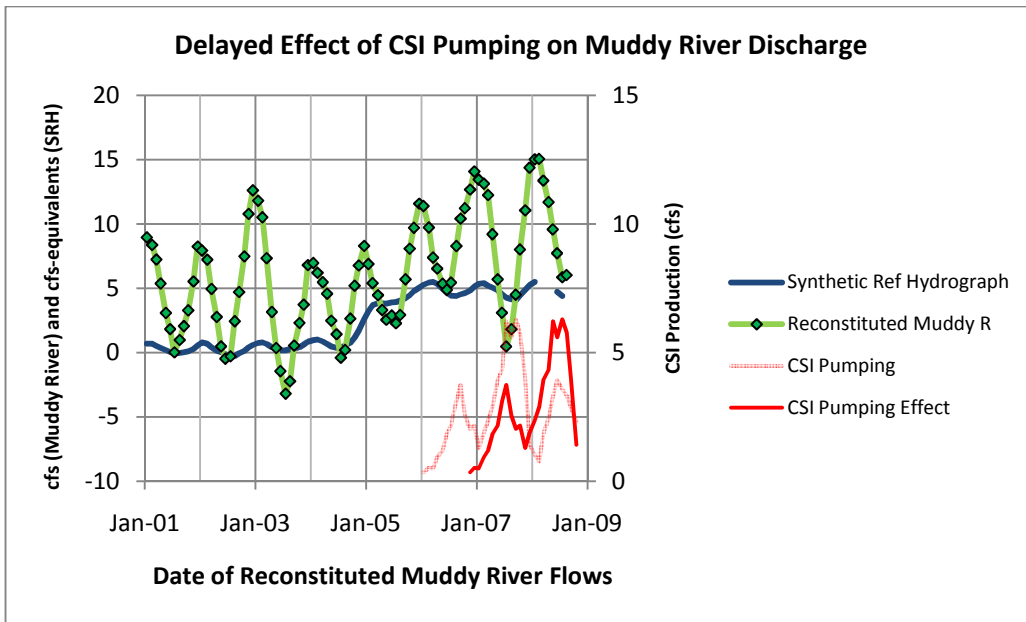


Figure 15. Divergence of reconstituted Muddy River discharge from baseline trend between April and September of 2007, corresponding (in terms of cfs-equivalents), to the production rate from CSI wells that first peaked in September of 2006, indicating a ten-month lag between cause and effect in the first phase of pumping. Zero reference is average of peak minima from 2002-2005. [file MuddyRivQ_2000-2010a.xls, Sheet 'CSImonthly']

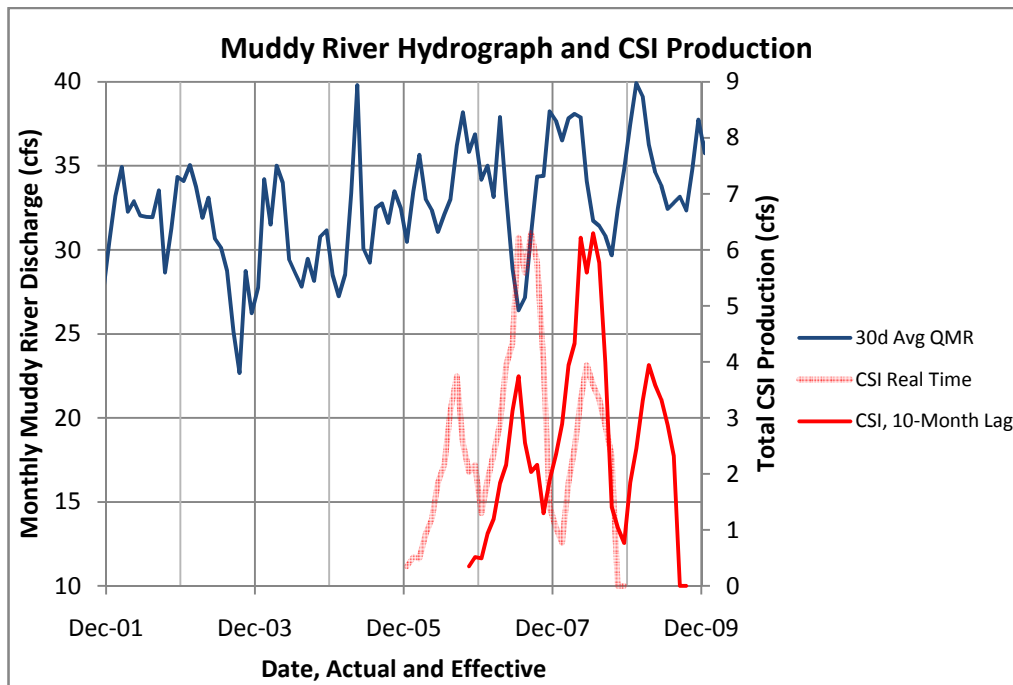


Figure 16. Raw Muddy River hydrograph, monthly samples of 30-day moving average, censored for rain days, and CSI production history. [file MuddyRivQ_2000-2010a.xls, Sheet 'Narrow']

References

- Beck, D.A., R. Ryan, R.J. Veley, D.P. Harper, and D.J. Tanko, 2006, Water-surface elevations, discharge, and water-quality data for selected sites in the Warm Springs area near Moapa, Nevada: U.S. Geological Survey Open-File Report 2006-1311, 240 p.
- Eakin, T.E. 1966. A regional interbasin groundwater system in the White River area, southeastern Nevada. *Water Resources Research* 2, no. 2: 251-271.
- Ertec Western, Inc., 1981, MX siting investigation, water resources program, results of regional carbonate aquifer testing, Coyote Spring Valley, Nevada: unpublished report dated December 18, 1981.
- Johnson, Cady, and Mifflin, Martin, 2006, The AEM and regional carbonate aquifer modeling: *Ground Water* 44(1), 24-34.
- Johnson, Michael E., 2005a, Drilling and Development of CSI Well No. 1 for Coyote Springs Investments LLC, Coyote Spring Valley, Clark County, Nevada: unpublished report dated August, 2005. 55p.
- Johnson, Michael E., 2005b, Drilling and Development of CSI Well No. 2 for Coyote Springs Investments LLC, Coyote Spring Valley, Clark County, Nevada: unpublished report dated November, 2005. 93p.
- Johnson, Michael E., 2007, Drilling and Development of CSI Well No. 3 for Coyote Springs Investments LLC, Coyote Spring Valley, Clark County, Nevada: unpublished report dated January, 2007. 55p.
- Las Vegas Valley Water District, 2001, Water resources and ground-water modeling in the White River and Meadow Valley flow systems – Clark, Lincoln, Nye and White Pine Counties, Nevada: unpublished “Exhibit 54” in Nevada State Engineer’s hearing on Coyote Spring Valley applications.
- Mayer, T.D. and Congdon, R.D., 2008, Evaluating Climate Variability and Pumping Effects in Statistical Analyses: *Ground Water*, Vol. 46, No. 2, pp. 212-227.
- Mifflin, M.D. 1968. Delineation of groundwater flow systems in Nevada. Water Resources Center, Desert Research Institute, University of Nevada System. Publication no. 42004: 111 p.
- USFWS, Intra-Service Programmatic Biological Opinion for the Proposed Muddy River Memorandum of Agreement Regarding Groundwater Withdrawal of 16,100 Acre-Feet per Year from the Regional Carbonate Aquifer in Coyote Springs Valley and California Wash Basins, and Establishing Conservation Measures for the Moapa Dace, Clark County, Nevada, January 30, 2006 (File No. 1-5-05-FW-536).
- USFWS, Request for Formal and Informal Consultation on the Kane Springs Valley Groundwater Development Project in Lincoln County, Nevada (Biological Opinion), October 29, 2008 (File Nos. 84320-2008-F-007 and 84320-2008-I-0216).

Addendum to “Order 1169 Impacts” Consultation Draft of May 27, 2010

Mifflin & Associates, Inc.
September 8, 2010

Background

Recently, a question was raised concerning the possibility that pumping in the Apex area (Figure 1), which is strongly seasonal, has influenced the Paiutes ECP-1 hydrograph. Mifflin & Associates (MAI) has presented analyses that rely on a Synthetic Reference Hydrograph (SRH) based on ECP-1 to predict springflow reductions that will occur in Upper Moapa Valley as a consequence of increased pumping from the carbonate-rock aquifer several miles northwest of the headwaters of the Muddy River.

Paiutes ECP-1 is remote from present pumping centers north and south, but has been interpreted by us to have been affected more by pumping of the Arrow Canyon #1 well than was MX-4, which is closer to the northerly pumping centers, over the past decade. This somewhat counter-intuitive interpretation is consistent with the locations of ECP-1 and the Arrow Canyon #1 well within a north-trending transmissive zone, roughly coincident with the trace of the Dry Lake Thrust, that has been exploited for water-resource development in the region. Before considering several recently-prepared difference hydrographs and pumping histories in the southern area, we emphasize Figure 2 (same data as Figure 4 of our May 27 report) for the visual clues that reveal the relationship we propose. The goal is to establish the effects of Arrow Canyon #1 (and #2) pumping on the ECP-1 hydrograph, so that CSI activities can be resolved in springflow records as pumping effects continue to develop.

The observation that correlations of the phase-shifted signals are preserved between zero and maximum pumpage (Figure 3; same as Figure 6 from May 27) is not, in our opinion, fortuitous. Seasonal pumping of constant amplitude, anywhere, would correlate with a constant-amplitude, annually-periodic hydrograph if shifted in time as needed to make the match. When seasonal pumping stress from year to year varies and water-level signal strength also varies systematically from year to year, cause and effect are demonstrated when a correlation exists. Then magnitude and timing of impacts can be determined.

Analysis

Well hydrographs throughout the Moapa – Apex region are characterized by seasonal water-level cycles, with the most prominent features of the 2000-2010 decade multi-year net declines (2000 – late 2004 and late 2006 – 2010) and a recovery event beginning in late 2004 (the start of an unusually wet winter) and continuing at least into 2006. When comparing hydrographs, it is useful to perform a point-by-point subtraction to filter regional components including seasonality, climatic events, barometric effects, and earth-tide contributions to the records. The difference hydrograph therefore reveals local effects on water levels through time. The magnitude of such effects at various distances from suspected pumping-related forcing can be explored by comparing difference hydrographs across a region.

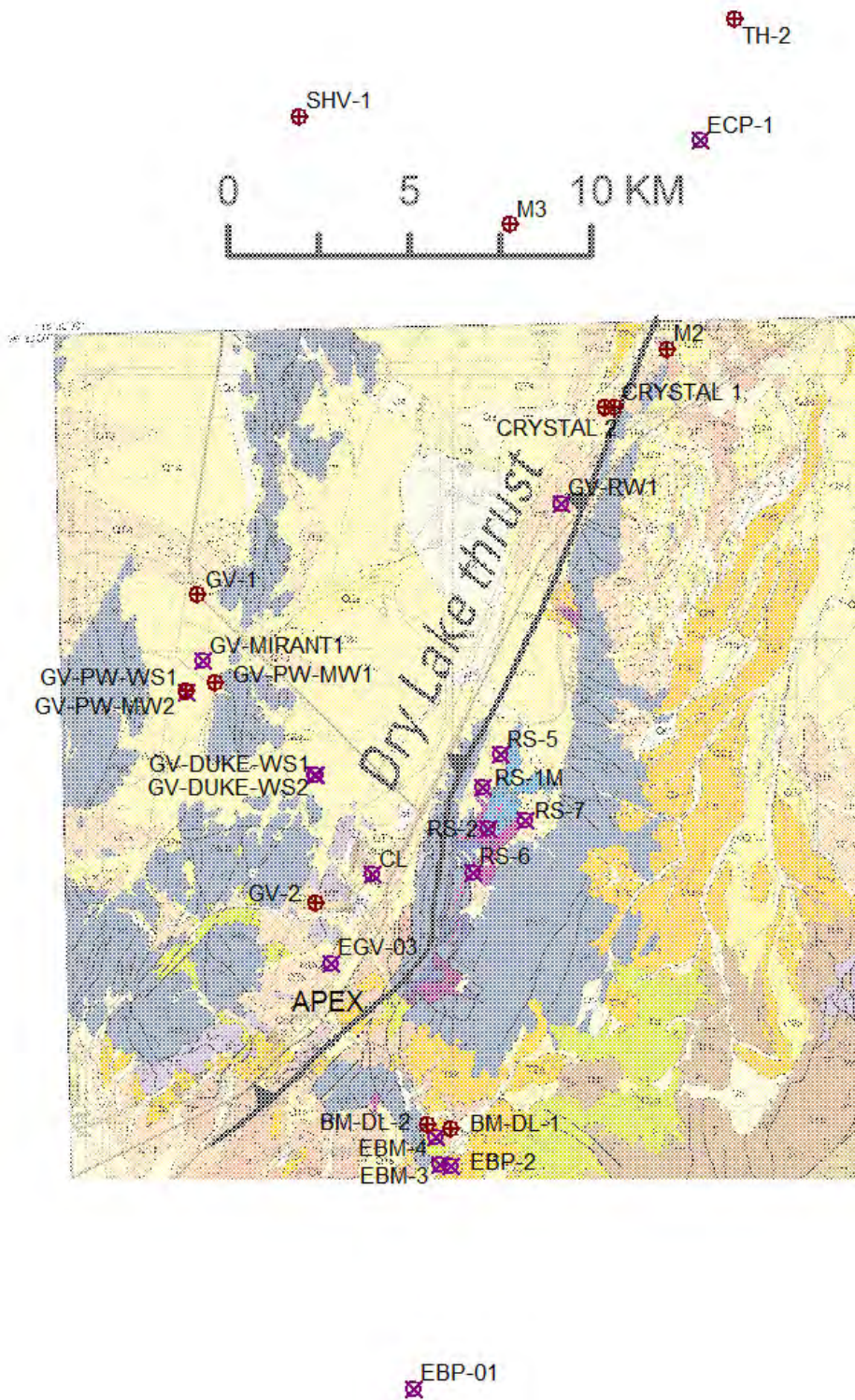


Figure 1. Well locations and general geology (Beard, et al., 2007) of evaluation area. Paiutes monitoring wells TH-2, ECP-1, and M2 are completed in the footwall of the Dry Lake Thrust, as inferred from strongly folded Permian rocks in sparse outcrops. Upper plate rocks are absent and presumably eroded north of Dry Lake Valley.

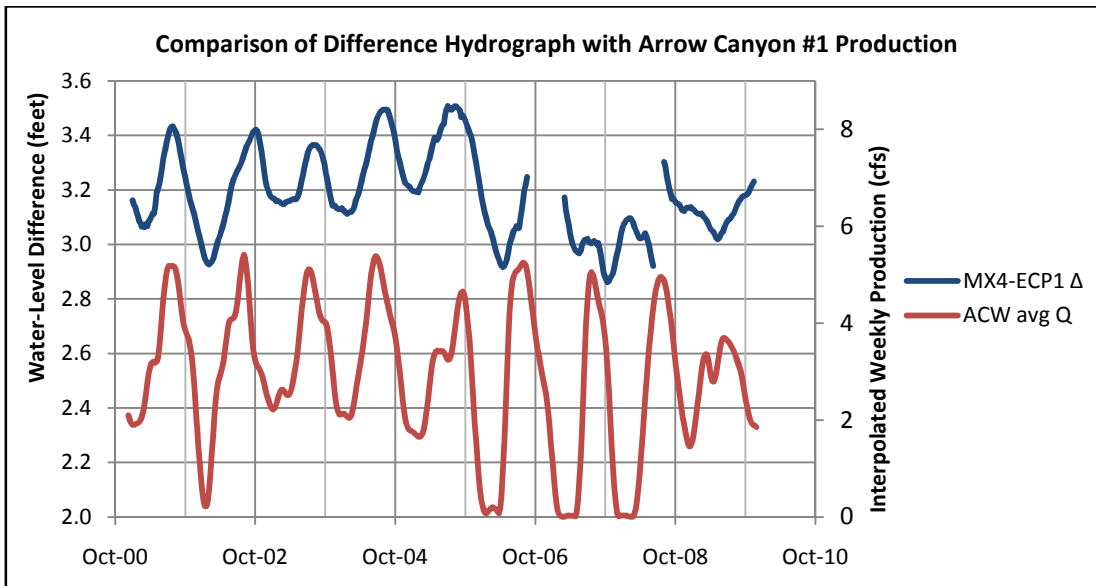


Figure 2. Difference hydrograph, obtained by subtracting weekly average water levels in ECP-1 from those in MX-4, compared with pumping rate of Arrow Canyon #1 well. The monthly well production totals were interpolated to weekly values with a cubic spline approximation. The relationship indicates that as well production increases the difference between the reference hydrographs increases, meaning that water levels in ECP-1 are being lowered relative to MX-4. **Note that peak-to-peak amplitude of difference hydrograph exceeds 0.5 feet in 2001-2004.** [file Production.xls, Sheet 'PrepRegressionData']

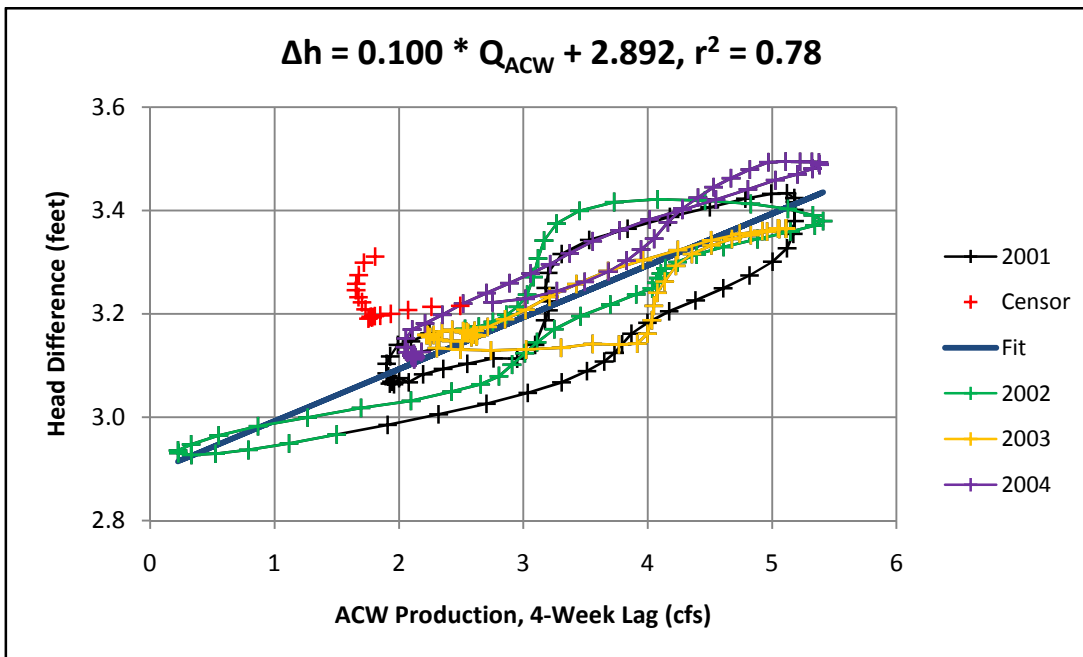


Figure 3. relations between Arrow Canyon #1 production and head difference between MX-4 and ECP-1 for 2001 through 2004. "Censor" indicates data from late 2004 not considered in the regression; heavy precipitation in that time frame may have caused a water-level rise in MX-4. **Note that the full range of long-term production variability is represented in the analysis interval.** [file Production.xls, Sheet 'PrepRegressionData']

We begin with an intercomparison of hydrographs (Figure 4) from the Paiutes TH-2, ECP-1, and M2 monitoring wells, which are 11.3, 13.4, and 17.0 miles (18.2, 21.6, and 27.4 km) south of Arrow Canyon #1, and 18.5, 16.4, and 13.0 miles (29.9, 26.4, and 20.9 km) north of Apex, respectively (Figure 1). Difference hydrographs for each well pair were prepared by subtracting the water level of the more southerly well from that of the more northerly well at corresponding times, allowing for comparison of relative water-level trends in northern (between TH-2 and ECP-1) and southern (between ECP-1 and M2) segments of an overall north-south evaluation transect.

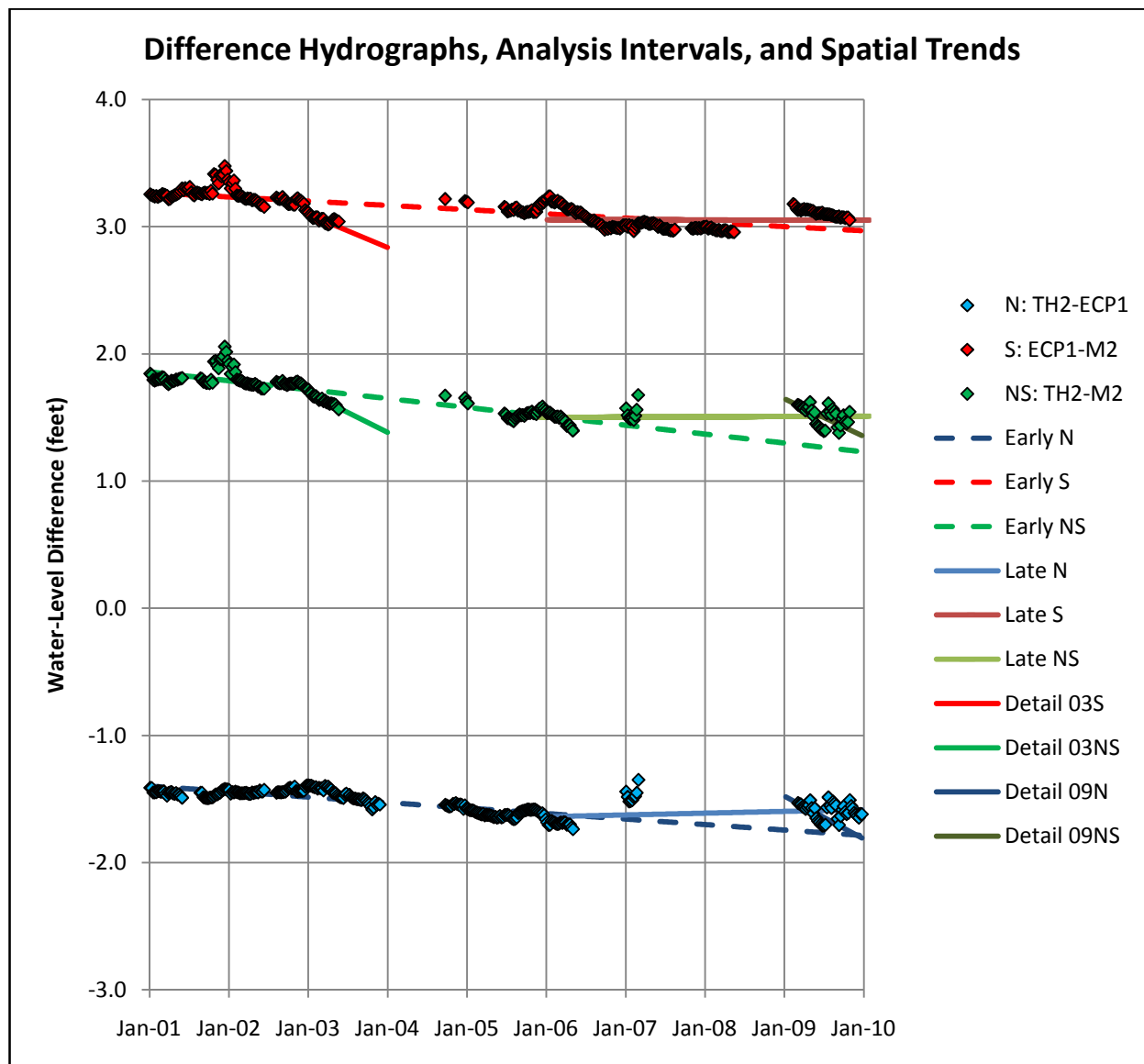


Figure 4. Difference hydrographs for well pairs TH-2/ECP-1 (northern segment), ECP-1/M2 (southern segment), and TH-2/M2 (combined northern and southern segments). Trends from 2000 through 2005 are shown as dashed lines and projected through 2009 for comparison with 2006-2009 trends, shown as solid lines. Weekly average water levels were used to establish the relations, except as indicated by short line segments in 2003 and 2009 where hourly data pairs were used. [file WeeklyDifferences.xlsx, Sheet Data&Plots]

In Figure 4, when the slope of a difference hydrograph is negative, water levels in the northern well of the well pair are decreasing with time relative to water levels in the southern well.

The difference hydrographs from the northern, southern, and combined evaluation areas are strikingly similar, both on multi-year time scales and for single years. For the multi-year interval 2000 through 2005, water levels in the northerly well of each well pair declined faster than water levels in the southerly well, imparting negative slopes to the difference hydrographs that indicate a predominance of local forcing ***from the north***. From 2006 through 2009, there appears to be a flattening or reversal of this relationship, suggesting some fundamental change in the state of the hydrologic system in the 2005-2006 time frame. Production increases by CSI and Nevada Energy (Duke facility) both occurred at about this time, but Nevada Energy's RW-1 well is a much closer "suspect" as pumping effects are sought in the water-level records. We find, however, that production and water-level records are inconsistent in two areas, near RW-1 and near the Duke facility.

Through the 9 years of record, RW-1 and the "Harvey Well" (254 feet from RW-1), produced intermittently (Figure 5). The Crystal-1 monitoring well is located 2.1 miles (3.4 km) north of RW-1 and only 1.2 miles (1.8 km) south of M2 (Figure 1). The ECP-1 – Crystal-1 difference hydrograph (Figure 6), prepared by comparing interpolated quarterly manual measurements at Crystal-1 (Figure 7) with closest-in-time weekly average transducer records from ECP-1, is very different from the ECP-1 – M2 difference hydrograph shown in Figure 4. A prominent oscillation of 1-foot magnitude in late 2006 is qualitatively uncorrelated with the reported pumping shown in Figure 5, and data quality uncertainties (Figure 7) are of insufficient magnitude to explain the oscillation as measurement error. RW-1 is capable of sustained production of well over 1000 gal/min, but 72-hours of pumping at >1100 gal/min in June-July, 2001 failed to elicit a detectable response in Crystal-1 (SRK, 2001, Tables 3 and 4). Aquifer tests have also been conducted at both Crystal-1 and Crystal-2 (SRK, 2001, Table 1) but the time frame of those tests is unknown.

If we ignore the problematic mid-decade results from Crystal-1, the overall rate of decline of ECP-1 relative to Crystal-1 from 2001 to 2009 is about $0.2 \text{ ft} / 8 \text{ yr} = 0.025 \text{ ft/yr}$, comparable to 0.23 ft/yr and 0.29 ft/yr for the northern and southern well pairs described above. It would be useful if the production history of RW-1 and the Harvey Well could be clarified, particularly for the winter seasons of 2001-2002 and 2005-2006, where "bumps" in the difference hydrographs (Figure 4) suggest effects at M2 that were not sensed at the more northerly wells.

Monitoring records from the Duke facility present a different set of issues. Reported water levels (Figure 8), specifically those from the GV-DUKE-WS2 supply well, appear to be inconsistent with what would be expected from a production well. The ECP-1 – GV-DUKE-WS2 difference hydrograph (Figure 9) does have some features suggestive of seasonal drawdown and recovery cycles, but the well was reportedly out of service until latest 2005 (Figure 10).

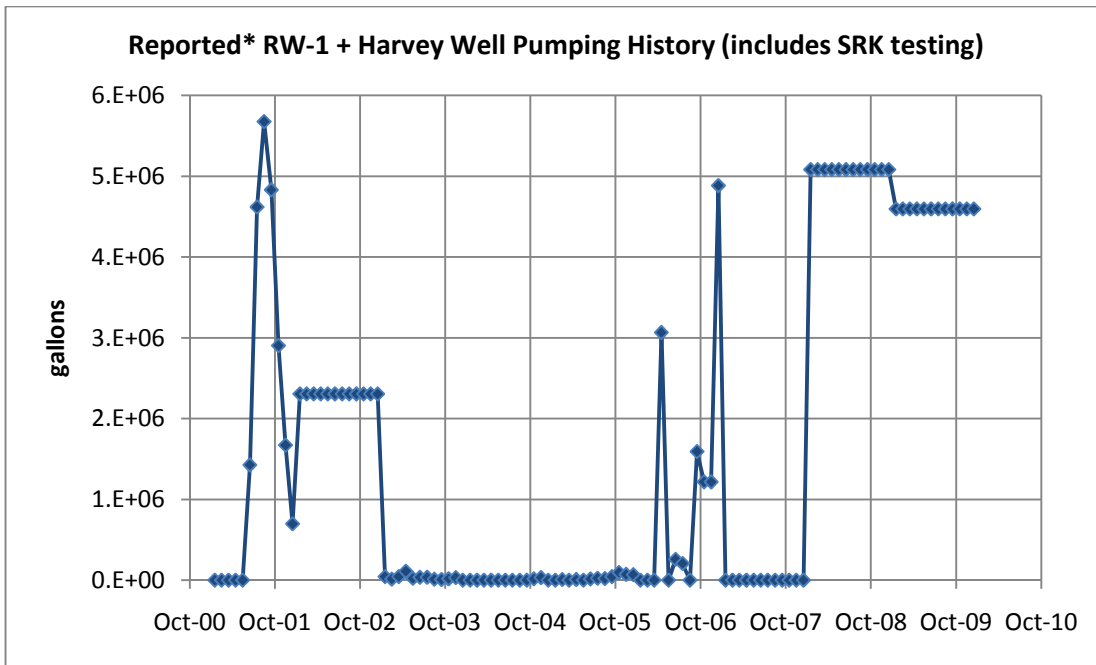


Figure 5. Reported monthly production from Nevada Energy RW-1, averaged in years when only annual production from Harvey Well is reported. Development and testing production in June and July of 2001 (SRK, 2001) has been added to the record. *2002, 2008, and 2009 annual reports attribute production to Harvey Well, 254 ft from RW-1; however, monthly reports for those years do not have a Harvey Well entry. [file RW1productionHistory.xlsx, Sheet1]

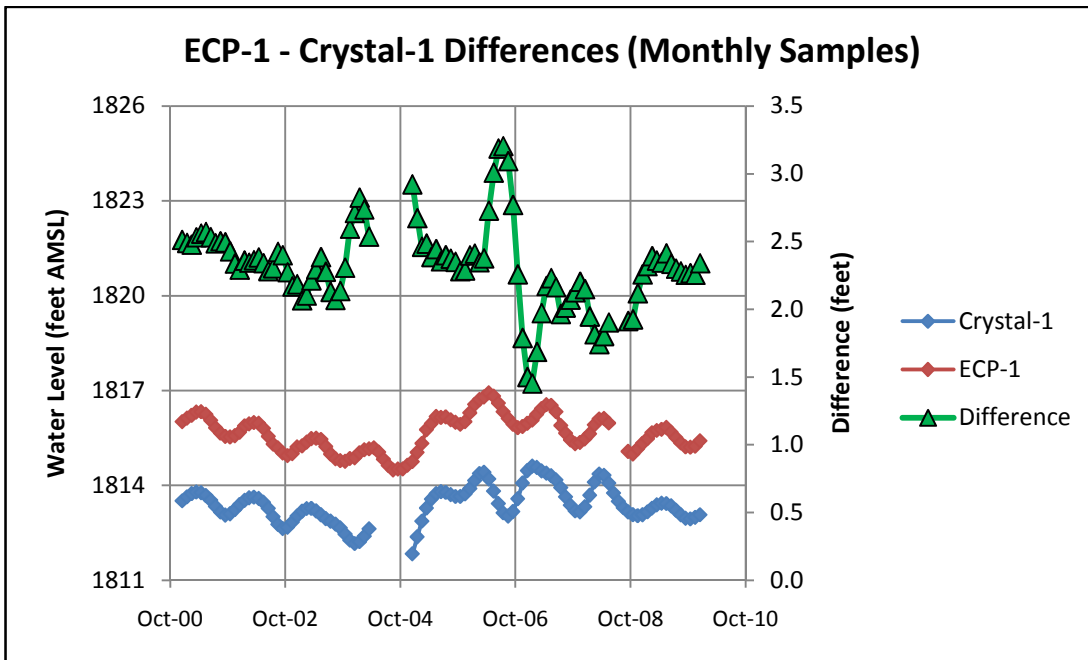


Figure 6. Weekly water levels from ECP-1 and Crystal-1, as reported to State Engineer, and derived water-level differences. [file WeeklyComparisons.xlsx, sheet ECP1-XL1MonthlyDiff]

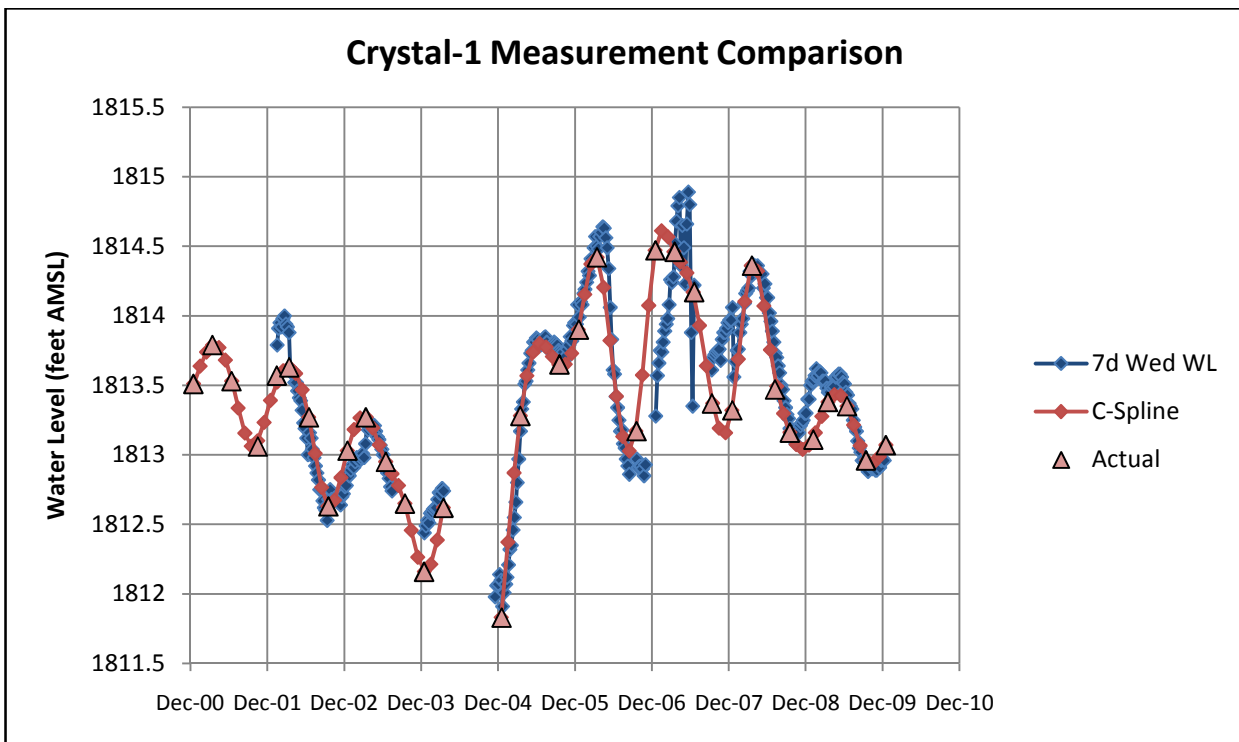


Figure 7. Monthly water levels interpolated from quarterly, mid-month measurements by cubic spline approximation, and weekly averages of hourly transducer measurements at Crystal-1. Both sets of measurements support a drawdown event in late 2006 of 1 foot or more. [file WeeklyComparisons.xlsx, sheet Crystal1_7dAvgWed]

Pumping in the Apex area is dominated by Nevada Cogeneration Associates (Figure 11), followed by Republic Services and LVVWD (Figure 12). Production is generally seasonal and quite uniform on an annualized basis for the larger producers (Figures 13-15), with the notable exceptions of Nevada Energy’s former Duke facility, which was inactive for most of 2003-2005 but has (with the exception of 2008) increased production each year thereafter (Figure 10). Pumping by Chemical Lime and Georgia-Pacific (Figures 16 and 17) shows less seasonality, and may therefore present opportunities for analyses of nearby monitoring records such as those from well GV-2 (Figure 1).

Point-by-point subtraction of the measured (monthly) water levels in GV-2 with closest-in-time measurements from ECP-1 provide a coarse but useful difference hydrograph (Figure 18) that may be representative of the Apex area since it is relatively remote from the largest pumping centers and equidistant from the less periodic forcing from Chemical Lime and Georgia-Pacific. Water levels *declined* in ECP-1 relative to GV-2 from 2002-2005, after which water levels at GV-2 declined relative to ECP-1. The ECP-1 – GV-2 difference hydrograph is an amplified version of the difference hydrographs derived from the Paiutes’ wells, described above.

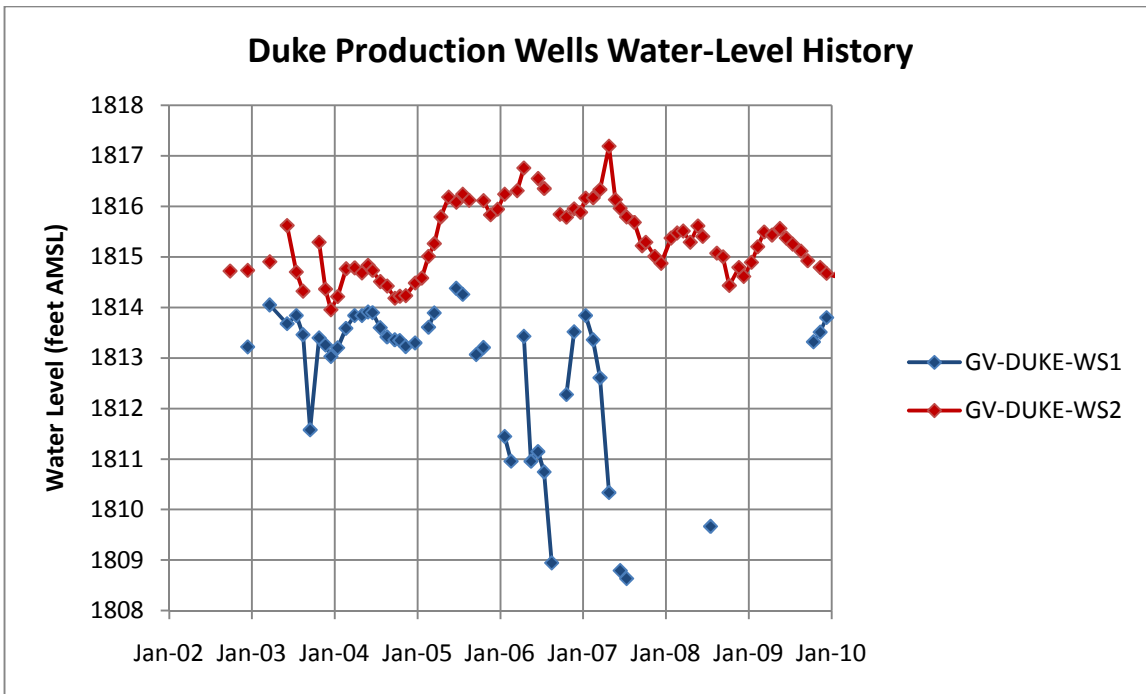


Figure 8. Water levels at Nevada Energy’s Duke facility as reported by SNWA [DukeProductionWellsWL.xlsx, Sheet ChartData]

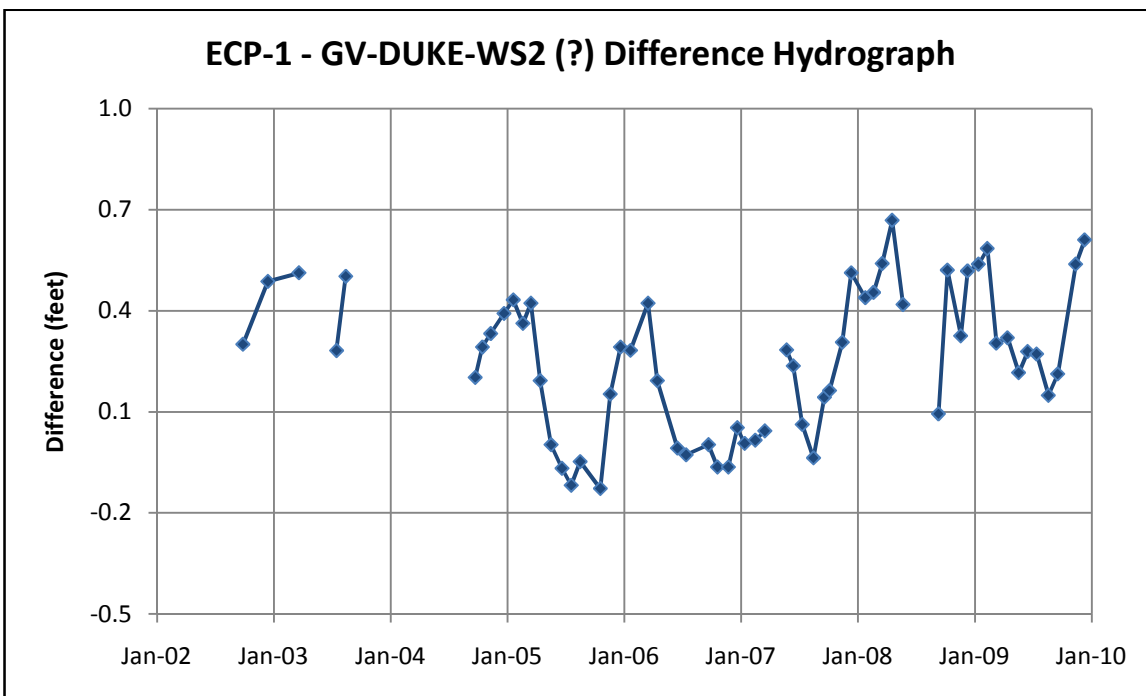


Figure 9. Difference between Paiutes ECP-1 and GV-DUKE-WS2 water levels, queried due to inconsistency of timing and magnitude of these very minor local effects with reported timing and magnitude of production from GV-DUKE-GV2. [file ECP1differences, Sheet ECP1-DukeWS2]

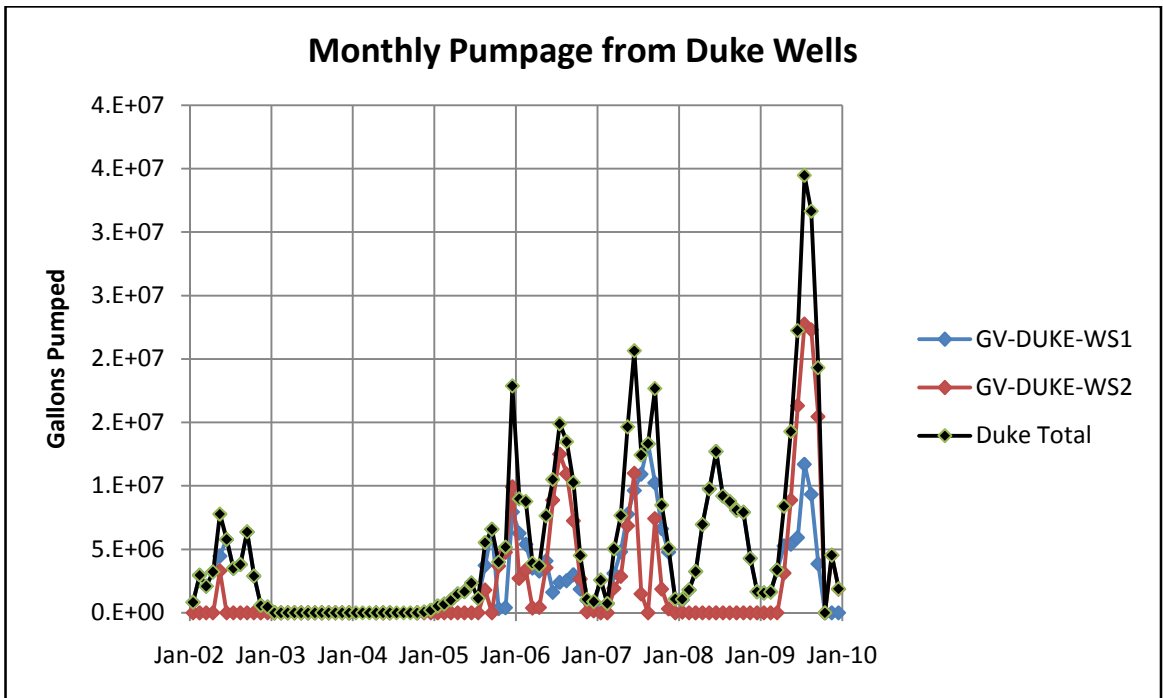


Figure 10. Monthly production from wells operated for power generation by Southern Nevada Water Authority [file SNWA_SFFmonthlyPumping.xlsx, Sheet1]

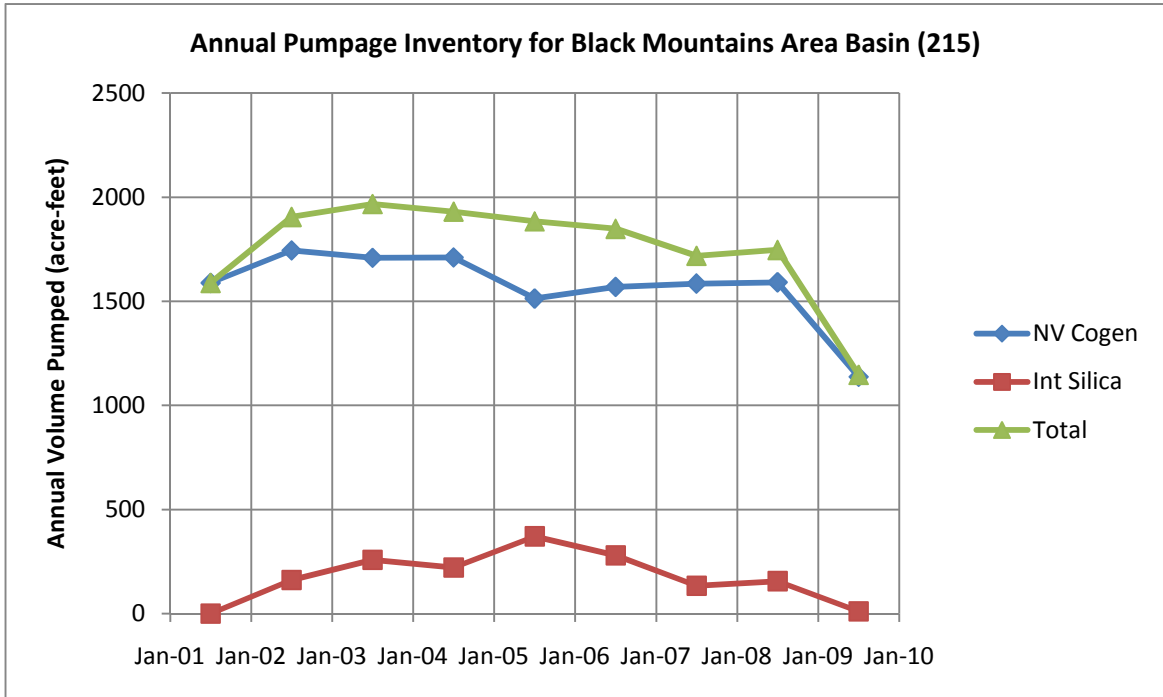


Figure 11. Annual production from Basin 215. [file SFFannualPumpageInventory.xlsx, Sheet GV215]

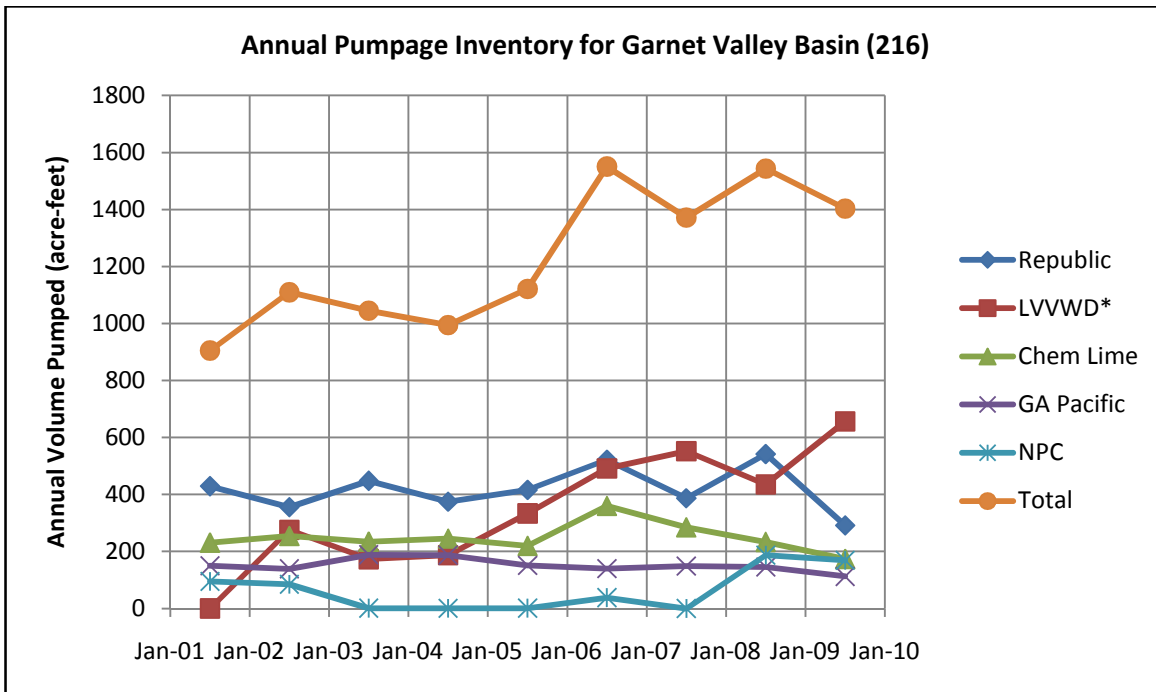


Figure 12. Annual production from Basin 216.[file SFFAnnualPumpageInventory.xlsx, Sheet GV216]

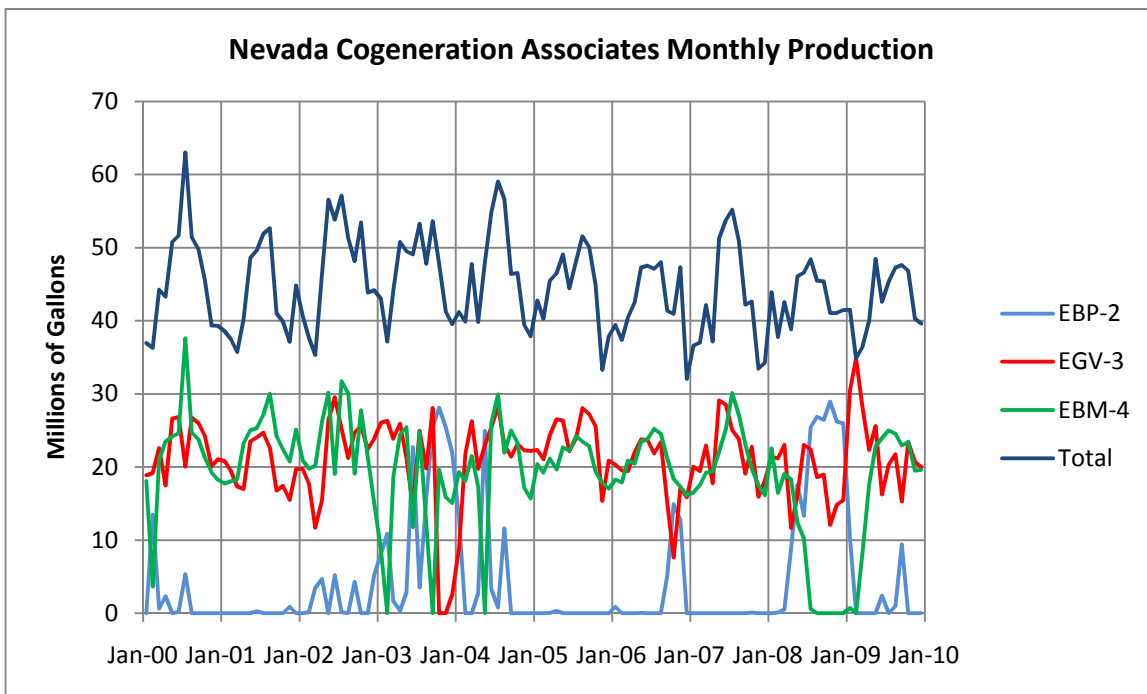


Figure 13. Monthly production by Nevada Cogeneration Associates [file NVcogenTransposeQ.xlsx, Sheet1]

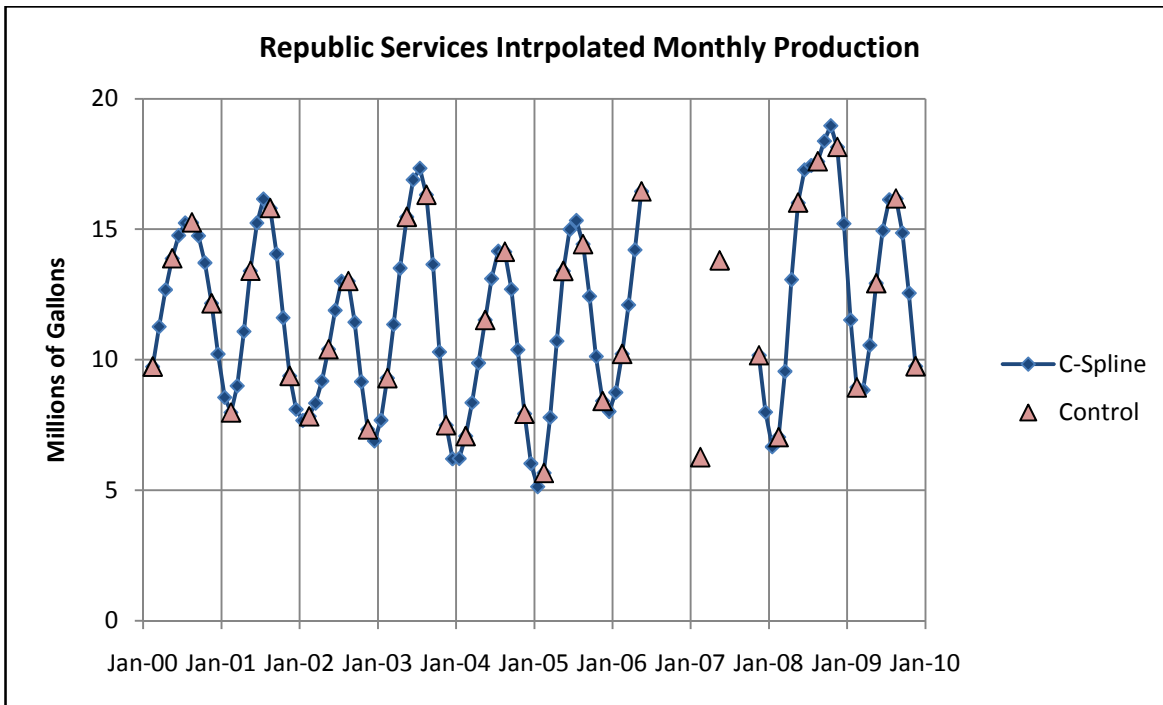


Figure 14. Monthly production by Republic Services interpolated from quarterly reports. [file RepublicTransposeQ.xlsx, Sheet Summary]

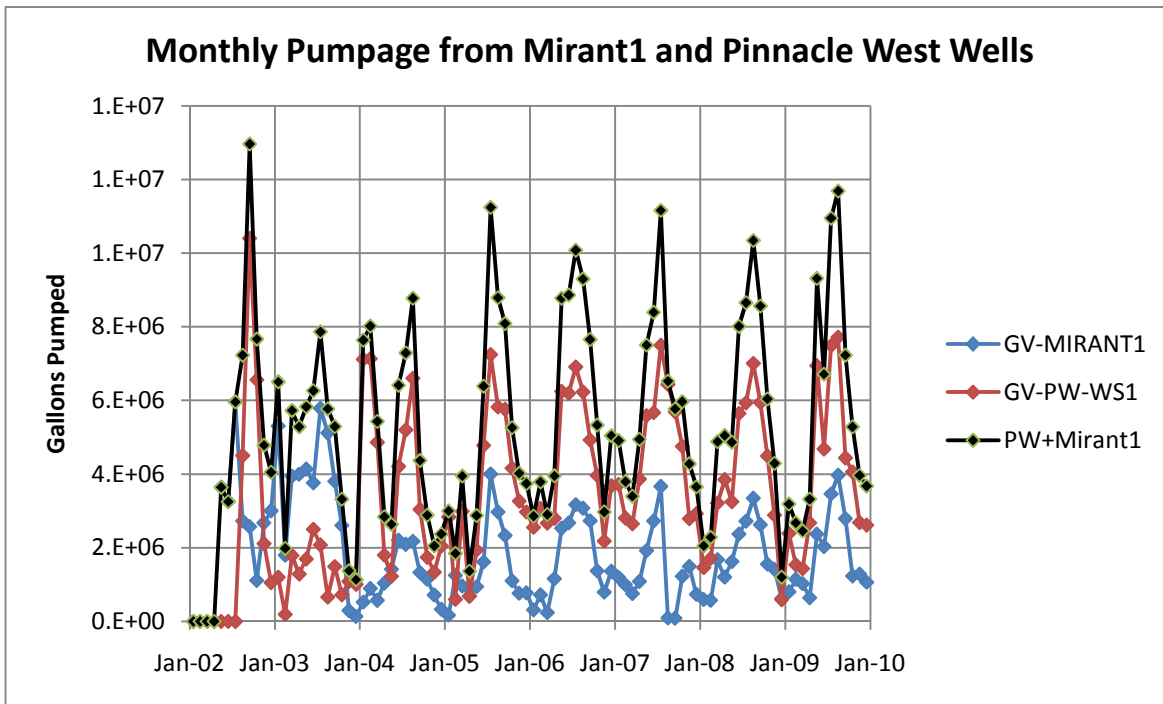


Figure 15. Monthly production from wells operated for power generation by Southern Nevada Water Authority [file SNWA_SFFmonthlyPumping.xlsx, Sheet1]

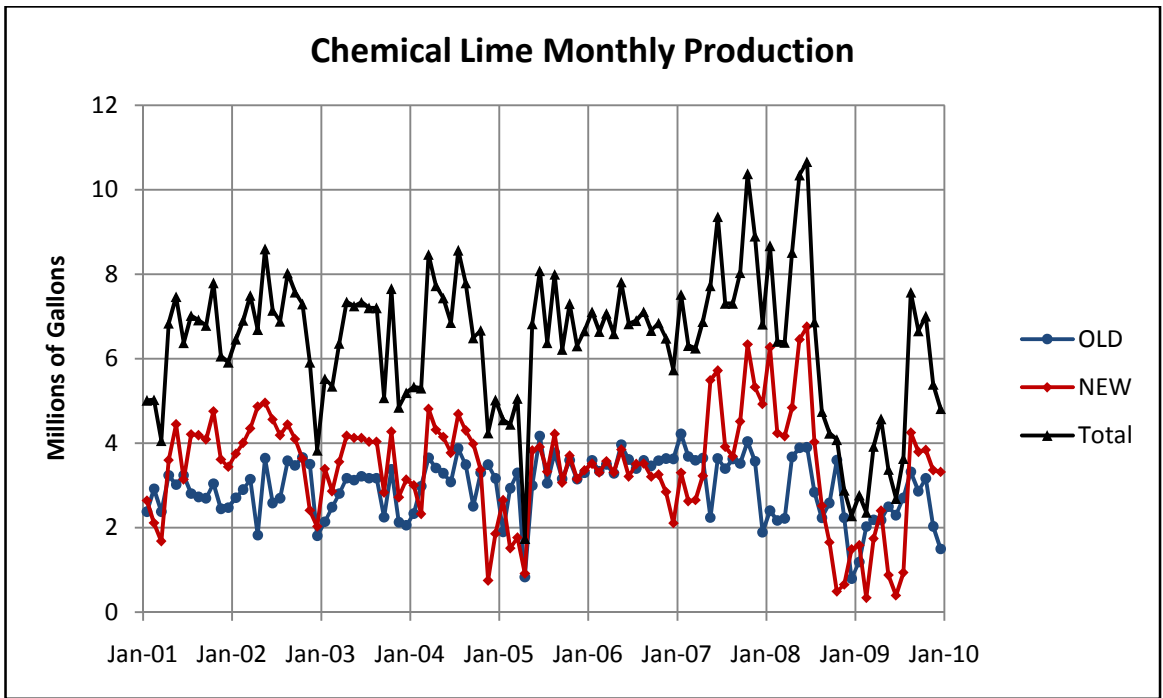


Figure 16. Monthly production by Chemical Lime. [file ChemLimeTranspose.xlsx, Sheet1]

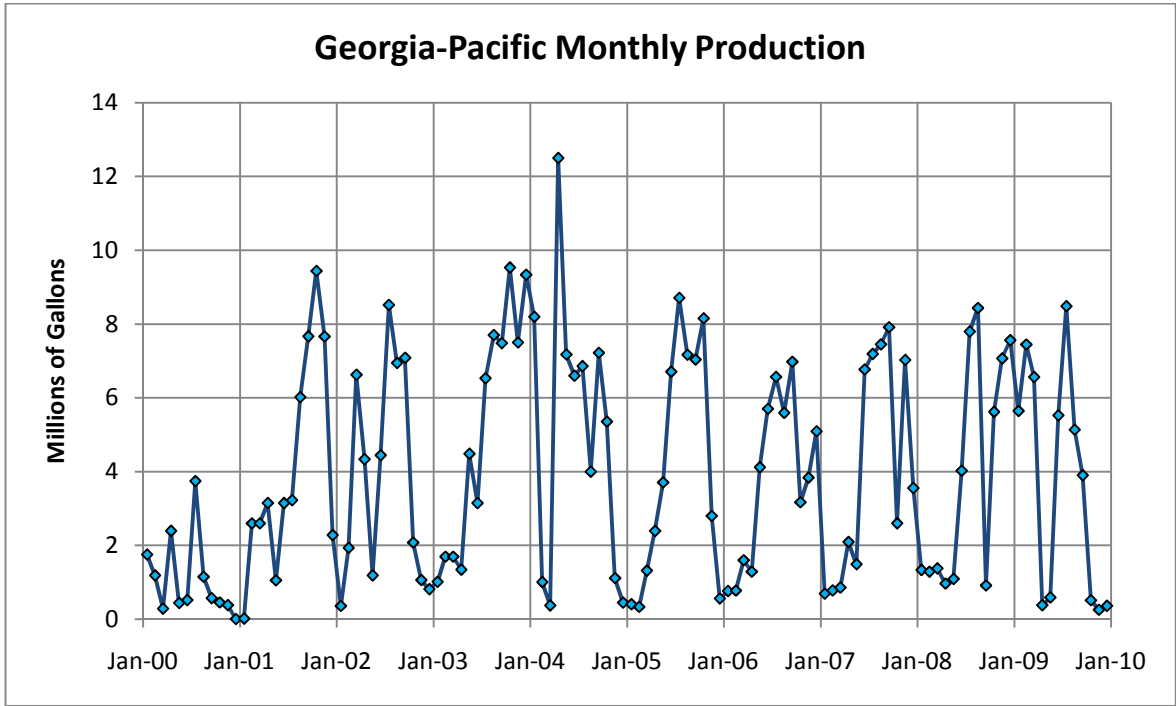


Figure 17. Monthly production by Georgia-Pacific. [file GeorgiaPacificTranspose.xlsx, Sheet1]

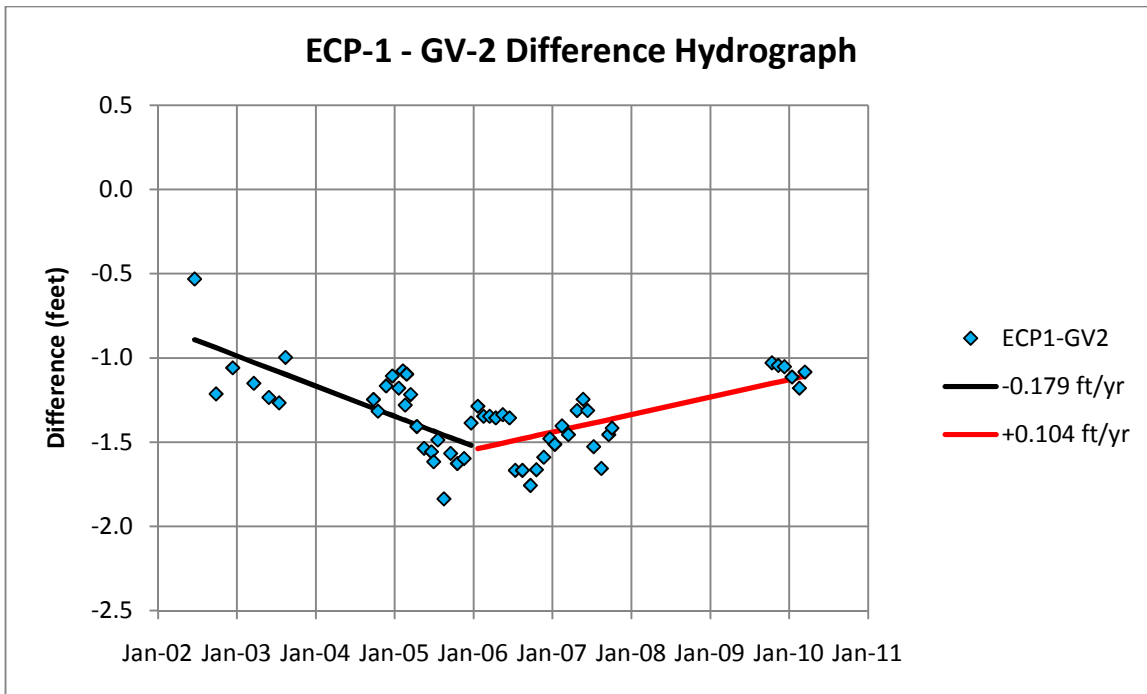


Figure 18. Point-by-point subtraction of GV-2 monthly water levels from those closest in time recorded at ECP-1. [file ECP1differences.xlsx, Sheet ECP1-GV2]

Discussion

Groundwater production for the Duke facility appears to be the only recognized agent that could be responsible for the character of the difference hydrographs presented here. As production from Duke levels off and the system approaches a new steady state, a new segment in the difference hydrographs will develop. Because the Paiutes’ water levels were affected in the pre-2006 era by a dominant *northerly* influence, the Synthetic Reference Hydrograph (SRH) provides a *conservative* baseline for evaluating water levels and springflow trends in more northerly areas. Between 2006 and 2009 the Paiutes’ wells may have begun to sense the effects of pumping in the Apex area, and the flattening of the difference hydrographs in this time frame suggests a balance between northern and southern pumping effects (reasonable to the extent hydraulic diffusivities are similar across the region, because the Paiutes’ wells are roughly mid-way between pumping centers of roughly equal strength, if Nevada Energy’s alluvial pumpage in upper Moapa Valley is ignored, which we believe is appropriate in this context). If so, there has been a transition from a *conservative* baseline (SRH) to a less conservative but, we believe, appropriate baseline, at least through 2008. If southern effects become predominant in the future, a detrending step will be necessary to extend the SRH forward in time. We note that if Duke production continues to increase as the Order 1169 Study is in progress, there will be justification for significantly enhanced monitoring efforts to better characterize southerly influences.

The possibility that pumping effects originating in the Apex area have contaminated the ECP-1 record is an extremely important consideration, and we consider the issue is only satisfactorily resolved for the pre-2009 time frame. It is clear to us that in 2001-2005, the interval on which our SRH is based, distance-drawdown relations were dominated by forcing from the north. A component of southerly forcing, if unrecognized, would not affect the overall conservatism of our analysis of Order 1169 impacts, but if seasonal in nature could invalidate the 9-10 month lag we estimate between pumping in

the CSI1 area and the onset of springflow reductions. The absence of seasonality in the difference hydrographs presented in Figures 4 and its apparent presence in Figure 18 suggests that seasonal effects from the Apex area, if not entirely damped out, are within the realm of measurement error in the Paiutes wells. It would have been helpful if, during the 2003-2004 hiatus in production from the Duke wells, GV-2 could have been monitored at a sufficiently high frequency to resolve pumping effects from nearby Chemical Lime and Georgia-Pacific, providing a synthetic hydrograph at that locality that could be used to isolate Duke effects, that now appear significant in the southern areas and may have appeared in the Paiutes' wells in 2006. Having moved beyond the initial hypothesis that ECP-1 presented a pristine and representative background hydrograph for the region, we have successfully (we believe) accommodated the effects of the most influential production well impacts (those from Arrow Canyon #1) on the ECP-1 record, producing our SRH. Additional influences are undoubtedly present, and efforts will continue to identify, quantify, and attribute such influences to their sources. To date, we have been unable to identify any such effects on and north of the Paiutes' Reservation that can be attributed to northward-propagating drawdown signals.

References

- Beard, L.S., R.E. Anderson, D.L. Block, R.G. Bohannon, R.J. Brady, S.B. Castor, E.M. Duebendorfer, J.E. Faulds, T.J. Felger, K.A. Howard, M.A. Kuntz, and V.S. Williams, 2007, Preliminary Geologic Map of the Lake Mead 30' x 60' Quadrangle, Clark County, Nevada, and Mohave County, Arizona: U. S. Geological Survey Preliminary Geologic Map of the Lake Mead 30' x 60' Quadrangle, Clark County, Nevada, and Mohave County, Arizona: U. S. Geological Survey Open-File Report 2007-1010, 109 p.
- SRK Consulting, Inc., 2001, Installation Report – Harvey Well Replacement – RW-1: unpublished report dated Sept. 28, 2001; Reno, Nevada, 87 p.



Techniques of Water-Resources Investigations
of the United States Geological Survey

Chapter B2

**INTRODUCTION TO
GROUND-WATER HYDRAULICS**

A Programed Text for Self-Instruction

By **Gordon D. Bennett**

Book 3

APPLICATIONS OF HYDRAULICS

SE ROA 38372

JA_9654

DEPARTMENT OF THE INTERIOR
MANUEL LUJAN, Jr., *Secretary*

U.S. GEOLOGICAL SURVEY
Dallas L. Peck, *Director*

Any use of trade, product, or firm names in this publication is for descriptive purposes only and does not imply endorsement by the U.S. Government

First printing, 1976
Second printing, 1978
Third printing, 1985
Fourth printing, 1989

UNITED STATES GOVERNMENT PRINTING OFFICE: 1989

For sale by the Books and Open-File Reports Section, U.S. Geological Survey,
Federal Center, Box 25425, Denver, CO 80225

SE ROA 38373

JA_9655

PREFACE

The series of manuals on techniques describes procedures for planning and executing specialized work in water-resources investigations. The material is grouped under major subject headings called books and further subdivided into sections and chapters; Section B of Book 3 is on ground-water techniques.

This chapter is an introduction to the hydraulics of ground-water flow. With the exception of a few discussions in standard text format, the material is presented in programed form. In this form, a short section involving one or two concepts is followed by a question dealing with these concepts. If the correct answer to this question is chosen, the reader is directed to a new section, in which the theory is further developed or extended. If a wrong answer is chosen, the reader is directed to a section in which the earlier material is reviewed, and the reasons why the answer is wrong are discussed; the reader is then redirected to the earlier section, to choose another answer to the question. This approach allows students who are either partially familiar with the subject, or well prepared for its study, to proceed rapidly through the material, while those who require more explanation are provided it within the sections that deal with erroneous answers.

In the preparation of any text, difficult choices arise as to the material to be included. Because this text is an introduction to the subject, the discussion has been restricted, for the most part, to the flow of homogeneous fluid through an isotropic and homogeneous porous medium—that is, through a medium whose properties do not change from place to place or with direction. Emphasis has been placed upon theory rather than application. Basic principles of ground-water hydraulics are outlined, their uses in developing equa-

tions of flow are demonstrated, representative formal solutions are considered, and methods of approximate solution are described. At some points, rigorous mathematical derivation is employed; elsewhere, the development relies upon physical reasoning and plausibility argument.

The text has been prepared on the assumption that the reader has completed standard courses in calculus and college physics. Readers familiar with differential equations will find the material easier to follow than will readers who lack this advantage; and readers familiar with vector theory will notice that the material could have been presented with greater economy using vector notation.

The material is presented in eight parts. Part I introduces some fundamental hydrologic concepts and definitions, such as porosity, specific discharge, head, and pressure. Part II discusses Darcy's law for unidirectional flow; a text-format discussion at the end of Part II deals with some generalizations of Darcy's law. Part III considers the application of Darcy's law to some simple field problems. The concept of ground-water storage is introduced in Part IV. A text-format discussion at the beginning of Part V deals with partial derivatives and their use in ground-water equations; the basic partial differential equation for unidirectional nonequilibrium flow is developed in the programed material of Part V. In Part VI, the partial differential equation for radial confined flow is derived and the "slug-test" solution, describing the effects of an instantaneous injection of fluid into a well, is presented and verified. A text-format discussion at the end of Part VI outlines the synthesis of additional solutions, including the Theis equation, from the "slug-test" solution. Part VII introduces the gen-

eral concepts of finite-difference analysis, and a text format discussion at the end of Part VII outlines some widely used finite-difference techniques. Part VIII is concerned with electric-analog techniques. The material in Part VI is not prerequisite to that in Parts VII and VIII; readers who prefer may proceed directly from Part V to Part VII.

A program outline is presented in the table of contents of this report. This outline indicates the correct-answer sequence through each of the eight parts and describes briefly the material presented in each correct-answer section. Readers may find the outline useful in review or in locating discussions of particular topics, or may wish to consult it for an overview of the order of presentation.

It is impossible, in this or any other form of instruction, to cover every facet of each development, or to anticipate every difficulty which a reader may experience, particularly in a field such as ground water, where readers may vary widely in experience and mathematical background. An additional difficulty inherent in the programed text approach is that some continuity may be lost in the process of dividing the material into sections. For all these reasons, it is suggested that the programed instruction presented here be used in conjunction with one or more of the standard references on ground-water hydraulics.

This text is based on a set of notes used by the author in presenting the subject of ground-water hydraulics to engineers and university students in Lahore, West Pakistan, while on assignment with the U.S. Agency for International Development. The

material has been drawn from a number of sources. The chapter by Ferris (1959) in the text by Wisler and Brater and that by Jacob (1950) in "Engineering Hydraulics" were both used extensively. Water-Supply Paper 1536-E (1962) by Ferris, Knowles, Brown, and Stallman was an important source, as was the paper by Hubbert (1940), "The Theory of Ground Water Motion." The text "The Flow of Homogeneous Fluids through Porous Media" by Muskat (1937) and the paper "Theoretical Investigation of the Motion of Ground Waters" by Slichter (1899) were both used as basic references. The development of the Theis equation from the "slug-test" solution follows the derivation given in the original reference by Theis (1935). The material on analog models is drawn largely from the book, "Analog Simulation," by Karplus (1958). In preparing the material on numerical methods, use was made of the book, "Finite-Difference Equations and Simulations," by Hildebrand (1968), and the paper "Selected Digital Computer Techniques for Groundwater Resource Evaluation," by Prickett and Lonquist (1971). A number of additional references are mentioned in the text.

The author is indebted to Messrs. David W. Greenman and Maurice J. Mundorff, both formerly Project Advisors, U.S. Geological Survey-U.S.A.I.D., Lahore, for their support and encouragement during preparation of the original notes from which this text was developed. The author is grateful to Patricia Bennett for her careful reading and typing of the manuscript.

CONTENTS

	Page
Preface -----	III
Program outline -----	VI
Instructions to the reader -----	1
Part	
I. Definitions and general concepts -----	3
II. Darcy's law -----	14
Beginning of programed instruction -----	14
Text-format discussion: Generalizations of Darcy's law -----	31
III. Application of Darcy's law to field problems -----	34
IV. Ground-water storage -----	53
V. Unidirectional nonequilibrium flow -----	69
Text-format discussion: Partial derivatives in ground-water-flow analysis -----	69
Beginning of programed instruction -----	72
VI. Nonequilibrium flow to a well -----	88
Beginning of programed instruction -----	88
Text-format discussion: Development of additional solutions by superposition -----	112
VII. Finite-difference methods -----	119
Beginning of programed instruction -----	119
Text-format discussion: Techniques of finite-difference solution of the ground-water-flow equation -----	136
VIII. Analog techniques -----	153
References -----	171

SYMBOLS

<i>Symbol</i>	<i>Dimensions (M, mass; L, distance; T, time)</i>	<i>Explanation</i>	<i>Symbol</i>	<i>Dimensions (M, mass; L, distance; T, time)</i>	<i>Explanation</i>
<i>A</i>	<i>L</i> ²	face area of aquifer, gross	<i>e</i>		base of natural logarithms
		cross-sectional area of flow	<i>F_g</i>	<i>MLT</i> ⁻²	gravitational force
<i>a</i>	<i>L</i>	node spacing in finite-difference grid	<i>f_l</i>	<i>MLT</i> ⁻²	component of gravitational force parallel to conduit
<i>b</i>	<i>L</i>	aquifer thickness	<i>f_n</i>	<i>MLT</i> ⁻²	component of gravitational force normal to conduit
<i>C</i>	farad (coulombs/ volt)	electrical capacitance	<i>g</i>	<i>LT</i> ⁻²	gravitational acceleration
			<i>h</i>	<i>L</i>	head; static head
			<i>h_p</i>	<i>L</i>	pressure head

<i>Symbol</i>	<i>Dimensions</i>	<i>Explanation</i>	<i>Symbol</i>	<i>Dimensions</i>	<i>Explanation</i>
<i>I</i>	amperes (coulombs/ second)	electrical current	<i>u</i>		$r^2S/4Tt$ —argument of the well function
<i>K</i>	LT^{-1}	hydraulic conductivity	∇	L^3	fluid volume
<i>k</i>	L^2	intrinsic permeability	<i>v</i>	LT^{-1}	velocity
<i>l</i>	L	length	$W(u)$		well function
<i>n</i>		porosity	<i>w</i>	L	width
<i>p</i>	$ML^{-1}T^{-2}$	pressure	<i>z</i>	L	elevation above datum
<i>Q</i>	L^3T^{-1}	volumetric fluid discharge	β		fraction of the total water in storage that can be drained by gravity
<i>q</i>	LT^{-1}	specific discharge—discharge per unit face area of aquifer, Q/A	$\Delta_x h$	L^{-1}	finite-difference approxima- tion to $\partial^2 h / \partial x^2$
<i>R</i>	ohms (volts/ ampere)	electrical resistance	$\Delta_y h$	L^{-1}	finite-difference approxima- tion to $\partial^2 h / \partial y^2$
<i>S</i>		storage coefficient	ϵ	coulomb	electrical charge
<i>S_s</i>	L^{-1}	specific storage	μ	$ML^{-1}T^{-1}$	dynamic viscosity
<i>S_y</i>		specific yield	ρ	ML^{-3}	fluid density
<i>T</i>	L^2T^{-1}	transmissivity (transmissi- bility)	ρ_e	ohm-metres	electrical resistivity
			σ	mhos/metre	electrical conductivity
			ϕ	volts	voltage or electrical potential

UNIT CONVERSION

<i>English</i>	<i>Factor for converting English units to international system of units</i>	<i>Metric SI</i>
ft (foot)	3.048×10^{-1}	m (metre)
gal (gallon)	3.785	l (litre)
ft ³ /s (cubic foot per second)	2.832×10^{-2}	m ³ /s (cubic metre per second)

PROGRAM OUTLINE

This program outline is provided to assist the reader in review, and to facilitate the location of particular topics or discussions in the text. Hopefully, it may also provide some feeling for the organization of the material and the order of presentation, both of which tend to be obscured by the programed format.

The section numbers in the left margin correspond to correct answers in the programed instruction; they give the sequence of sections which will be followed if no errors are made in answering the questions. An outline of the content of each of the correct-answer sections is given to the right of the section number. Two numbers are listed beneath each of these section outlines. These numbers identify the wrong-answer sections for the question presented in the outlined correct-answer section. The correct answer to this question is indicated by the next entry in the left margin.

The discussions written in standard text format are also outlined. For these discussions, page numbers corresponding to the listed material are given in parentheses in the left margin.

Part I. Definitions and general concepts:*Section:*

- 1 porosity
13; 18
- 9 effective porosity; saturation
12; 29
- 6 porosity, saturation (review); point velocity variations; tortuous path effects
4; 21
- 3 tortuous flow path effects (review); problems in determining actual cross-sectional flow area; relation of discharge per unit face area to flow velocity
28; 10
- 14 relation of discharge per unit face area to flow velocity (review); definition of specific discharge or specific flux; definition of head
11; 17
- 24 omission of velocity head in ground water; relation between pressure and height of fluid column (Pascal's law)
25; 19
- 16 Pascal's law (review); head as potential energy per unit weight; elevation head as potential per unit weight due to elevation; dimensions of pressure
7; 15
- 26 pressure as a component of potential energy per unit volume; pressure head as a component of potential energy per unit weight; total potential energy per unit weight (question)
20; 23
- 22 head as potential energy per unit weight (review); total potential energy per unit volume
5; 27
- 8 total potential energy per unit volume (review)

Part II. Darcy's law:*Section:*

- 1 outline of approach—method of balancing forces; friction force proportional to velocity; pressure force on face of a fluid element in a sand-packed pipe (question)
25; 16
- 8 relation between pressure and force; net pressure force on a fluid element (question)
23; 12
- 31 net pressure force on a fluid element (review); pressure gradient; net pressure force in terms of pressure gradient (question)
5; 14
- 26 net pressure force in terms of pressure gradient; gravitational force; mass of fluid element in terms of density, porosity, and dimensions (question)
3; 17
- 15 gravitational force in terms of density, porosity, and dimensions; component of gravitational

force contributing to the flow (question)
22; 18

- 33 resolution of gravitational force into components parallel and normal to the conduit; expression for magnitude of component parallel to the conduit (question)
6; 37
- 35 expression for component of gravitational force parallel to conduit (review); substitution of $\Delta z/\Delta l$ for cosine in this expression (question)
32; 4
- 11 substitution of $\Delta z/\Delta l$ for cosine in expression for gravity component along conduit (review); expression for total driving force on fluid element attributable to pressure and gravity (question)
24; 10
- 19 assumptions regarding frictional retarding force; expression for frictional retarding force consistent with assumptions (question)
2; 34
- 20 balancing of driving forces and frictional force to obtain preliminary form of Darcy's law
36; 27
- 28 Darcy's law in terms of hydraulic conductivity; replacement of

$$-\frac{1}{\rho g} \frac{dp}{dl} + \frac{dz}{dl}$$

by dh/dl (question)

9; 30

- 7 discussion of hydraulic conductivity and intrinsic permeability; flow of ground water in relation to differences in elevation, pressure, and head (question)
29; 13
- 21 Darcy's law as a differential equation; analogies with other physical systems; ground-water velocity potential

Text-format discussion—Generalizations of Darcy's law:

- (p. 31) specific discharge vector in three dimensions; definition of components of specific-discharge vector
- (p. 31) Darcy's law for components of the specific-discharge vector; Darcy's law using the resultant specific-discharge vector
- (p. 31) velocity potential; flownet analysis; Darcy's law for components of the specific-discharge vector in anisotropic media
- (p. 32) flowlines and surfaces of equal head in the anisotropic case; solution by transformation of coordinates
- (p. 32) anisotropy of stratified sedimentary material

- (p. 33) use of components of pressure gradient and components of gravitational force in each of the three major permeability directions; hydraulic conductivity tensor
- (p. 33) aquifer heterogeneity
- (p. 33) fluid heterogeneity; Darcy's law for a heterogeneous fluid in an anisotropic aquifer, using intrinsic permeability

Part III. Application of Darcy's law to field problems:

Section:

- 1 differential equations and solutions
15; 23
- 7 infinite number of solutions to a differential equation
29; 14
- 8 slope-intercept concept applied to solutions of differential equations
5; 20
- 10 application of Darcy's law to one-dimensional equilibrium stream seepage problem; selection of particular solution to satisfy the differential equation and to yield correct head at the stream (question)
22; 36
- 24 boundary conditions in differential equations; interpretation of head data observed in a field situation (question)
42; 21
- 25 application of Darcy's law to a problem of one-dimensional steady-state unconfined flow, using Dupuit assumptions
26; 43
- 9 substitution of
- $$\frac{1}{2} \frac{d(h^2)}{dx}$$
- for
- $$h \frac{dh}{dx}$$
- in the unconfined flow problem; testing for solution by differentiation and substitution of boundary conditions (question)
16; 4
- 41 parabolic steepening of head plot in the Dupuit solution; problem of radial flow to a well; cross-sectional area of flow at a distance r from the well (question)
12; 6
- 27 decrease in area along path of radial flow; relation between decreasing area and hydraulic gradient (question)
11; 32
- 40 signs in radial flow problem; application of Darcy's law to the flow problem (question)
33; 17

- 35 expression of radial flow differential equation in terms of

$$\frac{dh}{d(\ln r)}$$

39; 13

- 2 interpretation of radial flow differential equation expressed in terms of

$$\frac{dh}{d(\ln r)}$$

18; 31

- 38 interpretation of radial flow differential equation (review); solution equation as taken from a plot of h versus $\ln r$; conversion to common logs; characteristics of the semilog plot
34; 37
- 19 logarithmic cone of depression; equation for drawdown at the well (question)
28; 30
- 3 applications of the drawdown equation; general characteristics of well-flow problems

Part IV. Ground-water storage:

Section:

- 1 relation between volume of water stored in a tank and water level in the tank
10; 9
- 11 relation between volume of water stored in a sand-packed tank and water level in the tank
31; 12
- 14 slope of V versus h graph for sand-packed tank
17; 22
- 26 capillary effects; assumption that a constant amount of water is permanently retained; relation between volume of water in recoverable storage and water level, under these conditions (question)
18; 2
- 16 slope of V versus h graph for sand-packed tank with permanent capillary retention
4; 29
- 33 slope of V versus h graph for prism of unconfined aquifer
28; 19
- 32 dependence of V , h relationship on surface area, A ; definition of specific yield (question)
7; 27
- 6 confined or compressive storage; V , h relationship for a prism in a confined aquifer
23; 30
- 21 dependence of V , h plot for a prism of confined aquifer on base area
3; 34
- 20 definition of confined or compressive storage coefficient; specific storage
5; 15

- 25 storage equation—relation between time rate of change of volume of water in storage and time rate of change of head
8; 24
- 13 relation between time rate of change of volume in storage and time rate of change of head (review)

Part V:

Text-format discussion—Partial Derivatives in Ground-Water-Flow Analysis:

- (p. 69) Partial derivatives; topographic map example
- (p. 70) Calculation of partial (space) derivatives
- (p. 70) Partial derivative with respect to time
- (p. 70) Space derivatives as components of slope of the potentiometric surface; dependence on position and time; time derivative as slope of hydrograph; dependence on position and time
- (p. 72) Vector formulation of the specific discharge; Darcy's law for components of the specific discharge vector

Unidirectional nonequilibrium flow:

Section:

- 1 relation between inflow and outflow for a tank
29; 17
- 21 equation of continuity; relation of $\partial h/\partial t$ for a prism of aquifer to difference between inflow and outflow (question)
6; 5
- 30 combination of continuity and storage equation to obtain relation between $\partial h/\partial t$ and inflow minus outflow (review); expression for inflow through one face of a prism of aquifer (question)
8; 3
- 22 implications of difference between inflow and outflow in a prism of aquifer (question)
14; 26
- 33 expression for inflow minus outflow, for one dimensional flow, in terms of difference in head gradients (question)
18; 15
- 9 change in a dependent variable expressed as a product of derivative and change in independent variable (question)
25; 20
- 16 change in a dependent variable as product of derivative and change in independent variable (review); change in derivative as product of second derivative and change in independent variable (question)
31; 13
- 7 second derivatives and second partial derivatives; expression for change in $\partial h/\partial x$ in terms of second derivative (question)
4; 23

- 32 expression for change in $\partial h/\partial x$ in terms of second derivative (review); expression for inflow minus outflow using second derivative (question)
27; 2
- 34 definition of transmissivity; expression for inflow minus outflow for one dimensional flow through a prism of aquifer, in terms of T and $\partial^2 h/\partial x^2$; equating of this inflow minus outflow to rate of accumulation; expression for rate of accumulation in terms of storage coefficient (question)
28; 12
- 10 equating of rate of accumulation, expressed in terms of storage coefficient, to the expression for inflow minus outflow, to obtain the partial differential equation for one-dimensional nonequilibrium flow (question)
11; 24
- 19 partial differential equation for two-dimensional nonequilibrium flow; partial differential equations and their solutions; review of method of deriving partial differential equations of ground water flow

Part VI. Nonequilibrium flow to a well:

Section:

- 1 expression for flow through inner face of cylindrical element (question)
34; 36
- 15 combination of r and $\partial h/\partial r$ into a single variable; expression for inflow minus outflow for cylindrical element
30; 25
- 7 use of

$$\frac{\partial \left(r \frac{\partial h}{\partial r} \right)}{\partial r} \Delta r$$

in place of

$$\left(r \frac{\partial h}{\partial r} \right)_2 - \left(r \frac{\partial h}{\partial r} \right)_1$$

expression for

$$\frac{\partial \left(r \frac{\partial h}{\partial r} \right)}{\partial r}$$

- 26; 8
- 28 final expression for inflow minus outflow for cylindrical element; expression for rate of accumulation in storage in the element (question)
12; 16
- 37 combination of inflow minus outflow term with rate of accumulation term to obtain partial differential equation
22; 32
- 27 procedure of testing a function to determine whether it is a solution to the partial differential equation; calculation of first radial derivative of test function
4; 2

5 calculation of second radial derivation of test function
23; 9

35 calculation of time derivation of test function
3; 31

20 expressions for

$$\frac{S}{T} \frac{\partial h}{\partial t}$$

and

$$\frac{\partial^2 h}{\partial r^2} + \frac{1}{r} \frac{\partial h}{\partial r}$$

for test function

17; 24

21 verification that test function is a solution; instantaneous injection (slug test) problem; development of boundary conditions required at $t = 0$
10; 19

18 verification that test function satisfies the boundary conditions for $t = 0$; graphical demonstration of its behaviour as $t \rightarrow 0$; development of boundary condition for $r \rightarrow \infty$
29; 6

33 relation between condition that $(\partial h / \partial r) \rightarrow 0$ as $r \rightarrow \infty$ and condition that $h \rightarrow 0$ as $r \rightarrow \infty$; demonstration that test function also satisfies $h \rightarrow 0$ as $t \rightarrow \infty$; development of condition

$$V = \int_{r=0}^{\infty} S \cdot h_{r,t} \cdot 2\pi r dr$$

11; 14

13 demonstration that the test function satisfies

$$V = \int_{r=0}^{\infty} S \cdot h_{r,t} \cdot 2\pi r dr;$$

discussion of significance of slug test solution

Text-format discussion—Development of additional solutions by superposition:

(p. 112) Linearity of radial equation; superposition; equation for head at t due to injection at $t' = 0$

(p. 112) superposition to obtain effect of two injections

(p. 112) expression for head change due to instantaneous withdrawal; superposition to obtain effect of repeated bailing

(p. 113) variable rate of continuous pumping as a sequence of infinitesimal withdrawals; effect of withdrawal during an infinitesimal time dt' ; use of superposition to obtain head change due to pumping during a finite time interval

(p. 114) implementation of superposition by integration of the expression for head change due to instantaneous withdrawal, for case of variable pumping rate

(p. 115) transformation of integral into exponential integral, for case of constant pumping rate

(p. 116) definition of u ; evaluation of the exponential integral by means of series

(p. 116) definition of well function; equation for case where $h \neq 0$ prior to pumping; equation in terms of drawdown; This equation

(p. 117) development of the modified nonequilibrium (semilog approximation) formula

(p. 117) review of assumptions involved in derivation of the partial differential equation for radial flow

(p. 117) review of assumption involved in the instantaneous injection solution and in the continuous pumpage (constant rate) solution

(p. 118) review of assumptions involved in the semilog approximation; citations of literature on extensions of well-flow theory for more complex systems

Part VII. Finite-difference methods:

Section:

1 finite-difference expression for first space derivative (question)
7; 26

12 finite-difference expression for second space derivative (question)
27; 22

15 finite-difference expression for

$$\frac{\partial^2 h}{\partial x^2} + \frac{\partial^2 h}{\partial y^2}$$

(question)

28; 24

3 finite-difference expression for

$$\frac{\partial^2 h}{\partial x^2} + \frac{\partial^2 h}{\partial y^2}$$

(review);

notation convention for head at a node

14; 5

2 expression for

$$\frac{\partial^2 h}{\partial x^2} + \frac{\partial^2 h}{\partial y^2}$$

- using subscript notation convention
20; 18
- 4 third subscript convention for time axis
9; 23
- 10 expression for

$$\frac{\partial^2 h}{\partial x^2} + \frac{\partial^2 h}{\partial y^2}$$

- at a particular point and time using the subscript notation; approximations to $\partial h/\partial t$; finite forward-difference approximation to the ground water flow equation, using the subscript notation (question)
8; 19
- 16 application of forward-difference equation in predicting head values; iterative (relaxation) techniques (definition); finite-difference equation for steady-state two-dimensional flow (question)
11; 13
- 25 solution of the steady-state equation by iteration
21; 6
- 17 general discussion of numerical methods

Text-format discussion—Finite difference methods:

- (p. 136) Forward-difference and backward difference approximations to time derivative
- (p. 137) Forward-difference simulation of the ground-water flow equation; explicit method of solution
- (p. 137) Errors; stable and unstable techniques
- (p. 138) Backward-difference simulation of the ground-water flow equation; simultaneous equation sets
- (p. 139) Solution by iteration or relaxation techniques
- (p. 139) Solution of the steady-state equation by iteration
- (p. 139) Solution of the nonequilibrium equation, backward-difference simulation, by iteration
- (p. 140) Iteration levels; superscript notation; iteration parameter
- (p. 140) Successive overrelaxation; alternating direction techniques
- (p. 141) Forward-difference and backward-difference simulations of the ground-water flow equation using Δ notation
- (p. 141) Alternating direction implicit procedure
- (p. 144) Thomas algorithm for solution of equation sets along rows or columns

- (p. 147) Iteration of the steady-state equation using alternating direction method of calculation
- (p. 149) Iterative solution using the backward-difference simulation and the alternating direction technique of computation

Part VIII. Analog techniques:

Section:

- 1 Ohm's law; definitions of current and resistance
19; 8
- 6 definitions of resistivity and conductivity; Ohm's law in terms of resistivity
24; 3
- 28 Ohm's law in terms of conductivity; analogy between Ohm's law and Darcy's law for one-dimensional flow
12; 7
- 26 analogy between Darcy's law and Ohm's law for one-dimensional flow; extension to three dimensions; current density; flow of charge in a conducting sheet
25; 23
- 11 analogy between flow of charge in a conducting sheet and flow of water through a horizontal aquifer; method of setting up a steady-state analog; parallel between line of constant voltage and line of constant head (question)
16; 17
- 21 nonequilibrium modeling; storage of charge in a capacitor, and analogy to storage of ground water; capacitor equations
13; 10
- 9 relation between time rate of change of voltage and time rate of accumulation of charge for a capacitor; relation between current toward a capacitor plate and time rate of change of voltage
20; 18
- 4 relation between time rate of change of voltage and time rate of accumulation of charge for a capacitor (review); electrical continuity relation; relation between currents and time rate of change of capacitor voltage, for a system of four resistors connected to a capacitor; transformation of this relation to an equation in terms of voltages and $d\phi/dt$ (question)
15; 27
- 22 analogy between equation for capacitor—four resistor system with finite-difference form of two-dimensional ground-water flow equation; method of nonequilibrium modeling
2; 14
- 5 general discussion of the analog technique; heterogeneity; cross-sectional analogs; radial flow analogs

TECHNIQUES OF WATER-RESOURCES INVESTIGATIONS OF THE U.S. GEOLOGICAL SURVEY

The U.S. Geological Survey publishes a series of manuals describing procedures for planning and conducting specialized work in water-resources investigations. The manuals published to date are listed below and may be ordered by mail from the **U.S. Geological Survey, Books and Open-File Reports Section, Federal Center, Box 25425, Denver, Colorado 80225** (an authorized agent of the Superintendent of Documents, Government Printing Office).

Prepayment is required. Remittance should be sent by check or money order payable to U.S. Geological Survey. Prices are not included in the listing below as they are subject to change. **Current prices can be obtained** by writing to the USGS, Books and Open File Reports Section. Prices include cost of domestic surface transportation. For transmittal outside the U.S.A. (except to Canada and Mexico) a surcharge of 25 percent of the net bill should be included to cover surface transportation. When ordering any of these publications, please give the title, book number, chapter number, and "U.S. Geological Survey Techniques of Water-Resources Investigations."

- TWI 1-D1. Water temperature—influential factors, field measurement, and data presentation, by H.H. Stevens, Jr., J.F. Ficke, and G.F. Smoot, 1975, 65 pages.
- TWI 1-D2. Guidelines for collection and field analysis of ground-water samples for selected unstable constituents, by W.W. Wood. 1976. 24 pages.
- TWI 2-D1. Application of surface geophysics to ground water investigations, by A.A.R. Zohdy, G.P. Eaton, and D.R. Mabey. 1974. 116 pages.
- TWI 2-D2. Application of seismic-refraction techniques to hydrologic studies. F.P. Haem. 1988. 86 pages.
- TWI 2-E1. Application of borehole geophysics to water-resources investigations, by W.S. Keys and L.M. MacCary. 1971. 126 pages.
- TWI 3-A1. General field and office procedures for indirect discharge measurements, by M.A. Benson and Tate Dalrymple. 1967. 30 pages.
- TWI 3-A2. Measurement of peak discharge by the slope-area method, by Tate Dalrymple and M.A. Benson. 1967. 12 pages.
- TWI 3-A3. Measurement of peak discharge at culverts by indirect methods, by G.L. Bodhaine. 1968. 60 pages.
- TWI 3-A4. Measurement of peak discharge at width contractions by indirect methods, by H.F. Matthai. 1967. 44 pages.
- TWI 3-A5. Measurement of peak discharge at dams by indirect methods, by Harry Hulsing. 1967. 29 pages.
- TWI 3-A6. General procedure for gaging streams, by R.W. Carter and Jacob Davidian. 1968. 13 pages.
- TWI 3-A7. Stage measurements at gaging stations, by T.J. Buchanan and W.P. Somers. 1968. 28 pages.
- TWI 3-A8. Discharge measurements at gaging stations, by T.J. Buchanan and W.P. Somers. 1969. 65 pages.
- TWI 3-A9. Measurement of time of in streams by dye tracings, by F.A. Kilpatrick and J.F. Wilson, Jr. 1989. 27 pages.
- TWI 3-A10. Discharge ratings at gaging stations, by E.J. Kennedy. 1984. 59 pages.
- TWI 3-A11. Measurement of discharge by moving-boat method, by G.F. Smoot and C.E. Novak. 1969. 22 pages.
- TWI 3-A12. Fluorometric procedures for dye tracing, Revised, by James F. Wilson, Jr., Ernest D. Cobb, and Frederick A. Kilpatrick. 1986. 41 pages.
- TWI 3-A13. Computation of continuous records of streamflow, by Edward J. Kennedy. 1983. 53 pages.
- TWI 3-A14. Use of flumes in measuring discharge, by F.A. Kilpatrick, and V.R. Schneider. 1983. 46 pages.
- TWI 3-A15. Computation of water-surface profiles in open channels, by Jacob Davidian. 1984. 48 pages.
- TWI 3-A16. Measurement of discharge using tracers, by F.A. Kilpatrick and E.D. Cobb. 1985. 52 pages.
- TWI 3-A17. Acoustic velocity meter systems, by Antonius Laenen. 1985. 38 pages.
- TWI 3-A18. Determination of stream reaeration coefficients by use of tracers, by F.A. Kilpatrick, R.E. Rathbun, N. Yotsukura, G.W. Parker, and L.L. DeLong. 1989. 52 pages.
- TWI 3-B1. Aquifer-test design, observation, and data analysis, by R.W. Stallman. 1971. 26 pages.
- TWI 3-B2.¹ Introduction to ground-water hydraulics, a programmed text for self-instruction, by G.D. Bennett. 1976. 172 pages.
- TWI 3-B3. Type curves for selected problems of flow to wells in confined aquifers, by J.E. Reed. 1980. 106 pages.
- TWI 3-B5. Definition of boundary and initial conditions in the analysis of saturated ground-water flow systems—an introduction, by O. Lehn Franke, Thomas E. Reilly, and Gordon D. Bennett. 1987. 15 pages.

¹Spanish translation also available.

- TWI 3-B6. The principle of superposition and its application in ground-water hydraulics, by Thomas E. Reilly, O. Lehn Franke, and Gordon D. Bennett. 1987. 28 pages.
- TWI 3-C1. Fluvial sediment concepts, by H.P. Guy. 1970. 55 pages.
- TWI 3-C2. Field methods of measurement of fluvial sediment, by H.P. Guy and V.W. Norman. 1970. 59 pages.
- TWI 3-C3. Computation of fluvial-sediment discharge, by George Porterfield. 1972. 66 pages.
- TWI 4-A1. Some statistical tools in hydrology, by H.C. Riggs. 1968. 39 pages.
- TWI 4-A2. Frequency curves, by H.C. Riggs. 1968. 15 pages.
- TWI 4-B1. Low-flow investigations, by H.C. Riggs. 1972. 18 pages.
- TWI 4-B2. Storage analyses for water supply, by H.C. Riggs and C.H. Hardison. 1973. 20 pages.
- TWI 4-B3. Regional analyses of streamflow characteristics, by H.C. Riggs. 1973. 15 pages.
- TWI 4-D1. Computation of rate and volume of stream depletion by wells, by C.T. Jenkins. 1970. 17 pages.
- TWI 5-A1. Methods for determination of inorganic substances in water and fluvial sediments, by M.W. Skougstad and others, editors. 1979. 626 pages.
- TWI 5-A2. Determination of minor elements in water by emission spectroscopy, by P.R. Barnett and E.C. Mallory, Jr. 1971. 31 pages.
- TWI 5-A3. Methods for the determination of organic substances in water and fluvial sediments, edited by R.L. Wershaw, M.J. Fishman, R.R. Grabbe, and L.E. Lowe. 1987. 80 pages. This manual is a revision of "Methods for Analysis of Organic Substances in Water" by Donald F. Goerlitz and Eugene Brown, Book 5, Chapter A3, published in 1972.
- TWI 5-A4. Methods for collection and analysis of aquatic biological and microbiological samples, edited by P.E. Greeson, T.A. Ehlike, G.A. Irwin, B.W. Lium, and K.V. Slack. 1977. 332 pages.
- TWI 5-A5. Methods for determination of radioactive substances in water and fluvial sediments, by L.L. Thatcher, V.J. Janzer, and K.W. Edwards. 1977. 95 pages.
- TWI 5-A6. Quality assurance practices for the chemical and biological analyses of water and fluvial sediments, by L.C. Friedman and D.E. Erdmann. 1982. 181 pages.
- TWI 5-C1. Laboratory theory and methods for sediment analysis, by H.P. Guy. 1969. 58 pages.
- TWI 6-A1. A modular three-dimensional finite-difference ground-water flow model, by Michael G. McDonald and Arlen W. Harbaugh. 1988. 586 pages.
- TWI 7-C1. Finite difference model for aquifer simulation in two dimensions with results of numerical experiments, by P.C. Trescott, G.F. Pinder, and S.P. Larson. 1976. 116 pages.
- TWI 7-C2. Computer model of two-dimensional solute transport and dispersion in ground water, by L.F. Konikow and J.D. Bredehoeft. 1978. 90 pages.
- TWI 7-C3. A model for simulation of flow in singular and interconnected channels, by R.W. Schaffranek, R.A. Baltzer, and D.E. Goldberg. 1981. 110 pages.
- TWI 8-A1. Methods of measuring water levels in deep wells, by M.S. Garber and F.C. Koopman. 1968. 23 pages.
- TWI 8-A2. Installation and service manual for U.S. Geological Survey monometers, by J.D. Craig. 1983. 57 pages.
- TWI 8-B2. Calibration and maintenance of vertical-axis type current meters, by G.F. Smoot and C.E. Novak. 1968. 15 pages.

INTRODUCTION TO GROUND-WATER HYDRAULICS—A PROGRAMED TEXT FOR SELF-INSTRUCTION

By Gordon D. Bennett

Instructions to the Reader

This programed text is designed to help you learn the theory of ground-water hydraulics through self-study. Programed instruction is an approach to a subject, a method of learning; it does not eliminate mental effort from the learning process. Some sections of this program need only be read; others must be worked through with pencil and paper. Some of the questions can be answered directly; others require some form of calculation. You may have frequent occasion, as you work through the text, to consult standard texts or references in mathematics, fluid mechanics, and hydrology.

In each of the eight parts of the text, begin the programed instruction by reading Section 1. Choose an answer to the question at the end of the section, and turn to the new sec-

tion indicated beside the answer you have chosen. If your answer was correct, you will turn to a section containing new material and another question, and you may proceed again as in Section 1. If your answer was not correct, you will turn to a section which contains some further explanation of the earlier material, and which directs you to go back for another try at the question. Usually, in this event, it will be worthwhile to reread the material of the earlier section. Continue in this way through the program until you reach a section indicating the end of the part. Note that although the sections are arranged in numerical order within each of the eight parts, you would not normally proceed in numerical sequence (Section 1 to Section 2 and so on) through the instruction.

Part I. Definitions and General Concepts

Introduction

In Part I, certain concepts which are frequently used in ground-water hydraulics are introduced. Among these are porosity, specific discharge, hydraulic head, and fluid pressure. Rigorous development of theorems

relating to these terms is not attempted. The material is intended only to introduce and define these terms and to provide an indication of their physical significance.

The porosity of a specimen of porous material is defined as the ratio of the volume of open pore space in the specimen to the bulk volume of the specimen.

0.5 cubic feet
0.2 cubic feet
0.8 cubic feet

Turn to Section:
13
18
9

QUESTION

What volume of solid material is present in 1 cubic foot of sandstone, if the porosity of the sandstone is 0.20?

1.

Nowhere in Part I is there an instruction to turn to Section 2. Perhaps you have just read Section 1 and have turned to Section 2 without considering the question in Section 1. If so, return to Section 1, choose an answer

to the question, and turn to the section indicated opposite the answer you select.

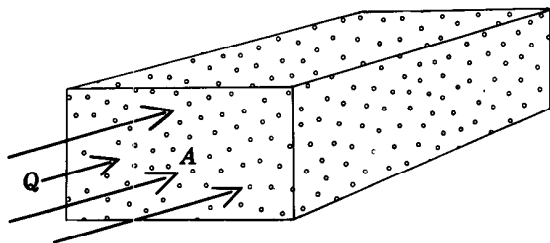
2.

Your answer in Section 6 is correct. Any flow path between *A* and *B* will be longer than the linear distance *AB*; it is generally impossible to know the actual distance that a particle of fluid travels in moving through a section of porous material.

In the same way, it is difficult to know the actual cross-sectional area of the flow, when dealing with flow in a porous medium. Any cross-sectional area selected will be occupied partly by grains of solid material and partly by pores containing the fluid. For this reason,

a problem may arise if we attempt to define average fluid velocity as a ratio of discharge to cross-sectional area, as is customarily done in open-flow hydraulics.

Con.— 3.



QUESTION

In the block of saturated porous material in the figure, a fluid discharge, Q , is crossing the area, A , at right angles. A represents the gross area of the block face, including both solid particles and fluid-filled pore space. The quotient Q/A would be:

less than	14
equal to	28
greater than	10

Turn to Section:

the average velocity of the fluid particles

3.—Con.

Your answer in Section 6 is not correct. The particle would move a distance equal to the linear interval AB if the two points were

connected by a straight capillary tube, but the probability of such a connection is essentially zero in a normal porous medium. In general, the possible paths of flow between any two points will be tortuous in character.

Return to Section 6 and select another answer.

4.

Your answer in Section 22 is not correct. Pressure does represent potential energy per unit volume due to the forces transmitted

through the surrounding fluid, but z represents potential energy per unit *weight* due to elevation. The question asked for total potential energy per unit volume.

Return to Section 22 and select another answer.

5.

Your answer in Section 9 is correct. Thirty percent of the interconnected pore space in a porous medium whose effective porosity is 0.20 is 6 percent of the bulk volume, or 0.06 cubic feet. In the remainder of this program, fully saturated conditions will be assumed unless unsaturated flow is specifically mentioned.

Variation in the flow velocity of an individual fluid particle is inherent in the nature of flow through porous media. Within an individual pore, boundary resistance causes the velocity to decrease from a maximum along

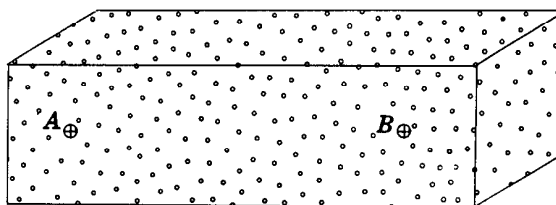
the centerline to essentially zero at the pore wall. Another form of velocity variation is imposed by the tortuous character of the flow—that is, the repeated branching and reconnecting of flow paths, as the particles of fluid make their way around the individual grains of solid. This anastomizing or braided pattern causes the velocity of a fluid particle to vary from point to point in both magnitude and direction, even if its motion occurs along the centerline of the pore space. However, if we view a small segment of the medium but one which is still large enough to contain a great number of pores, we find that the microscopic components of motion cancel in all except one resultant direction of flow.

6.—Con.

QUESTION

In the porous block in the figure, a particle of fluid moving from point A to point B would travel a distance:

	Turn to Section:
greater than the linear distance AB	3
equal to the linear distance AB	4
less than the linear distance AB	21



Con.— 6.

Your answer in Section 16 is not correct. If we were considering the height of a static column of water above a point, which as we have seen is given by $p/\rho g$, we would be dealing with dimensions of potential energy per unit weight. The question in Section 16, however, relates to the units of pressure alone. These units are force per unit area—for example, pounds of force per square foot of area, which can be written

in the form pounds/ft². Now we may “multiply” these units by the term ft/ft to obtain an equivalent set of units applicable to pressure.

Return to Section 16 and choose another answer.

7.

Your answer, $p + \rho g z$, in Section 22 is correct. We have seen that pressure is equivalent to potential energy per unit volume attributable to forces transmitted through the surrounding fluid. Potential energy per unit volume due to elevation is obtained by multiplying the potential energy per unit weight due to elevation—that is, z —by the weight per unit volume, ρg . The total potential energy per unit volume is then the sum of these two terms, that is, $p + \rho g z$.

No discussion of flow energy would be complete without mention of kinetic energy. In the mechanics of solid particles, the kinetic energy, KE, of a mass, m , moving with a velocity v , is given by

$$KE = mv^2/2.$$

Now suppose we are dealing with a fluid of mass density ρ . We wish to know the kinetic energy of a volume V of this fluid which is moving at a velocity v . The mass of the volume is ρV , and the kinetic energy is thus

$$\rho V v^2 / 2.$$

If we divide by the volume, V , we obtain

$$\rho v^2 / 2$$

as the kinetic energy per unit volume of fluid; and dividing this in turn by the weight per unit volume, ρg , gives $v^2/2g$ as the kinetic energy per unit weight of fluid. Each of these kinetic energy expressions is proportional to the square of the velocity. The velocities of flow in ground-water movement are almost always extremely low, and therefore the kinetic energy terms are extremely small compared to the potential energy terms. Consequently, in dealing with ground-water problems we can generally neglect the kinetic energy altogether and take into account only the potential energy of the system and the losses in potential energy due to friction. This is an important respect in which ground-water hydraulics differs from the hydraulics of open flow.

This discussion concludes Part I. In Part II we will consider Darcy's law, which relates the specific discharge, q , to the gradient of hydraulic head, in flow through porous media.

8.

Your answer in Section 1 is correct; if 0.20 of the cube is occupied by pore space, 0.80 of its volume must be solid matter. In ground-water studies we are normally interested in the interconnected, or effective, porosity, which is the ratio of the volume of interconnected pore space—excluding completely isolated pores—to the bulk volume. As used in this text the term “porosity” will always refer to the interconnected or effective porosity. Ground water is said to occur under saturated conditions when all interconnected pore space is completely filled with water,

9.

Your answer in Section 3 is not correct. The area A represents the gross cross-sectional area of the porous block, normal to the direction of flow. A part of this area is occupied by grains of solid, and a part by open pore space. Let us say that 20 percent of the area A represents pore space; the actual

10.

Your answer in Section 14 is not correct. The column of water in the piezometer is static, but h_p is the elevation of the top of this column above the point of measurement,

11.

Your answer in Section 9 is not correct. Saturation is expressed here as a percentage of the interconnected pore space, not as a percentage of the sample volume; that is,

12.

and it occurs under unsaturated conditions when part of the pores contain water and part contain air. In problems of unsaturated flow, the degree of saturation is often expressed as a percentage of the interconnected pore space.

QUESTION

What volume of water is contained in 1 cubic foot of porous material, if the effective porosity is 0.20 and saturation expressed as a percentage of the interconnected pore space is 30 percent?

Turn to Section:

0.30 cubic feet	12
0.06 cubic feet	6
0.20 cubic feet	9

cross-sectional area available for the flow is thus $0.2 A$. If we were willing to take the ratio of discharge to *flow* area as equal to the average velocity, without considering any other factor, we would have to use the ratio $Q/0.2A$. The actual average particle velocity would presumably exceed even this figure, because of the excess distance traveled in tortuous flow.

Return to Section 3 and choose another answer.

0 (h_p is sometimes referred to as the pressure head at point 0). We have defined *head* as the elevation *above datum* of the top of a static column of water that can be supported at the point.

Return to Section 14 and choose another answer.

30 percent of the interconnected pore space is occupied by water. Since the effective porosity was given as 0.20, and the sample volume as 1 cubic foot, the volume of interconnected pore space is 0.20 cubic feet.

Return to Section 9 and choose another answer.

Your answer in Section 1 is not correct. Porosity is defined by the equation

$$n = \frac{V_p}{V_g} = \frac{V_p}{V_s + V_p}$$

where V_p is the volume of pore space in the specimen, V_g is the gross volume of the specimen, and V_s is the volume of solid material in the specimen (note that $V_g = V_s + V_p$). The

question in Section 1 asked for the volume of solid material, V_s , in a specimen for which the gross volume, V_g , is 1 cubic foot and the porosity, n , is 0.20.

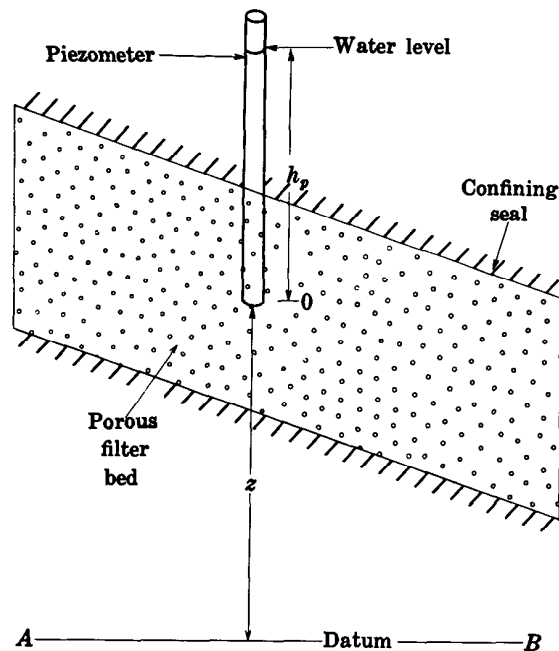
Return to Section 1 and choose another answer.

13.

Your answer in Section 3 is correct. Q/A will be less than the average velocity of fluid motion since the gross cross-sectional area, A , will be greater than the actual cross-sectional area of flow. In many porous media, the ratio of actual area of flow to gross cross-sectional area can be taken as equal to the interconnected porosity of the material.

We have seen that it is generally difficult or impossible to know or measure the actual velocity of fluid motion or the actual cross-sectional area of flow in a porous medium. For this reason, we usually work in terms of discharge and gross cross-sectional area. That is, we use the quantity Q/A , where Q is the discharge through a segment of porous material, and A is the gross cross-sectional area of the segment. This quantity is referred to as the specific discharge, or specific flux, and is designated by the symbol q .

Another quantity we will use frequently is the static head, or simply the head. In ground-water problems, the head at a point is taken as the elevation, above an arbitrary datum, of the top of a static column of water that can be supported above the point. In using this definition, we assume that the density of the water in the measuring column is equal to that of the ground water, and that the density of the ground water is uniform.



QUESTION

The diagram represents an enclosed porous filter bed; the plane AB is taken as the datum and a piezometer is inserted to the point 0. What is the head at point 0?

- The distance h_p
- The distance z
- The distance $h_p + z$

Turn to Section:

11

17

24

14.

Your answer in Section 16 is not correct. Pressure is usually expressed as force per unit area—for example, as pounds per square foot, which may be written pounds/ft². A term having units of work or energy per unit area, such as ft-pounds/ft², would represent

15.

Your answer, $p/\rho g$, in Section 24 is correct. The column of water inside the pipe is static and must obey the laws of hydrostatics. Thus the pressure at the bottom of the pipe is related to the height of the column of water in the pipe by Pascal's law, which here takes the form

$$p = \rho g h_p,$$

or

$$h_p = p/\rho g$$

h_p thus actually serves as a measure of the pressure at the point occupied by the end of the pipe and, for this reason, is termed the pressure head at that point. It is added to the elevation of the point to yield the head at the point.

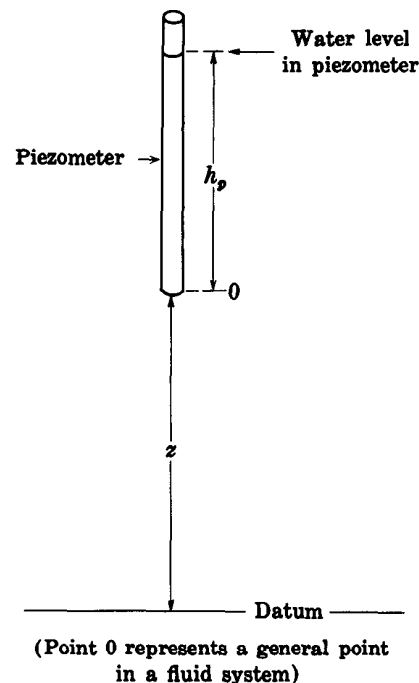
Head in ground water is actually a measure of the potential energy per unit weight of water. This is an important concept.

The elevation term, z , in the diagram represents the potential energy of a unit weight of water at point 0 that accrues from the position of the point above the datum. For example, if z is 10 feet, 10 pounds of water in the vicinity of point 0 could accomplish 100 foot-pounds of work in falling to the datum; the potential energy per unit weight of water at point 0 due to the elevation of the point alone would thus be 10 feet. Similarly, the pressure term, h_p , represents the potential energy of a unit weight of water at point 0 originating from the forces exerted on the point through the surrounding fluid. This concept is considered further in the following sections.

16.

the product of pressure and a term having units of distance, feet. We are interested here in an equivalent set of units for pressure alone. Now note that if a pressure term were multiplied by a dimensionless factor having "units" of ft/ft, we would obtain a result still having the units of pressure.

Return to Section 16 and select another answer.



QUESTION

Pressure is normally thought of as force per unit area. Dimensionally this is equivalent to:

energy per unit weight	7
energy per unit volume	26
work per unit area	15

Turn to Section:

Your answer in Section 14 is not correct. z is the elevation of the point above the datum; we defined head as the elevation, above datum, of the top of a static column of water that can be supported at the point. The column of water in the piezometer is static

when conditions in the porous medium are at equilibrium.

Return to section 14 and choose another answer.

17.

Your answer in Section 1 is not correct. If the porosity is 0.20, there will be 0.20 cubic foot of pore space in a specimen of 1-cubic-foot volume. The question asked for the volume of solid material in the specimen.

Return to Section 1 and choose another answer.

18.

Your answer in Section 24 is not correct. The column of water inside the pipe is static and must obey the laws of hydrostatics. The pressure at a depth d beneath the water surface, in a body of static water, is given by Pascal's law as

$$p = \rho g d$$

where again ρ is the mass density of the water, g is the acceleration due to gravity, and the pressure at the water surface is taken as zero. This relation may be applied

to the water inside the pipe in the question of Section 24. If you are not familiar with Pascal's law it would be useful to read through a discussion of hydrostatics, as given in any standard physics text, before proceeding further in the program.

Return to Section 24 and choose another answer.

19.

Your answer in Section 26 is not correct. Potential energy is a scalar term; when it consists of contributions from different sources, these are simply added to obtain the total potential energy. The potential energy of the unit weight of water due to its eleva-

tion is z , while that due to the forces exerted on it through the surrounding water is h_p .

Return to Section 26 and choose another answer.

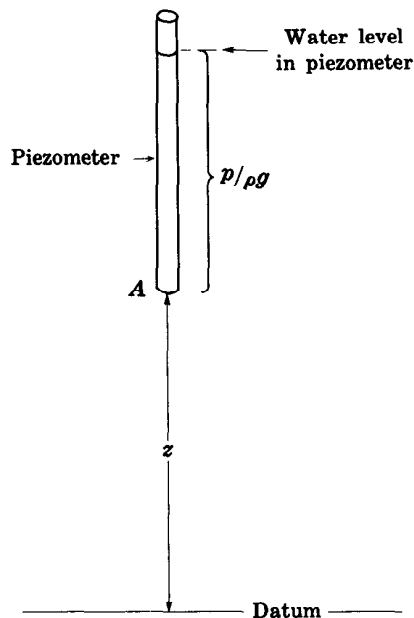
20.

Your answer in Section 6 is not correct. The line AB is, of course, the shortest distance between the two points, and no flow path could be any shorter than this.

Return to Section 6 and select another answer.

21.

Your answer in Section 26 is correct. The unit weight of water has hydraulic potential energy due to its elevation and due to the forces exerted on it by the surrounding fluid. The potential energy due to its elevation is z , and the potential energy due to the forces exerted on it through the surrounding fluid is $p/\rho g$ or h_p . The sum of z and h_p is of course the head, h , (as used in ground-water hydraulics) at the point in question. The two terms making up the head at a point—the elevation of the point itself above datum and the elevation of the top of a static column of water that can be supported above the point—measure respectively the two forms of hydraulic potential energy per unit weight. Their sum indicates the total hydraulic potential energy per unit weight of fluid at the point.



QUESTION

Which of the following expressions would indicate total hydraulic potential energy of a unit *volume* of fluid in the vicinity of point A in the diagram?

22.

- $p + \rho g z$
- $p + z$
- $p/\rho g + z$

Turn to Section:	
	8
	5
	27

Your answer in Section 26 is not correct. z represents the potential energy of a unit weight of water in the vicinity of point 0, due to its elevation above the datum. A unit

23.

weight of water in this vicinity will also possess potential energy because of the forces exerted upon it through the surrounding water. The question asked for total hydraulic potential energy.

Return to Section 26 and select another answer.

Your answer in Section 14 is correct. Head consists of two terms in ground-water systems: the elevation of the point itself above datum, and the height of a static column of

24.—Con.

water that can be supported above the point. In this case, the column of water in the piezometer is the static column above the point.

The height of the column of water above the point is a measure of the pressure at the point and is sometimes termed the pressure

head. Readers familiar with open flow hydraulics may recognize that the head we have defined here differs from the total head used in open flow hydraulics in that the velocity term, $v^2/2g$, is missing. Velocities of flow are usually small in ground-water systems, and the term $v^2/2g$ is almost always negligible in comparison to the elevation and pressure terms.

QUESTION

Suppose a pipe, open only at the top and bottom, is driven into the ground. The bottom of the pipe comes to rest at a point below the water table where the pressure is p . Water rises inside the pipe to a height h_p above the

lower end of the pipe. The pressure on the water surface within the pipe (which is actually the atmospheric pressure) is here taken as zero. The height of the column of water inside the pipe, above the bottom of the pipe, will be given by:

$h_p = p/\rho g$	Turn to Section: 16
$h_p = g/\rho p$	25
$h_p = \rho p g$	19

where ρ is the water density, or mass per unit volume, and g is the gravitational constant.

Con.— 24.

Your answer in Section 24 is not correct. Pressure within a body of static water varies in accordance with Pascal's law, which may be stated

$$p = \rho g d$$

where ρ is the mass density of water, g is the acceleration due to gravity, and d is the depth below the surface at which the pressure is measured. The pressure on the upper surface of the water (sometimes denoted p_0 in textbooks of hydraulics) is here considered to be zero. If you are not familiar with this relation, it would be a good idea to read through

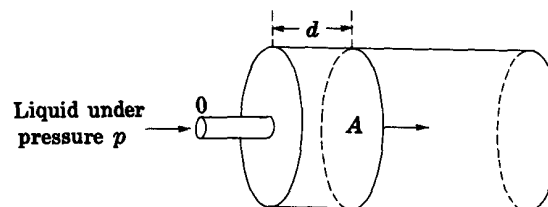
a discussion of hydrostatics, as presented in any standard physics text, before proceeding further with the program.

In the problem of Section 24, the column of water in the pipe is static, and Pascal's law may be used to give the pressure at any point within this column—even at its base, where it joins the ground-water system.

Return to Section 24 and choose another answer.

25.

Your answer in Section 16 is correct. Pressure may in fact be thought of as potential energy per unit volume of liquid. Physically, this concept is perhaps most easily appreciated using the example of a simple hydraulic cylinder, or hydraulic press, shown schematically in the diagram. Liquid under a pressure p is fed in through the port at 0. As the liquid enters, the piston is displaced to the right. Pressure is a measure of force per unit area, and it follows that the total force on the piston is given by the product of the pressure, p , and the face area of the



Con.— 26.

piston, which we designate A . Thus, $F = p \times A$, where F is the force on the piston.

The work accomplished in moving the piston is given as the product of the force and the distance through which it acts. If the piston moves a distance d , the work done is given by

$$W = F \times d = p \times A \times d$$

where W is the work accomplished in moving the piston. The product $A \times d$ is the volume of fluid in the cylinder at the completion of the work; and we could say that this volume of liquid is capable of doing the work W , provided the liquid is at the pressure p .

Potential energy is often termed the ability to do work. That is, if a system is capable of doing 10 foot-pounds of work, we say that it possesses a potential energy of 10 foot-pounds. In the case of our cylinder, the potential energy we assign depends upon how far we are willing to let the piston travel. If the piston is allowed to travel a distance $d = 5$, the work that can be done is $p \times 5A$; if the piston is allowed to travel a distance $d = 10$, the work that can be done is $p \times 10A$. Thus the assignment of a potential energy in this case is not altogether straightforward, since the distance which the piston will travel—or, equivalently, the volume of fluid which will be admitted to the cylinder under the pressure p —must be specified before the potential energy can be assigned. In this case, therefore, it is more convenient to talk about a potential energy per unit volume of liquid. For example, if we are told that the potential energy is 10 foot-pounds per cubic foot of water in the cylinder, we can calculate the particular potential energy associated with the admission of any specified volume of fluid to the cylinder. The work which can be done if a volume $A \times d$ of liquid is admitted is $p \times A \times d$; dividing this by the volume $A \times d$ gives the work which can be done per unit volume of liquid—that is, the potential energy per unit volume of liquid. This potential energy per unit volume turns out to be

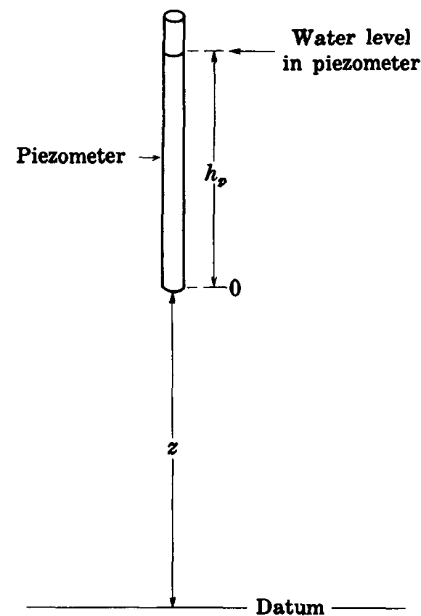
the pressure, p , under which the fluid is admitted to the cylinder.

This concept of pressure as potential energy per unit volume can be extended to general systems of flow, provided that we understand this potential energy to be only that due to forces exerted on a fluid element by the surrounding fluid. To obtain total potential energy, we would have to add the potential energy due to the force of gravity acting directly on the fluid element.

If pressure, representing potential energy per unit volume, is in turn divided by ρg , weight per unit volume, we obtain $p/\rho g$ —or simply h_p , the height of a static column of water above the point—as the potential energy per unit weight that is due to the forces transmitted through the surrounding fluid.

QUESTION

Referring to the diagram, which of the following expressions will give the total hy-



draulic potential energy of a unit weight of water located in the vicinity of point 0?

Turn to Section:

z	23
$h_p + z$	22
$h_p - z$	20

26.—Con.

Your answer in Section 22 is not correct. We have already seen that $p/\rho g + z$ was equal to the total potential energy per unit weight of water. To obtain potential energy per unit volume, we must multiply by weight per unit volume.

Return to Section 22 and choose another answer.

27.

Your answer in Section 3 is not correct. The quotient, Q/A , would yield an average velocity if we were dealing with an open flow. Here, however, A is not the cross-sectional area of flow; it is, rather, the cross-sectional area of the porous block normal to the flow. Only that fraction of this area which consists of open pore space can be considered the cross-sectional area of flow. Suppose, for

example, that this pore area represents 20 percent of the total face area, A . The flow area would then be $0.2 A$.

Return to Section 3 and choose another answer.

28.

Your answer in Section 9 is not correct. The volume of interconnected pore space is 0.20 cubic feet, but since saturation is less than 100 percent, the volume of water in the specimen cannot equal the volume of interconnected pore space. Keep in mind that we are expressing saturation as a percentage of the interconnected pore space.

Return to Section 9 and choose another answer.

29.

Part II. Darcy's Law

Introduction

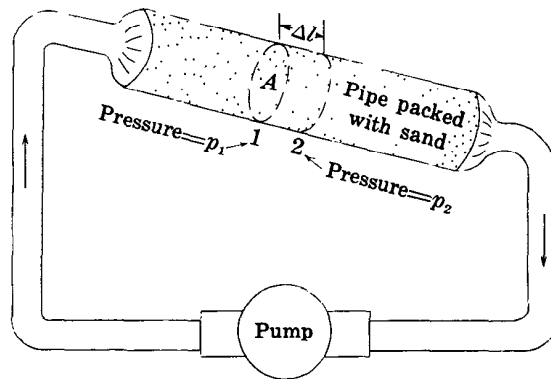
Part II gives a development of Darcy's law. This law relates specific discharge, or discharge per unit area, to the gradient of hydraulic head. It is the fundamental relation governing steady-state flow in porous media. The development given here should not be taken as a rigorous derivation; it is no more

than a plausibility argument, and is presented in order to give the reader some appreciation for the physical significance of the relation.

Following the program section of Part II a short discussion on generalization of Darcy's law is given in text format.

(I)

In mechanics, when considering the steady motion of a particle, it is customary to equate the forces producing the motion to the frictional forces opposing it. The same approach may be followed in considering the steady movement of fluid through a porous medium. In studying the motion of a solid particle through a fluid, we find that the force of friction opposing the motion is proportional to the velocity of the particle. Similarly, in flow through a porous medium, we will assume that the frictional forces opposing the flow are proportional to the fluid velocity. Our approach, then, will be to obtain expressions for the forces driving a flow and to equate these to the frictional force opposing the flow, which will be assumed proportional to the velocity. More exactly, we will take the vector sum of the forces driving and opposing the flow and set this equal to zero. What we are saying is that because the fluid motion is steady—that is, because no acceleration is observed—the forces on the fluid must be in balance, and therefore that their vector sum is zero, at all points. The equation that we obtain from this process of balancing forces



will be a form of Darcy's law. We begin by considering the forces which drive the flow.

QUESTION

Suppose we have a pipe packed with sand, as in the diagram. The porosity of the sand is n . Liquid of density ρ is circulated through the pipe by means of a pump. The dotted lines mark out a small cylindrical segment in the pipe, of length Δl , and of cross-sectional area A , equal to that of the pipe. A

(1)—Con.—

small volume, or element, of the moving fluid occupies this segment. The fluid pressure at point 1, at the upstream side of the segment, is p_1 .

Which of the following expressions would best represent the force exerted on the up-

stream face of the fluid element by the adjacent fluid element?

$p_1 A$	Turn to Section:	25
$p_1 n A$		8
$p_1 \rho g$		16

(2)—

Your answer in Section 19,

$$-\frac{1}{k} \mu Q (\Delta l \cdot n \cdot A),$$

is not correct. Our assumptions were that the frictional retarding force would be proportional in some way to the dynamic viscosity (μ), to the volume of fluid in the element ($\Delta l \cdot n \cdot A$), and to the specific discharge, or flow per unit area (Q/A). While the answer

which you have chosen is not incompatible with these assumptions, it does not fit them as well as one of the other answers. Your answer assumes the retarding force to be proportional more particularly to the full discharge, Q , than to the specific discharge, Q/A .

Return to Section 19 and choose another answer.

(3)—

Your answer in Section 26 is not correct. The term $\Delta l \cdot n \cdot A$ gives the volume of fluid in the element; the question asked for the mass of fluid in the element. Keep in mind that ρ ,

the density of the fluid, represents its mass per unit volume.

Return to Section 26 and choose another answer.

(4)—

Your answer in Section 35 is not correct. The term $\sqrt{(\Delta z)^2 + (\Delta x)^2}$ is obviously equal to Δl , so that the answer you selected is equivalent to the term $\rho \cdot n \cdot A \cdot g \cdot \Delta l$. But as we saw in Section 15, this term gives the magnitude of the *total* gravitational force on our fluid element; what we want here is an ex-

pression for the *component* of this total force in the direction of flow. We have seen that this component is given by the expression $\rho \cdot n \cdot A \cdot g \cdot \Delta l \cdot \cos \gamma$; the idea of the question is to find a term equivalent to $\cos \gamma$ and to substitute it into the above expression.

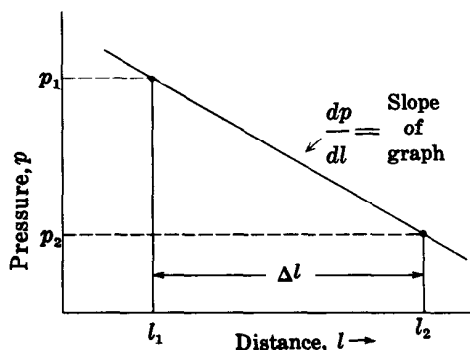
Return to Section 35 and choose another answer.

(5)

Your answer in Section 31,

$$\frac{dp}{dl}nA,$$

is not correct. The expression obtained previously for the net force was $(p_1 - p_2)nA$, or $-\Delta p nA$. You have substituted the pressure *gradient*, or rate of pressure change per foot, for the small pressure *change*, $-\Delta p$. To obtain a net change, or increment, from a gradient, or rate of change per unit distance, we must multiply the rate per unit distance by the distance over which this change takes place. For example, dp/dl in the figure represents the slope of a graph of pressure, p , versus distance, l . To obtain the pressure *change*, $p_2 - p_1$, we must multiply this slope by the length of the interval, Δl ; and since we actually require the quantity $p_1 - p_2$, we must insert a negative sign. (In the situation shown at left, p_1 is greater than p_2 —that is, pressure is decreasing in the direction of flow, l . The derivative dp/dl is therefore an



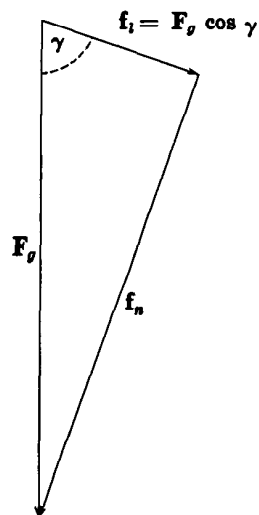
$$p_2 - p_1 = \text{Pressure change, } \Delta p = \frac{dp}{dl} \times \Delta l$$

intrinsically negative quantity itself—the graph has a negative slope. By inserting another negative sign, we will obtain a positive result for the term $p_1 - p_2$.)

Return to Section 31 and choose another answer.

(6)

Your answer in Section 33 is not correct. The term $\rho \cdot n \cdot \Delta l \cdot A \cdot g$ gives the magnitude of the total gravitational force vector, F_g . However, we require the component of this force vector in the direction l since only this component is effective in producing flow along the pipe. In the vector diagram, the length of the arrow representing the gravitational force, F_g , is proportional to the magnitude of that force, and the length of the arrows representing the two components, f_i and f_n , are proportional to the magnitudes of those components. Using a diagram to show the resolution of a vector into its components makes it easy to visualize the following general rule: the magnitude of the component of a vector in a given direction is obtained by multiplying the magnitude of the vector by the cosine of the angle between the direction of the vector and the direction in which the component is taken.



Return to Section 33 and choose another answer.

(7)

Your answer in Section 28,

$$\frac{Q}{A} = -K \frac{dh}{dl},$$

is correct. This relation between specific discharge and head gradient, or hydraulic gradient, dh/dl , was obtained experimentally by Henri Darcy (1856) and is known as Darcy's law for flow through porous media. The constant K , in the current usage of the U.S. Geological Survey, is termed the hydraulic conductivity and has the dimensions of a velocity. The constant k , again in the current usage of the Geological Survey, is termed the intrinsic permeability; its dimensions are $(\text{length})^2$, and its units depend upon the units of density and viscosity employed. In the current usage of the Geological Survey, where ρ is measured in kg/m^3 , g in m/s^2 , and μ in $\text{kg}/(\text{m s})$, k would have the units of m^2 .

As noted in Section 28, hydraulic conductivity, K , is related to intrinsic permeability, k , by the equation

$$K = k \frac{\rho g}{\mu}$$

where ρ is the fluid density, μ the dynamic viscosity of the fluid, and g the gravitational constant. Hydraulic conductivity thus incorporates two properties of the fluid and cannot be considered a property of the porous medium alone. Intrinsic permeability, on the other hand, is normally considered to be only a property of the porous medium. In ground-water systems, variations in density are normally associated with variations in dis-

solved-mineral content of the water, while variations in viscosity are usually due to temperature changes. Thus in problems involving significant variations in mineral content or in water temperature, it is preferable to utilize intrinsic permeability.

The entire theory of steady-state flow through porous media depends upon Darcy's law. There are certain more general forms in which it may be expressed to deal with three-dimensional motion; some of these are considered in the text-format discussion at the end of this chapter. The development presented in this chapter involves numerous arbitrary assumptions, and thus should not be considered a theoretical derivation of Darcy's law. It has been presented here to illustrate, in a general way, the physical significance of the terms appearing in the law.

QUESTION

Consider the following statements:

- ground water flows from higher elevations to lower elevations.
- ground water flows in the direction of decreasing pressure.
- ground water moves in the direction of decreasing head.

Based on Darcy's law as given in this chapter, which of these statements should always be considered true?

all three	Turn to Section: 29
(b) and (c) but not (a)	13
only (c)	21

(8)

Your answer, $p_1 n A$, in Section 1 is correct. The overall cross-sectional area of the upstream face of the segment is A . The area of fluid in the upstream face is nA , if we assume the ratio between fluid area and overall area to be equal to the porosity. The pressure, or force per unit area, multiplied

by the fluid area then gives the total force on the fluid element through the upstream face. Similarly, if p_2 is the fluid pressure at the downstream face, $p_2 n A$, gives the magnitude of the force exerted on the downstream face of the fluid element by the adjacent downstream element.

(8)—**Con.**—

QUESTION

Let us assume that the pressure p_1 is greater than the pressure p_2 . Which of the following expressions would best represent the *net* pressure-force on the element in the direction of flow?

$$p_1 n A + p_2 n A$$

$$\frac{p_1 n A + p_2 n A}{2}$$

$$p_1 n A - p_2 n A$$

Turn to Section:

23

12

31

(9)—

Your answer in Section 28 is not correct. We saw in Part I that head, h , was given by

$$h = \frac{p}{\rho g} + z.$$

It follows that

$$\frac{dh}{dl} = \frac{d(p/\rho g)}{dl} + \frac{dz}{dl}.$$

Use this result in selecting a new answer to the question of Section 28.

(10)—

Your answer in Section 11 is not correct. We have obtained expressions for two forces acting in the direction of flow—the net pressure force, which was calculated as the difference between forces exerted on the upstream and downstream faces of the element by adjacent elements of fluid (see Section 26); and the component of the gravitational force in the direction of flow (see Section 11). The question asks for the combined net force due to both pressure and gravity.

Forces are combined by means of vector addition. In this case, however, the net pressure force and the component of gravity we are considering are oriented in the same direction—in the direction of flow. Vector addition in this instance therefore becomes a simple addition of the magnitudes of the two terms.

Return to Section 11 and choose another answer.

(11)—

Your answer,

$$\rho \cdot n \cdot \Delta l \cdot A \cdot g \frac{\Delta z}{\Delta l},$$

in Section 35, is correct. $\Delta z/\Delta l$ is the equivalent of $\cos \gamma$; it simply gives the change in elevation per unit distance *along the path of flow*. (It thus differs from *slope* which by definition is the change in elevation per unit horizontal distance.) In the notation of calculus, $\Delta z/\Delta l$ would be represented by the derivative, dz/dl , implying the limiting value

of the ratio $\Delta z/\Delta l$ as smaller and smaller values of Δl are taken. The force component along the pipe must be positive, or oriented in the direction of flow, if z decreases in the direction of flow—that is, if dz/dl is negative. It must be negative, or oriented against the flow, if z increases in the direction of flow—that is if dz/dl is positive. We therefore introduce a negative sign, so that we have finally

$$f_1 = -\rho \cdot n \cdot A \cdot \Delta l \cdot g \cdot dz/dl$$

where f_1 is the component of the gravitational

(11)—**Con.**—

force parallel to the pipe, as in Section 33. The total force driving the flow is the sum of this gravity component and the pressure force.

QUESTION

Which of the following expressions would give the net force on the fluid in the direction of flow, due to pressure and gravity together?

$$\left(-\frac{dp}{dl} - \rho g \frac{dz}{dl} \right) \Delta l \cdot n \cdot A$$

Turn to Section:

19

$$-\frac{dp}{dl} \cos \gamma + \rho \cdot n \cdot \Delta l \cdot A \cdot g \cdot \frac{dz}{dl}$$

24

$$-\rho \cdot n \cdot \Delta l \cdot A \cdot g \cdot \frac{dz}{dl} - \frac{dp}{dl}$$

10

(12)—

Your answer in Section 8 is not correct. The expression $(p_1 n A + p_2 n A)/2$ would be approximately equal to the force in the direction of flow against a cross-sectional area taken at the midpoint of our fluid element; it does not give the *net* force on the element itself in the direction of flow.

The fluid element extends along the pipe a short distance. Over this distance, pressure decreases from p_1 at the upstream face to p_2 at the downstream face. The force on the element at the upstream face is the force acting in the direction of flow; the force on

the element at the downstream face is a force acting against the direction of flow. That is, it is a "back push" from the adjacent fluid element, against the element we are considering. Its magnitude is again given as a product of pressure, porosity, and face area, $p_2 n A$, but we now insert a negative sign to describe the fact that it acts in opposition to the force previously considered. The net force in the direction of flow is obtained by algebraic addition of the two force terms.

Return to Section 8 and choose another answer.

(13)—

Your answer in Section 7 is not correct. Ground water frequently percolates downward from the water table; the pressure is greater at depth than at the water table, so in these cases water is moving in the direction of increasing pressure. Keep in mind

that Darcy's law relates flow per unit area to the gradient of head, not to the gradient of pressure.

Return to section 7 and choose another answer.

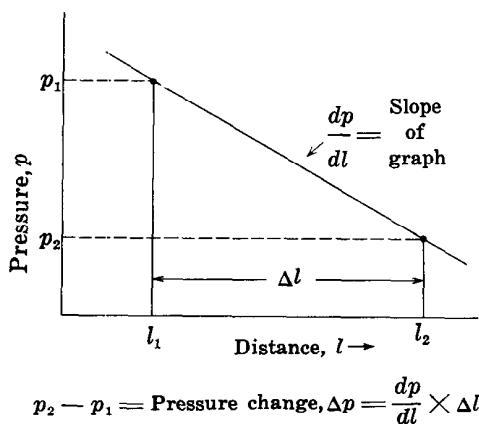
(14)—

Your answer in Section 31 is not correct. We have seen that the net pressure force was equal to $-\Delta p n A$. It cannot be equal to this and to $\Delta p (dp/dl) n A$ (unless dp/dl happens to equal -1 , in a particular case).

We wish to substitute an expression involving the derivative, dp/dl , in place of the

pressure change term, $-\Delta p$. To obtain an expression for a change, or an increment, from a derivative, it is necessary to multiply the derivative—that is, the rate of change per unit distance—by the distance over which the increment or change occurs. For example, the diagram shows a graph of pres-

(14)—Con.



sure versus distance. The slope of this graph is the derivative, dp/dl . If we wish to obtain the change in pressure, $p_2 - p_1$ occurring over the interval Δl , we must multiply the rate of change per unit distance, dp/dl , by the distance Δl . Since we actually require the negative of this quantity, $p_1 - p_2$, we must insert a negative sign. (As shown on the graph, p_1 exceeds p_2 —pressure is decreasing in the direction of flow, l . The derivative of pressure with respect to distance, dp/dl , is therefore a negative quantity itself—that is, the graph has a negative slope. By inserting another negative sign, we will obtain a positive result for the term $p_1 - p_2$.)

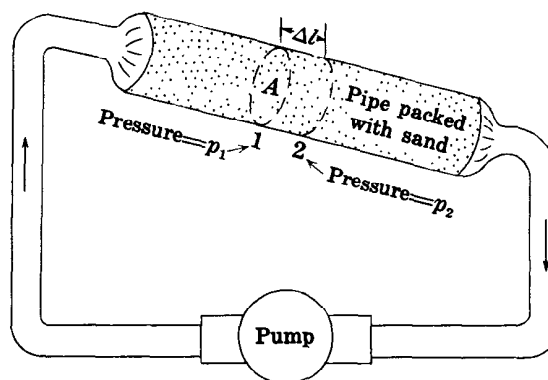
Return to Section 31 and choose another answer.

(15)

Your answer, $m = \rho \cdot \Delta l \cdot n \cdot A$, in Section 26 is correct; mass density, ρ , times volume of fluid, $n \cdot \Delta l \cdot A$, where n is porosity, gives the mass of fluid. The magnitude of the total force of gravity on our fluid element will, therefore, be $\rho \cdot \Delta l \cdot n \cdot A \cdot g$. This gravitational force acts vertically downward. As a force, however, it is a vector quantity; and like any other vector quantity it can be resolved into components acting in other directions.

QUESTION

The diagram again shows the flow system we have postulated. Which of the following statements is correct?



Turn to Section:

- The entire gravitational force is effective in causing flow along the pipe. 22
- Only the component of the gravitational force parallel to the axis of the pipe contributes to flow along the pipe. 33
- Only the horizontal component of the gravitational force contributes to flow along the pipe. 18

(16)

Your answer in Section 1 is not correct. The force on the element will be given by the pressure, or force per unit area, multi-

plied by the area of fluid against which the pressure acts.

Return to Section 1 and choose another answer.

(17)

Your answer in Section 26 is not correct. The term $\rho \cdot \Delta l \cdot A$ would give the mass of a fluid element having a volume $\Delta l \cdot A$. In our problem, however, only a part of the volume

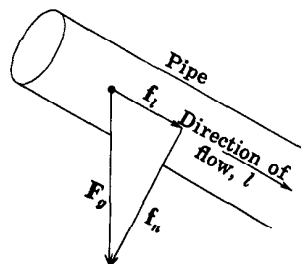
$\Delta l \cdot A$ is occupied by fluid; the balance is occupied by solid sand grains, so that the actual volume of fluid is less than $\Delta l \cdot A$.

Return to Section 26 and choose another answer.

(18)

Your answer in Section 15 is not correct. Gravity, as we are considering it, has no horizontal component. No vector can have a component perpendicular to its own direction. For our purposes we consider the gravitational force vector, F_g , to be always directed vertically downward; there can be no horizontal component of this force.

The diagram shows the gravitational force vector resolved into two components—one parallel to the direction of flow, f_i , and one perpendicular to the direction of flow, f_n . Fluid velocity itself may be considered a vector, in the direction l . As such, it has no component in the direction of f_n , normal to the pipe—and a force component normal to the



pipe could not contribute in any way to the fluid velocity.

Return to Section 15 and choose another answer.

(19)

Your answer in Section 11,

$$\left(-\frac{dp}{dl} - \rho g \frac{dz}{dl} \right) \Delta l \cdot n \cdot A$$

is correct. The net force *per unit volume of fluid* due to pressure and gravity would thus be

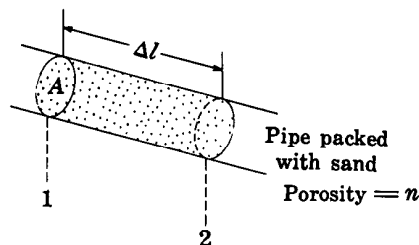
$$-\left(\frac{dp}{dl} + \rho g \frac{dz}{dl} \right),$$

since $\Delta l \cdot n \cdot A$ gives the volume of the fluid element.

Our approach in this development is to equate the net force driving the flow to the frictional force opposing it; more exactly, we will obtain the vector sum of these opposing forces and set the result equal to zero. The resulting equation will be a statement of Darcy's law. We have obtained an expression for the net force driving the flow. We now consider the force opposing the motion. This force is due primarily to friction between the moving fluid and the porous medium. In some

(19)—Con.

other systems of mechanics—for example in the case of a particle moving through a viscous fluid at moderate speed—the frictional retarding force is observed to be proportional to the velocity of movement. By analogy we assume a similar relation to hold for our element of fluid. However, as indicated in Part I, the actual (pore) velocity varies from point to point and is difficult or impossible to determine. For practical purposes therefore, we consider the frictional force on our fluid element to be proportional to the specific discharge, or flow per unit cross-sectional area, through the porous material. (See Section 14, Part I.) The specific discharge, which has the dimensions of a velocity (and is in fact a sort of apparent velocity), is determined by the statistical distribution of pore velocities within the fluid element; and we are, in effect, assuming that the total frictional retarding force on the element is likewise determined by this statistical distribution of pore velocities. In addition, we assume the total frictional retarding force on the fluid element to be proportional to the volume of fluid in the element, on the theory that the total area of fluid-solid contact within the element, and therefore the total frictional drag on the element, increases in proportion to the volume of the element. Finally, we assume that the retarding force is proportional to the dynamic viscosity of the fluid, since we would expect a fluid of low viscosity to move through a porous medium more readily than a highly viscous liquid.

**QUESTION**

Following the various assumptions outlined above, which of the following expressions would you choose as best representing the frictional retarding force on the fluid element of Section 1. (Shown again in the diagram.)

Turn to Section:

$-\frac{1}{k}\mu Q (\Delta l \cdot n \cdot A)$	2
$-\frac{1}{k} \cdot \frac{Q^2 \mu}{\Delta l \cdot n \cdot A}$	34
$-\frac{1}{k}\mu (\Delta l \cdot n \cdot A) \frac{Q}{A}$	20

where $1/k$ indicates a constant of proportionality, μ is the dynamic viscosity of the fluid, and Q is the fluid discharge through the pipe.

(20)

Your answer in Section 19,

$$-\frac{1}{k}\mu (\Delta l \cdot n \cdot A) \frac{Q}{A},$$

is correct. The negative sign is employed to indicate that the frictional retarding force will be opposite in direction to the fluid movement. We assume that our fluid motion is steady—that is, that the fluid velocity is not

changing with time, or in other words, that there is no fluid acceleration. In this condition, the forces producing the motion must be in balance with the frictional retarding force. The vector sum of these forces must therefore be zero; and because the force components contributing to the motion are all directed along the pipe, this vector sum is simply an algebraic sum.

(20)—Con.—

QUESTION

We have seen that the net driving force on the fluid element—that is, the net force in the direction of flow due to pressure and gravity together—is given by

$$-\left(\frac{dp}{dl} + \rho g \frac{dz}{dl}\right) \Delta l \cdot n \cdot A.$$

Suppose we take the algebraic sum of this force and our retarding force, and set the result equal to zero. Which the following

equations may then be derived from the result?

Turn to Section:

$$\frac{dp}{dl} + \rho g \frac{dz}{dl} + \frac{\mu}{k} \cdot \frac{Q}{A} = \Delta l \cdot n \cdot A \quad 36$$

$$-\frac{k}{\mu} \left(\frac{dp}{dl} + \rho g \frac{dz}{dl} \right) = \frac{Q}{A} \quad 28$$

$$\left(\frac{dp}{dl} + \rho g \frac{dz}{dl} \right) \Delta l \cdot n \cdot A = \frac{\mu}{k} \frac{Q}{A} \quad 27$$

(21)—

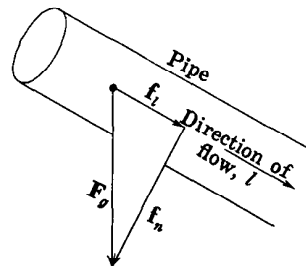
Your answer in Section 7 is correct. Darcy's law, as an equation containing a derivative, is actually a differential equation. It relates flow per unit area, or flux, to the energy consumed per unit distance by friction. Analogies can readily be recognized between Darcy's law and the differential equations governing the steady flow of heat or electricity. The hydraulic conductivity, K , is analogous to thermal or electrical conductivity; while hydraulic head, h , is a po-

tential analogous to temperature or voltage. (To be more correct, the term Kh constitutes a ground-water velocity potential—that is, a function whose derivative yields the flow velocity—provided both the fluid and the porous medium are homogeneous and the medium is isotropic.)

This concludes the programed instruction of Part II. A discussion in text format dealing with generalizations of Darcy's law begins on the page following Section 37.

(22)—

Your answer in Section 15 is not correct. The diagram shows the gravitational force vector, F_g , resolved into two components, one parallel to the direction of flow, f_t , and one perpendicular to it, f_n . If the flow were vertically downward,—that is, colinear with F_g —the entire gravitational force would be effective in producing flow. In the situation shown, however, one component of the gravitational force— f_n , or that perpendicular to the flow—is balanced by static forces exerted by the walls of the pipe. To view this in another way, we may note that the fluid velocity itself is a vector, in the direction l . No vector can have a component perpendicular to its own direction; so the velocity vector



has no component in the direction of f_n . The force component f_n can therefore contribute nothing to the fluid velocity.

Return to Section 15 and choose another answer.

(23)

Your answer in Section 8 is not correct. The pressure at a point in a fluid is a scalar quantity; it is not directional in character, and we say that it "acts in all directions." However, if we choose any small cross-sectional area within the fluid, we can measure a force against this area attributable to the pressure, regardless of the orientation of the area. This force is a vector, or directed quantity; it acts in a direction normal to the small area and has a magnitude equal to the product of the pressure and the area. In the example of Sections 1 and 8, we consider the pressure at two points, the upstream and downstream faces of our fluid element. At the upstream face we write an expression

$p_1 nA$ for the magnitude of the force in the direction of the flow. At the downstream face we are interested in a force opposing the flow—that is, acting in a direction opposite to the flow. The magnitude of this force is again given as a product of pressure, porosity, and face area, $p_2 nA$; but because we are interested in the force acting *against* the flow, or in a direction opposite to that originally taken, we now introduce a negative sign. The *net* force on the fluid element along the axis of the pipe can now be obtained by algebraic addition of the two force expressions.

Return to Section 8 and choose another answer.

(24)

Your answer in Section 11 is not correct. The idea here is simply to combine the expressions obtained for the net pressure force (see Section 26) and for the component of the gravitational force parallel to the pipe (see Section 11). Forces are always combined by means of vector addition. In this case, however, the two vectors we are considering are oriented in the same direction. That is,

both the net pressure force and our component of the gravitational force are oriented in the direction of the flow. In this case, therefore, vector addition amounts to no more than the simple scalar addition of the magnitudes of the two components.

Return to Section 11 and choose another answer.

(25)

Your answer in Section 1 is not correct. If we were dealing with open flow in the pipe, the force on the fluid element would indeed be given by the term $p_1 A$. Here, however, a part of the area A is occupied by solid sand grains and the remainder by the upstream

face of the fluid element. For our purposes here, we may assume that the ratio of fluid area to total area is equal to the porosity, n .

Return to Section 1 and choose another answer.

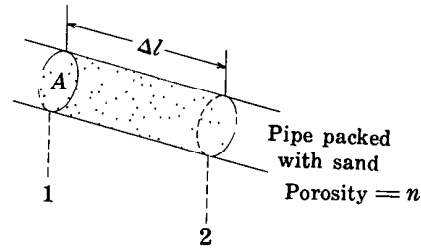
(26)

Your answer in Section 31,

$$-\frac{dp}{dl} \Delta l n A,$$

is correct. The gradient or derivative of pressure, dp/dl , multiplied by the length interval, Δl , gives the change in pressure, $p_2 - p_1$, occurring in that interval. Since we require the term $p_1 - p_2$, we use a negative sign. Multiplication by the fluid area, nA , then gives the net pressure force on the element.

Our purpose in this chapter is to develop Darcy's law by equating the forces driving a flow to the frictional force retarding it. We have considered the pressure force, which is one of the forces driving the flow. In addition to this pressure force, the element of fluid is acted upon directly by the force of gravity. The total gravitational force on the element is given by the acceleration due to gravity, g , multiplied by the mass, m , of fluid in the element.



QUESTION

Which of the following equations for the mass of fluid in our element, which is shown again in the diagram, is correct?

$$m = \Delta l \cdot n \cdot A$$

$$m = \rho \cdot \Delta l \cdot A$$

$$m = \rho \cdot \Delta l \cdot n \cdot A$$

Turn to Section:

3

17

15

(27)

Your answer,

$$\left(\frac{dp}{dl} + \rho g \frac{dz}{dl} \right) \Delta l \cdot n \cdot A = \frac{\mu}{k} \frac{Q}{A}$$

in Section 20 is not correct. Each of the force terms—the net driving force and the retarding force—contains the expression $\Delta l \cdot n \cdot A$

representing the volume of fluid in the element. When these force terms are added and their sum set equal to zero, the term $\Delta l \cdot n \cdot A$ may be divided out of the equation.

Return to Section 20 and choose another answer.

(28)

Your answer in Section 20,

$$-\frac{k}{\mu} \left(\frac{dp}{dl} + \rho g \frac{dz}{dl} \right) = \frac{Q}{A},$$

is correct. For the case of a fluid of uniform density and viscosity, the terms μ and ρ are constants and may be combined with the other constants in the problem to form a new constant, K , defined as

$$K = \frac{k \rho g}{\mu}.$$

Using this new constant we may rewrite our equation in the form

$$-K \left(\frac{1}{\rho g} \frac{dp}{dl} + \frac{dz}{dl} \right) = \frac{Q}{A}.$$

(continued on next page)

(28) — Con.

QUESTION

Keeping in mind that the term $1/\rho g$ is a constant, so that

$$\frac{1}{\rho g} \frac{dp}{dl} = \frac{d\left(\frac{p}{\rho g}\right)}{dl},$$

which of the equations given below constitutes a valid expression of the equation we have just obtained?

Turn to Section:

$$\frac{Q}{A} = -K \frac{dh}{dl} \quad 7$$

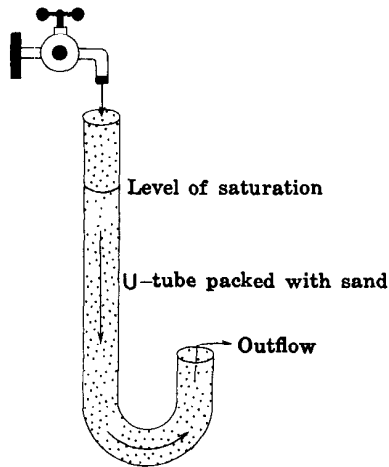
$$\frac{Q}{A} = -K \left\{ \frac{dp}{dl} + \frac{dz}{dl} \right\} \quad 9$$

$$\frac{Q}{A} = -K \left\{ \frac{1}{\rho g} \frac{dp}{dl} + \frac{dh}{dl} \right\} \quad 30$$

h represents the head as defined in Part I—that is,

$$h = \frac{p}{\rho g} + z.$$

(29)



Your answer in Section 7 is not correct. Ground water frequently discharges upward into stream valleys; and in the figure, upward flow occurs in the shorter arm of the U-tube. Thus statement (a) of Section 7 cannot always be true.

Return to Section 7 and choose another answer.

(30)

Your answer in Section 28 is not correct. We saw in Part I that hydraulic head, h , was given by

$$h = \frac{p}{\rho g} + z.$$

The derivative of h with respect to distance, l , is therefore given by

$$\frac{dh}{dl} = \frac{d\left\{ \frac{p}{\rho g} + z \right\}}{dl}.$$

Using this relation, return to Section 28 and choose another answer.

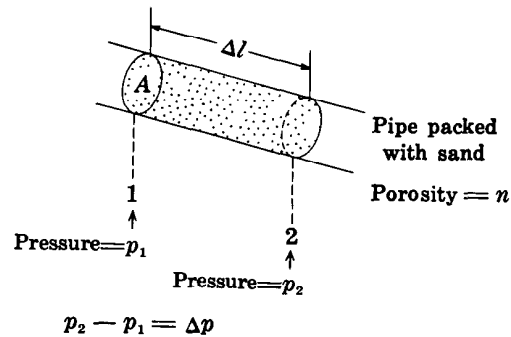
(31)

Your answer in Section 8 is correct. The net force in the direction of flow is given by the difference between the two opposing forces exerted upon the opposite faces of the element by the adjacent elements of fluid. We may now factor out the common term nA and obtain as our expression for net pressure force $(p_1 - p_2)nA$, or $-\Delta p nA$, where Δp indicates the small pressure difference, $p_2 - p_1$, between the downstream face of the fluid element and the upstream face.

Since pressure is varying from point to point within our system, we may speak of a pressure gradient; that is, a rate of change of pressure with distance, l , along the flow path. This gradient might be expressed, for example, in pounds per square inch (of pressure) per foot (of distance); it is represented by the symbol dp/dl , and is referred to as the derivative of pressure with respect to distance in the direction l . If we were to plot a graph of pressure versus distance, dp/dl would represent the slope of the graph.

QUESTION

Which of the following expressions is approximately equivalent to the net pressure



force, $-\Delta p nA$, on our element of fluid (shown again in the diagram)?

Turn to Section:

$\frac{dp}{dl} \Delta l nA$	26
$\frac{dp}{dl} nA$	5
$\Delta p \frac{dp}{dl} nA$	14

(32)

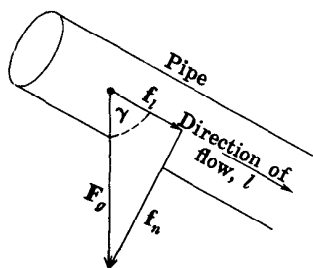
Your answer, $\rho \cdot n \cdot \Delta l \cdot A \cdot g \cdot \sin \gamma$, in Section 35 is not correct. We have already seen that the magnitude of our force component is given by $\rho \cdot n \cdot \Delta l \cdot A \cdot g \cdot \cos \gamma$. In the answer you have chosen, $\sin \gamma$ has been substituted for $\cos \gamma$ in our original expression—and this can be true only for a particular value of the

angle γ . It is true, however, that the idea of this question is to find an equivalent term for $\cos \gamma$ and substitute it in our previous expression for the force component.

Return to Section 35 and choose another answer.

(33)

Your answer in Section 15 is correct; we may resolve the gravitational force, F_g , into two orthogonal components, f_t and f_n , parallel to and perpendicular to the axis of the pipe as shown in the figure. There is no movement perpendicular to the pipe; the component of the gravitational force in this direction is



balanced by static forces exerted against the fluid element by the wall of the pipe. The component parallel to the pipe does contribute to the motion and must be taken into account in equations describing the flow.

QUESTION

The magnitude of the total gravitational force upon the element is given by the mass of the element multiplied by the acceleration due to gravity; that is, $F_g = mg$, where m is the mass of the fluid element. Referring to the diagram shown, which of the following expressions gives the magnitude of the component of the gravitational force parallel to the axis of the pipe?

Turn to Section:

$f_t = \rho \cdot n \cdot \Delta l \cdot A \cdot g$	6
$f_t = \rho \cdot n \cdot \Delta l \cdot A \cdot g \cdot \cos \gamma$	35
$f_t = n \cdot \Delta l \cdot A \cdot g \cdot \tan \gamma$	37

(34)

Your answer in Section 19,

$$\frac{1}{k} \frac{Q^2 \mu}{\Delta l \cdot n \cdot A},$$

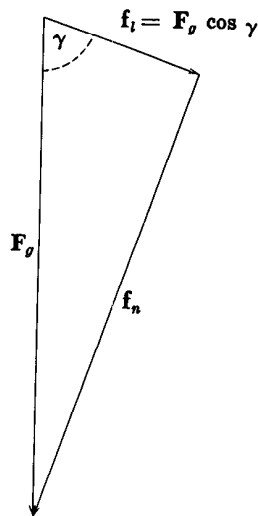
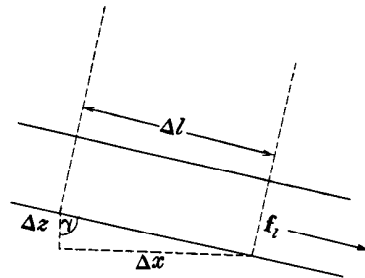
is not correct. Our assumptions were that the retarding force would be proportional in some way to the dynamic viscosity (μ), to the volume of fluid in the element ($\Delta l \cdot n \cdot A$), and to the specific discharge, or flow per unit area (Q/A). Your answer represents the retard-

ing force as proportional to the square of fluid discharge, which might be compatible with the assumptions, but as inversely proportional to the volume of fluid in the element, which is not compatible with the assumptions.

Return to Section 19 and choose another answer.

(35)

Your answer, $\rho \cdot n \cdot \Delta l \cdot A \cdot g \cdot \cos \gamma$, in Section 33 is correct. The mass of the fluid element, as we have seen, is $\rho \cdot n \cdot \Delta l \cdot A$; multiplication by the acceleration, g , gives the total gravitational force on the element. The component of this force parallel to the pipe, as indicated by the vector diagram, will be found by multiplying the total force by the cosine of γ .



QUESTION

Suppose we now draw a small right triangle, taking the hypotenuse as Δl , the length of our fluid element, and constructing the two sides Δz and Δx as in the diagram. Which of the following expressions may then be used for the magnitude (without regard to sign) of the component of gravitational force parallel to the flow?

- | | |
|---|------------------|
| | Turn to Section: |
| $\rho \cdot n \cdot \Delta l \cdot A \cdot g \cdot \sin \gamma$ | 32 |
| $\rho \cdot n \cdot A \cdot g \cdot \sqrt{(\Delta x)^2 + (\Delta z)^2}$ | 4 |
| $\rho \cdot n \cdot \Delta l \cdot A \cdot g \cdot \frac{\Delta z}{\Delta l}$ | 11 |

(36)

Your answer in Section 20 is not correct. If the sum of the two force expressions is set equal to zero, we have

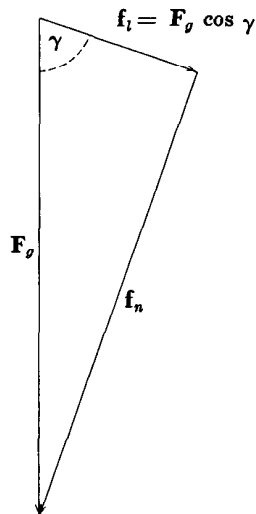
$$-\left(\frac{dp}{dl} + \rho g \frac{dz}{dl}\right)(\Delta l \cdot n \cdot A) - \frac{1}{k} \mu (\Delta l \cdot n \cdot A) \frac{Q}{A} = 0.$$

We may divide through by the term $\Delta l \cdot n \cdot A$, representing the volume of fluid in the element, and rearrange the resulting equation to obtain the required result.

Return to Section 20 and choose another answer.

(37)

Your answer in Section 33 is not correct. The total gravitational force on the element is given by mg , where m is the mass of fluid in the element and g is the acceleration due to gravity. The mass of fluid in the element is in turn given by the volume of fluid in the



element multiplied by the mass per unit volume, or mass density, of the fluid, which we have designated ρ . The volume of fluid in the element, as we have seen is $n \cdot \Delta l \cdot A$, where n is the porosity. The mass is therefore $\rho \cdot n \cdot \Delta l \cdot A$; and the total force of gravity on the fluid element is given by

$$F_g = \rho \cdot n \cdot \Delta l \cdot A \cdot g.$$

We require the component of this gravitational force parallel to the axis of the pipe. The sketch shows a vector diagram in which the length of each arrow is proportional to the force or component it represents. The gravitational force is represented by the arrow F_g and the components are represented by the arrows f_i and f_n . The rule for the resolution of a vector into components can be visualized from geometric considerations. The magnitude of the component of a vector in a given direction is the product of the magnitude of the vector and the cosine of the angle between the direction of the vector and the given direction.

Return to Section 33 and choose another answer.

Generalizations of Darcy's Law

The form of Darcy's law considered in the preceding program is useful only for one-dimensional flow. The discussion in this section indicates, in general outline, the manner in which Darcy's law is extended to cover more complex situations. Vector notation is used for economy of presentation, and this discussion is intended primarily for readers familiar with this notation. Those concepts which are essential to material covered later in the program are treated again as they are required in the development—without the use of vector notation. The material presented here is not difficult, and readers not familiar with vector notation may find it possible to follow the mathematics by reference to a standard text on vector analysis. However, those who prefer may simply read through this section for familiarity with qualitative aspects of the material and may then proceed directly to Part III.

For three-dimensional flow, we may consider the specific discharge, q or Q/A , to be a vector quantity, with components $i q_x$, $j q_y$, and $k q_z$ in the three coordinate directions. i , j , and k represent the standard unit vectors of the Cartesian system. We consider a small area, A_x , oriented at right angles to the x axis at a point 0, and observe the fluid discharge through this area to be Q_x ; the limiting value of the ratio Q_x/A_x , as A_x is made to shrink toward the point 0, gives the value of q_x applicable at point 0. q_y and q_z are similarly defined for the y and z directions. The specific discharge at point 0 is given by the vector sum

$$q = \frac{Q}{A} = i q_x + j q_y + k q_z.$$

q is thus a vector point function; its magni-

tude and direction may vary with location in steady flow and with location and time in unsteady flow.

If the porous medium is homogeneous and isotropic and if the fluid is of uniform density and viscosity, the components of the specific-discharge vector are each given by a form of Darcy's law, utilizing the partial derivative of head with respect to distance in the direction in question. That is, the components are given by

$$q_x = -K \frac{\partial h}{\partial x}$$

$$q_y = -K \frac{\partial h}{\partial y}$$

$$q_z = -K \frac{\partial h}{\partial z}$$

where K is the hydraulic conductivity.

It follows that the specific-discharge vector in this case will be given by

$$q = -K \left\{ i \frac{\partial h}{\partial x} + j \frac{\partial h}{\partial y} + k \frac{\partial h}{\partial z} \right\}$$

or

$$q = -K \nabla h$$

where ∇h denotes the head-gradient vector.

Thus, if the medium is isotropic and homogeneous, $-Kh$ constitutes a velocity potential; and the various methods of potential theory, as applied in studying heat flow and electricity, may be utilized in studying the ground-water motion. Since the specific-discharge vector is colinear with ∇h , it will be oriented at right angles to the surfaces of equal head, and flownet analysis immediately suggests itself as a useful method of solving field problems.

In practice, one does not usually find homogeneous and isotropic aquifers with which to work; frequently, however, simply for lack of more detailed data, aquifers are assumed to be homogeneous and isotropic in obtaining initial or approximate solutions to ground-water problems.

The situation in many aquifers can be represented more successfully by a slightly more general form of Darcy's law, in which a different hydraulic conductivity is assigned to each of the coordinate directions. Darcy's law then takes the form

$$q_x = -K_x \frac{\partial h}{\partial x}$$

$$q_y = -K_y \frac{\partial h}{\partial y}$$

$$q_z = -K_z \frac{\partial h}{\partial z}$$

where K_x , K_y , and K_z represent the hydraulic conductivities in the x , y , and z directions, respectively, and again

$$q = i q_x + j q_y + k q_z.$$

This form of Darcy's law can be applied only to those anisotropic aquifers which are characterized by three principal axes of hydraulic conductivity (or permeability) which are mutually orthogonal, so that the direction of maximum hydraulic conductivity is at right angles to the direction of minimum hydraulic conductivity. These axes must correspond with the x , y , and z axes used in the analysis. The implication is that one of the principal axes of conductivity must be vertical; for unless the z axis is taken in the vertical direction, the term $\partial h / \partial z$ cannot be used to represent the sum of the vertical pressure gradient and the gravitational force term.

It is easily demonstrated that the specific-discharge vector and the lines of flow are no longer orthogonal to the surfaces of equal head in this anisotropic case, and that the conditions for the existence of a velocity potential are no longer satisfied. Formal mathematical solutions to field problems are essentially as easy to obtain as in the isotropic case, however, since a relatively simple

transformation of scales can be introduced which converts the anisotropic system to an equivalent isotropic system (Muskat, 1937). The problem may then be solved in the equivalent isotropic system, and the solution retransformed to the original anisotropic system.

Probably the most common form of anisotropy encountered in the field is that exhibited by stratified sedimentary material, in which the permeability or hydraulic conductivity normal to the bedding is less than that parallel to the bedding. If the bedding is horizontal, the form of Darcy's law given above may be applied, using $K_x = K_y$. The anisotropy in this case is two-dimensional, with the axis of minimum permeability normal to the bedding, and the axis of maximum permeability parallel to it. In many cases, aquifers are assumed to exhibit simple two-dimensional anisotropy of this sort when in fact they are characterized by heterogeneous stratification and discrete alternations of permeability. This type of simplifying assumption frequently enables one to obtain an approximate solution, where otherwise no solution at all would be possible.

For many problems, however, this generalized form of Darcy's law is itself inadequate. As an example, one may consider a stratified aquifer, exhibiting simple two-dimensional anisotropy, which is not horizontal, but rather is dipping at an appreciable angle. The direction of minimum permeability, normal to the bedding, does not in this case coincide with the vertical. One may choose new coordinate axes to conform to the new principal directions of conductivity. If this is done, the component of the specific discharge in each of these new coordinate directions must be expressed in terms of the pressure gradient in the direction concerned, and the component of the gravitational force in that direction. Reduction of the equations to the simple form already given, using the principal directional derivatives of h , is not possible. Alternatively, one may retain the horizontal-vertical coordinate system, in which case the principal axes of conductivity do not coincide with the coordinate axes. In this case, hydraulic conductivity must be ex-

pressed as a tensor; the component of the specific discharge in one coordinate direction will not depend solely on the head gradient in that direction, but upon the head gradients in the other coordinate directions as well.

In addition to these considerations regarding aquifer anisotropy, practical problems require that attention be paid to heterogeneity, both of the aquifer and of the fluid. If the aquifer is heterogeneous, hydraulic conductivity must be treated as a function of the space coordinates; in this case, hydraulic conductivity (or in some cases intrinsic permeability) is usually defined as a tensor which varies with position in the aquifer.

If the fluid is heterogeneous, its viscosity and density cannot be treated as constants, as was done in the program section of Part II. Equations cannot be reduced to terms of the hydraulic conductivity and head gradients, but must rather be retained in terms of specific permeability, viscosity, pressure gradients, and components of the gravitational force (which depend upon fluid density, and will vary with position, and possibly with time, as fluid density varies). A special case of some importance is that in which the aquifer is horizontal, with principal axes of permeability in the x , y , and z directions, but

the fluid varies in both density and viscosity. Darcy's law for this case may be written

$$q_x = -\frac{k_x}{\mu_{x,y,z}} \frac{\partial p}{\partial x}$$

$$q_y = -\frac{k_y}{\mu_{x,y,z}} \frac{\partial p}{\partial y}$$

$$q_z = -\frac{k_z}{\mu_{x,y,z}} \left(\frac{\partial p}{\partial z} + \rho_{x,y,z} g \right)$$

and again

$$\mathbf{q} = \mathbf{i}q_x + \mathbf{j}q_y + \mathbf{k}q_z.$$

In these equations, k_x , k_y and k_z are the intrinsic permeabilities in the x , y , and z directions; $\mu_{x,y,z}$ is the dynamic viscosity function; $\rho_{x,y,z}$ is the density function; and the other terms are as previously defined. Since gravity is assumed to have no components in the horizontal plane, density does not enter into the expressions for q_x and q_y . In natural aquifers, variations in density are related primarily to variations in dissolved-solid content of the water, while variations in viscosity are related primarily to variations of ground-water temperature. The equations given above thus have utility in situations where water quality and water temperature are known to vary in an aquifer.

Part III. Application of Darcy's Law to Field Problems

Darcy's law, as mentioned in the discussion at the close of Part II, may be generalized to deal with three-dimensional flows; and it may be combined with other laws or concepts to develop equations for relatively complex problems of ground-water hydraulics. Even in the simple form developed in the program

of Part II, however, Darcy's law has direct application to many field problems. In Part III we shall consider a few examples of such direct application. Later, in Part V and VI, we will consider the combination of Darcy's law with other concepts to yield equations for more complex problems.

I □

In Part II we pointed out that Darcy's law is a differential equation—that is, an equation containing a derivative. It gives us some information about the rate at which head changes with distance, under given conditions of flow. In general, in dealing with ground-water problems, we will require expressions that relate *values* of head, rather than the rate of change of head, to flow conditions. To proceed from a differential equation, describing the rate of change of head, to an algebraic equation giving values of head, is to obtain a solution to the differential equation. There are various techniques for doing this. We need not go into these techniques of solution here. For our purposes, it will be sufficient if we can recognize a solution when we are given one—that is, if we can test an algebraic equation to determine whether it is a solution to a given differential equation. This is just a matter of differentiation. When we wish to know whether an algebraic equation is a solution to a differ-

ential equation, we may simply differentiate the algebraic equation. If we obtain a result which is equivalent to the given differential equation, then the algebraic equation is a solution to the differential equation. Should we fail to obtain an equivalent result, the algebraic equation is not a solution. Thus, for our present purposes at least, we may consider a solution to a differential equation to be an algebraic equation which, when differentiated, will yield the given differential equation.

QUESTION

Which of the following algebraic equations is a solution to the differential equation

$$\frac{dy}{dx} = K ?$$

$y = Kx^2$	15
$x = 2y + K$	23
$y = Kx + 5$	7

Turn to Section:

□ 2

Your answer in Section 35,

$$\frac{dh}{d(\ln r)} = \frac{Q}{2\pi Kb},$$

is correct. This equation is equivalent to the original differential equation for the problem and states that the rate of change of hydraulic head, with respect to change in the natural logarithm of radial distance, is constant and equal to

$$\frac{Q}{2\pi Kb}.$$

QUESTION

Suppose we were to plot a graph of hydraulic head versus the natural log of radial distance from the well, in our discharging well problem. Which of the following statements would apply to this graph?

- Turn to Section:
- (a) The plot would become progressively steeper with decreasing values of $\ln r$ —that is, as the well is approached. 18
- (b) Equal changes in head would be observed over intervals representing equal changes in r . 31
- (c) The plot would be a straight line. 38

□ 3

Your answer in Section 19 is correct. If the head in the well (and throughout the aquifer) prior to pumping is equal to h_e , the term $h_e - h_w$ is actually the drawdown in the pumping well (assuming that there are no additional losses in head associated with flow through the well screen, or within the well itself). Thus the equation in your answer allows us to predict the drawdown associated with any discharge, Q . Alternatively, the equation can be viewed as a method of calculating the hydraulic conductivity, K , of the aquifer on the basis of field measurements of Q and $h_e - h_w$, or on the basis of head measurements at any arbitrary radii, r_1 and r_2 , using observation wells. The theory of steady-state flow to a well as developed here is often referred to as the Thiem theory, after G. Thiem, who contributed to its development (Thiem, 1906).

While it would not be common, in practice, to find a well conveniently located at the center of a circular island, the example is a very useful one. The hydraulic operation of any well is similar, in many important respects, to that of the well on the island. In

particular, the decrease in cross-sectional area of flow as the well is approached, leading to the logarithmic "cone of depression" in the potentiometric surface, is a feature of every discharging well problem. It is in fact the dominant feature of such problems, since the head losses close to the well, within this "cone of depression" are normally the largest head losses associated with the operation of a well. The radial symmetry assumed in the Thiem analysis usually prevails, at least in the area close to the well, in most discharging well problems.

Readers familiar with differential equations will note that the equations of radial flow developed here can be obtained more directly by separating variables in the differential equation

$$\frac{Q}{2\pi br} = K \frac{dh}{dr},$$

and integrating between the limits r_1 and r_2 , or r_w and r_e . That is, these radial-flow equations, which state that head will vary with the logarithm of radial distance, are actually solutions to this differential equa-

3 □ —Con.

tion; if they are differentiated with respect to r , the differential equation is obtained. Again readers familiar with the general concepts of potential theory will recognize the pattern of head loss around the well as an example of the "logarithmic potential" asso-

ciated with potential-flow problems involving cylindrical symmetry in other branches of physics.

You have completed Part III. You may go on to Part IV.

4 □

Your answer in Section 9,

$$h = h_0 - \frac{2Q}{Kw}x$$

is not correct. If we differentiate this equation, treating h_0 as a constant, we obtain the result

$$\frac{dh}{dx} = -\frac{2Q}{Kw}$$

which is not the differential equation we de-

veloped for the problem. Keep in mind that in order to find a solution to the differential equation

$$\frac{d(h^2)}{dx} = -\frac{2Q}{Kw}$$

we must find an expression which will yield this equation upon differentiation.

Return to Section 9 and choose another answer.

5 □

Your answer in Section 8 is not correct. The differential equation tells us that any solution we obtain, giving h as a function of x , must be such that the derivative of h with respect to x , dh/dx is a constant, $-(Q/KA)$. Thus we know that (1) since the derivative is a constant (does not involve x), the plot of h versus x for any solution must have a constant slope—that is, the plot must be a straight line; and (2) since the constant has

the same value for any solution, the graphs of different or distinct solutions must all have the same slope—that is, these plots must be parallel straight lines. A family of curves all intersecting the x axis at a common point, as in the answer which you chose, could not have these characteristics.

Return to Section 8 and choose another answer.

6 □

Your answer in Section 41 is not correct. The direction of flow in this problem is radial, toward the well as an axis. The cross-sectional area of flow must be taken at right angles to this radial flow direction; that is, it must be a cylindrical surface within the aquifer having the centerline of the well as its

axis. At a radial distance r from the well, the cross-sectional area of flow will be the area of a cylindrical surface of radius r and of height equal to the thickness of the aquifer.

Return to Section 41 and select another answer.

□ 7

Your answer, $y = Kx + 5$, in Section 1 is correct; of the three expressions given, it is the only one which yields $dy/dx = K$ upon differentiation. However, $y = Kx + 5$ is obviously not the only equation which will give this result upon differentiation. For example, differentiation of the equations $y = Kx + 7$, $y = Kx - 3$, or $y = Kx$ will also yield $dy/dx = K$. The constant term which is added or subtracted on the right does not affect the differentiation; regardless of the value of the constant, the derivative of y with respect to x always turns out to be K . Since we have an infinite choice of constants to add or subtract, there are an infinite number of algebraic equations which qualify as solutions to our differential equation. This is a general characteristic of differential equations—the solutions to a differential equation are always infinite in number.

QUESTION

Given the following three algebraic equations relating head, h , to distance, x .

$$(a) \quad h = -\frac{Q}{KA}x$$

$$(b) \quad h = h_0 - \frac{Q}{KA}x$$

$$(c) \quad h = h_0 - \frac{Q}{KA}x^2 + 7$$

where h_0 , Q , K , and A are constants; which of the equations are solutions to the differential equation

$$\frac{Q}{A} = -K \frac{dh}{dx} ?$$

all three

only (a)

(a) and (b) but not (c)

Turn to Section:

29

14

8

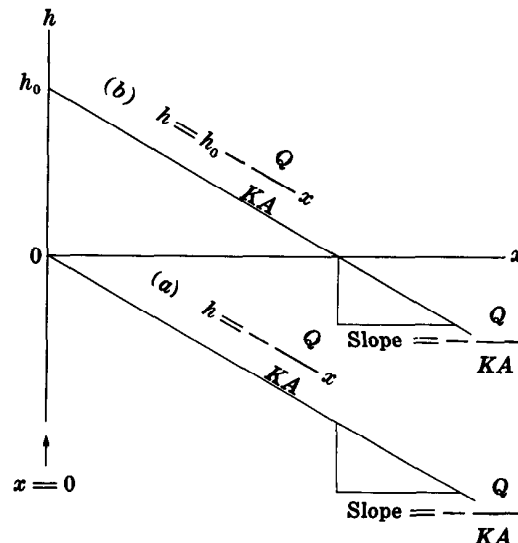
□ 8

Your answer in Section 7 is correct. Either (a) or (b), when differentiated and rearranged, will yield the equation

$$\frac{Q}{A} = -K \frac{dh}{dx}$$

Differentiation of (c) leads to an entirely different equation.

In the preceding example, the algebraic equations deal with values of hydraulic head, h , at various distances from some reference point; while the differential equation deals with the rate of change of head with distance. The differential equation is, of course, Darcy's law and states that if head is plotted versus distance, the slope of the plot will be constant—that is, the graph will be a straight



SE ROA 38420

8 □ —Con.

line. The graphs of equations (a) and (b) of Section 7 are shown in the diagram. Each is a straight line having a slope equal to

$$-\frac{Q}{KA};$$

the intercept of equation (a) on the h axis is $h=0$, while the intercept of equation (b) on the h axis is $h=h_0$. These intercepts give the values of h at $x=0$; they provide the reference points from which changes in h are measured.

QUESTION

If we were to graph all possible solutions to the differential equation

$$\frac{dh}{dx} = -\frac{Q}{KA},$$

the result would be:

Turn to Section:

A family of curves, infinite in number, each intersecting the x axis at

$$x = -\frac{Q}{KA} \quad 5$$

An infinite number of parallel straight lines, all having a slope

$$-\frac{Q}{KA},$$

and distinguished by different intercepts on the $x=0$ axis. 10

A finite number of parallel straight lines, all having a slope

$$-\frac{Q}{KA},$$

which intersect the $x=0$ axis at various positive values of h . 20

9 □

Your answer in Section 25,

$$Q = -Kwh \frac{dh}{dx},$$

is correct. From the rules of differentiation, the derivative of h^2 with respect to x is given by

$$\frac{d(h^2)}{dx} = 2h \frac{dh}{dx}.$$

Therefore, substituting

$$\frac{1}{2} \frac{d(h^2)}{dx}$$

for $h(dh/dx)$ in the equation

$$Q = -Kwh \frac{dh}{dx}$$

and rearranging, we have

$$\frac{d(h^2)}{dx} = \frac{-2Q}{Kw}.$$

In this rearranged form, the differential equation states that the derivative of h^2 with respect to x must equal the constant term

$$\frac{-2Q}{Kw}.$$

QUESTION

Which of the following expressions, when differentiated, yields the above form of the differential equation—that is, which of the following expressions constitutes a solution to the differential equation? (h_0 is a constant, representing the value of h at $x=0$.)

Turn to Section:

$$h^2 = h_0^2 - \frac{2Q}{Kw} x^2 \quad 16$$

$$h^2 = h_0^2 - \frac{2Q}{Kw} x \quad 41$$

$$h = h_0 - \frac{2Q}{Kw} x \quad 4$$

Your answer in Section 8 is correct. Any straight line having the slope

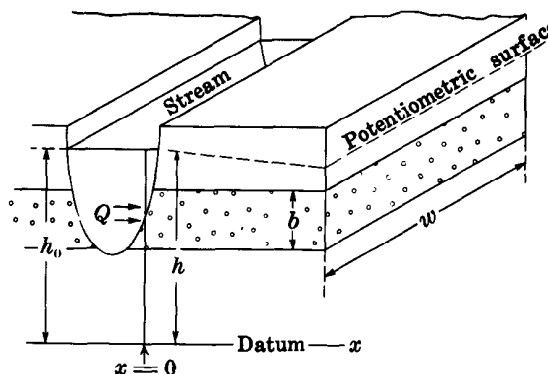
$$-\frac{Q}{KA}$$

will be the graph of a solution to the differential equation

$$\frac{dh}{dx} = -\frac{Q}{KA}$$

There are an infinite number of lines which may have this slope, corresponding to the infinite number of solutions to the differential equation.

The figure shows a confined aquifer of thickness b . The aquifer is completely cut by a stream, and seepage occurs from the stream into the aquifer. The stream level stands at an elevation h_0 above the head datum, which is an arbitrarily chosen level surface. The direction at right angles to the stream is denoted the x direction, and we take x as 0 at the edge of the stream. We assume that the system is in steady state, so that no changes occur with time. Along a reach of the stream having length w , the total rate of seepage loss from the stream (in, say, cubic feet per second) is denoted $2Q$. We assume that half of this seepage occurs through the right bank of the stream, and thus enters the part of the aquifer shown in our sketch. This seepage then moves away from the stream in a steady flow along the x direction. The resulting distribution of hydraulic head within the aquifer is indicated by the dashed line marked "potentiometric surface" in the sketch. This surface, sometimes referred to as the "piezometric surface," actually traces the static water levels in wells or pipes tapping the aquifer at various points. The differential equation applicable to this problem is obtained by applying Darcy's law to the



flow, Q , across the cross-sectional area, bw , and may be written

$$\frac{dh}{dx} = -\frac{Q}{Kbw}$$

where K is the hydraulic conductivity of the aquifer. The head distribution—that is, the potentiometric surface—is described by one of the solutions to this differential equation. In addition to satisfying the differential equation, the required solution must yield the correct value of h at the edge of the stream—that is, at $x=0$.

QUESTION

Which of the following expressions gives the particular solution (to the above differential equation) which applies to the problem described in this section?

Turn to Section:

$$h = -\frac{Q}{Kbw}x \quad 22$$

$$h = 2Q - \frac{Q}{Kbw}x \quad 36$$

$$h = h_0 - \frac{Q}{Kwb}x \quad 24$$

11 □

Your answer in Section 27 is not correct. The decrease in radius does not compensate for the decrease in cross-sectional area; it is, rather, the cause of this decrease in cross-sectional area. The decreasing cross-sectional area, along the path of flow, is a fundamental

characteristic of the problem we are considering. It has a major—in fact, dominant—effect upon the solution to the problem.

Return to Section 27 and choose another answer.

12 □

Your answer in Section 41 is not correct. The flow of water is directed radially inward toward the well. Any cross-sectional area of flow, taken normal to this radial direction of movement, would be a cylindrical surface in the aquifer, having the centerline of the well

as its axis. The area of flow at a radial distance r from the well would thus be the area of a cylindrical surface of radius r , having a height equal to the thickness of the aquifer.

Return to Section 41 and choose another answer.

13 □

Your answer in Section 35,

$$(\ln r) \frac{dh}{dr} = \frac{Q}{2\pi Kb}$$

is not correct. The differential equation as given in Section 35 was

$$r \frac{dh}{dr} = \frac{Q}{2\pi Kb}$$

In your answer, $\ln r$ has simply been substituted for r . This is obviously not what we

want; $\ln r$ is not equal to r . The relations given in Section 35 can be used to obtain an expression which is equivalent to dh/dr . This expression can then be substituted for dh/dr in the above differential equation to obtain the required result.

Return to Section 35 and choose another answer.

14 □

Your answer in Section 7 is not correct. It is true that expression (a),

$$h = -\frac{Q}{KA}x,$$

yields the result

$$\frac{dh}{dx} = -\frac{Q}{KA}$$

upon differentiation and is thus a solution to the given equation. However, it is not the only one of the given expressions which yields the required result upon differentiation.

Return to Section 7 and test the remaining expressions, by differentiation, in order to find the correct answer.

□ 15

Your answer, $y = Kx^2$, in Section 1 is not correct. If we differentiate the equation $y = Kx^2$, we obtain

$$\frac{dy}{dx} = 2Kx,$$

which is not the differential equation with which we started. Our differential equation was

$$\frac{dy}{dx} = K,$$

and we are looking for a solution to this differential equation—that is, we are looking for an algebraic expression which, when differentiated, will produce the differential equation $(dy/dx) = K$.

Return to Section 1 and test the remaining choices, by differentiating them, to see which will yield the given differential equation.

□ 16

Your answer in Section 9,

$$h^2 = h_0^2 - \frac{2Q}{Kw}x^2,$$

is not correct. If we differentiate this answer, treating h_0^2 as a constant, we obtain

$$\frac{d(h^2)}{dx} = -\frac{2Q}{Kw} \cdot 2x,$$

since the derivative of x^2 with respect to x

is $2x$. This result is not the differential equation with which we started, so the equation of your answer is not the solution we require.

Return to Section 9 and choose another answer. Keep in mind that the equation you select must yield the result

$$\frac{d(h^2)}{dx} = -\frac{2Q}{Kw}$$

when it is differentiated.

□ 17

Your answer in Section 40,

$$\frac{Q}{2\pi rb} = K \frac{d(h^2)}{dr},$$

is not correct. Darcy's law states that flow, divided by cross-sectional area, must be proportional to the head gradient. Your answer

states that flow, divided by cross-sectional area, is proportional to the gradient of the square of head. Thus it cannot be a valid application of Darcy's law to the problem.

Return to Section 40 and choose another answer.

□ 18

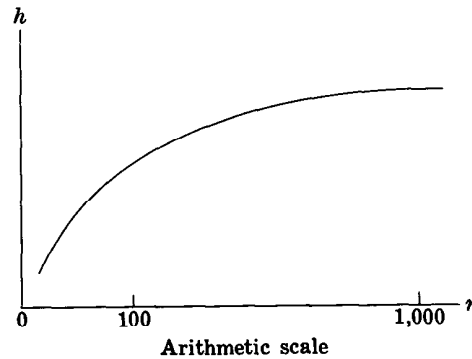
Your answer in Section 2 is not correct. The equation in Section 2 states that the derivative of head with respect to $\ln r$ is a constant. This derivative is simply the slope of a plot of h versus $\ln r$. If such a plot changes

slope, as in the answer you chose, the derivative cannot be constant.

Return to Section 2 and choose another answer.

19

Your answer in Section 38 is correct; inasmuch as $\log r$ changes by the same amount between 10 and 1 as it does between 1,000 and 100, the head changes by the same amount in these two intervals. If we were to replot head directly versus radius, r , rather than versus $\log r$, we would no longer have a straight line, but rather a "logarithmic" curve, as shown in the sketch. The gradient becomes progressively steeper as we approach the well, to compensate for the decreasing cross-sectional area of flow. This logarithmic pattern of head decline is sometimes referred to as the "cone of depression" in the potentiometric surface around the well.



QUESTION

The equation obtained in Section 38 can be applied between the radius of the island, r_e , and the radius of the well, r_w , to obtain an expression for the head difference between the well and edge of the island. If h_e represents the head at the edge of the island (that is, the level of the open water surrounding the island) and h_w represents the head in the

well which of the following expressions would result from this procedure?

Turn to Section:

$$h_e - h_w = \frac{2.3Q}{2\pi K b} \log \frac{r_w}{r_e} \quad 28$$

$$h_e - h_w = \frac{2.3Q}{2\pi K b} \log \frac{r_e}{r_w} \quad 3$$

$$h_e - h_w = \frac{2.3Q}{2\pi K b} (\log r_w - \log r_e) \quad 30$$

20

Your answer in Section 8 is not correct. If we were to write the solution to the equation

$$\frac{Q}{A} = -K \frac{dh}{dx}$$

in the most general form, we would write

$$h = -\frac{Q}{KA}x + c$$

where c could represent any constant term we wish. No matter what value we assign c , so long as it is constant (not dependent on x) its derivative with respect to x will be zero. Thus regardless of the value of c , differentiation will yield the result

$$\frac{dh}{dx} = -\frac{Q}{KA}$$

which is equivalent to our given differential equation. Clearly we can assign an infinite number of values to the term c , and obtain an infinite number of distinct equations (solutions) which we can differentiate to obtain our differential equation. Each of these solutions is the equation of a straight line; that is, each has a slope, dh/dx , equal to $-(Q/KA)$, and each has a distinct intercept on the h axis, where $x=0$. This intercept is simply the value of the constant c , since if we set $x=0$ in the solution we obtain $h=c$.

Return to Section 8 and choose another answer.

□ 21

Your answer in Section 24 is not correct. According to Darcy's law, the specific discharge, Q/A , is given by

$$\frac{Q}{A} = -K \frac{dh}{dx}$$

If the specific discharge increases as the stream is approached, the head gradient dh/dx must also increase—that is, become

steeper—as the stream is approached. A plot of h versus distance would thus be some sort of curve. In the statement of the problem in Section 24, however, head was described as increasing *linearly* with distance away from the stream. Since head increases in a linear fashion, dh/dx is constant.

Return to Section 24 and choose another answer.

□ 22

Your answer in Section 10,

$$h = -\frac{Q}{Kbw}x,$$

is not correct. It is true that differentiation of this equation yields the result

$$\frac{dh}{dx} = -\frac{Q}{Kbw}$$

which is our given differential equation; but this in itself is not enough to make it the answer to our problem. If we set x equal to zero in the expression

$$h = -\frac{Q}{Kwb}x,$$

we obtain the result $h=0$. That is, this equation says that where x is zero, at the edge of the stream, hydraulic head is also zero. Ac-

cording to the statement of our problem, however, head is equal to h_0 , the elevation of the stream surface above datum, at $x=0$. The solution which we require must not only have the property of yielding the given differential equation

$$\frac{dh}{dx} = -\frac{Q}{Kbw}$$

when it is differentiated; it must also have the property that when x is set equal to zero in the solution, hydraulic head will be h_0 . This is an example of what is meant by a *boundary condition*; the solution must satisfy a certain condition ($h=h_0$) along a certain boundary ($x=0$) of the problem.

Return to Section 10 and choose another answer.

□ 23

Your answer, $x=2y+K$, in Section 1 is not correct. We can rearrange the equation you selected as follows

$$y = \frac{1}{2}x - \frac{K}{2}$$

Now if we differentiate this equation, we obtain

$$\frac{dy}{dx} = \frac{1}{2},$$

which is not the differential equation with

which we started. We were asked to find a solution to the differential equation

$$\frac{dy}{dx} = K;$$

that is, we were asked to find an algebraic equation which, when differentiated, would yield the result $dy/dx = K$.

Return to Section 1 and test the remaining answers by differentiation, to see which one satisfies this condition.

24 □

Your answer in Section 10,

$$h = h_0 - \frac{Q}{Kbw}x$$

is correct. The differential equation tells us that a plot of h versus x will be a straight line with slope

$$-\frac{Q}{Kbw};$$

while from the other information given, we know that at $x=0$, h is equal to h_0 . Thus, to describe h as a function of x we require the equation of a straight line, with h_0 as the intercept and $-(Q/Kbw)$ as the slope. We can make two tests to verify that we have obtained the correct solution; first, we may differentiate the solution with respect to x , to see whether we obtain the differential equation; second, we may let x equal 0 in the solution to see whether the condition that h is h_0 at $x=0$ is satisfied. Only if our equation meets both of these tests is it the solution we require. The condition that h must be h_0 at $x=0$ is an example of what is commonly termed a *boundary condition*; it is a condition which states that h must have a certain value along one or another of the boundaries of our problem. The differential equation,

$$\frac{dh}{dx} = -\frac{Q}{Kbw},$$

is in itself insufficient to define head as a function of x . It establishes that the graph of h versus x will be a straight line with slope

$$-\frac{Q}{Kbw},$$

25 □

Your answer in Section 24 is correct. This serves to illustrate the dual utility of flow equations in ground-water hydraulics—they enable us to predict the head distributions associated with various conditions of flow and they enable us to draw conclusions regarding ground-water flow on the basis of head distributions observed in the field.

but there are an infinite number of such straight lines which we might draw. The additional information given by the boundary condition—that h must be h_0 at $x=0$ —permits us to pick out the particular straight line we require, by giving us its intercept. A boundary condition is thus a bit of information on the value of head at a known point; it provides a reference from which the changes in head indicated by a differential equation may be measured. The processes of (1) differentiation to establish that a given equation is a solution to a differential equation and (2) application of boundary conditions to establish that it is the particular solution that we require may be applied to problems much more complex than the one we have considered here.

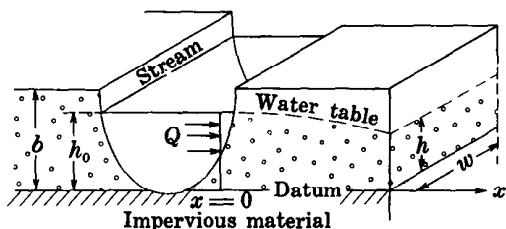
QUESTION

Suppose that, in measuring observation wells tapping a confined aquifer, we observe a linear increase in head with distance away from a stream or channel which cuts completely through the aquifer; and suppose this pattern remains unchanged through a considerable period of time. Which of the following conclusions could we logically draw on the basis of this evidence?

- | | |
|--|------------------------|
| There is no flow within the aquifer. | Turn to Section:
42 |
| There is a steady flow through the aquifer into the stream. | 25 |
| A flow which increases in specific discharge as one approaches the stream occurs in the aquifer. | 21 |

Suppose we now consider an aquifer in which the flow is unconfined, so that the upper limit of the flow system at any point is the water surface, or water table, itself. Again we consider uniform flow away from a stream, as shown in the diagram. It is convenient in this case to take the base of the unconfined aquifer as our head datum. We

Con.— □ 25



assume that vertical components of flow are negligible. This assumption is never wholly satisfied, as movement cannot be entirely lateral in and near the free surface, owing to the slope of the surface itself. Frequently, however, the vertical velocity component is slight compared to the lateral and therefore can be neglected, as we are doing here. An important difference between this problem and the confined-flow problem is that here the cross-sectional area of flow diminishes along the path of flow, as h decreases, whereas in the confined problem it remains constant.

Along a reach of the stream having a length w , seepage into the aquifer occurs at a rate $2Q$; and we assume that half of this seepage moves to the right, into the part of the aquifer shown in the sketch.

QUESTION

According to the assumptions outlined above, which of the following relations is obtained by applying Darcy's law to this problem?

Turn to Section:

- $Q = -Kxw \frac{dh}{dx}$ 26
- $\frac{Q}{bw} = -K \frac{dh}{dx}$ 43
- $Q = -Kwh \frac{dh}{dx}$ 9

□ 26

Your answer in Section 25,

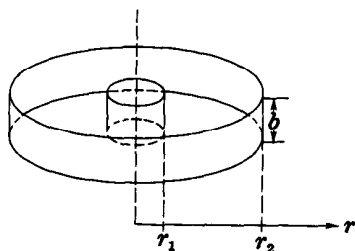
$$Q = -Kxw \frac{dh}{dx}$$

is not correct. Darcy's law states that the flow is the product of the hydraulic conductivity, the cross-sectional area of flow, and the (negative) head gradient. Referring to

the diagram of Section 25, the cross-sectional area of the flow—that is, the cross-sectional area taken at right angles to the direction of movement—can be seen to be equal to wh . In the answer which you chose, the term xw appears as the area of flow.

Return to Section 25 and choose another answer.

□ 27



Your answer, $2\pi r b$, in Section 41 is correct. The flow is radially inward in the (negative) r direction—that is, parallel to the r axis of

polar coordinates. The cross-sectional area of flow is a surface which is everywhere normal to this direction of flow; hence it is a cylindrical surface, and its area is given by the expression for the area of a cylinder.

As we proceed inward along the path of flow in this problem, the cylindrical area of flow becomes smaller and smaller, as illustrated in the sketch. This is also evident from our expression for the cross-sectional area, which tells us that as r decreases, the area must decrease.

27 □ —Con.

QUESTION

Which of the following statements is correct?

(a) Although cross-sectional area is decreasing, radius is also decreasing. These factors combine in such a way that the hydraulic gradient remains constant.

11

(b) Cross-sectional area decreases along the path of flow, while discharge remains constant; therefore, the hydraulic gradient must increase along the path of flow.

40

(c) Cross-sectional area of flow decreases along the path of flow, but this is offset by convergence of the flowlines toward the well, and no increase in the hydraulic gradient occurs.

32

Turn to Section:

28 □

Your answer in Section 19,

$$h_c - h_w = \frac{2.3Q}{2\pi Kb} \log \frac{r_w}{r_c},$$

is not correct. If we let h_c and r_c be represented by h_2 and r_2 , and if we let h_w and r_w be represented by h_1 and r_1 , your answer can be restated in the form

$$h_2 - h_1 = \frac{2.3Q}{2\pi Kb} \log \frac{r_1}{r_2}.$$

Comparison with the equations in Section 38 will show that this is not the form which we require.

Return to Section 19 and choose another answer.

29 □

Your answer in Section 7 is not correct. The given differential equation

$$\frac{Q}{A} = -K \frac{dh}{dx}$$

can be rearranged to

$$\frac{dh}{dx} = -\frac{Q}{KA}$$

In order for all three of the given expressions to be solutions to this equation, all three would have to yield $-(Q/KA)$ as the derivative of h with respect to x . But if we differentiate expression (c), for example, which was

$$h = h_0 - \frac{Q}{KA} x^2 + 7,$$

we obtain

$$\frac{dh}{dx} = -\frac{2Q}{KA} x,$$

which is not the given differential equation. Thus we can see that at least expression (c) does not satisfy the given equation.

Return to Section 7 and test the remaining expressions, by differentiation, in order to find the correct answer.

□ 30

Your answer in Section 19,

$$h_e - h_w = \frac{2.3Q}{2\pi K b} (\log r_w - \log r_e),$$

is not correct. The term $\log r_e$ will obviously be greater than $\log r_w$, since r_e is much greater than r_w . Thus the expression on the

right in your answer will be negative, implying that h_w is greater than h_e . This does not make sense; the head in a discharging well cannot be greater than the head at the radius of influence of the well.

Return to Section 19 and choose another answer.

□ 31

Your answer in Section 2 is not correct. If equal changes in head were observed over intervals representing equal changes in r , we could write

$$\frac{\Delta h}{\Delta r} = \text{constant}$$

where Δh is the change in head which is always observed over any interval of radial width Δr . In derivative form this would be

$$\frac{dh}{dr} = \text{constant},$$

and this is not the condition which has been shown to apply to this problem. The condition our plot must satisfy, rather, is

$$\frac{dh}{d(\ln r)} = \text{constant}.$$

Return to Section 2 and choose another answer.

□ 32

Your answer in Section 27 is not correct. The convergence of flowlines toward the well does not compensate for the decrease in flow area; it is, rather, caused by this decrease in flow area. The decrease in flow area as the well is approached is a fundamental charac-

teristic of the discharging well problem; in effect the decreasing flow area has a dominant influence on the form of the head distribution around the well.

Return to Section 27 and select another answer.

□ 33

Your answer in Section 40,

$$\frac{Q}{A} = K \frac{dh}{dx},$$

is not correct. The x coordinate was not used in our analysis of this problem; we did not

set up an x axis along which head could vary. The answer which you selected involves a derivative of head with respect to x and thus cannot apply to our problem.

Return to Section 40 and choose another answer.

34 □

Your answer in Section 38 is not correct. The equation

$$h_2 - h_1 = \frac{2.3Q}{2\pi Kb} \cdot \log \frac{r_2}{r_1}$$

indicates that if the ratio r_2/r_1 —that is, the ratio of the outer radius to the inner radius—

is the same for two different intervals, then the head drops across those intervals must be equal. For the two intervals mentioned in the answer which you chose, these ratios are 10/1 and 1000/100.

Return to Section 38 and choose another answer.

35 □

Your answer in Section 40 is correct. The hydraulic gradient here is dh/dr , since flow is in the r direction. We assume radial symmetry around the well, so that the angular polar coordinate, θ , need not appear at all. We now rewrite the equation which you selected in the form:

$$r \frac{dh}{dr} = \frac{Q}{2\pi Kb},$$

and we focus our attention for a moment on the left-hand member. According to the rules of differentiation we may write:

$$\frac{dh}{dr} = \frac{dh}{d(\ln r)} \cdot \frac{d(\ln r)}{dr}$$

where $\ln r$ denotes the natural logarithm of r ; and we may recall from introductory calculus that the derivative of $\ln r$ with respect to r is given by

$$\frac{d(\ln r)}{dr} = \frac{1}{r}$$

QUESTION

Using these expressions, which of the following may be obtained as a correct restatement of the differential equation for the problem?

Turn to Section:

$\frac{dh}{dr} = \frac{Q(\ln r)}{2\pi Kb}$	39
$\frac{dh}{d(\ln r)} = \frac{Q}{2\pi Kb}$	2
$(\ln r) \frac{dh}{dr} = \frac{Q}{2\pi Kb}$	13

36 □

Your answer in Section 10,

$$h = 2Q - \frac{Q}{Kwb}x,$$

is not correct. This answer is indeed a solution to our differential equation, for when we differentiate it we obtain the differential equation

$$\frac{dh}{dx} = -\frac{Q}{Kbw}$$

However, if we set x equal to zero in the answer which you chose, we find that hydraulic head, h , is equal to $2Q$ at the point where x is zero—that is, at the edge of the

stream. In the discussion of Section 10, however, it was stated that hydraulic head was equal to h_0 at the edge of the stream— h_0 being the elevation of the stream surface above datum. This problem illustrates what is meant by the term *boundary condition*; the solution must satisfy a condition along one boundary ($h = h_0$ at $x = 0$) in addition to satisfying the given differential equation. There are an infinite number of possible solutions to the above differential equation, but only one which satisfies this required boundary condition.

Return to Section 10 and choose another answer.

□ 37

Your answer in Section 38 is not correct. If the equation

$$h_2 - h_1 = \frac{2.3Q}{2\pi Kb} \log \left(\frac{r_2}{r_1} \right)$$

is applied to the two intervals in question, we have

$$h_{10} - h_1 = \frac{2.3Q}{2\pi Kb} \log \left(\frac{10}{1} \right) = \frac{2.3Q}{2\pi Kb} \cdot 1$$

and

$$h_{100} - h_{10} = \frac{2.3Q}{2\pi Kb} \log \left(\frac{100}{10} \right) = \frac{2.3Q}{2\pi Kb} \cdot 1.$$

Return to Section 38 and choose another answer.

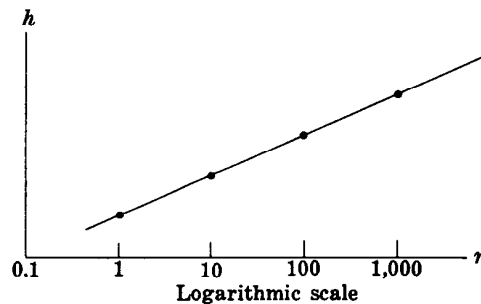
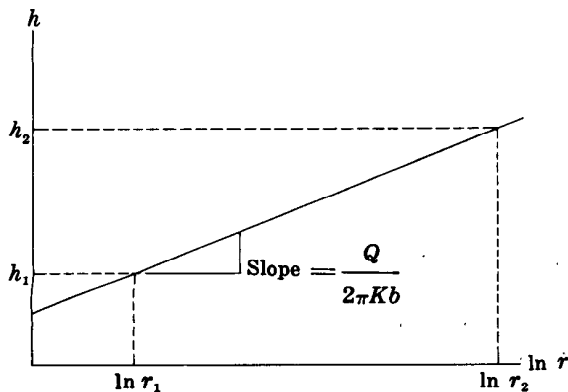
□ 38

Your answer in Section 2 is correct. The equation states that the derivative of h with respect to $\ln r$ is a constant. Thus a graph of h versus $\ln r$ will be a straight line, which will have a slope equal to

$$\frac{Q}{2\pi Kb}.$$

The sketch shows such a graph. As $\ln r$ changes from $\ln r_2$ to $\ln r_1$, head decreases from h_2 to h_1 ; and as with any straight line function, the change in head can be obtained by multiplying the change in the independent variable by the slope of the line; that is,

$$h_2 - h_1 = \frac{Q}{2\pi Kb} (\ln r_2 - \ln r_1).$$



This can be written in the equivalent form

$$h_2 - h_1 = \frac{Q}{2\pi Kb} \ln \frac{r_2}{r_1}$$

inasmuch as the difference between $\ln r_2$ and $\ln r_1$ is simply the log of the quotient $\ln (r_2/r_1)$. At this point it is convenient to change from natural logs to common logs. This involves only multiplication by a constant—that is $\ln r = 2.3 \log r$, where $\log r$ denotes the common logarithm, or log to the base 10. Making this change, our equation takes the form

$$h_2 - h_1 = \frac{2.3Q}{2\pi Kb} \log \left(\frac{r_2}{r_1} \right)$$

or

$$h_2 - h_1 = \frac{2.3Q}{2\pi Kb} (\log r_2 - \log r_1).$$

Again a graph can be plotted of h versus $\log r$ —or, to do the same thing more con-

38 □ —Con.

veniently, a graph can be plotted of h versus r on semilog paper, as shown in the sketch. Since we have only multiplied by a constant, the graph remains a straight line.

QUESTION

On the basis of the graph shown in the figure and the equations given above, which of the following statements is correct?

- Turn to Section:
- (a) The head drop between $r=10$ and $r=1$ is equal to that between $r=1,000$ and $r=100$. 19
- (b) The head drop between $r=10$ and $r=1$ is less than that between $r=1,000$ and $r=100$. 34
- (c) The head drop between $r=10$ and $r=1$ is much greater than that between $r=100$ and $r=10$. 37

39 □

Your answer in Section 35,

$$\frac{dh}{dr} = \frac{Q(\ln r)}{2\pi Kb}$$

is not correct. The following relations were given in Section 35:

$$\frac{dh}{dr} = \frac{dh}{d(\ln r)} \cdot \frac{d(\ln r)}{dr}$$

and

$$\frac{d(\ln r)}{dr} = \frac{1}{r}$$

Combining these,

$$\frac{dh}{dr} = \frac{1}{r} \cdot \frac{dh}{d(\ln r)}$$

In the question of Section 35, the idea is to substitute the term

$$\frac{1}{r} \cdot \frac{dh}{d(\ln r)}$$

for the term

$$\frac{dh}{dr}$$

in the differential equation for our problem.

Return to Section 35 and choose another answer.

40 □

Your answer in Section 27 is correct. The decrease in cross-sectional area must, according to Darcy's law, be accompanied by a steepening of the hydraulic gradient. When we apply Darcy's law to this problem, we will omit the customary negative sign. This is done because Q , the well discharge, must itself carry a negative sign in this problem, since it is oriented toward the well, in the direction of decreasing values of r . The negative sign on Q combines with the negative sign used by convention in Darcy's law to yield an equation in positive terms.

QUESTION

Which of the following expressions is a valid application of Darcy's law to this problem, and hence a valid differential equation for the problem?

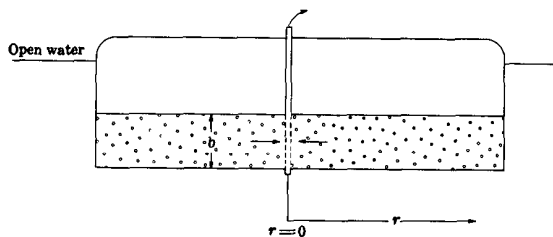
- Turn to Section:
- $\frac{Q}{A} = K \frac{dh}{dx}$ 33
- $\frac{Q}{2\pi r b} = K \frac{dh}{dr}$ 35
- $\frac{Q}{2\pi r b} = K \frac{d(h^2)}{dr}$ 17

□ 41

Your answer in Section 9,

$$h^2 = h_0^2 - \frac{2Q}{Kw}x,$$

is correct. The solution indicates that h will have the form of a parabola when plotted versus x in this case. The parabolic steepening of the hydraulic gradient compensates for the progressive decrease in flow area, in such a way that Darcy's law is always satisfied. This approximate theory of unconfined flow was introduced by Dupuit (1863) and the assumptions involved in it are frequently referred to as the Dupuit assumptions. If the method is used in cases where these assumptions do not apply, serious errors can be introduced.



We next consider another problem in which the cross-sectional area of flow diminishes along the path of flow, leading to a progressive steepening of the hydraulic gradient. In this case, however, the decrease in area is generated by cylindrical geometry rather than by the slope of a free surface.

The figure shows a well located at the center of a circular island. The well taps a confined aquifer which is recharged by the open water around the perimeter of the island. During pumping, water flows radially inward toward the well. We assume that the open water around the island maintains the head at a constant level along the periphery of the aquifer and that the recharge along this periphery equals the well discharge. Since the well is at the center of the island and the island is circular, we can assume that cylindrical symmetry will prevail; we can therefore introduce polar coordinates to simplify the problem.

QUESTION

If b represents the thickness of the aquifer, which of the following expressions represents the cross-sectional area of flow at a radial distance r from the axis of the well?

	Turn to Section:
$2\pi rb$	27
$\pi r^2 b$	12
$2\pi r^2$	6

□ 42

Your answer in Section 24 is not correct. The statement that there is a linear increase in head with distance away from the stream implies that there is a *non-zero* slope, dh/dx , in the potentiometric surface, and this in turn implies that flow exists in the aquifer. Darcy's law states that

$$Q = -KA \frac{dh}{dx}$$

Hydraulic conductivity, K , may be very low,

but cannot be considered equal to zero as long as we are dealing with an aquifer in the normal sense of the word. Thus in order for Q to be zero, through a given area A , the head gradient dh/dx normal to A must be zero. In this case we have observed a head gradient which is not zero in the aquifer, so we know that flow of some magnitude must exist in the aquifer.

Return to Section 24 and choose another answer.

43 □

Your answer in Section 25,

$$\frac{Q}{bw} = -K \frac{dh}{dx},$$

is not correct. You have taken the cross-sectional area of flow to be bw —that is, the product of aquifer thickness and width of section. An examination of the figure in Sec-

tion 25 will show that this does not represent the actual area of flow. The aquifer is not saturated through its full thickness, but rather to a distance h above the base of the aquifer. Thus, the cross-sectional area of flow is wh , rather than bw .

Return to Section 25 and choose another answer.

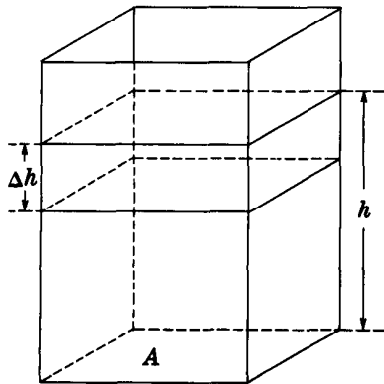
Part IV. Ground-Water Storage

Introduction

In Parts II and III we dealt with aquifers and porous media only as conduits—that is, we discussed only their properties relating to the transmission of water in steady flow. Aquifers have another very important hydraulic property—that of water storage. In Part IV we will examine this property of ground-water storage and develop an equation to describe it. In Part V we will develop

the differential equations for a simple case of nonequilibrium flow by combining the storage equation with Darcy's law, by means of the equation of continuity, which is simply a statement of the principle of conservation of mass. In Part VI, we will repeat this process for the case of nonequilibrium radial flow to a well and will obtain an important solution to the resulting differential equation.

1



The picture shows an open tank, having a square base of area A . If a volume of water, ΔV , is poured into this tank, the water level will rise by an increment, Δh , such that

$\Delta V = A \cdot \Delta h$. The total volume, V , of water in storage in the tank at any time can be determined by measuring the depth, h , of water in the tank and multiplying this depth by A .

QUESTION

Suppose the total volume of water in storage is plotted as a function of the level of water in the tank, so that the volume associated with any water level can be read directly from the plot. The graph will be:

Turn to Section:

- | | |
|--|----|
| (a) a parabola with slope $\frac{\Delta V}{\Delta h}$ | 10 |
| (b) a straight line with slope $\frac{\Delta V}{\Delta h} = A$ | 11 |
| (c) a logarithmic curve | 9 |

2

Your answer in Section 26 is not correct. The volume of water present in the sand initially was hAn . A certain fraction, β , of this fluid volume was drained off by gravity, leaving the fraction $1-\beta$ still occupied by fluid. β thus represents the fraction of the total pore space, below the level h , which does not already contain water, and which

must be refilled in order to resaturate the sand to the level h . That is, in order to resaturate the sand to the level h , a volume of water equal to this unoccupied pore volume must be pumped into the tank.

Return to Section 26 and choose another answer.

3

Your answer in Section 21 is not correct. In the imaginary experiment described in Section 21, it was stated that doubling the base area of the prism had the effect of doubling the slope of the V,h plot—that is, of doubling the term dV/dh . Thus, dV/dh

depends upon the size of the prism considered, as well as upon the type of aquifer material; it cannot be considered a constant representative of the aquifer material.

Return to Section 21 and choose another answer.

4

Your answer in Section 16,

$$\frac{\Delta V}{\Delta h} = \frac{dV}{dh} = n\beta,$$

is not correct. It neglects the effect of the base area, A , of the tank.

We have seen that when the tank is drained by gravity and then resaturated to the level h , the relation between V and h is

$$V = hAn\beta$$

where n is the porosity of the sand and β the fraction of the water in the sand that can be drained out by gravity. Now if, instead of

draining the sand to the bottom of the tank, we simply remove a small volume of water, ΔV , so that the water level in the tank falls by a small amount Δh , we should expect ΔV and Δh to be related in the same way as V and h in our previous experiment. If we are resaturating the sand by increments, when it has previously been saturated and then drained by gravity, the same relation should hold.

Return to Section 16 and choose another answer.

5

Your answer in Section 20 is not correct. If each well penetrated both aquifers, there would be no reason for the responses of the two wells to differ. The form of the response might be difficult to predict, but at least it should be roughly the same for each well.

Keep in mind that the storage coefficient of the artesian zone will probably be smaller than the specific yield of the water-table aquifer by at least two orders of magnitude.

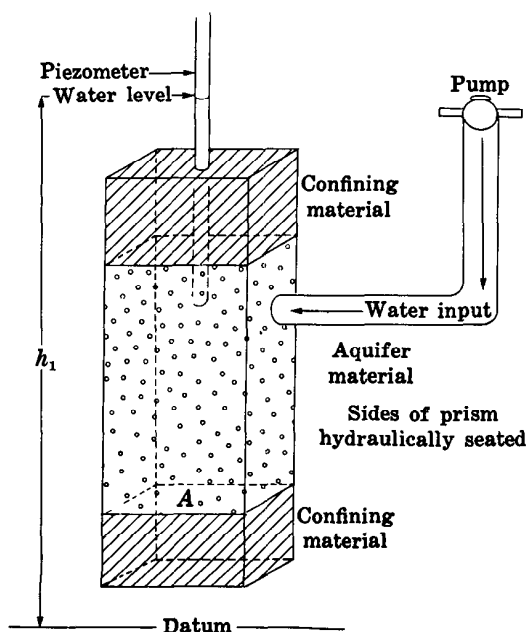
Return to Section 20 and choose another answer.

6

Your answer in Section 32 is correct. Specific yield figures for normal aquifer materials may range from 0.01 to 0.35. It is common to speak of the specific yield of an unconfined aquifer as a whole; but it should be noted that the process of release from unconfined storage really occurs at the water table. If the water table falls or rises within an aquifer, into layers or strata having different hydraulic properties, specific yield must change. In addition, of course, specific yield can vary with map location, in response to local geologic conditions.

Unconfined storage is probably the most important mechanism of ground-water storage from an economic point of view, but it is not the only such mechanism. Storage effects have also been observed in confined or artesian aquifers. The mechanism of confined storage depends, at least in part, upon compression and expansion of the water itself and of the porous framework of the aquifer; for this reason confined storage is sometimes referred to as compressive storage. In this outline we will not attempt an analysis of the mechanism of confined storage, but will concentrate instead on developing a mathematical description of its effects, suitable for hydrologic calculations. A discussion of the mechanism of confined storage is given by Jacob (1950, p. 328-334), and by Cooper (1966).

The diagram shows a vertical prism extending through a uniform confined aquifer. The base area of the prism is A . Although the prism remains structurally a part of the confined aquifer, we suppose it to be isolated hydraulically from the rest of the aquifer by imaginary hydraulic barriers, so that water added to the prism remains within it. We further imagine that we have some method of pumping water into the prism in measured increments, and that we have a piezometer, as shown in the diagram, through which we can measure the head within the prism.

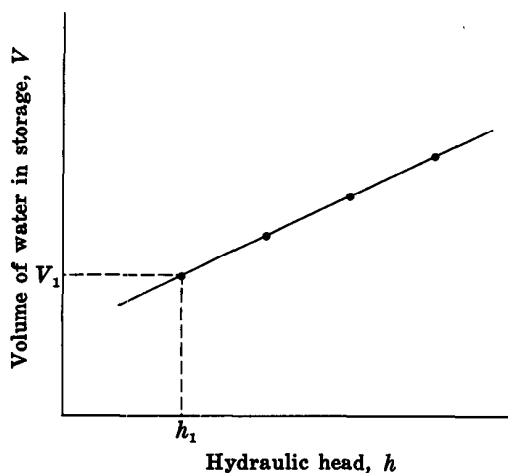


(continued on next page)

6—Con.

QUESTION

Suppose that head is initially at the level h_1 , which is above the top of the aquifer, indicating that the prism is not only saturated, but under confined hydrostatic pressure. We



designate the volume of water in storage in this initial condition as V_1 . Now suppose more water is pumped into the prism by increments; and that the head is measured after each addition, and a graph of the volume of water in storage versus the hydraulic head in the prism is plotted. If the resulting plot had the form shown in the figure, which of the following statements would you accept as valid?

Turn to Section:

- (a) The rate of change of volume of water in confined storage, with respect to hydraulic head, h , is constant; that is $\frac{dV}{dh} = \text{constant}$ 21
- (b) The rate of change of hydraulic head with respect to volume in storage, depends upon the volume in storage. 23
- (c) The rate of change of volume in storage, with respect to the base area of the prism, is equal to Δh . 30

7

Your answer in Section 32 is not correct. One important concept which is missing from the definition you selected is that specific yield refers to a unit base area of the aquifer. The definition you selected talks about the volume of water which can be drained from the aquifer—this would vary with extent of the aquifer and would normally be a

very large quantity. As we wish specific yield to represent a property of the aquifer material, we define it in terms of the volume that can be drained per unit map area of aquifer.

Return to Section 32 and choose another answer.

8

Your answer in Section 25 is not correct. The relation given in Section 25 for the rate of release of water from storage was

$$\frac{dV}{dt} = SA \frac{dh}{dt}$$

where S is the storage coefficient, A the area of aquifer under study, and dh/dt the rate

of change of head with time within that area of aquifer. In the question of Section 25, the specific yield of the water-table aquifer was given as 0.20, and the rate of decline of water level in the shallow well was given as 0.5 foot per day. The surface area of a section of the aquifer within a 10 foot radius of the well would be $\pi \times 10^2$, or 314 square feet. The

8—Con.

rate of release from storage in this section would therefore be

$$\frac{dV}{dt} = SA \frac{dh}{dt} = 0.2 \times 314 \times 0.5$$

$$= 31.4 \text{ cubic feet per day.}$$

Return to Section 25 and choose another answer.

9

Your answer in Section 1 is not correct. Whenever we add a fixed volume of water—say 10 cubic feet—to the tank, the water level must rise by a corresponding fixed amount. If the base area of the tank is 5 square feet, the addition of 10 cubic feet of water must always produce an increase of 2 feet in h ; the addition of 15 cubic feet of water must produce an increase of 3 feet in h ; and so on. The ratio $\Delta V/\Delta h$ in this case must always

be 5. In other words, the ratio $\Delta V/\Delta h$ is constant and is equal to the base area, A , of the tank.

Now if we plot V versus h , the slope of this plot will be $\Delta V/\Delta h$, by definition. This slope, as we have seen above, must be a constant. A logarithmic curve does not exhibit a constant slope.

Return to Section 1 and choose another answer.

10

Your answer in Section 1 is not correct. The increment in the volume of water within the tank, resulting from an increase in water level of Δh , is given by $\Delta V = A\Delta h$. Thus,

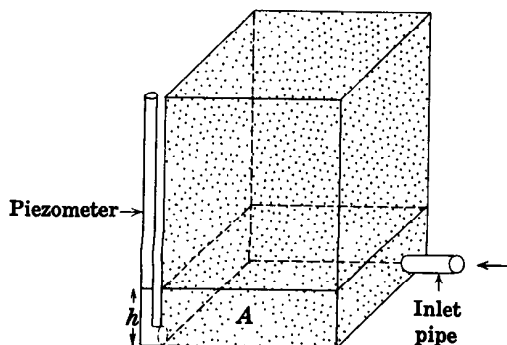
$$\frac{\Delta V}{\Delta h} = A$$

where A , the base area of the tank, is a constant. If we construct a plot of V , the vol-

ume of water in the tank, versus h , the level in the tank, the slope of the plot will by definition be $\Delta V/\Delta h$; but since $\Delta V/\Delta h$ is a constant, the plot cannot be a parabola. The slope of a parabola changes continuously along the graph.

Return to Section 1 and choose another answer.

11



Your answer in Section 1 is correct. The slope of the graph, $\Delta V/\Delta h$ or dV/dh , is constant and equal to A . Thus the volume of water in storage per foot of head (water level) in the tank is A .

Now consider the tank shown in the sketch. It is similar to the one we just dealt with, except that it is packed with dry sand having an interconnected (effective) porosity denoted by n . The tank is open at the top and has a base of area A . Water can be

11—Con.

pumped into the tank through a pipe connected at its base, and the water level within the tank—that is, the level of saturation in the sand—can be measured by means of a piezometer, also connected at the base of the tank.

QUESTION

Suppose we pump a small volume of water, V , into the tank and observe the level, h , to

which water rises in the piezometer. Neglecting all capillary effects, which of the following expressions would constitute a valid relation between the volume of water pumped into the tank and the rise in water level above the base of the tank?

$$V = Ah$$

$$h = VAn$$

$$V = hAn$$

Turn to Section:

31

12

14

12

Your answer in Section 11 is not correct. If the water rises to a level h above the base of the tank, the bulk volume of saturated sand (neglecting capillary effects) will be hA . This bulk volume must be multiplied by the porosity to obtain the total volume of sat-

urated pore space. A review of the definition of porosity as given in Part I may help to clarify this.

Return to Section 11 and choose another answer.

13

Your answer in Section 25 is correct. The release from storage in a given area in the water-table aquifer is given by

$$\frac{dV}{dt} = S_v A \frac{dh}{dt} = 0.2 \times A \times 0.5 = 0.1A.$$

The release from storage in an equal area in the artesian aquifer would be

$$\frac{dV}{dt} = SA \frac{dh}{dt} = 2 \times 10^{-4} \times A \times 5 = 0.001A.$$

Thus the water-table contribution exceeds the artesian release by a factor of 100.

This completes our introductory discussion of aquifer storage. You may go on to Part V, in which we will combine the concept of aquifer storage with Darcy's law, using the equation of continuity, to develop the differential equation for a simple problem in non-equilibrium ground-water flow.

14

Your answer, $V = hAn$, in Section 11 is correct. Now suppose water is added to the tank in increments, and h is measured after the addition of each increment; and suppose a graph of V versus h is plotted, where V is the total or cumulative volume which has been added, and h is the water level in the tank.

QUESTION

Again neglecting all capillary effects, the resulting graph would be:

- | | Turn to Section: |
|---|------------------|
| (a) a straight line with slope $\frac{\Delta V}{\Delta h} = \frac{1}{An}$ | 17 |
| (b) a straight line with slope $\frac{\Delta V}{\Delta h} = An$ | 26 |
| (c) a logarithmic curve with slope depending on h | 22 |

15

Your answer in Section 20 is not correct. The specific yield of the water-table aquifer would normally be greater than the storage coefficient of the artesian zone by at least two orders of magnitude. A seasonal fluctuation in pumpage would usually involve a brief withdrawal from storage, or a brief period of accumulation in storage. The two aquifers are pumped at about the same rate, so presumably seasonal adjustments in the pumpage will be of the same order of magnitude

for each. However, the response of the two aquifers to withdrawal (or accumulation) of a similar volume of water would be completely different, and would be governed by their storage coefficients. The aquifer with the higher storage coefficient could sustain the withdrawal with less drawdown of water level than could the aquifer with the lower storage coefficient.

Return to Section 20 and choose another answer.

16

Your answer, $V = hAn\beta$, in Section 26 is correct. This expression gives the volume of water withdrawn in draining the tank by gravity, and the volume which must be added to resaturate the sand to the original level, under our assumption that the fraction held by capillary forces is constant.

QUESTION

Suppose, subject to the same assumption, that the tank is drained by removing increments of water (or resaturated by adding increments of water) and a graph of the volume of water in storage, V , versus the level

of saturation, h , is plotted from the results of the experiment. Which of the following expressions would describe the slope of the resulting graph?

	Turn to Section:
$\frac{\Delta V}{\Delta h} = \frac{dV}{dh} = n\beta$	4
$\frac{\Delta V}{\Delta h} = \frac{dV}{dh} = An\beta$	33
$\frac{\Delta V}{\Delta h} = \frac{dV}{dh} = hAn\beta$	29

17

Your answer in Section 14 is not correct. We have seen that if a volume of water, V , is pumped into the tank when it is initially dry, the equation

$$V = h \cdot A \cdot n$$

describes the relation between V and h , the level of water in the sand. If the sand is

already saturated to some level, and an additional volume of water, ΔV , is pumped in, the water level will rise by an increment Δh , such that

$$\Delta V = \Delta h \cdot A \cdot n.$$

Return to Section 14 and use this relation in choosing another answer.

18

Your answer in Section 26 is not correct. $h \cdot A \cdot n$ would represent the volume of water required to raise the water level to a distance h above the base of the tank, *if the sand were initially dry*. In this case, however, the sand is not initially dry. Some of the pore space is already occupied by water at the beginning of the experiment, since after drainage by gravity, capillary effects cause some water to be held in permanent retention. The volume of water which must be added to resaturate the sand to the level h is equal to the volume of pore space below the level h which

does not already contain water. The total volume of pore space below the level h is $h \cdot A \cdot n$; when the sand was initially saturated, this entire volume contained water. When the sand was drained, a certain fraction of this water, which we designate β , was removed. The remaining fraction, $1 - \beta$, was held by capillary retention in the sand. Thus β represents the *fraction of the pore space* which is empty when we begin to refill the tank.

Return to Section 26 and choose another answer.

19

Your answer in Section 33 is not correct. Because the aquifer material is identical to the sand of our tank experiments and because the base area of our prism of aquifer is equal to the base area of our tank, we should expect the relation between volume released from storage and decline in water level within the prism to be identical to that obtained for the tank. In the answer which you selected, how-

ever, there is no description of the effect of capillary retention. Remember that the factor β , which was used in the tank experiment to describe the fraction of the water which could be drained by gravity, as opposed to that held in capillary retention, must appear in your answer.

Return to Section 33 and choose another answer.

20

Your answer in Section 21 is correct. The results of the imaginary experiment suggest that the term

$$\frac{1}{A} \frac{dV}{dh}$$

is a constant for the aquifer material.

In practice, in dealing with the confined or compressive storage of an aquifer, it is usually *assumed* that the quantity $(1/A)(dV/dh)$ is a constant for the aquifer, or is at least a constant for any given location in the aquifer. This quantity, $(1/A)(dV/dh)$, is denoted S and is called the *confined or compressive storage coefficient*, or simply the *storage coefficient*, of the aquifer.

It would of course be difficult or impossible to perform the experiment described in Section 6. However, if storage coefficient is defined by the equation

$$S = \frac{1}{A} \frac{dV}{dh},$$

a nonequilibrium theory can be developed from this definition which explains many of the observed phenomena of confined flow.

The following points should be noted regarding confined storage coefficient:

- (1) The storage coefficient is the volume of water released from storage in a prism of unit area, extending through the full thickness of the aquifer, in

20—Con.

response to a unit decline in head. This statement can be appreciated by a review of the hypothetical experiment described earlier, or by letting $A=1$ in the finite-difference form of the definition, $S = (1/A) (\Delta V/\Delta h)$.

- (2) The definition of storage coefficient is similar to that of specific yield, in the sense that each is defined as the term $(1/A) (dV/dh)$, for a prism extending through an aquifer. Thus in many applications, the two terms occupy the the same position in the theory. In the case of an unconfined aquifer the specific yield is often referred to as the storage coefficient.
- (3) It should be noted, however, that the processes involved in the two types of storage are completely different. Withdrawal from or addition to unconfined storage takes place at the water table; it is spoken of as occurring in a prism of aquifer because it is usually the only significant form of storage within such a prism in most water-table situations. Confined storage effects, on the other hand, are distributed throughout the vertical thickness of an aquifer.
- (4) Confined storage coefficient values are generally several orders of magnitude less than specific yield values. Specific yields range typically from 0.01 to 0.35, whereas confined storage values usually range from 10^{-5} to 10^{-3} .

The definition of confined storage in terms of a prism extending through the aquifer is adequate where the flow is entirely horizontal—that is, where no differences in head or in lithology occur along a vertical within the

aquifer. Where vertical differences do occur, one must allow for the possibility of different patterns of storage release at different points along the vertical, and a storage definition based on a prism is no longer adequate. Use is therefore made of the *specific storage*, S_s , which is defined as the volume of water released from confined storage in a unit *volume* of aquifer, per unit decline in head. In a homogeneous aquifer, S_s would be equal to S divided by the thickness of the aquifer.

QUESTION

Consider a small ground-water basin that has both an artesian aquifer and a water-table aquifer. Regional withdrawal from the artesian aquifer is about equal to that from the water-table aquifer, and seasonal fluctuations in pumpage are similar. Records are kept on two observation wells, neither of which is in the immediate vicinity of a discharging well. One well shows very little fluctuation in water level in response to seasonal variations in pumpage, while the other shows great fluctuation. Which of the following statements would more probably be true?

Turn to Section:

- (a) The well showing little fluctuation taps the water-table aquifer, while that showing great fluctuation taps the artesian zone. 25
- (b) Each well penetrates both aquifers. 5
- (c) The well showing great fluctuation taps the water-table aquifer, while that showing little fluctuation taps the artesian zone. 15

21

Your answer in Section 6 is correct. The plot is a straight line, so the slope, dV/dh , is a constant. Now suppose the prism is expanded to twice its original base area, and our imaginary experiment is repeated; and suppose we observe that, as a result of the increase in base area, the slope of our V, h plot is twice its original value.

QUESTION

Let A now represent the base area of any general (vertical) prism through the aquifer; or in general, let A represent the surface area of the section of the aquifer we are isolating for discussion. On the basis of the evidence described, which of the following statements would you be inclined to accept?

- Turn to Section:
- (a) $\frac{dV}{dh}$
is a constant for the aquifer material 3
- (b) The term $\frac{1}{A} \frac{dV}{dh}$
is a constant for the aquifer material 20
- (c) The term $A \frac{dV}{dh}$
is a constant for the aquifer material 34

22

Your answer in Section 14 is not correct. We have seen that, neglecting capillary effects, there is a linear relationship between the volume of water, V , pumped into the tank when it is initially dry, and the level of water, h , above the base of the tank. That is, a constant coefficient, An , relates these two quantities: $V = h \cdot A \cdot n$. This linearity holds

as well if the water is added to the tank in increments. Each incremental volume of water, ΔV , pumped into the tank produces an increment in head, Δh , such that

$$\Delta V = \Delta h \cdot A \cdot n.$$

Return to Section 14 and choose another answer.

23

Your answer in Section 6 is not correct. The ratio of the change of volume of water in storage, to the change in hydraulic head is by definition the slope, $\Delta V/\Delta h$ or dV/dh , of a plot of V versus h . If this rate of change of V with h were to depend upon V , the plot of V versus h would show a different slope

at different values of V . The plot, in other words, would be some sort of curve. The plot shown in Section 6, however, is a straight line—it has a constant slope, the same for any value of V .

Return to Section 6 and choose another answer.

24

Your answer in Section 25 is not correct. The relation given in Section 25 for the rate of release of water from storage was

$$\frac{dV}{dt} = SA \frac{dh}{dt}$$

where S is the storage coefficient, A the area of aquifer under study, and dh/dt the rate of change of head with time within that area of aquifer. In the question of Section 25, S was given as 2×10^{-4} for the artesian aquifer, and dh/dt , as measured in the deep well,

was 5 feet per day. A section of the aquifer within a 10 foot radius of the observation well would have a surface area of $\pi \times 10^2$, or 314 square feet. The rate of release of water from storage in this section would therefore be

$$\begin{aligned} \frac{dV}{dt} &= SA \frac{dh}{dt} = 2 \times 10^{-4} \times 314 \times 5 \\ &= 0.314 \text{ cubic feet per day.} \end{aligned}$$

Return to Section 25 and choose another answer.

25

Your answer in Section 20 is correct. Because of the higher storage coefficient of the water-table aquifer, release or accumulation of a comparable volume of water will cause a much smaller fluctuation of water level in the water-table aquifer than in the artesian aquifer. In effect, we have introduced time variation into the problem here, since we are discussing changes in head with time. To bring time into the equations, we may proceed as follows.

Let S represent either specific yield or storage coefficient. Then according to our definitions we may write, using the finite-difference form,

$$S = \frac{1}{A} \frac{\Delta V}{\Delta h}$$

The relation between the volume of water taken into or released from aquifer storage in a prism of base area A and the accompanying change in head, is therefore:

$$\Delta V = SA \Delta h.$$

Now let us divide both sides of this equation by Δt , the time interval over which the decline in head was observed. We then have:

$$\frac{\Delta V}{\Delta t} = SA \frac{\Delta h}{\Delta t}$$

or, if we are talking about a vanishingly small time interval,

$$\frac{dV}{dt} = SA \frac{dh}{dt}$$

Here dV/dt is the time rate of accumulation of water in storage, expressed, for example, in cubic feet per day; and dh/dt is the rate of increase in head, expressed, for example, in feet per day. If we are dealing with release from storage, head will decline, and both dV/dt and dh/dt will be negative. The partial derivative notation, $\partial h/\partial t$, is usually used instead of dh/dt , because head may vary with distance in the aquifer as well as with time. This equation is frequently referred to as the storage equation.

The equation can also be obtained using the rules of differentiation. For the case we are considering we have

$$\frac{dV}{dt} = \frac{dV}{dh} \cdot \frac{dh}{dt},$$

but from the definition of storage coefficient, $dV/dh = SA$, so that by substitution

$$\frac{dV}{dt} = SA \frac{dh}{dt}.$$

(continued on next page)

25—Con.

QUESTION

Suppose we record the water levels in a deep observation well, penetrating a confined aquifer which has a storage coefficient of 2×10^{-4} , and a shallow observation well, tapping a water-table aquifer which has a specific yield of 0.20. The water level in the deep well falls at a rate of 5 feet per day, while that in the shallow well falls at a rate of 0.5 foot per day. Considering the release of water from storage in each aquifer within a radius of 10 feet of the observation well, which of the following statements would be most accurate?

- (a) within a radius of 10 feet of the shallow well, water is being released from storage in the water-table aquifer at a rate of 5 cubic feet per day. 8
- (b) the rate of release of water from storage in the water-table aquifer, within 10 feet of the shallow well, is 100 times as great as that in the artesian aquifer, within 10 feet of the deep well. 13
- (c) within a radius of 10 feet of the deep well, water is being released from storage in the artesian aquifer at a rate of 1 cubic foot per day. 24

26

Your answer in Section 14 is correct. If there were no capillary effects, the result of filling the tank with sand would simply be to take up some of the volume available for storage of water. Thus the slope of the plot of V versus h for the sand-filled tank would differ from that for the open tank (Section 1) only by the factor n , which is the ratio of the storage volume available in the sand-filled tank to that available in the open tank.

In practice, of course, capillary effects cannot be neglected. In this development we will take a simplified view of these effects, as a detailed examination of capillary phenomena is beyond the scope of our discussion. Let us assume that due to capillary forces, a certain constant fraction of the water in the sand is permanently retained. That is, we assume that following the initial saturation of the sand, we can never drain off by gravity the full volume of water which was added during the initial saturation. A part of this initially added water remains permanently held in the pore spaces by capillary attrac-

tion; thus the amount of water which can be alternately stored and recovered is reduced.

QUESTION

Suppose the tank is initially saturated to a level h and is then drained by gravity. Suppose further that the ratio of the volume of water drained to that initially added is observed to be β ; that is, the fraction of the added water which can be drained is β , while the fraction retained in the sand by capillary forces is $(1 - \beta)$. Subject to our assumption that the fraction retained is a constant, which of the following expressions gives the volume of water which would have to be restored to the tank, after draining, in order to resaturate the sand to the same level, h , as before?

	Turn to Section:
$V = hAn$	18
$V = hA \frac{n}{\beta}$	2
$V = hAn\beta$	16

27

Your answer in Section 32 is not correct. Your answer defines specific yield as the quantity (presumably the total quantity) of water which can be drained by gravity from a unit area of the aquifer. In the preceding analysis, we developed the concept of specific yield in terms of the quantity of water which can be drained *per unit decline in water level*.

A verbal definition of specific yield must therefore include this latter concept in some manner—that is, it must indicate that we are referring to the quantity released from storage per unit decline in head.

Return to Section 32 and choose another answer.

28

Your answer in Section 33 is not correct. The aquifer material was given as identical to the sand of the tank experiments described previously, and the base area of the prism was taken as equal to the base area of the tank. We are considering only storage within the prism itself, in relation to water level in the prism, and are not concerned with what goes on in the aquifer beyond the boundaries

of the prism. At this rate, we should expect the relation between the volume of water drained from storage and the accompanying decline in water level to be the same for our prism of aquifer as for the tank of the earlier experiments.

Return to Section 33 and choose another answer.

29

Your answer in Section 16,

$$\frac{\Delta V}{\Delta h} = \frac{dV}{dh} = hAn\beta$$

is not correct. This answer would indicate that the relation between V and h —that is, the slope of a plot of V versus h —is a function of h . However, we have already seen that if we refill the tank after it has been drained by gravity, we will find V and h to be related by a constant $An\beta$. That is, we

will find that $V = hAn\beta$ or that the ratio of V to h is the constant $An\beta$. If the tank is drained by increments, or refilled by increments after draining, we would expect the same relationship to hold between the increments of fluid volume, ΔV , and the increments of head, Δh , as was observed between V and h in the initial problem. That is, we would expect to find that $\Delta V = \Delta h \cdot An\beta$.

Return to Section 16 and choose another answer.

30

Your answer in Section 6 is not correct. Δh represents a simple change in the hydraulic head, h . It does not represent any form of rate of change; when we describe a rate of change, we always require two variables, since we always consider the ratio of change of one variable to that of another. At this point of our discussion, moreover,

we are considering the relation between the volume of water in storage and the hydraulic head. We have not yet taken into consideration the effect of varying the base area of our prism of aquifer.

Return to Section 6 and choose another answer.

31

Your answer in Section 11 is not correct. The sand-filled tank of Section 11 differs from the open tank of Section 1, in that any quantity of water pumped into the sand-filled tank can utilize only the interconnected pore volume as its storage space; in the open tank of Section 1 the full capacity of the tank was available. If the sand-filled tank is initially empty and a volume of water, V , is pumped in, this water will occupy the total volume of interconnected space between the base of the tank and the height to which the sand is saturated (neglecting capillary

effects). If the water level in the sand is a distance h above the base of the tank, the bulk volume of the saturated part of the sand will be $h \cdot A$, where A is the base area of the tank. However, the volume of injected water will not equal this bulk saturated volume, but rather the interconnected pore volume within the saturated region. A review of the definition of porosity as given in Part I may help to clarify this.

Return to Section 11 and choose another answer.

32

Your answer in Section 33,

$$\frac{dV}{dh} = An\beta,$$

is correct. The aquifer material is assumed to be identical to the sand in the tank experiments; if the area of the prism is equal to that of the tank, the two plots of storage versus water level should be identical. Note, however, that area is a factor in the expression for dv/dh ; if we were to choose a prismatic section of larger area, it would provide more storage, per foot of head change, than one of smaller area, just as a tank of larger base area would provide more storage, per foot of water-level change, than a tank of smaller area. If the base of our prism of aquifer were unity, the expression for dV/dh would be simply $n\beta$; and in general, an expression could be written for the change in storage volume per unit head change, *per unit area of aquifer*, as

$$\frac{1}{A} \cdot \frac{dV}{dh} = n\beta.$$

The term $n\beta$ is referred to as the specific yield of an aquifer, and is usually designated S_y . Because we have assumed $(1-\beta)$, the fraction of water retained by capillary forces, to be constant, we obtain the result that S_y is a constant; and for many engineering applications, this is a satisfactory approximation. It should be noted, however, that it is only an approximation; the fraction of water held in capillary retention may change with time, for various reasons, leading to apparent variations in S_y with time.

Specific yield describes the properties of an aquifer to store and release water (through unconfined storage) just as permeability describes its properties of transmitting water. Mathematically, specific yield is equivalent to the term $(1/A)(dV/dh)$ for an unconfined aquifer.

(continued on next page)

32—Con.

QUESTION

On the basis of the above discussion, which of the following statements would you select as the best verbal definition of specific yield?

Turn to Section:

- | | |
|--|--|
| <p>(a) The specific yield of an unconfined aquifer is the volume of water which can be drained by gravity from the aquifer in response to a unit decline in head. 7</p> | <p>(b) The specific yield of a horizontal unconfined aquifer is the volume of water which is drained by gravity from a vertical prism of unit base area extending through the aquifer, in response to a unit lowering of the saturated level. 6</p> <p>(c) The specific yield of an unconfined aquifer is the quantity of water which can be drained from a unit area of the aquifer. 27</p> |
|--|--|

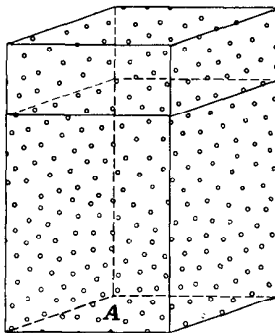
33

Your answer in Section 16,

$$\frac{\Delta V}{\Delta h} = \frac{dV}{dh} = An\beta,$$

is correct. The slope of the graph of volume of water in storage versus water level—or in other words, the derivative of V with respect to h —would be constant and equal to $An\beta$.

Now suppose that we are dealing with a prismatic section taken vertically through a



uniform unconfined aquifer as shown in the figure. The base area of the prism is again denoted A . Suppose the aquifer material is identical in its hydraulic properties to the sand of our tank experiments. We wish to construct a graph of the water in recoverable storage within the prism versus the level of saturation, or water-table level, in the aquifer in the vicinity of the prism. We are interested only in water which can be drained by gravity; water in permanent capillary retention will not be considered part of the storage.

QUESTION

Which of the following expressions would describe the slope of this graph?

Turn to Section:

- | | |
|----------------------------|----|
| $\frac{dV}{dh} = Ahn\beta$ | 28 |
| $\frac{dV}{dh} = An$ | 19 |
| $\frac{dV}{dh} = An\beta$ | 32 |

34

Your answer in Section 21 is not correct. In the imaginary experiment described in Section 21, it was stated that doubling the base area, A , of the prism had the effect of doubling the slope, dV/dh , of the V, h plot. Thus the term $A(dV/dh)$ would be four times as great for the prism of doubled area, as for the original prism. That is, the term

$A(dV/dh)$ would depend upon the size of the prism considered, as well as upon the type of aquifer material, and could not be considered a constant representative of the aquifer material.

Return to Section 21 and choose another answer.

Part V. Unidirectional Nonequilibrium Flow

Introduction

In Part V, our purpose is to develop the differential equation for a problem of non-equilibrium flow. To do this, we utilize the storage equation,

$$\frac{dV}{dt} = SA \frac{dh}{dt},$$

developed in Part IV, and we utilize Darcy's law. These two relations are linked by means of a relation called the equation of continuity, which is a statement of the principle of conservation of mass.

In Part VI we will develop the same type of equation in polar coordinates and will discuss a solution to this equation for a particular flow problem. In the course of working through Parts V and VI, the reader may realize that the relations describing the storage and transmission of ground water can be combined to develop the differential equa-

tions for many other types of flow; and that solutions to these equations can be developed for a variety of field problems.

Before the start of the program of Part V, there is a brief discussion, in text form, of the significance of partial derivatives, their use in ground-water equations, and in particular their use in a more general form of Darcy's law. This form of Darcy's law was introduced in the text-format discussion at the end of Part II. The discussion here is intended primarily for readers who may not be accustomed to using partial derivatives and vector notation. It may be omitted by readers conversant with these topics. This discussion is not intended as a rigorous treatment of partial differentiation. Readers who are not familiar with the subject may wish to review such a treatment in any standard text of calculus.

Partial derivatives in ground-water flow analysis

When a dependent variable varies with more than one independent variable, the partial derivative notation is used. A topographic map, for example, may be considered a representation of a dependent variable (elevation) which is a function of two independent variables—the two map directions, which we will call x and y , as shown in figure *i*. If elevation is denoted E , each contour on the map represents a curve in the x - y plane along which E has some constant value. In general, if we move in the x direction, we will cross elevation contours—that is, E will change. Let us say that if we move a distance Δx parallel to the x axis, E is observed to change by an amount ΔE_x . We may

form a ratio, $\Delta E_x/\Delta x$, of this change in elevation to the length of the x interval in which it occurs. If the interval Δx becomes vanishingly small, this ratio is designated $\partial E/\partial x$ and is termed the partial derivative of E with respect to x . $\partial E/\partial x$ is actually the slope of a plot of E versus x , at the point under consideration, or the slope of a tangent to this plot, as shown in figure *i*. Note that in obtaining $\partial E/\partial x$ we move parallel to the x axis—that is, we hold y constant, considering only the variation in E due to the change in x .

Similarly, if we move a small distance, Δy , parallel to the y axis, E will again change by some small amount, ΔE_y . We again form a ratio, $\Delta E_y/\Delta y$; if the distance taken along

the y axis is vanishingly small, this ratio is designated $\partial E/\partial y$ and is termed the partial derivative of E with respect to y . Note that this time we have moved parallel to the y axis; in effect we have held x constant and isolated the variation in E due to the change in y alone.

If it happened that land surface varied so regularly over the map area that we could actually write a mathematical expression giving elevation, E , as a function of x and y , then we could compute $\partial E/\partial x$ simply by differentiating this expression with respect to x , treating y as a constant. Similarly, we could compute $\partial E/\partial y$ by differentiating the expression with respect to y , treating x as a constant. For example, suppose that after studying the contour map, we decide that elevation can be expressed approximately as a function of x and y by the equation

$$E = 5x^2 + 10y + 20.$$

Differentiating this equation with respect to x , treating y as a constant, gives

$$\frac{\partial E}{\partial x} = 10x.$$

We could, therefore, compute $\partial E/\partial x$ at any point by substituting the x -coordinate of that point into the above equation. Differentiating the equation with respect to y , treating x as a constant, gives

$$\frac{\partial E}{\partial y} = 10,$$

indicating that $\partial E/\partial y$ has the same value, 10, at all points of the map. In this example, $\partial E/\partial x$ turned out to be independent of y and $\partial E/\partial y$ turned out to be independent of both x and y . In general, however, $\partial E/\partial x$ may depend on both x and y , and $\partial E/\partial y$ may also depend on both x and y . For example, if E were described by the equation

$$E = 5x^2 + 5y^2 + 8xy + 20,$$

differentiation with respect to x would give

$$\frac{\partial E}{\partial x} = 10x + 8y$$

while differentiation with respect to y would give

$$\frac{\partial E}{\partial y} = 10y + 8x.$$

In the topographic-map example, $\partial E/\partial x$ and $\partial E/\partial y$ are space derivatives—that is, each describes the variation of E in a particular direction in space. In the discussion given in this chapter we will use the space derivative of head, $\partial h/\partial x$, giving the change in hydraulic head with respect to distance in the x direction. In addition, however, we will use the time derivative of head, $\partial h/\partial t$, giving the change in head with respect to time, if position is held fixed. $\partial h/\partial t$ is a partial derivative, just as is $\partial h/\partial x$, and it is computed according to the same rules, by considering all independent variables except t to be constant. We could in fact make a “map” of the variation of head with respect to distance and time by laying out coordinate axes marked x and t , and drawing contours of equal h in this x, t plane. The discussion given for directional derivatives in the topographic-map example could then be applied to $\partial h/\partial t$ in this example.

The partial derivative of head with respect to distance, $\partial h/\partial x$, gives the slope of the potentiometric surface in the x direction at a given point, x , and time, t . This is illustrated in figure *ii*. If x or t are varied, then in general $\partial h/\partial x$ will vary, since the slope of the potentiometric surface changes, in general, both with position and with time.

The partial derivative of head with respect to time, $\partial h/\partial t$, gives the time rate at which water level is rising or falling—that is, the slope of a hydrograph—at a given point, x , and time, t . This is shown in figure *iii*. Again, if x or t are varied, then in general $\partial h/\partial t$ will vary. In other words, $\partial h/\partial x$ is a function of both x and t , and $\partial h/\partial t$ is also a function of both x and t , in the general case.

Physically, $\partial h/\partial x$ may be thought of as the slope of the potentiometric surface which

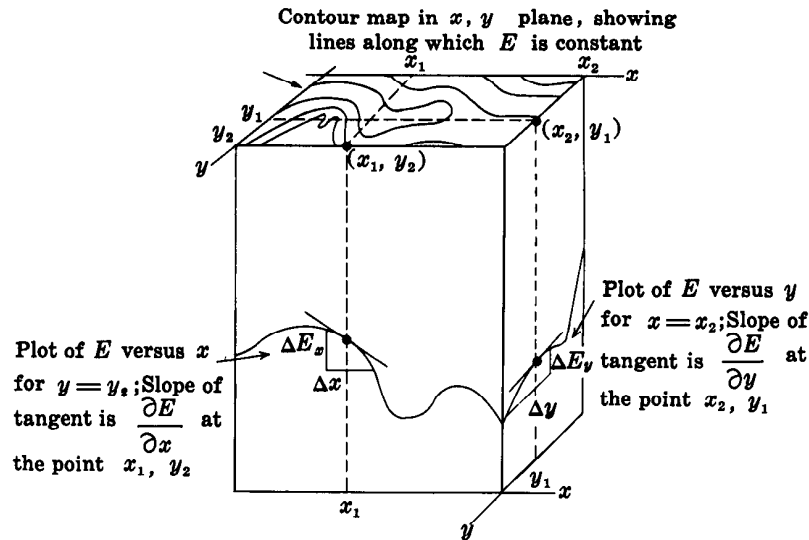


fig. i

will be observed if time is suddenly frozen at some value. If an expression is given for h , as a function of x and t , $\partial h / \partial x$ can be calculated by differentiating this expression with respect to x , treating t as a constant. In the same way, $\partial h / \partial t$ may be visualized as the slope of a hydrograph recorded at a particu-

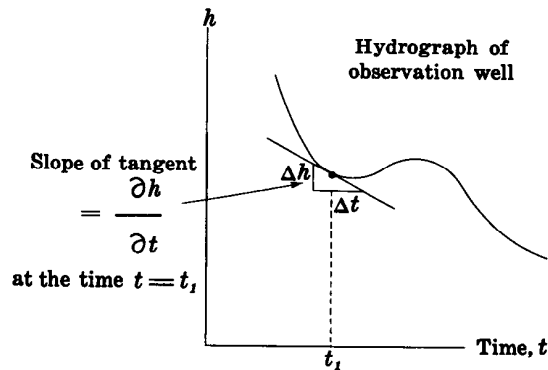


fig. iii

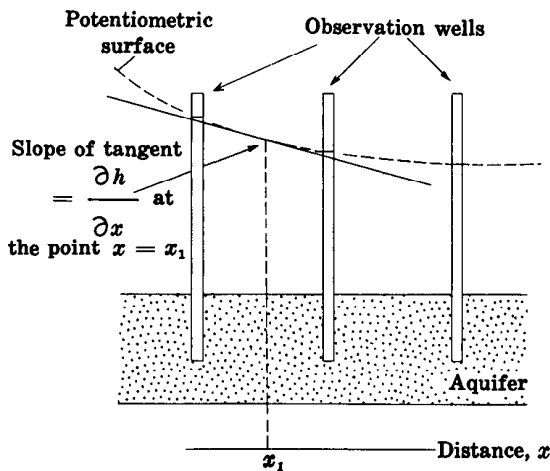


fig. ii

lar location (x value). If h is given as a function of x and t , an expression for $\partial h / \partial t$ may be obtained by differentiating with respect to t , treating x as if it were a constant.

In the discussion in Part V the problem is restricted to only one space derivative, $\partial h / \partial x$, and the time derivative. In the general case, we would have to consider all three space derivatives— $\partial h / \partial x$, $\partial h / \partial y$, and

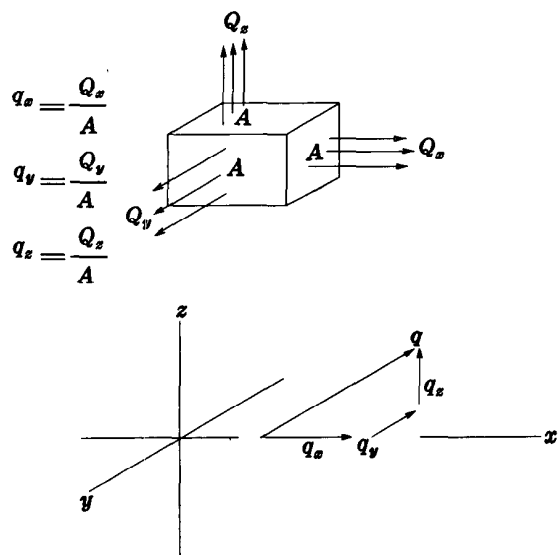


fig. iv

$\partial h/\partial z$ —in addition to the time derivative. In such a case, as noted in the discussion at the close of Part II, we would utilize Darcy's law in a somewhat more general form. When flow may occur in more than one direction, we consider the specific discharge, $q = Q/A$ to be a vector, having the three components q_x , q_y , and q_z . If the medium is isotropic, each of these components is given by a form of

Darcy's law, in which the partial derivative of head in the direction concerned is employed. The expressions for the apparent velocity components are

$$q_x = -K \frac{\partial h}{\partial x}$$

$$q_y = -K \frac{\partial h}{\partial y}$$

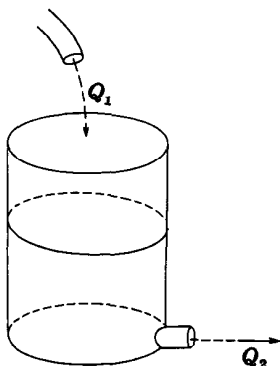
$$q_z = -K \frac{\partial h}{\partial z}$$

where K is the hydraulic conductivity.

q_x actually represents the fluid discharge per unit area in the x direction—that is, the discharge crossing a unit area oriented at right angles to the x axis. Similarly, q_y and q_z represent the discharges crossing unit areas normal to the y and z axes, respectively. The three components are calculated individually and added vectorially to obtain the resultant apparent velocity of the flow. (See figure iv.)

We now proceed to the programmed material of Part V.

I''



The picture shows an open tank with an inflow at the top and an outlet pipe at the base. Water is flowing in at the top at a rate Q_1 and is flowing out at the base at a rate Q_2 .

QUESTION

Suppose we observe that the volume of water in the tank is increasing at a rate of 5 cubic feet per minute. Which of the following equations could we consider correct?

$Q_1 = 5$ cubic feet per minute	29
$\frac{Q_1 + Q_2}{2} = 2.5$ cubic feet per minute	17
$Q_1 - Q_2 = 5$ cubic feet per minute	21

Turn to Section:

Your answer in Section 32,

$$Q_1 - Q_2 = K \frac{\partial h}{\partial x},$$

is not correct. The inflow through face 1 of the prism is given, according to Darcy's law, as a product of the hydraulic conductivity, the head gradient at face 1, and the cross-sectional area, $b\Delta y$, of face 1; that is,

$$Q_1 = -K \left(\frac{\partial h}{\partial x} \right)_1 b\Delta y.$$

Similarly, the outflow through face 2 is given as a product of hydraulic conductivity, head gradient at face 2, and the cross-sectional area of face 2, which is again $b\Delta y$; that is

$$Q_2 = -K \left(\frac{\partial h}{\partial x} \right)_2 b\Delta y.$$

Inflow minus outflow is thus given by

$$Q_1 - Q_2 = Kb\Delta y \left\{ \left(\frac{\partial h}{\partial x} \right)_2 - \left(\frac{\partial h}{\partial x} \right)_1 \right\}.$$

In the preceding sections, we have seen that the term

$$\left\{ \left(\frac{\partial h}{\partial x} \right)_2 - \left(\frac{\partial h}{\partial x} \right)_1 \right\}$$

can be written in an equivalent form using the second derivative.

Return to Section 32 and use this second derivative form in the above equation to obtain the correct answer.

" 2

Your answer in Section 30,

$$Q_1 = \frac{-K}{b\Delta y} \left(\frac{\partial h}{\partial x} \right)_1,$$

is not correct. Darcy's law states that the flow through a given plane—in this case, face 1 of the prism—is given as the product of hydraulic conductivity, area, and head gradi-

ent. Your answer gives the flow as the product of hydraulic conductivity and head gradient, divided by area.

Return to Section 30 and choose another answer.

" 3

Your answer in Section 7,

$$\frac{\partial^2 h}{\partial x^2} \cdot \frac{\partial h}{\partial x},$$

is not correct. We wish to find the change in the quantity $\partial h/\partial x$ over a small interval, Δx , of the x -axis. We have seen in the preceding sections of Part V that the change in a variable over such an interval is given by the derivative of the variable times the length

of the interval. Here, the variable is $\partial h/\partial x$ and the interval is Δx ; thus we require the derivative of $\partial h/\partial x$ with respect to x and must multiply this by the interval Δx .

Return to Section 7 and choose another answer.

" 4

5 "

Your answer in Section 21 is not correct. A falling water level in the piezometer would indicate that water was being released from storage in the prism of aquifer. The slope of a plot of piezometer level versus time would in this case be negative; that is, $\partial h/\partial t$ would be negative, since h would decrease as t increased. According to the storage equation,

$$\frac{dV}{dt} = SA \frac{\partial h}{\partial t}$$

and therefore the rate of accumulation in storage, dV/dt , would also have to be negative. That is, we would have depletion from storage, rather than accumulation in storage. The question in Section 22, however, states that inflow to the prism exceeds outflow; thus, according to the equation of continuity, accumulation in storage should be occurring.

Return to Section 21 and choose another answer.

6 "

Your answer in Section 21 is not correct. If the water level in the piezometer were constant with time, a plot of the piezometer readings versus time would simply be a horizontal line. The slope of such a plot, $\partial h/\partial t$, would be zero. From the storage equation, then, the rate of accumulation of water in storage in the prism would have to be zero, for we would have

$$\frac{dV}{dt} = SA \frac{\partial h}{\partial t} = SA \cdot 0 = 0.$$

The question states, however, that inflow to the prism exceeds outflow; according to the equation of continuity, then, the rate of accumulation of water in storage cannot be zero. Rather, it must equal the difference between inflow and outflow.

Return to Section 21 and choose another answer.

7 "

Your answer in Section 16,

$$\left(\frac{dy}{dx}\right)_2 - \left(\frac{dy}{dx}\right)_1 = \left(\frac{d\left(\frac{dy}{dx}\right)}{dx}\right)_{1-2} (x_2 - x_1),$$

is correct. In this case, the derivative itself is the variable whose change is required, and for this we must use the derivative of the derivative,

$$\frac{d\left(\frac{dy}{dx}\right)}{dx},$$

evaluated at an appropriate point within the interval. This term is called the second derivative of y with respect to x , and the notation d^2y/dx^2 is used for it. That is,

$$\frac{d^2y}{dx^2} = \frac{d\left(\frac{dy}{dx}\right)}{dx}$$

= slope of a plot of $\frac{dy}{dx}$ versus x .

The terms and notations used in the case of partial derivatives are entirely parallel. The notation $\partial^2h/\partial x^2$ is used to represent the second *partial* derivative of h with respect to x , which in turn is simply the partial derivative of $\partial h/\partial x$ with respect to x . That is,

Con.— " 7

$$\frac{\partial^2 h}{\partial x^2} = \frac{\partial \left(\frac{\partial h}{\partial x} \right)}{\partial x}$$

= slope of a plot of $\frac{\partial h}{\partial x}$ versus x .

Again, the partial derivative notation indicates that we can expect $\partial h/\partial x$ to vary with t (or some other variable) as well as with x ; $\partial^2 h/\partial x^2$ measures only its change due to a change in x , all other independent variables being held constant.

QUESTION

In Section 9, we saw that inflow minus outflow for our prism of aquifer could be expressed in the form

$$Q_1 - Q_2 = Kb\Delta y \left\{ \left(\frac{\partial h}{\partial x} \right)_2 - \left(\frac{\partial h}{\partial x} \right)_1 \right\}$$

and that the term

$$\left\{ \left(\frac{\partial h}{\partial x} \right)_2 - \left(\frac{\partial h}{\partial x} \right)_1 \right\}$$

represented the change in the hydraulic gradient occurring across the prism. If the width of the prism in the x direction (that is, parallel to the x -axis) is Δx , which of the following expressions could most reasonably be substituted for

$$\left\{ \left(\frac{\partial h}{\partial x} \right)_2 - \left(\frac{\partial h}{\partial x} \right)_1 \right\}?$$

Turn to Section:

$$\frac{\partial^2 h}{\partial x^2} \cdot \frac{\partial h}{\partial x} \quad 4$$

$$\frac{\partial \left(\frac{\partial h}{\partial x} \right)}{\partial x} \quad 23$$

$$\frac{\partial^2 h}{\partial x^2} \cdot \Delta x \quad 32$$

Your answer in Section 30,

$$Q_1 = -Kb\Delta x\Delta y \left(\frac{\partial h}{\partial x} \right)_1,$$

is not correct. According to Darcy's law, the flow through face 1 should equal the product of the hydraulic conductivity, the cross-sectional area of the face, and the head gradi-

ent at face 1. The cross-sectional area of face 1 is simply $b\Delta y$.

Return to Section 30 and choose another answer.

" 8

Your answer in Section 33,

$$Q_1 - Q_2 = -Kb\Delta y \left\{ \left(\frac{\partial h}{\partial x} \right)_1 - \left(\frac{\partial h}{\partial x} \right)_2 \right\},$$

is correct. We may change the term in braces to $(\partial h/\partial x)_2 - (\partial h/\partial x)_1$ and drop the negative sign to obtain the form

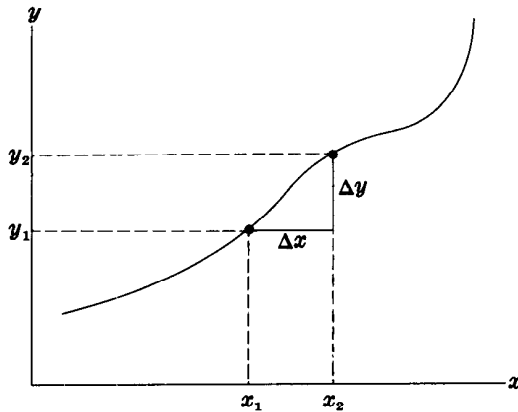
$$Q_1 - Q_2 = Kb\Delta y \left\{ \left(\frac{\partial h}{\partial x} \right)_2 - \left(\frac{\partial h}{\partial x} \right)_1 \right\}.$$

The term $(\partial h/\partial x)_2 - (\partial h/\partial x)_1$ represents the change in hydraulic gradient from one side of the prism of aquifer to the other. We wish now to express this change in hydraulic gradient in a slightly different form.

(continued on next page)

" 9

9" —Con.



QUESTION

In the figure, a variable y is plotted as a function of an independent variable, x . As x changes from x_1 to x_2 , y changes from y_1 to y_2 ; $(dy/dx)_{1-2}$ represents the slope of the plot at a point between x_1 and x_2 . If the change in x is small, which of the following expressions would you use to obtain an approximate value for the change in y ?

Turn to Section:

$$y_2 - y_1 = \left(\frac{dy}{dx} \right)_{1-2} (x_2 - x_1) \quad 16$$

$$y_2 - y_1 = \left(\frac{dy}{dx} \right)_{1-2} + (x_2 - x_1) \quad 25$$

$$y_2 - y_1 = m(x_2 - x_1) + \frac{\Delta y}{\Delta x} \quad 20$$

10"

Your answer in Section 34,

$$\frac{dV}{dt} = S \Delta x \Delta y \frac{\partial h}{\partial t}$$

is correct. (We should note that for a finite prism, $\partial h / \partial t$ may vary from point to point between the two faces; and we require an average value, which will yield the correct value of dV/dt for the prism. In fact there is always at least one point within the prism at which the value of $\partial h / \partial t$ is such an average, and we assume that we can measure and use $\partial h / \partial t$ at such a point. If we allow the prism to become infinitesimal in size, only one value of $\partial h / \partial t$ can be specified within it, and this

value will yield an exact result for dV/dt .)

Using the equation of continuity we may now set this expression which we have obtained for rate of accumulation equal to our expression for inflow minus outflow.

QUESTION

Which of the following equations is obtained by equating the above expression for dV/dt to that obtained in Section 34 for $Q_1 - Q_2$?

Turn to Section:

$$\frac{\partial^2 h}{\partial x^2} = \frac{S}{T} \frac{\partial h}{\partial t} \quad 19$$

$$T \frac{\partial^2 h}{\partial x^2} \Delta x \Delta y = S \frac{\partial h}{\partial t} \quad 11$$

$$T \Delta y \Delta x \frac{\partial h}{\partial x} = S \Delta x \Delta y \frac{\partial h}{\partial t} \quad 24$$

Your answer in Section 10 is not correct. We used Darcy's law to obtain expressions for inflow and outflow from the prism of aquifer, and we used the second derivative notation to express the difference between inflow and outflow. This led, in Section 34, to the equation

$$Q_1 - Q_2 = T \Delta x \Delta y \frac{\partial^2 h}{\partial x^2}$$

for inflow minus outflow. According to the equation of continuity, inflow minus outflow must equal rate of accumulation in storage; that is

$$Q_1 - Q_2 = \frac{dV}{dt}$$

We obtained an expression for dV/dt through the storage equation, which states that rate of accumulation in storage must equal the product of storage coefficient, surface (or base) area, and time rate of change of head; that is

$$\frac{dV}{dt} = S \Delta x \Delta y \frac{\partial h}{\partial t}$$

Substitution of the first and third equations into the second will yield the correct result.

Return to Section 10 and choose another answer.

" 11

Your answer in Section 34,

$$\frac{dV}{dt} = \frac{S}{K} \frac{\partial h}{\partial t},$$

is not correct. The storage equation tells us that the rate of accumulation of water in storage within the prism of aquifer must equal the product of storage coefficient, rate of change of head with time, and base area of the prism. Hydraulic conductivity, K , is

not involved in the storage equation. In the answer which you selected, there is no term describing the base area of the prism, and hydraulic conductivity appears on the right side of the equation.

Return to Section 34 and choose another answer.

" 12

Your answer in Section 16,

$$\left(\frac{dy}{dx} \right)_2 - \left(\frac{dy}{dx} \right)_1 = \left(\frac{dy}{dx} \right)_{1-2}^2 (x_2 - x_1),$$

is not correct. In this case, the dependent variable, plotted on the vertical axis, is dy/dx . As we have seen in preceding sections, the change in the dependent variable is given by the slope of the graph, or derivative of the dependent variable with respect to x ,

multiplied by the change in x . Thus we require the derivative of dy/dx with respect to x in our answer. In the answer shown above, however, we have only the square of the derivative of y with respect to x .

Return to Section 16 and choose another answer.

" 13

14 "

Your answer in Section 22 is not correct. It is true that if inflow differs from outflow

the water level in the prism of aquifer must change with time. However, it need not rise; if inflow is less than outflow, it will fall.

Return to Section 22 and choose another answer.

15 "

Your answer in Section 33,

$$Q_1 - Q_2 = \frac{S}{K} \left(\frac{\partial h}{\partial x} \right)_2$$

is not correct. This answer associates storage coefficient, S , with a space derivative of head, $(\partial h / \partial x)_2$; this in itself should be sufficient

to indicate that it is incorrect. In the storage equation, S is associated with the time derivative of head, $\partial h / \partial t$. Again, the answer chosen involves only the head gradient at the outflow face. Since we are seeking an expression for inflow *minus* outflow, we would expect head gradients at both faces to be involved in the answer.

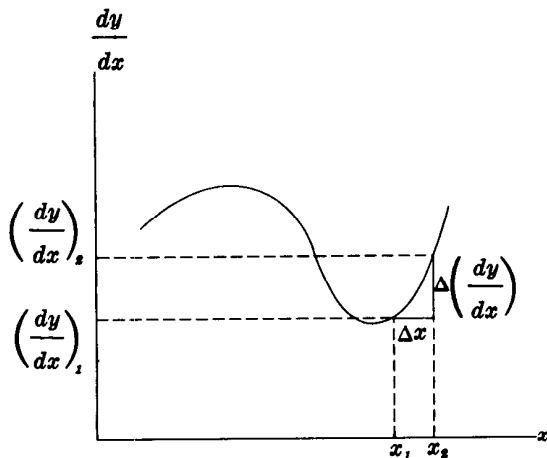
Return to Section 33 and choose another answer.

16 "

Your answer in Section 9,

$$y_2 - y_1 = \left(\frac{dy}{dx} \right)_{1-2} (x_2 - x_1),$$

is correct. The change in the dependent variable, y , is found by multiplying the change in the independent variable, x , by the slope of the plot, dy/dx . Note that dy/dx must be the slope in the vicinity of the interval x_1 to x_2 ;



frequently, it is considered to be the slope at the midpoint of this interval. The approximation becomes more and more accurate as the size of the interval, $x_2 - x_1$, decreases. The above equation is often written in the form

$$\Delta y = \frac{dy}{dx} \cdot \Delta x.$$

(In a more formal sense, it can be demonstrated that if y is a continuous function of x and if dy/dx exists throughout the interval from x_1 to x_2 , then there is at least one point somewhere in this interval at which the derivative, dy/dx , has a value such that

$$\frac{dy}{dx} = \frac{y_2 - y_1}{x_2 - x_1}$$

or

$$y_2 - y_1 = \frac{dy}{dx} (x_2 - x_1).$$

This is known as the law of the mean of differential calculus. It guarantees that the approximation can always be used, provided we are careful about the point within the interval at which we take dy/dx . Further, since this law must hold no matter how small

(continued on next page)

the interval $(x_2 - x_1)$ is taken, the approximation must become exact as the interval is allowed to become infinitesimal.)

QUESTION

Now suppose we measure the slope of our curve, dy/dx , at various points, and construct a plot of dy/dx versus x , as shown in the figure. Again, suppose we wish to know the change in dy/dx which occurs as x changes from x_1 to x_2 . The subscript 1-2 is again used to denote evaluation at a point between x_1 and x_2 . Which of the following expressions would give an approximate value for this change?

$$\left(\frac{dy}{dx}\right)_2 - \left(\frac{dy}{dx}\right)_1 = (x_2 - x_1) \left(\frac{dy}{dx}\right)_{1-2} \quad 31$$

$$\left(\frac{dy}{dx}\right)_2 - \left(\frac{dy}{dx}\right)_1 = \left(\frac{dy}{dx}\right)_{1-2}^2 (x_2 - x_1) \quad 13$$

$$\left(\frac{dy}{dx}\right)_2 - \left(\frac{dy}{dx}\right)_1 = \left(\frac{d\left(\frac{dy}{dx}\right)}{dx}\right)_{1-2} (x_2 - x_1) \quad 7$$

Turn to Section:

Con.— " 16

Your answer in Section 1 is not correct. The rate of accumulation in the tank does depend upon both Q_1 and Q_2 , but not in the way that your answer implies. The inflow to the tank must be balanced by outflow, by ac-

cumulation of water in the tank, or by a combination of these factors.

Return to Section 1 and choose another answer.

" 17

Your answer in Section 33,

$$Q_1 - Q_2 = K \left(\frac{\partial h}{\partial x}\right)_1 - K \left(\frac{\partial h}{\partial x}\right)_2$$

is not correct. The answer treats both inflow and outflow as products of hydraulic conductivity and head gradient; but we have seen, in our application of Darcy's law to the

problem, that each should be a product of hydraulic conductivity, head gradient, and flow area.

Return to Section 33 and choose another answer.

" 18

Your answer in Section 10,

$$\frac{\partial^2 h}{\partial x^2} = \frac{S}{T} \frac{\partial h}{\partial t},$$

is correct. This equation describes groundwater movement under the simple conditions which we have assumed—that is, where the aquifer is confined, horizontal, homogeneous, and isotropic, and the movement is in one direction (taken here as the x direction).¹ If horizontal components of motion normal to

¹A rigorous and more general development of the ground water equation is given by Cooper (1966).

the x -axis were present, we would have to consider inflow and outflow through the other two faces of the prism; that is, the two faces normal to the y -axis. We would find this inflow minus outflow to be

$$Q_{y1} - Q_{y2} = Kb \Delta x \Delta y \frac{\partial^2 h}{\partial y^2}.$$

The total inflow minus outflow for the prism would then be $(Q_{x1} - Q_{x2}) + (Q_{y1} - Q_{y2})$,

" 19

19 " —Con.

where $Q_{x_1} - Q_{x_2}$ represents the term we obtained previously, $Kb\Delta x\Delta y (\partial^2 h / \partial x^2)$. Finally, equating this total inflow minus outflow to the rate of accumulation, we would have

$$Kb\Delta x\Delta y \frac{\partial^2 h}{\partial x^2} + Kb\Delta x\Delta y \frac{\partial^2 h}{\partial y^2} = S\Delta x\Delta y \frac{\partial h}{\partial t}$$

or, using the notation $T = Kb$, and dividing through by $T\Delta x\Delta y$,

$$\frac{\partial^2 h}{\partial x^2} + \frac{\partial^2 h}{\partial y^2} = \frac{S}{T} \frac{\partial h}{\partial t}$$

These equations are *partial differential equations*; that is, they are equations containing partial derivatives. The relation given above for two-dimensional flow is a partial differential equation in three independent variables x , y , and t . For simplicity, we continue the discussion in terms of the equation for unidirectional flow,

$$\frac{\partial^2 h}{\partial x^2} = \frac{S}{T} \frac{\partial h}{\partial t}$$

This is a partial differential equation in two independent variables, x and t . It relates the rate of change of head with time, to the rate at which the slope of the potentiometric surface, $\partial h / \partial x$, changes with distance. When we say that we require a *solution* to this partial differential equation, we mean that we are looking for an expression giving head,

h , as a function of position, x , and time, t , such that when this expression is differentiated twice with respect to x (to obtain $\partial^2 h / \partial x^2$) and once with respect to t (to obtain $\partial h / \partial t$), the results will satisfy the condition

$$\frac{\partial^2 h}{\partial x^2} = \frac{S}{T} \frac{\partial h}{\partial t}$$

As with ordinary differential equations, there will always be an infinite number of expressions which will satisfy a partial differential equation; the particular solution required for a given problem must satisfy, in addition, certain conditions peculiar to that problem. As in ordinary differential equations, these additional conditions, termed boundary conditions, establish the starting points from which the changes in h described by the differential equation are measured.

This concludes Part V. In Part VI, we will make a development similar to the one made in Part V, but using polar coordinates, and dealing with the problem of non-equilibrium flow to a well. Our approach will be the same: we will express inflow and outflow in terms of Darcy's law and rate of accumulation in terms of the storage equation; we will then relate these flow and storage terms through the equation of continuity. We will go on to discuss a particular solution of the resulting partial differential equation and will show how this solution can be used to build up other solutions, including the well-known Theis equation.

20 "

Your answer in Section 9,

$$y_2 - y_1 = m(x_2 - x_1) + \frac{\Delta y}{\Delta x},$$

is not correct. If y is plotted as a function of

x , the change in y corresponding to a small change in x is given by the relation

Change in $y =$ (Slope of curve)

\cdot (Change in x),

where the slope of the curve is measured in the vicinity in which the change is sought. This follows directly from the definition of the slope of the curve.

Return to Section 9 and choose another answer.

" 21

Your answer in Section 1 is correct. If water is accumulating in the tank at a rate of 5 cubic feet per minute, inflow must exceed outflow by this amount. This is essentially a statement of the principle of conservation of mass. Since matter cannot be destroyed (except by conversion into energy, which we need not consider here), the difference between the rate at which mass enters the tank and that at which it leaves the tank must equal the rate at which it accumulates in the tank. Further, because compression of the water is not significant here, we may use volume in place of mass. In general terms, the relation with which we are dealing may be stated as:

Inflow - Outflow = Rate of accumulation.

This relation is often termed the equation of continuity.

Note that if outflow exceeds inflow, the

rate of accumulation will be negative—that is, we will have depletion rather than accumulation. An important special case of this equation is that in which inflow and outflow are in balance, so that the rate of accumulation is zero. As an example, consider a tank in which the inflow is just equal to the outflow. Rate of accumulation in the tank is zero, and the water level does not change with time. The flow is said to be in equilibrium, or in the steady state. The problems which we considered in Part III were of this sort; no changes of head with time were postulated, so the assumption that inflow and outflow were in balance was implicit. The flow pattern could be expected to remain the same from one moment to the next.

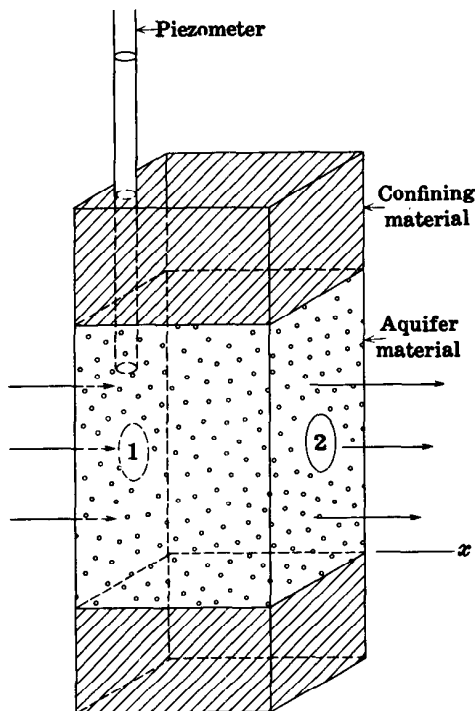
Forms of the equation of continuity occur in all branches of physics. In electricity, for example, if the flow of charge toward a capacitor exceeds that away from it, charge must accumulate on the capacitor plate, and voltage must increase. In heat conduction, if the flow of heat into a region exceeds that leaving it, heat must accumulate within the region, and the temperature within the region must rise.

QUESTION

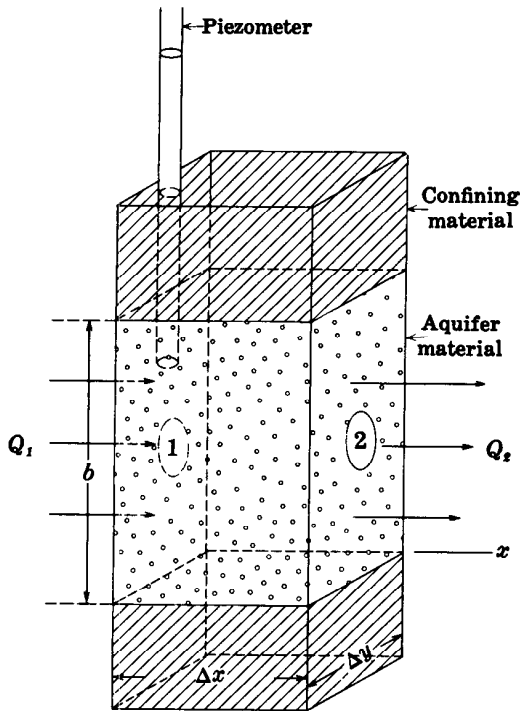
The sketch shows a prismatic section through a confined aquifer. Water is flowing in the x direction, that is, into the prism through face 1 and out of the prism through face 2. A piezometer or observation well measures the hydraulic head within the prism. Let us suppose that the volumetric rate at which water is entering through face 1 exceeds that at which it is leaving through face 2. The water level in the piezometer will then:

Turn to Section:

remain constant with time	6
fall steadily	5
rise	30



22 "



Your answer in Section 30,

$$Q_1 = -Kb\Delta y \left(\frac{\partial h}{\partial x} \right)_1,$$

is correct. $(\partial h/\partial x)_1$ is the hydraulic gradient at the particular point and time in which we are interested. We simply insert it in Darcy's law to obtain the required flow rate.

We are dealing with nonequilibrium flow here; that is, in general, inflow and outflow will not be equal. Flow occurs only in the x direction; thus the outflow from our prism of aquifer must take place entirely through face 2, as shown in the sketch.

QUESTION

Assuming that outflow differs from inflow and that the hydraulic conductivity and thickness of the aquifer are constant, which of the following statements is correct?

Turn to Section:

- The water level in the prism must rise 14
- The hydraulic gradient at face 2 of the prism must differ from that at face 1 of the prism 33
- The rate of withdrawal from storage must be given by Darcy's law. 26

23 "

Your answer in Section 7,

$$\frac{\partial \left(\frac{\partial h}{\partial x} \right)}{\partial x},$$

is not correct. As we have seen in earlier sections of this chapter, the change in a

dependent variable, over a small interval of the x -axis, Δx , is given by the derivative of the variable times the length of the interval. Here, the variable is $\partial h/\partial x$ and the term $\partial(\partial h/\partial x)/\partial x$ of your answer is certainly its derivative. However, this derivative is not multiplied by the interval along the x -axis; thus the answer gives only the *rate* of change of $\partial h/\partial x$ with distance—not its actual change across the interval Δx .

Return to Section 7 and choose another answer.

24 "

Your answer in Section 10 is not correct. The rate of accumulation in storage is given by

$$S\Delta x\Delta y \frac{\partial h}{\partial t},$$

as in the answer which you chose. However, the expression for inflow minus outflow requires a second derivative, as it deals with

the difference between two flow terms, each of which incorporates a first derivative. In the answer which you chose, inflow minus outflow is expressed in terms of a first derivative.

Con.—" 24

Review Sections 9, 32, and 34 and then return to Section 10 and choose another answer.

Your answer in Section 9,

$$y_2 - y_1 = \left(\frac{dy}{dx} \right)_{1-2} + (x_2 - x_1),$$

is not correct. From the definition of slope, the change in y can be found by multiplying the change in x by the slope of the curve, measured in the interval x_1 to x_2 . In the an-

swer which you chose, the slope of the curve is added to the change in x .

Return to Section 9 and choose another answer.

" 25

Your answer in Section 22 is not correct. Darcy's law describes the transmission of ground water, not its withdrawal from storage. The storage equation, developed in Part IV, deals with changes in the quantity of water in storage.

Return to Section 22 and choose another answer.

" 26

Your answer in Section 32,

$$Q_1 - Q_2 = K \frac{\partial^2 h}{\partial x^2} \Delta x,$$

is not correct. Your answer includes the hydraulic conductivity, K , and the term

$$\frac{\partial^2 h}{\partial x^2} \Delta x,$$

which, as we have seen, is equal to

$$\left\{ \left(\frac{\partial h}{\partial x} \right)_2 - \left(\frac{\partial h}{\partial x} \right)_1 \right\}.$$

Thus if we were to expand your answer, expressing it in the original head gradient terms, we would have

$$Q_1 - Q_2 = K \left\{ \left(\frac{\partial h}{\partial x} \right)_2 - \left(\frac{\partial h}{\partial x} \right)_1 \right\} = K \left(\frac{\partial h}{\partial x} \right)_2 - K \left(\frac{\partial h}{\partial x} \right)_1.$$

This states that inflow is a product of hydraulic conductivity and head gradient, and that outflow is similarly a product of hydraulic conductivity and head gradient. We know from Darcy's law, however, that both inflow and outflow must be given as products of hydraulic conductivity, head gradient, and flow area. Your answer thus fails to incorporate flow area into the expression for inflow minus outflow.

Return to Section 32 and choose another answer.

" 27

28 "

Your answer in Section 34,

$$\frac{dV}{dt} = Sb\Delta x \frac{\partial h}{\partial t},$$

is not correct. The storage equation states that the rate of accumulation of water in

storage in the prism of aquifer is equal to the product of storage coefficient, rate of change of head with time, and *base* area of the prism. In your answer the rate of accumulation is equated to the product of the storage coefficient, the rate of change of head with time, and the area, $b\Delta x$, of one of the vertical faces of the prism.

Return to Section 34 and choose another answer.

29 "

Your answer in Section 1 is not correct. Some of the inflow to the tank is balanced by outflow at the base. In order for your an-

swer to be correct, the outflow, Q_2 , would have to be zero. Only in that case would the rate of accumulation in the tank equal the inflow.

Return to Section 1 and choose another answer.

30 "

Your answer in Section 21 is correct. According to the equation of continuity, if inflow to the prism of aquifer exceeds outflow, water must be accumulating in storage within the prism. According to the storage equation, if water is accumulating in storage within the prism, hydraulic head in the prism must be increasing with time. Specifically, we have

$$\text{Inflow} - \text{Outflow} = \text{Rate of accumulation,}^1 \\ \frac{dV}{dt}$$

and

$$\frac{dV}{dt} = SA \frac{\partial h}{\partial t}$$

where A is the base area of the prism. Therefore,

$$\text{Inflow} - \text{Outflow} = SA \frac{\partial h}{\partial t}.$$

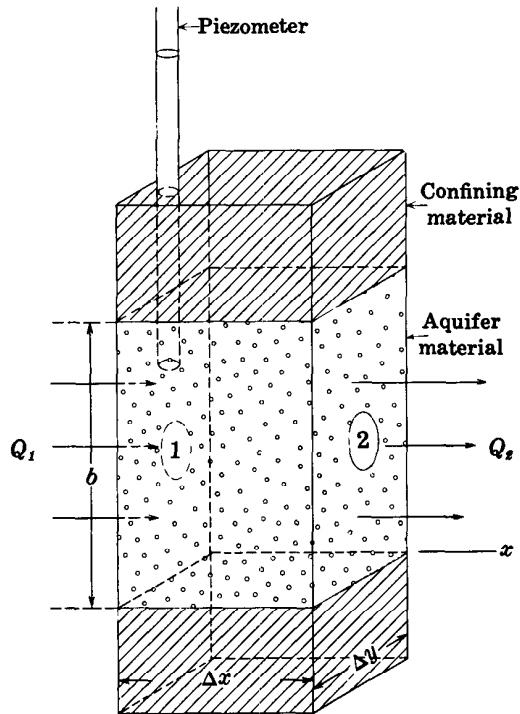
If the term (Inflow-Outflow) is positive—that is, if inflow exceeds outflow—then $\partial h/\partial t$ must be positive, and water levels must be increasing with time. In the above equations, we have used the partial derivative of head with respect to time, $\partial h/\partial t$; and in the equations that follow, we will use the partial derivative of head with respect to distance, $\partial h/\partial x$. These notations are used because, in this problem, head will vary both with time and with distance.

QUESTION

The sketch again shows the prism of Section 21. We assume this prism to be taken in a homogeneous and isotropic aquifer which is horizontal and of uniform thickness. Suppose we let $(\partial h/\partial x)_1$ represent the hydraulic gradient (in the x direction, which is the direction of the flow) at face 1 of the prism. We wish to write an expression for the inflow through face 1 of the prism. Let

¹ Here again we use volume in place of mass in the equation of continuity, even though slight compression and expansion of the water can be a factor contributing to confined storage. The changes in fluid density from point to point in a normal ground-water situation are sufficiently small to permit this approximation. In fact, if this were not the case, it would not be possible to use the simple formulation of storage coefficient, defined in terms of fluid volume, which we have adopted.

Con.— " 30



us denote this inflow Q_1 , and let us further denote the height of the prism (thickness of the aquifer) by b . The width of the prism normal to the x axis is denoted Δy , the length of the prism along the x axis is denoted Δx , and the hydraulic conductivity of the aquifer is denoted K . Which of the following equations gives the required expression for the inflow at face 1?

Turn to Section:

$$Q_1 = -Kb\Delta y \left(\frac{\partial h}{\partial x} \right)_1 \quad 22$$

$$Q_1 = -Kb\Delta x\Delta y \left(\frac{\partial h}{\partial x} \right)_1 \quad 8$$

$$Q_1 = \frac{-K}{b\Delta y} \left(\frac{\partial h}{\partial x} \right)_1 \quad 3$$

Your answer in Section 16,

$$\left(\frac{dy}{dx} \right)_2 - \left(\frac{dy}{dx} \right)_1 = (x_2 - x_1) \left(\frac{dy}{dx} \right)_{1-2},$$

is not correct. In the preceding sections we saw that the change in the dependent variable is given by the change, $x_2 - x_1$, in the independent variable, times the derivative of the dependent variable with respect to x . Here the dependent variable is dy/dx ; but

in your answer we do not have the derivative of this dependent variable with respect to x —we have, rather, only the derivative of y with respect to x .

Return to Section 16 and choose another answer.

" 31

Your answer in Section 7,

$$\frac{\partial^2 h}{\partial x^2} \cdot \Delta x,$$

is correct. This term is equivalent to the term

$$\left\{ \left(\frac{\partial h}{\partial x} \right)_2 - \left(\frac{\partial h}{\partial x} \right)_1 \right\},$$

provided that we choose a suitable point within the interval $x_2 - x_1$ at which to evalu-

ate $\partial^2 h / \partial x^2$. The product $(\partial^2 h / \partial x^2) \Delta x$ represents the slope of a plot of $\partial h / \partial x$ versus x , multiplied by the interval along the x -axis, Δx , and thus gives the change in $\partial h / \partial x$ over this interval.

(continued on next page)

" 32

32 " —Con.

QUESTION

Using this expression for

$$\left\{ \left(\frac{\partial h}{\partial x} \right)_2 - \left(\frac{\partial h}{\partial x} \right)_1 \right\},$$

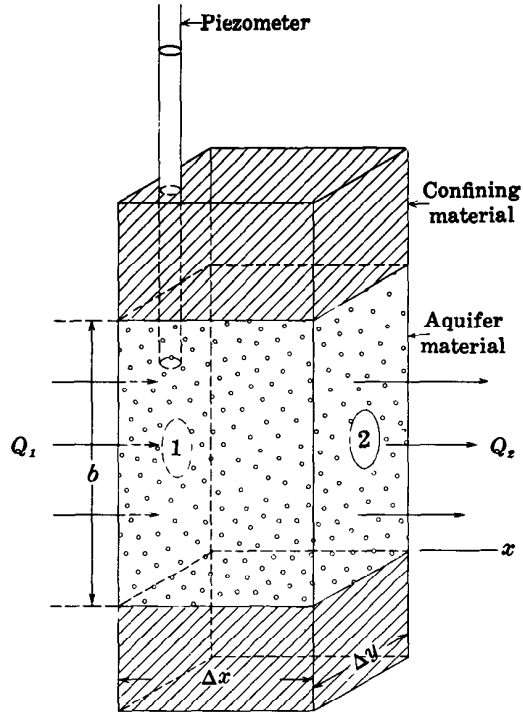
which of the following forms is the correct expression for inflow minus outflow, $Q_1 - Q_2$, for our prism of aquifer, which is shown again in the diagram?

Turn to Section:

$$Q_1 - Q_2 = K \frac{\partial^2 h}{\partial x^2} \Delta x \quad 27$$

$$Q_1 - Q_2 = Kb \Delta y \Delta x \frac{\partial^2 h}{\partial x^2} \quad 34$$

$$Q_1 - Q_2 = K \frac{\partial h}{\partial x} \quad 2$$



33 "

Your answer in Section 22 is correct. If we apply Darcy's law at face 2, we have

$$Q_2 = -Kb \Delta y \left(\frac{\partial h}{\partial x} \right)_2$$

where at face 1 we had

$$Q_1 = -Kb \Delta y \left(\frac{\partial h}{\partial x} \right)_1$$

K , b , and Δy do not change. Thus if the outflow, Q_2 , is to differ from the inflow, Q_1 , the hydraulic gradients at the inflow and outflow

faces must differ—that is, $(\partial h / \partial x)_2$ must differ from $(\partial h / \partial x)_1$.

QUESTION

Using the expressions we have developed for inflow and outflow, which of the following terms would describe inflow *minus* outflow for the prism?

Turn to Section:

$$Q_1 - Q_2 = K \left(\frac{\partial h}{\partial x} \right)_1 - K \left(\frac{\partial h}{\partial x} \right)_2 \quad 18$$

$$Q_1 - Q_2 = \frac{S}{K} \left(\frac{\partial h}{\partial x} \right)_2 \quad 15$$

$$Q_1 - Q_2 = -Kb \Delta y \left\{ \left(\frac{\partial h}{\partial x} \right)_1 - \left(\frac{\partial h}{\partial x} \right)_2 \right\} \quad 9$$

Your answer in Section 32,

$$Q_1 - Q_2 = Kb\Delta y\Delta x \frac{\partial^2 h}{\partial x^2},$$

is correct. The term Kb , representing the hydraulic conductivity of the aquifer times its thickness, is called the transmissivity or transmissibility of the aquifer, and is designated by the letter T . Using this notation, the expression for inflow minus outflow becomes

$$Q_1 - Q_2 = T\Delta y\Delta x \frac{\partial^2 h}{\partial x^2}.$$

Now according to the equation of continuity, this inflow minus outflow must equal the rate of accumulation of water in storage within the prism of aquifer, which is shown in the figure.

QUESTION

We represent the average time rate of change of head in the prism of aquifer by $\partial h/\partial t$ and note that the base area of the prism is $A = \Delta x\Delta y$. Using the storage equation, which of the following expressions gives the rate of accumulation in storage within the prism?

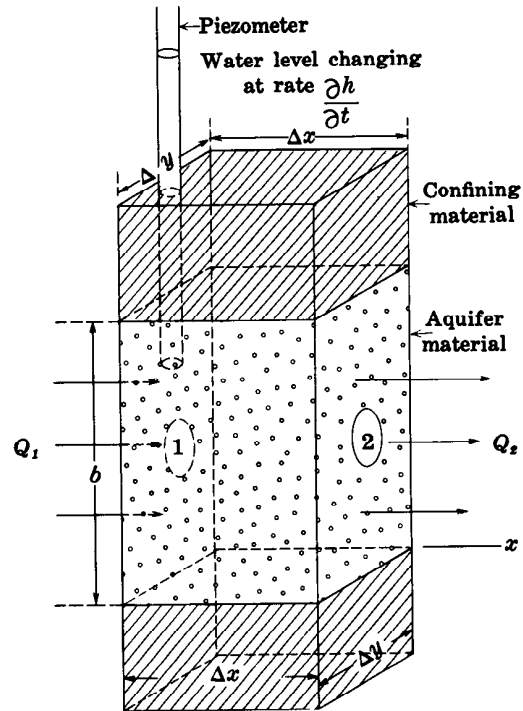
$$\frac{dV}{dt} = Sb\Delta x \frac{\partial h}{\partial t} \quad 28$$

$$\frac{dV}{dt} = \frac{S}{K} \frac{\partial h}{\partial t} \quad 12$$

$$\frac{dV}{dt} = S\Delta x\Delta y \frac{\partial h}{\partial t} \quad 10$$

Turn to Section:

" 34



Part VI. Nonequilibrium Flow to a Well

Introduction

In Part V we developed the equation

$$\frac{\partial^2 h}{\partial x^2} = \frac{S}{T} \frac{\partial h}{\partial t}$$

for one-dimensional nonequilibrium flow in a homogeneous and isotropic confined aquifer. We indicated, in addition, that extension to two-dimensional flow would yield the equation

$$\frac{\partial^2 h}{\partial x^2} + \frac{\partial^2 h}{\partial y^2} = \frac{S}{T} \frac{\partial h}{\partial t}$$

In Part VI we consider a problem involving flow away from (or toward) a well in such an aquifer. As in the steady-state problem of flow to a well, which we considered in Part III, we will find it convenient here to use polar coordinates. The two-dimensional differential equation

$$\frac{\partial^2 h}{\partial x^2} + \frac{\partial^2 h}{\partial y^2} = \frac{S}{T} \frac{\partial h}{\partial t}$$

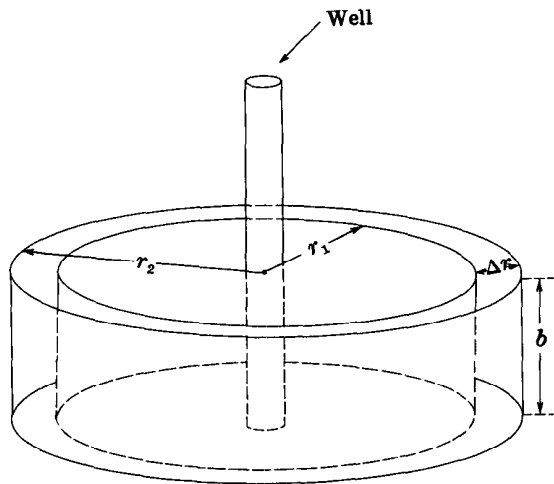
can be transformed readily into polar coordinates by using standard methods. However, it is both easy and instructive to derive the

equation again from hydraulic principles in the form in which we are going to use it. After we have developed the differential equation in this way, we will consider one of its solutions, corresponding to an instantaneous disturbance to the aquifer. In the terminology of systems analysis, this solution will give the "impulse response" of the well-aquifer system. In considering this solution, we will first show by differentiation that it satisfies the given differential equation; we will then develop the boundary conditions applicable to the problem and show that the solution satisfies these conditions. Following the programed section of Part VI, a discussion in text format has been added showing how the "impulse response" solution may be used to synthesize solutions corresponding to more complex disturbances to the aquifer. In particular, solutions are synthesized for the case of repeated withdrawal, or bailing, of a well and for the case of continuous pumping of a well. The latter solution, for the particular case in which the pumping rate is constant, is the Theis equation, which is commonly used in aquifer test analysis.



The figure shows a well penetrating a confined aquifer. A cylindrical shell or prism, coaxial with the well and extending through the full thickness, b , of the aquifer has been outlined in the diagram. The radial width of this cylindrical element is designated Δr ;

the inner surface of the element is at a radius r_1 from the axis of the well, which is taken as the origin of the polar coordinate system; and the outer surface of the element is at a radius r_2 from this axis. We assume all flow to be in the radial direction, so that

1 + —Con.—


we need not consider variation in the vertical or angular directions. We further assume that we are dealing with injection of water into the aquifer through the well, so that flow is outward, away from the well, in the positive r direction. The hydraulic conductivity of the aquifer is denoted K , the transmissivity T , and the storage coefficient S .

QUESTION

If $(\partial h / \partial r)_1$ represents the hydraulic gradient at the inner face of the cylindrical element, which of the following expressions will be obtained for the flow through this face, by an application of Darcy's law?

Turn to Section:

$$Q_1 = -K\pi r_1^2 \left(\frac{\partial h}{\partial r} \right)_1 \quad 34$$

$$Q_1 = -K2\pi r_1 b \left(\frac{\partial h}{\partial r} \right)_1 \quad 15$$

$$Q_1 = \frac{-Kb \left(\frac{\partial h}{\partial r} \right)_1}{2\pi r_1} \quad 36$$

2 + —

Your answer in Section 27,

$$\frac{\partial h}{\partial r} = \frac{V}{4\pi T t} e^{-(Sr^2/4Tt)},$$

is not correct.

You are correct in your intention to multiply the derivative of $e^{-(Sr^2/4Tt)}$ by the "constant" coefficient $V/(4\pi T t)$ to obtain the derivative of the product

$$\frac{V}{4\pi T t} e^{-(Sr^2/4Tt)},$$

with respect to r . However, your differentiation of $e^{-(Sr^2/4Tt)}$ is not correct. The deriva-

tive of e raised to some power is not simply e raised to the same power, as you have written, but the product of e raised to that power times the derivative of the exponent. That is,

$$\frac{de^u}{dr} = e^u \frac{du}{dr}$$

Thus, in this case, we must obtain the derivative of the exponent, $-(Sr^2/4Tt)$, and multiply $e^{-(Sr^2/4Tt)}$ by this derivative to obtain the derivative of $e^{-(Sr^2/4Tt)}$ with respect to r .

Return to Section 27 and choose another answer.

3 +

Your answer in Section 35,

$$\frac{\partial h}{\partial t} = \frac{V}{4\pi Tt} \cdot e^{-(Sr^2/4Tt)} \left(\frac{Sr^2}{4Tt^2} \right),$$

is not correct. In your answer, the term $e^{-(Sr^2/4Tt)}$ is differentiated correctly with respect to time. However, your answer gives only the derivative of this factor times the first factor itself, $V/(4\pi Tt)$. According to the rule for differentiation of a product, we must add to this the second factor, $e^{-(Sr^2/4Tt)}$,

times the derivative of the first factor. The first factor, $V/(4\pi Tt)$ was treated as a constant coefficient when we were differentiating with respect to r , since it does not contain r . It does, however, contain t and cannot be treated as a constant when we are differentiating with respect to t . Its derivative with respect to t is given in the discussion of Section 35.

Return to Section 35 and choose another answer.

4 +

Your answer in Section 27,

$$\frac{\partial h}{\partial r} = e^{-(Sr^2/4Tt)} \cdot \left(\frac{-2Sr}{4Tt} \right),$$

is not correct.

When an expression is multiplied by a constant coefficient, the derivative of the product is simply the constant coefficient times the derivative of the expression. For example, the derivative of the expression x^2 , with respect to x , is $2x$; but if x^2 is multiplied by the constant coefficient c , the derivative of the product, cx^2 , is $c \cdot 2x$.

In the question of Section 27, the term $e^{-(Sr^2/4Tt)}$ is actually the expression in which

we must differentiate with respect to r . The term $V/(4\pi Tt)$, represents a constant coefficient—constant with respect to this differentiation, because it does not contain r . Thus whatever we obtain as the derivative of $e^{-(Sr^2/4Tt)}$ must be multiplied by this coefficient, $V/(4\pi Tt)$, to obtain the derivative of the product

$$\frac{V}{4\pi Tt} e^{-(Sr^2/4Tt)}.$$

Your differentiation of $e^{-(Sr^2/4Tt)}$ is correct, but your answer does not contain the factor $V/(4\pi Tt)$ and thus cannot be correct.

Return to Section 27 and choose another answer.

5 +

Your answer in Section 27,

$$\frac{\partial h}{\partial r} = \frac{V}{4\pi Tt} e^{-(Sr^2/4Tt)} \cdot \left(\frac{-2Sr}{4Tt} \right),$$

is correct.

We now wish to differentiate this expression for $\partial h/\partial r$, in order to obtain $\partial^2 h/\partial r^2$. To do this, we treat the expression as the product of two factors. The first is the function we just differentiated,

$$\frac{V}{4\pi Tt} e^{-(Sr^2/4Tt)};$$

the second is

$$\left(\frac{-2Sr}{4Tt} \right).$$

Once again we are differentiating with respect to r , so that t is treated as a constant.

5 + —Con.—

QUESTION

If we follow the rule for differentiation of a product (first factor times derivative of second, plus second factor times derivative of first), which of the following results do we obtain for $\partial^2 h / \partial r^2$?

- | | |
|---|------------------------|
| $\frac{\partial^2 h}{\partial r^2} = \frac{V}{4\pi Tt} \left\{ e^{-(Sr^2/4Tt)} \cdot \left(\frac{-2S}{4Tt} \right) + \left(\frac{-2Sr}{4Tt} \right) \cdot e^{-(Sr^2/4Tt)} \cdot \left(\frac{-2Sr}{4Tt} \right) \right\}$ | Turn to Section:
35 |
| $\frac{\partial^2 h}{\partial r^2} = \frac{V}{4\pi Tt} \cdot e^{-(Sr^2/4Tt)} \cdot \left(\frac{-2S}{4Tt} \right) + \left(\frac{-2Sr}{4Tt} \right) \cdot e^{-(Sr^2/4Tt)} \cdot \left(\frac{-2Sr}{4Tt} \right)$ | 23 |
| $\frac{\partial^2 h}{\partial r^2} = \frac{V}{4\pi Tt} \left\{ e^{-(Sr^2/4Tt)} \cdot \left(\frac{-2S}{4Tt} \right) + \left(\frac{-2Sr}{4Tt} \right) \cdot e^{-(Sr^2/4Tt)} \right\}$ | 9 |

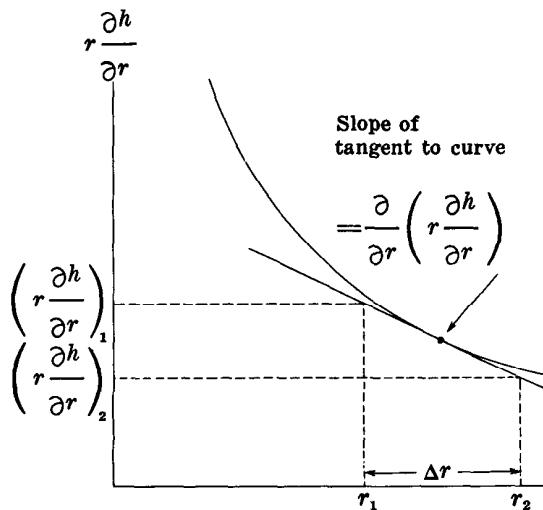
6 +

Your answer in Section 18 is not correct. The answer which you chose states that head becomes infinite as radial distance becomes small. The behavior which we are trying to describe is that in which head dies

out, or approaches zero, as radial distance becomes very large.

Return to Section 18 and choose another answer.

7 +



Your answer in Section 15,

$$Q_1 - Q_2 = 2\pi T \left\{ \left(r \frac{\partial h}{\partial r} \right)_2 - \left(r \frac{\partial h}{\partial r} \right)_1 \right\},$$

is correct. The term

$$\left\{ \left(r \frac{\partial h}{\partial r} \right)_2 - \left(r \frac{\partial h}{\partial r} \right)_1 \right\}$$

actually represents the change in the variable $r(\partial h / \partial r)$ between the radial limits, r_1 and r_2 , of our element. If we imagine a plot of $r(\partial h / \partial r)$ versus r , as in the figure, we can readily see that this change will be given approximately by the slope of the plot times
(continued on next page)

7 + —Con.

the radial increment, Δr . That is, approximately

$$\left(\frac{\partial h}{\partial r}\right)_2 - \left(\frac{\partial h}{\partial r}\right)_1 = \frac{\partial\left(\frac{\partial h}{\partial r}\right)}{\partial r} \cdot \Delta r$$

where the derivative

$$\frac{\partial\left(\frac{\partial h}{\partial r}\right)}{\partial r}$$

represents the slope of our plot, at an appropriate point within the element. This slope, or derivative, is negative in our illustration, so that

$$\left(\frac{\partial h}{\partial r}\right)_1 > \left(\frac{\partial h}{\partial r}\right)_2$$

The approximation inherent in the above equation becomes progressively more accurate as Δr decreases in size.

QUESTION

Recalling that the rule for differentiation of a product is "first factor times derivative of second plus second factor times derivative of first," which of the following equations gives the derivative of $r(\partial h/\partial r)$ with respect to r ?

Turn to Section:

$$\frac{\partial\left(\frac{\partial h}{\partial r}\right)}{\partial r} = r \frac{\partial\left(\frac{\partial h}{\partial r}\right)}{\partial r} + \frac{\partial h}{\partial r} \quad 26$$

$$\frac{\partial\left(\frac{\partial h}{\partial r}\right)}{\partial r} = r \frac{\partial^2 h}{\partial r^2} + \frac{\partial h}{\partial r} \quad 28$$

$$\frac{\partial\left(\frac{\partial h}{\partial r}\right)}{\partial r} = 2r \frac{\partial^2 h}{\partial r^2} \quad 8$$

8 +

Your answer in Section 7,

$$\frac{\partial\left(\frac{\partial h}{\partial r}\right)}{\partial r} = 2r \frac{\partial^2 h}{\partial r^2}$$

is not correct. We are required to take the derivative of the product $r(\partial h/\partial r)$. The rule for differentiation of a product is easy to remember: first factor times derivative of second, plus second factor times derivative of first; that is

$$\frac{d(uv)}{dx} = u \frac{dv}{dx} + v \frac{du}{dx}$$

A derivation of this formula can be found in any standard text of calculus. Our first factor is r , and our second factor is $\partial h/\partial r$. Thus we must form the expression: r times the derivative of $\partial h/\partial r$ with respect to r , plus $\partial h/\partial r$ times the derivative of r with respect to r .

Return to Section 7 and choose another answer.

 9 +

Your answer in Section 5,

$$\frac{\partial^2 h}{\partial r^2} = \frac{V}{4\pi Tt} \left\{ e^{-(Sr^2/4Tt)} \cdot \left(\frac{-2S}{4Tt} \right) + \left(\frac{-2Sr}{4Tt} \right) \cdot e^{-(Sr^2/4Tt)} \right\},$$

is not correct. If we remove the braces and separate your answer into two terms, we have

$$\frac{\partial^2 h}{\partial r^2} = \frac{V}{4\pi Tt} \cdot e^{-(Sr^2/4Tt)} \cdot \left(\frac{-2S}{4Tt} \right) + \left(\frac{-2Sr}{4Tt} \right) \cdot \frac{V}{4\pi Tt} \cdot e^{-(Sr^2/4Tt)}.$$

The first term, according to the rule for differentiation of a product, is correct, since it represents the first factor,

$$\frac{V}{4\pi Tt} \cdot e^{-(Sr^2/4Tt)}$$

multiplied by the derivative of the second (with respect to r), which is simply

$$\frac{-2S}{4Tt}.$$

The second term of your answer, however, is not correct.

$$\frac{-2Sr}{4Tt}$$

is the second factor of the product we wish to differentiate but

$$\frac{V}{4\pi Tt} \cdot e^{-(Sr^2/4Tt)}$$

does not represent the derivative of the first factor. This first factor is itself

$$\frac{V}{4\pi Tt} \cdot e^{-(Sr^2/4Tt)}$$

and its derivative with respect to r was obtained in answer to the question of Section 27.

Return to Section 5 and choose another answer.

10

Your answer in Section 21 is not correct. We established in the discussion of Section 21 that the rise in head within the well at $t=0$, due to injection of the volume V , would be given by V/A_w , where A_w is the cross-sectional area of the well bore. If the well radius approaches zero, A_w must approach zero. The smaller A_w becomes, the larger the quotient V/A_w must become; for example, $1/0.001$ is

certainly much greater than $1/1$. Your answer, that the head change is zero, could only be true if the area of the well were immeasurably large, so that the addition of a finite volume of water would produce no measurable effect.

Return to Section 21 and choose another answer.

11

Your answer in Section 33 is not correct. The integration in the equation

$$V = \int_{r=0}^{r=\infty} S \cdot h_{r,t} \cdot 2\pi r dr$$

cannot be carried out until we substitute some clearly defined function of r for the term $h_{r,t}$. Until this is done, we do not even know what function we are trying to integrate. But even if the integration could be carried out and the result were found to be

$$\frac{V}{4\pi T t} e^{-(r^2 S/4Tt)}$$

then we would be left with the result

$$V = \frac{V}{4\pi T t} e^{-(r^2 S/4Tt)}$$

which clearly can never be satisfied except perhaps at isolated values of r and t .

Return to Section 33 and choose another answer.

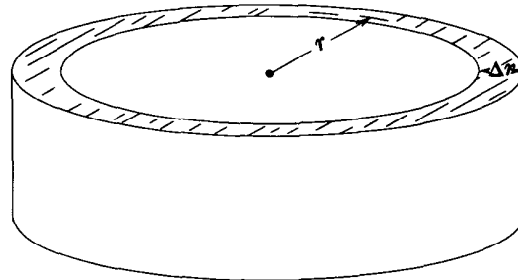
12

Your answer in Section 28,

$$\frac{dV}{dt} = S\pi r^2 \frac{\partial h}{\partial t},$$

is not correct. The storage equation states that the rate of accumulation in storage is equal to the product of storage coefficient, rate of change of head with time, and base area of the element (prism) of aquifer under consideration. Your answer contains the storage coefficient, S , and the time rate of change, $\partial h/\partial t$. However, the base area of the prism which we are considering is not given by πr^2 .

This term gives the area of a circle extending from the origin to the radius r ; our prism is actually a cylindrical shell, extending from



the radius r_1 to the radius r_2 . Its base area is the area of the shaded region in the figure. This region has a radial width of Δr and a mean perimeter of $2\pi r$.

Return to Section 28 and choose another answer.

13 +

Your answer in Section 33 is correct. Our proposed solution, giving h as a function of r and t is

$$h_{r,t} = \frac{V}{4\pi Tt} e^{-(r^2S/4Tt)}.$$

To test this solution for conformity with the required condition we substitute

$$\frac{V}{4\pi Tt} e^{-(r^2S/4Tt)}$$

for $h_{r,t}$ in the equation

$$V = \int_{r=0}^{r=\infty} S \cdot h_{r,t} \cdot 2\pi r dr$$

and evaluate the integral to see whether the equation is satisfied. The substitution gives

$$V = \int_{r=0}^{r=\infty} S \cdot \frac{V}{4\pi Tt} \cdot e^{-(r^2S/4Tt)} \cdot 2\pi r dr.$$

Constant terms may be taken outside the integral; in this case, we are integrating with respect to r , so t may be treated as a constant and taken outside the integral as well. We leave the factor 2 under the integral for the moment and take the remaining constants outside to give

$$V = \frac{SV}{4Tt} \int_{r=0}^{r=\infty} e^{-(r^2S/4Tt)} \cdot 2r dr.$$

To evaluate the integral in this form, we make use of a simple algebraic substitution. Let

$$z = r^2;$$

then

$$dz = 2r dr;$$

and let

$$a = \frac{S}{4Tt}.$$

Substituting these terms in the above equation, we obtain:

$$V = aV \int_{z=0}^{z=\infty} e^{-az} dz.$$

The indefinite integral of e^{-az} is simply

$$-\frac{1}{a} e^{-az};$$

that is,

$$\int e^{-az} dz = -\frac{1}{a} e^{-az} + c$$

where c is a constant of integration. The infinite upper limit in our problem is handled by the standard method; the steps are as follows

$$\begin{aligned} \int_{z=0}^{z=\infty} e^{-az} dz &= \lim_{b \rightarrow \infty} \int_0^b e^{-az} dz \\ &= \lim_{b \rightarrow \infty} \left\{ -\frac{1}{a} e^{-az} \Big|_{z=0}^{z=b} \right\} = \lim_{b \rightarrow \infty} \left\{ -\frac{1}{a} \cdot \frac{1}{e^{ab}} \right. \\ &\quad \left. - \left(-\frac{1}{a} \cdot \frac{1}{e^0} \right) \right\} \\ &= -\frac{1}{a} \left(\lim_{b \rightarrow \infty} \left\{ \frac{1}{e^{ab}} \right\} \right) + \frac{1}{a} \end{aligned}$$

but

$$\lim_{b \rightarrow \infty} \left\{ \frac{1}{e^{ab}} \right\} = 0,$$

so that

$$\int_{z=0}^{z=\infty} e^{-az} dz = \frac{1}{a}.$$

Therefore

$$aV \int_{z=0}^{z=\infty} e^{-az} dz = aV \cdot \frac{1}{a} = V.$$

This verifies that our function

$$\frac{V}{4\pi Tt} e^{-(r^2S/4Tt)}$$

(continued on next page)

13 + —Con.

actually satisfies the required condition—that is, that when we substitute this term for $h_{r,t}$ in the expression

$$\int_{r=0}^{r=\infty} S \cdot h_{r,t} \cdot 2\pi r dr$$

and perform the integration, the result is actually equal to V , the volume of injected water, as required by the condition.

We have shown, then, that the expression

$$h = \frac{V}{4\pi T t} e^{-(r^2 S / 4 T t)}$$

satisfies the differential equation for radial flow in an aquifer and satisfies as well the boundary conditions associated with the instantaneous injection of a volume of water through a well at the origin, at $t=0$. It is, therefore, the particular solution required for this problem. It is an important solution for two reasons. First, it describes approximately what happens when a charge of water is suddenly added to a well in the

standard “slug test” (Ferris and Knowles, 1963) and provides a means of estimating transmissivity through such a test.¹ Second, and more importantly, it gives the “impulse response” of the well-aquifer system—the solution corresponding to an instantaneous disturbance. Solutions for more complicated forms of disturbance, such as repeated injections or withdrawals, or continuous withdrawal, can be synthesized from this elementary solution. Following Section 37, a discussion is given in text format outlining the manner in which solutions corresponding to repeated bailing and continuous pumping of a well may be built up from the impulse response solution.

This concludes the programed instruction of Part VI. You may proceed to the text-format discussion following Section 37. Readers who prefer may proceed to Part VII.

¹A subsequent publication (Cooper, Bredehoeft, and Papadopoulos, 1967) has provided a more accurate description of the actual effect of adding a charge of water to a well, by considering the inertia of the column of water in the well. This factor was neglected in the original analysis.

14 +

Your answer in Section 33 is not correct. The condition to be satisfied was

$$V = \int_{r=0}^{r=\infty} S \cdot h_{r,t} \cdot 2\pi r dr.$$

A solution to our differential equation is by definition an expression giving the head, h , at any radius, r , and time, t , in a form that satisfies the differential equation. Here, the idea is to test such a solution to see if it *also* satisfies the condition phrased in the above

equation. The solution actually represents the head, $h_{r,t}$; if we substitute it for the quantity $2\pi r$, as your answer suggests, there will be two terms, $h_{r,t}$ and our solution, both representing head in the resulting equation. Moreover if the result of the integration were $2\pi S$ we would be left with the result $V = 2\pi S$, which does not satisfy the required condition.

Return to Section 33 and choose another answer.

15 +

Your answer in Section 1,

$$Q_1 = -K 2\pi r_1 b \left(\frac{\partial h}{\partial r} \right)_1,$$

is correct. The terms 2π , K , and b are all constants; we will denote the product Kb by

T , as before. The variable terms, r and $\partial h / \partial r$, may be combined and treated as a single variable, $r(\partial h / \partial r)$. The value of this variable at the inner face of the cylindrical element will be designated $(r \partial h / \partial r)_1$. Using these notations, our expression for inflow

15 + —Con.—

through the inner face of the cylindrical element is now

$$Q_1 = -2\pi T \left(r \frac{\partial h}{\partial r} \right)_1.$$

QUESTION

Suppose we continue to treat the product $r(\partial h/\partial r)$ as a single variable, and let $(r\partial h/\partial r)_2$ denote the value of this variable at the outer face of the cylindrical element. The expression for the outflow, Q_2 , through the outer cylindrical surface can then be written in terms of $(r\partial h/\partial r)_2$, in a form similar to

that for the inflow. Which of the following equations would we then obtain for the inflow minus outflow, $Q_1 - Q_2$, for our cylindrical element?

Turn to Section:

$$Q_1 - Q_2 = 2\pi T \left\{ \left(r \frac{\partial h}{\partial r} \right)_2 - \left(r \frac{\partial h}{\partial r} \right)_1 \right\} \quad 7$$

$$Q_1 - Q_2 = 2\pi T \left(r \frac{\partial h}{\partial r} \right)_1 \cdot \left(r \frac{\partial h}{\partial r} \right)_2 \quad 30$$

$$Q_1 - Q_2 = 2\pi T \left\{ \left(\frac{\partial h}{\partial r} \right)_2 - \left(\frac{\partial h}{\partial r} \right)_1 \right\} \quad 25$$

16 +

Your answer in Section 28,

$$\frac{dV}{dt} = \frac{S \frac{\partial h}{\partial t}}{2\pi r \Delta r},$$

is not correct. The storage equation tells us that rate of accumulation in storage should equal the *product* of storage coefficient, rate of change of head with time, and base area

of the element (prism) of aquifer with which we are dealing. Our element, or prism, of aquifer is a cylindrical shell extending from the radius r_1 to the radius r_2 . Its base area is given by the term $2\pi r \Delta r$. However, in your answer this area term is divided into the term $S(\partial h/\partial t)$.

Return to Section 28 and choose another answer.

17 +

Your answer in Section 20,

$$\frac{\partial^2 h}{\partial r^2} + \frac{1}{r} \frac{\partial h}{\partial r} = \frac{V}{4\pi T t} e^{-(Sr^2/4Tt)} \left\{ \frac{-2S}{4Tt} + \frac{2S^2 r^2}{16T^2 t^2} \right\},$$

is not correct. The mistake in this answer results from an algebraic error in simplifying the second term of the expression for $\partial^2 h/\partial r^2$. The product

$$\left(\frac{-2Sr}{4Tt} \right) \cdot \left(\frac{-2Sr}{4Tt} \right)$$

is not equal to

$$\frac{2S^2 r^2}{16T^2 t^2}.$$

Return to Section 20 and choose another answer.

18 +

Your answer in Section 21 is correct; head is immeasurably great, or infinite, at the well at $t=0$. Taking this result together with our requirement that head must be zero elsewhere in the aquifer at $t=0$, we may phrase the boundary condition for $t=0$ as follows

$$h \rightarrow \infty, \text{ for } r=0 \text{ and } t=0$$

$$h = 0, \text{ for } r > 0 \text{ and } t=0.$$

We now test our solution to see if it satisfies this requirement. Probably the easiest way to do this is to expand the term $e^{-(Sr^2/4Tt)}$ in a Maclaurin series. The theory of this type of series expansion is treated in standard texts of calculus; the result, as applied to our exponential function, has the form

$$e^x = 1 + x + \frac{x^2}{2!} + \frac{x^3}{3!} + \dots$$

or for a negative exponent,

$$e^{-x} = \frac{1}{1 + x + \frac{x^2}{2!} + \frac{x^3}{3!} + \dots}$$

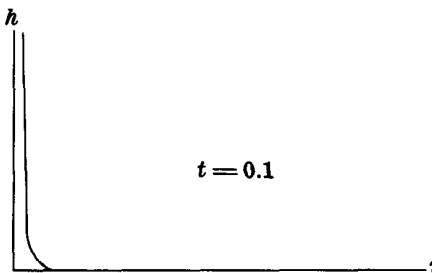
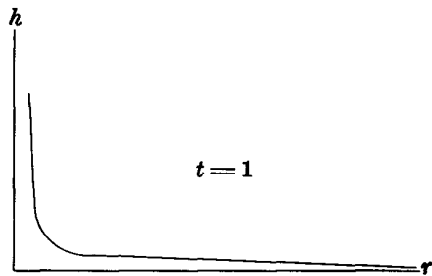
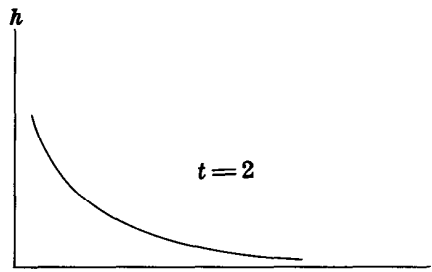
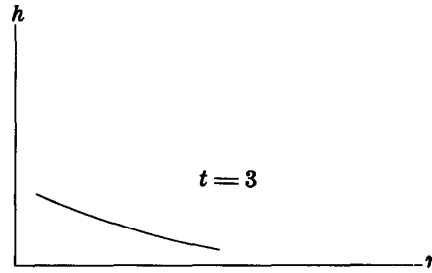
In our case, x is the term $r^2S/4Tt$, and

$$e^{-(r^2S/4Tt)} = \frac{1}{1 + \left(\frac{r^2S}{4Tt}\right) + \frac{\left(\frac{r^2S}{4Tt}\right)^2}{2!} + \frac{\left(\frac{r^2S}{4Tt}\right)^3}{3!} + \dots}$$

so that

$$\frac{V}{4\pi Tt} e^{-(r^2S/4Tt)} = \frac{V}{4\pi Tt + r^2S + \frac{r^4S^2\pi}{4Tt \cdot 2!} + \frac{r^6S^3\pi}{16T^2t^2 \cdot 3!} + \dots}$$

Now as t approaches zero, the first term in the denominator approaches zero; the second remains constant, and the third and all higher terms become infinite, provided r does not also approach zero. If any term in the



18 + —Con.—

denominator is infinite, the fraction as a whole becomes zero. Thus the expression

$$\frac{V}{4\pi T t} e^{-(r^2 S/4Tt)}$$

is zero for $t=0$ and $r \neq 0$, and satisfies the first part of our condition.

If r and t are both allowed to approach zero, the first two terms in the denominator of our fraction will be zero. The third will behave in the same manner as the fraction cx^4/kx behaves as x approaches zero, since r and t are both approaching zero in the same way. The limit of cx^4/kx as x approaches zero is 0, since

$$\frac{cx^4}{kx} = \frac{c}{k} x^3.$$

Therefore the third term in the denominator must also approach the limit zero as r and t approach zero. By a similar analysis it can be shown that the limit of every succeeding term in the denominator is zero as r and t approach zero. Thus the entire denominator is zero, and the fraction as a whole is infinite, so that the term

$$\frac{V}{4\pi T t} e^{-(r^2 S/4Tt)}$$

is infinite when r and t are both zero, satisfy the second part of our condition.

Another and very instructive way to in-

vestigate the behavior of the function

$$\frac{V}{4\pi T t} e^{-(r^2 S/4Tt)}$$

is to construct plots of this function versus r , for decreasing values of time. The figures show the form that such a series of plots will take. It may be noted that as time approaches zero the function approaches the shape of a sharp "spike," or impulse, at $r=0$. The shape of these curves suggests a head distribution which we might sketch intuitively, if we were asked to describe the response of an aquifer to the injection of a small volume of water. It is suggested that the reader construct a few of these plots, in order to acquire a feeling for the behavior of the function.

QUESTION

The aquifer is assumed to be infinite in extent, and the volume of water injected is assumed to be small. We would therefore expect the effects of the injection to die out at great radial distances from the well. Which of the following expressions is a mathematical formulation of this behavior and could be used as a boundary condition for our problem?

Turn to Section:

$h \rightarrow 0$ as $r \rightarrow \infty$	33
$h \rightarrow \infty$ as $t \rightarrow \infty$	29
$h \rightarrow \infty$ as $r \rightarrow 0$	6

19 +

Your answer in Section 21 is not correct. We established in the discussion of Section 21 that the rise in water level in the well at $t=0$ should be given by the expression $h = V/A_w$, where A_w is the cross-sectional area of the well bore and V is the volume of water injected. In order for h to have the instantaneous value of 1 foot, V , in cubic feet, would have to be numerically equal to A_w , in square feet. However, we are assuming

the well to have an infinitesimally small radius, so that A_w , its cross-sectional area, approaches zero. If smaller and smaller values are assigned to the denominator, A_w , while the numerator, V , is held constant, the fraction V/A_w must take on larger and larger values.

Return to Section 21 and choose another answer.

20

Your answer in Section 35,

$$\frac{\partial h}{\partial t} = \frac{V}{4\pi Tt} e^{-(Sr^2/4Tt)} \left(\frac{Sr^2}{4Tt^2} \right) + e^{-(Sr^2/4Tt)} \left(\frac{-V}{4\pi Tt^2} \right),$$

is correct. If the term

$$\frac{V}{4\pi Tt} e^{-(Sr^2/4Tt)}$$

is factored from this expression we have

$$\frac{\partial h}{\partial t} = \frac{V}{4\pi Tt} e^{-(Sr^2/4Tt)} \left\{ \frac{Sr^2}{4Tt^2} - \frac{1}{t} \right\}$$

and if we multiply this equation by S/T , we obtain

$$\frac{S}{T} \frac{\partial h}{\partial t} = \frac{V}{4\pi Tt} e^{-(Sr^2/4Tt)} \left\{ \frac{S^2 r^2}{4T^2 t^2} - \frac{S}{Tt} \right\}.$$

Our expression for $\partial h/\partial r$, obtained in answer to the question of Section 27 was

$$\frac{\partial h}{\partial r} = \frac{V}{4\pi Tt} e^{-(Sr^2/4Tt)} \left(\frac{-2Sr}{4Tt} \right).$$

The term $(1/r)(\partial h/\partial r)$ is therefore given by

$$\frac{1}{r} \frac{\partial h}{\partial r} = \frac{V}{4\pi Tt} e^{-(Sr^2/4Tt)} \cdot \left(\frac{-2S}{4Tt} \right).$$

In answering the question of Section 5, we saw that the expression for $\partial^2 h/\partial r^2$ was

$$\frac{\partial^2 h}{\partial r^2} = \frac{V}{4\pi Tt} \left\{ e^{-(Sr^2/4Tt)} \cdot \left(\frac{-2S}{4Tt} \right) + \left(\frac{-2Sr}{4Tt} \right) e^{-(Sr^2/4Tt)} \left(\frac{-2Sr}{4Tt} \right) \right\}$$

20 + —Con.—
QUESTION

Which of the following expressions is obtained for

$$\frac{\partial^2 h}{\partial r^2} + \frac{1}{r} \frac{\partial h}{\partial r},$$

by combining the two expressions given above and factoring out the term

$$\frac{V}{4\pi T t} \cdot e^{-(Sr^2/4Tt)} ?$$

Turn to Section:

$$\frac{\partial^2 h}{\partial r^2} + \frac{1}{r} \frac{\partial h}{\partial r} = \frac{V}{4\pi T t} e^{-(Sr^2/4Tt)} \left\{ \frac{-S}{Tt} + \frac{S^2 r^2}{4T^2 t^2} \right\} \quad 21$$

$$\frac{\partial^2 h}{\partial r^2} + \frac{1}{r} \frac{\partial h}{\partial r} = \frac{V}{4\pi T t} e^{-(Sr^2/4Tt)} \left\{ \frac{-2S}{4Tt} + \frac{2S^2 r^2}{16T^2 t^2} \right\} \quad 17$$

$$\frac{\partial^2 h}{\partial r^2} + \frac{1}{r} \frac{\partial h}{\partial r} = \frac{V}{4\pi T t} e^{-(Sr^2/4Tt)} \left\{ \frac{-4S}{Tt} + \frac{S^2 r^2}{8Tt} \right\} \quad 24$$

21 + —

Your answer in Section 20,

$$\frac{\partial^2 h}{\partial r^2} + \frac{1}{r} \frac{\partial h}{\partial r} = \frac{V}{4\pi T t} e^{-(Sr^2/4Tt)} \left\{ \frac{-S}{Tt} + \frac{S^2 r^2}{4T^2 t^2} \right\},$$

is correct. Now note that this expression is identical to that given for $(S/T) (\partial h / \partial t)$ in Section 20. Thus we have shown that if head is given by

$$h = \frac{V}{4\pi T t} \cdot e^{-(Sr^2/4Tt)}$$

then it is true that

$$\frac{\partial^2 h}{\partial r^2} + \frac{1}{r} \frac{\partial h}{\partial r} = \frac{S}{T} \frac{\partial h}{\partial t}.$$

21 + —Con.

In other words, the expression

$$h = \frac{V}{4\pi Tt} e^{-(Sr^2/4Tt)}$$

satisfies the partial differential equation, or constitutes one particular solution to it. In fact, this expression is the solution which describes the hydraulic head in an infinite, horizontal, homogeneous, and isotropic artesian aquifer, after a finite volume of water, V , is injected suddenly at $t=0$ into a fully penetrating well of infinitesimal radius located at $r=0$, assuming that head was everywhere at the datum prior to the injection—that is, assuming h was everywhere zero prior to $t=0$.

Proof that our function is the solution corresponding to this problem requires, in addition to the demonstration that it satisfies the differential equation, proof that it satisfies the various boundary conditions peculiar to the problem. We now wish to formulate these conditions.

The charge of fluid is added to the well at the instant $t=0$. At this instant, there has been no time available for fluid to move away from the well, into the aquifer. Therefore, at all points in the aquifer except at the well (that is, except at $r=0$), the head at $t=0$ must still be zero. In the well, on the other hand, the addition of the volume of

water produces an instantaneous rise in head. For a well of measurable radius, this instantaneous head buildup, Δh , would be given by

$$\Delta h = \frac{V}{A_w} = \frac{V}{\pi r_w^2},$$

where A_w is the cross-sectional area of the well bore, and r_w is the well radius. For example, if A_w is 1 square foot and we inject 1 cubic foot of water, we should observe an instantaneous rise in head of 1 foot in the well; and because head was originally at 0 (datum level), we can say that the head in the well at $t=0$ should be 1 foot. If A were 0.5 square foot, the head in the well at $t=0$ should be 2 feet; and so on.

QUESTION

For purposes of developing the boundary conditions, we have assumed the radius of our well to be infinitesimally small—that is, to approach zero. Which of the following statements describes the behavior of head at the well at $t=0$, subject to this assumption?

	Turn to Section:
head at the well will be 0 feet at $t=0$	10
head at the well will be 1 foot at $t=0$	19
head at the well will be immeasurably large—that is, infinite—at $t=0$	18

22 +

Your answer in Section 37 is not correct. The expression obtained in Section 28 for inflow minus outflow was

$$Q_1 - Q_2 = 2\pi T \left\{ r \frac{\partial^2 h}{\partial r^2} + \frac{\partial h}{\partial r} \right\} \Delta r.$$

Our expression for dV/dt was

$$\frac{dV}{dt} = S 2\pi r \Delta r \frac{\partial h}{\partial t}.$$

The expression for inflow minus outflow may be equated to that for dV/dt , and the result simplified to yield the correct answer.

Return to Section 37 and choose another answer.

Your answer in Section 5,

$$\frac{\partial^2 h}{\partial r^2} = \frac{V}{4\pi Tt} \cdot e^{-(Sr^2/4Tt)} \left(\frac{-2S}{4Tt} \right) + \left(\frac{-2Sr}{4Tt} \right) \cdot e^{-(Sr^2/4Tt)} \cdot \left(\frac{-2Sr}{4Tt} \right),$$

is not correct. The rule for differentiation of a product is: first factor times derivative of second plus second factor times derivative of first. The two factors, in this case, are

$$\frac{V}{4\pi Tt} e^{-(Sr^2/4Tt)}$$

(which we have already differentiated in the question of Section 27) and

$$\frac{-2Sr}{4Tt}.$$

The first term of your answer is correct; the first factor,

$$\frac{V}{4\pi Tt} e^{-(Sr^2/4Tt)}$$

is multiplied by the derivative of the second, which is

$$\frac{-2S}{4Tt}$$

(t is simply treated as part of the constant coefficient of r , since we are differentiating with respect to r). The second term of your answer, however, is not correct; you have written the derivative of the first factor as

$$e^{-(Sr^2/4Tt)} \cdot \left(\frac{-2Sr}{4Tt} \right).$$

Compare this with the correct answer to the question of Section 27 and you will see that it does not represent the derivative of

$$\frac{V}{4\pi Tt} e^{-(Sr^2/4Tt)}.$$

Return to Section 5 and choose another answer.

24 +

Your answer in Section 20,

$$\frac{\partial^2 h}{\partial r^2} + \frac{1}{r} \frac{\partial h}{\partial r} = \frac{V}{4\pi T t} e^{-(Sr^2/4Tt)} \left\{ \frac{-4S}{Tt} + \frac{S^2 r^2}{8Tt} \right\},$$

is not correct. This answer contains algebraic errors, both in the addition of the two terms

$$\left(\frac{-2S}{4Tt} \right)$$

and in the multiplication of the two terms

$$\left(\frac{-2Sr}{4Tt} \right).$$

Return to Section 20 and choose another answer.

25 +

Your answer in Section 15,

$$Q_1 - Q_2 = 2\pi T \left\{ \left(\frac{\partial h}{\partial r} \right)_2 - \left(\frac{\partial h}{\partial r} \right)_1 \right\},$$

is not correct. The expression for inflow through the inner cylindrical face was shown to be

$$Q_1 = -2\pi T \left(r \frac{\partial h}{\partial r} \right)_1.$$

Applying Darcy's law in a similar fashion to the outer cylindrical face, at radius r_2 , the

expression for outflow through this face is found to be

$$Q_2 = -2\pi T \left(r \frac{\partial h}{\partial r} \right)_2.$$

These two equations may be subtracted to obtain an expression for inflow minus outflow. The radius, r , does not disappear in this subtraction. Your answer, which does not include radius, must therefore be wrong.

Return to Section 15 and choose another answer.

26 +

Your answer in Section 7,

$$\frac{\partial \left(r \frac{\partial h}{\partial r} \right)}{\partial r} = r \frac{\partial \left(\frac{\partial h}{\partial r} \right)}{\partial r} + \frac{\partial h}{\partial r} \cdot r,$$

is not correct. The derivative of a product is given by the first factor multiplied by the derivative of the second, plus the second factor multiplied by the derivative of the first. Your first term, above is correct; the first factor, r , is multiplied by the derivative of $\partial h / \partial r$, although it would be more conventional to use the second derivative notation,

$$\frac{\partial^2 h}{\partial r^2},$$

rather than

$$\frac{\partial \left(\frac{\partial h}{\partial r} \right)}{\partial r}.$$

Your second term, however, is not correct. The derivative of r with respect to r is not equal to r .

Return to Section 7 and choose another answer.

27 +

Your answer in Section 37 is correct. The basic differential equation for the problem is

$$\frac{\partial^2 h}{\partial r^2} + \frac{1}{r} \frac{\partial h}{\partial r} = \frac{S}{T} \frac{\partial h}{\partial t}.$$

In seeking a solution to this equation, we are seeking an expression giving h as a function of r and t , such that when $\partial h/\partial r$, $\partial^2 h/\partial r^2$, and $\partial h/\partial t$ are obtained by differentiation and substituted into this equation, the equation is found to be satisfied. For example, consider the function

$$h = \frac{V}{4\pi T t} \cdot e^{-(Sr^2/4Tt)}$$

in which V (as well as S and T) is constant and e is the base of natural logarithms. This happens to be an important function in the theory of well hydraulics, as we shall see; and we wish now to test it, to see whether it satisfies the above differential equation. To do this we must differentiate the expression once with respect to t and twice with respect to r ; these operations are not difficult if the rules of differentiation are applied carefully. First we will differentiate with respect to

r ; in doing so, we treat t as a constant, so that the factor $V/(4\pi T t)$ becomes simply a constant coefficient. In the exponent, as well, the term $-(S/4Tt)$ may be considered a constant coefficient of r^2 ; and the problem is essentially one of finding the derivative of $e^{-(S/4Tt)r^2}$ and multiplying this by the constant factor $V/(4\pi T t)$. The derivative of a function e^u with respect to a variable r is given simply by $e^u \cdot (du/dr)$. Here, u is the term $-(S/4Tt)r^2$.

QUESTION

Following the procedure outlined above, which of the following expressions is found for $\partial h/\partial r$?

	Turn to Section:
$\frac{\partial h}{\partial r} = e^{-(Sr^2/4Tt)} \cdot \left(\frac{-2Sr}{4Tt} \right)$	4
$\frac{\partial h}{\partial r} = \frac{V}{4\pi T t} e^{-(Sr^2/4Tt)} \cdot \left(\frac{-2Sr}{4Tt} \right)$	5
$\frac{\partial h}{\partial r} = \frac{V}{4\pi T t} e^{-(Sr^2/4Tt)}$	2

28 +

Your answer in Section 7,

$$\frac{\partial \left(r \frac{\partial h}{\partial r} \right)}{\partial r} = r \frac{\partial^2 h}{\partial r^2} + \frac{\partial h}{\partial r},$$

is correct. Our expression for

$$\left(r \frac{\partial h}{\partial r} \right)_2 - \left(r \frac{\partial h}{\partial r} \right)_1$$

may therefore be written

$$\left(r \frac{\partial h}{\partial r} \right)_2 - \left(r \frac{\partial h}{\partial r} \right)_1$$

$$= \frac{\partial \left(r \frac{\partial h}{\partial r} \right)}{\partial r} \Delta r = \left\{ r \frac{\partial^2 h}{\partial r^2} + \frac{\partial h}{\partial r} \right\} \Delta r.$$

Our expression for inflow minus outflow therefore becomes

(continued on next page)

28 + —Con.

$$Q_1 - Q_2 = 2\pi T \left\{ \left(r \frac{\partial h}{\partial r} \right)_2 - \left(r \frac{\partial h}{\partial r} \right)_1 \right\}$$

$$= 2\pi T \left\{ r \frac{\partial^2 h}{\partial r^2} + \frac{\partial h}{\partial r} \right\} \Delta r.$$

As before, we wish to equate this expression for inflow minus outflow to the rate of accumulation of water in storage in our element. The surface area of the cylindrical element is given approximately by

$$A = 2\pi r \Delta r.$$

The term $2\pi r$ is the perimeter of a circle taken along the midradius of the element; multiplication by the radial width, Δr gives the surface area, or base area, of the cylindrical shell.

QUESTION

Using this expression for the surface area of the cylindrical element, and letting $\partial h / \partial t$ denote the time rate of head buildup in the element, which of the following expressions is obtained for the rate of accumulation of water in storage in the element?

Turn to Section:

$$\frac{dV}{dt} = S 2\pi r \Delta r \frac{\partial h}{\partial t} \quad 37$$

$$\frac{dV}{dt} = S \pi r^2 \frac{\partial h}{\partial t} \quad 12$$

$$\frac{dV}{dt} = \frac{S \frac{\partial h}{\partial t}}{2\pi r \Delta r} \quad 16$$

29 +

Your answer in Section 18 is not correct. The behavior we are trying to describe is the disappearance of the effect of injection, at great radial distances from the well. The answer which you chose describes head, h ,

as going to infinity, rather than disappearing; and it describes a restriction on h with time, rather than with distance.

Return to Section 18 and choose another answer.

30 +

Your answer in Section 15,

$$Q_1 - Q_2 = 2\pi T \left(r \frac{\partial h}{\partial r} \right)_1 - \left(r \frac{\partial h}{\partial r} \right)_2,$$

is not correct. We established in Sections 1 and 15 that inflow through the inner cylindrical face of the element is given by Darcy's laws as

$$Q_1 = -2\pi T \left(r \frac{\partial h}{\partial r} \right)_1.$$

Using a similar approach, we can show that outflow through the outer cylindrical face is given by

$$Q_2 = 2\pi T \left(r \frac{\partial h}{\partial r} \right)_2.$$

These two equations can be subtracted to obtain an expression for inflow minus outflow for the cylindrical element.

Return to Section 15 and choose another answer.

31 +

Your answer in Section 35,

$$\frac{\partial h}{\partial t} = \frac{V}{4\pi Tt} \cdot \frac{Sr^2}{4Tt^2} + e^{-(Sr^2/4Tt)} \cdot \left(\frac{-V}{4\pi Tt^2} \right),$$

is not correct. Application of the product rule—first factor times derivative of second plus second factor times derivative of first—is correct; but your expression for the time derivative of $e^{-(Sr^2/4Tt)}$ is not correct.

Recall that the derivative of an exponential, e^u , with respect to t is given by $e^u du/dt$. Letting u represent $-(Sr^2/4Tt)$, your answer gives only $\partial u/\partial t$ in the place where it should give

$$e^u \frac{\partial u}{\partial t}.$$

Return to Section 35 and choose another answer.

32 +

Your answer in Section 37 is not correct. In Section 28, we saw that the expression for inflow minus outflow could be written

$$Q_1 - Q_2 = 2\pi T \left\{ r \frac{\partial^2 h}{\partial r^2} + \frac{\partial h}{\partial r} \right\} \Delta r$$

while the expression we obtained for dV/dt was

$$\frac{dV}{dt} = S2\pi r \Delta r \frac{\partial h}{\partial t}.$$

If we equate the terms

$$2\pi T \left\{ r \frac{\partial^2 h}{\partial r^2} + \frac{\partial h}{\partial r} \right\} \Delta r$$

and

$$S2\pi r \Delta r \frac{\partial h}{\partial t}$$

and then divide through the resulting equation by

$$2\pi T r \Delta r,$$

we obtain the correct answer to the question of Section 37.

Return to Section 37 and choose another answer.

33 +

Your answer in Section 18, $h \rightarrow 0$ as $r \rightarrow \infty$ is correct. From a mathematical point of view, we should perhaps have used, instead, the condition that $(\partial h/\partial r) \rightarrow 0$ as $r \rightarrow \infty$. This condition is required as r increases toward infinity, because the cross sectional area of flow within the aquifer—a cylindrical area coaxial with the well—expands toward infinity. Thus if we were to apply Darcy's law to determine the flow of the injected water away from the well, we would obtain the result that this flow increases toward an infinite value with increasing distance from the well, unless we postulated that the head

gradient, $\partial h/\partial r$, decreased toward zero with increasing r . However, the condition that h approaches a constant, 0, as $r \rightarrow \infty$ implies that $\partial h/\partial r$ must also approach zero as r increases; and it is a somewhat easier condition to establish.

Our task, then, is to show that the function

$$\frac{V}{4\pi Tt} e^{-(r^2 S/4Tt)}$$

satisfies this condition—that is, we must test

33 + —Con.

this function to see whether its value approaches zero as r approaches infinity. It is easy to show that for any finite value of time the condition is satisfied. However, we are also interested in what happens as t approaches infinity along with r —that is, we would like our condition to be satisfied for all times, even those immeasurably large. For this reason, it is convenient to use the series expansion form given in Section 18; that is we use

$$\frac{V}{4\pi Tt} e^{-(r^2S/4Tt)}$$

$$= \frac{V}{4\pi Tt + r^2S\pi + \frac{r^4S^2\pi}{4Tt \cdot 2!} + \frac{r^6S^3\pi}{16T^2t^2 \cdot 3!}}$$

In order that the fraction on the right approach zero, it is sufficient that any one of the individual terms in the denominator becomes infinite. If r and t both approach infinity, the first two terms clearly become infinite; in fact, the remaining terms become infinite as well, although we need not show this. If one term is infinite, the entire denominator is infinite, and the fraction is zero. For a finite value of t , all terms except the first clearly become infinite as $r \rightarrow \infty$, and again the expression as a whole tends to zero. Thus the expression

$$\frac{V}{4\pi Tt} e^{-(r^2S/4Tt)}$$

satisfies the condition of tending to zero as $r \rightarrow \infty$, for any value of time. Again, this can be demonstrated by extending the plots described in Section 18 to large values of r .

We could also add the condition that h must approach zero as time becomes infinite, everywhere in the aquifer—that is, that the effect of the injection must eventually die out with time everywhere throughout the aquifer, since we are injecting a finite vol-

ume of water into an aquifer which is assumed to be infinite in extent. We have just shown that h approaches zero at infinite time, as r also becomes infinite; we need only show that this behavior holds when r is finite. We will show this through direct use of the function, although it is also evident using the series expansion form. As t becomes infinitely large the factor

$$\frac{V}{4\pi Tt}$$

must approach zero; the factor

$$- e^{-(r^2S/4Tt)}$$

which is equivalent to

$$\frac{1}{e^{(r^2S/4Tt)}}$$

must approach the value

$$\frac{1}{e^{r^2S/\infty}}$$

or

$$\frac{1}{e^0},$$

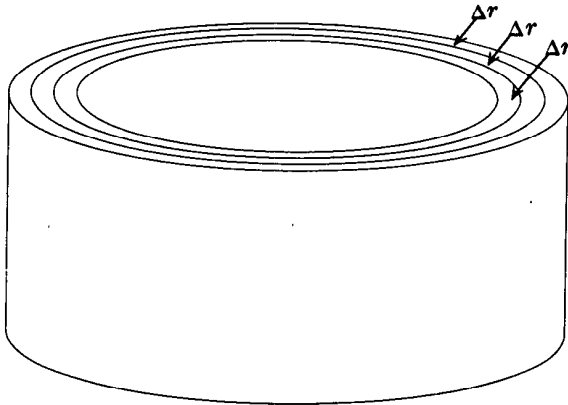
if r is finite. But e^0 is simply 1, so that the product

$$\frac{V}{4\pi Tt} \cdot e^{-(r^2S/4Tt)}$$

must approach zero as t becomes infinitely large, at any finite value of r .

We now consider the last condition which our function should satisfy. In the sketch, the aquifer has been divided into cylindrical elements of radial width Δr , coaxial with the well. At any given time t after injection, the injected volume of fluid, V , is distributed in some way among these cylindrical elements.

33 + —Con.—



We assumed head to be at the datum, or zero, prior to injection, so that h actually represents only the head increase due to the injection. From the definition of storage coefficient, the quantity of the injected fluid contained within a given cylindrical element will be given by

$$\Delta V = S \cdot h_{r,t} \cdot 2\pi r \Delta r$$

where r is the median radius of the element, so that $2\pi r \Delta r$ is the base area of the element; $h_{r,t}$ gives the average head in the element (that is, at the radius r) at the time in question; and S is the storage coefficient. (Recall the definition of storage coefficient—the volume in storage is the product of storage coefficient, head, and base area.) Now if we sum the volumes in storage in every cylindrical element in the aquifer, the total must equal the injected volume, V , at any time after injection. That is,

$$V = \Sigma \Delta V = \Sigma S \cdot h_{r,t} \cdot 2\pi r \Delta r$$

where the summation is carried out over all of the cylindrical elements in the aquifer. Again, it should be kept in mind that $h_{r,t}$ represents only the head increase associated with the injection, so that its use in the storage equation leads only to the volume of water injected, not to the total volume in storage. Now since we are dealing with a continuous system, we replace the summation in the above equation by an integration.

That is, we let the width of each element become infinitesimally small, denoting it dr , so that the number of elements becomes infinitely great; and we rewrite our equation as

$$V = \int_{r=0}^{r=\infty} S \cdot h_{r,t} \cdot 2\pi r dr.$$

The limits of integration extend from $r=0$ to $r=\infty$, indicating that the cylindrical elements extend over the entire aquifer. This equation then is the final condition which our function should satisfy if it is in fact the solution we are seeking.

QUESTION

How do you think our proposed solution should be tested to see if it satisfies this boundary condition?

Turn to Section:

The integration indicated in the equation should be carried out. The result should equal

$$\frac{V}{4\pi T t} e^{-(r^2 S / 4 T t)}, \quad 11$$

The expression

$$\frac{V}{4\pi T t} e^{-(r^2 S / 4 T t)}$$

should be substituted for

$$2\pi r$$

in the equation, and the integration should be carried out; the result should be

$$2\pi S. \quad 14$$

The expression

$$\frac{V}{4\pi T t} e^{-(r^2 S / 4 T t)}$$

should be substituted for

$$h_{r,t}$$

in the equation, and the integration should be carried out; the result should equal

$$V. \quad 13$$

34 +

Your answer in Section 1,

$$Q_1 = -K\pi r_1^2 \left(\frac{\partial h}{\partial r} \right)_1$$

is not correct. Darcy's law states that flow is given by the product of hydraulic conductivity, head gradient in the direction of flow, and cross-sectional area normal to the direction of flow. In this problem as in the steady flow to a well treated in Part III, the

direction of flow is the radial, or r , direction. An area which is everywhere normal to the radial coordinate would be a cylindrical area, coaxial with the well. That is, the flow area that we require here is a cylindrical area—in particular, the inner face of the cylindrical prism shown in Section 1. The area of a cylinder is given by the product of its height and its perimeter.

Return to Section 1 and choose another answer.

35 +

Your answer in Section 5,

$$\frac{\partial^2 h}{\partial r^2} = \frac{V}{4\pi T t} \left\{ e^{-(Sr^2/4Tt)} \cdot \left(\frac{-2S}{4Tt} \right) + \left(\frac{-2Sr}{4Tt} \right) \cdot e^{-(Sr^2/4Tt)} \cdot \left(\frac{-2Sr}{4Tt} \right) \right\},$$

is correct. We now wish to differentiate the equation

$$h = \frac{V}{4\pi T t} \cdot e^{-(Sr^2/4Tt)}$$

with respect to time, to obtain an expression for $\partial h / \partial t$. In doing this, we consider r to be a constant, and treat our expression as the product of the two functions of t ,

$$\frac{V}{4\pi T t}$$

and

$$e^{-(Sr^2/4Tt)}.$$

The derivative of

$$\frac{V}{4\pi T t}, \text{ or } \frac{V}{4\pi T} \cdot t^{-1}$$

with respect to t is

$$-\frac{V}{4\pi T} \cdot t^{-2}, \text{ or } \frac{-V}{4\pi T t^2}.$$

To differentiate

$$e^{-(Sr^2/4Tt)}$$

we again apply the rule

$$\frac{de^u}{dt} = e^u \frac{du}{dt},$$

where u is

$$\frac{-Sr^2}{4Tt}, \text{ or } \frac{-Sr^2}{4T} \cdot t^{-1},$$

and its derivative with respect to t is

$$\frac{Sr^2}{4T} \cdot t^{-2}, \text{ or } \frac{Sr^2}{4T t^2}.$$

QUESTION

Applying the rule for differentiation of a product, together with the above results, which of the following expressions is obtained for $\partial h / \partial t$?

35 + —Con.—

Turn to Section:

$$\frac{\partial h}{\partial t} = \frac{V}{4\pi T t} \cdot e^{-(Sr^2/4Tt)} \cdot \left(\frac{Sr^2}{4Tt^2} \right) \quad 3$$

$$\frac{\partial h}{\partial t} = \frac{V}{4\pi T t} \cdot e^{-(Sr^2/4Tt)} \left(\frac{Sr^2}{4Tt^2} \right) + e^{-(Sr^2/4Tt)} \cdot \left(\frac{-V}{4\pi T t^2} \right) \quad 20$$

$$\frac{\partial h}{\partial t} = \frac{V}{4\pi T t} \cdot \frac{Sr^2}{4Tt^2} + e^{-(Sr^2/4Tt)} \left(\frac{-V}{4\pi T t^2} \right) \quad 31$$

36 + —

Your answer in Section 1,

$$Q_i = \frac{-Kb \left(\frac{\partial h}{\partial r} \right)_1}{2\pi r_1}$$

is not correct. Darcy's law tells us that flow is given by the product of hydraulic conductivity, head gradient in the direction of flow, and cross-sectional area normal to the direction of flow. In this case, as in the steady state flow to a well in Part III, the direction

of flow is the radial direction and the cross-sectional area normal to the flow is a cylindrical surface—the inner surface of the cylindrical shell shown in Section 1. In your answer, however, there is no factor representing the area of this surface. The height of the cylinder, which is b , appears in the numerator of your answer; its perimeter, which is $2\pi r_1$, appears in the denominator of the answer which you chose.

Return to Section 1 and choose another answer.

37 + —

Your answer in Section 28,

$$\frac{dV}{dt} = S 2\pi r \Delta r \frac{\partial h}{\partial t}$$

is correct. As before, we will next use the equation of continuity to link the storage and flow equations.

QUESTION

If the expression obtained for inflow minus outflow is equated to that given above

for rate of accumulation in storage, which of the following equations may be obtained?

Turn to Section:

$$r \frac{\partial^2 h}{\partial r^2} + \frac{1}{2\pi r} \frac{\partial h}{\partial r} = S \frac{\partial h}{\partial t} \quad 22$$

$$2\pi T \Delta r \left\{ \frac{\partial^2 h}{\partial r^2} + \frac{\partial h}{\partial r} \right\} = S \frac{\partial h}{\partial t} \quad 32$$

$$\frac{\partial^2 h}{\partial r^2} + \frac{1}{r} \frac{\partial h}{\partial r} = \frac{S}{T} \frac{\partial h}{\partial t} \quad 27$$

Development of Additional Solutions by Superposition

The differential equation

$$\frac{\partial^2 h}{\partial r^2} + \frac{1}{r} \frac{\partial h}{\partial r} = \frac{S}{T} \frac{\partial h}{\partial t}$$

is linear in h ; that is, h and the various derivatives of h occur only in the first power—they are not squared, cubed, or raised to any power except 1, in any term of the equation. Equations of this type have the property that solutions corresponding to two individual disturbances may be added to obtain a new solution describing the effect of the two disturbances in combination. This is termed superposition of solutions; it is a technique which is often used intuitively by hydrologists—for example when calculating the drawdown produced by several wells, by adding drawdowns calculated for individual operation.

The solution obtained in the preceding

programed instruction was developed for an injection of fluid at $t=0$. If the injection does not occur at $t=0$, the term t in the solution is simply replaced by Δt , the time interval between the injection and the instant of head measurement. For example, if the injection occurs at time t' , and the head change due to this injection is measured at some later time t , the interval $t-t'$ is used in the solution in place of t , giving

$$h_{r,t} = \frac{V}{4\pi T(t-t')} \cdot e^{-\left(\frac{r^2 S}{4T(t-t')}\right)}$$

Now suppose two injections occur, one at t_1' and one at t_2' , and the head is measured at some time t following both injections. Using superposition, the head change due to the combined disturbances is

$$h_{r,t} = \frac{V_1}{4\pi T(t-t_1')} \cdot e^{-\left(\frac{r^2 S}{4T(t-t_1')}\right)} + \frac{V_2}{4\pi T(t-t_2')} \cdot e^{-\left(\frac{r^2 S}{4T(t-t_2')}\right)}$$

where V_1 is the volume injected at t_1' and V_2 is the volume injected at t_2' .

If we consider removal of a volume of water from the well, rather than injection, we need only introduce a change of sign, taking V as negative. For example, if a bailerfull of water is removed at $t=t_1'$, the head change at time t , due to this removal is

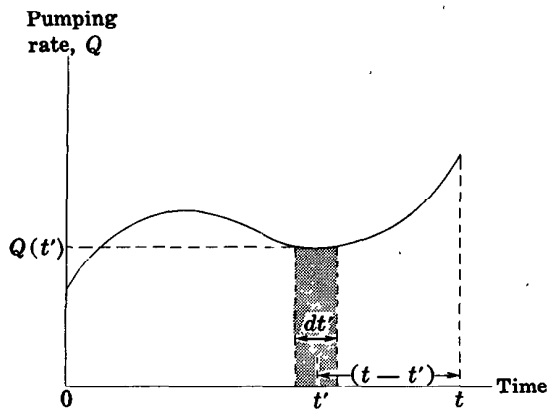
$$h_{r,t} = \frac{-V_1}{4\pi T(t-t_1')} \cdot e^{-\left(\frac{r^2 S}{4T(t-t_1')}\right)}$$

where V_1 is the volume removed by the bailer. If the well is bailed repeatedly, as may happen during completion, the head change due to bailing is obtained by super-

posing the disturbances due to each individual withdrawal:

$$h_{r,t} = -\frac{V_1}{4\pi T(t-t_1')} \cdot e^{-\left(\frac{r^2 S}{4T(t-t_1')}\right)} - \frac{V_2}{4\pi T(t-t_2')} \cdot e^{-\left(\frac{r^2 S}{4T(t-t_2')}\right)} \\ - \frac{V_3}{4\pi T(t-t_3')} \cdot e^{-\left(\frac{r^2 S}{4T(t-t_3')}\right)} \dots - \frac{V_n}{4\pi T(t-t_n')} \cdot e^{-\left(\frac{r^2 S}{4T(t-t_n')}\right)}$$

where t is the time at which h is measured; $t_1', t_2', t_3', \dots, t_n'$ are the times at which the individual withdrawals are made; and $V_1, V_2, V_3, \dots, V_n$ are the volumes removed by the bailer in the successive withdrawals. The "bailer method" of determining transmissivity from the residual drawdown of a well that has been bailed was developed from this equation (Skibitzke, 1963).



Now suppose a well is pumped continuously during the time interval from zero to t , and we wish to know the head change at

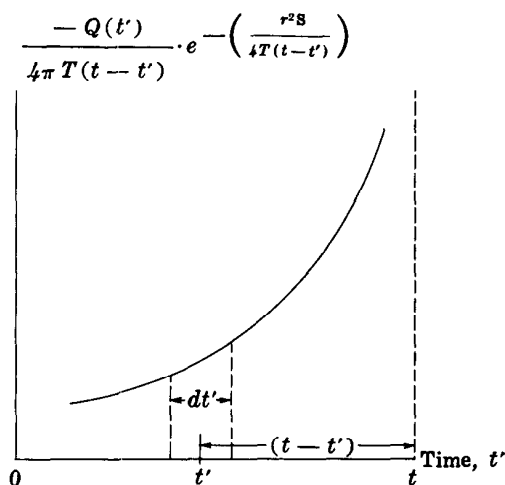
time t due to this continuous withdrawal. The rate of pumping, in volume of water per unit time, may vary from one instant to the next. The figure shows a plot of pumping rate versus time for a hypothetical case. Pumping starts at time = 0 and extends to time = t , the instant at which we wish to know the head change. We consider first the head change at t due to the action of the pump at one particular instant, t' , during the course of pumping. We consider an infinitesimal time interval, dt' , extending to either side of the instant t' ; the average rate of pumping during this interval is denoted $Q(t')$. The volume of water withdrawn from the well during the interval is the product of the pumping rate, $Q(t')$, and the time interval, dt' ; that is,

$$-V = -Q(t') dt'$$

Again negative signs are used to indicate withdrawal as opposed to injection. The product $Q(t') dt'$ is equal to the area of the shaded element in the graph shown in the preceding figure; the height of this element is $Q(t')$, and its width is dt' . The time interval between the instant of withdrawal and the instant of head measurement is $t-t'$. Using the solution obtained in the programmed instruction for the head change due to instantaneous withdrawal of a volume of water, the head change at time t due to the withdrawal at t' is given by

$$\frac{-V}{4\pi T(t-t')} \cdot e^{-\left(\frac{r^2 S}{4T(t-t')}\right)} = \frac{-Q(t') dt'}{4\pi T(t-t')} \cdot e^{-\left(\frac{r^2 S}{4T(t-t')}\right)}$$

The total head change at t , due to the continuous withdrawal from zero to t , is obtained through superposition, by adding the head changes due to the instantaneous withdrawals throughout the interval from zero to t .



The figure shows a graph in which, instead of plotting only discharge versus time, we plot the entire function

$$\frac{-Q(t')}{4\pi T(t-t')} \cdot e^{-\left(\frac{r^2 S}{4T(t-t')}\right)}$$

versus time. The area of the element at t' is now

$$\frac{-Q(t')}{4\pi T(t-t')} \cdot e^{-\left(\frac{r^2 S}{4T(t-t')}\right)} \cdot dt'$$

—thus it is just equal in magnitude to the head change at t , caused by the withdrawal at t' . If elements of the type shown in the figure are constructed all along the time axis, from zero to t , the area of each element will give the head change at t due to operation of the pump during the time interval represented by the element; the total head change at t due to all of the instantaneous withdrawals throughout the interval from zero to t will therefore be equal to the sum of these areas, or the total area under the curve from zero to t . This total area is the integral of the function

$$\frac{-Q(t')}{4\pi T(t-t')} \cdot e^{-\left(\frac{r^2 S}{4T(t-t')}\right)}$$

over the interval from zero to t , that is, the total head change is given by

$$h = \int_{t'=0}^{t'=t} \frac{-Q(t')}{4\pi T(t-t')} \cdot e^{-\left(\frac{r^2 S}{4T(t-t')}\right)} dt'$$

It should be noted that we are now using t' to denote the time *variable* or variable of integration, rather than to specify one particular instant. The function being integrated involves the difference, $t-t'$, between the upper limit of integration and the variable of integration. Evaluation of the integral will yield a function of the upper limit, t , and of r ; that is, the head change due to the pumping will be specified as a function of r and of t (the time of head measurement.)

For the particular case when the rate of discharge is a constant, Q , the integral equation can be transformed directly into a form suitable for computation. We have

$$h = \int_{t'=0}^{t'=t} \frac{-Q}{4\pi T(t-t')} \cdot e^{-\left(\frac{r^2 S}{4T(t-t')}\right)} dt'.$$

The term $-Q/4\pi T$ is a constant and may be taken outside the integral, giving

$$h = \frac{-Q}{4\pi T} \int_{t'=0}^{t'=t} \frac{1}{t-t'} \cdot e^{-\left(\frac{r^2 S}{4T(t-t')}\right)} dt'.$$

We introduce the algebraic change of variable,

$$\psi = \frac{r^2 S}{4T(t-t')}.$$

We differentiate this expression with respect to t' , treating t , at this stage, as a constant; this gives

$$\begin{aligned} \frac{d\psi}{dt'} &= \frac{r^2 S \cdot 4T}{(4T(t-t'))^2} = \frac{r^2 S}{4T(t-t')} \cdot \frac{1}{t-t'} \\ &= \frac{r^2 S}{4T(t-t')} \left\{ \frac{\frac{r^2 S}{4T(t-t')}}{\frac{r^2 S}{4T}} \right\} = \frac{\psi^2}{\frac{r^2 S}{4T}} \end{aligned}$$

Therefore

$$d\psi = \frac{\psi^2}{\frac{r^2 S}{4T}} \cdot dt'$$

and

$$dt' = \frac{r^2 S}{4T} \frac{d\psi}{\psi^2}.$$

The value of ψ corresponding to the upper limit of integration, $t'=t$, is

$$\psi_t = \frac{r^2 S}{4T(t-t)} = \infty.$$

While the value of ψ corresponding to the lower limit of integration, $t'=0$, is

$$\psi_0 = \frac{r^2 S}{4T(t-0)} = \frac{r^2 S}{4Tt}.$$

We now return to our integral equation and substitute ψ for

$$\frac{r^2 S}{4T(t-t')};$$

$$\frac{r^2 S}{4T} \cdot \frac{d\psi}{\psi^2}$$

for

$$dt';$$

and the values obtained above for the limits of integration. This gives

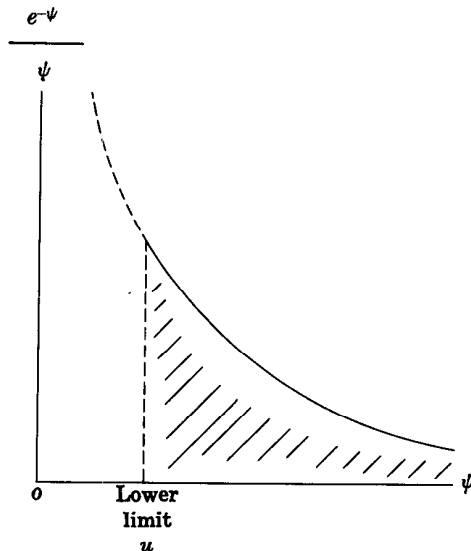
$$h = \frac{-Q}{4\pi T} \int_{\frac{r^2 S}{4Tt}}^{\infty} \frac{1}{t-t'} \cdot e^{-\psi} \cdot \frac{r^2 S}{4T} \cdot \frac{d\psi}{\psi^2}.$$

But since

$$\frac{1}{t-t'} \cdot \left(\frac{r^2 S}{4T} \right) = \psi,$$

the above integral becomes

$$h = \frac{-Q}{4\pi T} \int_{\frac{r^2 S}{4Tt}}^{\infty} \frac{e^{-\psi}}{\psi} d\psi.$$



This integral is called the exponential integral. It is a function of its lower limit, as suggested by the figure, which shows a graph of the function $e^{-\psi}/\psi$ versus ψ . The area under this graph is equal to the value of the integral. The upper limit is infinite, and the function $e^{-\psi}/\psi$ approaches zero as ψ becomes infinite; the area under the curve, or the value of the integral, depends only upon the point where the lower limit is taken—that is, upon the value of $r^2S/4Tt$. This term is often denoted u in the literature, so that the equation for head change is often written

$$h = \frac{-Q}{4\pi T} \int_u^\infty \frac{e^{-\psi}}{\psi} d\psi$$

where

$$u = \frac{r^2S}{4Tt}$$

It can be shown that the above integral is equal to an infinite series involving the lower limit. Specifically,

$$\int_u^\infty \frac{e^{-\psi}}{\psi} d\psi = -0.5772 - \ln(u) + u - \frac{u^2}{2 \cdot 2!} + \frac{u^3}{3 \cdot 3!} - \frac{u^4}{4 \cdot 4!} + \dots$$

Values of the integral for various values of the lower limit have been computed, using this series, and tabulated. In the hydrologic literature, the value of the integral is commonly referred to as $W(u)$ or “well function of u .” Tables of $W(u)$ versus u are available in the reference by Ferris, Knowles, Brown, and Stallman (1962) and in numerous other references. In the forms presented above, the equations yield the head change, or simply the head, assuming h was zero prior to pumping. If head was at some other constant level, h_0 , prior to pumping, the expressions are still valid for head change, $h - h_0$. That is, we have

$$h - h_0 = \frac{-Q}{4\pi T} \int_u^\infty \frac{e^{-\psi}}{\psi} d\psi = \frac{-Q}{4\pi T} \cdot W(u)$$

where

$$u = \frac{r^2S}{4Tt}$$

or in terms of drawdown, $h_0 - h$, we have

$$s = h_0 - h = \frac{Q}{4\pi T} \int_u^\infty \frac{e^{-\psi}}{\psi} d\psi = \frac{Q}{4\pi T} \cdot W(u)$$

The result we have obtained here is known as the Theis equation, after C. V. Theis who first applied it in hydrology (Theis, 1935). An excellent discussion of the significance of this equation in hydrology is given in another paper by Theis (1938).

It was recognized by Cooper and Jacob (1946) that at small values of u , (that is, at large values of t), the terms following $\ln(u)$ in the series expansion for

$$\int_{\mu}^{\infty} \frac{e^{-\psi}}{\psi} d\psi$$

become negligibly small. In this condition the value of the integral is given simply by

$$-0.5772 - \ln(u),$$

or

$$-0.5772 - \ln\left(\frac{r^2 S}{4Tt}\right).$$

The sign of the logarithmic term may be changed by inverting the expression in brackets,

$$-\ln\left(\frac{r^2 S}{4Tt}\right) = \ln\left(\frac{4Tt}{r^2 S}\right)$$

and the constant, 0.5772, may be expressed as the natural logarithm of another constant,

$$0.5772 = \ln\left(\frac{4}{2.25}\right)$$

so that

$$\begin{aligned} -0.5772 - \ln\left(\frac{r^2 S}{4Tt}\right) &= \ln\left(\frac{4Tt}{r^2 S}\right) - \ln\left(\frac{4}{2.25}\right) \\ &= \ln\left(\frac{2.25Tt}{r^2 S}\right) = 2.3 \log_{10}\left(\frac{2.25Tt}{r^2 S}\right). \end{aligned}$$

Thus when pumping has continued for a sufficient length of time so that u , or $r^2 S/4Tt$, is small we may write

$$s = \frac{Q}{4\pi T} \int_{\mu}^{\infty} \frac{e^{-\psi}}{\psi} d\psi \approx \frac{2.3Q}{4\pi T} \log_{10}\left(\frac{2.25 \cdot Tt}{r^2 S}\right).$$

This is the modified nonequilibrium formula, which forms the basis of the "semilog plot" techniques often used by hydrologists in the analysis of pumping test data. These techniques are generally applied for values of u less than 0.01.

The Theis equation and the modified nonequilibrium formula are extremely useful hydrologic tools, provided they are used within the limits of application established by the assumptions made in their derivation. Before leaving this subject, we will briefly review the assumptions that have been accumulated during the course of the derivation. We first developed the equation

$$\frac{\partial^2 h}{\partial r^2} + \frac{1}{r} \frac{\partial h}{\partial r} = \frac{S}{T} \frac{\partial h}{\partial t}$$

by assuming that:

1. The aquifer was confined;
2. There was no vertical flow;
3. All flow was directed radially toward (or away from) the origin;
4. S and T were constant—that is, the aquifer was homogeneous and isotropic;
5. There was no areal recharge applied to the aquifer

In writing the solution corresponding to instantaneous discharge or input of a volume of water, V , we added the assumptions that:

6. The aquifer was infinite in extent;
7. There was no lateral discharge or recharge except at the well
8. The head was uniform and unchanging throughout the aquifer prior to $t=0$.
9. All of the injected water was taken into storage (or conversely, all discharged water was derived from storage).
10. The well was of infinitesimal radius.

Finally, when we integrated the above solution to obtain the continuous discharge solution

$$s = h_0 - h = \frac{Q}{4\pi T} \int_{\frac{r^2 S}{4Tt}}^{\infty} \frac{e^{-\psi}}{\psi} d\psi$$

we added the condition that

11. The discharge, Q , was constant throughout the duration of pumping.

These assumptions should be kept in mind whenever the Theis equation is applied. The assumption that all flow is lateral implies that the well must fully penetrate the aquifer and that the aquifer is horizontal.

If the semilog approximation is used, we add the assumption that the time is great enough and radius small enough that the term $r^2S/4Tt$ is less than 0.01, and the later terms in the series expression for the integral can therefore be neglected.

The Theis equation was the first equation to describe flow of water to a well under nonequilibrium conditions. In subsequent work, Papadopulos and Cooper (1967) have accounted for the effects of a finite well radius; Jacob (1963) and several other writ-

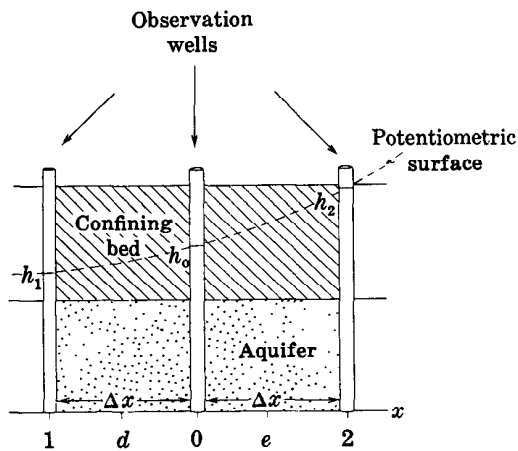
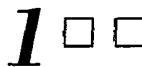
ers have examined the problem of discharge from partially penetrating wells; Stallman (1963a), Lang (1963), and numerous other investigators have utilized image theory to account for lateral aquifer boundaries; Jacob and Lohman (1952) have analyzed discharge at constant drawdown, rather than at constant rate; numerous writers, including in particular Jacob (1946), Hantush (1959, 1960 1967a 1967b) and Hantush and Jacob (1955) have treated the problem of discharge from an aquifer replenished by vertical recharge through overlying and underlying strata; and several writers, including Boulton (1954), have attacked the general problem of three-dimensional flow to a well. Weeks (1969) has applied various aspects of the theory of flow toward wells to the problem of determining vertical permeability from pumping test analysis.

Part VII. Finite-Difference Methods

Introduction

In preceding chapters we have considered formal mathematical solutions to the differential equations of ground-water flow. In practice, however, we find that such formal solutions are available only for a small minority of field problems, representing relatively simple boundary conditions. In most

cases, we are forced to seek approximate solutions, using methods other than direct formal solution. In Part VII, we consider one such method—the simulation of the differential equations by finite difference equations, which in turn can be solved algebraically or numerically.



Three observation wells tap a confined aquifer. The wells are arranged in a straight line in the x direction at a uniform spacing, Δx . The water levels in the three wells are designated h_1 , h_0 , and h_2 as indicated in the figure.

QUESTION

Which of the following equations gives a reasonable approximation for the derivative, $\partial h / \partial x$, at point d , midway between well 1 and well 0?

- Turn to Section:
- | | |
|--|----|
| $\left(\frac{\partial h}{\partial x}\right)_d \approx \frac{h_1 - h_2}{\Delta x}$ | 7 |
| $\left(\frac{\partial h}{\partial x}\right)_d \approx \frac{h_2 - h_1}{2\Delta x}$ | 26 |
| $\left(\frac{\partial h}{\partial x}\right)_d \approx \frac{h_0 - h_1}{\Delta x}$ | 12 |

2 □ □

Your answer, $h_{i,j}$, in Section 3 is correct.

QUESTION

Following the same conventions, which of the following expressions would serve as a finite-difference approximation to the term

$$\frac{\partial^2 h}{\partial x^2} + \frac{\partial^2 h}{\partial y^2}$$

at the point $h_{i,j}$?

$$\frac{\partial^2 h}{\partial x^2} + \frac{\partial^2 h}{\partial y^2} \approx \frac{h_{i-2,j} + h_{i-1,j} + h_{i+1,j} + h_{i+2,j} - 4h_{i,j}}{a^2}$$

Turn to Section:

20

$$\frac{\partial^2 h}{\partial x^2} + \frac{\partial^2 h}{\partial y^2} \approx \frac{h_{i,j+1} + h_{i+1,j} + h_{i,j+2} + h_{i+2,j} - 4h_{i,j}}{a^2}$$

18

$$\frac{\partial^2 h}{\partial x^2} + \frac{\partial^2 h}{\partial y^2} \approx \frac{h_{i-1,j} + h_{i+1,j} + h_{i,j-1} + h_{i,j+1} - 4h_{i,j}}{a^2}$$

4

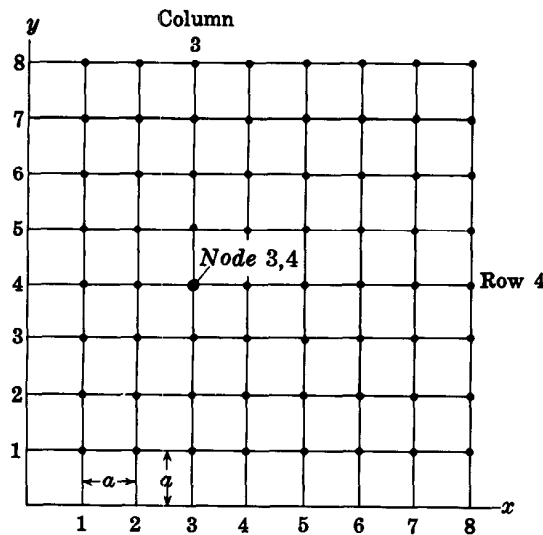
3 □ □

Your answer in Section 15,

$$\frac{\partial^2 h}{\partial x^2} + \frac{\partial^2 h}{\partial y^2} \approx \frac{h_1 + h_2 + h_3 + h_4 - 4h_0}{a^2},$$

is correct. These approximations to $\partial^2 h / \partial x^2$ and $\partial^2 h / \partial y^2$ can be obtained more formally through the use of Taylor series expansions. A certain error is involved in approximating the derivatives by finite differences, and we can see intuitively that this error will generally decrease as a is given smaller and smaller values.

Now let us place a rectangular grid of intersecting lines, as shown in the diagram



over the x, y plane. The lines are drawn at a uniform spacing, a , and are numbered successively from the origin. Lines parallel to the x -axis are termed rows, while lines parallel to the y -axis are termed columns. The intersections of the grid lines are termed nodes and are identified by the numbers associated with the intersecting lines. For example, the node 3, 4 is that formed by the intersection of the third column to the right of the y -axis with the fourth row above the x -axis. The spacing a , may be thought of as a unit of measurement; the node numbers then give the number of units of distance of a given node from the x and y axes. The head at a given node is indicated by using the node numbers for a subscript notation; for example, the head at node 3, 4 would be indicated by $h_{3,4}$.

QUESTION

Following this convention, how would we indicate the head at a node located i units to the right of the y axis and j units above the x axis (that is, at the point $x = i \cdot a, y = j \cdot a$, in the conventional Cartesian notation)?

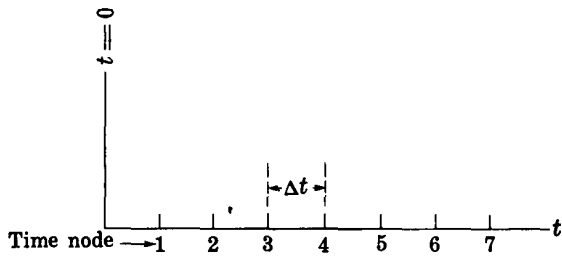
Turn to Section:

- $h_{j,i}$
- $h_{i,j}$
- $h_{ia,ja}$

- 14
- 2
- 5

4 □ □

Your answer in Section 2 is correct. We next consider the time axis and divide it as shown in the sketch into segments of length Δt , again numbering the division marks successively from $t=0$. We also introduce a third subscript, indicating the time at which a given head value is observed; for example,



$h_{i,j,n}$ refers to the head at the node i, j of the x, y plane at the time indicated by the n th division mark on the time axis.

QUESTION

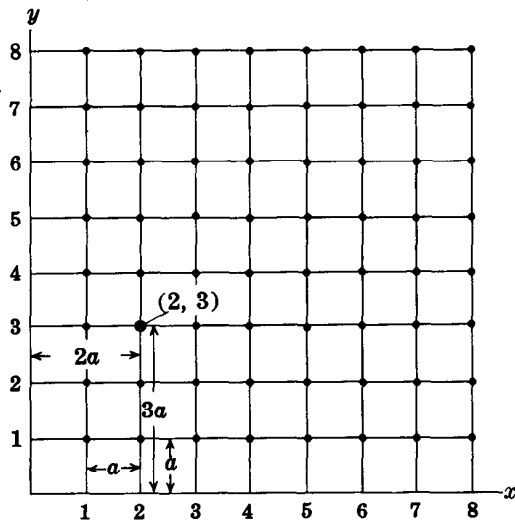
Again assuming $\Delta x = \Delta y = a$, which of the following would give the actual coordinate distances and time of measurement associated with the term $h_{i,j,n}$?

Turn to Section:

- $h_{i,j,n}$ = head at $x = i \cdot a, y = i \cdot \Delta t$, time = $n \cdot \Delta t$ 9
- $h_{i,j,n}$ = head at $x = i \cdot \Delta x, y = i \cdot \Delta y$, time = $n \cdot a$ 23
- $h_{i,j,n}$ = head at $x = i \cdot a, y = j \cdot a$, time = $n \cdot \Delta t$ 10

5 □ □

Your answer, $h_{ia,ja}$, in Section 3 is not correct. You have used the distances from the two coordinate axes as subscripts. That is,



you have used ia , which is actually the x coordinate of the node, or its distance from the y axis, as the first subscript; and you have used ja , which is actually the y coordinate of the node, or its distance from the x axis, as the second subscript. The convention introduced in Section 3, however, does not have this form. If the finite-difference grid is superimposed on the x, y plane, as in the sketch, then the subscript associated with the point $x = 2a, y = 3a$ is simply 2, 3; the head at this point is designated $h_{2,3}$. If we number the lines of the grid in succession along each axis, starting with the axis as 0, we can obtain the subscript of a given node, or grid intersection, by looking at the numbers assigned to the two grid lines which intersect there; point 2, 3 is at the intersection of vertical line number 2 and horizontal line number 3.

Return to Section 3 and choose another answer.

6 □ □

Your answer in Section 25 is not correct. Your formulation for the calculation of the new value of $h_{i,j}$ in the first step is incorrect. The finite-difference equation which we developed stated that the value of $h_{i,j}$ should be the average of the values of h at the four surrounding nodes, that is

$$h_{i,j} = \frac{1}{4} (h_{i-1,j} + h_{i+1,j} + h_{i,j-1} + h_{i,j+1}).$$

The idea in the relaxation process is to compute a new value of $h_{i,j}$ as the average of the previous values of h at the four surrounding nodes. That is

$$h_{i,j}(\text{New Value}) = \frac{1}{4} (h_{i-1,j} + h_{i+1,j} + h_{i,j-1} + h_{i,j+1}) (\text{Previous Values}).$$

When this calculation has been made, the idea is to compare the new value of $h_{i,j}$ with the previous value of $h_{i,j}$. If these two are very close, everywhere in the grid, there is no point in continuing the process further, since additional iterations will produce little additional change. The solution, in other words, has converged to values of h which satisfy the difference equation. In the second step, therefore, rather than setting $R_{i,j}$ equal to the average of the new and previous values of $h_{i,j}$ as in the answer you selected, $R_{i,j}$ should be set equal to the difference between $h_{i,j}$ (New Value) and $h_{i,j}$ (Previous Value). This difference may then be tested throughout the grid, and if it is sufficiently small at all points, the iteration process can be terminated.

Return to Section 25 and choose another answer.

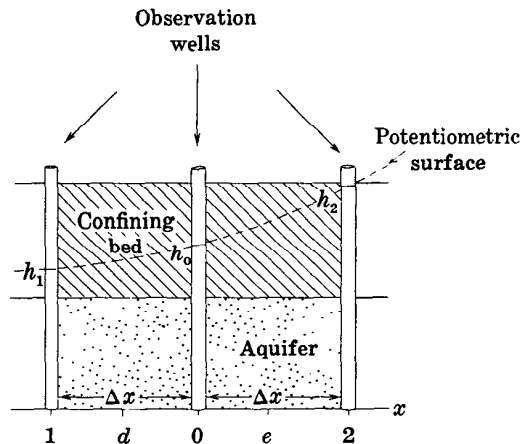
7 □ □

Your answer in Section 1,

$$\frac{h_1 - h_2}{\Delta x}$$

is not correct. In introducing the notion of a derivative, it is customary to begin with the finite-difference form—that is, to consider the finite change in h , Δh , occurring over a finite interval, Δx , along the x axis. The derivative notation, dh/dx , is then introduced to represent the value of the ratio $\Delta h/\Delta x$, as Δx becomes infinitesimal in size. Here, the idea is to move in the opposite direction. We started with the derivative, $\partial h/\partial x$, and we wish to approximate it by a ratio of finite differences. Moreover, we want an expression which applies at point d , midway between well 0 and well 1. The finite change in h occurring between these two wells is $h_0 - h_1$. The finite distance separating them is Δx .

Return to Section 1 and choose another answer.



8 □ □

Your answer in Section 10 is not correct. You have used the correct formulation for the forward-difference approximation to $\partial h / \partial t$ —that is,

$$\frac{\partial h}{\partial t} \approx \frac{h_{i,j,n+1} - h_{i,j,n}}{\Delta t}$$

—but your approximation for $(\partial^2 h / \partial x^2) + (\partial^2 h / \partial y^2)$ is not correct. To obtain an approximation for $\partial^2 h / \partial x^2$, we move along the x axis, holding y constant. In this process i , the subscript denoting node position on the x axis will change, whereas j , the subscript denoting node position in the y direction, will remain unchanged. Our result will be

$$\frac{\partial^2 h}{\partial x^2} \approx \frac{\frac{h_{i+1,j,n} - h_{i,j,n}}{a} - \frac{h_{i,j,n} - h_{i-1,j,n}}{a}}{a} = \frac{h_{i+1,j,n} + h_{i-1,j,n} - 2h_{i,j,n}}{a^2}$$

Similarly, in obtaining an approximation for $\partial^2 h / \partial y^2$, we move along the y axis, so that i remains fixed, while the y -subscript, j , varies. The result is

$$\frac{\partial^2 h}{\partial y^2} \approx \frac{\frac{h_{i,j+1,n} - h_{i,j,n}}{a} - \frac{h_{i,j,n} - h_{i,j-1,n}}{a}}{a} = \frac{h_{i,j+1,n} + h_{i,j-1,n} - 2h_{i,j,n}}{a^2}$$

Addition of these two expressions will give the correct approximation for $(\partial^2 h / \partial x^2) + (\partial^2 h / \partial y^2)$.

Return to Section 10 and choose another answer.

9 □ □

Your answer in Section 4 is not correct. The subscripts i, j, n tell us that head $h_{i,j,n}$ occurs at a certain node, i, j of the finite-difference grid on the x, y plane and at a certain point, n , of the finite-difference scale along the time axis. The coordinate values are found by multiplying the number of nodes along a given axis by the node spacing. Along the x axis the node i, j lies a distance $i \cdot a$ from the origin (i nodes, each with

spacing a). Along the time axis, the point n occurs at a time $n \cdot \Delta t$ (n time marks, each at a spacing Δt). The same procedure should be applied in determining the y coordinate, keeping in mind that there are j nodes along the y axis between the origin and point i, j , and that these nodes fall at a spacing a .

Return to Section 4 and choose another answer.

10 □ □

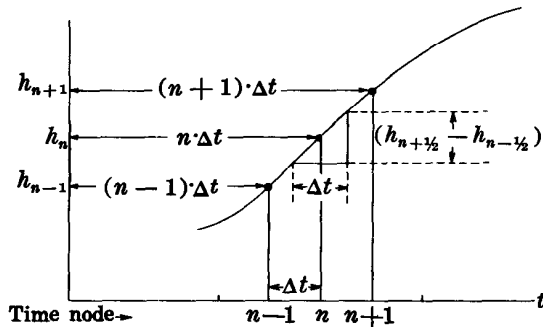
Your answer in Section 4 is correct. On each axis, x , y , and t , the value of the independent variable is found by multiplying the subscript, or node number, by the node spacing along the axis. Using the conventions we have adopted, therefore, the approximation

$$\left(\frac{\partial^2 h}{\partial x^2} + \frac{\partial^2 h}{\partial y^2}\right)_{n\Delta t} \approx \frac{h_{i-1,j,n} + h_{i+1,j,n} + h_{i,j-1,n} + h_{i,j+1,n} - 4h_{i,j,n}}{a^2}$$

Now in order to simulate the differential equation

$$\frac{\partial^2 h}{\partial x^2} + \frac{\partial^2 h}{\partial y^2} = \frac{S}{T} \frac{\partial h}{\partial t}$$

at the instant $t = n\Delta t$ we require in addition an approximation to $\partial h / \partial t$ at this instant.



The sketch shows a graph of h versus t in the vicinity of this time. A reasonable approximation to $\partial h / \partial t$ in the vicinity of the n th time mark would obviously be

$$\frac{\partial h}{\partial t} = \frac{h_{(n+1/2)} - h_{(n-1/2)}}{\Delta t}$$

to

$$\frac{\partial^2 h}{\partial x^2} + \frac{\partial^2 h}{\partial y^2}$$

at the time $t = n\Delta t$, and at the point $x = i \cdot a$, $y = j \cdot a$ would be given by

In practical methods of computation, however, the approximations

$$\left(\frac{\partial h}{\partial t}\right)_{n\Delta t} \approx \frac{h_{n+1} - h_n}{\Delta t}$$

or

$$\left(\frac{\partial h}{\partial t}\right)_{n\Delta t} \approx \frac{h_n - h_{n-1}}{\Delta t}$$

are often found preferable. Here, we are simulating the derivative at $t = n\Delta t$ by, respectively, a "forward difference" taken between the times $n \cdot \Delta t$ and $(n+1) \cdot \Delta t$, and a "backward difference," taken between $(n-1) \cdot \Delta t$ and $n \cdot \Delta t$. The error involved will depend largely upon our choice of Δt , and can be reduced to tolerable limits by choosing Δt sufficiently small.

QUESTION

Using the forward-difference approximation to $\partial h / \partial t$ given above, which of the following results is obtained as a finite-difference simulation of the equation

$$\frac{\partial^2 h}{\partial x^2} + \frac{\partial^2 h}{\partial y^2} = \frac{S}{T} \frac{\partial h}{\partial t}$$

at the point $x = ia$, $y = ja$, and at the time $t = n\Delta t$?

10 □ □ —Con.

Turn to Section:

$$\frac{h_{i-1,j,n} + h_{i+1,j,n} + h_{i,j-1,n} + h_{i,j+1,n} - 4h_{i,j,n}}{a^2} = \frac{S}{T} \frac{h_{i,j,n+1} - h_{i,j,n}}{\Delta t} \quad 16$$

$$\frac{h_{i-1,j-1,n} + h_{i+1,j+1,n} + h_{i,j-1,n} - h_{i-1,j+1,n} - 4h_{i,j,n}}{a^2} = \frac{S}{T} \frac{h_{i,j,n+1} - h_{i,j,n}}{\Delta t} \quad 8$$

$$\frac{h_{i-1,j,n} + h_{i+1,j,n} + h_{i,j-1,n} + h_{i,j+1,n} - 4h_{i,j,n}}{a^2} = \frac{S}{T} \frac{h_{i,j,n+\frac{1}{2}} - h_{i,j,n-\frac{1}{2}}}{\Delta t} \quad 19$$

11 □ □

Your answer in Section 16 is not correct. For the steady-state condition, $\partial h / \partial t = 0$; so, our equation,

$$\frac{\partial^2 h}{\partial x^2} + \frac{\partial^2 h}{\partial y^2} = \frac{S}{T} \frac{\partial h}{\partial t}$$

becomes simply

$$\frac{\partial^2 h}{\partial x^2} + \frac{\partial^2 h}{\partial y^2} = 0.$$

To obtain a finite-difference approximation to this equation, we need only take our finite-difference approximation to $(\partial^2 h / \partial x^2)$

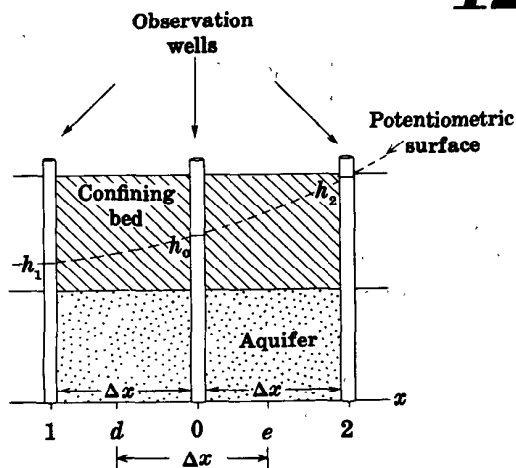
+ $(\partial^2 h / \partial y^2)$ and set it equal to zero. Our approximation to this sum, using the subscript notation associated with the finite-difference grid, was

$$\frac{h_{i-1,j} + h_{i+1,j} + h_{i,j-1} + h_{i,j+1} - 4h_{i,j}}{a^2}$$

This expression can be set equal to zero, and the resulting equation multiplied through by the constant a^2 to obtain the finite-difference equation which we require.

Return to Section 16 and choose another answer.

12 □ □



Your answer in Section 1,

$$\left(\frac{\partial h}{\partial x} \right)_a \approx \frac{h_0 - h_1}{\Delta x}$$

is correct. Similarly the derivative at point e , midway between well 0 and well 2 is approximated by

(continued on next page)

12 —Con.

$$\left(\frac{\partial h}{\partial x}\right)_e \approx \frac{h_2 - h_0}{\Delta x}$$

QUESTION

Which of the following expressions gives a reasonable approximation for the second derivative, $\partial^2 h / \partial x^2$, at point 0—that is, at the location of the center well?

$\frac{\partial^2 h}{\partial x^2} \approx \frac{h_2 - h_1}{2\Delta x}$	Turn to Section: 27
---	-------------------------------

$\frac{\partial^2 h}{\partial x^2} \approx \frac{h_1 + h_2 - 2h_0}{(\Delta x)^2}$	15
---	-----------

$\frac{\partial^2 h}{\partial x^2} \approx \frac{\frac{h_2 - h_0}{\Delta x} - \frac{h_0 - h_1}{\Delta x}}{2\Delta x}$	22
---	-----------

13

Your answer in Section 16 is not correct. The finite-difference expression approximating

$$\frac{\partial^2 h}{\partial x^2} + \frac{\partial^2 h}{\partial y^2}$$

was

$$\frac{h_{i-1,j} + h_{i+1,j} + h_{i,j-1} + h_{i,j+1} - 4h_{i,j}}{a^2}$$

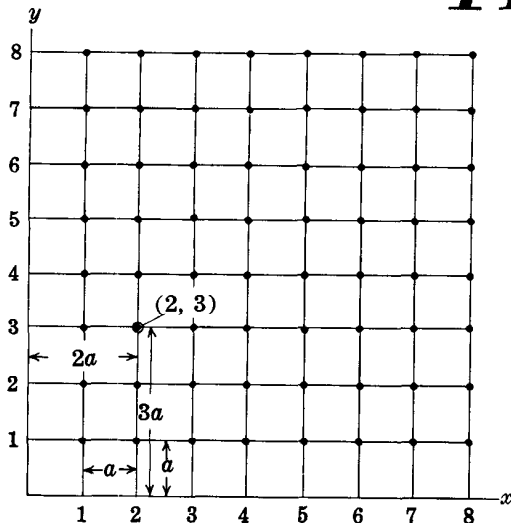
To approximate the equation

$$\frac{\partial^2 h}{\partial x^2} + \frac{\partial^2 h}{\partial y^2} = 0$$

this finite-difference expression need only be equated to zero. The resulting equation can be multiplied through by the constant a^2 .

Return to Section 16 and choose another answer.

14

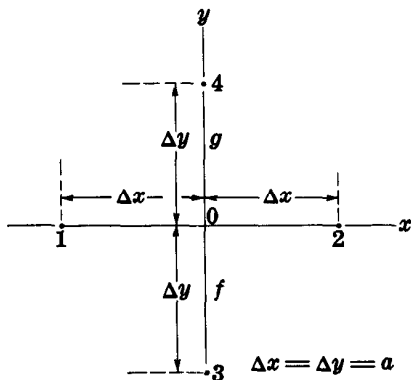


Your answer, $h_{j,i}$, in Section 3 is not correct. The sketch shows a diagram of the x , y plane, with the finite-difference grid superimposed upon it. Node 2, 3 is at a distance $2a$ from the y axis ($x=2a$) and a distance $3a$ from the x axis ($y=3a$). That is, the node having the coordinates $x=2a$, $y=3a$ is the node 2, 3; and the head at this node is designated $h_{2,3}$. The same rules apply for the node in the question of Section 3 which was at a distance $i \cdot a$ from the y axis and a distance $j \cdot a$ from the x axis. The coordinates of this node are $x=i \cdot a$, $y=j \cdot a$.

Return to Section 3 and choose another answer.

15 □ □

Map view



Your answer in Section 12,

$$\frac{\partial^2 h}{\partial x^2} \approx \frac{h_1 + h_2 - 2h_0}{(\Delta x)^2},$$

is correct. If we were to consider, in addition, the wells 3 and 4 along a line parallel to the y axis (see figure), we would similarly have as an approximation for $\partial^2 h / \partial y^2$ at point 0,

$$\frac{\partial^2 h}{\partial y^2} \approx \frac{h_3 + h_4 - 2h_0}{(\Delta y)^2}.$$

QUESTION

If the spacing of the wells in the diagram is uniform—that is, if $\Delta x = \Delta y = a$ —which of the following expressions may be obtained for

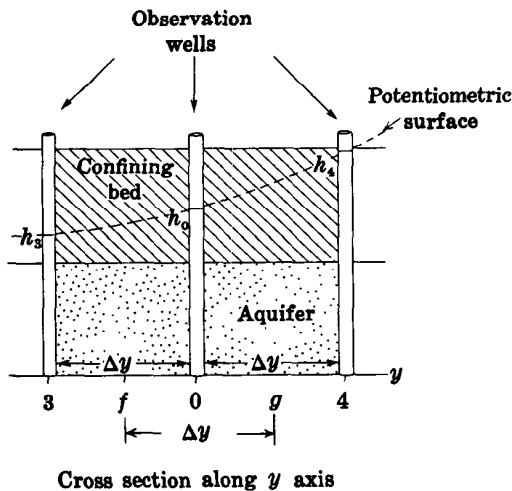
$$\frac{\partial^2 h}{\partial x^2} + \frac{\partial^2 h}{\partial y^2} ?$$

Turn to Section:

$$\frac{\partial^2 h}{\partial x^2} + \frac{\partial^2 h}{\partial y^2} \approx \frac{h_1 + h_2 + h_3 + h_4 - 4h_0}{a^2} \quad 3$$

$$\frac{\partial^2 h}{\partial x^2} + \frac{\partial^2 h}{\partial y^2} \approx \frac{h_1 + h_2 + h_3 + h_4}{a^2} \quad 28$$

$$\frac{\partial^2 h}{\partial x^2} + \frac{\partial^2 h}{\partial y^2} \approx \frac{(h_1 + h_2 - h_3 + h_4)}{a^2} \quad 24$$



16 □ □

Your answer in Section 10 is correct. Note that the equation which we have obtained is actually an algebraic equation, involving the terms $h_{i-1,j,n}$, $h_{i+1,j,n}$, $h_{i,j-1,n}$, $h_{i,j+1,n}$, $h_{i,j,n}$, and $h_{i,j,n+1}$; that is, we have simulated a differential equation by an algebraic equation. If the values of head are known at all nodes

of the x, y plane for some initial time, $t=0$, then the head value at each internal node for the succeeding time, $t=1 \cdot \Delta t$, can be obtained by applying the equation we have just obtained at the two times 0 and $1 \cdot \Delta t$ ($n=0$ and $n=1$). This would give

$$\frac{h_{i-1,j,0} + h_{i+1,j,0} + h_{i,j-1,0} + h_{i,j+1,0} - 4h_{i,j,0}}{a^2} = \frac{S}{T} \frac{h_{i,j,1} - h_{i,j,0}}{\Delta t}$$

16 □ □ —Con.

This equation is applied in turn at each internal node of the plane and solved for $h_{i,j,1}$ at each point, using the appropriate values of h from the $t=0$ distribution. Additional conditions must be given from which head values at nodes along the boundaries of the x, y plane at the new time can be determined. When the head values are determined throughout the plane for the new time ($n=1$), the procedure may be repeated to determine head values at the next point on the time axis ($n=2$); and so on.

This is termed the explicit procedure of solution. It suffers from the shortcoming that if Δt is chosen too large, errors may be introduced which grow in size as the stepwise calculation proceeds, so that for large values of time the solution bears no relation to reality, even as an approximation. To circumvent this difficulty, other schemes of computation are often used, some involving the backward-difference approximation to $\partial h/\partial t$, and others involving entirely different simulations of the differential equation.

Many of these schemes of solution involve iterative techniques, in which the differences between members of an equation are successively reduced by numerical adjustment. These techniques are sometimes termed re-

laxation methods; they are of sufficient importance that it will be worthwhile to see how they operate, through a simple example.

Suppose we are dealing with a problem of two-dimensional steady-state ground-water flow. For a steady state situation, the term $\partial h/\partial t$ of our differential equation, and therefore the term

$$\frac{h_{i,j,n+1} - h_{i,j,n}}{\Delta t}$$

of our finite-difference equation, is zero. The differential equation is simply

$$\frac{\partial^2 h}{\partial x^2} + \frac{\partial^2 h}{\partial y^2} = 0.$$

QUESTION

Using the notation developed above, but dropping the third subscript since time is not involved, which of the following would represent a valid finite-difference approximation to this steady-state equation?

Turn to Section:

$h_{i-1,j} + h_{i+1,j} + h_{i,j-1} + h_{i,j+1} - 4h_{i,j} = 0$	25
$h_{i-1,j} + h_{i+1,j} + h_{i,j-1} + h_{i,j+1} + 4h_{i,j} = a^2$	11
$h_{i-1,j} + h_{i+1,j} + h_{i,j-1} + h_{i,j+1} = \frac{4h_{i,j}}{a^2}$	13

17 □ □

Your answer in Section 25 is correct. If we were to "flow chart" the relaxation procedure for solution on a digital computer, we would have to incorporate these steps in some way.

Numerous other techniques exist for the numerical solution of the differential equations of flow. The efficiency of various methods, in terms of computational labor or machine time, varies widely depending upon the problem under study. Care must be exercised in selecting a method that is well suited to the problem, or unreasonable investments of time and effort may be required to obtain a solution.

In this discussion we have given only a brief indication of the way in which numerical methods may be applied in ground-water hydrology. Numerical analysis is a broad and complex field in itself. Interested readers will find an extensive literature dealing both with theory and with a wide range of applications. Examples of the use of numerical techniques in ground water may be found in the work of Prickett and Lonquist (1971), Stallman (1956), Remson, Appel, and Webster (1965), Pinder and Bredehoeft (1968), Rubin (1968), Bredehoeft and Pinder (1970), Freeze (1971), Prickett and Lonquist (1973), Trescott, Pinder, and

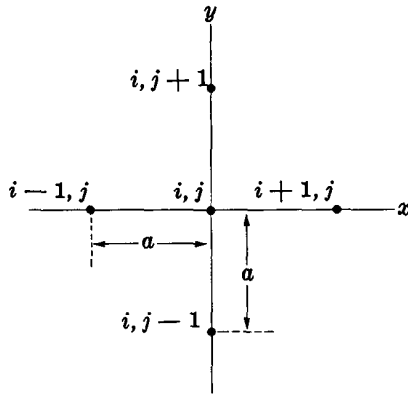
17 —Con.

Jones (1970), Trescott, (1973), and many others. An excellent summary of numerical methods as applied in ground-water hydrology is given by Remson, Hornberger, and Molz (1970).

You have completed the programed instruction of Part VII. A discussion giving further details of some of the standard finite-difference techniques is presented in standard text format following Section 28.

18

Your answer in Section 2 is not correct. The sketch shows the five-well array which we used earlier to develop an approximation for $(\partial^2 h / \partial x^2) + (\partial^2 h / \partial y^2)$, but with the wells now redesignated according to the scheme of subscripts associated with our



finite-difference grid. The head at the central well is designated $h_{i,j}$, rather than h_0 ; the heads at the two wells along the x axis are $h_{i-1,j}$ and $h_{i+1,j}$, rather than h_1 and h_2 ; and the heads at the two wells along the y axis are designated $h_{i,j-1}$ and $h_{i,j+1}$, rather than h_3 and h_4 . Our previous expression for

$$\frac{\partial^2 h}{\partial x^2} + \frac{\partial^2 h}{\partial y^2}$$

was

$$\frac{h_1 + h_2 + h_3 + h_4 - 4h_0}{a^2}$$

The question only requires that this be translated into the notation associated with the finite-difference grid.

Return to Section 2 and choose another answer.

19

Your answer in Section 10 is not correct. Your approximation for $(\partial^2 h / \partial x^2) + (\partial^2 h / \partial y^2)$ is correct, but you have not used the forward-difference formulation to approximate $\partial h / \partial t$, as required by the question. The approximation which you have used,

$$\frac{\partial h}{\partial t} = \frac{h_{i,j,n+\frac{1}{2}} - h_{i,j,n-\frac{1}{2}}}{\Delta t},$$

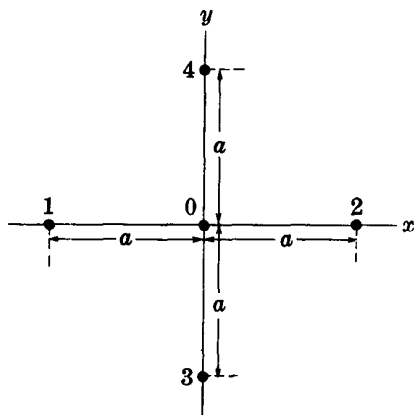
is normally a more accurate approximation to $\partial h / \partial t$ at i, j, n , than is the forward-difference formulation, since the difference is

taken symmetrically about the point at which $\partial h / \partial t$ is to be approximated. Unfortunately, however, it is not always as useful in the calculation of actual numerical solutions as is the forward-difference or backward-difference formulation. These formulations are unsymmetrical in the sense the difference is measured entirely to one side or the other of the time $t = n\Delta t$, which is the instant at which $\partial h / \partial t$ is to be approximated; but they are better suited to many techniques for computing solutions.

Return to Section 10 and choose another answer.

20 □ □

FIGURE A

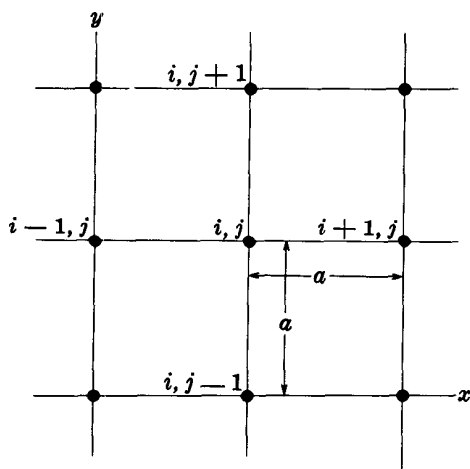


Your answer in Section 2 is not correct. The upper part of the figure shows the array which we used in developing our finite-difference approximation for $(\partial^2 h / \partial x^2) + (\partial^2 h / \partial y^2)$. The well at the center of the array was labeled 0; the surrounding wells were labeled as indicated. The expression we obtained for

$$\frac{\partial^2 h}{\partial x^2} + \frac{\partial^2 h}{\partial y^2}$$

was

$$\frac{h_1 + h_2 + h_3 + h_4 - 4h_0}{a^2}$$



Using the notation introduced for our finite-difference grid, shown in the lower part of the figure, the well at the center of the array would be denoted i, j ; the remaining wells would be designated: $i-1, j$; $i+1, j$; $i, j-1$; and $i, j+1$, as shown. It is simply a matter of substituting these designations for the designations, 0, 1, 2, 3, and 4 used in our earlier development.

Return to Section 2 and choose another answer.

21 □ □

Your answer in Section 25 is not correct. Your initial step, giving the formulation for computing the new value of $h_{i,j}$ using the previous values of $h_{i-1,j}$, $h_{i+1,j}$, $h_{i,j-1}$, and $h_{i,j+1}$, is correct. However, your second step is not correct. The idea is to continue the process until the difference between the previous value of $h_{i,j}$ and the new value of $h_{i,j}$

becomes very small everywhere in the grid. Thus $R_{i,j}$ should represent the difference between $h_{i,j}$ (New Value) and $h_{i,j}$ (Previous Value); and the process should be continued until $|R_{i,j}|$ is negligible throughout the grid.

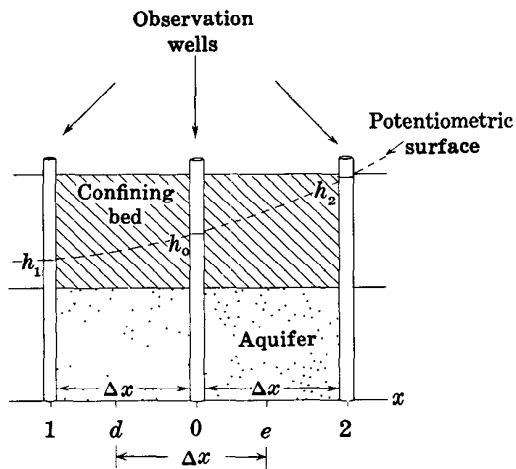
Return to Section 25 and choose another answer.

22 □ □

Your answer in Section 12,

$$\frac{\partial^2 h}{\partial x^2} \approx \frac{\frac{h_2 - h_0}{\Delta x} - \frac{h_0 - h_1}{\Delta x}}{2\Delta x},$$

is not correct. The numerator in your answer gives the difference between two terms: $(h_2 - h_0)/\Delta x$, which approximates $\partial h/\partial x$ at point e ; and $(h_0 - h_1)/\Delta x$, which approximates $\partial h/\partial x$ at point d .



The numerator thus represents the difference

$$\left(\frac{\partial h}{\partial x}\right)_e - \left(\frac{\partial h}{\partial x}\right)_d,$$

that is, it approximates the change in $\partial h/\partial x$ between point d and e . Thus if it were divided by Δx , the interval between points d and e , we would have an approximation to

$$\frac{\partial\left(\frac{\partial h}{\partial x}\right)}{\partial x},$$

that is, to $\partial^2 h/\partial x^2$ at the midpoint, 0, of the interval between d and e . In the answer which you selected, however, the quantity

$$\frac{h_2 - h_0}{\Delta x} - \frac{h_0 - h_1}{\Delta x}$$

is divided by $2\Delta x$, rather than by Δx .

Return to Section 12 and choose another answer.

23 □ □

Your answer in Section 4 is not correct. The coordinate of a point, in space or time, is found by multiplying the number of nodes between the origin and the point in question, along the appropriate axis, by the node spacing along that axis. Thus the x coordinate of a node i, j, n , is $x = i \cdot a$, since there are i nodes along the x axis from the origin

to i, j , and the node spacing is a . The same procedure may be applied along the y and t axes, keeping in mind that the node spacing along the y axis is a , while that along the time axis is Δt .

Return to Section 4 and choose another answer.

24 □ □

Your answer in Section 15,

$$\frac{\partial^2 h}{\partial x^2} + \frac{\partial^2 h}{\partial y^2} \approx \frac{(h_1 + h_2) - (h_3 + h_4)}{a^2}$$

is not correct. The approximate expression which we obtained for $\partial^2 h / \partial x^2$ was

$$\frac{h_1 + h_2 - 2h_0}{(\Delta x)^2}$$

or, since we have taken $\Delta x = a$,

$$\frac{h_1 + h_2 - 2h_0}{a^2}$$

The expression given in Section 15 for $\partial^2 h / \partial y^2$ was

$$\frac{h_3 + h_4 - 2h_0}{(\Delta y)^2}$$

or again, since we have taken $\Delta y = a$,

$$\frac{h_3 + h_4 - 2h_0}{a^2}$$

These two expressions need only be added algebraically to obtain an approximation for

$$\frac{\partial^2 h}{\partial x^2} + \frac{\partial^2 h}{\partial y^2}$$

Return to Section 15 and choose another answer.

25 □ □

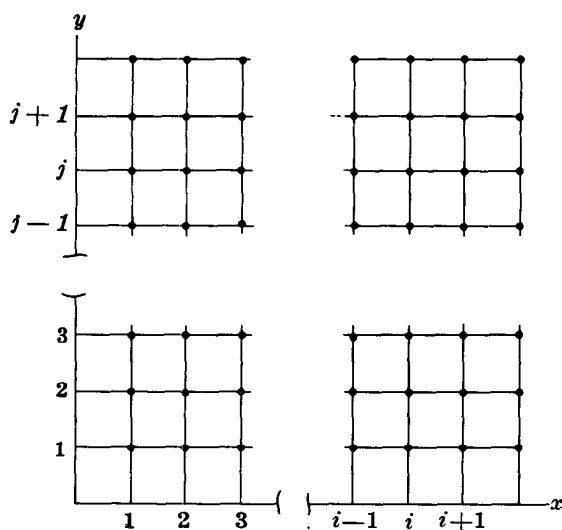
Your answer in Section 16

$$h_{i-1,j} + h_{i+1,j} + h_{i,j-1} + h_{i,j+1} - 4h_{i,j} = 0$$

is correct. To solve this by an iteration technique we rewrite the equation in the form

$$h_{i,j} = \frac{1}{4}(h_{i-1,j} + h_{i+1,j} + h_{i,j-1} + h_{i,j+1}),$$

and we divide the x, y plane into a grid as shown in the sketch, with the grid intersections forming the nodes at which we will compute values of h . In the form in which



we have written it, it is easy to see that what our equation actually says is that the head at each node must be the average of the heads at the four adjacent nodes. We begin by entering known values of head along the boundaries of the grid—that is, by applying the boundary conditions. We then insert assumed values of h at each interior grid point. These initial values of h may be anything we wish, although a great deal of work can be saved if we can choose them in a way that roughly approximates the final head distribution. We then move through the grid, in any order or direction, and at each interior node cross out the value of head, writing in its place the average of the head values at the four adjacent nodes. At each node we note not only the new value of h , but the *change* in h , from the initial value, resulting from the calculation. When we have completely traversed the grid, we start again, and proceed through the grid in the same way, replacing each h value by the average of the heads at the four adjacent nodes, and noting the change in h that this causes. After a number of repetitions we will find that the change in h caused by each new calculation becomes very small—in other words, that the value of head at each point is already essentially equal to the aver-

25 □ □ —Con.

age of those at the four neighboring points, so that inserting this average in place of h produces little or no additional change. At this point our head distribution represents an approximate solution to our difference equation and thus to the differential equation which the difference equation simulates.

The process just described, as noted earlier, is an example of a relaxation technique.

In general, since the head at each node is used in calculating the head at each of the four surrounding nodes, several complete traverses of the grid may be required before the changes in head are everywhere sufficiently small. This method can readily be used in hand calculation; it is also well adapted to solution by digital computer.

QUESTION

Which of the following would you choose as a "shorthand" description of the method of calculation described above?

Turn to Section:

$$h_{i,j} \text{ (New Value)} = \frac{1}{4} (h_{i-1,j} + h_{i+1,j} + h_{i,j-1} + h_{i,j+1}) \text{ (Previous Values)}$$

$$R_{i,j} = h_{i,j} \text{ (New Value)} - h_{i,j} \text{ (Previous Value)}$$

Continue calculation until $|R_{i,j}| \approx 0$ for all points in grid. 17

$$h_{i,j} \text{ (New Value)} = \frac{1}{4} (h_{i-1,j} + h_{i+1,j} + h_{i,j-1} + h_{i,j+1}) \text{ (Previous Values)}$$

$$R_{i,j} = h_{i,j} \text{ (New Value)}$$

Continue calculation until $|R_{i,j}| \approx 0$ for all points in grid. 21

$$h_{i,j} \text{ (New Value)} = \frac{1}{4} (h_{i+1,j} - h_{i-1,j} + h_{i,j+1} - h_{i,j-1}) \text{ (Previous Values)}$$

$$R_{i,j} = \frac{h_{i,j} \text{ (New Value)} + h_{i,j} \text{ (Previous Value)}}{2}$$

Continue calculation until $|R_{i,j}| \approx 0$ for all points in grid. 6

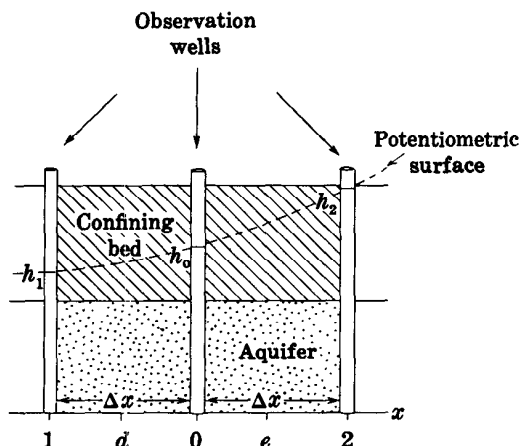
26 □ □

Your answer in Section 1,

$$\left(\frac{\partial h}{\partial x} \right)_a \approx \frac{h_2 - h_1}{2\Delta x}$$

is not correct. This answer would be a reasonable approximation for the derivative at point 0, in the center of the array, because it gives the ratio of a change in h , $h_2 - h_1$, to the corresponding change in distance, $2\Delta x$,

26 □ □ —Con.



over an interval which is centered at 0. For the derivative at point d , however, midway between well 1 and well 0, we can do a little better. The change in h over an interval centered at d is simply $h_0 - h_1$, and the corresponding interval of distance is simply Δx .

Return to Section 1 and choose another answer.

27 □ □

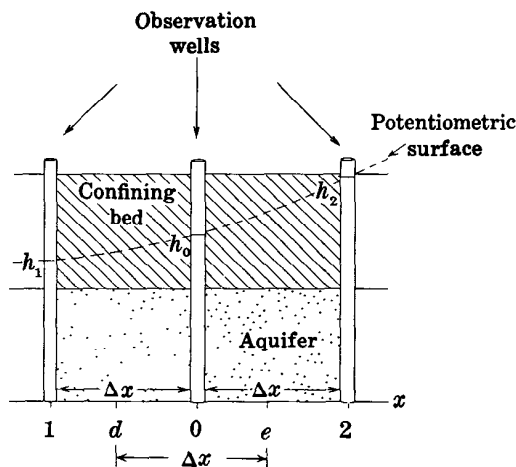
Your answer in Section 12,

$$\frac{\partial^2 h}{\partial x^2} \approx \frac{h_2 - h_1}{2\Delta x}$$

is not correct. $h_2 - h_1$ gives the change in h between points 1 and 2, and $2\Delta x$ gives the distance between these points. Thus the term $(h_2 - h_1)/2\Delta x$ is an approximation to the first derivative, $\partial h/\partial x$, at the midpoint of the distance interval—that is, at point 0. The question however, asked for a term approximating the second derivative, $\partial^2 h/\partial x^2$, at this point. The second derivative is actually the derivative of the first derivative; that is

$$\frac{\partial^2 h}{\partial x^2} = \frac{\partial \left(\frac{\partial h}{\partial x} \right)}{\partial x}$$

To obtain a finite-difference expression for this term, we must consider the change in the first derivative, $\partial h/\partial x$, between two points, and must divide this change in $\partial h/\partial x$ by the distance separating these two points. We have seen that $\partial h/\partial x$ at point d , midway between wells 1 and 0, can be approximated by the expression $(h_0 - h_1)/\Delta x$; and that $\partial h/\partial x$ at point e , midway between



wells 0 and 2 can be approximated by the term $(h_2 - h_0)/\Delta x$. Points d and e are themselves separated by a distance Δx , and point 0 is at the midpoint of this interval. Thus if we subtract our approximate expression for $\partial h/\partial x$ at d , from that for $\partial h/\partial x$ at e , and divide the result by the interval between d and e , Δx , we should obtain an expression for $\partial^2 h/\partial x^2$ at point 0.

Return to Section 12 and choose another answer.

28

Your answer in Section 15,

$$\frac{\partial^2 h}{\partial x^2} + \frac{\partial^2 h}{\partial y^2} \approx \frac{h_1 + h_2 + h_3 + h_4}{a^2}$$

is not correct. The term $-2h_0$ appeared in the numerator of both of our approximate

expressions —that for $\partial^2 h / \partial x^2$ and that for $\partial^2 h / \partial y^2$. When we add these two expressions to obtain an approximation for $(\partial^2 h / \partial x^2) + (\partial^2 h / \partial y^2)$, these terms in h_0 do not drop out.

Return to Section 15 and choose another answer.

Techniques of Finite-Difference Solution of the Ground-Water-Flow Equation

Certain techniques of numerical solution which are commonly used in ground-water modeling are described in the following discussion. No attempt has been made to discuss such topics as stability or rate of convergence in theoretical terms; the reader is referred to the paper by Peaceman and Rachford (1955) for discussion of these subjects. Similarly, no attempt has been made to give the details of the programming procedure. The paper by Prickett and Lonquist (1971) analyzes some typical programs and in addition provides an excellent summary of the hydrologic and mathematical foundations of digital modeling; the paper by Trescott (1973) describes a versatile program for areal aquifer simulation. The discussion presented here is limited to a description of some of the common techniques of approximation and calculation.

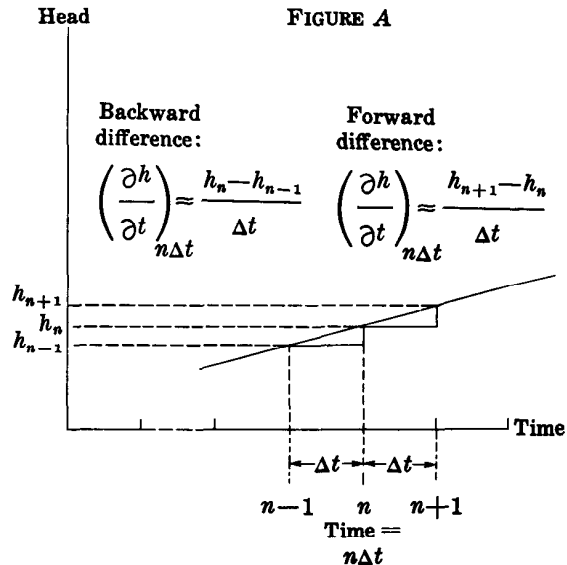
In Section 10 of Part VII we introduced two methods of approximating the time derivative in finite-difference simulations of the ground-water equation. One of these was termed the forward-difference approximation, and one the backward-difference approximation. Figure A shows a plot of head versus time which we may use to review these approximations. The time axis is divided into intervals of length Δt . The head at the end of the n th interval is termed h_n ; that at the end of the preceding interval is termed h_{n-1} ; and that at the end of the subsequent interval is termed h_{n+1} . We wish to approximate $\partial h/\partial t$ at the end of the n th interval, that is, at the time $n\Delta t$. If we utilize the head difference over the subsequent time interval, we employ the forward-difference approximation to the time derivative; if we utilize the head difference over the preced-

ing interval, we employ the backward-difference approximation. The forward-difference approximation is given by

$$\left(\frac{\partial h}{\partial t}\right)_{n\Delta t} \approx \frac{h_{n+1} - h_n}{\Delta t} \quad (1)$$

Where $(\partial h/\partial t)_{n\Delta t}$ represents the derivative at time $n\Delta t$. The backward-difference approximation is given by

$$\left(\frac{\partial h}{\partial t}\right)_{n\Delta t} \approx \frac{h_n - h_{n-1}}{\Delta t} \quad (2)$$



Forward-difference simulation: Explicit solution

The ground-water-flow equation, as it was given in Part V for two-dimensional flow, is

$$\frac{\partial^2 h}{\partial x^2} + \frac{\partial^2 h}{\partial y^2} = \frac{S}{T} \frac{\partial h}{\partial t} \quad (3)$$

where S represents storage coefficient and T transmissivity. In order to simulate this equation using either the forward-difference or backward-difference formulation, we would first write an approximate expression for the term

$$\frac{\partial^2 h}{\partial x^2} + \frac{\partial^2 h}{\partial y^2}$$

at the time $n\Delta t$ — that is, at point n on the time axis of figure A. Thus the forward-difference simulation is characterized by the fact that we approximate $\partial h/\partial t$ over a time interval which follows the time at which we approximate $(\partial^2 h/\partial x^2) + (\partial^2 h/\partial y^2)$, whereas the backward-difference simulation is characterized by the fact that we approximate $\partial h/\partial t$ over the time interval which precedes the time at which we approximate $(\partial^2 h/\partial x^2) + (\partial^2 h/\partial y^2)$. In the question of Section 10, Part VII, we obtained the following forward-difference simulation to equation 3:

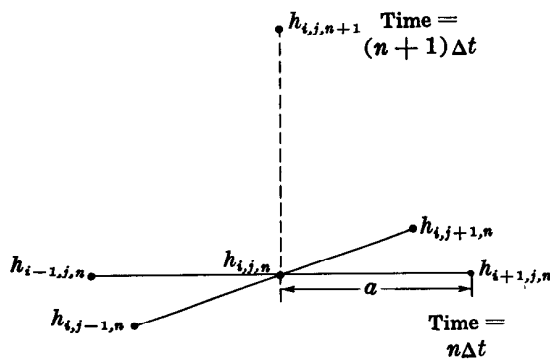
$$\frac{h_{i-1,j,n} + h_{i+1,j,n} + h_{i,j-1,n} + h_{i,j+1,n} - 4h_{i,j,n}}{a^2} = \frac{S}{T} \frac{h_{i,j,n+1} - h_{i,j,n}}{\Delta t} \quad (4)$$

where a is the node spacing, S is the storage coefficient, and T is the transmissivity. We wish to know the new value of head at the time $(n+1)\Delta t$ for the point i, j . Figure B shows the computation stencil for this simulation; the head at node i, j at the time $(n+1)\Delta t$ depends on the head in a five-node array at the preceding time, $n\Delta t$. The five values of h at the time $n\Delta t$ are all known. We need only to rearrange the equation, solving for $h_{i,j,n+1}$, and to insert the known

values of $h_{i-1,j,n}$, $h_{i+1,j,n}$, $h_{i,j-1,n}$, $h_{i,j+1,n}$, and $h_{i,j,n}$. There is no need to use simultaneous equations; the head at each node is computed explicitly, using the head at that node and the four neighboring nodes from the preceding time. The sequence in which we move through the x, y plane, calculating new values of head, is immaterial. The solution at one point does not require information on the surrounding points for the same time— only for the preceding time. For all these reasons, the forward-difference technique is computationally simpler than the backward-difference technique.

However, as we noted earlier, the forward-difference method does suffer from a serious drawback. Unless the ratio $\Delta t/a^2$ is kept sufficiently small, errors which grow in magnitude with each step of the calculation may appear in the result. More exactly, let us suppose that an error of some sort does arise, for whatever reason, at a certain node at a particular time step. Unless the ratio $\Delta t/a^2$ is sufficiently small, this error will increase in magnitude at each succeeding time

FIGURE B



step in the calculation until eventually the error completely dominates the solution. The term "error," as used here, refers to any difference between the computed head at a node i, j and time $n\Delta t$, and the actual value of head—that is, the value which would be given by the exact solution to the differential equation at that point and time. Such errors are inevitable in the normal application of finite-difference methods; they generally ap-

pear throughout the mesh in the first steps of the calculation. If the restriction on $\Delta t/a^2$ is satisfied, these errors will tend to die out as the computation sequence continues; the solution is then said to be stable. If the restriction is not satisfied, the errors will grow with each succeeding time step and will eventually destroy any significance which the solution might have; in this case, the solution is said to be unstable.

Backward-difference simulation: Solution by iteration

Because of this limitation in the forward-difference approach, attention has been given to a variety of alternative methods. One of these is simulation of the differential

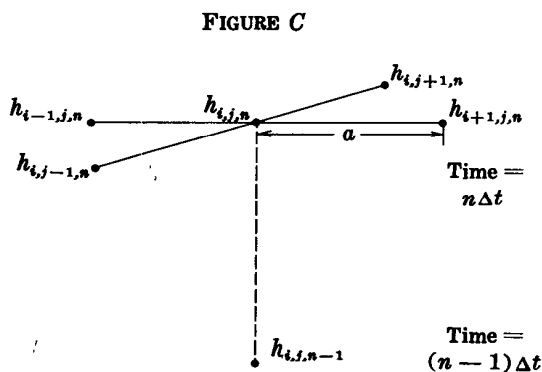
equation 3 through use of the backward-difference approximation to the time derivative as given in equation 2. The resulting finite-difference equation is

$$\frac{h_{i-1,j,n} + h_{i+1,j,n} + h_{i,j-1,n} + h_{i,j+1,n} - 4h_{i,j,n}}{a^2} = \frac{S}{T} \frac{h_{i,j,n} - h_{i,j,n-1}}{\Delta t} \quad (5)$$

Figure C shows a diagram of the computation stencil for equation 5. The time derivative is simulated over an interval which precedes the time at which $(\partial^2 h / \partial x^2) + (\partial^2 h / \partial y^2)$ is simulated; the equation incorporates five unknown values of head, corresponding to the time $n\Delta t$, and only one known value of head, corresponding to the time $(n-1)\Delta t$. Clearly we cannot obtain an

explicit solution to a single equation of the form of equation 5, the way we could to a single equation of the form of equation 4. We can, however, write an equation of the form of equation 5 for each node in the x, y plane; then since there is one unknown value of head (for time $t = n\Delta t$) at each node in the plane, we will have a system in which the total number of equations is equal to the total number of unknowns. We should therefore be able to solve the entire set as a system of simultaneous equations, obtaining the new value of $h_{i,j,n}$ at each node. The only drawback to this approach is that a great deal of work may be involved in solving the set of simultaneous equations; offsetting this drawback is the advantage that the technique is stable regardless of the size of the time step—that is, that errors tend to diminish rather than to increase as the computation proceeds, regardless of the size of Δt relative to a^2 .

The work required in utilizing the back-



ward-difference technique depends upon the size of the problem—that is, upon the number of equations in the simultaneous set. If this number becomes large, as it does in most ground-water problems, the work entailed becomes very great, particularly when the standard direct methods of solving simultaneous equations are used. For this reason it is worthwhile to look for efficient methods of solving these sets of equations; and it turns out that iteration or relaxation—the process described in Section 25 of Part VII, in connection with solution of the steady-state equation—provides us with a reasonably efficient approach.

The equation that we were trying to solve by iteration in Section 25 of Part VII rewritten here using the i, j subscript notation, is

$$\frac{1}{4}(h_{i-1,j} + h_{i+1,j} + h_{i,j-1} + h_{i,j+1}) = h_{i,j}. \quad (6)$$

This equation states that the head at the node i, j should be the average of the heads at the four surrounding nodes. No time subscripts are involved, since we are dealing with a steady-state situation. Our method is simply to move through the x, y plane, replacing the head at each node by the average of the heads at the four surrounding nodes. This process is continued until the head changes become negligible—that is, until the head at each node remains essentially unchanged after each traverse through the plane, indicating that equation 6 is satisfied throughout the plane.

In applying iteration to our nonequilibrium problem, the idea is to carry out a similar series of traverses of the x, y plane at every time step, using equation 5 rather than equation 6 as the basis of the calculation at each node. Thus to compute heads for the time $n\Delta t$ we would rearrange equation 5 as follows

$$h_{i,j,n} = \left(\frac{1}{\frac{4}{a^2} + \frac{S}{T\Delta t}} \right) \left\{ \frac{h_{i-1,j,n} + h_{i+1,j,n} + h_{i,j-1,n} + h_{i,j+1,n}}{a^2} + \frac{S}{T\Delta t} h_{i,j,n-1} \right\}. \quad (7)$$

We can envision an x, y plane for the time $n\Delta t$, initially containing specified values of $h_{i,j,n}$ at a few nodes, corresponding to the boundary conditions, and trial values of $h_{i,j,n}$ at the remaining nodes. We write an equation of the form of equation 7 for every node not controlled by a boundary condition; and we write equations expressing the boundary conditions for the nodes at which these conditions apply. In equation 7, the value of $h_{i,j,n}$ is expressed in terms of the head at the four surrounding nodes for the same time, and the head at the same node for the preceding time. In solving the set of equations for values of $h_{i,j,n}$ the values of $h_{i,j,n-1}$ actually constitute known or constant

terms, determined in the preceding step of the operation. Thus equation 7 relates the head at each node to the head at the four surrounding nodes, in terms of a set of constants or known quantities. The equation is a little more cumbersome than equation 6 in that instead of multiplying the sum of the heads at the surrounding nodes by $1/4$, we must now multiply by the term

$$\frac{1}{\left(\frac{4}{a^2} + \frac{S}{T\Delta t} \right) a^2}$$

and we must add the known term

$$\frac{\frac{S}{T\Delta t}}{\frac{4}{a^2} + \frac{S}{T\Delta t}} \cdot h_{i,j,n-1}$$

on the right side. These changes, however, do not make the equation appreciably more difficult to solve. We can still use the process of iteration; that is, we can move through the x, y plane, replacing each original trial value of $h_{i,j,n}$ by a new value, calculated from the four surrounding values by equation 7. At each node we note the difference between the new value of $h_{i,j,n}$ which we have calculated, and the trial value with which we started. If this difference turns out to be negligible at every node, we may conclude that our starting values already satisfied equation 7 and that further computation of new values is pointless. More commonly, however, we will note a measurable change in the value of h at each node, indicating that the initial values did not satisfy equation 7, and that the iteration procedure is producing an adjustment toward new values which will satisfy the equation. In this case we traverse the x, y plane again, repeating the procedure; each value of $h_{i,j,n}$ which we calculated in the first step (or iteration) is replaced by a new value calculated from the heads at the four surrounding nodes by equation 7. Again the difference between the new value and the preceding value at each node is recorded; and a test is made to see whether this difference is small enough to indicate that the new array of head values approximately satisfies equation 7. The process is continued until the difference between newly computed and preceding values is negligible throughout the array, indicating that equation 7 is essentially satisfied at all points.

The technique described above is often referred to as the Gauss-Seidel method; it is basically the same procedure that was applied in Section 25 of Part VII to the steady-state problem. It is an example of a relaxation technique—a method of computation in which the differences between the two sides

of an equation are successively reduced by numerical adjustment, until eventually the equation is satisfied. There are a number of varieties of relaxation techniques in use, differing from one another in the order or sequence in which the x, y plane is traversed in the calculation and in certain other respects.

It has been found that the number of calculations required to solve the set of finite-difference equations can frequently be reduced by the inclusion of certain “artificial” terms in these equations. These terms normally take the form

$$\lambda (h_{i,j,n}^{m+1} - h_{i,j,n}^m).$$

The superscripts m and $m+1$ indicate levels of iteration; that is, $h_{i,j,n}^m$ represents the value of $h_{i,j,n}$ after m traverses of the x, y plane in the iteration process, and $h_{i,j,n}^{m+1}$ represents the value of $h_{i,j,n}$ obtained in the next following calculation, after $m+1$ traverses. λ is termed an “iteration parameter”; it is a coefficient which, either on the basis of practical experience or theoretical analysis, has been shown to produce faster rates of solution. As the iteration process approaches its goal at each time step, the difference between the value of $h_{i,j,n}$ obtained in one iteration and that obtained in the next iteration becomes negligible—that is, the term $(h_{i,j,n}^{m+1} - h_{i,j,n}^m)$ approaches zero, so that the difference equation appears essentially in its original form, without the iteration parameter term; and the solution which is obtained thus applies to the original equation. In some cases, λ is given a sequence of different values in successive iterations, rather than a single constant value. Again, the particular sequence of values is chosen, either through theoretical analysis or through practical experience, in such a way as to produce the most rapid solution. When an iteration parameter or sequence of iteration parameters is utilized, the relaxation process is termed “successive overrelaxation” and is frequently designated by the initials *SOR*. Discussions of this technique are given by Forsythe and Wasow (1960) and many others.

Alternating-direction implicit procedure

The work required to obtain a solution by relaxation techniques is frequently tedious, particularly for a problem of large dimensions. For this reason, a great deal of effort has gone into the development of alternative approaches. Peaceman and Rachford (1955) proposed a technique of computation which has received wide use in a variety of forms. The name "alternating direction" has been applied to the general procedures of calculation which they proposed.

To simplify our discussion of their techniques we will introduce some new notation. We saw in Sections 12 and 15 of Part VII that an approximation to $\partial^2 h / \partial x^2$ is given by the term

$$\frac{h_1 + h_2 - 2h_0}{(\Delta x)^2};$$

or, in terms of our subscript notation,

$$\frac{h_{i-1,j} + h_{i+1,j} - 2h_{i,j}}{(\Delta x)^2}.$$

In the discussion which follows, we will let the symbol $\Delta_{xx}h$ represent this approximation to $\partial^2 h / \partial x^2$. That is, we say

$$\frac{\partial^2 h}{\partial x^2} \approx \Delta_{xx}h = \frac{h_{i-1,j} + h_{i+1,j} - 2h_{i,j}}{(\Delta x)^2}. \quad (8)$$

In addition, we will use a subscript to indicate the time at which the approximation is taken. For example, $(\Delta_{xx}h)_n$ will indicate an approximation to the second derivative at the time $n\Delta t$, or specifically

$$(\Delta_{xx}h)_n = \frac{h_{i-1,j,n} + h_{i+1,j,n} - 2h_{i,j,n}}{(\Delta x)^2}. \quad (9)$$

$(\Delta_{xx}h)_{n-1}$ will represent an approximation to the second derivative at time $(n-1)\Delta t$, and so on. Similarly, we will use the notation $\Delta_{yy}h$ to represent our approximation to $\partial^2 h / \partial y^2$, that is,

$$\frac{\partial^2 h}{\partial y^2} \approx \Delta_{yy}h = \frac{h_{i,j-1} + h_{i,j+1} - 2h_{i,j}}{(\Delta y)^2} \quad (10)$$

and again $(\Delta_{yy}h)_n$ will represent our approximation to $\partial^2 h / \partial y^2$ at the time $n\Delta t$, that is

$$(\Delta_{yy}h)_n = \frac{h_{i,j-1,n} + h_{i,j+1,n} - 2h_{i,j,n}}{(\Delta y)^2} \quad (11)$$

and so on.

Using this notation, our forward-difference approximation to the equation

$$\frac{\partial^2 h}{\partial x^2} + \frac{\partial^2 h}{\partial y^2} = \frac{S}{T} \frac{\partial h}{\partial t} \quad (3)$$

as given in equation 4, would be rewritten

$$(\Delta_{xx}h)_n + (\Delta_{yy}h)_n = \frac{S}{T} \frac{h_{i,j,n+1} - h_{i,j,n}}{\Delta t}. \quad (12)$$

In this formulation, $\partial^2 h / \partial x^2$ and $\partial^2 h / \partial y^2$ are simulated at the beginning of the time interval over which $\partial h / \partial t$ is simulated.

Again using the notation introduced above, our backward-difference approximation to equation 3, as given in equation 5, would be rewritten

$$(\Delta_{xx}h)_n + (\Delta_{yy}h)_n = \frac{S}{T} \frac{h_{i,j,n} - h_{i,j,n-1}}{\Delta t}. \quad (13)$$

In this formulation, $\partial^2 h / \partial x^2$ and $\partial^2 h / \partial y^2$ are simulated at the time $n\Delta t$, while $\partial h / \partial t$ is simulated over the time interval between $(n-1)\Delta t$ and $n\Delta t$; thus both $\partial^2 h / \partial x^2$ and $\partial^2 h / \partial y^2$ are approximated at the end of the time interval over which $\partial h / \partial t$ is approximated.

In the form in which it was originally proposed, Peaceman and Rachford's technique is usually termed the alternating-direction implicit procedure. In this form, the

simulation utilizes two equations, applicable over two successive time intervals. In the first equation, $\partial^2 h / \partial x^2$ is simulated at the beginning of a time interval, and $\partial^2 h / \partial y^2$ at the end of that interval; $\partial h / \partial t$ is simulated using the change in head occurring over the interval. The second equation applies over the immediately following time interval; here the order is reversed— $\partial^2 h / \partial y^2$ is simulated at the beginning of the time interval, $\partial^2 h / \partial x^2$ is simulated at the end, and again $\partial h / \partial t$ is simulated using the head difference occurring over the interval.

Using the notation introduced above, this simulation may be represented by the following equation pair

$$(\Delta_{xx}h)_{n-1} + (\Delta_{yy}h)_n = \frac{S}{T} \frac{h_{i,j,n} - h_{i,j,n-1}}{\Delta t} \quad (14)$$

$$(\Delta_{yy}h)_n + (\Delta_{xx}h)_{n+1} = \frac{S}{T} \frac{h_{i,j,n+1} - h_{i,j,n}}{\Delta t} \quad (15)$$

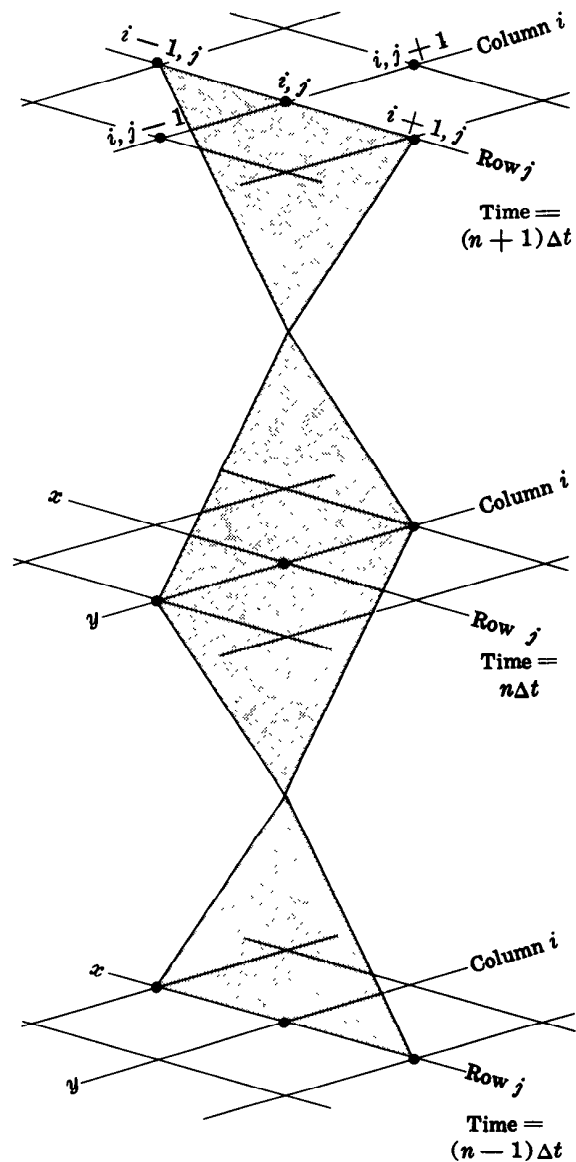
For the first time interval, $\partial^2 h / \partial x^2$ is simulated at $(n-1)\Delta t$; $\partial^2 h / \partial y^2$ is simulated at $n\Delta t$; and $\partial h / \partial t$ is simulated by the change in $h_{i,j}$ between $(n-1)\Delta t$ and $n\Delta t$. For the second time interval $\partial^2 h / \partial y^2$ is simulated at $n\Delta t$; $\partial^2 h / \partial x^2$ is simulated at $(n+1)\Delta t$; and $\partial h / \partial t$ is simulated by the change in $h_{i,j}$ between $n\Delta t$ and $(n+1)\Delta t$.

Figure D illustrates the form of this simulation. It may be recalled from Section 3 that lines parallel to the x -axis in the finite-difference grid are termed rows and that lines parallel to the y -axis are termed columns. As shown in figure D, then, three values of h are taken along row j at time $(n-1)\Delta t$ to simulate $\partial^2 h / \partial x^2$, while at the time $n\Delta t$ three values of h are taken along column i to simulate $\partial^2 h / \partial y^2$. The time derivative is simulated using the difference between the central h values at these two times. For the succeeding time interval, the three values of h along column i are taken first to simulate $\partial^2 h / \partial y^2$ at time $n\Delta t$; while at the time $(n+1)\Delta t$, three values of h are taken along row j to simulate $\partial^2 h / \partial x^2$. Again the time derivative is simulated using the

difference between the central h values.

The forward-difference and backward-difference techniques are characterized by symmetry in their simulation of the expression $(\partial^2 h / \partial x^2) + (\partial^2 h / \partial y^2)$. Both terms of this expression are simulated at the same time, using a five-node array centered about a single value of head, $h_{i,j,n}$. However, the

FIGURE D



simulation of $\partial h/\partial t$ in these formulations is asymmetrical, in the sense that it is not centered in time about $h_{i,j,n}$ but extends forward or backward from the time $n\Delta t$. In either case, however, if we allow Δt to become very small, the effects of this asymmetry die out; the approximation then approaches more and more closely the value of $\partial h/\partial t$ at the time $n\Delta t$. In the alternating-direction implicit procedure, by contrast, $\partial^2 h/\partial x^2$ and $\partial^2 h/\partial y^2$ are not simulated at the same time, and in this sense the simulation of $(\partial^2 h/\partial x^2) + (\partial^2 h/\partial y^2)$ cannot be termed symmetrical. It is again helpful, however, to visualize what will happen if Δt is allowed to become very small, so that the times $(n-1)\Delta t$ and $n\Delta t$ at which the individual simulations occur, fall more and more closely together. In this case, $(\Delta_{xx}h)_{n-1}$ should begin to approximate the value of $\partial^2 h/\partial x^2$ at $(n-1/2)\Delta t$, while $(\Delta_{yy}h)_n$ should begin to approximate the value of $\partial^2 h/\partial y^2$ at $(n-1/2)\Delta t$. In this sense, then, the expression

$$(\Delta_{xx}h)_{n-1} + (\Delta_{yy}h)_n$$

can be considered an approximation to

$$\frac{\partial^2 h}{\partial x^2} + \frac{\partial^2 h}{\partial y^2}$$

at the time $(n-1/2)\Delta t$. The simulation of $\partial h/\partial t$ is symmetrical with respect to this time, since it utilizes the head difference $h_n - h_{n-1}$. Thus even though a certain asymmetry exists in the expression by which $(\partial^2 h/\partial x^2) + (\partial^2 h/\partial y^2)$ is approximated in the alternating-direction technique, it can be argued that there is symmetry with respect to time in the simulation of $\partial h/\partial t$. Moreover, we may expect intuitively that if an error is generated by the fact that we simulate $\partial^2 h/\partial x^2$ prior to $\partial^2 h/\partial y^2$ during one time interval, some sort of compensating error should be generated during the following time interval, when we simulate $\partial^2 h/\partial y^2$ prior to $\partial^2 h/\partial x^2$; and in fact it turns out that this alternation in the order of simulation is essential to the stability of the method. If the order of simulation is reversed in

this way, then regardless of the size of the time step, the calculation will not be affected by errors which grow at each step of the calculation. A further condition for stability is that the time intervals represented in the two steps of the simulation (equations 14 and 15) must be equal. The length of the time interval may differ from one pair of time steps to the next, but within a given pair, as used in equations 14 and 15, the two values of Δt must be kept the same. Finally, there must be an even number of total time steps; $\partial^2 h/\partial y^2$ must be simulated prior to $\partial^2 h/\partial x^2$ as often as $\partial^2 h/\partial x^2$ is simulated prior to $\partial^2 h/\partial y^2$.

If equations 14 and 15 are written out using the earlier notation we have

$$\frac{h_{i-1,j,n-1} + h_{i+1,j,n-1} - 2h_{i,j,n-1}}{(\Delta x)^2} + \frac{h_{i,j-1,n} + h_{i,j+1,n} - 2h_{i,j,n}}{(\Delta y)^2} = \frac{S}{T} \frac{h_{i,j,n} - h_{i,j,n-1}}{\Delta t} \quad (16)$$

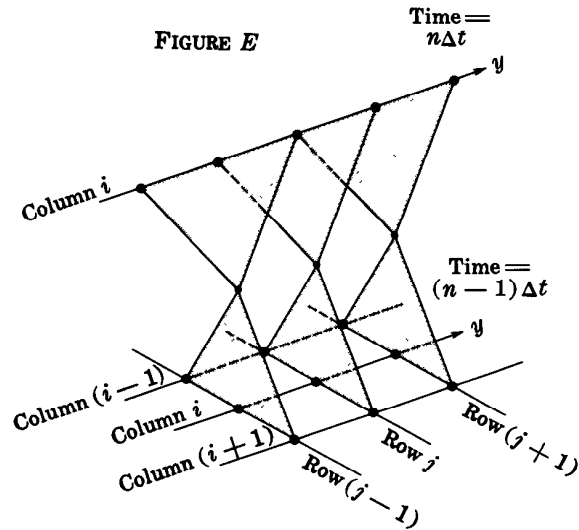
and

$$\frac{h_{i-1,j,n+1} + h_{i+1,j,n+1} - 2h_{i,j,n+1}}{(\Delta x)^2} + \frac{h_{i,j-1,n} + h_{i,j+1,n} - 2h_{i,j,n}}{(\Delta y)^2} = \frac{S}{T} \frac{h_{i,j,n+1} - h_{i,j,n}}{\Delta t} \quad (17)$$

Equation 16 involves three values of head along row j at time $(n-1)\Delta t$ and three values of head along column i at time $n\Delta t$. Let us assume that the head values for the earlier time, $(n-1)\Delta t$, have been calculated throughout the x, y plane and that we are concerned with calculation of head values for the time $n\Delta t$. Equation 16 then contains three known values of head, for the time $(n-1)\Delta t$ and three unknown, for the time $n\Delta t$. Since we have three unknowns in one equation, we will again need to use simultaneous equations. In this case the three unknowns occur along a single column; and by considering other equations which apply along this column we can develop a convenient method of solution.

Let us suppose that there are m nodes along column i and that the head is specified at the two end nodes by boundary conditions, but must be determined for all of the interior nodes. The first node is identified by the subscript $j=1$ (we assume that the x -axis, where $j=0$, lies outside the problem area); the final node is identified by the subscript $j=m$. Thus $h_{i,1,n}$ and $h_{i,m,n}$ are specified by boundary conditions, while $h_{i,2,n}$ through $h_{i,m-1,n}$ must be determined.

We can write an equation of the form of equation 16 for each interior node along column i . As we set up the equation at each node, we pick up three known values of head from the $(n-1)\Delta t$ "time plane"; these known values fall along a three-column band, as shown in figure E. Each equation also incorporates three values of head for the new time, $n\Delta t$, all lying along column i ; and when we have set up an equation of the form of equation 16 for each interior node along the column, we have a system of $m-2$ equations in $m-2$ unknowns, which can be solved simultaneously. The solution of this set of equations is undertaken independently from the solutions for adjacent columns in the mesh; thus, instead of dealing with a set of, say, 2,500 simultaneous equations in a 50 by 50 array, we deal in turn with separate sets of only 50 equations. Each of these sets corresponds to a column within the mesh; and



each is much easier to solve than the 2,500 equation set, not only because of the smaller number of equations, but also because a convenient order of computation is possible. We are able to utilize this order of computation through a technique developed by H. L. Thomas (1949) that is known as the Thomas algorithm.

To illustrate this method, we rearrange equation 16, putting the unknown values of head, corresponding to time $n\Delta t$, on one side, as follows:

$$\frac{h_{i,j-1,n}}{(\Delta y)^2} - \left(\frac{S}{T\Delta t} + \frac{2}{(\Delta y)^2} \right) h_{i,j,n} + \frac{h_{i,j+1,n}}{(\Delta y)^2} = - \frac{h_{i-1,j,n-1}}{(\Delta x)^2} - \left(\frac{S}{T\Delta t} - \frac{2}{(\Delta x)^2} \right) h_{i,j,n-1} - \frac{h_{i+1,j,n-1}}{(\Delta x)^2} \quad (18)$$

The right-hand side consists entirely of known terms, and it is convenient to replace this side of the equation by a single symbol, D_j , that is

$$D_j = - \frac{h_{i-1,j,n-1}}{(\Delta x)^2} - \left(\frac{S}{T\Delta t} - \frac{2}{(\Delta x)^2} \right) h_{i,j,n-1} - \frac{h_{i+1,j,n-1}}{(\Delta x)^2}, \quad (19)$$

The single subscript, j , is sufficient to designate D for our purposes. As suggested in figure E, the sequence of calculation is along the column i . At each node—that is, for each value of j —there is only one value of D , taken from the three-column band in the preceding time plane. We are limiting consideration here to one set of equations, corresponding to one column, and aimed at calculating the heads for one value of time; the subscripts designating the column and

time are therefore not required. Thus we can omit the subscripts i and n from the values of h on the left side of the equation. With these changes, equation 18 takes the form

$$A_j h_{j-1} + B_j h_j + C_j h_{j+1} = D_j \quad (20)$$

where, in the problem which we have set up

$$A_j = \frac{1}{(\Delta y)^2},$$

$$B_j = -\left(\frac{S}{T \Delta t} + \frac{2}{(\Delta y)^2} \right),$$

and

$$C_j = \frac{1}{(\Delta y)^2}.$$

The coefficients A , B , and C are constant for the problem which we have postulated. In some problems, however, where variation in T , S , or the node spacing is involved, they may vary from one node to another. To keep the discussion sufficiently general to cover such cases, the coefficients have been designated with the subscript j .

If we solve equation 20 for h_j , the central value of the three-node set represented in the equation, we obtain

$$h_j = \frac{D_j - A_j h_{j-1} - C_j h_{j+1}}{B_j}. \quad (21)$$

h_1 the head at the initial node of the column, is specified by the boundary condition. We apply equation 21 to find an expression for h_2 ; this gives

$$h_2 = \frac{D_2 - A_2 h_1 - C_2 h_3}{B_2}. \quad (22)$$

We rewrite this equation in the form

$$h_2 = g_2 - b_2 h_3 \quad (23)$$

where

$$g_2 = \frac{D_2 - A_2 h_1}{B_2} \quad (24)$$

and

$$b_2 = \frac{C_2}{B_2}. \quad (25)$$

b_2 consists of known terms, and since h_1 is known, g_2 can be calculated; equation 23 thus gives us an equation for h_2 in terms of the next succeeding value of head, h_3 . If we can continue along the column, forming equations which give the head at each node in terms of that at the succeeding node—that is, which give h_j in terms of h_{j+1} —we will eventually reach the next to last node in the column, where we will have an equation for h_{m-1} in terms of h_m , the head at the last node. Then since h_m is known, from the boundary condition, we will be able to calculate h_{m-1} ; using this value of h_{m-1} we can calculate h_{m-2} , and so on back down the column, until finally we can calculate h_2 in terms of h_3 using equation 23. This is the basic idea of the Thomas algorithm. We now have to see whether we can in fact obtain expressions for each head, h_j , in terms of the succeeding head, h_{j+1} , along the column.

We first apply equation 21 to find an expression for h_3 obtaining

$$h_3 = \frac{D_3 - A_3 h_2 - C_3 h_4}{B_3}. \quad (26)$$

To eliminate h_2 from this equation, we substitute from equation 23, obtaining

$$h_3 = \frac{D_3 - A_3 (g_2 - b_2 h_3) - C_3 h_4}{B_3}. \quad (27)$$

Equation 27 is now solved for h_3 as follows

$$h_3 - \frac{A_3 b_2}{B_3} h_3 = \frac{D_3 - A_3 g_2 - C_3 h_4}{B_3}$$

$$h_3 = \frac{D_3 - A_3 g_2 - C_3 h_4}{B_3 \left(\frac{B_3 - A_3 b_2}{B_3} \right)}$$

or

$$h_3 = \frac{D_3 - A_3 g_2}{B_3 - A_3 b_2} - \frac{C_3}{B_3 - A_3 b_2} h_4. \quad (28)$$

Now again we have an equation of the form

$$h_3 = g_3 - b_3 h_4 \quad (29)$$

where here

$$g_3 = \frac{D_3 - A_3 g_2}{B_3 - A_3 b_2} \quad (30)$$

and

$$b_3 = \frac{C_3}{B_3 - A_3 b_2}. \quad (31)$$

Since g_2 and b_2 are known from the preceding step of the calculation (equation 24 and 25), g_3 and b_3 can be calculated, and equation 29 then gives us an expression for h_3 in terms of h_4 . In effect, we have eliminated h_2 from equation 26, so that h_3 is expressed in terms of the succeeding value of head alone.

If we continue this process, we find that at each step we can obtain an equation of the form

$$h_j = g_j - b_j h_{j+1} \quad (32)$$

relating the head at each node to that at the succeeding node; and we find that g_j and b_j can always be determined from the preceding values of g and b by equations of the form of equations 30 and 31. That is, we find that

$$g_j = \frac{D_j - A_j g_{j-1}}{B_j - A_j b_{j-1}} \quad (33)$$

and

$$b_j = \frac{C_j}{B_j - A_j b_{j-1}}. \quad (34)$$

These general formulas apply even to the calculation of g_2 and b_2 if we specify the starting conditions $g_1 = h_1$ and $b_1 = 0$.

In summary, then, we may start at node 1 and move up the column calculating values of g_j and b_j . At each node, these values are calculated by equations 33 and 34, using the preceding values, g_{j-1} and b_{j-1} , and using the coefficients A_j , B_j , and C_j and the term D_j .

Ultimately, at the next to last node of the column, g_{m-1} and b_{m-1} are calculated; then since h_m is known from the boundary condition, h_{m-1} can be calculated from equation 32. We then proceed back down the column, calculating the value of h_j at each node from

the value of h_{j+1} using equation 32, until finally a value for h_2 has been calculated and heads have been determined throughout the column.

The whole process is actually one of Gaussian elimination, taking advantage of a convenient order of calculation. The solution of the difference equation 16 is obtained directly for points along the column through this process; we are not dealing with an iterative technique which solves the set of algebraic equations by successive approximation. When the head has been calculated at all nodes along column i , the process is repeated for column $i+1$, and so on until the entire plane has been traversed.

In a sense, this process of calculation stands somewhere between the forward-difference technique and the backward-difference technique. In the forward-difference technique the head at every node, for a given time level, is computed independently from the heads at the four adjacent nodes for that time level; the technique of computation is said to be explicit. In the backward-difference technique, the calculation of the head at each node incorporates the heads at the four adjacent nodes for the same time level; the method of calculation is termed implicit. In the alternating-direction technique the calculation of the head at a given node, as we move along a column, incorporates the heads for that time level at the two adjacent nodes along the column, but not at the two adjacent nodes in the adjoining columns. The method of calculation, for this step, is said to be implicit along the columns, but explicit in the transverse direction, along the rows.

When the heads have been calculated everywhere throughout the plane by the process of traversing the columns, calculations for the following time, $(n+1)\Delta t$ are initiated using equation 17. The procedure followed is the same as that described above, except that the calculation now moves along rows, rather than along columns. This alternation of direction again, is necessary in order to insure the stability of the method of calculation.

Solution of the steady-state equation by iteration using the alternating-direction method of calculation

In their initial paper proposing the alternating-direction implicit procedure, Peaceman and Rachford point out that the technique of solving alternately along rows and columns can be used effectively to iterate the steady-state equation. That is, suppose we must deal with the problem considered in Section 16 and 25 of Part VII, and reviewed earlier in the present discussion, in which the steady-state equation

$$\frac{\partial^2 h}{\partial x^2} + \frac{\partial^2 h}{\partial y^2} = 0 \quad (35)$$

is to be solved. In Section 25, we considered a technique of iteration, or relaxation, to solve this equation. In this technique we wrote the finite-difference approximation given in equation 6 as a simulation of equation 35; this gave

$$h_{i,j} = \frac{1}{4} (h_{i-1,j} + h_{i+1,j} + h_{i,j-1} + h_{i,j+1}). \quad (6)$$

To apply equation 6, we would move through the x, y plane replacing values of $h_{i,j}$ at each interior node by the average of the heads at the four surrounding nodes. At the end of one complete traverse of the plane we would have a set of values of $h_{i,j}$ which would be somewhat closer to satisfying equation 6 than were the values with which we started; and after several traverses, we would have a set of head values which would essentially satisfy equation 36 throughout the plane. This would be indicated by the fact that the values of $h_{i,j}$ obtained in each step would differ very little from those obtained in the preceding step.

Our objective here is to outline a more efficient technique of carrying out this itera-

tion process, based upon Peaceman and Rachford's method and the Thomas algorithm. We begin by introducing some nomenclature and notation. In our discussion of nonequilibrium problems, we spoke of "time planes"—that is, representations of the x, y plane in which the heads calculated for a given time were displayed. In discussing the solution of steady-state problems by iteration we can similarly speak of "iteration planes"—that is, representations of the x, y plane in which the values of head obtained after a certain number of iterations are displayed. Again, in our discussion of nonequilibrium problems we used the subscript n to designate the time level of a given head value— $h_{i,j,n}$ referred to a head value at the time $n\Delta t$. In a similar way, we will use a superscript m to denote the iteration level in the steady-state problem. $h_{i,j}^0$ will be used to designate the starting values of head, prior to any iterations; $h_{i,j}^1$ will indicate head values after one iteration—that is, the head values in the first iteration plane; and in general, $h_{i,j}^m$ will indicate head values after m iterations, or in the m th iteration plane.

Next we rewrite our approximation to equation 35 in a slightly different form. We rearrange equation 6 to give

$$h_{i-1,j} + h_{i+1,j} - 2h_{i,j} = -h_{i,j-1} - h_{i,j+1} + 2h_{i,j} \quad (36)$$

This can be obtained also by rewriting equation 35 in the form

$$\frac{\partial^2 h}{\partial x^2} = -\frac{\partial^2 h}{\partial y^2}$$

and then using the approximations given in equation 8 and 10 for $\partial^2 h / \partial x^2$ and $\partial^2 h / \partial y^2$.

We are interested in applying equation 36 to calculate head values for a new iteration level, using head values from the preceding

iteration level. In the procedure which we will employ it is necessary to consider two successive iteration steps. Using the superscript notation described above, and using $\Delta_{xx}h$ and $\Delta_{yy}h$ to represent our approximations to $\partial^2 h/\partial x^2$ and $\partial^2 h/\partial y^2$ as in equations 8 and 10, the method of calculation may be summarized as follows

$$-\Delta_{yy}h^m = \Delta_{xx}h^{m-1} \quad (37)$$

and

$$\Delta_{xx}h^{m+1} = -\Delta_{yy}h^m \quad (38)$$

or, in the notation of equation 36,

$$\begin{aligned} -h_{i,j-1}^m - h_{i,j+1}^m + 2h_{i,j}^m \\ = h_{i-1,j}^{m-1} + h_{i+1,j}^{m-1} - 2h_{i,j}^{m-1} \end{aligned} \quad (39)$$

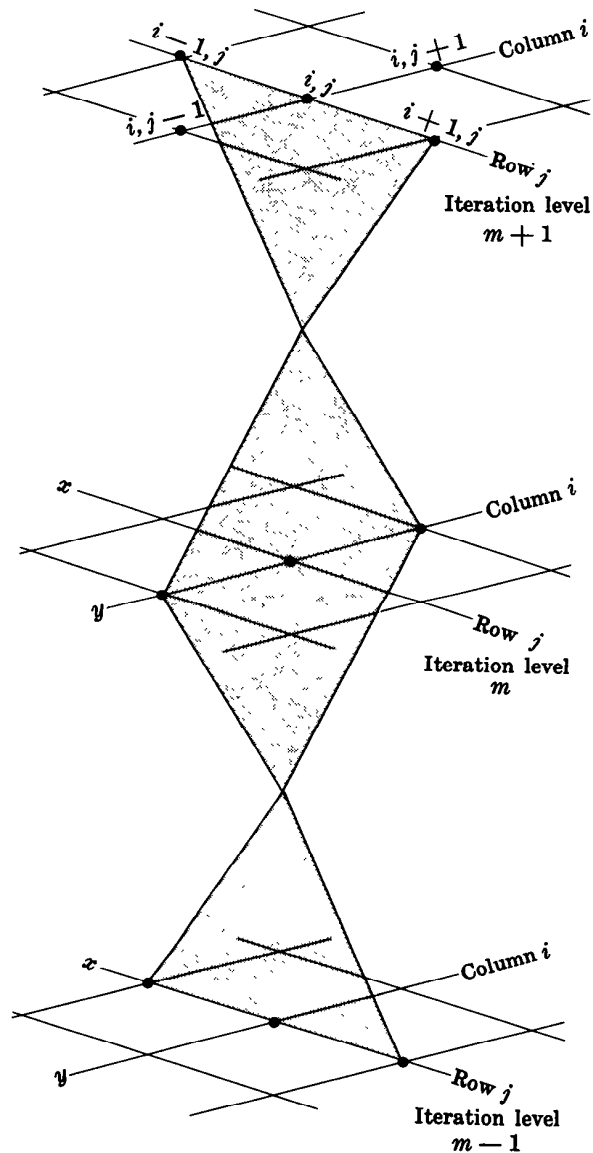
and

$$\begin{aligned} h_{i-1,j}^{m+1} + h_{i+1,j}^{m+1} - 2h_{i,j}^{m+1} \\ = -h_{i,j-1}^m - h_{i,j+1}^m + 2h_{i,j}^m \end{aligned} \quad (40)$$

As these equations indicate, the idea here is first to simulate $\partial^2 h/\partial x^2$ at one iteration level and $\partial^2 h/\partial y^2$ at the next; in the succeeding iteration, the order is reversed; $\partial^2 h/\partial y^2$ is simulated at the earlier iteration level, and $\partial^2 h/\partial x^2$ at the next. Figure D, which illustrated the simulation technique for the non-equilibrium problem, is reproduced as figure F, but with the time planes now relabeled as iteration planes. Equation 39 relates three values of head at iteration level m to three values at iteration level $m-1$; and, following the technique described above for the non-equilibrium case, we may move along column i in iteration plane m , at each node picking up three known values of h^{m-1} from a three column band in the preceding iteration plane, and thus generating a set of equations in which the unknowns are all values of h^m along column i .

As in the nonequilibrium case, the set of equations along a given column is solved directly by the Thomas algorithm—that is, by

FIGURE F



the process of Gaussian elimination outlined in equation 20 through 34. When this has been done for every column in the x, y plane, we have a new set of head values throughout the plane. These values, however do not necessarily constitute a solution to equation 35. The process we have described, of replacing the earlier head values with new values calculated through equation 39, accomplishes the same thing as the relaxation process of Section 25—it produces a new set of values which is closer to satisfying equation 35 than was the earlier set. This does not guarantee that the new set will constitute an acceptable solution. The test as to whether or not a solution has been found is carried out as in the relaxation technique of Section 25—

the values of head in iteration plane m are compared to those in iteration plane $m-1$. If the difference is everywhere negligible, equation 35 must be satisfied throughout the x, y plane; otherwise a new iteration must be initiated. In this new iteration we would utilize equation 40, moving along a row of the model to set up a system of equations for the head values along that row. As in the nonequilibrium problem this alteration of direction is necessary for stability. In summary then, we are utilizing an indirect iterative procedure of solution; but we use a direct method, Gaussian elimination, along each individual column or row, to move from one set of approximate head values to the next during the iterative process.

Backward-difference simulation: Solution by iteration using the alternating-direction method of calculation (iterative alternating-direction implicit procedure)

Peaceman and Rachford found that iteration of the steady-state equation by the alternating-direction procedure was considerably more efficient than the most rapid relaxation techniques that had been used prior to the time of their work. The use of the alternating-direction technique in this sense, as a method of iteration, has accordingly gained great popularity in recent years. As a method of solving the nonequilibrium equation 3, however, the alternating-direction implicit procedure, as embodied in equations 14 and 15 or 16 and 17, has not always proved advantageous. Although stability is assured, that is the calculation will not be affected by errors which necessarily increase in magnitude at each step, there is still a possibility for large error at any one time step and at any given node; and in many problems these errors have proved uncontrollable and unacceptable. This undesirable feature has inevitably led to renewed interest in the backward-difference formulation of equations 5 and 13. As we have noted,

solution by this method must generally be accomplished through iteration, for example using equation 7; the systems of simultaneous equations involved are usually too large to admit of an easy solution by direct methods. We have seen that the alternating-direction procedure of Peaceman and Rachford provides an effective method of iterating the steady-state equation; this suggests that the same technique may be used to iterate the backward-difference equation, 5 or 13. Equation 13, which utilized the abbreviated notation, is reproduced below

$$(\Delta_{xx}h)_n + (\Delta_{yy}h)_n = \frac{S}{T} \cdot \frac{h_{i,j,n} - h_{i,j,n-1}}{\Delta t} \quad (13)$$

$(\Delta_{xx}h)_n$ is an approximation to $\partial^2 h / \partial x^2$ at the time $n\Delta t$, while $(\Delta_{yy}h)_n$ is an approximation $\partial^2 h / \partial y^2$ at the time $n\Delta t$. We again introduce the superscript m to indicate the level of iteration; using this notation we rewrite equation 13 as it will be used in two

successive steps of the iteration process under consideration,

$$(\Delta_{xx}h)_n^{m-1} + (\Delta_{yy}h)_n^m = \frac{S}{T} \frac{h_{i,j,n}^m - h_{i,j,n-1}}{\Delta t} \quad (41)$$

$$(\Delta_{xx}h)_n^{m+1} + (\Delta_{yy}h)_n^m = \frac{S}{T} \frac{h_{i,j,n}^{m+1} - h_{i,j,n-1}}{\Delta t} \quad (42)$$

Several points about equations 41 and 42 should be noted carefully. The simulations of both $\partial^2 h / \partial x^2$ and $\partial^2 h / \partial y^2$, in both equations, are made at time $n\Delta t$; and again, in both equations, $\partial h / \partial t$ is simulated by the change in head at node i, j from time $(n-1)\Delta t$ to time $n\Delta t$. In equation 41, $(\partial^2 h / \partial x^2)_{n\Delta t}$ is simulated at the $(m-1)$ th iteration level, whereas $(\partial^2 h / \partial y^2)_{n\Delta t}$ is simulated at the m th iteration level; $h_{i,j,n}$, in the simulation of the time derivative, is represented at the m th iteration level. In equation 42, $(\partial^2 h / \partial y^2)_{n\Delta t}$ is simulated at the m th iteration level, while $(\partial^2 h / \partial x^2)_{n\Delta t}$ is simulated at the $(m+1)$ th iteration level; $h_{i,j,n}$, in the simulation of the time derivative, is again represented at the higher iteration level,

which is here $m+1$. No iteration superscript is attached to $h_{i,j,n-1}$ the head at the preceding time level, in either equation. The iteration process is designed to compute heads for the new time level, $n\Delta t$, and in this process the head at the preceding time level is simply a constant; it retains the same value throughout the series of iterations.

Rewriting equation 41 using the expanded notation for $\Delta_{xx}h$ and $\Delta_{yy}h$ (as given in equations 8 and 10), we have

$$\begin{aligned} & \frac{h_{i-1,j,n}^{m-1} + h_{i+1,j,n}^{m-1} - 2h_{i,j,n}^{m-1}}{(\Delta x)^2} \\ & + \frac{h_{i,j-1,n}^m + h_{i,j+1,n}^m - 2h_{i,j,n}^m}{(\Delta y)^2} \\ & = \frac{S}{T} \frac{(h_{i,j,n}^m - h_{i,j,n-1})}{\Delta t} \end{aligned} \quad (43)$$

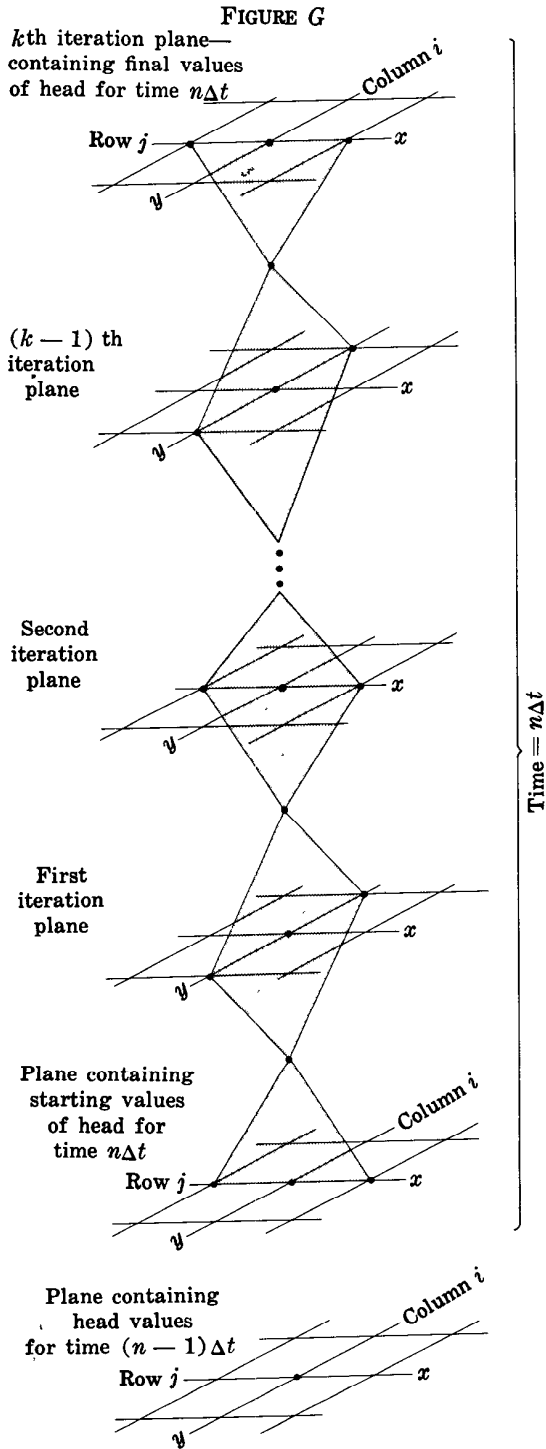
We wish to calculate head values at the new iteration level, m , on the basis of values which we already have for the preceding iteration level, $m-1$. We therefore rearrange equation 43, placing unknown terms on the left and known terms on the right. This gives

$$\begin{aligned} \frac{h_{i,j-1,n}^m}{(\Delta y)^2} + \frac{h_{i,j+1,n}^m}{(\Delta y)^2} - \left(\frac{S}{T\Delta t} + \frac{2}{(\Delta y)^2} \right) h_{i,j,n}^m = \\ - \frac{h_{i-1,j,n}^{m-1}}{(\Delta x)^2} - \frac{h_{i+1,j,n}^{m-1}}{(\Delta x)^2} + \frac{2}{(\Delta x)^2} h_{i,j,n}^{m-1} - \frac{S}{T\Delta t} h_{i,j,n-1} \end{aligned} \quad (44)$$

The unknown terms are the head values for iteration level m ; the known terms are the head values for the preceding iteration level, $m-1$, and one head value from the preceding time level, $n-1$. We may therefore proceed as in equation 19, replacing the entire right side by a single symbol, D_j , representing the known terms of the equation. We will then have an equation of the form of equation 20,

$$A_j h_{j-1}^m + B_j h_j^m + C_j h_{j+1}^m = D_j, \quad (45)$$

which can be solved by the Thomas algorithm, as outlined in equations 21-34. In the next step we utilize equation 42; here the unknown terms consist of three values of h for time $n\Delta t$ and iteration level $m+1$, while the known terms consist of three values of h for time $n\Delta t$ and iteration level m , and again one value of h for the time level $(n-1)\Delta t$. After this step, the heads which we obtain



are compared with those obtained in the preceding step. If the difference is everywhere negligible, the values of h^{m+1} are taken as a sufficiently close approximation to the heads for time $n\Delta t$.

It's important to note that while at each step we solve directly, (by Gaussian elimination, along columns or rows) to obtain a new set of head values, these new values do not generally constitute a solution to our differential equation. Rather, they form a new approximation to a solution, in a series of iterations which will ultimately produce an approximation close enough for our purposes. We may review the sequence of computation by referring to figure G, which illustrates the process of calculation schematically. The lowermost plane in the figure is a time plane, containing the final values of head for the preceding time level, $(n-1)\Delta t$. The plane immediately above this contains the initial assumed values of head for the new time, $n\Delta t$; we use three values of head, h_{i-1,j,n^0} , h_{i,j,n^0} , and h_{i+1,j,n^0} from this plane, together with one value of head $h_{i,j,n-1}$ from the $n-1$ time plane, on the right side of equation 44. On the left side of equation 44 we have three unknown values of head in the first iteration plane, $h_{i,j-1,n^1}$, h_{i,j,n^1} , and $h_{i,j+1,n^1}$. We set up equations of the form of equation 44 along the entire column i and solve by the Thomas algorithm (equations 21-34). We then repeat the procedure along all other columns, thus determining head values throughout the first iteration plane; these new head values constitute a somewhat closer approximation to the heads at time $n\Delta t$ than did the initial values. Next we set up a system of equations of the form of equation 42, arranged so that in each equation three head values from the first iteration plane and one from the $n-1$ time plane form the known terms, while three head values from the second iteration plane from the unknown terms. If we rewrite equation 42 in the expanded notation and rearrange it so that the unknown terms appear on the left and the known terms on the right we have

$$\frac{h_{i-1,j,n}^{m+1}}{(\Delta x)^2} + \frac{h_{i+1,j,n}^{m+1}}{(\Delta x)^2} - \left(\frac{S}{T\Delta t} + \frac{2}{(\Delta x)^2} \right) h_{i,j,n}^{m+1} = -\frac{h_{i,j-1,n}^m}{(\Delta y)^2} - \frac{h_{i,j+1,n}^m}{(\Delta y)^2} + \frac{2}{(\Delta y)^2} h_{i,j,n}^m - \frac{S}{T\Delta t} h_{i,j,n-1}. \quad (46)$$

Applying equation 46 between the first and second iteration planes, m would be taken as 1 and $(m+1)$ as 2. The four known terms on the right side of the equation would consist of three head values from the first iteration plane $h_{i,j-1,n}$, $h_{i,j,n}$, and $h_{i,j+1,n}$, and again one head value from the $n-1$ time plane, $h_{i,j,n-1}$. It is important to note that we return to the $n-1$ time plane—the lowermost plane in figure G—at each iteration level in the series, to pick up the constant values of $h_{i,j,n-1}$ that are used in simulating the time derivative. On the left side of equation 46 we would have the three unknown values of head corresponding to the new iteration level—that is, the second iteration plane). Again we would use the Thomas algorithm (equations 21–34) to solve for these new values of head throughout the plane. At the end of this solution procedure the head values in the second iteration plane are compared with those in the first iteration plane. If the difference is sufficiently small at all points, there is nothing to be gained by continuing to adjust the head values through further calculation—equation 3 is already approximately satisfied throughout the plane. If significant differences are noted, the procedure is continued until the differences between the head values obtained in successive iteration levels becomes negligible. At this point the heads for time $n\Delta t$ have been determined, and work is started on the next time step, computing heads for the time $(n+1)\Delta t$. Thus while direct solution and an alternating-direction feature both play a part in this procedure of calculation, the technique is basically one of iteration, in which, using the backward-difference formulation of equations 5 or 13, we progressively adjust head values for each time level until we arrive at a set of values which satisfies the equation. The method combines the advantages of the backward-

difference technique with the ease of computation of the alternating-direction procedure; it is the basis of many of the digital models presently used by the U.S. Geol. Survey. It is sometimes referred to as the iterative alternating-direction implicit procedure.

Prickett and Lonquist (1971) further modify this method of calculation by representing the central head value, $h_{i,j}$ only at the advanced iteration level; and by representing the head in the adjacent, previously processed column also at the advanced iteration level. That is, they do not simulate $\partial^2 h / \partial x^2$ and $\partial^2 h / \partial y^2$ in two distinct iteration planes, but rather set up the calculation as a relaxation technique, so that the new value of head at a given node is calculated on the basis of the most recently computed values of head in the surrounding nodes. They do, however, perform the calculations alternately along rows and columns using the Thomas algorithm.

In the discussions presented here we have treated transmissivity, storage coefficient, and the node spacings Δx and Δy , as constant terms in the x, y plane. In fact these terms can be varied through the mesh to account for heterogeneity or anisotropy in the aquifer or to provide a node spacing which is everywhere suited to the needs of the problem. Additional terms can be inserted into the equations to account for such things as pumpage from wells at specified nodes, retrieval of evapotranspiration loss, seepage into streams, and so on. Some programs have been developed which simulate three-dimensional flow (Freeze, 1971; Bredehoeft and Pinder, 1970; Prickett and Lonquist, 1971, p. 46); however, the operational problems encountered in three-dimensional digital modeling are sometimes troublesome.

The reader may now proceed to the programmed instruction of Part VIII.

Part VIII. Analog Techniques

Introduction

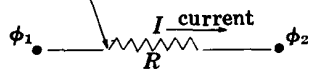
In Part VIII we consider another technique of obtaining solutions to the differential equation of ground-water flow. This is the method of the electric analog. It is a powerful technique which has been widely used. The technique depends upon the mathematical similarity between Darcy's law, describing flow in a porous medium, and Ohm's law, describing flow of charge in a conductor. In

the case of nonequilibrium modeling, it depends also upon the similarity between the ground-water storage-head relation and the equation describing storage of charge in a capacitor; and upon the similarity between the electrical continuity principle, involving the conservation of electric charge, and the equation of continuity describing the conservation of matter.

1 •

Ohm's law states that the electrical current through a conducting element is directly proportional to the voltage difference, or potential difference across its terminals. The sketch represents a conducting element, or resistor, across which the voltage difference is $\phi_1 - \phi_2$. That is, the voltage at one terminal of the resistor is ϕ_1 , while that at the other end is ϕ_2 . The current through the resistor is defined as the net rate of movement of positive charge across a cross-sectional plane within the resistor, taken normal to the direction of charge flow. The standard unit of charge is the coulomb, and current is normally measured as the number of coulombs per second crossing the plane under consideration. A charge flow of 1 coulomb per second is designated 1 ampere. The symbol I is frequently used to represent current.

Symbol representing a conducting element, or resistor



R represents value of resistance (ohms)

For the resistor shown in the diagram, Ohm's law may be stated as follows

$$I = \frac{1}{R}(\phi_1 - \phi_2)$$

where I is the current through the resistor, and $\phi_1 - \phi_2$, as noted above, is the voltage difference across its terminals. The term $1/R$ is the constant of proportionality relating current to voltage; R is termed the resistance of the element. It depends both upon the dimensions of the element and the electrical properties of the conductive material used. The unit of resistance is the ohm. A resistance of 1 ohm will carry 1 ampere of current under a potential difference of 1 volt.

QUESTION

Suppose the voltage at one terminal of a 500-ohm resistor is 17 volts, and the voltage at the other terminal is 12 volts. What would the current through the resistor be?

	Turn to Section:
10 amperes	19
0.10 ampere, or 100 milliamperes	8
0.01 ampere, or 10 milliamperes	8

2

Your answer in Section 22 is not correct. The finite-difference form of the equation for two-dimensional nonequilibrium groundwater flow is

$$h_1 + h_2 + h_3 + h_4 - 4h_0 = \frac{Sa^2 \Delta h_0}{T \Delta t},$$

while the equation for our resistance-capacitance network is

$$\phi_1 + \phi_2 + \phi_3 + \phi_4 - 4\phi_0 = RC \frac{d\phi_0}{dt}.$$

Comparison of these equations illustrates that resistance, R , may be considered to be analogous to the term $1/T$; voltage, ϕ , is analogous to head, h ; and capacitance, C , may be considered analogous to the term Sa^2 .

In the answer which you selected, voltage is treated as analogous to transmissivity, in that the procedure calls for increasing voltage in areas of high transmissivity.

Return to Section 22 and choose another answer.

3

Your answer in Section 6,

$$I = \frac{A}{RL} (\phi_1 - \phi_2),$$

is not correct. The idea here is to obtain an expression for the current which involves the resistivity, ρ_e , of the material composing the resistance. Your answer involves the resistance, R , rather than the resistivity. It is

not a valid statement of Ohm's law in any case, for Ohm's law in terms of resistance was given in Section 1 as

$$I = \frac{1}{R} (\phi_1 - \phi_2).$$

Return to Section 6 and choose another answer.

4

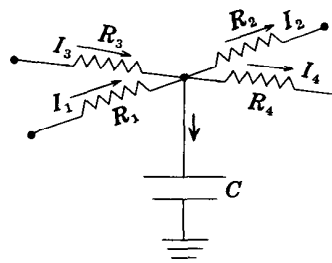
Your answer in Section 9,

$$\frac{1}{R} (\phi_1 - \phi_c) = C \frac{d\phi_c}{dt},$$

is correct. The quantity C , as we have seen, is actually the derivative $d\epsilon/d\phi_c$; thus $C(d\phi_c/dt)$ is equivalent to $(d\epsilon/d\phi_c) \cdot (d\phi_c/dt)$, or simply $d\epsilon/dt$.

Without referring to it explicitly, we made use in Section 9 of an electrical equivalent to the hydraulic equation of continuity. In an electric circuit, charge is conserved in the same way that fluid mass is conserved in a hydraulic system. Kirchoff's current law, which is familiar to students of elementary physics, is a statement of this principle. In the circuit of Section 9, we required that the rate of accumulation of charge in the capacitor

be equal to the time rate at which charge was transported to the capacitor plate through the resistor—that is, to the current through the resistor. In the circuit



shown in the figure, in which four resistors are connected to a single capacitor, the net

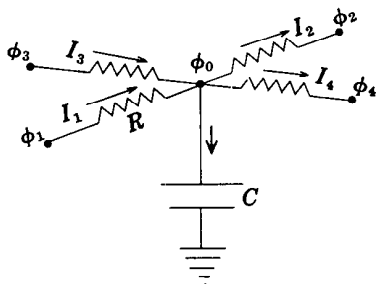
 Con.—4 •

inflow minus outflow of charge, through all four resistors, must equal the rate of accumulation of charge on the capacitor. Let I_1 and I_3 represent currents toward the capacitor, through resistors R_1 and R_3 ; and let I_2 and I_4 represent currents away from the capacitor, through resistors R_2 and R_4 . Then the time rate of inflow of charge, toward the capacitor, will be $I_1 + I_3$; the rate of outflow charge, away from the capacitor, will be $I_2 + I_4$. The net inflow minus outflow of charge will be $I_1 - I_2 + I_3 - I_4$; and this must equal the rate of accumulation of charge on the capacitor. That is, we must have

$$I_1 - I_2 + I_3 - I_4 = \frac{d\epsilon}{dt}.$$

QUESTION

The diagram again shows the circuit described above, but we now assume that the



four resistances are equal—that is, we assume

$$R_1 = R_2 = R_3 = R_4 = R.$$

Let ϕ_0 represent the voltage on the capacitor plate—this is essentially equal to the voltage at the junction point of the four resistors (the resistance of the wire connecting the capacitor to the resistor junction point is assumed negligible). The voltages at the extremities of the four resistors are designated ϕ_1 , ϕ_2 , ϕ_3 , and ϕ_4 , as shown in the diagram. If Ohm's law is applied to obtain an expression for the current through each resistor and the capacitor equation is applied to obtain an expression for the rate of accumulation of charge on the capacitor, which of the following equations will be obtained from our circuit equation

$$I_1 - I_2 + I_3 - I_4 = \frac{d\epsilon}{dt}?$$

Turn to Section:

$$\frac{\phi_1 - \phi_2 + \phi_3 - \phi_4}{R} = C \frac{d\phi_0}{dt} \quad 15$$

$$\frac{1}{C} (\phi_1 - \phi_2 + \phi_3 - \phi_4 + \phi_0) = R \frac{d\phi_0}{dt} \quad 27$$

$$\phi_1 + \phi_2 + \phi_3 + \phi_4 - 4\phi_0 = RC \frac{d\phi_0}{dt} \quad 22$$

 5 •

Your answer in Section 22 is correct. This is of course one indication of the power of the analog method, in that problems involving heterogeneous aquifers are handled as easily as those involving a uniform aquifer. Complex boundary conditions can also be accommodated, and three-dimensional problems may be approached by constructing networks of several layers. The method is applicable to water-table aquifers as well as to confined aquifers, provided dewatering

is small in relation to total saturated thickness. Some successful simulation has been done even for cases in which this condition is not satisfied, using special electrical components which vary in resistance as voltage changes.

Steady-state problems are sometimes handled by network models constructed solely of resistors—that is, not involving capacitors—rather than by analogs constructed of a continuous conductive mate-

5 • —Con.

rial. Such steady-state networks are particularly useful when heterogeneity is involved.

In some cases, the symmetry of a ground-water system may be such that a two-dimensional analog in a vertical plane—that is, representing a vertical cross section through an aquifer, or series of aquifers—may be more useful than a two-dimensional analog representing a map view. In this type of model, anisotropy is frequently a factor; that is, permeability in the vertical direction is frequently much smaller than that in the lateral direction. This is easily accommodated in a network by using higher resistances in the vertical direction; or, equivalently, by using a uniform resistance value but distorting the scales of the model, so that this resistance value is used to simulate different distances and cross-sectional areas of flow in the two directions.

An important special type of network analog is that used to simulate conditions in a vertical plane around a single discharging well. The cylindrical symmetry of the discharging well problem is in effect built into the network; the resistances and scales of

the model are chosen in such a way as to simulate the increasing cross-sectional areas of flow, both vertically and radially, which occur in the aquifer with increasing radial distance from the well.

This concludes our discussion of the electric-analog approach. We have given here only a brief outline of some of the more important principles that are involved. The technique is capable of providing insight into the operation of highly complex ground-water systems. Further discussion of the principles of simulation may be found in the text by Karplus (1958). The book "Concepts and Models in Ground-Water Hydrology" by Domenico (1972) contains a discussion of the application of analog techniques to ground water, as does the text "Ground-Water Resource Evaluation" by Walton (1970). Additional discussions may be found in papers by Skibitzke (1960), Brown (1962) Stallman (1963b) Patten (1965), Bedinger, Reed, and Swafford (1970), and many others.

This concludes the studies presented in this text.

6 •

Your answer in Section 1 is correct.

The resistance of an electrical element is given by the formula

$$R = \rho_e \cdot \frac{L}{A}$$

where L is the length of the element in the direction of the current, A is its cross-sectional area normal to that direction, and ρ_e is the electrical *resistivity* of the material of which the resistor is composed. The inverse of the resistivity is termed the conductivity of the material; it is often designated σ ; that is, $\sigma = 1/\rho_e$. Resistivity and conductivity are

normally taken as constants characteristic of a particular material; however, these properties vary with temperature, and the linear relationships usually break down at extremes of voltage. Moreover, a small change in the composition of some materials can produce a large change in electrical properties. Resistivity is commonly expressed in units of ohm·metre²/metre, or ohm-metres. With this unit of resistivity, the formula,

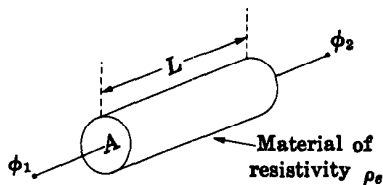
$$R = \rho_e \cdot \frac{L}{A},$$

 Con.—6•

will yield resistance in ohms if length is expressed in metres and area in square metres.

QUESTION

The sketch shows a resistor of cross-sectional area A and length L , composed of a



material of resistivity ρ_e . The potential difference across the resistor is $\phi_1 - \phi_2$. Which of the following expressions is a valid expression of Ohm's law, giving the current through the resistor?

Turn to Section:

$$I = \frac{A}{\rho_e L} (\phi_1 - \phi_2) \quad 28$$

$$I = \frac{\rho_e A}{L} (\phi_1 - \phi_2) \quad 24$$

$$I = \frac{A}{RL} (\phi_1 - \phi_2) \quad 3$$

 7•

Your answer in Section 28,

$$Q = \frac{K}{A_p} \cdot \frac{L_p}{h_1 - h_2}$$

is not correct. Darcy's law states that flow is directly proportional to cross-sectional area and to the (negative) gradient of head. In

the answer which you chose, flow is given as inversely proportional to cross-sectional area, and proportional to the term $L_p/h_1 - h_2$, which is actually the inverse of the negative head gradient.

Return to Section 28 and choose another answer.

 8•

Your answer in Section 1 is not correct. Ohm's law was given as

$$I = \frac{1}{R} (\phi_1 - \phi_2),$$

and the discussion pointed out that a resistance of 1 ohm would carry a current of 1 ampere under a potential difference of 1 volt. Thus when the voltage difference is ex-

pressed in volts and the resistance ohms, the quotient

$$\frac{\phi_1 - \phi_2}{R}$$

will give the correct current in amperes.

Return to Section 1 and choose another answer.

9

Your answer in Section 21 is correct.

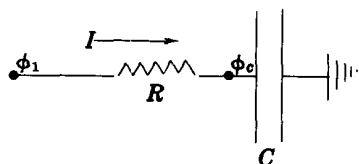
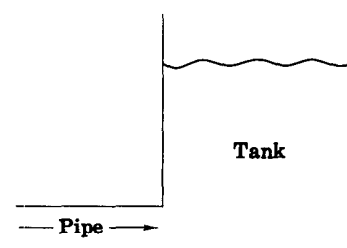
If we monitor the voltage on a capacitor plate in a given circuit and observe that it is changing with time, we know from the relations given in Section 21 that charge is accumulating on the capacitor plate with time. An expression for the rate at which charge is accumulating can be obtained by dividing the capacitor equation by a time increment, Δt . This gives

$$\frac{\Delta \epsilon}{\Delta t} = C \frac{\Delta \phi}{\Delta t}$$

or, in terms of derivatives,

$$\frac{d\epsilon}{dt} = C \frac{d\phi}{dt}$$

The figure shows a hydraulic system and an analogous electrical system. The rate of



accumulation of fluid in the tank is equal to the rate of flow of water through the pipe supplying it. Similarly, the rate of accumulation of charge on the capacitor plate is equal to the rate of flow of charge through the resistor connected to the plate. This rate of flow of charge is by definition the current through the resistor. (Recall that the units of current are charge/time—for example, coulombs/second.) We thus have

$$I = \frac{d\epsilon}{dt}$$

where I is the current through the resistor, and $d\epsilon/dt$ is the rate at which charge accumulates on the capacitor.

QUESTION

Suppose the voltage at the left terminal of the resistor is ϕ_1 , while the voltage at the right terminal, which is essentially the voltage on the capacitor plate, is ϕ_c . If we use Ohm's law to obtain an expression for I , in terms of the voltages, and the capacitor equation to obtain an expression for $d\epsilon/dt$, which of the following relations will we obtain. (R denotes the resistance of the resistor, and C the capacitance of the capacitor.)

Turn to Section:

$$\frac{1}{R}(\phi_1 - \phi_c) = C \frac{d\phi_c}{dt} \quad 4$$

$$R(\phi_c - \phi_1) = C \frac{d\phi_c}{dt} \quad 20$$

$$RC(\phi_c - \phi_1) = \frac{d\phi_c}{dt} \quad 18$$

10•

Your answer in Section 21 is not correct. The equation which we developed for the capacitor was

$$C = \frac{\Delta\epsilon}{\Delta\phi}$$

where C was the capacitance, $\Delta\epsilon$ the quantity of charge placed in storage in the capacitor, and $\Delta\phi$ the increase in the voltage difference across the capacitor plates, observed as the charge $\Delta\epsilon$ is accumulated. For the prism of aquifer used in developing the ground-water equations in Part V, we had

$$\Delta V = SA\Delta h$$

where ΔV was the volume of water taken into storage in the prism, Δh the increase in head associated with this accumulation in storage, S the storage coefficient, and A the base area of the prism. This equation can be rewritten

$$SA = \frac{\Delta V}{\Delta h}$$

to facilitate comparison with the capacitor equation.

Return to Section 21 and choose another answer.

11•

Your answer in Section 26 is correct. Note that this equation,

$$\frac{I}{w \cdot b} = -\sigma \frac{\partial \phi}{\partial x},$$

is analogous to the equation we would write for the component of specific discharge in the x direction, through a section of aquifer of width w and thickness b ; that is,

$$\frac{Q}{w \cdot b} = -K \frac{\partial h}{\partial x}.$$

In practice, steady-state electric-analog work may be carried out by constructing a scale model of an aquifer from a conductive material and applying electrical boundary conditions similar to the hydraulic boundary conditions prevailing in the ground-water system. The voltage is controlled at certain points or along certain boundaries of the model, in proportion to known values of head at corresponding points in the aquifer; and

current may be introduced or withdrawn in proportion to known values of inflow and outflow for the aquifer. When the boundary conditions are applied in this manner, voltages at various points of the model are proportional to heads at corresponding points in the aquifer, and the current density vector in various sections of the model is proportional to the specific-discharge vector in the corresponding sections of the aquifer.

QUESTION

Suppose an analog experiment of this type is set up, and the experimenter traces a line in the model along which voltage has some constant value. To which of the following hydrologic features would this line correspond?

	Turn to Section:
a flowline	16
a line of constant head	21
a line of uniform recharge	17

12 •

Your answer in Section 28,

$$Q = -K \frac{\partial^2 h}{\partial x^2} A_p,$$

is not correct. Darcy's law states that flow is equal to the product of hydraulic conductivity, cross-sectional area, and (negative) head gradient. The gradient of head is

by definition a first derivative—the derivative of head with respect to distance. The answer which you chose involves a second derivative. The correct answer must either include a first derivative, or an expression equivalent to or approximating a first derivative.

Return to Section 28 and choose another answer.

13 •

Your answer in Section 21 is not correct. We have seen in dealing with the analogy between steady-state electrical flow and steady-state ground-water flow that voltage is analogous to hydraulic head, whereas current, or rate of flow of charge, is analogous to the volumetric rate of flow of fluid. In the analogy between the capacitor equation and the storage-head relation, voltage must still be analogous to head, or capacitors

could not be used to represent storage in a model incorporating the flow analogy between Darcy's law and Ohm's law. Similarly, charge must represent fluid volume, so that rate of flow of charge (current) can represent volumetric fluid discharge. Otherwise the storage-capacitance analogy would be incompatible with the flow analogy.

Return to Section 21 and choose another answer.

14 •

Your answer in Section 22 is not correct. Increasing both R and C , as suggested in the answer which you chose, has the effect of increasing the factor RC in the equation

$$\phi_1 + \phi_2 + \phi_3 + \phi_4 - 4\phi_0 = RC \frac{d\phi_0}{dt}.$$

On the other hand, an increase in T in the aquifer causes the factor Sa^2/T to decrease, in the equation

$$h_1 + h_2 + h_3 + h_4 - 4h_0 = \frac{Sa^2 \Delta h}{T \Delta t}.$$

Thus the proposed technique fails to simulate the hydrologic system.

Notice that head and voltage are analogous and that increases in T can be simulated by decreases in R .

Return to Section 22 and choose another answer.

15 •

Your answer in Section 4 is not correct. The rate of accumulation of charge on the capacitor plate must equal the net rate at which charge is being transported to the capacitor through the four resistors. To set up the problem, we assume that the current is toward the capacitor in resistors 1 and 3, and away from the capacitor in resistors 2 and 4 in the diagram. The current toward the capacitor in resistor 1 is given by Ohm's law as

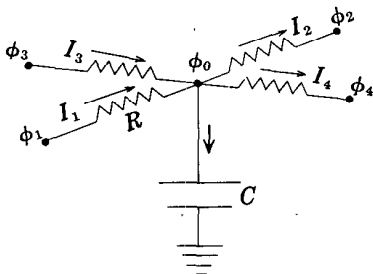
$$I_1 = \frac{1}{R}(\phi_1 - \phi_0),$$

while that in resistor 3 is given by

$$I_3 = \frac{1}{R}(\phi_3 - \phi_0).$$

The current away from the capacitor in resistor 2 is given by

$$I_2 = \frac{1}{R}(\phi_0 - \phi_2),$$



while that in resistor 4 is given by

$$I_4 = \frac{1}{R}(\phi_0 - \phi_4).$$

If it turns out that any of these currents are not actually in the direction initially assumed, the current value as computed above will be negative; thus the use of these expressions remains algebraically correct whether or not the assumptions regarding current direction are correct.

The net rate of transport of charge toward the capacitor will be the sum of the inflow currents minus the sum of the outflow currents, or

$$I_1 + I_3 - I_2 - I_4.$$

This term must equal the rate of accumulation of charge on the capacitor plate, $d\epsilon/dt$,

$$\frac{d\epsilon}{dt} = C \frac{d\phi_0}{dt}.$$

That is we must have

$$I_1 + I_3 - I_2 - I_4 = C \frac{d\phi_0}{dt}.$$

The correct answer to the question of Section 4 can be obtained by substituting our expressions for I_1 , I_2 , I_3 , and I_4 into this equation and rearranging the result.

Return to Section 4 and choose another answer.

16 •

Your answer in Section 11 is not correct. In steady-state two-dimensional flows, one can specify a function which is constant along a flowline. However, this function—which is termed a stream function—is not analogous to voltage (potential) in electrical theory; thus a flowline, or line along which stream function is constant, cannot correspond to an equipotential, or line along

which voltage is constant. In developing the analogy between flow of electricity and flow of fluid through a porous medium, we stressed that voltage is analogous to head; current is analogous to fluid discharge; and electrical conductivity is analogous to hydraulic conductivity.

Return to Section 11 and choose another answer.

17 •

Your answer in Section 11 is not correct. The forms of Darcy's law and Ohm's law which we have used for comparison are repeated below:

Darcy's law:

$$\frac{Q}{w \cdot b} = -K \frac{\partial h}{\partial x}$$

where Q is the volumetric fluid discharge through a cross-sectional area of width w and thickness b , taken at right angles to the x direction; K is the hydraulic conductivity; and $\partial h/\partial x$ is the derivative of head in the x direction.

Ohm's law:

$$\frac{I}{w \cdot b} = -\sigma \frac{\partial \phi}{\partial x}$$

where I is the current through a cross-sectional area of width w and thickness b , taken at right angles to the x direction; σ is the electrical conductivity; and $\partial \phi/\partial x$ is the derivative of voltage, or potential, in the x direction.

A comparison of these equations shows that voltage, or potential, ϕ , occupies a position in electrical theory exactly parallel to head, h , in the theory of ground-water flow. Current, I , is analogous to discharge, Q ; while σ , the electrical conductivity, is analogous to the hydraulic conductivity, K . These parallels should be kept in mind in answering the question of Section 11.

Return to Section 11 and choose another answer.

18 •

Your answer in Section 9 is not correct. The question concerns a capacitor which is connected to a resistor. The idea is to equate the rate of accumulation of charge on the capacitor plate to the rate at which charge is carried to the capacitor through the resistor—that is, to the current through the resistor. The rate at which charge accumulates on the capacitor plate is given by the capacitor equation as

$$\frac{d\epsilon}{dt} = C \frac{d\phi_c}{dt}$$

The current through the resistor, or rate at which charge flows through the resistor, is given by Ohm's law as

$$I = \frac{1}{R} (\phi_1 - \phi_c).$$

Return to Section 9 and choose another answer.

19 •

Your answer in Section 1 is not correct. Ohm's law was given in the form

$$I = \frac{1}{R} (\phi_1 - \phi_2).$$

If R is in ohms and the difference $\phi_1 - \phi_2$ is

in volts, current, I will be in amperes. In the example given, $\phi_1 - \phi_2$ was 5 volts and R was 500 ohms. Substitute these values in the equation to obtain the amount of current through the resistor.

Return to Section 1 and choose another answer.

20 •

Your answer, in Section 9,

$$R(\phi_0 - \phi_1) = C \frac{d\phi_0}{dt},$$

is not correct. The rate of accumulation of charge on the capacitor, $d\epsilon/dt$, is equal to $C(d\phi_0/dt)$, and this part of your answer is correct. However, the idea is to equate this rate of accumulation of charge on the capacitor to the rate of transport of the charge

toward the capacitor, through the resistor—that is, to the current through the resistor. This current is to be expressed in terms of resistance and voltage, using Ohm's law; and this has not been done correctly in the answer which you chose. Ohm's law states that the current through a resistance is equal to the voltage drop across the resistance divided by the value of the resistance in ohms.

Return to Section 9 and choose another answer.

21 •

Your answer in Section 11 is correct. The line of constant voltage, or equipotential line, is analogous to the line of constant head in ground-water hydraulics.

The analogy between Darcy's law and Ohm's law forms the basis of steady-state electric-analog modeling. In recent years, the modeling of nonequilibrium flow has become increasingly important; and just as Darcy's law alone is inadequate to describe nonequilibrium ground-water flow, its analogy with Ohm's law is in itself an inadequate basis for nonequilibrium modeling. The theory of nonequilibrium flow is based upon a combination of Darcy's law with the storage equation, through the equation of continuity. To extend analog modeling to nonequilibrium flow, we require electrical equations analogous to the storage and continuity equations.

The analog of ground-water storage is provided by an electrical element known as a capacitor. The capacitor is essentially a storage tank for electric charge; in circuit diagrams it is denoted by the symbol shown in figure A. As the symbol itself suggests, capacitors can be constructed by inserting two parallel plates of conductive material into a circuit, as shown in figure B. When the switch is closed, positive charge flows from the battery to the upper plate and ac-

cumulates on the plate in a manner analogous to the accumulation of water in a tank. At the same time, positive charge is drawn from the lower plate, leaving it with a net negative charge. Figure C shows a hydraulic circuit analogous to this simple capacitor circuit; when the valve is opened, the pump delivers water to the left-hand tank, draining the right-hand tank. If the right-hand tank is connected in turn to an effectively limitless water supply, as shown in figure D, both the volume of water and the water level in the right-hand tank will remain essentially constant, while water will still accumulate in the left-hand tank as the pump operates. The analogous electrical arrangement is shown in figure E; here the additional symbol shown adjacent to the lower plate indicates that this plate has been grounded—that is, connected to a large mass of metal buried in the earth, which in effect constitutes a limitless reserve of charge. In this situation, the quantity of charge on the lower plate remains essentially constant, as does the voltage on this plate, but the battery still causes positive charge to accumulate on the upper plate. The voltage on the lower plate is analogous to the water level in the right-hand tank, which is held constant by connection to the unlimited water supply.

21 • --Con.

FIGURE A



FIGURE B

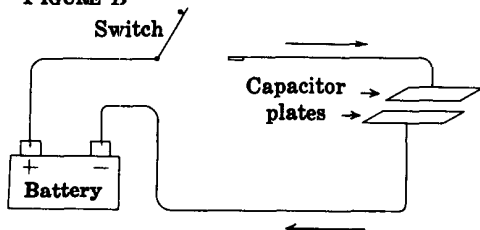


FIGURE C

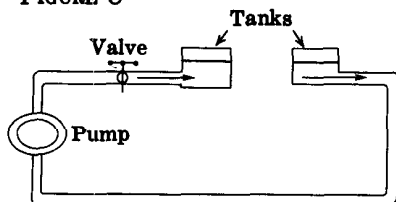


FIGURE D

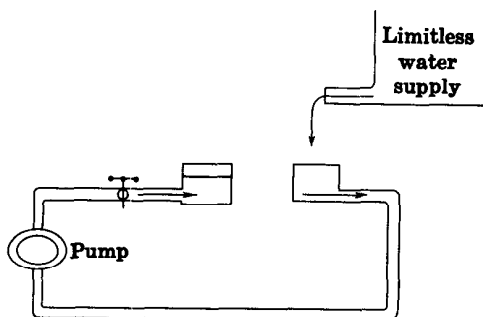
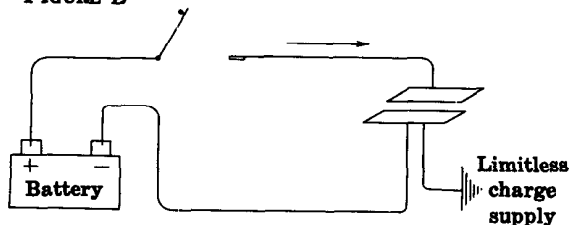


FIGURE E



In a circuit such as that shown in figure E, it is customary to designate the constant voltage of the ground plate as zero. This is done arbitrarily—it is equivalent for example, to setting head equal to zero at the constant water level of the right-hand tank of figure D. With the voltage of the grounded plate taken as zero, the voltage difference between the plates becomes simply the voltage, ϕ , measured on the upper plate. In the circuit of figure E, this voltage is equal to the voltage produced by the battery.

Now suppose an experiment is run in which the battery in the circuit of figure E is replaced in turn by batteries of successively higher voltage. At each step the charge on the positive plate is measured in some way, after the circuit has reached equilibrium. The results will show that as the applied voltage is increased, the charge which accumulates on the positive plate increases in direct proportion. If a graph is constructed from the experimental results in which the charge, ϵ , which has accumulated on the positive plate is plotted versus the voltage in each step, the result will be a straight line, as shown in the figure. The slope of this line, $\Delta\epsilon/\Delta\phi$, is termed the capacitance of the capacitor, and is designated C ; that is,

$$C = \frac{\Delta\epsilon}{\Delta\phi}, \quad C = \frac{d\epsilon}{d\phi},$$

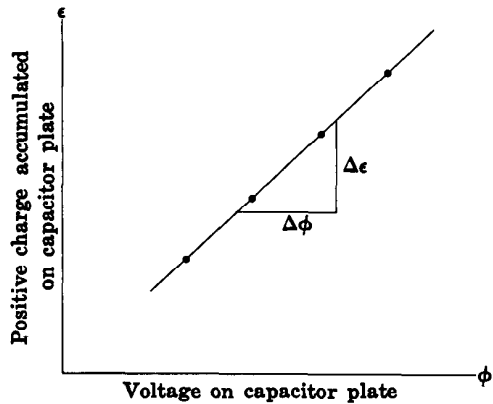
or simply

$$C = \frac{\epsilon}{\phi}.$$

Capacitance is measured in farads, or more commonly in microfarads; a farad is equal to 1 coulomb per volt.

These equations serve to define the operation of a capacitor and provide the analog we require for the equation of ground-water storage. It will be recalled that the relation between volume in storage and head can be written

$$\Delta V = S \cdot A \cdot \Delta h$$



where ΔV is the volume of water taken into or released from storage in a prism of aquifer of base area A , as the head changes by an amount Δh .

QUESTION

Which of the following statements correctly describes the analogy between the capacitor equation and the ground-water-storage—head relation?

Turn to Section:

Charge is analogous to head, voltage is analogous to volume of water, and capacitance, C , is analogous to the factor SA . 13

Charge is analogous to volume of water, voltage is analogous to head, and capacitance, C , is analogous to the factor SA . 9

Charge is analogous to volume of water, voltage is analogous to head, and capacitance, C , is analogous to the factor $\frac{1}{SA}$. 10

Your answer in Section 4,

$$\phi_1 + \phi_2 + \phi_3 + \phi_4 - 4\phi_0 = RC \frac{d\phi_0}{dt},$$

is correct. In Part VII, we obtained a finite-difference approximation to the differential equation for two-dimensional non-steady-state ground-water flow,

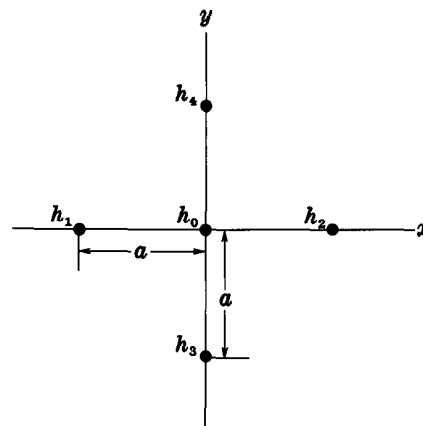
$$\frac{\partial^2 h}{\partial x^2} + \frac{\partial^2 h}{\partial y^2} = \frac{S}{T} \frac{\partial h}{\partial t}.$$

This approximation can be written

$$\frac{h_1 + h_2 + h_3 + h_4 - 4h_0}{a^2} = \frac{S}{T} \frac{\Delta h_0}{\Delta t}.$$

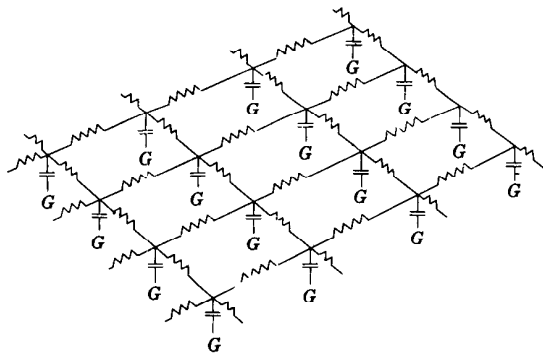
or

$$h_1 + h_2 + h_3 + h_4 - 4h_0 = \frac{Sa^2}{T} \frac{\Delta h_0}{\Delta t}.$$



22 • —Con.

where h_0 , h_1 , h_2 , h_3 , and h_4 represent the head values at the nodes of an array such as that shown in the sketch; a is the node spacing; S is storage coefficient; T is transmissivity; and $\Delta h_0/\Delta t$ represents the rate of change of head at the central node. The circuit equation which we have just obtained is directly analogous to this finite-difference form of the ground-water equation, except for the use of the time derivative notation $d\phi_0/dt$ as opposed to the finite-difference form, $\Delta h_0/\Delta t$. In other words, the circuit element composed of the four resistors and the capacitor behaves in approximately the same way as the prism of confined aquifer which was postulated in developing the ground-water equations. It follows that a *network* composed of circuit elements of this type, such as that shown in the figure, should behave



G indicates grounded terminal

in the same way as a two-dimensional confined aquifer of similar geometry. The non-equilibrium behavior of such an aquifer may be studied by constructing a model of the aquifer, consisting of a network of this type; electrical boundary conditions similar to the observed hydraulic boundary conditions are imposed on the model, and voltage is monitored at various points in the network as a function of time. The voltage readings constitute, in effect, a finite-difference solution to the differential equation describing head

in the aquifer. The time scale of model experiments is of course much different from that of the hydrologic regime. A common practice is to use a very short time scale, in which milliseconds of model time may represent months in the hydrologic system. When time scales in this range are employed, the electrical excitations, or boundary conditions, are applied repeatedly at a given frequency, and the response of the system is monitored using oscilloscopes. The sweep frequency of each recording oscilloscope is synchronized with the frequency of repetition of the boundary-condition inputs, so that the oscilloscope trace represents a curve of voltage, or head, versus time, at the network point to which the instrument is connected.

QUESTION

Suppose we wish to model an aquifer in which transmissivity varies from one area to another, while storage coefficient remains essentially constant throughout the aquifer. Which of the following procedures would you consider an acceptable method of simulating this condition in a resistance-capacitance network analog?

Turn to Section:

- | | |
|---|----|
| Construct a network using uniform values of resistance and capacitance, but apply proportionally higher voltages in areas having a high transmissivity. | 2 |
| Construct a network in which resistance and capacitance are both increased in proportion to local increases in transmissivity. | 14 |
| Construct a network in which resistance is varied inversely with the transmissivity to be simulated, while capacitance is maintained at a uniform value throughout the network. | 5 |

23 •

Your answer in Section 26,

$$\frac{I}{w \cdot l} = -\sigma \frac{\partial \phi}{\partial z},$$

is not correct. The answer which you chose actually expresses the component of current density in the z direction. $w \cdot l$ is an area taken normal to the z direction. If I represents the current through this area, $I/w \cdot l$ will give the component of current density in the z direction; and this should equal $-\sigma$

times the directional derivative of voltage in the z direction, $\partial \phi / \partial z$. However, the question asked for the current density component in the x direction; and in fact, the problem stated that the current flow was two dimensional confined to the x, y plane. This implies that the current component in the vertical direction is zero, and thus that $\partial \phi / \partial z$ is zero as well.

Return to Section 26 and choose another answer.

24 •

Your answer in Section 6 is not correct. Ohm's law was given in Section 1 as

$$I = \frac{1}{R} (\phi_1 - \phi_2)$$

where $\phi_1 - \phi_2$ is the voltage difference across a resistance, R , and I is the current through the resistance. In Section 6 the expression

$$R = \rho_e \cdot \frac{L}{A}$$

was given for the resistance, where ρ_e is the electrical resistivity of the material of which the resistance is composed; L is the length of the resistance, and A is its cross-sectional area. This expression for resistance should be substituted into the form of Ohm's law given above to obtain the correct answer.

Return to Section 6 and choose another answer.

25 •

Your answer in Section 26,

$$\frac{I}{w \cdot l} = -\sigma \frac{\partial \phi}{\partial y},$$

is not correct. The component of current density in a given direction is defined as the charge crossing a unit area taken normal to that direction, in a unit time. Here we are concerned with the current density component in the x direction; we must accordingly use an area at right angles to the x direc-

tion. In your answer, the area is $w \cdot l$, which is normal to the z direction. Again, the component of current density in a given direction is proportional to the directional derivative of voltage in that direction. Since we are dealing with the component of current density in the x direction, we require the derivative of voltage in the x direction. The answer which you chose, however, uses the derivative of voltage with respect to y .

Return to Section 26 and choose another answer.

26

Your answer in Section 28 is correct. The term

$$\frac{h_1 - h_2}{L_p}$$

is equivalent to the negative of the head gradient, $-\partial h/\partial x$, so that this formulation of Darcy's law is equivalent to those we have studied previously. Now let us compare this form of Darcy's law with Ohm's law.

Our expression for Darcy's law was

$$Q = K \cdot \frac{h_1 - h_2}{L_p} \cdot A_p.$$

Our expression for Ohm's law in terms of electrical conductivity was

$$I = \sigma \cdot \frac{\phi_1 - \phi_2}{L} \cdot A.$$

In terms of electrical resistivity, we obtained

$$I = \frac{1}{\rho} \cdot \frac{\phi_1 - \phi_2}{L} \cdot A.$$

In these forms, the analogous quantities are easily identified. Voltage takes the place of head, current takes the place of fluid discharge and as noted in the preceding section σ , or $1/\rho$, takes the place of hydraulic conductivity. We note further that since current is defined as the rate of movement of electric charge across a given plane, while fluid discharge is the rate of transport of fluid volume across a given plane, electric charge may be considered analogous to fluid volume.

In Part II, we noted that Darcy's law could be written in slightly more general form as

$$q_x = \frac{Q_x}{A} = -K \frac{\partial h}{\partial x}$$

$$q_y = \frac{Q_y}{A} = -K \frac{\partial h}{\partial y}$$

and

$$q_z = \frac{Q_z}{A} = -K \frac{\partial h}{\partial z}$$

where q_x is the component of the specific-discharge vector in the x direction, or the discharge through a unit area at right angles to the x axis; q_y is the component of the specific-discharge vector in the y direction, and q_z is the component in the z direction. The three components are added vectorially to obtain the resultant specific discharge. $\partial h/\partial x$, $\partial h/\partial y$, and $\partial h/\partial z$ are the directional derivatives of head in the x , y , and z directions; and K is the hydraulic conductivity, which is here assumed to be the same in any direction. We may similarly write a more general form of Ohm's law, replacing the term $\phi_1 - \phi_2/L$ by derivatives of voltage with respect to distance, and considering components of the current density, or current per unit cross-sectional area, in the three space directions. This gives

$$\left(\frac{I}{A}\right)_x = -\sigma \frac{\partial \phi}{\partial x} = -\frac{1}{\rho_e} \frac{\partial \phi}{\partial x}$$

$$\left(\frac{I}{A}\right)_y = -\sigma \frac{\partial \phi}{\partial y} = -\frac{1}{\rho_e} \frac{\partial \phi}{\partial y}$$

$$\left(\frac{I}{A}\right)_z = -\sigma \frac{\partial \phi}{\partial z} = -\frac{1}{\rho_e} \frac{\partial \phi}{\partial z}$$

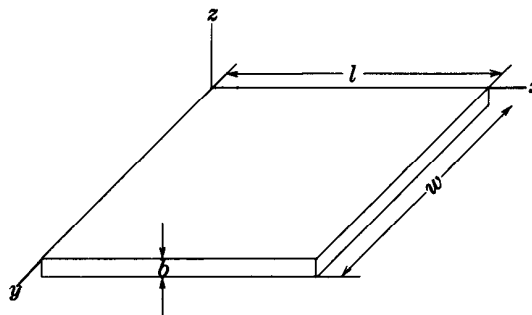
Here $(I/A)_x$ is the current through a unit area oriented at right angles to the x axis, $(I/A)_y$ is current through a unit area perpendicular to the y axis, and $(I/A)_z$ is the current through a unit area perpendicular to the z axis. These terms form the components of the current density vector. $\partial \phi/\partial x$, $\partial \phi/\partial y$, and $\partial \phi/\partial z$ are the voltage gradients, in units of volts/distance, in the three directions. These three expressions simply represent a generalization to three dimensions of the equation given in Section 1 as Ohm's law.

QUESTION

The picture shows a rectangle in a conductive sheet, in which there is a two-dimensional flow of electricity. The flow is in the plane of the sheet, that is, the x, y plane; the thickness of the sheet is b , and the dimensions of the rectangle are l and w . Which of the following expressions gives the magnitude of the component of current density in the x direction?

$\frac{I}{w \cdot b} = -\sigma \frac{\partial \phi}{\partial x}$	11
$\frac{I}{w \cdot l} = -\sigma \frac{\partial \phi}{\partial y}$	25
$\frac{I}{w \cdot l} = -\sigma \frac{\partial \phi}{\partial z}$	23

Turn to Section:



(I represents the current through the area utilized in the equation, $w \cdot b$ or $w \cdot l$.)

Your answer in Section 4 is not correct. The essential idea here is that the rate of accumulation of charge on the capacitor must equal the net inflow minus outflow of charge through the four resistors. The inflow of charge through resistor 1 is the current through that resistor, and is given by Ohm's law as

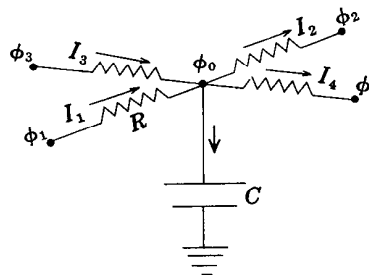
$$I_1 = \frac{1}{R}(\phi_1 - \phi_0).$$

The outflow through resistor 2 is similarly given by

$$I_2 = \frac{1}{R}(\phi_0 - \phi_2).$$

The inflow through resistor 3 is

$$I_3 = \frac{1}{R}(\phi_3 - \phi_0),$$



27 • —Con.

while the outflow through resistor 4 is

$$I_4 = \frac{1}{R}(\phi_0 - \phi_4).$$

The net inflow minus outflow of charge to the capacitor is

$$I_1 + I_3 - I_2 - I_4,$$

and this must equal the rate of accumulation of charge on the capacitor, $d\epsilon/dt$, that is

$$I_1 + I_3 - I_2 - I_4 = \frac{d\epsilon}{dt}.$$

According to the capacitor equation, $d\epsilon/dt$ is given by

$$\frac{d\epsilon}{dt} = C \frac{d\phi_0}{dt}.$$

The answer to the question of Section 4 can be obtained by substituting the appropriate expressions for I_1, I_2, I_3, I_4 and $d\epsilon/dt$ into the relation

$$I_1 + I_3 - I_2 - I_4 = \frac{d\epsilon}{dt},$$

and rearranging the result.

Return to Section 4 and choose another answer.

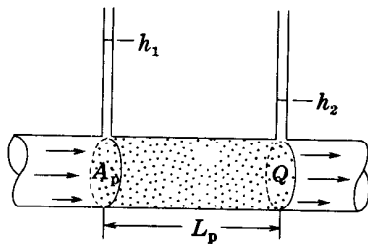
28 •

Your answer in Section 6 is correct.

Electrical conductivity, or 1/resistivity, is the electrical equivalent of hydraulic conductivity. In terms of electrical conductivity, Ohm's law for the problem of Section 6 becomes

$$I = \frac{\sigma A}{L}(\phi_1 - \phi_2)$$

where σ is electrical conductivity.



The analogy between Darcy's law and Ohm's law is easily visualized if we consider the flow of water through a sand-filled pipe, of length L_p and cross-sectional area A_p , as shown in the diagram. The head at the inflow end of the pipe is h_1 , while that at the outflow end is h_2 . The hydraulic conductivity of the sand is K .

QUESTION

Which of the following expressions is obtained by applying Darcy's law to this flow? (Q represents the discharge through the pipe.)

Turn to Section:

$$Q = -K \cdot \frac{\partial^2 h}{\partial x^2} \cdot A_p \quad 12$$

$$Q = K \cdot \frac{h_1 - h_2}{L_p} \cdot A_p \quad 26$$

$$Q = \frac{K}{A_p} \cdot \frac{L_p}{h_1 - h_2} \quad 7$$

References

- Bedinger, M. S., Reed, J. E., Wells, C. J., and Swafford, B. F., 1970, Methods and applications of electrical simulation in ground-water studies in the lower Arkansas and Verdigris River valleys, Arkansas and Oklahoma: U.S. Geol. Survey Water-Supply Paper 1971, 71 p.
- Boulton, N. S., 1954, The drawdown of the water table under nonsteady conditions near a pumped well in an unconfined formation: Proc. Civil Engineers (British), p. 564-579.
- Bredehoeft, J. D., and Pinder, G. F., 1970, Digital analysis of areal flow in multi-aquifer ground water systems: A quasi three-dimensional model: Water Resources Research, v. 6, no. 3, p. 883-888.
- Brown, R. H., 1962, Progress in ground water studies with the electric analog model: Am. Waterworks Assoc. Jour., v. 54, no. 8, p. 943.
- Cooper, H. H., 1966, The equation of ground water flow in fixed and deforming coordinates: Jour. Geophys. Research, v. 71, no. 20, p. 4785-4790.
- Cooper, H. H., Bredehoeft, J. D., and Papadopoulos, S. S., 1967, Response of a finite diameter well to an instantaneous charge of water: Water Resources Research, v. 3, no. 1.
- Cooper, H. H., and Jacob, C. E., 1946, A generalized graphical method of evaluating formation constants and summarizing well-field history: Am. Geophys. Union Trans., v. 27, no. 4, Aug. 1946, p. 526-534.
- Darcy, Henri, 1856, Les fontaines publiques de la ville de Dijon (The water supply of Dijon): Paris, Victor Dalmont, 647 p.
- Domenico, P. A., 1972, Concepts and models in ground water hydrology: New York, McGraw-Hill Book Co., 405 p.
- Dupuit, Jules, 1863, Etudes théoriques et pratiques sur le mouvement des eaux courantes (Theoretical and practical studies on the movement of running water): Paris, Carillon-Goery et V. Dalmont, 275 p.
- Ferris, J. G., 1959, Ground water, Chapter 6 in Wisler, C. O., and Brater, E. F., Hydrology (2d edition): New York, John Wiley and Sons.
- Ferris, J. G., and Knowles, D. B., 1963, The slug-injection test for estimating the transmissibility of an aquifer in Methods of determining permeability, transmissibility, and drawdown: U.S. Geol. Survey Water-Supply Paper 1536-I, 299 p.
- Ferris, J. G., Knowles, D. B., Brown, R. H., and Stallman, R. W., 1962, Theory of aquifer tests: U.S. Geol. Survey Water-Supply Paper 1536-E, 174 p.
- Forsythe, G. E., and Wasow, W. R., 1960, Finite difference methods for partial differential equations: New York, John Wiley and Sons.
- Freeze, R. A., 1971, Three-dimensional, transient, saturated-unsaturated flow in a ground water basin: Water Resources Research, v. 7, no. 2, p. 347-366.
- Hantush, M. S., 1959, Nonsteady flow to flowing wells in leaky aquifers: Jour. Geophys. Research, v. 64, no. 8, p. 1043.
- 1960, Modification of the theory of leaky aquifers: Jour. Geophys. Research, v. 65, no. 11, p. 3713-3725.
- 1967a, Flow of ground water in relatively thick leaky aquifers: Water Resources Research, v. 3, no. 2, p. 583.
- 1967b, Flow to wells in aquifers separated by a semipervious layer: Jour. Geophys. Research, v. 72, no. 6, p. 1709.
- Hantush, M. S., and Jacob, C. E., 1955, Nonsteady radial flow in an infinite leaky aquifer: Am. Geophys. Union Trans., v. 36, no. 1, p. 95.
- Hildebrand, F. B., 1968, Finite-difference equations and simulations: Englewood Cliffs, N.J., Prentice-Hall Inc., 338 p.
- Hubbert, M. K., 1940, The theory of ground-water motion: Jour. Geology, v. 48, no. 8, pt. 1, p. 785-944.
- Jacob, C. E., 1946, Radial flow in a leaky artesian aquifer: Am. Geophys. Union Trans., v. 27, no. 2, p. 198.
- 1950, Flow of ground water, Chapter 5 in Rouse, Hunter, Engineering Hydraulics: New York, John Wiley and Sons, 1039 p.
- 1963, Correction of drawdown caused by a pumped well tapping less than the full thickness of an aquifer in Methods of determining permeability, transmissibility, and drawdown: U.S. Geol. Survey Water-Supply Paper 1536-I, p. 272-282.
- Jacob, C. E., and Lohman, S. W., 1952, Nonsteady flow to a well of constant drawdown in an extensive aquifer: Am. Geophys. Union Trans., v. 33, no. 4, p. 559-569.
- Karplus, W. J., 1958, Analog simulation: New York, McGraw-Hill Book Co., 434 p.
- Lang, S. M., 1963, Drawdown patterns in aquifers having a straight line boundary in Shortcuts and special problems in aquifer tests: U.S. Geol. Survey Water-Supply Paper 1545-C.
- Muskat, M., 1937, The flow of homogeneous fluids through porous media: Ann Arbor, Mich., J. W. Edwards, Inc. [repr. 1946].

- Papadopoulos, S. S., and Cooper, H. H., 1967, Drawdown in a well of large diameter: *Water Resources Research*, v. 3, no. 1.
- Patten, E. P., 1965, Design, construction and use of electric analog models, in Wood, L. A., and Gabrysch, R. K., Analog model study of ground water in the Houston District, Texas: *Texas Water Comm. Bull.* 6508.
- Peaceman, D. W., and Rachford, H. H., 1955, The numerical solution of parabolic and elliptic differential equations: *Jour. Soc. Indust. Appl. Math.*, v. 3, no. 1, March, 1955.
- Pinder, G. F., and Bredehoeft, J. D., 1968, Applications of digital computer for aquifer evaluation: *Water Resources Research*, v. 4, no. 5, p. 1069-1093.
- Prickett, T. A., and Lonquist, G. C., 1971, Selected digital computer techniques for groundwater resource evaluation: *Illinois State Water Survey Bull.* 55, 62 p.
- 1973, Aquifer simulation model for use on disk supported small computer systems: *Illinois State Water Survey Circ.* 114, 21 p.
- Remson, Irwin, Appel, C. A., and Webster, R. A., 1965, Ground water models solved by digital computer: *Jour. Hydr. Div., Am. Soc. Civil Engineers*, v. 91, no. HY3, p. 133-147.
- Remson, Irwin, Hornberger, G. M., and Molz, F. J., 1971, Numerical methods in ground water hydrology: New York, Wiley Interscience Division, John Wiley and Sons, 389 p.
- Rubin, Jacob, 1968, Theoretical analysis of two-dimensional transient flow of water in unsaturated and partly unsaturated soils: *Soil Sci. Soc. America Proc.*, v. 32, no. 5, p. 607-615.
- Skibitzke, H. E., 1960, Electronic computers as an aid to the analysis of hydrologic problems: *Internat. Assoc. Scientific Hydrol. Pub.* 52, *Comm. Subterranean waters*, Gentbrugge, Belgium, p. 347.
- 1963, Determination of the coefficient of transmissibility from measurements of residual drawdown in a bailed well in *Methods of determining permeability, transmissibility, and drawdown: U.S. Geol. Survey Water-Supply Paper* 1536-I, p. 293.
- Slichter, C. S., 1899, Theoretical investigation of the motion of ground waters: *U.S. Geol. Survey, 19th Ann. Rept.*, pt. 2, p. 295.
- Stallman, R. W., 1956, Numerical analysis of regional water levels to define aquifer hydrology: *Am. Geophys. Union Trans.*, v. 37, no. 4, p. 451-460.
- 1963a, Type curves for the solution of single boundary problems in Shortcuts and special problems in aquifer tests: *U.S. Geol. Survey Water-Supply Paper* 1545-C, p. 45-47.
- 1963b, Electric analog of three dimensional flow to wells and its application to unconfined aquifers: *U.S. Geol. Survey Water-Supply Paper* 1536-H, 38 p.
- Theis, C. V., 1935, The relation between the lowering of the piezometric surface and the rate and duration of discharge of a well using ground water storage: *Am. Geophys. Union Trans.*, pt. 2, Aug. 1935, p. 519-524.
- 1938, The significance and nature of the cone of depression in ground water bodies: *Econ. Geology*, v. 33, no. 8, p. 889-902.
- Thiem, Gunther, 1906, *Hydrologische methoden (Hydrologic methods)*: Leipzig, J. M. Gebhardt, 56 p.
- Thomas, L. H., 1949, Elliptic problems in linear differential equations over a network: *Watson Scientific Computing Laboratory, Columbia Univ., N.Y.*
- Trescott, P. C., 1973, Iterative digital model for aquifer evaluation: *U.S. Geol. Survey open-file rept.*, June 1973, 63 p.
- Trescott, P. C., Pinder, G. F., and Jones, J. F., 1970, Digital model of alluvial aquifer: *Jour. Hydr. Div., Proc. Am. Soc. Civil Engineers*, HY5, p. 1115-1128.
- Walton, W. C., 1970, Ground water resource evaluation: New York, McGraw-Hill Book Co., 664 p.
- Weeks, E. P., 1969, Determining the ratio of horizontal to vertical permeability by aquifer-test analysis: *Water Resources Research*, v. 5, no. 1, p. 196-214.



GROUNDWATER

R. Allan Freeze / John A. Cherry

CARY JOHNSON

SE ROA 38556

JA_9838